

207

Dec 17 8/13

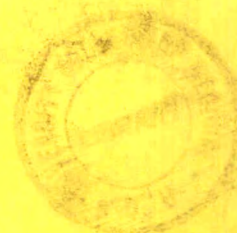
190

# AJR

32

CUK- H08510-32-1024459

American  
Journal of  
Roentgenology

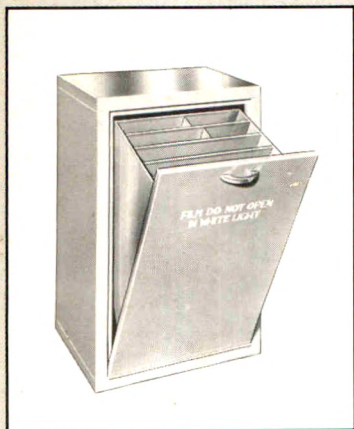


January 1991

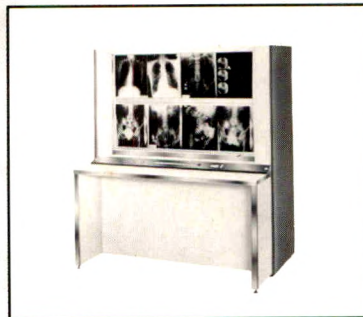
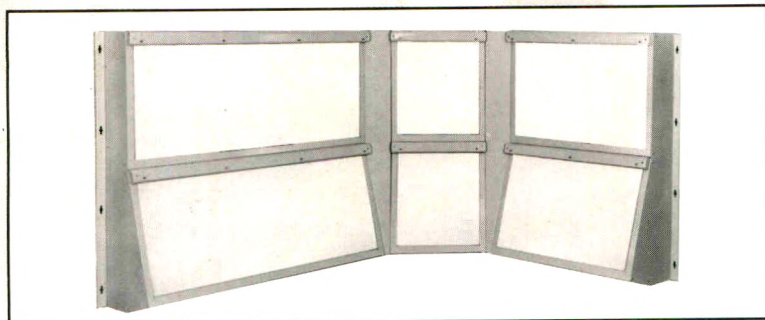


# X-RAY ACCESSORIES

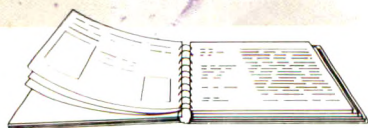
## The Difference is Clear



**T**ried, tested and trusted for over 40 years, S & S x-ray products deliver maximum proficiency and economy -- backed by quality, dependability and innovation.



**F**or a FREE copy of our fully illustrated, 100+ page catalog, contact S & S directly or your local x-ray dealer.



**X-RAY Film Viewers** ◆

**X-RAY Protection** ◆

**X-RAY Files** ◆

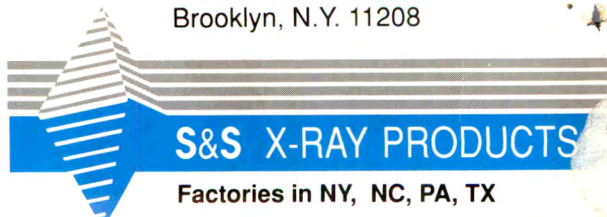
**X-RAY Darkroom Equipment** ◆

**X-RAY Cabinets** ◆

**X-RAY Accessories** ◆

**Phone:** 718/649-8500  
**FAX:** 718/257-0219  
**Toll Free:** 800/347-XRAY

1101 Linwood Street  
Brooklyn, N.Y. 11208



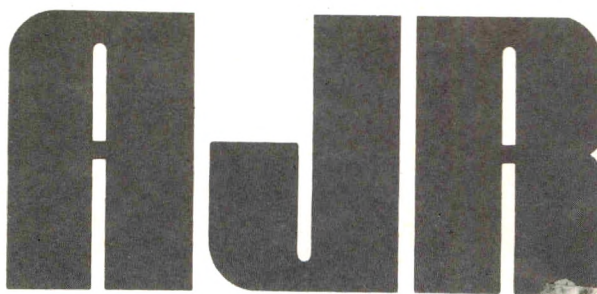
**S&S X-RAY PRODUCTS**

Factories in NY, NC, PA, TX



Official Journal of the American Roentgen Ray Society

Dec 17 <sup>8</sup>/<sub>93</sub>



**American Journal of Roentgenology**  
Diagnostic Imaging and Related Sciences

**Editor-In-Chief** Robert N. Berk, *La Jolla, California*  
*University of California, San Diego*  
*School of Medicine and Medical Center*

**Editor Emeritus** Melvin M. Figley, *Seattle, Washington*

**Associate Editor** Saskia von Waldenburg Hilton, *San Diego, California*

**Consulting Editor** Michael S. Huckman, *Chicago, Illinois*

**Statistician** Charles C. Berry, *San Diego, California*

P 24 459

**Editorial Board**

John R. Amberg  
Itamar Aviad  
Mark E. Baker  
Lawrence W. Bassett  
Michael A. Bettmann  
Felix S. Chew  
N. Reed Dunnick  
David K. Edwards  
Ronald G. Evens  
David S. Feigin  
Sandra K. Fernbach  
Richard H. Gold  
William R. Hendee

John R. Hesselink  
Charles B. Higgins  
Melvyn T. Korobkin  
Faye C. Laing  
Thomas L. Lawson  
Robert G. Levitt  
Bruce L. McClennan  
Richard P. Moser  
Albert A. Moss  
Jeffrey H. Newhouse  
Donald L. Resnick  
Stewart R. Reuter  
Charles A. Rohrmann, Jr.

Peter M. Ronai  
Sjef H. J. Ruijs  
Stuart S. Sagel  
David J. Sartoris  
Stefan C. Schatzki  
William P. Shuman  
Edward A. Sickles  
Barry A. Siegel  
David D. Stark  
Edward T. Stewart  
Murali Sundaram  
Eric vanSonnenberg  
Robert K. Zeman

**Editorial Staff:** Margaret Levene, *managing editor*; Katie L. Spiller, Barbara Rose, Barbara L. Halliburton, and Janine Anderson, *manuscript editors*; Nancy Rydbeck, *office manager*; Sheri Smith, *administrative assistant*; Linda J. Waggoner, *administrative secretary*.

AJR, AMERICAN JOURNAL OF ROENTGENOLOGY (ISSN 0361 803X) is the official journal of the American Roentgen Ray Society and is published monthly by Williams & Wilkins, 428 E. Preston St., Baltimore, MD 21202. Annual dues include \$50 for journal subscription. Second-class postage paid at Baltimore, MD, and at additional mailing offices. Postmaster, send address changes (Form 3579) to AJR, 428 E. Preston St., Baltimore, MD 21202. Subscription rates \$125 (\$180 foreign); institutions \$135 (\$190 foreign); in training \$25 (\$80 foreign); single copy \$18 (\$22 foreign). Airmail rates furnished on request. Indexed by *Current Contents* and *Index Medicus*. Copyright © 1990 by American Roentgen Ray Society.

0361-803X/90\$3.00





**e basically  
s of laser  
systems.**



# AJR Guidelines for Authors

Address new and revised manuscripts, correspondence, and classified ads to the Editor:

AJR Editorial Office  
2223 Avenida de la Playa, Suite 103  
La Jolla, CA 92037-3218

Telephone: (619) 459-2229; FAX: (619) 459-8814

Inquiries regarding subscriptions, display advertising, reprints, or permission to republish *AJR* material should be addressed to the publisher:

The Williams & Wilkins Co.  
428 E. Preston St.

Baltimore, MD 21202 Telephone: 1-800-638-6423

The *AJR* publishes original contributions to the advancement of medical diagnosis and treatment. Submitted manuscripts should not contain previously published material and should not be under consideration for publication elsewhere. Papers dealing with neuroradiology should be addressed to: American Journal of Neuroradiology, Dept. of Radiology, Massachusetts General Hospital, Boston, MA 02114. At the discretion of the *AJR* Editor, *AJNR* articles that are of interest to the general reader may be republished in the *AJR*. Neuro-radiologic papers sent to the *AJR* will be forwarded to the Editorial Office of the *AJNR*.

Manuscript decisions are based on peer review. Reviewers receive manuscripts without title pages to ensure an unbiased review. Statements made in the article, including changes made by the Editor or manuscript editor, are the responsibility of the author and not of the *AJR* or its publisher. Authors will be sent the edited manuscript, galley proof, and proofs of illustrations. If the corresponding author will be unavailable to review galleys, arrangements should be made for a coauthor or colleague to read and return the proof.

The following guidelines are based on instructions set forth in the **Uniform Requirements for Manuscripts Submitted to Biomedical Journals** (*Ann Intern Med* 1988;108:258-265). Articles will be edited, however, to conform to the individual style of *AJR*.

## General Guidelines for Major Papers

**Abstract.** Clearly state (in 200 words or less) the purpose, methods, results, and conclusions of the study. Include actual data.

**Introduction.** Briefly describe the purpose of the investigation and explain why it is important.

**Methods.** Describe the research plan, the materials (or subjects), and the methods used, in that order. Explain in detail how disease was confirmed and how subjectivity in observations was controlled.

**Results.** Present results in a clear, logical sequence. If tables are used, do not duplicate tabular data in text, but do describe important trends and points.

**Discussion.** Describe the limitations of the research plan, materials (or subjects), and methods, considering both the

purpose and the outcome of the study. When results differ from those of previous investigators, explain the discrepancy.

## AUTHOR'S CHECKLIST

**For priority handling, complete the following checklist, sign the copyright form on the reverse side of this page, and include both with the manuscript.**

\_\_\_\_\_ Two copies of the manuscript (the original and a photocopy) and two complete sets of figures are submitted. One copy has been retained by the author.

\_\_\_\_\_ If appropriate, *AJR* Guidelines for case reports, technical notes, pictorial essays, or letters to the Editor have been followed. (See page A11.)

\_\_\_\_\_ The manuscript, including references, figure legends, and tables, is typed double-spaced on 8½ × 11 in. (21.6 × 27.9 cm) *nonerasable* paper. Right-hand margins are not justified.

\_\_\_\_\_ All manuscript pages are numbered consecutively beginning with the abstract. Authors' names do not appear on the manuscript pages.

\_\_\_\_\_ The manuscript is organized as follows: title page, blind title page (title only), abstract, introduction, methods, results, discussion, acknowledgments, references, tables, figure legends, and figures.

\_\_\_\_\_ Informed consent has been obtained from patients who participated in clinical investigations. If experiments were performed on animals, authors complied with NIH guidelines for use of laboratory animals.

\_\_\_\_\_ Use of unfamiliar acronyms and abbreviations is kept to a minimum. When abbreviations are used they are defined at first mention, followed by the abbreviation in parentheses.

\_\_\_\_\_ Metric measurements are used throughout, or the metric equivalent is given in parentheses.

\_\_\_\_\_ Names and locations (city and state only) of manufacturers are given for equipment and nongeneric drugs.

## Title Page

\_\_\_\_\_ The following information is given: title of article; names and complete addresses (including zip code) of all authors; current addresses of authors who have moved since study; acknowledgment of grant or other assistance. The corresponding author is clearly identified, and a current address, phone number, and FAX number are given.

\_\_\_\_\_ Two copies of a blind title page are included giving only the title (without the authors' names) for use in the review process.

## Abstract

\_\_\_\_\_ An abstract of approximately 200 words concisely states the purpose, methods, and results of the study in one paragraph. Actual data are included. Conclusions are stated in a second, summary paragraph.

\_\_\_\_\_ No abbreviations or reference citations are used.



References

References (not to exceed 35) are typed double-spaced starting on a separate page and are **numbered consecutively in the order in which they appear in the text**. All references are cited in the text and are enclosed in brackets and typed on line with the text (not superscript). Unpublished data are not cited in the reference list, but are cited parenthetically in the text, for example, (Smith DJ, personal communication), (Smith DJ, unpublished data). This includes papers submitted, but not yet accepted, for publication. Inclusive page numbers (e.g., 333–335) are given for all references. Journal names are abbreviated according to *Index Medicus*. Style and punctuation of references follow the format illustrated in the following examples (all authors are listed when six or fewer; when seven or more authors, the first three are listed, followed by “et al.”):

Journal article

1. Long RS, Roe EW, Wu EU, et al. Membrane oxygenation: radiographic appearance. *AJR* 1986;146:1257–1260

Book

2. Smith LW, Cohen AR. *Pathology of tumors*, 6th ed. Baltimore: Williams & Wilkins, 1977:100–109

Chapter in a book

3. Breon AJ. Serum monitors of bone metastasis. In: Clark SA, ed. *Bone metastases*. Baltimore: Williams & Wilkins, 1983:165–180

Paper presented at a meeting

4. Lau FS, Kirk AN. MR imaging of the spine. Presented at the annual meeting of the American Roentgen Ray Society, Washington, DC, April 1986

Tables

Each table is typed double-spaced on a separate page without vertical or horizontal rules; each has a short, descriptive title. Tables do not exceed two pages in length and contain at least four lines of data. Tables are numbered in the order in which they are cited in the text.

Abbreviations are defined in an explanatory note below each table. Tables are self-explanatory and do not duplicate data given in the text or figures. All arithmetic (percentages, totals, differences) has been double checked for accuracy, and tabular data agree with data given in the text.

Figures and Legends

Two complete sets of original figures are submitted unmounted in labeled envelopes. Figures are clean, unscratched, 5 × 7 in. (13 × 18 cm) glossy prints with **white borders**. A separate print is submitted for each figure part. All figure parts relating to one patient have the same figure number. Each figure is labeled on the back with the figure number and an arrow indicating “top.” For black-and-white figures, labeling is done on a gummed label, which is then affixed to the back of the print. **Never** use labels on **color figures**, but write figure number on the back lightly in pencil. **Never** use ink on front or back of any figures. Author’s names are *not* written on the backs of figures. Only removable (rub-on) arrows and letters are used on the figures. Symbols are uniform in size and style and are not broken or cracked. Images are uniform in size and magnification. Line drawings are done in black ink on a white background. They are professional in quality, and all use the same size type. (Only glossy prints are acceptable.) Written permission has been obtained for use of all previously published illustrations (and copies of permission letters are included), and an appropriate credit line is given in the legends. Legends are typed double-spaced, and figure numbers correspond with the order in which the figures are cited in the text.

Transfer of Copyright Agreement, Conflict of Interest Acknowledgment, Certification of Coauthors, and Exclusive Publication Statement

Complete copyright to the article entitled: \_\_\_\_\_

is hereby transferred to the American Roentgen Ray Society (for United States government employees to the extent transferable), effective if and when the article is accepted for publication in the *American Journal of Roentgenology*. In the case of the authors who are officers or employees of the United States government, the American Roentgen Ray Society recognizes that works prepared by officers or employees of the United States government as part of their official government duties are in the public domain. Authors reserve all proprietary rights other than copyright, such as patent rights and the right to use all or part of this article in future works of their own. The authors retain the right of replication, subject only to crediting the original source of publication and receiving written permission from the publisher. Authors guarantee that this manuscript contains no matter that is libelous or otherwise unlawful, invades individual privacy, or infringes any proprietary rights. Authors understand that they will receive no royalty or other compensation from the American Roentgen Ray Society or the publisher. Authors guarantee that the editor has been or will be informed of any proprietary or commercial interest or conflicts of interest the authors may have that relate directly or indirectly to the subject of this article. All authors certify that they have made substantive and specific intellectual contributions to the article and assume public responsibility for its content. Finally, the authors certify that none of the material in this manuscript has been published previously or is currently under consideration for publication elsewhere.

_____	_____	_____
First author/date	Second author	Third author
_____	_____	_____
Fourth author	Fifth author	Sixth author

This agreement must be signed by all authors in order for the manuscript to be published.



### Case Reports

A case report is a brief description of a special case that provides a message that transcends the individual patient.

**Format.** There is no abstract. The introduction should be a short paragraph giving the general background and the specific interest of the case. No more than one case should be described in detail (similar ones can be mentioned briefly in the discussion). Emphasis should be on the radiologic aspects; clinical information must be limited to that necessary to provide a background for the radiology. The discussion should be succinct and should focus on the specific message and relevance of radiologic methods. A review of the literature is not appropriate.

**Length.** Maximum of five double-spaced, typewritten pages, including the references but not the title page or figure legends.

**References.** Maximum of eight.

**Figures.** Maximum of three or four, unless the text is shortened accordingly. Legends must not repeat the text.

**Tables and Acknowledgments.** Not appropriate in case reports.

### Technical Notes

A technical note is a brief description of a specific technique or procedure, modification of a technique, or equipment of interest to radiologists.

**Format.** No abstract, headings, or subheadings are required. If headings are used, they should be a combination of "Case Report," "Materials and Methods," "Results," and "Discussion." A brief one-paragraph introduction should be included to give the general background. Discussion should be limited to the specific message, including the uses of the technique or equipment. Literature reviews and lengthy case reports are not appropriate.

**Length.** Maximum of five double-spaced, typewritten pages, including the references but not the title page or figure legends.

**References.** Maximum of eight.

**Figures.** Maximum of two, unless the text is shortened accordingly.

**Tables and Acknowledgments.** Not appropriate in technical notes.

### Pictorial Essays

A pictorial essay is an article that conveys its message through illustrations and their legends. Unlike other *AJR* articles, which are based on original research, pictorial essays serve primarily as teaching tools, like exhibits at a scientific meeting. They are not encyclopedic book chapters. The abstract should be a short, introductory paragraph.

**Length.** Maximum of four double-spaced, typewritten pages, including the references but not the title page or figure legends.

**References.** Maximum of four.

**Figures.** Maximum of 30 figure parts. Number should be as few as necessary to convey the message of the paper.

**Tables and Acknowledgments.** Not appropriate in pictorial essays.

### Letters to the Editor and Replies

Letters to the Editor and Replies should offer objective and constructive criticism of published articles. Letters may also discuss matters of general interest to radiologists. Do not end a letter with a hand-written signature.

**Format.** All letters should be typed double-spaced on nonletterhead paper, with no greeting or salutation. Name and affiliation should appear at the end of the letter. Titles for letters should be short and pertinent. The title for a reply is simply "Reply."

**Length.** Maximum of two double-spaced, typewritten pages, including references.

**References.** Maximum of four.

**Figures.** Maximum of two.

**Tables and Acknowledgments.** Not appropriate in Letters to the Editor and Replies.

### Opinions, Commentaries, and Perspectives

Opinions, commentaries, and perspectives are special articles dealing with controversial topics or issues of special concern to radiologists.

**Format.** Include a title page but no abstract. Headings may be used to break up the text.

**Length.** Maximum of five double-spaced, typewritten pages.

**References.** Maximum of five.

**Tables and Figures.** Maximum of four.

### Computer Page Articles

Articles published on the computer page deal with practical computer applications to radiology.

**Format.** Include a title page but no abstract.

**Length.** Maximum of eight double-spaced, typewritten pages.

**References.** Maximum of five.

**Figures and Tables.** Maximum of five. Computer printouts are not acceptable. Figures must be submitted as 5 × 7 in. glossy prints.

**All submissions to the *AJR* must be accompanied by a completed copy of the Author's Checklist and the signed Copyright Agreement.**



F R O M M A L L





## AJR Business and Subscriber Information

### The American Roentgen Ray Society

*AJR*, *American Journal of Roentgenology*, is published monthly to disseminate research on current developments in the radiologic sciences and commentary on topics related to radiology. It is published by the American Roentgen Ray Society, 1891 Preston White Dr., Reston, VA 22091; (703) 648-8992. Inquiries regarding society business, the annual ARRS meeting, and membership should be addressed to the Society at the above address.

### Correspondence Concerning the *AJR*

Correspondence regarding display (not classified) advertising, subscriptions, address changes, reprints, and permission requests should be addressed to Williams & Wilkins, 428 E. Preston St., Baltimore, MD 21202; (301) 528-4000.

Correspondence regarding editorial matters and classified advertising should be addressed to Editorial Office, *AJR*, 2223 Avenida de la Playa, Ste. 103, La Jolla, CA 92037-3218; telephone (619) 459-2229; FAX (619) 459-8814. For information on manuscript submission, see Guidelines for Authors, pages A3-A5.

### Subscriber Information

Subscription requests and inquiries should be sent to Williams & Wilkins, 428 E. Preston St., Baltimore, MD 21202. ARRS annual dues include \$50 for journal subscription. Subscription rates are as follows: nonmembers, \$125/year (\$180 foreign); institutions, \$135 (\$190 foreign); nonmember in-training, \$25 (\$80 foreign). Single copies of the Journal may

be purchased for \$18 (\$22 foreign). Airmail rates will be furnished on request.

Call toll-free, 1-800-638-6423 (in Maryland call 1-800-638-4007), with subscription questions or problems. Please have the mailing label from your latest issue available when you call.

If a subscriber receives a damaged copy of the *AJR* or fails to receive an issue, the subscriber should notify Williams & Wilkins (428 E. Preston St., Baltimore, MD 21202) within 60 days of publication (90 days for foreign subscribers) and that issue will be replaced.

Change of address information should be sent to Williams & Wilkins, 428 E. Preston St., Baltimore, MD 21202. Allow 90 days for address changes.

### Copyrights, Permissions, and Reprints

The American Roentgen Ray Society holds the copyright for all material published in the *AJR*. No part of this publication may be reproduced without permission from the ARRS. Requests for such permission should be addressed to Williams & Wilkins, 428 E. Preston St., Baltimore, MD 21202.

For reprints of a particular article, please contact the author designated in the footnotes for that article.

### Indexes

The *AJR* provides volume and yearly indexes (subject and author) in the June and December issues each year. *AJR* articles are also indexed in *Current Contents*, *Index Medicus*, and the cumulative index published by *Radiology*.



## How can the VESS Chair help you do a better Swallow Study?

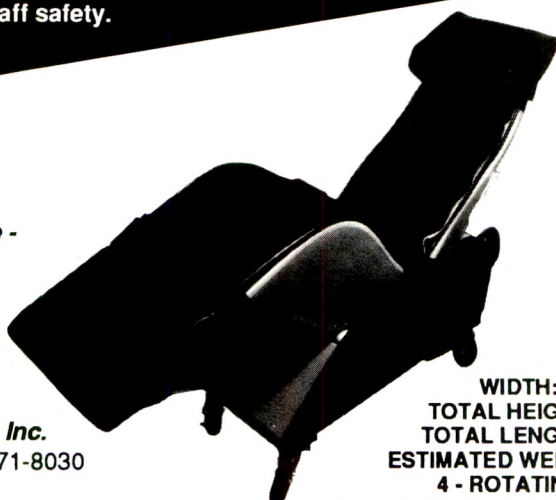
The VESS Chair is an adaptive seating device for the Modified Barium Swallow Study. For reliable Swallow Study outcomes, proper patient positioning and alignment of the head and neck is necessary. The VESS Chair provides Departments of Imaging and Speech/Language Pathology with positioning capability to effectively assess the more difficult or mobility-impaired patient.

The VESS Chair allows for both lateral and anterior-posterior viewing during videofluoroscopy. The VESS Chair's ergonomic design, narrow size, tilting flexibility and transportability will reduce the time needed in the fluoroscopy suite and contribute to patient and staff safety.



### New Features Include -

- IV Stand Holder
- Chart Holder
- Oxygen Tank Holder
- Foley Bag Holder
- Removeable Arms



For More Information Call or Write To: **VESS Chairs, Inc.**  
2938 North 61st Street Milwaukee, WI 53210 (414) 871-8030  
**Demonstration Video Available.**

**WIDTH:** 15-1/2 inches  
**TOTAL HEIGHT:** 50 inches  
**TOTAL LENGTH:** 52 inches  
**ESTIMATED WEIGHT:** 110 lbs.  
**4 - ROTATING CASTORS**

## Minding our P's & Q's is a high priority at Williams & Wilkins



People and Quality are the P's and Q's Williams & Wilkins represents. We put the two together because we believe the people who are important to us—our valued, longstanding subscribers—deserve the best quality products and services we can provide.

For customer service,  
call TOLL FREE:  
**1-800-638-6423**

(from anywhere in the U.S.)

Or write:

Subscription Fulfillment  
Department  
**Williams & Wilkins**  
428 East Preston Street  
Baltimore, MD 21202

### INFORMATION FOR SUBSCRIBERS

- |   |   |
|---|---|
| <p><input type="checkbox"/> <b>CHANGE OF ADDRESS.</b> Please notify us eight weeks in advance. Send us your mailing label or your account number, along with your new address, and the date the change of address is to take effect.</p> <p><input type="checkbox"/> <b>GIFT SUBSCRIPTIONS.</b> Do you have a friend or colleague who shares your professional interests? Give him or her a gift subscription to your journal. For assistance with your order, contact Customer Service, using our toll-free number (1-800-638-6423).</p> | <p><input type="checkbox"/> <b>RENEWALS.</b> To ensure uninterrupted service, please renew your subscription two months prior to the expiration date of your current subscription. Current rates are available for up to three years.</p> <p><input type="checkbox"/> <b>CLAIMS OR CANCELLATIONS.</b> Claims for missing or damaged issues are honored for three months after the mailing date of the issue. If, for any reason, you are not satisfied with your subscription, you may cancel and receive a full refund on all unmailed issues.</p> |
|---|---|

To order back issues, bound volumes, reprints of journal articles, microfilm, microfiche, CD-ROM: Call or write Williams & Wilkins, 428 East Preston Street, Baltimore, MD 21202. Toll-free number: 1-800-638-6423.



## Commentary

# Barium Enemas, Latex Balloons, and Anaphylactic Reactions

David W. Gelfand<sup>1</sup>

Most radiologists are aware that the United States Food and Drug Administration (FDA) has ordered a recall of latex balloon-equipped enema tips used for barium enemas. The recall was prompted by an increasing number of severe anaphylactic reactions, including fatalities, during barium enemas, reported to the FDA.

Allergy to latex products is a growing problem because of increased exposure of both medical personnel and lay people to latex since the emergence of the AIDS epidemic. Several recent publications document allergic and anaphylactic reactions to latex gloves [1-5], and an anaphylactic reaction to a condom also has been reported. Of particular interest in the matter of latex balloon-equipped enema tips is a report of an anaphylactic reaction occurring during rectal manometry in which the finger of a latex glove was used to cover the transducer [6].

It was not recognized at first that the latex balloon on enema tips might be the source of allergic and anaphylactic reactions. These reactions were included among the allergic reactions reported as occurring during barium enemas and were attributed to the suspending agents in the barium suspension. However, reports were recently received of fatal anaphylactic reactions occurring after insertion of a balloon-equipped tip but before administration of the barium suspension. At that point, attention was redirected toward the latex balloon.

Latex is a natural product derived from the sap of the rubber tree, and consists of long-chain molecules with an average molecular weight of several hundred thousand. However, the liquid latex supplied to manufacturers also contains small amounts of water-soluble proteins of lesser molecular weight. After the latex rubber product is formed by heating

the liquid latex, water-soluble proteins remain in the product and can be eluted from its surface. It is believed that absorption of these proteins by the rectal mucosa triggers the allergic and anaphylactic reactions.

Although historical evidence suggests that protein elutable from latex products is the allergen, more specific evidence has been provided by Dennis R. Ownby of the Division of Allergy of Henry Ford Hospital of Detroit (personal communication). Blood samples of six patients suspected of having severe allergic or anaphylactic reactions to latex balloons on enema tips were obtained. In vitro tests for latex-specific IgE antibodies were positive in five of the six patients, which provides presumptive evidence that the important allergen in these reactions is the protein elutable from latex. To confirm these initial results, Dr. Ownby requests that radiologists with patients who have had an allergic or anaphylactic reaction in connection with a barium enema contact him so that historical information and a blood sample can be obtained.

Latex allergy is particularly likely to be found in medical personnel and in atopic persons. A 1987 survey of medical personnel in Finland found that 3% were allergic to latex and that 67% of these were atopic [1]. It is therefore advisable to question patients for indications of allergy or asthma before performing a barium enema because of the potential for rapid absorption of allergens through the rectal mucosa. An obvious precaution is that the materials necessary to treat allergic, anaphylactic, and vasovagal reactions should be available where barium enemas are being performed.

The extent of the problem of allergy to balloon-equipped enema tips is reflected in the data base supplied to this author by E-Z-EM Company, which includes all incidents reported from December 1988 through September 1990. During this

<sup>1</sup> Department of Radiology, Bowman Gray School of Medicine, 300 S. Hawthorne Rd., Winston-Salem, NC 27103. Address reprint requests to D. W. Gelfand.



22-month period, 158 incidents related to barium examinations were reported, of which 148 (nine fatal) were associated with barium enema examinations and 10 (none fatal) were associated with oral barium administration. Five of the nine deaths were believed to be unrelated to allergy, with two due to myocardial infarction, and one each due to pulmonary edema, vasovagal reaction, and colonic perforation. In five fatal reactions, three of which were anaphylactic, no barium suspension had been administered; the reactions occurred after insertion of a balloon-equipped tip. It is believed very likely that an undetermined number of the nonfatal "barium" reactions reported in this data base also may be due to the latex balloons. Notably, only 10 reactions to orally administered barium were reported, and only one was severe.

These statistics emphasize the far greater risk associated with barium enema examinations than oral barium examinations. This is probably due to the ability of the rectal mucosa to absorb large molecules into the circulation almost instantaneously. It may be recalled that rectal administration of medications in the form of enemas or suppositories was common practice before the advent of IV therapy.

These data also indicate that fatal reactions due to anaphylaxis are rare. In the available data, four fatal anaphylactic reactions associated with barium enema examinations are recorded. During the reporting period, approximately eight million barium enemas were performed in the United States, suggesting a fatality rate from anaphylactic reactions of less than one in two million examinations.

This extremely low fatality rate raises the question of whether the recall of the enema tips may have adverse consequences greater than the danger posed by anaphylactic reactions occurring during barium enemas. The recall primarily affects elderly, incontinent patients, who are extremely difficult to examine without use of a balloon tip. An unknown number of such patients are likely to be diverted from having a barium enema to undergoing colonoscopy. These patients will be subjected to the far more dangerous colonoscopic examination, which has a mortality rate an order of magnitude greater than the barium enema. A recent publication summarizing reported complications indicates that colonoscopy has a major complication rate of 0.2% (1:500) and a fatality rate of 0.02% (1:5000) [7].

Several possibilities exist to circumvent the inconvenience caused by the recall of balloon enema tips. First, the largest manufacturer of such devices (E-Z EM) has developed a presumably less allergenic silicone rubber balloon tip that should be available in the near future, assuming that no problems are encountered during the FDA approval process. Second, the nondisposable Bardex rubber catheter (C. R.

Bard, Murray Hill, NJ) is still available and remains the most effective of all balloon catheters for helping the incontinent patient retain a barium enema. This particular catheter can be repeatedly cleaned, sterilized, and reused, although the process is less convenient than using a disposable balloon tip.

Apart from these substitutes, radiologists can and should make greater use of the ordinary nonballoon tip, and the patient will be better served by this. Most balloon-equipped enema tips are used for convenience in retaining the tip within the rectum rather than for incontinence. However, nonballoon tips are available with and without the air line required for double-contrast enemas. Retention of these tips can be ensured by properly taping the tip to the patient's buttocks. After insertion of the tip, a strip of adhesive tape is pasted to one buttock, run around the tube below the enema tip, and pasted to the other buttock. This forms a V-shaped sling that retains the tip in the rectum far more successfully than the more common method of taping straight across the buttocks. Apart from minimizing the danger of allergic reactions, use of nonballoon tips also minimizes perforation of the rectum by an enema tip being forced through the anterior wall as the balloon is inflated.

The latex balloon tip recall is a serious inconvenience. However, it may result in safer barium enema examinations, because it seems very likely that many presumed allergic reactions to barium suspensions have all along been due to latex allergy. In time, the silicone rubber balloon tip will be available and should provide greater safety. Also, to the extent that radiologists may learn to forgo the use of balloon tips, fewer rectal perforations are likely to occur.

## REFERENCES

1. Turjanmaa K. Incidence of immediate allergy to latex gloves in hospital personnel. *Contact Dermatitis* 1987;17:270-275
2. Gerber AC, Jörg W, Zbinden S, Seger RA, Dangel PH. Severe intraoperative anaphylaxis to surgical gloves: latex allergy, an unfamiliar condition. *Anesthesiology* 1989;71:800-802
3. Leynadier F, Pecquet C, Dry J. Anaphylaxis to latex during surgery. *Anaesthesia* 1989;44:547-550
4. Turjanmaa K, Räsänen L, Lehto M, Mäkinen-Kiljunen S, Reunala T. Basophil histamine release and lymphocyte proliferation tests in latex contact urticaria. *Allergy* 1989;44:181-186
5. Spaner D, Dolovich J, Tarlo S, Sussman G, Butto K. Hypersensitivity to natural latex. *Clin Immunol* 1989;83:1135-1137
6. Sondheimer JM, Pearlman DS, Bailey WC. Systemic anaphylaxis during rectal manometry with a latex balloon. *Am J Gastroenterol* 1989;84:975-977
7. Habr-Gama A, Waye JD. Complications and hazards of gastrointestinal endoscopy. *World J Surg* 1989;13:193-201



## Review Article

# Color Doppler Flow Imaging

W. Dennis Foley<sup>1</sup> and Scott J. Erickson

**The performance requirements and operational parameters of a color Doppler system are outlined. The ability of an operator to recognize normal and abnormal variations in physiologic flow and artifacts caused by noise and aliasing is emphasized. The use of color Doppler flow imaging is described for the vessels of the neck and extremities, upper abdomen and abdominal transplants, obstetrics and gynecology, dialysis fistulas, and testicular and penile flow imaging.**

Cardiac and vessel wall motion can be recorded by real-time sonography. However, except for the unusual instances in which sluggish venous blood flow can be recognized by recording the rouleaux phenomena, amplitude-dependent sonography is incapable of evaluating blood flow. The advent of duplex Doppler techniques in the late 1970s opened up a new field of sonographic investigation, namely, the direct recording of peripheral, abdominal, and cardiac blood flow, albeit limited to a relatively small sample volume. Normal and abnormal blood flow characteristics were defined by duplex Doppler techniques, setting the stage for clinical acceptance of a new generation of sonographic imaging devices, namely, color Doppler units capable of displaying regional physiologic and pathophysiologic arterial and venous flow in the familiar anatomic format of a gray-scale sonographic image [1]. The inherent visual appeal of color Doppler flow imaging accounts in some measure for the ready acceptance of this technique by both technologists and physicians alike. However, the advantage of visual imagery has also been matched by clinical

usefulness. Not only has color Doppler flow imaging expanded the role of Doppler sonography significantly, but, in a number of instances, it is now being used as a definitive diagnostic test without requirement for correlative angiography.

In this review, important practical aspects of the instrumentation and applications of color Doppler flow imaging are discussed.

### Instrumentation

Peripheral vascular color Doppler flow imaging is best performed with a linear probe, and abdominal color Doppler flow imaging, depending on anatomic area, with either a sector or linear probe. In peripheral vascular imaging, an angle must be made between the face of the transducer and blood flowing in vessels that are parallel to the skin surface. This can be achieved either by using a mechanical plastic sleeve offset (or wedge) or alternatively by electronic beam steering. An advantage of the attached wedge device is that color flow can be appreciated throughout the full longitudinal extent of a vessel included within the field of view. Color flow frame rates of 18 frames/sec for a 4-cm depth of field and 9 frames/sec for a 9-cm depth of field provide a physiologic real-time display of vascular motion. A more complete global display of color flow imaging is provided. This is an advantage either when imaging a selected anatomic area such as the carotid bifurcation or, more particularly, when "tracking" selected extremity vessels, such as the femoral artery, in the longitudinal plane.

Received April 30, 1990; accepted after revision June 28, 1990.

<sup>1</sup> Both authors: Department of Radiology, Medical College of Wisconsin, 8700 W. Wisconsin Ave., Milwaukee, WI 53226. Address reprint requests to W. D. Foley.

AJR 156:3-13, January 1991 0361-803X/91/1561-0003 © American Roentgen Ray Society



### Color Assignment

Color assignment is dependent on the flow direction determined by recorded phase shift. Color hue is dependent on the frequency shift determined by both the velocity of the moving reflectors (RBCs) as well as the angle of insonation between the ultrasound beam and the moving blood. In general, a light color hue is used to encode greater frequency shift. With a linear probe, a vessel with uniform flow velocity and direction and constant angle to the ultrasound beam will provide a uniform color encoding in the image. No color signal will be recorded in a vessel that is parallel to the face of the transducer (Fig. 1A) [2]. With a sector probe, color flow assignment is more complex (Fig. 1B). A vessel with uniform flow velocity and direction will result in a differential frequency shift being recorded along the longitudinal axis of the vessel as this vessel is interrogated by the diverging sound beam. Thus, color hue will change along the longitudinal axis of this vessel despite uniform flow velocity. A vessel that is parallel to the central elements in a curved sector probe will cause phase and frequency shift to be recorded only in the more peripheral elements of the probe. Furthermore, although there is unidirectional uniform flow velocity, color assignment will be at the opposite ends of the spectrum for either end of the vessel and color hue will change also. This again reflects the interaction of flowing RBCs with the diverging sound beam. When sector probes are used for abdominal imaging, it is customary to narrow the "Doppler window" and to angle the sound beam to avoid the effects just described. A narrow Doppler window also provides a faster frame rate.

### Choice of Probe

Peripheral vascular color Doppler flow imaging is performed with transducers varying in the frequency between 5.0 and 7.5 MHz. Higher frequency produces better anatomic resolution in the relatively short depth of field required. Although

high frequency is associated with relatively greater tissue attenuation than is lower frequency, this is compensated by more effective back scattering at higher frequency. In abdominal imaging, insonating frequency varies between 2.5 and 5.0 MHz. Lower frequencies produce greater tissue penetration. In general, a good standard for a deep abdominal Doppler probe is the capability of imaging at 18–20 cm of depth and recording a color flow signal at 13–15 cm of depth.

### Doppler Signal

The Doppler signal has two components, namely, amplitude and phase and frequency shift. Amplitude is dependent on the intensity of the insonating sound beam and its attenuation in tissue, as well as the reflectivity of RBCs. In general, flow sensitivity is increased when sound beam intensity and spatial pulse length are both increased. However, a longer spatial pulse length will degrade, to some extent, the axial resolution within the gray-scale image. Beam intensity should be modulated so that the projected intensity levels in vivo should remain within currently accepted standards, particularly when color Doppler flow imaging is performed in obstetric cases. The current Food and Drug Administration (FDA) recommendation for obstetric pulsed Doppler examination is for a projected spatial peak temporal average intensity of 94 mW/cm<sup>2</sup>.

### Flow Sensitivity

Flow rate sensitivity can be varied by changing the pulse repetition rate for the recorded Doppler signal. When the sampling rate is decreased, the system becomes more sensitive to slower flow. This is an advantage when performing venous studies of the extremities. However, operators must be careful to set the range of recorded frequency shifts so that physiologic flow can be recorded while avoiding color aliasing. Aliasing occurs when blood flow velocity results in a

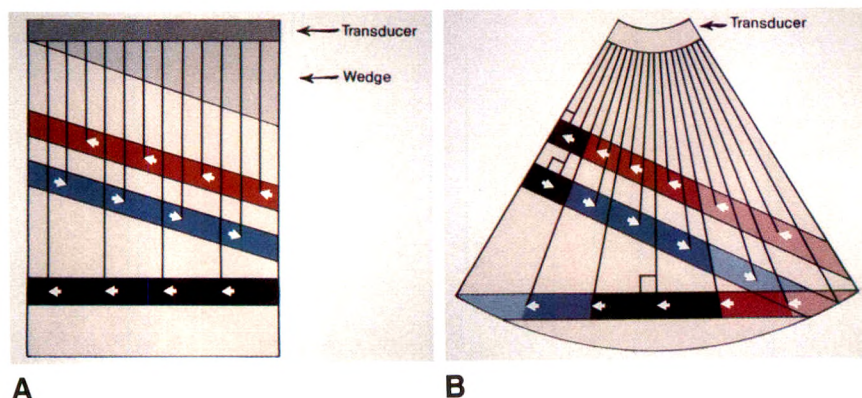


Fig. 1.—Schematic demonstration of color flow assignment for linear and sector format systems.

A, Linear system uses a mechanical plastic sleeve offset (wedge) to create a Doppler angle between face of transducer and vessels that are parallel to skin. Vessels that are parallel to transducer have no Doppler signal. Vessels that make an angle with transducer are assigned red (flow right to left) and blue (flow left to right). Flow is of uniform velocity across cross-sectional area and throughout length of each vessel. Doppler angle is equivalent at all points. Vessels are assigned a uniform color.

B, In sector format, vessels that are parallel to the transducer demonstrate a sequential color change and change in color hue reflecting flow toward and away from "line of sight" of sonic beam and a change in perceived Doppler angle that is greater at each end of the vessel than in the center. Obliquely angled vessels with uniform flow velocity show a change in recorded frequency shift from left to right. At left margin, vessels form a right angle with sonic beam, and no Doppler shift is recorded.

(Reprinted with permission from Foley [2].)



frequency shift that is more than half the pulse repetition rate for the recorded Doppler frequency. This phenomenon is well recognized in duplex Doppler imaging as a "folding over" of the frequency spectrum. In color Doppler flow imaging, aliasing results in the reverse color assignment. Aliasing is likely to occur in arteries with fast flow rates imaged with a narrow Doppler angle (Fig. 2) and with high-velocity flow jets associated with both significant stenoses and arteriovenous fistulas [3]. Aliasing can be either diminished or prevented by baseline shift correction, by increasing the angle between the sound beam and the flowing blood, by increasing the pulse repetition rate for the Doppler signal, and by decreasing insonating sound frequency.

### Operational Parameters

When beginning a color Doppler study, the important operational parameters are to select an appropriate anatomic window, depth-of-field, frame rate, and flow sensitivity. The appropriate anatomic window is usually self-evident, though care should be taken to image the vessels of interest at a Doppler angle varying between 30° and 80°. The color flow frame rate will vary depending on the width of the anatomic window and depth of field. The chosen frame rate should allow the operator to appreciate physiologic phenomena such as carotid bifurcation flow reversal (Fig. 3) [4] and hepatic vein bidirectional flow on the real-time video display. In addition, flow sensitivity should be adjusted so that, with appropriate gain settings, recorded color flow should occupy the full anteroposterior diameter or cross-sectional area of the vessel being imaged during the phase of maximum flow (Fig. 4) [5]. This should be accomplished without color flow aliasing and without the appearance of color noise in the surrounding tissues. In addition, differential flow sensitivity should allow

demonstration of the faster-flowing central systolic arterial streamline, both in medium-sized and small vessels down to the order of 2 mm (Fig. 5).

An important attribute of a color flow system, in addition to absolute and differential flow sensitivity, is color flow resolution, that is, the pixel size for the color flow display. It is the combination of differential flow sensitivity and color flow resolution that is important in imaging small-diameter vessels, such as the interlobar arteries of the kidney and the cavernosal penile vessels. By analogy to radiographs, differential flow sensitivity may be considered equivalent to contrast sensitivity and color flow resolution equivalent to spatial resolution (Fig. 6).

Two additional attributes of a color flow system are important. These are flow registration and motion discrimination (Fig. 6). Flow registration is the recording of color flow signal only within the vessel lumen. Motion discrimination is the differentiation of an intravascular flow signal from perivascular tissue motion. A color flow system should distinguish motion of a high-amplitude tissue reflector from motion of a low-amplitude intravascular RBC reflector. However, when perivascular tissue vibration reaches a critical threshold value, a characteristic color "bruit" is recorded as a phasic indeterminate color assignment in the perivascular tissues (Fig. 7). This finding is associated with high-grade stenoses and arteriovenous fistulas, though it has also been recorded in high-flow states associated with tortuous vessels. When perivascular tissue vibrations are imaged, careful attention should be directed to searching for an underlying vascular abnormality.

Although extremity and abdominal venous studies can be performed by using color Doppler flow imaging only, most arterial studies are performed with a combination of color Doppler flow imaging and selective spectral analysis. By using the graphic real-time portrayal of color flow as a guide, the

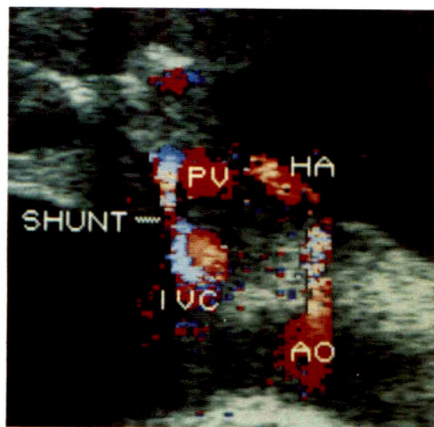


Fig. 2.—Patent portacaval shunt. Transverse subxiphoid sonogram. Shunt is seen as a direct vascular communication between portal vein (PV) and inferior vena cava (IVC). There is color flow aliasing in celiac artery, in which flow is color encoded white and light blue. This reflects both the zero Doppler angle and the rapid arterial flow rate. Local turbulence is seen in inferior vena cava at shunt insertion site. HA = hepatic artery, AO = aorta. (Reprinted with permission from Foley [2].)

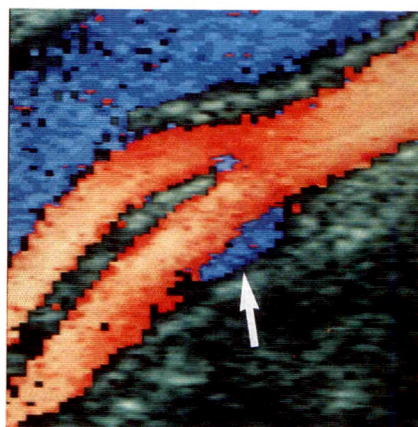


Fig. 3.—Longitudinal sonogram of carotid bifurcation obtained during systole. Physiologic flow reversal is in proximal internal carotid artery (arrow). This typically occurs in posterior lateral aspect of lumen away from takeoff of external carotid artery. Notice that systolic streamline flow in proximal internal carotid artery is eccentric.



Fig. 4.—Longitudinal sonogram of proximal thigh. Color flow occupies full anteroposterior diameter of femoral vein during phase of maximum venous flow (expiration). Minimal color flow signal is seen in deep femoral artery, which is almost parallel to face of transducer. ART = artery.



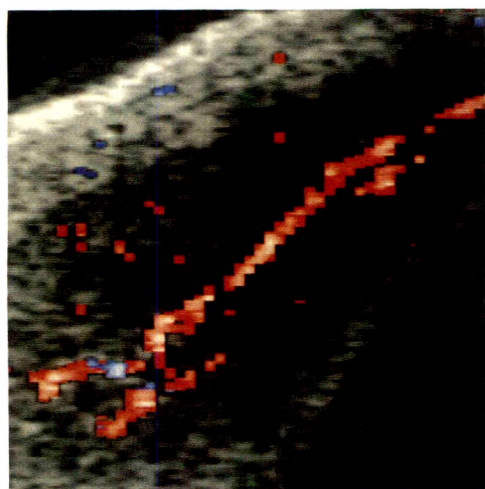


Fig. 5.—Right cavernosal penile artery imaged sonographically after intracorporal injection of papaverine. Differential systolic streamline flow is appreciated in segments of this 2-mm-diameter vessel. Color flow signal is also seen in some helicine vessels traversing image plane.

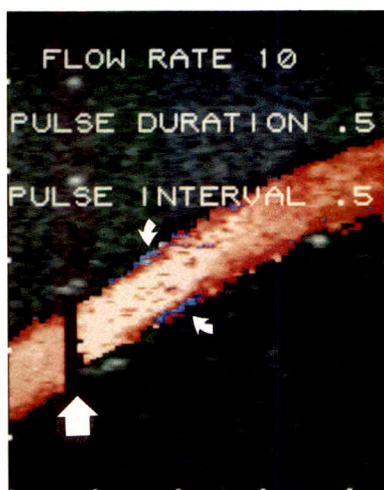


Fig. 6.—Longitudinal sonogram obtained during phase of maximum flow in color flow phantom (Radiation Measurements, Inc., Madison, WI) with a hemodynamically insignificant stenosis (straight arrow). Pulse duration and interval are both 0.5 sec. Cycle rate is 120/min. Note central rapid streamline flow of a whiter hue with differentiation between rapid and slower flow components downstream from stenosis. Eccentric eddy current formation is at vessel margins distal to stenosis (curved arrows). Color signal in small-diameter pixels is recorded up to edge of vessel; there is no color assignment in perivascular pixels. This is a good example of resolution, differential flow sensitivity, and flow registration.

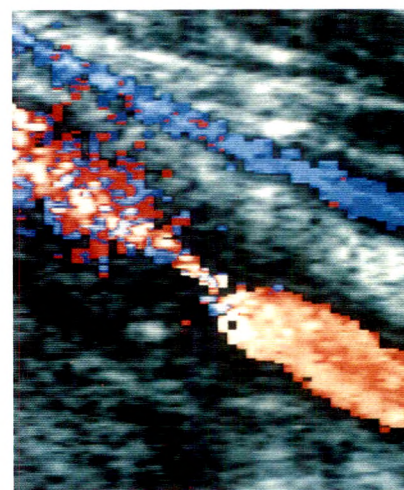


Fig. 7.—Longitudinal sonogram of common carotid artery with segmental high-grade stenosis in patient with atherosclerosis and prior neck irradiation. Sonography was performed during systole (note color bruit); indeterminate color assignment in perivascular tissues is caused by systolic vibration. Intravascular color flow aliasing is present. During diastole, there was a persistent flow jet, but no evidence of aliasing or perivascular tissue bruit.

operator may expeditiously place the sample volume at the site of maximum flow velocity or flow disturbance as appropriate (Fig. 8). This directed placement avoids the repetitive, somewhat undirected placement of sample volumes that occurs with duplex Doppler instruments searching for the site of maximum frequency shift. When spectral analysis is being obtained, the color flow image may be upgraded at rates varying between 0.5 and 2.0 frames/sec.

### Recording

An immediate "cine loop" playback function using built-in random access memory is a significant advantage. With cine loop, up to 10 sec of the previous recording can be played back at real-time acquisition rates or slower. This immediate review capability, when associated with image measurement and spectral analysis capabilities, allows the operator to categorize an abnormality and obtain an appropriate image for recording on hard copy, whether it be Polaroid or color print. A permanent real-time image recording can be obtained on videotape. In fact, it is preferable to record either a color Doppler flow imaging segment or a color Doppler flow imaging plus spectral analysis segment on videotape and then, immediately after recording this segment, to access the same information through the cine loop function for analysis and possible hard-copy recording. A significant advantage of one

vendor's videotape system is that, on replay, the information can be redigitized and reanalyzed. Thus, both direct anatomic measurements from the image and reanalysis of the spectral trace can be performed on the videotape replay. This is useful in case demonstrations, in tutorials, and for slide production. In the future, the large bandwidth of high-quality gray-scale and color images may exceed the bandwidth of reasonably priced commercial videocassette recorders. An alternative approach is real-time digital videodisk recording. For this to be practically feasible, reversible image compression and internal hard wiring may be necessary to allow real-time data transfer without interrupting patient scanning. Digital image transfer to a videodisk system will allow off-line image analysis and recording at an electronic workstation.

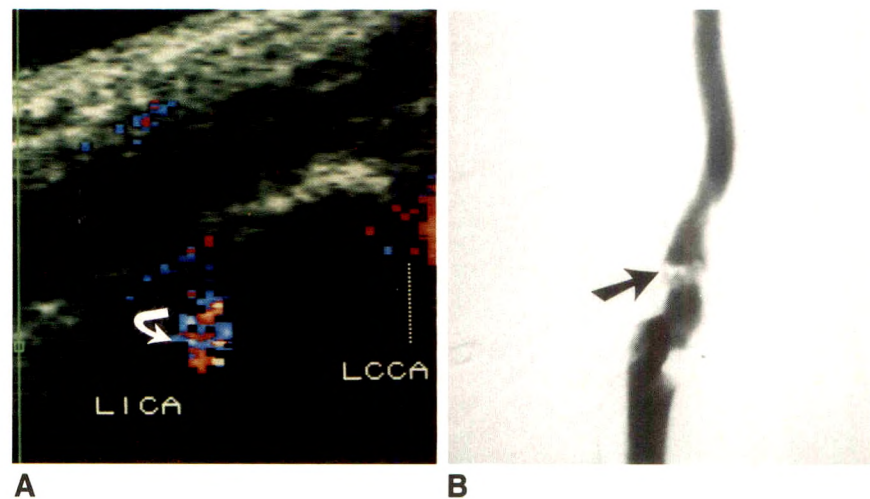
### Clinical Applications

#### Extracranial Carotid and Vertebral Arteries

Color Doppler flow imaging has not expanded the indications for noninvasive testing but has refined the technique. The study is best performed with a high-frequency linear-array probe with a relatively small footprint, a useful attribute when examining the high cervical bifurcation near the neck of the mandible. We perform a real-time color flow study of the common carotid artery, carotid bifurcation, internal and exter-



Fig. 8.—*A* and *B*, High-grade stenosis of left internal carotid artery (LICA) with external carotid artery occlusion. On color Doppler sonogram (*A*), calcified plaque in proximal internal carotid artery obscures underlying lumen for 1.2 cm. Turbulent flow (arrows) is distal to shadowing calcified plaque. Flow disturbance is an indication of hemodynamically significant stenosis seen on arteriogram (*B*). Image of calcified plaque is removed by subtraction process. LCCA = left common carotid artery.



nal carotid arteries, and vertebral arteries before proceeding to selective spectral analysis. In addition, the surface and internal characteristics of plaques are analyzed for the presence of obvious ulceration and internal plaque hemorrhage. On the color Doppler flow imaging display, normal physiologic flow reversal at the carotid bifurcation (Fig. 3) [4], as well as abnormal flow jets and turbulence, can be recognized. In addition, internal carotid artery occlusion may be recognized by early diastolic flow reversal at the stump of an occluded internal carotid artery, and subclavian steal phenomenon can be recognized by reversed flow in a vertebral artery. Reversed flow in the ipsilateral external carotid artery has been noted in patients with common carotid artery occlusion and collateral reconstitution of the internal carotid artery.

Spectral analysis with a display cursor to assign the angle between the sound beam and the axis of flowing blood is used to record real-time flow velocity. Internal carotid artery velocity and internal/common carotid artery velocity ratios provide complementary information to direct measurement of the percent arterial stenosis from the real-time color flow image. Provided that the underlying lumen is not obscured by calcific shadowing plaque, there is good agreement between the measured internal carotid artery stenosis obtained from the color Doppler flow imaging display and that determined by angiography [6]. When the underlying lumen is obscured by calcific shadowing plaque, the characteristics of the flow stream distal to the shadowing plaque are evaluated. If the shadowing plaque obscures the lumen for less than 1 cm and there is no evidence of a flow jet or turbulence distal to the plaque, then it is considered unlikely that a hemodynamically significant stenosis is present. Conversely, the presence of disturbed flow distal to a plaque, whether shorter or longer than 1 cm, is good evidence of an underlying hemodynamically significant stenosis (Fig. 8). In these situations, selective spectral analysis distal to the plaque may underestimate peak systolic velocity as the flow jet beneath the plaque cannot be imaged or interrogated.

Disturbed flow may be associated with tortuosity of the internal carotid artery and at carotid bifurcation thrombo-

endarterectomy sites, particularly those performed with patch angioplasty. The turbulence and nonaxial flow phenomena associated with these conditions probably have led to many overestimations of internal carotid artery stenosis by duplex Doppler studies. Color Doppler flow imaging can clearly differentiate tortuosity from significant stenosis.

The extracranial vertebral arteries are imaged in the mid and lower neck between the foramina transversaria. Flow direction, pulsatility, and internal vessel diameter can be recognized on color Doppler flow imaging. Subclavian steal phenomenon can be demonstrated in both symptomatic and asymptomatic patients. The abnormal vertebral artery flow in the resting state may be either reversed or bidirectional. With bidirectional flow, there is reversed flow in systole and antegrade flow in diastole (Fig. 9). The use of handgrip exercise or imaging after sphygmomanometer cuff release on the upper extremity can convert bidirectional vertebral artery flow to unidirectional reversed flow. The lower arterial resistance in the upper extremity caused by vasodilatation causes the augmented reversed flow. After successful subclavian artery angioplasty, color Doppler flow imaging can demonstrate normal antegrade flow in the ipsilateral vertebral artery.

If only the vertebral vein is imaged, then it is likely that the ipsilateral vertebral artery is occluded, provided that optimal technique, including appropriate power, gain, and sensitivity settings, is used. However, this has not been demonstrated in a sufficiently large patient series to assess its clinical utility. We have not seen a patient with verified bilateral vertebral artery occlusion. The origins of the vertebral arteries from the subclavian arteries in the supraclavicular fossa are difficult to image. We do not believe that color Doppler flow imaging will be of value in diagnosing or excluding stenosis at the orifice of the vertebral artery.

Noninvasive imaging of the extra- and intracranial cerebrovascular system will be possible by using a combination of color Doppler flow imaging and MR imaging. It is possible that the combination of color Doppler flow imaging of the extracranial carotid and vertebral vessels and MR imaging of the intracranial circulation [7] could, in the future, provide



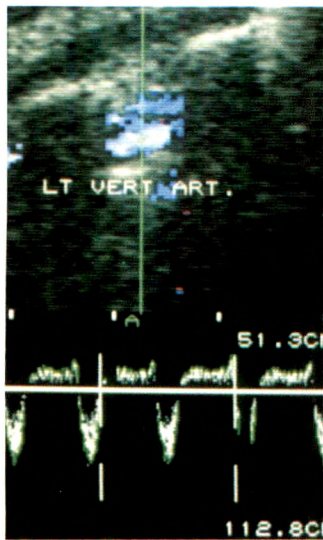


Fig. 9.—Left subclavian artery stenosis with subclavian steal phenomenon. Real-time color flow sonography shows antegrade flow in vertebral artery in diastole and retrograde flow during systole with flow in vertebral artery and vertebral vein in same direction. Selective spectral waveform demonstrates retrograde systolic flow and antegrade diastolic flow. Antegrade diastolic flow presumably reflects greater resistance of resting extremity circulation in comparison with cerebral circulation.

images of sufficient anatomic clarity and diagnostic accuracy to supersede the use of selective carotid arteriography in patients being evaluated for possible carotid endarterectomy.

#### Abdomen

The liver, spleen, and extrahepatic portal venous system are best imaged with a small footprint probe with a sector image format. The probe may be either phased array or curved linear array. This allows imaging of the upper abdominal anatomy through the rib interspaces. The upper abdominal aorta, celiac and superior mesenteric arteries, and renal vessels can be evaluated either with a sector or linear probe. A linear probe is preferred for evaluating the superficial renal and pancreatic transplants and the pregnant uterus.

**Examination technique.**—There are four imaging planes for hepatic imaging that provide the best combination of anatomic display and Doppler flow sensitivity in the insonated vessels. These are a right coronal oblique, transverse epigastric, transverse midclavicular line, and sagittal midline. The right coronal oblique view, when aimed at the hepatic hilum, demonstrates the extrahepatic portal vein and hepatic artery and the right intrahepatic branches of these vessels. The intrahepatic vessels should be followed out to their third-order branches. The right hepatic vein can be imaged in a slightly more posterior and cephalad plane and the middle hepatic vein in a slightly more anterior and cephalad plane.

With the transverse epigastric approach, the left intrahepatic portal vein and accompanying artery are imaged. If there is a prominent left hepatic lobe, then the celiac and common hepatic arteries can be imaged as well as the portal venous confluence. With cephalad angulation, a transverse view of the left hepatic vein can be obtained.

With a transverse imaging plane centered on the midclavicular line overlaying the hepatic hilum, the anterior and posterior branches of the right portal vein and the proximal left portal vein can be imaged. With cephalad angulation, the right

and middle hepatic veins can be imaged to the hepatic venous confluence.

The sagittal midline imaging plane through the left hepatic lobe demonstrates the left portal vein and accompanying hepatic artery and provides a longitudinal view of the left hepatic vein. This imaging plane also can demonstrate left gastric varices and umbilical vein collaterals.

The spleen is examined in a coronal imaging plane directed to the splenic hilum to demonstrate the main splenic artery and vein. Again, intrasplenic vessels should be demonstrated to their third-order branches.

**Portal hypertension.**—The main indications for upper abdominal color Doppler flow imaging are evaluation of portal hypertension, particularly with suspected thrombosis of the portal vein; evaluation of portacaval and splenorenal surgical anastomosis; evaluation of suspected thrombosis of the hepatic vein; and imaging of hepatic transplant recipients, both pre- and postoperatively.

The normal portal vein has hepatopetal flow with flow velocity between 10 and 30 cm/sec and mild changes with respiration. Prominent changes during the cardiac cycle may be noted in patients with severe right heart failure, particularly tricuspid regurgitation.

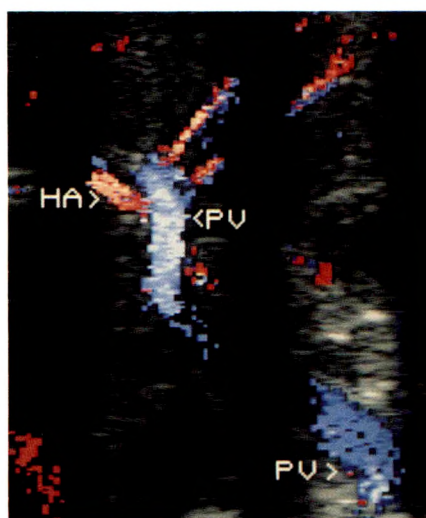
In severe portal hypertension, flow of the portal vein can be reversed. In this situation the portal vein will not be imaged with conventional arterial portography, unless selective hepatic artery injection is performed. Color Doppler flow imaging is a necessary complement to arterial portography in these patients, as a nonthrombosed vessel with hepatofugal flow makes portacaval shunting feasible (Fig. 10).

The prevalence of thrombosis of the portal vein in patients with cirrhosis and gastrointestinal bleeding who have not had surgery is probably on the order of 5%. Thrombosis of the portal vein, either partial or complete, is diagnosed more readily with color Doppler flow imaging than with duplex Doppler imaging as the diagnosis can be made from the real-time display alone. Difficulty can arise in the presence of relatively stagnant or "balanced" flow of the portal vein. Such patients may have transient reversals between hepatopetal and hepatofugal flow. It may not be possible to exclude partial thrombosis of the portal vein in these patients, and in these circumstances, dynamic contrast-enhanced CT scanning is advised. Diagnosis or exclusion of thrombosis of the portal vein in potential hepatic transplant recipients is critical. Complete extrahepatic thrombosis of the portal vein precludes hepatic transplantation.

Patency of side-to-side and end-to-side portacaval shunts can be established by Doppler sonography with a high level of reliability. Evidence of shunt patency is either direct imaging of a patent anastomosis or indirect evidence of appropriate flow direction in the venous limbs draining to the shunt site [8]. After a side-to-side H-type portacaval shunt, there should be hepatopetal flow in the proximal extrahepatic portal vein and hepatofugal flow in the distal extrahepatic portal vein, with both oppositely directed flow channels meeting at the shunt site (Fig. 11). At the site of inflow to the inferior vena cava, there is disturbed flow. With an end-to-side portacaval shunt, there is direct inflow from the extrahepatic portal vein

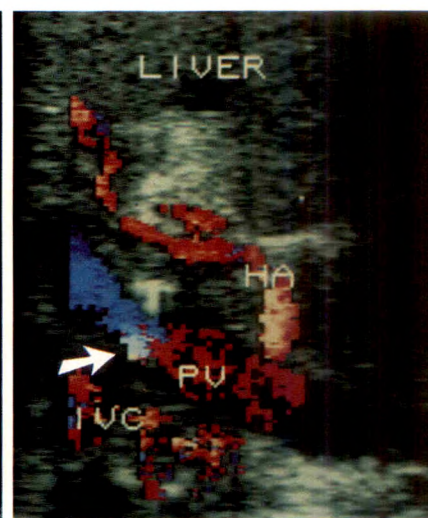


Fig. 10.—Reversed flow of portal vein. Right coronal oblique sonogram of hepatic hilum. Central streamline systolic flow is in a prominent hepatic artery (HA) and intrahepatic arterial branches. Main and intrahepatic portal vein branches are color-encoded blue, indicating flow reversal. Part of extrahepatic portal vein is obscured by a rib shadow. PV = portal vein. (Reprinted with permission from Foley [2].)



10

Fig. 11.—Patent portacaval shunt. Longitudinal parasagittal sonogram shows hepatopetal flow in proximal portal vein (red) and hepatofugal flow in distal portal vein (blue). Portal vein orifice of shunt (arrow). Hepatic artery (HA) is hypertrophied. A 50% "windows function" was used. This explains sharp vertical cutoff in color flow mapping on this image. PV = portal vein, IVC = inferior vena cava.



11

into the inferior vena cava. In most patients who have had a distal end-to-side splenorenal shunt, the actual shunt anastomosis is difficult to image because of intervening adipose tissue or bowel gas. If the two venous limbs, that is, the distal splenic vein and the left renal vein, are patent with appropriate flow direction, then it is likely that the shunt itself is patent.

Thrombosis of the hepatic vein can be diagnosed or excluded reliably by color Doppler flow imaging [9], obviating dynamic contrast-enhanced CT scanning or MR imaging. Aberrant hepatic venous collaterals also can be imaged.

**Mesenteric and renal imaging.**—Imaging the proximal celiac and superior mesenteric arteries is critical in patients with suspected mesenteric insufficiency. This is possible in patients in whom adequate acoustic access is supplied by the left hepatic lobe. Color Doppler flow imaging can be used to evaluate patients after superior mesenteric artery angioplasty.

The renal vascular pedicle from the central retroperitoneum to the renal hilum is difficult to image by using an anterior approach in adult patients. Patency of the renal vein at the renal hilum can be assessed with a coronal imaging approach and may be useful in patients with nephrotic syndrome or renal cell carcinoma. However, screening for renal artery stenosis in the adult population is unlikely to be successful owing to difficulty in acoustic access and the presence of small accessory arteries in 25–40% of the population.

**Abdominal transplantation.**—Patency of the hepatic artery is a critical issue after a liver transplantation. Thrombosis of the hepatic artery or severe stenosis can lead to biliary necrosis, bile leak, and sepsis. The diagnosis should be entertained in any patient with early posttransplantation hepatic dysfunction. Although normal patency of the hepatic artery at the hepatic hilum excludes thrombosis, it does not exclude possible stenosis at the donor-to-recipient arterial anastomosis, which is frequently obscured by bowel gas [10]. Thus, in a patient with hepatic dysfunction without evidence of rejection on liver biopsy and cholangiography showing nonobstructing biliary strictures, hepatic arteriography

may still need to be considered. Thrombosis of the portal and hepatic veins can also occur in hepatic transplant recipients.

The superficially located renal transplant is ideal for color Doppler flow imaging. The main, segmental, and interlobar arteries and accompanying veins to the level of the arcuate vessels can be imaged. This allows relatively rapid acquisition of flow-velocity waveforms from selected sampling sites for determination of resistivity and pulsatility indexes (Fig. 12). Although these indexes are nonspecific [11], they are of prognostic value in differentiating severe vascular rejection from interstitial rejection, in guiding appropriate therapy, and in assessing response to treatment. Main and segmental renal artery stenosis can be diagnosed by the presence of narrowing associated with flow jet turbulence and perivascular tissue vibration [12]. These studies may be repeated after angioplasty to assess response. In addition, postbiopsy arteriovenous fistulas are readily recognized [13].

Color Doppler flow imaging has been used in a less quantitative manner to evaluate patency of the peripancreatic and intrapancreatic vasculature after pancreatic transplantation. Normal resistivity and pulsatility indices have been associated with normal transplant function [14].

#### Extremity Veins

Techniques for noninvasive evaluation of suspected lower extremity venous thrombosis have been continuously refined in the past few years. Impedance plethysmography and continuous-wave Doppler are tests that evaluate venous patency by indirect means; are relatively insensitive to incompletely occluding thrombus; and may produce false-positive results in the presence of stagnant venous flow, as in right heart failure [15]. Compression sonography, a direct imaging study, is reported to be as accurate as contrast venography in the diagnosis or exclusion of femoropopliteal venous thrombosis [16]. Color Doppler imaging, in which the RBCs provide their



own intrinsic "color contrast," makes compression unnecessary, as, with adequate flow sensitivity, color flow signal should occupy the full anteroposterior diameter or cross-sectional area of the vein during the phase of maximum venous flow [5]. Incompletely occluding thrombus is readily recognized (Fig. 13).

Evaluation of suspected thrombosis of the calf veins by color Doppler imaging is under active investigation at this time (Fig. 14). In our practice, studies of the calf veins are performed with augmentation achieved by a mechanical plastic sleeve compressor cycling once every 5 sec. Initial results suggest that in those patients in whom technically adequate studies of the calf veins can be accomplished (60% of patients), color Doppler imaging is as accurate as contrast venography [17]. However, this will need to be corroborated in a large series of patients. The prevalence of clinically significant pulmonary embolus in patients with proved thrombosis of the calf veins is relatively negligible [18]. In general,

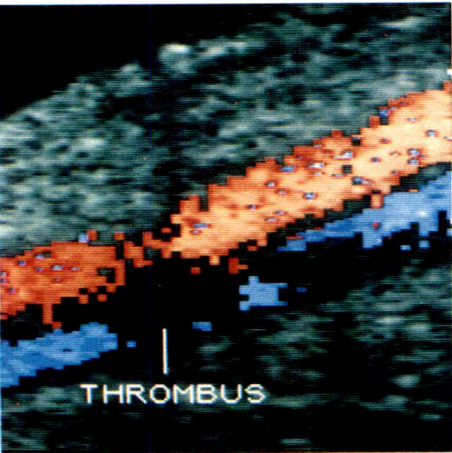
anticoagulants can be withheld from these patients unless there is evidence, provided by noninvasive testing, of proximal progression to the femoropopliteal system. Alternatively, patients with proved thrombosis of the calf veins may receive a course of anticoagulant therapy, particularly if there is significant local discomfort. If color Doppler imaging were accurate in the diagnosis or exclusion of thrombosis of the calf veins, the use of contrast venography or further noninvasive testing by serial study of the femoropopliteal system might be unnecessary.

Color Doppler imaging can be performed with 5.0- or 7.5-MHz linear-array probes, dependent on the patient's leg size. In patients with positive studies, it is important to map the anatomic extent of thrombus involving the femoropopliteal system. This is useful as a baseline when serial studies are required for evaluation of suspected proximal progression while a patient is on anticoagulant therapy. In addition, the appropriate venous insertion site for passage of an inferior vena caval filter umbrella device can be determined. If thrombosis of the femoral vein is limited to the superficial femoral vein, the ipsilateral common femoral vein can still be used as a suitable insertion site. Current studies suggest that there is no greater likelihood of thrombosis of the common femoral vein after vena caval filter placement if the ipsilateral superficial femoral vein is thrombosed [19].

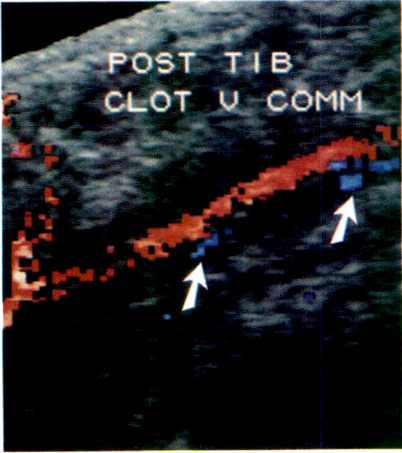
An important issue is distinction of chronic and possibly recanalized deep venous thrombosis from acute venous thrombosis [20]. Acute thrombi are hypoechoic and expand the venous lumen. Chronic thrombi are usually associated with venous wall thickening and luminal narrowing with the residual lumen serpiginous in outline. Patients with prior confirmed deep venous thrombosis who develop recurrent leg swelling may do so on the basis of venous insufficiency or recurrent deep venous thrombosis. However, it may not be possible to diagnose acute on chronic deep venous thrombosis, particularly if the acute thrombus does not result in expansion of the fibrotic vein. MR, by demonstrating perivenous edema and inflammation, may be of value in distinguishing acute from chronic deep vein thrombosis in these circumstances [21].



Fig. 12.—Renal transplant with selective spectral waveform obtained from interlobar artery. Note prominent cortical medullary differentiation. Black stripes in spectral waveform (arrows) represent time intervals for 1/sec image upgrade. Accurate pulsatility index can be obtained only in a "continuous record mode," in which there are no color flow upgrades during selective spectral analysis.



13



14

Fig. 13.—Partial femoral vein thrombosis. Color flow signal is recorded in eccentric venous channels in partly thrombosed vein. This finding is typical of recanalized venous thrombosis.

Fig. 14.—Patient with thrombosed posterior tibial venae comitantes (POST TIB V COMM). Venous thrombosis results in a hypoechoic expansile intraluminal defect. Note partial canalization (arrows).



Upper extremity venous thrombosis is increasing in prevalence in the inpatient population after use of central venous catheters for hyperalimentation, chemotherapy, and antibiotic treatment. Other common causes are mass compression, effort thrombosis, and IV drug abuse. Patients with dialysis fistulas in whom Mahurkar catheters have been placed in the subclavian vein for temporary dialysis may also develop upper extremity swelling caused by venous stenosis at the insertion site.

Upper extremity color Doppler imaging can be performed with 7.5-MHz probes for the basilic and axillary veins and the internal jugular veins and innominate veins at the thoracic inlet. A 5.0-MHz probe is used for evaluating the subclavian vein at the thoracic outlet by using an infraclavicular transpectoral approach.

Color Doppler imaging appears accurate in the diagnosis of both acute and chronic deep venous thrombosis [22]. However, thrombosis of the superior vena cava cannot be diagnosed by direct imaging as the central veins are hidden by the sternum. Obstruction of the superior vena cava may be inferred by diminished flow response of the subclavian and jugular veins to respiratory maneuvers. In addition, the retroclavicular segment of the subclavian vein cannot be clearly imaged with a linear-array probe, and small footprint sector probes can be useful for complete imaging of the subclavian vein.

As with the lower extremities, treatment of upper extremity deep venous thrombosis, either with anticoagulants or thrombolytic therapy, can be instituted after diagnosis with color flow imaging. Venography can be reserved for equivocal cases in which collateral venous drainage is identified, but segments of the subclavian vein are obscured by the clavicle.

### *Extremity Arteries*

Color Doppler flow imaging has three primary roles in the evaluation of lower extremity arterial disease: (1) evaluation of suspected localized disease, such as pseudoaneurysm or arteriovenous fistula; (2) sequential studies after angioplasty or surgical bypass grafting; and (3) a potential screening technique in patients with claudication.

Femoral artery pseudoaneurysm usually occurs after arterial catheterization or bypass grafting, either aortobifemoral or femoropopliteal. Both duplex Doppler and color Doppler are very accurate in distinguishing pulsatile perivascular hematoma from pseudoaneurysm [23]. The graphic portrayal of regional arterial anatomy and aneurysm lumen and the identification of the focal arterial communication provided by color Doppler imaging provide sufficient information for a definitive preoperative study. Arteriovenous fistulas, which can also be posttraumatic or postsurgical, likewise can be definitively diagnosed and treated on the basis of color Doppler imaging [24]. Perivascular tissue vibration may be associated with both pseudoaneurysm and arteriovenous fistula.

Patients who have had balloon and/or laser angioplasty for focal femoropopliteal arterial disease may be followed up by serial measurements of the ankle-to-brachial index, segmental lower limb pressures, and imaging studies. However, it is

useful to do color Doppler imaging before and after angioplasty to demonstrate the changes in lumen caliber and local hemodynamics that occur after angioplasty. The color Doppler imaging study done immediately after angioplasty can then serve as a baseline for serial studies. This should enable detection of restenosis in these patients.

Most femoral distal arterial bypass grafts are now performed with in situ venous bypass grafting. The superficial saphenous vein is readily accessible to color flow imaging and can be tracked from its proximal to its distal anastomotic site. Anastomotic and midgraft stenosis, residual valves, and arteriovenous fistulas can be detected. Decisions on angioplasty or surgical graft revision can then be performed, even in asymptomatic patients.

Patients with claudication are generally not considered candidates for percutaneous intervention or surgery unless claudication severely interferes with life-style or employment. Noninvasive evaluation by ankle-to-brachial indexes, segmental lower limb pressures, and determination of pulsatility index in the common femoral arteries is useful in localizing the level of disease but does not indicate the exact site or extent of disease nor distinguish stenosis from segmental occlusion. Color Doppler flow imaging provides a direct noninvasive imaging study that can characterize focal stenosis as hemodynamically insignificant or significant and distinguish focal stenosis from segmental occlusion [25]. Preliminary experience with color Doppler flow imaging is promising, but further validation of the accuracy of the test when performed independently and compared with angiography is necessary. A bilateral femoropopliteal arterial color Doppler study, including documentation by videotape recording, can be completed in 30 min. In our experience, dense arterial calcification, particularly in long segments of the distal superficial femoral artery, may preclude satisfactory imaging and result in both over- and underdiagnosis of disease. In addition, diagnosis of aortoiliac disease is inferential depending on demonstration of collateral inflow into the common femoral arteries and abnormal pulsatility index in the common femoral artery.

Patients with claudication without distal ischemic changes do not usually have significant tibioperoneal arterial disease. Accurate mapping of femoropopliteal arterial disease and inferential diagnosis of aortoiliac disease could result in the selection of patients who could benefit from percutaneous intervention. This may be a viable treatment option in a selected subgroup of patients who would otherwise not undergo arteriography and therapy.

### **Miscellaneous**

#### *Obstetrics and Gynecology*

The prevalence of ectopic pregnancy has been increasing. In our experience with transvaginal sonography, definitive diagnosis of a viable ectopic gestation by demonstration of fetal heart motion was possible in 35% of cases [26]. This is higher than has been recorded in previous series, reflecting clinical sensitivity to the diagnosis of ectopic gestation and the use of transvaginal sonography. The other patients had



nonviable or ruptured ectopic gestations. Although transvaginal sonography should allow clear distinction between a corpus luteum cyst and chorionic mass, this distinction may be more obvious with duplex or color Doppler imaging [27]. However, the incremental gain of using either duplex Doppler or color Doppler imaging in this situation needs to be assessed by a prospective study.

Color Doppler can be applied during routine obstetric sonography, provided that the spatial peak temporal average beam intensity does not exceed the arbitrary threshold of 94 mW/cm<sup>2</sup> set by the FDA. Pulsed Doppler spectral analysis in which higher output intensities are needed is currently reserved for studies in which intrauterine growth retardation or congenital heart disease is suspected. The value of color Doppler flow imaging in routine obstetric sonography is still under evaluation. Potential uses are more rapid identification of the umbilical cord insertion site at the fetal abdomen, distinction of decidual veins from placental abruption, localization of the umbilical vein in the fetal abdomen for determination of volume flow rate, and localization of the fetal aorta for selective spectral analysis in fetuses with suspected intrauterine growth retardation. Determination of flow resistance indexes (pulsatility index and resistivity index) in the fetal thoracic aorta, carotid and intracranial vessels, as well as the umbilical artery is facilitated by color Doppler imaging and may provide useful information in the assessment of suspected intrauterine growth retardation.

#### *Testicular Imaging*

Distinction of testicular torsion from epididymo-orchitis is important in patients with unilateral scrotal pain and swelling. This distinction can be made with a high degree of reliability by isotope techniques. The same diagnosis can be made rapidly and accurately with superior anatomic precision by color Doppler flow imaging [28, 29]. However, experience at this stage is somewhat limited and physicians should be careful to assess the sensitivity of their color flow instrument by examining normal testicles to be certain that they can record normal intratesticular blood flow before using color Doppler sonography in this clinical situation.

#### *Penile Color Flow*

Interest in the evaluation of suspected vasculogenic impotence has been increasing in the past several years. A vascular cause of impotence is thought to be responsible for this condition in more than 50% of patients. At this stage, color Doppler flow imaging and selective spectral analysis is used to evaluate the adequacy of arterial inflow. The accepted normal standard is that, after injection of 60 mg of intracorporal papaverine, peak systolic flow velocity in the cavernosal artery should be greater than 25 cm/sec [30]. This flow rate can be achieved at any time between 2 and 25 min after injection. The time of onset and peak effectiveness of intracorporal papaverine appears to vary among individuals. Although 25 cm/sec has been accepted as the lower limit of normal for peak systolic flow velocity after injection [30], this

has been determined in only a small number of normal volunteers and by correlation with penile arteriography in less than 50 patients in the world literature. The major value of color Doppler flow imaging is ready identification of the cavernosal arteries for selective spectral analysis.

Most patients with vasculogenic impotence have venous leak. In the laboratory setting, the semirigid tumescence resulting from intracorporal papaverine does not match the penile rigidity necessary for successful penetration. Continuous diastolic flow is associated with semirigid tumescence; in patients who develop rigid tumescence, diastolic flow is absent or reversed [31]. However, in patients who develop semirigid tumescence, some investigators have correlated the degree of persistent diastolic flow 10–15 min after papaverine injection with the presence or absence of venous leak, as demonstrated with cavernosography [32]. Persistent end-diastolic flow of >5 cm/sec is said to be associated with a high rate of venous leak. However, some normal patients may also exhibit prominent end-diastolic flow. Unchanged diameter and flow in the dorsal vein demonstrated on real-time color flow imaging also may be indicative of venous leak. Detection of venous leak and its anatomic identification by cavernosography may lead to cure of erectile dysfunction by selective venous ligation or retrograde coil embolization. However, the efficacy of this therapy has not yet been determined.

#### *Dialysis Fistulas*

Upper extremity dialysis fistulas may be end-to-side venoarterial and use either the radial or brachial artery. Alternatively, a prosthetic loop fistula connecting brachial artery to basilic vein may be performed in the antecubital fossa and proximal forearm. Complications that occur are venous stenosis, either proximal to or at the fistula site; pseudoaneurysm at the fistula site; and distal arterial steal with peripheral ischemia caused by proximal arterial obstruction and retrograde flow in the distal artery to the fistula site [33]. Venous drainage from the fistula site may be complex owing to multiple connections with the main draining vein. It is difficult with color Doppler flow imaging to diagnose either localized stenosis at the fistula site or proximal venous stenosis. Patients in whom flow is inadequate for satisfactory dialysis are best evaluated by a fistulogram [33]. However, patients with a localized pulsatile mass or distal ischemia can be evaluated by color Doppler imaging. Both pseudoaneurysm and proximal arterial obstruction with distal arterial steal can be diagnosed definitively.

Patients who have adequate fistula function but have ipsilateral upper extremity swelling may have subclavian venous stenosis, a condition that may be diagnosed by color Doppler flow imaging. In selected circumstances, these venous stenoses may be dilated by balloon angioplasty [34].

#### **Summary**

In this review, the performance requirements and operational parameters of a color Doppler flow system are outlined.



An operator's ability to recognize normal physiologic flow variations, pathophysiologic flow states, and artifacts such as noise and aliasing is emphasized. Major fields of application are the neck and extremity vessels; upper abdomen and abdominal transplants; and a miscellaneous group that includes obstetrics and gynecology, dialysis fistulas, and testicular and penile flow imaging.

The practical advantages of color Doppler flow imaging in comparison with duplex Doppler imaging are (1) direct measurement of flow lumen reduction in a manner analogous to arteriography, (2) venous studies that may be considered color contrast venograms not requiring spectral Doppler and that are more sensitive than compression sonography in the diagnosis of incompletely occluding thrombus or venous collaterals, and (3) a definitive preoperative study not requiring angiography in selected patients with pseudoaneurysm or suspected renal transplant arterial occlusion. In addition, accurate location and angle correction of sample volumes in medium-sized vessels such as the carotid and extremity arteries, and hepatic and renal arteries, is facilitated by color Doppler flow imaging. Finally, the more generalized application of Doppler techniques to analysis of flow in small vessels such as the penile and testicular circulation would not be possible without color Doppler flow imaging.

## REFERENCES

- Merritt CRB. Doppler color flow imaging. *JCU* 1987;15(9):591-597
- Foley WD. Abdominal color flow ultrasound imaging. *Ultrasound Q* 1989;7:271-291
- Middleton WD, Kellman GM, Melson GL, Madrazo BL. Postbiopsy renal transplant arteriovenous fistulas: color Doppler ultrasound characteristics. *Radiology* 1989;171:253-257
- Middleton WD, Foley WD, Lawson TL. Flow reversal and the normal carotid bifurcation: color Doppler flow imaging analysis. *Radiology* 1988;167:207-210
- Foley WD, Middleton WD, Lawson TL, Erickson SJ, Quiroz FA, Macrander SJ. Color Doppler ultrasound imaging of lower extremity venous disease. *AJR* 1989;152(2):371-376
- Erickson SJ, Mewissen MW, Foley WD, et al. Stenosis of the internal carotid artery: assessment using color Doppler imaging compared with angiography. *AJR* 1989;152:1299-1305
- Masaryk TJ, Modic MT, Ross JS, et al. Intracranial circulation: preliminary clinical results with three dimensional (volume) MR angiography. *Radiology* 1989;171:793-799
- Grant EG, Tessler FN, Gomes AS, et al. Color Doppler imaging of porto-systemic shunts. *AJR* 1990;154:393-397
- Grant EG, Errella R, Tessler FN, Lois J, Busuttill R. Budd-Chiari syndrome: the results of duplex and color Doppler imaging. *AJR* 1989;152:377-381
- Longley D, Skolnick ML, Zajko AB, Bron KM. Duplex Doppler sonography in the evaluation of adult patients before and after liver transplantation. *AJR* 1988;151:687-696
- Don S, Kopecky KK, Filo RS, et al. Duplex Doppler ultrasound of renal allografts: causes of elevated resistive index. *Radiology* 1989;171:709-712
- Middleton WD, Erickson SJ, Melson GL. Perivascular color artifact: pathological significance and appearance in color Doppler ultrasound images. *Radiology* 1989;171:647-652
- Middleton WD, Kellman GM, Melson GL, Madrazo BL. Postbiopsy renal transplant arteriovenous fistulas: color Doppler ultrasound characteristics. *Radiology* 1989;171:253-257
- Patel B, Wolverson MK, Mahanta B. Pancreatic transplant rejection: assessment with duplex ultrasound. *Radiology* 1989;173:131-135
- Ramchandani P, Soulen R, Fedullo L, Gaines V. Deep vein thrombosis: significant limitations of noninvasive tests. *Radiology* 1985;156:47-49
- Vogel P, Laing FC, Jeffrey RB, Wing VW. Deep venous thrombosis of the lower extremity: ultrasound evaluation. *Radiology* 1987;163:747-751
- Rose SC, Zwiebel WJ, Nelson BD, et al. Symptomatic lower extremity deep venous thrombosis: accuracy, limitations, and role of color duplex flow imaging in diagnosis. *Radiology* 1990;175:639-644
- Hull R, Hirsh J, Sackett DL. Replacement of venography in suspected venous thrombosis by impedance plethysmography and <sup>125</sup>I-fibrinogen leg scanning: a less invasive approach. *Ann Intern Med* 1981;94:12-15
- Mewissen MW, Erickson SJ, Foley WD, et al. Thrombosis at venous insertion sites after inferior vena caval filter placement. *Radiology* 1989;173:155-157
- Cronan JJ, Leen B. Recurrent deep vein venous thrombosis: limitations of ultrasound. *Radiology* 1989;170(3):739-742
- Erdman WA, Jayson HT, Redman HC, Miller GL, Parkey RW, Peshock RW. Deep venous thrombosis of extremities: role of MR imaging in diagnosis. *Radiology* 1990;174:425-431
- Knudson GJ, Wiedmeyer DA, Erickson SJ, et al. Color Doppler sonographic imaging in the assessment of upper extremity deep venous thrombosis. *AJR* 1990;154:399-403
- Mitchell DG, Needleman L, Bezzin M, et al. Femoral artery pseudoaneurysm: diagnosis with conventional duplex and color Doppler ultrasound. *Radiology* 1987;165:687-690
- Igdbashian UN, Mitchell DG, Middleton WD, Schwartz RA, Goldberg BB. Iatrogenic femoral arteriovenous fistula: diagnosis with color Doppler imaging. *Radiology* 1989;170:749-752
- Cossmann DV, Ellison JE, Wagner WH, et al. Comparison of contrast arteriography to arterial mapping with color flow duplex imaging in the lower extremities. *J Vasc Surg* 1989;10:522-529
- Thorsen MK, Lawson TL, Aiman EJ, et al. Diagnosis of ectopic pregnancy: comparison of endovaginal and transabdominal sonography (in press).
- Taylor KJW, Ramos IM, Feyock AL, et al. Ectopic pregnancy: duplex Doppler evaluation. *Radiology* 1989;173:93-97
- Middleton WD, Thorne DA, Melson GL. Color Doppler ultrasound of the normal testes. *AJR* 1989;152:293-297
- Middleton WD, Melson GL. Testicular ischemia: color Doppler sonographic findings in five patients. *AJR* 1989;152:1237-1239
- Lue TF, Hricak H, Marich KW, Tanagho EA. Vasculogenic impotence evaluated by high resolution ultrasonography and pulsed Doppler spectrum analysis. *Radiology* 1985;155:777-781
- Schwartz AN, Wang KY, Mack LA, et al. Evaluation of normal erectile function with color flow Doppler sonography. *AJR* 1989;153:1155-1160
- Quam JP, King BF, James EM, et al. Duplex and color Doppler sonographic evaluation of vasculogenic impotence. *AJR* 1989;153:1141-1148
- Middleton WD, Picus DD, Marx MV, Melson GL. Color Doppler sonography of hemodialysis vascular access: comparison with angiography. *AJR* 1989;152:633-639
- Ingram TL, Reid SH, Tismado J, Cho S-R, Posner MP. Percutaneous transluminal angioplasty of brachiocephalic vein stenosis in patients with dialysis shunts. *Radiology* 1988;166:45-47



## Book Review

**Two-dimensional Echocardiography and Cardiac Doppler**, 2nd ed. Edited by Jay N. Schapira and John G. Harold. Baltimore: Williams & Wilkins, 670 pp., 1990. \$99.50

Over the past two decades, echocardiography has established itself as an important diagnostic tool. Technologic advances have resulted in significant improvements in image quality, and newer techniques such as Doppler imaging, color flow imaging, and transesophageal imaging have opened up new dimensions by providing previously unavailable information. This text, which has several contributors, is the second edition of a book on two-dimensional echocardiography. Suffice it to say that in the 7 years since the first edition, enormous changes have occurred in echocardiography and its technology; these have been chronicled in this text. The editors have tried to present practical experience simply without compromising important basic information.

The text has 32 chapters and an appendix. The authors begin with a historical perspective of echocardiography, delving into fairly long details about development of different echo techniques. This is followed by a well-written chapter on the physical principles of cardiac sonography. Chapters 3 and 4 list the terminology and imaging planes of Doppler echocardiography recommended by the American Society of Echocardiography. This is followed by an excellent chapter detailing image orientation and the anatomic-echocardiographic correlates with tomographic planes. This is one of the most valuable sections of the text, particularly for beginning echocardiographers. Chapter 6 is a quick reference of basic conventional Doppler imaging parameters and how to identify basic valve abnormalities. The subsequent chapters discuss basic real-time color flow imaging, its pitfalls, and its role in evaluation of acquired valvular lesions; the role of intraoperative color flow imaging in the assessment of valvuloplasties and surgical repair of congenital heart disease; Doppler and two-dimensional echocardiographic patterns of valvular heart disease and mitral valve prolapse; evaluation of prosthetic valve function by Doppler echocardiography; and correlation data between Doppler and invasive hemodynamics in assessment of valvular lesions.

Assessment of ischemic heart disease by stress echocardiography and supine stress exercise echocardiography and the important

application of two-dimensional echocardiography in acute coronary care are discussed in chapters 13–15. The next three chapters discuss the role of echo Doppler imaging in the evaluation of cardiomyopathy, systolic cardiac function, and hypertrophic cardiomyopathy. Chapters 19–29 review echocardiography of the right ventricle, infective endocarditis, transesophageal imaging, fetal echocardiography, congenital heart disease, importance of two-dimensional echocardiography in evaluation of pericardial diseases and cardiac masses, advances in experimental echocardiography, echocardiographic changes related to space travel, and application of Doppler echocardiography in animals. Biological effects of ultrasound as well as authors' recommendations for training the sonographer are reviewed in chapters 30 and 31. The text concludes with a review of the recent application of peripheral vascular duplex imaging. A richly informative appendix provides case illustrations and listings of Doppler calculations.

This text alternates between well-written chapters and others that lack specific focus or fail to address crucial issues. This may be because the authors tried to cover almost every topic related to echocardiography. The rationale behind the sequence of the individual chapters is often not apparent. The quality of the two-dimensional echocardiograms is variable, and sometimes the authors have used obviously degraded images. Often figures are presented first without color and then shown again in color at the end of the book. As would be expected, continuity and orientation with the relevant subject matter are lost. Portions of this work will be quite useful, but as a comprehensive text, it lacks consistency and cohesion.

Taher Elkadi  
David J. Sahn

*University of California, San Diego, Medical Center  
San Diego, CA 92103*



## Review Article

# The Evaluation of Coronary Bypass Graft Patency: Direct and Indirect Techniques Other Than Coronary Arteriography

William Stanford,<sup>1</sup> Jeffrey R. Galvin,<sup>1</sup> David J. Skorton,<sup>2</sup> and Melvin L. Marcus<sup>3</sup>

Patients having one or more coronary artery bypass graft operations constitute an important part of the practice of cardiac radiology. Bypass graft patency can be determined by indirect and direct methods. The indirect imaging methods include radionuclide ventriculography, thallium-201 scintigraphy, and positron emission tomography. The direct methods include conventional CT, ultrafast CT, MR imaging, digital subtraction angiography, and Doppler sonography.

This review discusses the advantages and limitations of these methods and attempts to define the relative importance of each of these techniques in the evaluation of bypass graft patency.

Coronary artery bypass grafting (CABG) is performed in 165,000 Americans annually [1]. Follow-up studies have shown that 10–30% of these grafts are occluded 1–2 years and 45–55% are occluded 10–12 years after grafting [2–4]. Therefore, the follow-up and subsequent treatment of these patients constitute a significant medical and surgical problem.

Graft patency can be evaluated by indirect and/or direct methods. The definitive study of graft patency is coronary angiography, and it is against this technique that other procedures must be judged. The indirect imaging methods infer

graft patency/occlusion by changes in regional perfusion and/or myocardial wall contraction patterns. These indirect, noninvasive or minimally invasive methods include rest and exercise radionuclide ventriculography (RVG), thallium-201 scintigraphy, and positron emission tomography (PET). The direct, noninvasive or minimally invasive methods include specific graft identification with conventional CT, ultrafast CT (UFCT), MR imaging, digital subtraction angiography (DSA), and Doppler sonography.

In this paper, we discuss these imaging methods of evaluating bypass graft patency and emphasize the advantages and shortcomings of each technique as compared with coronary angiography.

### Rest and Exercise Radionuclide Ventriculography

Rest and exercise equilibrium radionuclide ventriculography (RVG) is performed by IV injection of <sup>99m</sup>Tc-labeled RBCs followed by gamma camera imaging 20–120 min later [5]. Individual grafts are not seen with this technique, but left ventricular ejection fraction at rest and peak exercise can be

Received June 4, 1990; accepted after revision August 6, 1990.

Presented in part at the 61st Scientific Session of the American Heart Association, Washington, DC, November 1988.

This work was supported in part by Specialized Center of Research in Ischemic Heart Disease Grant #HL32295 from the National Institutes of Health and by Research Career Development Award HL01290 from the National Heart, Lung, and Blood Institute.

<sup>1</sup> Department of Radiology, The University of Iowa College of Medicine, Iowa City, IA 52242. Address reprint requests to W. Stanford.

<sup>2</sup> Department of Internal Medicine (Cardiology), The University of Iowa College of Medicine, Iowa City, IA 52242.

<sup>3</sup> Deceased.



assessed along with abnormalities of regional wall motion. Graft patency is indirectly inferred by determining how well the ventricle contracts in response to exercise. End-diastolic volumes, end-systolic volumes, and stroke volumes also can be determined. Patients with patent grafts should show an increase in their stroke volumes and ejection fractions in response to exercise. Failure to do so or the detection of new abnormalities in wall motion suggests graft occlusion or incomplete revascularization [6–9].

Taylor and coworkers [10] used gated RVG to assess 56 consecutive bypass patients before and 6 weeks after CABG. In 52 postbypass asymptomatic patients, the exercise ejection fraction increased significantly and prebypass abnormalities in regional wall motion were abolished. Angina persisted in four postbypass patients, and the preoperative ejection fraction and wall motion abnormalities were not improved—implying incomplete revascularization. Kawasuji et al. [6] reported similar findings. Floyd and associates [11] also evaluated patients before and after CABG. In 104 patients in whom new electrocardiographic Q waves developed after CABG, they found no consistent impairment of left ventricular global function as determined by RVG. Others [6, 9] have reported similar findings; however, many of these reports did not have angiographic controls. One study with controls was that by Kent and coworkers [12], who evaluated 23 consecutive patients of whom 20 had postoperative coronary arteriograms. Fourteen of these patients had improved post-exercise ventricular function after the surgery. In the six that did not, one patient had wall motion abnormalities in the distribution of occluded grafts, three in the distribution of ungrafted vessels, and two in the distribution of patent grafts.

Exercise first-pass RVG also has been used to evaluate ventricular function. The test is performed by injecting a bolus of  $^{99m}\text{Tc}$ -labeled RBCs or DTPA through a peripheral vein. Multicrystal camera imaging is immediately carried out in the 30° right anterior oblique projection as the radionuclide tracer bolus traverses the right and left ventricles [5]. After successful revascularization, the exercise ejection fraction should increase, and there should be no wall motion abnormalities. Hellman and colleagues [8] correlated postoperative first-pass RVG studies with preoperative studies and with coronary angiography in 29 patients. In 21 of these patients with patent grafts, the ventricular function improved. Eight patients had an abnormal ventricular response. Seven of these had either closed grafts or incomplete revascularization; no explanation was found for this finding in the remaining patient. Hellman and coworkers thought that failure to abolish exercise-induced functional instability suggests incomplete revascularization. Lewis and associates [7] also used first-pass RVG techniques in 66 patients. In seven patients, both the preoperative resting and postexercise left ventricular function tests were normal. In the remaining 59 patients, 33 had normal resting but abnormal postexercise left ventricular function tests, whereas 26 had both resting and postexercise left ventricular abnormalities. After bypass grafting, no change occurred in those patients with normal preoperative left ventricular function; however, left ventricular function during exercise improved significantly in those who had preoperative abnormalities.

#### *Comment*

Radionuclide ventriculography is of some value in the assessment of graft patency but has limitations. One fundamental problem is the inability to differentiate single- from multiple-graft occlusion. Another problem is the inability to differentiate between nonrevascularized areas and disease progression. An additional problem is the inability of some patients to exercise intensively. Often postoperative patients cannot or will not exert themselves maximally. Also, postoperative patients may be on antianginal drugs, and these may severely compromise the level of exercise obtainable. Left bundle branch block or cardiac arrhythmias may distort the contraction pattern and interfere with the interpretation of a contraction abnormality. Last, previous myocardial infarction may preclude interpretation of wall motion abnormalities. For these reasons, equilibrium and first-pass RVG techniques are infrequently used in the evaluation of specific bypass graft patency.

#### **Thallium-201 Imaging**

Thallium-201 scintigraphy more closely estimates individual graft patency by identifying relative deficits in regional myocardial perfusion. In this method, thallium-201 chloride is injected IV at peak exercise and this is followed by immediate tomographic or planar gamma camera imaging. Postexercise radioisotope uptake in an area perfused by a bypass graft is indicative of bypass graft patency.

Several authors [13–19] have compared the sensitivity and specificity of thallium-201 scintigraphy with coronary angiography in postcoronary artery bypass graft patients. Starling et al. [15] studied 19 consecutive patients with chest pain after bypass grafting. His group found stress thallium studies had sensitivity of 75% and specificity of 86% as compared with coronary angiography. Greenberg et al. [13] in a similar study evaluated 27 patients postoperatively and found stress thallium had a sensitivity of 77% and a specificity of 100% as compared with coronary angiography for identifying incomplete revascularization. The results of several such studies are seen in Table 1. Overall sensitivities ranged from 64% to 100% and specificities from 73% to 100%.

#### *Comment*

Thallium-201 scintigraphy has been shown to identify accurately areas of poor myocardial perfusion due to incomplete revascularization. This is especially true with stress thallium studies. In certain instances the test results may be nonspecific, for example, the reason for decreased local myocardial perfusion may not be graft occlusion, but previous myocardial infarction, nonrevascularized areas of myocardium, or the progression of native coronary stenosis. All these can occur in spite of an open graft. The best indicator of graft patency would be when the stress thallium study was abnormal preoperatively and normal soon after surgery. In these instances, it is likely that at least one graft is patent. Exercise limitations also frequently occur in the postoperative patient, and this may preclude the usual exercise thallium study. Both dipyri-



TABLE 1: Thallium-201 in Coronary Bypass Graft Patency

Reference	No. of Patients	Sensitivity <sup>a</sup> (%)	Specificity <sup>a</sup> (%)
Starling et al. [15]	19	75	86
Heikuri et al. [16]	51	77	78
Greenberg et al. [13]	27	77	100
Kolibash et al. [14]	38	82	73
Engelstad et al. [17]	24	100	78
Zimmermann et al. [18]	34	64	77
Rasmussen et al. [19]	41	71	94

<sup>a</sup> Compared with coronary angiography.

damole and adenosine have been used as vasodilators to increase coronary blood flow and thus permit image-based identification of regions of relative perfusion deficit. Thus, pharmacologic stress also may be a useful method of identifying regional perfusion defects due to graft occlusion.

Positron Emission Tomography

Positron emission tomography (PET) is a radioactive tracer technique that allows in vivo measurements of regional myocardial blood flow, fuel substrate uptake, and other aspects of myocardial metabolism. In the technique, positron-emitting isotopes of carbon, nitrogen, oxygen, fluorine, rubidium, and other atoms are injected into the body and tomographic images are produced that represent the quantitative distribution of the positron-emitting tracer within the target organ [20]. PET can be used to evaluate regional myocardial perfusion and to distinguish between normal, ischemic, and infarcted myocardium [21, 22]. In particular, PET imaging with both a blood flow tracer (e.g., N-13 ammonia) and a tracer of fuel substrate uptake (e.g., F-18 deoxyglucose) may give unique insight into myocardial viability. If a region of myocardium supplied by a graft shows a deficit in blood flow but normal or enhanced glucose uptake, the tissue is viable. However, if both blood flow and glucose uptake are compromised, the tissue is most likely nonviable (because of infarction or scar). Clinically, PET also has been used to detect coronary artery stenosis [20] and to assess coronary artery flow reserve by comparing myocardial flow before and after coronary vasodilatation [23].

At least one study specifically assessed PET in the evaluation of graft patency after coronary bypass surgery. In 20 patients, Konishi et al. [24] compared <sup>13</sup>N-ammonia PET imaging with coronary arteriography and found that 91% of segments with normal PET perfusion were supplied by patent grafts. However 38% of ischemic segments and 57% of fibrotic segments also were supplied by patent grafts. No other reports were found specifically addressing the use of PET in assessing bypass graft patency.

Comment

PET presently appears to show promise in assessing areas of myocardium that might benefit from bypass graft surgery; however, the high cost and limited availability has restricted its use. Its potential in imaging coronary bypass grafts has

not been adequately examined; however, the ability of the technique to evaluate perfusion and metabolism suggests potential in this application.

Infrequently Used Direct Imaging Methods

Several direct imaging techniques have been used to evaluate graft patency: digital subtraction angiography, transthoracic Doppler sonography, and conventional CT. At the present time, these methods are infrequently used.

Digital Subtraction Angiography

Digital subtraction angiographic (DSA) evaluation of coronary bypass graft patency can be accomplished either by the IV (IV-DSA) or intraarterial (IA-DSA) administration of contrast material. With IA-DSA, a catheter is placed with its tip positioned in the aortic root via a technique similar to that of coronary angiography. With IV-DSA, a transvenous catheter is inserted and its tip is positioned at the caval/atrial junction. Imaging at up to 30 frames per second is done before, during, and after contrast administration. A "mask" or precontrast image is then subtracted from postcontrast images and the resultant images (depicting the contrast distribution) are played back in a cine viewing mode.

The advantages of DSA are similar to those of conventional angiography and consist of the immediate viewing of images, the ability to freeze individual images for study, and availability of digital images that may be processed and analyzed by computer.

The disadvantages include degradation of the subtracted images by respiratory, cardiac, or other patient motion and the requirement for either a central venous or an aortic root catheter. The degradation is particularly marked in the distal parts of the grafts, which have more spatial displacement due to the cardiac motion; it is less of a problem in the proximal parts of the grafts, which are more stationary. Figure 1 shows a representative IA-DSA image of a patent bypass graft.

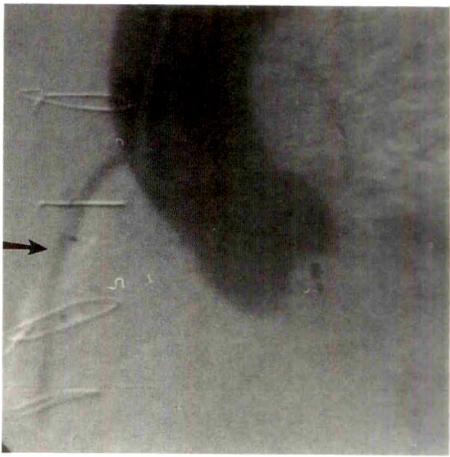


Fig. 1.—Intraarterial digital subtraction angiogram of a patent right coronary artery bypass graft (arrow). (Courtesy Robert F. Wilson, University of Minnesota.)



TABLE 2: Digital Subtraction Angiography in Coronary Bypass Graft Patency

Reference	No. of Grafts	Sensitivity <sup>a</sup> (%)	Specificity <sup>a</sup> (%)
Intraarterial Administration			
Goldberg et al. [25]	24	100	100
Drury et al. [26]	17	100	100
Hayward & Hunter [27]	26	100	100
Steffenino et al. [28] <sup>b</sup>	75	83	50
Guthaner et al. [29] <sup>c</sup>	103	92	
Intravenous Administration			
Drury et al. [26]	26	69	100
Guthaner et al. [29] <sup>d</sup>	32	41	
Lupon-Roses et al. [30] <sup>e</sup>	108	98	100
Guiraudon et al. [31] <sup>f</sup>	44	98	100
Kempton et al. [32]	24	75	
Magotteaux and Trotteur [33]	31	77	
Myerowitz et al. [34]	26	73	100

<sup>a</sup> Compared with coronary angiography.  
<sup>b</sup> Internal mammary artery (IMA) sensitivity 20% (five grafts).  
<sup>c</sup> Five IMA grafts (no coronary angiography).  
<sup>d</sup> Compared with IA-DSA controls (no coronary angiography).  
<sup>e</sup> Seven IMA grafts.  
<sup>f</sup> All (44) were IMA grafts.

The sensitivities and specificities of IA-DSA and IV-DSA are summarized in Table 2 [25–34]. Generally, the IA-DSA images had good sensitivities whereas IV-DSA, with the exception of results reported by Lupon-Roses and associates [30] and Guiraudon and associates [31], had poor sensitivities.

Comment

At the present time IA-DSA appears satisfactory for the evaluation of CABG patency but requires an aortic root catheter and, with the exception of requiring slightly less contrast material, has little advantage over selective graft angiography. With few exceptions, IV-DSA has little application in evaluating CABG patency.

Transthoracic Echocardiography/Doppler Sonography

Transthoracic Doppler sonography can directly detect graft patency by sending and receiving an ultrasound signal from a transducer placed on the chest wall [35]. The technique requires the positioning of a probe so as to detect and record an auditory signal from graft flow. The advantages are that the technique is noninvasive, rapid, and inexpensive. The disadvantages are that it requires considerable expertise and that it is difficult to differentiate the graft flow signal from that generated by the aorta and pulmonary arteries. The technique is less applicable for circumflex grafts. Additional sources for error are diastolic flow signals originating from the superior vena cava, internal mammary veins, tricuspid valve, mitral valve, and right ventricle. The sensitivities and specificities of this technique are summarized in Table 3 [35–37]. Overall sensitivities ranged from 83% to 92% and specificities from 56% to 100%.

Two-dimensional echocardiography also has been used to evaluate bypass grafts. Sheiban and coworkers [38] accu-

TABLE 3: Transthoracic Doppler in Coronary Bypass Graft Patency

Reference	No. of Grafts	Sensitivity <sup>a</sup> (%)	Specificity <sup>a</sup> (%)
Diebold et al. [35]	163	92	56
Gould et al. [36]	41	83	
Pisko-Dubienski et al. [37]	34	90	100

<sup>a</sup> Compared with coronary angiography.

rately determined the status of graft patency in 21 of 23 grafts. Newer echocardiographic imaging methods such as transesophageal echocardiography may broaden the role of echocardiography in the assessment of bypass graft patency, but experience is still limited. Additionally, the measurement of blood flow in selected internal mammary artery and saphenous vein grafts by two-dimensional and Doppler echocardiography is beginning to be reported [39].

Comment

At the present time, transthoracic Doppler sonography may be suitable for right coronary and left anterior descending coronary artery grafts but less so for circumflex grafts. Internal mammary and sequential grafts have not been extensively evaluated. Because standard transthoracic echocardiography does not permit sufficiently reliable determination of graft patency, the technique is infrequently used. Transesophageal echocardiography is just beginning to be used, and this technique may be useful in demonstrating graft patency, especially in grafts to the circumflex and posterior descending coronary artery distributions.

Conventional CT

Conventional CT also has been used to evaluate graft patency. It requires only a peripheral injection of contrast material. The advantages are that it is minimally invasive and CT scanners are available in most medical centers. The disadvantages are the slow scanning times (approximately 2–5 sec), poor graft opacification, the inability to measure flow, and interference from clip artifacts. The technique consists of multiple peripheral IV injections of approximately 50 ml of contrast material at 8–15 ml/sec. Localization of the scanning plane is critical and must be at the aortic root or at a marker clip; 8- or 10-mm thick sections are taken repetitively to identify bolus arrival and washout. Radiation exposure may be large and multiple levels may need to be imaged. The results of conventional CT studies are seen in Table 4 [40–47]. Sensitivities as compared with coronary arteriography ranged from 79% to 97% and specificities from 69% to 100%.

Comment

Although conventional CT may visualize coronary artery bypass grafts, the slow scanning times, poorer resolution, increased radiation exposure, and considerable motion artifact have relegated this technique to a relatively minor role in



**TABLE 4: Conventional CT in Coronary Bypass Graft Patency**

Reference	No. of Grafts	Sensitivity <sup>a</sup> (%)	Specificity <sup>a</sup> (%)
Daniel et al. [40]	125	91	88
Brundage et al. [41]	62	93	95
Godwin et al. [42]	47	79	77
Wilson et al. [43]	63	85	100
Kahl et al. [44]	100	82	69
Kawasuji et al. [45]	43	97	100
Foster et al. [46]	65	96	83
Moncada et al. [47]	33	96	91

<sup>a</sup> Compared with coronary angiography.

the evaluation of bypass graft patency. The majority of the published studies have not addressed the evaluation of internal mammary grafts.

### Potentially Useful Newer Direct Imaging Methods

Newer imaging techniques that are potentially useful for detecting CABG patency are ultrafast CT (UFCT), MR imaging, and Doppler catheter. These approaches have the advantage of direct visualization of graft patency/occlusion (UFCT and MR imaging) or direct measurement of coronary flow reserve (Doppler catheter).

#### Ultrafast CT

The UFCT scanner electromagnetically deflects a beam of electrons onto one of four target rings located in the gantry below the patient. X-rays produced from these target rings pass through the patient onto detector rings located in the gantry above the patient. The advantages of UFCT as compared with conventional CT are 50-msec scanning times, 0.75- to 1.50-mm resolution, and reduced motion and clip artifact. The disadvantages are similar to conventional CT and consist of radiation exposure and a requirement for administration of contrast media; however, the radiation exposure is approximately 1/10 that of conventional CT and

considerably less than cardiac catheterization. The average dose of contrast material is approximately 80 ml (two 40-ml injections) and is administered via a peripheral vein.

Figure 2 shows representative UFCT tangential and cross-sectional images of patent bypass grafts to the left anterior descending and circumflex systems. A multicenter study by Stanford and colleagues [48] showed a sensitivity of 93% for detecting angiographically patent grafts and a specificity of 89% for determining angiographically closed grafts. The overall accuracy was 92%. The number of technically adequate studies was more than 94%. Subsequently, three other studies have reported sensitivities of 95% [49], 96% [50], and 94% [51] (Table 5).

#### Comment

Ultrafast CT shows considerable promise in imaging bypass graft patency. The limited number of scanners and the inability to detect distal graft stenoses are drawbacks. The measurement of bypass graft flow in humans is not yet clinically available; however, recent work by Rumberger et al. [52] appears promising.

#### MR Imaging

MR imaging is noninvasive, requires no radiation exposure or administration of contrast media, and may be done in multiplanar views. The disadvantages are that the technique is time consuming, there is poorer image resolution as compared with CT, and patients with pacemakers are excluded.

Two imaging modes are used to evaluate bypass graft patency. In the spin-echo T1-weighted images, patent grafts appear as flow voids (Fig. 3A). The other sequence is the cine MR imaging mode, which uses gradient refocused echoes and fast scanning sequences. In these images, flowing blood within the grafts gives an enhanced signal (Fig. 3B).

The sensitivity, specificity, and accuracy for each of these sequences have been evaluated by White and coworkers. They reported a sensitivity in the spin-echo images of 91%,

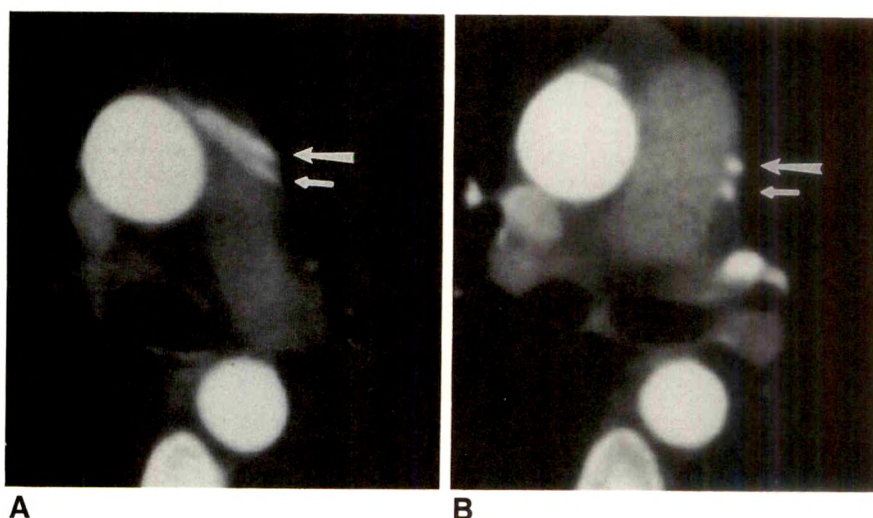


**Fig. 2.—Representative ultrafast CT scans.**

**A.** A patent left anterior descending coronary artery bypass graft (*long arrow*) and circumflex graft (*short arrow*) are seen tangentially as they exit aorta.

**B.** Grafts in left anterior descending coronary artery distribution (*long arrow*) and left circumflex artery distribution (*short arrow*) are seen in cross section.



TABLE 5: Ultrafast CT in Coronary Bypass Graft Patency

Reference	No. of Grafts	Sensitivity <sup>a</sup> (%)	Specificity <sup>a</sup> (%)
Stanford et al. [48] <sup>b</sup>	127	93	89
Bateman et al. [49]	39	95	86
Bateman et al. [50]	80	96	97
Stanford et al. [51] <sup>c</sup>	21	94	100

<sup>a</sup> Compared with coronary angiography.  
<sup>b</sup> Eleven internal mammary artery grafts.  
<sup>c</sup> Fifteen internal mammary artery grafts.

specificity of 72%, and overall accuracy of 86%; 10% of the studies were indeterminate [53]. The study included nine internal mammary grafts. One problem with spin-echo images is that other structures such as fibrous tissue and calcification also appear as flow voids, and these artifacts interfere with image interpretation. White et al. [54] also reported a sensitivity of 93%, specificity of 86%, and overall accuracy of 89% in cine MR imaging studies. The number of indeterminate studies was not stated; there was only one internal mammary graft in their series.

A problem with gradient refocused images is that spatial resolution is often poorer and, as with CT, distal graft insertions and stenoses cannot be visualized. Additionally the obliquity of the grafts often preclude seeing long segments in any one image plane. The results of these and other MR imaging studies of bypass graft patency are summarized in Table 6 [53–58]. Sensitivities ranged from 88% to 93% and specificities from 72% to 100%. As in the case of UFCT, investigations are in progress attempting to measure graft flow [57–59].

Comment

MR imaging, particularly with strategies that use cine MR imaging, presently shows some promise for imaging in CABG patients; however, the resolution is poorer than with CT and much poorer than with coronary angiography. Graft stenoses and distal anastomoses cannot be assessed, and artifacts

TABLE 6: MR Imaging in Coronary Bypass Graft Patency

Reference	No. of Grafts	Sensitivity <sup>a</sup> (%)	Specificity <sup>b</sup> (%)
Spin Echo			
White et al. [53] <sup>b</sup>	65	91	72
Rubinstein et al. [55]	47	90	72
Jenkins et al. [56]	60	90	90
Frija et al. [57] <sup>c</sup>	52	93	100
Cine MR Imaging			
White et al. [54] <sup>d</sup>	28	93	86
Aurigemma et al. [58] <sup>e</sup>	45	88	100

<sup>a</sup> Compared with coronary angiography.  
<sup>b</sup> Nine internal mammary artery (IMA) grafts.  
<sup>c</sup> Ten IMA grafts.  
<sup>d</sup> One IMA graft.  
<sup>e</sup> Four IMA grafts.

such as wires and native vessel calcification can interfere with the interpretation of spin-echo images. Because MR does not have the dynamic flow kinetics that identify the contrast bolus at arrival and washout, and because the spatial resolution is poorer, MR imaging does not appear as satisfactory as UFCT in evaluating coronary bypass graft patency. However, work is in progress to develop kinetic MR imaging strategies, and these may improve graft patency detection. At present, the role of MR imaging in the detection of coronary bypass graft patency is still unclear.

Doppler Catheter

The Doppler catheter is an invasive method whereby a 3-French catheter with a 1-mm outer diameter is introduced into the graft ostium. This technique has the advantage of being able to determine coronary bypass graft flow reserve directly. The disadvantages are its invasiveness and inapplicability to study mammary grafts. Figure 4 is a schematic of the Doppler catheter, and Figure 5 is a representative tracing of a flow reserve response to vasodilators before and after coronary artery angioplasty. At present, few patients have been studied, and its application is limited [60–62].

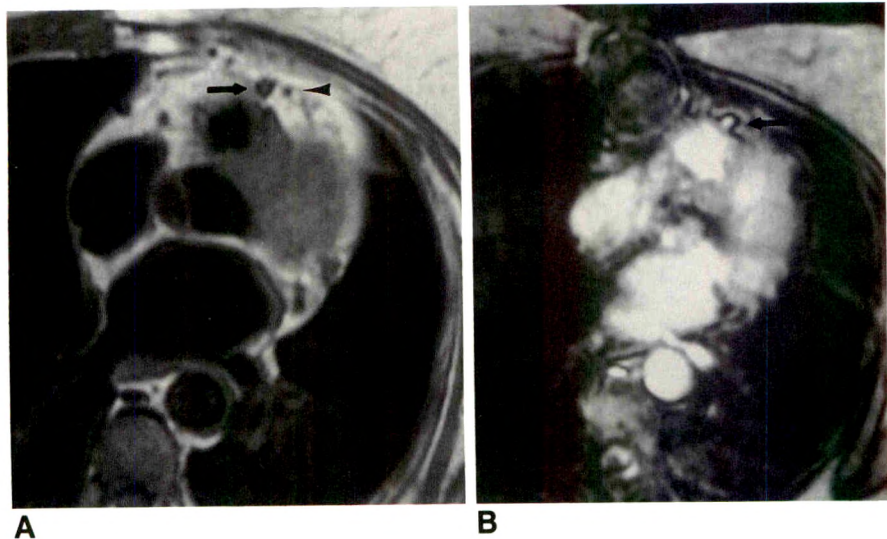


Fig. 3.—A, Spin-echo image of an angiographically proved patent saphenous vein bypass graft to left anterior descending (LAD) coronary artery. A signal void of flowing blood is seen within graft, indicating its patency (arrow). That graft appears patent in segment imaged does not necessarily imply that distal graft is open. Arrowhead denotes native LAD coronary artery. B, Cine MR image of same patent saphenous vein bypass graft shows high signal intensity in heart chambers and in bypass graft (arrow).



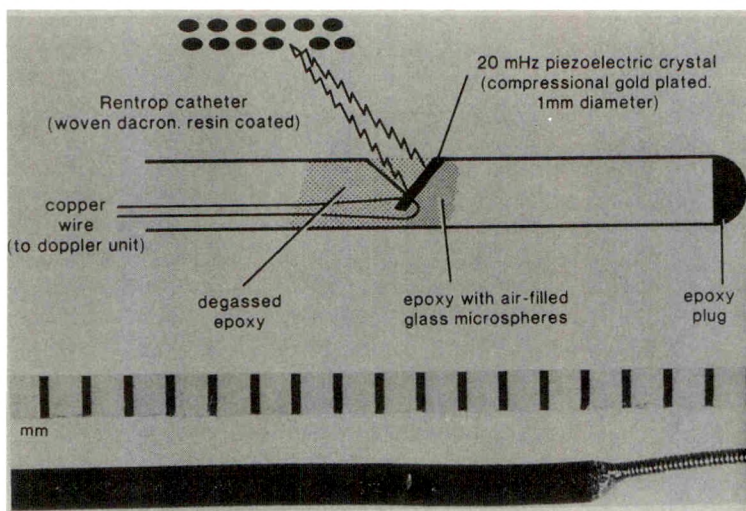


Fig. 4.—Schematic diagram (top) of distal portion of coronary Doppler catheter. Photograph (bottom) of distal 3 cm of catheter. (Reprinted with permission from Wilson et al. [60].)

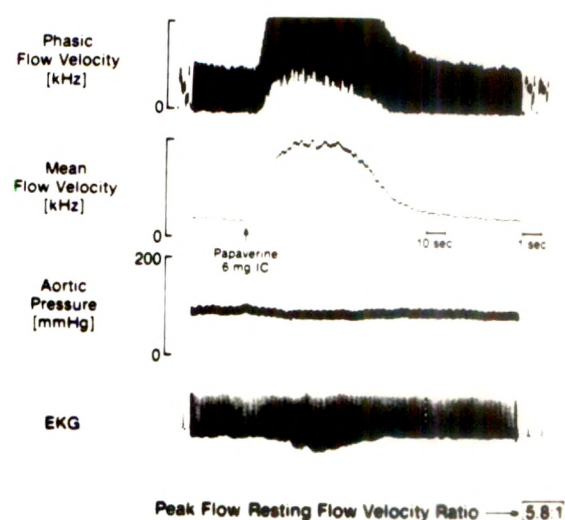


Fig. 5.—A record obtained from a patient undergoing Doppler catheter flow reserve study of a saphenous vein bypass graft. Top tracing shows phasic coronary blood flow velocity, second tracing shows mean coronary blood flow velocity, and bottom two tracings show arterial pressure and an electrocardiogram. Administration of 6 mg of intracoronary papaverine resulted in a fivefold increase in blood flow velocity, thus demonstrating no physiologically significant obstruction to vein bypass graft.

P24,459

#### Comment

The Doppler catheter presently can accurately measure coronary bypass graft flow reserve; however, the method is invasive and experience is very limited.

#### Conclusions and Future Directions

None of the newer methods compares to coronary arteriography in the ability to visualize graft stenoses and distant anastomoses. The noninvasive techniques are primarily used for screening patients with chest pain after coronary bypass grafting. The techniques do not replace coronary arteriography and are not sensitive enough to determine specific graft anatomy. Future developments need to quantitate graft flow noninvasively and to improve resolution to allow detailed observations of graft anatomy. Experimental techniques that use UFCT and MR imaging show some promise in this regard, but are not yet available clinically.

#### ACKNOWLEDGMENTS

The authors thank LuAnn Osdoba, Jan Widmer, Cheryel Reyhons, and Nicole Raitt for typing the manuscript and Marilyn Krachmer for helping with the data collection.

#### REFERENCES

- Trafford A. American's \$39 billion heart business. *US News & World Report* 1982;(March 15):53-57
- Loop FD. Progress in surgical treatment of coronary atherosclerosis (Part 1). *Chest* 1983;84:611-622
- Campeau L, Enjalbert M, Lesperance J, et al. Atherosclerosis and late closure of aortocoronary saphenous vein grafts; sequential angiographic studies at two weeks, 1 year, 5-7 years and 10-12 years after surgery. *Circulation* 1983;68[suppl II]:11-1-11-7
- Laurie GM, Morris GC Jr, Chapman DW, et al. Patterns of patency of 596 grafts up to seven years after aorto-coronary bypass. *J Thorac Cardiovasc Surg* 1977;73:443-448
- Mettler FA, Guiberteau MJ. *Essentials of nuclear medicine imaging*. Orlando, FL: Grune & Stratton, 1983:103-139
- Kawasuji M, Sawa S, Sakakibara N, et al. Serial assessment of left ventricular function following coronary artery bypass surgery by radionuclide angiocardiology. *Jpn Circ J* 1988;52:1149-1155
- Lewis RL, Videll JS, Strong MD, et al. Exercise radionuclide assessment of left ventricular function before and after coronary bypass surgery. *Angiology* 1987;38:601-607
- Hellman CK, Kamath ML, Schmidt DH, et al. Improvement in left ventricular function after myocardial revascularization: assessment by first-pass rest and exercise nuclear angiography. *J Thorac Cardiovasc Surg* 1980;79:645-655
- Newman GE, Rerych SK, Jones RH, Sabiston DC Jr. Noninvasive assessment of the effects of aorto-coronary bypass grafting on ventricular function during rest and exercise. *J Thorac Cardiovasc Surg* 1980;79:617-624
- Taylor NC, Barber RW, Crossland P, et al. Effects of coronary artery bypass grafting on left ventricular function assessed by multiple gated ventricular scintigraphy. *Br Heart J* 1983;50:149-156
- Floyd RD, Wagner GS, Austin EH, et al. Relation between QRS changes and left ventricular function before and after coronary artery bypass grafting. *Am J Cardiol* 1983;52:943-949
- Kent KM, Borer JS, Green MV, et al. Effects of coronary-artery bypass on global and regional left ventricular function during exercise. *N Engl J Med* 1978;298:1434-1439
- Greenberg BH, Hart R, Botvinick EH, et al. Thallium-201 myocardial perfusion scintigraphy to evaluate patients after coronary bypass surgery. *Am J Cardiol* 1978;42:167-176
- Kolibash AJ, Call TD, Bush CA, et al. Myocardial perfusion as an indicator of graft patency after coronary artery bypass surgery. *Circulation* 1980;61:882-887
- Starling MR, Walsh RA, Dehmer GJ, et al. Value of tomographic thallium-201 imaging in patients with chest pain following coronary artery bypass grafting. *Clin Nucl Med* 1987;12:134-139



16. Heikuri HV, Ikaheimo J, Korhonen UR, et al. Thallium scintigraphy in prediction of occlusion of bypass grafts in asymptomatic and symptomatic patients. *Acta Med Scand* **1987**;222:311-318
17. Engelstad BL, Wagner S, Herfkens R, et al. Evaluation of the postcoronary bypass patient by myocardial perfusion scintigraphy and computed tomography. *AJR* **1983**;141:507-512
18. Zimmermann R, Tillmanns H, Knapp WH, et al. Noninvasive assessment of coronary artery bypass patency: determination of myocardial thallium-201 washout rates. *Europ Heart J* **1988**;9:319-327
19. Rasmussen SL, Amtorp D, Folke K, Fritz-Hansen P, et al. 201-Thallium imaging as an indicator of graft patency after coronary bypass surgery. *Europ Heart J* **1984**;5:494-499
20. Jacobstein MD. Magnetic resonance imaging and positron emission tomography. In: Adams FH, Emmanouilides GC, Reimenschneider TA, eds. *Heart disease in infants, children and adolescents*, 4th ed. Baltimore: Williams and Wilkins, **1989**:114-129
21. Lerch RA, Ambos HD, Bergmann SR, et al. Localization of a viable ischemic myocardium by positron-emission tomography with 11C-palmitate. *Circulation* **1981**;64:689-699
22. Tillisch J, Brunken R, Marshall R, et al. Reversibility of cardiac wall-motion abnormalities predicted by positron tomography. *New Engl J Med* **1986**;314:884-888
23. Schelbert HR, Weisenberg G, Phelps ME, et al. Non invasive assessment of coronary stenosis by myocardial imaging during pharmacologic coronary vasodilation: detection of coronary artery disease in human beings with intravenous N13 ammonia and positron computed tomography. *Am J Cardiol* **1982**;49:1197-1207
24. Konishi Y, Ban T, Okamoto Y, et al. Myocardial positron tomography with N-13 ammonia in assessment of aortocoronary bypass surgery. *Japan Circ J* **1988**;52:411-416
25. Goldberg HL, Moses JW, Borer JS, et al. The role of digital subtraction angiography in coronary and bypass graft arteriography. *Circulation* **1982**;66[suppl II]:II-229
26. Drury JK, Gray R, Diamond GA, et al. Computer enhanced digital angiography visualizes coronary bypass grafts without need for selective injection. *Circulation* **1982**;66[suppl II]:II-229
27. Hayward R, Hunter GJS. Digital subtraction angiography in coronary artery bypass graft assessment: clinical applicability. *Br Heart J* **1985**;54:357-361
28. Steffenino G, Meier B, Bopp P, et al. Non-selective intra-arterial digital subtraction angiography for the assessment of coronary artery bypass grafts. *Int J Card Imaging* **1985**;1:209-215
29. Guthaner DF, Wexler L, Bradley B. Digital subtraction angiography of coronary grafts: optimization of technique. *AJR* **1985**;145:1185-1190
30. Lupon-Roses J, Montana J, Domingo E, et al. Venous digital angiography: an accurate and useful technique for assessing coronary bypass graft patency. *Eur Heart J* **1986**;7:979-986
31. Guiraudon GM, Rankin RN, Kostuk WJ, et al. Visualization of internal mammary artery bypass graft by digital intravenous angiography: experience with 42 consecutive patients. *J Am Coll Cardiol* **1986**;7:152A
32. Kempter H, Felix R, Benzer D. Digitale Subtraktionsangiographie (DSA): Darstellung von aortokoronaren venenbypassen. *ROFO* **1983**;138:137-139
33. Magotteaux P, Trotteur G. Controle de la permeabilite des greffons aortocoronaires par angiographie numerisee. *Rev Med Liege* **1984**;29:204-207
34. Myerowitz PD, Turnipseed WD, Shaw CG, et al. Computerized fluoroscopy: new technique for the noninvasive evaluation of the aorta, coronary artery bypass grafts, and left ventricular function. *J Thorac Cardiovasc Surg* **1982**;83:65-73
35. Diebold B, Theroux P, Bourassa MG, et al. Noninvasive assessment of aortocoronary bypass graft patency using pulsed Doppler echocardiography. *Am J Cardiol* **1979**;43:10-16
36. Gould JKL, Mozersky DJ, Hokanson DE, et al. A noninvasive technic for determining patency of saphenous vein coronary bypass grafts. *Circulation* **1972**;46:595-600
37. Pisko-Dubienski A, Baird RJ, Wilson DR. Noninvasive assessment of aortocoronary saphenous vein bypass graft patency using directional Doppler. *Circulation* **1975**;51 & 52[suppl I]:I-188-I-197
38. Sheiban I, Trevi G, Casarotto D, et al. Direct visualization of aortacoronary bypass grafts by two-dimensional echocardiography: a new clinical application. *Cardiovasc Intervent Radiol* **1988**;11:14-17
39. Fusejima K, Takahara Y, Sudo Y, et al. Comparison of coronary hemodynamics in patients with internal mammary and saphenous vein coronary bypass grafts: a non-invasive approach using combined two dimensional and Doppler echocardiography. *J Am Coll Cardiol* **1990**;15:131-139
40. Daniel WG, Dohring W, Stender HS, Lichtlen PR. Value and limitations of computed tomography in assessing aortocoronary bypass graft patency. *Circulation* **1983**;67:983-987
41. Brundage BH, Lipton MJ, Herfkens RJ, et al. Detection of patent coronary bypass grafts by computed tomography: a preliminary report. *Circulation* **1980**;61:826-831
42. Godwin JD, Califf RM, Korobkin M, et al. Clinical value of coronary bypass evaluation with CT. *AJR* **1983**;140:649-655
42. Wilson PC, Gutierrez O, Moss A. Early evaluation of coronary artery bypass grafts: CT or selective angiography. *Eur J Radiol* **1984**;4:22-27
44. Kahl FR, Wolfman NT, Watts LE. Evaluation of aortocoronary bypass graft status by computed tomography. *Am J Cardiol* **1981**;48:304-310
45. Kwasuji M, Aoyama T, Iwa T, Suzuki M. Noninvasive evaluation of aortocoronary bypass graft patency by contrast-enhanced computed tomography: incrementation mode and dynamic mode. *Jpn Circ J* **1984**;48:611-619
46. Foster CJ, Sekiya T, Brownlee WS, Isherwood I. Computed tomographic assessment of coronary artery bypass grafts. *Br Heart J* **1984**;52:24-29
47. Moncada R, Salinas M, Churchill R, et al. Patency of saphenous aortocoronary-bypass grafts demonstrated by computed tomography. *N Engl J Med* **1980**;303:503-505
48. Stanford W, Brundage BH, MacMillan, R, et al. Sensitivity and specificity of assessing coronary bypass graft patency with ultrafast computed tomography: results of a multicenter study. *J Am Coll Cardiol* **1988**;12:1-7
49. Bateman TM, Gray RJ, Whiting JS, et al. Cine computed tomographic evaluation of aortocoronary bypass graft patency. *J Am Coll Cardiol* **1986**;8:693-698
50. Bateman TM, Gray RJ, Whiting JS, et al. Prospective evaluation of ultrafast cardiac computed tomography for determination of coronary bypass graft patency. *Circulation* **1987**;75:1018-1024
51. Stanford W, Rooholamini M, Rumberger J, Marcus M. Evaluation of coronary bypass graft patency by ultrafast computed tomography. *J Thorac Imaging* **1988**;3:52-55
52. Rumberger JA, Feiring AJ, Hiratzka LF, et al. Quantification of coronary artery bypass graft patency by ultrafast computed tomography. *J Thorac Imaging* **1988**;2:194-202
53. White RD, Caputo GR, Mark AS, et al. Coronary artery bypass graft patency: noninvasive evaluation with MR imaging. *Radiology* **1987**;164:681-686
54. White RD, Pflugfelder PW, Lipton MJ, Higgins CB. Coronary artery bypass grafts: evaluation of patency with cine MR imaging. *AJR* **1988**;150:1271-1274
55. Rubinstein RI, Askenase AD, Thickman D, et al. Magnetic resonance imaging to evaluate patency of aortocoronary bypass grafts. *Circulation* **1987**;76:786-791
56. Jenkins JPR, Love HG, Foster CJ, et al. Detection of coronary artery bypass graft patency as assessed by magnetic resonance imaging. *Br J Radiol* **1988**;61:2-4
57. Fria G, Schouman-Claeys E, Lacombe P, et al. A study of coronary artery bypass graft patency using MR imaging. *J Comput Assist Tomogr* **1989**;13:226-232
58. Aurigemma GP, Reichek N, Axel L, et al. Non invasive determination of coronary artery bypass graft patency by cine magnetic resonance imaging. *Circulation* **1989**;80:1595-1602
59. Underwood SR, Firmin DN, Klipstein RH, et al. Toward MR flow measurements in the coronary arteries and coronary bypass grafts. *Radiology* **1986**;161(P):224
60. Wilson RF, Laughlin DE, Ackell PH, et al. Transluminal subselective measurement of coronary artery blood flow velocity and vasodilator reserve in man. *Circulation* **1985**;72:82-92
61. Wilson RF, Johnson MR, Marcus ML, et al. The effect of coronary angioplasty on coronary flow reserve. *Circulation* **1988**;77:873-885
62. Wilson RF, White CF. Does coronary artery bypass surgery restore normal maximal coronary flow reserve? *Circulation* **1987**;76:563-571



## Review Article

# CT of the Gastrointestinal Tract: Principles and Interpretation

Emil J. Balthazar<sup>1</sup>

The experience accumulated in daily abdominal CT scanning and CT evaluation of gastrointestinal lesions has generated helpful technical guidelines and some reliable principles of interpretation. These general principles are briefly discussed in this review, and the importance of performing a CT examination that is adequate for the detection and evaluation of gastrointestinal lesions is stressed. CT features useful in differentiating benign from malignant lesions, limitations and pitfalls in CT interpretation, overlap in the CT appearance, and classical CT features leading to specific diagnoses are described and illustrated.

Although CT is established as one of the most important techniques for imaging the gastrointestinal tract, it should be used selectively and only in the context of appropriate clinical and conventional radiologic examination. CT should not be regarded as competing with, but as complementing, barium examination of the gastrointestinal tract.

Technological advances in CT have changed the practice of gastrointestinal radiology. With the development of high-resolution scanners, technical refinements in obtaining better quality studies, and the accumulated clinical experience leading to better interpretation, the role, indications, and accuracy of CT of the gastrointestinal tract have dramatically enlarged and improved.

Today the indications for gastrointestinal examinations encompass a steadily expanding list of abnormalities based on CT's usefulness for (1) diagnosing or suggesting the presence of primary gut disease; (2) evaluating the nature and extent of disease in patients with known gastrointestinal lesions; and (3) determining the presence, location, and severity of complications associated with primary gastrointestinal lesions

such as phlegmons, abscesses, and perforations. Conventional barium examinations remain superior to CT for evaluating intraluminal and mucosal disease, but CT is far more accurate for evaluating the intramural and extraintestinal components, including involvement of the mesentery, peritoneal cavity, retroperitoneum, and solid organs. CT therefore should not be regarded as competing with, but as complementing, barium examinations of the gastrointestinal tract. Contrast examinations should be performed in all patients in whom the presence, origin, or nature of the abnormality is unknown or uncertain at the time of the CT examination. Conversely, CT examinations are often required to elucidate and evaluate gastrointestinal abnormalities detected or suspected on conventional examinations.

The purpose of this review is to emphasize principles of performing adequate CT examinations and formulate general rules of interpretation and differential diagnosis of gastrointestinal lesions. Common pitfalls in CT interpretation, limitations in the diagnosis, and the characteristic CT appearance of some of the primary gastrointestinal lesions are discussed and illustrated.

### Technical Considerations

Routine CT examinations of the abdomen usually result in the inadequate evaluation of most primary gastrointestinal lesions, unless a special effort is made to enhance their visualization. Techniques used to achieve this objective vary and have been described in the literature [1]. The goal of obtaining a high-resolution study can be accomplished only

Received May 29, 1990; accepted June 26, 1990.

<sup>1</sup> Department of Radiology, New York University—Bellevue Medical Center, 550 First Ave., New York, NY 10016. Address reprint requests to E. J. Balthazar.

*AJR* 156:23-32, January 1991 0361-803X/90/1561-0023 © American Roentgen Ray Society



by a determined attempt to follow several general principles of CT examination:

1. Visualization of the intestinal lumen and its mucosal surface and evaluation of the true thickness of the intestinal wall require the gastrointestinal tract to be empty and clean and its lumen to be opacified and distended. Patients should fast, and adequate preparation of the colon is essential, particularly in patients in whom colonic disease is suspected or known to be present. Visualization of intestinal lumen is achieved by the oral administration of 700–800 ml of 2% diluted barium or Gastrografin (diatrizoate meglumine, Squibb, Princeton, NJ) at least 1 hr before scanning. The terminal ileal loops and cecum should be filled with contrast material in all patients because the right lower quadrant is a common site for primary intestinal disease. This can be facilitated by the oral administration of 10 mg of Metoclopramide or, when necessary, by a second pelvic examination 15–30 min later. Stomach and colon may be filled with diluted barium or Gastrografin. We prefer, however, the use of air (EZ gas for the stomach and air insufflation for the colon) because the procedure can be achieved easily and rapidly, it is well tolerated by the patients, and air provides an excellent CT contrast medium [1]. Detection of subtle gastric, duodenal, or colonic lesions can be enhanced by repeated scans obtained with the patient prone or in the left or right lateral decubitus positions, depending on the location of the lesion, and by using well-established guidelines for fluoroscopic examination of the gastrointestinal tract [1].

2. Imaging of a primary gastrointestinal lesion should be done, whenever possible, during the arterial phase of a bolus IV injection of iodinated contrast material by using the sequential incremental table movement technique. With a rapid 2-sec scanner, this objective can be achieved with the help of an automatic power injector with a 22-gauge angiocath, and by injecting 50 ml of 43% diatrizoate at a rate of 1.5 ml/sec followed by 140 ml at a rate of 0.8 ml/sec. When the

location of the lesion is known or clinically suspected, the technique can be appropriately tailored, and the examination must be monitored before it is considered completed. For a pelvic lesion, for instance, one can start with a bolus of 50 ml of 43% contrast material at 1.5 ml/sec at the level of the diaphragm followed by 75 ml at 0.8 ml/sec. Delay the second bolus for 60 sec and again inject 75 ml of contrast material at 1.5 ml/sec while scanning over the pelvis. This technique allows imaging of the intestinal lesion at the peak of contrast enhancement, while permitting excellent visualization of the entire region during the arterial and venous return phase. The presence, degree, and pattern of enhancement are some of the important criteria used in the differential diagnosis of primary gastrointestinal lesions and should always be considered in the CT evaluation.

3. The successful acquisition of high-resolution images requires the liberal use of thin (5-mm) sections over the area suspected or known to be pathologically involved. This can be done, during the initial scanning, when the location of the lesion is known, or during repeated scanning at the end of the examination, when an abnormality is suspected but is inadequately imaged. At this time, 1 mg IV glucagon to inhibit peristalsis, additional barium or air in the stomach or colon, and proper positioning of the patient should be considered before repeated thin (5-mm) sections over the area of interest are obtained.

### Common Pitfalls in CT Interpretation

Most of the pitfalls in the CT detection and evaluation of gastrointestinal lesions are related to technical failures. Among them, inadequate contrast filling of the intestinal lumen and incomplete intestinal distension during CT scanning are the most common. Empty, collapsed intestinal loops or fluid-filled bowel can present as soft-tissue density mimicking

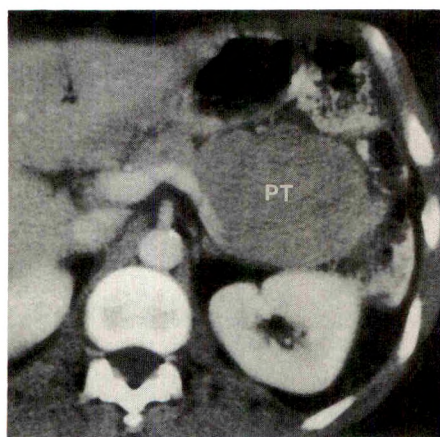
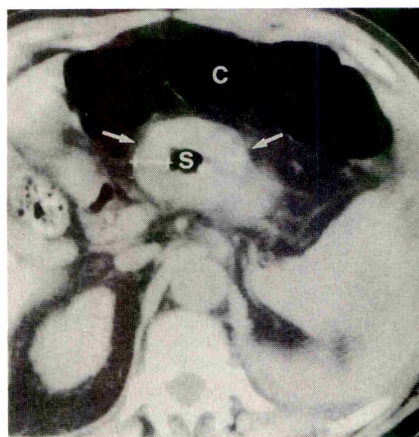
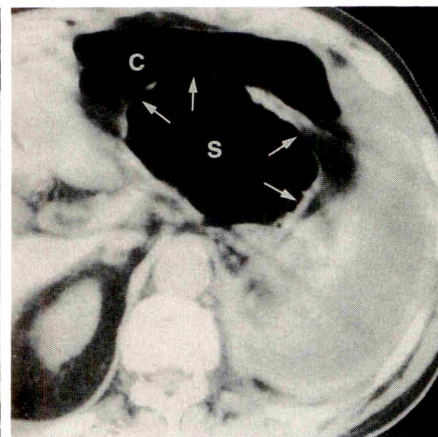


Fig. 1.—CT scan of pseudotumor (PT) in left upper abdomen produced by nonopacified, fluid-filled jejunal loops. Homogeneous appearance and higher density of intestinal contents mimics soft-tissue tumor.



A



B

Fig. 2.—Correlation of bowel thickness with degree of luminal distension on CT.  
A, Collapsed stomach (S) located posterior to transverse colon (C) shows 1.8-cm-thick gastric wall (arrows). Note perfect symmetry and homogeneous density.  
B, After luminal distension with air, stomach (S) shows a gastric wall thickness of only 1–2 mm (arrows).



mesenteric tumor (Fig. 1). Although they usually involve proximal jejunal loops, these pseudotumors may be located throughout the intestinal tract depending on the amount and/or timing of oral contrast administration before the CT examination. Furthermore, partial filling of the intestinal lumen can lead to false-positive or false-negative examinations because of inability to determine the true thickness of the intestinal wall. On CT, the normal thickness of the gastrointestinal wall varies greatly with the degree of luminal distension. The wall is barely perceptible and no more than 1–2 mm thick in a distended segment and appears thicker (3–4 mm) when the intestine is collapsed or partially distended. This is particularly true in the stomach, where the wall thickness varies considerably between 1 mm when distended to as much as 2 cm when it is collapsed (Fig. 2). If the wall is perceived to be evenly, concentrically, and symmetrically thickened and it is homogeneously enhancing, the clinical significance of this finding should be cautiously interpreted and related to the degree of distension of the gastrointestinal segment analyzed.

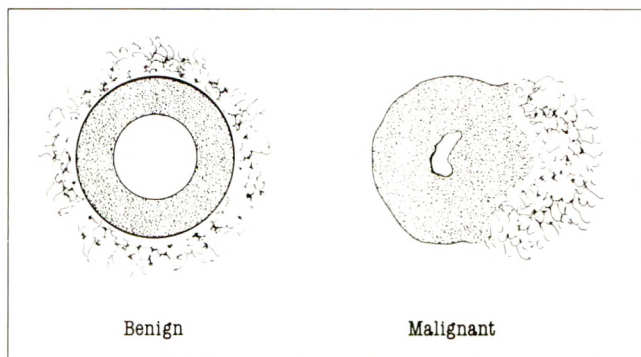


Fig. 3.—Cross section of abnormal bowel on CT. Benign disease shows mild (0.3–1.0 cm), circumferential, and symmetric wall thickening and adjacent mesenteric inflammatory response. Neoplastic disease exhibits thicker bowel wall (>2 cm), asymmetric involvement, lobulated contour, and narrowing of intestinal lumen.

### CT Assessment of Gastrointestinal Lesions

Once a gastrointestinal lesion is detected, its radiologic features are analyzed by using criteria employed in conventional radiology as well as observations specific to CT imaging. Important considerations are location, size, and length of involvement. It is particularly important to define the abnormality as focal, segmental, or diffusely affecting an entire intestinal segment (i.e., stomach, colon, or small bowel). CT features include degree of thickening of intestinal wall, symmetry of involvement, smooth vs irregular or lobulated inner or outer contour, and pattern of enhancement. Associated findings such as exophytic component, lymphadenopathy, distal metastases, adjacent mesenteric inflammatory response, phlegmon, or abscess are additional important features that are helpful in the differential diagnosis.

#### Benign Intestinal Disease

The hallmark of the CT appearance of a benign intestinal lesion is the circumferential and symmetric thickening of the bowel wall, usually not exceeding 1 cm from the luminal to the serosal surface (Fig. 3). The process is usually segmental or diffusely involves the entire colon or small bowel, and adjacent inflammatory reaction manifesting as thickened mesenteric fat with a streaky higher density appearance is common. Depending on the cause and the severity of the abnormality, the intestinal wall may occasionally be thicker (1–2 cm). However the circumferential involvement, relative symmetry, and segmental distribution are maintained. The involved bowel wall has a homogeneous soft-tissue density (Fig. 4) or exhibits alternate rings of low and high attenuation referred to as a “double halo” (two rings) or “target” (three rings) sign (Figs. 5 and 6).

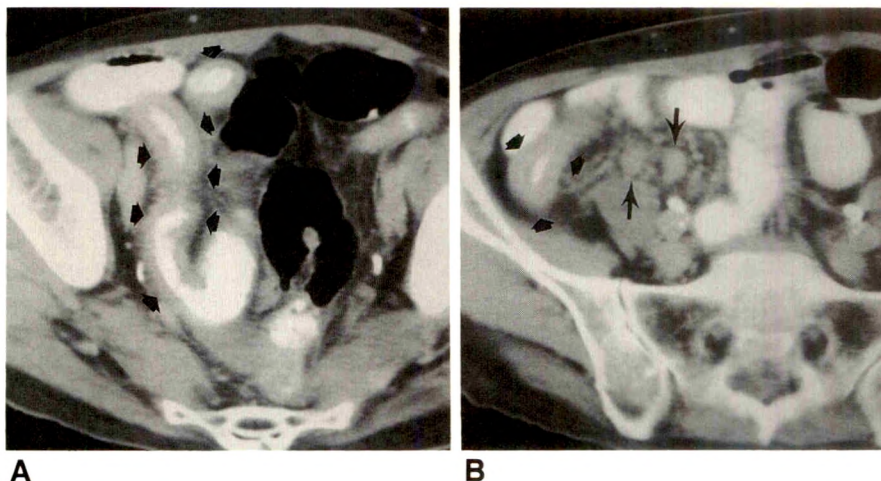
#### Double Halo and Target Sign

This CT appearance has been shown to be associated with submucosal edema, inflammation, and/or fat deposition [2],

Fig. 4.—CT of Crohn disease affecting terminal ileum with associated mesenteric lymphadenopathy.

A, Segmental involvement of distal ileum with mild, circumferential, and symmetric wall thickening showing a homogeneous density (arrows).

B, Unusual regional mesenteric lymphadenopathy (long arrows) adjacent to thick-walled intestine (short arrows). Crohn disease and large inflammatory nodes were proved at surgery.





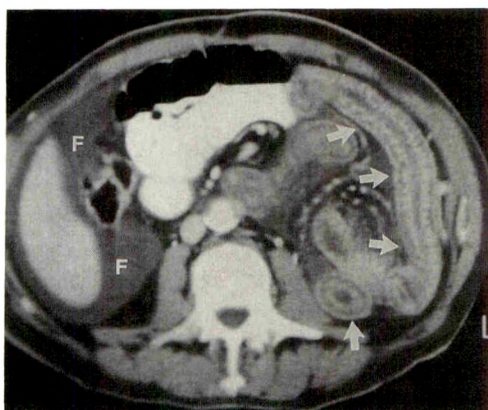


Fig. 5.—CT scan of ischemic enteritis showing alternate rings of high, low, and high attenuation in a symmetrical, circumferential, and slightly thickened bowel wall (arrows). Distribution is segmental, and there is associated intraperitoneal hemorrhagic fluid (F).

and it is helpful in the differential diagnosis of benign vs malignant disease. The different ring densities are better appreciated during the arterial phase of enhancement and may be totally absent on examinations performed without IV contrast material or with slow, low-volume drip infusions. Although originally reported in Crohn disease [3], it has since been observed in other benign entities (Table 1) and is therefore not specific. In our experience it is more commonly present in ischemic disease, but its significance should be judged in the context of the clinical presentation and the associated intestinal and mesenteric CT findings. Furthermore, the detection of this sign does not signify active disease because it may occur in a burned-out inflammatory or ischemic process in asymptomatic persons.

#### Inflammatory Disease

The CT prototype of a typical inflammatory lesion is Crohn disease. Because mucosal disease cannot be detected on CT, conventional barium studies remain the procedures of choice for the initial diagnosis of Crohn disease. With CT, however, this entity often can be diagnosed on the basis of the symmetric thickening of the bowel wall (Fig. 4), segmental distal ileal distribution, skipped areas of involvement, fistulas, and other commonly associated mesenteric abnormalities [4, 5]. Fibrofatty proliferation of the mesenteric fat is seen in about 40% of patients with various degrees of streakiness, poorly defined heterogeneous mesenteric densities (phlegmons), and/or well-margined collections of fluid sometimes containing bubbles of air representing abscesses. Small regional mesenteric nodes are present in about 20% of patients (Fig. 4). It is in the evaluation and management of these complications that CT has had the greatest impact [5].

Mild inflammatory colitides such as ulcerative and infectious colitis affect only the colonic mucosa and are not optimally evaluated or diagnosed with CT. Forms of severe colitis, on the other hand, are easily recognized. They are characterized by their diffuse distribution, marked concentric thickening of

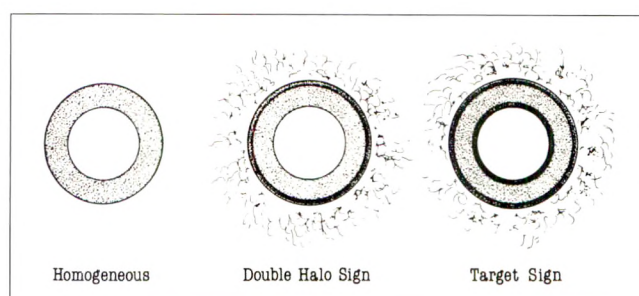


Fig. 6.—Cross section of benign intestinal disease. Involved segment may exhibit a homogeneous enhancing soft-tissue density, two concentric rings of low and high attenuation (double halo sign), or three concentric rings of high, low, and high density (target sign). Presence of two or three concentric rings has a similar clinical significance. Degree of density difference is related to severity of mucosal hyperemia, submucosal edema, inflammation, or fat deposition and to quality of CT examination.

TABLE 1: Double Halo and Target Sign

- |  |
|--|
| 1. Ischemic enteritis                              |
| 2. Crohn disease                                   |
| 3. Ulcerative colitis                              |
| 4. Infectious colitis                              |
| 5. Radiation enteritis                             |
| 6. Shönlein-Henoch purpura                         |
| 7. Bowel edema associated with portal hypertension |

the colonic wall, altered or absent haustral pattern, deep transmural ulcerations, and significant pericolic inflammatory changes (Fig. 7). We have found CT to be particularly valuable in the initial diagnosis of pseudomembranous colitis affecting debilitated persons on broad-spectrum antibiotic therapy and cytomegalovirus colitis in AIDS patients [6, 7]. These patients are often referred for examination because of sepsis and nonspecific abdominal complaints with the diagnosis unsuspected at the time of CT scanning.

#### Intramural Hemorrhage and Intestinal Ischemia

Intramural hemorrhage and intestinal ischemia have CT features similar to those of Crohn disease as far as their segmental distribution and the symmetrical, circumferential thickening of the affected bowel wall (Fig. 5).

Intramural hemorrhage due to anticoagulant therapy, bleeding diathesis, or trauma can be reliably visualized with CT. The high-density wall thickening usually involves a more proximal intestinal segment, and small amounts of mesenteric and/or free intraperitoneal blood may be present (Fig. 8). In the context of a proper history, these findings are characteristic of intramural hemorrhage. Furthermore, follow-up CT examination in these patients shows the typical and rapid resolution with return to a normal configuration in 7–14 days [8]. Because of its high sensitivity, noninvasiveness, and ability to image the entire peritoneal cavity, pelvis, and retroperitoneum, CT has become the imaging technique of choice in patients with abnormal clotting factors who develop acute abdominal symptoms or a sudden decrease in hematocrit.



Fig. 7.—Pseudomembranous colitis affecting entire colon. CT scan of transverse colon shows circumferential wall thickening, distortion of haustral pattern, and pericolic inflammation (arrows). Findings are consistent with a severe form of universal colitis but are not etiologically specific.

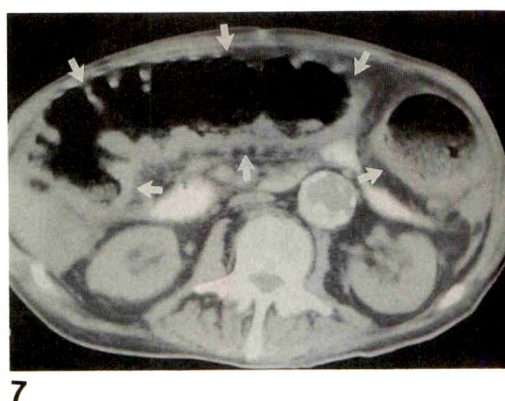
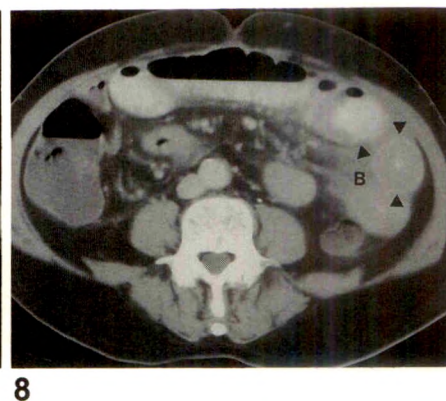


Fig. 8.—Intramural hemorrhage associated with anticoagulant therapy. CT scan of jejunal segment in left upper abdomen shows concentric wall thickening (arrowheads) and high-density fluid (blood, B) in adjacent mesentery.



Similar findings of mild (0.5–1.0 cm), circumferential, and symmetric thickening, with segmental distribution and homogeneous or “double halo” density, is often seen in ischemic bowel disease (Fig. 5). Free intraperitoneal blood, when present, is extremely useful in the differential diagnosis from inflammatory disease and in securing an early diagnosis. The sensitivity of CT in ischemic bowel disease is unknown but appears to be limited to the more severe forms of involvement [9–11]. The role of CT in this entity is still emerging and remains somewhat controversial. Although original reports were very encouraging, later clinical investigations have shown that nonspecific abnormalities (small-bowel dilatation, congestive changes in mesentery) are present in 50–56%, whereas a specific diagnosis can be made in only 26–39% of patients [9–11]. On good-quality examinations, CT can sometimes establish the cause of ischemia by showing arterial occlusion or thrombosis in the superior mesenteric or portal vein.

Advanced cases of ischemia in which bowel infarction has already developed are more reliably diagnosed by the detection of air in the wall of bowel (pneumatosis) associated with air in the regional mesenteric venous branches and/or intrahepatic portal veins.

Radiation enteritis has CT features very similar to inflammatory and ischemic disease and can be diagnosed mainly in the context of a proper history. The disease, in addition, has a characteristic distribution in most persons, with involvement of the pelvic structures including rectosigmoid and low-lying pelvic small-bowel loops.

#### Neoplastic Intestinal Disease

The hallmark of a malignant lesion on CT is eccentric or asymmetric thickening of the bowel wall, the irregular and lobulated inner and outer contour, and/or the focal soft-tissue mass usually exceeding 2 cm from the luminal to serosal surface (Fig. 3). The area of involvement varies in size. There is abrupt transition, luminal narrowing, and sometimes a spiculated outer contour. Regional adenopathy and distal mesenteric, retroperitoneal, and liver metastases, when present, confirm the neoplastic nature of the primary lesion. The contrast-enhanced soft-tissue mass may have a homogeneous density or, with certain lesions, appears heterogeneous

because of patchy irregular areas of lower densities related to zones of decreased blood supply and tumor necrosis [12].

#### Primary Adenocarcinoma

Carcinoma is by far the most common tumor affecting mainly the colon and stomach. In the small bowel, it is more common in the proximal duodenojejunal segment, often associated with proximal intestinal obstruction. The tumor usually involves only a short intestinal segment (3–5 cm) and on CT presents as an eccentric focal mass or as a circumferential asymmetric and irregular thickening of the bowel wall (Fig. 9). Larger lesions, when examined during the bolus arterial phase and imaged with narrow windows, show the characteristic patchy areas of low density representing tumor ischemia. The sensitivity of CT in detecting primary adenocarcinoma varies greatly depending on the size of the lesion and the quality of the examination. In the colon, it was reported to be 68% on routine CT examination and 95% on examinations performed on clean and air-distended colons [12]. CT cannot be used as a primary technique in diagnosing adenocarcinoma; how-

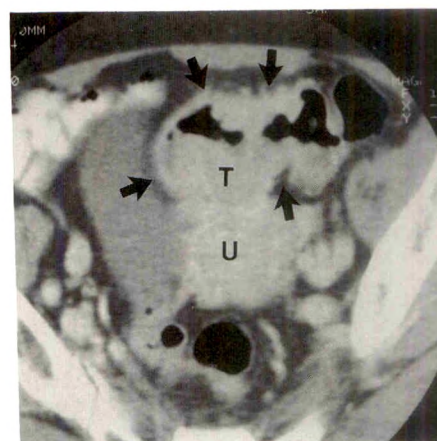


Fig. 9.—Adenocarcinoma of sigmoid colon. Magnified CT scan shows narrowed irregular sigmoid lumen and circumferential infiltration by a lobulated and asymmetric soft-tissue mass (arrows). Colonic tumor (T) is compressing uterus (U), and expected intermediary fat plane is obliterated.



ever, in our experience it has been useful in detecting tumors that were clinically unsuspected and in patients with nonspecific abdominal complaints.

### Lymphosarcoma

In most patients, at the time of the examination, gastrointestinal lymphosarcoma presents as a large infiltrating submucosal tumor. In these cases, two CT features allow a highly reliable preoperative diagnosis (Fig. 10). First, there is striking mural soft-tissue thickening concentrically infiltrating a segment of bowel. The segment involved is longer than most adenocarcinomas (5–15 cm). The tumor may be lobulated but sharply defined, and as a rule, it has a homogeneous density throughout (Fig. 11). Second, in most persons there is mas-

sive regional and distal retroperitoneal and/or mesenteric adenopathy [13]. Intestinal obstruction is unusual, but large ulcerations filled with contrast material and air may be present. Small incipient gastrointestinal lesions cannot be differentiated from adenocarcinoma.

### Leiomyosarcoma

Gastrointestinal leiomyosarcoma is a bulky tumor arising from the wall of bowel and developing into a large, lobulated, exophytic soft-tissue mass. The characteristic CT features are unusually large size and very common central necrosis and liquefaction (Fig. 10). A large irregular central zone of lower attenuation and fluid/fluid levels are detected with CT (Fig. 12). The tumor has an oval or round configuration, and when totally liquefied, it appears as a fluid-filled cyst with a slightly thickened and irregular outer wall attached to an intestinal segment [14]. If the site of attachment is not detected, the lesion may be misdiagnosed as pancreatic pseudocyst or mesenteric or ovarian cyst (Fig. 12). Lymphadenopathy is not seen in patients with leiomyosarcoma because this neoplasm spreads locally and by hematogeneous dissemination and not by lymphatic permeation.

### Limitations in the CT Diagnosis of Gastrointestinal Lesions

The CT characteristics of benign and malignant intestinal lesions heretofore described are helpful in the differential diagnosis of the majority of cases encountered in clinical practice. There remains, however, a good number of gastrointestinal lesions in which the atypical CT appearance, similarities and overlap in the CT presentation, and technical failures in CT performance and interpretation lead to an erroneous

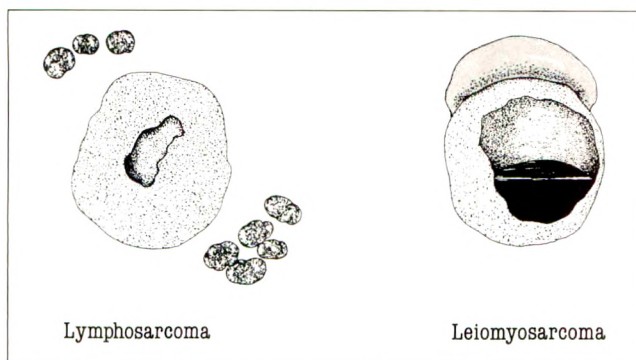


Fig. 10.—Differential diagnosis of lymphosarcoma vs leiomyosarcoma. Lymphosarcoma shows focal or circumferential massive wall thickening (5–10 cm), homogeneous enhancement, and extensive regional and distal lymphadenopathy. Leiomyosarcoma presents as a bulky, exophytic mass with large central zones of low density (ischemia, necrosis), or total liquefaction. There is no associated lymphadenopathy.

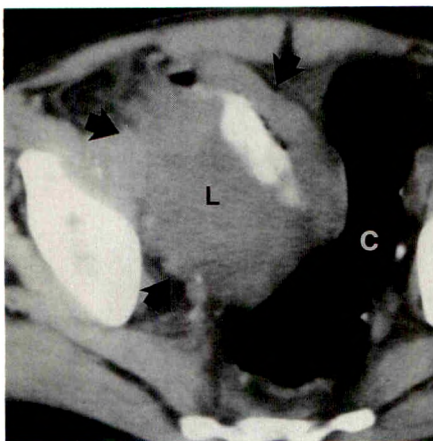
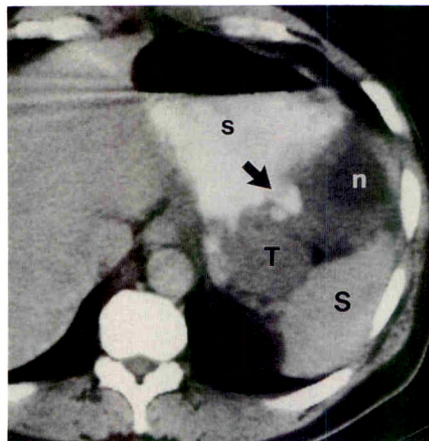
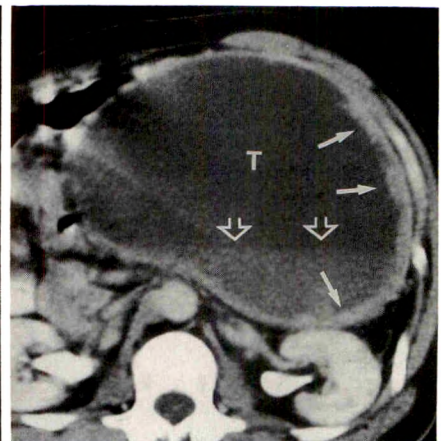


Fig. 11.—Distal ileal lymphosarcoma (L). CT scan shows an infiltrating circumferential, asymmetric soft-tissue mass of homogeneous density (arrows) compressing and displacing sigmoid colon (C). Barium-filled intestinal lumen is slightly distended and featureless, and bowel is not obstructed.



A



B

Fig. 12.—Gastric leiomyosarcoma presenting as a large encapsulated cystic mass. A, CT scan of stomach (s) shows a deep ulcer (arrow) along proximal greater curvature posterior wall. Attached to wall and surrounding ulcer is a lobulated soft-tissue tumor (T) exhibiting irregular patchy areas of necrosis (n). Tumor extends to anterior edge of spleen (S). B, Midabdominal CT scan shows large cystic component of tumor (T), with liquefaction, fluid-fluid level (open arrows), and a slightly thickened irregular wall (solid arrows).



diagnosis. Among some of the more common and most important entities leading to potential pitfalls in the CT diagnoses are the following:

1. Infiltrating scirrhous carcinoma (linitis plastica), presents as a plaquelike or circumferential wall thickening that mimics benign disease (Fig. 13). The bowel wall is 3–10 mm thick, the segment involved is long (10–15 cm) without abrupt transition, and the wall's inner and outer contour is smooth and symmetric. Despite its benign appearance, this lesion is easily recognized in the stomach because of its common involvement of this organ. When it involves the distal colon (rectosigmoid), it may be misdiagnosed as a form of segmental colitis or diverticulitis (Fig. 13). In most instances, however, rigidity with significant narrowing of the intestinal lumen occurs, and regional adenopathy and/or distal metastases secure the correct diagnosis.

2. Lymphosarcoma can have protean CT manifestations. It appears as a focal intraluminal lesion (Fig. 14) or as an infiltrating segmental intestinal lesion leading to slight circumferential wall thickening (Fig. 14). When focal, it can be misinterpreted as a mesenchymal tumor or as adenocarcinoma. It can be mistaken for an inflammatory or ischemic lesion when its involvement is segmental. In most cases however, the slight asymmetry in wall thickening, absence of the double

halo sign, and particularly the presence of significant associated adenopathy are clues leading to the correct diagnosis (Fig. 14).

3. The differential diagnosis of diverticulitis vs sigmoid carcinoma remains an important, common, and controversial clinical problem. Even in the presence of diverticula and pericolic inflammation, the configuration and degree of wall thickening remain the crucial CT indicators of the nature of the abnormality. The true thickness and configuration of the abnormal sigmoid segment can be assessed only when the bowel lumen is clearly visualized and well distended, and often only with thin (5 mm) sections obtained in the middle of the suspected lesion (Fig. 15).

The diagnosis of diverticulitis on CT can be made by demonstrating mild wall thickening (3–5 mm), symmetry of involvement, short segment (4–5 cm), colonic diverticula, and especially pericolic inflammation, phlegmon, or abscess [15, 16] (Fig. 16). In about 10% of patients, however, there is significant overlap in colonic wall thickness in diverticulitis and carcinoma, particularly with lesions between 1 and 3 cm in thickness [17]. In diverticulitis the wall thickening is seen mainly in chronic, long-standing disease, and it is the result of muscle hypertrophy, fibrosis, edema, intramural inflammation, or organized intramural inflammatory mass (Fig. 17). In

Fig. 13.—Scirrhous carcinoma exhibiting circumferential and symmetric wall thickening and homogeneous density of intestinal wall on CT.

A, Gastric lumen (S) is narrowed, wall is thickened (solid arrows), and numerous large lymph nodes are in lesser omentum (open arrows).

B, Sigmoid colon (C) reveals circumferential wall thickening (arrows) misdiagnosed as inflammatory or ischemic bowel disease.

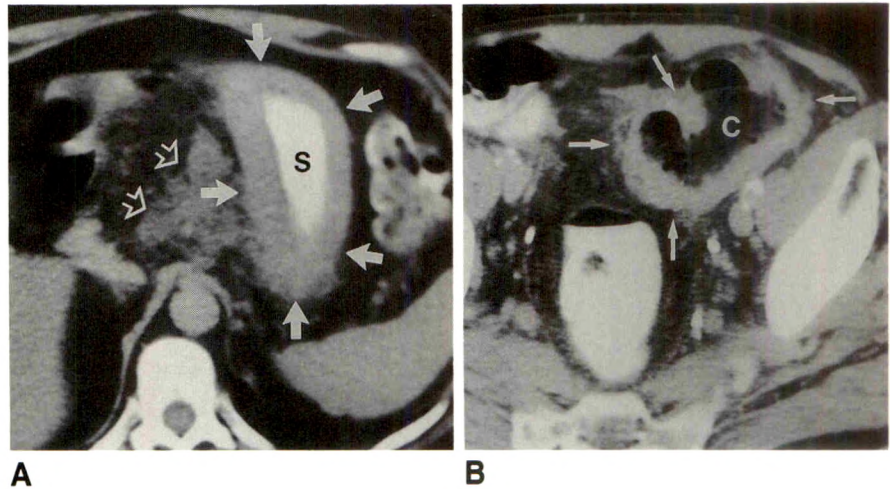
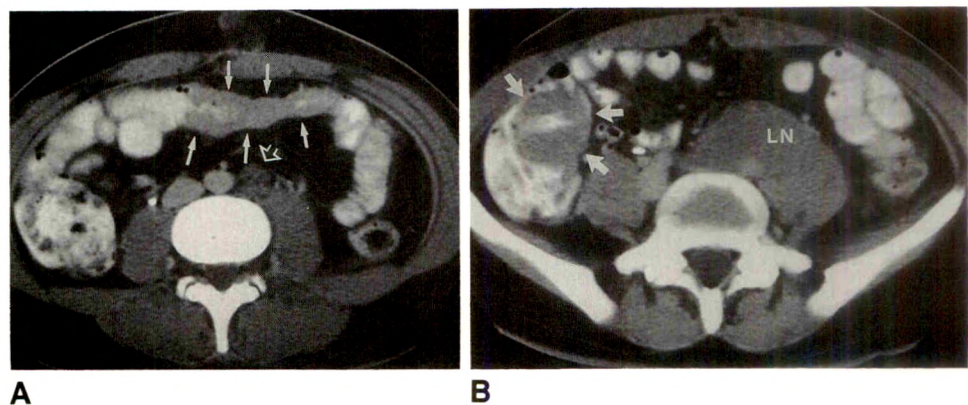


Fig. 14.—Lymphosarcoma with involvement of small intestine, colon, and lymph nodes.

A, CT scan of segment of distal ileum shows circumferential wall thickening (solid arrows) with slight asymmetry of involvement. Retroperitoneal adenopathy is visible at same level (open arrow).

B, CT scan of upper pelvis reveals focal homogeneous soft-tissue mass in cecum (arrows) and massive retroperitoneal lymphadenopathy (LN).





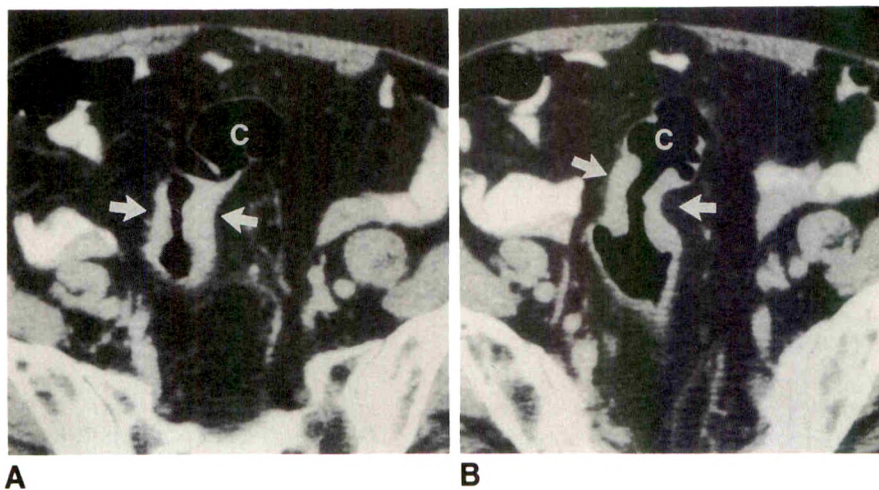


Fig. 15.—Sigmoid adenocarcinoma optimally imaged with air distension and thin (5 mm) section in middle of lesion.

A, Initial CT scan through sigmoid colon (c) reveals abnormally narrowed lumen and nonspecific circumferential thickened wall (arrows). Diagnosis includes diverticular disease with muscle hypertrophy and adenocarcinoma.

B, Repeated thin-section (5 mm) CT scan through sigmoid lumen (c) shows circumferential infiltrating lesion with overhanging edge and abrupt transition typical of adenocarcinoma (arrows).

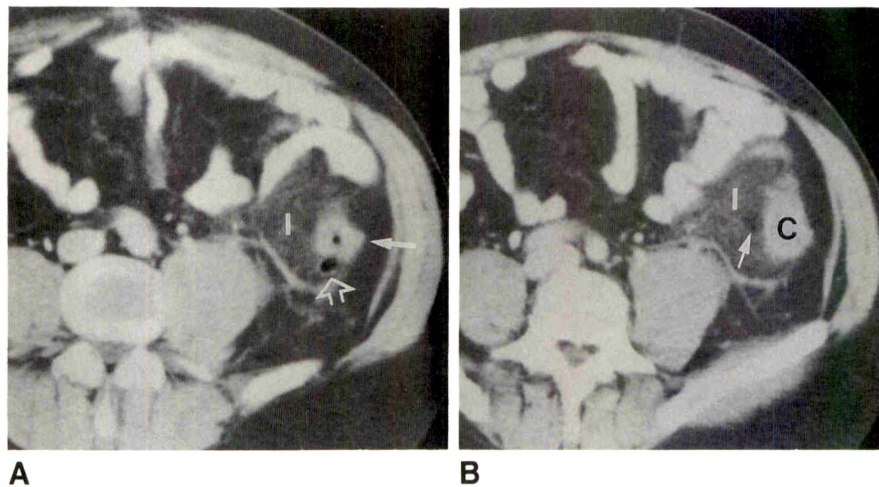


Fig. 16.—CT scans of acute diverticulitis of distal descending colon.

A, Typical appearance with mild circumferential wall thickening (solid arrow), air-filled diverticulum (open arrow), and pericolic inflammatory response (I).

B, Adjacent cross section shows fluid-filled colon (C), pericolic inflammation, and bubbles of air (arrow) indicating sealed-off perforation. CT findings were proved at surgery.

these patients, CT cannot confidently be used to differentiate diverticulitis from colonic carcinoma. Perforated sigmoid carcinoma should be suspected when the CT features are atypical, equivocal, or unusual. In our experience, if the colon is clean, with luminal visualization, air distension, and high-resolution (5-mm-section) scanning, this differential diagnosis can be made in most instances (Fig. 18) [18]. In the remaining uncertain cases, however, barium enema should be used liberally as an important complementary examination, to avoid potential CT errors. In addition, when the acute abdominal findings subside, and if surgical resection is not contemplated, sigmoidoscopy or barium enema should be performed to confirm the CT diagnosis.

#### Typical CT Appearance of Gastrointestinal Lesions

A few primary gastrointestinal lesions present with CT features that are virtually pathognomonic. They have no differential diagnosis and do not require endoscopy or barium studies for confirmation. In our experience, CT has been very helpful and specific in the diagnosis of the following lesions:

1. Gastrointestinal lipoma may occur throughout the gastrointestinal tract. It is commonly seen in the colon and small bowel and can be suspected on conventional barium studies because of its intraluminal location, sharply defined contour, and change in shape with compression. The lesion may be sessile when small (1–2 cm), or pedunculated when it is larger. CT can easily confirm the diagnosis with the demonstration of a homogeneous, low-density (–50 to –100 H) intraluminal defect (Fig. 19). With small lesions, thin sections (5 mm) and adequate contrast filling of the bowel lumen are required for a successful evaluation [19].

2. Small-bowel carcinoid. The sensitivity of CT in the detection and diagnosis of gastrointestinal carcinoids is not known. On the basis of their morphologic features, CT's sensitivity should be low for small intramural lesions, and its specificity should be unimpressive for the colonic or gastric lesions. Some of the primary small-bowel lesions, however, have exhibited characteristic CT features allowing a reliable and specific diagnosis to be made. The primary lesion located commonly in the terminal ileum appears as a small, round, and slightly lobulated soft-tissue mass that may contain central calcifications (Fig. 20). A radiating soft-tissue pattern



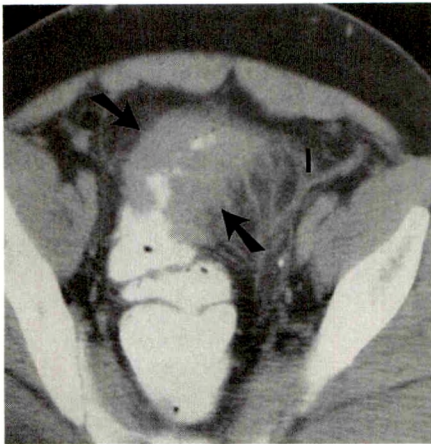
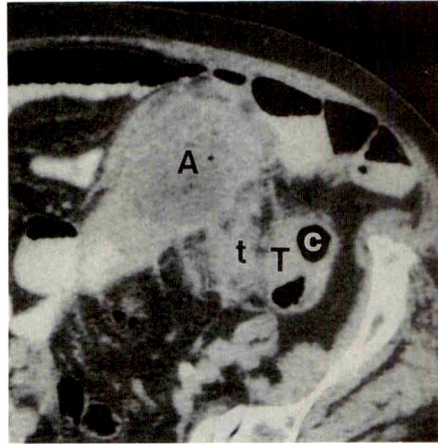
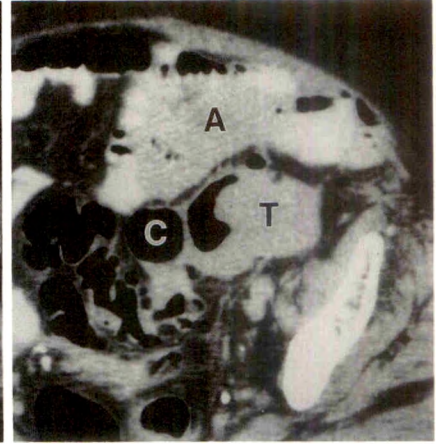


Fig. 17.—Sigmoid diverticulitis exhibiting neoplastic CT features. Note significant circumferential wall thickening (*arrows*), narrowed lumen with apparent abrupt transition, and pericolic inflammation (*I*). CT was suggestive of adenocarcinoma; barium enema showed diverticulitis.

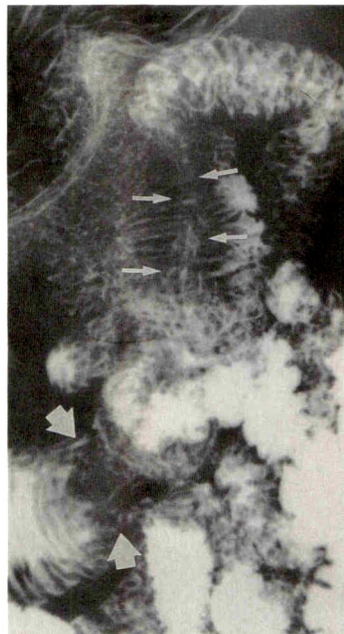


A

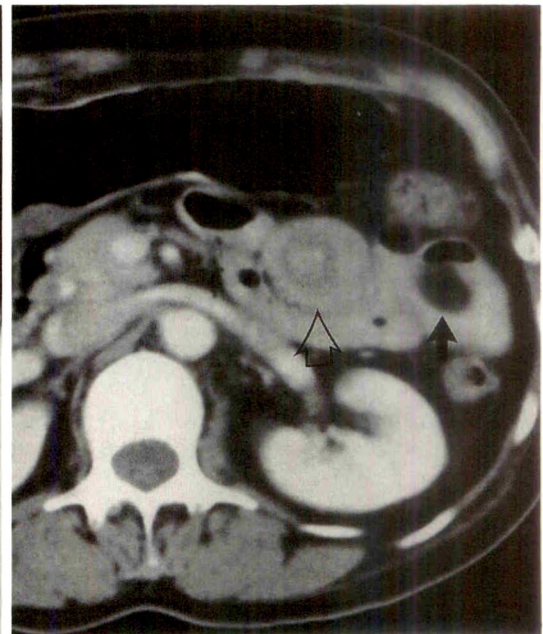


B

Fig. 18.—CT scans of perforated sigmoid adenocarcinoma.  
A, Pelvic CT scan shows poorly encapsulated abscess (*A*) and asymmetric thickening of adjacent sigmoid colon (*c*). Intramural tumor (*T*) has spread through serosa into adjacent pericolic fat (*t*).  
B, Bulk of primary sigmoid (*C*) tumor is better seen on a more caudal pelvic cross section. Pelvic abscess (*A*) is present anterior to sigmoid tumor (*T*).



A



B

Fig. 19.—Intussuscepted jejunal lipoma.  
A, Barium examination revealed a jejunal intussusception (*small arrows*) with leading intraluminal mass (*large arrows*) of unknown cause.  
B, Thin-section (5 mm) CT scan shows concentric layers of intussusception (*open arrow*) and a fat-containing intraluminal tumor (*solid arrow*) representing jejunal lipoma. Radiologic findings were proved at surgery.

reminiscent of a sunburst is seen in the periphery of the lesion and in the adjacent mesenteric fat (Fig. 20). Loops of small bowel are displaced and sharply angulated in the vicinity of the primary lesion, betraying the dermoplastic mesenteric reaction common in this entity. In our experience, these features have been highly reliable for intestinal carcinoids.

3. Intestinal intussusception in adults occurs rarely, but it is often associated with a benign or malignant neoplasm necessitating surgical intervention. In most of these patients, CT can rapidly and reliably establish the diagnosis by showing a characteristic intestinal complex, targetlike mass [20] (Fig. 21). On cross section, the inner central density of the mass

represents the invaginated intestinal loop (intussusceptum). Eccentrically and adjacent to it is the invaginated low-density mesentery. The peripheral outer contour is formed by the receiving intestinal loop (intussusciens), which is sharply defined (Fig. 21). Luminal contrast material may be seen trapped between the two loops. The underlying neoplasm may or may not be detected on CT depending on its size and density [20]. Although the CT detection of intestinal intussusception is reliable, its cause and clinical significance should be evaluated in the context of the clinical presentation and in association with other pertinent CT findings such as small-bowel obstruction or metastases.



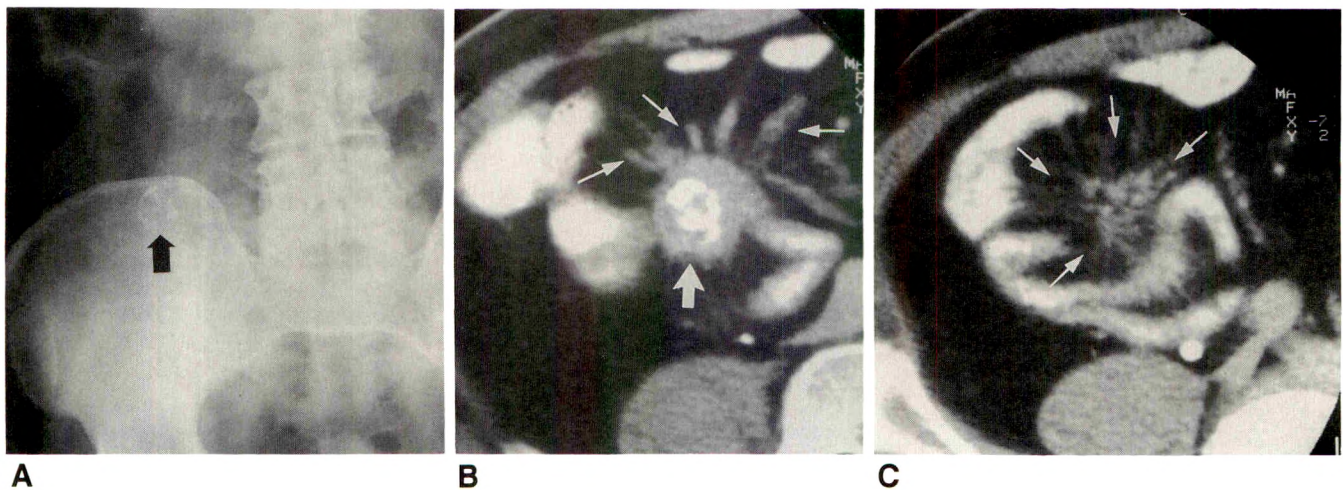


Fig. 20.—Distal ileal carcinoid tumor with mesenteric spread and desmoplastic reaction.

A, Plain abdominal film reveals ringlike calcification (arrow) in right side of lower abdomen.

B, CT scan shows soft-tissue intestinal tumor containing central calcifications (large arrow) and a radiating pattern resembling sunburst (small arrows).

C, Adjacent cross section reveals striated, radiating mesenteric reaction (arrows) displacing and kinking adjacent intestinal loops.

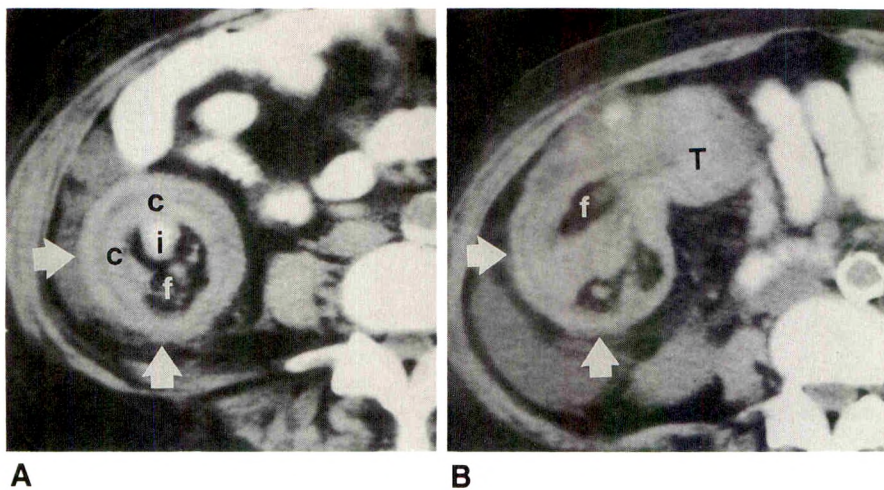


Fig. 21.—CT scans of ileocolocolic intussusception due to cecal carcinoma.

A, Ascending colon shows two concentric rings (c) representing intussuscepted colon. Central loop of small intestine (i) and adjacent luminal mesenteric fat (f) complete typical-appearing complex mass (arrows).

B, More cranial section reveals soft-tissue mass of adenocarcinoma (T) and associated proximal intussusception (arrows) containing mesenteric fat (f).

## REFERENCES

- Megibow AJ, Balthazar EJ. *Computed tomography of the gastrointestinal tract*. St. Louis: Mosby, 1986:1-31
- Jones B, Fishman EK, Hamilton SR, et al. Submucosal accumulation of fat in inflammatory bowel disease: CT/pathologic correlation. *J Comput Assist Tomogr* 1986;10:759-763
- Frager DH, Goldman M, Beneventano TC. Computed tomography in Crohn's disease. *J Comput Assist Tomogr* 1983;7:819-824
- Goldberg HI, Gore RM, Margulis AR, et al. Computed tomography in the evaluation of Crohn disease. *AJR* 1983;140:277-282
- Fishman EK, Wolf EJ, Jones B, et al. CT evaluation of Crohn's disease: effect on patient management. *AJR* 1987;148:537-540
- Megibow AJ, Streiter ML, Balthazar EJ, et al. Pseudomembranous colitis: diagnosis by computed tomography. *J Comput Assist Tomogr* 1984;8:281-283
- Balthazar EJ, Megibow AJ, Fazzini E, et al. Cytomegalovirus colitis in AIDS: radiographic findings in 11 patients. *Radiology* 1985;155:585-589
- Balthazar EJ, Hulnick D, Megibow AJ, et al. Computed tomography of intramural intestinal hemorrhage and bowel ischemia. *J Comput Assist Tomogr* 1987;11:67-72
- Perez C, Llauger J, Puig J, et al. Computed tomographic findings in bowel ischemia. *Gastrointest Radiol* 1989;14:241-245
- Alpern MB, Glazer GM, Francis IR. Ischemic or infarcted bowel: CT findings. *Radiology* 1988;166:149-152
- Smerud MJ, Johnson CD, Stephens DH. Diagnosis of bowel infarction: a comparison of plain films and CT scans in 23 cases. *AJR* 1990;154:99-103
- Balthazar EJ, Megibow AJ, Hulnick D, et al. Carcinoma of the colon: detection and preoperative staging by CT. *AJR* 1988;150:301-306
- Megibow AJ, Balthazar EJ, Naidich DP, et al. Computed tomography of gastrointestinal lymphoma. *AJR* 1983;141:541-547
- Megibow AJ, Balthazar EJ, Hulnick DH, et al. CT evaluation of gastrointestinal leiomyomas and leiomyosarcomas. *AJR* 1985;144:727-731
- Hulnick DH, Megibow AJ, Balthazar EJ, et al. Computed tomography in the evaluation of diverticulitis. *Radiology* 1984;152:491-495
- Johnson CD, Baker ME, Rice RP, et al. Diagnosis of acute colonic diverticulitis: comparison of barium enema and CT. *AJR* 1987;148:541-546
- Balthazar EJ, Megibow AJ, Schinella RA, et al. Limitations in the CT diagnosis of acute diverticulitis: comparison of CT, contrast enema, and pathologic findings in 16 patients. *AJR* 1990;154:281-285
- Hulnick DH, Megibow AJ, Balthazar EJ, et al. Perforated colorectal neoplasms: correlation of clinical, contrast enema and CT examinations. *Radiology* 1987;164:611-615
- Megibow AJ, Redmond PE, Bosniak MA, et al. Diagnosis of gastrointestinal lipomas by CT. *AJR* 1979;133:743-745
- Merine D, Fishman EK, Jones B, et al. Enterointestinal intussusception: CT findings in nine patients. *AJR* 1987;148:1129-1132



## Progress in Radiology

### Selective Salpingography and Fallopian Tube Recanalization

Amy S. Thurmond<sup>1</sup>

Obstruction of the uterine (proximal) end of the fallopian tube is noted on up to 20% of hysterosalpingograms and has a variety of underlying causes. Definitive diagnosis and treatment in the past have required laparoscopy or laparotomy with tubal resection. Selective salpingography and fallopian tube recanalization with fluoroscopically guided catheters has emerged as an improved method both for diagnosis and treatment in these patients. Technical success rates for overcoming the obstruction and visualizing distal tubal anatomy range from 76% to 95%. Pregnancy rates after the procedure vary depending on the patient populations studied; however, early results indicate a greater than 50% intrauterine pregnancy rate by 1 year. The rate of ectopic pregnancy is approximately 10% and that of early tubal reocclusion is less than 30%. Selective salpingography and fallopian tube recanalization is recommended as the first intervention in patients with obstruction of the proximal fallopian tube.

The prevalence of infertility in the United States is 15–20%, or one out of every five or six couples [1]. Fallopian tube disease is a major cause of infertility, and was estimated to affect more than 300,000 American women in 1987 [1]. Tubal obstruction, both at the distal fimbriated (ovarian) end and at the proximal (uterine) end, results from infection by chlamydia or gonorrhea, or from endometriosis. In the proximal portion of the tube, obstruction can also result from salpingitis isthmica nodosa [2]. Pathologic findings in the proximally occluded oviduct are fibrosis, adhesions, or amorphous debris

in the tubal lumen [3]. There is also the phenomenon of tubal "spasm" or "pseudoobstruction" [4]. This is the explanation for pathologically normal tubes despite a history of multiple preoperative examinations showing obstruction. No effective medication for reversing tubal spasm has been identified [5]. Recent data suggest that some of these cases of presumed spasm or pseudoobstruction may actually be mechanical occlusion from a discrete plug of debris in the proximal portion of the tube, which may be easily dislodged and missed at the time of pathologic examination [3]. The prevalence of a small discrete tubal plug of amorphous material in association with proximal tubal obstruction may be as high as 77% [3].

Proximal tubal obstruction is seen on 10–20% of hysterosalpingograms [4]. Because underfilling of the tube, tubal spasm, and mechanical obstruction from a variety of causes cannot be differentiated on conventional hysterosalpingography and inhibit visualization of the distal tube, the radiologist's task is frustrating. Similarly frustrating for the infertility surgeon has been resection of a tube that is subsequently shown to be normal or only minimally abnormal.

Fallopian tube catheterization with fluoroscopic guidance and a coaxial system of guidewires and catheters has been used for the purpose of selective salpingography to improve visualization of tubal anatomy. At the same time, the system can be used for fallopian tube recanalization as a nonsurgical method to dislodge debris and break adhesions in the proximal tube.

Received May 17, 1990; accepted after revision July 17, 1990.

This work was supported by the Research and Education Fund of the Radiological Society of North America and the Medical Research Foundation of Oregon.

<sup>1</sup> Departments of Diagnostic Radiology and Obstetrics and Gynecology, L-340, Oregon Health Sciences University, 3181 S.W. Sam Jackson Park Rd., Portland, OR 97201. Address reprint requests to Amy S. Thurmond.

AJR 156:33–38, January 1991 0361–803X/91/1561–33 © American Roentgen Ray Society



### Technique

Women in whom unilateral or bilateral proximal tubal obstruction is demonstrated on conventional hysterosalpingography or laparoscopy are candidates for selective salpingography and fallopian tube recanalization. Figures 1 and 2 illustrate the radiologic and microscopic anatomy of the fallopian tube in an autopsy specimen.

The technique has been described in detail [5]. Briefly, the method consists of gaining access to the uterus with a vacuum cup hysterosalpingography device (Fig. 3). With fluoroscopic guidance and the appropriate guidewires, a 5.5-French catheter is initially placed into the tubal ostium, followed by placement of a 3-French catheter in the interstitial or isthmic portion of the tube. Confirmation of correct catheter placement and documentation of tubal anatomy is performed by selective injection of contrast material. Recanalization of the tube is occasionally achieved via forceful injection into the tubal ostium, but more commonly by probing with the guidewire.

Performance of this procedure in close to 200 women has not resulted in any clinically significant complications. In our early experience, the radiation dose to the ovaries was  $8.5 \pm 5.6$  Gy ( $0.85 \pm 0.56$  rad), which is equivalent to estimated ovarian doses for a barium enema or excretory urogram [6].

### Results

With the equipment and technique described above, reported success rates for catheterization of the fallopian tubes and visualization of distal tubal anatomy range from 76% to 95% (Table 1) [5, 7–9] (Platia et al., presented at the annual meeting of the American Fertility Society, November 1989). Once the proximal obstruction is overcome and the distal tube visualized by selective salpingography, there are a variety of findings (Fig. 4) [5, 9–11]. Approximately one third of patients have normal-appearing tubes after the procedure. Another one third have normal tubes; however, the appear-

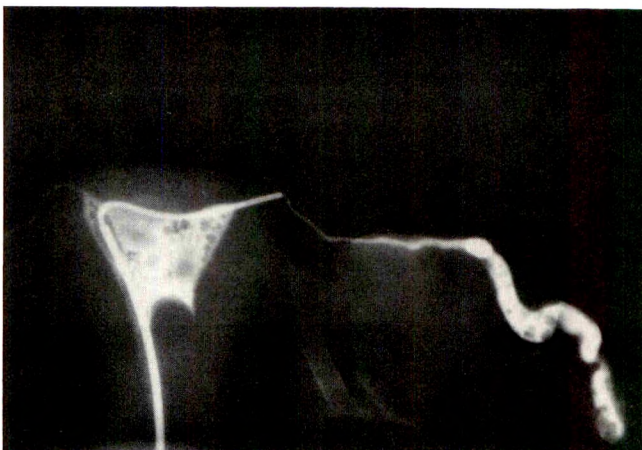


Fig. 1.—Fallopian tube catheterization in an autopsy specimen shows fallopian tube anatomy relative to uterus and other adnexal structures. Tip of catheter is at junction of interstitial and isthmic portions of left tube.

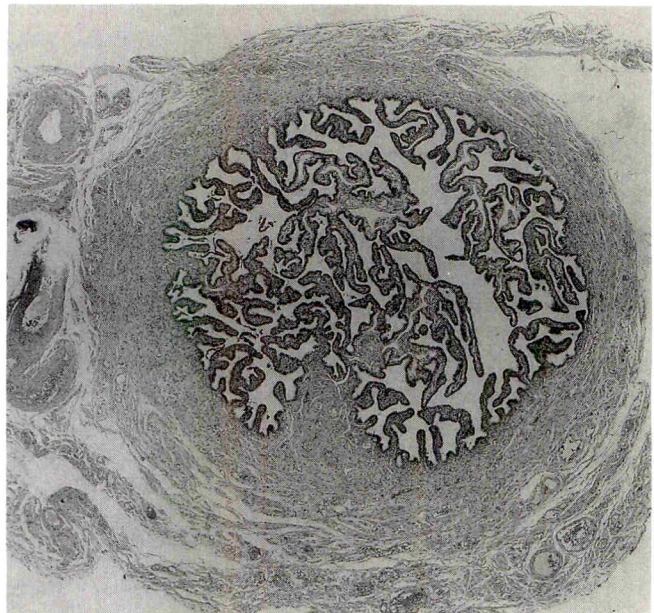


Fig. 2.—Light microscopy of cross section of isthmic portion of fallopian tube shows three distinct regions. Innermost is ciliated epithelium, which forms villi in lumen of tube. Surrounding this are smooth muscle layers. Outermost is serosa containing vessels and nerves.

ance of the peritoneal spill suggests peritubal adhesions. Of the remaining patients, approximately 8% have a small, focal, fusiform dilatation at the site of the recanalization. Approximately 8% have frank salpingitis isthmica nodosa. Distal occlusion is demonstrated in about 8% and attempts at recanalization are unsuccessful in about 8%. The latter group usually comprises patients with obstruction more distal in the tubes in the isthmic region or patients with severe salpingitis isthmica nodosa.

We evaluated the therapeutic effect of fallopian tube catheterization in 20 carefully selected patients [5]. All had bilateral proximal tube obstruction on at least two hysterosalpingograms and by laparoscopy; no distal tubal disease or pelvic adhesions were detected by laparoscopy. The average duration of infertility was 4 years; seven of the 20 women had additional infertility factors. All 20 patients had been recommended for tubal microsurgery or in vitro fertilization, but underwent catheter recanalization instead. Recanalization of one or both tubes was successful in 19 women (95%). Fifty-eight percent of the women conceived by 1 year without receiving any other therapy, and all pregnancies were intrauterine. Evaluation of a similar group of patients at another institution revealed comparable pregnancy results (Table 1) (Platia et al., AFS, November 1989).

In a more clinically heterogeneous group of women with unilateral or bilateral proximal tubal obstruction (100 consecutive patients), in which the primary goal was improved tubal diagnosis, pregnancy results were somewhat different (Table 1). We found catheterization was technically successful in visualizing the tubes in 86% [5]. Short-term follow-up in the women with patent tubes after the procedure revealed a 39% intrauterine pregnancy rate and a 6% ectopic pregnancy rate



Fig. 3.—Selective salpingography and recanalization of left fallopian tube.  
A, Injection via 5.5-French catheter wedged in tubal ostium confirms obstruction approximately 5 mm from uterine cavity in interstitial portion of tube.  
B, Guidewire and small catheter were passed just beyond level of obstruction. Injection through small catheter (tip indicated by radiopaque bead) confirms successful recanalization.  
C, Small catheter was removed, and injection through larger catheter still wedged in tubal ostium reveals more of tubal anatomy. There are no abnormalities at site of previous obstruction, and distal fallopian tube looks normal.  
D, Postprocedure hysterosalpingogram with all catheters removed confirms tubal patency.

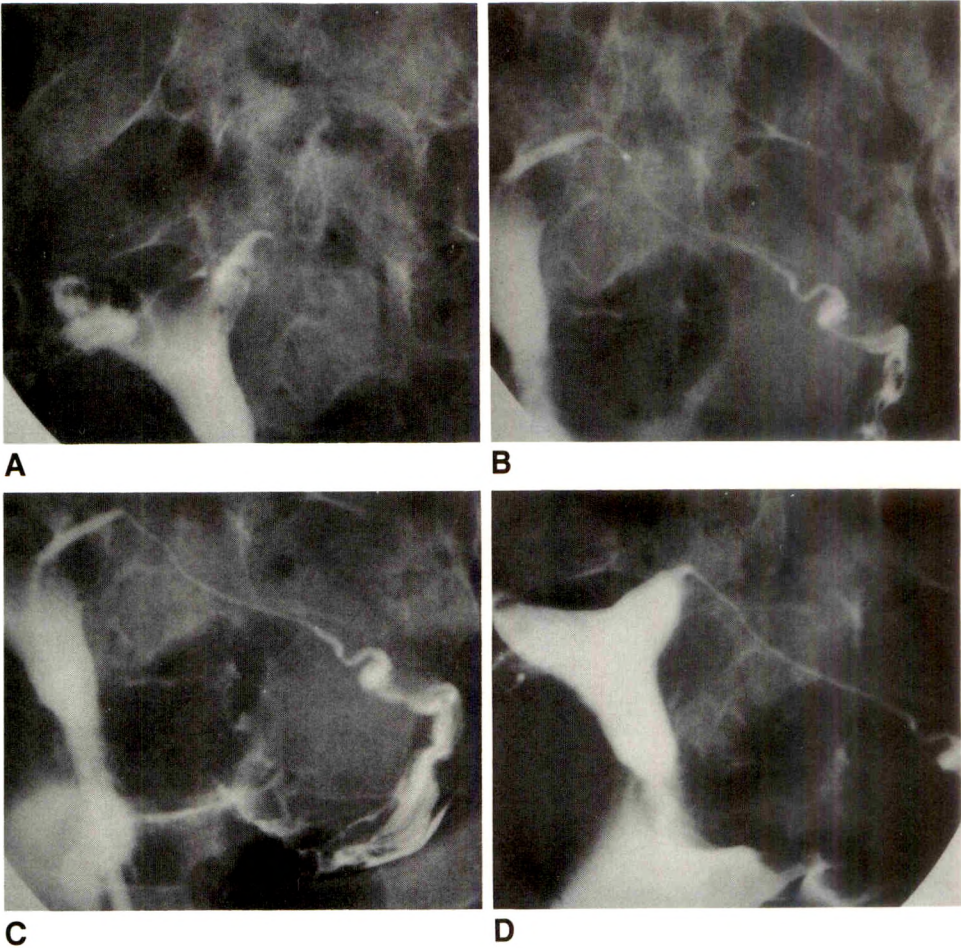


TABLE 1: Success Rates of Selective Salpingography and Fallopian Tube Recanalization

Indication/ Reference Source	No. of Patients	Rate (%)			
		Recanalization	Early Pregnancy (Months of Follow-up)	Ectopic Pregnancy	Reocclusion (Estimated)
Primarily for diagnosis					
Thurmond and Rosch [5]	100	86	39 (8)	6	30
Kumpe et al. [9]	22	88	23 (8)	9	30
Winfield et al. [7]	20	NA	15	5	NA
Amendola et al. [8]	12	89	17	0	NA
Primarily for treatment					
Thurmond and Rosch [5]	20	95	48 (9) 58 (12)	0 0	25
Platia et al. <sup>a</sup>	21	76	38	13	25
Confino et al. <sup>a</sup>	54	93	18 (<8)	0	Low

Note.—Diagnostic indications included unilateral or bilateral obstruction, presence of distal disease, and other factors not controlled. Indications for treatment included bilateral obstruction and absence of significant distal disease or pelvic adhesions by laparoscopy. The technique used by all researchers, with the exception of Confino et al., was a vacuum cup hysterosalpingography device with nonballoon fallopian tube catheters. Confino et al. used a balloon hysterosalpingography device with balloon fallopian tube catheters. NA = not available.

<sup>a</sup> Presented at the annual meeting of the American Fertility Society, November 1989.

(average follow-up, 8 months). All of the patients with ectopic pregnancies had either known peritubal adhesions or a history of tubal surgery, both of which are risk factors for ectopic pregnancy. All ectopic pregnancies were located in the am-

pulla of the tube, several centimeters distal to the site of catheterization.

The rate of tubal reocclusion is difficult to determine. In patients who do not conceive, it appears that 37–48% have



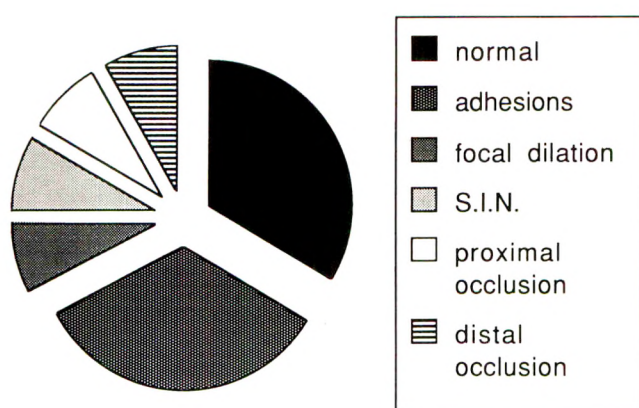


Fig. 4.—Findings after selective salpingography of fallopian tubes in consecutive women referred for proximal tubal obstruction. S.I.N. = salpingitis isthmica nodosa.

one or both tubes reocclude within 6 months [5, 9] (Platia et al., AFS, November 1989). If we assume that the tubes are patent in the patients who conceive, this gives an approximate reocclusion rate of 25–30% (Table 1). Repeated catheter recanalization is technically possible, and pregnancies have resulted after the second procedure.

## Discussion

The diagnostic and therapeutic aspects of fluoroscopically guided fallopian tube catheterization are closely related. Placement of the catheter over a guidewire into the tubal ostium or deeper into the proximal tube with forceful injection, for the purpose of selective salpingography, in many cases may actually dislodge debris and/or break up fine adhesions, resulting in recanalization. It is not possible in all cases to determine the nature of the underlying disease. We assume that a patient who has several examinations documenting proximal obstruction, as well as a thorough evaluation that reveals no other significant causes for infertility, probably has a mechanical obstruction and does not have tubal spasm or a false-positive hysterosalpingogram. Helpful information about the cause of the blockage may also be obtained at the time of the catheterization. Often in performing fallopian tube catheterization, one visualizes and also "feels" with the guidewire a clear point of obstruction that can be passed with gentle probing movements of the guidewire. We assume that this latter finding is related to a mechanical obstruction, particularly if there is some irregularity of the tube at this level, though many tubes thought to have a mechanical obstruction by the above criteria look completely normal after recanalization. At the other extreme, we also assume that if a tube is clearly patent on repeat hysterosalpingography, which is always performed prior to selective salpingography and recanalization, that the tube was not affected by a mechanical obstruction, and that the tube was not visualized because of tubal spasm, preferential spill from the contralateral tube, or

technical problems with the hysterosalpingogram. Between these two extremes, with which one can feel comfortable about diagnosing the presence or absence of tubal disease, there is a spectrum of historical factors and catheterization findings that must be interpreted and a judgment made as to the probable cause of the initial proximal tubal obstruction.

Because nonvisualization of the fallopian tubes is an indication for laparoscopy, followed by laparotomy if necessary, visualization of the fallopian tubes on selective salpingography is clearly beneficial in patient management. If normal anatomy is demonstrated, surgical evaluation of the tubes may be deferred. If abnormalities are visualized, the appropriate management can be discussed. Fimbrial disease or peritubal disease may require surgical correction. The presence of a hydrosalpinx greater than 15 mm in diameter [12], or the absence of ampullary rugal folds [13], has been correlated with poor surgical outcome, and in these patients in vitro fertilization may be recommended instead of surgery. Interestingly, selective salpingography may actually be more reliable than laparoscopy in the diagnosis of fimbrial disease and distal occlusion, though we can expect that it will have some of the same limitations as conventional hysterosalpingography in the diagnosis of peritubal disease [9].

The therapeutic nature of selective salpingography and fallopian tube recanalization is more difficult to prove, partly because the underlying disease cannot be reliably determined and can only be surmised as described above. Also, infertility is often a multifactorial problem, and, in addition to ovulation and sperm disorders, can be caused by advanced age, psychological problems, and idiopathic factors, which cannot be controlled. Pregnancy rates after surgical interstitial-to-isthmic anastomosis are 41–77%, with higher rates found in the series with longer follow-up and among patients with less extensive disease [14–16]. Approximately 15–30% of patients have proximal tubal reocclusion after surgery [14]. The ectopic pregnancy rate after tubal surgery is approximately 10% [12]. Early pregnancy rates after catheter recanalization in patient populations comparable to those described in the surgical literature are 38–58% (Table 1) [5] (Platia et al., AFS, November 1989). Tubal reocclusion rates after fluoroscopic catheterization are 30%, and ectopic pregnancy rates are approximately 10% [5, 9] (Platia et al., AFS, November 1989). Definitive proof of the efficacy of fluoroscopic fallopian tube recanalization could come only from a randomized controlled study of fluoroscopic fallopian tube recanalization vs proximal tubal microsurgery vs no intervention in patients with bilateral proximal obstruction. Because of both ethical and logistical difficulties in conducting such a study, it will probably never be done. Therefore, we must rely on the above data, which uses patients who in the past would have had proximal tubal microsurgery, and who instead have fluoroscopic catheterization. Early evaluation of these patients clearly indicates a therapeutic benefit, with results similar to those in the surgical literature.

Opinions vary as to the optimal method of performing selective salpingography and fallopian tube recanalization, both as to the best hysterosalpingography device as well as to the most effective catheterization system. The options for



a hysterosalpingography device consist of a vacuum cup cannula [17], an intrauterine balloon [18] (Confino et al., presented at the annual meeting of the American Fertility Society, November 1989; Sholkoff S, personal communication), or an acorn-tipped cannula with tenaculum [19]. The disadvantage of an intrauterine balloon is that in my experience it interferes with uterine visualization and the maneuverability of the catheters [20]. The disadvantage of a tenaculum device is that it causes pain and cervical bleeding. The disadvantage of a vacuum cup device is that in general it is harder to apply than the other two devices, and some experience is required to obtain an optimal relationship between the acorn tip and the vacuum cup so that a good cervical seal is maintained. Helpful maneuvers include opening the speculum wide and maneuvering the cervix so that one obtains a clear "bull's-eye" view of the external os. My experience with residents and fellows indicates that after four or five procedures they feel comfortable with the vacuum cup device, and we use it routinely for diagnostic hysterosalpingography.

The debate about which catheters to use in the fallopian tube revolves around whether a balloon catheter or a non-balloon catheter is more appropriate [18] (Confino et al., AFS, November 1989). The underlying disease is usually intraluminal, either an amorphous plug of debris or fine adhesions [3] or in some cases dense fibrous obliteration of the tubal lumen [3]. Strictures of the fallopian tube, such as those found in blood vessels, have not been demonstrated. For this reason, there is no clear rationale for balloon dilatation. It has been proposed that repeated inflation of a balloon just proximal to the site of obstruction in the fallopian tube may increase long-term patency rates [18]. Results so far, however, are comparable to those of recanalization without a balloon (Table 1), and because of the added expense and potential risk of balloon catheters, I do not believe their routine use is justified. Some investigators have had technical success with hydrophilically coated guides in the fallopian tubes; however, the hydrophilic material is quite toxic to embryos in vitro (Bosley R, personal communication), and therefore their use in the uterus and fallopian tubes is not recommended.

Attempts to recanalize tubes obstructed more distally than the interstitial or isthmic segments are not recommended. This is based on the observation that obstruction of the tube in the ampulla or infundibulum is related to fimbrial phimosis and/or dense peritubal adhesions, and attempts at catheter recanalization, though probably not harmful, will almost certainly be unsuccessful.

#### *Other Applications and Future Directions*

Guidance systems other than fluoroscopy have been used for fallopian tube catheterization. Hysteroscopic placement of the catheters in the tubal ostium with laparoscopic guidance has been used successfully in the operating room under general anesthesia. This may be a preferred method when the woman has proximal tubal obstruction as well as known distal tubal disease or pelvic adhesions. Surgical correction of the latter can then be performed at the same time as

proximal fallopian tube recanalization [21] (Novy, presented at the annual meeting of the American Fertility Society, November 1989).

Sonographically guided transvaginal fallopian tube catheterization for treatment of diseased tubes has been performed by others in a small number of patients (Confino et al., presented at the annual meeting of the American Fertility Society, November 1989). In my opinion, the relatively poor visualization of the equipment and of the tubal anatomy limits this application.

Sonography has been used to guide transvaginal catheterization of normal fallopian tubes. Radiologists may be asked to assist in these procedures, which are performed for potential treatment of infertility caused by sperm disorders or idiopathic factors. It appears that transvaginal placement of gametes or developing embryos in the fallopian tube may result in a higher pregnancy rate than does intrauterine placement; however, what optimally should be put in the tube and at which time in the cycle has not been completely established [21, 22].

The most exciting future application of fallopian tube catheterization may be nonsurgical tubal sterilization, for which there would be significant worldwide demand [23]. Successful laser ablation of the tubes has already been performed by using fluoroscopic guidance and the same catheter system used for selective salpingography and fallopian tube recanalization (Bylsma P, personal communication).

#### **Conclusions**

Fluoroscopic transvaginal fallopian tube catheterization in patients with proximal tubal obstruction results in improved diagnosis of tubal disease and is a proven successful treatment for infertility. Fluoroscopically guided tube catheterization causes less patient morbidity and is less expensive than diagnostic laparoscopy, tubal microsurgery, or in vitro fertilization. For this reason it should be the first intervention in patients with obstruction of the proximal fallopian tube. The more invasive therapies should be reserved for patients with distal tubal disease or for the small number of patients with proximal obstruction in whom fluoroscopic catheterization is not successful.

#### **ACKNOWLEDGMENTS**

I thank Marla Jones and Richard Katzberg, who read the manuscript and provided helpful suggestions.

#### **REFERENCES**

1. Serafini P, Batzofin J. Diagnosis of female infertility, a comprehensive approach. *J Reprod Med* 1989;34:29-40
2. Winfield AC, Wentz AC. *Diagnostic imaging of infertility*. Baltimore: Williams & Wilkins, 1987:105-125
3. Sulak PJ, Letterie GS, Coddington CC, Hayslip CC, Woodward JE, Klein TA. Histology of proximal tubal occlusion. *Fertil Steril* 1987;48:437-440
4. Thurmond AS, Novy M, Rosch J. Terbutaline in diagnosis of interstitial fallopian tube obstruction. *Invest Radiol* 1988;23:209-210
5. Thurmond AS, Rosch J. Nonsurgical fallopian tube recanalization for



- treatment of infertility. *Radiology* **1990**;174:371-374
6. Hedgpeth PL, Thurmond AS, Fry R, Schmidgall JR, Rosch J. Ovarian radiation dose in radiologic fallopian tube recanalization. *Radiology* (in press)
  7. Winfield AC, Moore D, Segars J, Holburn G, Herbert C. Selective fallopian tube canalization (abstr). *AJR* **1990**;154:195
  8. Amendola MA, Banner MP, Pollack HM, Sondheimer S. Preliminary experience with fluoroscopic transcervical fallopian tube recanalization (abstr). *AJR* **1990**;154:196
  9. Kumpe DA, Zwerdlinger SC, Rothbarth LJ, Durham JD, Albrecht BH. Proximal fallopian tube occlusion: diagnosis and treatment with transcervical fallopian tube catheterization. *Radiology* **1990**;177:183-187
  10. Thurmond AS, Rosch J, Patton PE, Burry KA, Novy M. Fluoroscopic transcervical fallopian tube catheterization for diagnosis and treatment of female infertility caused by tubal obstruction. *RadioGraphics* **1988**;8:621-640
  11. Lang EK, Dunaway HE, Roniger WE. Selective osteal salpingography and transvaginal catheter dilatation in the diagnosis and treatment of fallopian tube obstruction. *AJR* **1990**;154:735-740
  12. Jacobs LA, Thie J, Patton PE, Williams TJ. Primary microsurgery for postinflammatory tubal infertility. *Fertil Steril* **1988**;50:855-859
  13. Young PE, Egan JE, Barlow JJ, Mulligan WJ. Reconstructive surgery for infertility at the Boston Hospital for Women. *Am J Obstet Gynecol* **1970**;108:1092-1097
  14. Patton PE, Williams TJ, Coulam CB. Microsurgical reconstruction of the proximal oviduct. *Fertil Steril* **1987**;47:35-39
  15. Donnez J, Casanas-Roux F. Histology: a prognostic factor in proximal tubal occlusion. *Eur J Obstet Gynecol Reprod Biol* **1988**;29:33-38
  16. Gillett WR, Herbison GP. Tubocornual anastomosis: surgical considerations and coexistent infertility factors in determining the prognosis. *Fertil Steril* **1989**;51:241-246
  17. Thurmond AS, Uchida BT, Rosch J. Device for hysterosalpingography and fallopian tube catheterization. *Radiology* **1990**;174:571-572
  18. Confino E, Friberg J, Gleicher N. Preliminary experience with transcervical balloon tuboplasty. *Am J Obstet Gynecol* **1988**;159:370-375
  19. LaBerge JM, Poncet DJ, Gordon RL. Fallopian tube catheterization: modified fluoroscopic technique. *Radiology* **1990**;176:283-284
  20. Thurmond AS, Novy MJ, Uchida BT, Rosch J. Fallopian tube obstruction: selective salpingography and recanalization. *Radiology* **1987**;163:511-514
  21. Novy MJ, Thurmond AS, Patton PE, Uchida BT, Rosch J. Diagnosis of cornual obstruction by transcervical fallopian tube cannulation. *Fertil Steril* **1988**;50:434-440
  22. Jansen RPS. Nonoperative embryo transfer to the fallopian tube. *N Engl J Med* **1988**;319:288-291
  23. Jansen RPS, Anderson JC, Radonic I, Smit J, Sutherland PD. Pregnancies after ultrasound-guided insemination with cryostored donor semen. *Fertil Steril* **1988**;49:920-922
  24. Kessel E, Mumford SD. Potential demand for voluntary sterilization in the 1980's: the compelling need for a nonsurgical method. *Am J Steril* **1982**;37:725-733



## Detection of ACTH-Producing Bronchial Carcinoid Tumors: MR Imaging vs CT

John L. Doppman<sup>1,2</sup>  
 Harvey I. Pass<sup>3</sup>  
 Lynnette K. Nieman<sup>4</sup>  
 James W. Findling<sup>5</sup>  
 Andrew J. Dwyer<sup>1</sup>  
 Irwin M. Feuerstein<sup>1,2</sup>  
 Alexander Ling<sup>1,2</sup>  
 William D. Travis<sup>6</sup>  
 Gordon B. Cutler, Jr.<sup>4</sup>  
 George P. Chrousos<sup>4</sup>  
 D. Lynn Loriaux<sup>4</sup>

Adrenocorticotrophic hormone (ACTH)-producing bronchial carcinoid tumors tend to occur in the middle third of the lung adjacent to pulmonary vessels. Because they cause signs and symptoms when quite small (by virtue of their ACTH production), they may not be detected by CT. MR imaging was performed in 10 consecutive patients with surgically proved ACTH-producing bronchial carcinoid tumors in order to test the ability of MR to clarify equivocal or indeterminate findings on CT examinations. All bronchial carcinoid tumors had high signal intensity on T2-weighted and short-inversion-time inversion-recovery images, facilitating their distinction from pulmonary vasculature. In eight patients, the CT and MR images were equivalent in the detection of bronchial carcinoid tumors. In two patients, MR showed tumors in the middle third of the lung that were equivocal on CT.

MR imaging may distinguish small bronchial carcinoid tumors from adjacent pulmonary vessels in the central third of the lung at a time when the CT study is nondiagnostic or equivocal.

*AJR* 156:39-43, January 1991

In our experience [1], most of the ectopic adrenocorticotrophic hormone (ACTH)-producing tumors that elude detection for more than 1 year eventually prove to be small bronchial carcinoid tumors. We have always considered thin-section (5 mm) CT of the chest the most sensitive screening technique for the detection of small bronchial carcinoid tumors in patients with ectopic ACTH syndrome. Recently we have added MR imaging of the chest to our screening protocol on the theory that the high signal intensity or brightness of these tumors on T2-weighted and short-inversion-time inversion-recovery (STIR) images might permit distinction of small bronchial carcinoid tumors from normal pulmonary vasculature. Ten patients with ectopic ACTH syndrome due to surgically proved bronchial carcinoid tumors were studied prospectively.

The purpose of this presentation is twofold: to illustrate the conspicuity of small bronchial carcinoid tumors on MR imaging by virtue of their high signal intensity on T2-weighted and STIR sequences, and to suggest a role for MR imaging in screening for occult bronchial carcinoid tumors in patients with ectopic ACTH syndrome and equivocal CT examinations.

### Subjects and Methods

Seven women and three men with elevated levels of ACTH from a nonpituitary source were studied. Their average age was 46 years (range, 24-70). Nine patients had Cushing syndrome at the time of presentation. One patient had undergone bilateral adrenalectomy 10 years before admission.

All 10 patients had elevated levels of ACTH in peripheral blood samples. Nine patients had no ACTH gradients in selected samples from bilateral inferior petrosal sinuses. One patient did not undergo petrosal sinus sampling as she had no abnormal findings on pituitary

Received June 14, 1990; accepted after revision July 25, 1990.

<sup>1</sup> Department of Diagnostic Radiology, Warren G. Magnuson Clinical Center, Bldg. 10, Room 1C660, National Institutes of Health, Bethesda, MD 20892. Address reprint requests to J. L. Doppman.

<sup>2</sup> Department of Radiology, Georgetown University Medical Center, Washington, DC 20007.

<sup>3</sup> Surgery Branch, Division of Cancer Treatment, National Cancer Institute, National Institutes of Health, Bethesda, MD 20892.

<sup>4</sup> Developmental Endocrinology Branch, National Institute of Child Health and Human Development, National Institutes of Health, Bethesda, MD 20892.

<sup>5</sup> Department of Medicine, St. Luke's Medical Center, Milwaukee, WI 53215.

<sup>6</sup> Division of Cancer Biology and Diagnosis, Laboratory of Pathology, National Cancer Institute, National Institutes of Health, Bethesda, MD 20892.

0361-803X/91/1561-0039  
 © American Roentgen Ray Society



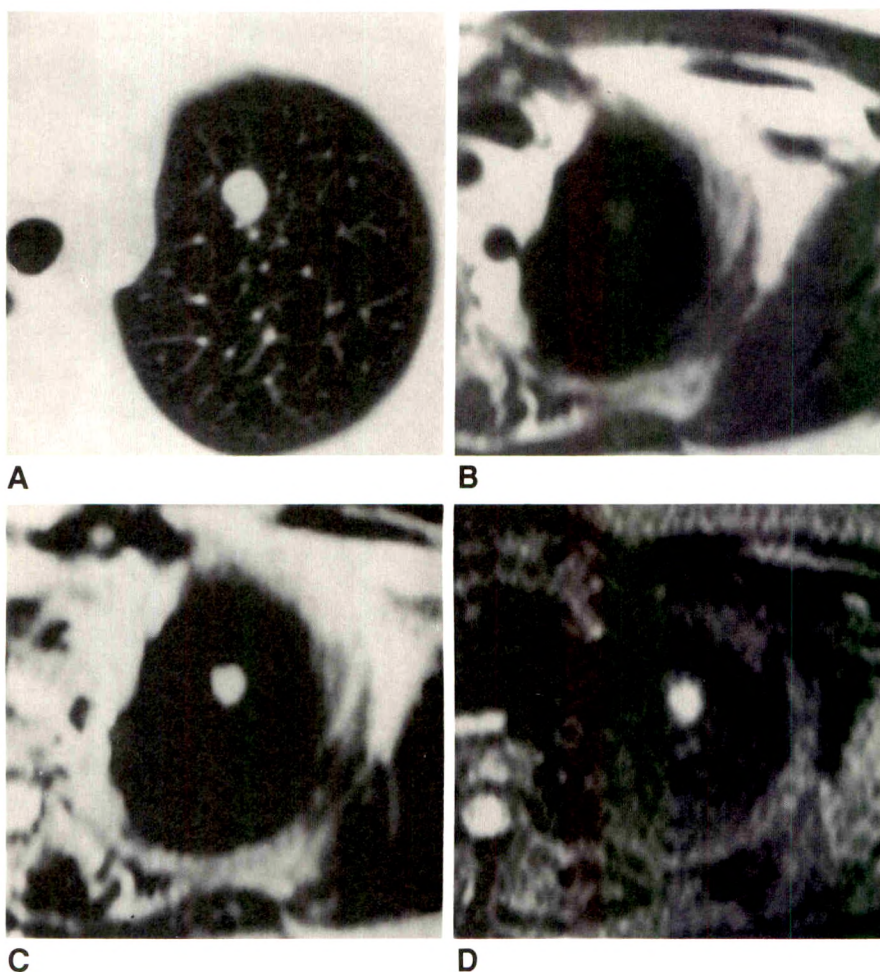


Fig. 1.—A, CT scan shows bronchial carcinoid tumor of left upper lobe.

B–D, Lesion has signal intensity comparable to that of muscle on T1-weighted MR image (B) but shows increasing brightness on T2-weighted (C) and STIR (D) images.

exploration 10 years before, and her pulmonary tumor was obvious on the chest radiograph obtained on admission.

The duration of Cushing syndrome ranged from 8 months to 22 years. Five patients had undergone a variety of treatments before referral to National Institutes of Health, including three transsphenoidal explorations with partial ( $n = 2$ ) or total ( $n = 1$ ) hypophysectomies and two bilateral adrenalectomies. We performed one transsphenoidal exploration and two bilateral adrenalectomies before bronchial carcinoid tumors were discovered.

Each patient was studied with CT (CT 9800, General Electric, Milwaukee, WI). Contiguous sections 5 mm thick from the pulmonary apices to the costophrenic sinuses were used. MR imaging was performed in nine patients on a 0.5-T scanner (Picker International, Highland Heights, OH); contiguous transaxial sections 10 mm thick from the pulmonary apices to the costophrenic sinuses were used. Coronal sections were obtained occasionally to verify a finding on the axial projection but were not obtained routinely. Spin-echo pulse sequences were obtained with T1-weighted, 300/10/8 (TR/TE/number of acquisitions), and T2-weighted, 2000/80/2, pulse sequences. In addition, a STIR pulse sequence with a 100-msec inversion time, 1600/100/30/2 (TR/TI/TE/number of excitations), was obtained routinely. One patient was scanned on a 1.5-T scanner (Signa, General Electric, Milwaukee, WI). T1-weighted, SE 800/20/2, and T2-weighted, SE 2800/70/1, images were obtained, but a STIR sequence was not performed.

All patients have undergone lobectomy ( $n = 9$ ) or segmentectomy

( $n = 1$ ) with removal of draining lymph nodes. Slides were reviewed from eight of 10 patients and showed typical bronchial carcinoid tumors (Kulchitzky-cell carcinoma, type I) [2]. In two patients, the pathologist's report was reviewed and was compatible with a typical bronchial carcinoid tumor.

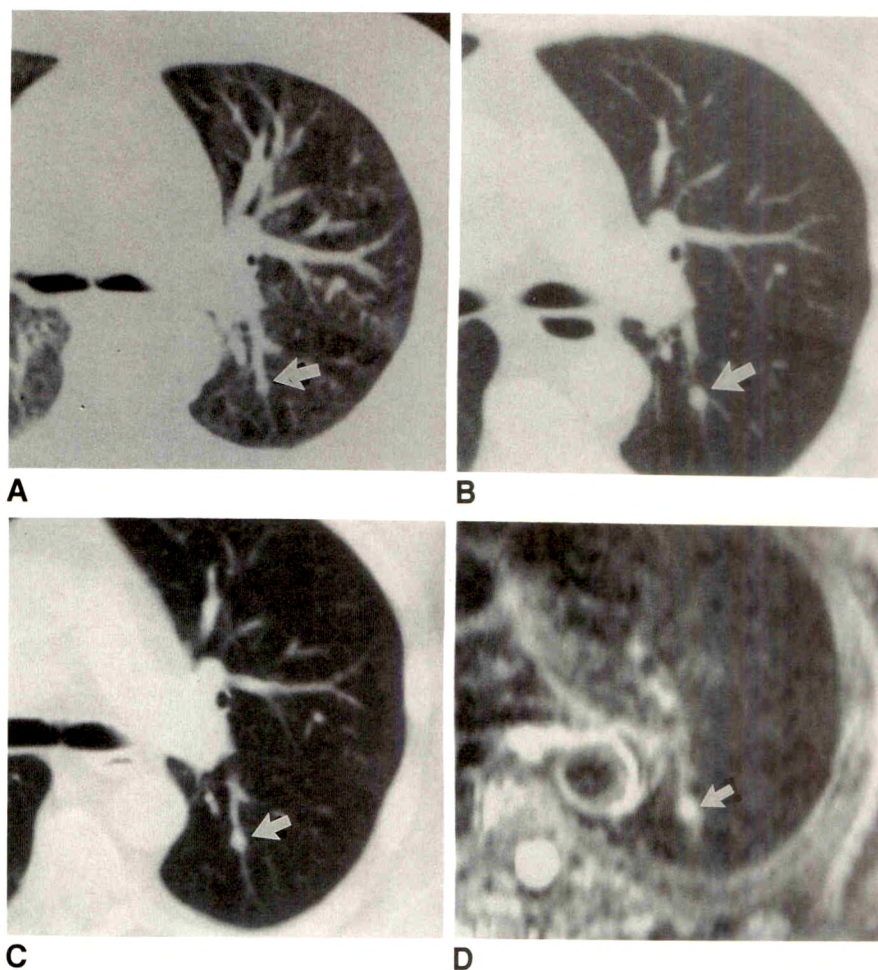
## Results

In six patients, pulmonary nodules or masses were detected on CT either on the initial ( $n = 5$ ) or on a serial semiannual follow-up study ( $n = 1$ ). In two patients, hilar or parenchymal lesions were first recognized on MR imaging, but were apparent retrospectively on CT. In the two remaining patients, parenchymal tumors were detected by MR in the presence of equivocal or nondiagnostic CT examinations.

All bronchial carcinoid tumors were visualized on the MR studies. They were similar to muscle in signal intensity on T1-weighted images, moderately bright on the T2-weighted sequences, and extremely bright on the STIR sequences (Fig. 1). Foci of high signal intensity due to flow artifacts in peripheral pulmonary vessels were not common and generally could be distinguished from bronchial carcinoid tumors by anatomic location and correlation with the CT scan. However, flow artifacts were much more common in the hilum; such hilar



**Fig. 2.—Bronchial adenoma in left lower lobe.**  
**A–C,** Serial CT scans 0 (**A**), 12 (**B**), and 31 (**C**) months after diagnosis of Cushing syndrome show gradual, but unrecognized, development of bronchial adenoma (arrows). Note tendency for bronchial adenomas to develop along course of branching normal vasculature (**B**).  
**D,** MR image (STIR sequence) obtained at time of final CT scan.



artifacts could not be distinguished from small metastatic lymph nodes. In this series, all primary bronchial carcinoid tumors were in the middle and peripheral thirds of the lung. All the involved hilar nodes in three patients were larger than 2 cm and readily distinguished from vessels on the CT/MR studies.

Serial CT scans permitted surveillance of the slow temporal evolution of these tumors and illustrated the difficulty of distinguishing them from pulmonary vasculature when the tumor occurs in the middle third of the lung. Figure 2 shows the gradual appearance of a nodule in the left lower lobe. The proximity of bronchial carcinoid tumors to vessels makes the distinction between branching vessels and tumor particularly difficult. In one additional patient, a parenchymal nodule was first seen on an MR study performed 2 years after the initial diagnosis of Cushing syndrome (Fig. 3).

## Discussion

Cushing syndrome due to ectopic production of ACTH remains a major diagnostic challenge to the endocrinologist [1, 3]. Although petrosal sinus sampling reliably differentiates pituitary from nonpituitary production of ACTH [4–6], it provides no clue to the site of the ectopic ACTH-secreting tumor.

In our experience, bronchial carcinoid tumors are the most common and elusive ectopic source [1]. Because of the malignant potential of these tumors [2, 7, 8], it is important to continue surveillance of these patients even after bilateral adrenalectomy has corrected the hypercortisolemia.

Although MR imaging reportedly has an accuracy comparable to that of CT in the detection of hilar and mediastinal masses [9–13], it generally is considered to contribute less to the detection of peripheral pulmonary nodules because of its prolonged acquisition time and poor spatial resolution. CT, on the other hand, can resolve pulmonary nodules as small as 3 mm in diameter [14]. In light of CT's outstanding sensitivity, few MR examinations of the chest are performed for the detection of pulmonary nodules.

The detectability of pulmonary parenchymal nodules by CT, however, depends somewhat on their location within the lung [15–18]. Metastases are usually multiple and tend to occur subpleurally, where they are distinguished easily from normal pulmonary vasculature. Normal subpleural lymph nodes may be mistaken for metastases [15], but this impugns CT's lack of specificity, not its sensitivity. In the inner and middle third of the lung, where many bronchial carcinoid tumors occur [19–21], differentiation of parenchymal nodules from normal vessels by CT is a problem. Although contrast-enhanced



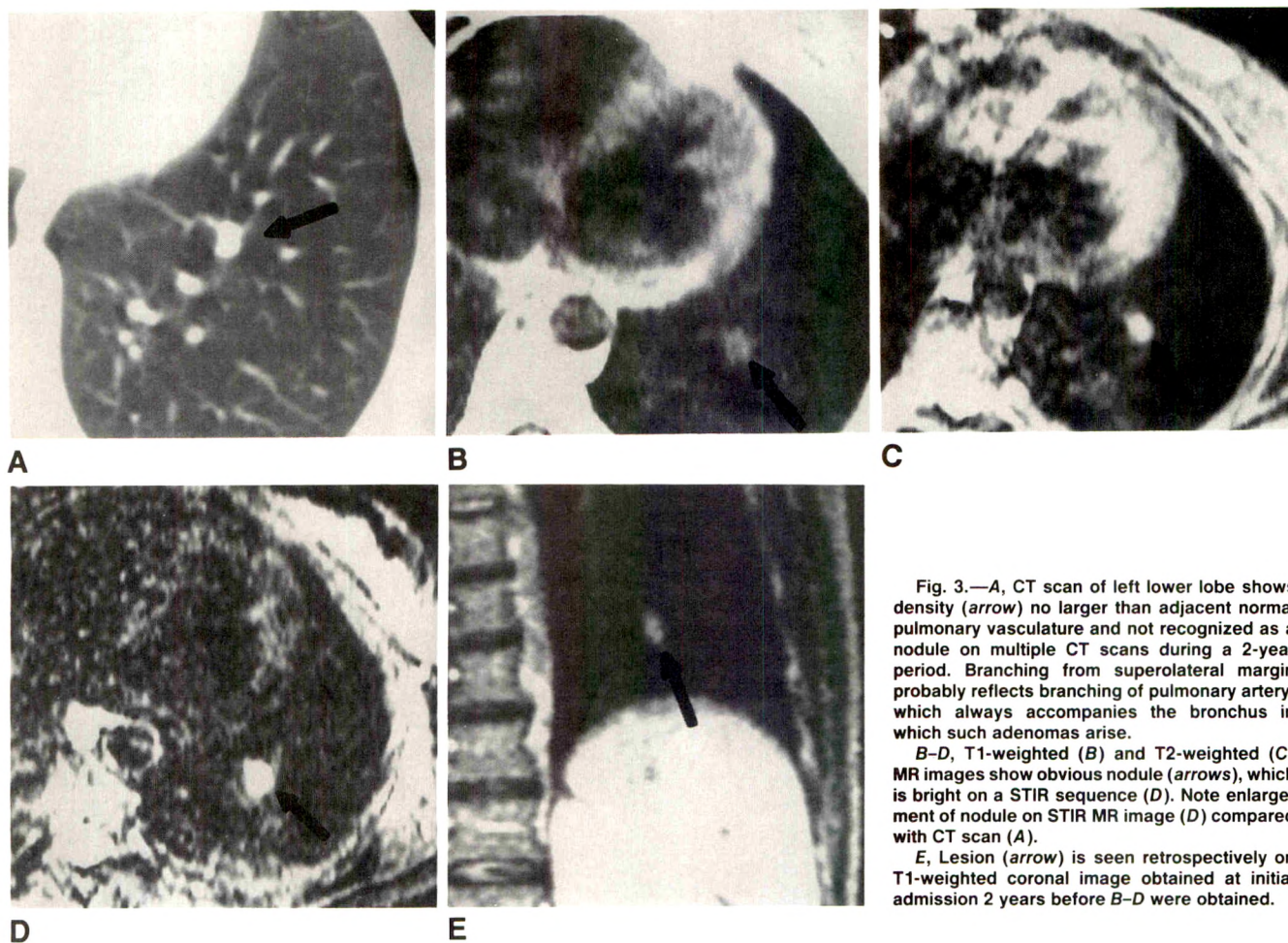


Fig. 3.—A, CT scan of left lower lobe shows density (arrow) no larger than adjacent normal pulmonary vasculature and not recognized as a nodule on multiple CT scans during a 2-year period. Branching from superolateral margin probably reflects branching of pulmonary artery, which always accompanies the bronchus in which such adenomas arise.

B–D, T1-weighted (B) and T2-weighted (C) MR images show obvious nodule (arrows), which is bright on a STIR sequence (D). Note enlargement of nodule on STIR MR image (D) compared with CT scan (A).

E, Lesion (arrow) is seen retrospectively on T1-weighted coronal image obtained at initial admission 2 years before B–D were obtained.

dynamic studies should allow this distinction, maximal enhancement is programmed generally to occur when scanning through the hilum. When the upper and lower lung fields are scanned, contrast enhancement may be insufficient to distinguish vessel from nodule. Mueller et al. [22] were the first to show that small nodules in the middle third of the lung may be more conspicuous on MR imaging than on CT.

Bronchial carcinoid tumors are of neuroendocrine origin [2, 7, 8], and, like islet cell tumors [23], pheochromocytomas [24], and medullary carcinoma of the thyroid [25], they are bright on T2-weighted and STIR sequences. Even though small bronchial carcinoid tumors may be smeared vertically over several contiguous axial slices by respiratory movements during the long acquisition times of an MR study (a phenomenon that tends to obscure small tumors in other organs such as the liver), the marked contrast between the high signal intensity of the nodule and the signal-free lungs and pulmonary vessels permits detection of the nodule.

The high signal intensity of bronchial carcinoid tumors also may account for their magnified appearance. We, as well as other authors, have observed a tendency for apparent enlargement of lesions on STIR images. Shuman et al. [26] noted enlargement of 26 lesions on STIR images; 10 of these were in the chest and the average increase in volume was

105%. These authors theorized that the apparent enlargement of lesions on STIR sequences was due to peritumoral edema. This, however, is an unlikely explanation for the enlargement of low-grade carcinoid tumors in the lung. Histologically, we saw no edema surrounding these slowly growing tumors. Enlargement probably is due to blooming of the high signal intensity of the bronchial carcinoid tumor into adjacent areas of absent signal (air-filled lung) because of the high contrast differential.

The detection of masses in the hilum of the lung is accomplished reliably by dynamic bolus-enhanced CT [27]. However, hypervascular masses close to the pulmonary artery may be difficult to resolve because of their enhancement and volume averaging with the pulmonary vasculature on axial scans. Aronchick et al. [28] have stressed the intense enhancement of bronchial carcinoid tumors on bolus-enhanced CT studies, which, in their case, allowed distinction from adjacent atelectatic lung but led to confusion with pulmonary vasculature. In one of our patients, a 2-cm hilar node was more obvious on MR than on bolus-enhanced dynamic CT and led to resection of an occult carcinoid tumor of the right upper lobe.

Bronchial carcinoid tumors may contain calcium. Shin et al. [29] recently reported an ossifying bronchial carcinoid tumor



that simulated broncholithiasis. As calcium reduces signal on MR images, it is possible that a bronchial carcinoid tumor containing significant amounts of calcium would provide less signal on T2-weighted and STIR images, thereby impairing the tumor's detection. However, the presence of calcium should enable its distinction from adjacent pulmonary vasculature on CT.

Despite the acknowledged sensitivity of CT in the detection of pulmonary nodules, few studies include pathologic correlation. Pass et al. [14] detected with CT (10-mm slice thickness) only 51% of nodules removed at the time of bilateral thoracotomy. Nodules smaller than 3 mm never were visualized on CT, and nodules up to 1–2 cm were missed sometimes. Possibly, many of these larger undetected nodules are in the middle third of the lung and are indistinguishable from normal pulmonary vessels. We currently are attempting to correlate the detectability of metastatic nodules on CT with their location within the lung as determined at the time of thoracotomy. It is for these central lesions that MR might be a particularly sensitive screening test, and for that reason we think that MR of the chest is indicated in patients with ectopic ACTH production when other localizing studies are normal.

## REFERENCES

- Doppman JL, Nieman L, Miller DL, et al. The ectopic ACTH syndrome: a review of localizing studies in 28 patients. *Radiology* **1989**;172:115–124
- Forster BB, Müller NL, Miller RR, Nelems B, Evans KG. Neuroendocrine carcinomas of the lung: clinical, radiologic and pathologic correlation. *Radiology* **1989**;170:441–445
- Findling JW, Tyrrell JB. Occult ectopic secretion of corticotropin. *Arch Intern Med* **1986**;146:929–933
- Findling JW, Aron DC, Tyrrell JB, et al. Selective venous sampling for ACTH in Cushing's syndrome: differentiation between Cushing's disease and the ectopic ACTH syndrome. *Ann Intern Med* **1981**;94:647–652
- Doppman JL, Oldfield E, Krudy AG, et al. Petrosal sinus sampling for Cushing syndrome: anatomical and technical consideration. *Radiology* **1984**;150:99–103
- Oldfield EH, Chrousos GP, Schulte HL. Preoperative lateralization of ACTH-secreting pituitary microadenomas by bilateral and simultaneous inferior petrosal venous sinus sampling. *N Engl J Med* **1985**;312(2):100–103
- Arrighi MG, Woolner LB, Bernatz PE. Atypical carcinoid tumors of the lung. *J Thorac Cardiovasc Surg* **1972**;64:413–421
- Paladugu RR, Benfield JR, Pak HY, Ross RK, Teplitz RL. Bronchopulmonary Kulchitsky cell carcinomas: a new classification scheme for typical and atypical carcinoids. *Cancer* **1985**;55:1303–1311
- Levitt RG, Glaser HS, Roper CL, et al. Magnetic resonance imaging of mediastinal and hilar masses: comparison with CT. *AJR* **1985**;145:9–14
- Webb WR, Jensen GB, Sollitto R, et al. Bronchogenic carcinoma staging with MR compared with staging with CT and surgery. *Radiology* **1985**;156:117–125
- Heelan RT, Martini N, Westcott JW, et al. Carcinomatous involvement of the hilum and mediastinum: computed tomographic and magnetic resonance evaluation. *Radiology* **1985**;156:111–115
- Musset D, Grenier P, Carette MF, et al. Primary lung cancer staging: prospective comparative study of MR imaging with CT. *Radiology* **1986**;160:607–611
- Poon PY, Bronskill MJ, Henkelman RM, et al. Mediastinal lymph node metastases from bronchogenic carcinoma: detection with MR imaging and CT. *Radiology* **1987**;162:651–656
- Pass HL, Dwyer A, Makuch R, Roth JA. Detection of pulmonary metastases in patients with osteogenic and soft tissue sarcomas. *Clin Oncol* **1985**;3:1261–1265
- Schaner EG, Chang AE, Doppman JL, Conkle DM, Flye MW, Rosenberg SA. Computed and whole lung tomography in detecting pulmonary nodules. *AJR* **1978**;131:51–54
- Muhm JR, Brown LR, Crowe JK. Use of computed tomography in the detection of pulmonary nodules. *Mayo Clin Proc* **1977**;52:345–348
- Muhm JR, Brown LR, Crowe JK, Sheedy PF II, Hattery RR, Stephens DH. Comparison of whole lung tomography and computed tomography for detecting pulmonary nodules. *AJR* **1978**;131:981–984
- Chang AE, Schaner EG, Conkle DM, Flye WM, Doppman JL, Rosenberg SA. Evaluation of computed tomography in the detection of pulmonary metastases: a prospective study. *Cancer* **1976**;43:913–916
- Naidich DP, McCauley DI, Siegelman SS. Computed tomography of bronchial adenoma. *J Comput Assist Tomogr* **1982**;6:725–732
- Magid D, Siegelman SS, Eggleston JC, Fishman EK, Zerhouni EA. Pulmonary carcinoid tumors: CT assessment. *J Comput Assist Tomogr* **1989**;13:244–247
- Rozenman J, Pausner R, Lieberman Y, Gamsu O. Bronchial adenoma. *Chest* **1987**;92:145–147
- Mueller DL, Gamsu G, Webb WR. Pulmonary nodules: detection using magnetic resonance and computed tomography. *Radiology* **1985**;155:687–690
- Frucht H, Doppman JL, Norton JA, et al. Gastrinomas: comparison of MR imaging with CT, angiography, and US. *Radiology* **1989**;171:713–717
- Fink IJ, Reinig JW, Dwyer AJ, Doppman JL, Linehan MW, Keiser HR. MR imaging of pheochromocytomas. *J Comput Assist Tomogr* **1985**;9:454–458
- Crow JP, Azar-Kia B, Prinz RA. Recurrent occult medullary thyroid carcinoma detected by MR imaging. *AJR* **1989**;152:1255–1256
- Shuman WP, Baron RL, Peters MJ, Tazioli PK. Comparison of STIR and spin-echo MR imaging at 1.5 T in 90 lesions of the chest, liver, and pelvis. *AJR* **1989**;152:853–859
- Naidich DP, Zerhouni EA, Siegelman SS. *Computed tomography of the thorax*. New York: Raven, **1984**
- Aronchick JM, Wexler BC, Wallace M, et al. Computed tomography of bronchial carcinoid. *J Comput Assist Tomogr* **1986**;10:71–74
- Shin MS, Berland LL, Myers JL, et al. CT demonstration of an ossifying bronchial carcinoid simulating broncholithiasis. *AJR* **1989**;153:51–52



## Book Review

**Nuclear Cardiovascular Imaging.** Current Clinical Practice. Edited by Milton J. Guiberteau. New York: Churchill Livingstone, 247 pp., 1990. \$65

Although some radionuclide imaging procedures have shown a decline in the number of studies performed, cardiovascular imaging has shown a consistent increase in the number of studies performed, the development of new radiopharmaceuticals, and the diversity of the kinds of cardiovascular disease that are evaluated. As a result of the rapid changes in the field, new textbooks reflecting current practice are needed. *Nuclear Cardiovascular Imaging: Current Clinical Practice* focuses on the "staples of nuclear cardiovascular imaging" as they are used on a day-to-day clinical basis and does not attempt to be a comprehensive textbook reviewing the whole field. Thus, it presents the physiology, instrumentation, and radiopharmaceuticals of cardiovascular imaging in the context of the examination of patients. For this reason, its major appeal is to physicians who are involved in using tried and true methods or to those residents or fellows who are learning fundamentals of cardiovascular imaging.

The book has 13 chapters dealing with planar, single-photon emission CT (SPECT) and positron emission tomographic cardiovascular imaging. The book is illustrated with both color and black-and-white images. Some of the chapters would benefit greatly by having more images. The overall quality of the illustrations, especially the black-and-white images, is modest at best, and in some cases, color images appear to have been printed in black and white. The chapter by Keith Fisher on qualitative SPECT thallium imaging is illustrated amply. Most chapters have abundant figures and graphs taken from original papers but lack adequate images to show the variety of normal, abnormal, and artifactual imaging results. The book was published in 1990, but many of the articles review the literature only through 1987. An area of major concern to practitioners is deciding whether to perform thallium imaging by using time-tested planar

techniques or newer tomographic methods. This issue is not addressed adequately, and the chapter on quantitative SPECT thallium imaging does not deal adequately with the low specificity that has been reported for SPECT methods in several large clinical studies. For some techniques, recent findings have changed clinical practice, and these changes are not discussed. As an example, diastolic function during rest or exercise is age dependent, and when analysis of this function is used to detect coronary artery disease, interpretation of the results must take this age dependency into consideration.

The last chapter in the book, on radionuclide venography, is out of context with the remainder of the book and could have been omitted. Overall, this book will be of value for clinical practitioners of nuclear cardiovascular imaging. The use of more and better quality illustrations would have been helpful, but then the price of the book would have increased, and this would have lessened its appeal. If you evaluate heart disease in a large number of patients, go buy the book. You will find it extremely useful.

Overall, this is an excellent review of the currently used clinical practice of cardiovascular nuclear medicine. It provides good details on the physiology of the various radionuclide tracers and on instrumentation and, for this reason, should appeal to those who deal with the procedures on a daily basis. A major limitation for the radiologic community is the general lack of good quality images to better illustrate the subtleties and nuances of imaging interpretation.

Manuel D. Cerqueira  
University of Washington School of Medicine  
Seattle VA Medical Center  
Seattle, WA 98108



## Pictorial Essay

# High-Attenuation Mediastinal Masses on Unenhanced CT

Harvey S. Glazer,<sup>1</sup> Paul L. Molina, Marilyn J. Siegel, and Stuart S. Sagel

On unenhanced CT scans, a variety of mediastinal masses contain areas with attenuation values higher than the attenuation value of the chest wall musculature. The increased attenuation may be diffuse or focal and may be a result of calcium deposition, high iodine content, or areas of acute hemorrhage. This report illustrates the gamut of high-attenuation mediastinal masses seen on unenhanced CT. Masses that are of high attenuation only on IV contrast-enhanced images (e.g., aberrant vessels) are not included.

### Calcification

#### Lymph Node

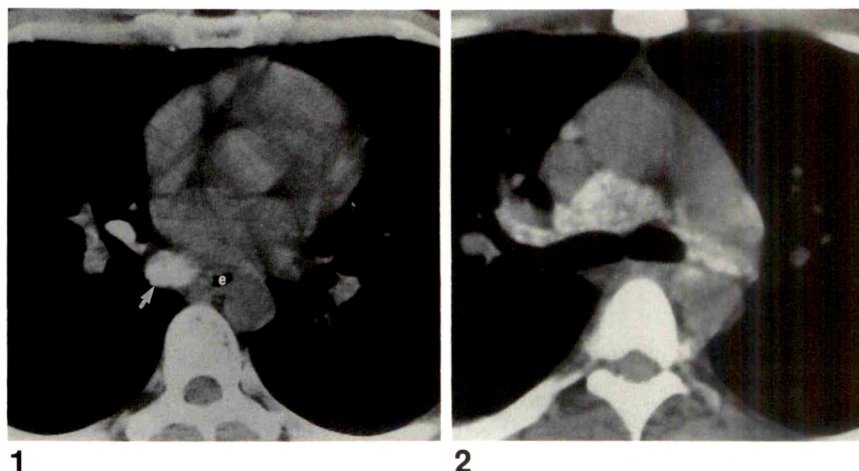
Calcification within lymph nodes is the most common cause of a high-attenuation mediastinal mass. In most cases it

represents a healed infectious process, especially granulomatous disease (e.g., histoplasmosis and tuberculosis) (Fig. 1). Calcified mediastinal lymph nodes also may occur in disseminated *Pneumocystis carinii* infection in patients with AIDS (Fig. 2) [1, 2]. These calcifications are believed to be caused by a necrotizing granulomatous reaction, since *Pneumocystis* organisms are frequently identified within calcified granulomas. Calcifications in extrapulmonary sites (e.g., spleen, liver, kidneys, and abdominal lymph nodes) are also common.

Inhalational diseases, such as coal worker's pneumoconiosis and silicosis, may cause lymphadenopathy that contains calcification (Fig. 3). Although classically described in silicosis, an eggshell pattern of lymph node calcification can be seen rarely in sarcoidosis, treated lymphoma, or healed

Fig. 1.—Healed granulomatous disease. CT scan shows large calcified subcarinal lymph node mass (arrow) adjacent to esophagus (e). Mass was removed because of dysphagia. Pathologic examination showed fibrous tissue, granulomas, and calcification. Fungal and acid-fast stains were negative.

Fig. 2.—*Pneumocystis carinii* infection in AIDS patient. Calcified hilar and mediastinal lymph nodes are seen. Other scans showed calcified axillary and intraabdominal nodes as well as hepatic, splenic, and renal calcifications. Biopsy of a calcified axillary node disclosed necrotizing granulomatous lymphadenitis, with *Pneumocystis carinii* organisms and dystrophic calcifications within the granulomas. (Courtesy of I. M. Feuerstein, Bethesda, MD.)

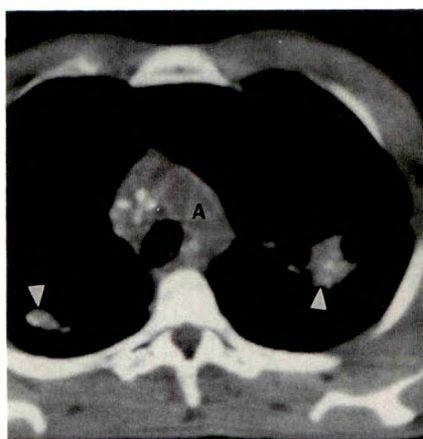


Received June 12, 1990; accepted after revision August 6, 1990.

<sup>1</sup> All authors: Mallinckrodt Institute of Radiology, Washington University School of Medicine, St. Louis, MO 63110. Address reprint requests to H. S. Glazer.

AJR 156:45-50, January 1991 0361-803X/91/1561-0045 © American Roentgen Ray Society





**A**



**B**

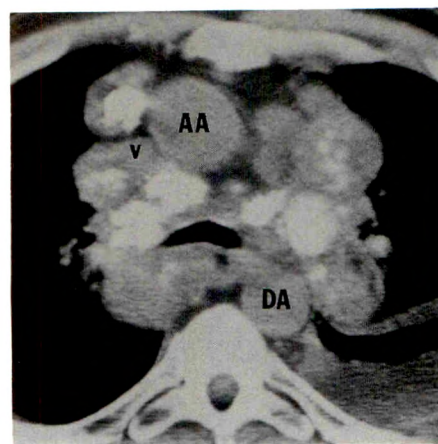
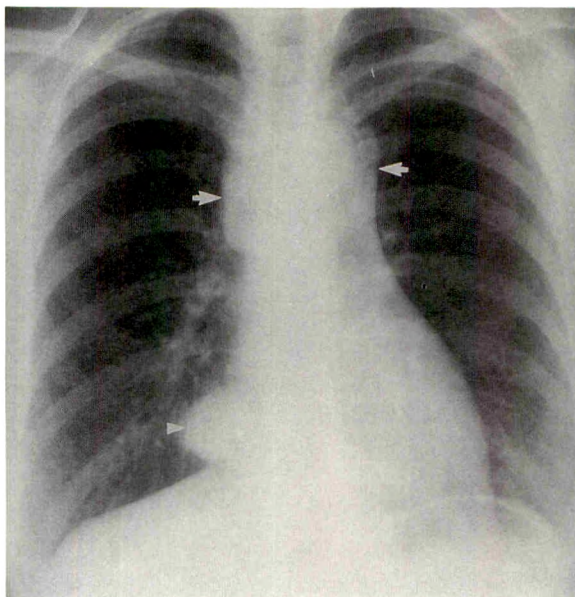


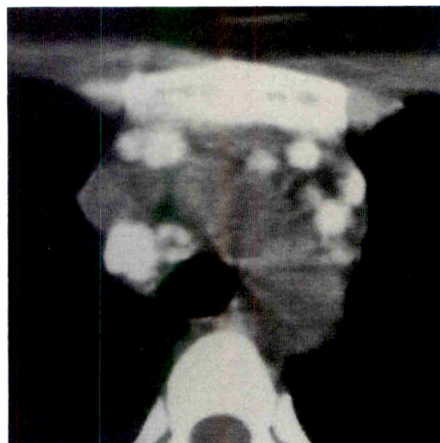
**Fig. 3.—Silicosis.**

A and B, CT scans show multiple calcified hilar and mediastinal lymph nodes, some of which show eggshell calcification (arrows). Areas of confluent infiltrate represent progressive massive fibrosis (arrowheads). A = aortic arch.

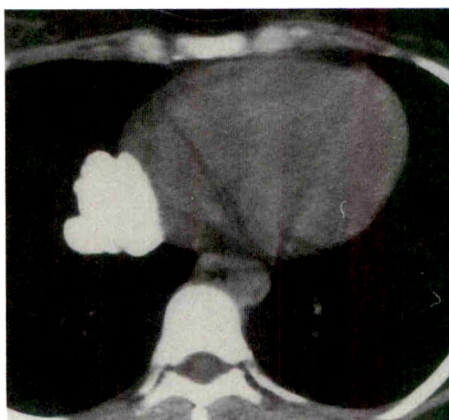
**Fig. 4.—Amyloidosis.** CT scan shows multiple, partially calcified lymph nodes in mediastinum and hila. Left pleural effusion is also present. v = superior vena cava, AA = ascending aorta, DA = descending aorta. (Courtesy of J. K. Aston and E. L. Saunders, Jonesboro, AR.)



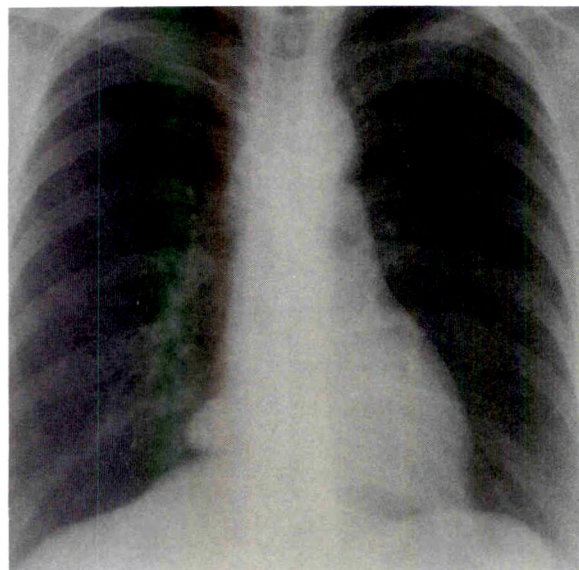
**A**



**B**



**C**



**D**

**Fig. 5.—Metastatic papillary carcinoma of ovary.**

A, Posteroanterior chest radiograph shows superior mediastinal (arrows) and right cardiophrenic angle (arrowhead) masses.

B and C, CT scans show multiple enlarged calcified lymph node metastases in superior mediastinum and right cardiophrenic angle.

D, Posteroanterior chest radiograph after chemotherapy shows decrease in size of superior mediastinal and right cardiophrenic lymphadenopathy.



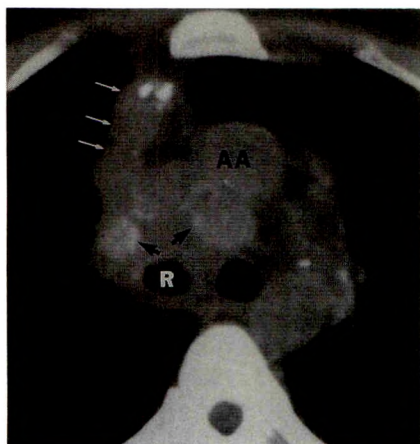


Fig. 6.—Bronchogenic carcinoma. CT scan shows areas of amorphous calcification (black arrows) within central right upper lobe mass and mediastinal lymphadenopathy. Scans through liver showed multiple, partially calcified liver metastases. Subsequent bronchoscopic biopsy of right main bronchus disclosed epidermoid carcinoma. Right upper lobe atelectasis (white arrows). AA = ascending aorta, R = right main bronchus.

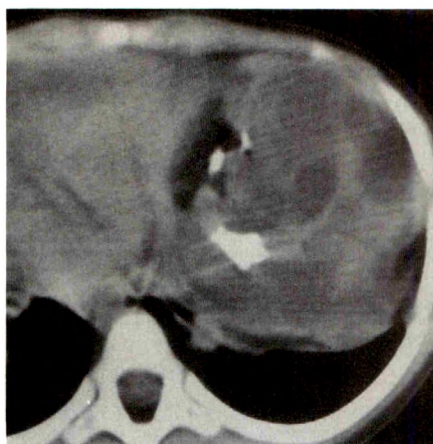


Fig. 7.—Benign mature teratoma. CT scan shows large mass containing fat, multiple cysts, and calcification. Heart is displaced to the right. Mass arose from left lobe of thymus and contained embryonic teeth.

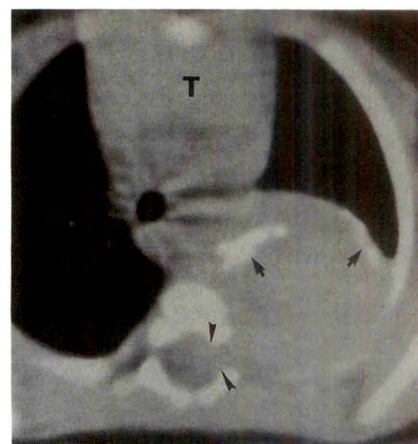
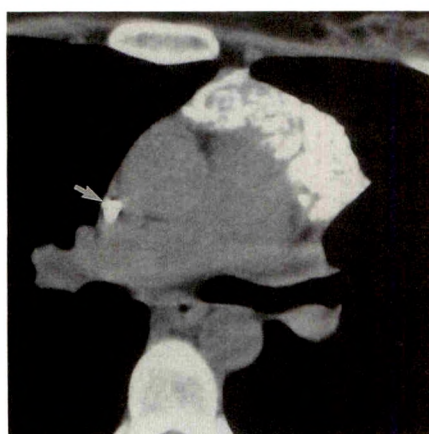


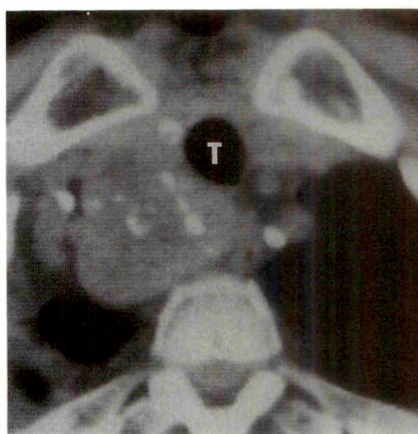
Fig. 8.—Neuroblastoma. CT scan shows large left posterior mediastinal mass extending into spinal canal (arrowheads) and destroying posterior rib. Calcification within mass (arrows). T = thymus.

Fig. 9.—Calcification after treatment for Hodgkin disease. CT scan at level of right pulmonary artery shows extensive calcification in anterior mediastinum. Previous studies before radiation and chemotherapy showed thymic infiltration by Hodgkin disease. Raaf catheter (arrow).



9

Fig. 10.—Goiter. CT scan at thoracic inlet shows large right-sided paratracheal mass containing multiple calcifications and deviating trachea (T) anteriorly. More cephalad images showed continuity of mass with right lobe of thyroid.



10

infectious granulomatous disease. Associated changes of progressive massive fibrosis should suggest the correct diagnosis. Angiofollicular lymph node hyperplasia (Castleman disease) and amyloidosis are other less common causes of calcified mediastinal lymph nodes (Fig. 4).

Mediastinal lymph node metastases calcify rarely (e.g., in mucinous ovarian or colonic carcinoma, bronchogenic carcinoma, papillary carcinoma of the thyroid, osteosarcoma) (Figs. 5 and 6) [3]. Treated lymph node metastases (after radiation therapy or chemotherapy) also may show areas of calcification. In most cases, the clinical history and other associated CT findings (e.g., pulmonary, adrenal, or liver metastases) should suggest the correct diagnosis.

#### Primary Neoplasm

Calcification can occur within a variety of primary mediastinal neoplasms (Figs. 7 and 8). Germ cell tumors, thymomas,

and neurogenic tumors can contain focal areas of calcification. The pattern of calcification generally is not helpful in terms of differential diagnosis. However, calcification within a fatty mass is highly suggestive of a benign mature teratoma, and a partially calcified mass adjacent to a widened intervertebral foramen usually represents a tumor of neurogenic origin. Although calcification in lymphomatous masses is almost always seen only after treatment (Fig. 9), occasionally it can occur at initial presentation [4].

#### Goiter

Intrathoracic goiters may contain focal deposits of calcium, a sequela of necrosis or hemorrhage within the mass (Fig. 10). Almost all intrathoracic goiters are continuous with the cervical part of the thyroid gland.



### Aneurysm

Aortic aneurysms typically contain peripheral curvilinear calcifications, which assist in identifying the mediastinal abnormality as vascular (Fig. 11). The calcification may be more centrally located if the intima is displaced (i.e., aortic dissection) (Fig. 12) or if there is mural thrombus calcification. Pseudodisplacement of intimal calcification can occur if the aorta is tortuous and crosses the CT imaging plane obliquely. Review of consecutive images and administration of IV contrast material should clarify such cases.

### Thrombosed Vein

A thrombosed vein may calcify and simulate a calcified lymph node (Fig. 13). Close scrutiny of consecutive images will show that the structure being imaged is vascular. Moreover, secondary signs of venous thrombosis (e.g., collateral vessels) usually will be present.

### Foregut Cyst

Foregut cysts usually are near water in attenuation. However, they may have high attenuation values if the fluid con-

tains calcium carbonate or calcium oxalate. Occasionally, calcifications may be present in the cyst wall.

### Miscellaneous

Focal areas of pericardial, myocardial, coronary artery, or mediastinal pleural calcification also can be seen on CT (Fig. 14). In most cases the calcification is linear and does not have the appearance of a mediastinal mass.

### High Iodine Content

#### Goiter

The attenuation value of the intrathoracic component of a goiter is generally less than that of the cervical thyroid gland, but greater than that of muscle (Fig. 15). This finding, however, is highly variable and relates to the iodine content of the goiter. If the iodine content is low, the attenuation value of the goiter may be similar to that of chest wall musculature.

### Residual Lymphangiographic Contrast Material

In most cases, CT images of the mediastinum after lymphangiography do not show residual lymphangiographic con-

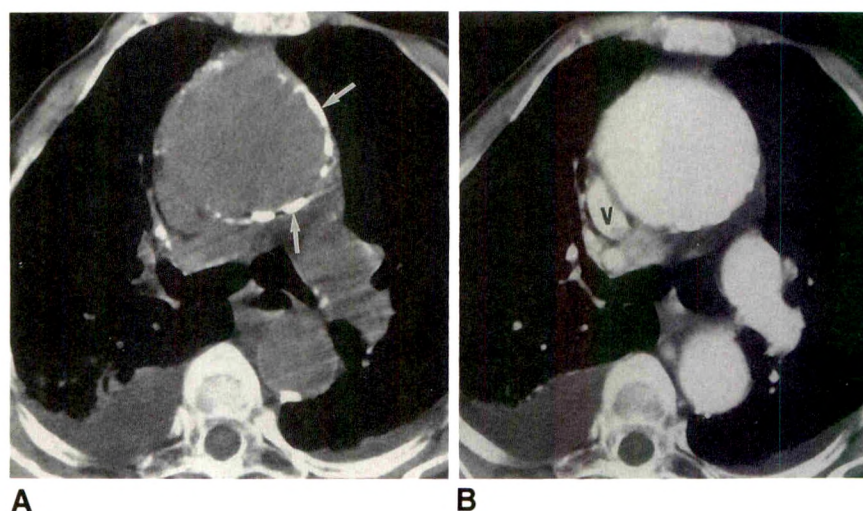


Fig. 11.—Aortic aneurysm.

A, Unenhanced CT scan shows 7-cm mass with peripheral calcification (arrows) in expected position of ascending aorta. Bilateral pleural effusions are also present.

B, After administration of contrast material, CT scan shows enhancement of aortic aneurysm, which compresses medial aspect of superior vena cava (V).

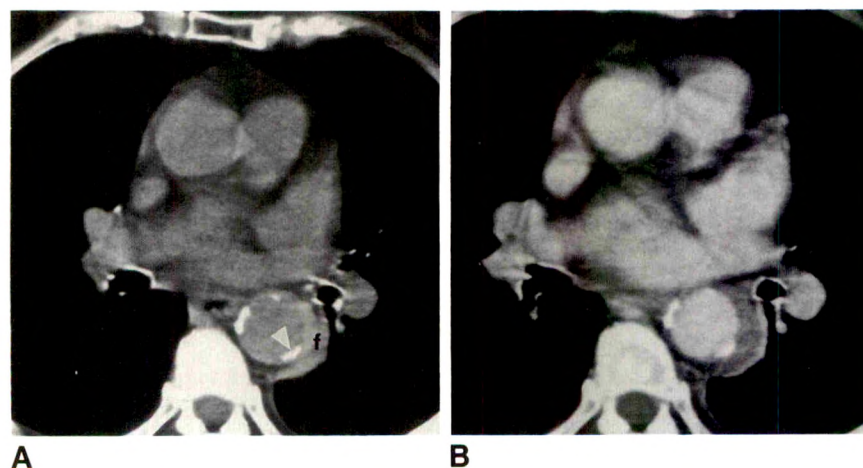
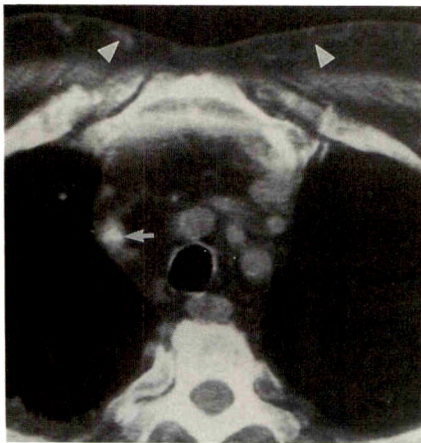


Fig. 12.—Type B aortic dissection.

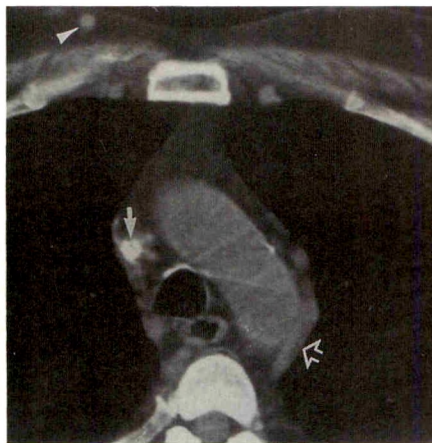
A, Unenhanced CT scan shows enlargement of descending aorta with internal displacement of intimal calcification (arrowhead). Note high-attenuation clotted blood in false lumen (f).

B, After administration of contrast material, CT scan shows enhancement of true lumen.





**A**



**B**

**Fig. 13.**—Calcified thrombus in superior vena cava.

**A and B,** CT scans show calcification (*arrows*) in superior vena cava. Multiple enlarged collateral vessels (*arrowheads*) are seen in anterior chest wall. Dilated left superior intercostal vein (*open arrow*).

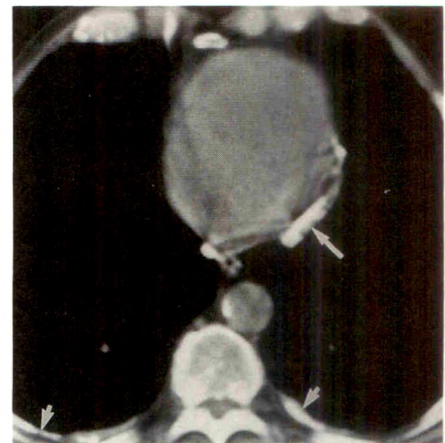
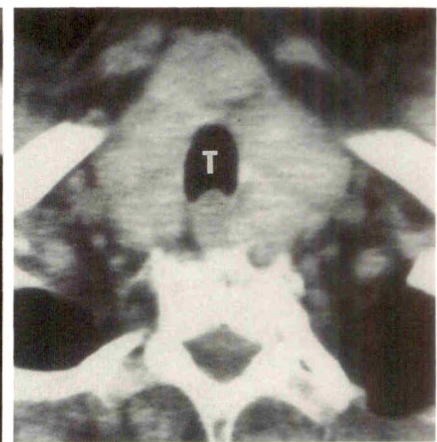


**Fig. 14.**—Calcified pleural plaque. CT scan in patient with prior asbestos exposure shows large, partially calcified plaque (*long arrow*) arising from mediastinal pleura adjacent to left side of heart. Thinner plaques (*short arrows*) are seen posteriorly in each hemithorax.



**A**

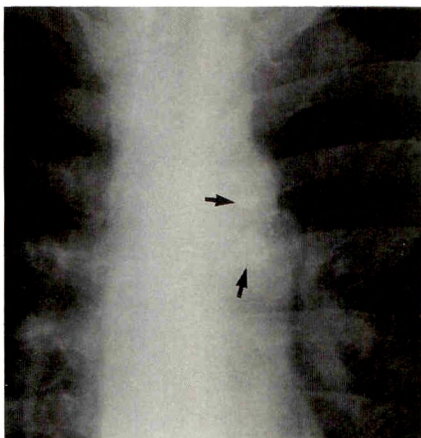


**B**

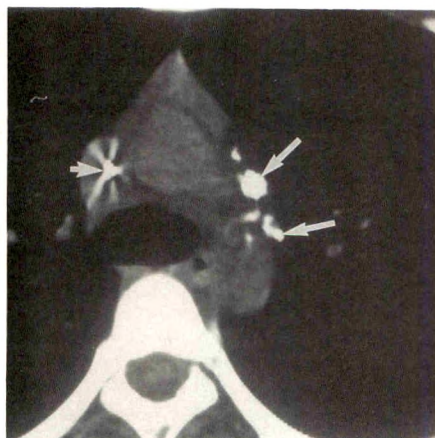
**Fig. 15.**—Goiter.

**A,** CT scan through superior mediastinum shows large mass on both sides of trachea (**T**). Mass has higher attenuation value than chest wall musculature and unenhanced blood vessels do.

**B,** More cephalad image shows continuity with enlarged cervical thyroid gland.



**A**



**B**

**Fig. 16.**—Residual lymphangiographic contrast material.

**A,** Posteroanterior chest radiograph after bipedal lymphangiography shows opacification of enlarged lymph nodes (*arrows*) in left side of mediastinum.

**B,** CT scan about 1½ years after treatment shows residual lymphangiographic contrast material (*long arrows*) in aortopulmonary window. Raaf catheter (*short arrow*).

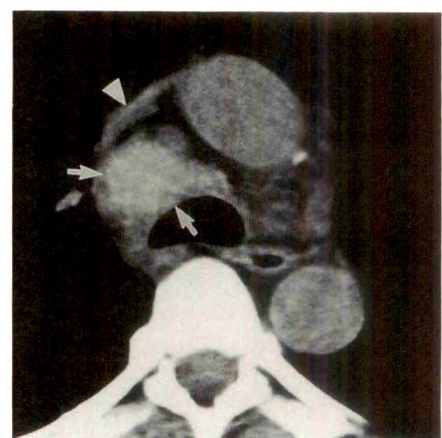


**Fig. 17.**—Mediastinal hematoma. CT scan obtained because mediastinal widening was seen on portable chest radiograph after mediastinoscopy shows high-attenuation hematoma (*arrows*) compressing superior vena cava (*arrowhead*).



trast material within mediastinal nodes. However, in some cases, residual contrast material may be seen within the involved nodes (Fig. 16). This may be difficult to distinguish from posttreatment lymph node calcification, unless appropriate history is provided.

### Hemorrhage

Hemorrhage can occur within any mediastinal mass, or after trauma (Figs. 12 and 17). Ninety percent of hematomas have areas of high attenuation during the first 72 hr, reflecting the high hemoglobin concentration of clotted blood [5]. The extent of alteration in the attenuation of the mass will depend on the degree and age of the hemorrhage as well as on the initial composition of the mass (e.g., fluid vs solid). As the hematoma ages, its attenuation decreases owing to hemoglobin lysis. This process often occurs in a centripetal fashion, creating a low-attenuation peripheral halo that increases in width over time.

### Miscellaneous

Masses that communicate with the esophagus (e.g., esophageal diverticulum) also will contain areas of high attenuation if oral contrast material has been administered.

Foreign bodies within the esophagus or other areas of the mediastinum also may be of high attenuation on CT. Even foreign bodies that are of relatively low attenuation (e.g., wood) may become calcified with time. Retained surgical sponges are usually identifiable by a radiopaque marker. Encapsulation with cyst formation and capsular calcification may occur when sponges have been retained for a long time.

### REFERENCES

1. Feuerstein IM, Francis P, Raffeld M, Pluda J. Widespread visceral calcifications in disseminated *Pneumocystis carinii* infection: CT characteristics. *J Comput Assist Tomogr* **1990**;14:149-151
2. Radin DR, Baker EL, Klatt EC, et al. Visceral and nodal calcification in patients with AIDS-related *Pneumocystis carinii* infection. *AJR* **1990**;154:27-31
3. Mahoney MC, Shipley RT, Corcoran HL, Dickson BA. CT demonstration of calcification in carcinoma of the lung. *AJR* **1990**;154:255-258
4. Panicek DM, Harty MP, Scicutella CJ, Carsky EW. Calcification in untreated mediastinal lymphoma. *Radiology* **1988**;106:735-736
5. Swensen SJ, McLeod RA, Stephens DH. CT of extracranial hemorrhage and hematomas. *AJR* **1984**;143:907-912



## Diaphragmatic Rupture Due to Blunt Trauma: Sensitivity of Plain Chest Radiographs

Russell Gelman<sup>1</sup>  
Stuart E. Mirvis<sup>1</sup>  
David Gens<sup>2</sup>

Preoperative diagnosis of diaphragmatic rupture caused by blunt injury is often difficult because of serious concurrent injuries, a lack of specific clinical signs, and simultaneous lung disease that may mask or mimic the diagnosis radiologically. Previous reports have suggested that a preoperative diagnosis is established on the basis of chest radiographs in only one third of patients. In order to assess the value of chest radiographs and other imaging techniques in diagnosing traumatic rupture of the diaphragm, we retrospectively reviewed all preoperative diagnostic imaging performed in 50 patients with surgically proved hemidiaphragmatic rupture due to blunt trauma. Chest radiographs were diagnostic in 20 (46%) of 44 patients with left-sided rupture and were considered suspicious enough to warrant further diagnostic studies in an additional eight patients (18%). Five patients with initially normal findings on chest radiographs had diagnostic findings on delayed chest radiographs. Chest radiographs were strongly suggestive in only one (17%) of six patients with right-sided hemidiaphragmatic rupture. CT was diagnostic for diaphragmatic rupture in only one (14%) of seven instances in which it was performed. MR was diagnostic in both patients in whom it was performed.

Our experience indicates that chest radiographs obtained at admission and repeated soon after are more valuable in suggesting the diagnosis of traumatic rupture of the diaphragm than previously reported, particularly in the more frequent, left-sided injuries. This increased sensitivity may be due to a greater level of suspicion maintained in a trauma referral center in which this injury is not uncommon.

*AJR* 156:51-57, January, 1991

The preoperative diagnosis of traumatic diaphragmatic rupture (TDR) due to blunt trauma is difficult. The injury may be initially overlooked because of other more immediate life-threatening conditions in the patient with multiple traumas. In addition, specific clinical signs are usually lacking, and results of initial radiologic studies may be normal or nonspecific [1-4]. Also, concurrent pulmonary abnormalities such as lower lobe contusion and/or laceration, lower lobe atelectasis, pleural effusion, phrenic nerve paresis, and hemidiaphragmatic eventration can mask or mimic diaphragmatic rupture with herniation of abdominal contents [2].

Previous reports have emphasized the limitations of chest radiographs in confidently establishing the preoperative diagnosis of TDR and have suggested using ancillary studies including fluoroscopy, gastrointestinal contrast studies, sonography, CT, and MR imaging to improve diagnostic accuracy. However, with the exception of MR imaging, where experience is limited, each has been shown to have significant limitations in making a confident diagnosis of TDR. All diagnostic imaging studies obtained in 50 patients with surgically proved TDR were reviewed retrospectively to evaluate the sensitivity of plain chest radiographs in detecting diaphragmatic rupture.

Received May 7, 1990; accepted after revision June 26, 1990.

<sup>1</sup> Department of Diagnostic Radiology, University of Maryland Medical System, 22 S. Greene St., Baltimore, MD 21201. Address reprint requests to S. E. Mirvis.

<sup>2</sup> Department of Surgery/Traumatology, Maryland Institute for Emergency Medical Services Systems, 22 S. Greene St., Baltimore, MD 21201.

0361-803X/91/1561-0051  
© American Roentgen Ray Society



## Methods and Materials

During a 6-year period (September 1983–September 1989), 169 patients admitted to the Shock Trauma Center of the Maryland Institute for Emergency Medical Services System had surgical treatment of acute TDR due to penetrating or blunt injury. Of this group, 82 patients (49%) had injuries due to blunt trauma. Of these, 50 patients (61%) had complete medical records including all radiologic studies available for review, and they make up the study population. There were 37 male and 13 female patients (age, 5–77 years; mean, 36 years). Mechanism of injury included 46 motor vehicle accidents, three pedestrian-vehicular accidents, and one patient crushed under a motor vehicle.

All imaging studies performed before surgical confirmation of the diagnosis were retrospectively reviewed by two radiologists and included one or more chest radiographs (all patients), CT (seven), gastrointestinal contrast studies (two), MR imaging (two), sonography (two), fluoroscopy (one), and diagnostic pneumoperitoneum (one). All interpretations were compared with the analyses performed at the time of the initial study. Chest radiographs were considered to be diagnostic or highly suggestive of TDR when definite air- or fluid-containing viscera were present above the left hemidiaphragm, or when the tip of a nasogastric tube was clearly above the level of the left hemidiaphragm. A very elevated diaphragm in the absence of any other cause also was considered diagnostic of diaphragmatic rupture. Findings suggestive of, but not diagnostic for, TDR include elevation of a hemidiaphragm in the absence of atelectasis and obscuration of a hemidiaphragm. In addition, evidence of mediastinal shift was noted, as well as evidence of ipsilateral lung disease including atelectasis, contusion, pleural effusion, and rib fractures.

CT scans were reviewed for evidence of fat- or air-containing viscera posterior, lateral, or anterior to the contour of the hemidiaphragm. Gastrointestinal contrast studies were reviewed for evidence of focal constriction of bowel at the level of the hemidiaphragm or obvious displacement of bowel into the thorax. MR images were reviewed for evidence of interruption of the low-signal-intensity hemidiaphragm or displacement of bowel or fat into the thoracic cavity. Coronal and axial MR images were performed on a Siemens Magnetom with T1 weighting (spin-echo 500/17 with four acquisitions).

Medical records of all patients were reviewed to ascertain in which cases TDR was diagnosed or strongly suggested by the chest radiograph or other imaging procedure and on which technique the diagnosis was based. Diagnosis of TDR by nonimaging studies or by celiotomy also was recorded. Results of diagnostic peritoneal lavage, if performed, and associated thoracic and/or abdominopelvic injuries also were recorded.

## Results

### Right Hemidiaphragmatic Rupture

Six (12%) of 50 patients had rupture of the right hemidiaphragm due to blunt trauma (Table 1). Associated injuries included liver lacerations (five), splenic laceration (two), small-bowel perforation (one), laceration of the inferior vena cava (one), and hemoperitoneum (two). The prospective and retrospective assessments of the findings on chest radiographs correlated in all six patients. Diagnosis of TDR was based on a diagnostic preoperative chest radiograph in one (17%) of the six patients (Fig. 1). The chest radiograph revealed marked elevation of the right hemidiaphragm (8 cm above the level of the left diaphragm) with the diaphragm being obscured. Mediastinal shift of 3 cm to the left occurred. A second

**TABLE 1: Results of Diagnostic Imaging in Six Patients with Ruptured Right Hemidiaphragm**

Imaging Technique/Finding	Number of Cases
Abnormal chest radiographs	2
Elevated right hemidiaphragm <sup>a</sup>	2 (4 cm and 8 cm)
Obscured right hemidiaphragm	1
Mediastinal shift <sup>b</sup>	1 (3 cm)
Ipsilateral rib fractures	0
Ipsilateral pleural effusion	1
Ipsilateral lung contusion	0
Other imaging studies	3
Sonography	1 (nondiagnostic)
CT	1 (nondiagnostic)
Diagnostic pneumoperitoneum	1 (positive)

Note.—Only two cases were diagnosed preoperatively.

<sup>a</sup> Elevation above level of left hemidiaphragm.

<sup>b</sup> Displacement of nasogastric tube to right of midline.

patient had a suggestive preoperative chest radiograph that showed the right hemidiaphragm elevated 4 cm above the level of the left hemidiaphragm. Sonography and CT were performed on this patient and results of both were normal, and a diagnostic pneumoperitoneum was then performed and results were positive. Both of these patients had negative diagnostic peritoneal lavage (DPL) results (<100,000 RBCs/ml). In the other four patients, the chest radiographs were interpreted as normal. DPL was positive in these four patients, leading to diagnosis of TDR by celiotomy. Table 1 summarizes results of radiologic and other ancillary imaging procedures performed in these six patients.

### Left Hemidiaphragmatic Rupture

Forty-four (88%) of 50 patients had traumatic rupture of the left hemidiaphragm. Associated injuries were present in 36 (82%) of these patients and included splenic rupture (21), pelvic fracture (17), and bladder rupture (eight), among others. In 20 (46%) of the 44 patients, chest radiographs were considered diagnostic or highly suspicious for TDR (Figs. 2–4). Five (25%) of these 20 patients had normal or minimally abnormal chest radiographs initially, but developed diagnostic or strongly suspicious findings on subsequent (second or third) chest radiographs obtained between 2 and 5 hr later, leading to celiotomy (Fig. 5). The prospective and retrospective assessments of the findings on chest radiographs correlated in all 20 patients. All 20 of these patients showed the presence of either air-containing bowel (16) or elevated nasogastric tube (four) above the level of the visualized diaphragm. The diaphragm was elevated in all 20 patients, with a range of 3–9 cm and an average of 6.2 cm.

Although not suggested on the initial interpretation, preoperative chest radiographs of an additional eight patients also were believed to be diagnostic of or strongly suggestive of TDR by retrospective review. Four patients showed the presence of air-containing viscera in the chest with elevation of the hemidiaphragm ranging from 3 to 6 cm (average, 4.2 cm). The other four patients showed marked elevation of the left hemidiaphragm in the absence of atelectasis and with me-



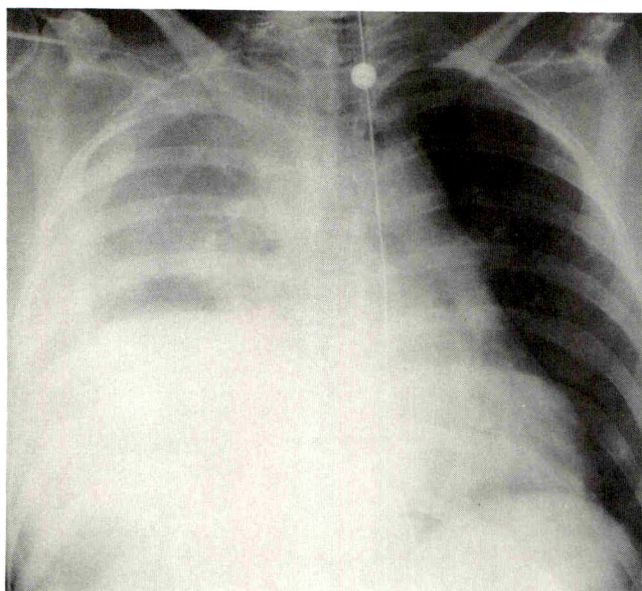


Fig. 1.—Chest radiograph shows elevated right hemidiaphragm, shift of mediastinum and nasogastric tube to left, and right-sided pleural effusion. Surgery revealed right diaphragmatic tear with herniation of liver into right hemithorax.

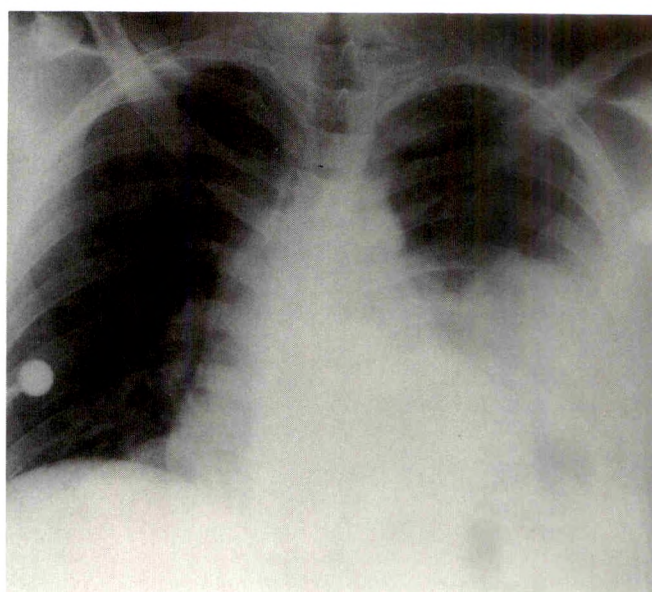


Fig. 2.—Chest radiograph shows marked apparent elevation of left hemidiaphragm with possible left lower lobe contusion or atelectasis. A moderate pleural effusion is present. Mediastinal shift to right is noted. An area of lucency is seen in lower left hemithorax. Surgery revealed a 10-cm tear of left hemidiaphragm with herniation of splenic flexure into left hemithorax.

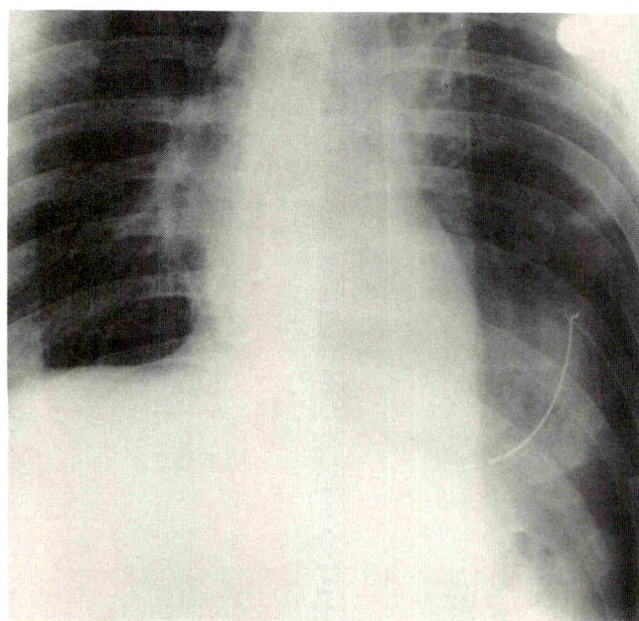


Fig. 3.—Chest radiograph reveals marked displacement of nasogastric tube into left lower hemithorax, suggesting gastric herniation. Contour of left hemidiaphragm is not clearly defined. An air lucency extends from abdomen into hemithorax. Fractures of seventh through ninth ribs were present on right side. Surgery revealed rupture of left hemidiaphragm with herniation of stomach, colon, and spleen into left hemithorax.

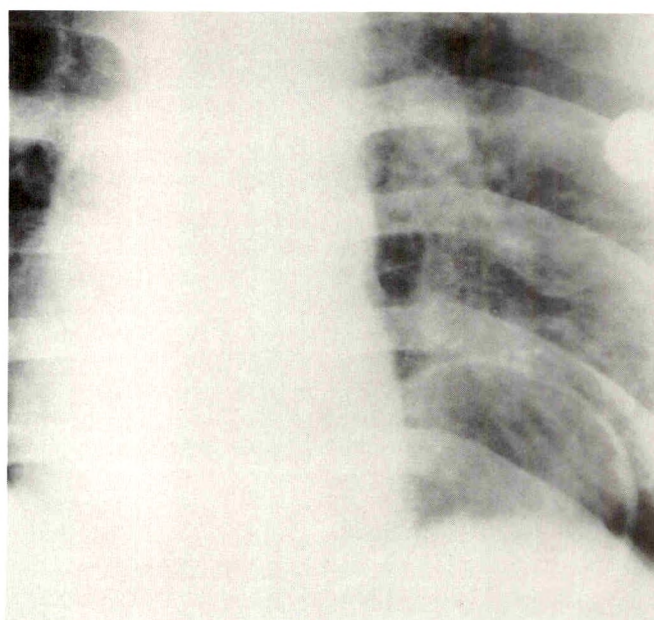


Fig. 4.—Chest radiograph shows a circular air lucency projecting above left hemidiaphragm, which appears to be in a normal position. Mediastinal shift toward right side is noted. Surgery revealed left hemidiaphragm rupture with herniation of colon into left hemithorax.



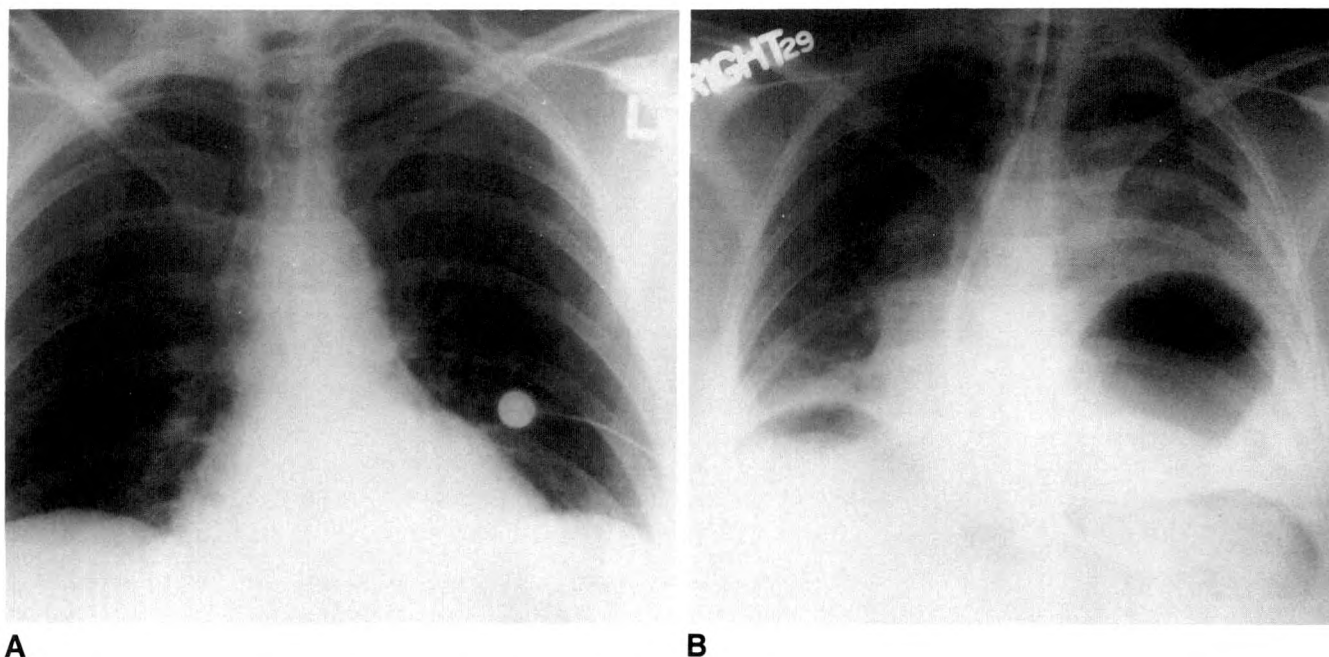


Fig. 5.—A, Chest radiograph shows normal contour and position of left hemidiaphragm. B, Chest radiograph obtained 2.5 hr after initial radiograph (A) shows loss of left hemidiaphragm contour, a large gas collection at left lung base, and a left pleural effusion. Mediastinum is shifted to right. A pneumoperitoneum has developed in interim. Surgery revealed an 8-cm rupture of left hemidiaphragm with herniation of gastric fundus into left hemithorax.

diastinal shift to the contralateral side. The range of diaphragmatic elevation was 7–13 cm with an average of 8.6 cm. It is difficult to explain the reasons for these cases not being diagnosed preoperatively, because the findings are consistent with the diagnosis of TDR. In all eight cases, celiotomy was performed because of positive findings on diagnostic peritoneal lavage. We believe that the chest radiologic findings determined retrospectively in these eight patients were either diagnostic or highly suggestive of TDR and cannot account for why the initial interpretations did not indicate this. Nonetheless, we believe these findings were obvious and therefore include them in our analysis of sensitivity of chest radiographs for diagnosing TDR. Thus, a total of 28 (64%) of the 44 patients had preoperative chest radiographs diagnostic of or strongly suggestive of TDR. Table 2 summarizes abnormal findings on chest radiographs in these 28 patients.

Retrospective review of the chest radiographs in the remaining 16 patients revealed six patients with radiographs suggestive of TDR. Left hemidiaphragmatic elevation ranged from 3 to 7 cm (average, 5.8 cm) above the right hemidiaphragm in these six patients, with five of the six showing possible but not definitive air-containing viscera in the chest. An obscured or disrupted outline of the left hemidiaphragm without elevation was present in an additional three patients. The chest radiograph was prospectively and retrospectively interpreted as normal in the seven other patients.

Ancillary diagnostic procedures were performed in eight patients and were helpful in confirming a diagnosis of TDR in five. Six of these eight patients had suggestive findings on

TABLE 2: Results of Diagnostic Imaging in 44 Patients with Ruptured Left Hemidiaphragm

Imaging Technique/Finding	Number of Cases
Diagnostic or suspicious chest radiograph	
Initial interpretation	20
Including retrospective review	28
Abnormal chest radiographs	
Elevated apparent hemidiaphragm <sup>a</sup>	27 (1–13 cm; mean, 6.1 cm; 61%)
Air-containing viscera in thorax	20 (45%)
Obscured or discontinuous diaphragm contour	17 (39%)
Mediastinal shift <sup>b</sup>	17 (1–4 cm; mean, 2.3 cm; 39%)
Elevated tip of nasogastric tube <sup>a</sup>	12 (1–5 cm; mean, 3 cm; 27%)
Ipsilateral rib fractures	12 (27%)
Ipsilateral pleural effusion	12 (27%)
Ipsilateral contusion/atelectasis	15 (36%)
Other imaging studies	
Fluoroscopy	1 (diagnostic)
Upper gastrointestinal series	2 (diagnostic)
Sonography	1 (nondiagnostic)
CT	6 (1 diagnostic, <sup>c</sup> 1 suspicious, <sup>d</sup> and 4 nondiagnostic)
MR	2 (diagnostic)

<sup>a</sup> Above level of dome of right hemidiaphragm.

<sup>b</sup> Shift of nasogastric tube to right of midline.

<sup>c</sup> Diagnostic in retrospect after MR performed.

<sup>d</sup> Confirmed as positive after MR performed.



chest radiographs, and two had normal chest radiographs, but positive DPL results. The procedures included fluoroscopy (one), upper gastrointestinal study (one), sonography (one), CT (six), and MR imaging (two) (Table 2). Fluoroscopy proved diagnostic of left hemidiaphragmatic rupture in the one patient in whom it was used. The upper gastrointestinal series also was diagnostic in both patients, showing a focal constriction of the stomach by the hemidiaphragm in one (Fig. 6) and marked elevation of the stomach in the other. Sonographic results in one patient were interpreted as negative for TDR. CT in one patient showed an air-fluid level at the left lung base with surrounding consolidation that was believed to be bowel or a traumatic lung cyst and was regarded as suggestive of TDR. Another patient's CT scan was initially interpreted as normal, but in retrospect revealed interruption of the left hemidiaphragm and herniation of omental fat into the thorax (Fig. 7A). CT scans in four other patients were nondiagnostic of TDR, showing only elevation of the hemidiaphragm in two. MR studies were performed in two patients and proved unequivocally diagnostic in both, showing interruption of the low-signal hemidiaphragm and herniation of bowel or omentum through the tear (Figs. 7B and 7C). The results of these ancillary procedures are summarized in Table 2.

Three patients had a preoperative diagnosis of TDR established by clinical means, including two with peritoneal lavage fluid draining through a thoracotomy tube and another with lung and omentum protruding through an open chest wound.

DPL was performed in 32 of these 44 patients, and results were positive in 26 (81%), 24 with hemoperitoneum and two

(noted above) with peritoneal lavage fluid draining through a thoracostomy tube. Fifteen patients (34%) who had had normal or minimally abnormal findings on chest radiographs underwent celiotomy for hemoperitoneum discovered at DPL. Of the 25 patients with preoperative diagnosis of TDR established by imaging methods, 14 also had DPL, the results of which were positive in nine patients and negative in five. Eleven of these patients did not undergo DPL. The remaining patient underwent celiotomy for severe abdominal pain and hemodynamic instability, but had negative findings on DPL.

Celiotomy revealed herniated abdominal organs in 19 (38%) of the patients with left-sided diaphragmatic rupture, including 11 with more than one herniated organ. The stomach was herniated in 11 patients, spleen in nine, colon in eight, omentum in four, and small bowel in four. All patients with abdominal viscera herniated into the thorax at surgery had the preoperative diagnosis established with chest radiographs or ancillary imaging investigations. The size of the diaphragmatic tear ranged from 2 to 20 cm with an average of 7.7 cm, and 75% of the ruptures were more than 5 cm long.

## Discussion

Traumatic rupture of the diaphragm may be due to penetrating or blunt trauma. Eighty-four percent of TDRs due to penetrating injury have a defect shorter than 2 cm, whereas diaphragmatic ruptures due to blunt trauma are more than 2 cm long, with the majority being over 10 cm long [3]. The diagnosis of TDR due to penetrating trauma is usually clinical,

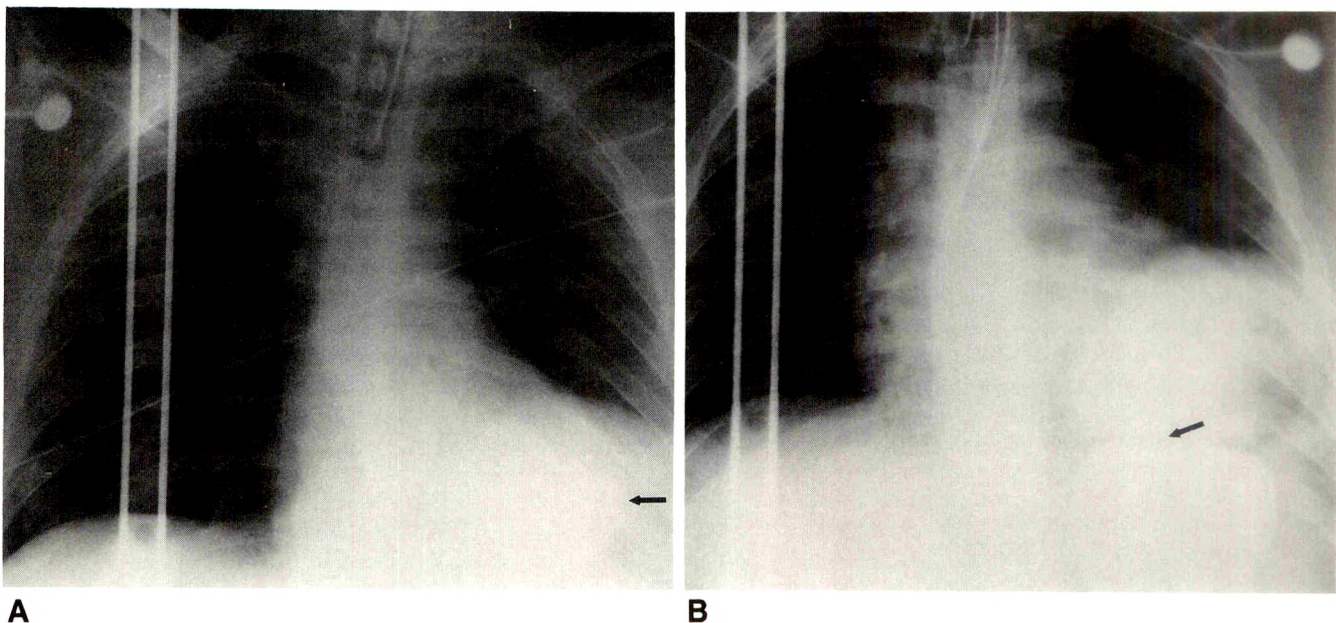


Fig. 6.—A, Chest radiograph reveals an apparently elevated left hemidiaphragm and a retrocardiac density suggestive of a fluid-filled gastric fundus (arrow). No mediastinal shift is present.

B, Upper gastrointestinal study verifies gastric fundus above left hemidiaphragm with a focal constriction at level of diaphragm (arrow). Surgery revealed a 6-cm laceration of left hemidiaphragm with gastric herniation.



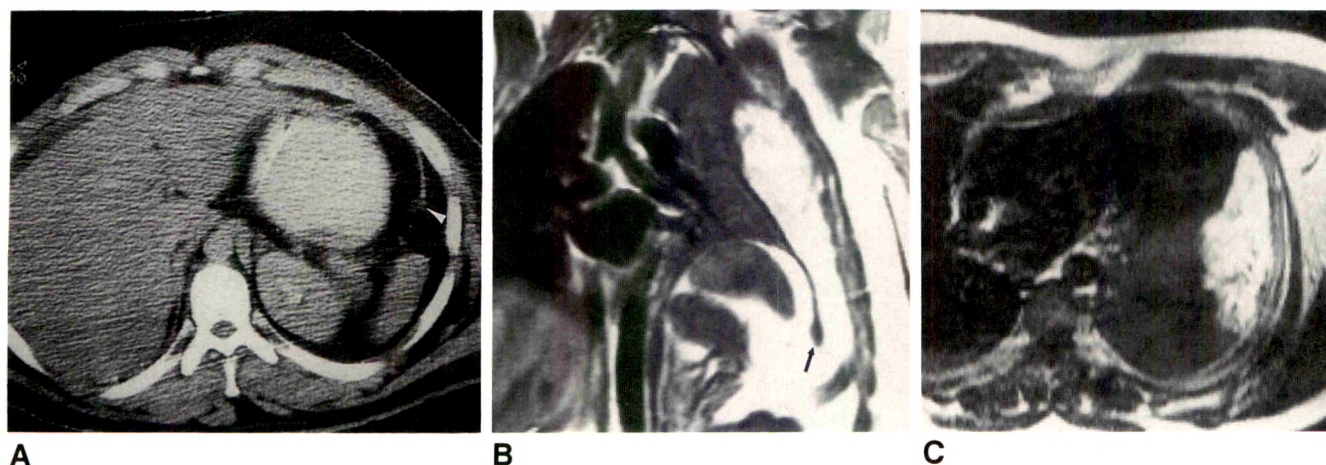


Fig. 7.—A, Axial CT scan at level of upper abdomen shows interruption of left hemidiaphragm (*arrowhead*), with fat present on both sides of diaphragm. Note small amount of perihepatic fluid. This injury was recognized after reviewing patient's MR images.  
B and C, Coronal (B) and axial (C) MR images with T1 weighting (SE 500/17) using cardiac and respiratory gating at 1.5 T. A defect in left hemidiaphragm is well shown on coronal image (*arrow*) with herniation of omental fat into thorax shown on both images. Lateral aspect of hemidiaphragm appears avulsed from thoracic wall. This was verified surgically.

relying on the entry site and direction of the wound, but TDR due to blunt trauma is much more difficult to diagnose [3].

Rupture of the hemidiaphragm is an uncommon injury occurring in from 0.8% to 1.6% of patients admitted with blunt force injury [5]. Left-sided hemidiaphragmatic injury predominates, probably because of the protective effect of the liver on the right hemidiaphragm and/or underdiagnosis of right-sided injuries [6, 7]. The clinical diagnosis of laceration of the hemidiaphragm with herniated viscera is difficult, but may be suggested by audible bowel sounds auscultated in the lower thorax, unilateral absence of breath sounds, respiratory distress, and/or a scaphoid abdomen [2, 8]. Often, bedside physical findings are masked by concurrent abnormalities, or these signs may be overlooked because of more apparent and life-threatening injuries in the acute posttrauma period. In our series of 50 patients with traumatic diaphragmatic rupture, 84% had severe multisystem injuries that demanded urgent treatment. The initial diagnosis of diaphragmatic injury after blunt trauma has been missed in from 7% to 66% of patients with multiple injuries [1–8]. Delayed presentation of diaphragmatic rupture with visceral herniation and strangulation is associated with higher morbidity and mortality rates than when the diagnosis is made and managed acutely [8].

Positive results of diagnostic peritoneal lavage may be helpful in suggesting the diagnosis of TDR, but this finding is nonspecific for site or severity of injury, and indiscriminate exploratory laparotomy based solely on the presence of a positive DPL results in an excessively high nontherapeutic laparotomy rate of up to 25% [9, 10]. In addition, DPL appears somewhat insensitive to the presence of a ruptured hemidiaphragm, as 21% (eight of 38) of our patients had false-negative DPL results. Of these, two showed lavage fluid draining from the thoracotomy tube, four showed the presence of bowel in the chest on plain radiographs, one had

diaphragmatic elevation of 8 cm, and one had positive findings on diagnostic pneumoperitoneum. Lack of sensitivity of DPL for injury to the hemidiaphragms has been reported by others [10].

Chest radiographs are the principal screening method for thoracic injury after blunt trauma [1, 3, 11, 12]. This study is often technically compromised by use of portable radiography units, supine projections, and limited patient cooperation [4]. Despite these limitations, chest radiographs are good screening images for detection of diaphragmatic injury. The preoperative diagnosis of TDR was made on the basis of chest radiographs in 20 (45%) of 44 patients with left-sided TDR and should have been made in an additional eight patients on the basis of our retrospective review. Thus, chest radiographs alone should have strongly suggested the diagnosis of TDR in 28 (64%) of 44 patients with left hemidiaphragmatic injury. Diagnostic or strongly suggestive findings include the definite presence of air-filled viscera or the tip of the nasogastric tube above the diaphragm, as well as a diaphragm that is "very elevated." A separate study to investigate the degree of diaphragmatic elevation that can occur in the patient with multiple traumas would be required to determine the upper limits of diaphragmatic elevation that can occur without TDR. Findings suggestive of TDR are elevation of the diaphragm not due to atelectasis, or obscuration of a nonelevated hemidiaphragm. Elevation of the hemidiaphragm was the most sensitive finding of diaphragmatic rupture, seen in 27 (61%) of 44 patients with left-sided TDR in our series, but is nonspecific in patients admitted with multiple system injuries because it also occurs in atelectasis and phrenic nerve paresis. The presence of air-containing viscera within the thorax was the most specific sign; it was diagnosed on chest radiographs in all cases in which herniation was proved surgically. As reported previously [6], the value of chest radiographs in diagnosing right-sided TDR is limited; they were diagnostic in



only one of six patients in our series and suggestive in one more. Both of these patients, however, had negative DPL results.

The benefits of serial chest radiographs have been reported [8, 12]. In our series, the progressive changes shown within 5 hr in five patients (11%) with left-sided TDR emphasizes the importance of repeating the chest radiograph before investigating further. Delayed or progressive visceral herniation through a diaphragmatic rent may result from the constant negative intrapleural pressure pulling on mobile abdominal viscera [12, 13]. The appearance of delayed herniation might thus be anticipated after patients with ruptured hemidiaphragms are removed from positive-pressure ventilatory support [13].

Other imaging methods that have been reported to be of value in evaluating the diaphragm include radiographs after nasogastric tube placement [14], fluoroscopy [6], upper and lower gastrointestinal contrast examination [15, 16], sonography [17, 18], CT [19, 20], MR imaging [21], contrast or air peritoneography [22], and liver-spleen scintigraphy [12]. The success of these imaging techniques depends largely on the demonstration of herniated abdominal contents, rather than a direct evaluation of the diaphragmatic tear. In our series, visceral herniation was found at surgery at 19 (43%) of the left-sided TDRs, which concurs with a previous report of 32% [13].

Fluoroscopy [6] and upper gastrointestinal contrast examinations [16, 17] have been reported to be useful in evaluating abnormal diaphragmatic motion and gastric herniation and were diagnostic in the three cases of left-sided TDR in which they were used.

The use of sonography for diagnosing TDR has been reported [17, 18], but is limited by subcutaneous emphysema, chest wall and abdominal pain, overlying bandages, and the presence of gas in stomach and splenic flexure. Sonographic performance is also highly operator-dependent. Although attempted only twice in our series, sonography was false-negative in both cases.

CT of the diaphragm has been reported to be useful in assessing for TDR [19, 20], but direct imaging is only available in the axial orientation, and superimposed effusions, atelectasis, and traumatic lung cysts can cause diagnostic confusion. In our series, CT was performed in seven patients with TDR and was interpreted as suggestive of the diagnosis in only one (14%), highlighting the limitations of CT in evaluating diaphragmatic abnormality.

MR evaluation of diaphragmatic injury also has been described [21]. The major advantages of MR over CT are the capacity for direct coronal and sagittal imaging, as well as direct visualization of the low-signal-intensity diaphragm. MR was unequivocally diagnostic for TDR in both patients in whom it was performed after nondiagnostic CT. One patient's CT scan was retrospectively interpreted as positive after obtaining the MR study, and the other CT was interpreted as suggestive, but not diagnostic, before the MR result.

In summary, our study indicates a sensitivity of 64% of initial and delayed chest radiographs in the diagnosis or

suggestion of diaphragmatic injury on the left side and 17% on the right side. We suggest that a second plain chest radiograph be obtained within 6 hr of the initial film in patients in whom the diagnosis is in doubt. Although used in a limited fashion, MR appears to be more accurate than CT in evaluating the diaphragm if serial chest radiographs and contrast opacification of the stomach are not diagnostic of TDR. As noted previously, many patients with rupture of the hemidiaphragms display normal or minimally abnormal imaging findings, and the rupture must be detected by clinical findings supplemented by diagnostic peritoneal lavage.

## REFERENCES

1. Shulman HS, Samuels TH. The radiology of blunt chest trauma. *J Can Assoc Radiol* **1983**;34:204-217
2. Hood RM. Traumatic diaphragmatic hernia. *Ann Thorac Surg* **1971**;12:311-324
3. Wise L, Connors J, Hwang YH, Anderson C. Traumatic injuries to the diaphragm. *J Trauma* **1973**;13:946-950
4. Wiencek RG, Wilson RF, Steiger Z. Acute injuries of the diaphragm: an analysis of 165 cases. *J Thorac Cardiovasc Surg* **1986**;92:989-993
5. Kearney PA, Rouhana SW, Burney RE. Blunt rupture of the diaphragm: mechanism, diagnosis and treatment. *Ann Emerg Med* **1989**;18:1326-1330
6. Estrera AS, Landay MJ, McClelland RN. Blunt traumatic rupture of the right hemidiaphragm: experience in 12 patients. *Ann Thorac Surg* **1985**;39:525-530
7. Hill LD. Injuries of the diaphragm following blunt trauma. *Surg Clin North Am* **1972**;52:611-624
8. Gourin A, Garzon AA. Diagnostic problems in traumatic diaphragmatic hernia. *J Trauma* **1974**;14:20-31
9. Haney PJ, Whitley NO, Brotman S, Cunant JS, Whitley J. Liver injury and complications in the post-operative trauma patient: CT evaluation. *AJR* **1982**;139:271-275
10. Freeman T, Fischer RP. The inadequacy of peritoneal lavage in diagnosing acute diaphragmatic injury. *J Trauma* **1976**;16:538-542
11. Aronoff RJ, Reynolds J, Thal ER. Evaluation of diaphragmatic injuries. *Am J Surg* **1982**;144:671-674
12. Estrera AS, Platt MR, Mills LJ. Traumatic injuries of the diaphragm. *Chest* **1979**;75:306-313
13. Rodriguez-Morales G, Rodriguez A, Shatney CH. Acute rupture of the diaphragm in blunt trauma: analysis of 60 patients. *J Trauma* **1986**;26:438-444
14. Perlman SJ, Rogers LF, Mintzer RA, Mueller CF. Abnormal course of nasogastric tube in traumatic rupture of left hemidiaphragm. *AJR* **1984**;142:85-88
15. Ball T, McCrory R, Smith JO, Clements JL Jr. Traumatic diaphragmatic hernias: errors in diagnosis. *AJR* **1982**;138:633-637
16. Fataar S, Schulman A. Diagnosis of diaphragmatic tears. *Br J Radiol* **1979**;52:375-381
17. Rao KG, Woodlief RM. Grey scale ultrasonic demonstration of ruptured right hemidiaphragm. *Br J Radiol* **1980**;53:812-814
18. Ammann AM, Brewer WH, Maull KI, Walsh JW. Traumatic rupture of the diaphragm: real time sonographic diagnosis. *AJR* **1983**;140:915-916
19. Heiberg E, Wolverson MK, Hurd RN, Jagannadharao B, Sundaram M. Case report: CT recognition of traumatic rupture of the diaphragm. *AJR* **1980**;135:369-372
20. Gurney J, Harrison WL, Anderson JC. Omental fat simulating pleural fluid in traumatic diaphragmatic hernia: CT characteristics. *J Comput Assist Tomogr* **1985**;9:1112-1114
21. Mirvis SE, Keramati B, Buckman R, Rodriguez A. MR Imaging of traumatic diaphragmatic rupture. *J Comput Assist Tomogr* **1988**;12:147-149
22. Efron G, Hyde I. Nonpenetrating traumatic rupture of the diaphragm. *Clin Radiol* **1967**;18:394-398



## Book Review



**Review of Radiology.** By the faculty of Duke University Medical Center, Department of Radiology. Edited by Carl E. Ravin and Cirrelda Cooper. Philadelphia: Saunders, 360 pp., 1990. \$35

This book was first conceived as the syllabus for the Duke University radiology review course, intended for both residents and practicing radiologists. It can be described as an annotated "gamuts," providing in outline form a framework for organizing and reviewing basic facts and concepts. This is an entirely different work from the abbreviated basic science textbooks favored by students (and frowned on by professors) that many will remember from medical school. Complex, involved subjects are summarized in three or four sentences. Subtleties and unusual manifestations of disease are by necessity ignored.

The material is divided into traditional categories of anatomy, pathology, and imaging. Tables of different diagnoses alternate with brief descriptive entries. Short reference lists are interspersed. No radiographs are provided; a few line drawings are. The book has a remarkable uniformity, cohesiveness, and clarity, especially for a work written by more than one author. A cogent discussion of reactions to

contrast media, including prophylaxis and treatment regimens, is particularly welcome.

The work succeeds on its own terms, but it is by no stretch of the imagination a substitute for general and subspecialty texts. Radiology residents at all levels of training will find it useful both as an aide-mémoire and as an indicator of what information, at an absolute minimum, needs to be mastered, particularly for review purposes for board examinations. Those who teach residents and medical students will find the work of value in organizing their lectures also. Other practicing radiologists will find the work less useful.

I personally know of no other similar general radiology review syllabus. Certainly this one can be recommended as a study guide for residents, to be used with the standard texts.

J. Eric Blum  
*Akron City Hospital*  
*Akron, OH 44309*



## Present Status of Residency Training in Mammography

Lawrence W. Bassett<sup>1</sup>  
Christopher I. Cassady  
Richard H. Gold

We conducted a telephone interview of all 207 accredited diagnostic radiology residency training programs listed in the American Medical Association's *Directory of Graduate Medical Education Programs*. Resident training in mammography was offered in 206 programs, and 35% of the programs had initiated this training within the past 3 years. Residents had an assigned block of time to do mammography in 84% of the programs. Of the 206 programs, 40% had rotations devoted exclusively to mammography, with 82% of the exclusive rotations lasting from 4 to 8 weeks. Residents were performing localization procedures in 91% of the programs and dictating cases in 81%. A distinction was made between screening and diagnostic examinations by 35% of the training institutions, at least in terms of the fee for the examination. Radiologists who devoted at least half of their practice to mammography taught in 52% of the programs. The American College of Radiology has granted accreditation in mammography to 29% of the programs.

Although almost all accredited residency training programs offer training in mammography, there are some deficiencies in this training. More residents need to gain the experience of dictating mammography reports and need to learn about the distinctions between screening and diagnostic mammography. Despite the anticipated deluge of screening examinations in the next decade, there were only 17 fellowships that included at least 6 months of mammography identified in 15 (7%) of the institutions; only 11 of these were full-time 1-year breast imaging fellowships.

*AJR* 156:59-62, January 1991

Mammography is burgeoning in almost every radiology practice [1]. Nevertheless, in 1987, more than 60% of American women older than 40 had never had a mammogram [2]. The National Cancer Institute has a goal of 80% use of mammography by eligible women by the year 2000 [3], and physicians with primary care responsibilities have progressively increased their referrals for screening mammography [4]. Training radiology residents to be proficient in mammography is an important challenge [5]. A 1980 survey revealed that radiology residency programs were providing insufficient training in mammography, and few had rotations devoted exclusively to mammography [6]. We undertook a telephone survey of all accredited radiology residency training programs to evaluate current mammography training.

### Methods

All 207 diagnostic radiology residency programs listed in the American Medical Association's *Directory of Graduate Medical Education Programs* [7] were surveyed. Between October 1989 and February 1990, one of the authors, working under the direct supervision of an experienced mammographer, spoke by telephone with a chief resident (189), training program director (12), or another faculty member (six) when chief residents or training directors were unavailable or unable to provide the requested information. Briefly, the following information was obtained: (1) whether training in mammography was offered; (2) the time assigned for

Received May 24, 1990; accepted after revision July 31, 1990.

Presented at the annual meeting of the American Roentgen Ray Society, Washington, D.C., May 1990.

<sup>1</sup> All authors: Iris Cantor Center for Breast Imaging at UCLA Medical Center, Department of Radiological Sciences, and the Jonsson Comprehensive Cancer Center, UCLA School of Medicine, Los Angeles, CA 90024. Address reprint requests to L. W. Bassett.

0361-803X/91/1561-0059  
©American Roentgen Ray Society



such training; (3) whether there was a formal rotation (a defined block of time) and, if so, whether it was devoted exclusively to mammography; (4) if the rotation was required; (5) the resident's role in the mammography section; (6) the type of mammography done; (7) whether a distinction was made between diagnostic and screening examinations at the institution (an affirmative response required at least a differentiation in fees for the two examinations); (8) whether the radiologists teaching mammography dedicated at least half of their practices to mammography; and (9) the availability of any full-time fellowships in breast imaging. We also identified the number of training programs that were accredited by the American College of Radiology (ACR) Mammography Accreditation Program as of March 7, 1990.

## Results

All 207 accredited residency training programs completed the telephone interview. Of these, 206 indicated that they offered some training in mammography: 19 (9%) had instituted mammography training within the last year, 72 (35%) instituted it within the past 3 years, and 134 (65%) had offered it for at least 4 years. Of the 206 programs that offered mammography training for residents, 173 (84%) had formal rotations with a defined period of time assigned to mammography, and 40% had rotations devoted exclusively to mammography (Table 1). Of the exclusive rotations, 82% lasted 4–8 weeks during the 4 years of residency training. In 44% of programs, mammography was combined with other radiology subspecialties: genitourinary (23%), chest (21%), bone (8%), sonography (8%), and others less frequently. Residents performed needle localizations in 91% of the programs and dictated the mammography reports in 81%. Film-screen mammography was used exclusively in 85% of the programs, both film-screen and xeromammography were used in 13%, and xeromammography was used exclusively in 2%. It was the practice to distinguish between screening and diagnostic examinations in 72 (35%) of the training programs. There were 217 radiologists at 107 (52%) of the training programs who dedicated at least half of their time to mammography. Our survey identified 17 fellowship positions with at least 6 months full-time in mammography offered at 15 (7%) of the training programs. Only 11 of these fellowships were devoted

exclusively to mammography for 1 year. Of the 206 training programs, 58 (29%) were accredited in mammography by the ACR.

Table 1 compares programs with rotations devoted exclusively to mammography with those combined with another subspecialty and with those with no formal rotation in mammography. Table 2 compares some aspects of the training programs found at university and nonuniversity facilities. A university facility was defined as one listed directly under the title of a university program in the *Directory of Graduate Medical Education Programs*; this would include the participating institutions at which the residents receive a significant portion of their training [7]. Table 3 compares institutions that perform more than 150,000 imaging examinations per year with those that perform fewer than 150,000.

## Discussion

In 1967 the ACR acknowledged that "mammography is here to stay and, with continued refinements in the technique and further improvements in the films and x-ray equipment, it will become a routine radiological procedure in the management of breast cancer" [8]. That year the ACR, working with the Cancer Control Branch of the U.S. Public Health Service, developed an extensive program for training in mammography for practicing radiologists and residents in radiology. Since then, the breadth of knowledge required to practice mammography has steadily increased. This includes knowledge that allows direct supervision of technical factors and meticulous image interpretation, knowledge to perform unique special procedures, such as prebiopsy needle localization, cyst aspiration and ductography, and knowledge of sonography, clinical correlation, epidemiology of breast cancer, and related socioeconomic issues.

Breast cancer is a relatively common disease with highly emotional implications, and mammography gets considerable attention from the news media, particularly when national figures, such as Mrs. Reagan, have breast cancer detected by mammography. Hence, the public and referring physicians have become increasingly aware of mammography and they expect it to be expertly rendered. For these reasons, and because of unreasonable expectations as well, medicolegal actions relating to mammography have burgeoned. A perception that residency training programs are not providing sufficient training in mammography has been stimulated by published data indicating that some training programs provided no exposure to mammography, and only a few programs had rotations devoted exclusively to mammography [6]. Additional pressure for more effective training of radiology residents in mammography comes from anticipated competition with non-radiologist physicians who believe that they should add mammography to the diagnostic procedures they offer [9]. This is another reason that our residents should be prepared to offer the most expert performance and interpretation of the examination.

Our telephone survey disclosed that all but one of the 207 programs offered some training in mammography, and in 35% this training had been initiated within the past 3 years. We

**TABLE 1: Description of Mammography Training in 206 (%) Programs**

Training	Type of Training		
	Exclusive Rotation	Combined Rotation	No Formal Rotation
Number	82 (39.8)	91 (44.2)	33 (16.0)
Duration (weeks)			
<4	5 (6.1)	1 (1.1)	0 (0.0)
4	44 (53.7)	17 (18.7)	1 (3.0)
4–8	23 (28.0)	20 (22.0)	0 (0.0)
>8	10 (12.2)	53 (58.2)	32 (97.0)
Residents dictate cases	68 (82.9)	72 (79.1)	26 (78.8)
Differentiate screening	35 (42.7)	32 (35.2)	9 (27.3)
Dedicated faculty	55 (67.1)	40 (44.0)	10 (30.3)
Fellowships offered <sup>a</sup>	12 (14.6)	3 (3.3)	0 (0.0)

<sup>a</sup> At least 6 months devoted exclusively to mammography.



**TABLE 2: Mammography Training in 206 (%) Programs: University vs Nonuniversity**

Training	All Programs	University (107)	Nonuniversity (99)	<i>p</i> <sup>a</sup>
No. with formal rotations	173 (84.0)	90 (84.1)	83 (83.8)	.960
Exclusively mammography	82 (39.8)	44 (41.1)	34 (34.3)	.320
Residents dictate cases	166 (80.6)	93 (86.9)	73 (73.7)	.002
Differentiate screening	72 (35.0)	44 (41.1)	28 (28.3)	.054
Dedicated faculty	107 (51.9)	69 (64.5)	38 (38.4)	<.001
Fellowships offered	15 (7.2)	12 (11.2)	3 (3.0)	.024
ACR accreditation <sup>b</sup>	59 (28.6)	33 (30.8)	26 (26.3)	.480

<sup>a</sup> *p* < .05 is statistically significant.<sup>b</sup> ACR = American College of Radiology.**TABLE 3: Mammography Training in 206 (%) Programs: ≥150,000 Examinations vs <150,000 Examinations Performed**

Training	All Programs	≥ 150,000 Exams (97)	< 150,000 Exams (109)	<i>p</i> <sup>a</sup>
No. with formal rotations	173 (84.0)	87 (89.7)	86 (78.9)	.036
Exclusive rotations	82 (39.8)	49 (50.5)	33 (30.3)	.003
Residents dictate cases	166 (80.6)	80 (82.5)	86 (78.9)	.520
Differentiate screening	72 (35.0)	35 (36.1)	37 (33.9)	.760
Dedicated faculty	107 (51.9)	67 (69.1)	40 (36.7)	<.001
Fellowships offered	15 (7.2)	12 (12.4)	3 (2.8)	.008

<sup>a</sup> *p* < .05 is statistically significant.

found that 40% of the training programs had rotations devoted exclusively to mammography, compared with 13% in 1980 [6]. Exclusive rotations were more likely to be found in programs located at institutions doing more than 150,000 radiologic examinations per year. In 44% of programs, the mammography rotation is combined with other subspecialties, most often genitourinary radiology (23%) or chest radiology (21%). Residents performed prebiopsy needle localizations in 91% of programs, but they were directly involved in the dictation of mammography reports in only 81%. Mammography training was optional in 11% of programs.

Many investigators have emphasized the importance of differentiating screening from diagnostic, problem-solving mammography. This type of distinction makes it possible for radiologists to make screening mammography a less expensive, faster, and more convenient procedure, particularly when it is performed in a facility dedicated to screening mammography [10, 11]. These steps can remove major barriers to mammography screening, including its relatively high cost [12] and a perception among many women that it is inconvenient [13]. Although some radiologists fear that this type of distinction leads to a double standard of care [14], other radiologists see the provision of reasonably priced screening as a benefit to society [15]. The Human Resources Division of the U.S. General Accounting Office (GAO) has reported that low-cost screening mammography services do not necessarily compromise the quality of the examination [16]. In fact, the GAO study found no relationship between the price charged for screening mammography and adherence to quality standards. In order to determine whether residents were gaining experience in screening mammography, we asked whether a distinction was made between the two types of examinations. There are many ways in which screening

and diagnostic examinations can differ, and in this survey we determined that a facility had to at least have a two-tiered fee system in order to qualify as distinguishing between screening and diagnostic mammography. This type of distinction was a policy in 52% of the programs, and in all of those programs the residents had training in both types of examinations.

As in other radiologic specialties [17], dedicated mammographers as teachers in academic institutions are in short supply. Only 52% of teaching institutions have radiologists who do mammography at least 50% of the time. Dedicated mammographers also are not being trained in large numbers in our residency training programs. Only 15 institutions offered fellowships that included at least 6 months dedicated to training in breast imaging, a number that has not increased since 1988 [18]. Only 11 full-time 1-year fellowships in breast imaging were available. This raises concern over our ability to meet the challenge of expert performance and interpretation of the rapidly expanding volume of mammography examinations. If training programs, radiology practices, and graduating residents are not willing to commit to the concept of full-time careers in mammography, it may become necessary to foster fellowships that combine mammography with another subspecialty. Another alternative, which may already be in effect in some programs, would be to offer a residency track wherein all elective time is devoted to mammography.

Several quality assurance problems relate to mammography. For example, problems in quality assurance related to the use of faulty equipment have been reported [19]. In addition, incorrect interpretation may result in missed cancers and lost opportunity for cure [20], whereas overreading creates anxiety and the time, trouble, added costs, and morbidity of unnecessary or avoidable biopsies [21, 22]. A perception that large numbers of unnecessary biopsies result from



screening mammography is cited as a barrier to its use [23]. Concerns over suboptimal quality control, technical performance, and interpretation have led the ACR to develop a Mammography Accreditation Program, which provides a means for referring physicians and patients to be sure that a facility meets minimal standards [24, 25]. As of March 1990, 29% of residency training programs in our survey had received ACR accreditation in mammography, a rate that is higher than the current estimate of 18% for all mammography facilities nationwide (Hendrick RE, personal communication). Of the radiology facilities that have applied for ACR accreditation, 29% have failed to be accredited in their first attempt [25]. The majority of failures have been due to poor image quality, and a smaller number to unacceptably high radiation dose. The accreditation process has revealed a wide range of image quality and doses in the practice of mammography, and these variations are attributed to a lack of standardized quality control procedures in the United States [25, 26]. As residents are expected to emulate the practices they encounter during their training, it is extremely important that training programs meet the requirements for ACR accreditation, complete the accreditation process, and train residents in quality control procedures.

This year, for the first time, mammography was included as a separate category in the oral examination of the American Board of Radiology. A preliminary analysis of the results indicates that residents' performance was consonant with that in other segments of the examination (Dodd GD, personal communication). This suggests that a satisfactory level of instruction is being achieved in most residency training programs. The inclusion of mammography in the oral examination underscores the increasing importance of mammography in radiologic practice and is expected to be a major impetus for improving training in mammography.

#### ACKNOWLEDGMENTS

We thank Gil Fine of the Department of Biostatistics, UCLA School of Public Health, for his statistical support.

#### REFERENCES

- Hall FM. Screening mammography: potential problems on the horizon. *N Engl J Med* 1986;314:53-55
- Center for Disease Control. Provisional estimates from the National Health Interview Survey, supplement on cancer control, United States, January-March 1987. *MMWR* 1988;37:417-420, 425
- National Cancer Institute. *Cancer control objectives for the nation: 1985-2000*. Bethesda, MD: US Department of Health and Human Services, Public Health Service, 1986; DHSS Publication No. (NIH) 86-2880. (NCI Monograph No. 2)
- American Cancer Society. 1989 survey of physician's attitudes and practices in early cancer detection. *CA* 1990;40:77-101
- McLelland R. Mammography 1984: challenge to radiology. *AJR* 1984;143:1-4
- Homer MJ. Mammography training in diagnostic radiology residency programs. *Radiology* 1980;135:529-531
- Directory of Graduate Medical Education Programs, 1989-1990. Chicago: American Medical Association, 1989
- Scott WG. Mammography and the training program of the American College of Radiology. *AJR* 1967;99:1002-1008
- Gleicher N. Breast disease programs in obstetrics and gynecology: a plea for training in mammography. *Am J Obstet Gynecol* 1989;161:267-270
- Sickles EA, Weber WN, Galvin HB, Ominsky SH, Solitto RA. Mammographic screening: how to operate successfully at low cost. *Radiology* 1986;160:95-97
- Bird RE, McLelland R. How to initiate and operate a low-cost screening mammography center. *Radiology* 1986;161:43-47
- American Cancer Society. Survey of physician's attitudes and practices in early cancer detection. *CA* 1985;35:197-213
- Rimer BK, Keintz MK, Kessler HB, Engstrom PF, Rosan JR. Why women resist screening mammography: patient-related barriers. *Radiology* 1989;172:243-246
- Robinson HM. A double standard of care in mammography? *ACR Bull* 1990;46:10
- Brenner RJ. High quality care despite differences in breast imaging. *ACR Bull* 1990;46:11
- United States General Accounting Office. *Screening mammography: low-cost services do not compromise quality*. Washington, DC: GAO Report HRD-90-32, January 1990
- Steiner RM, Rockoff SD, Stitik FP, et al. The current state of residency and fellowship training programs in pulmonary and cardiac radiology. *AJR* 1987;148:1081-1085
- Dunnick NR. Radiology residency training programs: current status. *Radiology* 1988;169:549-552
- Sienko DG, Osuch JR, Camburn JF. The need for quality assurance in mammography. *N Engl J Med* 1989;320:941
- Mann BD, Bassett LW, Giuliano AE. Delayed diagnosis as a result of normal mammograms. *Arch Surg* 1983;118:23-24
- Hall FM, Storella JM, Silverstone DZ, Wyshak G. Nonpalpable breast lesions: recommendations for biopsy based on suspicion of carcinoma at mammography. *Radiology* 1988;167:353-358
- Brenner RJ, Sickles EA. Acceptability of periodic follow-up as an alternative to biopsy for mammographically detected lesions interpreted as probably benign. *Radiology* 1989;171:645-646
- Howard J. Using mammography for cancer control: an unrealized potential. *CA* 1987;33:33-48
- Kaplan AS, Wollerton MA, Rachlin JA. Selecting a screening mammography facility. *Am Fam Physician* 1988;38:143-147
- Hendrick RE. Quality control in mammography: the American College of Radiology's Mammography Screening Accreditation Program. *Curr Opin Radiol* 1980;1:203
- Galkin BM, Feig SA, Muir HD. The technical quality of mammography in centers participating in a regional breast cancer awareness program. *RadioGraphics* 1988;8:133-145



## Pictorial Essay

# Endoscopic Sonography of the Upper Gastrointestinal Tract

Jose F. Botet<sup>1</sup> and Charles Lightdale<sup>2</sup>

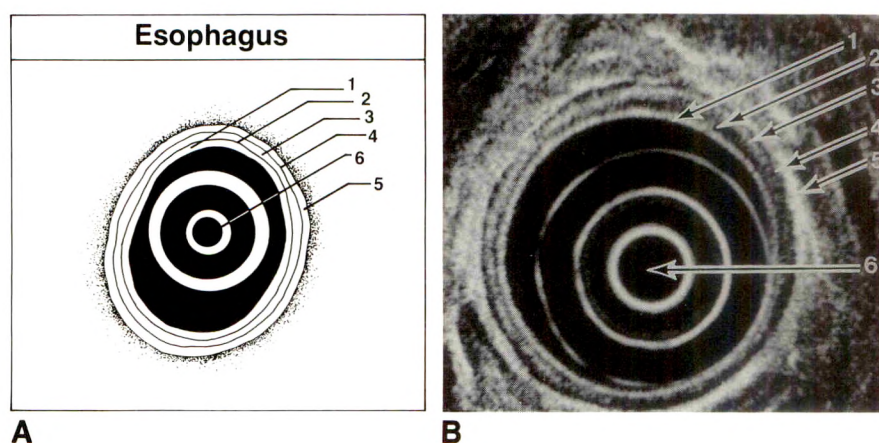
Endoscopic sonography was used to examine the upper gastrointestinal tract of 550 patients referred for evaluation of abnormal findings seen on conventional endoscopy, upper gastrointestinal series, and CT. This essay illustrates the potential uses and limitations of this technique. Special emphasis has been given to the use of landmarks to facilitate orientation of the transducer in both the esophagus and stomach. Specific examples demonstrate involvement of individual layers of the bowel wall in both benign and malignant processes. It is stressed that this is a combined procedure requiring both an endoscopist and a radiologist. Endoscopic sonography is a valuable new technology with substantial potential in the evaluation of the upper gastrointestinal tract.

Endoscopic sonography is a relatively new technique that combines the advantages of direct endoscopic visualization of the bowel wall with the capabilities of high-frequency sonography to visualize the layers of the bowel wall and the immediately surrounding spaces. The direct contact of the transducer with the bowel wall via a water-filled balloon in the esophagus or water filling the stomach makes it possible to circumvent the problem air presents with the use of sonography. Some of the earliest work in this field was done by Di Magno et al. [1], who published their preliminary experiences in 1980.

Fig. 1.—Endoscopic sonography of esophageal wall.

A, Diagram shows five-layered structure as depicted by endoscopic sonography. 1 = mucosal interface, highly echogenic; 2 = muscularis mucosa, hypoechoic; 3 = submucosa, highly echogenic; 4 = lamina propria, hypoechoic; 5 = adventitial interface, highly echogenic; 6 = transducer with inflated balloon.

B, Actual cross-sectional image of esophagus as visualized with endoscopic sonography (12-MHz transducer).



Received January 31, 1990; accepted after revision July 9, 1990.

Presented in part as an exhibit at the annual meeting of the American Roentgen Ray Society, New Orleans, LA, May 1989.

<sup>1</sup> Department of Medical Imaging, Memorial Sloan-Kettering Cancer Center, New York, NY 10021. Address reprint requests to J. F. Botet.

<sup>2</sup> Department of Medicine, Gastroenterology Service, Memorial Sloan-Kettering Cancer Center, New York, NY 10021.



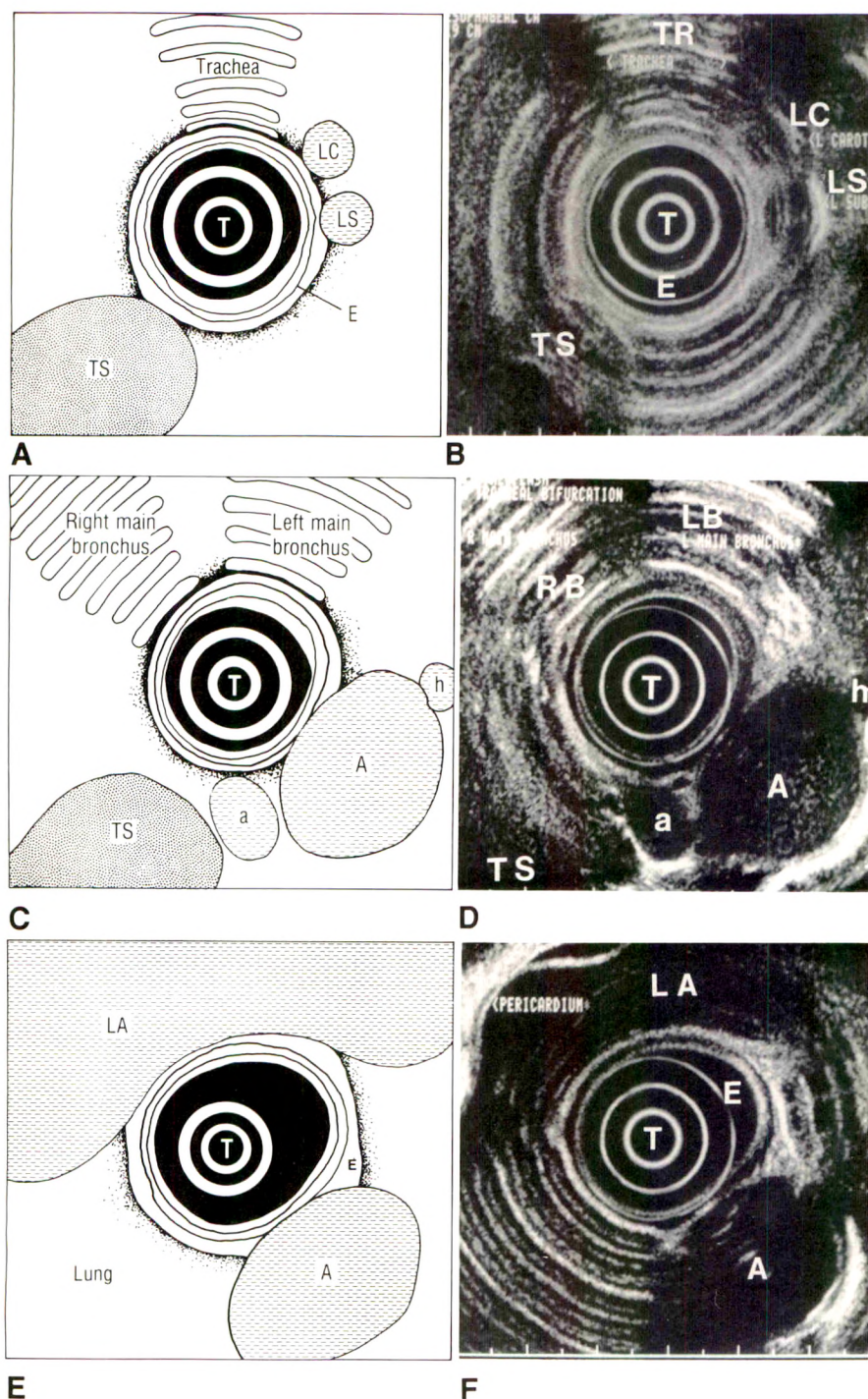


Fig. 2.—Endoscopic sonography of normal esophagus (E) with 12-MHz transducer (T).

A and B, Diagram (A) and sonogram (B) of upper portion of esophagus. Trachea (TR) is anterior; upper thoracic spine (TS) is posterior. LC = left carotid artery, LS = left subclavian artery.

C and D, Diagram (C) and sonogram (D) of middle portion of esophagus. Section just below carina shows both right (RB) and left (LB) main bronchi. Note elongation of aorta (A) at beginning of aortic arch; two hypoechoic vascular structures at both sides of aorta are azygous (a) and hemiazygous (h) veins.

E and F, Diagram (E) and sonogram (F) of lower portion of esophagus (E). Note close relationship of lower esophagus with left atrium (LA) anteriorly; aorta (A) lies posteriorly.

### Technique

The instrument used is a side-viewing endoscope measuring 13 mm in diameter, with a sonographic transducer at its tip. Two models are currently available, EU-M2 and EU-M3 (Olympus Corp., New Hyde Park, NY). The frequencies used are 7.5 MHz (EU-M2) and both 7.5 and 12 MHz (EU-M3). These mechanical probes provide real-time images with a 180° or 360° field of view orthogonal to the plane of the

endoscope. Depth of view is a maximum of a 7-cm radius with the 7.5-MHz transducer and a 3-cm radius with the 12-MHz transducer.

The procedures were performed by an endoscopist and a radiologist. The endoscopist introduced and manipulated the endoscope while the radiologist interpreted the images and guided the endoscopist in the positioning of the sonographic transducer.



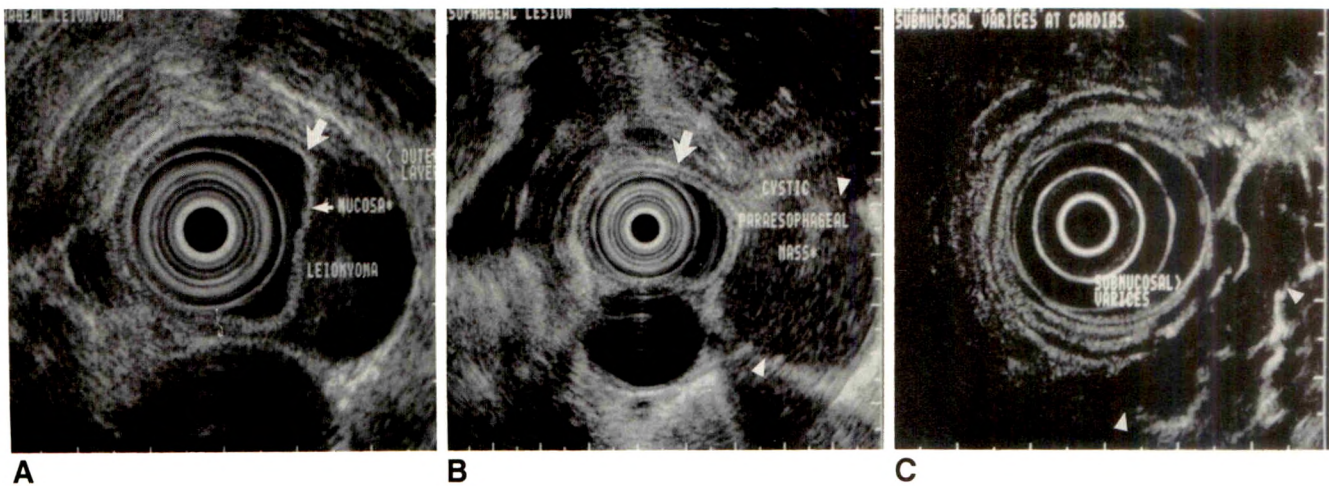


Fig. 3.—Endoscopic sonography of benign conditions of esophagus with 7.5-MHz transducer.  
**A**, Leiomyoma. Characteristic hypoechoic lesion arising from muscularis mucosa (large arrow). Overlying mucosa (small arrow) is intact.  
**B**, Duplication cyst. These usually hypoechoic lesions (arrowheads) may be differentiated from leiomyomas by their location outside of normal five-layered esophageal wall (arrow).  
**C**, Varices. Submucosal nature of esophageal varices (arrowheads) is not well demonstrated by endosonography because of compression by distended balloon. Extramural component at level of cardia appears as echo-free rounded structures.

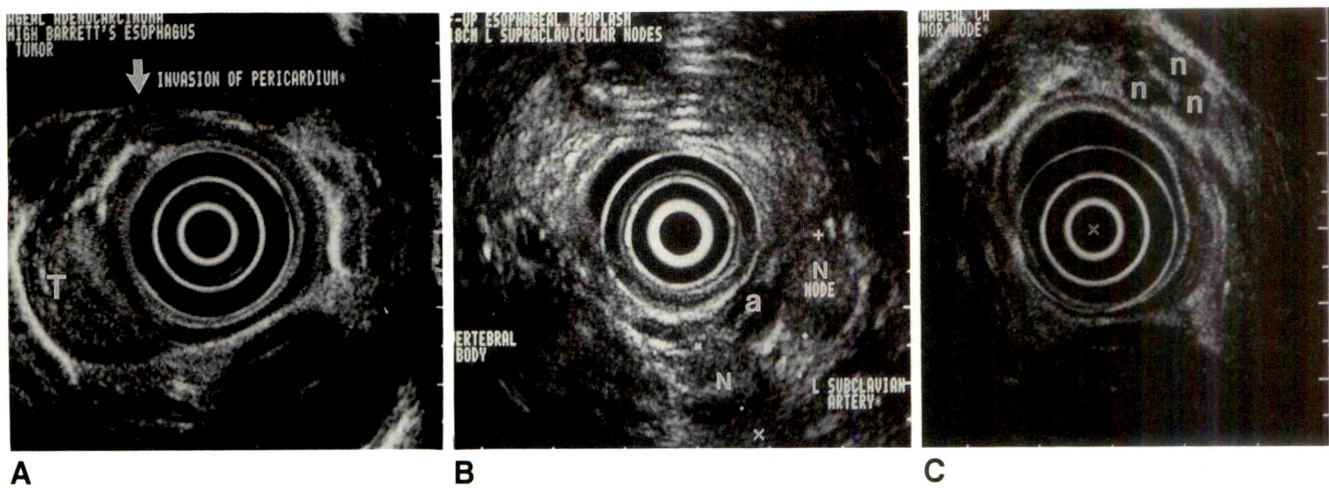


Fig. 4.—Endoscopic sonography of malignant processes.  
**A**, Tumor (12-MHz transducer). T4 tumor (T) of lower esophagus has invaded pericardium. Discontinuity in pericardial fat (arrow) was confirmed at surgery.  
**B**, Nodes (7.5-MHz transducer). Two 1.4-cm nodes (N) surround left subclavian artery (a). Although larger than 1 cm, they appear hyperechoic; they were found to be reactive at surgery.  
**C**, Small nodes (12-MHz transducer). Multiple small (4–6 mm) subcarinal nodes (n) with rounded and relatively low-level internal echoes were found to be involved by tumor at surgery.

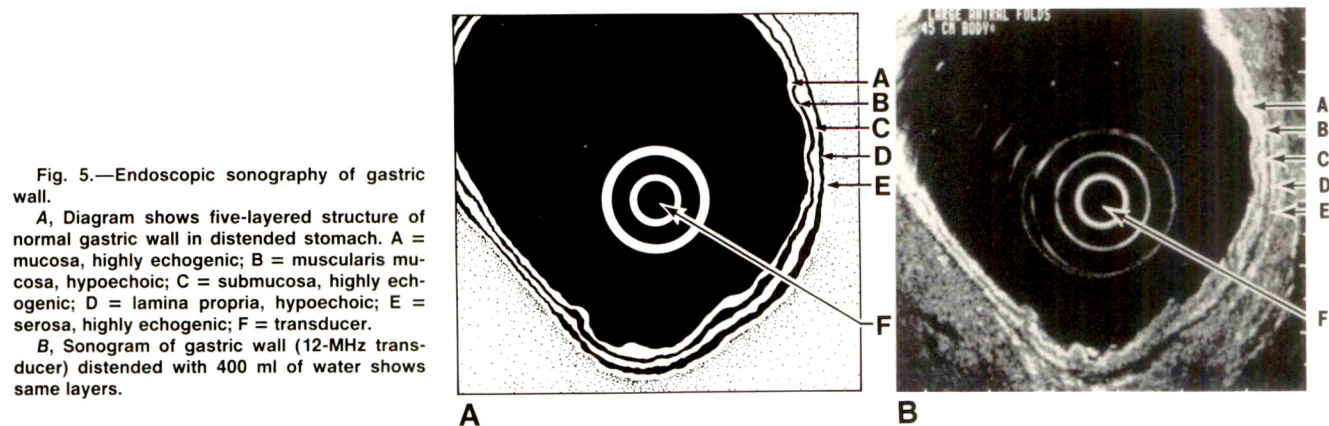


Fig. 5.—Endoscopic sonography of gastric wall.  
**A**, Diagram shows five-layered structure of normal gastric wall in distended stomach. A = mucosa, highly echogenic; B = muscularis mucosa, hypoechoic; C = submucosa, highly echogenic; D = lamina propria, hypoechoic; E = serosa, highly echogenic; F = transducer.  
**B**, Sonogram of gastric wall (12-MHz transducer) distended with 400 ml of water shows same layers.



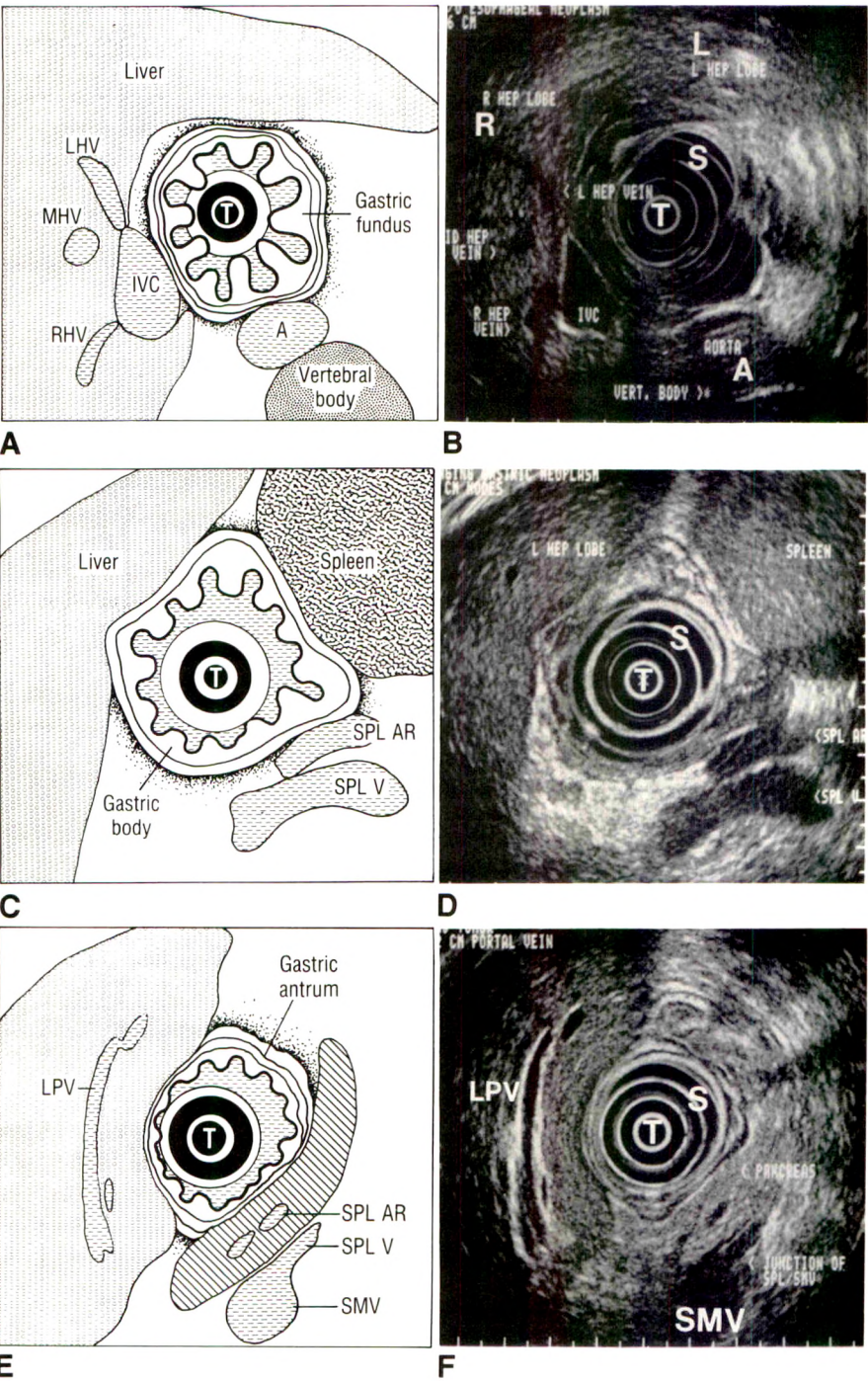


Fig. 6.—Endoscopic sonography of normal stomach with 7.5-MHz transducer (T).  
A and B, Diagram (A) and sonogram (B) of fundus. Left hepatic lobe (L) is anterior, right hepatic lobe (R) is to right. Left (LHV), middle (MHV), and right (RHV) hepatic veins drain into inferior vena cava (IVC). Aorta (A) is posterior. S = gastric fundus.  
C and D, Diagram (C) and sonogram (D) of body. Note relationship of gastric body to both splenic artery (SPL AR) and splenic vein (SPL V). S = gastric body.  
E and F, Diagram (E) and sonogram (F) of antrum. Pancreas body and part of head are seen posteriorly; at same level splenic (SPL V) and superior mesenteric (SMV) veins join to form portal vein. Splenic artery (SPL AR) is just anterior. LPV = left portal vein, S = gastric antrum.

Esophagus

The normal thickness of the esophageal wall when the lumen is distended with a 3-cm-diameter water-filled balloon is approximately 3 mm and is essentially uniform throughout. Five layers can be identified in the normal esophagus (Fig. 1). Sonographically, the esophagus can be divided into three parts: upper, middle, and lower. The upper portion of the esophagus extends from the oropharynx to the superior

aspect of the aortic arch; the most useful landmarks here are the vertebral column posteriorly and the tracheal air column anteriorly (Fig. 2A). The middle portion of the esophagus extends from the aortic arch to the subcarinal region, where the most useful relationships are the aortic arch and descending aorta posteriorly and the trachea and carina anteriorly (Fig. 2B). The lower portion of the esophagus extends from the subcarinal region to the cardia; the descending aorta is posterior and the left atrium is anterior (Fig. 2C).



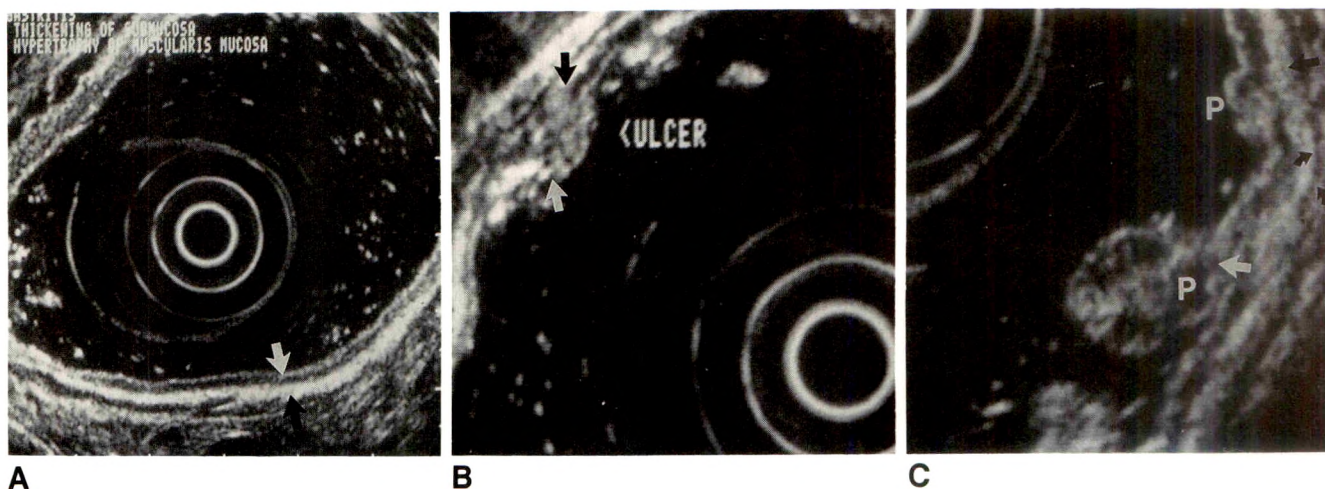


Fig. 7.—Endoscopic sonography of benign gastric processes with 12-MHz transducer.

A, Gastritis. There is significant thickening of all layers, especially mucosa (white arrow) and submucosa (black arrow), in distended stomach. Overall architecture is maintained.

B, Gastric ulcers. There is disruption of mucosal layer (white arrow) and associated inflammatory changes into submucosa and lamina propria (black arrow) in this small ulcer.

C, Gastric polyps. These benign hyperplastic polyps (P) arise only from mucosa (straight white arrow), whereas submucosa (straight black arrow) and lamina propria (curved arrows) appear normal.

Fig. 8.—Endoscopic sonography of gastric varices.

A, Gastric varices (7.5-MHz transducer) may arise within or outside gastric wall. They are more commonly seen in fundus along greater curvature (v). Anechoic rounded and elongated structures are seen from 10 o'clock to 6 o'clock positions.

B, Gastric varices (12-MHz transducer). These large varices are characterized as hypoechoic rounded or elongated structures with strong posterior wall enhancement when imaged with higher-frequency transducer.

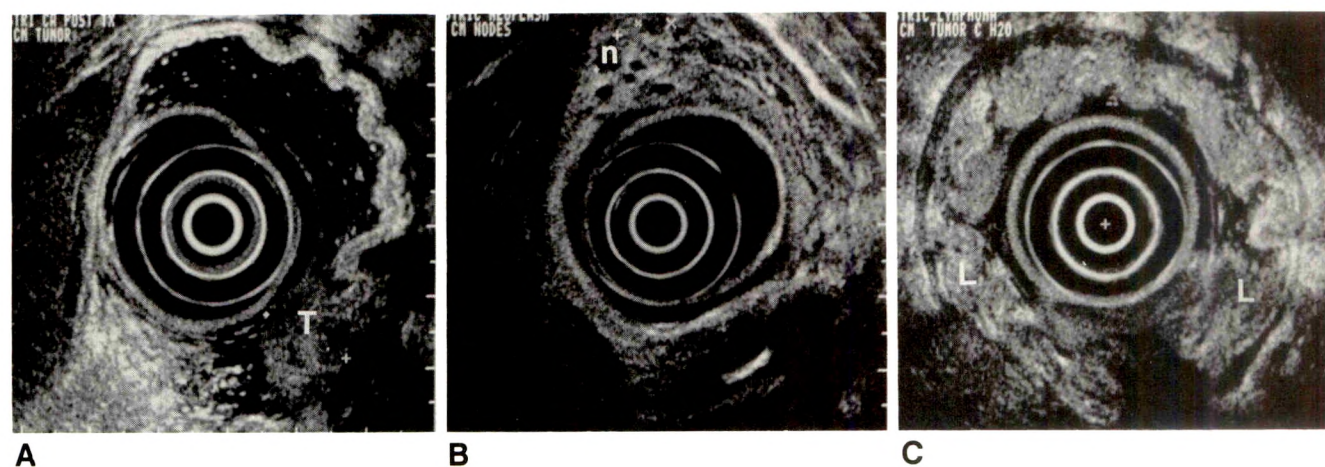
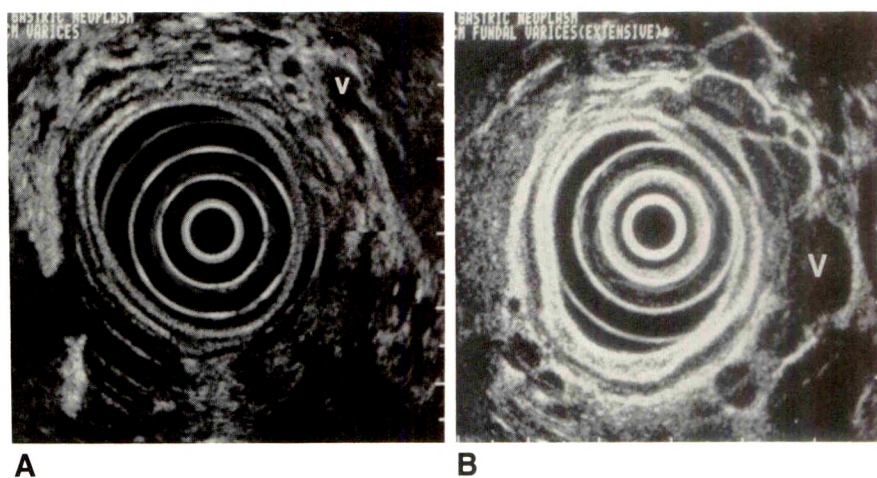


Fig. 9.—Endoscopic sonography of malignant gastric processes with 12-MHz transducer.

A, Adenocarcinoma. Tumor (T) involves all layers of gastric wall extending beyond serosa but not involving any adjacent structure.

B, Nodes. Multiple small nodes (n) in gastrohepatic ligament region, largest two measuring 5 and 6 mm at 11 and 12 o'clock positions. These round and hypoechoic nodes were found to be involved by tumor at surgery.

C, Gastric lymphoma. Folds (L) are thickened and prominent and there is circumferential involvement.



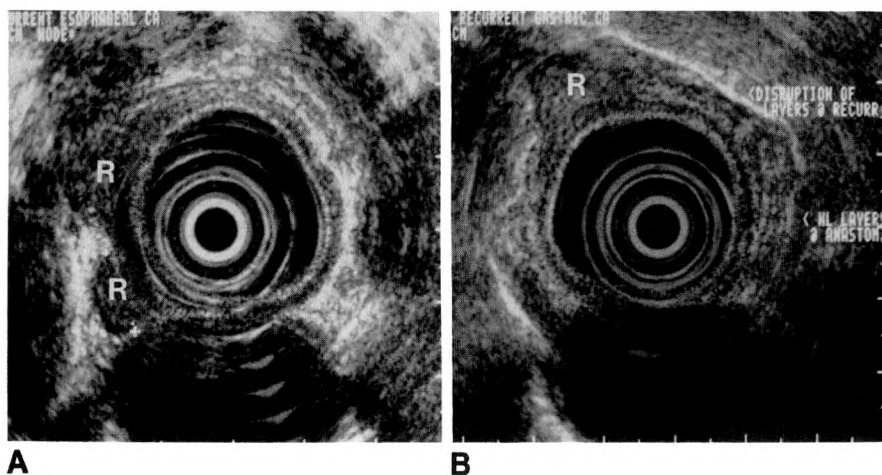


Fig. 10.—Endoscopic sonography of tumor recurrences with 7.5-MHz transducer.

A, Esophageal recurrence at anastomosis after pull-up surgery. Two areas of recurrence (R) are identified at 7 and 10 o'clock positions.

B, Gastric recurrence (R) after partial gastrectomy. There are a double set of layers at esophagogastric anastomosis at 3 o'clock position, and nodularity with disruption of normal layers between 7 and 12 o'clock positions. Biopsy proved this to be a recurrence of original gastric tumor.

Typical benign processes include leiomyomas (Fig. 3A), duplication cysts (Fig. 3B), and varices (Fig. 3C).

Sonograms of esophageal carcinoma are characterized by disruption of the layers of the esophageal wall, beginning with the mucosa, and possibly extending to involve all layers and invade the surrounding structures (Fig. 4A). Metastasis to lymph nodes as small as 2 mm in diameter can be visualized (Figs. 4B and 4C) [2]. On the basis of our experience in over 600 cases examined with endoscopic sonography, we have defined three criteria that suggest nodal involvement: Nodes that appear round are more likely to be malignant than those that appear elongated. Nodes that are hypo- or isoechoic with respect to the primary tumor also are more likely to be malignant. Those nodes that are hyperechoic are more commonly benign. Size is the least reliable predictor of malignant/benign involvement: nodes in the 3- to 5-mm range have been proved to be malignant, while nodes as large as 3 cm have been proved to be benign.

### Stomach

The normal thickness of the gastric wall varies according to the degree of gastric distension. In a fully distended water-filled stomach the thickness is approximately 3 mm. Sonograms show the five layers of the gastric wall (Fig. 5).

The stomach can be divided into the fundus, the body, and the antrum. The sonographic landmarks of the fundus are the aorta with the celiac axis posteriorly; the left hepatic lobe is seen to the right and the spleen is seen to the left (Fig. 6A). Sonograms of the body of the stomach will show the left hepatic lobe to the right and anteriorly, the body and tail of

the pancreas to the left and posteriorly (Fig. 6B). Sonograms of the antrum of the stomach show the left hepatic lobe anteriorly and the pancreas, splenic vein, and portal vein posteriorly. In the very distal antrum the gallbladder can be seen to the right (Fig. 6C).

Typical benign gastric lesions include gastritis (Fig. 7A), ulcer (Fig. 7B), polyps (Fig. 7C), and varices (Fig. 8).

Sonograms in cases of gastric carcinoma show disruption of the wall beginning with the mucosa (Fig. 9A). Nodal involvement of the gastric drainage areas may be shown by endoscopic sonography (Fig. 9B). Gastric involvement by lymphoma is not uncommon in the non-Hodgkin family of tumors; it arises from the lamina propria of the mucosa, which is rich in lymphoid tissue. Bolondi et al. [3] suggest that it may be differentiated on the basis of endoscopic sonography from carcinoma, because carcinoma may be more echogenic than lymphoma (Fig. 9C). Recurrences from both gastric and esophageal tumors can be detected by endoscopic sonography (Fig. 10) [4].

### REFERENCES

1. Di Magno EP, Regan PT, Clain JE, et al. Human endoscopic ultrasonography. *Gastroenterology* 1982;83:824-829
2. Tio TL, Cohen P, Coene P, et al. Endosonography and computed tomography of esophageal carcinoma. *Gastroenterology* 1989;96:1478-1486
3. Bolondi L, Casanova P, Caletti GC, Grigioni W, Zani L, Barbara L. Primary gastric lymphoma versus gastric carcinoma: endoscopic US evaluation. *Radiology* 1987;165:821-826
4. Lightdale CJ, Botet JF, Brennan M, Kelsen DP, Turnbull AD. Diagnosis of recurrent gastric cancer at the surgical anastomosis by endoscopic ultrasonography. *Gastrointest Endosc* 1989;35:407-412



# Thickening at the Root of the Superior Mesenteric Artery on Sonography: Evidence of Vascular Involvement in Patients with Cancer of the Pancreas

Tomoo Kosuge<sup>1</sup>  
Masatoshi Makuuchi  
Tadatoshi Takayama  
Junji Yamamoto  
Taira Kinoshita  
Hideo Ozaki

Thickening of the root of the superior mesenteric artery (SMA) was studied by using preoperative sonography in 23 patients with pancreatic cancer and in 10 healthy control subjects. Of the 23 with cancer, 11 had neoplastic involvement of the SMA and 12 did not. Prominent thickening of the area around the SMA with (six patients) or without (five patients) decreased echogenicity compared with the adjacent retropancreatic connective tissue was observed in patients with involvement of the SMA, a finding called the "cuff sign." Mean thickness of the periarterial area in the cancer patients with and without involvement of the SMA and in control subjects were 8.5 mm, 4.0 mm, and 2.9 mm, respectively. With an upper limit of normal of 7.0 mm for the thickness of the SMA, the sensitivity, specificity, and overall accuracy of this sign in the evaluation of involvement of the SMA were 91%, 100%, and 96%, respectively. Decreased echogenicity of the periarterial area was not observed in patients without involvement of the SMA or in control subjects.

Our results show that sonographic evidence of periarterial thickening of the root of the SMA (cuff sign), especially with decreased echogenicity, is a reliable finding of tumor infiltration of the SMA in patients with pancreatic carcinoma.

*AJR* 156:69-72, January 1991

Vascular involvement is one of the crucial determinants for surgical resectability of carcinoma of the pancreas. Although resection and reconstruction of the portal vein have become safe procedures [1, 2], resection of the superior mesenteric artery (SMA) still entails considerable risk [2]. Involvement of the SMA by locally advanced tumor growth is a determinant for unresectability, and thus estimation of such infiltration is required when candidates are evaluated for surgery.

Angiography has been the most widely used technique for determination of vascular involvement. CT evaluation also has been useful [3], and sonography has been considered merely complementary [4].

In our experience, prominent thickening of the periarterial area noted on sonography seems to correlate with involvement of the SMA. This finding was designated as the "cuff sign" because its appearance around the root of the SMA resembles an inflated cuff of an endotracheal tube (Figs. 1A and 1B). The present study was performed to evaluate this sonographic finding as an indication of SMA involvement in patients with pancreatic cancer.

## Subjects and Methods

Twenty-eight patients with pancreatic ductal carcinoma were admitted to the National Cancer Center Hospital, Tokyo, for surgery between June 1988 and December 1989. Results of preoperative workup with CT and sonography were considered contraindications to surgery in four patients. These four patients and one with cystadenocarcinoma of the pancreas were excluded from the study. The other 23 patients were included in the study. They were 11 men and 12 women with a mean age of 67 years (range, 51-78 years). None had associated

Received April 23, 1990; accepted after revision August 8, 1990.

This work was supported in part by a grant-in-aid for Cancer Research and a grant-in-aid for the Comprehensive 10-Year Strategy of Cancer Control from the Ministry of Health and Welfare of Japan.

<sup>1</sup> All authors: Department of Surgery, National Cancer Center Hospital, 1-1, Tsukiji 5-chome, Chuo-ku, Tokyo 104, Japan. Address reprint requests to T. Kosuge.

0361-803X/91/1561-0069  
© American Roentgen Ray Society



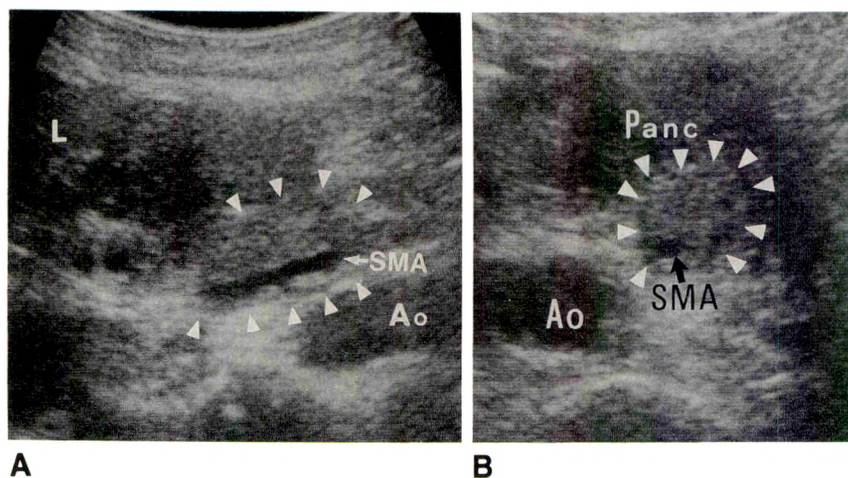


Fig. 1.—A, Cuff sign in a 68-year-old woman with cancer of pancreas and involvement of superior mesenteric artery (SMA). Longitudinal sonogram shows thickening of root of SMA measuring 10.2 mm. Lumen of SMA is preserved. Arrowheads indicate cuff. L = liver, Ao = aorta.

B, Transverse sonogram shows thickened area around SMA (arrowheads) that is hypoechoic compared with adjacent retropancreatic connective tissue. Panc = pancreas, Ao = aorta.

liver disease. All histologic confirmation was obtained from surgical specimens.

In addition, 10 healthy volunteers, six men and four women with a mean age of 55 years (range, 42–68 years), were examined with sonography as control subjects. They showed no sign of specific diseases within 1 year of follow-up.

Sonography was performed by using an electronic real-time scanning system, SSD-650 (Aloka, Tokyo, Japan), with a 3.5-MHz convex sector scanner. No information from previous CT or angiographic examinations was available. Vessels were identified on an anatomic basis without Doppler imaging. The thickness of the periarterial area around the SMA was measured as the distance from the dorsal edge of the pancreas or the splenic vein to the ventral edge of the SMA at the level of the splenic vein. Measurements were performed on longitudinal and transverse scans. When the two values were different, that of the longitudinal scan was taken as the thickness. The echogenicity of this region also was recorded by comparing it with that of the primary pancreatic mass and with that of the adjacent retropancreatic hyperechoic area.

CT was performed by using TCT-900S (Toshiba, Tokyo, Japan) with contiguous 5-mm-thick slices and 1.0-sec scanning times. Iodinated contrast medium (Iopamidol 300, Schering, Berlin) was administered as a 100-ml bolus via injector at a rate of 3.0 ml/sec. Selective arteriography of the SMA was performed by injecting 40 ml of contrast medium in 4 sec and by using serial films.

Laparotomies were performed within 2 weeks after all imaging examinations, and involvement of the SMA was confirmed or excluded. Direct extension of the pancreatic carcinoma around the SMA was confirmed in 11 patients. Nine of these had intraoperative irradiation or bypass operations or both. In two patients, palliative resections were performed, and tumor cells were shown in the dissected nerve plexus surrounding the SMA. The SMA was not infiltrated in the other 12 patients. Radical resections were performed in eight of these; all had associated obstructive pancreatitis. In the remaining four patients, multiple small liver metastases detected by clinical examination or intraoperative sonographic examination were contraindications for resection.

Values are expressed as means plus or minus the standard deviation. Wilcoxon's rank sum test was used for statistical analyses.

## Results

The root of the SMA was visualized sonographically in all instances. The thickness of the periarterial hyperechoic area

surrounding the SMA was  $8.5 \pm 1.2$  mm (range, 6.5–10.2 mm) in the 11 patients with SMA involvement at surgery,  $4.0 \pm 1.0$  mm (range, 2.5–6.0 mm) in the 12 patients without SMA involvement, and  $2.9 \pm 0.7$  mm (range, 2.0–4.0 mm) in the 10 control subjects. No overlap occurred between the patients with and without SMA involvement at surgery; the difference was statistically significant ( $p < .01$ ).

The echogenicity of the periarterial area involved was increased compared with that of the primary pancreatic mass in all 11 patients who had SMA involvement at surgery. In comparison with the adjacent retropancreatic area, the periarterial area was less echogenic in six patients (Figs. 1A and 1B) and isoechoic without definite borders or limits in the other five (Fig. 2). Decreased echogenicity of the periarterial area was not observed in patients without SMA involvement or in control subjects.

The diagnostic usefulness of the cuff sign was assessed by using an upper range of normal of 7.0 mm for thickness. In 10 of 11 patients with involvement of the SMA, the thickness was more than 7.0 mm. The 11th patient had periarterial thickness of 6.5 mm, but periarterial infiltration was considered mild, and the tumor was resected. The resectional margin of the dissected nerve plexus, however, showed tumor. In all 12 patients without SMA involvement at surgery, the cuff sign was negative; no patients had a periarterial thickness greater than 7.0 mm. The sensitivity of the cuff sign in estimating SMA involvement was 91% (10/11), specificity was 100% (10/10), and overall accuracy was 96% (22/23).

Angiography was performed in all 23 patients. Stricture or encasement of the main trunk of the SMA was observed in nine cases, and encasement of small branches of the SMA was shown in 10 of the 11 cases with SMA involvement at surgery. One patient with SMA involvement shown by sonography (Fig. 3) and CT had normal angiographic findings of the SMA. Periarterial infiltration was suspected in one case that showed no SMA involvement at surgery; this was the one false-positive result.

CT was performed in all 23 patients. One who had SMA involvement at surgery was excluded because of technical problems. SMA involvement was shown in nine of the other 10 patients who had SMA involvement at surgery. Evaluation



Fig. 2.—55-year-old woman with cancer of pancreas involving superior mesenteric artery (SMA). Transverse sonogram shows thickening of SMA. Distance between SMA and pancreas (Panc) is 8 mm (arrowheads), an example of isoechoic thickening. Ao = aorta.

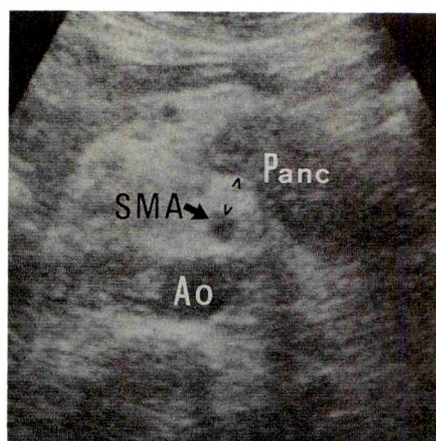


Fig. 3.—71-year-old man with cancer of pancreas and involvement of the superior mesenteric artery (SMA) not detected by angiography. Sonogram shows marked thickening of area around the SMA (arrowheads). Panc = pancreas.

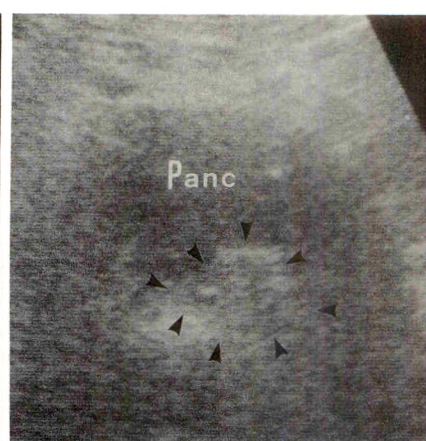


TABLE 1: Comparison of Diagnostic Value of the Three Imaging Techniques in Evaluating Involvement of the Superior Mesenteric Artery

	Sonography	CT	Angiography
Sensitivity (%)	91 (10/11)	90 (9/10)	91 (10/11)
Specificity (%)	100 (10/10)	100 (9/9)	91 (10/11)
Overall accuracy (%)	96 (22/23)	95 (21/22)	91 (21/23)

by CT was correct in all 12 patients who did not have SMA involvement at surgery.

The diagnostic values of sonography, CT, and angiography in the evaluation of SMA involvement are summarized in Table 1.

## Discussion

The usefulness of sonography in the detection and evaluation of the extent of pancreatic cancer, including vascular involvement, is widely accepted [4–10]. However, the precise sonographic appearance of possible SMA involvement has not been described before.

Compression or obliteration of the lumen and proximity to the tumor mass have been considered to be typical sonographic findings of vascular involvement. These findings frequently are observed when the portal venous system is involved [4]. In our experience, however, the morphologic change caused by cancer infiltration around the SMA is different from that seen in the portal venous system because occlusion is rare and stricture of the lumen is infrequent. Instead, prominent thickening of the periarterial area around the SMA with or without changes in echogenicity is observed. We have regarded this as a typical finding of SMA involvement by pancreatic cancer and called it the cuff sign.

Blurring of the SMA on CT with extension of the pancreatic mass around the SMA has been reported to indicate SMA

involvement by pancreatic cancer [3]. However, the sonographic appearance of SMA involvement is not similar to the findings on CT. Instead, a thickened periarterial area around the SMA appears to separate the tumor mass from the SMA; the echogenicity of the periarterial area was higher than that of both the primary pancreatic mass and the lumen of the SMA, even in the patients with the hypoechoic cuff sign. This feature is to be emphasized, because a radiologist who is not aware of it might interpret it as indicating that the SMA is intact, especially when the echogenicity of thickened periarterial area is similar to that of the retropancreatic connective tissue.

The present study showed the usefulness of the cuff sign in evaluating SMA involvement by pancreatic cancer. When the cutoff value of 7.0 mm for thickness was used, the specificity was 100%, and the sensitivity was 91%. These results were similar to those of CT and angiography. In addition to the thickness, lowered echogenicity of the periarterial area of the SMA compared with that of the surrounding retropancreatic connective tissue was observed in about half (6/11) of the patients with SMA involvement, facilitating recognition of the cuff sign. Such a finding was not observed in the patients without SMA involvement. In our series, thickening of the periarterial area in the patients with SMA involvement was so remarkable that even an isoechoic cuff could be recognized. However, recognition of isoechoic thickening might be difficult when the thickening is moderate. Therefore, the term cuff sign should be used only to refer to the hypoechoic thickening.

Thickening of the periarterial area around the SMA also has been observed in patients with invasive carcinomas originating from the gallbladder and the stomach. Thus, this sign per se is not specific to pancreatic cancer but simply represents carcinomatous infiltration around the SMA. Thickening of the periarterial area also might result from factors other than carcinomatous infiltration. Mitchell et al. [11] compared CT of the SMA in patients with pancreatitis with that in patients with pancreatic cancer. Occasionally, perivascular edema was shown in patients with pancreatitis; obliteration of the artery



never was observed. In our series, the periarterial area of patients with pancreatic cancer without SMA involvement was somewhat thicker than that of control subjects, maybe reflecting the influence of obstructive pancreatitis, although the difference in thickness was not statistically significant. Perivascular edema produced by acute pancreatitis may cause more prominent thickening of the periarterial area. Extreme obesity also might cause thickening of the periarterial area. Further study of the influence of these factors on sonographic appearance of the area around the SMA is required. Consequently, the cuff sign is not a definitive sign of pancreatic cancer but is valuable in estimating SMA involvement in patients with known pancreatic cancer.

#### REFERENCES

1. Fortner JG. The rationale, technique and results of treating pancreatic and peripancreatic cancer by regional pancreatectomy. *Acta Gastroenterol Belg* **1987**;40:121-127
2. Sindelar WF. Clinical experience with regional pancreatectomy for adenocarcinoma of the pancreas. *Arch Surg* **1989**;124:127-132
3. Megibow AJ, Bosniak MA, Ambos MA, Beranbaum ER. Thickening of the celiac axis and/or superior mesenteric artery: a sign of pancreatic carcinoma on computed tomography. *Radiology* **1981**;141:449-453
4. Garra BS, Shawker TH, Doppman JL, Sindelar WF. Comparison of angiography and ultrasound in the evaluation of the portal venous system in pancreatic carcinoma. *JCU* **1987**;15:83-93
5. Makie CR, Bowie J, Cooper MJ, Kunzmann A, Moossa AR. Prospective evaluation of gray scale ultrasonography in the diagnosis of pancreas cancer. *Am J Surg* **1978**;136:575-581
6. Hessel SJ, Siegelman SS, McNeil BJ, et al. A prospective evaluation of computed tomography and ultrasound of the pancreas. *Radiology* **1982**;143:129-133
7. Cohen MM, Switzer PJ, Copperberg PL. Sensitivity of ultrasonography in the diagnosis of pancreatic cancer. *Can Med Assoc J* **1979**;120:453-455
8. Tailor KJW, Buchin PJ, Viscomi GN, Rosenfield AT. Ultrasonographic scanning of the pancreas: prospective study of clinical results. *Radiology* **1981**;138:211-213
9. Pollock D, Taylor KJW. Ultrasound scanning in patients with clinical suspicion of pancreatic cancer: a retrospective study. *Cancer* **1981**;47:1662-1665
10. Campbell JP, Wilson SR. Pancreatic neoplasms: how useful is evaluation with US? *Radiology* **1988**;167:341-344
11. Mitchell DG, Hill MC, Cooper R, et al. The superior mesenteric artery fat plane: is obliteration pathognomonic of pancreatic carcinoma? *CT* **1987**;11:247-253



# Long-Term Soft-Tissue Effects of Biliary Extracorporeal Shock Waves: An Animal Study

Brijendra Rawat<sup>1</sup>  
Robert Wolber<sup>2</sup>  
H. Joachim Burhenne<sup>1</sup>

Although delayed effects of renal extracorporeal shock-wave lithotripsy (ESWL) have been reported, the long-term soft-tissue effects after biliary ESWL have not been investigated. We report soft-tissue effects seen up to 1 year after biliary extracorporeal shock waves were administered to 18 Yucatan pigs. The gallbladder received 4000 electromagnetic shock waves from a Siemens Lithostar overhead module. Blood samples were drawn from each pig for hematologic, coagulation, and biochemical profiles immediately before and then at prescribed time intervals after administration of shock waves. Autopsy and histopathologic examination of the gallbladder and surrounding organs were performed. Kidneys and adrenal glands also were examined in five pigs followed up for 1 year. There were no gross or microscopic abnormalities in 11 animals, including all five animals in the 1-year group in which kidneys and adrenal glands also were normal. One animal (3-week group) had two 2-mm foci of parenchymal necrosis in the right lobe of the liver, probably related to ischemia after shock-wave therapy. Transient rise in liver and pancreatic enzyme levels was seen in most animals after administration of shock waves. The levels returned to normal within 2 months in all but one animal.

We conclude that biliary ESWL with the Lithostar Plus does not produce long-term histologic evidence of organ damage in Yucatan pigs.

*AJR* 156:73–76, January 1991

Although cholecystectomy has been the traditional treatment for gallbladder stones, nonsurgical techniques such as biliary extracorporeal shock-wave lithotripsy (ESWL) have been proposed as alternatives [1]. Introduction of this new treatment for gallstone disease was preceded by successful demonstration of its efficacy and safety in experimental animals [2]. Other reports of short-term effects of biliary ESWL on animal and human soft tissues followed [3–8].

Long-term local and systemic effects of ESWL for renal calculi have been studied [9, 10] but to date, no such report has been published on biliary ESWL. We thus investigated the long-term soft-tissue and biochemical effects of biliary ESWL with the overhead module (Siemens Lithostar Plus) on Yucatan pig organs.

## Subjects and Methods

Extracorporeal shock waves were administered to 18 Yucatan pigs, targeted at their gallbladder. The mean weight of the animals at the time of administration was 39 kg. Each pig received 4000 shock waves delivered at energy level 5, which results in a focal positive peak pressure of approximately 450 bar (45 MPa) in vitro. The focal zone, within which more than 50% of the peak positive shock-wave pressure is delivered, was 40 mm in the long axis and 4 mm in the transverse axis. Because lung tissue is particularly susceptible to damage by shock waves [3], the path of the shock waves was directed away from the lungs. The animals were then randomized into five groups (A to E). The difference in the groups was the time interval between day of shock-wave administration and sacrifice. Three pigs of Group A were to be sacrificed at 3 weeks, three of Group B at 6 weeks, three of Group C at 12

Received May 23, 1990; accepted after revision July 23, 1990.

<sup>1</sup> Department of Radiology, University of British Columbia and Vancouver General Hospital, 855 W. 12th Ave., Vancouver, B.C., Canada V5Z 1M9. Address reprint requests to H. J. Burhenne.

<sup>2</sup> Division of Anatomic Pathology, University of British Columbia and Vancouver General Hospital, Vancouver, B.C., Canada V5Z 1M9.

0361-803X/91/1561-0073  
© American Roentgen Ray Society



weeks, three of Group D at 24 weeks, and six of Group E at 1 year after administration of shock waves. One of the pigs of Group E died 24 weeks after administration of shock waves because of infectious gastroenteritis. An autopsy was done immediately, and the results were added to those of the 24-week group (Group D). Group D then contained four pigs, and Group E contained five pigs.

Autopsies were performed by a pathologist within 3 hr of sacrifice. The lungs immediately were inflated with formalin. A detailed inspection of the lungs, liver, pancreas, gallbladder, bile ducts, and colon was made. An average of 42 blocks of tissue was obtained from each animal for microscopic examination. Sections were made from designated areas of all pulmonary lobes; the liver, particularly from the area around the gallbladder including the wall of the duodenum; the entire gallbladder and extrahepatic biliary ducts; the head, body, and tail of the pancreas; and the hepatic flexure of the colon. Both kidneys and adrenal glands also were examined in the five pigs belonging to the 1-year group, and an additional eight blocks of tissue were obtained from these organs. Histologic examination was performed on all sections after they were stained with hematoxylin and eosin.

Blood samples were obtained from each pig for routine hematologic and coagulation profiles. Biochemical tests also were performed for renal, liver, and pancreatic functions. These tests routinely were performed immediately before and 24 hr after administration of shock waves, and then were repeated at prescribed time intervals in all animals, which varied in different groups (Table 1). Chest radiographs also were obtained on all animals before and after lithotripsy.

Guidelines on the use of living animals in scientific investigations according to the Canadian Council on Animal Care were followed. All animals underwent endotracheal intubation after premedication with ketamine (20 mg/kg). This was followed by general inhalation anesthesia (halothane). Shock waves then were administered. For autopsy, all animals were premedicated with intramuscular ketamine (20 mg/kg) and then sacrificed by IV injection of pentobarbital (100 mg/kg).

## Results

No gross or microscopic changes related to the administration of shock waves were noted in the five animals that were followed up for 1 year. Also, no gross or microscopic changes in the kidneys and adrenal glands were seen in these five animals (Group E).

Twelve of the remaining 13 animals followed up for less than 1 year (Groups A, B, C, D) also showed no gross or microscopic changes related to administration of shock

waves. One animal in the 3-week group (Group A) had two 2-mm focal areas of parenchymal necrosis in the right lobe of the liver, which could be related to ischemia after shock-wave therapy.

Autopsy findings unrelated to administration of shock waves were seen in six of 18 animals: pulmonary epithelial granulomas and microabscesses from bronchopneumonia in three, focal hepatic granuloma in one, acute infectious enterocolitis with severe ulceration and hemorrhage in the bowel in one, and fresh patchy intraalveolar hemorrhage in all lobes of the right lung in one. This last animal was sacrificed after 6 weeks follow-up, and the fresh intraalveolar hemorrhage, which was negative for hemosiderin, was most likely an agonal event.

No evidence of gallbladder wall thickening, fibrosis, or hemorrhage was noted in any of the 18 animals.

The control biochemical and hematologic values varied widely. Thus, baseline values of each animal served as the animal's control values. A transient rise in the levels of serum amylase, lipase, alkaline phosphatase, and aspartate serum transaminase was seen in 12, 16, 17, and 16 animals, respectively, 24 hr after administration of shock waves (Fig. 1). Subsequent blood analyses showed return of these values to the baseline within 2 months time in all but one animal. In this pig, the serum amylase value remained high until the time of its sacrifice (12 weeks) (Fig. 1). The findings of other biochemical and hematologic tests remained unchanged in all animals. Chest radiographs performed immediately after administration of shock waves did not show any pulmonary or pleural changes.

## Discussion

An 8% prevalence of systemic arterial hypertension has been reported in patients after ESWL for renal calculi [11]. The main histopathologic abnormalities in the renal tissues after ESWL in the porcine model are interstitial and perivascular fibrosis. We thus thought it necessary to investigate possible long-term biological changes attributable to biliary ESWL. Animal studies described in the literature are limited to reports of short-term soft-tissue effects. As the overhead module had already proved its efficacy in fragmenting gallstones in our previous animal study [8] and in our clinical

TABLE 1: Protocol Synopsis

Group	No. of Pigs	No. of Shocks (Energy Level 5)	Schedule After Administration of Shock Waves	
			Blood Analysis	Time Before Sacrifice (wk)
A	3	4000	Day 1, 22 <sup>a</sup>	3
B	3	4000	Day 1, 30, 43 <sup>a</sup>	6
C	3	4000	Day 1, 30, 60, 85 <sup>a</sup>	12
D	3	4000	Day 1, 30, 60, 90, 169 <sup>a</sup>	24
E	6	4000	Day 1, 30, 60, 90, 365 <sup>a</sup>	52

Note.—Chest radiographs were taken before and after administration of shock waves in all animals. Energy level 5 produces 450 bar (45 MPa) of positive pressure in vitro at focus. Blood samples to serve as controls also were obtained before administration of shock waves in all animals.

<sup>a</sup> Day of sacrifice.



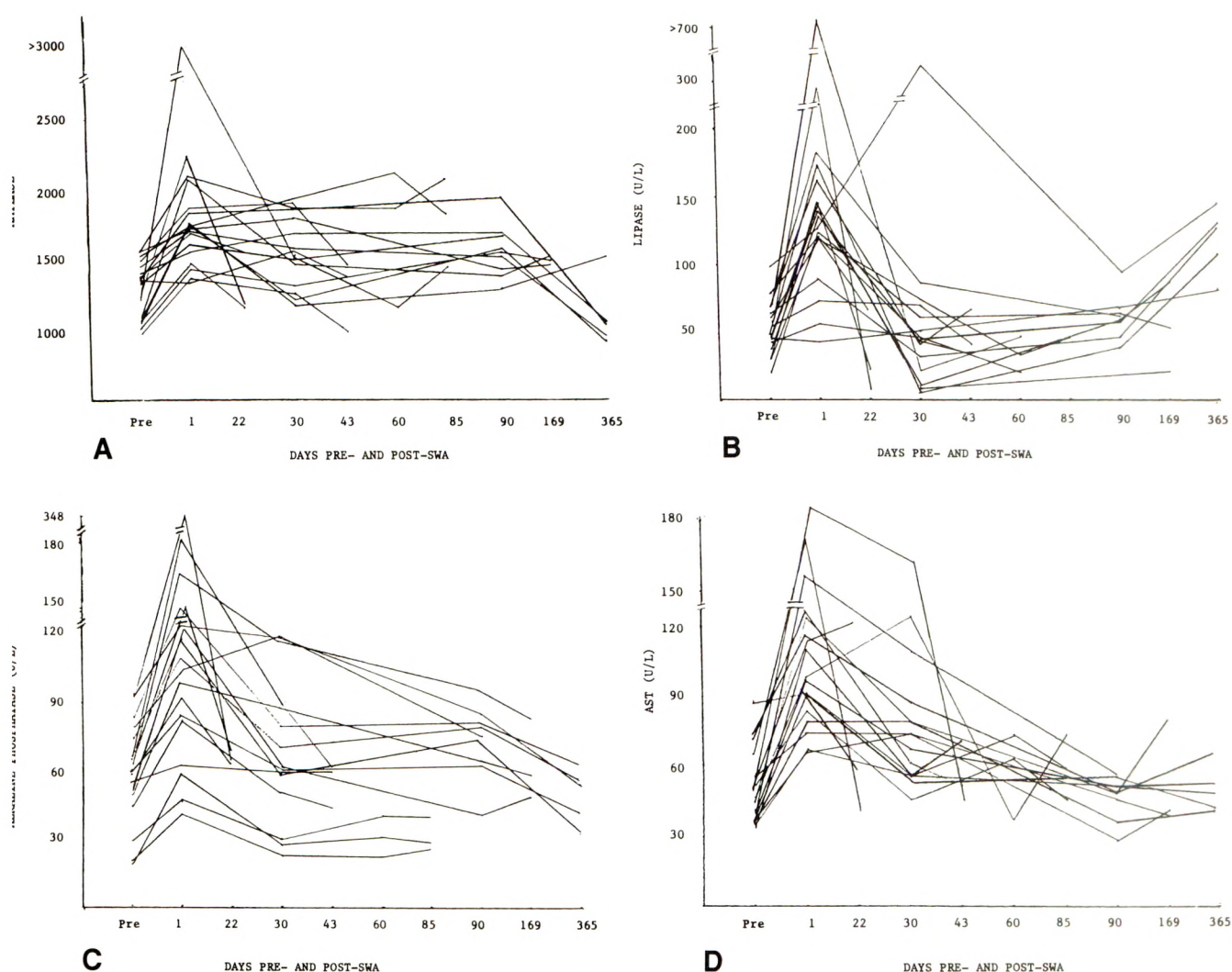


Fig. 1.—A–D, Graphs show serum levels of amylase (A), lipase (B), alkaline phosphatase (C), and aspartate serum transaminase (AST) (D) before and after administration of shock waves (SWA). Results of other biochemical and hematologic tests remained unchanged.

reports [12], we did not consider it necessary to implant calculi in the gallbladder in this long-term animal study. Thus, no absorption of shock-wave energy by gallbladder calculi was possible, and all of the focused shock-wave energy was delivered to the gallbladder and adjacent organs. The Lithostar Plus has a reduced shock-wave focal area when compared with the earlier Lithostar Model. This increases the pressure level within the focal volume but should reduce injury to surrounding tissue.

Pulmonary hemorrhage has been described as the most significant immediate soft-tissue effect of biliary ESWL in experimental animals [2, 3]. The change in acoustic impedance of the soft tissue and the gas-filled alveoli can lead to absorption of shock-wave energy in the lungs, producing hemorrhages [13]. Other short-term changes observed in soft tissues by earlier investigators were petechial hemorrhages in the gallbladder wall and the adjacent organs such as liver, pancreas, and duodenum [3]. These soft-tissue changes were observed with high-energy first-generation lithotripters with a

wide focal area. Some second-generation lithotripters, including the unit we used in our study, produce a low energy, and the high peak positive pressure, which is confined to a smaller focal area, causes less soft-tissue damage [14]. Ell et al. [15], however, who used second-generation piezoelectric shock waves, have observed significant hematomas in the gallbladder and liver of animals when shock waves were targeted at these organs. Similar changes were observed in human gallbladders and adjacent organs when they were subjected to shock waves immediately before elective cholecystectomy [16].

Our two previous short-term studies with a Siemens lithotripter showed only minor microscopic hemorrhages attributable to biliary ESWL in the gallbladder and right lung base in some animals [7, 8]. Amouretti et al. [6] observed significant soft-tissue hematomas in animals that were treated at 5.0 and 10.0 pulses/sec instead of the usual 2.5 pulses/sec, when no significant soft-tissue damages occurred. Our lithotripter delivers 2 pulses/sec, which is constant for both the



standard unmodified Lithostar unit and the overhead module.

Published results are for follow-up periods of 3 [15], 4 [4, 17], and 14 weeks [18]. Thus far, long-term effects of up to 1 year after biliary ESWL have not been reported. Our macro- and microscopic evaluation 1 year after ESWL of the gallbladder and surrounding structures (liver, small and large bowel, pancreas, bile ducts, and both kidneys and adrenal glands) revealed no abnormalities consistent with shock-wave changes in five animals. One animal sacrificed 3 weeks after administration of shock waves showed two minute necrotic foci in the right lobe of liver. No hemorrhage or fibrosis was seen. Further investigations ruled out an infectious cause of these lesions. The possible cause was thought to be a localized ischemic effect, and the indirect effect of the shock waves due to cavitation may have been responsible. Air microbubbles are formed in an aqueous medium (such as blood in the hepatic vessels) by shock waves [19]. These minute air bubbles can be observed as air contrast in small hepatic vessels in the liver bed on real-time sonography. Air bubbles could lodge in the hepatic microcapillaries and cause ischemic changes.

Pathologic changes in the lungs of some pigs not related to administration of shock waves are not unexpected. According to the veterinary physician at our institution, most pigs have bronchopulmonary inflammatory changes.

Recent reports on renal lithotripsy have indicated alteration in renal blood flow due to shock waves [11]. The investigators noticed a significant decrease in the percentage of effective renal plasma flow in treated kidneys and a significant increase in both systolic and diastolic blood pressure compared with pretreatment measurements. This effect is thought to be related to interstitial and perivascular fibrosis of renal blood vessels [20]. Damage to the right kidney also has been reported in one case of bile duct calculi [21]. Such injury also might occur after lithotripsy of gallbladder calculi, although it has not been reported to date. Our study examined kidneys in five pigs sacrificed 1 year after administration of shock waves to the gallbladder. We looked specifically for any perivascular or interstitial fibrotic changes. No abnormalities were noticed in the kidneys or adrenal glands of these animals.

We usually perform gallstone lithotripsy with the patient in the left posterior oblique position with the shock-wave head angled down, directing the central shock-wave path obliquely toward the spine. The right kidney is spared. Other investigators usually have the patient lie prone for targeting of gallbladder calculi. In this position, the gallbladder and right kidney lie in the same shock-wave path if the shockhead is not angled.

The periodic biochemical and hematologic blood analyses performed by us on all animals gave indication of mild traumatic changes to the liver and pancreas after administration of shock waves in the majority of cases. These changes were transient, and the values returned to normal within 8 weeks. In one pig, the serum amylase level remained high until the pig was sacrificed (12 weeks). No change occurred in the hematologic values, again ruling out the possibility of recognizable tissue hemorrhage or hemolysis.

Biliary lithotripsy equipment is evolving rapidly, with a variety of shock-wave generators, which differ in the shock-wave

energy and focal zone. These two parameters are important determinants of biological effects of shock waves. The results of our animal study indicate that electromagnetic shock waves are safe and produce no long-term effects on soft tissues.

#### ACKNOWLEDGMENTS

We thank Jim Love and his associates (Animal Care Lab, University of British Columbia) for technical assistance. Our thanks also to Betty Fowler for manuscript preparation.

#### REFERENCES

1. Sauerbruch T, Delius M, Paumgartner G, et al. Fragmentation of gallstones by extracorporeal shock waves. *N Engl J Med* 1986;314:818-822
2. Brendel W, Enders G. Shock waves for gallstones: animal studies (letter). *Lancet* 1983;1:1054
3. Delius M, Brendel W. In vivo parameters of gallstone fragmentation: experimental basis. In: Ferrucci JT, Delius M, Burhenne HJ, eds. *Biliary lithotripsy*. Chicago: Year Book Medical, 1989:49-58
4. Deaconson TF, Condon RE, Weitekamp LA, Kretzschmar S, Begun FP, Lawson RK. Biliary lithotripsy: determination of stone fragmentation success and potential tissue injury in swine. *Arch Surg* 1989;124:916-921
5. Stephenson TJ, Johnson AG, Ross B. Short-term effects of extracorporeal shock wave lithotripsy on the human gallbladder. *J Pathol* 1989;158:239-246
6. Amouretti M, Perissat J, Collet D, et al. Tissue effects of extracorporeal lithotripsy on a model of experimental biliary calculi in dogs. *Gastroenterol Clin Biol* 1989;13:489-494
7. Becker CD, Blake Gilks C, Burhenne HJ. Biological effects of biliary shock wave lithotripsy in swine. *Invest Radiol* 1989;24:366-370
8. Malone DE, Becker CD, Reich D, Quenville NF, Burhenne HJ. Soft-tissue effects of biliary extracorporeal shockwave lithotripsy in swine. *Br J Radiol* 1989;62:843-848
9. Rubin JI, Arger PH, Pollack HM, et al. Kidney changes after extracorporeal shock wave lithotripsy: CT evaluation. *Radiology* 1987;162:21-24
10. Ackaert KSJW, Schröder FH. Effects of extracorporeal shock wave lithotripsy (ESWL) on renal tissue: a review. *Urol Res* 1989;17:3-7
11. Williams CM, Kaude JV, Newman RC, Peterson JC, Thomas WC. Extracorporeal shock-wave lithotripsy: long-term complications. *AJR* 1988;150:311-315
12. Rawat B, Fache JS, Malone DE, Burhenne HJ. Biliary lithotripsy without oral chemolitholysis: the Vancouver experience. In: Burhenne HJ, Paumgartner G, Ferrucci JT, eds. *Biliary lithotripsy II*. Chicago: Year Book Medical, 1990:111-118
13. Brendel W. Shock waves: a new physical principle in medicine. *Eur Surg Res* 1986;18:177-180
14. Coleman AJ, Saunders JE. Shock wave generators in extracorporeal shock wave lithotripsy. In: Ferrucci JT, Delius M, Burhenne HJ, eds. *Biliary lithotripsy*. Chicago: Year Book Medical, 1989:17-21
15. Ell C, Kerzel W, Heyder N, et al. Tissue reactions under piezoelectric shockwave application for the fragmentation of biliary calculi. *Gut* 1989;30:680-685
16. Darzi A, Monson JRT, Kay E, et al. Extracorporeal shock wave therapy for gallstones may cause significant soft tissue damage (abstract). *Gastroenterology* 1988;94:A87
17. Ponchon T, Barkun AN. Experimental and clinical studies on extracorporeal shock wave biliary lithotripsy: the Lyon experience. In: Burhenne HJ, Paumgartner G, Ferrucci JT, eds. *Biliary lithotripsy II*. Chicago: Year Book Medical, 1990:83-87
18. Neisius D, Gebhardt TH, Seitz G, Ziegler M. Histological examination and laboratory analysis of the liver and gallbladder after application of extracorporeal shock waves to the gallbladder with the Piezolith 2200. *Lithotripsy Stone Dis* 1989;1:26-33
19. Zeman RK, Davros WJ, Garra BS, et al. Biliary lithotripsy: clinically relevant lessons learned from in vitro experiments (abstract). *Radiology* 1989;173(P):204
20. Begun FP, Lawson RK, Kearns CM, Tieu TM. Electrohydraulic shock wave induced renal injury. *J Urol* 1989;142:155-159
21. Williams CM, Thomas WC Jr, Newman RC, Bland KI. Right renal trauma: a side effect of biliary lithotripsy (letter). *N Engl J Med* 1989;320:739



## Technical Note

# Percutaneous Transluminal Biopsy of Biliary Strictures with a Bioprobe

Keith Terasaki,<sup>1</sup> Gerhard R. Wittich,<sup>1</sup> Gerhard Lycke,<sup>1</sup> Reinhard Walter,<sup>1</sup> Kent Nowels,<sup>2</sup> David Swanson,<sup>1</sup> and Daniel Lucas<sup>1</sup>

Several techniques are currently available to perform biopsy of biliary duct strictures. If an associated mass is seen on CT, sonography, or cholangiography, percutaneous fine-needle aspiration biopsy can often be performed, with a sensitivity of 50–90% for malignant obstruction [1, 2]. When biliary obstruction is due to a small tumor, endoluminal biopsy techniques may be preferable to standard percutaneous biopsy techniques. Cytologic examination of bile after percutaneous biliary drainage is easy to perform and inexpensive, but detects only 34% of malignant biliary strictures [3]. Brush biopsy performed via a percutaneous transhepatic transluminal approach or during endoscopic retrograde cholangiography is reported to yield malignant cells in 50–70% of malignant cases [4].

Because of the relatively low sensitivity of available methods for diagnosis of malignant biliary strictures, we performed percutaneous transluminal biopsy with a flexible bioprobe in six patients with biliary strictures.

### Subjects and Methods

The six patients in the study were all men, ranging in age from 46 to 72 years. Five patients had a history of malignant disease (colonic carcinoma, renal cell carcinoma, lymphoma, cholangiocarcinoma, and pancreatic carcinoma) that had been treated with either primary tumor resection or chemotherapy. One patient had a primary tumor in the head of the pancreas. Each patient then presented with obstructive jaundice. Sonographic and CT examinations showed biliary dilatation.

In three patients, a mass was seen near the porta hepatis. In the other three patients, no definite mass accounting for the biliary dilatation could be seen on CT or sonography.

Percutaneous transhepatic cholangiography was performed in each case and showed strictures involving the common bile duct in three patients, the main right duct in one patient, the main left duct in one patient, and both ducts in another patient. The obstruction appeared to be due to an extraluminal mass in five patients and was intrinsic to the duct in one patient. After cannulation of a peripheral biliary duct, a guidewire was passed through the stenosis and a 6- or 8-French soft-tip guiding catheter (Schneider-Shiley, Minneapolis, MN) was inserted through an 8-French peel-away sheath. The guiding catheter was advanced far enough to abut the area of stricture seen on the cholangiogram. A 50-cm, flexible, 3-French bioprobe (Cook, Bloomington, IN) or 5-French bioprobe (Cordis, Miami, FL, and Cook, Bloomington, IN) (Fig. 1) was then inserted through the guiding catheter, and biopsy of the stricture was performed under fluoroscopic guidance (Fig. 2). These bioprobes were designed primarily for transjugular endomyocardial biopsies. Their design is similar to an endoscopic wire forceps, but they are shorter and of smaller caliber. The biopsy specimens were 1 to 2 mm in diameter. In each patient, three to five biopsy samples were taken from different portions of the stricture and sent for cytologic and cell-block examination. After biopsy, an external-internal biliary drain was placed in five patients, and an endoprosthesis was placed in one patient. All patients received IV antibiotics before the procedure.

### Results

In all six patients, the biopsy results were positive for malignancy and correlated with the patient's known primary

Received February 7, 1990; accepted after revision June 14, 1990.

This work was supported in part by academic training grant HLO 7425 from the National Heart, Lung, and Blood Institute of the National Institutes of Health.

<sup>1</sup> Department of Diagnostic Radiology and Nuclear Medicine, Stanford University School of Medicine, Stanford, CA 94305-5105. Address reprint requests to K. Terasaki (Rm. H2321).

<sup>2</sup> Department of Pathology, Stanford University School of Medicine, Stanford, CA 94304.

AJR 156:77–78, January 1991 0361–803X/91/1561–0077 © American Roentgen Ray Society



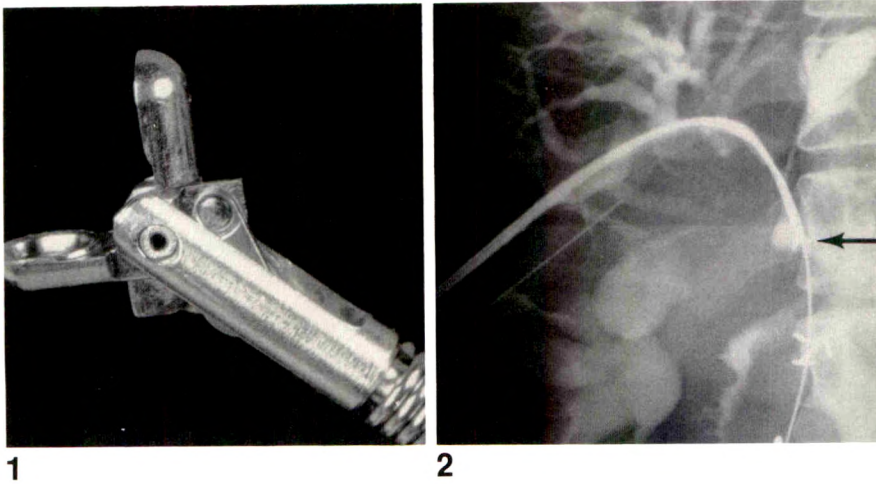


Fig. 1.—Flexible 5-French bioptome.

Fig. 2.—After percutaneous biliary drainage, a flexible bioptome (arrow) has been inserted through a 60-French guiding catheter for biopsy of a stricture in common bile duct.

tumor. The 3-French bioptome was used in two patients and the 5-French bioptome in four patients. In one patient with recurrent pancreatic carcinoma, separate biopsies were performed in both the right and left hepatic ducts; results of both biopsies were positive. In the patient with recurrent cholangiocarcinoma, multiple biopsies along the left hepatic duct were performed to determine the extent of cholangiocarcinoma. Results of biopsies at each of these sites were positive for carcinoma.

No major complications occurred. Minor hemobilia developed after biopsy in one patient and cleared within 24 hr.

### Discussion

Our initial experience with use of the flexible bioptome for percutaneous transluminal biopsy of biliary strictures has shown that the procedure is simple and easy to perform in conjunction with percutaneous biliary drainage and can be used to obtain tissue for pathologic diagnosis. As the bioptome is an intraluminal device, it allows accurate biopsy of lesions even when no mass is seen on CT or sonography. This is often the case in cholangiocarcinoma and when attempting to differentiate recurrent tumor from a postsurgical or a radiation-induced bile duct stricture.

Because the bioptome can be positioned accurately with use of the guiding catheter, the biopsy specimen can be obtained from the area of the stricture most narrowed or irregular on the cholangiogram. This presumably has the greatest chance of yielding malignant cells. As the site of biopsy can be determined, the extent of tumor involvement also can be ascertained. This could be important when determining the surgical resectability of certain tumors.

As the biopsy specimen is 1–2 mm thick, extramucosal, intramural lesions may be diagnosed. Biliary obstruction is often due to lymph node metastases to the porta hepatis with incomplete tumor invasion through the duct wall. In five of our cases, the stricture appeared to be due to an extrinsic mass, but biopsy with the bioptome obtained malignant tissue.

In patients with hemobilia or cholangitis, the biopsy should be deferred for several days because bioptome biopsy in-

creases the amount of bile duct manipulation. If percutaneous biliary access is impossible, or if the stricture is too difficult to reach, bioptome biopsy is not possible. If the stricture cannot be crossed with a guidewire, the bioptome can still be advanced up the stricture and a biopsy sample obtained there.

The theoretical risks of performing transmural biopsies of the common bile duct wall include injury to an adjacent blood vessel or development of a bile leak. This did not occur in our six patients.

Biopsy of biliary duct strictures with a forceps has been reported. Palayew and Stein [5] first used a postoperative T-tube tract to introduce a bronchial forceps for biopsy. Burhenne [6] also reported the use of a forceps biopsy via a subhepatic T-tube tract in 13 patients. Nishimura et al. [7] used a transhepatic access to introduce a 20-French choledochoscope and visually direct biopsy with a 7-French bioptome, while Elyaderani and Gabrielle [8] used a 12-French transhepatic catheter to introduce a biopsy forceps.

The advantage of our bioptome is that after external drainage of an obstructed biliary system, it can be quickly and easily used through an 8-French tract.

### REFERENCES

1. Cohan RH, Illescas FF, Braun SD, Newman GE, Dunnick NR. Fine needle aspiration biopsy in malignant obstructive jaundice. *Gastrointest Radiol* 1986;11:145–150
2. Teplick SK, Haskin PH, Kline TS, Sammon JK, Laffey PA. Percutaneous pancreaticobiliary biopsies in 173 patients using primarily ultrasound or fluoroscopic guidance. *Cardiovasc Intervent Radiol* 1988;11:26–28
3. Muro A, Mueller PR, Ferrucci JT, Taft PD. Bile cytology: a routine addition to percutaneous biliary drainage. *Radiology* 1983;149:846–847
4. Mendez G Jr, Russell E, Levi JU, Koolpe H, Cohen M. Percutaneous brush biopsy and internal drainage of biliary tree through endoprosthesis. *AJR* 1980;134:653–659
5. Palayew MJ, Stein L. Postoperative biopsy of the common bile duct via the T-tube tract. *AJR* 1978;130:287–289
6. Burhenne HJ. Biliary tract. In: Margulis AR, Burhenne HJ, eds. *Alimentary tract radiology*. St. Louis: Mosby, 1983:2334–2336
7. Nishimura A, Otsu H, Hiura T. Forceps biopsy of the bile duct under choledochoscopic control. *Endoscopy* 1980;12:23–29
8. Elyaderani MK, Gabrielle OF. Brush and forceps biopsy of biliary ducts via percutaneous transhepatic catheterization. *Radiology* 1980;135:777–778



## Duplex Doppler Sonography of the Hepatic Vein in Tricuspid Regurgitation

Monzer M. Abu-Yousef<sup>1</sup>

Patients with tricuspid regurgitation may present initially with vague abdominal symptoms and elevated liver enzymes. In the absence of diagnostic sonographic findings, patients may be subjected to an unnecessary invasive liver biopsy for an accurate diagnosis. We recently described the association of the pulsatile portal venous waveform on duplex Doppler sonography with tricuspid regurgitation in 15 patients. In this study I describe the changes in the hepatic venous waveform in these patients and compare the findings with the final diagnosis as determined by Doppler echocardiography ( $n = 14$ ) or ultrafast CT ( $n = 1$ ). All patients had clinical findings consistent with liver dysfunction and were referred for sonography to rule out diseases of the liver, biliary tree, or hepatic or portal veins. All patients had persistently dilated hepatic veins and inferior vena cavae. Twenty-four volunteers, 11 of whom had simultaneous ECG tracings, served as a control group. The main findings on the hepatic duplex sonogram in the disease group were a decrease in the size of the antegrade systolic wave with a systolic/diastolic flow velocity ratio of less than 0.6 ( $n = 4$ ) or reversal of the systolic wave ( $n = 10$ ). In all volunteers, systolic flow was antegrade and the ratio was more than 0.6. Two diagnoses were false positive and one was false negative.

In some patients with sonographic signs of congestive heart failure, duplex Doppler sonography of the hepatic vein may be helpful in the diagnosis of one of the causes of liver dysfunction, tricuspid regurgitation.

*AJR* 156:79-83, January 1991

The duplex Doppler examination has become an integral part of the sonographic evaluation of the upper abdomen. It is a useful technique in the diagnosis of Budd-Chiari syndrome, portal vein thrombosis, portal hypertension, venoocclusive disease, and liver transplant complications [1-8]. We recently described the pulsatile portal vein flow on duplex Doppler sonography and found it to be associated with tricuspid regurgitation in 13 of 15 patients with obscure abdominal symptoms and elevated liver enzymes [9]. The present study describes the changes in the duplex Doppler waveforms of the hepatic veins in these 15 patients, all of whom had correlation with Doppler echocardiography or ultrafast CT, and compares these waveforms with the Doppler sonograms of normal hepatic veins in 24 control subjects. Although these changes in the hepatic vein on duplex imaging have been discussed in the cardiology literature, to the best of my knowledge they have not been mentioned in the radiology literature [10-12].

The duplex Doppler spectral waveform of the normal hepatic vein is multiphasic and consists of large antegrade systolic and diastolic waves and small retrograde v, a, and, rarely, c waves (Fig. 1). The systolic wave, which occurs within 0.15 sec of the QRS complex on the ECG tracing, corresponds to the x' descent and trough on the right atrial pressure waveform and results from the negative pressure wave in the right atrium, caused by right atrial relaxation and movement of the tricuspid annulus toward the cardiac apex [13, 14]. In less than half of the subjects, this is followed by a small retrograde v wave that occurs toward the end of the T wave

Received March 19, 1990; accepted after revision August 6, 1990.

<sup>1</sup> Department of Radiology, The University of Iowa College of Medicine, Iowa City, IA 52242. Address reprint requests to M. M. Abu-Yousef.

0361-803X/91/1561-0079  
© American Roentgen Ray Society



on the ECG tracing and corresponds to a similar v wave on the right atrial pressure tracing [10]. It results from right atrial overfilling against a closed tricuspid valve. This is followed by an antegrade diastolic wave that occurs after the T wave on the ECG tracing and corresponds to the y descent and trough on the right atrial pressure tracing. It results from the negative pressure created in the right atrium from the opening of the tricuspid valve and flowing of blood from the right atrium to the right ventricle. In most subjects, this is either equal to or smaller than the systolic wave. In about two thirds of the subjects, this is followed by a small retrograde a wave that occurs after the P wave on the ECG tracing and corresponds to a similar a wave on the right atrial pressure tracing [10]. It results from elevated right atrial pressure caused by right atrial contraction. In a few subjects, another small positive c wave follows the a wave and results from a positive atrial pressure wave caused by the bulging of the tricuspid valve into the right atrium at the beginning of systole.

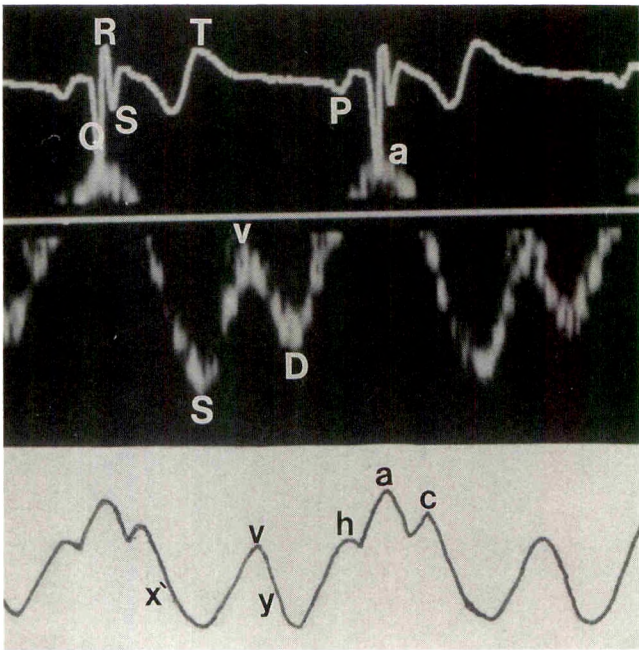


Fig. 1.—Simultaneous ECG tracing (top), duplex Doppler sonogram (middle), and line drawing of right atrial pressure tracing (bottom) of normal hepatic vein.

Subjects and Methods

From November 1987 to October 1989, most patients in whom sonography showed dilated hepatic veins and inferior venae cavae without significant variation in size with respiratory movements underwent duplex Doppler examinations of the portal and hepatic veins. The duplex Doppler spectral waveforms of the hepatic veins were analyzed retrospectively in 15 of these patients who were suspected of having tricuspid regurgitation because of findings on duplex Doppler sonograms of the portal veins. The diagnosis was correlated with Doppler echocardiography (*n* = 14) or ultrafast CT scans of the heart (*n* = 1). All 15 patients were referred for sonography to rule out diseases of the liver, biliary tree, or hepatic or portal vein. Most patients had biochemical liver abnormalities or vague abdominal signs and symptoms, including an increase in abdominal girth, weight gain, abdominal pain, and hepatomegaly. There were six men and nine women 38–77 years old (mean, 53 years).

The control group consisted of 24 volunteers with no known cardiac, hepatic, or biliary disease. There were nine men and 15 women 14–74 years old (mean, 29 years). In addition to the duplex Doppler examination of the hepatic veins, simultaneous ECG tracings for 11 subjects were displayed on the same hard copy as the duplex Doppler spectral waveform.

All examinations were performed with a 3.5-MHz phased-array transducer of a commercially available sonographic scanner with duplex Doppler capability (Acuson 128, Mountain View, CA). As part of an upper abdominal examination, all patients had fasted for 8–12 hr before the examination. The middle hepatic vein was examined in the longitudinal plane via a right intercostal approach or in the transverse plane with the patient supine via a subcostal approach. All measurements were recorded 1–2 cm proximal to the vein's entrance into the inferior vena cava. Subjects were asked to hold their breath during the Doppler examination.

The spectral Doppler waveform of the hepatic vein was analyzed for maximum systolic velocity ( $\bar{S}$ ), maximum diastolic velocity ( $\bar{D}$ ), v-wave maximum velocity ( $\bar{v}$ ), and a-wave maximum velocity ( $\bar{a}$ ). In patients with antegrade systolic flow, the  $\bar{S}:\bar{D}$  ratio was obtained. Antegrade flow, that is, toward the heart, was considered positive; retrograde flow, that is, away from the heart, was considered negative. The diameter of the hepatic vein was also measured at the same level at which the Doppler sample was taken.

Results

The middle hepatic vein was interrogated at a very small angle with good Doppler tracings in all subjects in the disease and control groups. The range of velocities, differences, ratios, and means in both groups are shown in Table 1.

TABLE 1: Diameters and Maximum Velocities of Various Components of Duplex Doppler Spectral Waveforms of Hepatic Veins

Variable	Control Group ( <i>n</i> = 24)			Disease Group ( <i>n</i> = 15)		
	Maximum	Minimum	Mean	Maximum	Minimum	Mean
Maximum systolic velocity ( $\bar{S}$ ) (cm/sec)	47	22	29.0	32	–55	–12.0
Maximum diastolic velocity ( $\bar{D}$ ) (cm/sec)	42	12	23.0	82	18	52.0
$\bar{S}:\bar{D}$	2.4	0.8	1.5	0.9	–0.9	–0.2
$\bar{S} - \bar{D}$ (cm/sec)	27	–2	7.8	–3	–132	–63.9
$\bar{v}$ -Wave velocity (cm/sec)	–11	0	–1.3	–55	–13	–30.0
$\bar{a}$ -Wave velocity (cm/sec)	–18	0	–10.0	–43	–10	–21.6
Hepatic vein diameter (mm)	10	3	7.0	18	8	10.0



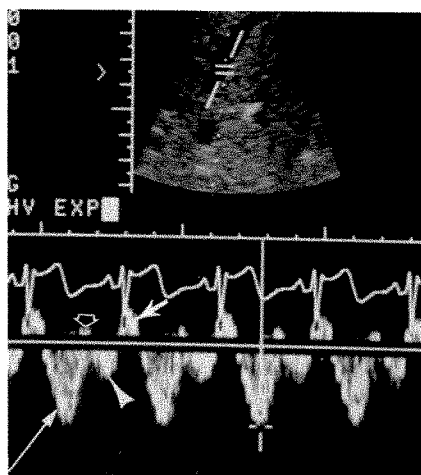


Fig. 2.—Normal hepatic vein duplex Doppler sonogram with simultaneous ECG tracing. Note larger antegrade systolic wave (long arrow) and slightly smaller antegrade diastolic wave (arrowhead). Note also small retrograde v wave at end of systole (open arrow) and larger retrograde a wave at end of diastole (short solid arrow).

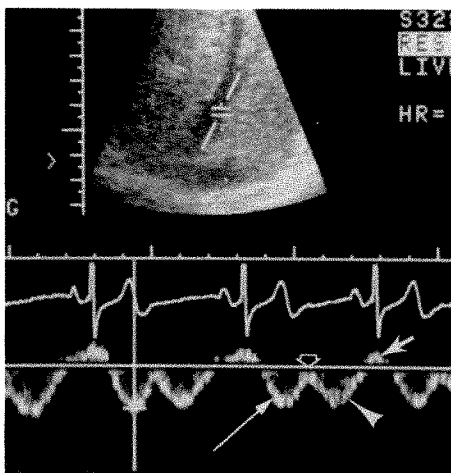


Fig. 3.—Normal hepatic vein duplex Doppler sonogram with simultaneous ECG tracing and absent retrograde v-wave flow (open arrow). Systolic wave (long arrow) is equal to diastolic wave (arrowhead). a wave (short solid arrow).

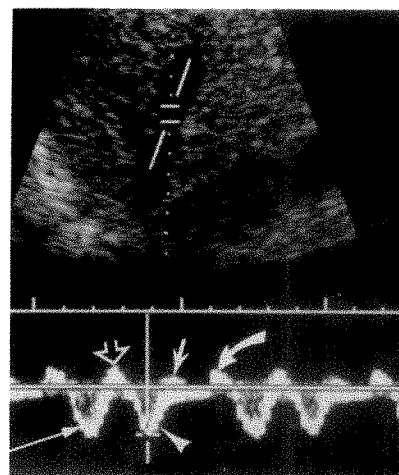


Fig. 4.—Normal hepatic vein duplex Doppler sonogram shows a c wave (curved arrow). Systolic wave (long straight arrow); v wave (open arrow); diastolic wave (arrowhead); a wave (short solid arrow).

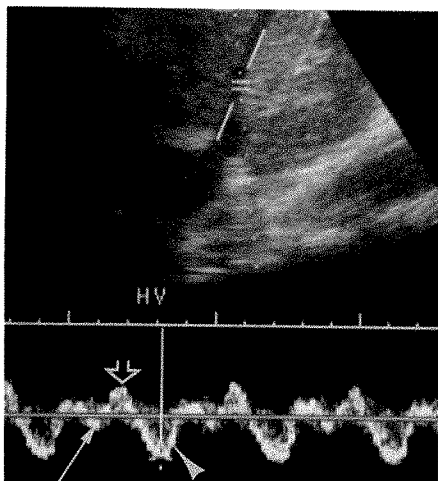


Fig. 5.—Hepatic vein duplex Doppler sonogram in tricuspid regurgitation shows a systolic wave (solid arrow) that is antegrade but very small (10 cm/sec); diastolic wave (arrowhead) is much larger (32 cm/sec). Note that v wave (open arrow) is now large (26 cm/sec).

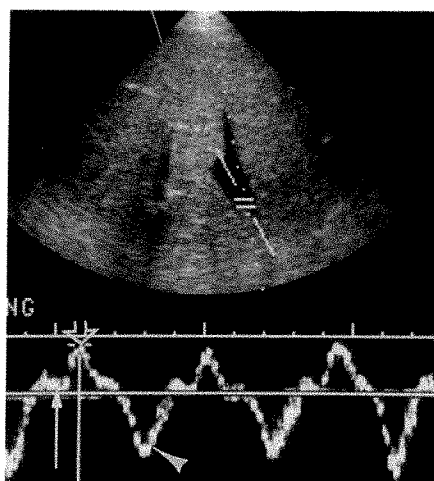


Fig. 6.—Hepatic vein duplex Doppler sonogram in tricuspid regurgitation shows a small retrograde systolic wave (solid arrow), large (55 cm/sec) antegrade diastolic wave (arrowhead), and large (−33 cm/sec) retrograde v wave (open arrow).

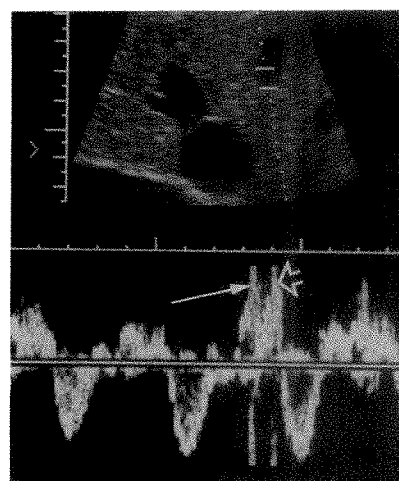


Fig. 7.—Hepatic vein duplex Doppler sonogram in aortic-right atrial fistula. Note very large retrograde systolic wave (solid arrow), which is combining with a very large retrograde v wave (open arrow). Note also large antegrade diastolic wave (>60 cm/sec).

#### Control Group

The systolic and diastolic waves in this group were antegrade in all subjects. Five subjects had a  $\bar{S}:\bar{D}$  value greater than 26 cm/sec. The systolic wave was larger than or equal to the diastolic wave in all but one subject. The retrograde v wave was seen in four subjects (17%) (Fig. 2) and was absent in 20 (Fig. 3). The retrograde a wave was seen in 21 subjects (88%) (Figs. 2 and 3) and was absent in three. In a few patients, a small retrograde c wave was seen after the a wave

and right before the systolic wave (Fig. 4). The diameter of the hepatic vein ranged from 3 to 10 mm (mean, 7 mm).

#### Disease Group

Five of the 15 patients in this group had an antegrade systolic flow wave; four of these five had an  $\bar{S}:\bar{D}$  ratio of less than 0.6 (Fig. 5), and the fifth, who had a ratio of 0.91, was considered not to have tricuspid regurgitation on Doppler



imaging of the hepatic vein. The remainder (10 patients) had a retrograde systolic flow wave. The maximum retrograde systolic velocity for four of these 10 was less than 16 cm/sec (Fig. 6) and for the other six was greater than 16 cm/sec (Fig. 7). The diastolic flow wave was antegrade in all patients.  $\bar{D}$  was greater than 26 cm/sec in all but one patient. A retrograde  $v$  wave was seen in all patients in the disease group and was more than 16 cm/sec in 12 patients. A retrograde  $a$  wave was seen in all patients and was more than 16 cm/sec in nine. The diameter of the hepatic vein in this group ranged from 8 to 18 mm (mean, 10 mm).

Thirteen patients were proved by Doppler echocardiography or ultrafast CT to have tricuspid regurgitation; one patient was proved by contrast ventriculography to have an aortic-right atrial fistula due to the rupture of a sinus of Valsalva aneurysm. The hepatic vein duplex Doppler findings were consistent with tricuspid regurgitation in 14 of 15 patients. The one patient with a false-negative diagnosis had an  $\bar{S}:\bar{D}$  ratio of 0.91. One patient with a positive Doppler examination of the hepatic vein was shown to be normal by Doppler echocardiography.

## Discussion

Tricuspid regurgitation occurs most frequently as a result of dilated cardiomyopathy and rarely as a result of primary valvular leaflet disease [15]. This complication of congestive heart failure often goes undetected. The retrograde flow of blood from the right ventricle to the right atrium, inferior vena cava, and hepatic veins under high pressure during systole often leads to liver congestion and dysfunction [16]. Most patients present with elevated liver enzyme levels or rapid onset of ascites and rapid increase in weight or abdominal girth. The sonographer, who often has to evaluate these patients, should be familiar with spectral Doppler waveforms of the hepatic vein in normal subjects and in patients with tricuspid regurgitation so an accurate diagnosis can be made.

The present study indicates that Doppler imaging of the hepatic vein can be helpful in the diagnosis of tricuspid regurgitation. The hepatic veins can be easily interrogated at a very small angle, both in normal subjects and in patients with tricuspid regurgitation. Although simultaneous ECG tracings can facilitate analysis of the spectral waveform of the hepatic vein, it is not necessary if a careful review of the various components of the normal hepatic vein Doppler waveform is made. This analysis is even easier in patients with tricuspid regurgitation.

During most the cardiac cycle, flow in the hepatic veins of normal subjects should be in the antegrade direction. During systole and diastole, a drop in pressure in the right atrium leads to two antegrade waves. In tricuspid regurgitation, owing to the incompetence of the tricuspid valve, the high right ventricular systolic pressure is transmitted to the right atrium. Depending on the degree of incompetence of this valve, the systolic flow in the hepatic veins may be either decreased or reversed. Sakai et al. [11] have divided hepatic vein Doppler waveforms in tricuspid regurgitation into three types according to systolic flow wave changes: type 1; in

which  $\bar{S}$  is decreased relative to  $\bar{D}$ ; type 2, in which there is no systolic flow; and type 3, in which systolic flow is reversed. They found good correlation between moderate and severe tricuspid regurgitation and type 3 and between types 1 and 2 and mild or absent tricuspid regurgitation. Although no attempt was made to grade this disease in the present study, four patients fit into type 1, one into type 2, and nine into type 3. None of the control subjects showed systolic flow reversal or an antegrade  $\bar{S}:\bar{D}$  ratio of less than 0.6. Only one normal subject had an  $\bar{S}$  less than  $\bar{D}$ , but the ratio was still within normal range at 0.9. Although the mean diameter of the hepatic vein was increased in the disease group compared with the control group, similar to the findings of Sakai et al. [11], there was some overlap between the two groups so that this finding did not prove helpful in the diagnosis of tricuspid regurgitation. In addition, the absence of variation in the size of the dilated hepatic veins and inferior venae cavae with respiration, which was used as an indication for the Doppler examination, was not by itself helpful in differentiating patients with congestive heart failure from those with tricuspid regurgitation.

These findings are also consistent with those of Pennestri et al. [10], who found that the presence of retrograde systolic flow or a decrease in antegrade systolic flow correlates well with the presence of tricuspid regurgitation (as depicted by ventriculography). Of their 47 patients with tricuspid regurgitation, 64% had retrograde systolic flow, whereas 66% of the 15 patients in the present study had this finding. In addition, 26% of their patients had an antegrade  $\bar{S}:\bar{D}$  ratio of less than 0.6, whereas 27% of the patients in the present study had a ratio of less than 0.6. It also appears from their study that the Doppler examination of the hepatic vein was at least as sensitive as Doppler echocardiography in detecting tricuspid regurgitation. In the present study, all but one of the patients with tricuspid regurgitation had either retrograde systolic flow or a ratio of antegrade systolic/diastolic flow velocity of less than 0.6. Moreover, all but one patient had an antegrade

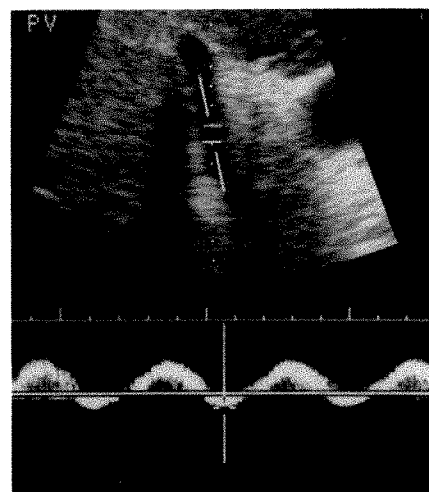


Fig. 8.—Portal vein duplex Doppler sonogram in tricuspid regurgitation shows pulsatile waveform with retrograde flow presumably during systole.



diastolic flow velocity greater than 26 cm/sec. A large retrograde v wave (more than 16 cm/sec) was also seen in 12 patients and a similar large a wave was seen in nine. The changes in the systolic velocity and  $\bar{S}:\bar{D}$  ratio were used as the main criteria for the diagnosis of tricuspid regurgitation. The  $\bar{D}$  value of greater than 26 cm/sec was not helpful, as it was seen in 21% of normal subjects. Similar findings also were reported by Pennestri et al. [10]. In addition to these findings, all 15 patients in the disease group exhibited a pulsatile portal venous waveform in which flow during systole dropped to or below the baseline (Fig. 8) [9].

One of the 15 patients had a false-negative diagnosis by the hepatic vein Doppler criteria I used. However, this patient had retrograde  $\bar{v}$  and  $\bar{a}$  velocities that were greater than 16 cm/sec and an antegrade  $\bar{D}$  greater than 26 cm/sec. Two diagnoses were false positive; one was due to an aortic-right atrial fistula, which essentially produced the same hemodynamic changes as tricuspid regurgitation. The exact reason for the other false-positive diagnosis is not known, but the Doppler waveform of the portal vein was consistent with tricuspid regurgitation, and this could represent a false-negative diagnosis of Doppler echocardiography.

In summary, this study shows that it is possible to diagnose tricuspid regurgitation by duplex Doppler examination of the hepatic vein in patients with liver dysfunction or rapid onset of ascites. Although a diagnosis of tricuspid regurgitation can be made by Doppler imaging of the portal vein, as shown in our previous study, the changes in the Doppler waveform of the hepatic vein in this disease may occur earlier than those in the portal vein, because of the direct communication of the hepatic veins with the right atrium. A thorough knowledge and accurate analysis of the various components of the normal spectral Doppler waveform of the hepatic veins and the nature and mechanics of waveform changes in tricuspid regurgitation are essential for detection of this disease and for initiation of appropriate and timely treatment.

#### ACKNOWLEDGMENTS

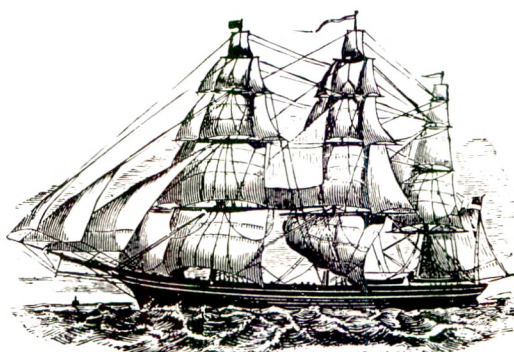
I thank the department sonographers for help in performing this study, Nicole Raitt for typing the manuscript, Phyllis Bergman for

editing efforts, and the department photographers for technical assistance.

#### REFERENCES

1. Hosoki T, Kuroda C, Tokunaga K, Marukawa T, Masuike M, Kozuka T. Hepatic venous outflow obstruction: evaluation with pulsed duplex sonography. *Radiology* **1989**;170:733-737
2. Keller MS, Taylor KJW, Riely CA. Pseudoportal Doppler signal in the partially obstructed inferior vena cava. *Radiology* **1989**;170:475-477
3. Miller VE, Berland LL. Pulsed Doppler duplex sonography and CT of portal vein thrombosis. *AJR* **1985**;145:73-76
4. Weltin G, Taylor KJW, Carter AR, Taylor CR. Duplex Doppler: identification of cavernous transformation of the portal vein. *AJR* **1985**;144:999-1001
5. Patriquin H, Lafortune M, Burns PN, Dauzat M. Duplex Doppler examination in portal hypertension: technique and anatomy. *AJR* **1987**;149:71-76
6. Nelson RC, Lovett KE, Chezmar JL, et al. Comparison of pulsed Doppler sonography and angiography in patients with portal hypertension. *AJR* **1987**;149:77-81
7. Brown BP, Abu-Yousef M, Farner R, LaBrecque D, Gingrich R. Doppler sonography: a noninvasive method for evaluation of hepatic venocclusive disease. *AJR* **1990**;154:721-724
8. Longley DG, Skolnick ML, Zajko AB, Bron KM. Duplex Doppler sonography in the evaluation of adult patients before and after liver transplantation. *AJR* **1988**;151:687-696
9. Abu-Yousef M, Milam SG, Farner RM. Pulsatile portal vein flow: a sign of tricuspid regurgitation on duplex Doppler sonography. *AJR* **1990**;155:785-788
10. Pennestri F, Loperfido F, Salvatori M, et al. Assessment of tricuspid regurgitation by pulsed Doppler ultrasonography of the hepatic veins. *Am J Cardiol* **1984**;54:363-368
11. Sakai K, Nakamura K, Satomi G, Kondo M, Hirokawa K. Evaluation of tricuspid regurgitation by blood flow pattern in the hepatic vein using pulsed Doppler technique. *Am Heart J* **1984**;108:516-523
12. Carreras F, Borrás X, Auge JM, Pons-Llado G. Pulsed Doppler assessment of tricuspid regurgitation: usefulness of regurgitant signal patterns for estimation of severity. *Angiology* **1988**;39:788-794
13. Cohen MV. Arterial and venous pulse recordings, apexcardiography, phonocardiography, and systolic time intervals. In: Goldberger E, ed. *Textbook of clinical cardiology*. St. Louis: Mosby, **1982**:83-122
14. Hurst JW, Schlant RC. Examination of the venous pulse. In: Hurst JW, Logue RB, Schlant RC, Wenger NK, eds. *The heart*, 3rd ed. New York: McGraw-Hill, **1974**:179-189
15. Hansing CE, Rowe GG. Tricuspid insufficiency: a study of hemodynamics and pathogenesis. *Circulation* **1972**;45:793-799
16. Blasco VV. Features of hepatic involvement in congestive heart failure. *Cardiovasc Rev Rep* **1983**;4:963-966





Come to the  
American Roentgen Ray Society

91<sup>st</sup>

ANNUAL MEETING

---

Boston, MA

---

Sheraton Boston Hotel  
May 5-10, 1991

---

---

Scientific Program (200 papers)

Instructional Courses (60 hours)

Categorical Course on Body MR Imaging

The Caldwell Lecture

Award Papers

Scientific Exhibits

Social, Golf, and Tennis Programs

Guest Programs





# Portal Venous System After Portosystemic Shunts or Endoscopic Sclerotherapy: Evaluation with Doppler Sonography

Scott Rice<sup>1</sup>  
Kevin P. Lee  
Meade B. Johnson  
Jacob Korula  
Philip W. Ralls

We sought to determine the usefulness of duplex Doppler sonography in the assessment of blood flow and clot formation in the portal vein in 44 patients with portal hypertension and bleeding esophageal varices who had undergone either endoscopic sclerotherapy (28 cases) or portosystemic shunt procedures (16 cases). The main, left, and right portal veins (collectively referred to as intrahepatic portal veins), superior mesenteric vein, splenic vein, and shunt were assessed for flow direction, presence of thrombi, and collaterals. Patent shunts were visualized in 12 (75%) of the 16 cases. Clot was detected in 27 (69%) of 39 intrahepatic portal veins in patients with end-to-side shunts, in six (67%) of nine intrahepatic portal veins in patients with distal splenorenal shunts, and in five (5%) of 92 intrahepatic portal veins in patients who had had endoscopic sclerotherapy. Flow in the main portal vein was hepatopetal in two (15%) of 13 patients with patent shunts (one end-to-side portacaval shunt and one distal splenorenal shunt). Flow in the main portal vein was hepatopetal in 26 (93%) of 28 patients who had had endoscopic sclerotherapy.

Our data suggest endoscopic sclerotherapy preserves antegrade portal flow and results in fewer portal vein clots than surgical portosystemic shunts do. Patterns of thrombosis and flow direction vary unpredictably from patient to patient. Shunt patency should not be inferred without direct visualization of the shunt.

*AJR* 156:85-89, January 1991

Patients with bleeding esophageal varices from portal hypertension require treatment to prevent life-threatening hemorrhage. Standard therapy includes decompression via surgical portosystemic shunts or endoscopic sclerotherapy.

The effects of surgical portosystemic shunt procedures on intrahepatic portal blood flow and clot formation have been addressed in the literature [1-5]. Several studies [6-9] have used Doppler sonography to evaluate the main portal vein, but only recently have data for intrahepatic portal veins been reported [10]. To our knowledge, no detailed information is available on Doppler sonographic studies of the portal system in patients who have had endoscopic sclerotherapy.

We report the results of Doppler sonography in patients with portal hypertension who had undergone either endoscopic variceal sclerotherapy or portosystemic shunting for bleeding esophageal varices.

## Patients and Methods

The study group consisted of 44 patients who had undergone either endoscopic sclerotherapy (28 patients) or surgical creation of portosystemic shunts (16 patients) for bleeding esophageal varices. Of 16 patients who had portosystemic shunts, 12 had end-to-side portacaval shunts, three had distal splenorenal shunts, and one had a mesocaval shunt. All patients had portal hypertension, esophageal varices, and clinical or histologic evidence of liver cirrhosis. Thirty-five had alcoholic cirrhosis, four had cryptogenic cirrhosis, and five had chronic active hepatitis with positive serologic tests for hepatitis B.

The 44 patients had 54 scans obtained. Thirty-four were scanned after esophageal

Received May 10, 1990; accepted after revision July 19, 1990.

<sup>1</sup> All authors: Department of Radiology, University of Southern California School of Medicine and the Los Angeles County-USC Medical Center, 1200 N. State St., Box 631, Los Angeles, CA 90033. Address reprint requests to P. W. Ralls.

0361-803X/91/1561-0085  
© American Roentgen Ray Society



sclerotherapy (26 patients) or creation of portosystemic shunts (eight patients). Ten other patients had 20 scans both before and after sclerotherapy (two patients, four scans) or creation of portosystemic shunts (eight patients, 16 scans).

Patients were scanned with an Acuson 128 computed sonography system (Mountain View, CA), operating at 3 MHz. Standard technique was used to assess vessel location and morphology and presence and direction of flow. A Doppler frequency of 3.5 MHz was used to obtain the flow information. Scanning was done with the patient supine and in the left lateral decubitus position. When necessary, the patients were given water orally to improve visualization of vessels. Recent food intake was not documented; however, patients were requested to fast [11]. The Doppler sample volume was placed fully within the vessel, and the angle of insonation was kept to less than 60 degrees, when possible. In some instances, obtaining a satisfactory Doppler angle was difficult. Assessment of flow volume was not attempted.

The main portal vein, right portal vein, left portal vein, superior mesenteric vein, splenic vein at the hilum or retropancreatic area, and the portacaval anastomosis in patients with shunts were assessed for flow direction and presence of clot. Three measurements were made of flow direction in each vessel studied. A tabulation was made of vessels that could be imaged and those that could not. Occluding clot was diagnosed when persistent intraluminal echoes were detected, the normal portal venous landmarks were obliterated, and Doppler signal was absent throughout [12]. Nonoccluding clot was diagnosed when Doppler flow was present around the thrombus [13].

## Results

Forty-four patients had one or more Doppler examinations from 1 week to 4 months after intervention. One patient with a shunt was evaluated 5 years after surgery. For all examinations, 263 (92%) of 286 vessels sought were visualized. The main portal, right portal, left portal, and splenic veins were imaged in 98% to 100% of examinations. The least frequently identified vessel was the superior mesenteric vein (36 of 54, 67%). It was often obscured by overlying bowel gas. Shunts were visualized in 12 (75%) of 16 scans and were, hence, the second least frequently visualized structures (Fig. 1). Four of 16 shunts were obscured by gas within the gastrointestinal tract. All three distal splenorenal shunts were seen. No significant difference in visualization rates was seen between patients treated with sclerotherapy and those with portosystemic shunts.

Flow direction was assessed in all visible vessels and is presented in Tables 1–3. All visualized surgical shunts had flow through patent anastomoses toward the inferior vena cava, as intended (Table 1). Overall, 33 (69%) of 48 intrahepatic portal veins in all patients with portosystemic shunts had clot. No predictable pattern of flow was seen in the remaining intrahepatic portal veins. Flow was hepatopetal in five vessels and hepatofugal in nine.

Occluding clot was present in 27 (69%) of 39 intrahepatic portal vessels in patients with end-to-side shunts. No clots were seen in the visualized superior mesenteric or splenic veins. Hepatofugal flow was present in nine (82%) of 11 remaining intrahepatic portal vessels without clot. Flow in the main portal vein stump was present in five (42%) of 12 end-to-side cases, even though the main portal vein is oversewn

as part of this procedure. Of these five patients, one had a partially occluded main portal vein with hepatofugal flow (Fig. 2). In this patient, flow in the left portal vein was hepatofugal, flow in the superior mesenteric vein was hepatopetal, and flow in the shunt was hepatofugal. One patient with a patent end-to-side shunt had hepatopetal flow in the main portal vein. The three remaining patients had hepatofugal flow in the main portal vein, and no clots were present. The only patient with a mesocaval shunt had occlusion of all intrahepatic portal veins. This shunt was not visualized.

Patients with distal splenorenal shunts had clot in six (67%) of nine intrahepatic portal vessels. One patient had thrombosis in all intrahepatic portal vessels, but the shunt was patent (Fig. 3).

Table 2 shows results of preoperative and postoperative scans done in seven patients with end-to-side shunts. These patients are a subset of those in Table 1. Occluding clot developed in 75% of preoperatively patent portal veins (15 new clots/20 vessels at risk) after the shunt procedure. Flow in the superior mesenteric and splenic veins remained hepatopetal in at least 90% of the vessels without clot in these patients. The distal splenorenal shunt procedure (one patient) resulted in thrombosis in the main portal vein with preservation of hepatopetal flow in the other portal vessels.

Patients examined both before and after sclerotherapy (four scans, two patients) had no changes in flow pattern. All flow was hepatopetal.

Of sclerotherapy patients (Table 3), flow in the main portal vein was hepatopetal in 26 (93%) of 28 cases. Occluding clot in the intrahepatic portal veins was seen in only five (5%) of 92 vessels. Only one patient had occluding clot in the main portal vein. Partial thrombosis of the main and right portal veins was observed in one case; the left portal vein was thrombosed. In no case were all of the intrahepatic portal veins thrombosed. Thus, this group had a higher percentage of persistent hepatopetal flow and a lower prevalence of clots than did the group who had shunts.

Our only instance of true bidirectional flow occurred in the right portal vein of a patient treated with sclerotherapy. Flow in the main portal vein was hepatofugal, and flow in the left portal vein was hepatopetal (Fig. 4).

## Discussion

The physiology of portal blood flow is complex and certainly not completely defined by angiography or scintigraphy [14, 15]. A noninvasive technique is desirable both for research purposes and for less-invasive examination of patients with liver disease. Recently, the results of duplex sonography have been shown to correlate well with those of portal angiography [10, 16]. Because of this and its noninvasive character, duplex sonography has been suggested as the appropriate screening test to assess the patency of portacaval shunts [6, 7, 10, 13, 17–20].

Direct evaluation of shunt patency was possible in 75% (12 of 16) of our cases, which is slightly better than or comparable to previous reports [7, 10, 19, 20, 21]. Overall, we were able to image 92% (263 of 286) of vessels. We agree with others



Fig. 1.—Longitudinal sonogram of patent end-to-side portacaval shunt (straight arrow) shows flow into inferior vena cava (curved arrow). Sample volume overlies anastomosis. Note cardiac influence on Doppler waveform.

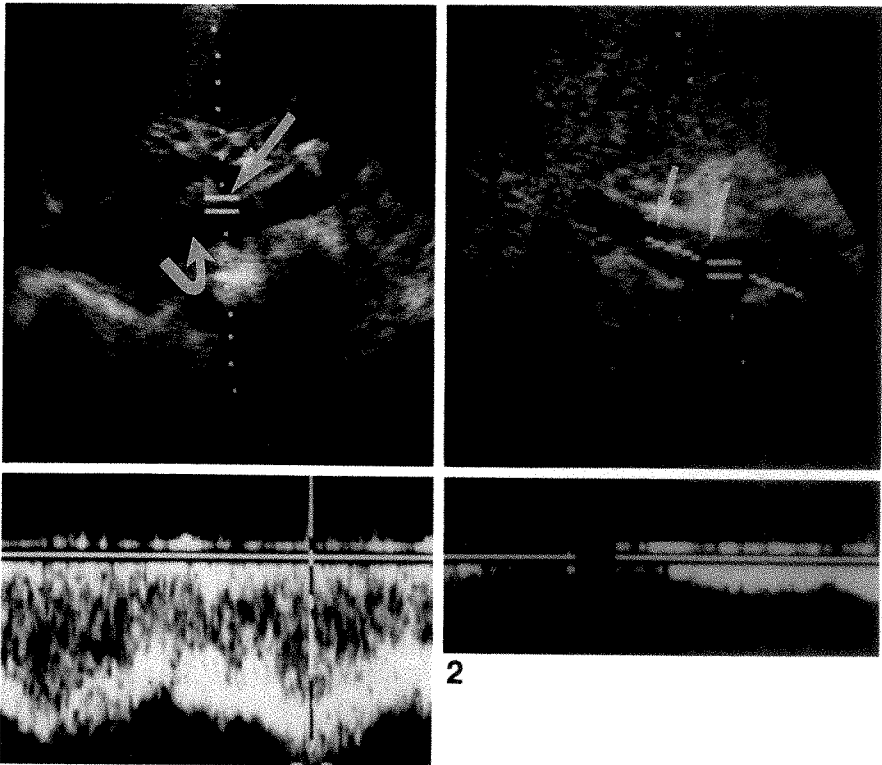


Fig. 2.—Longitudinal sonogram of partially occluded main portal vein stump shows intraluminal echoes (arrows) and low-velocity, intermittent reversed flow.

TABLE 1: Blood Flow Direction and Clot Prevalence in Patients with Portosystemic Shunts

Type of Shunt	MPV	RPV	LPV	SMV	SPV	PCA
End-to-side shunts (13 scans, 13 patients) <sup>a</sup>						
Hepatopetal	1	1	0	6	12	0
Hepatofugal	4	3	2	2	1	9
Clot	8 <sup>b</sup>	9	10	0	0	0
Gas	0	0	1	5	0	4
Distal splenorenal shunts (three scans, three patients)						
Hepatopetal	1	1	1	1	3	0
Hepatofugal	0	0	0	0	0	3
Clot	2	2	2	0	0	0
Gas	0	0	0	2	0	0

Note.—MPV = main portal vein, RPV = right portal vein, LPV = left portal vein; SMV = superior mesenteric vein, SPV = splenic vein, PCA = portacaval anastomosis, Clot = complete or partial clot, Gas = bowel-gas interference. No patients had bidirectional flow.

<sup>a</sup> One patient with mesocaval shunt is included (see text).  
<sup>b</sup> One patient had partially occluding clot with hepatofugal flow.

that duplex sonography should be the first test in evaluating shunt patency.

Our results indicate a high prevalence (69%, 33 of 48) of intrahepatic portal clots in the patients with end-to-side shunts and predominance of hepatofugal flow in the main portal vein and the remaining patent vessels. These results differ markedly from recent duplex sonography reports [9, 10] and previous angiography studies [3, 4].

Bookstein et al. [3] and Reuter and Orloff [4] showed a low prevalence of intrahepatic portal vein clots after creation of

TABLE 2: Preoperative and Postoperative Blood-Flow Direction and Clot Prevalence in Seven Patients with End-to-Side Shunts

Type of Shunt	Preoperative Flow/Postoperative Flow				
	MPV	RPV	LPV	SMV	SPV
Hepatopetal	6/0	6/0	6/0	5/4	7/7
Hepatofugal	1/2	1/1	0/1	0/1	0/0
Clot	0/5	0/6	1/6	0/0	0/0
Gas	0/0	0/0	0/0	2/2	0/0

Note.—MPV = main portal vein, RPV = right portal vein, LPV = left portal vein, SMV = superior mesenteric vein, SPV = splenic vein, Clot = complete or partial clot, Gas = bowel-gas interference. No patients had bidirectional flow.

TABLE 3: Blood-Flow Direction and Clot Prevalence in 28 Patients After Endoscopic Sclerotherapy

Type of Shunt	MPV	RPV	LPV	SMV	SPV
Hepatopetal	26	23	25	13	27
Hepatofugal	1	0	1	2	0
Clot	2 <sup>a</sup>	3 <sup>a</sup>	2 <sup>b</sup>	2 <sup>c</sup>	0
Bidirectional flow	0	1	0	0	0
Gas	0	1	0	11	1

Note.—MPV = main portal vein, RPV = right portal vein, LPV = left portal vein, SMV = superior mesenteric vein, SPV = splenic vein, Clot = complete or partial clot, Gas = bowel-gas interference.

<sup>a</sup> Includes one case with partial thrombosis and hepatopetal flow in the main portal vein and right portal vein.  
<sup>b</sup> All had nonoccluding clot.  
<sup>c</sup> Includes one scan with nonoccluding clot.



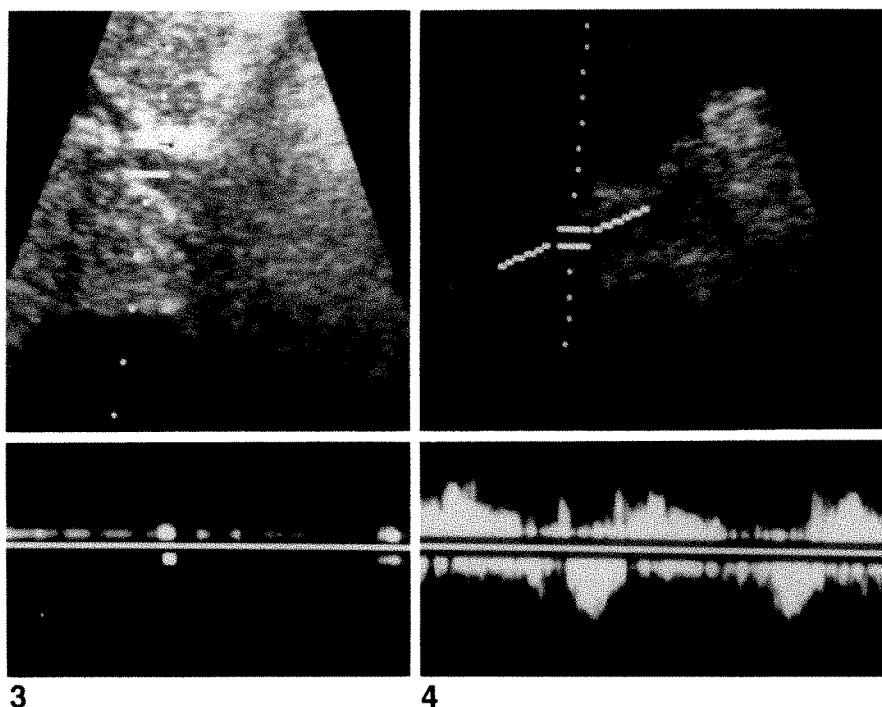


Fig. 3.—Longitudinal sonogram of thrombosed main portal vein shows no detectable flow and only random noise in this highly amplified duplex Doppler image. Distal splenorenal shunt was patent.

Fig. 4.—Doppler image of right portal vein shows signal alternating above and below baseline, consistent with bidirectional flow. Patient had undergone endoscopic sclerotherapy.

end-to-side portacaval shunts (approximately 10%). Hepatofugal or indeterminate flow was present in the majority of their cases. Bookstein et al. were able to determine the direction of flow in the main portal vein in only two of 17 patients by using celiac artery injections. We think carefully performed duplex sonography is reliable for determining patency and flow direction in patients who have shunts.

Lafortune et al. [10] recently concluded that hepatofugal flow in intrahepatic portal veins probably signals a patent shunt and that the presence of a thrombosed shunt resulted in hepatopetal portal flow. Although we did not visualize any thrombosed shunts in this series, our data suggest that shunt patency, or lack thereof, should not be inferred without direct visualization of the shunt; two of our cases (one distal splenorenal and one end-to-side shunt) showed hepatopetal flow in the main portal vein in the presence of a patent shunt.

Our three patients with distal splenorenal shunts had an overall thrombosis rate of 67%. Previous authors have used angiographic data to show a prevalence of thrombosis of 3–10% [10, 22–24] and perhaps up to 27% [1]. Using duplex sonography, previous authors have shown a prevalence of portal vein clot from 22% [7] to 75% [20] in patients with distal splenorenal shunts. Our data for prevalence of clot are similar to those in recent duplex sonography reports, but higher than angiographic data. Our data are too limited to support or refute findings that the distal splenorenal shunt is more likely to preserve patency of the portal vein [1, 2, 12]. Flow direction within the liver was variable, with approximately equal prevalence of hepatopetal and hepatofugal flow in the intrahepatic portal veins.

The clinical significance of intrahepatic portal thrombi is

uncertain, particularly because the biologic behavior of these thrombi, in terms of their persistence or disappearance, is not known. The potential contribution of these thrombi to the formation of postshunt ascites or to the eventual impairment of hepatic function after portosystemic shunt surgery are important clinical issues that require further study.

To our knowledge, this is the first report of duplex Doppler sonography used to evaluate the portal venous system in patients who have undergone endoscopic sclerotherapy. Our data strongly suggest endoscopic sclerotherapy results in significantly fewer portal system clots than portosystemic shunts do. Ohnishi et al. [6] reported findings in 20 patients who underwent transhepatic and endoscopic sclerotherapy for obliteration of varices. They noted increased portal flow at 1 and 18 months, but did not mention portal vein clots or flow reversal. It seems clear that hepatopetal flow is maintained in endoscopic sclerotherapy patients. The clinical significance of this finding is unknown.

Our results show that portal blood flow is complex. Variable flow direction, both hepatopetal and hepatofugal, and various patterns of clotting may occur. Sonographic evaluation can therefore be technically demanding in these patients. Subsequent data have shown us that color Doppler sonography allows more rapid evaluation of complex intrahepatic blood-flow patterns [25]. We think it is important to evaluate flow in all portal vessels that can be imaged to gather as much hemodynamic information as possible in these patients.

#### REFERENCES

1. Nabseth DC, Widrich WC, O'Hara ET, Johnson WC. Flow and pressure characteristics of the portal system before and after splenorenal shunts.



- Surgery* 1975;78:739-748
2. Henderson JM, Millikan WJ, Chipponi J, et al. The incidence and natural history of thrombus in the portal vein following distal splenorenal shunt. *Ann Surg* 1982;196:1-7
  3. Bookstein J, Boijesen E, Olin T, Vang J. Angiography after end-to-side portocaval shunt: clinical, laboratory and pharmacoangiographic observations. *Invest Radiol* 1971;6:101-109
  4. Reuter SR, Orloff MJ. Wedged hepatic venography in patients with end-to-side portocaval shunts. *Radiology* 1974;111:563-566
  5. Fulenwider JT, Nordlinger BM, Millikan WJ, Sones PJ, Warren WD. Portal pseudoperfusion: an angiographic illusion. *Ann Surg* 1979;189:257-268
  6. Ohnishi K, Nakata H, Terabayashi H, et al. The effects of endoscopic sclerotherapy combined with transhepatic variceal obliteration on portal hemodynamics. *Am J Gastroenterol* 1987;82:1138-1142
  7. Bolondi L, Gaiani S, Mazziotti A, et al. Morphological and hemodynamic changes in the portal venous system after distal splenorenal shunt: an ultrasound and pulsed Doppler study. *Hepatology* 1988;8:652-657
  8. Albertyn LT. Acute portal vein thrombosis. *Clin Radiol* 1987;38:645-648
  9. Kawasaki T, Moriyasu F, Nishida O, et al. Analysis of hepatofugal flow in portal venous system using ultrasonic Doppler duplex system. *Am J Gastroenterol* 1989;84:937-941
  10. Lafortune M, Patriquin H, Pomier G, et al. Hemodynamic changes in portal circulation after portosystemic shunts: use of duplex sonography in 43 patients. *AJR* 1987;149:701-706
  11. Pugliese D, Ohnishi K, Tsunoda T, Sabba C, Albano O. Portal hemodynamics after meal in normal subjects and in patients with chronic liver disease studied by echo-Doppler flowmeter. *Am J Gastroenterol* 1987;82:1052-1056
  12. Merritt CRB. Ultrasonographic demonstration of portal vein thrombosis. *Radiology* 1979;133:425-427
  13. Miller VE, Berland LL. Pulsed Doppler duplex sonography and CT of portal vein thrombosis. *AJR* 1985;145:73-76
  14. Rikkers LF, Miller FJ, Christian P. Effect of portosystemic shunt operations on hepatic portal perfusion. *Am J Surg* 1981;141:169-174
  15. Burns PN, Blei AT. More on Doppler flowmetry and portal hypertension. *Gastroenterology* 1988;95:260-261
  16. Nelson RC, Lovett KE, Chezmar JL, et al. Comparison of pulsed Doppler sonography and angiography in patients with portal hypertension. *AJR* 1987;149:77-81
  17. Nakamura T, Moriyasu F, Nobuyuki B, et al. Hemodynamic analysis of postsplenectomy portal thrombosis using ultrasonic Doppler duplex system. *Am J Gastroenterol* 1987;82:1212-1216
  18. Ohnishi K, Saito M, Sato S, et al. Direction of splenic venous flow assessed by pulsed Doppler flowmetry in patients with a large splenorenal shunt: relation to spontaneous hepatic encephalopathy. *Gastroenterology* 1985;89:180-185
  19. Berger LA, Sagor G, George P. The ultrasonic demonstration of portacaval shunts. *Br J Surg* 1979;66:166-168
  20. Ackroyd N, Gill R, Griffiths K, Kossof G, Reeve T. Duplex scanning of the portal vein and portosystemic shunts. *Surgery* 1986;99:591-597
  21. Foley WD, Gleysteen JJ, Lawson TL, et al. Dynamic computed tomography and pulsed Doppler ultrasonography in the evaluation of splenorenal shunt patency. *J Comput Assist Tomogr* 1983;7:106-112
  22. Rotstein LE, Makowka L, Langer B, et al. Thrombosis of the portal vein following distal splenorenal shunt. *Surg Gynecol Obstet* 1979;149:847-851
  23. Maillard JN, Flamant YN, Hay JM, Chandler JG. Selectivity of the distal splenorenal shunt. *Surgery* 1979;86:663-671
  24. Uribe M, Orozco H, Guevara L, et al. Selectivity of the distal splenorenal shunt. *Surgery* 1980;88:328-329
  25. Ralls PW. Color Doppler sonography of the hepatic artery and portal venous system. *AJR* 1990;155:517-525





The Radiology Outreach Foundation (ROF) is a nonprofit corporation whose goal is to help disadvantaged countries improve their health care by providing radiology equipment, books, consultation, education, and training to their practitioners. This assistance is on an application basis that is independent of political, ethnic, or religious orientation of the grantee. It depends on the need of the people and the ability of the ROF to meet that need. The ROF is approved by the U.S. Internal Revenue Service as a tax-exempt organization. It is endorsed by the following radiologic societies:

American Association of Women Radiologists  
American College of Radiology  
American Roentgen Ray Society  
Association of University Radiologists  
Radiological Society of North America  
Society of Chairmen of Academic Radiology Departments  
Society for Pediatric Radiology  
European Society of Pediatric Radiology

All donations to the ROF are tax deductible. Persons who would like to contribute financially to the ROF, would be interested in being a visiting professor, would like to send books or journals to any of the institutions supported by the ROF, or would like further information about the ROF should write to

Charles A. Gooding, M.D.  
President  
Radiology Outreach Foundation  
3415 Sacramento St.  
San Francisco, CA 94118 USA



## Case Report

# Peliosis Hepatis in a Patient with Human Immunodeficiency Virus Infection

D. Randall Radin<sup>1</sup> and Gary C. Kanel<sup>2</sup>

The AIDS epidemic in the United States was first recognized 10 years ago when *Pneumocystis carinii* pneumonia and Kaposi sarcoma were seen with alarming frequency in young homosexual men. Since then, more and more unusual diseases have become familiar to physicians caring for patients infected by the human immunodeficiency virus (HIV). Several reports indicate that peliosis hepatis (multiple blood-filled cavities in the liver) is another condition for which HIV-infected patients are at increased risk [1-3]. We wish to report the CT findings in an HIV-seropositive man with biopsy-proved peliosis of the liver and possible involvement of the spleen and abdominal lymph nodes.

### Case Report

A 34-year-old homosexual man had a several-month history of diarrhea with 20-kg weight loss. Medical history included syphilis, pulmonary tuberculosis, oral candidiasis, and positive serology for HIV antibodies. Physical examination showed hepatosplenomegaly. *Giardia lamblia* was present in the stool. Laboratory evaluation was remarkable for anemia, hypoalbuminemia, and moderate to marked elevation of serum levels of alkaline phosphatase, ranging from 350 to 1045 U/l (normal, 35-110 U/l) during 3 weeks.

Abdominal CT showed enlargement of the left hepatic lobe, dilatation of the portal vein, splenomegaly, diffuse small hepatic and splenic lesions, portal and retroperitoneal lymphadenopathy, ascites, and bilateral pleural effusions (Fig. 1). Most of the liver lesions, which were seen as hypodense nodules smaller than 1 cm in diameter on unenhanced CT, became isodense with IV contrast enhancement. Most of the splenic lesions were seen as nonenhancing hypodense nodules up to 1.5 cm in diameter. Small, central enhancing foci were

present within some of the splenic lesions. The enlarged lymph nodes were homogeneous, measured up to 2 cm in diameter, and showed significant contrast enhancement.

Fine-needle aspirations of hepatic and splenic lesions and paraaortic adenopathy were performed with CT guidance. Cytologic evaluation showed only blood. Smears and cultures for fungi, mycobacteria, and parasites were negative. Smears and cultures of blood, sputum, and urine specimens also were negative. Abdominal paracentesis yielded serosanguinous fluid with no evidence of infection or neoplasm. The ascites decreased with diuretic therapy.

Core biopsy of the liver revealed an intact basic architecture. Portal tracts were normal in size, with minimal fibrosis and a mild mononuclear inflammatory infiltrate. Bile ducts were unremarkable. The cord-sinusoid pattern of the parenchyma was intact. Numerous cystlike spaces were present within the lobules. The cysts were filled with RBCs and granular proteinaceous eosinophilic material, most likely representing plasma. Rarely, small new vessels, consistent with early organizing thrombi, were present within some of the cysts. In some areas the cysts had an endothelial lining, whereas in others, a lining was absent. In addition, dilated sinusoids occasionally merged into the cysts. No tumor cells were present. The pathologic diagnosis was peliosis hepatis. The patient denied use of or exposure to hepatotoxic agents, including alcohol, or drugs or chemicals known to be associated with peliosis hepatis.

The patient was alive and well when last seen, 9 months after presentation, but refused follow-up examination.

### Discussion

Peliosis hepatis is an uncommon condition characterized by multiple blood-filled cavities in the hepatic parenchyma [4]. These cavities range in size from less than 1 mm to

Received May 15, 1990; accepted June 12, 1990.

<sup>1</sup> Department of Radiology, University of Southern California School of Medicine, L.A. County-USC Medical Center, 1200 N. State St., Los Angeles, CA 90033-1084. Address reprint requests to D. R. Radin.

<sup>2</sup> Department of Pathology, University of Southern California School of Medicine, Rancho Los Amigos Medical Center, Downey, CA 90242.

AJR 156:91-92, January 1991 0361-803X/91/1561-0091 © American Roentgen Ray Society



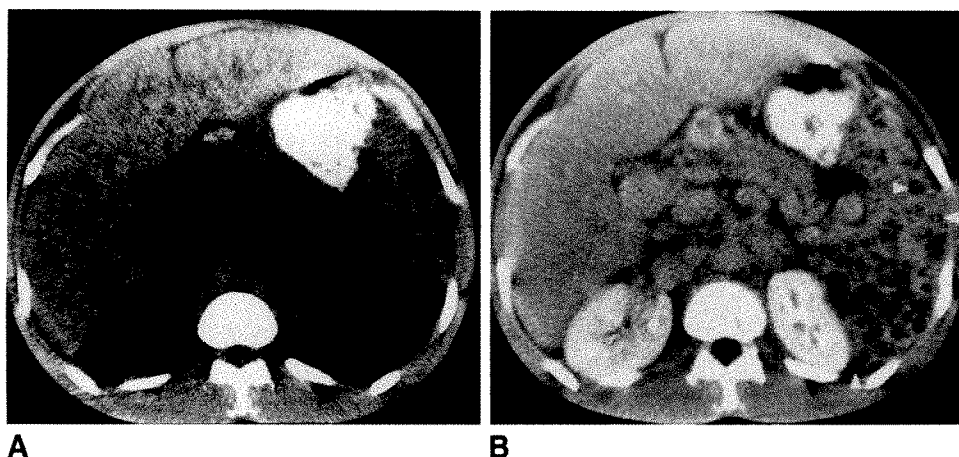


Fig. 1.—A, Unenhanced CT scan shows hypodense nodules in liver and spleen and enlarged retroperitoneal lymph nodes.

B, Enhanced CT scan shows small, central enhancing foci (arrowheads) within some hypodense splenic nodules. Most hepatic nodules are isodense. Retroperitoneal nodes are similar in density to aorta and vena cava.

several centimeters, may or may not have an endothelial lining, and may communicate with dilated sinusoids. Originally described as an incidental autopsy finding in patients with chronic wasting due to tuberculosis or cancer, peliosis hepatis has been reported in patients treated with a variety of drugs, including anabolic steroids, azathioprine, and corticosteroids, and may present with hepatomegaly, cirrhosis with portal hypertension, hepatic failure, or shock due to hepatic rupture [4, 5]. Pathogenetic theories include toxic effect of a substance on the sinusoidal wall, hepatic venous outflow obstruction, and hepatocellular necrosis [4].

Peliosis also has been reported in the rest of the reticulo-endothelial system and elsewhere. Although peliosis hepatis is also present in most of these cases, symptoms from extrahepatic involvement may predominate. In 24 patients with peliosis of the spleen, splenic rupture occurred in 25% of cases [2, 6, 7]. Peliosis of the liver, spleen, retroperitoneal lymph nodes, bone marrow, lungs, pleura, kidneys, adrenal glands, stomach, and ileum was found during autopsy in a man who presented with bilateral spontaneous pneumothorax followed by pulmonary hemorrhage and disseminated intravascular coagulation [8].

Peliosis hepatis has been reported in eight patients with AIDS or AIDS-related complex [1–3]. In one case, involvement of the spleen, porta hepatis lymph nodes, and bone marrow in addition to the liver was seen during autopsy [2]. In a patient with biopsy-proved peliosis hepatis, CT showed "hepatosplenomegaly with multiple zones of diminished density involving both lobes of the liver and the spleen" [2]. Because peliosis was diagnosed by liver biopsy in the other six patients, it is unknown whether or not extrahepatic sites were involved [1, 3]. Possible mechanisms for the development of peliosis in patients with HIV infection include direct or indirect cytopathic effect of the virus on sinusoidal endothelial cells. Inappropriate secretion of immunoregulatory factors acting on vascular endothelium has been suggested as the cause of both peliosis and Kaposi sarcoma [1, 3].

The CT appearance of peliosis hepatis can be suggested by the pathologic findings. If the peliotic cavities are much smaller than 1 cm in diameter, CT findings may be normal. Larger cavities that communicate with sinusoids will have the same attenuation characteristics as blood vessels. Thrombosed cavities will appear as nonenhancing nodules. Thus, in our patient, the CT demonstration of multiple, hypodense hepatic nodules that became isodense with IV contrast enhancement is consistent with (but not specific for) peliosis.

The additional findings of enlargement of the left hepatic lobe, dilatation of the portal vein, splenomegaly, and ascites indicate the presence of portal hypertension, a complication of peliosis hepatis.

Although not proved, it seems likely that the spleen and retroperitoneal lymph nodes in our patient also were involved by peliosis. No other evidence of infection or neoplasm was found, and multiple fine-needle aspirations yielded only blood. The enlarged lymph nodes were similar in density to the aorta and vena cava both before and after IV contrast enhancement. However, most of the splenic lesions did not enhance. This finding could be explained by thrombosis of the peliotic cavities, although the reason that thrombosis might involve predominantly the splenic lesions with relative sparing of the hepatic and nodal lesions is not known. The small, central, enhancing foci seen within some of the splenic nodules in our patient may represent recanalization of organized thrombi [7].

We expect that additional cases of peliosis will be encountered as the AIDS epidemic continues. Awareness of this entity by radiologists is important for three reasons. The CT findings in peliosis may be mistaken for a neoplastic or infectious process for which AIDS patients are at increased risk. Peliosis may have life-threatening complications, including hepatic failure, portal hypertension, and hemorrhage from hepatic or splenic rupture. And, finally, nonoperative diagnosis may require core biopsy rather than fine-needle aspiration.

## REFERENCES

1. Scoazec JY, Marche C, Girard PM, et al. Peliosis hepatis and sinusoidal dilatation during infection by the human immunodeficiency virus (HIV): an ultrastructural study. *Am J Pathol* 1988;131:38–47
2. Czapar CA, Weldon-Linne CM, Moore DM, Rhone DP. Peliosis hepatis in the acquired immunodeficiency syndrome. *Arch Pathol Lab Med* 1986;110:611–613
3. Devars du Mayne JF. Hepatic vascular lesions in AIDS. *JAMA* 1985;254:53–54
4. Simon DM, Krause R, Galambos JT. Peliosis hepatis in a patient with marasmus. *Gastroenterology* 1988;95:805–809
5. van Erpecum KJ, Janssens AR, Kreuning J, Ruiter DJ, Kroon HMJA, Grond AJK. Generalized peliosis hepatis and cirrhosis after long-term use of oral contraceptives. *Am J Gastroenterol* 1988;83:572–575
6. Diebold J, Audouin J. Peliosis of the spleen. *Am J Surg Pathol* 1983;7:197–204
7. Kubosawa H, Konno A, Komatsu T, Ishige H, Kondo Y. Peliosis hepatis: an unusual case involving the spleen and lymph nodes. *Acta Pathol Jpn* 1989;39:212–215
8. Ichijima K, Kobashi Y, Yamabe H, Fujii Y, Inoue Y. Peliosis hepatis: an unusual case involving multiple organs. *Acta Pathol Jpn* 1980;30:109–120



## CT of Acute Pancreatitis: Correlation Between Lack of Contrast Enhancement and Pancreatic Necrosis

C. Daniel Johnson<sup>1</sup>  
David H. Stephens<sup>1</sup>  
Michael G. Sarr<sup>2</sup>

This study was performed to determine if a correlation exists between pancreatic parenchymal enhancement or lack thereof on contrast-enhanced CT and surgical evidence of pancreatic necrosis. Accurate CT assessment of pancreatic vascular perfusion would be helpful in preoperative planning before pancreatic debridement and necrosectomy. The CT scans and medical records were blindly and retrospectively reviewed in 13 patients with the operative diagnosis of pancreatic necrosis. In all cases, CT examinations preceded surgery within 72 hr. Surgical and pathologic findings served as the gold standards for the diagnosis of pancreatic necrosis. Seven (54%) of 13 patients had a region or regions of parenchymal necrosis within the head, body, and/or tail of the pancreas seen during surgery. All seven of these patients had no pancreatic enhancement on CT in at least one region of the pancreas (CT sensitivity = 100%). In four of the seven, two regions were found to be necrotic at surgery, but only one of the two segments did not enhance on CT scans. In three of the seven patients, lack of contrast enhancement on CT (no enhancement of the pancreatic head and body in two patients and throughout the gland in another) correlated with necrosis in the same regions at surgery. The remaining six (46%) patients, who had peripancreatic or small, focal, and/or superficial areas of pancreatic necrosis at surgery, had normal pancreatic enhancement on CT.

Our results show that regions of pancreatic necrosis found surgically correlate with lack of enhancement of pancreatic parenchyma on CT. Peripancreatic necrosis and minor areas of focal or superficial parenchymal necrosis were not detected on CT.

*AJR* 156:93-95, January 1991

Necrotizing pancreatitis is a severe form of acute pancreatitis characterized by destruction of pancreatic parenchyma, peripancreatic tissues, or both [1]. Patients are usually severely ill, and pancreatic infection is a common complication, often responsible for the high mortality rate in these patients [2]. Early recognition of patients with pancreatic necrosis by using CT can be helpful in predicting the severity of pancreatitis and in identifying those patients likely to develop pancreatic infection [2, 3]. The purpose of this study was to correlate enhancement of pancreatic parenchyma on contrast-enhanced CT with necrosis found surgically in patients with suspected necrotizing pancreatitis.

### Materials and Methods

The medical records of 24 patients with the diagnosis of necrotizing pancreatitis confirmed intraoperatively between May 1983 and September 1989 were reviewed. Thirteen patients had contrast-enhanced CT scans obtained within 72 hr of the surgical diagnosis of necrotizing pancreatitis. Patients had a median age of 60 years (range, 24-73 years); all but two were men. Patients were selected for surgical intervention on the basis of their clinical findings. Patients either had sepsis or were not responding to medical therapy. The selection process was not influenced by Ranson's prognostic criteria [4] or by CT findings. Infected fluid obtained by using a CT-directed aspiration of peripancreatic fluid or pancreatic parenchyma was an important factor in the decision to operate.

Received March 28, 1990; accepted after revision July 17, 1990.

<sup>1</sup> Department of Diagnostic Radiology, Mayo Clinic and Mayo Foundation, Rochester, MN 55905. Address reprint requests to C. D. Johnson.

<sup>2</sup> Section of Gastroenterologic and General Surgery, Mayo Clinic and Mayo Foundation, Rochester, MN 55905.

0361-803X/91/1561-0093  
© American Roentgen Ray Society



The surgical and pathologic notes were reviewed without knowledge of the CT findings by a surgeon who carefully categorized the abnormality as either peripancreatic necrosis, small focal or superficial areas of pancreatic necrosis, or definite areas of segmental pancreatic necrosis. Peripancreatic and small focal areas of pancreatic necrosis were considered to represent less severe pancreatitis than definite necrosis in which at least one third of the gland was nonviable. The amount of definite pancreatic necrosis was estimated to involve a single region (pancreatic head, body, or tail), two regions, or three regions. Criteria for definite necrosis at surgery included absence of identifiable normal pancreatic tissue in patients whose major vessels (splenic or portal vein) were exposed in the course of debridement of necrotic tissues. After the pancreas is exposed during surgery, no other organ lies between it and the splenic/portal vein. Exposure of these vessels during surgical debridement implies that pancreatic parenchyma was excised. Peripancreatic and patchy pancreatic necrosis were considered present when tissue necrosis was obvious, but major vessels were not exposed, and histologic review of resected tissue revealed viable pancreatic tissue in the presence of peripancreatic necrosis of connective tissues.

All of the CT scans were obtained within 72 hr before surgery (seven within 24 hr, five within 48 hr, and one within 72 hr). All patients had clinical evidence of severe pancreatitis at the time of CT scanning. IV contrast material was given to all patients. Several radiologists were involved in directing the CT studies. In general, the contrast material was administered as a 50-ml bolus followed by a rapid 100-ml infusion of 60% iodinated contrast material. All scans were 10-mm thick, obtained at 10-mm intervals through the pancreatic bed. Three patients had scans both without and with contrast material, and the remaining patients had only contrast-enhanced scans.

The CT scans were reviewed by two radiologists who agreed on the CT findings without knowledge of the surgical classification. Pancreatic enhancement was categorized as normal (homogeneous enhancement throughout the gland) or abnormal. Abnormal scans were further categorized as to the regions (pancreatic head, body, or tail) of diminished enhancement and the number of regions involved. No attempt was made to compare the ratio of pancreatic to aortic enhancement in Hounsfield units because numerical data had not been saved for retrospective review and because of potential technical problems with partial-volume effect and accurate cursor placement.

Treatment included debridement of nonviable peripancreatic and pancreatic tissues (pancreatic necrosectomy). All patients survived; median hospital stay was 76 days (range, 21–144 days).

## Results

Seven (54%) of the 13 patients had surgical evidence of definite pancreatic necrosis. Two pancreatic regions were necrotic in six (86%) of these seven patients with definite

necrosis: the pancreatic body and head in three, and the body and tail in the other three. The other patient had necrosis of the entire gland. At least one region of the pancreas did not enhance on CT in all seven patients with definite necrosis seen during surgery (Fig. 1). Lack of contrast enhancement on CT correlated with multiple regions of necrosis seen during surgery in three (43%) of the seven patients. The pancreatic head and body were found to be necrotic during surgery and did not enhance in two patients, and the entire gland did not enhance and was totally necrotic in another. In the remaining four patients, only the pancreatic body did not enhance on CT, but during surgery both the pancreatic body and tail were found to be necrotic in three patients and the body and head in another.

Pancreatic necrosis was described by the surgeon at surgery in the remaining six patients, but on review of the surgical report and associated histopathology of resected tissues the disease extent was recategorized as peripancreatic necrosis. Indeed, two of these patients underwent distal pancreatectomy because the surgeon believed that the distal pancreas was necrotic; histologic review of the resected distal pancreas, however, showed viable pancreatic parenchyma and only peripancreatic necrosis. All six of these patients had normal pancreatic enhancement on CT.

The sensitivity and specificity of CT for segmental parenchymal necrosis was 100%. Seven of seven patients with large zones of necrosis had lack of enhancement on CT; and six of six patients with small, focal, or superficial areas of pancreatic or peripancreatic necrosis had normal pancreatic enhancement on CT (Fig. 2).

Pancreatic enlargement was present in all but one of the 13 patients. Peripancreatic fluid was present in all patients. Nine patients had a large amount of fluid at CT, three had a moderate amount, and one had a small amount. All of the patients with definite necrosis shown during surgery had a large amount of fluid at CT.

## Discussion

Necrotizing pancreatitis is a severe form of acute pancreatitis. The gland is swollen and indurated with destruction of pancreatic parenchyma and of peripancreatic tissues. Histologically, necrosis with destruction of interlobular septa is present with phlebitis, arterial thrombosis, capillary disruption, and occasionally hemorrhage [1]. In time, necrotic tissues may become superinfected with enteric organisms (infected necrosis), may be walled off and become infected abscess

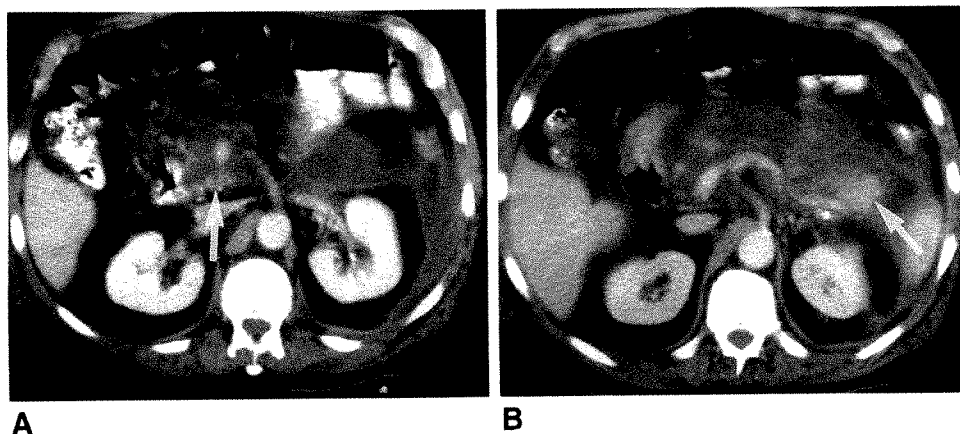


Fig. 1.—A and B, Necrotizing pancreatitis. Contrast-enhanced CT scan shows nonenhancement of majority of pancreas with enhancement of a small portion of pancreatic head and tail (arrows). These findings of severe necrotizing pancreatitis were confirmed at surgery.





Fig. 2.—Peripancreatic and patchy pancreatic necrosis. Contrast-enhanced CT scan shows a normally enhancing pancreatic body and tail. A large amount of fluid is present in anterior pararenal space and lesser sac (which contains a drain). Patient underwent surgery for presumed pancreatic necrosis; however, only small focal areas of pancreatic necrosis and peripancreatic necrosis were present.

collections (pancreatic abscess), or may be reabsorbed without infective or other local complications. Many investigators believe that the risk of infection and clinical severity of the episode increases with the extent of parenchymal necrosis [2, 5, 6]. Present clinical criteria [4] are useful but imperfect in separating patients with acute (self-limited) edematous pancreatitis from those with necrotizing pancreatitis. One study found 39% of 93 patients with necrotizing pancreatitis were initially classified as "mild" by using Ranson's criteria [7].

Kivisaari et al. [8] were the first to report lack of enhancement of the pancreas in patients with necrotizing pancreatitis by using dynamic, contrast-enhanced CT. Beger et al. [9] studied 77 patients and reported a sensitivity of 85% for detecting pancreatic necrosis. The majority of their patients had only partial enhancement of the pancreas. They also reported a false-negative rate of 15% and a false-positive rate of 50%. Bradley et al. [6] demonstrated that dynamic contrast-enhanced CT would reliably differentiate pancreatic necrosis from other pancreatic inflammatory disorders not affecting pancreatic perfusion (uncomplicated pancreatitis, pancreatic abscess, peripancreatic necrosis) and from normal control subjects. Balthazar et al. [3, 5] reported the value of CT in predicting prognosis in acute pancreatitis. Pancreatic necrosis (defined as lack of pancreatic enhancement during dynamic CT) carried the highest mortality and morbidity rates [3].

In this study we have demonstrated that in patients with pancreatic necrosis, contrast-enhanced CT findings correlate closely with findings at surgery. All patients with definite pancreatic necrosis found during surgery had lack of enhancement of one or more regions of the pancreas on CT. As pancreatic necrosis is associated with vascular thrombosis and capillary disruption, we assume that the lack of pancreatic enhancement at CT represents absent pancreatic perfusion. This information can be helpful to the surgeon, not only in predicting prognosis but also in planning surgery. If the findings from contrast-enhanced CT indicate a normally perfused pancreatic head and uncinate process, then the surgeon may elect not to open the pancreatic capsule in this region or to perform a Kocher maneuver to expose this region completely. Conversely, surgical debridement of a pancreatic region that did not enhance at CT could be planned by the surgeon.

Differentiation of pancreatic from peripancreatic necrosis can be difficult during surgery. Unless major vessels (splenic and portal vein) are exposed in the course of debridement, it may be impossible to differentiate intrapancreatic from extrapancreatic necrosis. Peripancreatic necrosis, consisting of necrotic peripancreatic fat and connective tissues, was not identified in any patients on CT. All of these patients had a normally enhancing gland on CT. Four of these six patients had small to moderately sized peripancreatic fluid collections, whereas all patients with pancreatic necrosis had large peripancreatic effusions. Except in predicting prognosis [3], the clinical significance of accurately judging the full extent of pancreatic necrosis is unknown. Currently, we use contrast-enhanced CT as a diagnostic and prognostic indicator, but not as an absolute indication for surgery. Our recent experience has shown that even extensive pancreatic nonenhancement may resolve spontaneously without surgery.

The limitations of CT are most apparent among patients with peripancreatic necrosis. Peripancreatic necrosis has no known specific findings. Its presence can be inferred if pancreatic necrosis is present, for it was always present in our patients with definite pancreatic necrosis. However, peripancreatic necrosis alone may become infected and require surgery. Thus the finding of normal pancreatic parenchymal enhancement on CT does not mean the patient will never require surgical debridement/necrosectomy.

Presently, patients are selected for surgery on the basis of their clinical findings. Most patients have sepsis and are believed to have either infected pancreatic necrosis or a pancreatic abscess. Further study is needed to determine if certain findings at CT are helpful in determining which patients will require surgery before pancreatic infection and its complications arise.

Lack of enhancement of a region of the pancreas on CT correlates reliably with pancreatic necrosis found during surgery. Peripancreatic necrosis and small areas of patchy pancreatic necrosis were not detected on CT.

## REFERENCES

1. Baggenstoss AH. Pathology of pancreatitis. In: Gambill EE, ed. *Pancreatitis*. St. Louis: Mosby, 1973:179-212
2. Beger HG, Krautzberger W, Bittner R, et al. Results of surgical treatment of necrotizing pancreatitis. *World J Surg* 1985;9:972-979
3. Balthazar EJ, Robinson DL, Megibow AJ, Ranson JHC. Acute pancreatitis: value of CT in establishing prognosis. *Radiology* 1990;174:331-336
4. Ranson JHC, Rifkind KM, Roses DF, Fink SD, Eng K, Spencer FC. Prognostic signs and the role of operative management in acute pancreatitis. *Surg Gynecol Obstet* 1974;139:69-81
5. Balthazar EJ, Ranson JH, Naidich DP, Megibow AJ, Caccavale R, Cooper MM. Acute pancreatitis: prognostic value of CT. *Radiology* 1985;156:767-772
6. Bradley EL III, Murphy F, Ferguson C. Prediction of pancreatic necrosis by dynamic pancreatography. *Ann Surg* 1989;210:495-504
7. Block S, Maier W, Bittner R, Buchler M, Malferteiner P, Beger HG. Identification of pancreatic necrosis in severe acute pancreatitis: imaging procedures vs clinical staging. *Gut* 1986;27:1035-1042
8. Kivisaari L, Somer K, Standertskjold-Nordenstam C-G, Schroder T, Kivilaakso E, Lempiinen M. A new method for the diagnosis of acute hemorrhagic-necrotizing pancreatitis using contrast-enhanced CT. *Gastrointest Radiol* 1984;9:27-30
9. Beger HG, Maier W, Block S, Buchler M. How do imaging methods influence the surgical strategy in acute pancreatitis? In: Malferteiner P, Ditschuneit H, eds. *Diagnostic procedures in pancreatic disease*. New York: Springer-Verlag, 1986:54-60



## Videotape Review

**RSNA Today**, Vol. 4, No. 2. Oak Brook, IL: The Radiological Society of North America, 1990. \$55; by subscription, 6 issues annually at \$185 for RSNA members and \$225 for nonmembers (videotape)

This issue of *RSNA Today* covers three topics: "Imaging of the Craniocervical Junction," "Acute Pancreatitis: Prognostic Value of CT," and "Imaging Insights: The Breast Lesion Seen in Only One View." *RSNA Today* continues its track record of high-quality educational products by providing three excellent discussions of practical topics by experts in the field.

Anton Hasso discusses the first topic, "Imaging of the Craniocervical Junction." His discussion is organized, comprehensive, and lucid. This is a concise and interesting presentation of an important area in radiology that has a wide spectrum of pathologic changes. Dr. Hasso's material is excellent, and his images, most of which are CT or MR, are well reproduced on the videotape.

The second segment is an interview with Emil Balthazar by Stanley Siegelman, editor of *Radiology*, concerning Dr. Balthazar's research into the prognostic value of CT in patients with acute pancreatitis. Dr. Siegelman, who himself has a long-standing interest in pancreatitis, leads Dr. Balthazar through the salient points of the thesis that CT can predict which patients might benefit from surgical intervention. Although this is a controversial area in radiology (a number of other centers have not had similar experiences), Dr. Balthazar's data are compelling. This topic is treated fairly, with both supporting data and opposing points of view well represented. With the interview format,

this segment exploits the advantages of videotape education. The CT images are well reproduced.

Edward Sickles hosts the third segment, "Imaging Insights: The Breast Lesion Seen in Only One View." Dr. Sickles's approach to this topic is clear and concise. For those of us who deal with this particular problem almost daily, this segment offers a great deal of practical help and insight. The prime weakness of videotape education, however, is illustrated by this segment. Breast images, which are difficult to reproduce in a slide format, or even on copy film, are not at all well produced on videotape. The inherent low resolution of the videotape format precludes high-quality plain film images for instruction. However, much of Dr. Sickles's approach in this segment is conceptual and is enhanced by line diagrams so that the information conveyed is not lost to the viewer.

In summary, this issue of *RSNA Today* is a good one, and I recommend it to practicing radiologists. The only drawback is the inherent limitations of image production in the videotape format.

Robert A. Clark  
H. Lee Moffitt Cancer Center and Research Institute  
Tampa, FL 33682-0179



## Case Report

# Pancreatitis with Pseudoaneurysm Formation: A Pitfall for the Interventional Radiologist

Michael J. Lee,<sup>1</sup> Sanjay Saini,<sup>1</sup> Stuart C. Geller,<sup>1</sup> Andrew L. Warshaw,<sup>2</sup> and Peter R. Mueller<sup>1</sup>

Interventional radiology has made significant contributions to the care of patients with severe pancreatitis since the introduction of percutaneous procedures for drainage of abscess and fluid collections [1]. Recently, aggressive radiologic intervention has been suggested as either a temporizing measure for stabilizing ill patients before surgery or as a primary treatment [2, 3].

We report the inadvertent placement, and consequent management, of a percutaneous 12-French catheter into a large pseudoaneurysm in a patient with pancreatitis and suspected abscess.

### Case Report

A 63-year-old woman was admitted with severe acute pancreatitis occurring de novo after ERCP. A dynamic CT scan, after bolus IV contrast administration, showed extensive, solid, phlegmonous pancreatitis involving the retroperitoneum and lesser sac. Conservative management was started, but surgical debridement was performed 2 weeks after admission because of the patient's worsening clinical condition.

The patient was initially stable postoperatively, but 10 days later sepsis and high-grade fever developed. A second CT scan showed a collection of fluid in the right anterior pararenal space containing pus, which resolved with percutaneous drainage. The patient improved temporarily, but fever recurred a week later, and resistant *Pseudomonas* was cultured from blood specimens. Despite multiple antibiotic regimens during the ensuing 4 weeks, acute respiratory distress syndrome developed, which eventually required tracheostomy, ventilation, and intensive-care support. Sepsis continued during this period with hypotension requiring treatment with vasopressors, ventilator dependence, and the development of acute renal failure. Multiple CT scans during this period revealed a residual phlegmon in the retroperitoneum without localized fluid collections amenable to percutaneous drainage. Surgery was contraindicated because of the patient's unstable clinical condition. A final CT scan was obtained with the intention of placing a percutaneous catheter into any drainable collection.

The CT scan was obtained without IV contrast material because of the patient's acute renal failure. An area of low attenuation (+10 Hounsfield units) was seen in the head of the pancreas, surrounded by a solid phlegmon (Fig. 1A). Under CT guidance, an 18-gauge sheath needle was advanced into this area and a small amount of brown hemorrhagic fluid was aspirated. After CT documentation of the needle within the collection, the patient had a percutaneous catheter placed under fluoroscopic guidance by use of the Seldinger method. A 0.038-in. (0.096 cm) torque guidewire was advanced through the sheath and coiled in a midline position. The tract was dilated with 8- and 10-French dilators, and a 12-French sump catheter was advanced over the guidewire into the phlegmon.

On placement of the catheter, pulsatile blood flow returned from the catheter. Contrast material was injected through the catheter, revealing a 5-cm pseudoaneurysm involving the pancreaticoduodenal arcade and communicating with the hepatic artery and branches of the superior mesenteric artery (Fig. 1B). The catheter was coiled in this pseudoaneurysm. To prevent retroperitoneal bleeding, we decided to embolize the pseudoaneurysm before withdrawing the percutaneous catheter. A 3-French catheter was advanced coaxially through the 12-French sump catheter into the pseudoaneurysm, and 4000 units of topical thrombin (Thrombinar, bovine, U.S.P., Armour Pharmaceutical Co., Kankakee, IL) were instilled. Consequently, pulsatile blood flow ceased, and the catheter was removed. The patient remained stable and was returned to the intensive-care unit.

The embolization of the pseudoaneurysm proved to be a temporizing measure only. Approximately 2 weeks later, bleeding recurred through existing surgical drains. Arteriography confirmed the presence of a pseudoaneurysm involving the pancreaticoduodenal arcade and frank arterial extravasation. Despite multiple attempts at embolization by means of tissue adhesive, gelatin sponges, and metal coils, the site of arterial bleeding could not be controlled. The patient died shortly after the procedure.

### Discussion

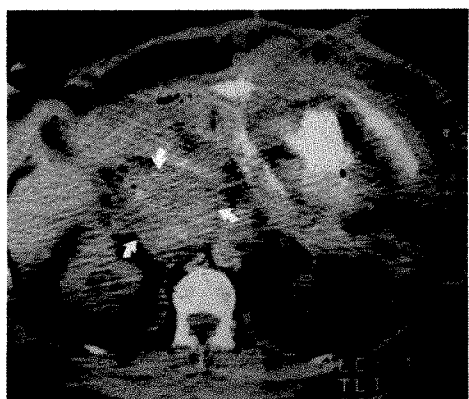
Pseudoaneurysms complicating pancreatitis have been reported extensively in the surgical literature [4, 5] but scant

Received April 30, 1990; accepted after revision June 12, 1990.

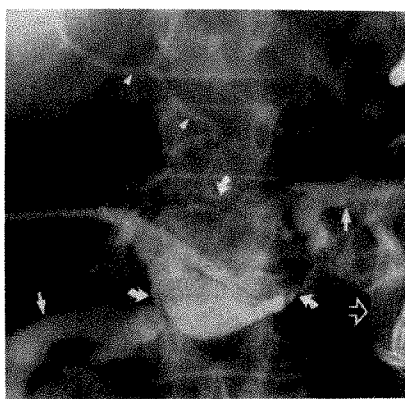
<sup>1</sup> Department of Radiology, Massachusetts General Hospital, Fruit St., Boston, MA 02114. Address reprint requests to P. R. Mueller.

<sup>2</sup> Department of Surgery, Massachusetts General Hospital, Fruit St., Boston, MA 02114.





A



B

Fig. 1.—Pancreatitis with pseudoaneurysm formation.

A, CT scan shows extensive, solid, abdominal phlegmon, with involvement of mesentery and thickening of bowel wall. One area of lower density is seen near pancreatic head (arrows). An 18-gauge needle was placed into this area under CT control, and patient was transferred to fluoroscopy. (Image quality is degraded because of breathing and motion artifact).

B, Radiograph shows contrast material injected through percutaneous catheter outlining a large pseudoaneurysm (curved arrows) with antegrade filling of hepatic artery (arrowheads). Pseudoaneurysm was embolized, bleeding ceased, and catheter was withdrawn. Surgical drains (open arrow) and contrast-filled bowel loops (straight arrows) overlie pancreatic bed.

radiologic literature exists about this topic. Although White et al. [6] estimated a 10% prevalence of pseudoaneurysm formation from a series of 73 patients undergoing arteriography for pancreatitis, to our knowledge, no reports have been published of significant complications from pseudoaneurysm puncture during radiologic intervention in pancreatitis.

Pseudoaneurysm formation in pancreatitis is thought to occur because of autodigestion of arterial walls by pancreatic enzymes, especially elastase, liberated in pancreatitis [7]. The splenic artery most commonly is involved; next are the gastroduodenal, inferior pancreaticoduodenal, and superior pancreaticoduodenal arteries. Involvement of the superior mesenteric, dorsal pancreatic, hepatic, and gastric arteries also has been shown to occur. Rupture of a pseudoaneurysm, either into the retroperitoneum or abdominal cavity, may have serious consequences (the estimated mortality is 37%) [4]. Although angiography remains the gold standard for detection of pseudoaneurysms, recent reports indicate that CT [8] and sonography [9, 10] also may be diagnostic.

CT requires bolus injection of IV contrast material followed by immediate scanning for optimal visualization of these vascular abnormalities. The demonstration of a homogeneously enhancing structure within or adjacent to a pseudocyst or contiguous with a vascular structure is highly suggestive of an associated pseudoaneurysm [8]. However, because many of the patients in whom pseudoaneurysms develop have associated renal and multiorgan failure, contrast-enhanced CT is often contraindicated.

Sonography detects pseudoaneurysms because of their pulsatile nature, except when perianeurysmal fibrosis or thrombosis is present. In the latter instance, Doppler imaging may reveal turbulent arterial flow consistent with pseudoaneurysm formation [9]. Sonographic findings include a hypoechoic cystic structure within a larger cyst, which is highly suggestive of a pseudoaneurysm within a pseudocyst [8]. However, adequate visualization of the pancreatic area with sonography can be problematic in obese patients and in patients with an associated ileus.

Our case emphasizes the typical situation that faces the interventional radiologist. It is often hazardous to administer IV contrast material to patients with severe pancreatitis because of associated renal failure. Thus, it may be difficult to ascertain the presence of a pseudoaneurysm before catheter placement. On the other hand, aggressive radiologic intervention offers the best hope of achieving a curative or temporizing effect in these patients [2, 3]. In this situation, inadvertent

puncture of pseudoaneurysms may occur. A limited, single-level CT scan, after a small bolus of IV contrast material, may help to solve this problem in the future. In our patient, we were reluctant to withdraw the catheter without embolization for fear of retroperitoneal bleeding or exsanguination. When embolization was performed, pulsatile backflow of blood through the catheter stopped, and the catheter was removed without consequence. More aggressive embolization attempts, such as leaving the catheter in situ and placing stainless steel coils into the pseudoaneurysm, or performing arteriography to embolize the feeding vessel, were not considered practical in this case because of the patient's terminally ill condition.

In conclusion, we think that patients with pancreatitis who are undergoing interventional procedures should have either CT with IV contrast administration or sonography to exclude the presence of pseudoaneurysms. If these are not feasible, and inadvertent puncture of a pseudoaneurysm occurs, embolization of the pseudoaneurysm through the percutaneous catheter may control bleeding and permit withdrawal of the catheter.

## REFERENCES

1. vanSonnenberg E, Wittich GR, Casola G, et al. Complicated pancreatic inflammatory disease: diagnostic and therapeutic role of interventional radiology. *Radiology* 1985;155:335-340
2. Freney PC, Lewis GP, Traverso LW, Ryan JA. Infected pancreatic fluid collections: percutaneous catheter drainage. *Radiology* 1988;167:435-441
3. Steiner E, Mueller PR, Hahn PF, et al. Complicated pancreatic abscesses: problems in interventional management. *Radiology* 1988;167:443-446
4. Stable BE, Wilson SE, Debas HT. Reduced mortality from bleeding pseudocysts and pseudoaneurysms caused by pancreatitis. *Arch Surg* 1983;118:45-51
5. Stroud WH, Cullom JW, Anderson MC. Hemorrhagic complications of severe pancreatitis. *Surgery* 1981;90:657-665
6. White AF, Baum S, Buranasiri S. Aneurysms secondary to pancreatitis. *AJR* 1976;127:393-396
7. Geokas MC. The role of elastase in acute pancreatitis. *Arch Pathol* 1968;86:135-141
8. Burke JW, Erickson SJ, Kellum CD, Tegtmeyer CJ, Williamson BRJ, Hansen MF. Pseudoaneurysms complicating pancreatitis: detection by CT. *Radiology* 1986;161:447-450
9. Falkoff GE, Taylor KJW, Morse S. Hepatic artery pseudoaneurysm: diagnosis with real time and pulsed Doppler ultrasound. *Radiology* 1986;158:55-56
10. Gooding GAW. Ultrasound of a superior mesenteric artery aneurysm secondary to pancreatitis: a plea for real time ultrasound of sonolucent masses in pancreatitis. *JCU* 1981;9:255-256



## Endoluminal Sonography of the Urinary Tract: Preliminary Observations

Barry B. Goldberg<sup>1</sup>  
 Demetrius Bagley<sup>2</sup>  
 Ji-Bin Liu<sup>1</sup>  
 Daniel A. Merton<sup>1</sup>  
 Archie Alexander<sup>1</sup>  
 Alfred B. Kurtz<sup>1</sup>

Endoluminal sonography of the urinary tract was performed by using endoluminal ultrasound transducers contained within 2-mm-diameter catheters. The catheters were inserted into the urinary bladder via the urethra and advanced into the ureters and renal pelvis under cystoscopic control; then, cross-sectional images of the bladder, ureters, and renal pelvis were obtained. Two dogs and seven human patients were studied. In one dog, a 4.5-mm pseudopolyp, which was surgically created in the bladder wall, was successfully imaged; in the other, stones 2 mm or larger inserted into the bladder were identified. Of the seven patients, sonography showed stones embedded in the renal parenchyma (one patient) and the mucosa of the distal ureter (one patient). These were ultimately confirmed by their eventual removal. In a third, sonography showed a tumor of the distal ureter and identified the depth of the tumor. This was confirmed by biopsy. In a fourth, sonography clearly showed a crossing vessel as the cause for narrowing of the proximal ureter. In a fifth, sonography showed that the cause of a ureteral stricture was idiopathic. In the last two cases, sonography did not reveal a cause for hematuria. In these last three cases, negative sonographic results were confirmed by direct ureteroscopic examinations and follow-up studies.

Our observations based on this limited study suggest that endoluminal sonography is a useful procedure for diagnosing diseases of the urinary tract. Further study is warranted.

*AJR* 156:99-103, January 1991

During the past year, we have used specially designed 6-French catheters containing 20-MHz transducers to evaluate a variety of lumina, including the urethra, urinary bladder, ureters, renal pelvis, endometrial canal, fallopian tubes, bile ducts, and bowel. Performed in animal models, this initial work has shown the feasibility of endoluminal sonography for detecting and evaluating a number of abnormalities [1]. Cross-sectional sonographic measurements of the wall have correlated closely with the actual thicknesses measured on anatomic specimens. Adjacent structures have been accurately identified. Because of this initial success, these specially designed catheters were used in additional animal models and human subjects to study a variety of urologic abnormalities. The goal of this preliminary study was to evaluate the potential usefulness of this procedure in a variety of urologic conditions.

### Subjects, Materials, and Methods

Specially developed, commercially available 6-French (outer diameter, 2 mm) flexible catheters containing sonographic transducers of 20 MHz were used in all of the procedures in both animal models and humans (Fig. 1). This frequency provided axial resolution of 0.1 mm and a maximum penetration of approximately 2 cm. The blunt-tipped or over-guidewire catheters (Meditech/Boston Scientific, Watertown, MA) were 95 cm long and attached to a sonographic unit (Diasonics IVUS, Milpitas, CA). The transducer inner core, when connected to a motor, allowed transducer rotation of 360°, producing cross-sectional sonographic

Received April 27, 1990; accepted after revision August 6, 1990.

Presented at the annual meeting of the American Roentgen Ray Society, Washington, DC, May 1990.

<sup>1</sup> Department of Radiology, Division of Diagnostic Ultrasound, Jefferson Medical College and Thomas Jefferson University Hospital, 7th Floor, Main Bldg., 132 S. 10th St., Philadelphia, PA 19107-5244. Address reprint requests to B. B. Goldberg.

<sup>2</sup> Department of Urology, Jefferson Medical College and Thomas Jefferson University Hospital, Philadelphia, PA 19107-5244.

0361-803X/91/1561-0099  
 © American Roentgen Ray Society



images at 10° off from true perpendicular. The rotational speed was approximately 30 frames per second, producing a real-time image recorded on videotape with individual images printed on thermal paper. The catheters were reused several times in the animals; in humans, the catheters were used only once. The catheters and inner-core transducers were sterilized by using standard gas sterilization techniques. The inner-core transducer could be resterilized. The catheter is made so that a 27-gauge needle can be inserted through the tip and sterile water injected to displace any air trapped near the transducer that might interfere with the propagation of the ultrasound beam.

Two dogs were studied. After induction of anesthesia, the catheter was placed through the urethra and advanced into the urinary bladder. Sonograms of the bladder wall were made and its thickness was measured. The catheter was then advanced under direct visualization into the ureter via a small suprapubic incision in the abdomen and bladder wall. Multiple images were recorded at various levels. The wall thickness of the ureters was measured at the various levels. After the animals were sacrificed, the ureteral sonographic measurements were repeated and compared with measurements from the anatomic specimens. Three small human renal stones measuring 2, 4, and 5 mm were surgically placed in the urinary bladder. A 4.5-mm

polyplike pseudomass was created in the urinary bladder by surgically invaginating a portion of the wall to simulate a tumor. Endoluminal sonography was then performed in an attempt to detect the stones and pseudomass.

Seven patients (two women and five men 40–72 years old) were then studied. All had previously been examined for specific indications with a variety of urologic tests. Radiographs had shown evidence of renal calculi in two of the seven patients, one in the region of the distal ureter and the other in the kidney. In these two cases, endoscopy could not visualize the location of the stones. In a third case, moderate hydronephrosis was seen on an excretory urogram, the result of extrinsic compression on the proximal ureter of unknown cause. In two other patients, excretory urography revealed moderate hydronephrosis with no apparent cause. The differential diagnosis included a stone, stricture, or tumor. In the last two cases, the patients had hematuria. In both cases the cause was not revealed by excretory urography or CT.

Each patient signed a consent form approved by the internal review board of the university for the additional sonographic study. The sonography was performed in the operating room. For abnormalities within the ureter, rigid cystoscopy was initially performed, followed by the use of a rigid or flexible ureteroscope if indicated. The endoluminal sonographic catheter was then advanced through the working port of the cystoscope into the ureter. The position was confirmed fluoroscopically. In one of the patients with a nephrostomy tube in place, a rigid nephroscope was placed within the renal pelvis with the endoluminal sonographic catheter advanced through the working port of the nephroscope into the renal pelvis. It was then positioned under direct observation.

In order to determine the exact anteroposterior and lateral positions of the transducer-containing catheter, several techniques were used. In the urethra, the region of the compression of the anterior surface could be seen on the cross-sectional sonographic image. With this information, the orientation of the image could be adjusted so that the relationships between right and left and anterior and posterior were accurate. With the catheter in the urine-filled bladder, pressure on the anterior abdominal wall caused distortion of the anterior surface of the bladder, allowing information to be recorded on the

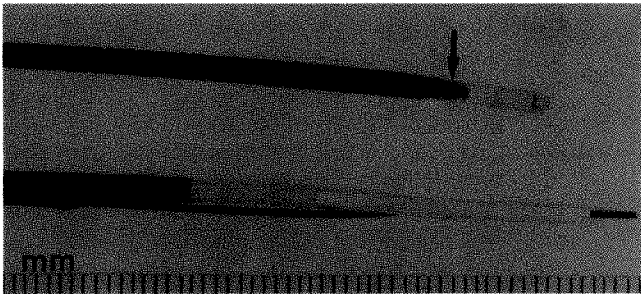


Fig. 1.—Transducer-containing catheters (blunt-tipped and over guide-wire). Tip of transducer (arrow).

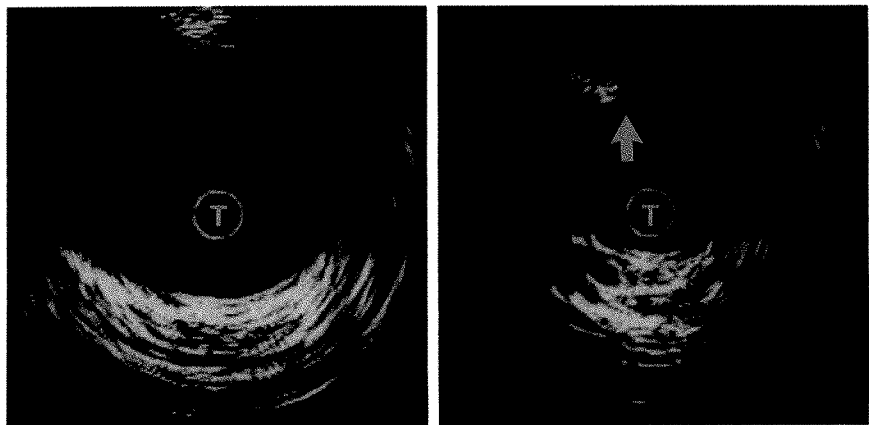


Fig. 2.—A, Cross-sectional sonogram of urine-filled bladder. Initial image without compression of anterior wall.  
B, Cross-sectional sonogram of urine-filled bladder after distortion of anterior wall (arrow) by pressure applied suprapubically in order to confirm proper orientation of transducer-containing catheter.  
T = transducer.

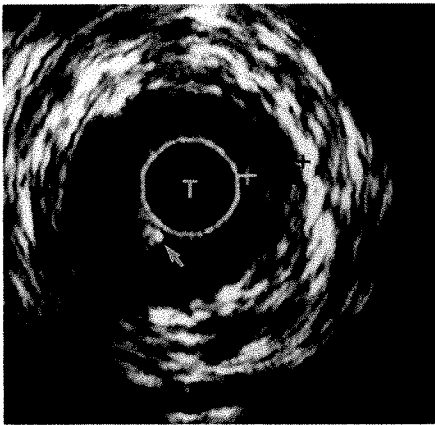


Fig. 3.—Cross-sectional sonogram of distal left ureter shows normal wall (2.3-mm width, cursors). Note bright reflector (arrow) with distal acoustic shadowing produced by guidewire. T = transducer.



position of the sonographic image relative to the correct anatomic orientation (Fig. 2). When the catheter was in the ureter and renal pelvis, proper orientation required the presence of a guidewire, which could be easily visualized by the sonographic transducer as a bright reflector, often producing a distinct acoustic shadow (Fig. 3). The position of this guidewire was easily determined by fluoroscopy or endoscopy. With this information, the relationship of the bright reflection on the sonogram relative to its true anatomic location could be determined and the image oriented appropriately.

## Results

No significant differences were found in the measurements of ureteral wall thickness between the sonograms and anatomic cross sections in the two dogs studied. Eight measurements at 10-mm intervals were recorded, with each paired measurement showing a difference no greater than  $\pm 0.2$  mm ( $p = .29$ ). The thickness of the ureteral wall as measured by sonography was  $1.25 \pm 0.26$  mm and by autopsy  $1.20 \pm 0.30$  mm (mean  $\pm$  SD). The endoluminal transducer was able to detect the stones ranging in size from 2 to 5 mm placed within the urinary bladder (Fig. 4). In the animal in which the mucosa of the urinary bladder was thickened by suturing, producing a 4.5-mm polypoid mass, the sonogram showed the abnormality (Fig. 5). Adjacent structures including lymph nodes, blood vessels, and muscles also could be imaged (Fig. 6).

In two of the seven patients examined, the question to be resolved was whether the stones that were suspected on radiographs were within or outside of the urinary tract. Initial ureteroscopic evaluation failed to detect the locations of the stones. However, endoluminal sonography showed both the size of the stones and their depth beneath the mucosal

surface (Fig. 7). In the other case, the sonogram showed a 4.5-mm stone in an area of eccentric mucosal thickening in the distal ureter (Fig. 8). A guidewire in the ureter initially used as a guide for placement of the ureteroscope and sonographic catheter also could be visualized, and its exact location relative to the area of thickened mucosa and the embedded stone could be determined and confirmed with a radiograph. With this information, the urologist was able to place a stone-removal instrument through the ureteroscope into the area, and the stone was exposed and removed. The actual stone size (5.0 mm) and the sonographic measurement (4.5 mm) correlated closely.

In the third case, the endoluminal catheter was placed cystoscopically into the left ureter in the region where a mass was seen endoscopically. A well-delineated solid hypoechoic area of focal thickening was imaged that measured 4.1 by 3.0 mm. Although there was bulging of the outer ureteral wall, no evidence was found of invasion or visualization of adjacent lymph nodes (Fig. 9). A biopsy was done and the lesion was fulgurated ureteroscopically and found to be a low-grade transitional cell carcinoma. In the fourth case, a suspected filling defect seen in the renal pelvis on a retrograde pyelogram and a CT scan was not confirmed by flexible ureteroscopy, but a shelflike area at the ureteropelvic junction was seen. The endoluminal sonogram of the proximal ureter showed that an artery was crossing perpendicular to the course of the ureter, causing the distortion seen on excretory urography (Fig. 10). In the remaining patients, no abnormality was detected by the endoluminal sonographic approach. In one, evidence of a stricture was seen on urography; the other two patients had a history of hematuria. Endoscopy and subsequent follow-ups failed to reveal any abnormalities.

In all of the patients, similar to the animal experiments, it was possible to visualize structures adjacent to the renal pelvis and ureter, including arteries, veins, and muscle. No

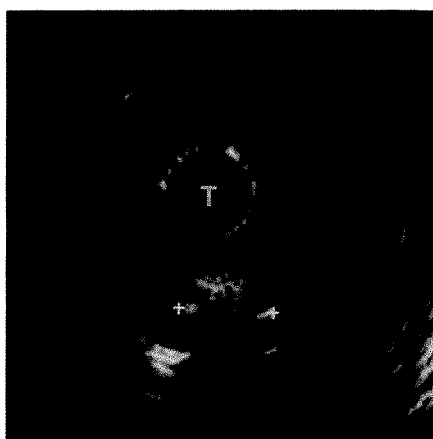


Fig. 4.—Cross-sectional sonogram of urine-filled bladder in a dog shows 4.1-mm stone (cursors) producing distal acoustic shadowing. T = transducer.

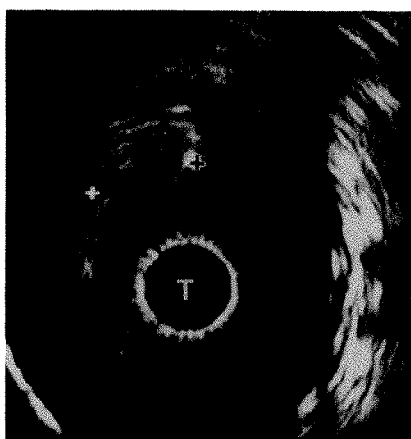


Fig. 5.—Cross-sectional sonogram within urinary bladder of a dog shows polypoid mucosal pseudomass measuring 4.5 mm in diameter (cursors). T = transducer.

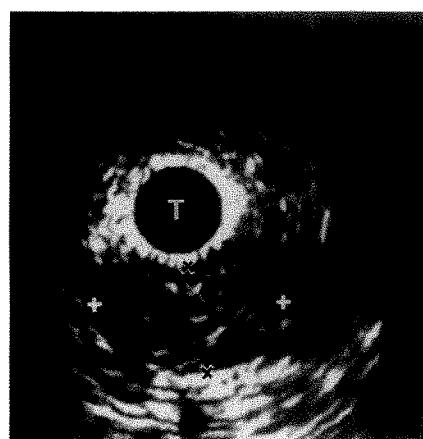
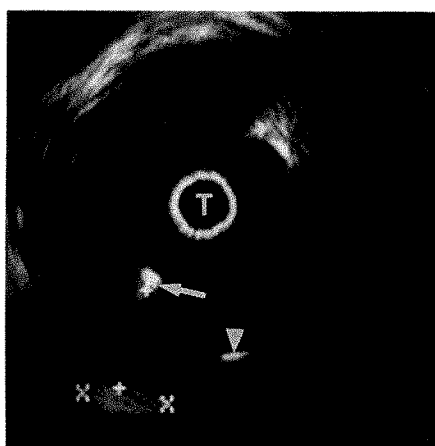
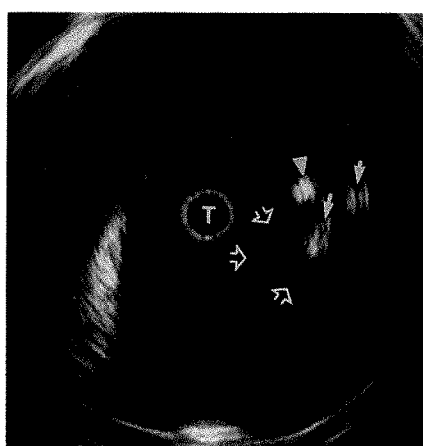


Fig. 6.—Cross-sectional sonogram within ureter shows normal-sized lymph node measuring 8.0 x 4.5 mm (cursors) adjacent to ureter. This was confirmed by dissection at completion of animal experiment. T = transducer.





A



B

Fig. 7.—A, Cross-sectional sonogram obtained from within renal pelvis in a human evaluated via nephrostomy. Note bright reflection from guidewire (arrow) located against mucosal surface. Within renal parenchyma, a stone (x cursors) measuring 6.2 mm in diameter was demonstrated at a distance of 7.5 mm from mucosal surface (plus cursors). Arrowhead delineates a superficial stone seen by endoscopy. At two o'clock, a reverberation echo is noted, the result of air within renal pelvis.

B, Cross-sectional sonogram obtained from within renal pelvis delineates renal papilla (open arrows) with two stones identified in submucosa (solid arrows). Note bright reflection from guidewire in contact with mucosal surface (arrowhead). A portion of another renal papilla is between 7 and 10 o'clock.

T = transducer.

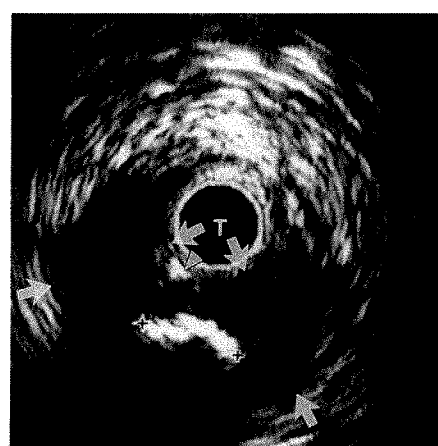
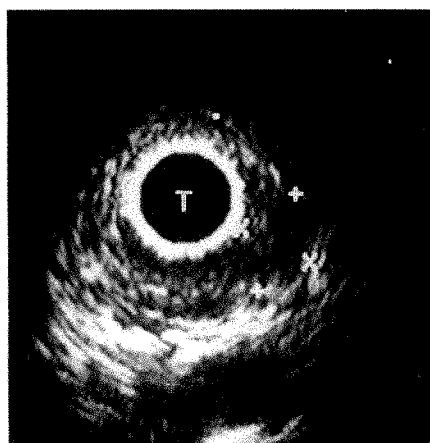
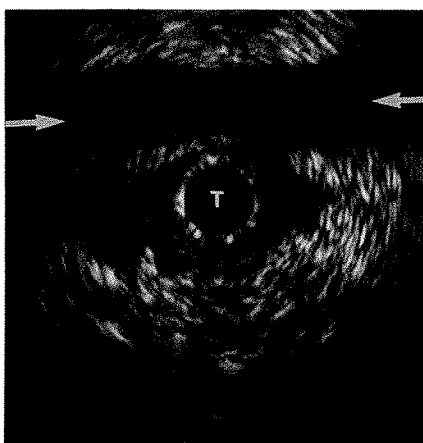


Fig. 8.—Patient with distal ureteral stone. Cross-sectional sonogram of distal left ureter shows thickened hypoechoic mucosa (arrows). Located within area of thickened mucosa was a calculus measuring 4.5 mm (cursors) with distal acoustic shadowing. Reflection from guidewire (arrowhead). T = transducer.



9



10

Fig. 9.—Sonographic transducer (T) located within distal ureter shows area of hypoechoic wall thickening with bulging (cursors) of outer ureteral wall measuring 4.1 x 3.0 mm. This was proved to be a low-grade transitional cell carcinoma.

Fig. 10.—Cross-sectional sonogram delineates a vessel (arrows) crossing perpendicular to course of proximal ureter. T = transducer.

complications occurred as a result of these endoluminal sonographic procedures.

### Discussion

Endoluminal sonography is ideally suited to supply information beyond that provided by other techniques. This procedure has already been used successfully in specially designed sonographic transducer-containing endoscopes for the upper gastrointestinal tract [2].

Our results suggest that endoluminal sonography is a useful procedure. These flexible sonographic transducers permit evaluation of the mucosal surface and walls of the bladder, ureters, and renal pelvis, as well as adjacent structures. The

sonograms produced by these probes allow the identification of areas of wall thickening or narrowing, calculi, and blood vessels. Within the urinary bladder, although rigid endoluminal sonographic probes can be used, the flexible nature of these catheters and their smaller diameters allow their easy passage without the need for urethral dilatation.

These specially developed transducers measuring 2 mm in diameter housed within catheters have limitations in terms of imaging capabilities. The high frequency (20 MHz) prevents penetration beyond a few centimeters. However, newer, relatively lower-frequency transducers (12.5 MHz) are now being developed, which should allow for a greater depth of imaging. The smallness of the transducer itself does limit the resolution, so that, unlike with larger endoluminal catheters placed in



such areas as the esophagus and stomach, it was not possible to delineate the multiple layers of the ureter and, to a lesser extent, the urinary bladder [3]. However, in the cases examined, the questions that were answered were not related to the ability to delineate multiple layers in the normal ureter.

Transducer-containing catheters can be guided into the ureter during the course of a cysto- or ureteroscopic examination. They have proven useful for detecting stones located beneath the surface of the mucosa in the ureter and kidney. The exact depth of the stones beneath the surface could be clearly documented and their size measured. In one case, the calculus of interest was found to be at a minimum of 7.5 mm beneath the surface, and, thus, no attempt was made to remove it. In one case where a mass was identified on ureteroscopy, neither its internal architecture nor its depth of invasion could be seen. The tumor was identified by endoluminal sonography, which showed it to be confined to the ureteral wall and eliminated the small possibility of an embedded stone. Minimal invasion would not be seen, and, of course, the possibility of spread beyond local lymph nodes could not be eliminated. More cases are needed to provide

enough evidence that this technique can be used for the staging of tumors.

#### ACKNOWLEDGMENTS

We thank Sandra M. Ehrlich for statistical analysis, Tessa Mueller and Ji-Wen Yu for typing the manuscript, and Frederic Ross and Kenneth Goodman for preparing the illustrations.

#### REFERENCES

1. Goldberg BB, Liu JB, Merton DA, Kurtz AB. Endoluminal US: experiments with nonvascular uses in animals. *Radiology* **1990**;175(1):39-43
2. Fukuda M, Hirata K, Saito K, et al. On the diagnostic use of echoendoscope in abdominal diseases. I. Diagnostic experiences with a new type of echoendoscope on gastric diseases. *Proc Jpn J Med Ultrasound* **1980**;37:409-410
3. Murata Y, Suzuki S, Hashimoto H. Endoscopic ultrasonography of the upper gastrointestinal tract. *Surg Endosc* **1988**;2:180-183



## Book Review

### **Radiology of Renal Failure, 2nd ed. By Harry J. Griffiths. Philadelphia: Saunders, 272 pp., 1990. \$50**

The target audience of this book is radiologists interested in the radiology of renal failure and clinicians who deal with patients in chronic renal failure. It is divided into eight chapters: genitourinary tract, gastrointestinal tract, cardiopulmonary diseases, bone disease, arthritis, avascular necrosis, soft-tissue calcification, and bone mineral analysis. The first edition (1976) was organized along different lines: initial diagnosis, dialysis, and renal transplantation. The images are mostly plain films; a few sonograms, CT scans, MR images, urograms, and barium studies are included. The quality of the images is excellent, with some exceptions. The quality of the cover, binding, and paper is first-rate. The price is reasonable. The references at the end of each chapter are extensive and current through 1987; some 1988 citations are given.

Chapter 1 includes material on excretory urography and contrast agents, excretory urographic technique, urography in renal failure, and renal calcification. Although well written, this chapter is largely irrelevant as urography no longer is performed intentionally in patients with chronic renal failure. The material on the imaging of diseases leading to renal failure is well written, but it is available in greater detail in urologic radiology texts. MR imaging is given short shrift. The section on imaging renal transplantation is good but brief. The second chapter discusses gastrointestinal radiologic problems in patients with renal failure. It is more interesting from a clinical standpoint than from a radiologic one. The images are single contrast and vary from fair to poor in quality. Many are coned down to such an extent that the findings are difficult to appreciate. Monilial esophagitis

is illustrated by two spot films from a single-contrast study with poor image contrast and nearly invisible findings. It is stated that "the irregularities and filling defects of monilial esophagitis are often as poorly seen as this." This is true only when high-quality double-contrast studies are not performed. A chest film showing free air is reversed left to right. The third chapter on cardiopulmonary diseases affecting patients who have chronic renal failure is well-written and of interest to clinicians and general radiologists. It would be improved by some discussion of CT, which is quite useful in selected instances (e.g., pulmonary calcification, pericardial effusion). The remaining 130 pages and five chapters discuss musculoskeletal aspects of chronic renal failure and are really the heart of this book. Although the coverage of disease processes is briefer than what might be found in the larger orthopedic radiology texts, the discussions and the illustrations are quite good. Radiology residents, interested general radiologists, and clinicians would benefit from reading these chapters.

Although overall this is an excellent text, its appeal will probably be limited because of its overlap between genitourinary, chest, gastrointestinal, and musculoskeletal radiology. I recommend it to radiology residents and training program libraries, general radiologists with referrals from dialysis and transplant centers, and clinicians who care for patients who have chronic renal failure.

Arnold C. Friedman  
Temple University Hospital  
Philadelphia, PA 19140



**1990 ARRS  
Executive Council  
Award**

**Renal Transplant Rejection:  
Diagnosis with  $^{31}\text{P}$  MR Spectroscopy**

Thomas M. Grist<sup>1</sup>  
H. Cecil Charles  
H. Dirk Sostman

We evaluated the role of  $^{31}\text{P}$  MR spectroscopy in the diagnosis of renal transplant allograft dysfunction. Thirty-six  $^{31}\text{P}$  MR spectroscopy examinations were prospectively performed in 35 patients with renal allografts. The study was performed in two phases. In the first phase, 12 transplant recipients with normal graft function were studied as normal controls. During phase two, 24  $^{31}\text{P}$  MR spectroscopy studies were performed in patients at the time of renal transplant biopsy for allograft dysfunction. Twenty-one of these studies were technically adequate. Pathologic analysis of the biopsy specimens showed evidence of allograft rejection in 14 and no rejection in seven. Various phosphorus metabolite ratios were calculated for each patient, including phosphodiester/phosphomonoesters (PDE/PME), phosphomonoesters/inorganic phosphate (PME/Pi), and inorganic phosphate/adenosine triphosphate (Pi/ATP). The PDE/PME and Pi/ATP ratios in the allografts with rejection differed significantly from the corresponding metabolite ratios in patients without rejection ( $p = .017$  and  $p = .024$ , respectively). A PDE/PME ratio exceeding 0.8 had a sensitivity of 100% and specificity of 86% for predicting rejection. A Pi/ATP ratio greater than 0.6 had a sensitivity of 72% and a specificity of 86% for predicting rejection.

We conclude that  $^{31}\text{P}$  MR spectroscopy may be useful as a noninvasive method for evaluating renal metabolism during episodes of transplant allograft dysfunction.

*AJR* 156:105-112, January 1991

Renal allograft failure has a number of causes, including rejection, obstruction, acute tubular necrosis, cyclosporine nephrotoxicity, and renal artery stenosis. Differentiation between these entities, particularly rejection, acute tubular necrosis, and cyclosporine toxicity, continues to be a diagnostic problem without a definitive clinical solution. The noninvasive diagnostic tests available to evaluate renal allograft failure are currently limited to sonography and scintigraphy [1]. No noninvasive diagnostic test exists that will determine definitively the cause of posttransplant graft failure when obstruction has been excluded. Renal transplant biopsy is the gold standard for differentiating allograft rejection from acute tubular necrosis and cyclosporine toxicity. Because different therapies are required for alternative diagnoses, it is very important that an accurate diagnosis is made.

MR spectroscopy has been widely investigated as a noninvasive tool for evaluating the metabolic parameters of various organs. In particular,  $^{31}\text{P}$  MR spectroscopy has been used to observe the relative concentrations of several high energy phosphorus metabolites, including adenosine triphosphate (ATP), inorganic phosphate (Pi), phosphocreatine (PCr), phosphomonoesters (PME), and phosphodiesters (PDE). Alterations in these metabolites have been observed in various pathologic states, including ischemia, enzyme deficiencies, and tumors [2-4]. The use of MR spectroscopy to evaluate disease is predicated on the hypothesis that metabolic changes may precede or be more specific than clinically detectable alterations in tissue morphology.

In vivo  $^{31}\text{P}$  MR spectroscopy has been used to evaluate renal ischemia, obstruction, and acid-base disturbances in animal models [5-8]. In addition,  $^{31}\text{P}$  MR

Received March 21, 1990; accepted after revision July 3, 1990.

Presented at the annual meeting of the American Roentgen Ray Society, Washington, DC, May 1990.

<sup>1</sup> All authors: Department of Radiology, Duke University Medical Center, P.O. Box 3808, Durham, NC 27710. Address reprint requests to T. M. Grist.

0361-803X/91/1561-0105  
© American Roentgen Ray Society



spectroscopy has been used to evaluate heterotopic renal allograft rejection in the rat [9, 10]. In this model, alterations in the relative concentrations of high energy phosphate metabolites correlated with histologic findings in rejecting and nonrejecting kidneys. In vitro  $^{31}\text{P}$  MR spectroscopy has been used to predict viability of cadaveric renal allografts [11, 12]. The feasibility of acquiring  $^{31}\text{P}$  MR spectra in patients with normally functioning renal transplants also has been demonstrated [13, 14]. However, to our knowledge, no investigation of  $^{31}\text{P}$  MR spectroscopy in allograft dysfunction has been reported in humans.

The objective of this work is to prospectively evaluate  $^{31}\text{P}$  MR spectroscopy of the kidney in renal transplant recipients with graft dysfunction as well as normally functioning allografts and to correlate the spectroscopic findings with results of transplant biopsy.

## Methods

### Population of Patients

Thirty-six  $^{31}\text{P}$  MR spectroscopy examinations were performed in 35 patients with renal allografts. The study was performed in two phases. The purpose of the first phase was to characterize the  $^{31}\text{P}$  MR spectroscopic findings in a group of 12 control subjects with normal allograft function. In addition, two different acquisition techniques were evaluated in the control group. In the second phase of the study, we prospectively performed 24 consecutive  $^{31}\text{P}$  MR spectroscopy studies in 23 renal transplant recipients referred to Duke University Medical Center for allograft dysfunction. These patients were identified at the time of referral to the department of radiology for sonographically guided transplant biopsy. Every attempt was made to recruit all renal transplant recipients undergoing biopsy in order to reduce selection bias. However, we were unable to perform the study in approximately 66% of patients because of an unwillingness to consent, superimposed medical emergencies, or limited availability of the MR system. Informed consent was obtained in all cases, and the protocol was approved by our institution review board.

Clinical data recorded at the time of MR spectroscopy included transplant type, (cadaveric or living related donor), duration of the transplant, patient's age, serum creatinine level at the time of biopsy, and baseline serum creatinine level. Ratios of serum creatinine level at the time of biopsy to baseline serum creatinine level were determined for each patient.

Renal cortex biopsy samples were obtained by using a 20-gauge cutting needle and were sent immediately for pathologic analysis. Gross and histologic examinations as well as immunofluorescence studies were performed by renal pathologists with extensive experience in transplant biopsies. The pathologists were unaware of the results of MR imaging and spectroscopy studies, although relevant clinical information was used while interpreting the results of biopsy specimens. On the basis of the pathologic reports, each of the 24 biopsy studies were separated into two categories, rejectors and nonrejectors. In addition, cases of rejection were assigned a relative grade of mild, moderate, and severe rejection. The MR spectroscopy studies were performed within 24 hr of the renal transplant biopsy, except in six cases. In this group of patients, the status of the transplant allograft was thought, on the basis of serial creatinine measurements and requirements for dialysis, not to differ significantly from the status of the graft at the time of biopsy. These delays were typically due to unavailability of the MR scanner and did not exceed 48 hr. The patients were typically on multiple medications at the time

of biopsy. No attempt was made to control for the type or dose of medications the patients were receiving at the time of renal transplant biopsy.

### MR Instrument and Imaging Techniques

All studies were performed on a 1.5-T MR imaging-spectroscopy system (GE Signa, Milwaukee, WI) equipped with the spectroscopy research accessory. The spectra were acquired with a dual-frequency transmit/receive surface coil (Medical Advances, Inc., Milwaukee, WI) tuned to the resonant frequencies of  $^{31}\text{P}$  and  $^1\text{H}$  on our system (25.86 and 63.91 MHz, respectively). The probe is a coplanar array with receiver-coil diameter of 7.5 cm and transmit-coil diameter of 20 cm [15]. In selected cases in which the renal allograft was small and close to the anterior abdominal wall, a smaller, single-frequency  $^{31}\text{P}$  transmit/receive coil (6-cm diameter) was used to acquire the  $^{31}\text{P}$  MR spectra.

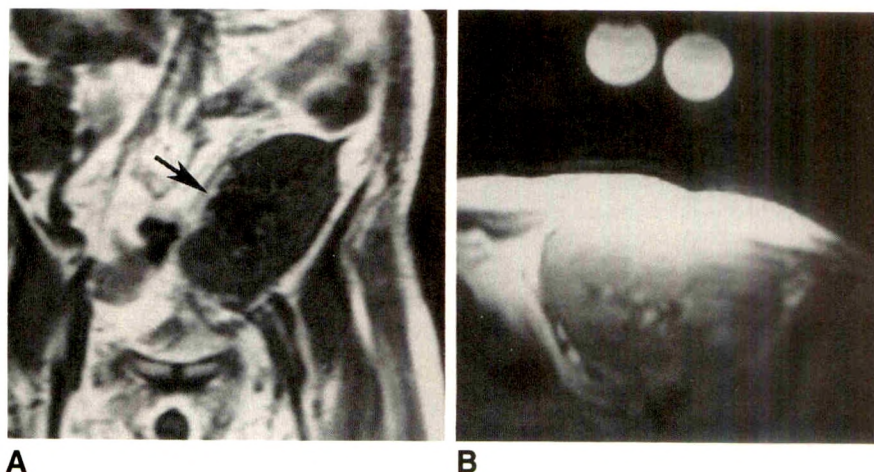
The patient was placed inside the magnet with the surface coil positioned directly over the renal allograft. A 50-ml, 50-mmol/l methylene diphosphonate (MDP) standard was placed on the coil surface opposite the patient's skin. In addition, later in the study four patients were asked to give a urine sample before the MR spectroscopy study for reasons explained in the Discussion section. In this group of patients, the 50-ml urine sample was placed adjacent to the MDP standard on the coil.

The imaging protocol consisted of axial and coronal T1-weighted proton images (500/30 [TR/TE], 1–2 excitations,  $256 \times 128$  acquisition matrix, 24- to 40-cm field of view). Coronal images were used to determine the location of the transplanted kidney within the pelvic fossa and aid in the placement of the surface coil (Fig. 1A). Subsequently, axial and coronal images were obtained with the surface coil in order to confirm that the region of sensitivity of the surface coil corresponded to the renal parenchyma (Fig. 1B). Using depth-resolved surface coil spectroscopy (DRESS) and the hydrogen signal from the surface coil, we adjusted the static magnetic field ( $B_0$ ) homogeneity over a 30-mm-thick slab within the kidney [16]. The homogeneity was altered by using the first-order x, y, or z magnetic-field-gradient shims. In each patient, the homogeneity was measured as the full width at half maximum (FWHM) of the water proton peak. The typical FWHM varied from 0.10 to 0.25 ppm. Then the MR spectrometer was tuned to the resonance frequency of  $^{31}\text{P}$ , and the transmit pulse amplitude was adjusted with a repetition time (TR) of 1500 msec. The optimal transmit pulse amplitude was determined by using an unlocalized RF pulse without an associated  $B_0$  field gradient. The transmit power was set to achieve maximal peak height for the PME peak at 6.9 ppm with reference to PCr. (All chemical shifts defined herein are referenced to PCr of surrounding skeletal muscle, which was assigned a chemical shift of 0 ppm.)

After adjusting the transmit power, localized  $^{31}\text{P}$  spectra were obtained with either DRESS [16] or one-dimensional chemical shift imaging (1D-CSI) [17]. Spectra were acquired by using DRESS in eight of the control subjects and none of the patients with abnormal graft function. The 1D-CSI sequence was used to acquire spectra from four control subjects and all of the patients with transplant dysfunction. During the first phase of the study,  $^{31}\text{P}$  MR spectra were acquired from eight control subjects with DRESS and four control subjects with 1D-CSI. These data were compared in order to determine which technique would be more appropriate for obtaining  $^{31}\text{P}$  spectra from patients with abnormal allograft function. DRESS is a single-voxel acquisition technique that uses a selective RF pulse in the presence of a magnetic-field gradient to obtain a spectrum from a volume of tissue at a given depth. The thickness of the volume of acquisition (12 mm in our study) is determined by the RF pulse and the strength of the  $B_0$  magnetic-field gradient, whereas the diameter



Fig. 1.—A and B, Coronal (A) and axial (B) T1-weighted MR images (500/20/2,  $256 \times 128$  matrix) obtained to position surface coil on kidney (arrow). Coronal image is obtained with body coil and is used to place surface coil. Axial image obtained with surface coil is important to confirm that region of sensitivity of surface coil is confined principally to renal parenchyma.



of the volume is set by the region of sensitivity of the receiver coil (Fig. 2). Typically, spectra were acquired by averaging 600 excitations at a TR of 1500 msec, resulting in a spectral acquisition time of 15 min.

In contrast, the 1D-CSI sequence is a multiple-voxel acquisition sequence. Spatial localization is accomplished by phase encoding in a plane parallel to the plane of the surface coil. For our sequence, 128 phase-encoding steps were acquired, and subsequently a two-dimensional Fourier transform was performed to yield up to 128 voxels containing  $^{31}\text{P}$  spectra. Typically, only the center 10 voxels contained MR spectra, owing to the limited region of sensitivity of the receiver coil. The phase-encoding gradient strength was adjusted to result in slices 1 cm thick in a coronal plane. The TR was 1500 msec, and four excitations were performed for each phase-encoding step. These acquisition parameters result in a total acquisition time of 12 min 53 sec. The 1D-CSI pulse sequence results in a series of contiguous slices 1-cm thick with a diameter that is also determined by the receiver coil's region of sensitivity (5- to 9-cm diameter depending on depth of the slice) (Fig. 3A). The spectral width was 2000 Hz, and 256 complex points were acquired for both sequences. With either sequence, the entire study was performed in approximately 1 hr.

#### Data Processing and Analysis

Each study resulted in axial and coronal T1-weighted MR images, a proton spectrum from the kidney indicating the relative degree of magnetic field homogeneity, an unlocalized phosphorus spectrum from the kidney and superimposed muscle tissue, and a phosphorus data set containing the localized  $^{31}\text{P}$  MR spectroscopy data. Adequacy of the study was determined at the time of examination by observing the signal-to-noise ratio of the spectra. If the signal-to-noise ratio of the phosphomonoester peak was less than three, the data were not included in the analysis. These data were processed, without knowledge of the pathologic results, in the following manner. First, the axial proton images were annotated to mark the location of each slice within the localized phosphorus data. The unlocalized phosphorus spectrum was processed by first applying a 16-Hz exponential filter, baseline correction, and performing a one-dimensional Fourier transform. The peak corresponding to phosphocreatine was assigned a chemical shift of 0 ppm, and this was used as a reference for the localized phosphorus spectra.

For the localized data sets, spectral processing was performed by applying a signal-to-noise enhancing filter, Fourier transforming the

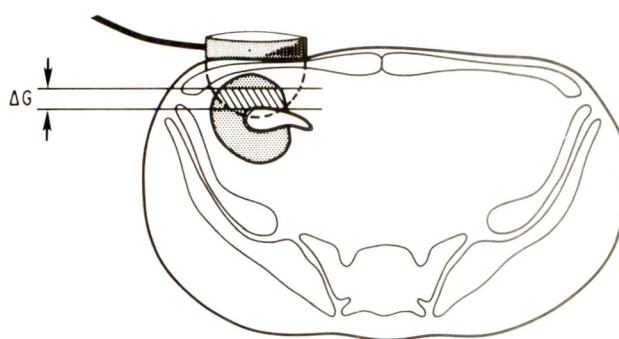


Fig. 2.—Line drawing shows principles of localization for depth-resolved surface-coil spectroscopy (DRESS) of renal transplant. As shown here, DRESS uses a slice-selective magnetic field gradient and a tailored RF excitation pulse to select a slice of tissue ( $\Delta G$ ) at a prescribed depth. Boundaries of acquisition volume are created by intersection of slice and region of sensitivity of surface coil. For one-dimensional chemical shift imaging (1D-CSI) acquisition technique, multiple slices are selected by phase encoding in a coronal plane. Volume of interest also is determined by slice thickness and region of sensitivity of receiver coil in 1D-CSI.

data, manual phasing, baseline correction, and line fitting each spectrum. A two-dimensional Fourier transform was performed on the data acquired with the 1D-CSI sequence. A 16-Hz line-broadening exponential filter was applied before Fourier transformation. Manual phasing compensated for the frequency-dependent phase shifts introduced by delaying data acquisition for slice selection or phase encoding. Typical acquisition delays were 0.5 msec for the 1D-CSI data and 3 msec for the DRESS data. Phase correction of the data results in the creation of baseline artifacts, which add an inverse sinc function to each spectrum. These baseline artifacts were removed by applying an interpolation correction routine, which uses a cubic spline function, added to the original spectrum to remove baseline error. The cubic spline function was determined by placing nine points in the spectrum at consistent positions for each spectrum. After phase correction and baseline fitting, the peak areas, chemical shifts, amplitudes, and line widths were manually determined with the GE peak-fitting routine. A 40% Gaussian line shape was used for each peak. Subsequent measurements were expressed as peak area ratios and as chemical shifts referenced to phosphocreatine.

Several different metabolite ratios were computed from the spectra. First, the ratio of Pi to ATP (Pi/ATP) was determined. In addition, the PDE/PME and PME/Pi ratios were calculated for each patient.



The mean and standard error of the various metabolite ratios were determined for each group including the control group, the group of patients with biopsy results showing rejection, and the group of patients with biopsies indicating normal kidneys or diseases other than rejection. The patients' data were statistically analyzed with a one-way analysis of variance (Kruskal-Wallis test) and the Dunn test to correct for multiple comparisons [18]. To determine the statistical significance of differences between the 1D-CSI and DRESS acquisition techniques in the control subjects, we used a Mann-Whitney test [18].

## Results

Twenty-three patients were referred for 24 MR spectroscopy studies after a sonographically guided biopsy was performed. In three of the 24 studies, we were unable to correlate the histologic findings with MR spectroscopic findings because of inadequate MR spectroscopy data. One of the three patients terminated the study because of claustrophobia. In the second patient, the kidney was 12 cm from the surface and therefore the spectral signal-to-noise ratio was insufficient for interpreting the data. Finally, adequate spectra could not be acquired from the third patient in this group because of an equipment failure during the study.

These exclusions left 21 studies with both spectroscopic and pathologic analysis. Of the 21 studies, 14 were interpreted as showing evidence of rejection and seven had no indication of rejection. In the seven patients without rejection, three showed changes consistent with cyclosporine toxicity, one had interstitial fibrosis probably related to past pyelonephritis, and one patient each had chronic arteriosclerosis, chronic ischemic injury, and a normal biopsy. In 14 patients with rejection, the biopsy results were reported as showing mild ( $n = 5$ ), moderate ( $n = 5$ ), and severe ( $n = 4$ ) rejection. In one patient, two biopsies and two MR spectroscopy studies were done 1 year apart. The first biopsy showed mild focal arterionephrosclerosis, and the second biopsy indicated moderate chronic allograft rejection. These studies were treated as independent samples in the data analysis.

The patients' ages ranged from 10 to 67 years old (mean, 31 years). Nineteen of the patients received cadaveric transplants, and four patients received grafts from living related donors. The average duration of the transplant was 31 months (range, 1–72 months). The mean elevation in serum

creatinine level, which prompted hospitalization for transplant failure, was 230% above the baseline creatinine level. Because patients who underwent biopsy were on several different antirejection prophylactic regimens, we made no attempt to control the differences. A wide variety of therapies were instituted for the treatment of graft failure after preliminary results of the transplant biopsy were obtained, and we made no attempt to account for these differences.

Figures 3A and 3B show a typical T1-weighted proton image and the corresponding  $^{31}\text{P}$  spectra obtained from the kidney of a transplant recipient. The 1D-CSI sequence results in a series of  $^{31}\text{P}$  spectra from contiguous slices (1-cm thick) in a coronal plane. The spectra characteristically contain seven peaks. From left to right, the peaks correspond to PME, Pi, PDE, PCr, and the  $\gamma$ -,  $\alpha$ -, and  $\beta$ -phosphates of ATP. The peak areas depend on the type of tissue and the concentrations of high-energy phosphorus metabolites within the tissue. The more superficial slices contain significant amounts of PCr, which is found in high concentrations within the skeletal muscle of the anterior abdominal wall. As the spectra are obtained from progressively deeper locations, the relative concentration of PCr is reduced, whereas the contribution of PME to the spectrum increases. PME is typically found in high concentrations within the kidney. The signal-to-noise ratio for each spectrum is highly dependent on the distance of the kidney from the coil. The signal-to-noise ratio decreases approximately in the proportion of 1:radius of the receiver coil. Therefore, we experienced a limitation to the sensitivity of the method for slices deeper than 10 cm. Slices deeper than this resulted in spectra with inadequate signal-to-noise ratios for suitable analysis. In addition, depth-dependent alterations in the reception field profile result in a reduction in the localization effectiveness for deeper slices.

Figure 4 shows spectra obtained from a patient with severe rejection, a patient with cyclosporine nephrotoxicity, and a normal control subject. The spectrum obtained from the patient with rejection shows an increase in PDE and Pi and a relative reduction in  $\beta$ -ATP compared with the patient with cyclosporine toxicity and the normal control subject. In Table 1, we have tabulated the relative concentrations of metabolites for the control subjects, for patients with biopsies showing no rejection, and for patients with histologic evidence of rejection. The mean and standard error of the PDE/PME,

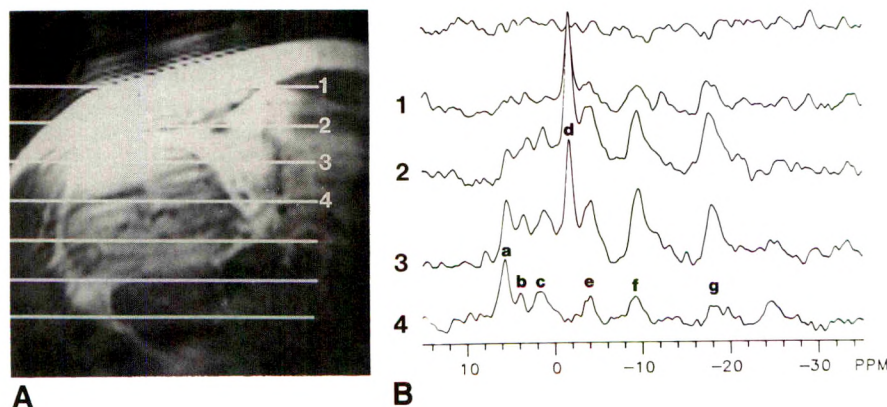


Fig. 3.—A, Axial T1-weighted (500/20) surface-coil image obtained with proton signal from surface coil. Horizontal lines show position of 1-cm-thick slices selected with one-dimensional chemical-shift imaging technique.

B, Contiguous  $^{31}\text{P}$  MR spectra obtained from slices shown in A. Note presence of significant phosphocreatine (PCr) at surface, consistent with muscle tissue. Deepest slice shows a large phosphomonoester peak and little PCr, consistent with renal tissue. Peaks from left to right correspond to phosphomonoesters (a), inorganic phosphate (b), phosphodiester (c), phosphocreatine (d), and  $\gamma$ - (e),  $\alpha$ - (f), and  $\beta$ - (g) phosphates of adenosine triphosphate.



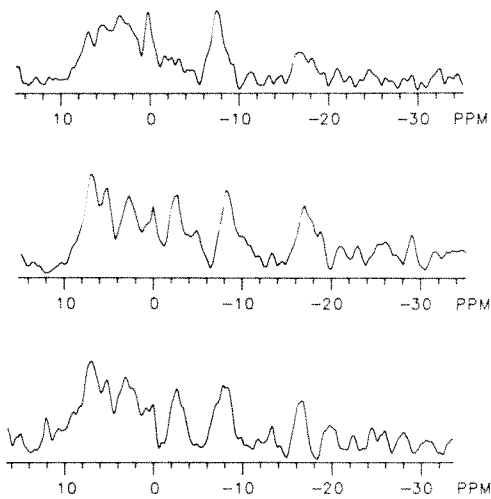


Fig. 4.—<sup>31</sup>P MR spectra from a patient with a normally functioning renal allograft (bottom), a patient with cyclosporine nephrotoxicity (middle), and a patient with moderate cellular rejection (top). Note increase in inorganic phosphate and phosphodiester in patient with rejection compared with normal control subject or patient with cyclosporine toxicity. Phosphocreatine is a contaminant from extrarenal tissue.

TABLE 1: Mean (Standard Error) of Metabolite Ratios

Patient Group	PDE/PME	PME/Pi	Pi/ATP
Rejection (n = 14)	1.43 (0.21)	1.04 (0.23)	1.10 (0.21)
No rejection (n = 7)	0.79 (0.42)	3.60 (0.86)	0.41 (0.07)
Normal control (n = 12)			
Dress (n = 8)	0.55 (0.10)	3.77 (0.44)	0.35 (0.05)
1D-CSI (n = 4)	0.47 (0.11)	1.87 (0.94)	0.67 (0.17)

Note.—PDE = phosphodiester, PME = phosphomonoester, Pi = inorganic phosphate, ATP = adenosine triphosphate, DRESS = depth-resolved surface-coil spectroscopy, 1D-CSI = one-dimensional chemical-shift imaging.

PME/Pi, and ATP/Pi ratios are shown. The relatively small sample size makes assumptions regarding a normal sample distribution invalid. Therefore, nonparametric tests were used in the data analysis. Table 2 shows the *p* value and the significance level for the differences in metabolite ratio means for the following groups: patients with biopsies showing rejection vs those with no rejection, control subjects vs patients with no rejection, and rejecting vs control kidneys. A statistically significant difference between the mean PDE/PME and the mean Pi/ATP ratios for the rejecting vs nonrejecting kidneys was observed (*p* = .024 and *p* = .017, respectively).

We attempted to compare the patients who had rejection with the small subgroup of patients with cyclosporine nephrotoxicity. The limited number of patients with cyclosporine toxicity (*n* = 3) in this study makes comparison of spectroscopic findings between the groups unreliable. Although there is a trend toward elevated PDE/PME in the patients with rejection as compared with those who had cyclosporine toxicity, the difference is not statistically significant (*p* = .085). The differences between the Pi/ATP or PME/Pi ratios of the rejection and cyclosporine toxicity groups also were not statistically significant.

TABLE 2: Significance of Differences Between Mean Metabolite Ratio Ranks

Comparison	Pi/ATP	PME/Pi	PDE/PME
Rejection vs no rejection <sup>a</sup>	<i>p</i> = .017	<i>p</i> = .180	<i>p</i> = .0240
Rejection vs controls <sup>a</sup>	<i>p</i> > .500	<i>p</i> = .046	<i>p</i> = .0027
No rejection vs controls <sup>a</sup>	<i>p</i> > .500	<i>p</i> > .500	<i>p</i> > .5000
Controls: DRESS vs 1D-CSI <sup>b</sup>	<i>p</i> = .040	<i>p</i> = .240	<i>p</i> = .7300

Note.—Pi = inorganic phosphate, ATP = adenosine triphosphate, PME = phosphomonoester, PDE = phosphodiester, DRESS = depth-resolved surface-coil spectroscopy, 1D-CSI = one-dimensional chemical-shift imaging.

<sup>a</sup> Results of Dunn's Test.

<sup>b</sup> Results of Mann-Whitney Test.

In Figure 5, the mean PDE/PME and Pi/ATP ratios are shown for the control subjects and for patients with mild, moderate, and severe rejection. There is a trend toward increasing PDE/PME ratios with increasing severity of rejection. The Pi/ATP ratio shows no clear correlation with the histologic grade.

Figure 6 shows the results of receiver-operating-characteristic analysis showing the relationship between sensitivity and specificity of various metabolite ratios for detecting rejection.

Discussion

The elevated Pi/ATP ratio observed in patients with rejection in this study is consistent with experimental results in animal models [9, 10]. Pi is a breakdown product resulting from the hydrolysis of high-energy phosphate bonds that is frequently associated with tissue ischemia. ATP, on the other hand, is an energy-storage phosphate that must be replenished in the kidney by oxidative phosphorylation. The Pi/ATP ratio has been shown to be a sensitive indicator of tissue ischemia in the kidney and other organs [2, 5]. We postulate that the elevated Pi/ATP ratio observed in patients with rejection is a result of tissue ischemia from reduced renal

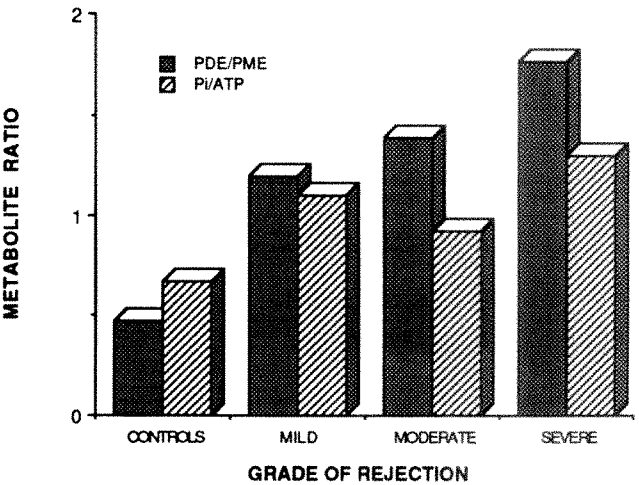


Fig. 5.—Mean phosphodiester/phosphomonoester (PDE/PME) and inorganic phosphate/adenosine triphosphate (Pi/ATP) ratios plotted as a function of rejection grade.



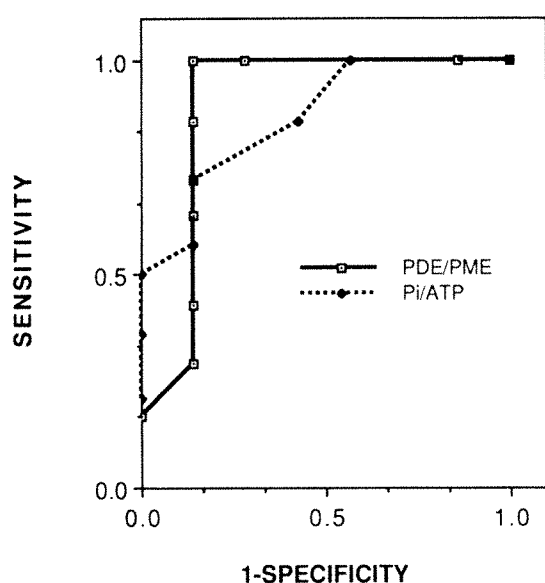


Fig. 6.—Receiver-operating-characteristic analysis shows relationship between sensitivity and specificity of phosphodiester/phosphomonoester (PDE/PME) and inorganic phosphate/adenosine triphosphate (Pi/ATP) ratios for detecting rejection.

perfusion. Although the differences in mean Pi/ATP ratios between the rejectors and the nonrejectors are statistically significant, considerable overlap between the two groups exists. For example, one of the nonrejectors and one control subject each had Pi/ATP ratios above 0.70 (0.72 and 1.14, respectively). On the other hand, two of the patients with rejection had Pi/ATP ratios less than 0.4.

The cause of an elevated ratio of PDE/PME in the patients with rejection is unknown; however, several possible explanations exist. In our study, the elevated PDE/PME ratio results principally from an increase in the PDE contribution to the spectra. The PME resonance is thought to have contributions from phosphorylethanolamine (PE), phosphorylcholine (PC), and adenosine monophosphate (AMP) [12]. The PDE resonance has been shown to be a combination of several compounds, including glycerophosphocholine (GPC), glycerophosphoethanolamine (GPE), the mobile fractions of large membrane phospholipid molecules, and Pi found in acidotic urine.

First, as a consequence of the low pH of urine, the Pi found in urine has a chemical shift similar to that of PDE [11]. Previous investigators have shown renal obstruction increases the observable PDE peak through an increase in the urine Pi [19]. However, none of the patients with rejection had sonographic evidence of obstruction, and therefore this explanation seems unlikely. Phosphate wasting due to a variety of factors has been observed in renal transplants [20]. To investigate this issue, we placed urine samples adjacent to the MDP standard in four patients, two of whom were found to have rejection on pathologic analysis. Although we observed a small peak that resonated in the region of PDE, the amplitude of the resonance was much smaller than the

amplitude of the PDE peak observed in the patients. Because of the close proximity of the urine sample to the receiver coil and the relatively small urine Pi peak, the urine Pi resonance is thought to contribute little to the PDE resonance for slices within the kidney.

As alternative explanation for the elevated PDE/PME ratio is that the increase is related to an increase in the intracellular GPC and GPE [21]. The PME and PDE metabolites are found on the biochemical pathways of phospholipid synthesis and catabolism, respectively. Therefore, changes in these metabolites may be linked to alterations in cell growth. Stimulus for cell growth is known to be associated with renal dysfunction [22].

Recent studies have suggested, however, that the contribution of GPC and GPE to the PDE peak is relatively small [23, 24]. These investigators suggest that the principal component of the PDE peak is related to the membrane phospholipids. This observation is based on the finding of substantial field dependence of the PDE peak, an effect of chemical-shift anisotropy associated with large, relatively immobile, membrane-bound phospholipids. We postulate that the elevated PDE in patients with rejection may be related to an alteration of membrane metabolism associated with the inflammatory changes in rejection. The trend toward increasing PDE/PME ratios associated with severity of rejection (Fig. 5) may represent the sequelae of membrane breakdown or a stimulus for cellular hypertrophy. The absence of a clear trend in the Pi/ATP ratios for different rejection grades is unknown and most likely reflects factors modifying the response of the kidney to renal ischemia.

The elevation of PDE/PME found in this study is consistent with observations made in previous animal models [9, 10]. Animal models have shown an increase in PDE associated with acute rejection, although no definitive explanation is given in two studies.

The difference in Pi/ATP ratios (Table 2) when DRESS is used compared with when 1D-CSI is used is most likely a result of significant differences in the acquisition parameters for the two sequences. For example, in the DRESS acquisition, a 3-msec delay occurs between the end of the RF pulse and the start of data acquisition. In the 1D-CSI sequence, the acquisition delay is 0.5 msec. The longer delay with the DRESS sequence results in greater phase-correction requirements when processing the spectra. The increased phase correction requirements introduce baseline artifacts into the spectra. These baseline artifacts cause error in the peak area measurements for certain metabolites, particularly ATP.

The spectral localization ability of the 1D-CSI technique was preferred to that of the DRESS sequence because of the multiple voxel data sets that were generated. These data sets allowed a choice of spectra that were least contaminated by extrarenal tissue. Both 1D-CSI and DRESS techniques were effective in localization; however, signal emanating from extrarenal tissues does contaminate the spectra. Contamination was easily assessed by noting the intensity of the PCr peak in the renal spectra, because the kidney contains no phosphocreatine [25]. In this study, the mean PCr area constituted less than 10% of the total  $^{31}\text{P}$  signal. Because very little PME



and PDE is found in muscle tissue, contamination was thought not to affect significantly the PDE/PME ratio. In addition, because typical PCr/Pi and PCr/ATP ratios exceed 4:1 in muscle, a PCr peak that constitutes 10% of the <sup>31</sup>P signal contributes less than 2.5% error to the phosphorus signal.

The small sample size in our study limits the applicability of the results in a clinical setting. Particularly, the small number of patients with no evidence of rejection on biopsy findings limits the determination of the specificity of an abnormal metabolite ratio. For example, in a clinical situation, the principal differential diagnosis is likely to include rejection, acute tubular necrosis, and cyclosporine toxicity. None of the non-rejectors had acute tubular necrosis, and only three of seven patients had cyclosporine toxicity.

Inclusion of the four normal control subjects with spectra acquired by 1D-CSI in the analysis is thought to be justified. The control subjects were studied during the same time interval as the patients, and the 1D-CSI acquisition technique was used in both groups. Although it was known that they were control subjects during processing and analysis, this was not thought to influence metabolite measurements significantly.

The sensitivity of this technique, as currently implemented, may be significantly limited by factors that prevent us from acquiring spectra with adequate signal-to-noise ratio for processing. We encountered this problem in one patient when the kidney was too deep for sufficient spectral signal-to-noise ratio. This problem may be circumvented in the future with implementation of more advanced RF coil technology, including quadrature surface coils and whole-volume coils used in conjunction with two-dimensional chemical-shift imaging [26, 27]. Inclusion of three patients with inadequate studies reduces the sensitivity of an elevated metabolite ratio for detecting rejection (i.e., for PDE/PME > 0.8, sensitivity was 82%, vs 100% sensitivity when these cases are excluded). Future efforts should be directed at improving the reliability and signal-to-noise ratio of the acquisition techniques.

The sensitivity and specificity of this test, on the other hand, may be improved by using combinations of metabolite ratios in the analysis. For example, if dual requirements of a PDE/PME ratio greater than 0.8 and a Pi/ATP ratio exceeding 0.6 are met, the sensitivity and specificity are equal to 100% in this small series. From a biochemical standpoint, we are probably justified in treating the PDE/PME and Pi/ATP ratios as independent variables because they are on different cellular metabolic pathways.

Although the number of patients in our study limits the determination of sensitivity and specificity, our results compare favorably with existing techniques. For example, the sensitivity of Doppler sonographic examination of the transplanted kidney is thought to be low (9–13%), whereas the specificity is comparable to our data (91%) [28]. Indium-111 platelet studies demonstrate similar sensitivity (86%) and specificity (93%) [29]. Direct comparison of these techniques is necessary in a larger, prospective trial.

In summary, we have demonstrated the feasibility of performing <sup>31</sup>P MR spectroscopy studies in renal transplant recipients with normally functioning grafts and in patients with

allograft dysfunction. The preliminary results described here indicate that elevated Pi/ATP and PDE/PME are associated with allograft rejection and may be useful in differentiating rejection from other causes of transplant failure. Hence, we encourage the prospective evaluation of a larger group of patients to determine the potential value of <sup>31</sup>P MR spectroscopy in assessing graft dysfunction.

#### ACKNOWLEDGMENTS

The authors are indebted to Mark Algabright for his patience and expertise demonstrated while performing the studies. We gratefully acknowledge B. Vernon, R. Bollinger, J. Clapp, C. Gunnells, S. Schwab, L. Quarrels, and J. Scheinman for referring patients. We also thank Cindy Lawrence for arranging the control studies and F. Sanfilippo for helpful discussions regarding the pathologic analysis. Craig Beam's assistance with statistical analysis of the data was very helpful. Finally, Mirjana Cudic's expertise in preparing the manuscript is greatly appreciated.

#### REFERENCES

1. Flye MW, Rigsby CM, Desire G, et al. Diagnosis of renal allograft rejection by radionuclide scintigraphy, pulse Doppler scanning, indium-111 labeled platelet scintigraphy, and renal biopsy. *Transplant Proc* 1986;18:705
2. Chance B, Eleff S, Leigh JS, Skolow D, Sapega A. Mitochondrial regulations of phosphocreatine/inorganic phosphate ratios in exercising human muscle: a gated P-31 NMR study. *Proc Natl Acad Sci USA* 1981;78:6714–6718
3. Ross BD, Radda GK, Gadian DG, Rocker G, Esiri M, Falconer-Smith J. Examination of a case of suspected McArdle's syndrome by P-31 nuclear magnetic resonance. *N Engl J Med* 1981;304:1338
4. Nidecker AC, Muller S, Ave WP. Extremity bone tumors: evaluation by P-31 MR spectroscopy. *Radiology* 1985;157:167–174
5. Siegel NJ, Avison MJ, Reill HF, et al. Enhanced recovery of renal ATP with post-ischemic infusion of ATP-MgCl<sub>2</sub> determined by P-31 NMR. *Am J Physiol* 1983;245:F530
6. Chan L, Waterton JC, Radda GK. Study of rat kidney in vivo during hypovolemic shock by P-31 NMR. *Biochem Soc Trans* 1981;9:239
7. Vigneron DB, Tzika AA, Hricak H, et al. Complete and partial ureteral obstruction: evaluation of renal effects with P-31 MR spectroscopy and Tc-DMSA scintigraphy. *Radiology* 1988;168:645–650
8. Freeman D, Lowry M, Radda G, et al. P-31 analysis of renal response to respiration acidosis. *Biochem Soc Trans* 1982;10:399
9. Shapiro JI, Haug CE, Weil R, Chan L. P-31 nuclear magnetic resonance study of acute renal dysfunction in rat kidney transplants. *Magn Reson Med* 1987;5:346–353
10. Shapiro JI, Haug CE, Shanley PF, Weil R, Chan L. P-31 nuclear magnetic resonance study of renal allograft rejection in the rat. *Transplantation* 1988;45:17–21
11. Bretan PN, Vigneron DB, James TL, et al. Assessment of renal viability by phosphorus-31 magnetic resonance spectroscopy. *Urology* 1986;135:866–871
12. Bretan PN, Baldwin N, Novick AC, et al. Pretransplant assessment of renal viability by phosphorus-31 magnetic resonance spectroscopy. *Transplantation* 1989;48:48–53
13. Grist TM, Charles HC, Herfkens RJ. P-31 MR spectroscopy in renal transplant recipients using chemical shift imaging. *Radiology* 1988;169(P):168
14. Grist TM, Kneeland JB, Jesmanowicz A, Froncisz W, Hyde JS. In vivo MRI and localized P-31 MRS of the kidney in renal transplant recipients. *Proceedings of the 6th annual meeting of the Society of Magnetic Resonance in Medicine*. Berkeley, CA: Society of Magnetic Resonance in Medicine, 1987:559
15. Grist TM, Jesmanowicz A, Froncisz W, Kneeland JB, Hyde JS. Doubly



- tuned local coils for MRI and MRS at 1.5T. *Magn Reson Med* **1988**;6:253-264
16. Bottomley PA, Foster TH, Darrow RD. Depth-resolved surface-coil spectroscopy (DRESS) for in vivo H-1, P-31 and C-13 NMR. *J Magn Reson* **1984**;59:338
  17. Brown TR, Kincaid BM, Ugurbil K. NMR chemical shift imaging in three dimensions. *Proc Natl Acad Sci USA* **1982**;79:3523-3526
  18. Zar JH. *Biostatistical analysis*, Englewood Cliffs, NJ: Prentice-Hall, **1984**:149-201
  19. Shapiro JL, Chan L. P-31 NMR of the kidney. A new method for diagnosing urinary tract obstruction. *Proceedings of the 5th annual meeting of the Society of Magnetic Resonance in Medicine*. Berkeley, CA: Society of Magnetic Resonance in Medicine, **1986**:178
  20. Parfitt AM, Kleerekoper M, Cruz C. Reduced phosphate reabsorption unrelated to parathyroid hormone after renal transplantation: implications for the pathogenesis of hyperparathyroidism in chronic renal failure. *Miner Electrolyte Metab* **1986**;12:356-362
  21. Daly PF, Lyon RC, Fausinto PJ, Cohen JS. Phospholipid metabolism in cancer cells monitored by P-31 NMR spectroscopy. *J Biol Chem* **1987**;262:14875
  22. Fine L. The biology of renal hypertrophy. *Kidney Int* **1986**;29:619
  23. Bates TE, Williams SR, Gadian DG. Phosphodiesterases in the liver: the effect of field strength on the P-31 signal. *Magn Reson Med* **1989**;12:145-150
  24. Murphy EJ, Rajagopalan B, Brindle KM, Radda GK. Phospholipid bilayer contribution to P-31 NMR spectra in vivo. *Magn Reson Med* **1989**;12:282-289
  25. Sehr PA, Bore PJ, Papatheofanis J, Radda GK. Nondestructive measurement of metabolites and tissue pH in the kidney by P-31 nuclear magnetic resonance. *Br J Exp Pathol* **1979**;60:632
  26. Hyde JS, Jesmanowicz A, Grist TM, Francis W, Kneeland JB. Quadrature detection surface coil. *Magn Reson Med* **1987**;4:179-184
  27. Charles HC, Prost R, Grist TM, MacFall JR. Exploring the limits of spatial resolution in phosphorus imaging: is hydrogen a good ruler? *Radiology* **1989**;173(P):165
  28. Jenkins SM, Sanfilippo FP, Carroll BA. Duplex Doppler sonography of renal transplants: lack of sensitivity and specificity in establishing pathologic diagnosis. *AJR* **1989**;152:535-539
  29. Collier BD, Adams MB, Kauffman HM, Trembath L, et al. Accurate diagnosis of renal transplant rejection by indium-111 platelet imaging despite postoperative cyclosporine therapy. *Clin Nucl Med* **1988**;13:606-610



# Failure of MR Imaging to Detect Reflex Sympathetic Dystrophy of the Extremities

Esther Koch<sup>1</sup>  
 Heinz O. Hofer<sup>2</sup>  
 Gregorio Sialer<sup>1</sup>  
 Borut Marincek<sup>1</sup>  
 Gustav K. von Schulthess<sup>1</sup>

Reflex sympathetic dystrophy of the extremities is a disease with a wide spectrum of clinical manifestations. It is characterized by pain, hyperthermia, and cutaneous changes and has been linked to an abnormality of regional blood flow. The disease is associated with previous injury or trauma including surgery, but also has been found in association with myocardial infarctions and tumors. The final diagnosis can be made only on the basis of the clinical course, which is characterized either by regression without sequel or the appearance of aponeurotic and tendinous retractions including bony sclerosis in the affected region occurring over many months to years. The literature and our own results show that MR imaging has high sensitivity for diagnosing transient osteoporosis of the hip, which is generally thought to be a form of reflex sympathetic dystrophy. Therefore we investigated the usefulness of MR imaging for diagnosing sympathetic dystrophy of the extremities. Twenty-five patients underwent T1- and T2-weighted MR imaging of the affected body region. They were selected on the basis of the initial clinical findings and positive findings on scintigraphy, which is known to be a sensitive, but not very specific, imaging method for sympathetic dystrophy. The final diagnosis was established on the basis of the clinical course in 17 of the 25 patients. In 10 of these, findings on MR images were completely normal, in six the MR images showed only nonspecific soft-tissue changes or bone marrow sclerosis, and in one patient they showed changes in bone marrow signal. Of the remaining eight patients without a final diagnosis of sympathetic dystrophy, MR showed soft-tissue or bone marrow alterations in six.

MR imaging appears to be of little value in establishing the diagnosis of sympathetic dystrophy, but it may improve diagnostic specificity when used in conjunction with scintigraphy.

*AJR* 156:113-115, January 1991

Reflex sympathetic dystrophy is a disease with a wide range of clinical manifestations. Thus, before it was recognized as a single disease, it received a large number of names, such as algodystrophy, Sudeck atrophy, shoulder-hand syndrome, and causalgia. Transient osteoporosis of the hip also is thought by many authors to be a form of reflex sympathetic dystrophy [1, 2]. The etiology is unclear but is related to trauma, injuries including surgery, and may be due to a neuronal abnormality affecting regional blood flow.

Sympathetic dystrophy is commonly divided into three stages. The initial (inflammatory) stage (I) lasts from 1 to 7 weeks and is characterized by diffuse locoregional pain, inflammation, edema, and hypothermia or hyperthermia. In the second (dystrophic) stage (II), which lasts from 3 to 24 months, the principal clinical findings are pain on exercise, increased sensitivity of the skin to temperature and pressure changes, and the beginning of skin and muscle atrophy. In the final (atrophic) stage (III), pain on exercise persists and scleroderma-like skin changes and aponeurotic or tendinous retractions may occur. These changes are irreversible. The final diagnosis of sympathetic dystrophy is established on the basis of the clinical course and radiologic signs by either noting complete remission without clinical sequelae in

Received May 17, 1990; accepted after revision August 6, 1990.

<sup>1</sup> Department of Medical Radiology, University Hospital, CH-8091 Zurich, Switzerland. Address reprint requests to G. K. von Schulthess, Department of Medical Radiology, Division of Nuclear Medicine, Universitätsspital, Rämistr. 100, CH-8091 Zurich, Switzerland.

<sup>2</sup> Department of Rheumatology and Institute for Physical Medicine, University Hospital, CH-8091, Zurich, Switzerland.

0361-803X/91/1561-0113  
 © American Roentgen Ray Society



the large majority of cases or progression to stage III [3, 4]. Treatment with calcitonin, beta-blockers, or corticosteroids in stages I and II often results in marked improvement [5].

Even though bone scintigraphy has long been recognized to be a highly sensitive method for the early detection of the disease [6], it is not specific. As MR imaging has proved to be valuable in diagnosing transient osteoporosis of the hip [7–12], we initiated this study to determine if MR imaging can contribute to the early diagnosis of reflex sympathetic dystrophy of the extremities.

### Subjects and Methods

Twenty-five patients with the tentative diagnosis of reflex sympathetic dystrophy of the extremities were studied. The patients were selected for the study if sympathetic dystrophy was suggested clinically and findings on bone scintigraphy were consistent with this diagnosis. This procedure for selecting patients ensured that a larger number of the study participants had reflex sympathetic dystrophy. However, because of the relatively low specificity of the initial clinical and scintigraphic findings, the patients did not have a definitive diagnosis of reflex sympathetic dystrophy. The final diagnosis was made solely on the basis of clinical follow-up and late radiologic findings, and this combination was taken as the gold standard. Hence scintigraphy was used merely to increase the prevalence of sympathetic dystrophy in the study group. Sympathetic dystrophy was diagnosed eventually in 17 of the 25 patients. Of these 17, 12 were women and five were men. Eight had involvement of the hand, eight had involvement of the foot, and one had involvement of the knee. In two patients, the event initiating the sympathetic dystrophy was a fracture in the affected region, the others had different forms of trauma such as contusions or surgery.

The final diagnoses in the study group were as follows: Four patients had stage I disease, six patients had stage I–II disease, and seven patients had stage II disease. The remaining eight patients had the following final diagnoses: one had reactivated osteoarthritis, one had ankylosing spondylitis, and three had synovitis, one case of which was villonodular. One patient had palmoplantar pustulosis, one had avascular necrosis of the talus, and one diagnosis remained unclear, although sympathetic dystrophy was excluded.

Bone scans were obtained with approximately 500 MBq of  $^{99m}\text{Tc}$ -labeled diphosphonate (DPD, Behring, Mannheim, Germany). Two- or three-phase scintigraphy was performed on a Picker Dyna SX-500 or a GE Maxi II large-field camera acquiring analog images only. The perfusion phase was observed under the camera while the radiopharmaceutical was injected. A sequence of analog images at 10-sec intervals was used for this purpose. Blood-pool-phase scintigra-

phy of the affected extremities was performed within the first 15 min after injection, while bone-phase images were obtained between 150 and 200 min after injection. The perfusion phase was considered positive when a distinct difference in radioactivity was seen between the affected and the unaffected limb. Blood-pool and bone-phase scans were considered positive when there was a diffuse asymmetry in the soft tissues and the bony structures, respectively (Fig. 1). The soft-tissue phase abnormality and the diffuseness of the activity distribution in the bone phase were used to distinguish reflex sympathetic dystrophy from mere bone uptake abnormalities after a fracture.

MR imaging was done within 3 weeks of scintigraphy, thus presumably during the same disease stage. The MR imager was a Philips Gyroscan S15 with a field strength of 1.5 T and local coils. T1- and T2-weighted images were acquired with spin-echo 450–700/20–30 (TR/TE) and 1500–2000/60–100 sequences, respectively. The scans were examined by three radiologists, and the presence of bone marrow alterations, joint effusions, and soft-tissue changes was noted. As only patients with positive clinical findings and bone scans were referred, the tentative diagnosis of reflex sympathetic dystrophy was known to the radiologists interpreting the MR images.

### Results

In the 17 patients with reflex sympathetic dystrophy, the MR findings were as follows: Ten patients had completely normal findings on MR imaging (Fig. 1). Bone marrow was abnormal in three patients, two of whom had had a fracture. In these cases, the bone marrow abnormality was focal and corresponded to the region of bony sclerosis on the radiographs. Low signal intensity was noted on T1- and T2-weighted images. The third case (Fig. 2) showed diffuse decrease in signal intensity of the talus on T1-weighted images and an increase on T2-weighted images. This was the only case with bone marrow abnormalities similar to the ones found in transient osteoporosis of the hip. Three patients showed soft-tissue changes on MR imaging, one of them had edema and two had muscular atrophy. Two patients showed joint effusions in the affected region.

The eight patients in whom a final diagnosis of sympathetic dystrophy was not established on the basis of clinical follow-up had various diseases. One patient with reactivated osteoarthritis had no MR changes. One patient with ankylosing spondylitis showed a calcaneal spur on MR imaging. A patient with proved villonodular synovitis had no bone marrow changes, but areas without signal in the synovia of the

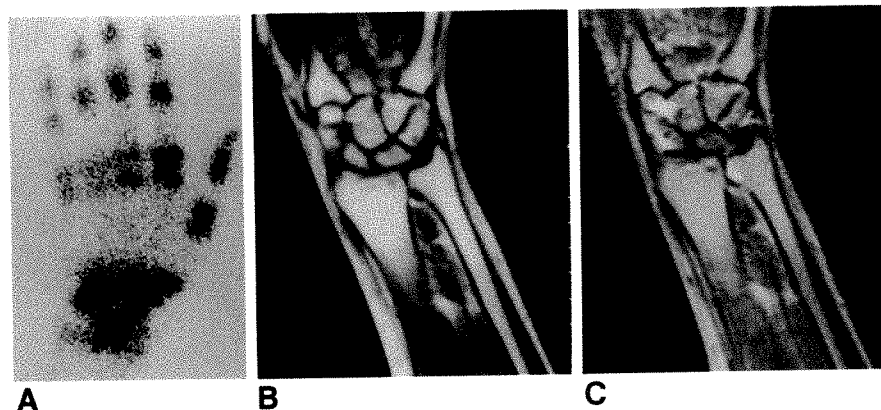


Fig. 1.—Bone scan and MR images show typical findings of reflex sympathetic dystrophy of upper extremity. A 38-year-old woman had pain in left wrist. Perfusion and blood-pool scans showed increased activity on left side.

A, On bone-phase scan, disease affects distal radius and ulna, entire wrist, and joints of digits I–III.

B, T1-weighted MR image, 525/20, shows normal bone marrow in left arm, but muscular atrophy in left forearm.

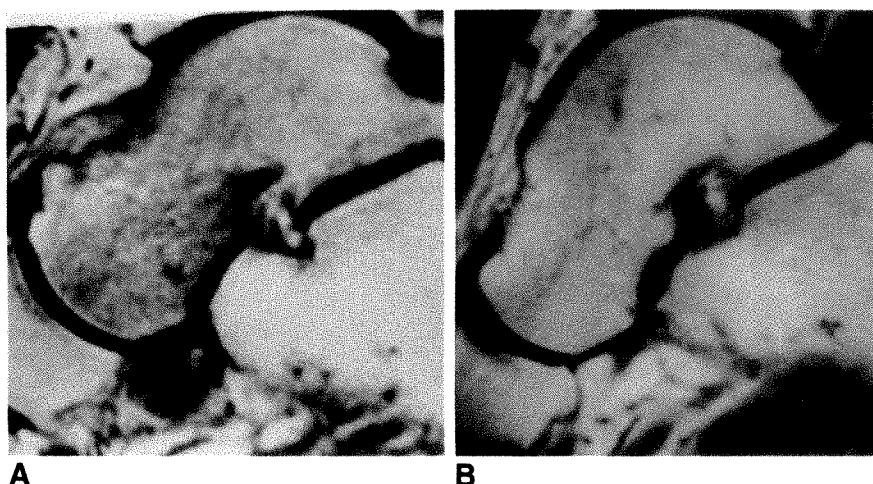
C, On T2-weighted MR image, only finding is minimal signal increase in some muscles of left forearm and fluid accumulation in medial wrist. Bone marrow remains normal.



Fig. 2.—Only case with final clinical diagnosis of reflex sympathetic dystrophy in which MR images showed abnormal bone marrow. A 21-year-old man had minor trauma to right foot. MR images suggest that patient may have had talar contusion, although clinical course tended to exclude this diagnosis.

A, T1-weighted MR image, 500/25, shows diffuse signal intensity decrease in bone marrow of talus.

B, MR image obtained 14 months later shows signal intensity has reverted to normal.



affected joint were typical for iron deposits, and the diagnosis of villonodular synovitis was made prospectively by MR imaging. Another patient had a palmoplantar pustulosis and no MR findings. One patient with synovitis had a joint effusion, and one with a tenosynovitis had inflammatory changes confined to a tendon. One patient with a proved avascular necrosis of the talus showed soft-tissue edema in conjunction with bone marrow changes of avascular necrosis on MR images, and one patient showed edema and necrosis. His final diagnosis could not be established, but the clinical course excluded reflex sympathetic dystrophy.

With these results and the criterion of bone marrow signal intensity that decreased on T1-weighted images and increased on T2-weighted images, MR imaging is a poor method for diagnosing reflex sympathetic dystrophy in the extremities. In fact, because with this criterion there were 16 false-negative, six true-negative, one true-positive, and two false-positive cases, the sensitivity, specificity, and diagnostic accuracy are 6%, 75%, and 28%, respectively.

## Discussion

The diagnosis of reflex sympathetic dystrophy remains a clinical one and can be made only after a clinical follow-up lasting several months to more than a year. The etiology is still uncertain, and the relationship between transient osteoporosis of the hip and sympathetic dystrophy is still questioned, but substantial evidence has accumulated linking the two [3]. Our working hypothesis, that MR findings in peripheral sympathetic dystrophy should be similar to those in the hip was therefore reasonable.

The 17 patients with proved sympathetic dystrophy included in this study showed hardly any abnormality on MR imaging. Only one of them had MR findings comparable to those found in transient osteoporosis of the hip, namely, low signal intensity on T1-weighted images and high signal intensity on T2-weighted images (Fig. 2). The findings in this case were somewhat atypical on scintigraphy because the area of increased signal intensity was relatively well circumscribed. Nevertheless, reflex sympathetic dystrophy was diagnosed in this patient on the basis of the clinical course. In fact, an MR image showing bone marrow abnormalities in the extremities would tend to exclude the diagnosis of sympathetic dystro-

phy. This is particularly true if the alterations had an appearance suggestive of avascular necrosis.

The MR findings relating to soft-tissue and joint changes also were not helpful in making the diagnosis of sympathetic dystrophy. Muscular atrophy is simply a result of decreased mobility, and a joint effusion is a nonspecific sign found in many circumstances.

There are two possible reasons that findings on MR images in patients with sympathetic dystrophy are normal despite striking changes on MR in patients with transient osteoporosis of the hip [10–12]. One is that the two diseases are not related. The other is that because of anatomic differences between the hip and the extremities, a kind of compartment syndrome leading to bone marrow edema can develop in the former but not in the latter case. Further investigations clarifying the relation between reflex sympathetic dystrophy and transient osteoporosis of the hip are warranted.

## REFERENCES

1. Resnick D, Niwayama G. Transient osteoporosis of the hip. *Diagnosis of bone and joint disorders*, 2nd ed. Philadelphia: Saunders, 1988:2034–2053
2. Feine U, Müller-Schauenburg W. *Skelettszintigraphie: Knochendiagnostik mit neuen Verfahren*. Stuttgart: Wachholt-Verlag, 1989
3. Doury P, Dirheimer Y, Pattin S. *Algodystrophy*. Berlin: Springer-Verlag, 1981
4. Genant HK, Kozin F, Bekerman C, McCarty DJ, Sims J. The reflex sympathetic dystrophy syndrome. *Radiology* 1975;117:21–32
5. Kozin F, McCarty CJ, Sims J, Genant HK. Reflex sympathetic dystrophy syndrome: I. Clinical and histological evidence of articular involvement and response to corticosteroid. *Am J Med* 1976;60:321–331
6. Hunder GG, Kelly PJ. Bone scans in transient osteoporosis. *Ann Intern Med* 1971;75:134–139
7. Glickstein MF, Lawrence BD, Schiebler ML, et al. Avascular necrosis versus other diseases of the hip: sensitivity of MR imaging. *Radiology* 1988;169:213–215
8. Coleman BG, Kressel HY, Dalinka MK, Scheibler ML, Lawrence BD, Cohen EK. Radiographically negative avascular necrosis: detection with MR imaging. *Radiology* 1988;168:525–528
9. Beltran J, Herman LJ, Burk JM, et al. Femoral head avascular necrosis: MR imaging with clinical, pathologic and radionuclide correlation. *Radiology* 1988;166:215–220
10. Higer HP, Grimm J, Pedrosa P, Apel R, Bandilla K. Transitorische Osteoporose oder Femurkopfnekrose? Frühdiagnose mit der MRT. *Fortschr Röntgenstr* 1989;150:407–412
11. Wilson AJ, Murphy WA, Hardy DC, Totty WG. Transient osteoporosis: transient bone marrow edema? *Radiology* 1988;167:757–760
12. Bloem JL. Transient osteoporosis of the hip: MR imaging. *Radiology* 1988;167:753–755



## Book Review

### **Skeletal Radiology. The Bare Bones.** By Felix S. Chew. Rockville, MD: Aspen, 262 pp., 1989. \$65

Each year a crop of new residents and medical students asks for a reading list on musculoskeletal disorders. They prefer a single textbook on bone conditions that is readable and relatively inexpensive. Dr. Chew met the challenge by writing *Skeletal Radiology: The Bare Bones*. It is a simplified approach to a broad spectrum of skeletal problems.

The book is divided into four sections: trauma, tumors, articular disorders, and a miscellaneous section that includes a discussion of dysplasias, deformities, hematogenous infections, and metabolic bone disease. All of this information is compressed into 14 chapters and 262 pages. The book is well illustrated with quality prints, tables, diagrams, and figures. The cost is only \$65. The purpose of the book is to present a credible approach to the diagnosis of skeletal lesions so that the need for "memorization and pattern recognition" can be discarded. The writing is succinct and easily understood.

Part I is devoted to trauma. The opening chapter addresses the biomechanics of fractures and how excessive loading of the bone can induce specific injuries. The chapter on trauma teaches how to apply the principles of injury to an understanding of fractures. An important section is the author's method for describing a fracture and how to formulate a radiologic report. This message is all too often neglected in residency training. The most common fractures that occur in adults and children are discussed, and the section on the wrist, foot, and ankles in adults is excellent. A chapter on axial injuries is weakened by the omission of a discussion of unstable spinal fractures and the principles of the "three-column concept." I hope the author will address unstable spinal fractures in the revision of the book.

Part II introduces bone tumors with a chapter on the analytic or pragmatic approach to neoplasms. A clear attempt is made to define a pattern of aggressiveness of the tumor and illustrate signs of benignity and malignancy. This section addresses the most frequent

benign and malignant tumors seen in younger and older age groups. Some of the illustrations, particularly the ones on fibrous dysplasia, are questionable. Fibrous dysplasia is rare in the vertebral bodies (Fig. 7-14), yet the author shows this as a representative print. The book includes a second print that is labeled fibrous dysplasia, but is a fairly classic illustration of nonossifying fibromatosis.

Part III on articular disease is also well developed. The presentation of joint involvement in degenerative osteoarthritis and the pertinent and inflammatory articular disorders are well illustrated and are supplemented by tables outlining both the radiologic hallmarks and the critical laboratory data.

Part IV, a potpourri of miscellaneous conditions, opens with a review of the most frequent skeletal dysplasias. Although it begins with a well-organized approach to dysplasias, it then makes an about-face and indicates that after examination of the radiograph reveals that the lesion is a bone dysplasia, then the radiologist should consult an atlas of developmental anomalies and match the proband to the image for the correct diagnosis, just as would be done in the "Aunt Minnie" approach. Although this is not a serious defect, it is a departure from the pragmatic convictions embraced throughout the rest of the book. Nevertheless, I praise the succinct discussions of congenital hip dysplasias, Legg-Calvé-Perthes disease, and congenital hip deformities. Last, the chapter on postsurgical imaging is masterfully done. It is a fine introduction to the subject of prostheses, osteotomy, grafting, and spinal instrumentation.

I recommend this book to residents and medical students. It is an excellent introduction to skeletal radiology and deserves a spot on the library shelf in any teaching program.

Alex Norman  
New York Medical College  
Valhalla, NY 10595



# Sagittal MR Images of the Knee: A Low-Signal Band Parallel to the Posterior Cruciate Ligament Caused by a Displaced Bucket-Handle Tear

Kenneth L. Weiss<sup>1</sup>  
Helen T. Morehouse<sup>1</sup>  
I. Martin Levy<sup>2</sup>

A low-signal band parallel and anterior to the posterior cruciate ligament has been noted on sagittal MR images of the knee in some patients with other evidence for medial meniscal tears. It was hypothesized that this low-signal band represented the mesially displaced fragment of a bucket-handle tear. To verify this, we retrospectively reviewed MR and arthroscopic findings in 54 consecutive patients. Arthroscopy showed a bucket-handle tear of the medial meniscus in seven patients and was considered diagnostic. Sagittal MR images were reviewed without knowledge of the arthroscopic results. The presence of a curvilinear low-signal band above the tibial cortex anterior, inferior, and parallel to the posterior cruciate ligament was identified on MR images in all seven of the patients in whom the presence of a bucket-handle medial meniscal tear was confirmed by arthroscopy.

Our findings suggest that a low-signal band anterior and parallel to the posterior cruciate ligament on sagittal MR images of the knee is caused by a mesially displaced bucket-handle tear of the medial meniscus.

*AJR* 156:117-119, January 1991

MR imaging has been shown to be a sensitive and specific technique for the noninvasive detection of meniscal tears [1-3], and the criteria for diagnosis of the tears has been firmly established [4-8]. A clinically important subset of these tears, the "bucket handle," usually involves the medial meniscus and represents a full-thickness longitudinal tear that propagates anteriorly and posteriorly. This type of tear has been described as a vertical tear in both the anterior and posterior horns of the meniscus [4]; however, difficulty in detecting the linear defect of a tear when it is oriented parallel to the plane of the image has been stressed [5]. Failure to detect the body of the medial meniscus or visualizing two separate fragments on a coronal image infers a bucket-handle tear [4, 6]. The mesial fragment may be displaced into the intercondylar notch by compressive forces. This displaced mesial fragment might be visualized on sagittal MR images and account for a low-signal band anterior and parallel to the posterior cruciate ligament. To test this hypothesis, we reviewed sagittal MR images of the knee and compared the MR findings with the arthroscopic findings in 54 consecutive cases.

## Materials and Methods

Sagittal MR images were retrospectively reviewed in 54 consecutive patients who underwent preoperative MR evaluations of the knee and subsequent arthroscopic surgery from January to July 1989. All patients were considered to have significant physical findings that would require arthroscopic evaluation. Most cases (47 of 54) were studied with routine clinical MR protocols on a Signa 1.5-T unit with a commercial extremity coil (General Electric, Milwaukee, WI). The leg was positioned in less than 20° external rotation. Sagittal images were obtained with both spin-echo (SE) sequencing (5-mm-thick contiguous sections, 256 × 256 matrix, 16-cm field of view, 2000/25, 80 [TR/TE], contiguous slice multiecho multiplanar,

Received March 23, 1990; accepted after revision July 23, 1990.

<sup>1</sup> Department of Radiology, Albert Einstein College of Medicine, Rm. 4N16 Jacobi Hospital, Pelham Pkwy. 50, Bronx, NY 10461. Address reprint requests to K. L. Weiss.

<sup>2</sup> Department of Orthopedics, Albert Einstein College of Medicine, 1300 Morris Park Ave., Bronx, NY 10461.

0361-803X/91/1561-0117

© American Roentgen Ray Society



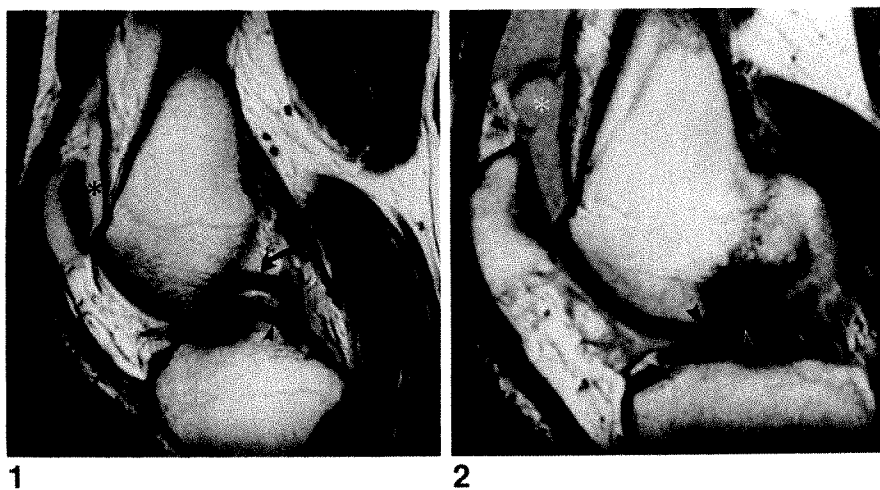


Fig. 1.—37-year-old man who injured his left knee at work 1 week before imaging studies. Bucket-handle tear of medial meniscus was proved by arthroscopy. SE 2000/25 sagittal MR image shows displaced fragment of torn medial meniscus (arrowheads) just anterior to posterior cruciate ligament (curved arrow). Asterisk = joint effusion.

Fig. 2.—30-year-old man who twisted his knee 8 days before imaging studies. SE 2000/25 sagittal MR image shows mesial displaced fragment (arrowheads) just above cortex of medial tibial plateau. Adjacent mesial image showed posterior cruciate ligament. Asterisk = joint effusion.

one excitation) and three-dimensional gradient-echo (GRE) sequencing (1.5- to 1.7-mm-thick contiguous sections,  $256 \times 256$  matrix, 20-cm field of view, 33/15, flip angle  $20^\circ$ ). All MR sequences included T1-weighted (800/20, 5-mm-thick sections with 1-mm gap) coronal images.

The remaining seven of 54 MR imaging studies were performed on other units operating at from 0.3 to 1.5 T. All studies included T1-weighted or proton-density sagittal sequences as well as coronal sequences with 5 mm or less thickness.

The presence or absence on sagittal MR images of a low-signal band anterior and parallel to the posterior cruciate ligament was noted by two authors reviewing the studies in concert. The coronal images also were reviewed, and bucket-handle tears of the medial meniscus were confirmed in all cases.

All arthroscopic studies were performed by one author, who used standard technique. Tear types and anatomic locations of abnormalities were recorded at the time of surgery.

## Results

Seven cases showed a low-signal band parallel and anterior to the posterior cruciate ligament on sagittal images. Although extensive medial meniscal tears were prospectively detected in these cases, only three of seven were initially categorized as bucket-handle tears. All cases were proved by arthroscopy to be medial bucket-handle meniscal tears. Six of the seven cases showed the displaced mesial fragment of the medial meniscal bucket-handle tear within the intercondylar notch in the same sagittal section in which the posterior cruciate ligament was identified (Fig. 1). In one of the seven positive cases, the displaced mesial fragment was seen on a sagittal section adjacent to the section on which the posterior cruciate ligament was seen, thus requiring the examination of two adjacent sagittal MR images for the finding (Fig. 2).

Typically, the displaced fragment could be traced on contiguous sagittal images to a classic meniscal tear with abnormal high signal communicating with an articular surface. Additionally, in all positive cases, the displaced mesial meniscal fragment of the bucket-handle tear (Fig. 3A) could be shown

in the coronal projection to be inferior to a cross section of the posterior cruciate ligament, providing a tangential analogue to the finding on sagittal views (Fig. 3B).

The sagittal three-dimensional GRE images often showed the finding as well or better than the spin-echo images did.

One of the seven cases was studied both before and after partial meniscectomy (Fig. 4). The sagittal MR images in this case showed the low-signal band parallel and anterior to the posterior cruciate ligament on sagittal images before partial meniscectomy and did not show this finding after surgery. This also was readily distinguished from the ligament of Humphry (Fig. 4). Twenty-six of the 54 cases were thought to show this ligament.

No additional medial meniscal bucket-handle tear was identified in the remaining 47 cases examined arthroscopically. Of two lateral meniscal tears noted arthroscopically, sagittal MR imaging of one showed a small, crumpled, displaced nonlinear fragment extending anterior to the posterior cruciate ligament. This, however, did not have the configuration of a mesially displaced fragment, as is seen with bucket-handle tears of the medial meniscus.

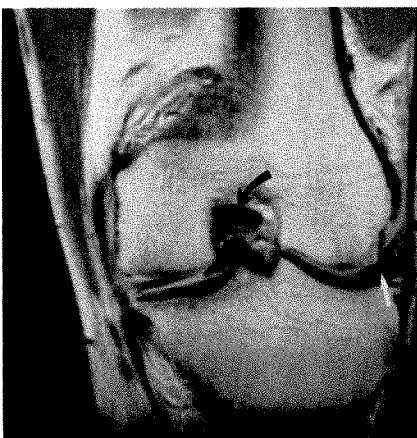
## Discussion

MR imaging has been demonstrated to be accurate in detecting meniscal tears. A bucket-handle tear can be difficult to diagnose [5]. Review of both sagittal and especially coronal views has been emphasized in the literature [3–6]. The bucket-handle tear is a full-thickness longitudinal tear, usually of the medial meniscus. The mesial fragment may be displaced into the region of the intercondylar notch by compressive forces. The presence of a bucket-handle tear may be inferred by nonvisualization of the body of the medial meniscus on sagittal MR or by detecting two fragments of the medial meniscus on coronal MR images [4, 6]. On sagittal MR images, we had visualized a low-signal band anterior and parallel to the posterior cruciate ligament in patients with





A



B

Fig. 3.—A, 26-year-old man who injured his knee while jogging 1 week before imaging studies. SE 2000/25 sagittal MR image shows low-signal band (arrowhead) anterior and paralleling posterior cruciate ligament (curved arrow). Asterisk = joint effusion.

B, SE 800/20 coronal MR image shows mesial displaced fragment of bucket-handle tear of medial meniscus (arrowhead) is in same sagittal plane as posterior cruciate ligament (black arrow). Incidental tear of lateral meniscus is also identified (white arrow).



Fig. 4.—18-year-old woman imaged 2 months after trauma to left knee. SE 2000/25 sagittal MR image shows low-signal band (black arrowhead) anterior to and paralleling posterior cruciate ligament (arrow) proved to be a mesial displaced fragment of a bucket-handle tear at surgery. This finding was not present on follow-up MR 7 days after surgery. Ligament of Humphry is identified (white arrowhead). Asterisk = joint effusion.

prominent medial meniscal tears. This band is in the same sagittal plane as the posterior cruciate ligament and may simulate a "second posterior cruciate ligament" or "third cruciate ligament." We tested the hypothesis that this low-signal band was the mesially displaced fragment of a bucket-handle tear by reviewing 54 cases in patients who had undergone both MR imaging and arthroscopy.

Because of the retrospective nature of this study, and the relatively small number of cases, the study population may be skewed, yielding an unusually high prevalence (seven of 54 cases) of mesially displaced bucket-handle tears, and high sensitivity and specificity (100%) of MR imaging. We are undertaking a larger prospective study to determine the reliability of the linear low-signal band anterior and parallel to the posterior cruciate ligament as an indicator of displaced medial meniscal bucket-handle tears.

#### REFERENCES

1. Beltran J, Noto AM, Mosure JC, Weiss KL, Christoforidis AS. Surface coil MR imaging at 1.5T: the knee. *Radiology* 1986;159:747-751
2. Crues JV III, Mink JH, Levy TL, Lotvich M, Stoller W. Meniscal tears of the knee: accuracy of MR imaging. *Radiology* 1987;164:445
3. Reeder JD, Matz SO, Becker L, et al. MR imaging of the knee in the sagittal projection: comparison of three-dimensional gradient echo and spin-echo sequences. *AJR* 1989;153:537
4. Bellon EM, Keith MW, Coleman PE, Shah ZR. Magnetic resonance imaging of internal derangements of the knee. *RadioGraphics* 1988;8:95
5. Herman LJ, Beltran J. Pitfalls in MR imaging of the knee. *Radiology* 1988;167:775
6. Stoller DW, Martin C, Crues JV III, Kaplan L, Mink JH. Meniscal tears: pathologic correlation with MR imaging. *Radiology* 1987;163:731
7. Ricklin P, Ruttimann A, DelBun MS. *Meniscus lesions*, 2nd ed. New York: Thieme Verlag, 1983
8. Watanabe AT, Carter BC, Teitelbaum GP, et al. Normal variations in MR imaging of the knee: appearance and frequency. *AJR* 1989;153:341-344

## Book Review

**Edeiken's Roentgen Diagnosis of Diseases of Bone**, 4th ed., vols. 1 and 2. By Jack Edeiken, Murray Dalinka, and David Karasick. Baltimore: Williams & Wilkins, 1832 pp., 1990. \$195

It is a nostalgic exercise for me to review the fourth edition of *Edeiken's Roentgen Diagnosis of Diseases of Bone*, as the 1973 (second) edition provided my original foundation in the musculoskeletal area. Although the current edition is updated in several respects, the book retains its personality, including both its strengths and weaknesses.

The two-volume fourth edition contains the same chapter headings as the third edition: "Basic Considerations of Bone and Cartilage;" "General Radiologic Approach to Bone Lesions;" "New Bone Production and Periosteal Reaction;" "Bone Tumors and Tumor-Like Conditions;" "Arthritides;" "Bone Ischemia and Osteochondroses;" "Osteomyelitis;" "Metabolic and Dystrophic Bone Disease;" "The Anemias;" "Congenital Hip Dislocation;" "Spondylolisthesis;" "Calcinosis, Calcifications, and Myositis Ossificans;" "Osseous Manifestations of Metal Poisoning;" "Skeletal Maturation;" "Dysplasia;" "Mucopolysaccharidoses;" "Chromosomal Abnormalities;" and "Lipidoses." Emphasis is placed on tumors and arthritis; a total of 873 pages is devoted to these areas, representing more than 45% of the book. The fourth edition includes updated material in several areas, including osteoporosis and ischemic necrosis. A discussion of MR in ischemic necrosis and some examples of MR of tumors and other conditions have been added.

Two strengths of this book stand out and make it a worthwhile purchase even now when several competitive volumes are available. The first is its readability. Vast numbers of necessary facts are conveyed with unusual clarity and in an unusually easy-to-read style. If you are looking for a book to read cover to cover, this is probably the one. The second strength is the large number of illustrations provided, particularly in the chapter on bone tumors. Thus, for example, the book has 15 examples of osteoblastoma and more than

40 examples of chondrosarcoma. This is an unusually large number of figures for a general textbook.

The weaknesses of this text are perhaps not as significant as its strengths. The first is the omission of areas such as fractures or surgical intervention. This is by design, however, and excellent textbooks are available to fill this gap. The second weakness relates to the difficulty in ensuring that a textbook is up-to-date. An obvious effort was made to include MR images, but, nonetheless, the number of such images is limited and they are not fully described. This dearth of MR images is a common problem with recent textbooks, but it is unfortunate in a text that covers bone tumors so extensively. The authors have made valiant attempts to include up-to-date material, such as the excellent description of methods of evaluating osteoporosis. Unfortunately, presumably because of limitations in publication time, dual-energy radiography, the newest technique for the assessment of osteoporosis, is not discussed. The most recent references are from 1986. The third weakness, and the most minor, refers to production errors, such as having some figures upside-down and incorrect matching of figure legends with figures. Such errors were present in the second edition of this textbook, and presumably the publisher should have been more careful now.

In summary, this edition is well written and well illustrated and is an excellent textbook, particularly for residents who want an overview of bone disease. Additional sources will be necessary to fill in the gaps in the areas covered and in the current roles of newer imaging techniques.

Barbara N. Weissman  
Brigham and Women's Hospital  
Boston, MA 02115



# MR Imaging of Displaced Bucket-Handle Tear of the Medial Meniscus

Rolando D. Singson<sup>1</sup>  
 Frieda Feldman<sup>2</sup>  
 Ronald Staron<sup>2</sup>  
 Howard Kiernan<sup>3</sup>

A bucket-handle tear of the meniscus is a vertical or oblique tear with longitudinal extension toward the anterior horn in which the inner fragment is frequently displaced toward the intercondylar notch with resultant mechanical locking of the knee joint. A precise MR diagnosis requires identification of the centrally displaced fragment because the peripheral nondisplaced component may have only a subtle truncated or foreshortened appearance that may escape detection. Eighteen consecutive cases of displaced bucket-handle tears of the medial meniscus diagnosed by MR had a characteristic low-signal band extending across the joint and projecting over the medial tibial eminence. The posterior portion was parallel and beneath the posterior cruciate ligament on both sagittal and coronal images. Arthroscopy confirmed the presence and location of the displaced fragment in all 18 cases.

Awareness of this characteristic MR finding may increase the sensitivity of MR imaging in the diagnosis of bucket-handle tears of the medial meniscus.

*AJR* 156:121-124, January 1991

A bucket-handle tear commences as a vertical or oblique tear at the posterior horn of the meniscus. Longitudinal extension toward the anterior horn often allows the inner segment to undergo varying degrees of displacement into the intercondylar notch. The term *bucket handle* is derived from the appearance of the tear, in which the inner displaced fragment of the meniscus resembles a handle, and the peripheral nondisplaced portion has the appearance of a bucket. The medial meniscus is usually involved. The injury is commonly seen in young adults with a history of locking, extension block, or "slipping out of joint" due to displacement of the central fragment toward the intercondylar notch [1, 2].

Preoperative MR studies of 18 knees accurately depicted the medial meniscal tear as well as the centrally displaced fragment in the intercondylar notch. The findings, apparent on both sagittal and coronal images, appear to serve as reliable indicators of the displaced bucket-handle component of medial meniscal tears.

Received June 18, 1990; accepted after revision August 13, 1990.

<sup>1</sup> Department of Radiology, St. Luke's/Roosevelt Hospital Center, 420 W. 59th St., New York, NY 10019. Address reprint requests to R. D. Singson.

<sup>2</sup> Department of Radiology, Columbia-Presbyterian Medical Center, College of Physicians and Surgeons, New York, NY 10032.

<sup>3</sup> Department of Orthopedic Surgery, Columbia-Presbyterian Medical Center, College of Physicians and Surgeons, New York, NY 10032.

0361-803X/91/1561-0121  
 © American Roentgen Ray Society

## Materials and Methods

Twenty-eight displaced bucket-handle tears of the medial meniscus were diagnosed from a total of 677 consecutive MR imaging studies of the knee. Arthroscopic confirmation of displaced bucket-handle tear was obtained in 18 of the 28 cases. Follow-up was unavailable in the 10 remaining cases. Among those confirmed arthroscopically, four had associated complete anterior cruciate ligament tears, two had posterior ruptures of the bucket-handle fragment, and one had a discoid medial meniscus that was not recognized on the MR images.

## Results

In all 28 cases, the centrally displaced fragment of the bucket-handle tear appeared as a low-signal structure extending over the tibial surface. The anterior

portion of the bucket handle was displaced toward the infrapatellar fat pad, and the posterior portion was deflected superiorly toward the extrasynovial surface of the posterior cruciate ligament by the medial tibial eminence. The displaced fragment could be identified on both sagittal and coronal images between the posterior cruciate ligament and the medial tibial eminence. On the sagittal view, the fragment was seen as a smaller, low-signal, longitudinally oriented band lying beneath and parallel to the larger and thicker posterior cruciate ligament so that the latter appeared to have a double configuration (Fig. 1).

The meniscal origin of the displaced fragment was almost always apparent. The anterior and/or posterior portions of the displaced fragment could be traced on slices sequential to the peripheral nondisplaced anterior and/or posterior portions of the torn meniscus (Fig. 2). The nondisplaced portion, including the peripheral segment of the body of the meniscus, had a truncated or foreshortened appearance.

### Discussion

Two parallel low-intensity bands within the intercondylar notch simulating a double posterior cruciate ligament on both sagittal and coronal MR images appear to be indicative of a displaced bucket-handle tear of the medial meniscus. An

otherwise subtle additional finding relies on the more peripheral nondisplaced meniscal segment appearing as a truncated triangle [3, 4]. Reliance solely on the visualization of a fragment lodged within the femorotibial joint space leads to the erroneous diagnosis of an isolated loose body.

The size of the displaced fragment varies with the size of the tear. It is usually thick since the longitudinal tear occurs at or near the periphery of the meniscus. On coronal images, the low-intensity band of the bucket handle and the posterior cruciate ligament are correspondingly smaller since they are imaged end-on in their transverse diameter. It is on the coronal images that the bucket-handle fragment can be mistaken for a loose body (Figs. 1C and 1D).

Other normal and abnormal low-intensity structures within the intercondylar notch on MR images should not be mistaken for the abnormality described here. This includes the ligament of Humphry, which is a normal accessory meniscofemoral ligament. It extends from the posterior horn of the lateral meniscus to the lateral aspect of the medial femoral condyle and is closely related to the anterior margin of the posterior cruciate ligament. On MR, it commonly appears as a small, rounded, low-signal structure. Occasionally, a short segment of it may appear linear (Fig. 3). It is a much smaller and thinner band than the bucket-handle fragment, and its close relationship to the cruciate ligament serves to differentiate among

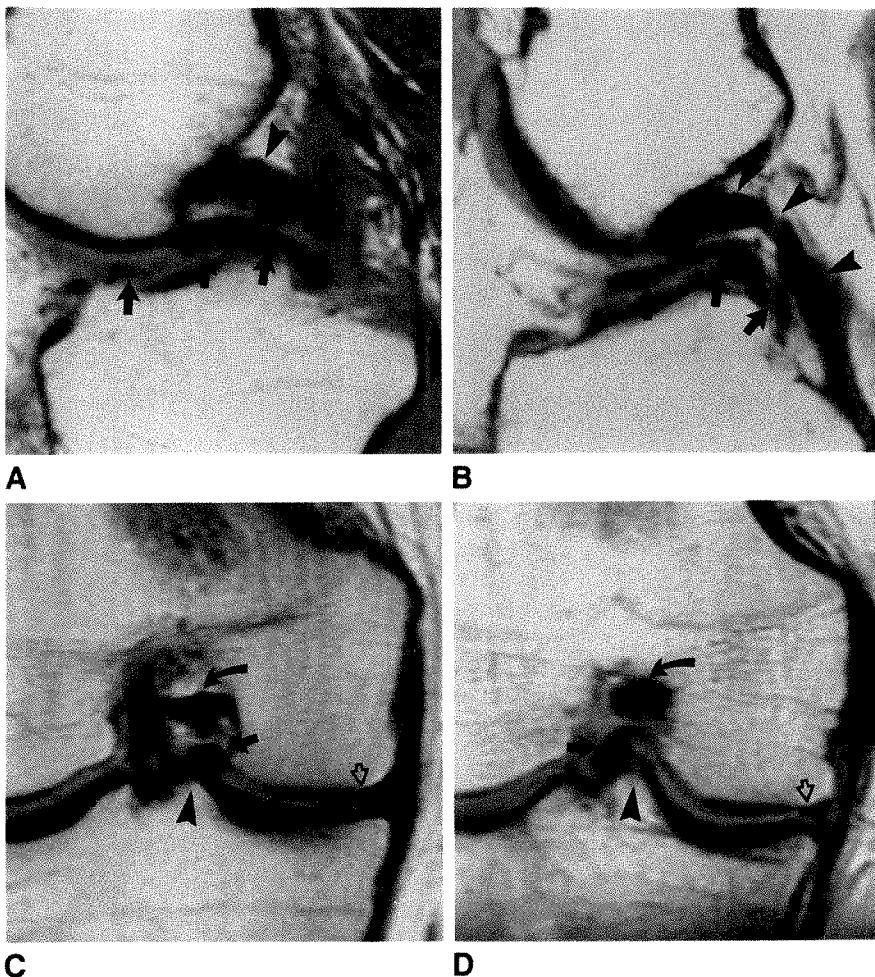


Fig. 1.—A and B, Sagittal T1-weighted MR images of displaced bucket-handle tears of medial meniscus confirmed at arthroscopy in two patients. Centrally displaced longitudinal fragment (arrows) is oriented anteroposteriorly over tibial surface. Smaller low-intensity band of posterior half of fragment is parallel and underneath larger low-signal band of posterior cruciate ligament (arrowheads). Duplicated posterior cruciate outline is simulated.

C and D, Corresponding coronal proton-density MR images show displaced fragment (long straight solid arrows) between medial tibial eminence (arrowheads) and posterior cruciate ligament (curved arrows). Peripheral nondisplaced portion of meniscus (open arrows) has subtle foreshortened outline. Note intact anterior cruciate ligament (short straight solid arrow) on C.



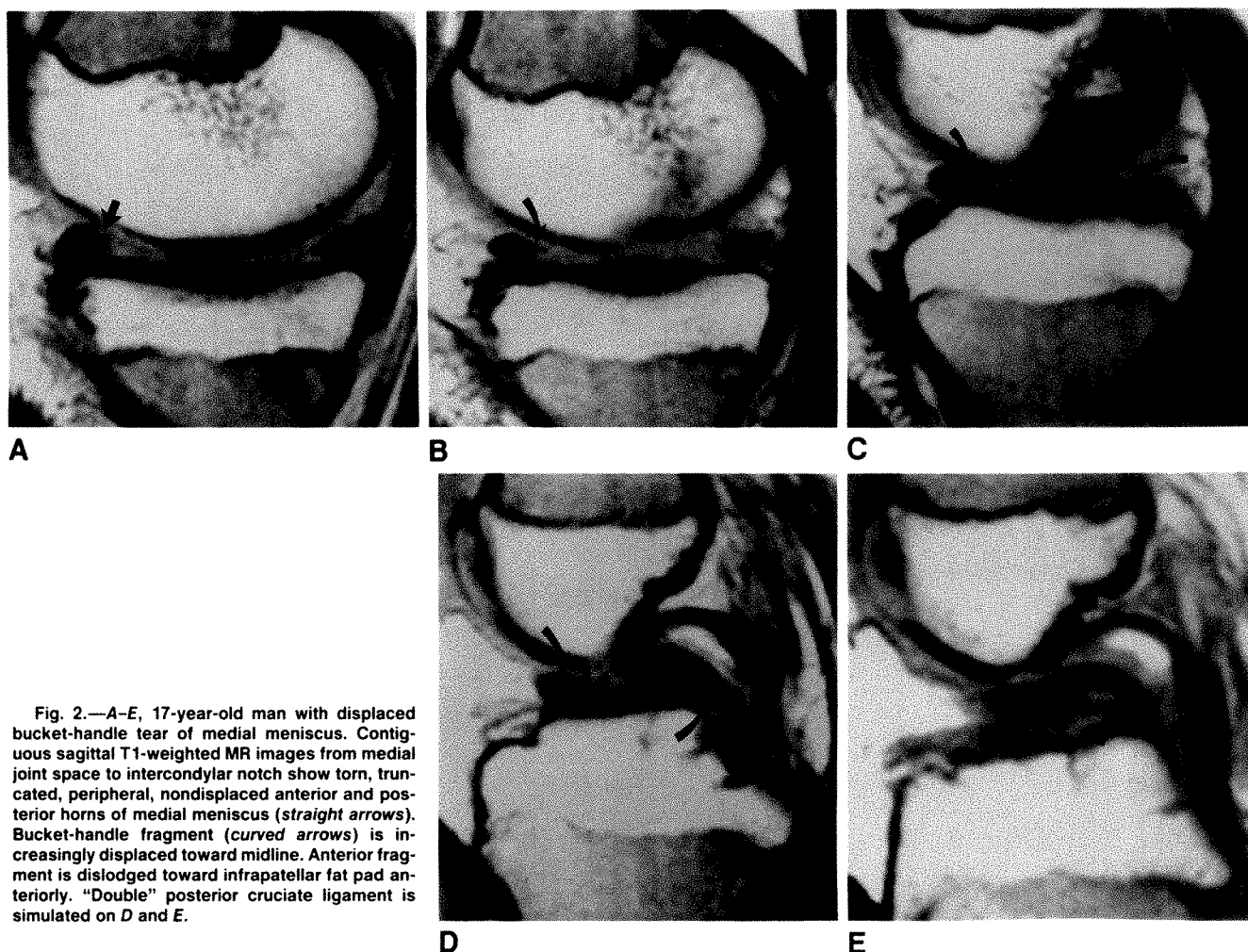


Fig. 2.—A–E, 17-year-old man with displaced bucket-handle tear of medial meniscus. Contiguous sagittal T1-weighted MR images from medial joint space to intercondylar notch show torn, truncated, peripheral, nondisplaced anterior and posterior horns of medial meniscus (straight arrows). Bucket-handle fragment (curved arrows) is increasingly displaced toward midline. Anterior fragment is dislodged toward infrapatellar fat pad anteriorly. “Double” posterior cruciate ligament is simulated on D and E.



Fig. 3.—Sagittal T1-weighted MR image shows relatively thin ligament of Humphry (arrow) closely apposed to anterior margin of posterior cruciate ligament.

them. It is never seen in the coronal plane. Its prevalence on MR has been reported as 34% [5]. A torn anterior cruciate ligament can appear as a low-signal linear band within the intercondylar notch [6, 7]. Although most tears occur at its

midportion, when it is detached from its femoral insertion, the ligament can flop over to the medial compartment. It may appear as fine, linear strands of low signal intensity that are transversely oriented over the tibial surface. The anterior cruciate ligament usually has higher signal characteristics compared with a homogeneously low-signal meniscal fragment. Loose bodies lying underneath the posterior cruciate ligament, osteophytes, and fracture fragments are other abnormalities that should be considered. Their true nature should be apparent after careful analysis of sequential multiplanar images as well as routine radiographs.

Three of our cases of displaced bucket-handle tears of the lateral meniscus did not display the described two parallel bands. Perhaps the meniscal fragment was not sufficiently displaced for it to occupy the same plane as the posterior cruciate ligament, which courses more medially than the anterior cruciate ligament. Also, tears of the lateral meniscus are commonly radial, involve the posterior horn, and usually do not lead to a bucket-handle type of deformity [1, 8].

#### REFERENCES

1. Shakespeare DT, Rigby HS. The bucket-handle tear of the meniscus. A clinical and arthrographic study. *J Bone Joint Surg [Br]* 1983;65-B:383–387

2. O'Connor RL, Shahriaree H. Meniscal lesions and their treatment. In: Shahriaree H, ed. *O'Connor's textbook of arthroscopic surgery*. Philadelphia: Lippincott, **1984**:99-162
3. Crues JV, Stoller DW. The menisci. In: Mink JK, Reicher MA, Crues JV, eds. *Magnetic resonance imaging of the knee*. New York: Raven, **1987**:55-88
4. Mink JH. Pitfalls in interpretation. In: Mink JK, Reicher MA, Crues JV, eds. *Magnetic resonance imaging of the knee*. New York: Raven, **1987**:141-155
5. Watanabe AT, Carter BC, Teitelbaum GP, Seeger LL, Bradley WG. Normal variations in MR imaging of the knee: appearance and frequency. *AJR* **1989**;153:341-344
6. Mink JH, Levy T, Crues JV III. Tears of the anterior cruciate ligament and menisci of the knee: MR imaging evaluation. *Radiology* **1988**;167:769-781
7. Mink JH. The ligaments of the knee. In: Mink JH, Reicher MA, Crues JV, eds. *Magnetic resonance imaging of the knee*. New York: Raven, **1987**:103-111
8. Manco LG, Berlow ME, Csajka J, Alfred R. Bucket-handle tears of the meniscus: appearance at CT. *Radiology* **1988**;168:709-712

### **American Roentgen Ray Society Residents' Award Papers, 1991**

The ARRS announces competition for the 1991 President's Award and two Executive Council Awards for the best papers concerning the clinical application of the radiologic sciences.

#### **Awards**

The winner of the President's Award will receive a certificate and a \$2000 prize. The winners of the two Executive Council Awards will each be given a certificate and a prize of \$1000. The winners will be announced on March 15, 1991. Winning papers will be presented at the ARRS annual meeting at the Sheraton Boston Hotel, Boston, MA, May 5-10, 1991. Winning papers will be submitted for early publication in the *American Journal of Roentgenology*. All other papers will be returned to the authors.

#### **Regulations**

Eligibility is limited to residents or fellows in radiology who have not yet completed 4 years of approved training in a radiologic discipline. A letter from the resident's department chairman attesting to this status must accompany the manuscript. The resident must be the sole or senior author and be responsible for all or most of the project.

Submitted manuscripts must not exceed 5000 words and have no more than 10 illustrations. Four copies of the manuscript and illustrations are required. Submitted manuscripts should not contain previously presented or published material and should not be under consideration for publication elsewhere.

Deadline for submissions is February 15, 1991. Send papers to

Nancy O. Whitley, M.D.  
Chairman, Committee on Education & Research  
American Roentgen Ray Society  
Department of Radiology  
University of Maryland Medical Systems Hospital  
22 South Greene St.  
Baltimore, MD 21201



# Rheumatoid Arthritis of the Knee: Value of Gadopentetate Dimeglumine- Enhanced MR Imaging

Gerhard Adam<sup>1</sup>  
Manfred Dammer<sup>1</sup>  
Klaus Bohndorf<sup>1</sup>  
Rolf Christoph<sup>2</sup>  
Franz Fenke<sup>2</sup>  
Rolf W. Günther<sup>1</sup>

In an attempt to differentiate among joint effusion, synovitis, pannus, and subchondral sclerosis in patients with clinically proved chronic rheumatoid arthritis, we used gadopentetate dimeglumine-enhanced MR imaging to examine 23 patients with acute knee symptoms. All patients had had rheumatoid arthritis for more than 6 months and satisfied four or more of the criteria of the American Rheumatism Association for rheumatoid arthritis. MR imaging was performed on a 1.5-T machine by using unenhanced T1-weighted spin-echo imaging, unenhanced T2\*-weighted gradient-echo imaging, and unenhanced and enhanced T1-weighted gradient-echo imaging. Signal intensities of the synovium and bone marrow were measured with the region-of-interest technique on unenhanced and enhanced T1-weighted gradient-echo scans. Conventional radiographs were available for each patient. Joint effusion, synovitis, intraarticular pannus, subchondral sclerosis, and subchondral pannus had the same signal intensities on unenhanced T1-weighted spin-echo, unenhanced T1-weighted gradient-echo, and unenhanced T2\*-weighted gradient-echo MR images, and could not be differentiated from one another. On enhanced T1-weighted gradient-echo sequences, pannus and synovitis showed marked enhancement in 15 patients, whereas joint effusion and sclerosis did not. Synovitis was diagnosed if the synovial membrane showed high enhancement; pannus was diagnosed if enhancing masses were seen within the joint space or in the subchondral area. In eight of the 23 joints, there was no enhancement of the synovium or intraarticular or subchondral tissue.

We conclude that gadopentetate dimeglumine-enhanced MR imaging allows differentiation between synovitis and joint effusion and between subchondral pannus and subchondral sclerosis. Enhancement of the synovium and pannus indicates acute inflammation of the joint.

*AJR* 156:125-129, January 1991

There are only a few reports in the literature describing the use of MR imaging for assessment of rheumatoid arthritis [1-6]. On unenhanced MR images it is impossible to distinguish synovitis and pannus from synovial fluid [2] and bony erosions [1]. Only Reiser et al. [5] described the use of gadopentetate dimeglumine-enhanced MR imaging for assessment of synovitis and pannus formation.

The diagnosis of rheumatoid arthritis is made by using clinical, laboratory, and plain film findings. However, MR imaging may play an important role in the assessment of the disease because it displays the joint abnormalities, including changes in the cartilages and soft tissues, directly and in their entirety. Furthermore, MR may be helpful in preoperative planning for patients in whom synovectomy is necessary.

We studied gadopentetate dimeglumine-enhanced MR imaging of the knee in 23 patients with chronic rheumatoid arthritis and acute symptoms to determine the usefulness of the procedure for assessing the disease.

## Subjects and Methods

Twenty-three knees in 23 consecutive patients 19-79 years old (mean age, 55), six men

Received April 20, 1990; accepted after revision August 6, 1990.

<sup>1</sup> Department of Diagnostic Radiology, Aachen University of Technology, Pauwelsstrasse, 5100 Aachen, Germany. Address reprint requests to G. Adam.

<sup>2</sup> Hospital for Rheumatic Diseases, Burtscheider Markt 24, 5100 Aachen, Germany.

0361-803X/91/1561-0125  
© American Roentgen Ray Society

and 17 women, were examined by MR imaging from October 1988 to August 1989. The patients had had rheumatoid arthritis for more than 6 months. The mean duration of rheumatoid arthritis was 5.8 years (range, 9 months to 11.4 years). All patients had positive findings on hand radiographs. Involvement of the knee was supposed in all patients because of pain, tenderness, or swelling. In all patients, four or more of the criteria of the American Rheumatism Association [7] for rheumatoid arthritis were satisfied: morning stiffness, arthritis of three or more joint areas, arthritis of hand joints, symmetric arthritis, rheumatoid nodules, serum rheumatoid factor, and changes on radiographs. Conventional radiographs of the knee in two different planes were obtained within 1 week before the MR examination.

MR imaging was performed on a 1.5-T magnet (Magnetom, Siemens, Erlangen, Germany) with a knee coil capable of transmitting and receiving. After a spin-echo scout view, we used a T1-weighted spin-echo sequence (600/15 [TR/TE]) and an unenhanced T2\*-weighted gradient-echo sequence with a three-dimensional Fourier transform (3DFT) fast imaging with steady precession (FISP) technique (40/13/40° [TR/TE/flip angle]). Finally, a relatively T1-weighted gradient-echo sequence, a two-dimensional Fourier transform (2DFT) fast low-angle shot (FLASH) technique (400/10/60°), was used before and after IV administration of 0.1 mmol of gadopentetate dimeglumine (Magnevist, Schering, Germany) per kilogram of body weight. Slice thickness was 3 mm with a 0.6-mm interslice gap for both T1-weighted sequences and 1 mm without interslice gap for the 3DFT FISP sequence. In the FISP sequence, rephasing gradients are used to destroy transverse magnetization prior to a subsequent RF pulse, whereas in FLASH, transverse magnetization is destroyed by a spoiling gradient. In FISP, once the echo has been recovered by gradients, additional gradients are used to rephase spins that have been dephased for purposes of phase encoding. Consequences of maintaining transverse coherence are that subsequent RF pulses not only will flip a longitudinal component out of the z direction, as in FLASH, but will now also flip the remaining coherent transverse component out of the x-y plane. By doing so the signal produced by each RF pulse will be influenced by the rate of T1 longitudinal recovery of the tissue and by the rate of T2\* decay of the tissue. FLASH assumes that no transverse component remains to be affected by making T2\* approach zero with a spoiler gradient [8, 9]. Total examination time for this protocol was about 30 min.

Before reviewing MR images, conventional radiographs were analyzed for erosions, joint space narrowing, effusions or soft-tissue swelling, and periarticular osteoporosis. In addition, features of degenerative disease such as subchondral sclerosis, osteophytes, and cyst formation were analyzed. Four of the 23 joints were classified as normal on plain films. The remaining 19 joints showed narrowing of the joint space, medial or lateral or both (15); osteophytes (11); femoropatellar osteoarthritis (seven); periarticular osteoporosis (seven); destruction of the intercondylar tubercles (five); and soft-tissue swelling (three). Erosions were seen on plain films in two of 19 patients, and subcortical sclerosis was evident in three. On conventional radiographs we classified eight of 19 joints as rheumatoid arthritis without secondary osteoarthritis and the remaining were classified as rheumatoid arthritis with secondary osteoarthritic changes.

MR images were interpreted with respect to the bone marrow signal of the subchondral area, changes of the hyaline and fibrous cartilage, intraarticular and subchondral soft-tissue masses, effusions, and ligamentous disorders. Unenhanced and enhanced images were compared with each other. Synovitis was diagnosed if the synovium showed marked enhancement. Pannus formation was considered if enhancing soft-tissue masses were seen within the joint or in the subchondral area. The relative signal intensities, measured with the region-of-interest technique, were compared on unenhanced and enhanced scans. The signal intensities were measured within the

metaphyseal bone marrow and synovium. No pathologic correlation was available, because none of the patients underwent arthroscopy or arthrotomy after the MR examination.

## Results

### *Patients with Normal Radiographs*

MR studies in four patients with normal radiographs showed small joint effusions that were of low signal intensity on T1-weighted images and high signal intensity on T2\*-weighted images. Two patients had circumscribed loss of subchondral bone marrow signal on both T1- and T2\*-weighted images. Decreased thickness of the articular cartilage was identified in two patients. In these patients, the cartilage had signal inhomogeneities. The menisci were thinned in all patients, particularly in the intermediate parts, and had signal inhomogeneities that were classified as meniscal degeneration. This was seen on both T1-weighted and T2\*-weighted images. The synovial membrane of these joints displayed only a small signal increase after administration of gadopentetate dimeglumine. It was of low signal on unenhanced T1-weighted images and of intermediate signal intensity or isotense compared with effusion on unenhanced T2\*-weighted images. In the absence of joint effusion, the synovial membrane was not visible on unenhanced images. Enhancement of subchondral areas that exhibited low signal on T1-weighted images was not observed. The mean increase in relative synovial signal as measured at the suprapatellar recess was 9.4% (mean relative signal intensity on unenhanced images, 650; mean relative signal intensity on enhanced images, 711). The mean increase in relative signal of the metaphyseal bone marrow was 1.2% (mean relative signal intensity on unenhanced images, 427; mean relative signal intensity on enhanced images, 432). On the basis of MR findings, diagnosis of early osteoarthritis was possible in these four patients with normal radiographs.

### *Patients with Abnormal Radiographs*

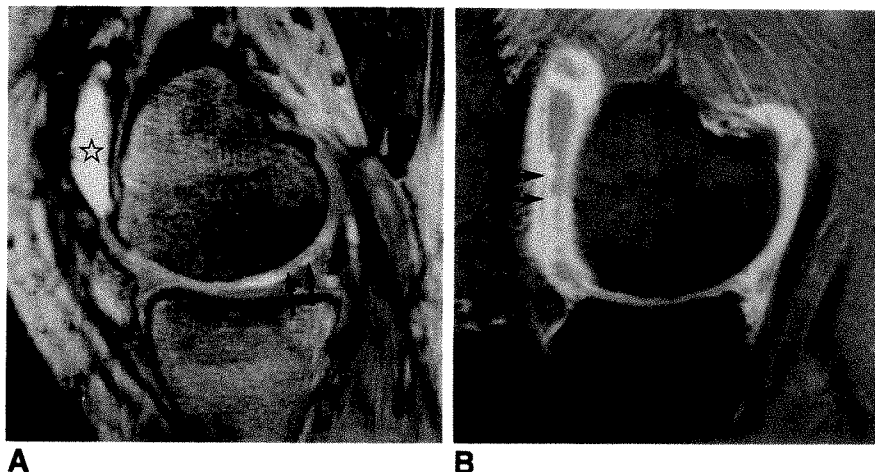
Of the remaining 19 joints in which abnormalities were visible on plain films, MR showed joint effusions in 16, hyaline cartilage defects in 12, and thinned menisci with irregular signal in 10. Hyaline cartilage defects were diagnosed if the cartilage layer was thinned and the signal inhomogeneous on T1- and T2\*-weighted images or if gross defects were seen. The meniscal changes also appeared as thinning and signal inhomogeneities on all sequences. The synovium was swollen in all cases and showed nodular transformation, but displayed a large increase in signal in only 15 patients. Exact delineation of the synovium, which appeared isointense relative to joint effusions on unenhanced T1- and T2\*-weighted scans, was possibly only on enhanced images (Fig. 1). The increase in the relative signal intensity of the synovium was 82% (mean relative signal intensity on unenhanced images, 703; mean relative signal intensity on enhanced images, 1279). The mean increase in the signal intensity of the metaphyseal bone marrow in these patients was 3.4% (mean relative signal intensity on unenhanced images, 447; mean relative signal



Fig. 1.—Sagittal MR images of the knee from a 45-year-old woman known to have rheumatoid arthritis for 1 year.

A, 3DFT FISP MR image. Effusion (star) has high signal intensity. Note signal irregularities and thinning of articular cartilage (arrows). Delineation of synovium is impossible.

B, Gadopentetate dimeglumine-enhanced 2DFT FLASH image shows hyperintensity and nodular transformation (arrows) of synovium.



intensity on enhanced images, 462). In four patients the synovium showed only a small increase in signal of 9.0% (mean relative signal intensity on unenhanced images, 680; mean relative signal intensity on postcontrast images, 741).

Nineteen joints demonstrated diffuse or circumscribed lesions of low signal intensity on T1-weighted images in the subcortical space. All but six of these areas also had low signal intensity on T2\*-weighted images except for small, focal areas of increased signal intensity. The remaining became hyperintense on T2\*-weighted scans and were classified as subchondral cysts. After enhancement, the areas of low signal on T1- and T2\*-weighted images revealed a high, particularly inhomogeneous signal increase; pannus formation was diagnosed (Figs. 2 and 3). Two of the subchondral cysts also showed enhancement at their outer margins after administration of gadopentetate dimeglumine; this was classified as synovitis. The cruciate ligaments of 10 knee joints were surrounded by tissue of low signal on unenhanced T1- and T2\*-weighted scans. After administration of gadopentetate dimeglumine, however, a marked increase in signal intensity was observed in this tissue.

On the basis of the signal behavior of the synovium and the enhancing soft tissues in the joint space and subchondral bone, four of the 19 patients with abnormal radiographs were classified as having inactive rheumatoid arthritis with secondary osteoarthritis. The other 15 were classified as having active rheumatoid arthritis with secondary osteoarthritis, because these joints demonstrated marked enhancement of the synovium and/or the intraarticular and subchondral pannus.

## Discussion

In addition to clinical and laboratory tests, the diagnosis of rheumatoid arthritis is based on findings on conventional radiographs. Radiographs depict bony changes directly, whereas disease of the articular cartilage, menisci, ligaments, and synovium are identified only indirectly.

MR imaging has proved to be useful in evaluating rheumatoid arthritis [1–4]. Because of its high soft-tissue contrast, MR demonstrates cartilaginous, soft-tissue, and bone marrow

abnormalities. Beltran et al. [2] indicated that it was difficult to differentiate between pannus and synovial fluid since both had low signal intensity on T1-weighted images and high signal intensity on T2-weighted images.

We also observed low signal intensities in the thickened synovium on T1-weighted images and a moderately high signal on T2\*-weighted scans. Therefore, without gadopentetate dimeglumine enhancement, differentiation of the synovium from the effusions was not possible in areas in which the synovium became hyperintense. The signal behavior of subchondral pannus was similar. On unenhanced T1- and T2\*-weighted scans, areas of relatively low signal or of moderate hyperintensity were seen.

Enhancement with gadopentetate dimeglumine differentiated these areas from sclerotic bone or subchondral cysts. We cannot agree with Yulish et al. [1] that T1-weighted images adequately display subchondral bone lesions. For an exact evaluation, T1- and T2-weighted imaging as well as contrast-enhanced T1-weighted images are necessary.

Furthermore, in joints in which only degenerative changes are present, absence of inflammation is established by the minimal signal increase after administration of gadopentetate dimeglumine. As Yulish et al. [1] described, the normal synovial membrane was not visible or was difficult to detect on unenhanced scans.

Reiser et al. [5] evaluated the use of gadopentetate dimeglumine-enhanced MR imaging in 31 patients with rheumatoid arthritis and related diseases such as juvenile rheumatoid arthritis, psoriatic arthropathy, systemic lupus erythematosus, ankylosing spondylitis, and septic arthritis. They also found on unenhanced MR images inadequate contrast between the synovium and joint effusion. After administration of gadopentetate dimeglumine, enhancement of the synovium occurred. We also found marked signal increase in pannus and synovitis. The contrast between effusions and the synovium involved by rheumatoid arthritis allowed their differentiation after administration of gadopentetate dimeglumine.

In the four patients in this study with normal plain films, the signal in the synovium did not increase. Signs of osteoarthritis were represented on MR by thinning of the articular cartilage

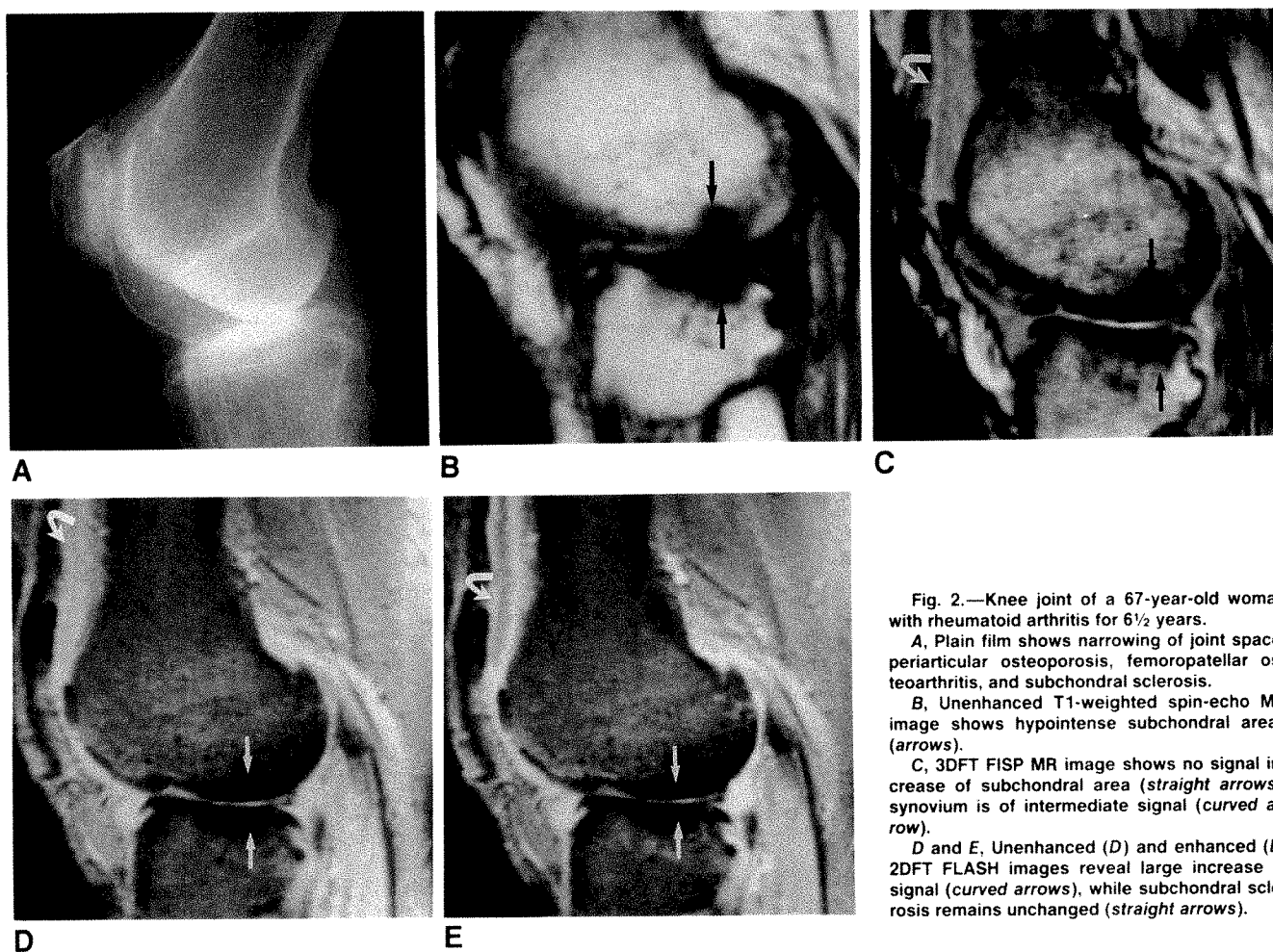


Fig. 2.—Knee joint of a 67-year-old woman with rheumatoid arthritis for 6½ years.

A, Plain film shows narrowing of joint space, periarticular osteoporosis, femoropatellar osteoarthritis, and subchondral sclerosis.

B, Unenhanced T1-weighted spin-echo MR image shows hypointense subchondral areas (arrows).

C, 3DFT FISP MR image shows no signal increase of subchondral area (straight arrows); synovium is of intermediate signal (curved arrow).

D and E, Unenhanced (D) and enhanced (E) 2DFT FLASH images reveal large increase in signal (curved arrows), while subchondral sclerosis remains unchanged (straight arrows).

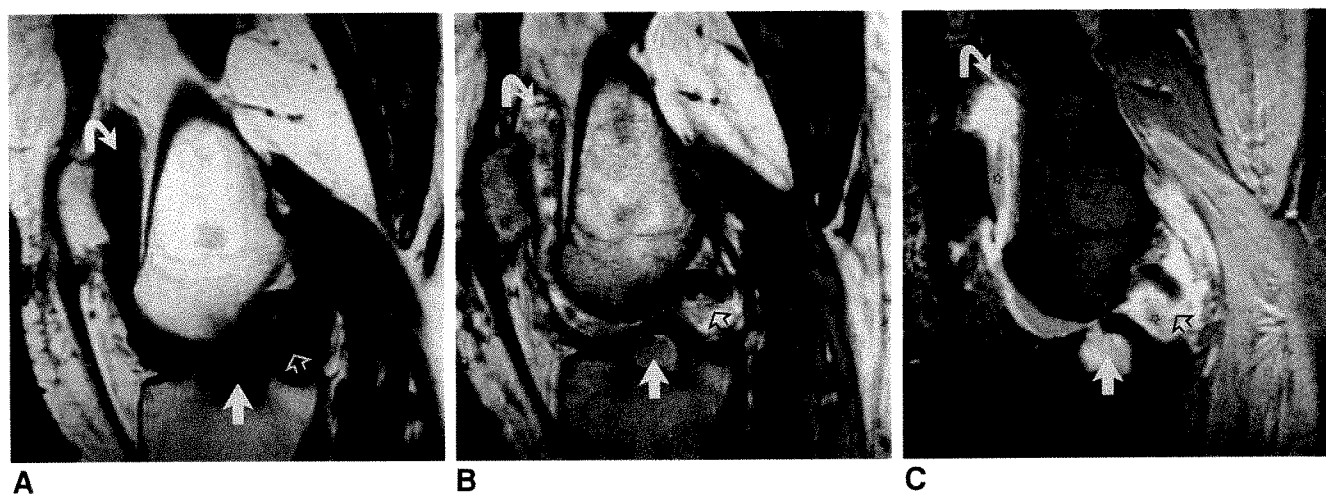


Fig. 3.—Knee joint of a 72-year-old woman with rheumatoid arthritis for 7 years.

A, Unenhanced T1-weighted spin-echo MR image shows tissue of low signal intensity within suprapatellar recess (curved arrow) and around posterior cruciate ligament (open arrow); there is reduction in subchondral bone marrow signal (solid straight arrow).

B, 3DFT FISP MR image shows signal increase appearing like an effusion around posterior cruciate ligament (open arrow) and within recess (curved arrow). Subchondral defect (solid straight arrow) is isointense relative to surrounding bone marrow.

C, 2DFT FLASH MR image shows enhancement (arrows) of synovium and subchondral and intraarticular pannus after administration of gadopentetate dimeglumine. Effusion (stars).



and menisci. In addition, areas of low signal visible subchondrally on T1- and T2\*-weighted images indicated subchondral sclerosis, and enhancement was not seen after administration of contrast medium.

Gadopentetate dimeglumine is distributed in the extracellular space, which is enlarged in inflammatory diseases [10]. Therefore, the signal increase of the synovium indicates non-specific inflammation and allows differentiation of an unaffected from an affected joint. As Reiser et al. [5] described, no differences were seen between the different inflammatory disorders they examined.

This study has several shortcomings. First, the MR diagnoses were made retrospectively, with knowledge of the findings on conventional radiographs and the clinical diagnosis of rheumatoid arthritis. Second, MR images were not correlated to histopathologic data, because none of the patients underwent subsequent arthroscopy or arthrotomy. Nevertheless, we believe that the signal behavior of the inflamed knee joint tissue reflects the hyperemia occurring in acute rheumatoid arthritis.

The study demonstrates that gadopentetate dimeglumine-enhanced MR imaging allows differentiation between synovitis and effusion, distinction between normal and inflammatory synovium, and differentiation of subchondral pannus from subchondral sclerosis. The diagnosis of rheumatoid arthritis is usually made by clinical, laboratory, and plain film findings. Enhanced MR imaging might be helpful for the detection of acute synovitis and for preoperative planning in patients in whom synovectomy becomes necessary, and for evaluation of response to drug therapy.

#### ACKNOWLEDGMENT

We thank Harry K. Genant, University of California, San Francisco, for careful review of this work.

#### REFERENCES

1. Yulish BS, Lieberman JM, Newman AJ, et al. Juvenile rheumatoid arthritis: assessment with MR imaging. *Radiology* **1987**;165:149-152
2. Beltran J, Caudill JL, Herman LA, et al. Rheumatoid arthritis: MR imaging manifestations. *Radiology* **1987**;165:153-157
3. Bundschuh C, Modic MT, Kearny E, et al. Rheumatoid arthritis of the cervical spine: surface coil MR imaging. *AJNR* **1988**;9:565-571
4. Senac MO Jr, Deutsch D, Bernstein BH, et al. MR imaging in juvenile rheumatoid arthritis. *AJR* **1988**;150:873-878
5. Reiser MF, Bongartz GP, Erlemann R, et al. Gadolinium-DTPA in rheumatoid arthritis and related diseases: first results with dynamic magnetic resonance imaging. *Skeletal Radiol* **1989**;18:591-597
6. Reiser M, Kahn T, Rupp N, Allgayer B. Ergebnisse der MR Tomographie in der Diagnostik der Osteomyelitis und Arthritis. *ROFO* **1988**;145,6:661-666
7. Arnett FC, Edworthy SM, Block DA, et al. The American Rheumatism Association 1987 revised criteria for the classification of rheumatoid arthritis. *Arthritis Rheum* **1988**;31:315-324
8. Haase A, Frahm D, Matthaei D, Hänicke W, Merboldt KD. FLASH imaging. Rapid NMR imaging using low flip angle pulses. *J Magn Reson* **1986**;67:258-266
9. Oppelt A, Graumann R, Barfuss H, et al. FISP: eine neue schnelle Pulssequenz für die Kernspintomographie. *Electromed* **1986**;54:15-18
10. Terrier F, Hricak H, Revel D, et al. Magnetic resonance imaging and spectroscopy of the periarthritic inflammatory soft tissue changes in experimental arthritis of the rat. *Invest Radiol* **1985**;20:813-823

## Book Review

**Osteoporosis. Physiological Basis, Assessment, and Treatment.** Edited by Hector F. DeLuca and Richard Mazess. New York: Elsevier, 346 pp., 1990. \$95

This important new book summarizes the proceedings of the 19th Steenbock Symposium, which was held June 5–8, 1989, at the University of Wisconsin in Madison. The symposium was organized specifically to bring together outstanding clinical investigators to discuss current understanding of osteoporosis, assessment of the extent of the disease, the risks of diminished bone density, and the means by which this disease can be treated or prevented. Work was presented on the use of estrogens as replacement therapy in postmenopausal women, the use of calcitonin to diminish bone pain and block bone resorption, the use of the vitamin D compounds to increase calcium absorption, and the importance of exercise and the need for adequate calcium intake throughout life. This symposium also underlined the need for understanding additional factors and new modes of therapy. This book should reach far beyond the symposium to educate and provide information to the medical world as to how this disease can be managed as of 1989.

The book begins with a section on the physiologic and cellular basis of osteoporosis, which includes consideration of the pathogenesis of postmenopausal osteoporosis, causes of age-related bone loss and fractures, therapy-induced osteoporosis, and the metabolic basis of osteoporosis. A section on the risk of fracture discusses fracture patterns, assessment and modification of the risk of hip fracture by using predictions of a stochastic model, and prediction of fractures. Methods of assessment, including bone densitometry for clinical diagnosis and monitoring, quantitative CT, bone histomorphometry, and biochemical assessment of bone turnover in osteoporosis, are covered. A section on estrogen includes the following topics: estrogens in prevention and treatment of osteoporosis; prevention of postmenopausal bone loss by long-term parenteral administration of 17-estradiol; comparison of percutaneous and transdermal routes; prophylaxis of bone loss: long-term effects of continuous and sequential estrogen/progestin administration and identification of women at risk; and a current perception of the risks and benefits of hormone replacement therapy. With regard to fluoride, consideration is given to developing a benefit-risk ratio of fluoride therapy in vertebral osteoporosis via comparison of sodium fluoride with mono-

fluorophosphate and to showing that fluoride and calcium therapy for osteoporosis increases trabecular vertebral bone density above the fracture threshold. Articles on vitamin D include the basis for using 1, 25-dihydroxyvitamin D to treat osteoporosis, a pathophysiologic study of women with postmenopausal osteoporosis who are on long-term treatment with calcitriol, the benefits and risks of using 1,25-dihydroxyvitamin D<sub>3</sub> to treat osteoporosis, and long-term use of 1 $\alpha$ -hydroxyvitamin D<sub>3</sub> in involutional osteoporosis. A section devoted to calcitonin covers recent developments, secretion, metabolism, and action of endogenous calcitonin in humans; use of calcitonin in the treatment of postmenopausal osteoporosis; intranasal calcitonin for prevention and treatment of osteoporosis; and calcitonin and bone pain. The following topics on exercise and calcium are discussed: physical activity and bone mass, exercise and bone mass, calcium and bone loss in postmenopausal women, and calcium requirements. ADFR (activate-depress-free-repeat), or coherence therapy, for osteoporosis and the possible use of bisphosphonates in osteoporosis are considered also. Finally, the book addresses the question of whether dermal losses explain the difference between absorbed and excreted calcium in normal subjects with high intake of calcium and provides an overview of abstracts presented at the symposium.

The book is a handy size and contains a large number of useful charts and graphs, comprehensive reference lists, and an index to the topics covered. The book would be a useful acquisition for any biomedical or departmental library. It will be most beneficial to clinical physicians who see patients with osteoporosis and metabolic bone disease and to radiologists who are interested in measurements of bone density and longitudinal follow-up of patients. The book is well worth its moderate cost; is edited by two of the leading authorities in the field; and compares favorably with other recent books on the subject, including *Osteoporosis: A Clinical Guide*, by Woolf and Dixon, and *Osteoporosis: Etiology, Diagnosis, and Management*, by Riggs and Melton.

David J. Sartoris  
University of California, San Diego Medical Center  
San Diego, CA 92103



## Pictorial Essay

# MR Imaging of the Lateral Collateral Ligament of the Ankle

Scott J. Erickson,<sup>1</sup> Judith W. Smith,<sup>2,3</sup> Mario E. Ruiz,<sup>1</sup> Steven W. Fitzgerald,<sup>1,4</sup> J. Bruce Kneeland,<sup>1,5</sup> Jeffrey E. Johnson,<sup>2</sup> Michael J. Shereff,<sup>2</sup> and G. F. Carrera<sup>1</sup>

The ankle is stabilized by three sets of ligaments: the medial collateral (deltoid) ligament, the syndesmotous complex, and the lateral collateral ligament. Of these three, the lateral collateral ligament is the one most often injured in ankle sprains. Assessment of the extent of injury has classically relied on clinical evaluation; plain film radiographs (including stress views); and, in some acute situations, ankle arthrography and/or peroneal tenography. In this report we illustrate the use of MR in the evaluation of the lateral collateral ligament. The normal anatomy, pitfalls in image interpretation, and findings in cases of ligamentous injury are demonstrated.

## Subjects and Methods

We performed MR imaging in two normal subjects and also reviewed the MR examinations of over 50 patients with various types of ankle abnormalities. The scans were obtained on a 1.5-T Signa MR unit (General Electric Medical Systems, Milwaukee, WI) in conjunction with the extremity coil provided with the system or a specialized saddle configuration coil. T1-weighted images were obtained with 500/20 (TR/TE), a 256 × 256 acquisition matrix, a 10- to 12-cm field of view, and two excitations. T2-weighted images were obtained with 2500/20,80, a 256 × 192 acquisition matrix, a 12-cm field of view, and one excitation. In all cases, the slice thickness was 3 mm. For T1-weighted images, we either obtained contiguous slices or used a 1-mm interslice gap. For T2-weighted images, a 1-mm interslice gap was used routinely. In the normal subjects we obtained

axial, sagittal, coronal, and oblique axial images. In patients, the scanning plane varied depending on the specific clinical indication.

Normal anatomic images were selected from both normal subjects and also from patients without signs or symptoms of ligamentous injury in whom studies were performed for other clinical indications. The normal images were compared with corresponding cryomicrotome sections and with standard anatomic texts [1-3]. Cases of ligamentous injury were correlated with surgical findings.

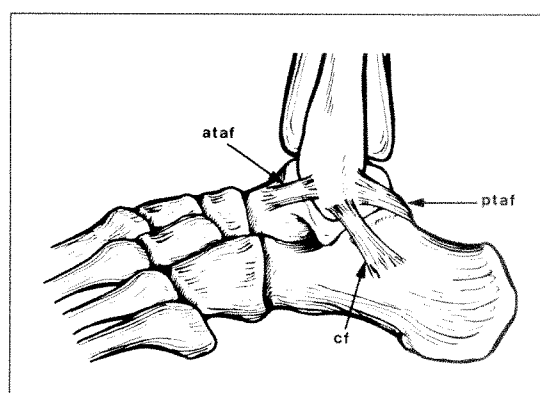


Fig. 1.—Drawing of lateral aspect of ankle shows components of lateral collateral ligament. See abbreviation key on page 132.

Received June 14, 1990; accepted after revision August 9, 1990.

Presented as an exhibit at the annual meeting of the American Roentgen Ray Society, Washington, DC, May 1990.

<sup>1</sup> Department of Radiology, Medical College of Milwaukee, Milwaukee County Medical Complex, 8700 W. Wisconsin Ave., Milwaukee, WI 53226. Address reprint requests to S. J. Erickson.

<sup>2</sup> Department of Orthopaedic Surgery, Medical College of Wisconsin, Milwaukee, WI 53226.

<sup>3</sup> Present address: Department of Orthopaedic Surgery, Emory University, Atlanta, GA 30322.

<sup>4</sup> Present address: Department of Radiology, Northwestern Memorial Hospital, Northwestern University Medical School, Chicago, IL 60011.

<sup>5</sup> Present address: Department of Radiology, Hospital of the University of Pennsylvania, Philadelphia, PA 19104.

AJR 156:131-136, January 1991 0361-803X/91/1561-0131 © American Roentgen Ray Society

Key to Abbreviations and Symbols Used in Figures	
ataf	anterior talofibular ligament
atif	anterior tibiofibular ligament
c	calcaneus
cf	calcaneofibular ligament
f	fibula
pbt	peroneus brevis tendon
plt	peroneus longus tendon
ptaf	posterior talofibular ligament
ptif	posterior tibiofibular ligament
sn	sural nerve
spr	superior peroneal retinaculum
ta	talus
ti	tibia
open arrows	malleolar fossa

Normal Anatomy

The lateral collateral ligament of the ankle includes the following structures: the anterior talofibular ligament, the posterior talofibular ligament, and the calcaneofibular ligament (Fig. 1). With the ankle in neutral position, the two talofibular ligaments are approximately in the same plane, the anterior talofibular ligament extending from the anterior aspect of the fibula to the lateral talar neck, and the posterior talofibular ligament from the distal aspect of the malleolar fossa to the lateral tubercle of the posterior talar process (Figs. 2 and 3). The anterior talofibular ligament is actually located within the anterior joint capsule, analogous to the anterior glenohumeral ligaments of the shoulder. While the anterior talofibular ligament appears homogeneously hypointense on all MR sequences, the posterior talofibular ligament often appears inhomogeneous, similar to the anterior cruciate ligament of the

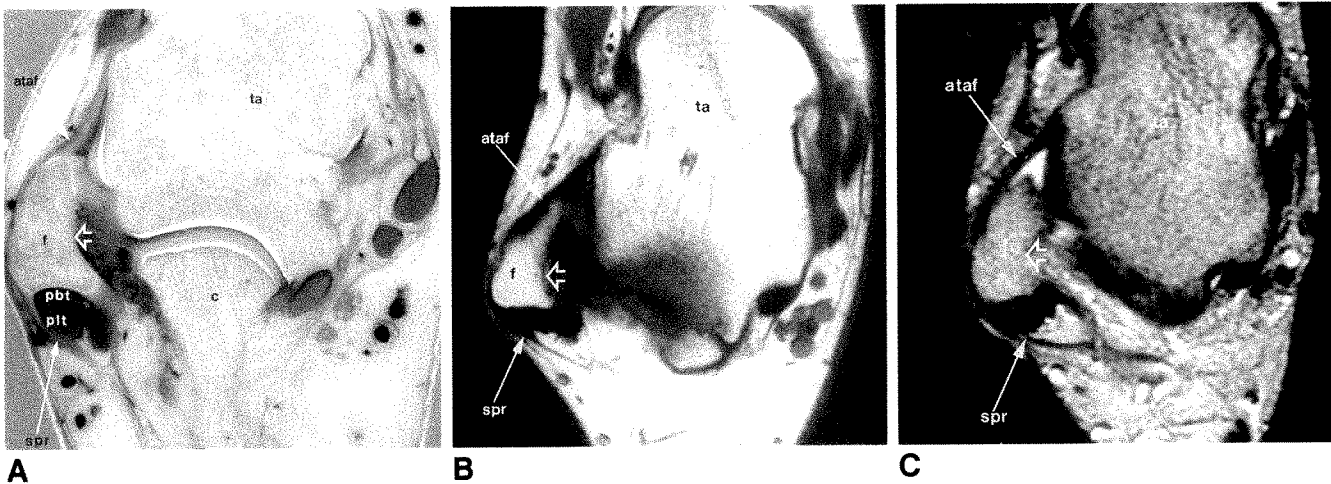


Fig. 2.—Normal anterior talofibular ligament, axial plane. See abbreviation key on this page.  
A, Cryomicrotome section.  
B, T1-weighted image, 500/20.  
C, T2-weighted image, 2500/80.

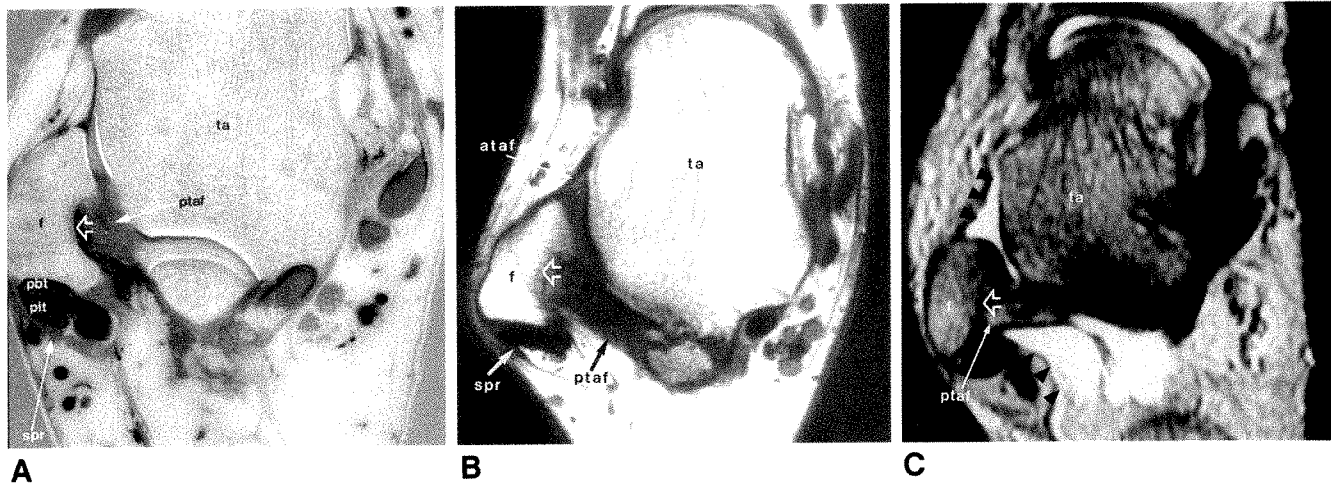
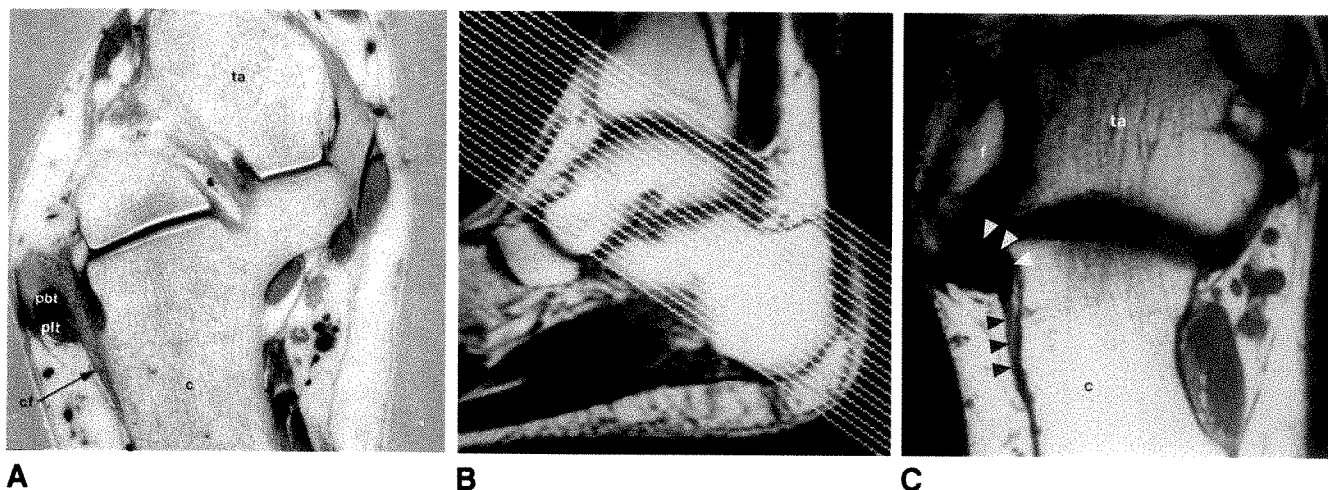
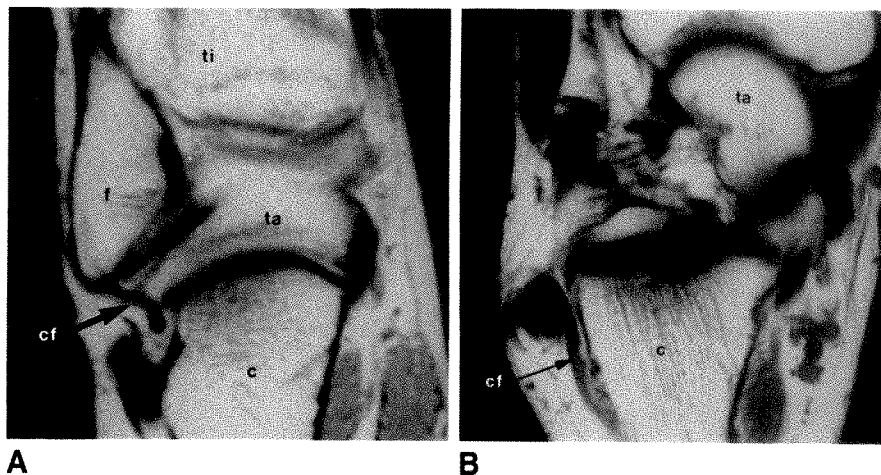


Fig. 3.—Normal posterior talofibular ligament, axial plane. See abbreviation key on this page.  
A, Cryomicrotome section.  
B, T1-weighted image, 500/20.  
C, T2-weighted image, 2500/80. Note fluid within joint (arrowheads).



**Fig. 4.—Normal calcaneofibular ligament.** See abbreviation key on page 132.  
**A,** Coronal spin-density image, 2500/20.  
**B,** Axial T1-weighted image, 500/20.



**Fig. 5.—Normal calcaneofibular ligament.** See abbreviation key on page 132.  
**A,** Cryomicrotome section.  
**B,** Sagittal localizer demonstrates oblique axial plane.  
**C,** Oblique axial T1-weighted image, 500/20, shows entire course of calcaneofibular ligament (arrowheads).

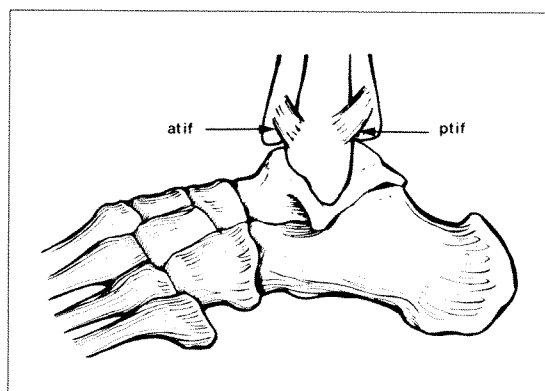


**Fig. 6.—Drawing of lateral aspect of ankle shows tibiofibular ligaments.** See abbreviation key on page 132.

knee (Fig. 3C). These two ligaments are best demonstrated in the axial plane, although with experience they may be identified in either the coronal or sagittal plane. The calcaneofibular ligament courses deep to the peroneus brevis and peroneus longus tendons, extending from the tip of the lateral malleolus to a small tubercle on the lateral aspect of the calcaneus. This ligament is often seen in part on either coronal or axial images (Fig. 4), but is best identified by using an oblique axial scanning plane (Fig. 5), or by scanning in the axial plane with the foot in plantar flexion [4].

#### Pitfalls in MR Image Interpretation

The talofibular ligaments can be easily confused with the adjacent anterior and posterior tibiofibular ligaments on MR

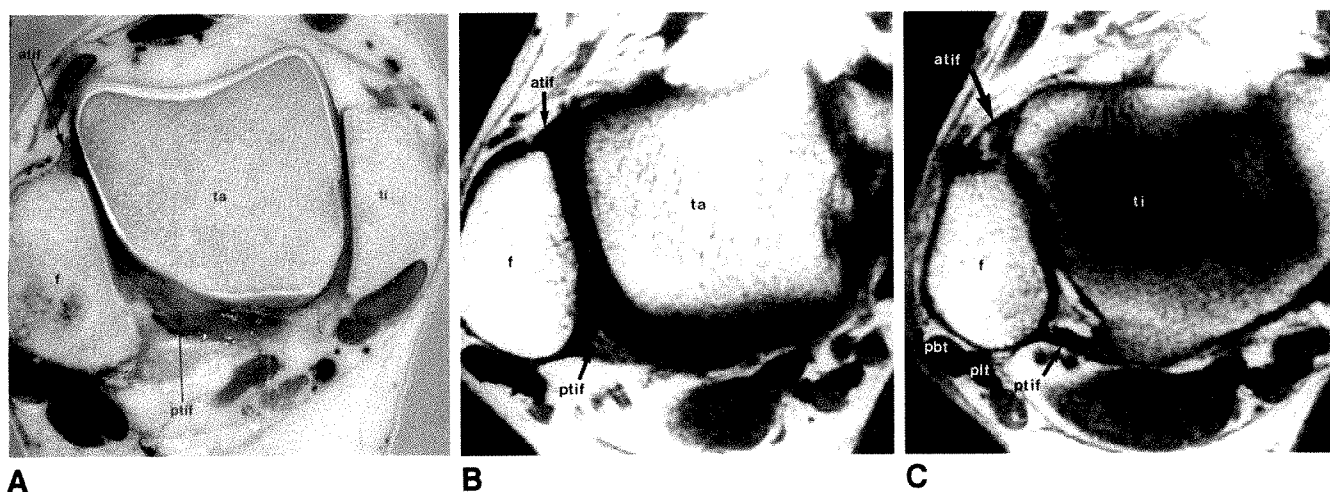


Fig. 7.—Normal tibiofibular ligaments, axial plane. See abbreviation key on page 132.

A, Cryomicrotome section.

B, Corresponding T1-weighted image, 500/20.

C, T1-weighted image, 500/20, obtained at level of ankle joint, slightly superior to B.

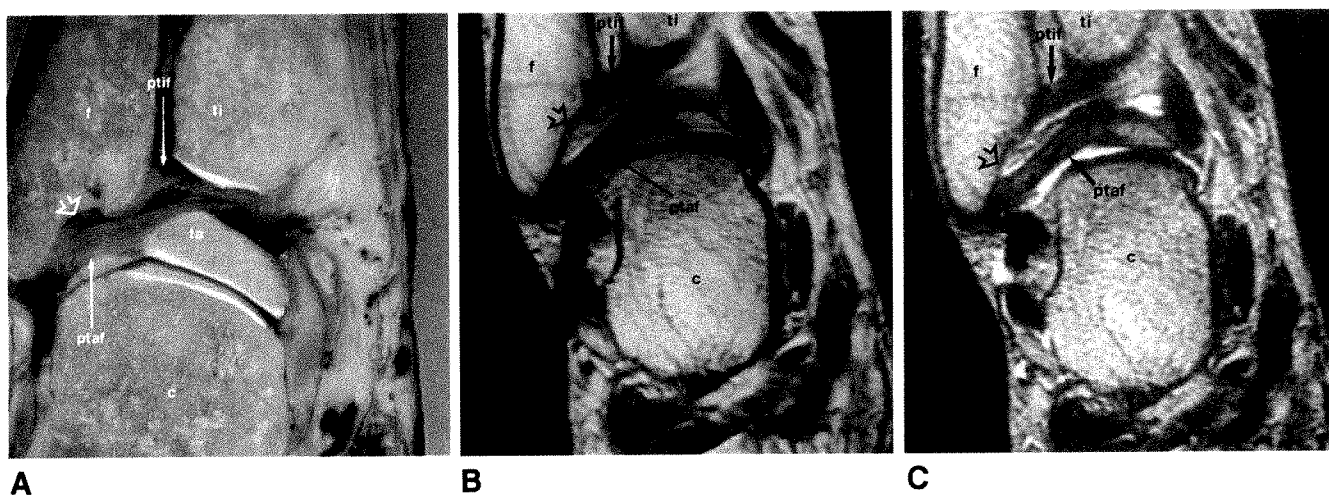


Fig. 8.—Distinction of talofibular from tibiofibular ligaments, coronal plane. See abbreviation key on page 132.

A, Cryomicrotome section.

B, Spin-density image, 2500/20.

C, T2-weighted image, 2500/80.

images (Fig. 6). The latter course obliquely from the anterior and posterior aspects of the distal tibia to insert onto the anterior and posterior aspects of the fibula (Fig. 7). The fibular sites of attachment are superior to the attachments of the talofibular ligaments, that is, above the level of the malleolar fossa (Fig. 8). The configuration of the fibula, therefore, can be used to distinguish the tibiofibular from the talofibular ligaments on axial images.

The inferior transverse ligament and the tibial slip of the posterior talofibular ligaments are diminutive structures situated between the posterior talofibular and tibiofibular liga-

ments. These structures are difficult to demonstrate with MR and should not cause diagnostic confusion.

The normal talofibular ligaments may be mistaken for abnormal conditions, particularly in the sagittal plane. For example, these hypointense structures can simulate loose bodies (Fig. 9). Such errors can be avoided by tracing the structures on adjacent slices to their sites of attachment.

#### Ligamentous Injury

The lateral collateral ligament is commonly injured with inversion stress. The weak anterior talofibular ligament is



Fig. 9.—Posterior talofibular and tibiofibular ligaments mimicking loose bodies, sagittal plane. See abbreviation key on page 132.

A, Cryomicrotome section.  
B, Corresponding spin-density image, 2500/20.  
C, Spin-density image, 2500/20, lateral to B.  
D, T2-weighted image, 2500/80, at same level as C.

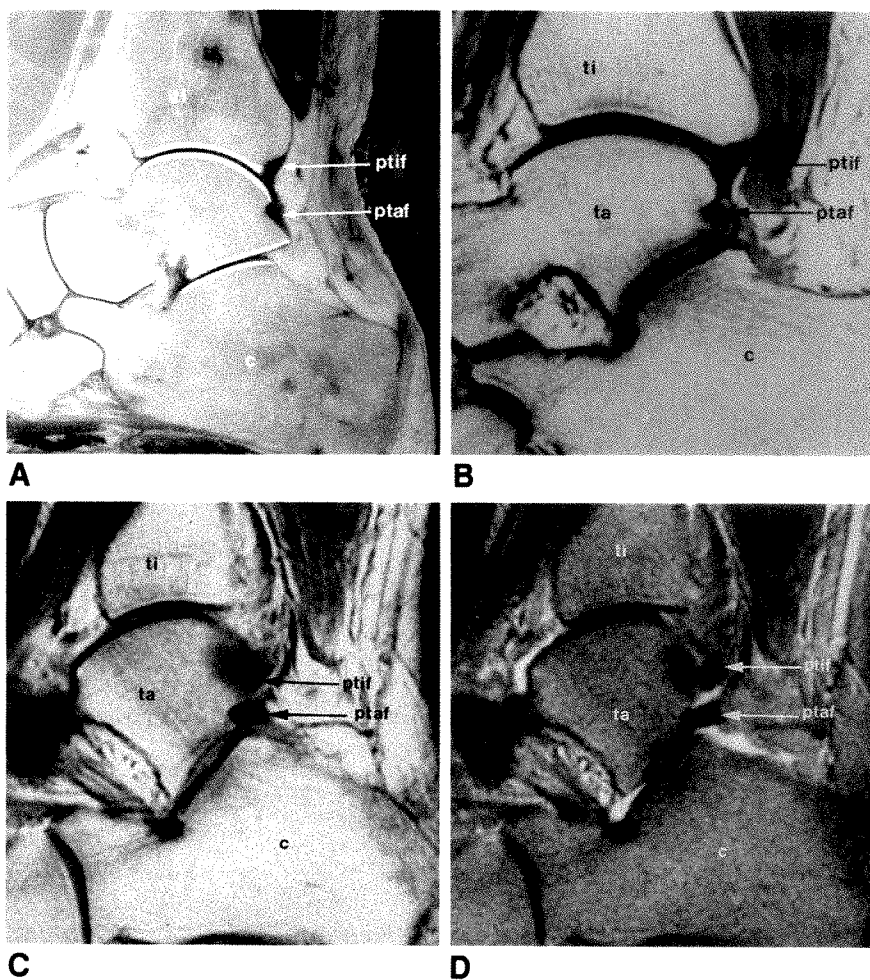
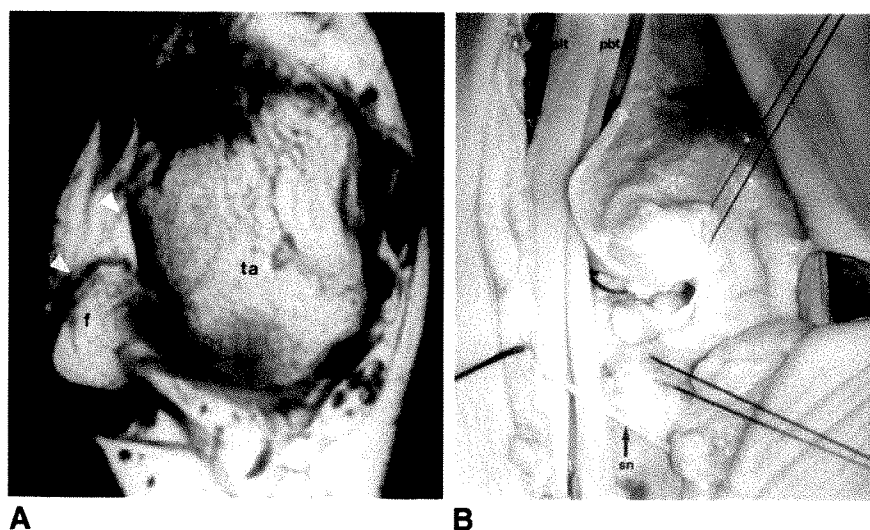


Fig. 10.—Anterior talofibular ligament injury. See abbreviation key on page 132.

A, Axial spin-density image, 2500/20, shows ligamentous discontinuity (arrowheads).  
B, Intraoperative image shows torn ends of ligament (marked by sutures).



usually injured first. MR imaging may show the anterior talofibular ligament to be attenuated, lax, or discontinuous (Figs. 10 and 11). In acute cases, there may be accompanying high signal intensity within the joint or adjacent soft tissues (Fig.

11). In one chronic case, a "mass" probably representing organizing hematoma was identified (Fig. 12).

The calcaneofibular ligament may be injured with more severe inversion stress, and is almost always associated with

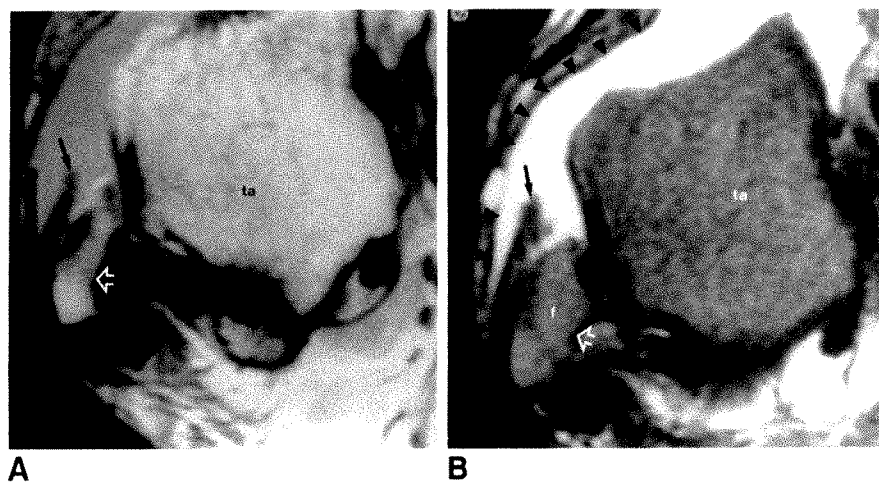


Fig. 11.—Acute anterior talofibular ligament injury. See abbreviation key on page 132. (Case courtesy of S. F. Quinn, Portland, OR.)

A, Axial spin-density image, 2500/20, shows torn end of ligament (solid arrow).

B, Axial T2-weighted image, 2500/80, shows torn end of ligament (solid arrow) with adjacent fluid (arrowheads).

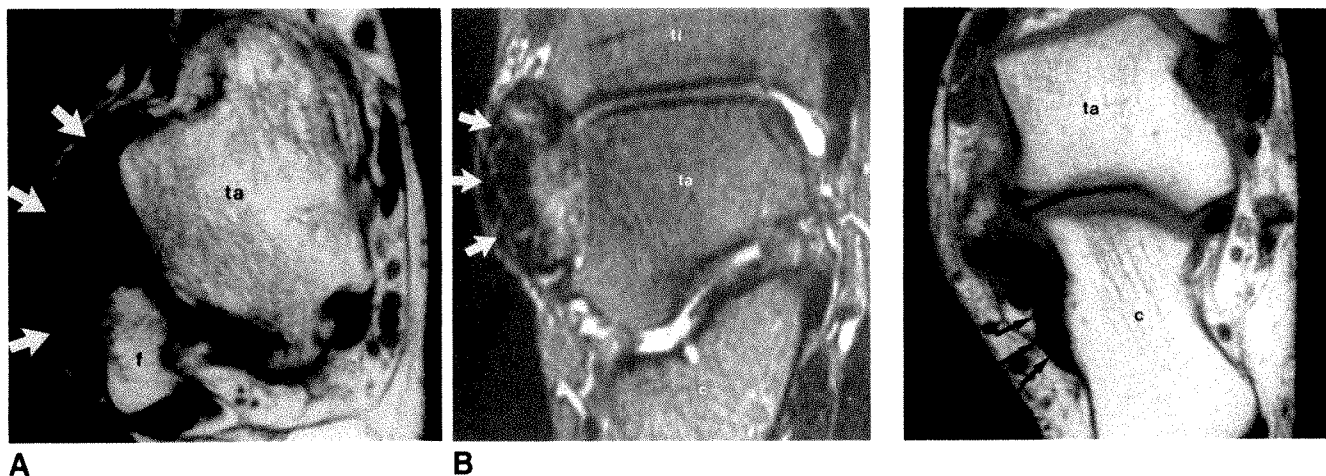


Fig. 12.—Anterior talofibular ligament injury with probable organizing hematoma. See abbreviation key on page 132.

A, Axial T1-weighted image, 500/20, shows absent ligament and hypointense hematoma (arrows).

B, Coronal T2-weighted image, 2500/80, shows predominantly hypointense hematoma (arrows).

Fig. 13.—Calcaneofibular ligament injury. Oblique axial T1-weighted image, 500/20, shows abnormal thickening of ligament (arrows). See abbreviation key on page 132.

an anterior talofibular injury. MR imaging may show attenuation or abnormal thickening of the ligament (Fig. 13). Anatomic variability in the configuration of the ligament, combined with relative difficulty in identification, may make assessment of injury a diagnostic challenge.

Posterior talofibular ligament injury is uncommon, and is almost always associated with injury to both the anterior talofibular and calcaneofibular ligaments.

#### REFERENCES

1. Netter FH. *The Ciba collection of medical illustrations*, vol. 8. *Musculoskeletal system*, part I. *Anatomy, physiology and metabolic disorders*. Summit, NJ: Ciba-Geigy, 1987.
2. Anderson JE. *Grant's atlas of anatomy*, 7th ed. Baltimore: Williams & Wilkins, 1978.
3. Williams PL, Warwick R, Dyson M, Bannister LH. *Gray's anatomy*, 37th ed. Edinburgh: Churchill Livingstone, 1989.
4. Rijke AM. Acute ankle sprains: What is the role of the radiologist? *Appl Radiol* 1989;18:11-16.



## Urethral Abnormalities in Male Neonates with VATER Association

Sandra K. Fernbach<sup>1</sup>

In the past 3 years, eight of 20 male neonates with stigmata of the VATER association were found to have significant urethral abnormalities. Three had megalourethra, two had duplication of the urethra, and one each had an anterior urethral valve, congenital stricture, and hypospadias. In only five of eight was the extent of the abnormality clinically apparent. All three infants with megalourethra and imperforate anus died because of the coexistence of other severe congenital anomalies. Prior literature has described but not stressed the increased prevalence of urethral abnormalities in children with the VATER association.

Because of the high prevalence (eight of 20) of significant urethral anomalies, we perform voiding cystourethrography on all males with the stigmata of the VATER association, even in the absence of clinical symptoms.

*AJR* 156:137-140, January 1991

The VATER association is the name given to a specific concurrence of congenital anomalies: vertebral (or vascular), anorectal, tracheoesophageal, and radial/renal [1]. Since the original description, the anomalies found in each of these organ systems have been more completely defined, and additional anomalies have been described. The association between both upper and lower gastrointestinal malformations and genitourinary anomalies has been investigated and reported [2-7].

Upper urinary tract abnormalities are more common with supralevator imperforate anus than with infralevator imperforate anus [5]. These anomalies include unilateral renal agenesis, renal dysplasia, ureteropelvic junction obstruction, and renal ectopia. Belman and King [5] also reported a high prevalence of lower urinary tract anomalies in children with the supralevator type of imperforate anus [5]. The lesion most frequently detected was a fistulous communication between the imperforate colon and the posterior portion of the male urethra or the female vagina [5]. It is unclear how many children in their series could be classified as having VATER association.

When duplication of the urethra has been reported in larger series, the stigmata of VATER association have been given only incidental mention [8, 9]. In the literature on the VATER association, only a few urethral abnormalities, such as hypospadias and chordee, have been described [2-6]. None of the prior papers has stressed the increased occurrence of urethral anomalies in the VATER association, and none has specifically looked at the prognosis of infants with imperforate anus and megalourethra.

### Materials and Methods

In the past 3 years, eight male neonates with the VATER association were identified as having a urethral abnormality. Each neonate had a gastrointestinal abnormality and at least two other classically described malformations. A minimum of three abnormalities was chosen to define affected children, the same criteria used by Barnes and Smith [6]. The medical

Received March 8, 1990; accepted after revision August 6, 1990.

<sup>1</sup> Department of Radiology, The Children's Memorial Hospital and Northwestern University Medical School, Chicago, IL 60611. Address reprint requests to S. K. Fernbach, Department of Radiology #9, The Children's Memorial Hospital, 2300 Children's Plaza, Chicago, IL 60614.

0361-803X/91/1561-0137  
© American Roentgen Ray Society

records and radiologic films of these children were reviewed. To identify the total number of male neonates seen with the VATER association, we reviewed the medical records and radiologic films of all male neonates with tracheoesophageal fistula, esophageal atresia, or imperforate anus.

Results

The data of the neonates with urethral anomalies are summarized in Table 1. Of those without urethral abnormalities, two had esophageal atresia as the gastrointestinal malformation and eight had imperforate anus. Only two neonates had both an imperforate anus and esophageal atresia.

Three neonates, each with imperforate anus, had a grossly abnormal phallus typical of megalourethra. These three neonates died of severe, multiple renal anomalies (Table 1). One of these, with a solitary pelvic kidney, underwent vesicostomy after which voiding cystourethrography (VCUG) showed a megalourethra and meatal stenosis (Fig. 1).

Two neonates (one with esophageal atresia, one with imperforate anus) had urethral duplication, one complete and one incomplete. In both the duplication was initially occult but became apparent in the neonatal period (Figs. 2 and 3).

Two neonates with imperforate anus had no clinical deformity of the phallus and no voiding symptoms to suggest abnormality. However, during VCUG performed to diagnose or exclude fistulous connections between the gastrointestinal and genitourinary tracts, congenital stricture of the urethra was identified in one and an anterior urethral valve (Fig. 4) in the other. A third was noted clinically to have hypospadias and a rectourethral fistula, which were shown by VCUG.

Discussion

Common urethral congenital anomalies such as hypospadias have been reported in children with VATER association. It remains unclear whether the frequency of hypospadias is truly increased in this population, although recent reports suggest this may be so [4].

Complete urethral duplication is a rare anomaly. Its presence in children with VATER association has received little attention. In a report of 16 children with complete urethral duplication, Psihramis et al. [9] mention two children with

TABLE 1: Abnormalities in the Eight Neonates with Urethral Anomalies

Type	Patient Number							
	1	2	3	4	5	6	7	8
Urethral	Fusiform	Fusiform	Fusiform	Complete duplication	Incomplete duplication	Congenital stricture	Anterior urethral valve	Hypospadias
Gastrointestinal	IA	IA, DA, EA-TEF	IA	EA-TEF, absent gall-bladder	IA	IA	IA	IA
Genitourinary	Absent kidneys	Left kidney absent, right multicystic dysplastic kidney	Left kidney absent, right kidney pelvic, prune belly syndrome	Large urachal remnant, segmental renal dysplasia (at autopsy)	Double urethral duplication, incomplete proximal and distal channels	Left-sided UPJO and UVJO, bifid scrotum	Right ectopic kidney	Right kidney absent
Tracheal	—	Tracheal rings	Tracheal rings	Tracheal rings	—	—	—	—
Musculoskeletal	Hands: cutaneous syndactyly	Narrow pelvis, short sterum	—	Bifid distal phalanx of right thumb, 11 ribs bilateral	Hypoplastic 4th left rib	—	13 ribs	—
Vertebral	Sacral segmentation anomalies	Partial sacral agenesis	Partial sacral agenesis	—	Sacral segmentation anomalies	—	Thoracic spine segmentation anomalies	—
Cardiac	—	—	—	PDA, PFO, MR	TOF	VSD	—	TAPVR
Other	—	—	—	—	—	Low-set ears	—	—
Karyotype	Normal	Normal	Normal	Normal	Normal	Normal	Normal	—

Note.—IA = imperforate anus, DA = duodenal atresia, EA-TEF = esophageal atresia and tracheoesophageal fistula, UPJO = ureteropelvic junction obstruction, UVJO = ureterovesical junction obstruction, — = not present, PDA = patent ductus arteriosus, PFO = patent foramen ovale, MR = mitral regurgitation, TOF = tetralogy of Fallot, VSD = ventricular septal defect, TAPVR = total anomalous pulmonary venous return.



Fig. 1.—Voiding cystourethrogram of megalourethra in infant with imperforate anus. Contrast material introduced through suprapubic tube flows into distensible fusiform megalourethra. Meatal stenosis, clinically present, is preventing antegrade flow of contrast material.

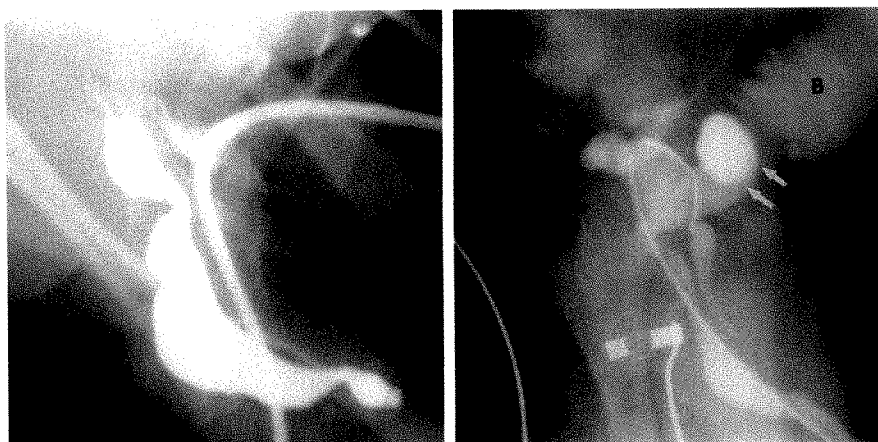


Fig. 2.—Voiding cystourethrogram of duplicated urethra shows deformity of distal sacrum (black arrows). This spot film obtained near end of voiding shows incompletely emptied trabeculated bladder (B), reflux into seminal vesicles (arrowheads), and incompletely formed dorsal urethra. Rounded density at bladder base (white arrows) is a periureteral diverticulum (Hutch diverticulum) seen en face.



Fig. 3.—Voiding cystourethrogram of duplicated urethra. Catheter defines rectal urethra. A second urethral channel arises from posterior urethra and follows expected course of a normal penile urethra. Enlarged refluxing distal ureters are seen on sides of bladder (arrows).

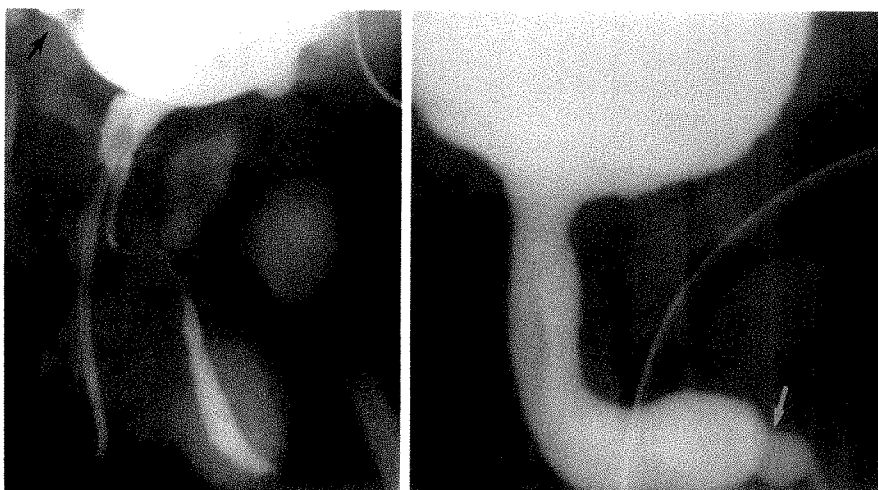


Fig. 4.—Voiding cystourethrogram of male infant with imperforate anus shows an anterior urethral valve causing an abrupt change in urethral caliber (arrow). Note distension of posterior urethra.



imperforate anus. One child, a girl, also had vaginal atresia; the other, a boy, had an ectopic kidney.

The type of complete duplication seen in the neonate with esophageal atresia has been variously called an H-type urethroanal fistula or duplication with a perineal (hypospadiac) channel. Three of the five male neonates with this lesion who are well-described in the literature also had esophageal atresia with distal tracheoesophageal fistula [10–12]. In all, the perineal or rectal urethra was the dominant uriniferous channel. This is expected, as the ventral urethra, regardless of location, is generally the main urethra. The possibility that these multiple anomalies of septation (esophageal atresia, imperforate anus, duplication of the urethra) may have a common cause is intriguing but unproved.

The type of double incomplete duplication detected in the neonate with imperforate anus was unexpected and, according to Effmann et al. [8], is very rare. At the time of catheterization, before VCUG began, this child would have been thought to have an incomplete distal duplication because of

the glanular meatus. The incomplete proximal urethra could not have been anticipated.

Fusiform megalourethra occurs when there is marked deficiency or absence of the corpus spongiosum and the corpora cavernosa (Fig. 1). In general it is an ominous sign and is seen in children with severe, life-threatening anomalies [13]. In our series, all three neonates with this anomaly died of severe renal anomalies causing renal insufficiency in the perinatal period.

The association of imperforate anus, severe urethral or penile abnormalities, and intrauterine death has recently been reported in the radiologic literature [14]. Oligohydramnios complicated almost all these pregnancies, but none of the fetuses or neonates had renal agenesis. Although children with imperforate anus generally undergo VCUG to detect rectourinary fistula, reflux, and abnormal bladder function, the VCUG may, in children with VATER association, show many other abnormalities. This appears to be true in those children with esophageal atresia and imperforate anus.

## ACKNOWLEDGMENT

The author thanks Sally Gartman for her help in preparing the manuscript.

## REFERENCES

1. Quan L, Smith DW. The VATER association. Vertebral defects, anal atresia, T-E fistula with esophageal atresia radial and renal dysplasia: a spectrum of associated defects. *J Pediatr* **1973**;82:104-107
2. Uehling DT, Gilbert E, Chesney R. Urologic implications of the VATER association. *J Urol* **1983**;129:352-354
3. Hoekstra WJ, Scholtmeijer RJ, Molenaar JC, Schreeve RH, Schroeder FH. Urogenital tract abnormalities associated with congenital anorectal abnormalities. *J Urol* **1983**;130:962-963
4. Berkhoff WBC, Scholtmeyer RJ, Tibboel D, Molenaar JC. Urogenital tract abnormalities associated with esophageal atresia and tracheoesophageal fistula. *J Urol* **1989**;141:362-363
5. Belman AB, King LR. Urinary tract abnormalities associated with imperforate anus. *J Urol* **1972**;108:823-824
6. Barnes JC, Smith WL. The VATER association. *Radiology* **1978**;126:445-449
7. Weaver DD, Mapstone CL, Yu P. The VATER Association: analysis of 46 patients. *Am J Dis Child* **1986**;140:225-229
8. Effmann EL, Lebowitz RL, Colodny AH. Duplication of the urethra. *Radiology* **1976**;119:179-185
9. Psihramis KE, Colodny AH, Lebowitz RL, Retik AB, Bauer SB. Complete patent duplication of the urethra. *J Urol* **1986**;136:63-67
10. Bruce R, Alton D. Duplication of urethra with communication to the rectum. *Pediatr Radiol* **1986**;16:79-81
11. deVries PA, Friedland GW. Congenital "H-type" ano-urethral fistula. *Radiology* **1974**;113:397-407
12. Stephens FD, Donnellan WL. "H-type" urethroanal fistula. *J Pediatr Surg* **1977**;12:95-102
13. Firlit CF. Urethral abnormalities. *Urol Clin North Am* **1978**;5:31-54
14. Hayden SA, Russ PD, Pretorius DH, Manco-Johnson ML, Clewell WH. Posterior urethral obstruction: prenatal sonographic findings and clinical outcome in fourteen cases. *J Ultrasound Med* **1988**;7:371-375



# Sonography in Neonatal Congenital Adrenal Hyperplasia

Carlos J. Sivit<sup>1,2</sup>  
Wellington Hung<sup>2,3</sup>  
George A. Taylor<sup>1,2</sup>  
Linda M. Catena<sup>1</sup>  
Cathy Brown-Jones<sup>1</sup>  
David C. Kushner<sup>1,2</sup>

Adrenal gland size was evaluated in six infants with congenital adrenal hyperplasia. All of the infants had a severe deficiency of the 21-hydroxylase enzyme resulting in the salt-losing form of congenital adrenal hyperplasia. The adrenal measurements were compared with those of 40 consecutive age-matched, asymptomatic infants. Mean adrenal length was 14.4 mm and width was 1.9 mm in asymptomatic infants, whereas in infants with congenital adrenal hyperplasia, mean adrenal length was 23.7 mm and width was 5.3 mm.

Although infants with congenital adrenal hyperplasia may have normal-sized adrenal glands, mean length measurements of 20 mm or greater and mean width measurements of 4 mm or greater suggest the diagnosis.

*AJR* 156:141-143, January 1991

Congenital adrenal hyperplasia (CAH) results from an inborn enzyme deficiency in the biosynthetic pathway of adrenal steroid metabolism. This deficiency causes ineffective production of adrenal steroids; overproduction and accumulation of cortisol precursors, some of which produce androgenic effects; and hyperplasia of the adrenal cortex. The overproduction of androgens results in inhibition of differentiation of the embryonic genital tract along female lines, resulting in masculinization in females. In approximately 30% of cases, mineralocorticoid production also is impaired, resulting in hyponatremia, hyperkalemia, hypoglycemia, and hypotension [1]. The diagnosis should be considered in any infant with salt-losing crisis.

The most common enzymatic abnormality, accounting for over 90% of cases, is 21-hydroxylase deficiency [1]. The diagnosis is confirmed biochemically by elevated serum levels of 17-hydroxyprogesterone and testosterone levels, as well as elevated urine levels of 17-ketosteroid and pregnanetriol levels. Unfortunately standard biochemical assays may require days to complete and cause delay in diagnosis and subsequent therapy by 1 week or more.

The severity of illness in affected neonates requires the institution of therapy as soon as possible. This study evaluates the role of adrenal sonography in the diagnosis of CAH.

## Materials and Methods

Sonographic examinations were obtained with a real-time sector scanner (Acuson, Mountain View, CA) with the use of a 5-MHz transducer. The presence, echo-pattern, and size of both adrenal glands were evaluated. Measurements of adrenal gland length and width were made to the nearest tenth of a millimeter on sagittal projections according to the method described by Oppenheimer et al. (Fig. 1) [2]. The length of the gland was defined as the maximal cephalocaudal dimension. The width was defined as the maximum dimension perpendicular to the length of the posterior wing. The width measurement was obtained near the base of the gland.

Received November 13, 1989; accepted after revision July 10, 1990.

<sup>1</sup> Department of Diagnostic Imaging and Radiology, Children's National Medical Center and the George Washington University School of Medicine and Health Sciences, 111 Michigan Ave. N.W., Washington, DC 20010. Address reprint requests to C. J. Sivit.

<sup>2</sup> Department of Pediatrics, Children's National Medical Center and the George Washington University School of Medicine and Health Sciences, 111 Michigan Ave N.W., Washington, DC 20010.

<sup>3</sup> Department of Endocrinology, Children's National Medical Center and the George Washington University School of Medicine and Health Sciences, 111 Michigan Ave. N.W., Washington, DC 20010.

0361-803X/91/1561-0141  
© American Roentgen Ray Society

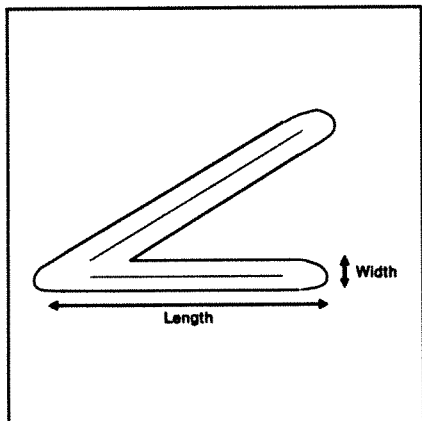


Fig. 1.—Method of adrenal gland measurement on coronal and sagittal projections.



Fig. 2.—Longitudinal sonogram through left upper quadrant of abdomen shows a markedly enlarged right adrenal gland (arrows). S = spleen, K = left kidney.

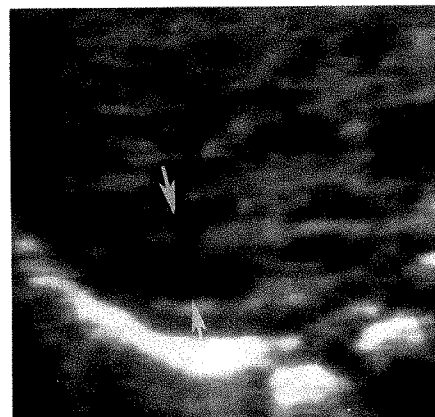


Fig. 3.—Longitudinal sonogram of a normal left adrenal gland (arrows).

A retrospective analysis was made of the records of all infants diagnosed with CAH at our institution between March 1985 and May 1989 (six patients). Mineralocorticoid deficiency was established by the presence of hyponatremia, hyperkalemia, and/or elevated plasma renin activity. Biochemical confirmation of CAH consisted of elevated serum levels of testosterone and 17-hydroxyprogesterone and elevated urinary excretion of 17-ketosteroids and pregnanetriol.

Sonographic images on hard copy were independently reviewed by two examiners on two separate occasions. The scans were given to each examiner mixed in with 40 additional cases of normal infants, who were matched for age. The examiners did not know the identity of the patients.

The asymptomatic group represented abdominal sonograms of 40 consecutive full-term infants, ranging in age from 2 days to 8 weeks postterm. Indications for sonography in this group included: urinary tract infection (19), vomiting (six), congenital anomaly (six), jaundice (four), suspected abdominal mass (four), and sibling reflux (one).

Adrenal gland size in infants with CAH and in normal infants was compared. Differences in mean adrenal gland length and width between the two groups were analyzed by *t* test.

## Results

There were six infants with CAH. Five were girls and one was a boy. Sonography was performed between 2 days and 8 weeks of life (mean age, 1.9 weeks). All of the infants had a deficiency of 21-hydroxylase resulting in the salt-losing form of CAH. All infants had electrolyte imbalance and shock. The female infants also had ambiguous genitalia.

Both adrenal glands were identified in all infants with CAH. The normal corticomedullary pattern, consisting of the echogenic central medulla and peripheral hypoechoic cortex (Fig. 2), was preserved. Additionally the typical adrenal shape, which resembles a triangle or Y, was maintained. Adrenal lengths and widths were measured by the first examiner to be 14.0, 20.5, 26.5, 27.5, 29.0, and 28.5 mm length and 4.0, 6.0, 5.0, 6.5, 4.5, and 6.0 mm width. Examiner two measured the same glands as follows: 14.0, 20.0, 27.0, 20.0, 28.0, and 28.0 mm length and 4.0, 6.0, 5.5, 6.0, 4.5, and 6.0 mm width.

Interobserver variability in adrenal measurement was as-

sessed in these infants by calculating agreement in absolute measurements of width and length. Agreement was defined as 0.5 mm or smaller difference in measurement. Much less variability was noted in measurement of width than length. All width measurements agreed within 0.5 mm, and half of the length measurements were in agreement.

There were 22 girls and 18 boys in the asymptomatic group. The mean age was 2.2 weeks. The right adrenal gland was identified in all asymptomatic infants, and the left was identified in 39 (98%). No statistically significant difference in size was seen between the right and left adrenal glands. Mean adrenal length and width were significantly greater ( $p = .0001$  by two-tailed, unpaired *t* test) in infants with CAH than in asymptomatic infants (Table 1, Fig. 3). Five of six infants with CAH had a mean length of 20 mm or greater, whereas only one of 40 asymptomatic infants had a mean width of 20 mm or greater. Five of six infants with CAH had a mean width of 4 mm or greater, whereas only one of 40 asymptomatic infants had a mean width of 4 mm or greater.

## Discussion

Sonography has been shown to be an effective technique for evaluating the neonatal adrenal gland [2-4]. Our data support previous reports that the neonatal adrenal gland can usually be identified sonographically. We visualized the right adrenal gland in all infants studied. The left adrenal gland was identified in all infants with CAH and in 98% of asymptomatic infants.

The neonatal adrenal gland is distinctly different from the adult gland. The absolute thickness of the cortex is greater than the thickness in older children and adults [2]. It is composed of the fetal zone, comprising 80% of the thickness, and the thin peripheral zone that comprises 20% of the thickness and becomes the adult cortex [2, 3]. After birth, involution of the fetal zone occurs, which is accomplished by hemorrhagic necrosis [2, 4]. In normal neonates, the size of



**TABLE 1: Comparison of Adrenal Gland Size in Infants with Congenital Adrenal Hyperplasia vs Normal Infants**

Dimension	Normal		Congenital Adrenal Hyperplasia	
	Mean <sup>a</sup>	Standard Error	Mean <sup>a</sup>	Standard Error
Length (mm)	14.4	0.81	23.7	1.40
Width (mm)	1.9	0.12	5.3	0.60

Note.— $p = .0001$  by two-tailed, unpaired  $t$  test.

<sup>a</sup> Average value of two independent examiners.

the adrenal glands may decrease by 50% between 1 and 3 weeks of life [5–7].

The neonatal adrenal gland has a characteristic sonographic appearance. The shape resembles a triangle or inverted Y. The pattern consists of a central echogenic stripe surrounded by a peripheral hypoechoic rim. The echogenic core correlates histologically with the adrenal medulla, and the peripheral hypoechoic region represents the adrenal cortex, which is larger in neonates than in older children or adults [2].

Various sonographic measurements of adrenal size have been described [2, 6–8]. These include measurements of adrenal length, width, area, and circumference. We noted less interobserver variability in adrenal width than in adrenal length, as has been reported [9].

Our data indicate that sonography can detect adrenal enlargement in infants with CAH. Adrenal length and width measurements were greater in infants with CAH than in asymptomatic infants. Although the two populations overlap somewhat, mean length measurements of 20 mm or greater and mean width measurements of 4 mm or greater suggest the diagnosis of CAH. Some neonates who have biochemically proved CAH may have normal sonographic findings. Thus, identification of sonographically normal-sized adrenal glands does not exclude CAH.

Adrenal enlargement associated with CAH has characteristics that permit differentiation from other adrenal diseases. Adrenal hemorrhage is characterized by a different clinical presentation and sonographic enlargement that is usually

asymmetric with associated loss of the normal corticomedullary differentiation [10]. The sonographic pattern of hemorrhage may vary from an anechoic to a hyperechoic mass [10, 11]. Rare adrenal tumors also would be asymmetric and would result in loss of the normal adrenal architecture [12, 13].

In summary, sonography can be an effective, noninvasive tool in the diagnosis of adrenal enlargement due to CAH. It should be the technique of choice for making this diagnosis. If symmetric enlargement is present, the presumptive diagnosis of CAH can be made and therapy initiated while awaiting confirmation by laboratory studies. The presence of normal-sized glands, however, does not exclude the diagnosis.

#### REFERENCES

1. Sommers SC. Adrenal glands. In: Kissane JM, ed. *Anderson's pathology*, 8th ed. St. Louis: Mosby, 1985:1429–1450.
2. Oppenheimer DA, Carroll BA, Yousem S. Sonography of the normal neonatal adrenal gland. *Radiology* 1983;146:157–160.
3. McIntosh AD. The human fetal adrenal: a morphologic and histochemical study with comment on the problem of function. *Scot Med J* 1960;5:242–249.
4. Zurbrugg RP. Congenital adrenal hyperplasia. In: Gardner LI, ed. *Endocrine and genetic diseases of childhood*, 2nd ed. Philadelphia: Saunders, 1975:476–499.
5. Gardner LI. Development of the normal fetal and neonatal adrenal. In: Gardner LI, ed. *Endocrine and genetic diseases of childhood*, 2nd ed. Philadelphia: Saunders, 1975:460–475.
6. Scott EM, Thomas A, McGarrigle HG, Lachelin GCL. Serial adrenal ultrasonography in normal neonates. *J Ultrasound Med* 1990;9:279–283.
7. Schulz DM, Giordano DA, Schulz DH. Weights of organs of fetuses and infants. *Arch Pathol* 1962;74:244–250.
8. Kangaroo H, Diamant MJ, Gold RH, et al. Sonography of adrenal glands in neonates and children: changes in appearance with age. *JCU* 1986;14:43–47.
9. Bryan PJ, Caldamone AA, Morrison SC, Yulish BS, Owens R. Ultrasound findings in the adreno-genital syndrome. *J Ultrasound Med* 1988;7:675–679.
10. Mittelstaedt CA, Volberg FM, Merten DF, Brill PW. The sonographic diagnosis of neonatal adrenal hemorrhage. *Radiology* 1979;131:453–457.
11. Nissenbaum M, Jequier S. Enlargement of adrenal glands preceding adrenal hemorrhage. *J Clin Ultrasound* 1988;16:349–352.
12. Yeh H, Mitty HA, Rose J, Wolf BS, Gabrilove JL. Ultrasonography of adrenal masses: usual features. *Radiology* 1978;127:467–474.
13. Davies RP, Lam AH. Adrenocortical neoplasm in children: ultrasound appearance. *J Ultrasound Med* 1987;6:325–328.

# International Pediatric Radiology '91

## Conjoint Meeting: SPR and ESPR, Stockholm, Sweden, May 27–31, 1991

The members, officers, and program committee of the IPR Conjoint Meeting proudly announce the second conjoint meeting of the SPR and ESPR (European Society of Pediatric Radiology). Meeting registration and hotel reservation request forms will be available for **SPR members** from: Lynne Tiras, I.M.M., 4550 Post Oak Place, Ste. 248, Houston, TX 77027.

Further information about the meeting and registration can be obtained from Carol M. Rumack, M.D., Secretary, The Society for Pediatric Radiology, University of Colorado Health Sciences Center, 4200 E. 9th Ave., Box A030, Denver, CO 80262-0030; telephone (303) 270-4512.

**ESPR members** should contact: IPR'91 Congress, c/o Stockholm Convention Bureau, Box 6911, S-102 39, Stockholm, Sweden, for request forms.

### Sunday, May 26

1:00–7:00 p.m.  
6:00–8:00 p.m.

Registration  
Early Bird Reception (wine and cheese)

### Monday, May 27

7:45–8:00 a.m.  
8:00–9:40 a.m.  
9:40–10:20 a.m.  
10:20–12:20 p.m.  
12:20–1:20 p.m.  
1:20–3:20 p.m.  
3:40–5:00 p.m.  
5:00–5:40 p.m.  
8:00–5:40 p.m.  
7:00–9:00 p.m.

Opening Ceremony  
**Symposium** (1–5)  
Poster Session 1 (posters 1–10)  
**Scientific Session 1** (papers 1–12)  
Lunch  
**Scientific Session 2** (papers 13–24)  
**Scientific Session 3** (papers 25–32)  
Swedish Society of Medicine Pediatric Radiology Lecture  
Poster Exhibits  
Stockholm Town Hall Welcome Reception

### Tuesday, May 28

8:00–9:40 a.m.  
9:40–10:20 a.m.  
10:20–12:20 p.m.  
8:00–12:20 p.m.  
Afternoon free

**Symposium** (6–10)  
Poster Session 2 (posters 11–20)  
**Scientific Session 4** (papers 33–44)  
Poster Exhibits  
Shopping, Sightseeing, Dining

### Wednesday, May 29

8:00–9:40 a.m.  
9:40–10:20 a.m.  
10:20–12:20 p.m.  
12:20–1:20 p.m.  
1:20–3:20 p.m.  
3:40–5:40 p.m.  
8:00–5:40 p.m.  
7:00–8:30 p.m.

**Symposium** (11–15)  
Poster Session 3 (posters 21–30)  
**Scientific Session 5** (papers 45–56)  
Lunch  
**Scientific Session 6** (papers 57–68)  
**Scientific Session 7** (papers 69–76, short papers 1–8)  
Poster Exhibits  
Stockholm Concert Hall Reception & Concert

### Thursday, May 30

8:00–9:40 a.m.  
9:40–10:20 a.m.  
10:20–12:20 p.m.  
12:20–1:20 p.m.  
1:20–3:00 p.m.

**Symposium** (16–20)  
Poster Session 4 (posters 31–40)  
**Scientific Session 8** (papers 77–88)  
Lunch  
Annual General Meetings  
Society for Pediatric Radiology (Room A)  
European Soc. of Pediatric Radiology (Berns' Lecture Hall)  
Australasian Society of Pediatric Imaging (Room C)  
**Scientific Session 9** (short papers 9–22)  
Neuhauser Lecture  
Awards Ceremony  
Poster Exhibits  
Dinner Dance Grand Hotel (Winter Garden Room)

3:20–4:30 p.m.  
4:30–5:30 p.m.  
5:30–6:00 p.m.  
8:00–6:00 p.m.  
7:30–12:00 a.m.

### Friday, May 31

8:00–9:40 a.m.  
9:40–10:20 a.m.  
10:20–12:20 p.m.  
8:00–12:20 p.m.  
12:20 p.m.

**Symposium** (21–25)  
Poster Session 5 (posters 41–50)  
**Scientific Session 10** (short papers 23–46)  
Poster Exhibits  
Closing Ceremonies & Post-Congress Tours (long/short)



# Mediastinal Pseudomass Caused by Compression of the Thymus in Neonates with Anterior Pneumothorax

Francis N. O'Keeffe<sup>1</sup>  
Leonard E. Swischuk<sup>1,2</sup>  
Susan D. Stansberry<sup>1</sup>

We studied the radiographs of 115 neonates with anterior pneumothoraces to determine how often the pneumothorax created the impression of a mediastinal pseudomass. The pseudomass results from compression of the thymus gland by air under pressure. To the unwary, the resulting configuration can lead to an erroneous diagnosis of a mediastinal mass. In experienced hands, however, it can serve as a strong clue to the presence of an underlying anterior pneumothorax. A pseudomass was present in 27 (33%) of 82 neonates with unilateral pneumothoraces and in 29 (88%) of the 33 patients with bilateral anterior pneumothoraces. A free lung edge was visualized in 26% of the patients with a unilateral pseudomass and in 55% of the neonates with a bilateral pseudomass. The pseudomass was large enough to potentially lead to a misdiagnosis in one third of the cases. In the other neonates the mass was smaller and not particularly problematic. The majority of the neonates with pseudomasses were large, not intubated, and not on positive-pressure assisted ventilation. Over half had no underlying pulmonary disease.

The appearance of a mediastinal pseudomass on radiographs of neonates can obscure a pneumothorax, and lead to an erroneous diagnosis. Recognition of the pseudomass as a manifestation of pneumothoraces is important.

*AJR* 156:145-148, January 1991

Anterior pneumothorax is a well-known phenomenon in neonates [1-4]. The accumulation of air over the anterior surface of the lung results in the radiologic appearance of a hyperlucent hemithorax with increased sharpness of the ipsilateral mediastinal edge [4]. When the pneumothorax also is under tension, the thymus gland is compressed, and this can result in a variety of mediastinal configurations and distortions. Unfortunately, these mediastinal distortions often are so striking and bizarre that the underlying pneumothorax can be overlooked. This is especially apt to occur when the free edge of the lung is not delineated.

We reviewed the chest radiographs of 115 cases of neonatal anterior pneumothorax from 1987 to 1990 to determine the frequency and type of mediastinal pseudomass configurations that occurred. We alert radiologists to the potential of the pseudomass to distract the observer from the real problem—the pneumothorax.

## Materials and Methods

The chest radiographs of 430 consecutive neonates with neonatal pneumothorax studied between the years of 1987 and 1990 were reviewed. The radiographs were inspected retrospectively to determine what type of pneumothorax was present, and those with anterior pneumothoraces were separated to form our study group. The diagnosis of anterior pneumothorax was made by noting the presence of hyperlucency of the involved hemithorax and increased sharpness of the ipsilateral mediastinal edge [4]. When there was diagnostic uncertainty, cross-table lateral or decubitus films were obtained routinely. In addition, it is customary for all neonates with pneumothorax to have follow-up radiographs. Thus, the presence of the pneumothorax was confirmed in every case by documenting its disappearance

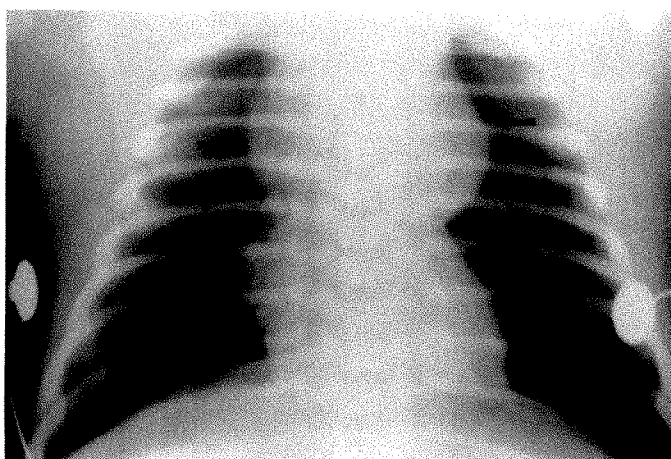
Received June 4, 1990; accepted after revision July 27, 1990.

Presented at the annual meeting of the American Roentgen Ray Society, Washington, DC, May 1990.

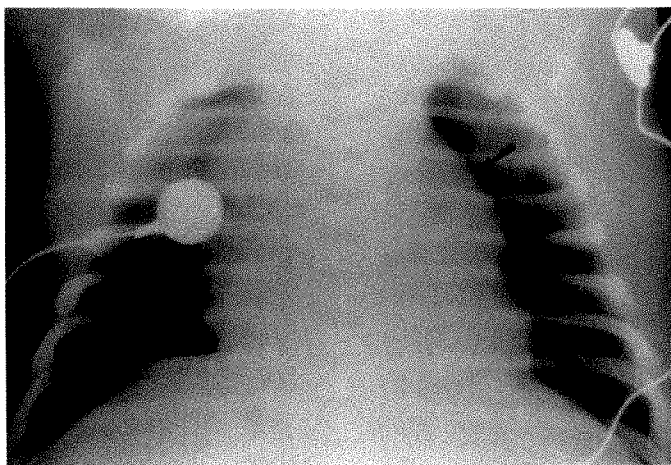
<sup>1</sup> Department of Radiology, Division of Pediatric Radiology, The University of Texas Medical Branch, Child Health Center C-65, Galveston, TX 77550. Address reprint requests to L. E. Swischuk.

<sup>2</sup> Department of Pediatrics, The University of Texas Medical Branch, Galveston, TX 77550.

0361-803X/91/1561-0145  
© American Roentgen Ray Society



A



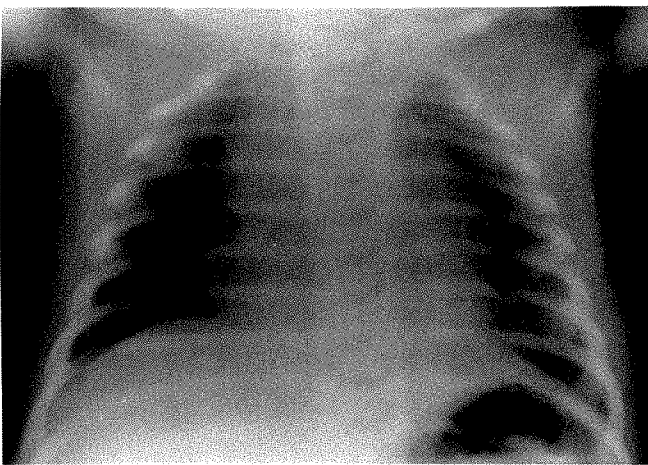
B

Fig. 1.—Bilateral anterior pneumothorax: evidence of thymic compression.

A, Hemithoraces appear large and hyperlucent on chest radiograph as a result of bilateral anterior pneumothoraces. Note snowman configuration (arrows) and free lung edge in right apex.

B, 1 day later. Right-sided pneumothorax is no longer evident, and right lobe of thymus gland assumes a normal configuration. A small left-sided anterior pneumothorax remains, resulting in residual unilateral pseudomass configuration (arrows).

C, 1 day later (day 3). Both pneumothoraces are no longer evident, and thymus gland now appears entirely normal on both sides.



C

on radiographs. A mediastinal pseudomass was considered present when any masslike configuration deviating from the normal appearance of the mediastinum was seen.

The hospital records of the neonates with mediastinal pseudomasses were reviewed to determine whether (1) the neonates weighed more or less than 2000 g, (2) any underlying pulmonary disease was present, and (3) they were breathing spontaneously or intubated and on positive-pressure ventilation. The radiologic findings assessed were whether (1) the pneumothorax was unilateral or bilateral, (2) the free edge of the lung could be visualized, (3) mediastinal shift was present, and (4) a mediastinal pseudomass was present.

### Results

Of the initial 430 neonates with radiologic documentation of pneumothoraces, we found 115 with evidence of anterior pneumothoraces on radiographs. There were 71 boys and 44 girls. Nine (8%) of these neonates weighed less than 2000 g, whereas the remaining 106 (92%) weighed more than 2000 g. Underlying pulmonary disease was present in 51 (44%) of the neonates (hyaline membrane disease in 18, meconium aspiration in 23, and miscellaneous in 10). The last consisted of hypoplastic/immature lung in four neonates, sepsis in three neonates, and transient respiratory distress of the newborn (wet-lung syndrome) in three neonates. The remaining 64

neonates (56%) had no underlying pulmonary disease. Eighty-five (74%) of the neonates were breathing on their own when the pneumothoraces were detected and 30 (26%) were intubated and being ventilated with positive-pressure ventilation.

Of the 115 patients with anterior pneumothoraces, the pneumothoraces were bilateral in 33 (29%) and unilateral in 82 (71%). Of the unilateral pneumothoraces, 39 were on the right side and 43 were on the left. A unilateral pseudomass was present in 27 (33%) of the 82 neonates with unilateral pneumothoraces. A bilateral pseudomass was present in 16 (49%) of the 33 neonates with bilateral pneumothoraces and a unilateral pseudomass was present in 13 (39%) of these 33 patients. Therefore, a pseudomass of some type was present in 29 (88%) of 33 patients with bilateral anterior pneumothoraces. A free lung edge was visualized in only seven (26%) of 27 patients with unilateral pseudomasses and was seen on one side or the other in 16 (55%) of 29 patients with bilateral mediastinal pseudomasses. Mediastinal shift was present in 48 (59%) of 82 neonates with unilateral pneumothoraces and eight (24%) of 33 neonates with bilateral pneumothoraces.

### Discussion

Anterior pneumothoraces are commonly seen on chest radiographs of newborn infants examined in the supine posi-



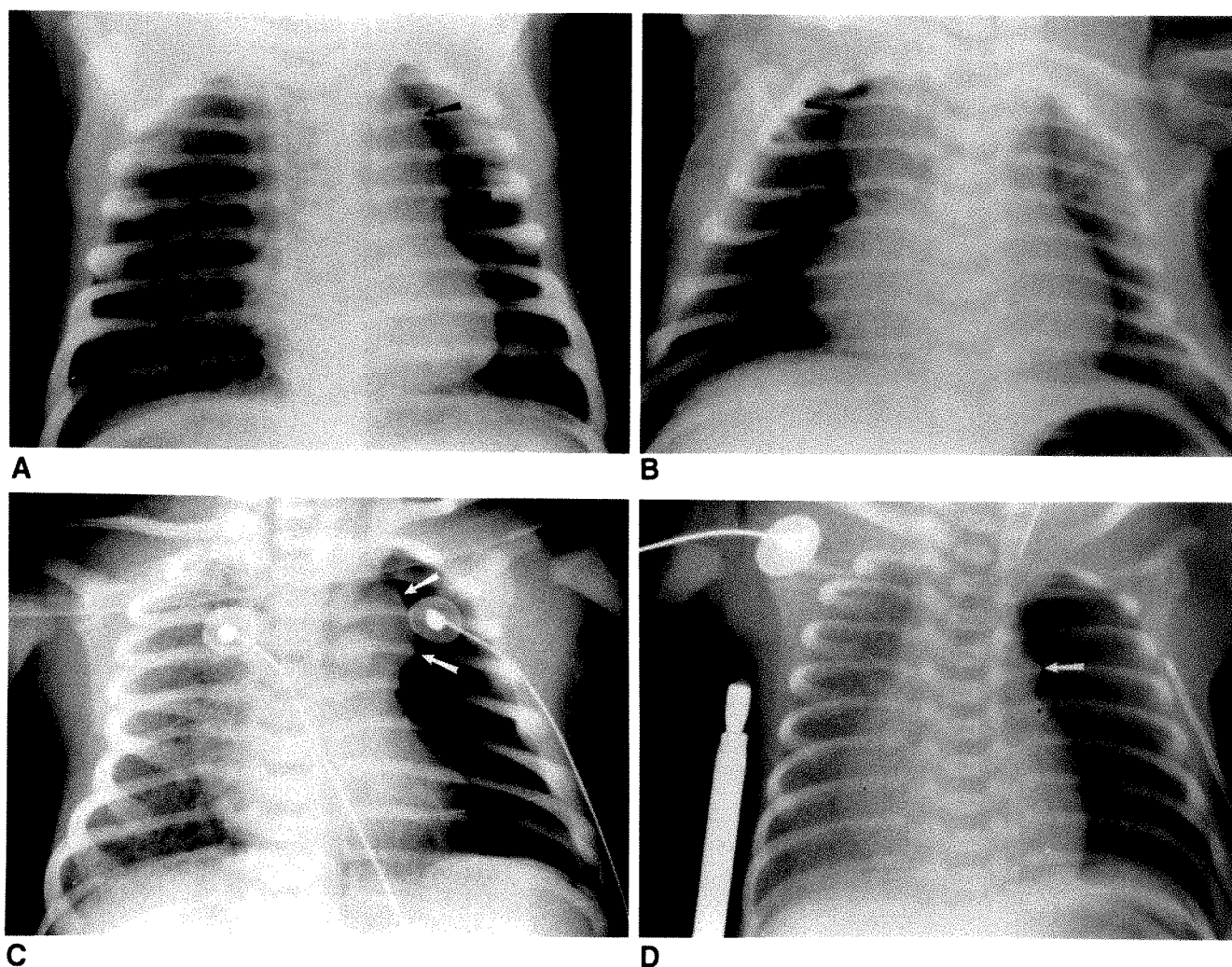


**Fig. 2.—Unilateral pseudomass: various configurations.**  
**A,** Chest radiograph reveals hyperlucent left hemithorax and increased sharpness of ipsilateral mediastinal edge. Anterior pneumothorax is present, and thymus gland is compressed into a pseudomass (arrows).  
**B,** Another patient with a similar configuration on right (arrows). A minimal anterior pneumothorax is present on left side (note increased sharpness of lower cardiac edge and adjacent halo of radiolucency). However, no pseudomass configuration is present on this side.  
**C,** Bulging left thymic lobe (arrows) produces a pseudomass. Extremely hyperlucent hemithorax is caused by anterior pneumothorax.  
**D,** Left anterior pneumothorax produces contralateral shift of mediastinum and small, compressed thymic pseudomass (arrow).

tion. The characteristic findings of an anterior pneumothorax are increased lucency of the involved hemithorax and increased sharpness of the ipsilateral mediastinal edge [4]. If a free lung edge is identified, the diagnosis is usually obvious. However, when this is not the case, the pneumothorax can be overlooked. This is even more apt to occur if a bizarre and distracting mediastinal pseudomass is present also. On the other hand, if one is aware of this phenomenon, the pseudomass can be used as a strong signal for the presence of the underlying pneumothorax. This is important, because a classic free lung edge was visualized in only 26% (7/27) of our patients with unilateral pseudomasses and in 55% (16/29) of patients with bilateral mediastinal pseudomasses.

A mediastinal pseudomass, either unilateral or bilateral, results from compression of the normal thymus gland. This can be appreciated as the pneumothorax dissipates and the thymus gland slowly returns to a normal configuration (Fig. 1). Depending on the size of the underlying thymus and the degree of tension produced by the anterior pneumothorax, a wide variety of unilateral pseudomass configurations can arise

(Fig. 2). The most common of these is a smooth-edged mass that has a rounded appearance. However, the size of the mass and the degree of roundness are somewhat variable (Fig. 2). One third of our neonates demonstrated thymic pseudomasses large enough to cause potential diagnostic problems (Figs. 1A, 2A, and 2B).

When the pseudomass configuration is bilateral, the overall mediastinal appearance often erroneously suggests the "figure eight" or "snowman" heart of total anomalous pulmonary venous return type I (Figs. 1 and 3). In other instances, the thymus can appear more like a mediastinal mass of noncardiac origin (Fig. 3B). Once again, the final configuration depends on the original size of the thymus gland and the degree of compression. In extreme cases, the gland may be so compressed that virtually no mass is present, but rather the mediastinum along with the thymus gland are squeezed into a very narrow configuration (Fig. 3C).

It is interesting that the vast majority of our patients (92%) were large, weighing over 2000 g. In addition, the lungs in 56% were completely normal. These neonates were exam-

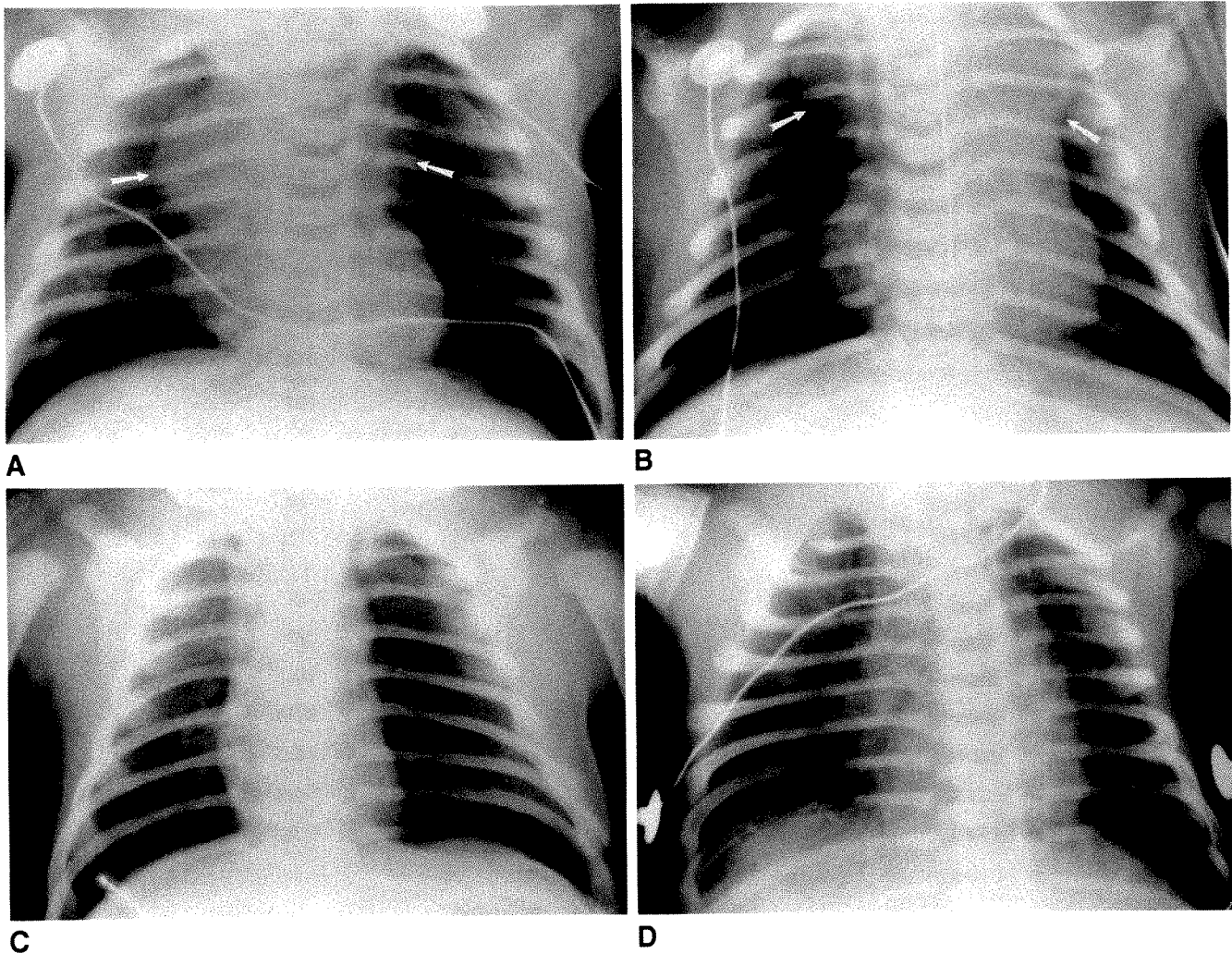


Fig. 3.—Bilateral pseudomasses: various configurations.

A, Bilateral anterior pneumothoraces produce snowmanlike configuration of heart (arrows) on chest radiograph. Note free lung edge in left apex.  
 B, Another patient with no visible free lung edge on either side and bilateral thymic pseudomass mimicking anterior mediastinal mass (arrows).  
 C, Another patient in whom bilateral anterior pneumothoraces, under tension, squeeze thymus and heart, producing a narrow mediastinal silhouette. A free lung edge is visible in left apex.  
 D, 1 day later, after resolution of pneumothoraces. Normal thymus gland and heart have expanded to normal proportions.

ined because of respiratory distress, but no underlying pulmonary disease was present. In the remaining 44% of neonates, the most common underlying pulmonary problems were meconium aspiration and hyaline membrane disease (respiratory distress syndrome). Seventy-four percent of our neonates were breathing spontaneously when their pneumothoraces were discovered, whereas only 26% were intubated and on positive-pressure assisted ventilation.

There are three possible explanations as to why most of our cases of anterior pneumothorax with associated thymic pseudomass formation were in larger neonates. First, many of the smaller neonates had thymic atrophy because of the stress associated with their underlying pulmonary disease. It is possible that not enough thymic tissue remained to result in a pseudomass. Another possible explanation centers on pulmonary compliance. If a lung with normal compliance is distended to normal size, it will occupy most of the hemithorax. Therefore, air that accumulates anteriorly may find it difficult to track along the lateral aspect of the lung to produce a visible lung edge. On the other hand, when pulmonary compliance is diminished, as in hyaline membrane disease,

for example, the lung does not distend to normal size. Consequently, even though air from a pneumothorax might at first accumulate anteriorly, it would be very easy for it to track laterally, and indeed surround the lung to produce a clearly visible free lung edge. The third explanation concerns the volume of free air present. In most of our neonates who were intubated and on positive-pressure ventilation, the volumes of free air were large and clearly surrounded the entire lung. With such large volumes of air, the chances of the air accumulating in, and being confined to, the anterior pleural space are minimal.

#### REFERENCES

1. MacEwan DW, Dunbar JS, Smith RD, Brown B. Pneumothorax in young infants; recognition and evaluation. *Can Assoc Radiol J* 1971;22:264-269
2. Hoffer FA, Ablow RC. The cross-table lateral view in neonatal pneumothorax. *AJR* 1984;142:1283-1286
3. Moskowitz PS, Griscom NT. The medial pneumothorax. *Radiology* 1976;120:143-147
4. Swischuk LE. Two lesser known but useful signs of neonatal pneumothorax. *AJR* 1976;127:623-627



## Case Report

# Normal Sonographic Appearance of a Thanatophoric Dwarf Variant Fetus at 13 Weeks Gestation

Marian B. Macken,<sup>1</sup> Edward B. Grantmyre,<sup>1</sup> David L. Rimoin,<sup>2</sup> and Ralph S. Lachman<sup>3</sup>

The prenatal diagnosis of many types of short-limbed dwarfism by real-time sonographic examination has been well documented [1–4]. This report describes a fetus with a form of lethal, neonatal short-limbed dwarfism (thanatophoric variant, San Diego type) whose limbs were normal in appearance and measurement on sonography at 13 weeks gestational age. A variant of thanatophoric dwarfism was then diagnosed at 32 weeks gestational age when sonographic examination showed that the limbs were significantly shortened and the thorax was much reduced in size.

### Case Report

A 25-year-old gravida 2, para 0 woman had a sonographic examination at 13 weeks gestation. The fetus was normal in appearance; fetal limbs were well visualized and were normal in appearance (Fig. 1A). Biparietal diameter was 2.2 cm, which is the mean diameter for 12.3 weeks gestational age. Femur length was 1.2 cm, which is the mean for 13.4 weeks gestational age [5].

The patient presented at 32 weeks gestation in premature labor. Sonographic examination showed hydramnios. The head appeared large with a biparietal diameter of 8.9 cm, equal to the mean for 36 weeks gestational age. No evidence of hydrocephalus or cloverleaf skull was present. The thorax appeared small; the thoracic circumference was 22.7 cm. Abdominal circumference was 30.8 cm.

The long bones were seen to be markedly shortened and bowed with abundant soft tissue (Fig. 1B). Femur length was 3.7 cm, equal to the mean for 21.5 weeks gestational age. The humerus was 2.5 cm long, equal to the mean for 17 weeks gestational age (Fig. 1C).

A diagnosis of severe short-limbed dwarfism was made, with a presumptive diagnosis of thanatophoric dysplasia.

A few hours later the patient delivered a live-born female neonate weighing 1750 g. The neonate died shortly after birth, and postmortem radiologic and pathologic studies were performed. Radiographs (Figs. 1D and 1E) showed marked shortening and bowing of the long bones; the bowing was particularly marked in the distal long bones. The long bones also were wider than is seen in thanatophoric dysplasia. The spine was very hypoplastic with ovoid vertebral bodies. The pelvis was hypoplastic, with flaring of the iliac bones, horizontal acetabular roofs, and medial ischial spurs. The sacrosciatic notches were wider than those seen in thanatophoric dysplasia.

Thanatophoric dysplasia was diagnosed initially, but review of histologic findings and radiographs at the International Skeletal Dysplasia Registry indicated that the diagnosis was that of a variant of thanatophoric dysplasia [6].

### Discussion

Lethal neonatal platyspondylic dwarfism is increasingly being recognized as a heterogeneous group of disorders [6–8]. At present, two forms of classic thanatophoric dysplasia are recognized. However, it is likely that this represents variability rather than true heterogeneity. Type 1, which appears to be sporadic, has curved femora and very flat vertebral bodies. Type 2 has straighter femora, wider bones, flatter vertebral bodies, and cloverleaf skull deformity [7].

Several reports have described variants of lethal neonatal short-limbed dwarfism that have many features in common with thanatophoric dysplasia but have some distinct radiologic features and clearly distinct histologic features [6, 8]. Our case appears to be closest to the San Diego variety as described by Horton and associates [6]. Many reports of the

Received March 17, 1988; accepted after revision July 2, 1990.

This work was supported in part by U.S. Public Health Service NIH Program Project Grant HD 22657.

<sup>1</sup> Department of Diagnostic Imaging, Dalhousie University, Halifax, Nova Scotia, Canada. Address reprint requests to M. B. Macken, Department of Diagnostic Imaging, IWK Children's Hospital, P.O. Box 3070, Halifax, Nova Scotia, Canada B3J 3G9.

<sup>2</sup> Ahmanson Pediatric Center, Cedars-Sinai Medical Center, UCLA School of Medicine, Los Angeles, CA 90048.

<sup>3</sup> Division of Pediatric Radiology, Harbor/UCLA Medical Center, 1000 W. Carson St., Torrance, CA 90509.

*AJR* 156:149–150, January 1991 0361–803X/91/1561–0149 © American Roentgen Ray Society

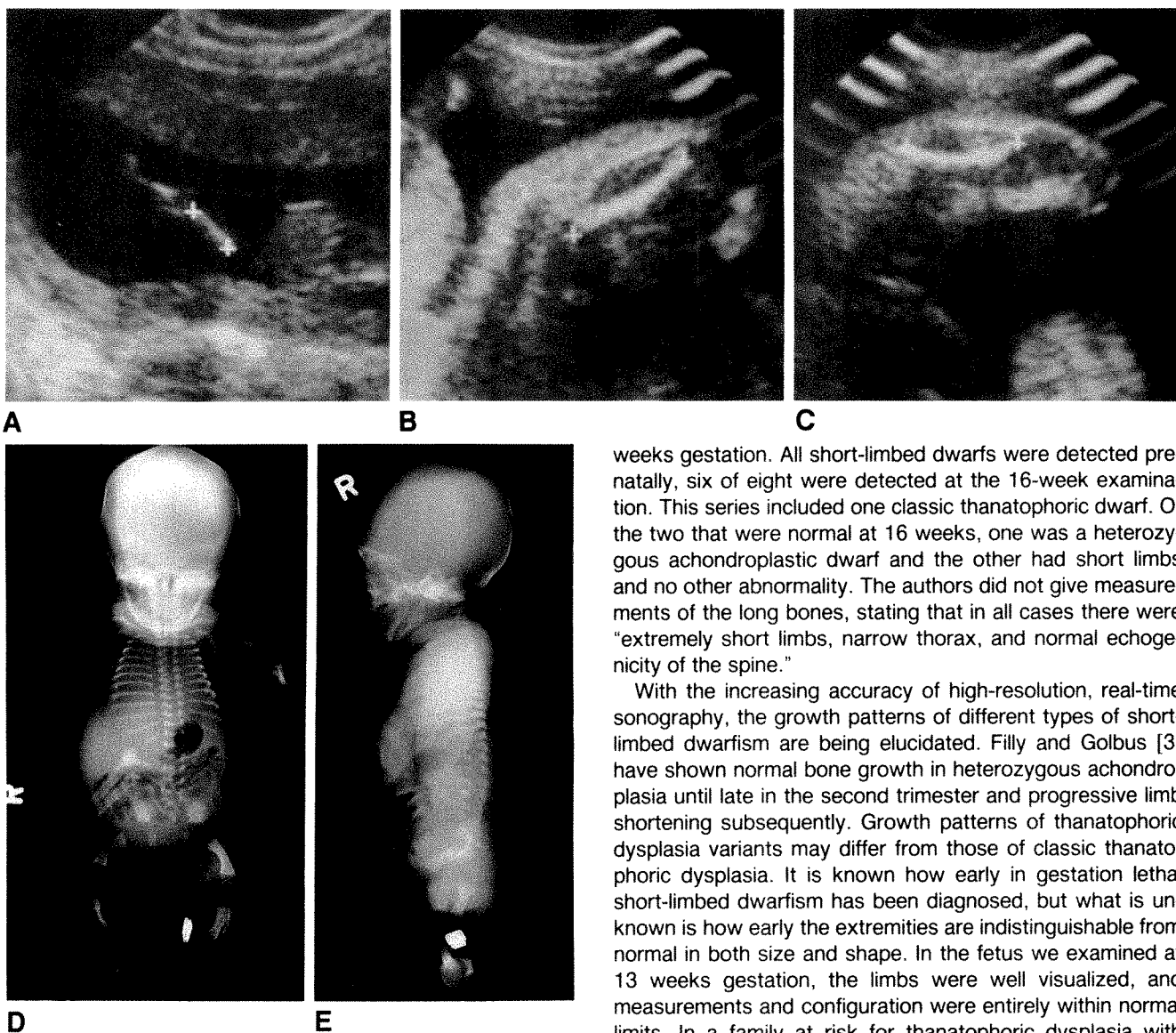


Fig. 1.—A, Sonogram of leg of fetus at 13 weeks shows absence of bowing and normal proportion of femur to lower leg.  
 B, Sonogram of femur at 32 weeks shows bowing and redundant soft tissue.  
 C, Sonogram of humerus at 32 weeks shows marked shortening and bowing with prominent soft tissue.  
 D and E, Postmortem anteroposterior (D) and lateral (E) radiographs show wide long bones and bowing more pronounced distally, mild platyspondylitis with ovoid vertebral bodies, and relatively wide sacrosciatic notches.

diagnosis of lethal short-limbed dwarfism by prenatal sonography have been published [1–4]. The reported sonographic features in utero include hydramnios and marked shortening of the major long bones. Most reported cases indicate that long-bone measurements are at least two standard deviations below the mean for the gestational age. Bowing of the extremities can be seen. The narrow thorax, which results in a protuberant abdomen, is usually easily seen.

It has been difficult to diagnose platyspondylitis in utero. This has been true in several case reports and our own experience [2, 4].

In 1985 Weldner and associates [4] reviewed 12,453 pregnant women examined sonographically at 16 weeks and 32

weeks gestation. All short-limbed dwarfs were detected prenatally, six of eight were detected at the 16-week examination. This series included one classic thanatophoric dwarf. Of the two that were normal at 16 weeks, one was a heterozygous achondroplastic dwarf and the other had short limbs and no other abnormality. The authors did not give measurements of the long bones, stating that in all cases there were “extremely short limbs, narrow thorax, and normal echogenicity of the spine.”

With the increasing accuracy of high-resolution, real-time sonography, the growth patterns of different types of short-limbed dwarfism are being elucidated. Filly and Golbus [3] have shown normal bone growth in heterozygous achondroplasia until late in the second trimester and progressive limb shortening subsequently. Growth patterns of thanatophoric dysplasia variants may differ from those of classic thanatophoric dysplasia. It is known how early in gestation lethal short-limbed dwarfism has been diagnosed, but what is unknown is how early the extremities are indistinguishable from normal in both size and shape. In the fetus we examined at 13 weeks gestation, the limbs were well visualized, and measurements and configuration were entirely within normal limits. In a family at risk for thanatophoric dysplasia with normal findings on early sonographic examination, a second sonographic examination at around 20 weeks gestation is indicated.

Radiographs of the fetus in utero can be helpful in making a specific diagnosis of skeletal dysplasia.

#### REFERENCES

1. Mahony BS, Filly RA, Callen PW, Golbus MS. Thanatophoric dwarfism with the cloverleaf skull: a specific antenatal sonographic diagnosis. *J Ultrasound Med* 1985;4:151–154
2. Pretorius DH, Rumack CM, Manco-Johnson ML, et al. Specific skeletal dysplasias in utero: sonographic diagnosis. *Radiology* 1986;159:237–242
3. Filly RA, Golbus MS. Ultrasonography of the normal and pathologic fetal skeleton. *Radiol Clin North Am* 1982;20:311–323
4. Weldner BM, Persson PH, Ivarsson SA. Prenatal diagnosis of dwarfism by ultrasound screening. *Arch Dis Child* 1985;60:1070–1072
5. Hadlock FP, Harrist RB, Deter RL, Park SK. Fetal femur length as a predictor of menstrual age: sonographically measured. *AJR* 1982;138:875–878
6. Horton WA, Rimoin DL, Hollister DW, Lachman RS. Further heterogeneity within lethal neonatal short-limbed dwarfism: the platyspondylic types. *J Pediatr* 1979;94:736–742
7. Langer LO, Yang SS, Hall JG, et al. Thanatophoric dysplasia and cloverleaf skull. *Am J Med Genet Suppl* 1987;3:167–179
8. Knowles S, Winter R, Rimoin D. A new category of lethal short-limbed dwarfism. *Am J Med Genet* 1986;25:41–46



## Case Report

# CT of Acute Splenic Torsion in Children with Wandering Spleen

Thomas E. Herman<sup>1</sup> and Marilyn J. Siegel

Wandering spleen is an uncommon condition characterized by laxity or absence of the supporting splenic ligaments [1]. Patients with torsion of the wandering spleen may have acute, chronic, or intermittent symptoms. Although several reports of the sonographic and scintigraphic features of torsion both in children and adults have been published [2–9], little information is available on the CT appearance of torsion, particularly acute torsion [10, 11]. We report two cases of acute splenic torsion in children to show the characteristic CT findings of this condition.

### Case Reports

#### Case 1

The first patient was a 2½-year-old girl who had a body temperature of 37°C, vomiting, and severe crampy abdominal pain of several hours duration. Physical examination revealed a tender mass in the left upper quadrant. Laboratory studies showed only leukocytosis. Plain radiographs showed an ileus. Because an abscess was suspected, CT was performed. CT showed absence of the spleen in the left upper quadrant and an avascular, homogeneous, nonenhancing mass below the lower pole of each kidney, leading to the diagnosis of splenic torsion (Fig. 1). The pancreatic tail was in normal position. During surgery, a 360° torsion of the splenic pedicle resulting in complete splenic infarction was found. The spleen was not attached to the stomach, retroperitoneum, or colon. The tail of the pancreas was not involved, and the remainder of the abdomen appeared normal. Pathologic examination confirmed splenic infarction.

#### Case 2

The second patient was a 2½-year-old girl who had had low grade fever and abdominal pain for 1 week. Exploration laparotomy was performed for suspected appendicitis and showed a normal appendix but an enlarged spleen. A postoperative CT scan was obtained for evaluation (Fig. 2). On reexploration, the splenic pedicle was torsed 270° and splenic ligaments were absent. Pathologic analysis showed a hemorrhagic necrotic spleen with a thick pseudocapsule.

### Discussion

Wandering spleen is a rare condition. In a review of 1413 splenectomies in children, only four instances of splenectomy for a wandering spleen were noted by Erkalis and Filler [12]. Furthermore, in a review of surgical pathology records at Boston Children's Hospital, Broker et al. [4] reported only three cases in 24 years. A more recent review of the English literature by Allen and Andrews [2] found 35 cases of wandering spleen in children less than 10 years old. Eighteen of these patients presented as acute surgical emergencies, and of these, only eight had the diagnosis of splenic torsion established preoperatively.

Children with wandering spleens are typically between 3 months and 10 years old; the most frequent age at presentation is less than 1 year [2]. Affected patients may be asymptomatic and present with an incidental mass on physical examination, may have mild abdominal pain due to vascular

Received April 26, 1990; accepted after revision June 20, 1990.

<sup>1</sup> Both authors: Mallinckrodt Institute of Radiology, Washington University School of Medicine, 510 S. Kingshighway Blvd., St. Louis, MO 63110. Address reprint requests to T. E. Herman.

AJR 156:151–153, January 1991 0361–803X/91/1561–0151 © American Roentgen Ray Society

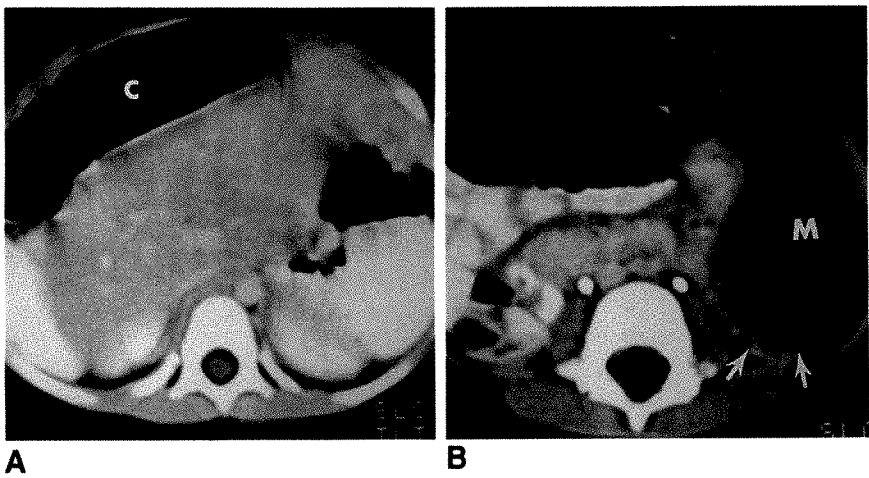


Fig. 1.—A, CT scan at level of upper poles of kidney shows absence of splenic tissue. An air-filled dilated transverse colon (C) is present anterior to liver, reflecting a marked ileus.  
B, CT scan below level of kidneys shows a nonenhancing spleniform mass (M) in left lower quadrant, anterior to partially air-filled colon (arrows).

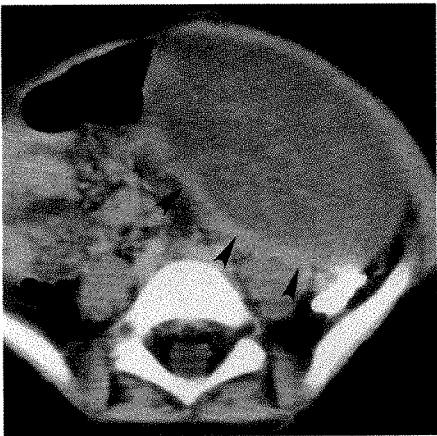


Fig. 2.—CT scan shows low-density, slightly heterogeneous spleniform mass with thick capsule (arrowheads) in left lower quadrant, displacing bowel loops to right. No splenic tissue was present on more cephalad sections. Heterogeneity within spleen reflects areas of hemorrhage within infarcted spleen.

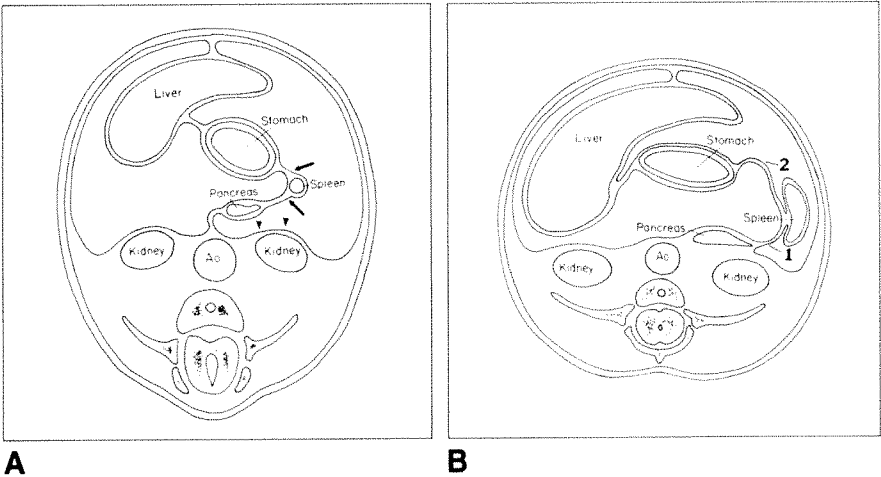


Fig. 3.—Line drawings of normal development of mesogastrium. (Adapted from Sadler [14].)  
A, Fifth week of fetal life. Primordial spleen and tail of pancreas form within leaves of dorsal mesogastrium (arrows), which extends from stomach to aorta (Ao). Parietal peritoneum (arrowheads) covers retroperitoneum.  
B, Sixth week of fetal life. Dorsal portion of pancreas becomes retroperitoneal, with fusion of parietal peritoneum and posterior leaf of dorsal mesogastrium. Unfused portion of dorsal mesogastrium persists as lienorenal ligament (1) and gastrolial ligament (2) form attachments of spleen.

congestion or intermittent torsion and spontaneous detorsion, or may present with an acute abdomen due to torsion of the splenic pedicle with subsequent infarction. With acute torsion, the condition can be confused with appendicitis or ovarian torsion. Other clinical findings include nausea, vomiting, fever, leukocytosis, peritoneal signs, and a palpable mass in the abdomen or pelvis. Complications of acute splenic torsion include gangrene, abscess formation, local peritonitis, intestinal obstruction, and necrosis of the pancreatic tail.

In adults, particularly women of childbearing age, splenic torsion has usually been attributed to acquired abnormalities such as ligamentous laxity, splenomegaly, trauma, and hormonal effects of pregnancy. Splenic torsion in children is believed to be congenital and due to abnormal development of the dorsal mesogastrium [2, 4, 9, 13]. Normally the dorsal mesogastrium gives rise to the spleen and its supporting structures, the lienorenal and gastrolial ligaments [14] (Fig. 3). The most important attachment is the lienorenal ligament,

which arises after fusion of the posterior leaf of the dorsal mesogastrium with the parietal peritoneum in front of the left kidney (Fig. 3B). This ligament attaches the spleen to the posterior body wall and contains the splenic artery. The lienorenal ligament and the gastrolial ligament allow some mobility of the spleen normally, but prevent its displacement from a position posterior to the stomach and anterior to the left kidney. Incomplete fusion or formation of the dorsal mesogastrium results in an abnormally mobile spleen with a long vascular pedicle that is predisposed to torsion. The dorsal pancreatic bud also develops within the dorsal mesogastrium. When the parietal peritoneum and posterior leaf of the dorsal mesogastrium fuse, the pancreas becomes a retroperitoneal organ [14] (Fig. 3B). If the dorsal mesogastrium is incomplete or fails to fuse with the parietal peritoneum, portions of the pancreatic tail may be intraperitoneal and can be involved in splenic torsion. This did not occur in our patients. The normal lienorenal and gastrolial ligaments can



occasionally be seen on CT in patients with abundant intra-abdominal fat. However, in children who have a relative paucity of fat, splenic ligaments are not visualized on CT.

Multiple imaging techniques have been used to diagnose wandering spleen, including plain radiographs, barium studies, scintigraphy, sonography, angiography, and more recently CT [2-12]. Plain radiographs of the abdomen usually have nonspecific findings, but they can suggest the diagnosis by showing an abdominal mass in conjunction with absence of a splenic shadow in the left upper quadrant. Barium enema findings may be normal or can show displacement by an extrinsic mass. Scintigraphy can be valuable in the evaluation of splenic function and may show either absence of radionuclide uptake due to splenic torsion or normal uptake of radionuclide by an abnormally positioned spleen. However, scintigraphy has poor anatomic resolution and hence little advantage over studies such as sonography or CT. Sonography and CT are able to show the typical comma shape of the spleen in an ectopic position and lack of splenic tissue in the left upper quadrant. However, sonography can be hampered by a large amount of bowel gas. Because CT is not degraded by bowel gas and has an added advantage of being able to establish the presence or absence of perfusion rapidly [10-12, 15], it is the preferred study for diagnosing wandering spleen and torsion suspected clinically or on other imaging studies. Angiography also can provide definite evidence of splenic torsion and ectopic splenic location, but it is invasive and no longer indicated for diagnosis.

The CT manifestations of wandering spleen with acute torsion include (1) absence of the spleen anterior to the left kidney and posterior to the stomach, (2) a lower abdominal or pelvic mass with homogeneous or heterogeneous parenchyma and an attenuation value less than that of normal splenic tissue, and (3) secondary findings such as ascites and necrosis of the pancreatic tail. In reported cases and in the two cases described here, the decreased attenuation was associated with infarction. A thick, enhancing pseudocapsule, representing omental and peritoneal adhesions, has been observed with chronic or intermittent torsion [15]. In the second of our two cases, it was associated with acute torsion. When the pancreatic tail is involved, a whorl of pancreatic tissue and fat at the medial border of the displaced spleen

may be seen on CT [11]. This was not observed in either of our two cases. The CT appearance of a torsed spleen may be similar to that seen with other cystic lesions, such as an abscess or mesenteric or omental cysts, but the absence of a spleen in its normal position in the left upper quadrant should suggest the diagnosis.

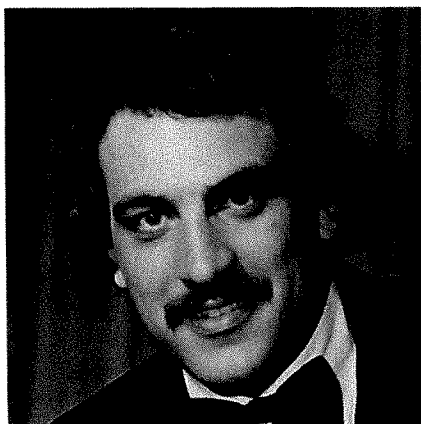
Although rare, splenic torsion should be recognized as a cause of an acute abdomen. Splenectomy is the treatment for acute splenic torsion with infarction. Splenopexy can be performed in patients who have chronic or intermittent symptoms in whom the diagnosis is made before splenic infarction [2].

#### REFERENCES

1. Abell J. Wandering spleen with torsion of the pedicle. *Ann Surg* 1933;98:722-735
2. Allen KB, Andrews G. Pediatric wandering spleen—the case for splenopexy: review of 35 reported cases in the literature. *J Pediatr Surg* 1989;24:432-435
3. Barki Y, Bar-Ziv J. Wandering spleen in two children: the role of ultrasonic diagnosis. *Br J Radiol* 1984;57:267-270
4. Broker FHL, Fellows K, Treves S. Wandering spleen in three children. *Pediatr Radiol* 1978;6:211-214
5. Gordon DH, Burrell MI, Levin DC, Mueller CF, Becker JA. Wandering spleen: the radiological and clinical spectrum. *Radiology* 1977;125:39-46
6. Hunter TB, Haber K. Sonographic diagnosis of a wandering spleen. *Radiology* 1977;129:925-926
7. Rosenthal L, Lisbona R, Banerjee K. A nucleographic and radioangiographic study of a patient with torsion of the spleen. *Radiology* 1974;110:427-428
8. Setiawan H, Harrell RS, Perret RS. Ectopic spleen: a sonographic diagnosis. *Pediatr Radiol* 1982;12:152-153
9. Thompson JS, Ross RJ, Pizzaro ST. The wandering spleen in infancy and childhood. *Clin Pediatr* 1980;19:221-224
10. Parker LA, Mittelstaedt CA, Mauro MA, Mandell VS, Jaques PF. Torsion of a wandering spleen: CT appearance. *J Comput Assist Tomogr* 1984;8:1201-1203
11. Sheflin JR, Lee CM, Kretchmar KA. Torsion of wandering spleen and distal pancreas. *AJR* 1984;142:100-104
12. Erkal AJ, Filler RM. Splenectomy in childhood: a review of 1413 cases. *J Pediatr Surg* 1972;7:382-388
13. Woodward DAK. Torsion of the spleen. *Am J Surg* 1967;114:953-955
14. Sadler TW. *Langman's medical embryology*, 5th ed. Baltimore: Williams & Wilkins, 1967:953-955
15. Shiels WE, Johnson JF, Stephenson SR, Huang YC. Chronic torsion of the wandering spleen. *Pediatr Radiol* 1989;19:465-467

## Memorial

### Andrew N. Schwartz, 1950–1989



Andrew N. Schwartz died on April 27, 1989, after a long illness. Andy was born in Lawrence, MA, on April 11, 1950. After graduating magna cum laude from Tufts University in 1972 and from Tufts University School of Medicine in 1976, he interned in medicine at the Medical College of Virginia Hospitals and completed a junior assistant residency in medicine at Albert Einstein College of Medicine in New York. The following year he

completed a National Library of Medicine fellowship in computer medicine at Mount Sinai Hospital in New York. Convinced by a friend and co-intern to specialize in diagnostic radiology, he began his residency program at the Massachusetts General Hospital in July of 1979. After completing the program in 1982, he spent a fellowship year as the chief resident in pediatric radiology at the Children's Hospital Medical Center in Boston.

Leaving the comfortable and familiar confines of Boston, he ventured forth to Connecticut to accept a position as a pediatric radiologist with the Jefferson X-ray Group at Hartford Hospital. Shortly thereafter, he became chief of pediatric radiology at Hartford Hospital, assistant director of radiology at Newington Children's Hospital, and assistant clinical professor of radiology at the University of Connecticut Health Center. During this time, he was a member of the New England Roentgen Ray Society, the Radiological Society of North America, the Radiological Society of Connecticut, the American College of Radiology, and the Society for Pediatric Radiology. In this environment, Andy flourished. His love for pediatric radiology, his caring for his patients, and his enthusiasm for teaching were bountiful. His morning be-

gan with breakfast with colleagues, occasionally uncovering the newest political news in the hospital. Fortified—necessary to keep his 6 ft. 5 in. (2 m) frame energized—he eagerly began his day. Whether it was to run a cardiac catheterization conference or to begin a pediatric fluoroscopy schedule, Andy was charged and ready to go. His concern for his patients and their families was intense, and this attribute made other staff members, whether technologist or radiologist, similarly attuned. His patience with residents and the care he took in preparing conferences did not go without notice.

Anyone who found Andy, a naturally gregarious animal, lumbering down the hall could always engage him in conversation. Besides radiology, discussions frequently would turn to sports, especially the Boston Celtics; music from the 60s and 70s; and his beloved family.

Andy is survived by his wife, Deborah, his daughter, Lauren, and his son, Daniel. He leaves behind his father, mother, and brother as well as all those who had the privilege to know and love him.

Hugh S. Vine  
M. B. Ozonoff  
Hartford, CT 06106



## Case Report

# Pulmonary Emboli As a Primary Manifestation of Wilms Tumor

Dorothy I. Bulas,<sup>1</sup> Raleigh Thompson,<sup>2</sup> and Gregory Reaman<sup>3</sup>

Wilms tumor or nephroblastoma is the most common urinary tract neoplasm and one of the most frequent solid abdominal malignant tumors of childhood. Up to 40% of Wilms tumors have invaded the renal vein by the time of diagnosis. Vena caval or atrial thrombus is less common; the reported prevalence is 4% [1]. Although pulmonary metastases may already be present in up to one fourth of cases at the time of initial diagnosis, it is exceedingly rare for pulmonary emboli to develop as a first manifestation of Wilms tumor [1, 2].

We describe a child who initially had signs and symptoms of pulmonary emboli; later Wilms tumor was diagnosed.

### Case Report

A 6-year-old girl was in her usual state of good health until 3 days before admission when she suddenly became pale and limp after being hugged. She recovered within a few seconds but had a second episode 5 min later. After these two events, she was alert and awake but complained of shortness of breath and chest tightness. At initial hospitalization the patient was hypoxic, with an arterial pH of 7.42,  $PO_2$  of 85 mm Hg, and  $P_{CO_2}$  of 35 mm Hg while on 50% oxygen. Physical examination revealed tachypnea and tachycardia. The lungs were clear to auscultation. The results of the remainder of the physical examination were normal except for a 2/6 systolic ejection murmur. Laboratory results included a hematocrit of 32%, platelet count of 343,000/ $\mu$ l, normal levels of electrolytes, and normal urinalysis. A chest radiograph showed a slightly enlarged cardiac silhouette with clear lungs. Results of ECG, EEG, and cranial CT were all normal. An echocardiogram showed right ventricular hypertrophy and tricuspid regurgitation. Findings on a  $^{99m}Tc$ -DTPA aerosol ventilation scan

were normal. A technetium-99m macroaggregated albumin perfusion scan showed multiple perfusion defects in the right lung (Fig. 1A). No therapy was started because no source for emboli was found. Clinical condition slowly improved, but the patient continued to require oxygen support. She was transferred to our hospital 2 days later for further evaluation.

On admission, the patient was still tachypneic and tachycardic. The lungs remained clear to auscultation, and a 2/6 systolic ejection murmur was still present. Abdominal examination revealed a palpable liver edge 2.5 cm below the costal margin. Laboratory results included a  $PO_2$  of 26 mm Hg in room air and 126 mm Hg on 50% oxygen. Prothrombin time and fibrinogen level were normal.

Sonography performed on arrival showed a large mass within the lower pole of the right kidney extending into the right renal vein. A separate 1.5-cm mass was seen in the inferior vena cava below the hepatic veins (Fig. 1B). No connection could be seen between the intraluminal inferior vena caval mass and the renal vein mass. Chest CT showed asymmetry in size of pulmonary vessels suggestive of hypoperfusion to the right lung. Several pleurally based nodules were identified as well. Abdominal CT showed a right renal mass originating in the lower pole and extending into the right renal vein (Figs. 1C and 1D). An echocardiogram showed no thrombi within the cardiac chambers.

At surgery, the suprahepatic inferior vena cava was isolated and clamped. During dissection of the renal tumor and vessels, the patient became hypotensive and the inferior vena cava clamp was partially released. The patient suddenly went into asystole but was resuscitated and placed on cardiopulmonary bypass. The right kidney and inferior vena cava thrombus were removed successfully. The main pulmonary artery was then opened, and large clots were removed from the main and right pulmonary arteries. The patient was successfully weaned from bypass and did well postoperatively.

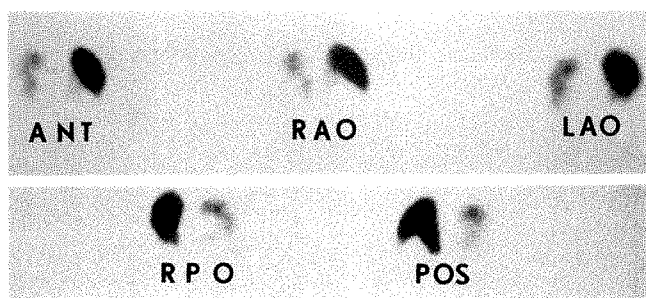
Received April 30, 1990; accepted after revision June 13, 1990.

<sup>1</sup> Department of Diagnostic Imaging and Radiology, Children's National Medical Center, and Department of Pediatrics, George Washington University School of Medicine and Health Sciences, 111 Michigan Ave., N.W., Washington, DC 20010. Address reprint requests to D. I. Bulas.

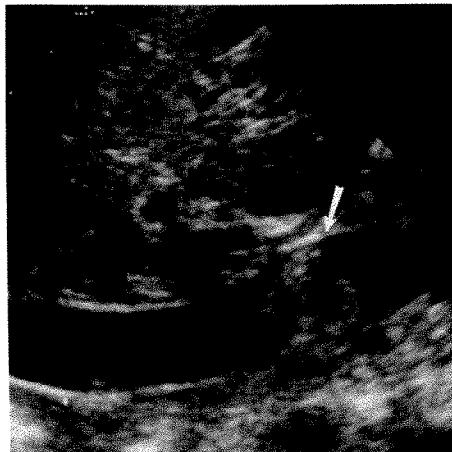
<sup>2</sup> Department of Surgery, Children's National Medical Center, and George Washington University School of Medicine and Health Sciences, Washington, DC 20010.

<sup>3</sup> Department of Hematology Oncology, Children's National Medical Center, and Department of Pediatrics, George Washington University School of Medicine and Health Sciences, Washington, DC 20010.

*AJR* 156:155-156, January 1991 0361-803X/91/1561-0155 © American Roentgen Ray Society



A



B



C



D

Fig. 1.—Pulmonary emboli in a 6-year-old girl with Wilms tumor.

A,  $^{99m}\text{Tc}$ -macroaggregated albumin (MAA) perfusion scans show multiple segmental and subsegmental perfusion defects of right lung consistent with "high probability" pulmonary emboli. ANT = anterior, RAO = right anterior oblique, LAO = left anterior oblique, RPO = right posterior oblique, POS = posterior.

B, Longitudinal sonogram of intrahepatic inferior vena cava shows a 1.5-cm, well-circumscribed intraluminal mass (arrow) and no evidence of intraatrial extension.

C, CT scan shows a large mass within lower pole of right kidney.

D, CT scan shows a low-attenuation filling defect within an enlarged right renal vein (arrow) that represents direct tumor extension. Separate intraluminal mass within intrahepatic portion of inferior vena cava was not well shown by CT.

Pathologic examination of surgical specimens showed a triphasic Wilms tumor of the right kidney. Intracaval and intrapulmonary arterial clots contained tumor thrombi.

The patient has done well in the past 6 months, with no evidence of disease after therapy with vincristine and actinomycin D, in addition to flank and whole-lung irradiation in accordance with the National Wilms Tumor Study-4 protocol.

## Discussion

Wilms tumor is one of the most common tumors in infants and children. Typically, it is manifested as an asymptomatic upper abdominal mass. Abdominal pain, fever, anemia, hematuria, and hypertension are less frequent presenting signs and symptoms [1, 2]. The initial presentation of acute pulmonary tumor emboli without surgical manipulation has not been described before.

Pulmonary embolism remains one of the most difficult diagnoses to make on the basis of clinical findings. Although rare in infants and children, pulmonary emboli occur more frequently than commonly is recognized [3]. Clinically, symptoms and signs may be absent or minimal or attributed to causes other than emboli. When pulmonary emboli are considered a possible cause of respiratory distress, the availability of radionuclide perfusion and ventilation scans allows rapid and accurate diagnosis.

Once the diagnosis is made, the source of emboli needs to be determined. Forty percent of children with pulmonary emboli have venous thrombosis of the vena cava, heart, mesenteric veins, or extremity veins [3]. Sonography is a valuable noninvasive method for examining many of these vessels. Other sources to be considered include fat emboli from fractures, septic emboli, air, and foreign material [4].

Massive tumor emboli are a rare cause of acute respiratory distress in children. Only three cases of Wilms tumor embolizing to the lungs have been reported; all occurred during intraoperative manipulation [5–7]. Preoperatively, sonography is useful in showing the cranial extent of tumor thrombus, allowing proper intraoperative approach [8]. As it is now standard practice to ligate veins before surgical handling of the tumor, massive pulmonary emboli should be a rare complication.

In our patient, a portion of the tumor may have embolized after the hug she received just before her first collapse. Although the source of these emboli was unusual, this case demonstrates that Wilms tumor can embolize preoperatively, and this may occur more commonly than has been recognized.

## REFERENCES

- Kobrinsky NL, Talgoy M, Shuckett B, Gritter HL. Wilms tumor. *Pediatr Ann* 1988;17:240–250
- Ritchey ML, Kelalis PP, Breslow N, Offord KP, Shochat SJ, D'Angio GJ. Intracaval and atrial involvement with nephroblastoma: review of National Wilms Tumor Study-3. *J Urol* 1988;140:1113–1118
- Jones DRB, MacIntyre IMC. Venous thromboembolism in infancy and childhood. *Arch Dis Child* 1975;50:153–155
- Buck JR, Connors RH, Coon WW, Weintraub WH, Wesley JR, Coran AG. Pulmonary embolism in children. *J Pediatr Surg* 1981;16:385–391
- Akyon MG, Arslan G. Pulmonary embolism during surgery for a Wilms tumour (nephroblastoma). *Br J Anaesth* 1981;53:903–904
- Shurin SB, Gauderer MWL, Dahms BB, Conrad WG. Fatal intraoperative pulmonary embolization of Wilms tumor. *J Pediatr* 1982;101:559–561
- Suqueni HL, Suarez JMC, Roca IC, Casquero CR, Landeira JMV. Massive intraoperative pulmonary embolism in a case of Wilms tumor. *Rev Esp Anestesiol Reanim* 1985;32:303–305
- Didier D, Racle A, Etievent JP, Weill F. Tumor thrombus of the inferior vena cava secondary to malignant abdominal neoplasms: US and CT evaluation. *Radiology* 1987;162:83–89



# Focal High Signal on MR Scans of the Midbrain Caused by Enlarged Perivascular Spaces: MR-Pathologic Correlation

Allen D. Elster<sup>1</sup>  
Dan N. Richardson

Punctate and linear foci of abnormal signal were observed near the substantia nigra in the midbrains of 32 (20%) of 157 patients undergoing high-resolution MR imaging of the brainstem. The lesions were most easily seen on long TR/long TE images, where they were of high signal intensity. Their location was consistently in the lower mesencephalon near the junction of the substantia nigra and cerebral peduncle. Unilateral lesions were observed in 18 cases, while bilateral lesions were noted in 14.

A review of anatomic specimens revealed the constant presence of penetrating branches of the collicular or accessory collicular arteries in this location. Enlarged perivascular spaces around these vessels were frequently seen in the specimens and probably account for punctate and linear foci observed on high-resolution MR images of the midbrain.

*AJNR* 11:1119-1122, November/December 1990; *AJR* 156:157-160, January 1991

Punctate foci of high signal on T2-weighted images of the brain have long excited curiosity and interest. Initially dubbed "UBOs," or "unidentified bright objects," the anatomic and pathologic correlates of these lesions are gradually being explained. Known causes of these lesions include enlarged perivascular spaces, atrophic perivascular demyelination, white matter infarctions, capillary telangiectasias, congenital brain cysts, ventricular diverticula, ependymitis granularis, and isomorphic gliosis [1-9]. When no particular causative factor is identified, the descriptive term "leuko-araiosis" has been applied to these lesions [10].

Although these lesions were initially observed supratentorially, several investigators have noted that similar-appearing lesions may also be found in the brainstem [1, 6]. These brainstem lesions are relatively common in elderly patients, are located predominantly in the pons, and frequently possess ill-defined margins. Recently, we began to observe a different type of brainstem lesion in several young patients undergoing high-resolution MR imaging of the posterior fossa. These lesions were punctate and linear foci typically located near the substantia nigra and cerebral peduncle in the lower mesencephalon (Fig. 1). Because of their consistent location and shape, we speculated that these midbrain lesions represented anatomic structures rather than being merely nonspecific white matter abnormalities. We therefore set out to investigate systematically the frequency of these lesions and to establish their true identity.

## Materials and Methods

During an 18-month period, 157 patients were referred to us for high-resolution MR studies of the cerebellopontine angle and temporal bone. The patients ranged in age from 28 to 82 years old (median, 45 years). Approximately 90% (141/157) of these patients were referred from our otolaryngology service for hearing loss or vertigo, with the principal clinical injunction to "rule out acoustic neuroma." The remaining patients were referred for a variety of lesions involving the temporal bone, including postoperative complications, infections, and neoplasms.

Received May 3, 1990; revision requested June 4, 1990; revision received June 18, 1990; accepted July 2, 1990.

<sup>1</sup> Both authors: Department of Radiology, Bowman Gray School of Medicine, Wake Forest University, 300 S. Hawthorne Rd., Winston-Salem, NC 27103. Address reprint requests to A. D. Elster.

0361-803X/91/1561-0157  
© American Roentgen Ray Society

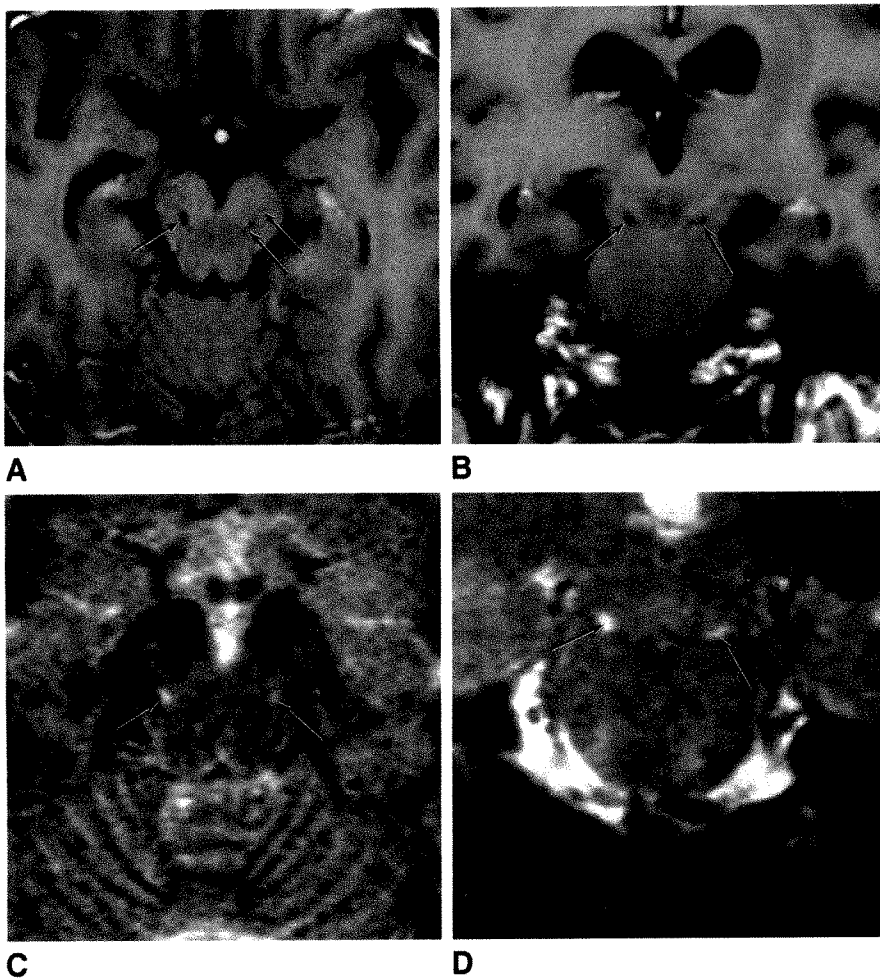


Fig. 1.—Punctate and linear foci (arrows in A–D) of abnormal signal seen in midbrain.  
 A, Axial T1-weighted image (600/20/2). Lesion on left has a more linear configuration.  
 B, Coronal T1-weighted image (600/20/2).  
 C and D, Axial and coronal T2-weighted images (2000/120/2).

No patient in this series had symptoms or signs referable to the midbrain, as determined by review of a three-page medical questionnaire completed by each patient prior to imaging.

All scans were acquired at 1.5 T (Picker Vista MR, Highland Heights, OH). The scans analyzed were from a triple-echo protocol with parameters of 2000/40, 80, 120/2 (TR/TEs/excitations). Slices were 3.5-mm thick with a 0.5-mm gap, and the images analyzed were exclusively from the coronal plane. Other scan parameters included a field of view of 20 cm and an image acquisition matrix of  $192 \times 256$ . Axial T2- and T1-weighted images were inconsistently obtained through the upper midbrain, so these were not used in the statistical tabulation. Where available and appropriate, however, images from these sequences were retained for purposes of illustration. Similarly, since all patients were referred for suspected disease involving primarily the cerebellopontine angles or temporal bone, complete images of the rest of the brain were obtained only occasionally in fewer than 15 patients.

The MR scans were retrospectively reviewed by the authors to determine the frequency of punctate and linear foci seen in the lateral and inferior mesencephalon as illustrated in Figure 1. High-signal foci were scored by consensus of the readers as either present or absent in each case. If present, the lesions were further scored as being present unilaterally or bilaterally.

Following the retrospective analysis of the MR scans, we reviewed serial midbrain sections from 25 cadaver brains. These specimens were selected at random from a medical school anatomy laboratory

collection, the ages and clinical status of the donors being unknown. All brains were fixed in formalin, then embedded in paraffin, sectioned at  $40 \mu\text{m}$ , and stained with H and E. The sections were viewed with low-power light microscopy using magnification of up to  $\times 200$ . Reference to a major brainstem anatomy text was made in order to assign specific identities to the structures visualized [11].

## Results

Punctate and linear foci of high signal on T2-weighted MR images were identified in the midbrains of 32 (20.4%) of 157 patients. In 18 cases the lesions were unilateral and in 14 cases they were bilateral. The lesions were consistently located in the lower mesencephalon near the substantia nigra, cerebral peduncle, and decussation of the brachium conjunctivum. Representative examples are shown in Figure 1.

The lesions seen were approximately 1–1.5-mm in greatest dimension and were frequently more ovoid or linear than round. They were best seen on the TE 120 images, and (when performed) also on the T1-weighted images. On all pulse sequences used they maintained isointensity with CSF.

Since our study was not prospectively designed and since complete images of the rest of the brain were not routinely obtained, we did not attempt to correlate the presence of these midbrain lesions with supratentorial white matter lesions



or enlarged perivascular spaces elsewhere in the brain. We found no significant differences in the ages of the patients with midbrain lesions (28–79 years) and those without such lesions (29–82 years). Since nearly all patients in both groups were referred for suspicion of acoustic neuroma, there were likewise no significant differences between the two groups with regard to clinical symptomatology. Enlarged perivascular spaces near the anterior commissure were seen in association with the midbrain lesions in several patients who had complete brain studies; conversely, several patients had midbrain lesions as an isolated finding.

Review of the anatomic specimens revealed the constant (25/25 cases) presence of small, penetrating vessels in the inferolateral midbrain (Fig. 2). The vessels seen were identified as branches of the collicular and accessory collicular arteries, which are themselves branches of the posterior cerebral artery. In six of these specimens, prominent perivascular spaces measuring larger than 1 mm in greatest dimension were observed. These perivascular spaces were of the appropriate size, location, and orientation such that they could reasonably account for the punctate and linear foci of high signal seen on MR images of the midbrain.

## Discussion

Over the last 2 years, several investigators have noted that enlarged perivascular spaces are responsible for producing punctate lesions on MR scans in the brains of otherwise healthy individuals [1, 2, 7–9]. These enlarged perivascular (Virchow-Robin) spaces are commonly seen in two locations: along the anterior commissure into the lower basal ganglia and at the brain vertex. The MR signal characteristics of these perivascular spaces are such that they maintain isointensity with CSF on all pulse sequences used. The midbrain lesions we observed have MR signal characteristics entirely consistent with that reported for perivascular spaces elsewhere in the brain.

Review of serial anatomic specimens and the anatomic

literature reveals that the enlarged perivascular spaces in the midbrain we have observed most likely surround penetrating branches of the collicular and accessory collicular arteries (Fig. 3). The crus cerebri and anterolateral midbrain are supplied primarily by rami of these arteries. The collicular artery is a small but constant vessel that arises from the posterior cerebral artery in the interpeduncular fossa [11]. Here the artery lies in close relation to radicles of the oculomotor nerve.

Exiting the interpeduncular fossa the collicular artery first traverses the anterior surface of the crus cerebri, closely following the pontomesencephalic sulcus. Upon reaching the lateral margins of the crus, the collicular artery ascends across its lateral side reaching the lateral mesencephalic sulcus. Thereafter, the artery inclines sharply posteriorly to reach the brachium of the inferior colliculus. Here it divides into its two terminal branches that supply the superior and inferior colliculi, respectively.

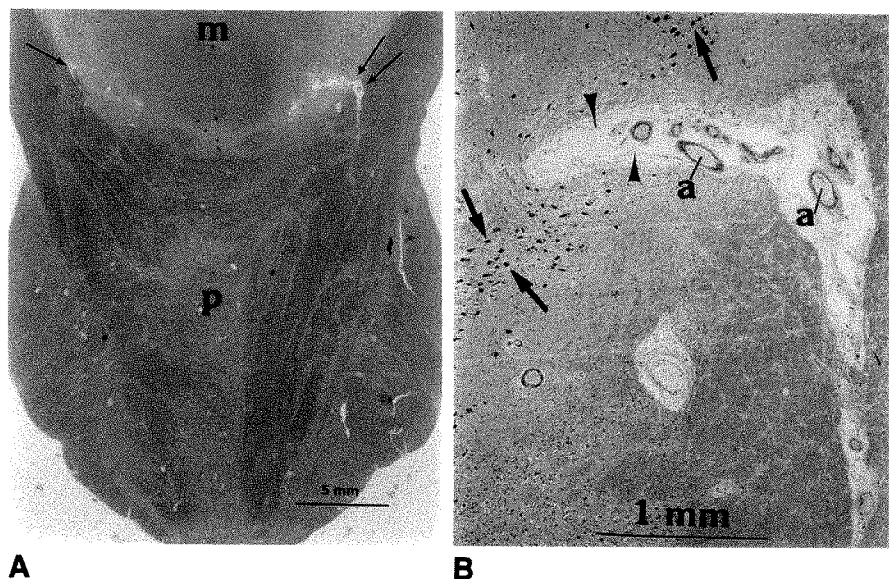
In most specimens an accessory collicular artery may also be found. This vessel branches from the proximal segment of the main collicular artery, following it closely upon its upper side as far as the lateral mesencephalic sulcus. Both the main and accessory collicular arteries give rise to numerous penetrating branches that supply the cerebral peduncle, substantia nigra, and lateral portion of the red nucleus. These arteries have a steeply oblique course through the brainstem, accounting for their segmental visualization on serial MR images.

Each penetrating mesencephalic artery is often closely accompanied by a satellite vein. Frequently, several veins and arteries are seen grouped into a small pedicle for some distance after penetrating the lateral margin of the crus cerebri. The penetrating veins drain outward to the lateral mesencephalic vein. This vessel in turn links the basal vein to the superior petrosal vein. We were unable to observe any venous structures of size comparable to the perivascular spaces surrounding the collicular arteries in any of our anatomic specimens. It remains possible, however, that in some cases signal from slowly flowing blood in the satellite veins described

Fig. 2.—Anatomic specimens (H and E stain) of midbrain (m) and pons (p).

A, Coronal section (×5). Enlarged perivascular spaces surrounding collicular artery are seen on left (double arrows). A normally sized perivascular space is noted on right (single arrow).

B, Higher power view of A (×50). Branches of collicular artery (a) are seen surrounded by enlarged Virchow-Robin space. The perivascular space is lined by pia (arrowheads). Note pigmented cells of substantia nigra nearby (arrows).



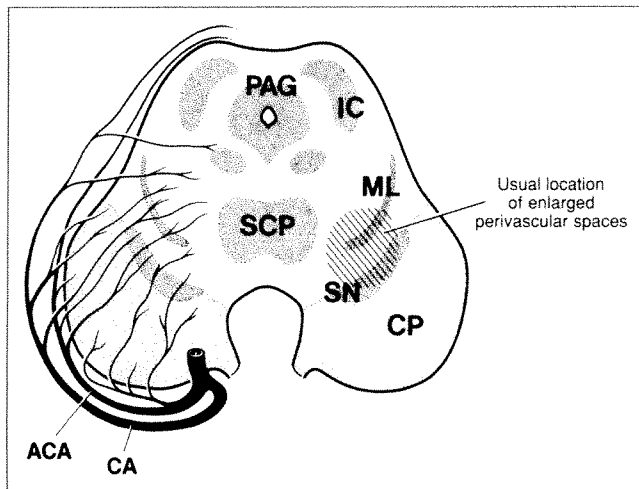


Fig. 3.—Diagram of blood supply to lateral midbrain. Penetrating branches of collicular artery (CA) and accessory collicular arteries (ACA) routinely supply the region where enlarged perivascular spaces are found. CP = cerebral peduncle, SN = substantia nigra, ML = medial lemniscus, SCP = decussation of superior cerebellar peduncle, IC = inferior colliculus, PAG = periaqueductal gray matter.

above may contribute to the linear and punctate midbrain lesions we have described.

In conclusion, we believe that small foci of high signal seen in the inferior and lateral midbrain represent enlarged perivascular spaces associated with penetrating branches of the collicular and accessory collicular arteries. Such lesions

should not be mistaken for lacunar infarcts or nonspecific white matter changes when seen in this characteristic location.

#### REFERENCES

1. Braffman BH, Zimmerman RA, Trojanowski JQ, et al. Brain MR: pathologic correlation with gross and histopathology. 1. Lacunar infarction and Virchow-Robin spaces. *AJNR* 1988;9:621-628
2. Braffman BH, Zimmerman RA, Trojanowski JQ, et al. Brain MR: pathologic correlation with gross and histopathology. 2. Hyperintense white-matter foci in the elderly. *AJNR* 1988;9:629-636
3. Kirkpatrick JB, Hayman LA. White matter lesions in magnetic resonance imaging of clinically healthy brains of elderly subjects: possible pathologic basis. *Radiology* 1987;162:509-511
4. Zimmerman RD, Fleming CA, Lee BCP, Saint-Louis LA, Deck MDF. Periventricular hyperintensity as seen by magnetic resonance: prevalence and significance. *AJNR* 1986;7:13-20
5. Sze G, DeArmond SJ, Brant-Zawadzki M, et al. Foci of MRI signal (pseudo lesions) anterior to the frontal horns: histologic correlations of a normal finding. *AJNR* 1986;7:381-387
6. Salomon A, Yeates AE, Burger PC, Heinz ER. Subcortical arteriosclerotic encephalopathy: brain stem findings with MR imaging. *Radiology* 1987;165:625-629
7. Jungreis CA, Kanal E, Hirsch WL, et al. Normal perivascular spaces mimicking lacunar infarction: MR imaging. *Radiology* 1988;169:101-104
8. Drayer BR. Imaging of the aging brain. I. Normal findings. *Radiology* 1988;166:785-796
9. Heier LA, Bauer C, Schwartz L, Zimmerman RD, Deck MDF. Large Virchow-Robin spaces: MR-clinical correlation (abstr). *AJNR* 1988;9:1033.
10. Hachinski VC, Potter P, Merskey H. Leuko-araiosis. *Arch Neurol* 1987;44:21-24
11. Duvernoy HM. *Human brainstem vessels*. Berlin: Springer-Verlag, 1978:16-66



# Normal Venous Anatomy of the Brain: Demonstration with Gadopentetate Dimeglumine in Enhanced 3-D MR Angiography

Donald W. Chakeres<sup>1</sup>  
 Petra Schmalbrock<sup>2</sup>  
 Martha Brogan<sup>1</sup>  
 Chun Yuan<sup>2</sup>  
 Lance Cohen<sup>1</sup>

This investigation evaluates whether gadopentetate dimeglumine enhancement of three-dimensional (3-D) acquisition MR angiography can generate clinically useful images of the normal venous anatomy of the brain. 3-D MR angiography of normal cerebral arterial anatomy has made rapid progress, although demonstration of detailed venous anatomy with similar techniques has been much less revealing. To overcome the limitation of slow venous flow, IV gadopentetate dimeglumine contrast enhancement was used to alter the relaxation times of blood, thus augmenting the venous signal. Several groups of patients were evaluated: we studied eight patients both with and without contrast enhancement, 20 patients and volunteers with multiple techniques to determine optimal technical parameters, and seven patients in whom enhanced MR studies were compared with standard selective biplane cut-film arterial angiograms. Only the large dural sinuses (such as the transverse sinus) could be seen on unenhanced studies owing to the saturation of slowly flowing venous spins. With contrast enhancement, many of the important small and large cerebral venous structures were routinely seen with reasonable scanning times (7 min). The venous anatomy was well seen for approximately one-half hour after injection and correlated well with angiograms. There are several important limitations to this technique, including a limited field of view, variable visibility of specific veins owing to technical and physiologic factors, confusion of enhancing non-flow-related structures, and lack of detailed physiologic information.

Single excitation 3-D MR angiograms are insensitive in the evaluation of cerebral venous structures. Enhancement with gadopentetate dimeglumine affords rapid scanning and excellent visualization of the pertinent venous anatomy. The best image quality was obtained with a sequence of 50/7/30° (TR/TE/flip angle).

*AJNR* 11:1107-1118, November/December 1990; *AJR* 156:161-172, January 1991

A number of MR angiographic techniques have been proposed that use the advantages of flowing blood to differentiate moving from stationary spins. The two most common techniques are based on time-of-flight effects of moving spins or on motion-induced phase shifts [1-7]. The most time-efficient methods are those that use three-dimensional (3-D) volume and multiple thin two-dimensional (2-D) [8, 9] time-of-flight techniques, since they use only single excitation data and there is no need to subtract different data sets. Subtraction of 3-D MR angiograms with and without gadopentetate dimeglumine has been reported to improve visualization of the venous structures (Seider M, unpublished data). Phase-contrast MR angiographic techniques evaluate differences in phase induced by motion in the presence of magnetic field gradients [5]. 3-D volume phase-contrast techniques generally have long acquisition times, up to 40 min.

The 3-D time-of-flight volume MR angiographic technique has made rapid progress in the acquisition of images of normal cerebral arterial anatomy, yielding good correlation with standard angiography [10-13]; however, demonstration of detailed venous anatomy has been much less revealing. Only large venous structures such as the dural sinuses are seen routinely, and even then, not to the best advantage.

Received August 29, 1989; revision requested November 17, 1989; final revision received June 1, 1990; accepted June 4, 1990.

<sup>1</sup> Department of Radiology, Division of Neuroradiology, Ohio State University Hospital, Ohio State University College of Medicine, 410 W. 10th Ave., Columbus, OH 43210. Address reprint requests to D. W. Chakeres.

<sup>2</sup> General Electric Medical Systems, Milwaukee, WI 53201.

0361-803X/91/1561-0161  
 © American Roentgen Ray Society

Noninvasive evaluation of the cerebral venous structures is desirable in order to ensure a complete evaluation of the brain vasculature. Venous thrombosis, stricture, compression, displacement, and anomalies are all important angiographic findings that ordinarily are not visible on images designed to optimize single-excitation 3-D volume MR angiographic arterial studies.

The poor visualization of the venous anatomy with the 3-D MR angiographic technique is partially a result of slower moving venous spins that are saturated within the imaging volume. To avoid this problem, we generated MR angiograms that were not based entirely on flow effects, but improved by relaxation time differences between vascular structures and stationary tissues. For this purpose, the contrast between blood and brain tissue was enhanced by IV injection of gadopentetate dimeglumine. Because this investigation was primarily focused on development of the technique and so many different parameters were varied, this article does not attempt to address the utility and accuracy of visualization of specific veins and abnormalities. It is a study specifically to review the technical parameters that are optimal for gadopentetate-dimeglumine-enhanced venous MR angiography.

### Subjects and Methods

Thirty-five patients and volunteers 4–75 years old (mean age, 45 years) were evaluated. Almost all of the patients were adults. Images

were acquired on a 1.5-T General Electric Signa system using a gradient-echo 3-D volume imaging sequence, which allows very short TEs (Schmalbrock P, unpublished data). The sequence uses first-order flow-motion compensation in both read- and slice-selection directions. The slice thickness can be varied from 0.7 to 5 mm, and the field of view from 16 to 48 cm. Initially, the shortest possible TE (<7 msec) required field-of-view restrictions in the frequency-encoded direction. Later versions of the pulse sequence code avoided this limitation. In most cases, 60 1.5-mm-thick slices were acquired with a field of view of 20–24 cm and a 128 × 256 matrix resolution. Because only a single acquisition is required, scan times were typically under 7 min. Thirty slices could be acquired in 3½ min.

Angiographic displays were generated by using ray-tracing methods on a stack of thin sections [5, 7, 14]. In the computational algorithm, parallel rays through a chosen imaging volume selected the points with maximum signal from the stack of individual images. In this fashion, a new projection image was generated. By changing the direction of the parallel rays, projection images of various angles could be generated. A minimum of six different projections were calculated for any chosen stack of slices. The projections were created to correspond to standard anteroposterior and lateral angiograms.

We initially obtained unenhanced images to evaluate the visualization of venous structures (Fig. 1). Then, we compared eight MR angiographic studies with and without IV gadopentetate dimeglumine enhancement (10 ml, 4.7 g) in the same patient or volunteer to evaluate the visualization of cerebral venous anatomy with enhancement (Fig. 2).

Varying T1 contrast weighting on unenhanced and contrast-enhanced images was achieved by manipulating the TR and flip angle.

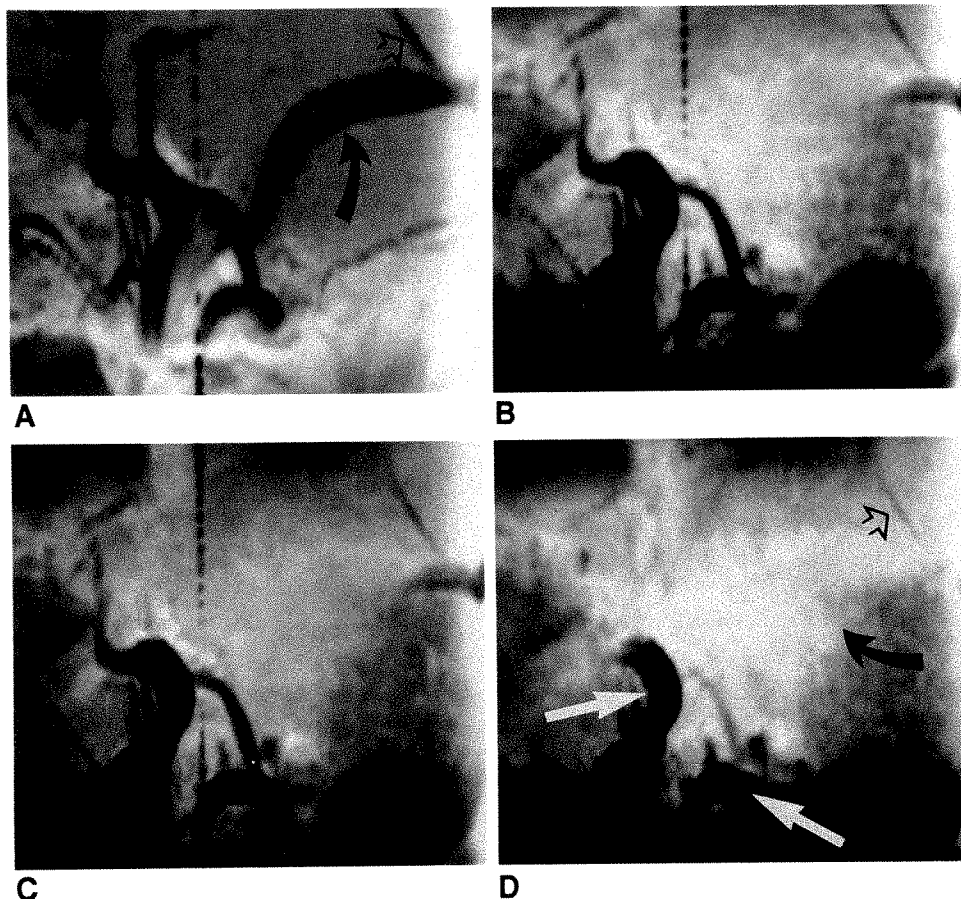


Fig. 1.—Effect of variable flip angle on unenhanced 3-D MR angiography.

A–D, Lateral projections from unenhanced axially acquired 3-D volume images, 50/7 (TR/TE), with variable flip angles of 15° (A), 30° (B), 45° (C), and 60° (D). Pixel size was 1.5 × 1.8 × 0.9 mm. Flow compensation was applied in both read- and slab-excitation directions. On lower-flip-angle image, visualization of venous structures, including transverse (solid black arrows) and straight (open arrows) sinuses, is faint. With larger flip angle, straight and transverse sinuses are almost completely absent. Even arterial structures (white arrows) are degraded by saturation effects.

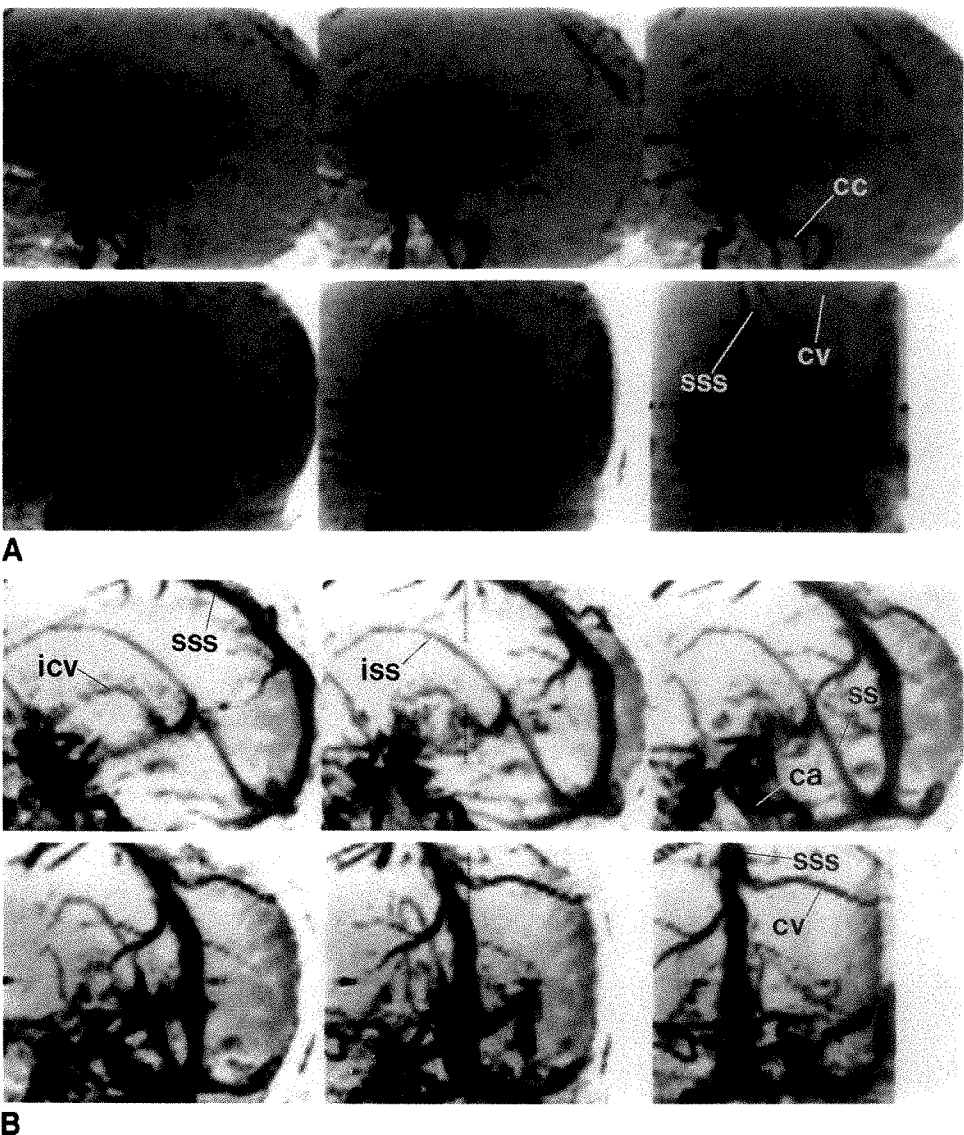


Fig. 2.—Multiple projections with and without contrast enhancement. 3-D MR angiograms, 47/7 (TR/TE), were acquired sagittally and are displayed in multiple projections (top left image is lateral; lower right is anteroposterior). Voxel size was 1.5 × 1.9 × 0.9 mm.

A, Unenhanced study, with a 15° flip angle, poorly displays venous anatomy, although proximal arterial system is visible.

B, Enhanced study, with a 30° flip angle for optimal results, shows a dramatic improvement in visualization of many venous structures.

cc = carotid canal, sss = superior sagittal sinus, cv = cortical vein, icv = internal cerebral vein, iss = inferior sagittal sinus, ca = carotid artery, ss = straight sinus.



Spoiler gradients on all axes allowed the generation of images that were more T1 weighted. We varied the TR from 33 to 50 msec. Initially, unenhanced MR angiograms with flip angles of 15°, 30°, 45°, and 60° were obtained in the same volunteer (Fig. 1). Then, similar series of images was obtained with gadopentetate dimeglumine in the same volunteer (Fig. 3).

The TE was varied from 7 to 14 msec to evaluate its effect on visualization of the veins, as well as fat suppression due to chemical shift [15].

To evaluate washout of contrast material over time, consecutive contrast-enhanced images in the same volunteer were completed (Fig. 4).

To evaluate the effect of section plane and image volume on venous visualization, consecutive section planes in the same volunteer were compared after contrast injection (Fig. 5).

A comparison was made of single- and multiple-image volume selection for ray-tracing projections (Fig. 6) and the original images were reviewed for anatomic detail (Fig. 7).

We directly compared standard selective biplane cut-film cerebral angiograms and MR angiograms from the same seven patients (Figs. 8–11). A general evaluation was made of the quality, extent of

visualization of the venous system, artifacts, and optimal imaging parameters with cerebral venous MR angiography. Because the examinations were done with many different techniques, a detailed quantitative evaluation of specific veins or abnormalities with varying techniques was not possible.

Results

The unenhanced MR angiograms displayed the venous structures poorly (Fig. 1). The images with higher flip angles further limited venous visualization. Comparison of enhanced and unenhanced scans of adult patients was done as soon as possible after injection of gadopentetate dimeglumine. There was remarkable improvement in the visualization of the venous system with enhancement (Fig. 2). Most of the major venous structures were well seen. Visualization of the arterial structures was not significantly improved with contrast material.

Changes in T1 weighing did have a noticeable impact on image quality in both enhanced and unenhanced examina-

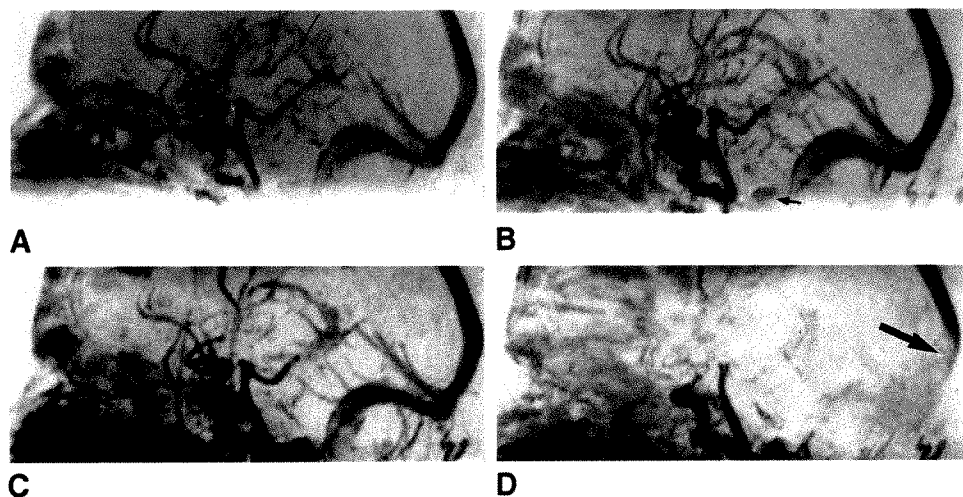


Fig. 3.—Variable-flip-angle contrast-enhanced MR angiograms.

A-D, Axially acquired images were obtained on two consecutive days to avoid changes related to contrast washout (A and B, one day; C and D, the next). The only acquisition parameter varied was the flip angle: 15° (A), 30° (B), 45° (C), and 60° (D). Images are displayed as lateral angiograms. Image with 60° flip angle (D) shows extensive saturation of superior sagittal sinus and transverse sinuses in inferior portion of image (arrow). Other images are of comparable quality, but there are subtle differences. Image with 15° flip angle (A) shows less detail of deep venous system (arrows). Original images showed less contrast between gray and white matter structures than did higher-flip-angle images. Choroid plexus is more prominent on image with 45° flip angle (C), leading to confusion with flowing structures. Enhancement of nasal mucosa is visible on all images.

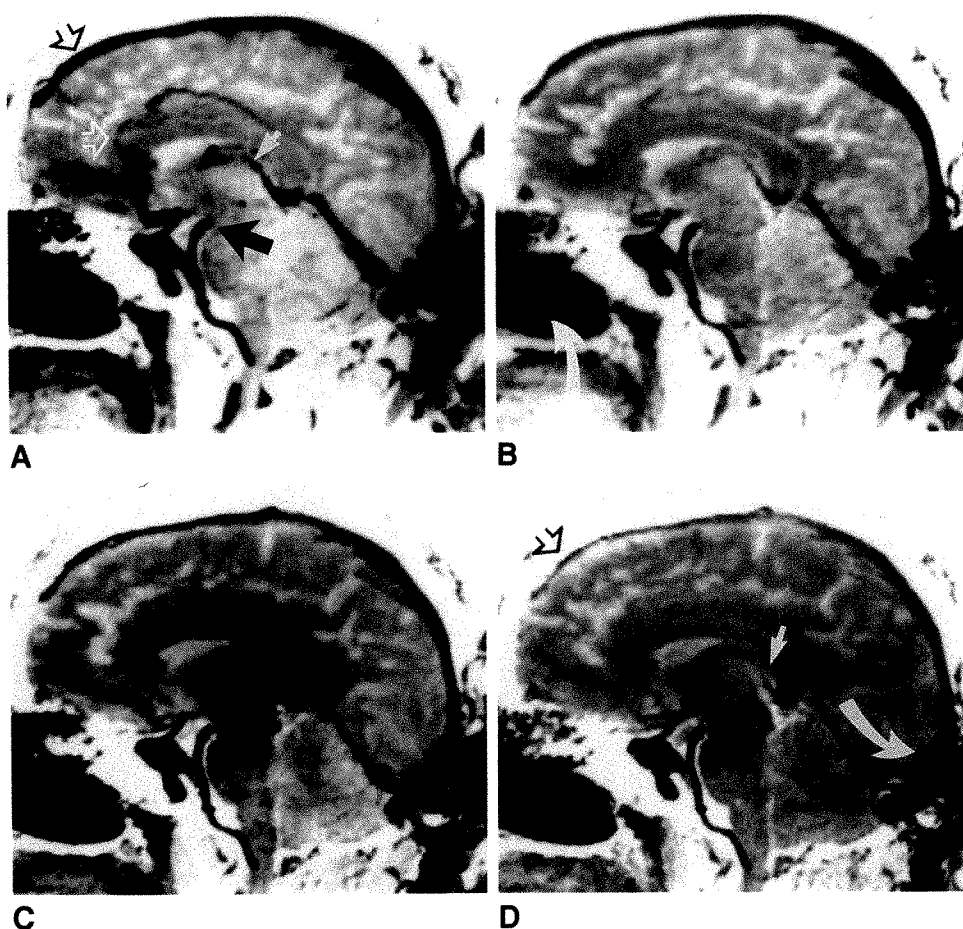


Fig. 4.—Time-related contrast washout.

A-D, Four consecutive sagittally acquired images, 50/11/30°, at 4 (A), 17 (B), 31 (C), and 44 (D) min after injection of 10 ml of gadopentetate dimeglumine. Voxel size was 1.5 × 1.6 × 0.8 mm. Only the central 22 images of a total of 60 were postprocessed for ray-tracing projection images shown. Best venous image contrast is seen on 4-min study (A). Midline venous structures, including superior sagittal sinus (open black arrows) and internal cerebral veins (solid white arrows), are seen well (A). A number of important arterial structures, including pericallosal (open white arrow) and basilar (solid black arrows) arteries, are seen on 4-min image also. With longer post-injection delays, smaller vascular structures are not seen as well (D). Venous quality of 44-min image (D) is marginal. There is minimal change in visualization of large arterial structures (solid black arrows) with time. Extensive enhancement of nasal mucosa and wraparound artifact is noted (curved white arrows).

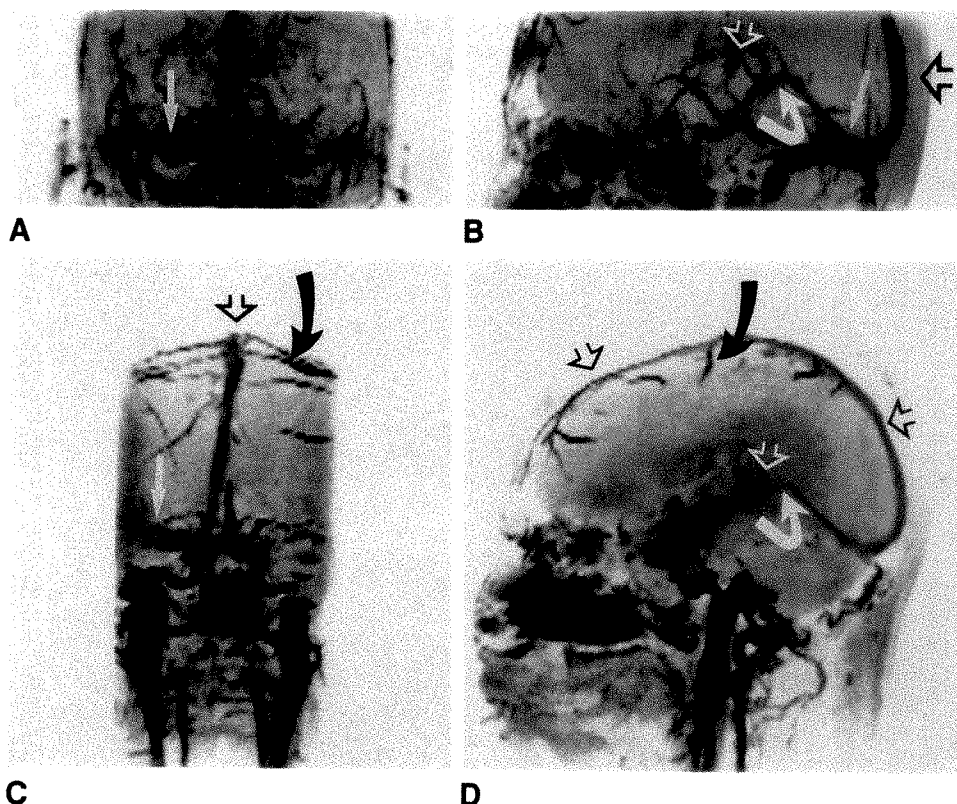
tions. Varying the TR from 33 to 50 msec did not significantly alter the results except for changing the total examination time. Longer TRs were not considered because of the prolonged examination time, and shorter TRs were not considered owing to technical limitations and expected decrease in

signal to noise. On unenhanced studies with lower flip angles, only the large dural sinuses (such as the superior sagittal and transverse sinuses) could be seen (Fig. 1A). Owing to saturation of the slow-flowing venous spins, the larger the flip angle, the worse the venous visualization (Figs. 1B-1D). On



Fig. 5.—Comparison of axial and sagittal acquisitions.

A–D. Contrast-enhanced images, 52/11/30°, were obtained with both axially (A and B) and sagittally (C and D) acquired techniques, then postprocessed with ray tracing to generate similar anteroposterior (A and C) and lateral (B and D) projections. Each acquisition has advantages for visualization of specific vessels. Deep venous system is better seen on axially acquired series (A and B), including vein of Galen (curved white arrows), transverse sinus (straight white arrows), and internal cerebral veins (open white arrow). On sagittally acquired images (C and D), superior sagittal sinus (open black arrows), jugular fossa, and cortical veins (curved black arrows) are seen best.



the contrast-enhanced studies, large flip angles also led to more venous saturation (Fig. 3). Increase in background signal from non-flow-related enhancing tissues (nasal mucosa and brain) became more pronounced with higher flip angles (Fig. 3D). A flip angle of approximately 30° was optimal, though there was a wide range that was adequate. The lower-flip-angle original images had less T1 weighting. The higher-flip-angle original images were less attractive.

The effect of the various TEs on image quality was important. No substantial signal loss for the venous structures was observed when increasing TEs from 7 to 15 msec. Modification of the TE between 7 and 11 msec, however, caused a variation in the background signal intensity of the fatty tissues (Fig. 7). Best results were obtained with a TE of 7 or 11 msec, where the magnetization of fat and water aligns in an antiparallel fashion, while a TE of 9–10 msec with parallel magnetization increased the background signal [15]. This was important in the suppression of unwanted signal from the scalp on the ray-tracing projection images.

The improvement in venous visualization lasted approximately 30 min after injection (Fig. 4). The sooner the examination followed the injection, the better the result, but the contrast load was adequate for at least two acquisitions.

Orientation of the acquisition section plane, slice thickness, and total number of slices were important factors, since they defined the total imaging saturation volume. When the imaging volume completely encompassed the majority of a venous territory, the results were compromised (Fig. 5). This indicates that the signal intensity is not entirely due to T1 contrast, but is also dependent on inflow effects. For example, rostral axial sections of the vertex did not demonstrate the superior sag-

ittal sinus as well as a direct sagittal series did (Fig. 5A). However, the deep venous system was usually seen better on axial images that did not include the vertex of the brain than on direct sagittal images (Fig. 5B). Coronal acquisitions, though possible, were not frequently used since they did not correspond with the venous anatomy in terms of covering a wide area.

The angiographic ray-tracing projection generated from smaller processed volumes best demonstrated smaller structures (Fig. 6) [14]. The larger structures (for example, the superior sagittal sinus) were less sensitive to the size of the reconstructed volumes.

The original slice images were of good quality, with T1-weighted contrast similar to that of spin-echo images (Figs. 7 and 11). Diagnosis of soft-tissue disease was possible (Figs. 7 and 11). The images were not clearly better than standard spin-echo images; however, the thin slice thickness was advantageous in the visualization of small structures.

Comparison of the MR and standard angiograms confirmed that, on the enhanced images, many of the important cerebral venous structures were seen routinely. In most instances, MR angiography correlated well with standard selective cerebral angiography (Figs. 8–11), although the results varied among patients. Routinely visualized structures included superior and inferior sagittal sinuses (Fig. 2), transverse and sigmoid sinuses (Fig. 11), vein of Galen (Fig. 9), basal vein of Rosenthal (Fig. 9), internal cerebral and thalamostriate veins (Fig. 8), lateral mesencephalic and jugular veins (Fig. 5), and cortical veins (Figs. 5 and 6). Occasionally, the septal (Fig. 6), precentral cerebellar, and other smaller veins were visible. Contrast enhancement helped define the extent of disease in

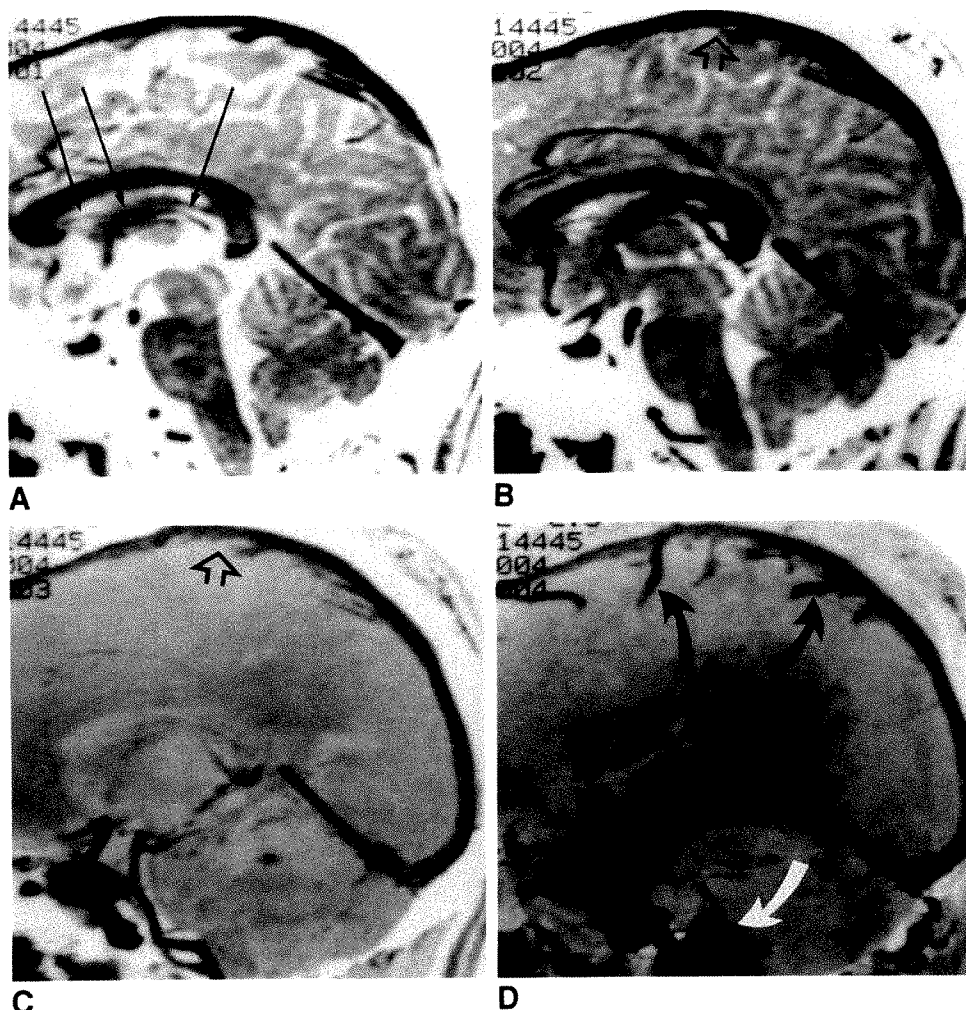


Fig. 6.—Effects of ray tracing post-processing.

A-D, Four images generated from one set of contrast-enhanced sagittally acquired images, 52/11/30°, show effects of different postprocessing techniques on visualization of various venous structures. A is single midline section from imaging block. Visualization of even small veins, such as internal cerebral and septal veins (straight solid arrows), is superb. B was processed from central four images. C and D were processed from 22 and 60 images, respectively. Most smaller midline veins are not visible on thicker slabs (C and D). On large imaging block (D), cortical veins (curved black arrows), complete superior sagittal sinus (open arrows), and jugular fossa (curved white arrow) are better displayed than on narrow midline image.

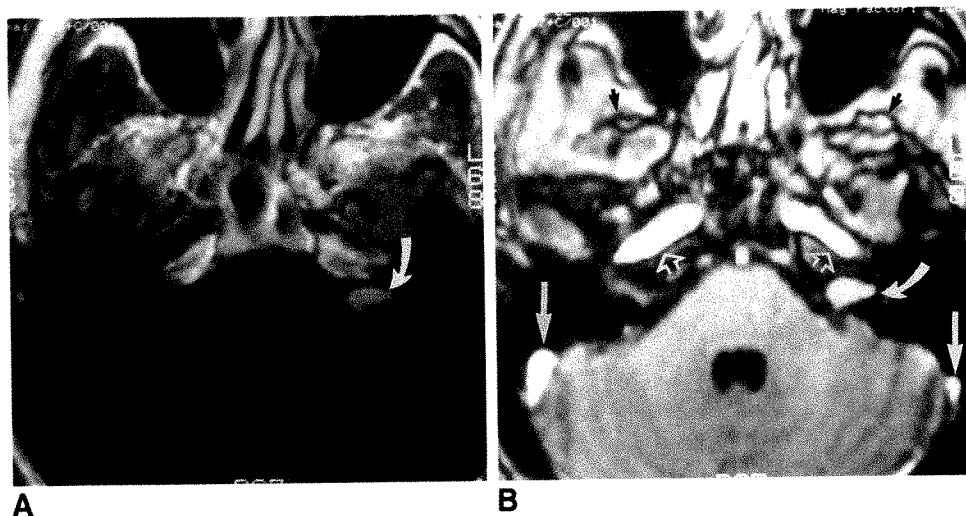


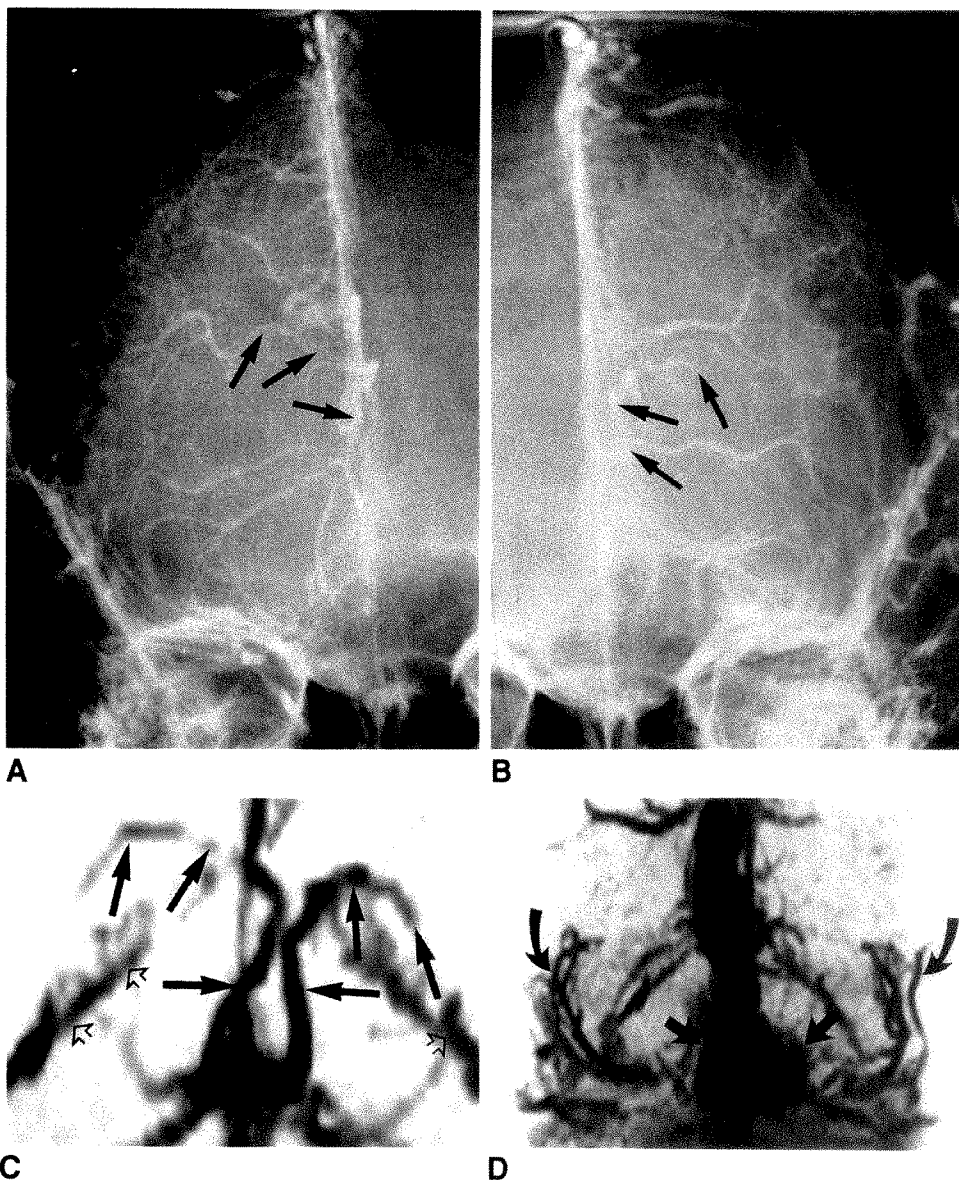
Fig. 7.—Comparison of spin-echo and 3-D images.

A and B, Gadopentetate-dimeglumine-enhanced axial images in patient with acoustic neuroma. Spin-echo image, 600/30, with a 256 × 256 matrix and 5-mm-thick section (A) and single 1.5-mm 256 × 128 section from a 60-slice 3-D MR angiogram, 47/11/30° (B), were compared. Both show enhancing intracanalicular mass on left (curved arrows). MR angiogram (B) shows high signal from carotid arteries (open arrows) and sigmoid sinuses (solid straight white arrows). Black interface of sub-temporal fossa fat and adjacent muscles is seen secondary to chemical-shift effect (black arrows).



Fig. 8.—Direct comparison of anteroposterior standard and MR angiograms.

A–D, Standard cut-film selective bi-lateral anteroposterior common carotid angiograms (A and B) and axially acquired MR angiograms, 40/7/30°, ray-tracing projections (C and D). Only central volume of brain surrounding deep venous system was processed on C to better display deep venous anatomy. Complete volume was processed on D. An enhancing suprasellar craniopharyngioma is seen (straight arrows, D). Mild subfalcine herniation to left is seen by distortion of internal cerebral and thalamostriate veins (solid arrows, A–C). MR angiogram (C) accurately reflects local distortion. Complete data reconstruction on D shows superior sagittal sinus and middle cerebral arteries (curved arrows) better. Choroid plexus of lateral temporal horns is seen also (open arrows, C).



cases of an arteriovenous malformation (Fig. 10), acoustic neuroma (Fig. 7), and metastatic tumor obstructing the jugular vein (Fig. 11).

### Discussion

Most MR angiographic techniques exploit one of two strategies to obtain sensitivity to flowing blood. The first strategy relies on changes in the phase of the transverse magnetization, which are introduced when blood moves in the presence of magnetic field gradients. Those spins moving in the direction of increasing gradient strength will advance in phase, while those moving in the opposite direction will fall behind the phase of stationary tissue. Phase-sensitive techniques usually involve subtraction of data obtained with different gradient schemes, such as bipolar gradient pairs [4], with and

without first-order motion compensation [3], or use of different first-moment magnetic field gradients (Pelc NJ, unpublished data). Investigation of complex blood flow requires acquisition of three separate data sets for the three gradient directions, thus leading to long examination times (up to 40 min). Since the changes in the phases are directly related to the velocity of flow, physiologic information can be obtained. Phase-sensitive techniques are capable of detecting relatively slow flow over large fields of view, since they are less sensitive to saturation. They are sensitive only to the component of flow coincident with the direction of the applied magnetic field gradient. For routine clinical studies they are very slow, partially because multiple acquisitions are needed. Because of the multiple acquisitions, high-resolution studies take even longer. We initiated our study to find technical parameters that would eliminate as many of these limitations as possible.

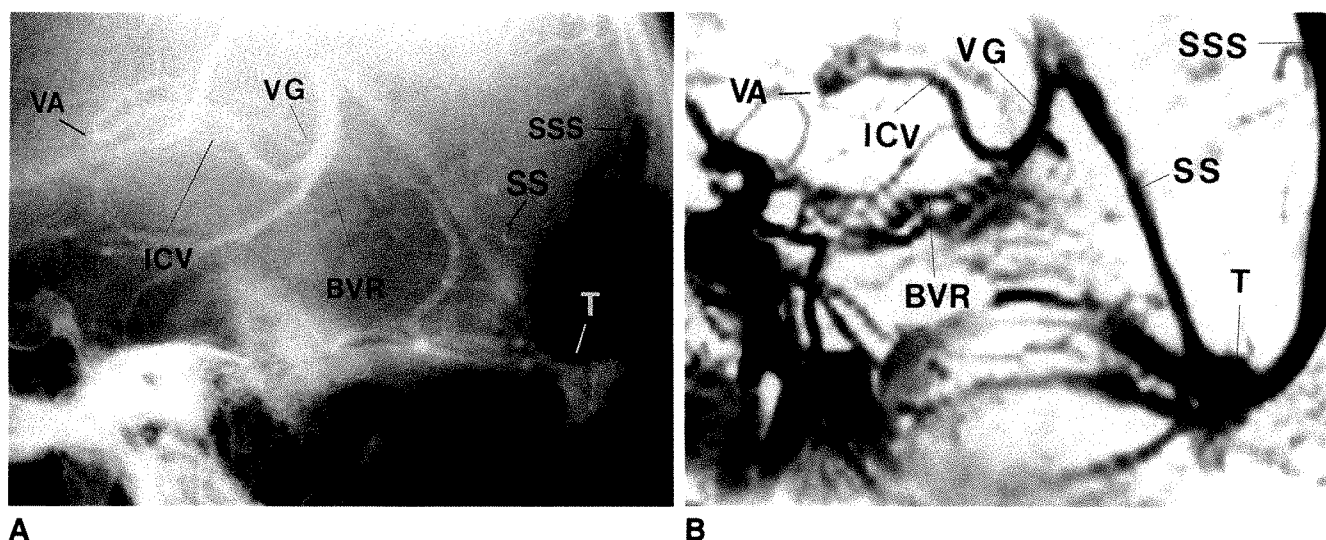


Fig. 9.—Direct comparison of a lateral standard and MR angiograms.  
 A, Standard cut-film selective carotid lateral angiogram shows much of deep venous system.  
 B, Corresponding axially acquired MR angiogram, postprocessed lateral projection.  
 Deep venous system is well seen on both studies. Carotid arteries are well seen. VA = venous angle, ICV = internal cerebral vein, VG = vein of Galen, BVR = basal vein of Rosenthal, SSS = superior sagittal sinus, SS = straight sinus, T = torcular Herophili.

The second MR angiographic strategy relies on time-of-flight effects to transport flowing spins with a different RF excitation history than the stationary tissue into the imaging region. The different excitation history can consist of selective presaturation [16] or inversion pulses (Wright GA, unpublished data), which are used to "tag" the signal of inflowing spins. Another time-of-flight technique takes advantage of the inflow of "fresh" unsaturated spins in a volume of saturated stationary spins, as in 2-D and 3-D time-of-flight angiography.

Acquisition of a single 2-D time-of-flight MR angiogram that highlights the signal from moving spins is possible in just a few seconds. The direction of flow should be perpendicular to the section plane for ideal results. Marked differences in signal between moving spins and stationary tissue are common with this technique. Flow parallel to the section plane can induce saturation. The original 2-D MR angiograms are of poor quality with respect to anatomic detail, since the signal of the stationary tissue has a poor signal-to-noise ratio. Also, the resolution (slice thickness) is limited by gradient strength. To create a ray-tracing projection, multiple images are needed, increasing the acquisition time. Motion between sections can degrade image quality [9], similar to CT postprocessing artifacts. The time-of-flight methods also are limited to the investigation of relatively fast flow (arteries or high-velocity veins) and/or small imaging regions, since the inflow of initially "fresh" spins is rapidly saturated as the imaging volume is traversed. For example, slow moving spins in the internal cerebral veins would be more saturated with sagittal than with coronal images. These differences can produce regions of low signal that are not related to a true stenosis. Because of the limitations of 2-D MR angiographic techniques, we decided to investigate the visualization of the venous anatomy with our techniques.

Other investigators have reported early results on the use

of gadopentetate dimeglumine with 3-D MR angiographic time-of-flight imaging techniques (Seiderer M, unpublished data). They subtracted two separate series of 3-D MR angiograms before and after contrast enhancement. It was found that visualization of the venous system was particularly improved. It was also reported that the anatomic information obtained with this technique was comparable to that obtained with digital subtraction angiography. The optimal technical parameters were similar to those we concluded to be optimal, 33/11/40° (TR/TE/flip angle); however, their technique has several major drawbacks: patient motion during or between the two series seriously degraded image quality, the acquisition time was at least twice that of a single acquisition, and each acquisition took 22 min.

We wished to develop a clinically useful single fast-acquisition MR angiographic technique that would provide high-resolution quality on the original and ray-tracing images. It was clear from prior experience with T1-weighted spin-echo imaging that the veins enhanced intensely following injection of contrast material. We attempted to take advantage of this phenomenon with a 3-D MR angiographic technique. Our approach can be classified as a hybrid time-of-flight T1-weighted method. We use a 3-D pulse sequence variation that could be used for arterial studies, but it is more T1 weighted. The 3-D techniques include high resolution with slice thickness potentially thinner than with 2-D MR angiography, short acquisition times (30 sections in 3½ min), and excellent original T1-weighted images owing to the improved signal-to-noise ratio of the 3-D MR angiographic technique.

This study demonstrates that unenhanced single-excitation 3-D MR angiography is an insensitive examination for demonstrating venous anatomy (Fig. 1). The venous flow rates in even the large dural sinuses are much slower than the arterial rates; thus, the spins reach saturation before they exit the

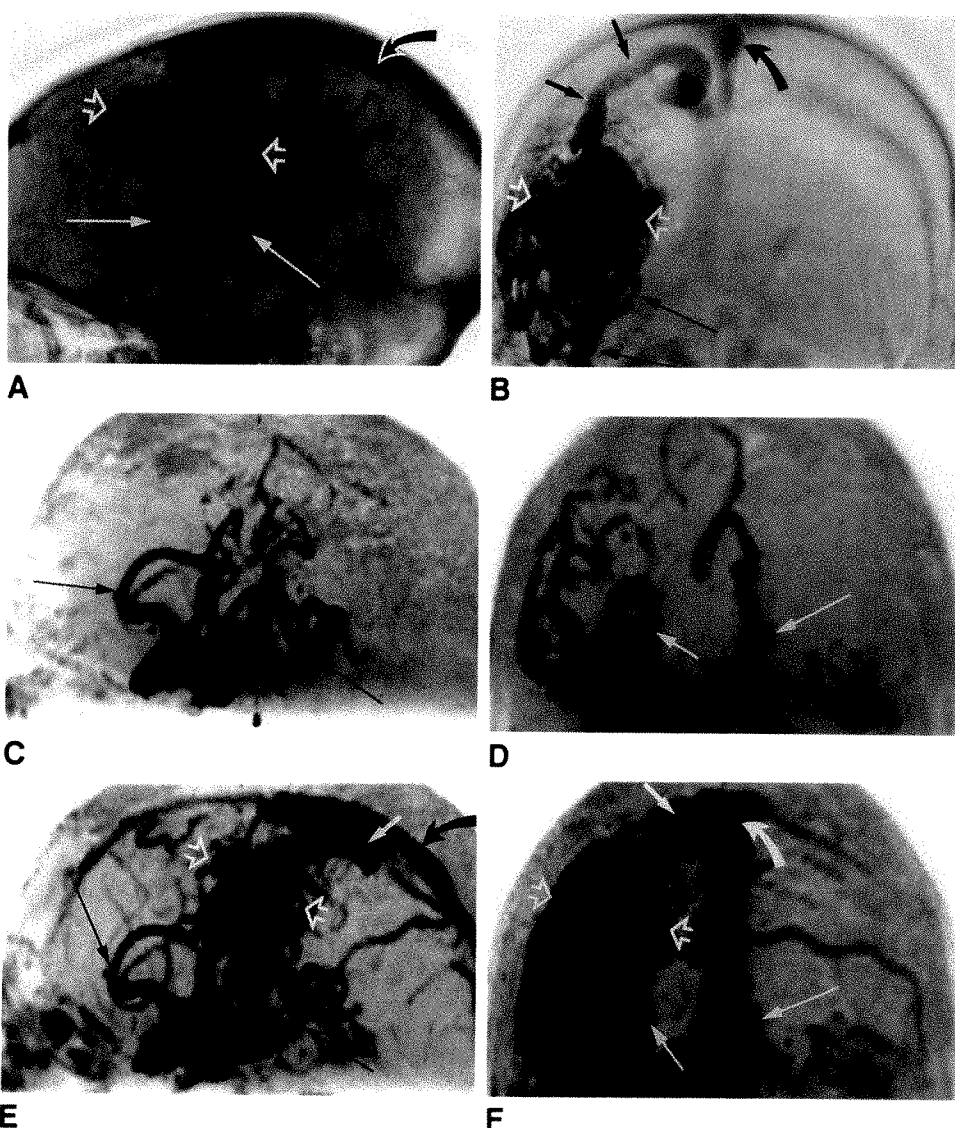


Fig. 10.—Comparison of standard and MR angiograms in patient with frontoparietal arteriovenous malformation (AVM) demonstrates importance of contrast enhancement.

A and B, Lateral (A) and anteroposterior (B) late arterial right carotid artery angiograms show large AVM (open arrows). Large arterial feeders (long thin arrows). Huge dilated draining veins (shorter straight arrows) are seen coursing superiorly to empty into superior sagittal sinus (curved arrows).

C and D, Unenhanced 3-D MR angiograms, 47/11/30°, lateral (C) and anteroposterior (D) ray-tracing images, display enlarged arterial feeders from anterior and middle cerebral arteries (arrows) toward AVM. AVM and its large draining veins, however, are not visible.

E and F, Contrast-enhanced 3-D MR angiograms, 47/11/30°, lateral (E) and anteroposterior (F) ray-tracing images, better display large cluster of draining veins (solid white arrows). Without contrast enhancement, complete extent of abnormality would be underestimated.



imaging slab. This is particularly the case for thick-volume slabs, short TRs, and higher flip angles (Fig. 1). Very little significant clinical information relating to the venous system was generated from 3-D MR angiographic techniques used for optimal arterial visualization. The limited visualization of the veins is not a disadvantage if the goal is to display the arteries only.

To overcome the limitations of unenhanced single-excitation 3-D MR angiography, we demonstrated that contrast enhancement markedly improves venous visualization by altering the relaxation times of venous blood rather than relying solely on rapid flow velocities (Figs. 2–11). Because an intact blood-brain barrier excludes contrast material from the brain, there is limited enhancement of the brain itself (Figs. 2 and 3). The contrast agent was concentrated in the blood pool, causing large changes in the relaxation times of the venous blood in comparison with the surrounding brain. This technique may not be useful outside of the brain. The image contrast for arterial structures was not significantly altered

with gadopentetate dimeglumine, since the signal generated by rapid flow-related enhancement alone produces nearly maximum contrast (Fig. 2).

The degree of T1 weighting was an important factor affecting venous visualization. The short T1 relaxation time of blood following enhancement allows for more rapid recovery of longitudinal magnetization and, therefore, increased signal intensity on T1-weighted images. Consequently, better differentiation of brain tissue from veins is expected when the flip angle is increased, up to a point. This was observed in the images with 15–30° flip angles (Figs. 1 and 3). Increasing the flip angle to 60° decreased venous image quality, primarily owing to large saturation losses of the flowing spins. There were also larger signal contributions from other tissues, such as fat and contrast-enhancing structures (nasal mucous), obscuring the veins. A flip angle around 30° was found to be optimal for both the original and projection images.

The choice of TE was important since it indirectly affected the overall quality of the images. Changes in the TE did not

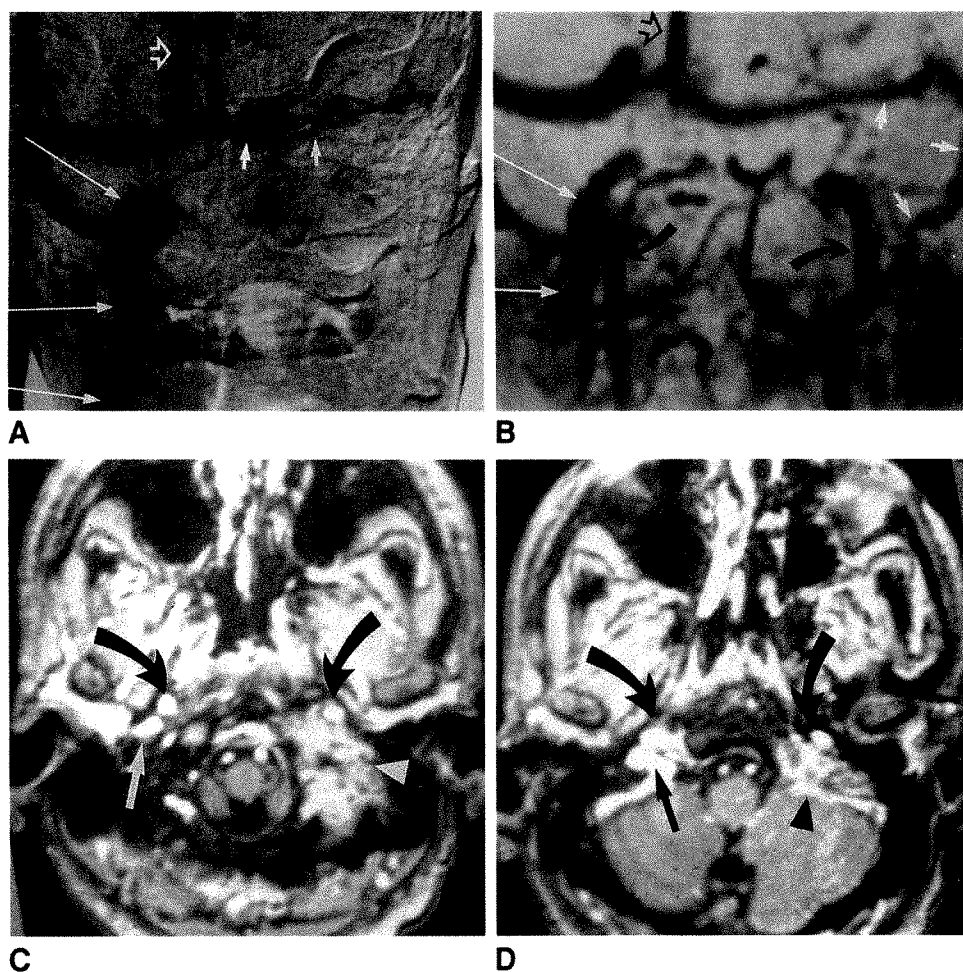


Fig. 11.—Comparison of standard and MR angiography of jugular occlusion in elderly man with a history of multiple left lower cranial nerve palsies, suggesting a jugular fossa lesion. Biopsy showed metastatic small cell carcinoma.

A, Anteroposterior digital subtraction angiogram from late venous phase of aortic arch injection shows complete occlusion of left jugular fossa and vein (short white arrows). Open arrow = superior sagittal sinus.

B, Anteroposterior ray-tracing image from 3-D MR angiogram, contrast-enhanced axially acquired series, displays patent right jugular bulb and vein (long white arrows) and normal carotid arteries (curved arrows) with complete occlusion of left jugular vein (shorter white arrows). Open arrow = superior sagittal sinus.

C and D, Axial slices from same series show tumor invading left jugular fossa (arrowheads) without involvement of adjacent brain or carotid arteries (curved arrows). Straight arrows = jugular veins.

directly change the visualization of the venous structures, but rather they affected the regions containing fat and water (Fig. 7) [17]. TEs of 7 or 11 msec helped to suppress the fat signal, which can be a serious problem, particularly on ray-tracing images of the vertex of the skull. A TE of 7 or 11 msec corresponds with the antiparallel alignment of the fat and water magnetic vectors. For further image improvement it might be necessary to implement fat suppression in the image sequence.

The TE also may affect image contrast by dephasing effects, with potential loss of signal with longer TEs. Since image contrast is dominated in part by T1 effects, and since the venous flow is slow, signal loss due to dephasing for larger voxel sizes or longer TEs did not pose a significant problem, in contrast to arterial blood flow. For fast flow, larger voxel sizes yield lower signal, owing to the fact that the velocity distribution within the voxel causes spin dephasing. For more T1-based images and slow flow, however, larger voxels may yield improved signal to noise, and thus contrast to noise. Because the velocities of venous flow are slower than those of arterial flow, less higher-order motion is expected. Because of this, very short TEs are not as critical as they are with fast arterial flow to prevent spin dephasing [1]. On the other hand, the use of gadopentetate dimeglumine decreases not only T1 but also T2 relaxation, necessitating

an appropriately short TE to prevent potential signal loss from the vascular structures.

The physiologic excretion and redistribution of the gadopentetate dimeglumine contrast material did have a profound effect on image quality. The 3-D MR angiographic contrast-enhanced study must be completed rapidly after injection, since a high concentration in the blood pool is crucial to ensure a good study (Fig. 4). The quality of the venous anatomy is maintained for a relatively long interval after injection (approximately 30 min). Repeat injections of contrast material may also be used to ensure adequate contrast enhancement, as long as the total dose does not exceed recommendations.

Physiologic time-of-flight effects of both the venous and arterial vessels are very important. Even with contrast enhancement, influx of unsaturated spins is a component of the signal characteristic. Choice of the overall imaging volume in relation to normal venous flow is crucial because of saturation effects. There was gradual loss of signal from the sagittal, transverse, and sigmoid sinuses and jugular bulbs on the more inferior sections of axially acquired images (Figs. 3, 9, and 11), secondary to progressive saturation of venous spins flowing into the inferior parts of the image volume, since the spins remain in the excitation volume for an extended time. Another example of this saturation phenomenon is the fact



that the jugular fossae were better seen on sagittally than on axially acquired images because of inflow of spins from the transverse sinuses (which are outside the sagittal excitation region) (Fig. 5). The same phenomenon may account for better visualization of the deep veins on axially acquired rather than sagittally acquired images, in which case the superior portion of the brain is not included in the imaging volume, and thus allows for inflow of unsaturated spins (Figs. 5, 8, and 9). We found that a total combination of the imaging volume, direction, and velocity of venous flow has significant effects on visualization of the small and large veins.

Review of the originally acquired and postprocessed images is also essential, since nonvisualization of veins on the projection images may be artifactual and technique dependent rather than a true finding of occlusion or other disease (Fig. 6) [14]. Because the stationary background tissue has relatively high signal, a vein may well be visible on the original image but not evident on the ray-tracing projection (Fig. 6).

The correlation between the cut-film angiograms and the MR angiograms is quite compelling. For example, the major dural sinuses are well seen on MR angiography without the problem of partial venous filling seen on the selective angiograms (Figs. 8–11). An aortic arch injection or a direct venous catheterization is frequently needed for more complete venous angiographic filling (Fig. 11). The deep venous system is also well seen on MR angiography, which has lower resolution than standard angiography, but the 3-D display and the ability to select the processed volume proved to be a major advantage. For example, if the dural sinuses obscure a small vessel on the standard angiogram, it may not be resolved (Fig. 8). On MR angiography, a rotated or regional volume view may accurately display the small vessel.

Limitations inherent to the maximum-intensity ray-tracing technique accounted for nonvisualization of small vessels (such as the septal veins), which were seen on the original images but not on the angiographic projections of large volumes (Fig. 6). The smaller the ray-tracing volume, the more detailed the depiction of the enhancing structures. Trimming the volume down could exclude regions that were not of interest or that were troublesome, such as the enhancing mucosa of the sinuses.

The quality of the original brain images alone is very good, so this MR angiographic technique could substitute for other T1-weighted spin-echo images, saving time (Fig. 8) [17]. The contrast is similar to that of T1-weighted spin-echo images. There is some loss of signal from magnetic susceptibility differences seen at bone, air, and brain interfaces, but the changes were not severe since the TEs were relatively short. Clear definition of contrast-enhancing disease was possible (Figs. 7, 10, and 11).

This MR angiographic technique has several major limitations. The 3-D technique is not ideal for visualization of the complete cerebral venous system. The present imaging volume is inadequate to include the complete head, and saturation is a major problem (Figs. 2 and 5). With this technique it would be necessary to acquire at least two different imaging volumes in which the venous territory is not completely encompassed to allow inflow of unsaturated spins. This is not as serious a limitation with 2-D time-of-flight techniques, since

the imaging slice is small and there is little saturation effect. Also, saturation is not as serious a problem with phase-contrast imaging, where the complete head can be studied in one series.

Confusion of high-signal regions due to enhancement, other high-signal structures, and blood flow is a potentially serious problem (Figs. 3, 7, and 8) [18]. For example, an enhancing tumor may obscure a vascular stenosis, since the lesion may envelop the narrowed vessel, as when a superior sagittal sinus thrombosis is obscured by an enhancing falx meningioma. Confusion can also be caused by enhancement of normal tissues, including the dural structures, choroid plexus, nasal mucosa (Fig. 4), and other vascular structures without blood barriers (such as the pituitary stalk). Other high-signal tissues unaffected by contrast enhancement (such as scalp fat or subacute hemorrhage) also may be a problem [18]. An enhancing tumor in the location of normal venous channels could produce potentially confusing findings. Review of spin-echo or other images usually resolves the potential misinterpretation. Characterization of flow properties such as direction, quantitative velocity, and higher-order motion contributions is not obtainable with this technique. This is a disadvantage if physiologic information is desired.

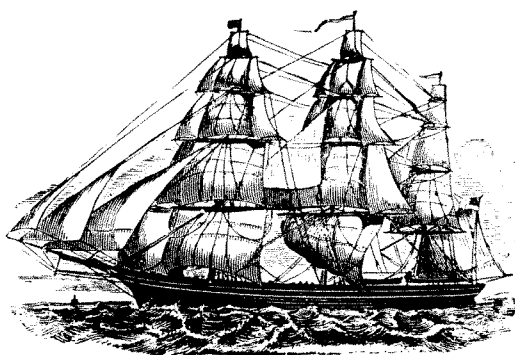
Possible indications for venous MR angiography include dural sinus thrombosis, venous angioma, varix, unexplained cerebral hemorrhage, arteriovenous malformation, venous anomaly, jugular paraganglioma, giant jugular bulb, contraindication to routine angiography, and demonstration of the normal venous anatomy for surgical planning. Complete assessment of both the venous and the arterial anatomy is important. If MR angiography is to be used for more than just a rough screening examination, extensive and consistent visualization of the entire cerebral vascular system is necessary.

In summary, unenhanced single-excitation 3-D MR angiography is quite insensitive in the evaluation of cerebral venous structures. Contrast enhancement allows for rapid scanning times and excellent visualization of most of the important venous anatomy. We documented good correlation of cut-film angiograms and MR angiograms. This technique could be used as a venous screening examination and could also substitute for a T1-weighted enhanced study so that the total examination time would not be seriously lengthened. We found the best image quality was obtained with a 50/7/30° sequence.

## REFERENCES

1. Nishimura DG, Macovski A, Pauly JM. Considerations of MRA by selective inversion recovery. *Magn Reson Med* 1988;7:472–484
2. Dumoulin CL, Cline HE, Souza SP, Wagie WA, Walker MF. 3-D time of flight MRA using spin saturation. *Magn Reson Med* 1989;11:35–46
3. Laub GA, Kaiser WA. MR angiography with gradient motion refocusing. *J Comput Assist Tomogr* 1988;122:377–382
4. Dumoulin CL, Hart HR. Magnetic resonance angiography. *Radiology* 1986;161:717–720
5. Dumoulin CL, Souza SP, Walker MF, Wagie W. Three-dimensional phase contrast angiography. *Magn Reson Med* 1989;9:139–149
6. Ruggieri PM, Laub GA, Masaryk TJ, Modic MT. Intracranial circulation: pulse sequence considerations in three-dimensional (volume) MR angiography. *Radiology* 1989;171:785–791
7. Masaryk TJ, Modic MT, Ross JS, et al. Intracranial circulation: preliminary

- clinical results with 3-D (volume) MRA. *Radiology* **1989**;171:793-799
8. Gullberg GT, Wehrli FW, Shimakawa A, Simons MA. MR vascular imaging with a fast gradient refocusing pulse sequence and reformatted images from transaxial sections. *Radiology* **1987**;165:241-246
  9. Keller PJ, Drayer BP, Fram EK, Williams KD, Dumoulin DL, Souza SP. MR angiography via 2-D acquisition and three-dimensional display. Work in progress. *Radiology* **1989**;173:527-532
  10. Hale JD, Valk PE, Watts JC, et al. MR imaging of blood vessels using three-dimensional reconstruction: methodology. *Radiology* **1985**;157:727-733
  11. Wedeen VJ, Mueli RA, Edelman RR, Frank LR, Brady TJ, Rosen BR. Projective imaging of pulsatile flow with magnetic resonance. *Science* **1985**;230:946-948
  12. Masaryk TJ, Ross JS, Modic MT, Lenz GW, Haacke EM. Carotid bifurcation: MR imaging. *Radiology* **1988**;166:461-466
  13. Tsuruda J, Halbach VV, Higashida RT, Mark AS, Hieshima GB, Norman D. MR evaluation of large intracranial aneurysms using cine low flip angle gradient-refocused imaging. *AJNR* **1988**;9:415-424
  14. Anderson CM, Saloner D, Tsuruda JS, Shapeero LG, Lee RE. Artifacts in maximum-intensity-projection display of MR angiograms. *AJR* **1990**;154:623-629
  15. Wehrli FA, Perkins DG, Shimakawa A, et al. Chemical shift induced amplitude modulations in images obtained with gradient refocusing. *Magn Reson Imaging* **1987**;5:157-158
  16. Edelman RR, Mattie HP, Kleefield J, et al. Quantification of blood flow with dynamic MR imaging and presaturation bolus tracking. *Radiology* **1989**;171:551-556
  17. Steinberg PM, Ross JS, Modic MT, Tkach J, Masaryk TJ, Haacke EM. The value of fast gradient-echo MR sequences in the evaluation of brain disease. *AJNR* **1990**;11:59-67
  18. Yousem DM, Balakrishnan J, Debrun GM, Bryan RN. Hyperintense thrombus on GRASS MR images: potential pitfall in flow evaluation. *AJNR* **1990**;11:51-58



Scientific Program (200 papers)  
Instructional Courses (60 hours)

Categorical Course on  
Body MR Imaging

The Caldwell Lecture

Award Papers

Scientific Exhibits

Social, Golf, and Tennis Programs

Guest Programs



# Come to the American Roentgen Ray Society 91<sup>st</sup> ANNUAL MEETING

Boston, MA

Sheraton Boston Hotel  
May 5-10, 1991



## Technical Note

# Atherectomy Facilitated by Long Vascular Sheaths

David H. Porter,<sup>1</sup> Ducksoo Kim,<sup>1</sup> Jeffrey B. Siegel,<sup>1,2</sup> Janet M. Storella,<sup>1,3</sup> and Daniel Z. Silverstone<sup>1,4</sup>

The Simpson Peripheral AtheroCath (Devices for Vascular Intervention, Inc., Redwood City, CA) has been used increasingly since 1987, when it first became commercially available for use in the iliac, femoral, and popliteal arteries [1-6]. The atherectomy catheter's short 0.018-in. (0.046-cm), fixed floppy guidewire tip and the cutter's stiff metal housing can negotiate most stenoses in the fairly straight superficial femoral and popliteal arteries and venous bypass grafts. The relatively tortuous, more acutely angled course of the external and common iliac arteries, however, can offer significant resistance to or prevent smooth advancement of the rigid cutter housing/collection chamber assembly. With resultant buckling and kinking of the leading floppy guidewire, further advancement of the atherectomy device often is not possible and risks significant trauma to the artery. Atherectomy must usually be abandoned in these situations. Additionally, the floppy guidewire tip usually will not cross an occluded segment that has not already been partially recanalized by other instruments. We have been able to avoid these difficulties by using long 25- to 70-cm vascular sheaths for both introducing and positioning the atherectomy catheter. These sheaths have enabled atherectomy to be performed in situations that would otherwise have been limited to treatment by conventional balloon angioplasty.

## Materials and Methods

The atherectomy catheter requires an introducer sheath with a hemostasis valve for vascular access. For approach to femoropopliteal and to mid or distal external iliac stenoses, we use standard short 10- to 13-cm vascular sheaths. For common iliac and proximal external iliac stenoses and for short femoropopliteal occlusions, we

now use long 25- to 70-cm sheaths, depending on the distance of the lesion from the femoral puncture site.

### *Proximal Iliac Stenoses (Figs. 1 and 2)*

After retrograde puncture of the ipsilateral common femoral artery, an angiographic guidewire is negotiated through the iliac artery stenosis and up into the abdominal aorta. Depending on which size atherectomy catheter will be used, a 9-, 10-, or 11-French by 25- to 30-cm-long introducer sheath (Bard, Tewksbury, MA; UMI Corp., Ballston Spa, NY) is then inserted coaxially over its corresponding tapered dilator and advanced as a unit over the guidewire into the distal abdominal aorta. The guidewire and dilator are removed (Fig. 1B). The sidearm of the sheath is connected to a constant infusion of heparinized saline flush solution. The patient is also given 5000 units of heparin as a bolus once the sheath has been placed.

The atherectomy catheter is then introduced into the long sheath and passed up through it until the cutting window of the device lies at the level of the stenosis (Fig. 1C). This is determined from a previous arteriogram or by digital road mapping. After the atherectomy catheter is fixed in this position, the sheath is slowly withdrawn back along the shaft of the catheter until the working end of the device lies free within the artery a few centimeters beyond the sheath tip (Fig. 1D). The maneuver is similar to unsheathing an inferior vena caval filter during its delivery. Atherectomy is then performed as per the manufacturer's instructions.

When the collection chamber has been filled by resected material or when one wishes to check progress angiographically, the atherectomy catheter can be drawn back down into the sheath and removed. Contrast material can then be injected through the sheath sidearm, or a diagnostic catheter can be placed further upstream over a guidewire, and arteriography can be performed. If further passes with the atherectomy device are required, a guidewire is reintroduced into the aorta and the long sheath is advanced over its dilator back up into the aorta.

Received May 18, 1990; accepted after revision July 2, 1990.

<sup>1</sup> Department of Radiology, Beth Israel Hospital and Harvard Medical School, 330 Brookline Ave., Boston, MA 02215. Address reprint requests to D. H. Porter.

<sup>2</sup> Present address: Department of Radiology, Grossmont Hospital, La Mesa, CA 92044.

<sup>3</sup> Present address: Department of Radiology, Suburban Hospital, Bethesda, MD 20814.

<sup>4</sup> Present address: Department of Radiology, Massachusetts General Hospital, Boston, MA 02114.

Alternatively, before the atherectomy catheter is removed, the long sheath can be advanced forward over the cutter housing and extended collection chamber (Fig. 1E). This repositions the sheath back through the stenosis, reestablishing access for the catheter without having to renegotiate the lesion. The sheath should not be advanced beyond the extended collection chamber in order to avoid its tip

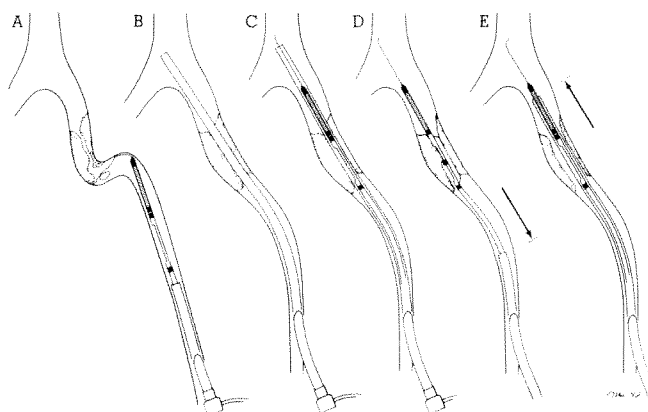


Fig. 1.—Use of long sheath for iliac atherectomy.

**A,** Stiff distal portion of atherectomy device is unable to traverse tortuous iliac artery with eccentric tight stenosis. Floppy wire tip has coiled and kinked.

**B,** After angiographic guidewire and catheter negotiation through stenosis, catheter and standard short introducer sheath have been exchanged over wire for a long 25- to 30-cm sheath placed into distal aorta.

**C,** Atherectomy catheter now passes without difficulty through sheath as it courses through tortuous portions of iliac artery, which are now somewhat straightened by presence of sheath and catheter.

**D,** After atherectomy device is positioned at stenosis, long sheath has been withdrawn back along catheter shaft (arrow). Balloon is inflated and atherectomy performed.

**E,** Before atherectomy catheter removal, long sheath is advanced forward over cutter housing and extended collection chamber (arrow), but not beyond nose cone. Catheter can then be removed, an arteriogram performed, and atherectomy device reintroduced for repeated atherectomy as needed.

scraping along the arterial intima because of the mismatch in caliber between the sheath and the atherectomy catheter's floppy guidewire.

#### Femoropopliteal Occlusions (Fig. 3)

After antegrade puncture of the ipsilateral common femoral artery, a guidewire and 5-French catheter are used to negotiate the short segmental occlusion. The upper and lower boundaries of the occlusion should be marked by radiopaque ruler or clamps. Once injection of contrast material confirms intraluminal position, the angiographic catheter is exchanged over a guidewire for a long sheath of appropriate size for the corresponding 7-, 8-, or 9-French atherectomy device. The atherectomy catheter is then introduced, positioned, and unsheathed as described earlier. The sheath should be no longer than 70 cm to allow the unsheathed cutter housing, which is located 76 cm down the working shaft of the catheter, to lie fully within the artery beyond the tip of the sheath once the sheath has been withdrawn. Sheaths up to 80 cm in length, originally designed for percutaneous aspiration thromboembolectomy [7], are commercially available (Cook, Inc., Bloomington, IN; Cordis Corp., Miami, FL).

#### Results

To date, we have used this technique in five separate procedures, each time successfully. In all four patients (one had bilateral iliac stenoses treated), we had not been able to negotiate the atherectomy catheter across the lesion by itself before placement of a long sheath. Two patients had three markedly eccentric, tight, proximal external iliac artery stenoses at near 90-degree bends in their arteries. The 9- and 11-French atherectomy catheters used passed without difficulty through the respective 9- and 11-French long sheaths, providing conduits through the tortuous portions of the iliac arteries. The other two patients had superficial femoral artery (SFA) occlusions.

Long sheaths have been necessary in 21% (three of 14) of the iliac lesions and 7% (two of 28) of the SFA lesions that we have treated with atherectomy. We have not encountered

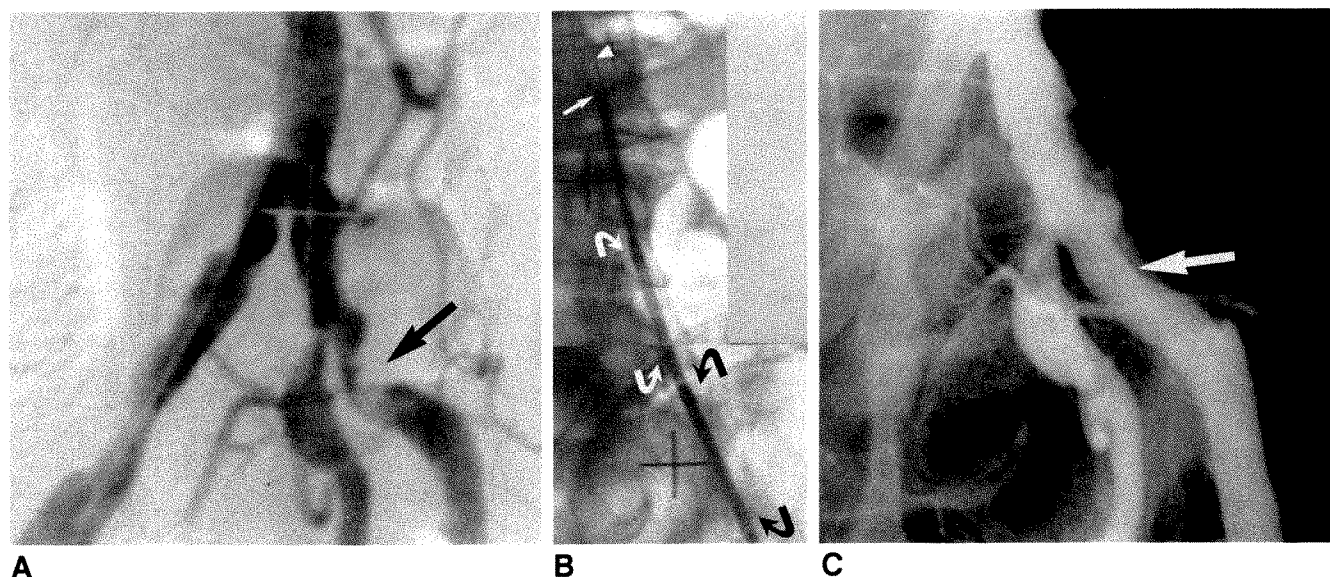


Fig. 2.—Markedly eccentric, tight stenosis in proximal left external iliac artery of a 69-year-old man with claudication.

**A,** Digital subtraction arteriogram of aortoiliac region in left posterior oblique (LPO) projection profiles stenosis (arrow) within a very tortuous arterial segment.

**B,** Digital fluoroscopic image of 9-French atherectomy device positioned in sheath across stenosis. Tip of atherectomy catheter guidewire (arrowhead) just beyond end of long 9-French sheath (straight arrow) in distal aorta. Note extended collection chamber (curved white arrows) and metal cutter housing (curved black arrows) at stenosis.

**C,** LPO arteriogram after atherectomy shows good technical result, with smooth, markedly improved angiographic lumen (arrow).



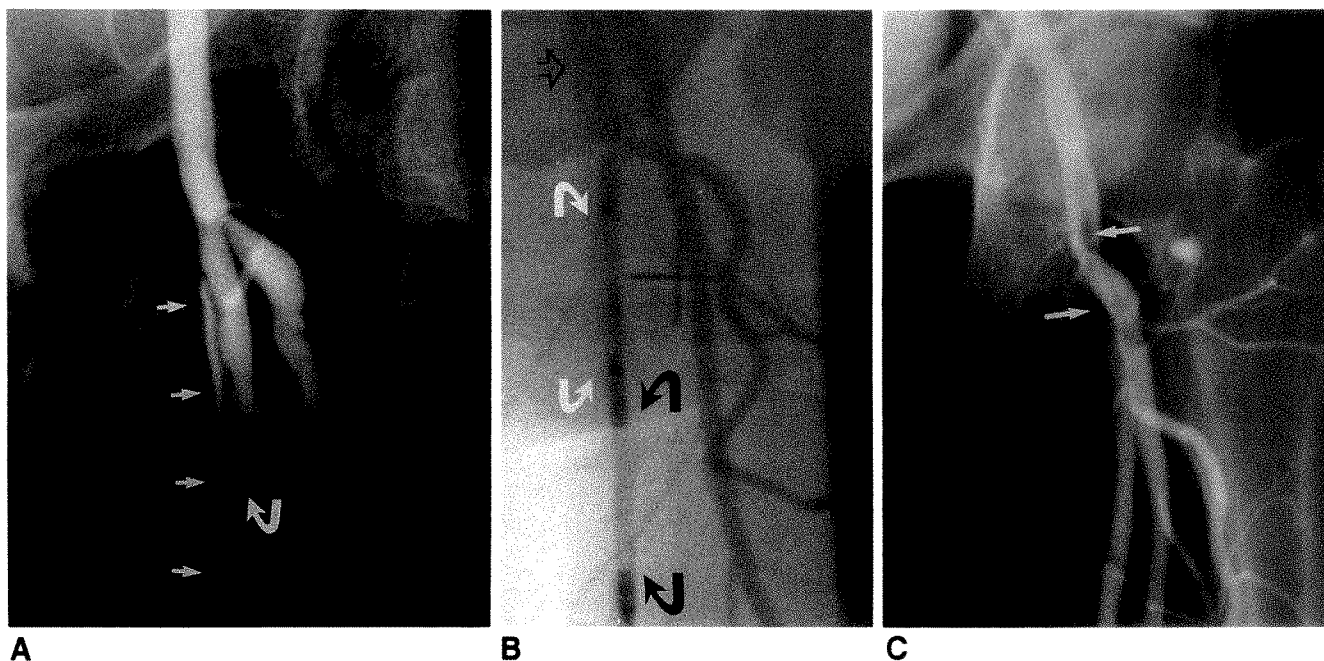


Fig. 3.—52-year-old man with residual 2.5-cm left superficial femoral artery (SFA) occlusion and 8-cm dissection after retrograde transpopliteal recanalization of 21-cm SFA occlusion 1 day earlier with rotational transluminal endarterectomy catheter (TEC - InterVentional Technologies, San Diego, CA).

A, Right posterior oblique arteriogram at level of left hip shows 8-cm false channel of dissection (short arrows) along anteromedial aspect of proximal left SFA. True lumen (curved arrow) is occluded. A steerable 0.035-in. (0.089-cm) guidewire/5-French catheter combination was needed to cross short residual SFA occlusion, after antegrade left common femoral artery puncture. A long, 30-cm, 9-French sheath was then placed across occlusion.

B, Digital fluoroscopic image of 9-French atherectomy device positioned with cutter housing (curved white arrows) at level of occlusion. Tip of sheath (open arrow) has been withdrawn into proximal SFA just below its origin. Note extended collecting chamber (curved black arrows).

C, Anteroposterior arteriogram after resection of short occluded segment and large dissection flap shows successful restoration of good-caliber SFA lumen. 9-French sheath (arrows) causes filling defect in left common and superficial femoral arteries, as injection was made through original diagnostic catheter placed across aortic bifurcation from right femoral approach.

any complications from using the long sheaths for atherectomy.

## Discussion

At present, it is unknown whether atherectomy with the Simpson atherectomy catheter will result in higher initial revascularization success rates, increased long-term patency, or lower restenosis rates compared with percutaneous balloon angioplasty. More data and comparison studies are needed. Meanwhile, the intuitive potential advantages of atherectomy favor its use when technically possible [1–4].

The use of long vascular sheaths is a technique with which most angiographers are familiar. Extension of their use to facilitate atherectomy is straightforward. Good fluoroscopic imaging is essential. Intimal damage could result if the tip of the sheath is advanced beyond the atherectomy catheter nose cone, as mentioned earlier. Additionally, the tip of the sheath could be resected during atherectomy if it is not withdrawn behind the cutter housing window. Vascular sheaths with a radiopaque band marking the tip of the sheath would be most helpful.

Recent manufacturer improvements include the extended collection chamber and replaceable guidewire tip assemblies. These allow slightly easier passage of the atherectomy device through bends in vessels and enable more rapid resection of the lesion, often with just one insertion of the atherectomy catheter, compared with the multiple insertions required when using the older model.

Until the development of over-the-wire or along-the-wire (“monorail”) iliac and femoral atherectomy catheters, however, the use of long sheaths for atherectomy can greatly facilitate the procedure and allow access to stenoses that the atherectomy device cannot now reach on its own. It also should facilitate supplemental atherectomy of arterial occlusions that can initially be crossed with standard guidewire-catheter techniques, rotational recanalization devices [8], or lasers.

## REFERENCES

1. Simpson JB, Selmon MR, Robertson GC, et al. Transluminal atherectomy for occlusive peripheral vascular disease. *Am J Cardiol* 1988;61:96G–101G
2. Schwarten DE, Katzen BT, Simpson JB, Cutcliff WB. Simpson catheter for percutaneous transluminal removal of atheroma. *AJR* 1988;150:799–801
3. Newman GE, Miner DG, Sussman SK, Phillips HR, Mikat EM, McCann RL. Peripheral artery atherectomy: description of technique and report of initial results. *Radiology* 1988;169:677–680
4. Maynar M, Reyes R, Cabrera V, et al. Percutaneous atherectomy with Simpson atherectomy device in the management of arterial stenosis. *Semin Intervent Radiol* 1988;5:247–252
5. Maynar M, Reyes R, Cabrera V, et al. Percutaneous atherectomy as an alternative treatment for postangioplasty obstructive intimal flaps. *Radiology* 1989;170:1029–1031
6. Dolmatch BL, Rholl KS, Moskowitz LB et al. Blue toe syndrome: treatment with percutaneous atherectomy. *Radiology* 1989;173:799–804
7. Starck EE, McDermott JC, Crummy AB, Turnipseed WD, Acher CW, Burgess JH. Percutaneous aspiration thromboembolectomy. *Radiology* 1985;156:61–66
8. Wholey MH, Jarmolowski CR. New reperfusion devices: the Kensey catheter, the atherolytic reperfusion wire device, and the transluminal extraction catheter. *Radiology* 1989;172:947–952

## Book Review

**Optimization of Image Quality and Patient Exposure in Diagnostic Radiology (BIR Report 20).** Edited by B. M. Moores, B. F. Wall, H. Eriskat, and H. Schibilla. London: British Institute of Radiology, 288 pp., 1989. \$60 (Available from Butterworths, Stoneham, MA)

Here is one aspect of European unification that may have escaped your attention. An objective of the Commission of the European Communities (CEC) is that from 1992 onward, every citizen who moves from one member state to another should be able to continue medical diagnostic examinations under similar conditions without needing to repeat radiographs previously taken in another location. In order to achieve this objective, member states would need to agree on verifiable criteria to define acceptable radiographs for given diagnostic examinations. These criteria encompass four major factors of a radiologic examination: image quality, equipment performance, radiographic technique, and patient dose.

In 1988, the CEC convened two workshops in an effort to identify criteria for acceptable radiographs. The first, held in Brussels in February 1988, addressed the influence of equipment performance and radiographic technique on acceptable radiographs (BIR Report 18). The proceedings described in BIR Report 20 are the product of a second meeting held in Oxford, England, in September 1988 that addressed the remaining factors: image quality and patient dose. These proceedings consist of 77 papers on the state of the art of research in radiologic image quality as reflected in British and European studies of image perception, image interpretation, and quantification of image quality and in evaluations of the optimization of radiation exposure, when optimization is interpreted as the use of the least radiation possible consistent with the acquisition of acceptable radiographs. Papers in the proceedings are grouped under several headings, including image perception, physical (and clinical) assessment of image quality, optimization of image quality and patient

dose in several clinical applications (pediatrics, mammography, chest, and technical factors), patient dose measurements and quality assurance, and the CEC Image Quality and Patient Exposure Criteria Trial.

Considerable information and insight into dose optimization and image quality are available in these papers and in those in the companion proceedings from the Brussels conference. However, the appendix to the present proceedings is of even greater interest. This appendix, entitled "Quality Criteria for Diagnostic Radiographic Images," offers specific guidelines on three factors—image quality, radiographic technique, and patient dose—for several common radiologic examinations (chest, skull, lumbar spine, urinary tract, pelvis, and breast). Member states are encouraged to adhere to these guidelines in order to achieve a comparable level of image quality throughout Europe by using optimal radiographic techniques and avoiding unnecessarily high doses of radiation to patients. Currently, radiology departments throughout the European community are being invited to help evaluate the applicability of the image quality criteria and test how well these criteria meet the quality requirements of radiologists.

These proceedings are not standard fare for everyone. However, for physicists in diagnostic radiology and radiologists interested in the technical features of image quality and dose optimization, they are definitely recommended reading.

William R. Hendee  
*American Medical Association*  
Chicago, IL 60610



## Perspective

# Analysis of the Cost-Effectiveness of PACS

Peter E. Hilsenrath,<sup>1</sup> Wilbur L. Smith,<sup>2</sup> Kevin S. Berbaum,<sup>2</sup> Edmund A. Franken,<sup>2</sup> and David A. Owen<sup>2</sup>

Picture archiving and communications systems (PACS) have emerged as an important part of digital imaging technology. However, the future of PACS is uncertain because its economic viability is in doubt. Cost-effectiveness analysis is an accepted technique for evaluating the economics of new technologies. This paper addresses the cost-effectiveness of PACS and identifies factors that are important in determining the cost of PACS relative to film-based radiology. These include the impact of PACS on physician productivity, maintenance costs, discount rates, and the time period for amortization of capital goods. The effectiveness of PACS is also explored in terms of improvements in diagnostic accuracy and timely diagnosis. Financial and clinical impacts should be integrated to provide information about how PACS expenditures will affect radiology departments, hospitals, and national research and development objectives.

Many radiology departments are considering the acquisition of picture archiving and communications systems (PACS) to modernize storage and processing of images and related information. PACS has the potential to replace film-based radiology and permit the use of image-processing techniques. The transformation of a film-based radiology department to an electronic one is costly and the issues underlying its justification may not be clear. A better understanding of the issues can improve resource allocation. This paper discusses how cost-effectiveness studies can help medical decision makers evaluate the economics of PACS.

### An Overview of Financial and Economic Viability

Until recently, medical decision makers could pass on costs of new technologies without much difficulty. Today, hospitals face diagnosis-related groups (DRGs) and other reimburse-

ment schemes that force more careful analyses of new acquisitions. Profitability is increasingly used as a criterion for investment in health care owing to economic pressures that limit the scope for cross-subsidization. Profits will erode if capital expenditures do not ultimately reduce costs, or alternatively, lead to an equivalent or greater increase in revenues. There is substantial uncertainty that PACS will do either.

The decision to buy PACS requires a careful assessment of its financial and economic impact. Benefits accrue at different levels of activity, and a layered approach to evaluation is important. A more complete set of benefits emerges as the domain of activity widens from the radiology department to the hospital and ultimately to the economy as a whole. For example, more timely diagnoses and treatment leading to shorter stays are clearly benefits, but those benefits may not appear on a radiology department's balance sheet. A recent study indicates that approximately \$32,000 of annual costs could be averted if PACS resulted in a 1% reduction in average length of stay for a volume of about 4000 inpatient procedures per year [1]. This suggests that PACS would cut costs by \$800,000 in a hospital with 100,000 inpatient procedures.

Failure to meet the financial test of profitability does not necessarily make acquisition of PACS an unsound economic decision. Economic conditions can inhibit proper functioning of markets, leading to inefficient levels of investment. One such condition is the presence of "external benefits," a form of market failure characterized by social demand exceeding market demand. Research and development (R&D) is an example of market underallocation due to external factors. Market mechanisms may not signal the true value of R&D when some parties benefit from the efforts of others without

Received May 17, 1990; accepted after revision August 13, 1990.

<sup>1</sup> Graduate Program in Hospital and Health Administration, University of Iowa College of Medicine, Iowa City, IA 52242.

<sup>2</sup> Department of Radiology (S703, GH), University of Iowa Hospitals and Clinics, Iowa City, IA 52242. Address reprint requests to P. Hilsenrath.

**AJR 156:177-180, January 1991** 0361-803X/91/1561-0177 © American Roentgen Ray Society

bearing any cost [2]. This is a well-recognized problem and helps explain why the federal government provided an estimated \$8.2 billion for R&D in the health sector in fiscal year 1990 [3].

This underscores the importance of clearly designating funds as R&D allocations and designating whether they are from public or private sources. For example, R&D activities that are financed from operating revenues may be subjected to undue pressure to show immediate performance. Potential long-term gains may be sacrificed for short-term financial objectives. The use of public funds should generate an even broader perspective of viability with a focus on social benefits as opposed to the narrower potential for private gain. Long-term economy-wide benefits in the form of lower costs or improved diagnostic accuracy may justify expensive investments that otherwise appear unsound.

### **Cost-Effectiveness: Basis for Economic Assessment**

Cost-effectiveness analysis can indicate whether an individual option has financial or economic merit and can help in the determination of which option is best if several alternatives are under consideration [4–6]. Cost and effectiveness are two distinct components of the analysis. Cost analysis measures expenses in dollars, whereas effectiveness analysis relies on nonmonetary measures.

Cost analysis helps to identify if and under what conditions PACS will reduce expenses. For example, the University of Washington evaluated a future military health care facility with an expected volume of 220,000 procedures annually and identified labor productivity and maintenance costs as two important factors affecting cost structure. A cost simulation found that a 1% increase in physician productivity could reduce the payback period by as much as 2 years. The base case analysis showed a positive cash flow after 9 years. Similarly a reduction in PACS maintenance expenses from 7% to 5% of acquisition cost reduced the payback period by about 1 year [7]. However, it should be noted that a great deal of uncertainty was attributed to the base case estimate, and a pessimistic scenario ignoring gains in labor productivity suggested that breaking even could take as long as 17 years. Similarly the use of 7% of acquisition costs for annual maintenance costs may be regarded as optimistic when other digital technologies commonly use 10%.

Other cost analysts have focused on storage and hardware costs [8]. Technical improvements may permit significantly lower acquisition costs in future years. Dutch investigators modeled the impact of anticipated reduction in acquisition costs and found that PACS would become practical by the turn of the century in a hospital performing 110,000 radiologic examinations a year [9].

Effectiveness analysis focuses on how the new technology affects clinical outcomes such as diagnostic accuracy and patients' outcomes. Most current research is looking at the more proximate impact of how, and under what conditions, PACS improves diagnostic accuracy. Research to determine patients' outcomes such as quality-adjusted life years will be most difficult to design for PACS technology.

### **Costs: Important Concepts for Analysis**

#### *Net Total Costs*

This is the difference between total cost in a PACS-oriented setting and in a film-based setting. Net total cost will be negative if switching to PACS results in savings. A film-based department should also consider sunk costs (money that has already been spent) and may find the status quo relatively more attractive than those acquiring PACS with no established radiology operations.

Equipment costs must be amortized over the useful life of the machinery so that total costs can be analyzed on an annual basis. The period of time that elapses before the equipment must be replaced can be an important variable in determining the viability of PACS. A related and potentially important factor is the discount rate, usually selected from prevailing market rates of interest. Positive returns that are foregone because of the allocation of funds to PACS must be considered and entered as a cost.

#### *Net Average Costs*

Average cost is defined by total costs divided by quantity and, when plotted against quantity, shows what kind of production economies exist. Favorable production economies exist if output grows faster than costs do. For example, suppose it costs \$3,000,000 to purchase and operate a filmless radiology department performing 10,000 procedures or \$300 per procedure. Then suppose it costs only \$200,000 to double output to 20,000 procedures. The average cost now falls sharply to \$160 per procedure.

Net average cost is the difference between the average cost of a procedure using PACS and the average cost of a procedure in a conventional setting. Net average costs can be developed to show at what level of output, if any, PACS is less costly per procedure than a film-based department. Avoided film costs and reduced personnel requirements may eventually offset capital and maintenance costs at a sufficiently large volume. For example, PACS may not be viable when costs are spread over 30,000 procedures per year but may well be cheaper than film when costs are distributed over 200,000 procedures a year.

#### *Net Marginal Costs*

This is the additional cost of PACS associated with expanding the scale of output minus avoided film-related costs. It is the net cost of extending PACS and further displacing film-based operations. Net marginal cost analyses are based on the assumption that the core of the system has already been purchased.

Economic viability of PACS is enhanced if the marginal costs of PACS are less than avoided film-related costs. Marginal costs, or incremental costs that are lower than average costs, will reduce average costs as output expands, just as a low procedure volume when a CT scanner is down for repair pulls down the CT unit's average study volume. Once the initial capital outlays have been made, it may be cheaper to extend PACS than to rely on conventional film-based



radiology. The average cost of PACS will eventually be lower than film at some level of output if the net marginal cost is negative.

A basis of output comparison between PACS and conventional systems is needed to measure marginal and net marginal costs. A lightbox is not a perfect substitute for a viewing station. It is important to identify how much more output results from the introduction of each of these units so that marginal costs can be evaluated. For example, the total cost resulting from the addition of two lightboxes should be compared to one viewing station if an extra viewing station results in twice as much output as an extra lightbox. The productivity and cost of viewing stations are thus important variables in evaluating the viability of PACS.

### Effects

The nonmonetary impact of switching to PACS-based radiology can be divided into two groups of effects, clinical and nonclinical. Clinical effects may be measured as changes in diagnostic accuracy, more timely treatment, and improved outcomes for patients.

Evaluations of diagnostic accuracy have tended to focus on spatial resolution requirements with detection of abnormalities requiring high spatial resolution, such as pneumothorax and interstitial lung disease, the topic of many experiments. Unfortunately, it is often difficult to generalize from the results of these studies to populations of patients because the cases are not sampled so as to be representative of those populations. Performance of PACS may be poorer in such studies than would actually be the case in practice because some cases that may benefit from image processing but that are unaffected by reduced spatial resolution are not included. For example, we found PACS depicted diagnostic features more clearly in 25% of the cases than hardcopy in a paired comparison of body CT scans. When PACS images were inspected after hardcopy, more clinically significant true-positive findings were found during second inspection than when hardcopy was viewed after PACS. PACS revealed 5% more findings when viewed after hard copy, whereas hard copy revealed 1% more findings when viewed after PACS.

The spatial resolution requirements for general PACS have been studied extensively with adult chest examinations. The detection of abnormalities involving fine detail, such as pneumothorax and interstitial lung disease (chronic obstructive pulmonary disease, emphysema) is degraded in 1024<sup>2</sup> digitized images [10, 11], in 2048<sup>2</sup> digitized images [12], and in 2048<sup>2</sup> computed radiographs [13]. There is little overall difference with digitized images of pulmonary nodules that do not involve fine detail (high spatial frequency information), even at 1024<sup>2</sup> resolution and improvement in detecting hilar and mediastinal abnormalities based on windowing and leveling [14–16]. These results also appear to hold at 2048<sup>2</sup> resolution [17, 18]. Investigations of other types of examinations by using 200- $\mu$ m digitization (equivalent to 2048<sup>2</sup> on an adult chest film) or computed radiography suggest that current monitor technology may be adequate for urography [19] and myelography [20], but perhaps not for mammography [21] or skeletal radiology [22, 23]. It has recently been suggested

that the weight of evidence favors a 2048<sup>2</sup> monitor requirement for a general PACS [24].

Other efforts have focused on the frequency and timeliness of image viewing. De Simone et al. [25] found that viewing occurred earlier more often when PACS was available. This was evaluated in a controlled experiment with chest radiographs in which most of the examinations occurred early in the morning. They found that 34% of the images were viewed between 8:00 and 10:00 a.m. with PACS, whereas less than 10% of the film images were seen during this interval.

Nonclinical aspects may be evaluated to account for important business considerations. Consumer, payers as well as providers, have difficulty gauging quality differentials in health care. Proxies of quality, such as technical sophistication, are often used to determine who provides the best care. Hospitals may find it necessary to stay abreast of technical developments in order to stay competitive in the medical arms race [26]. In this respect sophisticated technologies may yield value in the marketplace independently of clinical effectiveness. Recognition of these market considerations may prompt the profit- or prestige-maximizing decision maker to acquire PACS technology even if its usefulness is in doubt.

### Cost-Effectiveness

Costs and effects can be brought together to provide information telling the decision maker what one gets and how much it costs. The decision to buy is easy if analysis shows PACS leading to lower-cost operations with no effect on quality of care. Preliminary evidence suggests that this is not the case. It is also easy if no discernible benefits or advantages are identified and the acquisition simply drives up costs. The decision is more difficult if PACS is shown to reduce costs but with adverse effects or if it increases costs with corresponding positive effects. In these cases judgment must be rendered as to whether the acquisition is worth it. Cost-effectiveness analysis will provide useful information, but not the answer, when results are ambiguous.

### What to Watch Out for

It is important that all costs and effects are identified and measured. Failure to specify significant factors can lead to erroneous conclusions. It is also important to match costs with effects properly. For example, an expansion of PACS to neonatal intensive-care units involves specific costs such as additional viewing stations and their installation fees. These net costs should be compared with improved diagnosis of neonatal chest examinations and any significant changes in treatment or patients' outcomes. A mismatch of costs and effects will lead to inaccurate evaluation of extending PACs.

Uncertainty is a common problem in cost analyses. Many important variables such as improved labor productivity, maintenance costs, and storage medium costs are difficult to project accurately. The appropriate technique for addressing uncertainty is sensitivity analysis. A model can be built with spreadsheet software that permits the assessment of how different values assigned to uncertain variables affect costs. Modeling PACS costs can be a valuable tool and may provide insights that are not intuitively obvious. For example, higher



**TABLE 1: Important Elements in the Analysis of the Cost-Effectiveness of PACS**

Costs	Effects
Acquisition costs	Diagnostic accuracy
Future acquisition costs	More timely diagnosis and intervention
Period of amortization	Promotion of hospital image
Discount rates	Promotion of national research and development objectives
Procedure volume	
Potential reductions in length of stay	
Impact on labor costs	
Impact on film-related costs	

Note.—PACS = picture archiving and communication systems.

wage rates for physicians can actually enhance viability if PACS is found to increase productivity significantly [7]. Higher wages may be offset by reduced physician inputs. Alternatively, expected future cost savings associated with the new technology may not be sufficient to make acquisition attractive when discounting reduces the value of the future stream of cost savings. The lost income from investments forgone could offset any cost savings associated with PACS.

Sensitivity analyses can answer "what if" questions and improve understanding of how individual variables affect viability. This information can help decision makers frame resource allocation decisions in a larger, more complete context.

In summary, a thorough approach to assessing PACS requires a careful look at relative costs as well as clinical and nonclinical effects. Table 1 summarizes key elements for consideration in a cost-effectiveness analysis. Acquisition costs, both present and future, should be annualized by using appropriate periods of amortization and rates of discount. Net average costs should be established that spread total costs over procedure volume. Net average costs will be driven by net marginal costs, and particular attention should be paid to the cost and productivity of viewing stations in large hospitals.

The impact of PACS on labor costs resulting from changes in productivity and reduced film management costs needs to be assessed along with savings resulting directly from reductions in film requirements. These savings are the primary source of any cost reduction that PACS may bring radiology departments.

The nonmonetary effects also must be considered. The principal effects include improved diagnostic accuracy, more timely diagnosis, and an improved image in the marketplace. The long-term potential to achieve better and faster diagnosis with PACS should be assessed to allocate R&D funds better.

## Conclusion

Some new medical technologies may be assimilated into the fabric of the health sector without meeting the test of cost-effectiveness. Others that may be genuinely worthwhile risk being cast aside because of increasingly constrained financial environments. These problems suggest that we should consider new and more vigorous approaches to guide the development of new technologies and assist the diffusion of those that are genuinely cost-effective.

## REFERENCES

1. Stockburger W, King W. PACS: A financial analysis for economic viability. *Appl Radiol* **1990**;19:17-24
2. Mansfield E. *Microeconomics: theory and applications*, 6th ed. New York: Norton, **1988**:485-487
3. U.S. Bureau of the Census. *Statistical abstract of the United States*: 1990. Washington, DC: U.S. Government Printing Office, **1990**:585
4. Williams A. The role of economics in the evaluation of health technologies. In: Culyer AJ, Horisberger B, eds. *Economic and medical evaluation of health care technologies*. New York: Springer-Verlag, **1983**:38-50
5. Hutton J. Economic evaluation of medical technologies. *Int J Technol Assess Healthcare* **1986**;2:43-52
6. Weinstein MC. Economic assessments of medical practices and technologies. *Med Decis Making* **1981**;1:309-330
7. Saarinen AO, Haynor DR, Loop JW, et al. Modeling the economics of PACS: what is important? *SPIE* **1989**;1093:62-73
8. Dwyer SJ III, Templeton AW, Martin NL, et al. The cost of managing digital diagnostic images. *Radiology* **1982**;144:313-318
9. van Poppel BM, van Gennip EM, Bakker AR, Wilmink JB. First results with the software package CAPACITY for cost modeling of PACS. *SPIE* **1990**;1234:905-910
10. Goodman LR, Foley WD, Wilson CR, Rimm AA, Lawson TL. Digital and conventional chest images: observer performance with film digital radiography system. *Radiology* **1986**;158:27-33
11. Winter LHL, Romeny BMTH, Binkhuysen FHB, et al. Diagnostic evaluation of a PAC subsystem using phantom chest roentgenograms: an observer performance study. *SPIE* **1989**;1093:418-422
12. MacMahon H, Vyborny C, Metz CE, Doi K, Sabeti V., Solomon SL. Digital radiology of subtle pulmonary abnormalities: an ROC study of the effect of pixel size on observer performance. *Radiology* **1986**;158:21-26
13. Fajardo LL, Hillman BJ, Pond GD, Carmody RF, Johnson JE, Ferrell WR. Detection of pneumothorax: comparison of digital and conventional chest imaging. *AJR* **1989**;152:475-480
14. Lams PM, Cocklin ML. Spatial resolution requirements for digital chest radiographs: an ROC study of observer performance in selected cases. *Radiology* **1986**;158:11-19
15. Chakraborty DP, Breatnach ES, Yester MV, Soto B, Barnes GT, Fraser RG. Digital and conventional chest imaging: a modified ROC study of observer performance using simulated nodules. *Radiology* **1986**;158:35-39
16. Carterette EC, Fiske RA, Huang HK. Receiver operating characteristic (ROC) evaluation of a digital viewing station for radiologists. *SPIE* **1986**;626:441-446
17. Seeley GW, Fajardo LL, Ker M, et al. Evaluation of the DuPont Telera-diagnosis System. *SPIE* **1989**;1093:106-108
18. Newell JD, Seeley G, Hagaman RM, et al. Computed radiographic evaluation of simulated pulmonary nodules preliminary results. *Invest Radiol* **1988**;23:267-270
19. Hillman BJ, Fajardo LL. Scientific assessment of the clinical utility of phosphor plate computed radiography. *SPIE* **1989**;1091:245-249
20. Yang PJ, Seeley GW, Carmody RF, Seeger JF, Yoshino MT, Mockbee B. Conventional vs. computed radiography: evaluation of myelography. *AJNR* **1988**;9:165-168
21. Klessens PLM, Binkhuysen FHB, Ottens FP, Winter LHL, Willemse APP, deValk J-PJ. Diagnostic evaluation of a PACS subsystem using mammographs: an ROC analysis. *Med Inf* **1988**;13:323-326
22. Arenson RL, Seshadri SB, Kundel HL, DeSimone D. PACS at Penn. *SPIE* **1989**;1093:50-59
23. Dawood RM, Craig JOMC, Highman JH, et al. Clinical diagnosis from digital displays: preliminary findings of the St. Mary's evaluation project. *Clin Radiol* **1989**;40:369-373
24. Fraser RG, Sanders C, Barnes GT, et al. Digital imaging of the chest. *Radiology* **1989**;171:297-307
25. DeSimone DN, Kundel HL, Arenson RL. Effect of digital imaging network on physician behavior in an intensive care unit. *Radiology* **1988**;169:41-44
26. Robinson J. Hospital quality competition and the economics of imperfect information. *Milbank Q* **1988**;66:465-481



## Perspective

### Effective Audiovisual Presentation

Stuart S. Sagel<sup>1</sup> and Ruth G. Ramsey<sup>2</sup>

*The human brain starts working at birth  
and never stops,  
until you stand up to speak in public.*

—G. Jessel

Virtually every radiologist, whether in residency, academics, or private practice, eventually will need to address some audience. Such a presentation may be given at a national conference, or to a local group of physicians or medical students, or even to a nonmedical assemblage. Undoubtedly, every speaker desires to make a favorable impression and to have his/her message conveyed in an effective fashion. Unfortunately, lack of familiarity with basic educational techniques sometimes precludes such an accomplishment. Transmission of information may be lost in a morass of disorganized, incomprehensible, or irrelevant material. Slides may be used that are too complex to be understood or even read by the audience. Proper preparation can help almost anyone to correct and avoid such problems or to overcome the natural anxiety related to public speaking.

Preparing and delivering an effective audiovisual presentation is not a simple task. Expenditure of considerable time and effort is required for it to be successful. Even the most experienced speakers, who make their presentations look deceptively simple, have worked long and hard to perform in an excellent fashion. Abraham Lincoln's immortal Gettysburg Address, which contains 10 sentences, totals 271 words including 202 of one syllable, and takes 2 min to deliver, required 3 days of labored preparation (it was not jotted down on the back of an envelope while he was on a train).

This article is designed to provide practical and helpful

information in planning and preparing an effective presentation. Poor talks can be avoided if certain rules are obeyed. Our recommendations are offered really as guidelines, even if firmly expressed, dogmatic, or controversial on occasion. This advice is intended to improve the quality of your next talk.

#### Preparation

##### Audience

Whenever one is asked to give a presentation, the initial question should be, "What will be the composition of the audience: size, age range, experience, and knowledge level?" The topic and content then can be tailored for this group. The amount of technical detail, the types of examples, and the major goals will vary depending on whether the audience is composed of general or subspecialty radiologists, clinical colleagues, medical students, paramedical personnel, or even a group of lay persons. It is simply not feasible to deliver one particular canned talk on a subject to such disparate audiences. You don't want to show myriad histologic slides to a group of radiologists, nor a large series of angiograms to internists.

##### Topic

The topic chosen should be a problem/disease/technique that is not only relevant to the intended audience, but that can be discussed in the time allotted. The speaker must decide whether the topic will be broad and all inclusive or will be narrowly focused.

After selecting the topic, the next critical step is delineating

Received July 13, 1990; accepted after revision August 7, 1990.

<sup>1</sup> Mallinckrodt Institute of Radiology, Washington University School of Medicine, 510 S. Kingshighway Blvd., St. Louis, MO 63110. Address reprint requests to S. S. Sagel.

<sup>2</sup> Department of Radiology, University of Chicago School of Medicine, 5841 S. Maryland Ave., Chicago, IL 60637.

AJR 156:181-187, January 1991 0361-803X/91/1561-0181 © American Roentgen Ray Society



its proper boundaries. A somewhat limited scope must be maintained, and the information content must be tailored to the appropriate level. In deciding on the components, sins of commission are far more common than sins of omission. Most speakers, the experienced included, try to incorporate far too much information into their presentation. Afraid to leave out something important, the speaker tries to squeeze in the uncommon and the exceedingly rare along with the common. Emphasize the general rules. It is the exemplary teacher who, relying on his or her experience that the audience may lack, can omit the minutiae and stress what is probable and practical. Exhaustive details or encyclopedic lists and differentials are best left to textbooks, which must be relatively complete. Presenting a scientific paper is a special challenge, one as arduous as the research that precedes it. Countless research hours must be condensed into a fraction of an hour, usually 10–12 min. With so little time to enlighten, selectivity must be rigorous. The speaker should try not to fall into the trap of assuming that the audience will understand the subject as well as he or she does. It is far better to annoy a few sophisticates by stating that "complex mathematical formulas were used to analyze the statistical validity of the data" than to leave the majority of the audience bewildered by presenting laborious formulas.

Preparing a brief outline of the intended form of presentation is strongly recommended. It is the speaker's duty not only to gather the facts, but to present them in a cohesive fashion. The outline should provide a rough estimate of the number of examples required, their type, the supplementary word slides needed to enhance the message, and the intended method of gathering the appropriate illustrative examples and supporting data.

#### *Case Collection and Selection*

Appropriate illustrative cases can be acquired in a number of different ways. A simple method of personally collecting interesting and instructive cases is to list them in a small loose-leaf notebook for retrieval and review at a later date. A very brief note can be included as to why the case is instructive, and it might even be marked in a prospective fashion for potential inclusion in a particular forthcoming presentation. For the resident presenting at a conference, it is easiest to rely on a teaching file that has already been developed in a department.

Proper case selection is of vital importance. When creating the outline of the presentation, the speaker should have already decided whether the discussion will include normal and abnormal examples. In addition, a decision must be made about the types of abnormal cases to be presented so that the topic can be covered in a suitable fashion and in the required time frame. Will the type of abnormality be restricted (e.g., only neoplastic disease) or will it be more encompassing (e.g., also include inflammatory and congenital abnormalities)? Also, the proper balance between simple and more complex examples must be ascertained for the particular audience. It is important for a speaker not to become so enamored with a particular case that it cannot be discarded at some later

date if a better example, especially one with state-of-the-art imaging, is encountered. If a new technique is being presented, the speaker should strive to compare what he or she is discussing with more traditional methods (e.g., when illustrating an MR image of a hepatic neoplasm, contrast it with a CT scan at the same level). This not only helps keep the audience oriented, but allows them to test their usual way of doing things against this new approach and to comprehend the value, or the lack thereof, of the new technique.

In selecting illustrative cases, it is best to use examples in which the therapeutic outcome was affected, rather than choosing one simply because a brilliant diagnosis was achieved. Never show an intricate case with beautiful images and then state that the diagnosis is unproved. It is even worse for the speaker to state that he or she doesn't know the final pathologic results. When discussing a particular case, treat it as a patient rather than as a diseased piece of tissue. Interject some human elements into the problem. Mention the patient's age or occupation, or spend a few words describing the impact of his or her disease. The audience will better relate to your ideas if they have some empathy for the people you are discussing.

#### **Slides**

*Less is more.*

—Ludwig Mies van der Rohe

The architect of McCormick Place in Chicago was not talking about slides, but the same principle applies. Material originally designed for one format is not necessarily suitable for another. Simplification distinguishes a talk from a manuscript. Slides must be comfortably read and understood; the critical observation must be seen at a single glance. Only one main idea or finding should be on each slide. The key word is *few*: few slides, few lines per slide, few words per line.

Almost all educational presentations use 35-mm slides, which fit into carousel-type projectors. As a basic guideline, if a 35-mm slide can be easily read or the abnormality seen when held at arm's length, the audience seated near the back of any room should be able to see them projected on the screen. If the audience will most likely be unable to see a subtle finding, don't show the slide! It is crucial to remember the rectangular 2 × 3 format of the standard 35-mm slide. Because most screens are horizontal, an effort should always be made to try to keep the information on any slide oriented horizontally, so that the projected image will fit the screen and not have its top or bottom cut off. If feasible, information should be designed to fill this entire space, with proportions of three across by two down.

#### *Text Slides*

We remember best what we see. Visual aids complement the spoken word, enhance understanding, and boost retention. Although the written word often has a greater impact than mere verbal expression, the message must be short and to the point for the audience to quickly grasp the intent of the



speaker. Text slides need to be both legible (ease of seeing) and readable (ease of understanding). Legibility is dependent on such variables as type size and style, spacing between words, length of the lines of the text, and the vertical distance between lines. Readability is related to the organization of the text and the use of a vocabulary appropriate for the audience. If the information is complex, it needs to be broken up into several slides. The fewer the words, the better. Complete sentences are unnecessary. Short phrases, leaving out unnecessary verbiage, are both acceptable and preferable.

*"Rule of 7's."*—As a generalization, word slides should contain a maximum of seven lines of type, and individual lines should contain no more than seven words across. Long titles may need to be divided into two lines. Words should never be hyphenated. It is ideal to try to keep an entire phrase or concept on the same line. Abbreviations should be avoided, especially at an international presentation; if used, they need to be explained initially.

The text should be set in a mixture of upper and lower case letters for ease of understanding. All capital letters may be used for titles or short headings, or for acronyms or abbreviations (e.g., ACTH), so that they stand out clearly from the surrounding text. Only one simple bold typeface should be used. Italics and other fancy typefaces reduce reading speed and are appropriate only to emphasize a few key words or numbers. Underlining should not be used for emphasis with word processor-derived text; it is too close to descending letters.

A few variations can be used to make the data on a slide more readable. Numbers can be used to highlight various points that follow in a particular chronological sequence. If the pertinent points have no inherent logical order, but need to be uniquely identified, "bullets," little dots before each point, are a better alternative. They are especially helpful if some of the points on the slide take up more than one line. During the actual presentation, the listener's attention may be cued to each point by the use of an electronic or laser pointer.

Title slides (e.g., MRI of Pituitary Adenomas) are the audiovisual equivalent to chapter headings or subheadings in a book. They guide the audience through the talk and help make certain that transitions are clear. They allow introduction of a new topic without the slide from the previous case or theme remaining on the screen. And perhaps most important, title slides can be used to refresh the speaker's memory as to what to say next; they can obviate having a brief outline or notes on the podium.

### *Color*

High contrast is vital for good visibility. For continuous reading in a darkened room, white type on a black background is less fatiguing and more legible than black type on a white background. Slides with the latter format also are more prone to annoying dust or finger marks.

Color can add a certain amount of flair to a presentation by increasing the attention-attracting qualities of a slide. In addition, applied logically, consistently, and with restraint, color also can emphasize and divide information and make it more

understandable. The title on a slide may be one color and the text a different one. Colors have different luminances: white is 100%, yellow 89%, green 59%, red 30%, blue 11% and black 0%. With colored lettering on a dark colored background, high-luminance colors will be visible more easily than low-luminance colors. White or yellow are most suitable for display of text or data against a dark (deep blue is ideal) background. Remember that primary red is one of the least dominant colors against a dark background and should not be used. Red/green combinations should be avoided because some persons are color-blind to this mixture.

Particularly crucial information can be highlighted in a different color to draw attention to such items. In order not to lose impact, strive never to emphasize more than two words on a slide. Also, four should be the absolute maximum number of colors used in a slide.

### *Radiologic Material*

The area of interest should be appropriately cropped and properly centered and magnified. Depending on the sophistication of the audience and the complexity of the material presented, it may be useful to show an entire image for orientation (e.g., a posteroanterior chest radiograph) and then project a close-up view of the specific pertinent region (e.g., a retrocardiac nodule). When illustrating digital radiologic studies, be certain to mask (or delete) the name of the patient or other distracting alphanumeric during photography.

Don't ever show a poor-quality radiologic image. Such an approach is self-demeaning. The inference drawn is that the speaker is satisfied with poor technique. The unique case with inferior radiologic quality is superfluous; if it is so rare that it is the only case the expert speaker has available, it doesn't require emphasis. In addition, showing a poor-quality slide insults the audience; the implication is that they are not worth the time or effort for the speaker to seek out a better case or to have done an acceptable job of photography.

Try to use your own material and not borrow cases. The speaker is the alleged expert, and doesn't need to illustrate the exceedingly rare.

### *Charts, Tables, and Graphs*

These must be relatively rudimentary. Extensive legends and numerals that elucidate an illustration in a journal article or textbook can be confusing during the relatively quick glimpse required in a talk. A published graph may be understood and absorbed at the reader's own speed, whereas in a lecture, it is the speaker who dictates the pace. It is absolutely inexcusable for the speaker to state that he or she realizes that there is too much data on the slide, but only wants the audience to concentrate on column eight. In fact, only column eight should have been photographed.

### *Number of Slides*

Most presenters try to show too many slides. Time needs to be allotted for the audience to study the slide before it is

discussed. Depending obviously on the complexity of the material shown, each slide should take approximately 30 sec–1 min to present. Therefore, the maximum number of slides for a 30-min presentation generally should be 60; a better number would be 45, or 1.5 slides per minute.

Every slide should convey pertinent and necessary information. Be tough in your selection. Discard material that doesn't photograph well or is nonessential. If you are showing an adrenal mass on CT, there is no need to project a plain abdominal radiograph or an excretory urogram if these were normal or noncontributory. Not every number from a research project needs to be extracted and presented, just the ones of importance to the topic. Don't show myriad examples of the same abnormality to emphasize exactly the same point. Don't bore or irritate the listeners with multiple rudimentary or esoteric examples. When in doubt, throw the slide out.

#### *Photographic Techniques*

**Computer slide makers.**—Personal computers are not only ideal for preparing manuscripts, they are a superb tool to facilitate making 35-mm text and graphics slides. Personal computers are available in almost all radiology departments, can substantially shorten the time from concept to finished product, and when combined directly with a suitable film recorder, their slide quality rivals that of a professional photography service. Although virtually any word-processing software can be used to produce text slides, relatively inexpensive (\$100 to \$500) dedicated programs are available not only for text, but to integrate graphics and to drive various computer image recording systems. Inherent in such dedicated software is a feature called "nutshelling," which prohibits the user from creating slides with too many words. For generation of simple text slides, both Image Mate (Presentation Technologies, Sunnyvale, CA) and GEM Wordchart (Digital Research, Monterey, CA) software packages are extremely easy to learn and use. For more advanced applications requiring a variety of templates for sophisticated graphs and charts, either Harvard Graphics (Software Publishing Company, Mountain View, CA) or Freelance Plus (Lotus Development Corporation, Cambridge, MA) are advantageous.

Unfortunately, the final link in the personal slide production chain is not inexpensive, although excellent quality desktop digital film recorders can be purchased for less than \$10,000. Resolution is simply unacceptable if photography is done directly from the computer monitor. Dedicated film recorders generally contain their own 35-mm camera and a small high-resolution CRT monitor, capable of at least 2000 lines per inch, which eliminates amateurish jagged edges. Although sometimes called slide makers, their output could be prints or posters if negative film were used. An incredible array of products is available; suitable film-recording equipment includes the Image Maker Plus (Presentation Technologies), a relatively slow character-wheel system, ideal if text slides are the overwhelming need, and either the Montage FRI (Presentation Technologies) or Lasergraphics LFR (Irvine, CA), faster raster systems that are much better if graphics production is important.

**Film.**—Kodak T Max 100 Professional film (Rochester, NY), using the Direct Positive Film Developing Outfit (50 ASA), is strongly recommended for producing slides of all black and white radiologic material. High quality, continuous tone is uniformly achieved.

If typewritten text needs to be photographed for slides, the negative from Kodak Ektagraphic HC (8 ASA) produces the most ideal white lettering on a dark black background. Alternatively, mounting the negative from T Max 100 film with conventional development is acceptable. A colored background with white lettering can be achieved with Kodak Color Dupe film (2 ASA); the background color is determined by the filter used. This film resembles the aniline dye (diaz) technique. With the diazo technique, it is impossible to obtain uniformity of color if the slides are made at different times, and this film fades dramatically with repeated use and time. Polaroid Pola Blue BN (Cambridge, MA), which produces white lettering on a blue background, can be used when rapid developing is essential.

For color slide photography directly from film recorders, Kodak Ektachrome 100 H.C. or Professional is recommended for the brightest and most consistent colors. Fujichrome 100 (Tokyo, Japan) is a reasonable alternative. High-contrast Polaroid Polachrome HCP can be used when instant processing is essential; it costs more and the quality is not as good.

**Mounts.**—It is preferable to have all slides mounted in the same material to avoid refocusing problems during the presentation.

Glass-mounted slides are the easiest to keep clean; they also are expensive and relatively heavy. When these mounts are used it is advisable to tape an edge of the film to the slide mount; this will prevent subsequent movement of the film, especially during travel. If such slides are brought in from the cold to a large auditorium in which high-intensity xenon lamp arc projectors are used, contained water will vaporize, and the audience will see dark shadows slowly melting away on the screen. This distraction can be obviated by preheating the slides before presentation; a hair-dryer is adequate.

Cardboard mounts are the cheapest to use. The slide film should be cleaned with an airbrush before presentation to remove annoying dust or hair. With repeated use or when projectors become relatively hot, these mounts often bend and may jam within the carousel tray. Plastic mounts are a suitable compromise; they are relatively inexpensive and do not bend.

#### **Delivery**

The talk should be given as if the speaker were having a pleasant conversation with friends and professional associates, at a slightly slower pace than his or her normal speech pattern, with varied voice inflections. Be sure to face and establish eye contact with members of the audience, at least intermittently; do not constantly look at the slides or any notes. And never, ever, read word-for-word from a prepared text. Such an approach is guaranteed to create almost instantaneous dismay among the listeners. All spontaneity is lost; the speaker and the audience are no longer friends. The



attendees probably will consider their time and effort wasted, wondering why the speaker didn't simply distribute the written material that they could subsequently read at their leisure. On the other hand, expertise is not a license to stand before an audience without preparation and lecture impromptu. Key points are often omitted, minor ones belabored, and subjects addressed out of sequence in such an ad lib presentation. The gift of being a "natural speaker" is either extremely rare, or more likely, nonexistent. Most often, the apparent extemporaneous delivery is an illusion, belying the intense forethought and careful preparation, or sometimes derived from many years of talking on exactly the same subject.

In beginning a presentation, it is important to win the interest of the audience. Invest a few moments in describing why you believe the topic is important and briefly explain how you will accomplish your goals. Perhaps something like, "Today I'll be speaking about the usefulness of CT for the detection of liver metastases. First, I'll cover the basic techniques, then I'll show you some typical examples, and finally I'll present some unusual cases to you." The audience likes to know what to expect. Give them a reason to want to pay attention to the information you have gotten together. Such opening remarks also afford the speaker the opportunity to relate the topic to the specific audience being addressed. If you are talking to practicing physicians, they will appreciate knowing that the forthcoming material has practical daily usefulness. Academic audiences might be pleased to learn that you will describe the cutting-edge of a particular subject. Absolutely do not begin to talk by apologizing for potential shortcomings. Apologies are for inadvertent acts, not intentional errors that could have been avoided. The talk should have been prepared prospectively and rough edges smoothed out in advance.

While you are talking, always glance at every new slide you project. It is disconcerting to spend time talking about the wrong slide. During the discussion of text slides, try to use the same words as are projected. As the slides themselves may contain only phrases rather than complete sentences, fill in the additional words while talking. And talk about everything on the slide. Never include numeric data that are not referred to. In the presentation of radiologic images, it may be important to orient the audience initially. For example, "this slide shows a T2-weighted sagittal MR image of the pituitary fossa." Always describe the screen from the audience's perspective (e.g., on the left-hand slide). Use a light pointer to clearly show the audience what you wish them to see. Then turn the light off; do not wave the light around the room. If you are right-handed, place the slide advancer on the left and use your right hand for the pointer. The opposite is advocated for the left-handed person. To avoid the "trembling" pointer, it may be useful to brace the pointing wrist and forearm against another object (e.g., the podium or opposite hand/wrist) when the light is on.

In order to heighten interest, it is acceptable to occasionally ask the audience about the correct diagnosis regarding a projected image. This is best done in a rhetorical fashion with no single person expected to respond. Care must be taken not to overuse this technique so that it doesn't disrupt delivery of the message. Especially when addressing a relatively large

audience within a fixed time frame, the speaker should not solicit questions during the actual talk. Premature questions not only interrupt the flow, but often are answered by a later segment of a properly prepared talk. Therefore, as a rule, questions are best held until a lecture's close.

Avoid squandering your time with multiple "sneak previews" of what is to follow, and try not to defer messages. Mentioning a point in passing only to say "I'll come back to that later" leads the attention of the audience astray. It is even worse if the promise is not kept.

Handouts to the audience may be effective if the talk contains a lot of facts and statistics. This will ensure that the detailed supporting data will be conveyed accurately. A selective reference list also may be helpful for supplementary reading; compiling extensive written materials generally is a waste of time.

It is imperative that every talk be structured so that it ends at or before the allotted time. Exceeding your time limit reflects arrogance and bad manners, especially if other speakers are to follow. The speaker is implying that what he or she has to say is so important that the audience must sit through it regardless of any other commitment—or that the overall schedule be damned. The speaker should realize that, for example, a 1-hr lecture in reality is only about 50–55 min in length. He or she must consider the time necessary for the introduction, adjustment of the microphone, dimming of the lights, and so forth, as well as perhaps reserving a brief period at the end of the presentation for questions and answers to allow the audience to clarify any important conclusion. A potential option to help ensure finishing on time is to have several alternative endings for the presentation. After loading the essential slides, some expendable examples can be placed at the end for discussion if time permits.

### *Dual Projection*

Dual projection has only one purpose: to show comparisons. You can pair a posteroanterior chest radiograph on the left-hand screen with a lateral projection on the right-hand one, or a precontrast with a postcontrast CT scan, a CT scan with an MR image, or correlate a radiologic image with a gross pathologic specimen. The value of this technique is not to show more slides in an allotted time.

As the purpose of the technique is for comparison, the slide on the right-hand screen should always relate to that on the left. If there is no suitable companion, an opaque blank slide should be used in the right projector. The right-hand slot should never be filled with an extraneous slide showing some scenic vacation spot the speaker has visited, nor pictures of the speaker's children, pets, favorite artwork, or flowers. Although such a slide may be colorful and attractive and meant to set a relaxed mood, it is certain to divert attention from the informational slide on the left-hand screen. The viewer often wonders how the speaker will relate the slide to the text (which generally he or she doesn't).

When using dual projection, the set of slides should always be advanced simultaneously with each carousel on the same number. If you want the left-hand slide to remain on the

screen, while changing the one on the right, duplicate the former. Remember to talk about both slides.

### *Humor*

*You don't have to be solemn  
to be serious.*

William Safire

Used properly, humor can demonstrate your humanity, build a bond with the audience, and effectively drive home a point. But it must be used judiciously. Humorous remarks must be absolutely relevant to the topic and acceptable to the audience. Be aware of society's growing intolerance for cavalier comments; ethnic, sexist, or sexual gibes are verboten. Radiologic technologists should not be called "the girls."

Try never to tell a pure joke, especially when starting off a lecture. Don't try too hard to be funny; eliciting laughter is not an oratorical obligation. Audiences generally prefer hearing a carefully prepared presentation illustrated with good slides delivered in a relaxed manner rather than one full of "funny" stories. The germane anecdote, the pertinent cartoon—these are appropriate.

### *Rehearsal*

A concise, clear delivery is essential to keep the attention of the audience. There is no substitute for rehearsal to accomplish this goal. Rehearsal not only will enable the speaker to appreciate problems in structure but it also will help allay anxiety; overpreparation is the best cure for stage fright.

Initially, practice the talk alone. Avoid "ah" or "uhm" as a substitute for a brief pause, and phrases like "let's see here." However difficult, try to envision yourself as someone only slightly familiar with your subject. Project your slides in a room comparable in size to where the material will be presented. Sit down at the back of the room to ensure that all slides are visible; view them with dispassion. You may be surprised at what you see, but try to learn from it for the sake of the audience. Slides that are too busy or hard to see should now be sacrificed. Effective lecturing, like art, is partly performance, and the podium is, in effect, a stage. Belief in one's product is communicable. Enthusiasm is a vital ingredient of any successful talk, and the speaker should not say or show something relatively unimportant in a halfhearted fashion. Delete any element you are not enthralled about. Make certain that the talk consistently requires less time than that allotted; most speakers tend to embellish somewhat at the time of the actual presentation.

It is helpful to memorize the order of the slides, so that transitions between subjects or cases are smooth and you can quickly overcome any error in slide advancement. Knowing precisely what each picture shows and what the text states also is important, because part of the projected slide may be difficult to see from the podium. During the actual presentation it is best never to return to a previous slide. If you have forgotten to mention something important, try to discuss it without the slide. If you need to refer to a slide at different times in a talk, use duplicate slides.

After practicing alone, it is extremely helpful to solicit constructive criticism from a small group of colleagues. This should include persons both familiar and relatively unfamiliar with the subject matter to be presented, and at least someone with a background similar to the main composition of the intended audience. Your comrades also can time you. If your talk is too long, they can help you decide how to make it shorter. Listen to their comments, and try not to be defensive. Also, ask your colleagues to make up questions about the presentation, and practice answering them. The question period after a talk is often the most stressful portion, and it helps to be prepared. Obviously, these practice sessions should be conducted far enough in advance of the actual talk to allow time for corrections, or additions, if necessary.

### *Know Your Audiovisual Equipment*

If at all feasible, visit the room where you will be speaking before the actual presentation. See how big it is, and become familiar with the microphone, lighting, pointer, slide-advance buttons, presence of a timer and its type, lectern height, and the relationship of the podium to the screen. Locate the podium light, and turn it off during the presentation if possible. If available, wearing a clip-on microphone is preferable, because it allows the speaker to face the screen and speak. You should avoid turning your head alone without the rest of the body to prevent variation in sound level.

If there will not be a projectionist present, ensure that the projection equipment is functioning properly, and that spare batteries, bulb, and a pointer are available. The speaker should know how to fix common problems, particularly a jammed slide (which almost always results from warping of a cardboard mount). He or she should know how to remove the carousel tray quickly, after releasing it with a coin, and to retrieve and replace the jammed slide, turning a potential disaster into a deftly handled minor annoyance. Alternatively, a simple tongue depressor or a long knife can be used to guide the slide back into the carousel while the select button is pressed.

The speaker should personally load his or her slides into an 80-slide, universal carousel tray(s). Do not use the 140-slide tray, which is much more prone to jammed slides and almost never should be needed; talks are rarely longer than 50 min, and 80 slide slots, especially if dual projection is used, should be sufficient. At many meetings, there is a slide-ready room where you can verify that all of your slides are correctly oriented and in proper order. Slides that are projected upside-down or backward during the actual presentation immediately announce to the audience that the speaker is careless and make them query whether what he or she is saying can be trusted. Make certain that each slide is not bent, frayed, or dirty, and that it drops from and returns to the carousel tray correctly. Put your name and the time you are going to speak on a piece of tape and attach it to the outside of the tray. If using dual projection, label each carousel tray LEFT or RIGHT, respectively.

If you are flying to a meeting, carry the slides with you, preferably preloaded in a carousel tray or at least consecu-



tively ordered in plastic slide-mount holders. Absolutely never pack slides with your checked luggage, unless you don't care about them arriving at a destination disparate from where your presentation will be. It is advantageous to number the slides consecutively and to place a red dot on the lower left-hand corner of each slide when it is viewed in a hand-held position; this will enable quick replacement of the slide in the proper fashion if it becomes jammed or falls out of the carousel tray.

If a projectionist is available, give him or her the slides in enough time before the actual talk for discussion of any special instructions. Ascertain whether you or the projectionist will advance the first slide. If focusing or lighting assistance is needed during the presentation, courteously ask the projectionist for help.

### Conclusion

It is best to end the talk with a few brief comments repeating what you have tried to accomplish during the talk and a summary of the important points. This should be followed by a short statement of appreciation of the audience's attention, which hopefully will encourage the crowd to start applauding, and tell the projectionist to turn the slides off and the lights on.

If you ever intend to give the talk again, and want to improve it, listen carefully to any questions asked at the end of the presentation. They may suggest that certain subjects need more clarification or emphasis in the future. During the questioning, relax, be professional, and try not to be defensive. Keep answers as succinct as possible. If you do not know the answer to a question, simply say so. Be appreciative; if someone makes a very good point, tell him or her so. Realize that certain questions arise out of disagreement rather than lack of understanding, but strive to avoid argument. Be kind to the audience, and defer one-on-one confrontation until after they leave. Disagree vehemently only if the point being

made by the questioner is absolutely critical, and you are certain that he or she is wrong.

In addition, to enhance the future value of your presentation, solicit comments about the quality of the talk from individuals you know and respect in attendance. How the lecture and lecturer were perceived by the audience may be available through a more candid and nonconfrontational critique form.

Finally, remember that the word *doctor* comes from the Latin *docere*, meaning to teach. And teaching promotes learning. Instructing others will stimulate you to learn new facts and organize this updated knowledge and provides an opportunity for feedback and subsequent improvement. This old axiom is absolutely true: the person who gets the most out of a talk is the one who prepared it.

### SUGGESTED READINGS

1. Brown G, Tomlinson D. How to improve lecturing. *Med Teacher* 1979; 1:128-135
2. Chew FS. The use of a microcomputer to make rapid and inexpensive lecture slides. *AJR* 1989;152:185-188
3. Findley LJ, Antczak FJ. How to prepare and present a lecture. *JAMA* 1985;253:246
4. Garson A Jr, Gutgesell HD, Pinsky WW, McNamara DG. The 10-minute talk: organization, slides, writing, and delivery. *Am Heart J* 1986;111: 193-203
5. Hawkins C. *Speaking and writing in medicine*. Springfield, IL: Thomas, 1967
6. Hunter TB, Brewer M. Production of text and graphics slides on a personal computer. *AJR* 1985;144:1309-1312
7. Kroenke K. The lecture: where it wavers. *Am J Med* 1984;77:393-396
8. Kroenke K. The 10-minute talk. *Am J Med* 1987;83:329-330
9. Making effective lecture slides: guide to reproducing radiographic images. Rochester, NY: Eastman Kodak Publication No. M3-106, 1987
10. Simmonds D, Reynolds L. *Computer presentation of data in science*. Dordrecht, The Netherlands: Kluwer, 1989
11. The view from the back row: how to make legible slides (...and videographics too). Rochester, NY: Eastman Kodak Publication No. U9-225, 1986
12. Thompson WM, Mitchell RL, Halvorsen RA Jr, Foster WL Jr, Roberts L. Scientific presentations: what to do and what not to do. *Invest Radiol* 1987;223:244-245

## Books Received

Receipt of books is acknowledged as a courtesy to the sender. Books considered of sufficient interest are reviewed as space permits. If the book has been reviewed in the *AJR*, the date of its review is given in parentheses.

**Laser Angioplasty.** Edited by Timothy A. Sanborn. New York: Liss, 121 pp., 1989. \$49.50 (10/90)

**Computers in Diagnostic Radiology.** A Book of Selected Readings. Edited by Euclid Seeram. Springfield, IL: Thomas, 355 pp., 1989. \$58.75 (10/90)

**MRI of the Body.** Edited by Daniel Vanel and Michael T. McNamara. (Translated by Suzanne Assenat.) New York: Springer-Verlag, 385 pp., 1989. \$236.90 (10/90)

**Diagnosis of Diseases of the Chest,** 3rd ed., vol. III. By Robert G. Fraser, J. A. Peter Paré, P. D. Paré, Richard S. Fraser, and George P. Genereux. Philadelphia: Saunders, 831 pp., 1990. \$85 (10/90)

**Textbook of Interventional Cardiology.** Edited by Eric J. Topol. Philadelphia: Saunders, 954 pp., 1990. \$95 (10/90)

**How to Measure Angles from Foot Radiographs.** A Primer. By Alan E. Oestreich. New York: Springer-Verlag, 48 pp., 1990. \$19.95 (10/90)

**Magnetic Resonance Imaging of Central Nervous System Diseases.** Functional Anatomy, Imaging, Neurological Symptoms, Pathology. By W. J. Huk, G. Gademann, and G. Friedmann. (Translated by Terry Telger.) New York: Springer-Verlag, 450 pp., 1990. \$295 (10/90)

**The Nucleus of Cardiac Diagnosis.** Electrocardiography and Chest X-Ray. By William A. Schiavone. Philadelphia: Lea & Febiger, 287 pp., 1990. \$34 (10/90)

**Practical Color Atlas of Sectional Anatomy.** Chest, Abdomen, and Pelvis. By E. A. Lyons. New York: Raven, 320 pp., 1990. \$56, softcover (11/90)

**Genitourinary Radiology.** A Multimodality Approach. By Rosalyn Kutcher and Everett M. Loutin. New York: Gower Medical, 280 pp., 1990. \$95 (11/90)

**Progress in Cardiology.** Update on Cardiac Imaging. Edited by Douglas P. Zipes and Derek J. Rowlands. Philadelphia: Lea & Febiger, 1990;3(2):1-239, softcover; by subscription, 2 issues (1 year) for \$49.50; 4 issues (2 years) for \$85 (11/90)

**CT and MRI of the Thorax.** Edited by Elias A. Zerhouni. (Vol. 11 in Contemporary Issues in Tomography.) New York: Churchill Livingstone, 222 pp., 1990. \$62 (11/90)

**Duplex Doppler Ultrasound.** (Vol. 26 in Clinics in Diagnostic Ultrasound.) Edited by Kenneth J. W. Taylor and D. Eugene Strandness, Jr. New York: Churchill Livingstone, 182 pp., 1990. \$55 (11/90)

**New Techniques in Metabolic Bone Disease.** By John C. Stevenson. Stoneham, MA: Butterworths, 287 pp., 1990. \$175 (11/90)

**Magnetic Resonance Imaging of the Spine.** By Michael T. Modic, Thomas J. Masaryk, and Jeffrey S. Ross. Chicago: Year Book Medical, 280 pp., 1989. \$110 (11/90)

**Primer of Medical Radiobiology,** 2nd ed. By Elizabeth LaTorre Travis. Chicago: Year Book Medical, 302 pp., 1989. \$29.25, softcover (12/90)

**Nonionizing Radiation Protection,** 2nd ed. (WHO Regional Publications, European Series, No. 25.) Edited by Michael J. Suess and Deirdre A. Benwell-Morison. Copenhagen: World Health Organization, Regional Office for Europe, 346 pp. 1989. \$34.40 (12/90)

**Imaging Principles of Cardiac Angiography.** By Robert J. Moore. Rockville, MD: Aspen, 258 pp., 1990. \$59 (12/90)

**Magnetic Resonance Imaging and Computed Tomography of the Head and Spine.** By C. Barrie Grossman. Baltimore: Williams & Wilkins, 465 pp., 1990. \$125 (12/90)

**RSNA Today,** Vol. 4, No. 1. Oak Brook, IL: The Radiological Society of North America, 1990. \$55; by subscription, 6 issues annually at \$185 for RSNA members and \$225 for nonmembers (VHS videotape) (12/90)

**Stedman's Medical Dictionary,** 25th ed. Baltimore: Williams & Wilkins, 1784 pp., 1990. \$38.95 (12/90)

**Clinical Magnetic Resonance Imaging.** Edited by Robert R. Edelman and John R. Hesselink. Philadelphia: Saunders, 1192 pp., 1990. \$165 (12/90)

**Endosonography.** Edited by Bruno D. Fornage. Boston: Kluwer, 186 pp., 1989. \$129 (12/90)

**Radiology of Bone Diseases,** 5th ed. By George B. Greenfield. Philadelphia: Lippincott, 1024 pp., 1990. \$95 (12/90)

**MacDose.** Version 2.1; User's Manual. Edited by Russell K. Hobbie. Madison, WI: Medical Physics Publishing, 28 pp., 3.5-in. disk included. 1989. \$30 (12/90)

**The Radiology Word Book.** By Theresa Indovina and Wilburta Q. (Billie) Lindh. Philadelphia: Davis, 504 pp., 1990. \$22.95, softcover (12/90)

**Neuro-Oncology.** Primary Malignant Brain Tumors. Edited by David G. T. Thomas. Baltimore: The Johns Hopkins University Press, 303 pp., 1990. \$62.50

**Plasticity and Morphology of the Central Nervous System.** Edited by C. L. Cazzullo, E. Sacchetti, G. Conte, G. Invernizzi, and A. Vita. Boston: Kluwer, 256 pp., 1990. \$70

**Clinical Application of Radiolabelled Platelets.** Edited by Ch. Kessler, M. R. Hardeman, H. Henningsen, and J.-N. Petrovici. Boston: Kluwer, 295 pp., 1990. \$89

**Clinical Neutron Dosimetry.** Part I. Determination of Absorbed Dose in a Patient Treated by External Beams of Fast Neutrons. By ICRU. Bethesda, MD: ICRU, 90 pp., 1989. \$18



## Meeting News

### Tenth Meeting and Postgraduate Course of the Society of Uroradiology, September 1990

Elizabeth Whalen<sup>1</sup>

The tenth meeting and postgraduate course of the Society of Uroradiology was held September 8–14, 1990, at the Westin Bayshore Hotel, Vancouver, B.C., Canada. This report covers the first 2 days, which were devoted to the scientific session. During this session, 33 scientific papers were presented, including 25 from the United States and eight from other countries (including Denmark, England, France, Germany, Israel, and the Netherlands). Space limitations do not allow discussions of all the papers presented, but this report includes papers from the major topics covered: pediatric uroradiology, uroradiologic techniques (interventional uroradiology, contrast media, CT, MR imaging, and sonography), and uroradiologic terminology.

Sharing the award for best presentation at this year's scientific session were Henrik Thomsen, who reported on the effects of contrast material in rats with gentamicin-induced nephropathy, and Bruce L. McClennan, who discussed color Doppler imaging of the ureteral jet.

#### Pediatric Uroradiology

##### *Unsuspected Double Collecting Systems*

Robert L. Lebowitz (Children's Hospital, Boston) discussed the unsuspected double collecting system in children; he emphasized that some double collecting systems cannot be detected by today's imaging methods and that nondetection

should be neither a cause of consternation for surgeons nor a source of embarrassment for radiologists. At Children's Hospital between 1976 and 1989, unsuspected double collecting systems were found in six children (four girls, two boys; age range, 3.5–7.0 years). Urinary tract infection was present in five cases; in the other case, CT of the abdomen after trauma showed hydronephrosis. All six patients were thought to have reflux into a single system, and the double system was found only when the bladder was opened to reimplant the ureter. Double collecting systems were not shown on any of the preoperative imaging studies, which included voiding cystourethrography (six patients), cystoscopy (six), excretory urography (four), and sonography (two). In all cases, retrograde ureterography done at the time of surgery showed that the previously unsuspected upper-pole ureter ended blindly at the level of the kidney. Neither cystoscopy nor imaging tests are able to show this type of double collecting system. Radiologists should not be concerned about missing these duplex systems, however, because they do not cause problems for the patient. The occult double collecting system will either be found at surgery or, if no surgery is performed, will exist without harm to the patient.

##### *Spinning-Top Urethra*

Another of the pediatric uroradiology presentations concerned spinning-top urethra in boys with bladder instability.

<sup>1</sup> Contributing editor, *American Journal of Roentgenology*, Ste. 200, 2223 Avenida de la Playa, La Jolla, CA 92037.

Editor's note.—"Meeting News" articles report the highlights of important national radiology meetings. The intent is to provide Journal readers with succinct, substantive, and accurate reviews of topics of current interest, written in a readable fashion and published promptly after the meeting.

The articles will not undergo the peer review usually required of *AJR* publications, nor will they offer a critique of the information provided. The sole purpose of the series is to apprise *AJR* readers of topics of current concern in an interesting and timely fashion.

As Hugh M. Saxton (Guy's Hospital, London, United Kingdom) remarked, a spinning-top urethra, which looks like the child's toy on voiding cystourethrography, has been considered a normal variant in girls. His own recent studies, however, indicate that this appearance may be associated with bladder instability and sometimes with a wide bladder neck. Between 1987 and 1990, 153 children (<15 years old) were studied for urinary frequency; the group included 107 girls and 46 boys. Forty-eight (45%) of the girls and four (9%) of the boys had spinning-top urethra. The group discussed in this presentation included these four boys and two other boys, all of whom presented with symptoms that indicated bladder instability (urinary frequency, urgency, and sometimes daytime wetting). Bladder instability was confirmed by video urodynamic studies. No patient had evidence of prune-belly syndrome, obstruction, or neuropathy. Patients with spinning-top urethra experience large bladder contractions that are resisted by voluntary sphincter overactivity so that a little leakage of urine occurs during each contraction. Saxton stressed that urodynamic imaging is necessary to confirm the diagnosis.

### Uroradiologic Methods

#### *Interventional Uroradiology*

*Percutaneous endopyelotomy.*—Experience with percutaneous endopyelotomy (the endoscopic pyelotomy of the ureteropelvic junction and stenting via the percutaneous nephrostomy—essentially, a closed version of the Davis intubated ureterotomy) in 100 patients was reported by Won J. Lee (Long Island Jewish Medical Center, New Hyde Park, NY). The indication for the procedure was primary obstruction in 32 patients and secondary obstruction in 68 patients. Preoperative evaluation consisted of some combination of the following studies: excretory urography (100 patients), furosemide renography (62), retrograde pyelography (17), Whitaker test (11), and renal angiography (one). After the procedure, patients were evaluated by nephrostography at 48 hours and before removal of the stent and excretory urography at 3–6 months and at 1 year. If assessed by clinical criteria, the procedure was successful in 88% of the cases: 27 (84%) of the primary obstructions, 61 (90%) of the secondary obstructions. If the procedure was assessed by radiologic criteria, the success rate was 85%. Although this is a lower success rate than usually is achieved by open pyeloplasty, use of percutaneous endopyelotomy has the important advantages of minimal morbidity and significantly shorter hospital stay and convalescence time. The number of complications from percutaneous endopyelotomy decreased dramatically as experience with the procedure was gained. In the first 60 patients, five major complications and 30 minor complications occurred; in the next 40 patients, only one major complication and 14 minor complications occurred. This improvement probably resulted from experience with the difficult aspects of this procedure (e.g., large extravasation and small operative field) and stent evolution. Working closely with the urologist both to locate the ureteropelvic junction and to place the stent allows successful percutaneous endopyelotomies with few complications.

#### *Biopsy Complications*

John J. Cronan (Rhode Island Hospital, Providence) discussed the risks of renal biopsy for benign kidney disease. In a 5-year study, he and his colleagues have performed 307 CT-guided renal biopsies in 238 patients (age range, 4–79 years). The Franklin modification of the Vim-Silverman needle was used, and 1-cm-thick, enhanced, axial CT scans were obtained. A successful biopsy recovers 15–20 glomeruli; in this study, an average of 42 glomeruli per tissue sample was obtained. Moreover, the tissue-recovery rate was 100%; the amount of tissue was always sufficient for laboratory tests (even when special tests were required); and a final histopathologic diagnosis was obtained in every case. No instances of anuria, obstruction, hypertension, or infection occurred; one patient died. All patients experienced mild to moderate flank pain and microhematuria. In 18 cases, clinically evident hemorrhage occurred. Bleeding was seen more often in women (9%) than in men (7%) and more often in left-sided biopsies (9%) than in right-sided biopsies (6%). Patients undergoing hemodialysis were at greatest risk for developing hemorrhage (bleeding occurred in 24% of the hemodialysis patients but only in 6% of the other patients). These data confirm the necessity for screening patients who are being considered for large-bore renal biopsy and for monitoring the patients in the hospital for 1–2 days after the procedure. In answer to a question from a participant, Dr. Cronan said that CT was used rather than sonography for guidance because it is easier to use (especially in obese patients) and because CT is comparable in cost to sonography at his institution.

Another study concerning complications of biopsies was presented by John T. Cuttino (Lahey Medical Center, Burlington, MA). After performing a literature search to find the average complication rate reported after prostatic biopsy, these researchers reviewed patients' charts at least 3 months after the biopsy and then surveyed by telephone 214 patients who had undergone a sonographically guided prostatic biopsy (the median time at which these patients were contacted was 15 days after their procedures). The indications for prostatic biopsy in the patients studied included palpable mass/induration, abnormal results on transrectal sonography, and strong suspicion of prostatic cancer. The percentage of patients who experienced complications according to the telephone survey and chart review, respectively, were as follows: hematuria, 45.8% and 0.5%; blood clots in urine, 12.2% and 0.5%; hemospermia, 22.4% and 0.5%; hematochezia, 11.7% and 0.5%; dysuria, 7.5% and 0%; pain at biopsy site, 5.1% and 0%; and pain with bowel movement, 2.8% and 0%; urosepsis, 1.4% and 0.9%; orchitis, 0.9% and 0%; and uncomplicated urinary tract infection, 0.5% and 0.9%. In all but one category of complication, the chart review resulted in a sometimes serious underestimation of the complication rate. The telephone survey seems to be much more accurate; however, it is too time-consuming to do routinely.

#### *Contrast Material*

*Contrast material complications.*—Henrik S. Thomsen (Herlev Hospital, University of Copenhagen, Herlev, Denmark)



presented the award-winning study about the effects of IV administration of diatrizoate and iohexol in rats with gentamicin-induced nephropathy (tubulointerstitial nephritis). The urine profiles studied included albumin, glucose, sodium, and the enzymes NAG, OGT, and LDH; serum profiles and kidney histology also were examined. Daily injections of gentamicin into rats demonstrated the four stages of gentamicin-induced nephropathy: first week, no change; second week, degeneration phase; third week, regeneration phase; and fourth week, necrosis no longer present. In this study, one group of rats (control) received neither gentamicin nor contrast material; one group received gentamicin and saline but no contrast material; another group received gentamicin and diatrizoate (an ionic contrast agent); and another group received gentamicin and iohexol (a nonionic contrast agent). In one series, rats received the injections after 14 daily doses of gentamicin (at the beginning of the regeneration phase). In both series, tubular dysfunction was worsened more by iohexol than it was by diatrizoate, but no difference was seen in the glomerular effects of the two contrast media. Specifically, light-microscopy studies revealed a more prolonged occurrence of tubular necrosis and a more intensive round cell infiltration in the iohexol group than in either the saline or diatrizoate group. Dr. Thomsen applied his results to the clinical setting by noting that reduced renal function may be due to many factors (such as infection and dehydration, as well as contrast media) and that this study suggests that gentamicin and contrast media may be a harmful combination.

A study concerning the use of nonionic contrast media in patients who have had serious reactions to ionic agents was presented by Harry W. Fischer (Green Valley, AZ). The results included 1989–1990 (and prior) data from Rochester, NY, and showed that the use of nonionic contrast material in previous reactors dramatically reduces the risk of a second reaction. In 106 patients who had previously experienced reactions to ionic contrast material, only six (6%) reactions occurred, compared with an expected occurrence of up to 44% if ionic agents had been used. No deaths occurred, and all reactions observed were less severe than the reactions the patients had experienced with ionic contrast agents. Discussion after this presentation revealed that seven of the meeting attendees had seen deaths resulting from the administration of nonionic contrast material. Also, Dr. Fischer reported that he had seen three patients who did not have reactions to ionic contrast material react to the administration of a nonionic agent; the reason for this phenomenon is not yet known.

Richard H. Cohan (Eastern Virginia Medical Center, Norfolk) discussed the use of dilution to decrease the cutaneous toxicity of ionic contrast material should extravasation occur. Although large-volume extravasations of contrast material are rare, they are potentially catastrophic. Dr. Cohan and his colleagues studied the effects of extravasation of three different dilutions of contrast material 48 hr after injection. Sixty-four adult male Sprague-Dawley rats were anesthetized and given subcutaneous injections of nondiluted (0.5 ml) or diluted (with 0.1, 0.2, or 0.3 ml of sterile water) Renografin M60 into the distal thigh. At 48 hr after injection, the rats were sacrificed, and scores for necrosis, edema, and hemorrhage were

recorded. Only in one category did dilution of the contrast material improve symptoms significantly; the group receiving Renografin plus 0.3 ml of water had significantly less hemorrhage than did the group receiving undiluted Renografin. Some rats had severe skin reactions, and some had no reactions at all. Dilution of contrast material does not seem to be an effective method of preventing damage from contrast material extravasation.

*Measurement of glomerular filtration rate.*—Use of gadopentetate dimeglumine to determine glomerular filtration rate was studied by Peter L. Choyke and colleagues (National Institutes of Health, Bethesda, MD). Current filtration markers are either inaccurate or unavailable. Gadopentetate dimeglumine is readily filtered (not secreted) and is analogous to Tc-DTPA. Tc-DTPA is an accurate marker, but is radioactive, and therefore requires licensed facilities. A linear relationship has been found between concentrations of gadopentetate dimeglumine and T1 relaxivity (1/T1). Glomerular filtration rates of gadolinium and technetium were compared in 60 patients (37 with uveitis, 13 with multiple sclerosis, and 10 with membranous glomerulonephritis). Gadopentetate dimeglumine clearance methods showed excellent correlation with Tc-DTPA methods, and gadolinium is not radioactive.

#### CT

*CT of renal lymphoma.*—N. Reed Dunnick and colleagues (Duke University Medical Center, Durham, NC) retrospectively reviewed the records of 29 patients (28 with non-Hodgkin lymphoma and one with Hodgkin lymphoma) to investigate whether the most common CT manifestation of renal lymphoma (bilateral renal masses) usually is associated with retroperitoneal lymph node enlargement, as is suggested by some recent studies. Of the 29 patients studied, a solitary mass was seen in 3% and multiple masses were seen in 59%; 11% showed perirenal infiltration and 28% showed infiltration from adjacent tumor. Only 55% of all patients had accompanying disease; of the patients with multiple renal masses, only 41% had accompanying disease. These results indicate that radiologists may miss some renal lymphomas if they expect the bilateral renal masses of renal lymphoma always to be associated with retroperitoneal lymphadenopathy. Dr. Dunnick mentioned one patient whose unenhanced CT scans and MR images looked normal and whose sonograms looked nearly normal; only gadolinium-enhanced MR images showed the masses of Hodgkin lymphoma. On contrast-enhanced CT scans, renal masses are often homogeneous (60% in this group) or mildly heterogeneous (40%); also, contour deformity is missing in some (29%), mild in many others (49%), and obvious only occasionally (24%).

*CT after resection of rectal carcinoma.*—CT of the urinary tract after abdominoperineal resection for rectal carcinoma was the subject of a presentation by Marjorie Hertz (The Chaim Sheba Medical Center, Tel Hashomer, Israel). In the study group of 43 patients (26 men, 17 women; age range, 33–88; mean age, 62), the bladder was displaced postoperatively in 15 patients. Twenty-one patients developed a presacral mass after resection. Of these, seven were fibrotic

masses: in five of these patients, no change in the mass was seen at follow-up studies; in one, fibrosis was proved at surgery; and one patient was clinically normal at follow-up. Seven of the presacral masses proved to be inflammatory processes. The remaining seven presacral masses were recurrent carcinoma: two recurrences were indicated by mass enlargement, two by positive biopsy results, two by clinical observation, and one by proved bone destruction. In the 21 patients with a postoperative presacral mass, the patients with fibrosis all had normal collecting systems, those with inflammatory processes had slight dilatation of the upper collecting system, and all those with malignant tumors had dilatation (some had severe dilatation). These results suggest that hydronephrosis in the presence of a presacral mass after abdominoperineal resection indicates recurrent malignancy.

*Acquired renal cystic disease (ARCD) and renal cell carcinoma (RCC) in dialysis patients.*—This 7-year, prospective, longitudinal CT study sparked much controversy in the scientific session. Errol Levine (Bell Memorial Hospital, University of Kansas Medical Center, Kansas City) began his presentation by stating that because patients undergoing dialysis have an increased prevalence of RCC, some researchers have recommended periodic renal imaging for all dialysis patients; however, the influence of renal neoplasms on the morbidity and mortality of dialysis patients is unknown, and cost must be considered if annual renal CT examinations are to be recommended for the more than 100,000 patients being treated with dialysis in the United States. The study material consisted of 88 CT scans of 30 long-term dialysis patients (mean follow-up, 55 months). At the end of the study, 16 (53%) of the patients were alive, and 14 (47%) had died (cause of death was cancer in four patients, including RCC in one). ARCD was seen in 87% of patients (compared with 57% at the start of the study); two patients developed renal neoplasms (histologically proved invasive RCC), which indicates an annual RCC incidence in dialysis patients that is six times greater than that in the general population. On the basis of life expectancy of dialysis patients and costs of screening, these researchers concluded that routine annual screening is not justified. However, they suggested screening for select patients, including high-risk patients (e.g., those with hematuria or flank pain; unexplained fever or systemic illness; or predisposing factors to RCC, such as more than 3 years of dialysis, ARCD, and male gender) and patients whose general medical condition is good (e.g., patients who are young, fit, and potential transplant recipients). A lively discussion focused on two questions: a scientific question of whether the data gathered supported the researchers' conclusions and a social/ethical question about whether any patients should be denied the possible detection of disease.

*Detection of bladder rupture.*—In this study of CT evaluation of bladder injuries in trauma patients, Phil J. Kenney and colleagues (University of Alabama at Birmingham) reported on 16 patients with bladder rupture; 14 underwent both CT and cystography; in two patients with urethral disruption, cystography could not be performed. Most of these patients had other injuries indicating the need for CT studies, and these researchers investigated whether cystography adds any information about bladder injuries in patients who will be

studied with CT in any case. Imaging results were compared with surgical findings in 10 patients, autopsy results in one, and follow-up data in five. Nine patients had extraperitoneal ruptures, three had intraperitoneal ruptures, and two had both; the other two patients had interstitial leaks. CT findings were correct in 13 (81%) cases; in three cases, CT findings were false-negative. In 10 cases, correct diagnoses were derived from cystographic findings; in four cases, cystographic results were false-negative. In no case did cystography add information when CT showed a bladder rupture. However, in two cases in which CT missed an extraperitoneal rupture, cystography results were positive. Lack of bladder distension on CT was the apparent cause of the false-negative results. Dr. Kenney and colleagues concluded that if a patient requires CT, cystography need not be performed before the CT examination and can be eliminated if CT scans show positive results. False-negatives may be reduced by direct bladder distension (CT cystogram), although that was not done in the study.

*Hyperdense adrenal glands in trauma patients.*—Dr. Kenney also presented a study of enhanced CT scans in trauma patients. These investigators had noticed hyperdense adrenal glands on CT scans of six patients who, although initially stable, became hypotensive in the radiology department. To further evaluate this sign as a possible indication of a life-threatening injury, they retrospectively reviewed the records of 50 normotensive patients undergoing routine CT and 50 stable patients undergoing CT after blunt trauma. The definition used for "hyperdense adrenal" was an adrenal gland as dense as adjacent vessels (aorta and inferior vena cava) on IV bolus-enhanced CT (images were obtained about 90–120 sec after injection of the contrast material). Of the six index patients with hyperdense adrenal glands, four died (one soon after surgery, one 2 hr after CT, one 28.5 hr after surgery, and one 13 hr after CT) and two survived (one recovered well and was discharged 7 days after CT and one is comatose). Of the 50 patients undergoing routine CT, none had a hyperdense adrenal gland, and none died within 24 hr; of the 50 stable trauma patients, none had a hyperdense adrenal gland, but one died soon after the scan. Technique is important; four possible pitfalls were found during the study: (1) early imaging after the injection of the contrast material may show a pseudohyperdense adrenal gland, (2) late imaging—during contrast washout—may miss a hyperdense adrenal gland, (3) the presence of fatty liver may be confusing, and (4) an infarcted adrenal gland will not enhance. In conclusion, the hyperdense adrenal gland seems to be a significant indicator of a life-threatening condition.

#### MR Imaging

*Dynamic, contrast-enhanced RASE MR imaging of renal masses.*—The value of conventional MR imaging of the kidney is decreased by poor lesion conspicuity, suboptimal lesion characterization, and respiratory motion artifacts. Joseph K. T. Lee and colleagues (Mallinckrodt Institute of Radiology, St. Louis, MO) prospectively studied 18 patients with 67 renal masses with both standard T1- and T2-weighted spin-echo



sequences and rapid-acquisition, spin-echo (RASE) imaging. The RASE technique uses a short TR/TE spin-echo sequence with half-Fourier sampling; 11 slices can be obtained in 23 sec, and the entire kidney can be surveyed during suspended respiration. As gadopentetate dimeglumine (Magnevist, Berlex Imaging, Cedar Knolls, NJ) has now been approved by the FDA, these researchers also compared enhanced and unenhanced RASE images. Diagnoses of the 67 masses (58 simple renal cysts, eight solid renal neoplasms, and one pseudotumor) were confirmed by surgery or CT. In subjective evaluations of image quality, 93% of the enhanced RASE images were rated good or excellent, compared with 85% of unenhanced RASE images and 53% of enhanced T1-weighted images; dynamic enhanced RASE images were found to be useful in 72% of cases. For cysts, sensitivities for lesion detection of unenhanced T1-weighted, T2-weighted, and RASE images were 24%, 45%, and 26%, respectively; for solid neoplasms, the sensitivities were 75%, 57%, and 75%, respectively. In all cases, contrast enhancement increased these sensitivities; this was especially true for lesions smaller than 1 cm. A combination of pre- and post-gadolinium RASE images and T2-weighted images seems to be an excellent protocol to both detect and characterize renal masses.

**MR imaging of intraabdominal fluid collections.**—Annick Pinet (Hôpital Edouard Herriot, Lyon, France) presented a study to determine the value of MR imaging in the detection and discrimination of intraabdominal fluid collections in recipients of pancreatic or kidney transplants. They performed 31 MR studies in 29 patients (19 with both kidney and pancreas transplants, nine with kidney transplants only, and one with a pancreas transplant only). All 23 fluid collections in 16 patients were identified on MR images; the sensitivity of MR imaging was higher than that of CT in these cases. In 17 fluid collections verified by puncture, surgery, or fluid analysis, MR imaging helped locate the origin of the collection (pancreatic juice, six; lymphoceles, five; hematoma, three; abscess, two; and urinoma, one). On T1-weighted images, homogeneous urinelike signals were seen in urinoma, lymphoceles, pancreatic juice, and one of two abscesses. The same type of signal on T2-weighted images was seen in urinoma and abscess (single-echo studies) and in urinoma and one of five lymphoceles (double-echo studies). Homogeneous musculike signal on T1-weighted images indicated recent (<7 days) hematoma; one abscess also showed this type of signal. Abscesses also were shown by a heterogeneous urinelike signal on double-echo T2-weighted images. Hematomas were shown especially well on T2-weighted images by a heterogeneous hyperintense signal.

**MR imaging of testicular remnants.**—Identification and localization of the undescended testicle by MR imaging was studied by Peggy J. Fritzsche and colleagues (Loma Linda University Medical Center, Loma Linda, CA). In 20 patients with 23 nonpalpable testes, MR results were correlated with surgical and histologic findings. MR field strengths used were 1.0 T in 16 patients and 0.5 T in seven; in all patients, T2-weighted transverse and T1-weighted coronal images were obtained, and T1-weighted sagittal images also were obtained in 12 patients. Although the study was retrospective, the MR

images were interpreted without knowledge of the surgical or histologic results, and the confidence level of interpretation was rated for each plane. These researchers found that MR imaging can locate undescended testes (19/19 locations were proved correct at surgery) and can identify testicular remnants (MR imaging visualized seven remnants, six of which were confirmed and one of which was a false-positive finding). On T2-weighted images, low signal intensity correlated well with testicular remnants, and high signal intensity correlated well with the presence of a testis. Use of three planar views (with triangulation and with a confidence-level scoring system) and thorough knowledge of testicular and pelvic anatomy are needed for effective use of MR imaging of undescended testes and testicular remnants. Discussion focused on the use of sonography for locating undescended testes: Dr. Fritzsche pointed out that sonography is not very helpful for identifying structures above the internal inguinal ring, but she agreed it would be interesting to investigate color Doppler imaging for evaluation of vessels in this area, specifically in the inguinal canal.

**Experimental design of MR studies.**—John R. Thornbury (University Hospital & Clinics, Madison, WI) discussed ways to improve the scientific value of current studies in MR imaging. To date, three factors have limited the efficacy of MR research: insufficient sample size, referral bias, and biases related to the reference standard. In terms of sample size, analysis by receiver-operating-characteristic (ROC) curves requires a minimum of 50–70 patients. Referral bias taints studies when the patients imaged are different from the general population (e.g., when only patients with a high probability of having a condition are imaged); this bias limits the generalization of the results. The true-positive rate is artificially increased by three types of reference standard bias: (1) work-up biases, in which imaging results contribute to the inclusion or exclusion of a case from the study; (2) diagnostic review bias, in which the diagnosis is affected by imaging results; and (3) test review bias, in which the final diagnosis or comparison-examination result is used in interpreting MR results. Dr. Thornbury suggested several methods to offset the biases and shortcomings often seen in MR imaging research. Two helpful steps are performing both MR imaging and the competing technique in all patients and documenting the pretest probability of the diagnosis being studied in all patients. Also, results should be interpreted in a randomized, blinded fashion, and the true diagnosis should be determined by an interdisciplinary panel of experts (including clinicians). Whenever possible, use of histology results and a sufficiently large sample size will improve the validity of study results. Finally, researchers can expand data collection and analysis by determining diagnostic, therapeutic, and patient-outcome efficacy and by performing formal cost-effectiveness and cost-benefit analyses. After the presentation, Dr. Dunnick suggested that including a statistician at the beginning of a study helps avoid statistical biases.

### Sonography

**Color Doppler flow imaging of the prostate.**—Matthew D. Rifkin (Thomas Jefferson University Hospital, Philadelphia)

described an interesting study of color Doppler flow sonography of the prostate. Conventional duplex Doppler studies have not had promising results in this area, but because color Doppler studies have successfully revealed abnormal vascular patterns in a variety of nonprostatic diseases, these investigators studied color Doppler flow imaging in patients undergoing endorectal sonography for diagnosis and biopsy of the prostate. The preliminary results are based on 125 men, 16 of whom have undergone radical prostatectomy. Color Doppler flow results were surprisingly helpful, indicating that prostatic cancer may be a more vascular process than was previously thought. Although color Doppler flow imaging does not yet yield a definite diagnosis, these researchers have shown that the normal peripheral prostate has very little flow and that the normal neurovascular bundle shows a combination of arterial and vascular flow as well as variable resistance. Benign prostatic hyperplasia is seen as a combination of high-resistance (occasionally low-resistance) venous flow and, occasionally, surgical capsule flow; the color-flow appearance of prostatitis is increased flow and low resistance. In cancer patients, resistance is generally low, and surprisingly, focal increased flow is seen within the lesion or peripheral to the lesion. Dr. Rifkin concluded that color Doppler flow imaging is an effective adjunct to conventional gray-scale techniques; it may yield additional information, delineate lesions that need further evaluation, and provide data that is more tissue-specific than findings from conventional sonographic studies.

*Color Doppler imaging in renal transplant infarction.*—Ten recipients of kidney transplants who developed ischemia or infarction were studied by Syed Z. H. Jafri and colleagues (William Beaumont Hospital, Royal Oak, MI). Both gray-scale and color Doppler sonograms were obtained in the patients, prospectively in nine and postoperatively in one. All these patients had received cadaver allografts (donor ages—which may have significance—were 1–10 years in four, 11–20 years in one, 20–30 years in two, and unknown in three). Infarcts were located in the upper pole in five cases, both the upper and lower poles in three cases, upper and mid kidney in one, and the lower pole in one. On gray-scale sonography, early findings included increased parenchymal echogenicity (nine), loss of corticomedullary detail (eight), and hyperechoic vascular grooves (eight). Focal areas of liquefaction and loss of parenchymal substance were late findings. With color Doppler imaging, hypoperfusion was shown in nine cases, attenuated intrarenal vessels in eight, vessels within a hyperechoic groove in eight, and tissue vibrations in three (one case of arterial kink and two cases of renal artery stenoses). The causes of ischemia and infarction in these cases are not yet clear; however, possible mechanisms include surgical technique (e.g., use of renal artery dilators), harvesting technique, and use of kidneys from very young donors. The results of this study indicate that ischemia and focal infarction after renal transplantation can be detected by both color Doppler and gray-scale sonography.

*Color Doppler imaging of the ureteral jets.*—In his award-winning presentation, Bruce L. McClennan (Mallinckrodt Institute of Radiology, St. Louis, MO) reported the results of a study to determine whether color Doppler sonography can help characterize the ureteral jet in normal subjects and detect

ureteral obstruction in symptomatic patients. The efflux of contrast-laden urine (jet) from the ureteral orifice has long been recognized on urography. Gray-scale sonographic studies have described the ureteral jet phenomenon, and in vitro studies have shown its origin to be the reflections that arise from density differences between intravesicle urine and ureteral urine. Color Doppler imaging was used to study 17 normal subjects and 26 patients with ureteral stones and obstruction. In the normal subjects, ureteral jets were flame-shaped, with the highest frequency shift at the orifice; the frequency, duration, and shape of the ureteral jets were relatively symmetric in each normal subject. In patients with obstruction, color Doppler sonography showed three different patterns and asymmetry in the ureteral jets. In 12 patients, urine flow (ureteral jet) was completely absent; in four others, a continuous, low-level flow was seen from the symptomatic ureteral orifice. Obstruction correlated better with the appearance of the ureteral jets than it did with the degree of hydronephrosis seen on urography. These researchers concluded that unilateral ureteral obstruction causes asymmetry of ureteral jets and that color Doppler sonography allows simultaneous visualization of both jets. Potential uses for color Doppler imaging of ureteral jets include further evaluation of hydronephrosis, expediting of diagnoses of high-grade vs partial obstruction when urography shows that the pyelogram is delayed, and evaluation of ureteral obstruction in pregnant patients and in patients with either poor venous access or a history of reactions to contrast media.

*Duplex and color Doppler imaging in vasculogenic impotence.*—The cause of impotence may be psychogenic, organic, or a combination of the two. One type of organically caused impotence is related to vascular abnormalities; duplex color Doppler imaging is evolving as an effective noninvasive method to assess patients with possible vasculogenic impotence. Robert R. Hattery (Mayo Clinic, Rochester, MN) discussed this use of color Doppler sonography on the basis of experience with approximately 1000 patients. The standard sonographic examination of the penis includes gray-scale imaging, measurement of vessel diameter, peak systolic velocities, end-diastolic velocities, and analysis of the Doppler waveform of the cavernosal arteries at 5, 10, 15, and 20 min. Also, velocities in the dorsal arteries and dorsal vein may be of more significance than previously stressed. Dr. Hattery said that one indication of arterial disease may be a large difference in the blood-flow velocities of the right and left cavernosal arteries and systolic flow reversal. Some possible causes of these findings include arterial occlusive disease, Peyronie disease, arteriosinusoidal fistulas, collateral vessels, and variations in anatomy. Researchers are continuing to work to advance the art of detecting and treating vasculogenic impotence by use of duplex color Doppler evaluation of penile hemodynamics.

*Transvaginal color Doppler sonography of the ovary.*—In a presentation made by Arthur C. Fleischer (Vanderbilt University Medical Center, Nashville, TN), a study was described in which transvaginal imaging was used with color Doppler sonography to evaluate ovarian masses. In 30 patients and 12 control subjects, a 5.0-MHz curvilinear prototype probe was used to perform transvaginal color Doppler sonography.



In both patients and control subjects, the pulsatility indexes of intraovarian arteries were calculated, and the location and the velocities of venous flow were recorded. The range of the pulsatility indexes were as follows: 0.7–3.8 (mean, 1.8) for normal ovarian arteries and 0.3–0.9 (mean, 0.7) for 20 ovarian masses. Direct surgical correlation was obtained in all patients (all the masses were sufficiently large that the clinicians did not feel comfortable with “only observation” follow-up). Analysis of the results indicated that the pulsatility indexes and venous flow of benign ovarian masses differ from those of malignant ovarian masses; however, some diagnostic problems are caused by benign lesions that incite large peritoneal reactions, and some overlap occurs between vascular benign masses and relatively avascular malignant masses.

### Uroradiologic Terminology

Stanford M. Goldman (Francis Scott Key Medical Center, Baltimore, MD) provided an interesting discussion of the confused and confusing terms used to describe pyelonephritis. In the past 25 years, many new terms have been coined concerning this condition, including suppurative pyelonephritis; acute bacterial nephritis; acute pyelonephritis; focal bacterial nephritis; focal bacterial nephronia; preabscess, pseudoabscess, and chronic pyelonephritis; reflux nephropathy; chronic atrophic pyelonephritis; and interstitial nephritis. Little radiologic or pathologic correlation exists for so many distinct conditions; moreover, a review of radiologic, urologic, and pathologic textbooks showed that different definitions are used by different authors, and some terms are simply not used by some authors. The problem is further compounded by the physiologic facts about renal infection: the disease is not static in any given patient but changes constantly, the disease may affect one area of the kidney differently from another, the disease may affect each kidney differently, and two or more disease states may involve the same kidney simultaneously. Dr. Goldman suggested a return to the original pathologic terms in order to make textbook descriptions consistent. He proposed these four main classifications: (1) *diffuse acute infectious pyelonephritis* (including acute pyelitis, acute interstitial nephritis, and acute bacterial nephritis); one subgroup: *severe acute infectious pyelonephritis* (including acute bacterial nephritis and acute suppurative nephritis); (2) *focal acute infectious pyelonephritis* (including focal lobar nephronia and focal bacterial nephritis); (3) *the preabscess state* (including focal lobar nephronia and pseudoabscess); and (4) *intrarenal abscess*. Goldman also recommended using *chronic infectious pyelonephritis* to refer to changes in the scarred kidney that are caused by infections and, in turn, reserving other terms, such as ascending atrophic pyelitis and reflux nephropathy, to refer to scarring without infection. *Atrophic pyelonephritis* should not be used, as it could theoretically be due to obstruction.

A list of all papers presented at the meeting, in order of presentation, follows.

**In utero-vesico amnion shunts.** Glickman MG, Grannum PA, Beheshti M

**The unsuspected double collecting system.** Share JC, Lebowitz RL

**Neither minor nor rare urethral anomalies in neonates with imperforate anus and the VATER association.** Fernbach SK

**Spinning top urethra in male children with bladder instability.** Saxton HM, Borzyskowski M, Mundy AR

**Limited ureteral compliance causing functional obstruction at the uretero-pelvic junction.** Willi UV

**Percutaneous endopyelotomy. Analysis of 100 consecutive patients.** Lee WJ, Smith AD, Pillari GP

**Self-expandable metallic stents (Wallstents) in strictured urethras and Bricker ureters: first results.** van Waes PFGM, van Schaik JPJ, Mali WPTHM, Gort HBW, Boon TA, deHond JAPM, Lock MTWF

**Renal biopsy for benign disease: what are the risks?** Cronan JJ, Sateriale M, Lionel S

**The morbidity of transrectal ultrasound guided biopsy of the prostate: the value of telephone.** Krause R, Scholz FJ, Cuttino JT Jr, Larsen CR

**Color flow Doppler of the prostate.** Rifkin MD, Alexander AA, Merton DA

**Testis vs testicular remnants: MR imaging with surgical correlation.** Fritzsche PJ, Hopkins CR, Moorhead JD, et al.

**CT or renal lymphoma.** Dunnick NR, Cohan RH, Leder RA, Baker ME

**Urine profiles following intravenous diatrizoate and iohexol in gentamicin nephropathy.** Thomsen HS

**Use of nonionic contrast media in previous reactors.** Fischer HW

**Injuries produced by extravasation of radiographic contrast media: efficacy of local dilution.** Cohan RH, Leder RA, Herzberg AJ, Hedlund LT, Beam CA, Dunnick NR

**Gadolinium-DTPA clearance as a determinant of glomerular filtration rate (GFR).** Choyke PL, Frank JA, Gorton ME, Diggs RL, Miller LGS, Simon TR, Austin HA

**Vasculogenic impotence: duplex and color Doppler imaging.** Hattery RR, King BF, James EM, Lewis RW, McKusick MA

**Color Doppler ultrasound investigation of the ureteral jet phenomenon.** Burge HJ, Middleton WD, McClennan BL

**Intrarenal Doppler curves in renal artery stenosis.** Patriquin HB, Landriault J, O'Regan S, Filiatrault D, Garel L, Lafontaine A

**Doppler imaging of renal tumors.** Denys I, Helenon O, Attian E, Gay F, Souissi M, Moreau JF

**Important factors in the experimental design of formal clinical efficacy studies of MR in the genitourinary tract.** Thornbury JR

**Dynamic contrast enhanced MRI of renal masses.** Eilenberg SS, Lee JKT, Brown JJ, Heiken JP, Mirowitz SA

**Complications of renal transplants with children.** Lohr E, Sievers KW

**Segmental renal transplant ischemia/infarction: the value of color Doppler imaging.** Madrazo BL, Jafri SZH, Ellwood RA, Rocher LL

**MRI evaluation of intra-abdominal fluid collections in patients with pancreatic and/or kidney transplants.** Pinet A, Studniarek M, Tourasse C, Flinas B, Pelegrin I, Lapra C

**Evolution of acquired renal cystic disease and incidence of renal cell carcinoma in dialysis patients: a prospective longitudinal CT study.** Levine E, Slusher SL, Grantham JJ, Wetzel LH

**CT of the urinary tract after abdominoperineal resection for rectal carcinoma.** Hertz M, Apter S

**CT detection of bladder rupture: value and limitations.** Kenney PJ, Koslin DB, Berland LL, Stanley RJ, Mulligan S

**Lacunae: a little known urographic finding in chronic obstructive uropathy.** Talner LB, Webb JAH, Dail DH

**MRI of renal angiomyolipomas.** Amendola MA, Brown SM, Schnall M, Morillo G, Pollack HM, Kressel HR

**Transvaginal color Doppler sonography of normal and abnormal ovaries.** Fleischer AC, Rao BK, Kepple DM

**The hyperdense adrenal: a sign of life-threatening injury.** Kenney PJ, Berland LL, Stanley RJ, Koslin B

**The acute and subacute pyelonephritides: a crisis in terminology.** Goldman SM

**Self-referring vs radiologist-referring physicians' imaging of males with difficulty urinating.** Hillman BJ, Joseph CA, Babry MR, Sunshine JH, Kennedy SD, Noether M

## FORTHCOMING ARTICLES

### FELSON LECTURE

**Chronic interstitial lung disease of unknown cause: a new classification based on pathogenesis.** *Hogg JC*

### REVIEW ARTICLES

**Advances in contrast-enhanced MR imaging.** *Saini S, Modic MT, Hamm B, Hahn PF*

**The changing epidemiology of tuberculosis and other mycobacterial infections in the United States: implications for the radiologist.** *Buckner CB, Leithiser RE, Walker CW, Allison JW*

### CHEST RADIOLOGY

**Value of sonography in monitoring the therapeutic response of mediastinal lymphoma: comparison with chest radiographs and CT.** *Wernecke K, Vassallo P, Hoffmann G, et al.*

**Value of CT in determining the need for angiography in equivocal findings of mediastinal hemorrhage on chest radiographs.** *Richardson P, Mirvis SE, Scorpio R, Dunham CM*

**The pathogenesis of pulmonary edema during interleukin-2 therapy: correlation of chest radiograph and clinical findings in 54 patients.** *Saxon RR, Klein JS, Bar MH, et al.*

### BREAST RADIOLOGY

**Pictorial essay. Abnormalities of the breast caused by biopsy: the spectrum of mammographic findings.** *Stigers KB, King JG, Davey DD, Stelling CB*

### GASTROINTESTINAL RADIOLOGY

**Videofluoroscopy in elderly patients with aspiration: importance of evaluating both oral and pharyngeal stages of deglutition.** *Feinberg MJ, Ekberg O*

**Carcinoma of the esophagus: CT vs MR imaging in determining resectability.** *Takashima S, Takeuchi N, Shiozaki H, et al.*

**Expert advice. Radiologic detection of colonic neoplasms: benefits of a systems analysis approach.** *Gelfand DW, Chen YM, Ott DJ*

**Fatty infiltration of the liver: quantification with phase-contrast MR imaging at 1.5 T vs biopsy.** *Levenson H, Greensite F, Hoefs J, et al.*

**Periportal contrast enhancement on CT scans of the liver.** *Hammerman AM, Kotner LM Jr, Doyle TB*

**Focal nodular hyperplasia of the liver: MR findings in 35 proved cases.** *Lee MJ, Saini S, Hamm B, Taupitz M, Hahn PF, Ferrucci JT*

**Self-expandable stainless steel endoprostheses for treatment of malignant bile duct obstruction.** *Adam A, Chetty N, Roddie M, Yeung E, Benjamin IS*

**Pictorial essay. Choledochal cysts: classification and cholangiographic appearance.** *Savader SJ, Benenati JF, Venbrux AC, et al.*

### MUSCULOSKELETAL RADIOLOGY

**MR of the knee: the significance of high signal in the meniscus that does not clearly extend to the surface.** *Kaplan PA, Nelson NL, Garvin KL, Brown DE*

**Pictorial essay. MR imaging of synovial sarcoma.** *Morton MJ, Berquist TH, McLeod RA, Unni KK, Sim FH*

**Case report. Fournier's gangrene caused by a perforated retroperitoneal appendix: CT demonstration.** *Gaeta M, Volta S, Minutoli A, Bartiromo G, Pandolfo I*

**Technical note. Two-piece wrist surface coil.** *Totterman SM, Heberger R, Miller R, Rubens DJ, Blebea JS*

### FETAL AND PEDIATRIC RADIOLOGY

**Comparison of iohexol with barium in gastrointestinal studies of infants and children.** *Cohen MD, Towbin R, Baker S, et al.*

**The calcified ligamentum arteriosum in children: a normal finding on CT.** *Bisceglia M, Donaldson JS*

**Pictorial essay. Radiologic evaluation of limb lengthening procedures.** *Walker CW, Aronson J, Kaplan PA, Molpus WM, Seibert JJ*

**Unilateral hydrocephalus: prenatal sonographic diagnosis.** *Patten RM, Mack LA, Finberg HJ*

**Case report. Occult ectopic ureter in girls with urinary incontinence: diagnosis with CT.** *Braverman RM, Lebowitz RL*

**Technical note. Limited-slice CT in the evaluation of paranasal sinus disease in children.** *Gross GW, McGeady SJ, Kerut T, Ehrlich SM*

**Technical note. Measurement of the diameter of the tracheal lumen in children and adolescents with CT.** *Griscom NT*

### NEURORADIOLOGY

**Intracranial vascular abnormalities: value of MR phase imaging to distinguish thrombus from flowing blood.** *Nadel L, Braun IF, Kraft KA, Fatouros PP, Laine FJ*

**Paranasal sinuses on MR images of the brain: significance of mucosal thickening.** *Rak KM, Newell JD II, Yakes WF, Damiano MA, Luethke JM*

### ANGIOGRAPHY

**Angiography is useful in detecting the source of chronic gastrointestinal bleeding of obscure origin.** *Rollins ES, Picus D, Hicks ME, Darcy MD, Bower BL, Kleinhoffer MA*

**Iliac artery stenosis or obstruction after unsuccessful balloon angioplasty: treatment with a self-expandable stent.** *Günther RW, Vorwerk D, Antonucci F, et al.*

**Technical note. CT analysis of a safe approach for translumbar access to the aorta and inferior vena cava.** *Cazenave FL, Glass-Royal MC, Teitelbaum GP, Zuurbier R, Zeman RK, Silverman PM*

### TECHNICAL NOTES

**A new percutaneous access set for interventional procedures.** *McLellan GL*

**Improved needle tip visualization by color Doppler sonography.** *Hamper UM, Savader BL, Sheth S*



## Letters

### Hypersensitivity Reaction to Oral Iohexol

Hypersensitivity reactions after administration of intravascular ionic and nonionic contrast media, and even oral and rectal barium sulfate, are well recognized [1, 2]. We present a case of a previously unreported severe adverse reaction to orally administered nonionic contrast medium.

A fit 31-year-old man with an ileoanal pouch complained of abdominal bloating. He drank 100 ml of iohexol (350 mg/ml) (Omnipaque 350, Nycomed A.S., Oslo, Norway) for a follow-through study performed to exclude subacute obstruction and late anastomotic dehiscence. Approximately 1 hr later, he collapsed with cramping abdominal pains, vomiting, hypotension (supine blood pressure, 80/50 mm Hg), and a rapid low-volume pulse (120 beats/min). He also complained of mild tightness of the throat, but dyspnea did not develop. He was treated with plasma expanders, IV antihistamine, and corticosteroids, and he recovered completely. No bowel abnormality was shown in the study or subsequently.

An uneventful endoscopy of the pouch had been performed 2 hours before the administration of iohexol, but no medication had been given for 18 hr before the follow-through study. The patient had not eaten for 12 hr and had drunk only a little water 6 hr earlier. The only previous contrast examinations were a barium enema and two sodium trizoate and meglumine trizoate (Gastrografin, Schering AG, Berlin, Germany) pouchograms. Although the patient had no previous exposure to iohexol by any route and had no history of allergy, the contrast agent seems to be the only precipitating cause of the adverse reaction. The mechanism of the reaction remains obscure. Less than 2% of oral iohexol is absorbed from normal bowel [3], and, unlike barium preparations, it contains no additives. Consequently, any hypersensitivity must be to the contrast agent itself, mediated either by receptors in the bowel wall or via the small quantity absorbed into the circulation. In a recent large-scale study [4], IV nonionic contrast media was associated with such a low prevalence (0.04%) of severe adverse reactions that radiologists may tend to forget that the risks attached to all contrast media still apply, even if the contrast agent is given enterally. However, a risk of severe, and possibly even fatal, adverse reaction exists for even the safest available contrast media. Also, as in our case, this type of idiosyncratic response may occur in patients with no history of allergy and no previous exposure to the contrast medium.

Jonathan R. Glover  
Brian M. Thomas  
St. Mark's Hospital  
London EC1V 2PS, England

### REFERENCES

1. Feczko PJ, Simms SM, Bakirci N. Fatal hypersensitivity reaction during a barium enema. *AJR* 1989;153:275-276
2. Janower ML. Hypersensitivity reactions after barium studies of the upper and lower gastrointestinal tract. *Radiology* 1986;161:139-140
3. Stordahl A. Urinary excretion of enteral iohexol in rats with intestinal ischaemia. *Scand J Gastroenterol* 1988;23:983-990
4. Katayama H, Yamaguchi K, Kozuka T, Takashima T, Seez P, Matsuura K. Adverse reaction to ionic and nonionic contrast media. *Radiology* 1990;175:621-628

### Clinical History and Accurate Interpretation of Chest Radiographs

We read with interest the article by Good et al. [1], "Does Knowledge of the Clinical History Affect the Accuracy of Chest Radiograph Interpretation?" The results, which suggest that knowledge of clinical history does not affect the accurate interpretation of chest radiographs for the detection of interstitial disease, nodules, and pneumothoraces, seem counterintuitive and contrary to the findings of other investigators [2-5]. This, in part, may be related to (1) the study design and (2) the method of analysis.

A diagnosis might be missed for at least two reasons: Either the diagnosis never occurred to the radiologist, or a particular condition did occur, but the radiologist failed to detect or interpret findings consistent with it. The study by Good et al., which asked radiologists to rate the likelihood of interstitial disease, nodules, and pneumothoraces, effectively precluded the first possibility. Asking a radiologist to look for a specific finding may be as powerful an influence as providing a history that is "non-cuing." In other words, having a form requiring the radiologists to determine the likelihood of a pneumothorax being present or not biases them just as if they were provided with a clinical history of, for example, right-sided pleuritic chest pain. In both cases, the radiologist will be directed to search for a pneumothorax.

To determine whether clinical history altered the radiologist's interpretation, the authors compared the area under the receiver-operating-characteristic (ROC) curves generated with and without clinical information. Providing a history may have influenced the diagnosis without altering the shape of the ROC curve. The shape of, and therefore the area under, an ROC curve is determined by the ability of a detection system to discriminate normal from abnormal. It is independent of the particular cutoff point or threshold chosen. It is reasonable to presume that providing a history would bias the radiologist toward or away from a correct diagnosis, but this would not

alter the shape of or the area under the ROC curve. The literature cited by Good et al. demonstrates this observation. Doubilet and Herman [6] found a statistically significant increase in the rate of true-positive interpretations in the presence of a suggestive as compared with a nonsuggestive history and a concomitant increase in false positives. This corresponds to a shift of the detection threshold, and not to a change in the area under the ROC curve. Other studies [3, 5] also showed an increase in true-positive rates related to providing a history suggestive of a change in threshold; whether they resulted in a change in  $d'$  was not described.

We think that the manner in which the study was conducted—the fixed rating task, the lack of analytical distinction between positive and negative histories, and the exclusive focus on the area of the ROC curve—does not permit the conclusion that clinical history does not affect the accurate interpretation of chest radiographs.

Craig L. Coblenz  
Geoff Norman

McMaster University Medical Centre  
Hamilton, Ontario, Canada L8N 3Z5

#### REFERENCES

1. Gur D, Good B, Cooperstein LA. Reply. To: Black WC, Dwyer AJ. Knowledge of clinical history and the accuracy of interpretation of chest radiographs (letter). *AJR* 1990;155:1342–1343
2. Gur D, Good B, Cooperstein LA. Reply. To: Miller WT. Value of clinical history (letter). *AJR* 1990;155:653–654
3. Schreiber MH. The clinical history as a factor in roentgenogram interpretation. *JAMA* 1963;185:399–401
4. Berbaum KS, Franken EA, Dorfman DD, et al. Tentative diagnoses facilitate the detection of diverse lesions in chest radiographs. *Invest Radiol* 1986;21:532–539
5. Potchen EJ, Gard JW, Lazar P, Lahaie P, Andary M. The effect of clinical history data on chest film interpretation: direction or distraction (abstr). *Invest Radiol* 1979;14:404
6. Doubilet P, Herman PG. Interpretation of radiographs: effect of clinical history. *AJR* 1981;137:1055–1058

#### Reply

As we have noted in previous responses to similar criticisms of our work [1, 2], we think that the fact that we investigated three particular abnormalities (pneumothorax, nodule, and interstitial disease) during the study and the observers knew this does not constitute providing a history. Importantly, a number of cases in the study did contain abnormalities other than the three we investigated. In addition, the form that was provided to the observers for scoring purposes (on which they were to record findings) appeared as a checklist for *all* cases, something we think is quite different qualitatively from providing a particular history for a particular case.

We respectfully disagree with the comment of Coblenz and Norman on the significance of changing thresholds of detection *without* causing a change in the shape or area under the receiver-operating-characteristic (ROC) curve. In order to show a meaningful effect, the curve must change over at least some range of the false-positive fraction. As we have noted before, we provided only summary performance indexes ( $A_z$ ); however, ROC methods do provide detailed information on relative performance of observers at different false-positive fractions. If we had observed in our analyses significant differences between the two reading modes (i.e., with and without history) as a function of the false-positive fraction, we would have discussed them, but this was not the case. Our study included accurate and actual clinical histories of the patients whose images were used in the study. The images were selected before the study was run and without any knowledge of the clinical histories of the patients involved. No attempt was made to create positive or negative

histories for any of these cases, and we do not think that the histories should have been classified as such.

We are convinced, despite the last remark of Coblenz and Norman, that the scientific merit of our study and its resulting data do permit our carefully worded conclusions.

David Gur  
Barbara Good  
Lawrence A. Cooperstein  
University of Pittsburgh  
Pittsburgh, PA 15261

#### REFERENCES

1. Gur D, Good B, Cooperstein LA. Reply. To: Black WC, Dwyer AJ. Knowledge of clinical history and the accuracy of interpretation of chest radiographs (letter). *AJR* 1990;155:1342–1343
2. Gur D, Good B, Cooperstein LA. Reply. To: Miller WT. Value of clinical history (letter). *AJR* 1990;155:653–654

#### Defining Terms for Medical Decision Making

I was pleased to see the article by Phillips and Scott [1] on practical evaluation of diagnostic examinations and the application of these results to medical decision making. The authors are to be congratulated on the clarity of their presentation. Anything that can make the difficult subject of statistics and decision analysis easier to understand is certainly welcome.

I would like to offer several definitions for consideration. Other articles have referred to the false-positive ratio (FPR) and false-negative ratio (FNR) as representing (1—specificity) and (1—sensitivity), respectively [2–4]. Phillips and Scott use the same terms, FPR and FNR, as the inverse probabilities of their respective predictive values.

As we are discussing conditional probabilities, perhaps it would be useful to define terms on the basis of the condition applied. If specificity represents the pretest likelihood of obtaining a negative result, given that the disease is absent, and if sensitivity represents the pretest likelihood of obtaining a positive result, given that the disease is present, should the FPRs and FNRs under these conditions be referred to as pretest ratios? Conversely, if the positive predictive value (PV+) represents the posttest likelihood that a patient has the disease in question, given a positive test, and if the negative predictive value (PV−) represents the likelihood that a patient is free of disease, given a negative test, should the ratios as defined by Phillips and Scott be referred to as posttest ratios? Without such clarification, the receiver-operating-characteristic curves, inherent characteristics of imaging systems, as well as posttest probabilities for decision making, a function of disease prevalence, could be applied incorrectly.

H. G. Adams  
National Naval Medical Center  
Bethesda, MD 80814-5000

#### REFERENCES

1. Phillips WC, Scott JA. Medical decision making: practical points for practicing radiologists. *AJR* 1990;154:1149–1155
2. McNeil BJ, Keeler E, Adelstein SJ. Primer on certain elements of medical decision making. *N Engl J Med* 1975;293:211–215
3. Browner WS, Newman TB. Are all significant P values created equal? *JAMA* 1987;257:2459–2463
4. Metz CE. ROC methodology in radiologic imaging. *Invest Radiol* 1986;21:720–733

Note.—The opinions and assertions in the preceding letter are views of the author and should not be construed as official policy or views of the Department of Defense or the Department of the Navy.



TABLE 1: Terms Used in Medical Decision Making

Term	Reference
Probability of TP/FP	<i>Radiology</i> 1982;143:29 <i>Radiology</i> 1981;138:723
Proportion of TP/FP decisions	<i>AJR</i> 1982;138:485
Sensitivity vs nonspecificity	<i>Am J Clin Pathol</i> 1971;55:105
TP/FP fraction	<i>Semin Nucl Med</i> 1978;8:273 <i>Semin Nucl Med</i> 1978;8:283
TP/FP percentages	<i>Radiology</i> 1981;141:25
TP/FP rate	<i>AJR</i> 1982;138:977
TP/FP ratio	<i>Radiology</i> 1982;143:129 <i>N Engl J Med</i> 1975;293:211
TP/FP response	<i>Radiology</i> 1981;141:139
True positive/negatives	<i>Radiology</i> 1983;143:121

Note: TP = true positive, FP = false positive.

Reply

I appreciate the interest and comments of Dr. Adams. Dr. Scott and I have published two articles [1, 2] on medical decision making, and both times the issue of proper terminology has arisen. Unfortunately, no widely accepted set of definitions of terms has been adopted, and I think that this leads to much confusion. A few years ago I made a list of some of the terms and their sources that are used in analysis of receiver-operating-characteristic curves. Table 1 shows what I found. The list shows that a variety of terms are used to define the same thing.

The best solution to this dilemma would be to adopt a set of standardized definitions that are accepted by everyone. Until that time, the terms used by an author should be defined in the paper or book in which they appear.

Warren C. Phillips, Jr.  
Milford Memorial Hospital  
Milford, DE 19963

REFERENCES

1. Phillips WC, Scott JA, Blasczynski G. Statistics for diagnostic procedures. 1. How sensitive is "sensitivity"; how specific is "specificity"? *AJR* 1983;140:1265-1270

2. Phillips WC, Scott JA. Medical decision making: practical points for practicing radiologists. *AJR* 1990;154:1149-1155

Hypervascularity of Nontoxic Goiter as Shown by Color-Coded Doppler Sonography

In 1988, Ralls et al. [1] described hypervascularity in the thyroid gland in Graves disease and suggested that color-coded Doppler sonography might be a primary noninvasive technique for diagnosing thyrotoxicosis. Their data support the finding that many nontoxic nodular goiters, as well as solitary benign nodules, may be hypervascular, but this finding was not emphasized.

We recently observed, in two patients, striking increased blood flow in association with nontoxic nodular goiter, and we would like to give this finding more emphasis.

The first patient, a 32-year-old woman, had noticed swelling of the right lobe of the thyroid. She had no clinical signs of a toxic state, and laboratory tests for thyroid function were all within normal limits. Color-coded Doppler imaging showed markedly increased blood flow in the periphery of a inhomogeneous mass that involved the whole right lobe of the thyroid. Radionuclide scanning showed areas of hyper- and hypoactivity, indicative of thyroid adenoma with central degeneration.

The second patient was a 28-year-old woman in whom a 1.5-cm

nodular lesion had been discovered incidentally 1 year earlier. The lesion was hypoechoic and contained small calcifications. Again, blood flow in the lesion was increased. On radionuclide scanning, the lesion showed hyperactivity, indicative of benign adenoma. All laboratory tests for thyroid function were normal.

Many benign nodules, whether solitary or in a multinodular goiter, may show hypervascularity, and this finding has no relationship to thyrotoxicosis or malignancy.

Raul Barreda  
Juri V. Kaude  
Michael Fagien  
Walter E. Drane  
University of Florida, College of Medicine  
Gainesville, FL 32610-0374

REFERENCE

1. Ralls PW, Mayekawa DS, Lee KP, et al. Color-flow Doppler sonography in Graves disease: "thyroid inferno." *AJR* 1988;150:781-784

Mucocele of the Breast

We report two cases of benign mucocele of the breast that were manifested as suspicious clustered calcifications. The first patient, a 48-year-old woman, had had a modified left radical mastectomy 10 months earlier for an infiltrating ductal carcinoma with multifocal intraductal disease. A postoperative mammogram of the right breast had shown a cluster of three to four calcifications that were stable when compared with findings on previous examinations. A reevaluation mammogram obtained 6 months later showed an increase in the number of calcifications (Fig. 1). Stereotactic fine-needle aspiration yielded calcific debris in mucinous material and a few benign epithelial cells. Excisional biopsy showed a mucocele and fibrocystic changes. The second patient, a 54-year-old woman, had a cluster of calcifications in the left breast that had not been present 1 year earlier. The findings at mammography, fine-needle aspiration, and excisional biopsy were similar to those of the first case.

To our knowledge, the mammographic findings of mucocelelike lesions have not been discussed in the radiologic literature. These lesions recently have been described in the surgical-pathologic literature as mucin-filled, dilated ducts and cysts lined by simple flat to cuboidal epithelium with mucin focally dissecting into the surrounding stroma [1]. Aspiration of either mucinous carcinoma or mucocele may

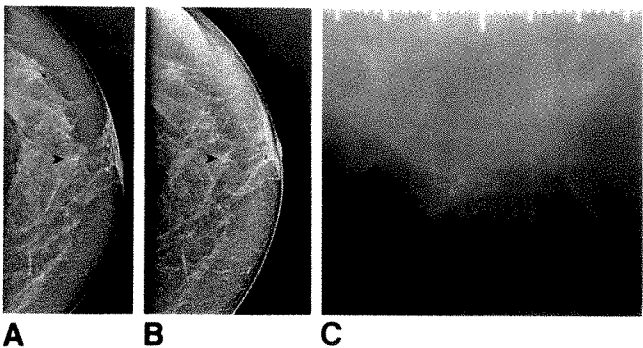


Fig. 1.—Breast mucocele.

A, Initial craniocaudal view of right breast shows a few rounded calcifications (arrowhead).

B, Similar view obtained 6 months later shows an increase in number of calcifications (arrowhead).

C, Enlarged close-up view shows calcifications before stereotactic biopsy.

yield mucin with a few epithelial cells. Excisional biopsy is required for differentiation [1].

The mammographic pattern of calcification in the mucocoeles in our two cases is quite similar to that of intralobular calcifications. These are described as single, tightly packed clusters of punctate calcifications that often overlap one another [2]. Although this pattern of calcification generally is due to adenosis, lobular carcinoma in situ has no specific mammographic pattern and may present in a similar manner. Thus, mucocoelelike lesions of the breast should be considered in the differential diagnosis of calcifications of the type sometimes associated with lobular carcinoma in situ. Accumulation of a sufficient number of cases may permit the mammographic differentiation of these mucocoelelike lesions.

I. Ray Kirk

Daniel S. Schultz

Ruth L. Katz

Herman I. Libshitz

The University of Texas, M. D. Anderson Cancer Center  
Houston, TX 77030

#### REFERENCES

1. Rosen PP. Mucocoelelike tumors of the breast. *Am J Surg Pathol* 1986;10:464-469
2. Martin JE. *Atlas of mammography: histologic and mammographic correlations*. Baltimore: Williams & Wilkins, 1988:194-195

#### Buckled Meniscus Revisited

In the July 1990 issue of the *AJR*, Chew [1] describes a phenomenon seen on MR imaging of the knee that he refers to as *meniscal flounce*: "an undulating, wavy appearance along the free edge" of the meniscus. This appearance has been described in the arthroscopic literature, but Chew states that "meniscal flounces were radiologically unobservable before the advent of MR imaging . . . and would not be visible at all at arthrography."

In 1978, I described the appearance of this phenomenon on arthrograms of the knee [2]. It is seen uncommonly, but by no means rarely, during routine arthrographic stress maneuvers. In one of the cases of meniscal buckling that I illustrated, the identical phenomenon was observed in the same meniscus on subsequent surgical arthroscopy.

I think the term *buckled meniscus* more accurately describes this physiologic phenomenon than *meniscal flounce* does. As Chew points out, the meniscus is attached along its periphery and at its anterior and posterior horns, which may permit the free internal edge to buckle during stress maneuvers applied to the knee. Such external stresses are applied routinely during arthrography and arthroscopy. However, the knee is not stressed during MR imaging. I am uncertain if the phenomenon that Chew illustrates is a buckled meniscus, but, if it is, it must be observed rarely.

Ferris M. Hall

Beth Israel Hospital

Harvard Medical School

Boston, MA 02215

#### REFERENCES

1. Chew FS. Medial meniscal flounce: demonstration on MR imaging of the knee (letter). *AJR* 1990;155:199
2. Hall FM. Buckled meniscus. *Radiology* 1978;126:89-90

#### Reply

I regret that I overlooked Dr. Hall's fascinating paper [1] on the arthrographic demonstration of transient meniscal buckling when I

was researching the meniscal flounce I observed on MR imaging [2]. Those of us who trained after the heyday of arthrography for diagnosis and arthrotomy for treatment of internal derangements of the knee have missed learning the nuances of a now lost art.

Felix S. Chew

Massachusetts General Hospital

Harvard Medical School

Boston, MA 02114

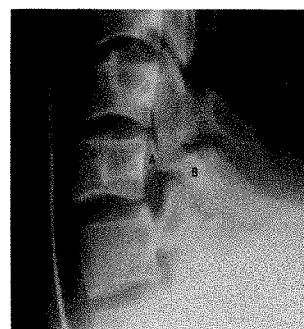
#### REFERENCES

1. Hall FM. Buckled meniscus. *Radiology* 1978;126:89-90
2. Chew FS. Medial meniscal flounce: demonstration on MR imaging of the knee (letter). *AJR* 1990;155:199

#### CT of Bilateral Cervical Spondylolysis

Forsberg et al. [1] recently reported a series of 12 patients with cervical spondylolysis. The authors carefully reviewed the plain film, plain tomographic, and CT appearances of this disorder. They presented one CT section showing an example of unilateral disease. My colleagues and I recently saw a patient with bilateral C6 spondylolysis that had most of the features described by Forsberg et al. We present this case as an example of cervical spondylolysis seen as a bilateral lesion on CT.

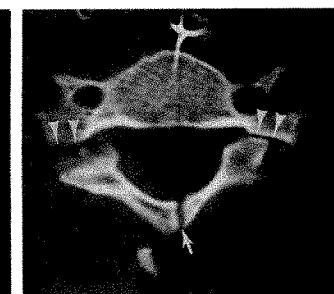
A 29-year-old man was the restrained driver in a high-speed motor vehicle accident. He was admitted to the hospital with amnesia about the accident, splenic and hepatic lacerations, a scalp laceration, and no focal neurologic complaints. His medical history was unremarkable. Specifically, he had no history of previous neck trauma. Physical examination showed abdominal tenderness. The results of serial neurologic examinations were entirely normal. Radiographs of the cervical spine (Fig. 1A) showed many of the features of cervical spondylolysis described by Forsberg et al.: (1) the "cleft-bow-tie" configuration formed by the triangular ventral and dorsal fragments that make up the articular masses, (2) mild anterolisthesis, (3) hypoplastic pedicles (better seen on oblique views), and (4) dysplastic (hyperplastic in this case) superior and inferior adjacent articular



A



B



C

Fig. 1.—Bilateral cervical spondylolysis.

A, Lateral radiograph of spine shows classic findings of C6 spondylolysis: "cleft-bow-tie" configuration of articular masses, mild anterolisthesis, hypoplastic pedicles, and dysplastic articular pillars. A = anterior fragment, B = posterior fragment.

B and C, Axial CT scans through C6 show well-corticated, smoothly margined spondylolytic clefts (arrowheads) through articular masses, small pedicles with enlarged vertebral foramina, and spina bifida occulta (arrows).



pillars. The abnormalities were at the C6 level, the most common level (74%) at which this lesion has been reported [1]. Unenhanced axial CT scans of the C6 vertebra (3-mm contiguous sections) obtained by using a bone algorithm showed well-corticated, smoothly margined spondylolytic defects through the articular masses bilaterally (Figs. 1B and 1C). Small pedicles with enlarged vertebral foramina also were seen bilaterally (findings more prominent on the left side). Spina bifida occulta was seen also. Incidentally noted on a lumbosacral spinal series was a definite spondylolytic defect on the left at L5, with findings suggestive of a similar defect on the right at L5.

In the absence of any focal neurologic deficit, these findings were considered diagnostic of long-standing spondylolysis. Lateral flexion/extension radiographs of the cervical spine showed no ligamentous instability. After 1 week of observation for his abdominal injuries, the patient was discharged from the hospital without any additional treatment.

Douglas J. Quint  
University of Michigan Hospitals  
Ann Arbor, MI 48109

#### REFERENCE

1. Forsberg DA, Martinez S, Vogler JB III, Wiener MD. Cervical spondylolysis: imaging findings in 12 patients. *AJR* 1990;154:751-755

#### Reply

We were interested to read Dr. Quint's case of bilateral C6 spondylolysis in a 29-year-old man who had been in a motor vehicle accident. The accompanying radiographs show quite well the diagnostic features of cervical spondylolysis. Three of the patients in our series [1] had bilateral spondylolytic defects, all at C6. Interestingly, Dr. Quint's patient also had spondylolysis at L5. We know of a 16-year-old woman who has cervical spondylolysis and abnormal posterior elements at L4 and L5 but not pars interarticularis defects [2].

It should be emphasized further that most patients with cervical spondylolysis have normal neurologic examinations. Like Dr. Quint's patient, they require no treatment.

David A. Forsberg  
Salutario Martinez  
Duke University Medical Center  
Durham, NC 27710

#### REFERENCES

1. Forsberg DA, Martinez S, Vogler JB III, Wiener MD. Cervical spondylolysis: imaging findings in 12 patients. *AJR* 1990;154:751-755
2. Barnes DA, Borns P, Pizzutillo PD. Cervical spondylolisthesis associated with the multiple nevoid basal cell carcinoma syndrome. *Clin Orthop* 1982;162:26-30

### Childproof Cap on Medicine Bottles as a Risk for Esophageal Foreign Body

A 71-year-old woman came to the emergency department because of dysphagia that had begun abruptly 2 days earlier. She did not recall any pertinent antecedent event. A lateral radiograph of the neck showed gas in the proximal part of the thoracic esophagus. An esophagogram (Fig. 1A) showed a circular filling defect in the cervical esophagus that was not apparent on the plain film. Endoscopy was done, and a foreign body was removed—the plastic inner liner from a childproof safety cap for a medicine bottle (Fig. 1B). After further discussion with the patient, it became apparent that she takes a number of daily medications. She habitually collects all the pills she is taking at one time in one of the medicine-bottle caps and then swallows all of the medications at once. She tosses the pills to the back of her throat and rinses them down with water.

Although placing pills in the cap of a medicine bottle is convenient,

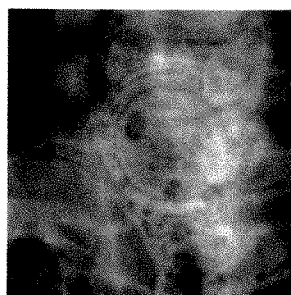
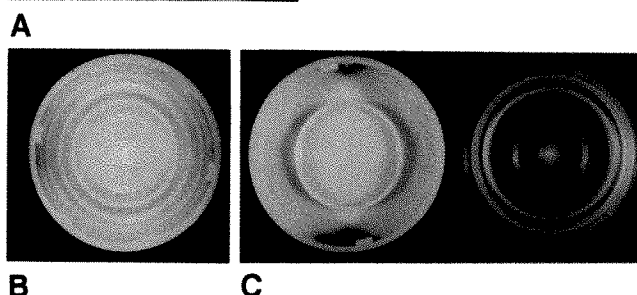


Fig. 1.—Childproof medicine-bottle cap as an esophageal foreign body.

A, Spot film from barium esophagogram shows a circular foreign body in the proximal thoracic esophagus.

B and C, Photographs show childproof safety cap with inner plastic lining in place (B) or removed (C).



and probably is a common practice, our case shows that there is a risk of swallowing the cap. Most medication containers have safety caps with a plastic inner liner that may dislodge from the main part of the cap.

Eric Brandser  
Claire Smith  
Rush-Presbyterian-St. Luke's Medical Center  
Chicago, IL 60612

### Coarctation of the Abdominal Aorta Associated with Malignant Hypertension and Collateral Mesenteric Circulation

Coarctation of the aorta is an abnormal narrowing sufficient to cause a serious disturbance in blood flow. The common site is the thoracic aorta near the junction of the ligamentum arteriosum. However, 2% of coarctations affect the abdominal aorta [1]. Fewer than 150 cases in the abdominal aorta have been reported in the English-language literature.

We encountered a case with an unusual presentation. A 52-year-old man had a blood pressure of 300/180 mm Hg and hypertensive encephalopathy. No abdominal bruits were noted, and femoral pulses were not diminished. He did not have claudication or abdominal angina. A flush aortogram (Fig. 1A) showed bilateral stenosis of the renal arteries and tapering of the aorta to a mild waist just below the renal arteries. The aortic bifurcation was higher than normal at the L2 level, suggesting a congenital anomaly. No significant pressure gradient was measured across the coarctation; however, complete ostial occlusion of the celiac and superior mesenteric arteries was present. A meandering mesenteric artery (Fig. 1B) originating from the infrarenal aorta provided collateral flow to the occluded vessels.

The level of renin in the left renal vein was elevated. Medical therapy was unsuccessful, and the patient had a right iliac to left renal artery bypass. At the time of surgery, the aorta was not thickened from fibrosis or hardened from atherosclerosis. A biopsy specimen of the intima of the iliac artery showed no pathologic changes. Minimal postoperative improvement in the patient's blood pressure occurred, but he refused further treatment, and his pressure has remained elevated.

Most authors reserve the term coarctation for a congenital anomaly. Acquired diseases that mimic this condition include Takayasu aortitis and other autoimmune diseases, tuberculosis of the aorta, radiation aortitis, fibromuscular dysplasia, and neurofibromatosis of the aorta. Abdominal coarctation is seen most often in childhood or

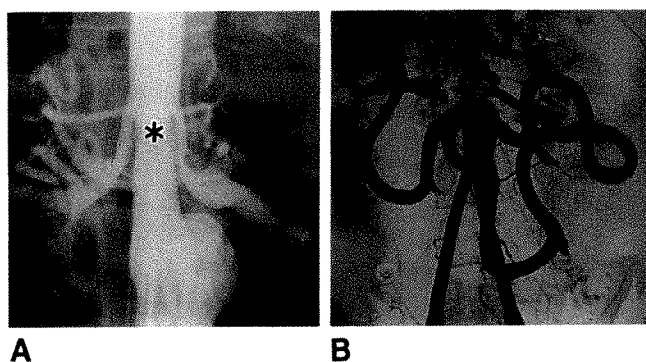


Fig. 1.—Coarctation of abdominal aorta associated with malignant hypertension.  
A and B, Angiograms show stenosis of renal arteries (A), mild infrarenal coarctation (A, asterisk), and meandering mesenteric artery (B).

early adulthood and is manifested as renovascular hypertension. Patients with this condition who reach their 40s most commonly have disease affecting the infrarenal part of the aorta, and claudication is the usual manifestation [2]. The average age at presentation is 21 years, with a second peak in the fourth or fifth decade [3].

Involvement of the renal and splanchnic vessels is common. This has been attributed to intimal hyperplasia due to the eddy currents in the narrowed zone [4]. Stenosis of the renal arteries is seen in nearly 85% of patients. The celiac artery, superior mesenteric artery, inferior mesenteric artery, or a combination of these is involved in one quarter of the cases. As in our case, collateral flow via the mesenteric artery occurs when the superior mesenteric or inferior mesenteric arteries are involved.

Abdominal coarctation can be classified on the basis of its type (segmental or hypoplastic) and location (suprarenal, interrenal, or infrarenal). The pattern most commonly encountered is interrenal (50%); next, in order, are infrarenal (25%), suprarenal (15%), and diffuse (about 10%). Ischemia of the viscera is rarely of clinical significance because of the development of extensive collaterals [1].

Thomas B. Poulton  
Barry S. Rose  
Aultman Hospital  
Canton, OH 44710

## REFERENCES

1. DeBakey ME, Garrett HE, Howell JF, Morris GC Jr. Coarctation of the abdominal aorta with renal arterial stenosis: surgical considerations. *Ann Surg* 1967;165:830-843
2. Bergqvist D, Bergentz S, Ekberg M, Jonsson K, Takolander R. Coarctation of the abdominal aorta in elderly patients. *Acta Med Scand* 1988;223:275-280
3. Cohen JR, Birnbaum E. Coarctation of the abdominal aorta. *J Vasc Surg* 1988;8:160-164
4. Edwards JE, Christensen NA, Clagett OT, McDonald JR. Pathologic considerations in coarctation of the aorta. *Proc Staff Meet Mayo Clin* 1948;23:324-332

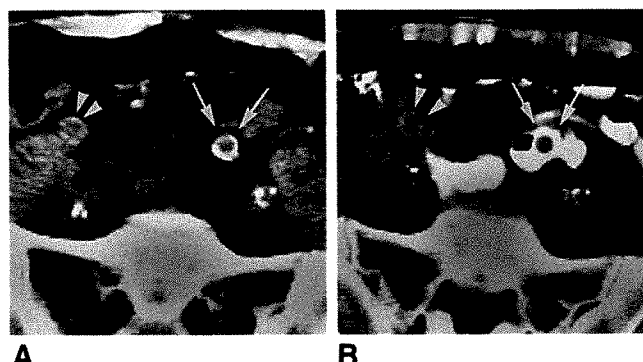


Fig. 1.—A and B, CT scans obtained before (A) and after (B) administration of rectal contrast material show intrasigmoidal course of left limit of aorta-bifurcation prosthesis (arrows). Arrowheads indicate right limit of graft.

## Intrasigmoidal Aorta-Bifurcation Prosthesis Diagnosed on CT

A 74-year-old man was admitted because of septicemia and pneumonia. Five years earlier, a Sauvage-velours prosthesis to replace the aortic bifurcation had been implanted for treatment of an aortic aneurysm with stenoses of both iliac vessels. Two weeks before admission, the patient had hematochezia on one occasion. Blood cultures were positive for *Escherichia coli*. An infected prosthesis with enteric fistulation was postulated as the cause of the septicemia, and antibiotics were administered.

Abdominal sonography and angiography of the aorta and iliac vessels were normal. A scintigram made with <sup>99m</sup>Tc-HMPAO-labeled leukocytes showed uptake in the left lower quadrant of the abdomen after 4 hr. A CT scan without rectal contrast material showed no abnormalities at the proximal and distal anastomoses of the vascular prosthesis. However, the left iliac limit of the prosthesis appeared to traverse the lumen of the sigmoid colon for about 3.5 cm (Fig. 1A). A CT scan obtained after rectal administration of contrast material confirmed this finding (Fig. 1B). At surgery, the prosthesis had eroded the sigmoid colon and had an intraluminal course of 4 cm. The left iliac limit of the prosthesis was replaced by a Dacron prosthesis, and the patient made an uneventful recovery.

To our knowledge, the only published example of a paraprosthesis-enteric fistula involving the sigmoid colon was diagnosed on the basis of a barium enema [1]. Although an intrasigmoidal aorta-bifurcation prosthesis is probably unique, we have shown that it can easily be demonstrated with CT.

Joan J. M. Peters  
Bernard Verbeeten, Jr.  
Jan Kromhout

University of Amsterdam, Academic Medical Center  
1105 AZ Amsterdam, the Netherlands

## REFERENCE

1. Thompson WM, Jackson DC, Johnsrude IS. Aortoenteric and paraprosthesis-enteric fistulas: radiologic findings. *AJR* 1976;127:235-242

Letters are published at the discretion of the Editor and are subject to editing.  
Letters to the Editor must not be more than two *double-spaced*, typewritten pages. One or two figures may be included. Abbreviations should not be used. See Author Guidelines, page A5.  
Material being submitted or published elsewhere should not be duplicated in letters, and authors of letters must disclose financial associations or other possible conflicts of interest.  
Letters concerning a paper published in the *AJR* will be sent to the authors of the paper for a reply to be published in the same issue. Opinions expressed in the Letters to the Editor do not necessarily reflect the opinions of the Editor.



## Review of Current Literature

Initials and addresses of corresponding authors are provided in parentheses for each article so that the reader can obtain reprints directly. Abstracts are printed verbatim from each journal.

### Cancer

**Some limitations of the radioisotope bone scan in patients with metastatic prostatic cancer: a subanalysis of EORTC trial 30853.** Smith PH, Bono A, Calais da Silva F, et al. (PHS, Dept. of Urology, St. James's University Hospital, Beckett St., Leeds LS9 7TF, United Kingdom). *Cancer* 66:1009-1016, 1990

This article reviews the serial bone scans of 149 of 327 patients entered into a randomized prospective trial comparing orchidectomy versus zoladex and flutamide in patients with metastatic prostatic cancer. Attention is drawn to the difficulty of evaluating the response rate and of the importance of tumor load in determining survival. The use of sequential bone scans once the diagnosis of metastatic disease has been confirmed is of questionable value as the scans are expensive and contribute little to the further management of the patient in the absence of symptoms requiring relief.

Reprinted by permission from the American Cancer Society.

### Chest

**Endoscopic ultrasound examination for mediastinal lymph node metastases of lung cancer.** Kondo D, Imaizumi M, Abe T, Naruke T, Suemasu K (DK, Dept. of Thoracic Surgery, Nagoya University School of Medicine, 65 Tsurumai, Showa-ku, Nagoya, Aichi 466, Japan). *Chest* 98(3):586-593, Sept. 1990

Among patients with primary lung cancer who were admitted to the National Cancer Center Hospital from July 1987 to April 1988 for surgical treatments, 132 underwent preoperative transesophageal endoscopic ultrasound examination (EUS) on mediastinal lymph nodes. Of the 132 patients, 101 were pathologically evaluated and studied in this article. A GF-UM2 radial scanner with 7.5-MHz (Olympus Co Ltd) was used for image examination. The lymph nodes were diagnosed as positive for metastasis when they had thickened images, clear contours, and low echoing images of fusion or lobulation. The results obtained from 509 sites were as follows: sensitivity, 53.6 percent; specificity, 97.5 percent; positive predictive accuracy, 77.1 percent; negative predictive accuracy, 93.1 percent; and overall accuracy, 91.6 percent. The sensitivity rate was 80.6 percent excluding the result of the right superior mediastinal lymph nodes that were difficult to examine for anatomic reasons. Although EUS was considered to be an excellent method in diagnosing lymph node metastases,

it had a blind angle in the field. More accurate diagnoses of mediastinal lymph node metastases could be achieved by using EUS and computed tomography (CT) together.

### Gastroenterology

**Effects of ursodeoxycholic acid on gallbladder contraction and cholecystokinin release in gallstone patients and normal subjects.** Van Erpecum KJ, Van Berge Henegouwen GP, Stolk MFJ, Hopman WPM, Jansen JBMJ, Lamers CBHW (KJVE, Dept. of Gastroenterology, University Hospital Utrecht, Utrecht, the Netherlands). *Gastroenterology* 99:836-842, 1990

It has been previously suggested that treatment with ursodeoxycholic acid leads to decreased gallbladder emptying. The proposed mechanism is decreased release of cholecystokinin through negative feedback control by an increased amount of intraduodenal bile acids. In the present study we examined cholecystokinin release and gallbladder contraction after oral administration of a commercial fatty meal (Sorbitract; Dagra, Diemen, The Netherlands) using ultrasonography in eight normal subjects and eight gallstone patients before and after 1 and 4 weeks of treatment with ursodeoxycholic acid (10 mg kg<sup>-1</sup>.day<sup>-1</sup>). Fasting gallbladder volume increased in 15 of 16 subjects during treatment ( $P < 0.01$ ). Minimal volume did not change. Therefore, both absolute and relative gallbladder emptying increased during therapy. Maximal decrement of gallbladder volume in milliliters and percentage as well as integrated gallbladder contraction during 90 minutes in milliliters and percentage were significantly increased after 1 and 4 weeks of treatment with ursodeoxycholic acid when compared with data before therapy. Gallstone patients tended to have larger fasting and residual gallbladder volumes than normal subjects, whereas parameters for the amount of bile expelled (maximal decrement of gallbladder volume and integrated gallbladder contraction in milliliters and percentage) did not differ. Release of cholecystokinin did not change during treatment and did not differ significantly between patients and normal subjects. Mean relative percentage of ursodeoxycholic acid in bile during treatment in 13 subjects consenting to have duodenal intubation was 47% (range 31%-60%). Changes of fasting gallbladder volume after institution of bile acid treatment correlated significantly ( $r = 0.74$ ,  $P < 0.01$ ) with changes of cholesterol saturation index but not with relative percentage of ursodeoxycholic acid in bile. This study indicates that gallbladder emptying does not decrease during treatment with ursodeoxycholic acid. Moreover, there is no evidence of decreased cholecystokinin release.

Reprinted with permission by the American Gastroenterological Association.

**Prevalence of columnar-lined (Barrett's) esophagus: comparison of population-based clinical and autopsy findings.** Cameron AJ, Zinsmeister AR, Ballard DJ, Carney JA (AJC, Division of Gastroenterology, Mayo Clinic, Rochester, MN). *Gastroenterology* 99:918-922, 1990

In this study, two different methods were used to investigate the prevalence of columnar-lined (Barrett's) esophagus. First, a population-based study of clinically diagnosed cases was performed in Olmsted County, Minnesota. Twenty-five residents of this county, who had undergone endoscopy and biopsy between 1969 and 1986, were diagnosed as having Barrett's esophagus. On January 1, 1987, 17 of these patients were still living in the county, representing an age- and sex-adjusted prevalence rate of 22.6 cases per 100,000 population (95% confidence interval, 11.7-33.6 cases). A prospective search of Mayo Clinic autopsy material for Barrett's esophagus was conducted using the same diagnostic criteria as in the clinical study. Over an 18-month period ending in September 1987, 7 cases of Barrett's esophagus were found in 733 unselected autopsies. In 5 of the 7 cases, Barrett's esophagus was first detected at the time of autopsy. Using the age- and sex-specific prevalence from the clinically diagnosed study, researchers expected to find 0.19 cases of Barrett's esophagus at the 226 autopsies performed on Olmsted County residents, although 4 were actually observed ( $P < 0.001$ ). This approximately 21-fold increase (95% confidence interval, 5-54 cases) corresponds to an autopsy estimated prevalence of 376 cases per 100,000 population (95% confidence interval, 95-967 cases). In conclusion, a majority of cases of Barrett's esophagus, a condition that predisposes to esophageal malignancy, remains unrecognized in the general population.

Reprinted with permission by the American Gastroenterological Association.

**Predictability of the postoperative course of Crohn's disease.** Rutgeerts P, Geboes K, Vantrappen G, Beyls J, Kerremans R, Hiele M (PR, Dept. of Medicine, University Hospital "Gasthuisberg," University of Leuven, Belgium). *Gastroenterology* 99:956-963, 1990

Eighty-nine patients who had been treated by ileal resection for Crohn's disease between 1979 and 1984 were included in a prospective cohort follow up to study the natural course of early postoperative lesions. Recurrent lesions were observed endoscopically in the neoterminal ileum within 1 year of surgery in 73% of the patients, although only 20% of the patients had symptoms. Three years after surgery, the endoscopic recurrence rate had increased to 85% and symptomatic recurrence occurred in 34%. The ultimate course of the disease was best predicted by the severity of the early postoperative lesions, as observed at ileoscopy. Clinical parameters that influenced outcome were preoperative disease activity, the indication for surgery, and the number of surgical resections. When patients were stratified for preoperative disease activity, the severity of lesions found at endoscopy remained a strong predictive factor for symptomatic recurrence. In 22 other patients submitted to "curative" ileal resection and ileocolonic anastomosis, the segment to be used as neoterminal ileum was carefully examined during surgery, and two large biopsies were taken before making the anastomosis. An ileoscopy was performed 6 months after surgery. Although all patients had a macroscopically normal neoterminal ileum and 19 had entirely normal biopsies at the time of surgery, 21 patients were found at ileoscopy to have developed ileitis involving a 15-cm segment (range, 4-30 cm), and 20 had unequivocal microscopic lesions on biopsies. These studies suggest that early lesions in the neoterminal ileum after Crohn's resection do not originate from microscopic inflammation present in this bowel segment at the time of surgery. The early postoperative lesions in the neoterminal ileum seem to be a suitable model to study the pathogenesis of Crohn's disease and also to evaluate new therapeutic modalities, either to prevent development of these early lesions or to treat progressive recurrence.

Reprinted with permission by the American Gastroenterological Association.

**Endoscopic laser lithotripsy of large bile duct stones.** Cotton PB, Kozarek RA, Schapiro RH, et al. (PBC, Duke University Medical Center, Durham, NC). *Gastroenterology* 99:1128-1133, 1990

Experimental work has established that the Candela (Candela Laser Corporation, Wayland, MA) flashlamp excited dye laser (wavelength, 504 nm) is a highly effective method for fragmenting biliary stones and has minimal potential for injuring the bile duct wall. This technique was evaluated in 25 complex patients whose stones, usually because of large size, did not respond to standard nonoperative treatment. The laser imaging was applied through a quartz fiber and aimed either under direct vision with choledochoscopes passed percutaneously or through a special "mother" duodenoscope or under fluoroscopic guidance at standard duodenoscopy. Laser treatment resulted in some fragmentation of stones in 23 cases. Subsequently, it proved that it was possible to clear the bile duct of stones in 20 patients, 12 of them receiving successful treatment during the same endoscopic procedure. There were no significant complications. This endoscopic technique seems to be a useful new alternative to surgery in patients with large and difficult bile duct stones.

Reprinted with permission by the American Gastroenterological Association.

## Digestive Diseases and Sciences

**Serum diatrizoate level during intraoperative cholangiography in patients without choledochal obstructions.** Sakahira K, Ebata T, Tsunoda Y, Amaha K, Meno K (KS, Tokyo Medical and Dental University, 5-45 Yushima, 1-Chome, Bunkyo-ku, Tokyo 113, Japan). *Dig Dis Sci* 35(9):1085-1088, Sept. 1990

To assess the degree of regurgitation of contrast media during intraoperative cholangiography, serum diatrizoate levels were measured in 15 patients without demonstrable bile duct obstructions. The maximum pressure achieved during the injection was measured in seven cases and ranged from 13 to 39 cm H<sub>2</sub>O (average  $21.7 \pm 9.3$  cm H<sub>2</sub>O). Only two of the 15 patients studied had detected serum diatrizoate (in one patient 7-14  $\mu\text{g/l/ml}$  and the other patient 119-200  $\mu\text{g/l/ml}$ ) after completion of the injection. The data suggest that regurgitation of contrast media into the blood during intraoperative cholangiography does not depend solely on injection pressure. Moreover the data suggest that in order to prevent adverse reactions to accidental intravenous contrast administration nonionic contrast media should be used in most, if not all, radiographic studies as some contrast media reaches the bloodstream.

## Clinical Orthopaedics and Related Research

**Reflex sympathetic dystrophy in children.** Dietz FR, Mathews KD, Montgomery WJ (FRD, Dept. of Orthopaedic Surgery, University of Iowa Hospitals and Clinics, Iowa City, IA 52242). *Clin Orthop* 258:225-231, Sept. 1990

Reflex sympathetic dystrophy (RSD) is an uncommonly reported entity in children. This paper reports five cases of RSD in children and summarizes 80 cases of pediatric RSD reported in the literature. The diagnosis is based on the clinical findings of pain, dysesthesia, and autonomic instability. *Tache cérébrale*, not previously described in the diagnosis of RSD, is a helpful sign of vasomotor dysfunction. RSD in childhood frequently affects the lower extremities, in contrast to the adult localization around the shoulders and hands. Noninvasive, nonpharmacologic management is generally successful. A simple outpatient program of massage and mobilization was beneficial in four of the five patients treated in this study.

## The Journal of Urology

**Computerized tomography in acute pyelonephritis: the clinical correlations.** Tsugaya M, Hirao N, Sakagami H, et al. (MT, Dept. of



Urology, Nagoya City University School of Medicine, Nagoya, Japan). *J Urol* 144:611-613, Sept. 1990

Computerized tomography was performed on 19 patients diagnosed as having uncomplicated acute pyelonephritis. The relationship was investigated among the laboratory findings, presence of flank pain, clinical course and severity of the lesions detected by computerized tomography. In patients febrile for less than 2 weeks healing as assessed by computerized tomography took an average of 76 days. However, in patients with repeated febrile episodes occurring for longer than 2 weeks healing was delayed until an average 232 days after onset. Computerized tomography findings generally correlated well with the erythrocyte sedimentation rate, C-reactive protein level, and presence of pyuria and flank pain. However, in patients with a prolonged course computerized tomography proved to be a more reliable indicator of progress than either the results of laboratory tests or the symptoms. In conclusion, computerized tomography was useful in the diagnosis, assessment of severity and evaluation of healing of acute pyelonephritis.

## Pediatrics

**Decreased bone density in adolescent girls with anorexia nervosa.** Bachrach LK, Guido D, Katzman D, Litt IF, Marcus R (LKB, Dept. of Pediatrics, Stanford University Medical Center, Stanford, CA 94305). *Pediatrics* 86(3):440-447, Sept. 1990

Osteoporosis develops in women with chronic anorexia nervosa. To determine whether bone mass is reduced in younger patients as well, bone density was studied in a group of adolescent patients with anorexia nervosa. With single- and dual-photon absorptiometry, a comparison was made of bone mineral density of midradius, lumbar spine, and whole body in 18 girls (12 to 20 years of age) with anorexia nervosa and 25 healthy control subjects of comparable age. Patients had significantly lower lumbar vertebral bone density than did control subjects ( $0.830 \pm 0.140$  vs  $1.054 \pm 0.139$  g/cm<sup>2</sup>) and significantly lower whole body bone mass ( $0.700 \pm 0.130$  vs  $0.955 \pm 0.130$  g/cm<sup>2</sup>). Midradius bone density was not significantly reduced. Of 18 patients, 12 had bone density greater than 2 standard deviations less than normal values for age. The diagnosis of anorexia nervosa had been made less than 1 year earlier for half of these girls. Body mass index correlated significantly with bone mass in girls who were not anorexic ( $P < .05$ ,  $.005$ , and  $.0001$  for lumbar, radius, and whole body, respectively). Bone mineral correlated significantly with body mass index in patients with anorexia nervosa as well. In addition, age at onset and duration of anorexia nervosa, but not calcium intake, activity level, or duration of amenorrhea correlated significantly with bone mineral density. It was concluded that important deficits of bone mass occur as a frequent and often early complication of anorexia nervosa in adolescence. Whole body is considerably more sensitive than midradius bone density as a measure of cortical bone loss in this illness. Low body mass index is an important predictor of this reduction in bone mass.

Reprinted by permission of PEDIATRICS © 1990.

## The Journal of Pediatrics

**Bone pain as an initial symptom of childhood acute lymphoblastic leukemia: association with nearly normal hematologic indexes.** Jonsson OG, Sartain P, Ducore JM, Buchanan GR (GRB, Dept. of Pediatrics, University of Texas Southwestern Medical Center, 5323 Harry Hines Blvd., Dallas, TX 75235-9063). *J Pediatr* 117:233-237, Aug. 1990

We reviewed the records of all patients with a diagnosis of ALL made at our center during a 13-year period to determine the relationship between bone pain and the hematologic findings at diagnosis of acute lymphoblastic leukemia. Of 296 eligible patients, 179 (60%) had no bone pain (group 1), 65 (22%) had some bone pain (group 2), and 52 (18%) had prominent bone pain that overshadowed other

manifestations of the leukemia (group 3). Statistically significant differences were found between the groups for hemoglobin concentration ( $p < 0.001$ ), leukocyte count ( $p = 0.014$ ), absolute neutrophil count ( $p = 0.002$ ), percentage of circulating blast cells ( $p = 0.009$ ), and platelet count ( $p < 0.001$ ). Children in group 3 had values closer to normal for all these values than those of patients in the other groups. Group 3 patients had symptoms an average of more than 2 weeks longer before diagnosis, and had significantly lower serum uric acid and higher calcium levels than patients in the other groups had. No differences were detected among the groups in age at diagnosis, gender, or survival rate. We conclude that children with acute lymphoblastic leukemia who have prominent bone pain preceding the diagnosis frequently have nearly normal hematologic values and that this feature may contribute to a delay in diagnosis.

## Gastrointestinal Radiology

**Local recurrence of rectosigmoid cancer: what about the choice of MRI for diagnosis?** Balzarini L, Ceglia E, D'Ippolito G, Petrillo R, Tess JDT, Musumeci R (LB, Istituto Nazionale Tumori, MRI Unit, Via Venezian, 1, 20133 Milano, Italy). *Gastrointest Radiol* 15:338-342, 1990

Local recurrence is a frequent event in the natural history of rectosigmoid cancer. The diagnostic possibilities, as well as the limits of computed tomography (CT) and transrectal ultrasonography (TRU), are well known in these conditions. The aim of our study was to define the possible role of magnetic resonance imaging (MRI). We considered 15 examinations carried out in 14 patients, seven of which were obtained before and after Gd-DTPA administration. MRI demonstrated a 93.3% accuracy, 100% sensitivity, and 83.3% specificity in relation to the presence of local recurrence. The presence of pelvic recurrence was suggested on the basis of morphological and signal criteria. The use of paramagnetic contrast gave additional information in four of seven patients. The use of Gd-DTPA may be most beneficial in patients suspected of recurrence, within 6 months of their last treatment, where the diagnosis is more difficult.

**Barium meal study for amyloidosis of the small intestine: measurements on radiograph.** Tada S, Iida M, Fuchigami T, et al. (ST, Second Dept. of Internal Medicine, Faculty of Medicine, Kyushu University, Maidashi 3-1-1, Higashi-ku, Fukuoka 812, Japan). *Gastrointest Radiol* 15:320-324, 1990

In order to determine barium meal radiographic findings characteristic of amyloidosis, we measured the jejunal diameter, valvular width, and intervalvular distance in 25 patients with small bowel amyloidosis and in 30 control individuals, and compared the two groups with each other. As a result, jejunal diameter demonstrated no difference between amyloidosis cases and controls, while there was a significant difference in valvular width or intervalvular distance between the two groups. Our results indicate that objective estimates of the thickening of the valvulae and the shortening of the intervalvular distance by means of measurements of the given roentgenograms greatly contribute to the clinical diagnosis of this disease.

**Esophageal squamous cell carcinoma: MRI evaluation of mediastinum.** Petrillo R, Balzarini L, Bidoli P, et al. (RP, MRI Unit, Istituto Nazionale Tumori, via Venezian No. 1, 20133 Milano, Italy). *Gastrointest Radiol* 15:275-278, 1990

Thirty-two patients with esophageal spinocellular (squamous cell) carcinoma were studied with superconductive magnet in order to evaluate local and extraluminal extent, as well as mediastinal lymph node spread of the disease. In the absence of adenopathy, the localized tumors were considered susceptible to surgical treatment. All patients were operated on within 21 days. The resectability criteria were correctly evaluated in 75% of cases; sensitivity and specificity were 86 and 67%, respectively. Unsatisfactory results were obtained in the evaluation of mediastinal adenopathies. We conclude that

magnetic resonance imaging (MRI) is useful in the preoperative evaluation of resectability criteria in patients with esophageal squamous cell carcinoma.

**CT detection of asymptomatic pancreatitis following ERCP.** Thoeni RF, Fell SC, Goldberg HI (RFT, Dept. of Radiology, University of California San Francisco, San Francisco CA 94143-0628). *Gastrointest Radiol* 15:291-295, 1990

Presence or absence of pancreatitis without symptoms attributable to pancreatitis was assessed by computed tomography (CT) in 31 patients who underwent CT following endoscopic retrograde cholangiopancreatography (ERCP) within a time interval of 0-9 days. Presence or absence of pancreatitis was proved by elevated or normal amylase, and/or surgery, and by symptoms related to pancreatitis. Twenty-five of the patients underwent ERCP without and six with sphincterotomies. Among the six patients, additional procedures included two stent placements, two balloon dilatations, and one basket retrieval. Eleven of 31 patients developed pancreatitis following ERCP. The incidence of pancreatitis was higher in the group with maneuvers (four of six patients or 66.7%) than that without maneuvers (seven of 25 or 28%). Asymptomatic pancreatitis was present in five of 31 patients or 16.1%, and three of these had CT evidence of severe pancreatitis. CT demonstration of pancreatitis following ERCP with or without maneuvers may not always indicate clinically relevant disease.

## Journal of Ultrasound in Medicine

**Sonographic appearance and ultrasound-guided fine-needle aspiration biopsy of breast carcinomas smaller than 1 cm<sup>3</sup>.** Fornage BD, Sneige N, Faroux MJ, Andry E (BDF, Dept. of Diagnostic Radiology, University of Texas M. D. Anderson Cancer Center, 1515 Holcombe Blvd., Houston, TX 77030). *J Ultrasound Med* 9:559-568, Oct. 1990

The purpose of this study was to review the sonographic appearance and the results of ultrasound-guided fine-needle aspiration biopsies of a series of 49 breast carcinomas smaller than 1 cm<sup>3</sup>. No tumor was found to be hyperechoic. Contours were irregular in 69% of cases. In 53%, an echogenic rim was present, and the echotexture was nonhomogeneous in 41%. Sound beam attenuation was present in 39%. The ratio of longitudinal diameter to anteroposterior diameter ranged from 0.67 to 2.25 (mean, 1.08 ± 0.28). Fine-needle aspiration biopsy under continuous real-time sonographic guidance was performed on 36 patients and yielded 30 positive and four suspicious results (sensitivity, 94%), one inadequate specimen, and one false-negative result. With high-resolution hand-held transducers, breast sonography can depict small carcinomas and provides accurate, cost-effective guidance for fine-needle aspiration biopsy.

Reprinted with permission by the American Institute of Ultrasound in Medicine.

## Journal of Computer Assisted Tomography

**Gadolinium-enhanced MR in spinal infection.** Post MJD, Sze G, Quencer RM, Eismont FJ, Green BA, Gahbauer H (MJDP, Dept. of Radiology [R-109], University of Miami School of Medicine, P. O. Box 016960, Miami, FL 33101). *J Comput Assist Tomogr* 14(5):721-729, Sept./Oct. 1990

The purpose of this study was to determine what advantages the use of paramagnetic contrast material might have in evaluating patients clinically suspected of having spinal infection. To determine this we prospectively examined with noncontrast and contrast magnetic resonance (MR) 33 such patients and correlated the MR diagnoses

with clinical and pathologic data. Our results showed the following advantages of gadolinium-enhanced MR: it (a) provided excellent anatomical delineation of all epidural abscesses, routinely differentiating them from the adjacent compressed thecal sac even when this was not possible by noncontrast MR; (b) increased observer confidence in the diagnosis of disk space infection and osteomyelitis in patients with equivocal noncontrast MR; (c) localized those portions of paraspinal masses most likely to yield a positive percutaneous biopsy; and (d) identified active infections from those that had responded adequately to antibiotic therapy. We conclude that contrast MR is a valuable adjunct to noncontrast MR when diagnosis, anatomical clarity, and/or lesion activity requires further elucidation.

**CT-pathology correlation of amiodarone lung.** Ren H, Kuhlman JE, Hruban RH, Fishman EK, Wheeler PS, Hutchins GM (GMH, Dept. of Pathology, The Johns Hopkins Hospital, Baltimore, MD 21205). *J Comput Assist Tomogr* 14(5):760-765, Sept./Oct. 1990

Eleven isolated lungs from patients who had received amiodarone therapy and 22 other lungs from age-race-sex-matched controls autopsied at The Johns Hopkins Hospital were inflation fixed, air dried, and examined by high resolution CT (HRCT). The HRCT findings were directly correlated with gross and histologic changes in these lungs. Intralobular septal thickening and visceral pleural thickening on postmortem HRCT were significantly more severe in the lungs from patients who had received amiodarone than in the controls ( $p < 0.05$ ). These HRCT findings were directly associated with the presence of mural foam cells and intraalveolar foam cells. These results suggest that amiodarone therapy may lead to the accumulation of mural and intraalveolar foam cells, and the accumulation of these foam cells may account for the changes seen on HRCT.

**Thoracic collateral venous channels: normal and pathologic CT findings.** Trigaux JP, Van Beers B (JPT, Service de Radiologie, Cliniques UCL Mont-Godinne, B-5180 Yvoir, Belgium). *J Comput Assist Tomogr* 14(5):769-773, Sept./Oct. 1990

Opacification of thoracic collateral venous channels (CVC) on chest CT is considered a useful sign of superior vena cava (SVC) obstruction, although its lack of specificity has occasionally been emphasized. We compared the degree of opacification of six various thoracic CVC in a group of 36 patients with SVC syndrome and in a control group of 50 patients; a dynamic incremental CT technique with bolus injection was used. Opacification of at least one CVC is inaccurate for the diagnosis of SVC obstruction, with a false-positive and false-negative rate of 34 and 31%, respectively. Only the opacification of the subcutaneous anterior channel provides a good specificity (96%), significantly higher ( $p < 0.05$ ) than that observed for the posterior collateral channels. In patients in whom the clinical records and other direct CT signs of vena cava obstruction are doubtful or absent, opacification of a subcutaneous anterior channel on chest CT should lead to a suspicion of obstruction of the SVC and cavography should be performed.

**MR and CT appearance of iliopsoas bursal distention secondary to diseased hips.** Pritchard RS, Shah HR, Nelson CL, FitzRandolph RL (RSP, Dept. of Radiology, Slot 581, University of Arkansas for Medical Sciences, 4301 W. Markham St., Little Rock, AR 72205). *J Comput Assist Tomogr* 14(5):797-800, Sept./Oct. 1990

Occasionally hip joint disease may extend into surrounding structures, including the retroperitoneum, via the iliopsoas bursa. The enlargement of this bursa may present as an inguinal or pelvic mass that may affect other surrounding structures and can result in a multitude of clinical presentations. The two cases presented herein of iliopsoas bursa distention secondary to hip disease demonstrate the excellent specificity of CT and magnetic resonance in differentiating this clinical entity from other causes of groin masses.



## News

### Swallowing Center Preceptorship

The Johns Hopkins Medical Institutions are sponsoring ongoing preceptorships at The Johns Hopkins Swallowing Center, The Johns Hopkins Hospital, in Baltimore. The program has been established to provide physicians and allied health professionals with practical observation and teaching research so that they might better evaluate the patient who has dysphagia and use a multidisciplinary approach to diagnosis and management of this disorder. Category 1 credit: 40 hr. Fee: 5 days, \$500; 2 days, \$200. Information: Program Coordinator, The Johns Hopkins Medical Institutions, Office of Continuing Education, Turner Bldg., 720 Rutland Ave., Baltimore, MD 21205; (301) 955-2959.

### Imaging Fellowship

Mount Sinai Medical Center of Greater Miami, Miami Beach, FL, is offering a 12-month fellowship that will provide training in all imaging techniques, including neurologic, body, and cardiac procedures. The program has two 6-month rotations, one in MR and CT and one in sonography, nuclear medicine, and nuclear cardiology. Information: Jerome J. Sheldon, M.D., Dept. of Radiology, Mount Sinai Medical Center, 4300 Alton Rd., Miami Beach, FL 33140; (305) 674-2690.

### Palm Beach Magnetic Resonance Imaging Update

The Depts. of Radiology, JFK Medical Center, Atlantis, FL, and University of Florida, College of Medicine, Gainesville, FL, are sponsoring the 6th annual Palm Beach Magnetic Resonance Imaging Update, Feb. 17-20, at the Breakers Hotel, Palm Beach. The course will instruct participants in basic principles and recent advances in clinical MR imaging. Category 1 credit: 20 hr. Fee: physicians, \$525; residents and technologists, \$350. Information: Christine McDonald, Seminar Coordinator, Dept. of Radiology, Box J-374, JHMHC, Gainesville, FL 32610; (904) 395-0288.

### Skeletal Radiology Symposium

The Dept. of Radiology, Hospital of the University of Pennsylvania, is sponsoring Skeletal Radiology Symposium, Feb. 18-22, at the Sun Valley Lodge and Inn, Sun Valley, ID. The symposium will emphasize practical aspects of bone and joint disease, including the latest imaging techniques. Papers will be accepted for presentation. Guest faculty: Robert Bucholz, Deborah Forrester, Harry Genant, Jeremy Kaye, Michael Pitt, Chitranjan Ranawat, and Donald Resnick. Category 1 credit (pending): 23 hr. Fee: physicians, \$495; residents, \$350. Information: Janice Ford, 3340 Market St., Ste. 420, Philadelphia, PA 19104; telephone: (215) 662-2904 or 662-6982; fax: (215) 349-5925.

### North American Society for Cardiac Imaging Annual Meeting

The 18th annual meeting of the North American Society for Cardiac Imaging will be held Feb. 22-24 at the Marriott Hotel on Market St. in San Francisco. The meeting will include a special focus section on cardiac interventional procedures in adults and children and a discussion of pathologic findings. Imaging of the aorta will be the focus of another session. Scientific presentations by the members of the society will be included. Program chairmen: Curtis Green and Larry Box. Information: Jean Parker, Parker and Parker Conferences, Seminars, Conventions; Consulting, Negotiating, and Planning, P. O. Box 7849, Breckenridge, CO 80424; (303) 453-2058.

### Advances in PET and SPECT Imaging

The Johns Hopkins Medical Institutions, Baltimore, are sponsoring Brain Chemistry and Behavior: Advances in PET and SPECT Imaging, March 14-16. The objective of this 7th annual course on imaging of brain chemistry is to inform participants of the latest uses of positron emission tomography (PET) and single-photon emission CT (SPECT) in studies of the brain. Advances in the preparation of radiotracers, instrumentation, quantification of data, measurements of cerebral blood flow, metabolism, and neurotransmission will be covered. The uses of PET and SPECT in various neurologic and psychiatric diseases will be discussed and illustrated with specific examples of case studies. Both clinical studies and current research will be covered. Course director: Henry N. Wagner, Jr. Category 1 credit: 18 hr. Fee: physicians, \$440; residents, \$340. Information: Patty Campbell, Program Coordinator, Office of Continuing Education, 720 Rutland Ave., Baltimore, MD 21205; (301) 955-3839; or Julia W. Buchanan, Course Codirector, (301) 955-8582.

### 1991 MRI Update at Vail

The Dept. of Radiology, Hospital of the University of Pennsylvania, is sponsoring 1991 MRI Update at Vail: Brain, Spine, Head and Neck, and Musculoskeletal, March 25-29, at the Westin Hotel, Vail, CO. The course will emphasize the latest advances in MR imaging techniques and pathologic alterations of the brain, spine, head and neck, and musculoskeletal system. Course director: Herbert I. Goldberg.

Category 1 credit (pending): 27 hr. Fee: physicians, \$525; residents, \$350. Information: Nancy Fedullo, 3440 Market St., Ste. 420, Philadelphia, PA 19104; (215) 662-6904 or 662-6982.

### CT Symposium

The Depts. of Radiology and Continuing Medical Education, University of Wisconsin, Medical School, are sponsoring the 5th annual CT Symposium, April 5-6, at the Edgewater Hotel, Madison, WI. The program will be a review and discussion of the latest developments in CT. Category 1 credits will be awarded. Information: Sarah Aslakson, Continuing Medical Education, 2715 Marshall Ct., Madison, WI 53705; (608) 263-2856.

### Differential Diagnosis in Radiology

The University of Michigan will present its 8th annual course, Differential Diagnosis in Radiology, April 6-8, in Ann Arbor, MI. The format of the course will emphasize a case-solving approach to the unknown radiograph. Differential diagnostic features of common radiologic abnormalities will be stressed in lectures and workshops. Course director: K. H. Vydareny. Category 1 credit: 19.5 hr. Fee: \$200. Information: Ms. Carol O'Connor, Dept. of Radiology, University of Michigan Hospital, Taubman Center 2910, 1500 E. Medical Center Dr., Ann Arbor, MI 48109-0326; (313) 936-4365.

### International Radiopharmaceutical Dosimetry Symposium

The Radiopharmaceutical Internal Dose Information Center, Oak Ridge Associated Universities, the U. S. Food and Drug Administration, and the U. S. Dept. of Energy are cosponsoring the 5th International Radiopharmaceutical Dosimetry Symposium, May 7-10, in Oak Ridge, TN. The symposium will focus on current developments in nuclear medicine that have an impact on calculations of internal doses. Topics will include microdosimetry; radiobiological considerations; and dosimetry of positron emitters, radiolabeled monoclonal antibodies, and new radiopharmaceutical agents. Invited speakers will present comprehensive papers on these and other pertinent subjects. The program committee is soliciting abstracts for contributed papers. Abstracts must be received by Jan. 11. Category 1 credits will be awarded. Fee: before March 1, \$150; March 1 and after, \$175. Information: Evelyn Watson, Program Committee, Radiopharmaceutical Dosimetry Symposium, Oak Ridge Associated Universities, P. O. Box 117, Oak Ridge, TN 37831-0117; telephone: (615) 576-3450; fax: (615) 576-3194.

### Thoracic Imaging 1991

The Society of Thoracic Radiology will present Thoracic Imaging 1991, May 13-17, at the Four Seasons Yorkville Hotel, Toronto. The course is designed to be a detailed review of the state of the science and art of cardiopulmonary radiology. Category 1 credit: 30 hr. Fee: physicians, \$500; residents, fellows, and technologists, \$350. Information: Dawne Ryals, Ryals & Associates, P. O. Box 1925, Roswell, GA 30077-1925; telephone: (404) 641-9773; fax: (404) 552-9859.

### International Workshop on Hypertrophic Osteoarthropathy

The 1st International Workshop on Hypertrophic Osteoarthropathy will be held Sept. 8-11 in Dubrovnik, Yugoslavia. The program will

include formal discussions on epidemiology, pathogenesis, pathology, radiology, disease associations, and therapy and presentations of papers by participants in the workshop. Information: Prof. Ivo Jajić, Secretariat of the First International Workshop on Hypertrophic Osteoarthropathy, Dept. of Physical Medicine and Rheumatology, Lovčenska 100, 41000 Zagreb, Yugoslavia; telephone: 41-572440.

### The American Board of Radiology Examinations

Written examinations for the American Board of Radiology (ABR) are scheduled for Oct. 3-4, 1991. Oral examinations will be held at the Executive West Hotel in Louisville, KY, June 3-7, 1991. The ABR will accept applications for admission to the examinations after July 1, but not later than Sept. 30, in the year *preceding* the year in which the examination is to be taken. For application forms and further information: Office of the Secretary, The American Board of Radiology, 300 Park, Ste. 440, Birmingham, MI 48009.

### Meeting and Course Review

For the reader's convenience, a summary of upcoming meetings and courses is provided. Detailed listings are given in the *AJR* issue given in parentheses.

**Cyanoacrylate Embolization Course**, times arranged, Baltimore (July 1990)

**Visiting Fellowships in Ultrasound**, times arranged, Baltimore (Aug 1990)

**Visiting Fellowships in Interventional Radiology**, times arranged, Baltimore (Oct 1990)

**Caribbean Cruise—MRI at Sea**, Jan. 5-12 (Dec 1990)

**MRI Fellowships at Johns Hopkins**, Jan. 7-11, April 8-12, and June 17-21, Baltimore (Oct 1990)

**Future and Present MRI**, Jan. 9-13, Naples, FL (Aug 1990)

**Caribbean Cruise—Breast Imaging at Sea**, Jan. 12-19 (Nov 1990)

**Physics and Instrumentation**, Jan. 14-18, Philadelphia (Dec 1990)

**Advanced Seminars in Diagnostic Imaging**, Jan. 19-21, Laguna Niguel, CA (Aug 1990)

**Seminars in MRI**, Jan. 19-26, Vail, CO (Nov 1990)

**Park City 1991: MRI Update**, Jan. 20-24, Park City, UT (Oct 1990)

**Diagnostic Imaging in Aruba**, Jan. 20-26, Aruba (Aug 1990)

**Cross-Sectional Anatomy**, Jan. 21-25, Philadelphia (Dec 1990)

**International Symposium on MR Imaging**, Jan. 23-27, Garmisch-Partenkirchen, Bavaria (Aug 1990)

**Society for Pediatric Radiology Research and Education Grants**, application deadline, Feb. 1 (Sept 1990)

**Midwinter Radiological Conference**, Feb. 1-3, Los Angeles (Nov 1990)

**Annual AFIP Neuroradiology Review Course**, Feb. 2-3, Bethesda, MD (Dec 1990)

**Practical Aspects of Diagnostic Radiology/Medical Imaging IV**, Feb. 2-8, Snowmass Village, CO (Nov 1990)

**Big Sky Radiology Conference**, Feb. 3-7, Big Sky, MT (Nov 1990)

**Practical Radiology 1991**, Feb. 3-8, near Vancouver, B.C. (Dec 1990)

**Angio-Interventional Radiology**, Feb. 4-5, Coronado (San Diego), CA (Oct 1990)

**Obstetrics and Gynecology**, Feb. 4-8, March 11-15, and April 22-26, Philadelphia (Dec 1990)

**Mid-Pacific Radiological Conference**, Feb. 5-9, Maui, HI (Nov 1990)

**Intraluminal Ultrasound Imaging**, Feb. 6, Coronado (San Diego), CA (Dec 1990)

**Duplex Imaging**, Feb. 6-9, Coronado (San Diego), CA (Dec 1990)



**Computed Body Tomography 1991—The Cutting Edge**, Feb. 7–10, Orlando, FL (Nov 1990)  
**Obstetric and Gynecology Sonographic Update**, Feb. 9–10, Coronado (San Diego), CA (Dec 1990)  
**Annual Intermountain Imaging Conference**, Feb. 9–16, Steamboat Springs, CO (Nov 1990)  
**Contemporary Diagnostic Imaging**, Feb. 11–15, Mauna Lani, HI (Oct 1990)  
**Current Topics in Diagnostic Imaging**, Feb. 11–15, Cerromar Beach, Puerto Rico (Dec 1990)  
**Mammographically Detected Early Breast Cancer**, Feb. 14–17, Naples, FL (Dec 1990)  
**Society of Gastrointestinal Radiologists Annual Meeting and Postgraduate Course**, Feb. 17–21, Carlsbad, CA (Oct 1990)  
**Imaging the Head, Spine, and Musculoskeletal System**, Feb. 17–22, Kauai, HI (Oct 1990)  
**MR Imaging Course at Disney World**, Feb. 17–22, Orlando, FL (Oct 1990)  
**Sun Valley Imaging Meeting**, Feb. 23–March 2, Sun Valley, ID (Nov 1990)  
**Positron Emission Tomography**, Feb. 24–27, Dana Point, CA (Dec 1990)  
**Principles and Practice of Clinical MRI**, Feb. 28–March 3, Lake Buena Vista, FL (Nov 1990)  
**Advanced Seminars in Diagnostic Imaging**, March 1–3, Laguna Niguel, CA (Nov 1990)  
**Winter Congress on Diagnostic Imaging**, March 2–9, Val D'Isere, France (Dec 1990)  
**Masters Diagnostic Radiology Conference**, March 3–8, Maui, HI (Dec 1990)

**Practicum in Diagnostic Ultrasound**, March 4–8 and April 22–26, Baltimore (Oct 1990)  
**Course on MR Imaging**, March 4–8, Coronado (San Diego), CA (Nov 1990)  
**Musculoskeletal Imaging**, March 4–8, Barbados (Nov 1990)  
**Update on Body Imaging and Neuroradiology**, March 4–8, Acapulco, Mexico (Dec 1990)  
**Pediatric Radiology Course**, March 11–15, Park City, UT (Dec 1990)  
**Breast Imaging Conference**, March 21–24, Lake Buena Vista, FL (Dec 1990)  
**Orthopedic Radiology 1991**, March 25–27, Boston (Nov 1990)  
**Ultrasound 1991**, April 2–5, Boston (Nov 1990)  
**National Council on Radiation Protection and Measurements Annual Meeting**, April 3–4, Washington, DC (Nov 1990)  
**Society for Magnetic Resonance Imaging Annual Meeting**, April 13–17 (Nov 1990)  
**San Diego Residents' Radiology Review Course**, April 21–26, La Jolla, CA (Dec 1990)  
**Clinical Nuclear Medicine 1991**, April 22–25, Boston (Nov 1990)  
**Introduction to Interventional Radiology**, April 27, La Jolla, CA (Dec 1990)  
**International Pediatric Radiology '91**, May 27–31, Stockholm (Aug 1990)  
**Leeds Gastroenterology Course for Radiologists**, July 1–5, Leeds, England (Dec 1990)  
**International Congress of Radiation Research**, July 7–12, Toronto. Deadline for abstracts, Jan. 15 (May 1990)  
**World Congress in Ultrasound**, Sept. 1–6, Copenhagen (Sept 1990)  
**European Congress of Radiology 1991**, Sept. 15–20, Vienna, Austria (Oct 1990)

### **Correction: Practical Aspects of Diagnostic Radiology/Medical Imaging IV**

Vanderbilt University Medical Center is sponsoring Practical Aspects of Diagnostic Radiology/Medical Imaging IV, Feb. 2–8, 1991, at the Snowmass Conference Center, Snowmass Village, CO. Emphasis will be on everyday problems, *not* on the research interests of the faculty. Category 1 credit: 25 hr. Fee: physicians, \$550; residents and fellows, \$350 (letter required). Information: Marilyn D'Asaro, Vanderbilt Division of CME, CCC-5316 Medical Center North, Nashville, TN 37232; (615) 322-4030.

*AJR* carries announcements of courses, symposia, and meetings of interest to its readers if received a minimum of 5 months before the event. There is no charge; receipt of items by the *AJR* Editorial Office is not acknowledged. Submit items for publication typed double-spaced. Provide title, date, location, brief description, sponsor, course directors, fees, category I credit, and address and telephone number for additional information. Faculty from the host institution will not be listed. Guest faculty names will appear **only** if initials are provided. Mail news items to *AJR* Editorial Office, 2223 Avenida de la Playa, Suite 103, La Jolla, CA 92037-3218.

# American Roentgen Ray Society: Officers, Committees, and Membership Information

## Officers

**President:** M. Paul Capp

**President-elect:** John A. Kirkpatrick, Jr.

**1st Vice-president:** A. Everette James, Jr.

**2nd Vice-president:** Andrew K. Poznanski

**Secretary:** Joseph T. Ferrucci, Jr.

**Treasurer:** Beverly P. Wood

**Executive Council:** R. J. Alfidi, R. N. Berk, M. P. Capp, W. J. Casarella, N. R. Dunnick, R. G. Evens, J. T. Ferrucci, Jr., A. E. James, Jr., J. A. Kirkpatrick, Jr., A. M. Landry, Jr., J. E. Madewell, A. A. Moss, A. K. Poznanski, L. F. Rogers, R. J. Stanley, J. H. Thrall, K. H. Vydareny, N. O. Whitley, B. P. Wood, G. R. Leopold, chairman

## Committees

**Editorial Policy:** R. N. Berk, E. Buonocore, Melvin M. Figley, S. v. W. Hilton, M. S. Huckman, C. A. Rohrmann, Jr., R. J. Stanley, R. I. White, W. J. Casarella, chairman

**Education and Research:** C. B. Higgins, B. J. Hillman, R. A. McLeod, R. J. Stanley, W. M. Thompson, N. O. Whitley, chairman

**Finance and Budget:** R. J. Alfidi, R. K. Gedgaudas-McClees, J. R. Thornbury, K. H. Vydareny, J. H. Thrall, chairman

**Nominating:** G. A. W. Gooding, L. F. Rogers, K. H. Vydareny, chairman

**Publications:** E. Buonocore, C. A. Rohrmann, Jr., R. J. Stanley, R. I. White, W. J. Casarella, chairman

**Membership:** J. E. Madewell, A. A. Moss, K. H. Vydareny, R. J. Alfidi, chairman

## Representatives to Other Organizations

**American Board of Radiology:** J. A. Kirkpatrick, Jr., E. C. Klatte, L. F. Rogers

**American College of Radiology:** J. M. Dennis, R. A. Gagliardi, J. E. Madewell, B. L. McClennan, R. J. Stanley

**American Medical Association:** S. F. Ochsner, delegate; K. L. Krabbenhoft, alternate; K. L. Kidd, CPT Advisory Committee

**American National Standards Institute:** M. E. Haskin

**National Council on Radiation Protection and Measurements:** F. Miraldi, E. L. Saenger

**Armed Forces Institute of Pathology:** J. E. Madewell

## Meeting Arrangements

**Annual Meetings:** May 5–10, 1991, Sheraton Boston, Boston; May 10–15, 1992, Marriott's World Center, Orlando, FL

**Annual Meeting Committee:** H. C. Carlson, J. K. Crowe, N. R. Dunnick, R. R. Lukin, R. J. Stanley, R. D. Steele, Jr., A. M. Landry, Jr., chairman

**Instructional Courses:** R. J. Stanley, chairman; Bruce McClennan, associate chairman

**Scientific Program:** P. Arger, E. Buonocore, D. O. Davis, K. B. Hunter, D. Kushner, T. C. McLoud, W. A. Murphy, Jr., L. B. Talner, J. H. Thrall, J. A. Kirkpatrick, Jr., chairman

**Scientific Exhibits:** J. R. Haaga, R. G. Ramsey, N. R. Dunnick, chairman

## ARRS Membership

An application form is printed in this issue of the Journal. For consideration at the 1991 ARRS meeting, send completed forms before February 1, 1991, to American Roentgen Ray Society, 1891 Preston White Dr., Reston, VA 22091. Active members are graduates of an approved medical or osteopathic school or hold an advanced degree in an allied science. They must practice radiology or work in an associated science in the United States or Canada and be certified by the American Board of Radiology, American Osteopathic Board of Radiology, or Royal College of Physicians of Canada or otherwise adequately document training and credentials. Corresponding members are foreign radiologists or scientists who are active in radiology or an allied science. Members-in-training are residents or fellows in radiology or postgraduate students in an allied science. Additional application forms can be obtained from the ARRS offices in Reston, VA.

## Business Office

Paul Fullagar, Executive Director, American Roentgen Ray Society, 1891 Preston White Dr., Reston, VA 22091; (703) 648-8992.



# Invitation to the 1991 American Roentgen Ray Society Meeting in Boston, MA, May 5–10, 1991

I am pleased to extend an invitation to all radiologists to attend the 91st annual meeting of the American Roentgen Ray Society in Boston, MA, May 5–10, 1991. In keeping with the ARRS tradition, outstanding scientific and social programs will be provided.

The excitement of a meeting set in Boston, MA, in the spring requires no further description. The opportunity for busy radiologists to attend a major national meeting while enjoying all that Boston, MA, has to offer is ideal.

The scientific program, instructional courses, and categorical course are certain to be interesting and informative (see schedule below).

## Scientific Program

Two hundred scientific papers have been selected from more than 400 abstracts. Scientific sessions will be devoted to all major body systems, angiography, interventional techniques, sonography, and mammography, as well as technologies. Special emphasis has been placed on discussion of new developments.

The innovative and timely Friday morning minisymposium is entitled "Breast Imaging Update 1991." An outstanding faculty has been assembled for what I am sure will be a very stimulating program.

## Instructional Courses

Robert J. Stanley, Chairman, and Bruce McClennan, Associate Chairman of the Instructional Course Committee, have put together 60 instructional courses. Faculty members have been drawn from across the country. A superlative educational experience is anticipated, and advance registration is recommended.

## Categorical Course

An extraordinary categorical course on spine and body MR imaging has been fashioned. The course covers all aspects of the field, including equipment and principles of diagnosis. This course is certain to be popular, and advance registration is advised.

## Summary of 1991 American Roentgen Ray Society Meeting

Sunday May 5	Monday May 6	Tuesday May 7	Wednesday May 8	Thursday May 9	Friday May 10
	8:00–9:30 Instructional courses	8:00–9:30 Instructional courses	8:00–9:30 Instructional courses	8:00–9:30 Instructional courses	8:00–10:00 Symposium: breast imaging update
10:00–12:30 Categorical course: spine and body MR imaging	10:00–10:30 Opening cere- monies				
	10:30–12:30 Scientific programs	10:00–12:30 Scientific programs	10:00–12:30 Scientific programs	10:00–12:30 Scientific programs	10:30–12:30 Symposium: breast imaging update
2:00–3:00 Categorical course: spine and body MR imaging	1:30–3:30 Categorical course: spine and body MR imaging	1:30–3:30 Scientific programs	1:30–3:30 Caldwell lecture and award session	1:30–3:30 Scientific programs	
3:30–5:00 Categorical course: spine and body MR imaging	4:00–5:30 Instructional courses and cate- gorical course: spine and body MR imaging	4:00–5:30 Instructional courses and cate- gorical course: spine and body MR imaging	4:00–5:30 Instructional courses and cate- gorical course: spine and body MR imaging	4:00–5:30 Instructional courses and cate- gorical course: spine and body MR imaging	

**Scientific Exhibits**

The more than 200 scientific exhibits coordinated by N. Reed Dunnick will cover the entire breadth of the field of diagnostic radiology. The technical exhibits will be integrated among the scientific exhibits to enhance the interaction of the attendees with technical exhibitors, a format that has proven to be very satisfactory.

**Caldwell Lecture**

N. Thorne Griscom, M.D., has agreed to present the Caldwell Lecture at the 1991 meeting. This promises to be one of the highlights of the meeting and is concerned with pediatric pulmonary disorders encountered in the adult.

**Social Events**

Boston, MA, offers an unlimited number of diversions, and Abner M. Landry, Jr., Chairman of the Annual Meeting Committee, has engaged a Boston-based tour consultant to plan a variety of tours. The annual golf and tennis tournaments for attendees and their companions are scheduled for Monday. The traditional cocktail party given by the society in the exhibit area for all registrants will be Sunday evening and will provide a convenient and early meeting place.

This promises to be a truly outstanding event in exceptional surroundings. I hope you will be able to accept our invitation. Plan now to attend.

John A. Kirkpatrick  
President-Elect, ARRS

**Forthcoming ARRS Meeting Information**

Details of the American Roentgen Ray Society Meeting in Boston, MA, May 5–10, 1991, will appear in the **February**, **March**, and **April** 1991 issues of the *AJR*. Information about the scientific program, instructional programs, and social events and hotel and travel forms will be published in the Journal.

See page 213 of this issue for more information concerning the meeting.



# 1991 ARRS Meeting Summary, May 5–10, 1991 Boston, MA

A comprehensive description of the meeting, including the instructional courses, categorical course, and the Friday symposium, will appear in the February issue of the *AJR*. Meeting and registration forms also will be found in the February and March issues. These may be photocopied.

## Accreditation

All courses and scientific sessions carry AMA Category 1 credit on an hour-for-hour basis.

## Meeting Format

*Scientific Program.* Sessions will be grouped in parallel sessions so that registrants may choose topics related to their interests. A total of 189 scientific papers will be presented, Monday–Thursday, May 6–9. In addition, on Wednesday, May 8, the afternoon session will feature award papers and the Caldwell Lecture, which will be delivered by N. Thorne Griscom, M.D. On Friday, May 10, there will be a special 4-hr symposium on breast imaging.

*Categorical Course on Spine and Body MR.* This 15.5-hr course will be held Sunday–Thursday.

*Luncheon Sessions.* Registrants may enroll in special luncheon sessions, Monday–Thursday. A box lunch will be provided.

## Exhibits

*Scientific and Technical Exhibits and Case of the Day* will be set up in the Hynes Convention Center, Hall A, adjacent to the Sheraton Boston Hotel, Monday–Thursday, May 5–9. The Case of the Day will be presented by John F. O'Connor of Boston University School of Medicine.

## Local Activities

*General Reception.* Sunday evening, May 5, for all registrants.

*Golf Tournament.* Monday, May 6 at a local country club.

*Men's and Women's Tennis Tournaments.* Monday, May 6, at the Winchester Tennis Club.

*Local Tours.* See February issue of the *AJR* for a description of the activities and registration forms.

## Meeting Registration

Preregistration will be accepted until April 20. There will be on-site registration. Official badges and program books will be available at the registration desk, Sheraton Boston Hotel. No confirmations will be mailed.

## Course Registration

Register early—enrollment is limited. List first, second, and third choices for each period. Also, indicate whether you wish to take the categorical course. Deadline for registration by mail is April 20. All ticket orders will be filled according to postmarked date. Course tickets *will not* be mailed. Tickets will be available beginning at 1:00 p.m. on Saturday, May 4, at the ARRS registration desk in the Sheraton Boston Hotel. There will be on-site registration for courses not already filled.

## Hotel Registration

Reservations are handled by the ARRS Housing Bureau, Sheraton Boston Hotel, Attn: Reservations Office, 39 Dalton St., Boston, MA 02199. These must be received by April 13. Make check payable to Sheraton Boston Hotel. See reservation form in February *AJR* for prices and complete instructions.

## Fees

### Meeting:

ARRS members and resident members . . . . .	No fee
Nonmembers . . . . .	\$250
Nonmember physicians in training (with verification) . . . . .	25
Categorical course . . . . .	75
Luncheon sessions/each . . . . .	12
Local tours . . . . .	20–75

## Cancellations and Fee Refunds (Excluding Hotel Fees)

Fees will be refunded only if cancellation is received by April 20, 1991. Send to American Roentgen Ray Society, 1891 Preston White Drive, Reston, VA 22091.

## Transportation Discounts

United Airlines is offering discounts of up to 40% on airfares. Call (800) 521-4041 and reference ARRS account number 429JW.

Hertz Rent A Car is offering special rates on car rentals. Reserve a Hertz car at these special rates through United Airlines when you make your plane reservations, or call Hertz directly at (800) 772-3773.

# Information and Application for Membership in the American Roentgen Ray Society

## General Information

The American Roentgen Ray Society, founded in 1900, has been a forum for progress in radiology since shortly after the discovery of X-rays. From its beginning and continuing to today, the ARRS has been guided by dedication to the goal of the advancement of medicine through the science of radiology and its allied sciences.

The goal of the ARRS is maintained through an annual scientific and educational meeting, and through publication of the *American Journal of Roentgenology*.

The annual meeting consists of instructional courses, scientific sessions, a symposium, scientific exhibits, and commercial exhibits. A special categorical course is also offered. Category I CME credits are available on an hour-for-hour basis.

The monthly *American Journal of Roentgenology* is a highly respected peer review journal with a worldwide subscription base. For over 75 years the *AJR* has been accepted as one of the best specialty journals available in the world, and this reputation grows each month.

A recently developed quarterly ARRS newsletter keeps members informed of events and general Society news.

## Application Instructions

### Candidates for Active Membership

1. An Active member must be a graduate of an approved medical school or hold an advanced degree in one of the physical, chemical or biological sciences and be certified by the American Board of Radiology, the American Osteopathic Board of Radiology, the Royal College of Physicians of Canada, or document training and credentials that are adequate to qualify for membership. Active members shall actively practice radiology or one of its branches in the United States or Canada. Such members are eligible to participate in all activities of the Society, including membership on committees, and have full voting privileges.
2. Application must be on an official form, signed by the applicant and at least two members of the American Roentgen Ray Society, active or emeritus, in good standing, who endorse the applicant.
3. Application fee is \$50 (payable when billed for dues).
4. Annual dues are \$150, payable on January 1 of each year following the initial year. First year dues will be invoiced following candidate election at the annual meeting. Of this amount, \$50 is for a 1-year subscription to the *American Journal of Roentgenology*, beginning with the July issue following election to membership.
5. Application must be received by February 1 for action during the current year's meeting.

### Candidates for In-Training Membership

1. In-training members must be serving in a radiology residency program approved by the Radiology Residency Review Committee, the American Osteopathic Board of Radiology, or the Royal College of Physicians of Canada, or in an approved post-residency fellowship, or be a postgraduate student in an allied science. Training status must be verified by the program director. In-training members have special consideration in fees and subscription rates to the Society journal. Such members cannot hold Society offices or vote.
2. Application must be on an official form and signed by the applicant and by the applicant's training or residency program director.
3. In-training status is limited to a maximum of five years starting with the entrance date into the radiology residency. In the last year, each in-training member will receive an application for active membership from the Society. Those who do not apply for transfer to active membership shall be dropped from membership at the end of the fifth year, but can later apply as a new member through the process outlined for active status.
4. There is no application fee. Annual dues are \$25. Membership includes a subscription to the *American Journal of Roentgenology* and admission to the annual meeting without payment of the registration fee.
5. Membership applications will be acted on when received.

### Corresponding Membership

A corresponding member must meet the qualifications of active membership, but reside and practice in a foreign country. Corresponding members shall pay dues and fees, but shall not have the privileges of voting nor of holding elective office.

#### All Applicants

1. Do not remit application fee or dues until requested.
2. Send completed forms to: American Roentgen Ray Society  
1891 Preston White Drive  
Reston, Virginia 22091



For ARRS  
Office Use

Date Rec'd \_\_\_\_\_

I.D.# \_\_\_\_\_

AMERICAN ROENTGEN RAY SOCIETY

APPLICATION FOR MEMBERSHIP

Date: \_\_\_\_\_

Category of Membership: ☐ Active  
(Check One) ☐ Corresponding  
☐ In-Training

Name (Please Print) \_\_\_\_\_  
First Initial Last

Degree(s) \_\_\_\_\_

Mailing Address \_\_\_\_\_  
Street/Box

Date of Birth \_\_\_\_\_

City/State/Country \_\_\_\_\_ Zip Code

Telephone ( ) \_\_\_\_\_

A. Education: (List name of institution, years attended, and degree and type received.)

Undergraduate: \_\_\_\_\_  
\_\_\_\_\_

Graduate (Medical School, Graduate School, etc.):  
\_\_\_\_\_  
\_\_\_\_\_

Postgraduate (Internship, Residency, Fellowship, etc.):  
\_\_\_\_\_  
\_\_\_\_\_  
\_\_\_\_\_

B. Licensure:

Licensed to practice \_\_\_\_\_ in \_\_\_\_\_ since \_\_\_\_\_  
(Type) (State, Province, etc.)

C. Appointments/Memberships: (In-Training applicants: skip to Section F on reverse.)

Present Appointments: Academic \_\_\_\_\_  
\_\_\_\_\_

Hospitals \_\_\_\_\_  
\_\_\_\_\_

Memberships in Scientific Societies: \_\_\_\_\_  
\_\_\_\_\_

Offices or Committee Assignments: \_\_\_\_\_  
\_\_\_\_\_

Government Service (Military or Civilian) \_\_\_\_\_  
(Position) (Years)

D. Credentials:

(To be completed by Active and Corresponding applicants only.)

I hereby certify that I was issued a certificate of qualification in \_\_\_\_\_  
(Specialty)  
in \_\_\_\_\_ by the \_\_\_\_\_  
(Year) (Name of Qualifying Board)  
Other Credentials: \_\_\_\_\_  
  
Signature: \_\_\_\_\_

E. References:

(To be completed by Active and Corresponding applicants only.)

We, active or emeritus members in good standing of the American Roentgen Ray Society, and acquainted with the applicant, do recommend him/her for membership in the Society. (Two references are required.)  
  
Name (Please Print) 1. \_\_\_\_\_ 2. \_\_\_\_\_  
Address \_\_\_\_\_  
\_\_\_\_\_  
  
Signatures: \_\_\_\_\_

F.

IN-TRAINING APPLICANTS MUST COMPLETE THIS SECTION

Credentials:

I certify that I am serving as a Resident/Fellow in \_\_\_\_\_  
(Specialty)  
at \_\_\_\_\_ Date program began (begins): \_\_\_\_\_  
(Name of Institution)  
date program to end: \_\_\_\_\_ I understand that in-training membership is limited to a maximum of 5 years.  
  
Applicant Signature: \_\_\_\_\_

Verification: (Program Director or Department Chairman only)

I certify that the applicant is in training at the institution named and qualifies for enrollment as a member-in-training of the American Roentgen Ray Society.  
  
Name (Please Print) \_\_\_\_\_  
Address: \_\_\_\_\_  
\_\_\_\_\_  
  
Signature \_\_\_\_\_

Send completed form to: American Roentgen Ray Society  
1891 Preston White Drive  
Reston, Virginia 22091



# Classified Advertisements

## Positions Available

**PEDIATRIC RADIOLOGIST**—The Dept. of Radiology at the University of Minnesota has a full-time position available in the pediatric section at the rank of tenure-track assistant professor or tenured associate professor, beginning March 16, 1991. At the assistant professor level, minimum requirements are board certification in radiology, a minimum of 1 yr postresidency specialty training or experience in pediatrics, and a demonstrated involvement in quality research accepted or published in peer-reviewed journals. Appointment at the rank of associate professor requires a minimum of 4 yr postresidency experience, a professional distinction in research and writing, and demonstrated effectiveness in teaching and advising. Responsibilities will include all facets of pediatric radiology as well as graduate and undergraduate medical instruction. Research performance will be strongly encouraged and evaluated. Salary is negotiable and competitive, and is dependent on past scholarly productivity and post-M.D. experience. Applicants must be licensed or able to obtain a license to practice medicine in the state of Minnesota before appointment date. Applications will be accepted through Feb. 28, 1991. Send letters to William M. Thompson, M.D., Professor and Chairman, Dept. of Radiology, Box 292 UMHC, University of Minnesota, 420 Delaware St., S.E., Minneapolis, MN 55455. The University of Minnesota is an equal opportunity educator and employer and specifically invites and encourages applications from women and minorities. 1a

**RADIOLOGIST NEEDED** with experience in CT, ultrasound, nuclear medicine, mammography, and general radiology to provide vacation coverage for 2 practices in rural western Montana. One practice requires some traveling. Position would be excellent for person who wishes to semiretire in a pleasant scenic area. Great opportunity for recreational activities. Send inquiries to Tyler H. Gill, M.D., 1200 Westwood Dr., Hamilton, MT 59840; (406) 363-2211. 1ap

**SEATTLE AND SUBURBS**—BC associate needed immediately for rapidly growing practice dedicated to mammography and breast diagnosis. Four offices; 2 also have general ultrasound. 85% OB-GYN. Mammography or ultrasound fellowship or extensive experience helpful. Association leading to partnership. Send letter and CV to Irwin Schiller, D.O. and Marita Acheson, M.D., c/o Breast Diagnostic Center, 411 Strander Blvd., #303, Seattle, WA 98188; (206) 575-9123. 1-3ap

**MUSCULOSKELETAL/MRI RADIOLOGIST, THOMAS JEFFERSON UNIVERSITY HOSPITAL** We are recruiting a faculty musculoskeletal radiologist (either junior or senior level) for an important and challenging position in our dept. The position encompasses MRI of the musculoskeletal system and other body applications, plain film musculoskeletal radiology, tomography, and arthrography. Jefferson currently operates 4 GE 1.5-T Signa MRI units and 3 CT scanners. Close relationships are maintained with busy orthopedic, rheumatology, trauma, and spinal cord injury services. A thriving clinical practice, active teaching program, and well-equipped research facilities all combine to make this an outstanding career opportunity. Excellent faculty incomes and many other benefits are provided. Interested applicants should contact David C. Levin, M.D., Chairman, Dept. of Radiology, Thomas Jefferson University Hospital, 11th and Walnut Sts., Philadelphia, PA 19107; (215) 955-7265. Jefferson is an equal opportunity/affirmative action employer. 1-4a

**SAN FRANCISCO BAY AREA**—Progressive BC/BE diagnostic radiologist sought to join 5 BC radiologists serving a 200-bed, acute-care hospital and outpatient clinic. Special competency in MRI and cross-sectional imaging desired. Quality practice in desirable suburban setting. We offer a competitive salary and generous benefits package. Send CV to Martin Portnoff, M.D., Dept. of Radiology, Kaiser Permanente Medical Center, 200 Muir Rd., Martinez, CA 94553; (415) 372-1100. EOE. 1-2a

**SALEM, MA**—July 1991 position available for BC, recently trained radiologist with strong interest in general diagnostic radiology and expertise in mammography and OB-GYN ultrasound for Women's Imaging Center to open next yr. Eleven radiologists practicing in a large, community teaching hospital on Boston's beautiful North Shore. Contact Courtney Neff, M.D.; (508) 741-1200, ext. 4420. 1-2ap

**DIAGNOSTIC RADIOLOGIST**—Fantastic practice opportunity in the beautiful setting of Lewistown, MT. Central Montana Medical Center is a 132-bed, combined facility (47 acute and 85 long-term) with a progressive and very well equipped hospital. The excellent 1-radiologist practice has little night or weekend call responsibilities, good locum tenens coverage for vacations, and excellent proven income. Imaging dept. does CT, nuclear medicine, MRI, ultrasound, etc. Comfortably paced practice working with high-caliber medical staff. Immediate opening. Contact Bob Conrad, CEO, Central Montana Medical Center, Box 580, Lewistown, MT 59457; (406) 538-7711. 1ap

**BC RADIOLOGIST, KANSAS CITY, MO**—Seven radiologists currently covering a 600-bed, tertiary medical center seek a radiologist with a special competency or fellowship in nuclear medicine. The position, open immediately, includes competitive salary and fringe benefits, and leads to full partnership. Send CV and letter of inquiry to J. M. Speckman, M.D., 6400 Prospect, Ste. 310, Kansas City, MO 64132. 1-4ap

**FACULTY OPENING IN THORACIC IMAGING** The Johns Hopkins University Hospital has an opening at the junior faculty level in the Division of Thoracic Imaging. The division is fully integrated across all modalities including MRI, CT, and interventional procedures. Research opportunities are exceptional with protected research time available to rapidly establish an academic career. Academic rank and salaries will be determined by previous experience. The candidate must be board-certified. Contact Elias A. Zerhouni, M.D., Director, Thoracic Imaging & MRI Divisions, Dept. of Radiology, Johns Hopkins Hospital, Baltimore, MD 21205; (301) 955-4062. 1-6a

**MAMMOGRAPHY FACULTY POSITION**—The Dept. of Radiology at Johns Hopkins University Hospital has a faculty position available in mammography. The mammography section is part of the thoracic imaging division. The section offers a strong potential for academic growth with emphasis on original research and teaching. Protected academic time is available for candidates interested in developing a strong academic career. Support, resources, and opportunities are available for creative research. The candidate can also participate in all other aspects of diagnostic imaging as desired. Academic rank and salary will be determined by previous experience. Candidate must be board-certified. Contact Elias A. Zerhouni, M.D., Director, Thoracic Imaging and MRI Divisions, Dept. of Radiology, Johns Hopkins Hospital, Baltimore, MD 21205; (301) 955-4062. 1-6a

**DIAGNOSTIC RADIOLOGIST IMMEDIATE OPENING AT ROSE MEDICAL CENTER (RMC), DENVER, CO**—A 7-person radiology group is recruiting a radiologist with fellowship training in interventional radiology. The practice involves all imaging modalities. Highly competitive first yr salary and generous fringe benefit package. Position leads to offer of equal shares in the professional corporation after 1 yr, if mutually agreed upon. RMC is affiliated with the University of Colorado. Contact David W. Wilder, M.D. or Jeffrey A. Levy, M.D.; (303) 320-2256. 1-3a

**FLORIDA, STAFF RADIOLOGIST**—Opportunity for board-certified diagnostic radiologist with experience in reading plain films, fluoroscopy, ultrasound, CT, nuclear medicine, and some angiography in the radiology service at this progressive, GM&S, Dept. of Veterans Affairs (VA) Medical Center. Potential academic appointment and affiliation in surgery with the University of Florida. Competitive salary plus incentive pay commensurate with qualifications. Excellent employment benefits including 30 days paid vacation and 15 days sick leave per yr; liberal life and health insurance benefits; malpractice insurance; and retirement program. Moving expenses paid. "Florida's new gateway city" is located in northern Florida with a mild climate yr round. Extensive outdoor recreational activities, reasonable cost of living, no state income tax, and fine schools and nearby universities provide opportunity for continuing education and cultural diversion. Florida license not required. Contact or send CV to Richard Parker, M.D., Chief of Radiology, VA Medical Center, Lake City, FL 32055-5892; (904) 755-3016, ext. 2543. An equal opportunity employer. 1a

**MUSCULOSKELETAL RADIOLOGIST**—The Dept. of Radiology, University of Texas Health Science Center at San Antonio, seeks a musculoskeletal radiologist. Salary and academic rank are commensurate with the candidate's experience. Excellent research opportunities are available in a new 30,000 sq. ft. research imaging center. The Health Science Center lies in the northern suburbs of San Antonio adjacent to excellent living areas and schools. Replies and CVs should be sent to Stewart R. Reuter, M.D., Chairman, Dept. of Radiology, 7703 Floyd Curl Dr., San Antonio, TX 78284-7800. Equal opportunity/affirmative action employer. 1-3a

**RADIOLOGY FACULTY POSITIONS**—The University of Tennessee, Memphis, in conjunction with UT Medical Group, Inc., is actively recruiting radiologists in diagnostic, pediatric, and interventional radiology, angiography, ultrasound, and MRI. The applicant must be board-certified or eligible. Competitive salaries, excellent benefits, and research/clinical opportunities. Blacks, women, handicapped, and other minorities are encouraged to apply. The University of Tennessee, Memphis, is an equal employment opportunity/Title IX/Section 504/affirmative action employer. Send CV to Barry Gerald, M.D., Chairman, Dept. of Radiology, The University of Tennessee, Memphis, 800 Madison Ave., Memphis, TN 38163. 1a

**CONNECTICUT**—Expanding group of 8 radiologists has a position available for an additional angio/interventional, BC/BE radiologist with expertise in general radiology also. Practice includes a 435-bed, fully equipped, university-affiliated, community hospital and a 47-physician, multispecialty clinic. Excellent salary and benefits leading to full partnership after second yr. For information, send CV to Paul C. Lakin, M.D., Dept. of Radiology, New Britain General Hospital, 100 Grand St., New Britain, CT 06050. 1-4ap

**DIAGNOSTIC RADIOLOGIST**—Recent fellowship or faculty status preferred. Early partnership. We are a private-practice group of 8 full- and 2 part-time, board-certified radiologists all with prior fellowship and/or faculty status. We practice general radiology with specialty interests accommodating all diagnostic and interventional modalities including MRI. Our 350-bed hospital is a primary teaching affiliate of the University of Massachusetts Medical School with year-round medical students and house staff in several depts. The Berkshire Mountains are a desirable summer, winter, and foliage resort community less than a 3-hr drive to Boston, New York City, Vermont skiing, and the ocean. The quality of our practice, hospital and affiliate office, and style of life are superior. Please respond with CV to Stuart J. Masters, M.D., Chairman, Dept. of Radiology, Berkshire Medical Center, 725 North St., Pittsfield, MA 01201. 1ap

**UCSD SCHOOL OF MEDICINE**—The Dept. of Radiology seeks a diagnostic radiologist to participate in clinical service, medical student and resident teaching, and research projects in the subspecialty of osteoradiology. Qualifications required are board-eligibility/certification, California medical license, and 1-yr fellowship in osteoradiology. One yr experience in osteoradiology, including MRI, in an academic program is preferred. Title series is assistant professor (in-resident or clinical series, not currently a tenure-track position); level based on years experience; salary commensurate with rank, and step of appointment based on the established salary schedule of the UCSD School of Medicine Faculty Compensation Plan. The University of California, San Diego, is an equal opportunity/affirmative action employer. All CVs received before Jan. 31, 1991, will be considered. Send to Donald Resnick, M.D., Chief of Radiology, VA Medical Center, 3350 La Jolla Village Dr., San Diego, CA 92161. 1a

**UCSD SCHOOL OF MEDICINE**—The Dept. of Radiology is seeking an ultrasonologist to assist in clinical service, medical student and resident teaching, and research projects. Participation in other diagnostic subspecialties is available. Qualifications required are board-eligibility/certification, California medical license, and 1 yr fellowship training in ultrasound. Title series is assistant or associate professor (in residence or clinical series, not currently a tenure-track position); level based on years experience; salary commensurate with rank, and step of appointment based on the established salary schedule of the UCSD School of Medicine Faculty Compensation Plan. The University of California, San Diego, is an equal opportunity/affirmative action employer. All CVs received before Jan. 1, 1991, will be given full consideration. Send to Dolores Pretorius, M.D., Chief of Ultrasound (H-759), UCSD Medical Center, 225 Dickinson St., San Diego, CA 92103. 1a

**VASCULAR/INTERVENTIONAL RADIOLOGIST** Large radiology group in western Massachusetts is seeking a BC vascular/interventional radiologist to join existing 5-person vascular/interventional team. Fellowship or equivalent experience required. Must also have expertise in CT and general diagnostic radiology. Primary assignment at 868-bed, tertiary-care hospital with radiology residency program. Practice also includes 3 community hospitals and 6 private offices. Full partnership after 1 yr. Available July 1991. Send CV to Director of Recruiting, Radiology and Imaging, Inc., 130 Maple St., Springfield, MA 01103. 1-3ap

**DIAGNOSTIC RADIOLOGIST**—Excellent opportunity in well-established, South Carolina hospital-based practice for BC/BE radiologist. Competitive salary. Full partnership in 1 yr. Send CV to Box H87, *AJR* (see address this section). 12-3ap

**THE UNIVERSITY OF TEXAS HEALTH SCIENCE CENTER AT SAN ANTONIO** announces formation of a Research Imaging Center. This center is designed to use modern imaging methods in evaluating pharmaceutical therapies in both animal and human models. Thirteen new positions are available in 1990/1991 and an equal number are anticipated the following yr. Applications are invited for the following faculty or administrative positions: Director of PET Facility—An M.D.- or Ph.D.-level scientist to provide overall direction of the PET facility operation, supervise personnel, and conduct an independent research program. Appointment at the assistant or associate professor level will depend on experience. Radiochemist—A Ph.D.-level scientist to direct operation of the cyclotron and radiochemistry hot lab in support of the PET operations and conduct an independent research program. Appointment at the assistant or associate professor level will depend on experience. Associate Radiochemist/Physicist—A Ph.D.-level scientist to be responsible for the operation of the cyclotron and related radiochemistry developments. Appointment as assistant professor or lecturer will depend on experience. Radiopharmacist—A Master's (or Ph.D.) level radiopharmacist who is licensed and certified to prepare, test, and certify radiopharmaceuticals for human use. The appointment will be at the assistant professor level. NMR Physicist or Chemist—A Master's (or Ph.D.) level scientist with a minimum of 2 yr experience operating and assisting others in the use of a 2-T (45-cm bore) MRI/MRS unit. The appointment will be at the level of lecturer. NMR Chemist or Biologist—A Master's (or Ph.D.) level scientist to operate high resolution NMR spectrometers and assist others in using these instruments. The appointment will be at the level of lecturer. All of the above faculty will have the opportunity to participate in both medical and graduate school (radiological sciences) educational programs with appointments depending on the interests and experience of the successful candidates. The University of Texas Health Science Center at San Antonio is an equal opportunity employer. Send cover letter/CV to Gary D. Fullerton, Ph.D., Dept. of Radiology, UTHSCSA, 7703 Floyd Curl Dr., San Antonio, TX 78284-7800. 12-2ap

**STAFF PHYSICIAN/RADIOLOGY**—Vacancies exist for 2 diagnostic radiologists, board-certified or in examining process, with experience in CT, ultrasound, and invasive diagnostic procedures. Hospital located in northeastern Tennessee near ski slopes and Appalachian Trail in Smoky Mountains. Great area for outdoor activities including hiking, golf, tennis, and all water sports. Affiliated with Quillen College of Medicine in Johnson City, TN. Direct inquiries to Harold Ross, M.D., Chief, Radiology Service, VA Medical Center, Mountain Home, TN 37684; (615) 926-1171 ext. 7401. An equal opportunity employer. 12-1a

**MAINE**—Excellent opportunity for BC/BE, fellowship-trained neuroradiologist with progressive, well-established, small group. Live and work in college community in southern region close to coast, mountains, and lakes. Competitive compensation package leading to partnership. Affiliated with 200-bed, modern community hospital. Send CV to New England Health Search, 63 Forest Ave., Orono, ME 04473; (207) 866-5680 or (207) 866-5685. 11-2ap

**MRI RADIOLOGIST**—An 8-person radiology group in southern New Jersey, 15 min from Philadelphia, seeks a board-certified radiologist with specialty training in body MRI to help run a new GE 1.5-T Signa MRI. Busy, dynamic practice consists of 2 hospitals as well as a full-service private office which also houses the MRI unit. Competitive compensation package will lead to full partnership. Send CV or call Steven Singer, M.D., Kings Highway and Princeton Ave., Woodbury, NJ 08096; (609) 848-4998. 11-1ap

**GENERAL DIAGNOSTIC RADIOLOGIST**—Position available to join 11-member, private-practice group in 500-bed, university-affiliated, tertiary-care hospital in Allentown, PA. The position offers a competitive salary benefit package commensurate with training leading to full partnership. The Radiology Dept. offers a fellowship in CT, ultrasound, and angiography/interventional. The hospital has active residency programs in medicine and surgery. Allentown is located in the Lehigh Valley (population 250,000) and is 2 hr from New York City, 1 hr from Philadelphia, and 1 hr from the Pocono Mountains. For information, please contact Robert Kricun, M.D., or Alan Wolson, M.D., Lehigh Valley Hospital Center, 1200 S. Cedar Crest Blvd., P.O. Box 689, Allentown, PA 18105; (215) 776-8088. 12-2ap

**ULTRASOUND RADIOLOGIST**—The Dept. of Radiology at the University of Arkansas for Medical Sciences is inviting applications for a faculty radiologist at the instructor or assistant professor level to do primarily ultrasound. The position would require someone with a reasonable amount of ultrasound experience. Also included would be participation in CT and nonvascular interventional procedures. The UAMS is the only medical school and teaching hospital in the state of Arkansas. There are approximately 1150 beds in our institution, which includes the University Hospital, an adjacent VA Hospital, and a large Children's Hospital. For further information or to apply, please contact Steven K. Teplick, M.D., Vice-Chairman, Dept. of Radiology; (501) 686-6902. The University of Arkansas is an equal opportunity employer. 12-1ap

**NUCLEAR MEDICINE OR INTERVENTIONAL RADIOLOGIST**—Progressive, 7-person group seeks to add an interventional radiology or nuclear medicine (special competency preferred) fellowship-trained radiologist for spring 1991. This busy, expanding practice is hospital- and recently full-service imaging center-based. Both institutions use leading edge technology. The proximity of Lake Tahoe, the gaming industry, the state capitol, and a major university provides many cultural, entertainment, and sporting opportunities. Send CV to Colby Laughlin, M.D., Reno Diagnostic Center, 590 Eureka Ave., Reno, NV 89512. 12-3a

**DIAGNOSTIC RADIOLOGIST**—Excellent opportunity for BC/BE radiologist to join established group of 4 in July 1991 providing all services for 380-bed hospital. Rewarding practice in university city of 200,000. Send CV and letter to N. Thomas Rice, M.D., Central Baptist Hospital, 1740 S. Limestone St., Lexington, KY 40503. 12-2ap

**PHILADELPHIA, PA**—Temple University Hospital and School of Medicine seeks the following board-certified radiologists: Vascular/Interventional Radiologists (2)—Section Head and staff positions available. Positions involve responsibilities in patient care and teaching. Candidates with fellowship training and research skills preferred. Abdominal imaging radiologist—Strong clinical skills in ultrasound, CT, MRI, urography, and gastrointestinal radiology. Fellowship training is preferred. An interest in medical student and radiology resident teaching is required. Interest in abdominal imaging research desirable. Pulmonary radiologist—Candidate should be a senior-level radiologist at the professor or associate professor level with a primary interest in pulmonary radiology. Ideal candidate will have fellowship training in pulmonary radiology and proficiency in all areas of radiologic practice. Candidates should have demonstrated skills as a teacher and an interest in research. Applicants should send current CV (indicate position of interest), bibliography, and 3 letters of recommendation to Temple University School of Medicine, Attn: Francis J. Shea, M.D., Deputy Chairman, Dept. of Diagnostic Imaging, Broad and Ontario Sts., Philadelphia, PA 19140. An equal opportunity/affirmative action employer. 1xa



**CHIEF, RADIOLOGY DEPT.**—The VA Medical Center in Louisville, a major affiliate of the University of Louisville, School of Medicine, is seeking applications for the Chief of Diagnostic Radiology. The radiology dept. is equipped with state-of-the-art equipment, which is the result of a recent \$13 million clinical and educational addition. The dept. includes facilities for digital vascular imaging, CT, ultrasound, and all noncardiac nuclear medicine imaging. The radiology dept. is now staffed by a group of 6 physicians and performs approximately 50,000 exams/yr. Qualifications include board certification in diagnostic radiology and eligibility for an academic appointment at the University of Louisville School of Medicine. Please send inquiries to Hollis A. Thomas, M.D., Professor and Chairman, Dept. of Diagnostic Radiology, Humana Hospital-University of Louisville, 530 S. Jackson St., Louisville, KY 40202. An equal opportunity/affirmative action employer. 12-1ap

**NEURORADIOLOGIST** with fellowship training in MR to join 7-member group in community practice. Candidate should be board-certified. Facilities include 2 community hospitals and several outpatient facilities, 2 MRI, 3 CT; installing new angio suite. Rapidly growing coastal community in southwest Florida with attractive cultural and recreational amenities. Generous salaried position leading to partnership. Reply to Box H83, *AJR* (see address this section). 12-1ap

**INTERVENTIONAL RADIOLOGIST** to join 7-member group in community practice. Candidate should be board-certified. Recent fellowship training preferred. Facilities include 2 community hospitals and several outpatient facilities. Installing new special procedure suite. Rapidly growing coastal community in southwest Florida with attractive cultural and recreational amenities. Generous salaried position leading to partnership. Reply Box H85, *AJR* (see address this section). 12-1ap

**CHIEF RADIOLOGIST AND RADIOLOGISTS**—In anticipation of the opening of our clinical addition, we are actively seeking BC radiologists for chief and staff positions. Facilities include fluoroscopy, tomography, diagnostic ultrasound, general radiology, CT, and angiography. Joint faculty appointment with our major affiliate, the Marshall University School of Medicine, dependent on candidate's clinical and academic experience. Our medical center is currently expanding to 250 beds and doubling facility size with a clinical addition. Radiology service will be located in new state-of-the-art facilities in the addition. Work with a rotating staff of radiologists, a chief technician, a permanent technical staff, and transitional residents in radiology. For more information on these challenging opportunities, please call or send your CV to Ms. R. Bookwalter, Office of the Chief of Staff, VA Medical Center, 1540 Spring Valley Dr., Huntington, WV 25704; (304) 429-6755, ext. 2517. 12-2a

**IMMEDIATE OPENING**—Radiologist needed to join 1 other in a 60-bed, hospital-based practice with GE 1.5-T MRI, 9800 CT, Doppler ultrasound, SPECT, nuclear, and biplane angio. Excellent salary leading to early partnership. Unique opportunity to join a sophisticated practice while living among the redwoods in a northern California coastal city with a referral population of over 100,000. Send CV to Dr. Jackson, 3560 N. St., Eureka, CA 95501; (707) 445-5993. 12-2ap

**DIAGNOSTIC RADIOLOGIST**—Eight board-certified radiologists in expanding, hospital-based private practice seek BC/BE general radiologist to associate. Competence in all modalities expected with need for MRI training emphasized for 2 MRI facilities in practice. Opportunity in midwestern city of 72,000 people offers generous compensation/vacation. Full partnership after 2 yr. Reply to Box H89, *AJR* (see address this section). 12-3ap

**WEST RIVER REGIONAL MEDICAL CENTER** of Hettinger, ND, is seeking a board-certified or eligible radiologist to join a progressive and innovative health-care team using state-of-the-art technology in a rural/frontier setting. General radiology including in-house mammography, ultrasound, nuclear medicine, echocardiography with color Doppler, and CT. MRI available. Unique medical staff (awarded 1982 Outstanding Rural Health Project Award) and 2 staff physicians (awarded North Dakota Physician of the Year). World-class upland game hunting, including pheasant, grouse, partridge, deer, and antelope. Superb fishing for walleye, trout, and salmon. Send CV and letter of inquiry to Bryon J. Dockter, President and CEO, West River Regional Medical Center, Rte. 2, Box 124, Hettinger, ND 58639; (701) 567-4561. 12-1ap

**DIAGNOSTIC RADIOLOGIST** needed in Conway Hospital, a community hospital located 10 mi. west of the resort/seaside community of Myrtle Beach, SC. The dept. performs 44,000 exams/yr including CT, MRI, nuclear medicine, ultrasound, mammography, and special procedures. All exams are done on state-of-the-art equipment. Our 3-person group offers a very strong financial package with all benefits including 17-wk vacation. Lovely, rapidly growing resort area includes 60 mi. of sandy beaches, 70 golf courses, and beautiful seaside homes. Contact Gary Rike, M.D., P.O. Box 917, Conway, SC 29526; (803) 347-7277. 12-5ap

**PART-TIME MAMMOGRAPHY/ULTRASOUND RADIOLOGIST**—Immediate opening for a half-time diagnostic radiologist with a 12-member group in a Pacific Northwest city of 60,000+. BC/BE with expertise/interest in mammography and ultrasound. Equipment is state-of-the-art. Competitive salary and benefits. Located amidst the recreational activities of the Puget Sound and Cascade Mountains. Send letter, personal sketch, and CV to J. W. Little, M.D., 3822 Colby Ave., Everett, WA 98201; (206) 259-3256. 12-2ap

**DIAGNOSTIC RADIOLOGIST, SAN FRANCISCO BAY AREA**—The Permanente Medical Group is seeking a progressive BC/BE diagnostic radiologist with special competency in MRI and cross-sectional imaging to join 5 other BC radiologists serving a 200-bed, acute-care hospital and outpatient clinic. This quality practice, located in a desirable suburban setting, offers all imaging modalities. Competitive salary and generous benefits. Send CV to Martin Portnoff, M.D., Kaiser Permanente Center, 200 Muir Rd., Martinez, CA 94553; (415) 372-1110. EOE. 12-2a

**FACULTY NEURORADIOLOGIST, THOMAS JEFFERSON UNIVERSITY HOSPITAL**—The Dept. of Radiology at Thomas Jefferson University Hospital in Philadelphia has an immediate opening for a faculty neuroradiologist. This can be either at a very senior or junior level. Our dept. currently operates 4 GE 1.5-T Signa MRI units, and also has a modern neurosciences imaging center. Aside from the MRI units, this facility has a Philips angio room with DSA, a myelography room, 2 CT scanners, reading rooms, and faculty offices. There are 6 faculty members in the neuro division, as well as 5 2-yr neuro fellows. Our practice is growing rapidly and close clinical and research relationships exist with neurosurgery, neurology, orthopedic surgery, and a large spinal-cord-injury center. The dept. also maintains experimental laboratories of its own. Candidates should ideally have broad clinical, research, and teaching interests. Excellent salary and fringe benefits. Interested persons should contact David C. Levin, M.D., Chairman, Dept. of Radiology, Thomas Jefferson University Hospital, Philadelphia, PA 19107; (215) 955-7264. Jefferson is an equal opportunity/affirmative action employer. 11-1a

**BOSTON, IMMEDIATE OPENING**—Radiologist wanted to join busy, well-established, private-practice group with 4 outpatient facilities. Expertise in ultrasound and mammography. No evening or weekend call. Excellent life-style, partnership opportunity. Send letter and CV to Box E49, *AJR* (see address this section). 9-2ap

**BC/BE DIAGNOSTIC RADIOLOGIST** with skills in all aspects of radiology, including CT, ultrasound, nuclear medicine, interventional, MR, and mammography sought to join a dynamic group of 6 BC radiologists covering a busy, progressive, community hospital, 2 private offices, and an outpatient women's center. Modern dept., state-of-the-art equipment, attractive vacation, CME, and benefits package. 30 min west of Philadelphia. Position available immediately but will wait for right person. Reply with CV to L. Griska, M.D., Dept. of Radiology, Montgomery Hospital, Powell and Farnance Sts., Norristown, PA 19401. 11-2ap

**IMMEDIATE OPENING, DIAGNOSTIC RADIOLOGIST**—Excellent opportunity for a young, dynamic, preferably board-certified radiologist to join an active, 9-member group. Growing practice includes a 700-bed hospital system with state-of-the-art equipment and excellent working facilities. Skills in all phases of diagnostic radiology desired. Attractive and competitive benefits package leading to full partnership. Contact Sanford E. Rabushka, M.D., 11133 Dunn Rd., Ste. 1017, St. Louis, MO 63136; (314) 653-4300. 11-4ap

**BROAD SPECTRUM RADIOLOGIST/UPSTATE NEW YORK**—Radiologist wanted for hospital-based practice 90 mi. northwest of New York City. Excellent recreational activities and easy access to metropolis. All modalities available. Excellent salary and benefits leading to early partnership. Immediate availability, but can wait for right applicant. Call G. Bilick; (914) 794-3300, ext. 2216 or send CV to P.O. Box 144, Harris, NY 12742. 11-2ap

**RADIOLOGIST**—Veterans Affairs Medical Center, Wilkes-Barre, PA, has an immediate vacancy for a board-certified radiologist. This 473-bed, teaching medical center with a 120-bed (plus 60 additional beds currently under construction) nursing home-care unit is affiliated with Temple University School of Medicine, Hahnemann University School of Medicine, and Episcopal Hospital, Philadelphia, PA. Wilkes-Barre is located near the Pocono Mountains resort area within a 2½-hr drive of New York City and Philadelphia. For additional information, contact William K. Grossman, M.D., Chief of Staff; (717) 821-7207. An equal opportunity employer. 11-1a

**NEW ORLEANS PARTNERSHIP OPPORTUNITY**—Would you like to live in "America's most interesting city"? Would you like to become a partner in a well-established, highly successful radiology group practice that has the latest technology, including a free-standing MRI center with a 1.5-T GE Advantage system? We are a large, multispecialty group practicing in hospital, outpatient offices, and a new breast center. We will offer a BC radiologist, with interest in MR and/or vascular procedures, an exciting job opportunity. Contact Harold R. Neitzschman, M.D., 4400 General Meyer Ave., Ste. 211, New Orleans, LA 70131; (504) 368-5074. 11-1ap

**RADIOLOGISTS**—Seven-member group seeks board-certified radiologists to join a progressive, hospital/clinic practice in scenic western Arkansas town of approximately 100,000. All modalities represented in practice. Competitive salary leading to early, full partnership. Liberal fringe benefits and vacation. At least 3 mo documented MRI training necessary. Interested parties please send CV to W. T. Huskison, M.D., P.O. Box 3887, Fort Smith, AR 72913; (501) 452-9416 collect. 11-1ap

**CHICAGO AREA**—Opening for full- or part-time radiologist to join progressive, 8-member group in a large, community hospital in Harvey, IL (southern suburb of Chicago), beginning July 1991. State-of-the-art equipment in CT, ultrasound, nuclear medicine, angiography, MRI, and diagnostic radiology is available. Approximately 120,000 exams/yr. We are looking for a well-trained, flexible radiologist interested in both general radiology and all facets of imaging. Nuclear cardiology and mammography experience is preferred. Interested parties should contact Jay Bronner, M.D., or Peter Kucharski, M.D., Ingalls Hospital, Harvey, IL 60426; (708) 333-2300, ext. 5600. 12-1ap

**RADIOLOGIST**—A second radiologist is needed for a 54-physician, multi-specialty group located in western Montana. Experience or formal training in mammography a must; general radiologic procedures excluding CT and MRI. Offered salary and benefits generous. Send CV to Administrator, Western Montana Clinic, P.O. Box 7609, Missoula, MT 59807. 12-1ap

**STAFF INTERVENTIONAL RADIOLOGIST SOUGHT** at the New York Hospital-Cornell University Medical Center for July 1991. The position includes clinical and teaching responsibilities as well as the opportunity for research. Equipment includes 3 state-of-the-art Philips digital labs and a 4-bed recovery room. Applicants should be trained in all aspects of peripheral vascular and nonvascular interventions. For further information, please contact Thomas A. Sos, M.D.; (212) 746-2600. 12-1a

**VASCULAR/INTERVENTIONAL RADIOLOGIST** The University of Texas Southwestern Medical School, Dept. of Radiology, is seeking BC/BE vascular/interventional radiologists at the rank of assistant/associate professor who have had a CVI fellowship or extensive experience in the subspecialty. Responsibilities will include clinical work in all aspects of the subspecialty at Parkland Memorial Hospital, Zale-Lipsky Hospital, and the VA Hospital as well as teaching of medical students, residents, and fellows. Clinical and basic research opportunities abound at this rapidly growing medical school complex. Salary negotiable and competitive and is dependent on the level of experience. Interested individuals should contact Helen C. Redman, M.D., Dept. of Radiology, The University of Texas Southwestern Medical School, 5323 Harry Hines Blvd., Dallas, TX 75235. UT Southwestern is an equal opportunity/affirmative action employer. 12-2a

**IMMEDIATE OPENING**—BC/BE radiologist to join medium-size group in Austin, TX. Practice covers major trauma center and outpatient radiology facility. In addition to general diagnostic services, outpatient facility also provides CT and MRI services on 2 GE 9800 scanners and on GE 1.5-T and 0.5-T MR units. Applicants are requested to contact Drs. Boyd, Gray, or Lava at 711 W. 38th St., Ste. B-8, Austin, TX 78705; (512) 454-8718. 12-5ap

**RADIOLOGY/NEURORADIOLOGY, GEORGIA** Group of 5 radiologists seeks individual with neuroradiology fellowship training and interest in continuing to practice other aspects of radiology. Well-established, private practice in 300-bed, acute-care hospital with neuro intensive care unit and private office. All imaging modalities are represented including MRI. Excellent benefits with full partnership in 2 yr. This is an opportunity to join an expanding practice in a beautiful coastal city with excellent recreational and cultural advantages. Send CV to Don Starr, M.D., Savannah Radiologists, P.A., 503 Eisenhower Dr., Savannah, GA 31499. 12-2ap

**RURAL RADIOLOGY PRACTICE**—Interested in being an extremely busy general radiologist in a rural midwest setting? We are seeking a fourth board-certified general radiologist to replace our recently retired senior partner. Hays is a town of 25,000 (5000 students at Fort Hays State University) in central Kansas, and functions as a regional medical center with 40-50 physicians. We are the sole radiology practice in northwest Kansas, reading about 70,000 exams/yr in Hays and surrounding towns. Equipment is state-of-the-art including 2 CT, a GE Signa MRI, 2 Acuson 128 color Doppler, angiography with DSA, nuclear medicine, and fluoro and plain films. The practice is egalitarian, with identical work schedules, call, and vacation times. Contact Robert F. Bowerman, M.D., Ph.D., for more details at Radiology Associates of Hays, P.A., P.O. Box 833, Hays, KS 67601; (913) 625-6521. 12-2ap

**RADIOLOGIST, CHICAGO AREA**—A 7-member radiology group in far southwest suburb of Chicago metropolitan area is currently interviewing BC/BE radiologists for a position available July 1991. Fellowship training attractive but not essential. A highly recommended candidate directly from residency will be given equal consideration. Expertise in general radiology, imaging, and angiography required. Radiology services are provided for 524-bed community hospital and soon-to-be-completed joint venture MRI center, together generating 85,000 exams/yr. Number of exams, as well as group revenue, has steadily increased in the past several years and is likely to continue as we are in a rapidly growing, middle/upper class area. We are oriented toward providing top-quality radiology to referring physicians, as well as a pleasant work environment and significant leisure time for ourselves. Features include competitive starting salary, full benefit package, full partnership after 3 yr, equal division of call among group members, generous vacation time (8 wk to start), and teleradiography. Equipment includes the following state-of-the-art items: Siemens Hi-Q CT; 2 Acuson units with color-flow Doppler and endovaginal probe (third unit ordered); Phillips ARC-14 DVI-S specials room with full digital capability; fully equipped nuclear medicine dept. with dual head bone table and third SPECT camera ordered; 1.5-T Siemens SP MRI with MR angiography; and GE Senographe 600-T mammography unit. Send CV to Box G73, AJR (see address this section). 11-1ap

**SKELETAL RADIOLOGIST**—A staff position is available at the Cleveland Clinic Foundation in the 4-member Section of Musculoskeletal Radiology. The Cleveland Clinic is a 1,000-bed, academic, tertiary-care facility with a large outpatient population and international referral base. The section provides CT and MR as applied to the musculoskeletal system. In addition, the section performs bone biopsies, quantitative bone densitometry, arthrography, and reads a large volume of plain films. There is a large radiology residency at the Cleveland Clinic. A musculoskeletal fellowship will begin in 1991. Applicants should be fellowship-trained or possess equivalent experience. Send CV to Bradford J. Richmond, M.D., Head, Section of Musculoskeletal Radiology, Clinic Radiology, Desk A21, Cleveland Clinic Foundation, 9500 Euclid Ave., Cleveland, OH 44195. The Cleveland Clinic is an equal opportunity employer. M-F-H-V. 11-1a

**RADIOLOGIST**—Seven-person group seeks general radiologist with fellowship training and special interest in MRI for 92-bed hospital and several imaging centers. Practice in the rapidly growing north San Diego and Temecula Valley areas. Send CV to North Coast Imaging Radiology Medical Group, Inc., 1582 W. San Marcos Blvd., Ste. 104, San Marcos, CA 92069; (619) 744-6442. 11-2ap

**MINNEAPOLIS, MINNESOTA**—Practice opportunity for a board-certified radiologist with subspecialty interest in musculoskeletal imaging. MR experience is required. Procedural skills are desirable, as there is a growing volume of invasive orthopedic procedures. Practice is based at a rapidly growing, privately owned, freestanding outpatient imaging center equipped with 2 GE 9800 CT scanners, 2 GE Signa 1.5-T MR scanners, and related fluoroscopic-radiographic and ultrasound equipment. Practice also includes coverage of a 750-bed, tertiary-care medical center and adjacent satellite clinic. Five radiologists in practice currently. One distant MR facility operating and plans for more. Investment opportunities for radiologists involved in the practice as well as academic orientation and opportunity for subspecialization. Excellent benefits. Send CV and responses to Cooper R. Gundry, M.D., Center for Diagnostic Imaging, 5775 Wayzata Blvd., Ste. 190, Minneapolis, MN 55416. No telephone calls please. All inquiries confidential. 11-1ap

**BODY MRI/ABDOMINAL IMAGING**—Board-certified radiologist with fellowship training in MRI needed for a position beginning July 1, 1991. Must have fellowship training in MRI, and an interest in CT and GI studies for practice in 578-bed, advanced, metropolitan, tertiary-care teaching hospital. Radiology group is an academically oriented private practice. Send inquiries to Harvey L. Neiman, M.D., Chairman, Dept. of Radiology, The Western Pennsylvania Hospital, 4800 Friendship Ave., Pittsburgh, PA 15224. 11-1a

**PHYSICIAN/RADIOLOGIST**—Large radiology group with 2 hospitals and multiple private offices with state-of-the-art equipment seeks a radiologist who is board-certified in nuclear medicine. Competitive salary and benefit package. Send CV to Radiology Associates of Burlington County, P.A., 175 Madison Ave., Mt. Holly, NJ 08060. 11-1ap

**TEN-PERSON RADIOLOGY GROUP** located in Corpus Christi is seeking a new associate to start July 1990 or as late as July 1991. Must be board-certified or eligible. Will perform all diagnostic studies, including interventional, CT, MRI, nuclear medicine, and ultrasound. Please send CV to Search Committee, P.O. Box 5608, Corpus Christi, TX 78465-5608. 1xa

**DIAGNOSTIC RADIOLOGISTS**—Owing to expansion and retirement, several positions are available with a large, dynamic radiology group in the Central New Jersey/Bucks County, PA, region. Openings for radiologists with expertise in 1 or more of the following: nuclear medicine, general, and angio/interventional. Immediate availability. Send letter and CV to E. Tarasov, M.D., 838 W. State St., Trenton, NJ 08618. 12-1a

**INDIANAPOLIS, IN**—Practice opportunity for a radiologist to serve as medical director of a new, freestanding, privately owned, high-field MR imaging center. Facility will be managed by and affiliated with the Center for Diagnostic Imaging in Minneapolis, MN. MR experience mandatory. Subspecialty experience in MR desirable. Board certification and licensure in Indiana required. Please send inquiries with CV to Cooper R. Gundry, M.D., Center for Diagnostic Imaging, 5775 Wayzata Blvd., Ste. 190, Minneapolis, MN 55416. All inquiries entirely confidential. No telephone calls please. 12-2a

**CHALLENGING LOCUM TENENS POSITIONS AVAILABLE NOW**—Work at your convenience, full- or part-time. Competitive compensation. No hassles, politics, or paperwork. Paid malpractice insurance, housing, and transportation. Put an experienced leader to work for you! Contact LOCUM Medical Group, 30100 Chagrin Blvd., Cleveland, OH 44124; (800) 752-5515. 1xa



**ULTRASOUND SECTION CHIEF, UNIVERSITY OF MARYLAND**

The University of Maryland Hospital seeks a chief for the ultrasound section of the Dept. of Radiology. Although already well-equipped, this position offers a great opportunity for expansion and development, both with the new all-digital Dept. of Radiology under construction at the adjoining VA Hospital and in a new planned all-digital Dept. of Radiology to be constructed at the University Hospital. Applicants should have specialist training and fellowship in ultrasound and a willingness to be involved in the teaching of residents and students. Academic rank and salary are commensurate with experience. The radiologists are organized as a professional corporation, offering excellent fringe benefits. Baltimore is a superb place to live and work. It has all the amenities of a large metropolitan center, yet is small enough to avoid most of the problems (traffic, inflated property values, etc.) of our largest cities. It is only 3 hr from the ocean and Washington, Philadelphia, and New York are readily accessible. Submit CV to Gerald S. Johnston, M.D., Dept. of Diagnostic Radiology, 22 S. Greene St., Baltimore, MD 21201; (800) 866-8667, ext. 3477. Affirmative action/equal opportunity employer encourages applications from members of minority groups. 9-2ap

**THE DEPT. OF RADIOLOGY AT TRIPLER ARMY MEDICAL CENTER, HONOLULU, HI**

is recruiting academic radiologists for several divisions of the dept. including ultrasound, chest, skeletal, neuro, and general diagnostic radiology. Our dept. offers a fully accredited residency program with 20 residents and 16 attending full-time staff. Numerous consultants from across the country lecture on a continuing and regular basis. The hospital is a modern, tertiary-care center serving Hawaii and the entire Pacific Basin. A strong residency program, diverse and interesting patient population, excellent equipment, and a tropical lifestyle are positive aspects of the practice. Academic credentials and/or experience are necessary. Recently graduated fellows are encouraged to apply. Board certification is mandatory. Candidates should be particularly interested in patient care, teaching, and research. Salary and benefits are competitive and generous. Tripler is an EO/EEO employer. Please contact Mark F. Hansen, M.D., Col., MC, Chief, Dept. of Radiology, TAMC, HI 96859-5000; (808) 433-6393. 8-7a

**FACULTY ULTRASOUND RADIOLOGIST, THOMAS JEFFERSON UNIVERSITY HOSPITAL**

Jefferson's Dept. of Radiology wishes to recruit a faculty radiologist to work in our division of diagnostic ultrasound. Candidates at all levels will be considered. This division is housed in 1 of the largest and best equipped facilities in the world and is extensively involved in the full range of ultrasound studies including obstetrical, vascular, echocardiography, invasive, endoluminal, and both biliary and kidney stone lithotripsy. A new outpatient ultrasound facility is under construction adjacent to the main campus. The position provides excellent salary and benefits, protected research time each wk, and an opportunity to become associated with 1 of the most academically productive ultrasound groups anywhere. Interested individuals should contact either Barry Goldberg, M.D. (Director of Ultrasound), or David C. Levin, M.D. (Dept. Chairman), at the Dept. of Radiology, Thomas Jefferson University Hospital, Philadelphia, PA 19107. Jefferson is an equal opportunity/affirmative action employer. 1xa

**FULL-TIME BC RADIOLOGIST** needed to staff outpatient women's diagnostic center in suburban Dallas. Experience in mammography and OB/GYN sonography preferred. No call responsibilities. Attractive compensation package. Send CV to Box Y56, AJR (see address this section). 1xa

**MAMMOGRAPHY, UNIVERSITY OF PENNSYLVANIA**

—Exceptional opportunity in academic mammography within a high-volume, rapidly expanding, breast imaging section. Ongoing screening and problem-solving mammography, breast ultrasound, and collaborative projects. Academic rank and salary commensurate with credentials. Resident and student teaching responsibilities along with negotiable participation in bone and chest outpatient radiology. Position available immediately. Applicant must be ABR-certified and able to obtain license in Pennsylvania. University of Pennsylvania is an affirmative action, equal opportunity employer and specifically encourages applications from women and minorities. Send letter and CV to Rosalind H. Troupin, M.D., Dept. of Radiology, H.U.P., 3400 Spruce St., Philadelphia, PA 19104. 10-1ap

**VASCULAR/INTERVENTIONAL RADIOLOGIST**

Progressive, private-practice group is seeking a second fellowship-trained vascular and interventional radiologist for its expanding interventional radiology service. We are currently performing more than 1000 procedures/yr. We are budgeted for 2 state-of-the-art vascular suites, the first to be installed early in 1991. We will break ground soon on a new imaging center to include 2 MRI and 2 CT (including a cine CT) scanners. We have a noninvasive lab and retain admitting privileges for our interventional service. We are located in Fresno, CA, at Saint Agnes Medical Center. Saint Agnes is a tertiary-referral center for the San Joaquin Valley, and Fresno is one of the fastest growing cities in CA. We are located 90 mi. from Yosemite National Park and less than 2 hr from excellent winter skiing and 2 hr from the coast. We offer 2 yr to full partnership with excellent salary and benefits. Please contact Art Fontaine, M.D., Dept. of Imaging, Saint Agnes Medical Center, 1303 E. Herndon, Fresno, CA 93710; (209) 449-3210. 10-3ap

**DIAGNOSTIC RADIOLOGIST, TEXAS**

—Progressive, well-diversified group (15 radiologists) has immediate opening for a BC/BE diagnostic radiologist with competence in a broad range of modalities. Additional consideration for fellowship. Excellent opportunity with excellent salary and benefits. Send CV with letter of inquiry to Will Gray, M.D., 1101 N. 19th St., Abilene, TX 79601. 10-1ap

**NEURORADIOLOGIST**

—Excellent, young, 12-person radiology group has an opening for a well-trained neuroradiologist. Practice is hospital-based with 2 GE CT 9800 scanners, 1 high-field MRI, 1 mid-field MRI, new GE angio. Please contact Richard D. Herman, M.D., Dept. of Radiology, St. Luke's Hospital, Bethlehem, PA 18015; (215) 691-4200. 10-1ap

**SALT LAKE CITY, UT**

—Opportunity for board-certified diagnostic radiologist, with recent MRI fellowship training, to join group of 7 board-certified radiologists. Experience in all aspects of general radiology required. Practice includes 2 hospitals, 2 private offices, and a freestanding MRI center. Send letter and CV to Neel E. Bennett, M.D., Medical Director and Chairman, Dept. of Radiology, Holy Cross Hospital, 1050 E. S. Temple, Salt Lake City, UT 84102; (801) 350-4636. 1xa

**THE NEW YORK HOSPITAL, CORNELL MEDICAL CENTER, DEPT. OF RADIOLOGY**

has a position available for a junior attending in an expanding urology section beginning July 1991. Position involves responsibilities in clinical aspects of GU imaging, teaching, and research. Applicants should be board-certified/eligible with experience in cross-sectional imaging. Please send CV to Susan Krysiwicz, M.D., Dept. of Radiology, NYH-CUMC, 525 E. 68th St., Starr 8A15, New York, NY 10021; (212) 746-2557. 10-1a

**DIAGNOSTIC RADIOLOGIST, IMMEDIATE OPENING: DENVER, CO, AT ROSE MEDICAL CENTER (RMC)**

—A 7-person radiology group is recruiting a radiologist with fellowship training in body imaging or invasive radiology. The practice involves all imaging modalities. RMC is affiliated with the University of Colorado. Salary, benefits, and location are highly attractive. Contact David W. Wilder, M.D., or Jeffrey A. Levy, M.D., at (303) 320-2256. 10-1ap

**PENN STATE UNIVERSITY, FACULTY POSITION IN CARDIOVASCULAR/INTERVENTIONAL RADIOLOGY**

—The Penn State University, Dept. of Radiology, is seeking a full-time faculty member in the Section of Cardiovascular/Interventional Radiology for July 1, 1991. The section provides a wide range of services in all aspects of diagnostic and interventional angiography (including neuro- and pulmonary angiography), percutaneous and combined percutaneous/peroral biliary interventions, genitourinary interventions, central and peripheral venography (with IVC filter placement), traumatic and oncological embolizations, foreign body retrievals, complex biopsy and drainage procedures (under multiple imaging modalities), and is currently an FDA test site for a new holmium:YAG intravascular laser. Clinical responsibility at the assistant professor level is required, necessitating a Pennsylvania medical license, University Hospital medical staff privileges, and ABR certification. Although seeking a junior faculty person at the assistant professor level, the academic rank will be commensurate with previous academic performance, recommendations, and Penn State University guidelines. Independent original research is expected and is amply funded, both in time and money. The animal research facility at Penn State University is one of the finest facilities of its kind in the country and is coupled with a dedicated MR research facility with angiographic and spectroscopic capability. Both research facilities are staffed by full-time research associates and research faculty, and are equipped with modern, state-of-the-art equipment. The position is open to persons who have completed an accredited residency program in radiology and an accredited fellowship in CV/I radiology, can obtain a Pennsylvania medical license, and have fulfilled ABR requirements for board certification. A generous and competitive salary and benefits package are offered. National meeting presentation is encouraged and fully supported. Exceptional academic, biophotographic, and secretarial support are also provided. Applicants should respond as soon as possible with a letter of interest and current CV. Please direct inquiries and requests for application forms to John F. Cardella, M.D., Associate Professor and Chief, Cardiovascular/Interventional Radiology Section, Penn State University/Hershey Medical Center, Box 850, Hershey, PA 17033. Penn State University is an affirmative action, equal opportunity employer. Women and minorities are encouraged to apply. 10-1a.

**PHYSICIAN/RADIOLOGIST**

—Large radiology group with multiple private offices seeks a board-certified radiologist interested in a full-time position. Responsibilities include general radiography. Special training in CT, ultrasound, and nuclear medicine is desirable but not required. Desirable southern New Jersey location. Competitive salary and benefit package. Send CV to RABC, P.O. Box 729, Mt. Holly, NJ 08060. 10-1ap

**DIAGNOSTIC RADIOLOGIST**

sought to join a fee-for-service group practice at 2 mid-Bronx hospitals. Board-certification with expertise in imaging and in special procedures/interventional radiology preferred. Please send CV to Arthur Avenue Radiology, P.O. Box 4332, Great Neck, NY 11027. 10-3ap

**THE DEPT. OF RADIOLOGY, MEDICAL CENTER HOSPITAL OF VERMONT**, Burlington, VT, is seeking board-certified radiologists for academic positions in neuroradiology, angio/interventional radiology, body imaging with substantial training or experience in MRI, and general diagnostic radiology. Applicants should send letters of interest to John P. Tampas, M.D., Professor and Chairman, Dept. of Radiology, Medical Center Hospital of Vermont, 111 Colchester Ave., Burlington, VT 05401-1435. 10-1ap

**BC/BE RADIOLOGIST, SUBURBAN PHILADELPHIA**—Tired of hospital-based radiology? Opportunity to join private imaging facility with state-of-the-art equipment, including fourth-generation CT. Competency in CT, ultrasound, mammography, and general radiography is a must. Compensation includes salary for the first yr with an opportunity for partnership after first yr. Send CV to Box F61, *AJR* (see address this section). 10-1ap

**IMMEDIATE OPENING, DIAGNOSTIC RADIOLOGY**—Midwest city of 55,000 in metropolitan area of 600,000. Abundant recreational opportunities to complement hospital-based, 3-person group practice with very up-to-date equipment including MRI, CT, color ultrasound, SPECT nuclear, and angio with DSA. University appointment may be available if desired. Medical staff is highly specialist oriented. Competitive salary and benefit package including pension, health and disability insurance, and time off. Contact Charles Morris, M.D., P.O. Box 279, Council Bluffs, IA 51502; (712) 328-7646 (office) or (712) 328-2074 (home). 10-1ap

**DIAGNOSTIC RADIOLOGIST**—A 4-member radiology group located in beautiful southwestern Montana is currently seeking an additional board-certified/eligible radiologist. Expertise in MRI preferred. Hospital-based and office practice. Excellent school system and outstanding, year-round recreational activities. Approximately 35,000 exams last yr. Hospital is acquiring MRI and updating CT services. One yr to full partnership. Contact Dennis L. Rich, M.D., 300 N. Willson, Bozeman, MT 59715; (406) 587-8631. 10-3ap

**RADIOLOGISTS**—New York City, combined private radiology practice, and fee-for-service hospital practice has an immediate opening for a board-certified radiologist with experience in CT, ultrasound, and interventional radiology. In addition, MRI and mammography experience is preferred. This well-established practice has 3 private offices on the upper East Side of Manhattan as well as operations in 2 hospitals in Manhattan. Other studies performed in the practice are diagnostic radiology, nuclear imaging, and vascular duplex imaging. The practice continues to expand in all imaging modalities with its recent opening of a second state-of-the-art MRI unit. Excellent benefit package includes health, life, disability, and malpractice insurance; profit sharing plan; continuing medical education; and a travel and entertainment account for professional use. Send CV to Box F67, *AJR* (see address this section). 1-3ap

**PEDIATRIC RADIOLOGIST, PORTLAND, OR**—Immediate opening for a pediatric radiologist at Emanuel Hospital in Portland, OR. Either a pediatric fellowship or significant work experience is required. Opportunity to do general radiology as well. The hospital is a Level I trauma center, as well as a major pediatric referral center. The position leads to full partnership after second year. Please send CV to Blaine E. Kozak, M.D., Chairman, Dept. of Radiology, Emanuel Hospital, 2801 N. Gantenbein, Portland, OR 97227; (503) 280-4032. 1ap

**ULTRASOUND/CT/MRI**—Opportunity for a board-certified radiologist specializing in ultrasound, body CT, and body MRI to pursue an academic career at the New York Hospital-Cornell Medical Center. Dept. provides state-of-the-art equipment, including Acuson ultrasound, GE 9800 CT, and GE Signa 1.5-T MR. Wide variety of ultrasound exams include abdominal, OB-GYN, color Doppler, small parts, neonatal head, transvaginal, and transrectal. Prefer candidate with prior fellowship in sectional imaging or ultrasound. Responsibilities include clinical practice, teaching, and research. Position available 7/1/91 or earlier. Please send CV to Elias Kazam, M.D., Dept. of Radiology, The New York Hospital-Cornell Medical Center, 525 E. 68th St., New York, NY 10021. 1-4ap

## Positions Desired

**PGY-2 RADIOLOGY RESIDENCY POSITION SOUGHT**—Radiology resident in second yr of training seeks position in University-based program. Interested in research and academic career. Strong credentials. Reply Box H93, *AJR* (see address this section). 12-1bp

## Fellowships and Residencies

**ABDOMINAL IMAGING FELLOWSHIP**—Opening for July 1, 1991. A 1-yr fellowship in abdominal imaging available at the George Washington University Medical Center. Training provided in diagnostic ultrasound, CT, and MR. Applicants must have completed an approved residency program in diagnostic radiology and be board-eligible/certified. Send letter of inquiry with CV to Michael C. Hill, M.D., The George Washington University Hospital, Dept. of Radiology, 901 23rd St. N.W., Washington, DC 20037; (202) 994-2980. The George Washington University Hospital is an EEO/affirmative action employer. 12c

**UNIVERSITY OF WASHINGTON FELLOWSHIP IN DIAGNOSTIC IMAGING SCIENCES**—The Diagnostic Imaging Sciences Center of the Dept. of Radiology at the University of Washington in Seattle is recruiting for 2 fellowship positions in radiology science research. The research fellowship program is funded by NCI Training Grant T32 CA 096552 and combines a 2-yr, fully funded, laboratory-based, educational and research program with a guaranteed clinical fellowship after successful completion of the radiology science program. Candidates should have successfully completed 2 or 3 yr of a diagnostic radiology residency and must have a strong interest and commitment to a career in academic radiology. The research fellowship program will combine academic courses and a thesis project that will lead to a masters degree in biomedical imaging at the University of Washington. A portion of each fellow's time will be spent in clinical subspecialty radiology training to keep the fellows clinically astute and to provide additional clinical experience. The Radiology Imaging Research Laboratory at the University of Washington consists of over 20,000 sq. ft. of dedicated research and includes more than 25 full-time scientists, state-of-the-art equipment in MRI, NMR spectroscopy, PET, SPECT, DIN/PACS, angiography, ultrasound, and image processing. Four MRI instruments, including a GE Signa system, are dedicated to research use. Candidates interested in the Radiology Research Sciences Program should contact James A. Nelson, M.D., Dept. of Radiology, SB-05, University of Washington, Seattle, WA 98195; (206) 543-3757. The University of Washington is an equal opportunity employer. 1-2c

**BODY IMAGING FELLOWSHIP (MRI, CT, ULTRASOUND)**—A 1-yr fellowship position is available commencing July 1, 1992, at St. Luke's-Roosevelt Hospital Center in New York City. We offer extensive clinical experience and opportunities for research using state-of-the-art equipment, including GE 1.5-T Signa MRI, GE 9800 CT, Siemens DRH, Acuson, ATL, and Diasonics ultrasound including color Doppler, small parts, and intracavitary studies. The hospital is a 1315-bed, voluntary university hospital of Columbia University College of Physicians and Surgeons. Applicants should be ABR-eligible or certified. Application requires CV and 3 letters of recommendation. Send inquiries to Benjamin Bashist, M.D., St. Luke's-Roosevelt Hospital Center, Dept. of Radiology, Special Procedures, 428 W. 59th St., New York, NY 10019. An equal opportunity employer M/F. 1cp

**FELLOWSHIP IN ABDOMINAL IMAGING AND INTERVENTIONS**—The Dept. of Radiology, Massachusetts General Hospital and Harvard Medical School, offers a 2-yr fellowship in abdominal imaging and interventions beginning July 1, 1992. Training covers all aspects of abdominal imaging (radiography, fluoroscopy, ultrasound, CT, and MR) and nonvascular interventions in the GI and GU tracts. Research is active and participation is encouraged. Candidates should be ABR-eligible or certified. Address inquiries to Peter R. Mueller, M.D. or Nicholas Papanicolaou, M.D., Dept. of Radiology, Massachusetts General Hospital, Boston, MA 02114. An equal opportunity employer. 1-3cp

**INTEGRATED CHEST RADIOLOGY FELLOWSHIP AT JOHNS HOPKINS UNIVERSITY HOSPITAL**—The Dept. of Radiology, Division of Thoracic Imaging, Johns Hopkins University is offering a 1- to 2-yr academically oriented fellowship in chest radiology. The fellowship offers an integrated experience in cross-sectional imaging, including over 4000 chest CT and 1000 thoracic MRI exams/yr. Strong research interests in high-resolution CT, MRI, digital imaging methods, and interventional thoracic radiology offer the candidate an exciting environment to work in. The fellowship is available starting July 1, 1991. Contact Elias A. Zerhouni, M.D., Director of Thoracic Imaging and MRI, Dept. of Radiology, Johns Hopkins Hospital, Baltimore, MD 21205; (301) 955-4062. 1-6c

**NEURORADIOLOGY FELLOWSHIP**—The Dept. of Radiology at the University of California, Davis, Medical Center in Sacramento offers a 1- or 2-yr fellowship position in neuroradiology starting July 1, 1991. Training is offered in neuroangiography (including interventional techniques), CT, MRI, and myelography. The UC Davis Medical Center is a 505-bed university hospital located in Sacramento, CA, 90 mi. east of San Francisco and 100 mi. west of Lake Tahoe. The dept. consists of 16 staff, 3 fellows, and 17 residents and does 180,000 exams/yr. The hospital is the major trauma center for northern California outside the San Francisco Bay area. The dept. is well equipped with 2 Toshiba CT, a 1.5-T GE MR, and a small-bore, 2.0-T unit for animal research on the Davis campus. The fellow will assist in the teaching of residents and medical students, will have opportunity to conduct basic or clinical research, and will be expected to participate in clinical conferences with the Depts. of Neurology and Neurosurgery. The candidate must be board-certified or qualified in diagnostic radiology and be able to obtain a California medical license. For further information, contact Stephen T. Hecht, M.D., Chief, Division of Neuroradiology, Dept. of Radiology, UC Davis Medical Center, 2516 Stockton Blvd., Sacramento, CA 95817; (916) 734-3608. UCD is an affirmative action/equal opportunity employer. 1cp



**NEURORADIOLOGY FELLOWSHIP**—The Dept. of Radiology, Strong Memorial Hospital, University of Rochester School of Medicine and Dentistry offers a 1- or 2-yr neuroradiology fellowship to begin July 1, 1991. Training is offered in MRI, CT, and special procedures, with the opportunity to perform both pediatric and carotid ultrasound. Assistance in teaching of medical students and residents is expected. Additional training in maxillofacial, dental, and ENT radiology also is available, as is the opportunity to perform both clinical and laboratory research. A very strong neuroscience community exists. The dept. consists of 25 radiologist faculty, 16 residents, and 3-5 fellows. State-of-the-art equipment is available in all modalities including new single and biplane angiographic systems, 3 third-generation CT, a 1.5-T MRI, and a midfield MR. Strong Memorial Hospital is a 750-bed, tertiary-care hospital with 100 beds dedicated to pediatric diseases. Candidates must have completed an accredited diagnostic radiology residency program, be board-certified or eligible, and have a New York state medical license by July 1, 1991. Send inquiries to Robert E. O'Mara, M.D., Box 648, University of Rochester Medical Center, Rochester, NY 14642; (716) 275-2733. EO/AA/M-F employer. 1-6c

**PEDIATRIC RADIOLOGY FELLOWSHIP**—The Dept. of Radiology at Children's Hospital of Philadelphia (CHOP) offers a 1- or 2-yr pediatric radiology fellowship beginning July 1, 1992. A 1-yr pediatric neuroradiology fellowship program is also offered and may be taken separately or in combination with a second yr adult neuroradiology fellowship at Jefferson University Medical Center in Philadelphia. A special (1-yr) cross-sectional imaging (CT, ultrasound, and MRI) fellowship may be arranged. CHOP is a 294-bed pediatric hospital affiliated with the University of Pennsylvania. Radiology has an attending faculty of 11 and performs 90,000 cases/yr (plain films, fluoroscopy, ultrasound, CT, nuclear medicine, neuroradiology, angiography/interventional radiology, and MRI). Our equipment is state-of-the-art and new since 1988 and includes ATL ultrasound equipment with duplex and color flow Doppler; gamma camera with SPECT; a high-resolution fast Siemens Somatom Plus CT scanner; and a 1.5-T Siemens Magnetom MRI installation with spectroscopy. A pediatric outpatient radiology facility has recently opened. We have an active teaching program for radiology residents and fellows. The patient population is large and varied, from routine emergencies to complicated tertiary care problems. The fellowship provides not only a broad clinical experience with subspecialty training, but offers opportunities for clinical and basic research and scholarship. Applicants must have completed a diagnostic radiology residency, be board-certified or eligible, and be able to obtain a Pennsylvania medical license. Salary and fringe benefits are highly competitive. Address inquiries to Sandra S. Kramer, M.D., Dept. of Radiology, The Children's Hospital of Philadelphia, 34th St. and Civic Center Blvd., Philadelphia, PA 19104; (215) 590-2575. The Children's Hospital of Philadelphia and the University of Pennsylvania are equal opportunity/affirmative action employers. 1-3cp

**FELLOWSHIP IN VASCULAR AND INTERVENTIONAL RADIOLOGY**—A 1-yr fellowship position is available at the New York Hospital-Cornell University Medical Center for July 1991. Training includes experience in all aspects of peripheral vascular and nonvascular interventions. Equipment includes 3 state-of-the-art Philips digital labs and a 4-bed recovery room. For further information, please contact Thomas A. Sos, M.D.; (212) 746-2600. 12-1c

**DUKE UNIVERSITY, DEPT. OF RADIOLOGY** offers 1- or 2-yr fellowship positions in chest radiology, neuroradiology, vascular/interventional radiology, musculoskeletal radiology, CT, ultrasound, MRI, abdominal imaging, mammography, pediatric radiology, and nuclear medicine beginning July 1991. The dept. runs an active clinical service with top quality equipment including 5 GE 9800 Quick CT scanners, 3 GE 1.5-T MRI units, and 4 fully equipped vascular/interventional laboratories. In addition to their clinical responsibilities, fellows are provided academic time to pursue investigational interests. Applications are due March 1, 1991, and interviews will be scheduled in the spring. For further information and application material, please contact Ms. Debbie Sykes at the Dept. of Radiology, Box 3808, Duke University Medical Center, Durham, NC 27710; (919) 660-2711, ext. 5228. Duke University is an equal opportunity/affirmative action employer. 12-2c

**FELLOWSHIP IN VASCULAR/INTERVENTIONAL RADIOLOGY 1991**—The University of New Mexico is offering a 1-yr fellowship in vascular/interventional radiology, beginning July 1, 1991. We perform all noncardiac diagnostic angiography, including neuroangiography, as well as a wide variety of vascular and nonvascular interventional procedures, with state-of-the-art equipment at the University Hospital (a level 1 trauma center) and the VA/Air Force Hospital. Applicants must have passed the ABR written exam, be eligible for ABR certification, and be eligible for medical licensure in the state of New Mexico. Contact Jerry King, M.D., University of New Mexico Hospital, Dept. of Radiology, Albuquerque, NM 87131; (505) 843-2269. 12-1c

**VASCULAR/INTERVENTIONAL RADIOLOGY FELLOWSHIP, ST. LOUIS VASCULAR INSTITUTE AT THE CHRISTIAN HOSPITAL, ST. LOUIS, MO**—A 1- to 2-yr fellowship in vascular and interventional radiology is offered beginning July 1, 1991. Training includes all aspects of diagnostic angiography and vascular and nonvascular interventional techniques. Candidates must have completed a diagnostic radiology residency in an accredited training program, must be certified by or eligible for certification by the ABR, and must be able to obtain a Missouri license. Direct inquiries to Saadoun Kadir, M.D., Dept. of Radiology, Christian Hospital Northeast, 11133 Dunn Rd., Ste. 1017, St. Louis, MO 63136. 11-4cp

**WOMEN'S IMAGING FELLOWSHIP**—A 1- or 2-yr comprehensive experience in women's imaging modalities is offered in Tucson, AZ. Procedures in which we expect the fellow to gain expertise include high-volume, low-cost screening mammography and its associated administrative, financial, and epidemiological aspects; problem-solving diagnostic mammography, including invasive mammographic procedures (e.g., stereotactic guided cytology and galactography); high-volume obstetric and gynecologic sonography. Annual stipend is \$50,000. Contact Arizona State Radiology, 7250 E. Ventana Canyon Dr., Tucson, AZ 85715; (602) 620-4911. 10-3cp

**IMMEDIATE UNEXPECTED OPENING FOR FELLOWSHIP IN CARDIOVASCULAR-INTERVENTIONAL RADIOLOGY**—One-yr fellowship program at 750-bed teaching hospital. Extensive clinical experience involving all aspects of cardiovascular imaging and interventional vascular and nonvascular procedures. Availability for clinical or animal research. Send CV and inquiries to Oscar H. Gutierrez, M.D., Dept. of Radiology, Box 648, University of Rochester Medical Center, Rochester, NY 14642. AA/EO/M-F employer. 10-1cp

**CARDIOVASCULAR/INTERVENTIONAL RADIOLOGY FELLOWSHIP, PENN STATE UNIVERSITY** The Penn State University, Dept. of Radiology, offers 1- or 2-yr fellowships in cardiovascular/interventional radiology, with a primary purpose of preparing graduates for academic careers in the subspecialty of CV/I radiology. Fellows will receive training in all aspects of diagnostic and interventional angiography (including neuro and pulmonary angiography), percutaneous and combined percutaneous/peroral biliary interventions, genitourinary interventions, central and peripheral venography (with IVC filter placement), traumatic and oncological embolizations, foreign body retrievals, and complex biopsy and drainage procedures (under multiple imaging modalities). Clinical responsibility at the instructor level is required, necessitating a Pennsylvania medical license, university hospital medical staff privileges, and ABR eligibility (at time of application) and certification (during first program yr). Independent original research is expected and is amply funded, both in time and money. The animal research facility at Penn State University is one of the finest facilities of its kind in the country and is coupled with a dedicated MR research facility with angiographic and spectroscopic capability. Both research facilities are staffed by full-time research associates and research faculty, and are equipped with modern state-of-the-art equipment. The fellowship is open to individuals who have completed an accredited residency program in radiology, can obtain a Pennsylvania medical license, and have fulfilled ABR requirements for board-certification or eligibility. A generous competitive salary and benefits package are offered. Academic, biophotographic, and secretarial support are also provided. Applicants should respond as soon as possible with a letter of interest and current CV. Please direct inquiries and requests for application forms to John F. Cardella, M.D., Associate Professor and Chief, Cardiovascular/Interventional Radiology Section, Penn State University/Hershey Medical Center, Box 850, Hershey, PA 17033. Penn State University is an affirmative action, equal opportunity employer. Women and minorities are encouraged to apply. 10-1c

**ABDOMINAL IMAGING FELLOWSHIP**—The Dept. of Radiology at the University of Florida is offering 1-yr fellowships in abdominal imaging beginning July 1, 1991, and July 1, 1992. Minimum requirements include successful completion of an accredited radiology residency. The fellowship includes training in all aspects of abdominal imaging (gastrointestinal and genitourinary radiology, CT, ultrasound, and MRI) by a 3-person subspecialty faculty. The program offers full clinical experience and research opportunities. Applicants must be eligible to obtain a license in the state of Florida. For additional information, contact Pablo R. Ros, M.D., Professor, Dept. of Radiology, Box J-374, Gainesville, FL 32610-0374; (904) 395-0288. The University of Florida is an equal opportunity/affirmative action employer and encourages applications from women and minorities. 10-6c

**FELLOWSHIP IN ULTRASOUND AND BODY CT/MRI**—July 1, 1992, to June 30, 1993, at the New York Hospital-Cornell Medical Center. Dept. provides state-of-the-art equipment including Acuson ultrasound, GE 9800 CT, and GE Signa 1.5-T MR. Wide variety of ultrasound exams include abdominal, OB-GYN, color Doppler, small parts, neonatal head, transvaginal, and transrectal. Applicant should be ABR eligible or certified. Send CV to Elias Kazam, M.D., Dept. of Radiology, The New York Hospital-Cornell Medical Center, 525 E. 68th St., New York, NY 10021. 1-4cp

**FELLOWSHIPS AT THOMAS JEFFERSON UNIVERSITY HOSPITAL**—The Dept. of Radiology at Thomas Jefferson University Hospital in Philadelphia offers the following fellowship programs each yr. **Ultrasound/CT/MRI** — Jefferson's ultrasound division is 1 of the largest in the world and performs all currently available exams including obstetric, vascular, lithotripsy, invasive, and endoluminal. We also operate 4 GE 1.5-T MRI units and 3 CT scanners. Contact Barry Goldberg, M.D., regarding this program. **Cardiovascular/interventional** — this division is housed in a new suite containing Philips angio units with DSA and performs the full range of vascular and non-vascular interventional procedures. Contact Geoffrey Gardiner, Jr., M.D. **Neuro/ENT radiology** — very active clinical services supply a wealth of material to this division, which is housed in a neurosciences imaging center containing all imaging modalities. Contact Carlos Gonzalez, M.D. **Breast imaging** — Jefferson's new breast imaging center performs approximately 85 studies/day including ultrasound and needle localizations. Contact Stephen Feig, M.D. **Chest** — includes biopsies and CT. Contact Robert Steiner, M.D. **MRI** — a dedicated body MRI program including excellent research opportunities in addition to a large clinical case load. Contact Matthew Rifkin, M.D. **Ultrasound** — a dedicated ultrasound program. Contact Barry Goldberg, M.D. **Musculoskeletal** — includes MRI of the musculoskeletal system. Contact David Karasick, M.D. All program directors listed above can be contacted at the Dept. of Radiology, Thomas Jefferson University Hospital, Philadelphia, PA 19107. Jefferson is an equal opportunity/affirmative action employer. 1x

Tutorials/Courses

**ALASKA 91/CRUISE THE INLAND PASSAGE** MRI at sea, July 6–13, 1991. For information, contact Medical Seminars International, Inc., 18981 Ventura Blvd., Ste. 303, Tarzana, CA 91356; (818) 774-9077, fax (818) 774-0244. 1–5d

**NINTH WINTER DIAGNOSTIC IMAGING CONGRESS, VAL D'ISERE, FRANCE**—March 2–9, 1991. MRI, CT, ultrasound. Medical Seminars International, 18981 Ventura Blvd., #303, Tarzana, CA 91356; (818) 700-9821. 10–2d

Other

**MRI/CT INTERPRETATIONS** — Overreads or primary reads of MRI/CT exams via teleradiology or overnight mail. Teleradiology Associates, P.A., One University Pl., Ste. 350, Durham, NC 27707; (919) 419-1000. 1ep

**VISITING PROFESSORSHIPS, THOMAS JEFFERSON UNIVERSITY HOSPITAL**—The Dept. of Radiology at Thomas Jefferson University Hospital in Philadelphia is offering visiting professorships over the next several yr, while some of our faculty members are on sabbatical leave. These positions can have either a 6-mo or 1-yr term. In particular, we are seeking candidates with expertise in either ultrasound or general diagnostic radiology, but emphasis in other areas may be acceptable as well. Funding for these positions is appropriate for a senior faculty member from another institution on sabbatical with partial funding of his/her own, or for a junior faculty member. These positions are also open to highly qualified foreign radiologists with current academic appointments at prestigious foreign medical schools. Visiting faculty members will do some clinical work in our dept. and also have access, for research or educational purposes, to state-of-the-art imaging modalities of all types, as well as well-equipped physics and physiology research laboratories. Interested persons should contact David C. Levin, M.D., Chairman, Dept. of Radiology, Thomas Jefferson University Hospital, Philadelphia, PA 19107. Jefferson is an equal opportunity/affirmative action employer. 1xe



AJR Classified Advertisements Information

Box Responses and Address for Ad Placement

Write Box \_\_\_\_\_, *AJR*, 2223 Avenida de la Playa, Suite 103, La Jolla, CA 92037-3218; Telephone: (619) 459-2229; FAX: (619) 459-8814.

How to Place an Ad

*AJR* accepts classified advertising for Positions Available, Positions Desired, Fellowships and Residencies, and Tutorials/Courses. Ads are accepted by mail or FAX.

**Rates:** \$6.00/line with a \$30 minimum charge. Box service is \$10 additional for each month the ad appears. There are discounts for multiple insertions: 10% for 2–3 insertions; 20% for 4 or more. To estimate lines, count all words and divide by 7.

**Billing:** Ads *must* be prepaid, or advertisers will be billed after the ad appears *providing* a purchase order number is submitted with the advertising copy. Terms are net 30 days.

**Deadlines:** 6 weeks prior to issue date. For specific deadlines, telephone the *AJR* editorial office.

Estimating Ad Charges

Line charge: divide total words by 7 and multiply by \$6.00	.....	\$	_____
Multiple insertions? If so, multiply by number	.....	x	_____
Subtotal	.....	\$	_____
Discount applies to two or more insertions. Subtract 10% if ad appears 2–3 months; 20% if 4 months or more	.....	–	_____
Subtotal	.....	\$	_____
Box response requested? If so, multiply number of months by \$10.00	.....	+	_____
Approximate advertising charge	.....	\$	_____



An informed approach to the great threats  
of our time from *Physicians for Social Responsibility*...



# THE PSR QUARTERLY



*A Journal of Medicine and Global Survival*

"After years of  
talking and writing  
about the role of  
medicine and public  
health in responding  
to the great threats  
of our time, the PSR  
physicians now  
intend to create a  
forum where such  
discussions can be  
captured in a single  
publication."

—Jennifer Leaning, M.D.  
Editor-in-Chief

Jennifer Leaning, M.D.  
EDITOR-IN-CHIEF

Christine K. Cassel, M.D.  
H. Jack Geiger, M.D.  
ASSOCIATE EDITORS

Drawing on the best traditions  
in medical science, *The PSR Quarterly* will publish peer-reviewed  
articles examining health-related  
aspects of nuclear, biological, and  
chemical warfare; environmental  
change; natural and technological  
disasters; and relevant social  
policies.

The PSR Quarterly welcomes  
articles, reports, and letters  
from authors with divergent  
views. Contributors who  
would like to submit manu-  
scripts or propose articles  
should write to the Editor:  
Jennifer Leaning, M.D.,  
10 Brookline Place West,  
Brookline Massachusetts  
02146.

## CHARTER SAVINGS!

SUBSCRIBE NOW, while charter  
rates are in effect! To order, call  
TOLL FREE:

**1-800-638-6423**  
Or complete and mail this coupon.

### THE PSR QUARTERLY

*A Journal of Medicine and Global Survival*  
Quarterly • Beginning March 1991

- |   |                                 |
|---|---------------------------------|
| <input type="checkbox"/> Individual \$48/yr.    | <input type="checkbox"/> 3 yrs. |
| <input type="checkbox"/> Institutional \$85/yr. | <input type="checkbox"/> 2 yrs. |
| <input type="checkbox"/> In-training* \$25/yr.  | <input type="checkbox"/> 1 yr.  |

Add \$15/yr for postage outside the U.S. Rates  
valid until October 31, 1991. Orders outside the  
U.S. must be prepaid in U.S. dollars. Maryland  
subscribers add 5% sales tax. Canadian sub-  
scribers add 7% GST.

Payment options: ☐ Bill me  
☐ Check enclosed (payable to Williams & Wilkins)  
☐ AmEX ☐ MasterCard ☐ VISA

Acct. # \_\_\_\_\_ Exp. date \_\_\_\_\_

Signature \_\_\_\_\_

Name \_\_\_\_\_

Address \_\_\_\_\_

City/State/Zip \_\_\_\_\_

\*Specify institution  
and training status \_\_\_\_\_

**Note: PSR members will receive the journal as a  
benefit of their membership.**

Return to: Williams & Wilkins, P.O. Box 23291,  
Baltimore, MD 21203-9990.

FORM 52541

J0079S01

PUBLISHED BY  
WILLIAMS & WILKINS



## SPECIAL ARTICLE

- 1 Commentary. Barium enemas, latex balloons, and anaphylactic reactions. *Gelfand DW*

## REVIEW ARTICLES

- 3 Color Doppler flow imaging. *Foley WD, Erickson SJ*  
 15 The evaluation of coronary bypass graft patency: direct and indirect techniques other than coronary arteriography. *Stanford W, Galvin JR, Skorton DJ, Marcus ML*  
 23 CT of the gastrointestinal tract: principles and interpretation. *Balthazar EJ*

## PROGRESS IN RADIOLOGY

- 33 Selective salpingography and fallopian tube recanalization. *Thurmond AS*

## CARDIOPULMONARY RADIOLOGY

- 39 Detection of ACTH-producing bronchial carcinoid tumors: MR imaging vs CT. *Doppman JL, Pass HI, Nieman LK, et al.*  
 45 Pictorial essay. High-attenuation mediastinal masses on unenhanced CT. *Glazer HS, Molina PL, Siegel MJ, Sagel SS*  
 51 Diaphragmatic rupture due to blunt trauma: sensitivity of plain chest radiographs. *Gelman R, Mirvis SE, Gens D*

## BREAST RADIOLOGY

- 59 Present status of residency training in mammography. *Bassett LW, Cassady CI, Gold RH*

## GASTROINTESTINAL RADIOLOGY

- 63 Pictorial essay. Endoscopic sonography of the upper gastrointestinal tract. *Botet JF, Lightdale C*  
 69 Thickening at the root of the superior mesenteric artery on sonography: evidence of vascular involvement in patients with cancer of the pancreas. *Kosuge T, Makuuchi M, Takayama T, Yamamoto J, Kinoshita T, Ozaki H*  
 73 Long-term soft-tissue effects of biliary extracorporeal shock waves: an animal study. *Rawat B, Wolber R, Burhenne HJ*  
 77 Technical note. Percutaneous transluminal biopsy of biliary strictures with a biptome. *Terasaki K, Wittich GR, Lycke G, et al.*  
 79 Duplex Doppler sonography of the hepatic vein in tricuspid regurgitation. *Abu-Yousef MM*  
 85 Portal venous system after portosystemic shunts or endoscopic sclerotherapy: evaluation with Doppler sonography. *Rice S, Lee KP, Johnson MB, Korula J, Ralls PW*  
 91 Case report. Peliosis hepatis in a patient with human immunodeficiency virus infection. *Radin DR, Kanel GC*  
 93 CT of acute pancreatitis: correlation between lack of contrast enhancement and pancreatic necrosis. *Johnson CD, Stephens DH, Sarr MG*  
 97 Case report. Pancreatitis with pseudoaneurysm formation: a pitfall for the interventional radiologist. *Lee MJ, Saini S, Geller SC, Warshaw AL, Mueller PR*

## GENITOURINARY RADIOLOGY

- 99 Endoluminal sonography of the urinary tract: preliminary observations. *Goldberg BB, Bagley D, Liu J-B, Merton DA, Alexander A, Kurtz AB*  
 105 Renal transplant rejection: diagnosis with <sup>31</sup>P MR spectroscopy. *Grist TM, Charles HC, Sostman HD*

## MUSCULOSKELETAL RADIOLOGY

- 113 Failure of MR imaging to detect reflex sympathetic dystrophy of the extremities. *Koch E, Hofer HO, Sialer G, Marincsek B, von Schulthess GK*  
 117 Sagittal MR images of the knee: a low-signal band parallel to the posterior cruciate ligament caused by a displaced bucket-handle tear. *Weiss KL, Morehouse HT, Levy IM*

- 121 MR imaging of displaced bucket-handle tear of the medial meniscus. *Singson RD, Feldman F, Staron R, Kiernan H*  
 125 Rheumatoid arthritis of the knee: value of gadopentetate dimeglumine-enhanced MR imaging. *Adam G, Dammer M, Bohndorf K, Christoph R, Fenke F, Günther RW*  
 131 Pictorial essay. MR imaging of the lateral collateral ligament of the ankle. *Erickson SJ, Smith JW, Ruiz ME, et al.*

## PEDIATRIC RADIOLOGY

- 137 Urethral abnormalities in male neonates with VATER association. *Fernbach SK*  
 141 Sonography in neonatal congenital adrenal hyperplasia. *Sivit CJ, Hung W, Taylor GA, Catena LM, Brown-Jones C, Kushner DC*  
 145 Mediastinal pseudomass caused by compression of the thymus in neonates with anterior pneumothorax. *O'Keeffe FN, Swischuk LE, Stansberry SD*  
 149 Case report. Normal sonographic appearance of a thanatophoric dwarf variant fetus at 13 weeks gestation. *Macken MB, Grantmyre EB, Rimoin DL, Lachman RS*  
 151 Case report. CT of acute splenic torsion in children with wandering spleen. *Herman TE, Siegel MJ*  
 155 Case report. Pulmonary emboli as a primary manifestation of Wilms tumor. *Bulas DI, Thompson R, Reaman G*

## NEURORADIOLOGY

- 157 Focal high signal on MR scans of the midbrain caused by enlarged perivascular spaces: MR-pathologic correlation. *Elster AD, Richardson DN*  
 161 Normal venous anatomy of the brain: demonstration with gadopentetate dimeglumine in enhanced 3-D MR angiography. *Chakeres DW, Schmalbrock P, Brogan M, Yuan C, Cohen L*

## TECHNICAL NOTE

- 173 Atherectomy facilitated by long vascular sheaths. *Porter DH, Kim D, Siegel JB, Storella JM, Silverstone DZ*

## PERSPECTIVE

- 177 Analysis of the cost-effectiveness of PACS. *Hilsenrath PE, Smith WL, Berbaum KS, Franken EA, Owen DA*

## RADIOLOGY TEACHING

- 181 Perspective. Effective audiovisual presentation. *Sagel SS, Ramsey RG*

## MEETING NEWS

- 189 Tenth meeting and postgraduate course of the Society of Uroradiology, September 1990. *Whalen E*

## OTHER CONTENT

- Book and videotape reviews 14, 44, 58, 96, 104, 116, 120, 130, 176  
 124 ARRS 1991 resident award papers information  
 154 Memorial, Andrew N. Schwartz  
 188 Books received  
 196 Forthcoming articles  
 197 Letters  
 203 Review of current literature  
 207 News  
 210 American Roentgen Ray Society information  
 211 Invitation to the 1991 ARRS meeting  
 213 Summary of the 1991 ARRS meeting  
 214 ARRS membership information and application  
 217 Classified advertisements  
 A9 Guidelines for authors  
 A17 AJR business and subscriber information



VCM

12<sup>11</sup>/<sub>92</sub>

# AJR

American  
Journal of  
Roentgenology



**February 1991**

This issue: ARRS Meeting Section



ELEMA-SCHONANDER

## New Efficiency For Your Angio Suite



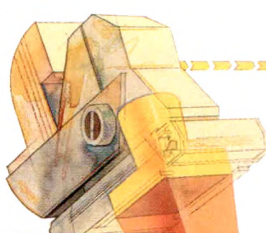
### PUCK® 90 M Filmchanger

Every change we made in this new PUCK helps you increase the return from your radiology operation. It speeds up examination time to permit greater patient throughput.

New 30 film stackloading magazine reloads faster and needs reloading less often.

Total positional independence takes away the mid-procedure pause to rotate the filmchanger.

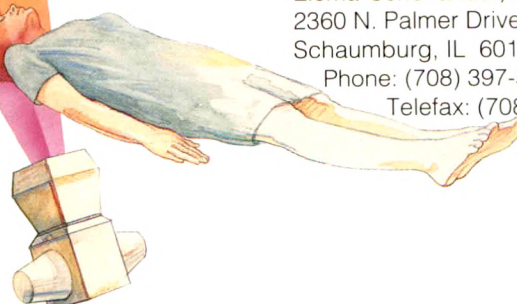
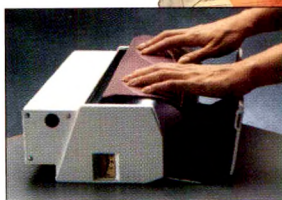
And exposure monitoring ends the "stop-and-wait" in the angio suite by delivering instant procedure verification.



Find out how the new PUCK 90 M filmchanger can help your bottom line. Contact Elema-Schonander or your X-ray distributor.



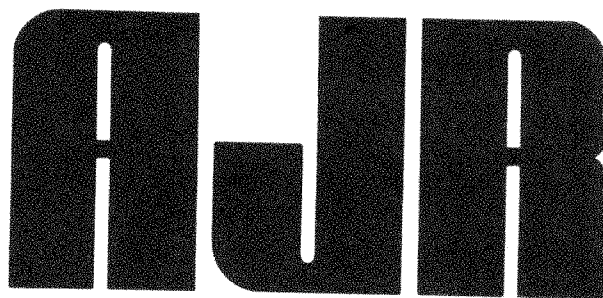
Elema-Schonander, Inc.  
2360 N. Palmer Drive  
Schaumburg, IL 60173-3887  
Phone: (708) 397-5931  
Telefax: (708) 397-5058



**Setting The Standards In Filmchangers**



Official Journal of the American Roentgen Ray Society



**American Journal of Roentgenology**  
Diagnostic Imaging and Related Sciences

- Editor-in-Chief** Robert N. Berk, *La Jolla, California*  
*University of California, San Diego*  
*School of Medicine and Medical Center*
- Editor Emeritus** Melvin M. Figley, *Seattle, Washington*
- Associate Editor** Saskia von Waldenburg Hilton, *San Diego, California*
- Consulting Editor** Michael S. Huckman, *Chicago, Illinois*
- Statistician** Charles C. Berry, *San Diego, California*

**Editorial Board**

- |                     |                          |                    |
|---------------------|--------------------------|--------------------|
| John R. Amberg      | John R. Hesselink        | Peter M. Ronai     |
| Itamar Aviad        | Charles B. Higgins       | Sjef H. J. Ruijs   |
| Mark E. Baker       | Melvyn T. Korobkin       | Stuart S. Sagel    |
| Lawrence W. Bassett | Faye C. Laing            | David J. Sartoris  |
| Michael A. Bettmann | Thomas L. Lawson         | Stefan C. Schatzki |
| Felix S. Chew       | Robert G. Levitt         | William P. Shuman  |
| N. Reed Dunnick     | Bruce L. McClennan       | Edward A. Sickles  |
| David K. Edwards    | Richard P. Moser         | Barry A. Siegel    |
| Ronald G. Evens     | Albert A. Moss           | David D. Stark     |
| David S. Feigin     | Jeffrey H. Newhouse      | Edward T. Stewart  |
| Sandra K. Fernbach  | Donald L. Resnick        | Murali Sundaram    |
| Richard H. Gold     | Stewart R. Reuter        | Eric vanSonnenberg |
| William R. Hendee   | Charles A. Rohrmann, Jr. | Robert K. Zeman    |

**Editorial Staff:** Margaret Levene, *managing editor*; Katie L. Spiller, Barbara Rose, Barbara L. Halliburton, and Janine Anderson, *manuscript editors*; Nancy Rydbeck, *office manager*; Sheri Smith, *administrative assistant*; Linda J. Waggoner, *administrative secretary*.

AJR, AMERICAN JOURNAL OF ROENTGENOLOGY (ISSN 0361 803X) is the official journal of the American Roentgen Ray Society and is published monthly by Williams & Wilkins, 428 E. Preston St., Baltimore, MD 21202. Annual dues include \$50 for journal subscription. Second-class postage paid at Baltimore, MD, and at additional mailing offices. Postmaster, send address changes (Form 3579) to AJR, 428 E. Preston St., Baltimore, MD 21202. Subscription rates \$125 (\$180 foreign); institutions \$135 (\$190 foreign); in training \$25 (\$80 foreign); single copy \$18 (\$22 foreign). Airmail rates furnished on request. Indexed by *Current Contents* and *Index Medicus*. Copyright © 1991 by American Roentgen Ray Society. 0361-803X/90\$3.00



# The Osler Institute

## Radiology Review Course

### May 27-June 1, 1991 — Louisville

### September 26-October 1, 1991 — Chicago

**Now, your review for written and oral exams offers unlimited mock orals**

#### OBJECTIVES

- Improve basic knowledge and clinical skills in radiology
- Assist residents and fellows to study efficiently
- Prepare recent graduates to meet their next milestones
- Provide practicing radiologists with a review and update

#### METHODS

- HOME STUDY MATERIALS consisting of a syllabus of assignments with questions and answers
- SEMINAR with projection slides and syllabus
- PRACTICE EXERCISES with oral and written parts

*"The faculty was outstanding. The most pleasant thing was learning a tremendous amount, not only from world-famous authorities but from people who are relatively unknown as well."*

Radiologic Physics	Nuclear Radiology	Bone and Joints
Radiation and Radiology	Decay and Detectors	Tumors and Trauma
X-rays and Imaging	Statistics & Instrumentation	Metabolic and Endocrine
Fluoroscopy	Radiopharmaceuticals	Infection
Tomography	Quality Control & Licensure	Dysplasia
Computed Tomography	Endocrine Scans and Tx	Articular Disorders
Ultrasonography	GI, GU, Bone, and Brain	<b>Neuro., Head and Neck</b>
MRI	Liver, Spleen, and Lung	Skull and Contents
Quality Assurance	Ga, In, and Heart	Spine, Disc and Cord
<b>Chest</b>	<b>Gastrointestinal</b>	Temporal and Facial Bones
Infiltrates and Cavities	Esophagus and Stomach	Sinuses
Nodules and Masses	Small Bowel and Colon	Larynx and Neck
Mediastinum	Liver and Gallbladder	<b>Pediatric</b>
Mammography	Pancreas and Spleen	Pediatric Chest
<b>Cardiovascular</b>	<b>Genitourinary</b>	Cardiovascular System
Heart and Aorta	Kidney and Ureter	Gastrointestinal Tract
Coronary Arteries	Bladder and Pelvis	Genitourinary Tract
Peripheral Arteries	Abdominal Ultrasound	Bones and Joints
Echocardiography	Ob. and Pelvic Ultrasound	Central Nervous System

#### Limited Enrollment: RADIOLOGY REVIEW REGISTRATION

Name \_\_\_\_\_  
 Address \_\_\_\_\_  
 City/State/Zip \_\_\_\_\_  
 Phone \_\_\_\_\_

#### Mail today to:

1094 Dawn Lane, Dept. 101  
 P.O. Box 2218  
 Terre Haute, IN 47802

For: ☐ May 27-June 1, '91 — Louisville  
☐ Sept. 26-Oct. 1, 1991 — Chicago

Check enclosed for \$ \_\_\_\_\_  
 Please send more information

*"Accommodations were comfortable...."*

**GOALS AND LOCATION:** These courses are designed, scheduled and located to serve the needs of radiology residents and recent graduates. Home study questions are sent upon registration. The courses include both lectures and question sessions — faculty and students both questioning and answering in practice for what will follow. The early fall courses are more theoretical and the spring courses are more clinical. Your best value is to repeat the seminar for half price. The fall course is in Chicago just before written boards and the spring course is in Louisville just before oral boards.

*"...and those little extras...."*

**LOWEST AIR FARES:** Please call toll-free 1-800-548-8185 for special group fares.

*"...the most education for the money."*

#### FEES AND COURSE HOURS:

- Physician or Resident: Phy. Res. hrs.
- May 26: Radiology Physics \$135 \$ 90 10
- May 27-June 1: Clin. Rad. \$660 \$440 50
- May 26-June 1: Full Course \$750 \$500 60
- Repeating within 2 years: \$375 \$375 60
- Mock oral exams: \$ 70 \$ 70 1/2
- Private mock orals: \$100 \$100 1/2
- Add 10% to fees within 10 days of the course.
- Attendees not in course hotel add \$20/day.
- \$50.00 will reserve your position.
- Most home study material will be mailed after half of the registration fee is received.

*"...home study material was extremely helpful."*

**REFUNDS:** Subject to a \$50 fee, refunds will be made up until the seminar begins.  
 • Cancellation after mailing home study material requires retention of half the fee.

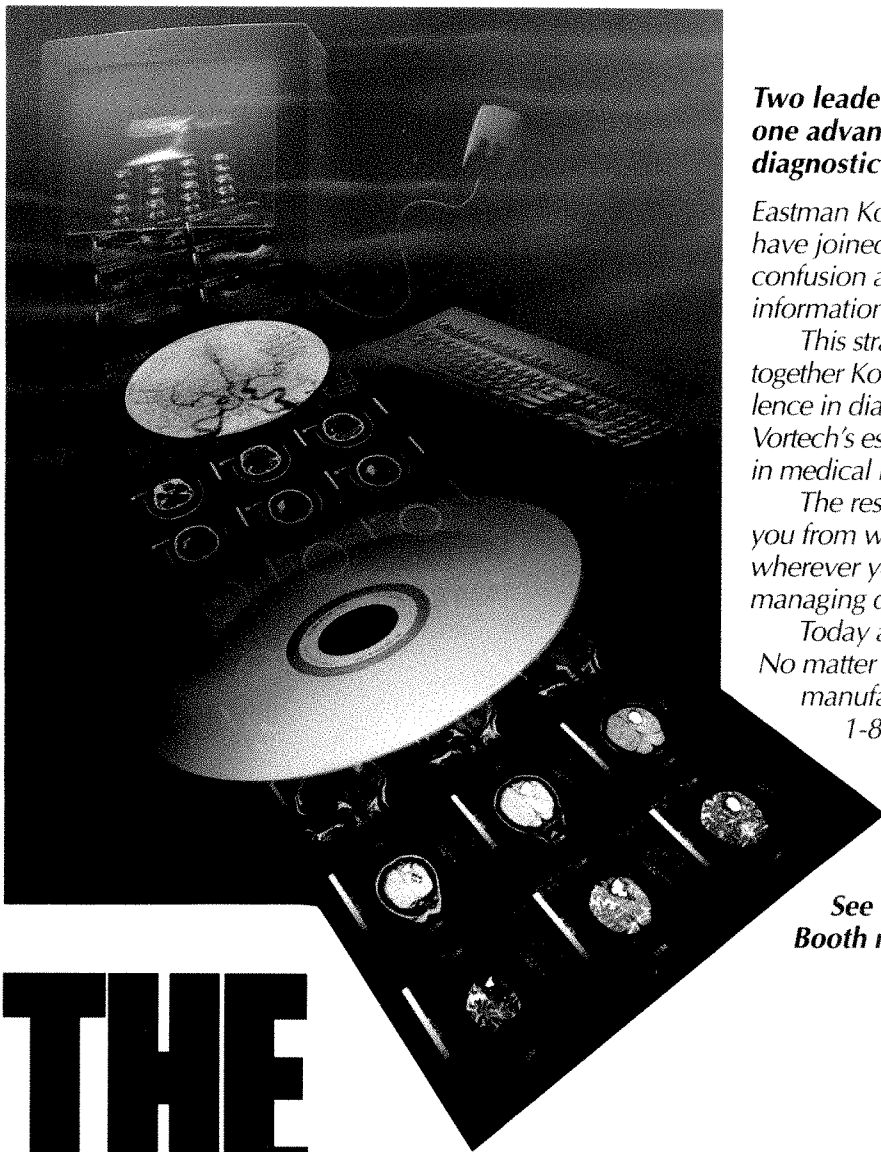
*"I feel [the course] helped me pass...."*

#### INFORMATION:

Joseph H. Selliken, Jr., M.D.  
**The Osler Institute**  
 1094 Dawn Lane, P.O. Box 2218  
 Terre Haute, IN 47802  
 (800) 356-7537 or (812) 299-5658

*\* Comments by past Osler participants*





***Two leaders in image technology present  
one advanced system for managing all your  
diagnostic imaging information.***

Eastman Kodak Company and Vortech Data, Inc.  
have joined forces to clear a path through the  
confusion and uncertainty of diagnostic imaging  
information management.

This strategic alliance brings  
together Kodak's proven excel-  
lence in diagnostic imaging with  
Vortech's established leadership  
in medical image management.

The result is a system to take  
you from wherever you are to  
wherever you want to be in  
managing diagnostic imaging information.

Today and tomorrow. Whatever your needs.  
No matter how many modalities you use. Or who  
manufactured the equipment. For details, call  
1-800-44KODAK, ext. 500.



***The resources are in place.  
The path is clear.  
The next step is yours.***

***See us at RSNA 1990.  
Booth no. 1126.***

# THE PATH IS CLEAR. KODAK

*Quality imaging worldwide*



## AJR Business and Subscriber Information

### The American Roentgen Ray Society

*AJR*, *American Journal of Roentgenology*, is published monthly to disseminate research on current developments in the radiologic sciences and commentary on topics related to radiology. It is published by the American Roentgen Ray Society, 1891 Preston White Dr., Reston, VA 22091; (703) 648-8992. Inquiries regarding society business, the annual ARRS meeting, and membership should be addressed to the Society at the above address.

### Correspondence Concerning the AJR

Correspondence regarding display (not classified) advertising, subscriptions, address changes, reprints, and permission requests should be addressed to Williams & Wilkins, 428 E. Preston St., Baltimore, MD 21202; (301) 528-4000.

Correspondence regarding editorial matters and classified advertising should be addressed to Editorial Office, *AJR*, 2223 Avenida de la Playa, Ste. 103, La Jolla, CA 92037-3218; telephone (619) 459-2229; FAX (619) 459-8814. For information on manuscript submission, see Guidelines for Authors, pages A3-A5.

### Subscriber Information

Subscription requests and inquiries should be sent to Williams & Wilkins, 428 E. Preston St., Baltimore, MD 21202. ARRS annual dues include \$50 for journal subscription. Subscription rates are as follows: nonmembers, \$125/year (\$180 foreign); institutions, \$135 (\$190 foreign); nonmember in-training, \$25 (\$80 foreign). Single copies of the Journal may

be purchased for \$18 (\$22 foreign). Airmail rates will be furnished on request.

Call toll-free, 1-800-638-6423 (in Maryland call 1-800-638-4007), with subscription questions or problems. Please have the mailing label from your latest issue available when you call.

If a subscriber receives a damaged copy of the *AJR* or fails to receive an issue, the subscriber should notify Williams & Wilkins (428 E. Preston St., Baltimore, MD 21202) within 60 days of publication (90 days for foreign subscribers) and that issue will be replaced.

Change of address information should be sent to Williams & Wilkins, 428 E. Preston St., Baltimore, MD 21202. Allow 90 days for address changes.

### Copyrights, Permissions, and Reprints

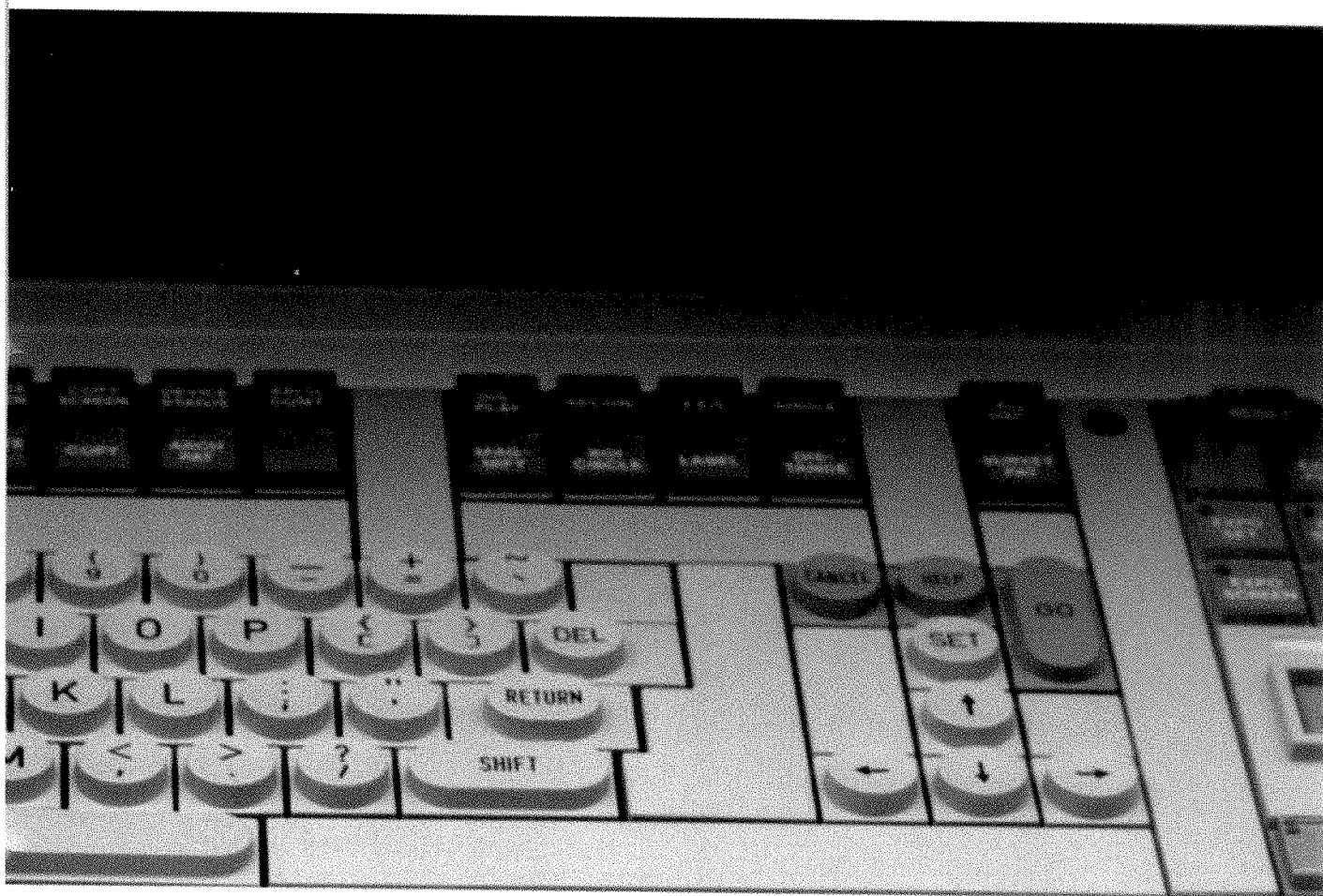
The American Roentgen Ray Society holds the copyright for all material published in the *AJR*. No part of this publication may be reproduced without permission from the ARRS. Requests for such permission should be addressed to Williams & Wilkins, 428 E. Preston St., Baltimore, MD 21202.

For reprints of a particular article, please contact the author designated in the footnotes for that article.

### Indexes

The *AJR* provides volume and yearly indexes (subject and author) in the June and December issues each year. *AJR* articles are also indexed in *Current Contents*, *Index Medicus*, and the cumulative index published by *Radiology*.





450-560 004 7952 © Siemens Medical Systems, Inc. 1990

Just three years ago, Siemens set a new standard for CT scanning with slip-ring technology. Now we've exceeded our own limits: the new SOMATOM® PLUS-S system cuts cycle times by 20%. To freeze motion and reveal greater detail... giving you more images... and more precise images... in less time.

With the SOMATOM PLUS-S you can run a routine scan in an eight-second cycle, including instant image reconstruction. Or scan any volume in a five-second cycle, using our Dynamic Screening software package.

**Speed saves even more than time.**

When scanning takes less time, it uses less

contrast media... and causes less patient discomfort. Think how much that will help geriatric patients. And trauma cases, where every second counts. Or pediatric patients, who'd rather wiggle than wait.

**Spiral your way through 29cm.** Capture images with no respiration artifacts or misregistration of slices. Because Spiral CT has both continuous table movement and data acquisition to let you scan an entire anatomical region in just 30 seconds — a single breath-hold. An imaging first, with the SOMATOM PLUS-S.

**Scan even more without repositioning.**

Head first or feet first, scan more of the body without moving the patient, using our

new 139cm scannable range, the longest and most convenient one available today.

To set new speed limits for scanning with the new SOMATOM PLUS-S, contact your local Siemens representative.

**Siemens Medical Systems, Inc.**

CT Marketing Division  
186 Wood Avenue South  
Iselin, NJ 08830  
(908) 321-4500

**Siemens...  
technology in caring hands.**

# AJR Guidelines for Authors

Address new and revised manuscripts, correspondence, and classified ads to the Editor:

AJR Editorial Office  
2223 Avenida de la Playa, Suite 103  
La Jolla, CA 92037-3218

Telephone: (619) 459-2229; FAX: (619) 459-8814

Inquiries regarding subscriptions, display advertising, reprints, or permission to republish *AJR* material should be addressed to the publisher:

The Williams & Wilkins Co.  
428 E. Preston St.

Baltimore, MD 21202 Telephone: 1-800-638-6423

The *AJR* publishes original contributions to the advancement of medical diagnosis and treatment. Submitted manuscripts should not contain previously published material and should not be under consideration for publication elsewhere. Papers dealing with neuroradiology should be addressed to: American Journal of Neuroradiology, Dept. of Diagnostic Radiology, 1653 W. Congress Pkwy., Chicago, IL 60612. At the discretion of the *AJR* Editor, *AJNR* articles that are of interest to the general reader may be republished in the *AJR*. Neuroradiologic papers sent to the *AJR* will be forwarded to the Editorial Office of the *AJNR*.

Manuscript decisions are based on peer review. Reviewers receive manuscripts without title pages to ensure an unbiased review. Statements made in the article, including changes made by the Editor or manuscript editor, are the responsibility of the author and not of the *AJR* or its publisher. Authors will be sent the edited manuscript, galley proof, and proofs of illustrations. If the corresponding author will be unavailable to review galleys, arrangements should be made for a coauthor or colleague to read and return the proof.

The following guidelines are based on instructions set forth in the **Uniform Requirements for Manuscripts Submitted to Biomedical Journals** (*Ann Intern Med* 1988;108:258-265). Articles will be edited, however, to conform to the individual style of *AJR*.

## General Guidelines for Major Papers

**Abstract.** Clearly state (in 200 words or less) the purpose, methods, results, and conclusions of the study. Include actual data.

**Introduction.** Briefly describe the purpose of the investigation and explain why it is important.

**Methods.** Describe the research plan, the materials (or subjects), and the methods used, in that order. Explain in detail how disease was confirmed and how subjectivity in observations was controlled.

**Results.** Present results in a clear, logical sequence. If tables are used, do not duplicate tabular data in text, but do describe important trends and points.

**Discussion.** Describe the limitations of the research plan, materials (or subjects), and methods, considering both the

purpose and the outcome of the study. When results differ from those of previous investigators, explain the discrepancy.

## AUTHOR'S CHECKLIST

**For priority handling, complete the following checklist, sign the copyright form on the reverse side of this page, and include both with the manuscript.**

\_\_\_\_\_ Two copies of the manuscript (the original and a photocopy) and two complete sets of figures are submitted. One copy has been retained by the author.

\_\_\_\_\_ If appropriate, *AJR* Guidelines for case reports, technical notes, pictorial essays, or letters to the Editor have been followed. (See page A17.)

\_\_\_\_\_ The manuscript, including references, figure legends, and tables, is typed double-spaced on 8½ × 11 in. (21.6 × 27.9 cm) *nonerasable* paper. Right-hand margins are not justified.

\_\_\_\_\_ All manuscript pages are numbered consecutively beginning with the abstract. Authors' names do not appear on the manuscript pages.

\_\_\_\_\_ The manuscript is organized as follows: title page, blind title page (title only), abstract, introduction, methods, results, discussion, acknowledgments, references, tables, figure legends, and figures.

\_\_\_\_\_ Informed consent has been obtained from patients who participated in clinical investigations. If experiments were performed on animals, authors complied with NIH guidelines for use of laboratory animals.

\_\_\_\_\_ Use of unfamiliar acronyms and abbreviations is kept to a minimum. When abbreviations are used they are defined at first mention, followed by the abbreviation in parentheses.

\_\_\_\_\_ Metric measurements are used throughout, or the metric equivalent is given in parentheses.

\_\_\_\_\_ Names and locations (city and state only) of manufacturers are given for equipment and nongeneric drugs.

### Title Page

\_\_\_\_\_ The following information is given: title of article; names and complete addresses (including zip code) of all authors; current addresses of authors who have moved since study; acknowledgment of grant or other assistance. The corresponding author is clearly identified, and a current address, phone number, and FAX number are given.

\_\_\_\_\_ A blind title page is included in each copy of the manuscript, giving only the title (without the authors' names) for use in the review process.

### Abstract

\_\_\_\_\_ An abstract of approximately 200 words concisely states the purpose, methods, and results of the study in one paragraph. Actual data are included. Conclusions are stated in a second, summary paragraph.

\_\_\_\_\_ No abbreviations or reference citations are used.



### Case Reports

A case report is a brief description of a special case that provides a message that transcends the individual patient.

*Format.* There is no abstract. The introduction should be a short paragraph giving the general background and the specific interest of the case. No more than one case should be described in detail (similar ones can be mentioned briefly in the discussion). Emphasis should be on the radiologic aspects; clinical information must be limited to that necessary to provide a background for the radiology. The discussion should be succinct and should focus on the specific message and relevance of radiologic methods. A review of the literature is not appropriate.

*Length.* Maximum of five double-spaced, typewritten pages, including the references but not the title page or figure legends.

*References.* Maximum of eight.

*Figures.* Maximum of four, unless the text is shortened accordingly. Legends must not repeat the text.

*Tables and Acknowledgments.* Not appropriate in case reports.

### Technical Notes

A technical note is a brief description of a specific technique or procedure, modification of a technique, or equipment of interest to radiologists.

*Format.* No abstract, headings, or subheadings are required. If headings are used, they should be a combination of "Case Report," "Materials and Methods," "Results," and "Discussion." A brief one-paragraph introduction should be included to give the general background. Discussion should be limited to the specific message, including the uses of the technique or equipment. Literature reviews and lengthy case reports are not appropriate.

*Length.* Maximum of five double-spaced, typewritten pages, including the references but not the title page or figure legends.

*References.* Maximum of eight.

*Figures.* Maximum of two, unless the text is shortened accordingly.

*Tables and Acknowledgments.* Not appropriate in technical notes.

### Pictorial Essays

A pictorial essay is an article that conveys its message through illustrations and their legends. Unlike other *AJR* articles, which are based on original research, pictorial essays serve primarily as teaching tools, like exhibits at a scientific meeting. They are not encyclopedic book chapters. The abstract should be a short, introductory paragraph.

*Length.* Maximum of four double-spaced, typewritten pages, including the references but not the title page or figure legends.

*References.* Maximum of four.

*Figures.* Maximum of 30 figure parts. Number should be as few as necessary to convey the message of the paper.

*Tables and Acknowledgments.* Not appropriate in pictorial essays.

### Letters to the Editor and Replies

Letters to the Editor and Replies should offer objective and constructive criticism of published articles. Letters may also discuss matters of general interest to radiologists. Do not end a letter with a hand-written signature.

*Format.* All letters should be typed double-spaced on nonletterhead paper, with no greeting or salutation. Name and affiliation should appear at the end of the letter. Titles for letters should be short and pertinent. The title for a reply is simply "Reply."

*Length.* Maximum of two double-spaced, typewritten pages, including references.

*References.* Maximum of four.

*Figures.* Maximum of two.

*Tables and Acknowledgments.* Not appropriate in Letters to the Editor and Replies.

### Opinions, Commentaries, and Perspectives

Opinions, commentaries, and perspectives are special articles dealing with controversial topics or issues of special concern to radiologists.

*Format.* Include a title page but no abstract. Headings may be used to break up the text.

*Length.* Maximum of five double-spaced, typewritten pages.

*References.* Maximum of five.

*Tables and Figures.* Maximum of four.

### Computer Page Articles

Articles published on the computer page deal with practical computer applications to radiology.

*Format.* Include a title page and an abstract.

*Length.* Maximum of eight double-spaced, typewritten pages.

*References.* Maximum of five.

*Figures and Tables.* Maximum of five. Computer print-outs are not acceptable. Figures must be submitted as 5 × 7 in. glossy prints.

**All submissions to the *AJR* must be accompanied by a completed copy of the Author's Checklist and the signed Copyright Agreement.**

References

References (not to exceed 35) are typed double-spaced starting on a separate page and are **numbered consecutively in the order in which they appear in the text**. All references are cited in the text and are enclosed in brackets and typed on line with the text (not superscript). Unpublished data are not cited in the reference list, but are cited parenthetically in the text, for example, (Smith DJ, personal communication), (Smith DJ, unpublished data). This includes papers submitted, but not yet accepted, for publication. Papers presented at a meeting are not cited in the reference list, but are cited parenthetically in the text (e.g., Smith DJ et al., presented at the annual meeting of the American Roentgen Ray Society, May 1990). After first mention, use (Smith DJ et al., ARRS meeting, May 1990). Inclusive page numbers (e.g., 333–335) are given for all references. Journal names are abbreviated according to *Index Medicus*. Style and punctuation of references follow the format illustrated in the following examples (all authors are listed when six or fewer; when seven or more authors, the first three are listed, followed by “et al.”):

*Journal article*  
1. Long RS, Roe EW, Wu EU, et al. Membrane oxygenation: radiographic appearance. *AJR* 1986;146:1257–1260

*Book*  
2. Smith LW, Cohen AR. *Pathology of tumors*, 6th ed. Baltimore: Williams & Wilkins, 1977:100–109

*Chapter in a book*  
3. Breon AJ. Serum monitors of bone metastasis. In: Clark SA, ed. *Bone metastases*. Baltimore: Williams & Wilkins, 1983:165–180

Tables

Each table is typed double-spaced on a separate page without vertical or horizontal rules; each has a short, descriptive title. Tables do not exceed two pages in length and contain at least four lines of data.

Tables are numbered in the order in which they are cited in the text. Abbreviations are defined in an explanatory note below each table. Tables are self-explanatory and do not duplicate data given in the text or figures. All arithmetic (percentages, totals, differences) has been double checked for accuracy, and tabular data agree with data given in the text.

Figures and Legends

Two complete sets of original figures are submitted unmounted in labeled envelopes. Figures are clean, unscratched, 5 × 7 in. (13 × 18 cm) glossy prints with **white borders**. A separate print is submitted for each figure *part*. All figure parts relating to one patient have the same figure number. Each figure is labeled on the back with the figure number and an arrow indicating “top.” For black-and-white figures, labeling is done on a gummed label, which is then affixed to the back of the print. **Never** use labels on **color** figures, but write figure number on the back lightly in pencil. **Never** use ink on front or back of any figures. Author’s names are *not* written on the backs of figures. Only removable (rub-on) arrows and letters are used on the figures. Symbols are uniform in size and style and are not broken or cracked. Images are uniform in size and magnification. Line drawings are done in black ink on a white background. They are professional in quality, and all use the same size type. (Only glossy prints are acceptable.) Written permission has been obtained for use of all previously published illustrations (and copies of permission letters are included), and an appropriate credit line is given in the legends. Legends are typed double-spaced, and figure numbers correspond with the order in which the figures are cited in the text.

Transfer of Copyright Agreement, Conflict of Interest Acknowledgment, Certification of Coauthors, and Exclusive Publication Statement

Complete copyright to the article entitled: \_\_\_\_\_

is hereby transferred to the American Roentgen Ray Society (for United States government employees to the extent transferable), effective if and when the article is accepted for publication in the *American Journal of Roentgenology*. In the case of the authors who are officers or employees of the United States government, the American Roentgen Ray Society recognizes that works prepared by officers or employees of the United States government as part of their official government duties are in the public domain.

Authors reserve all proprietary rights other than copyright, such as patent rights and the right to use all or part of this article in future works of their own. The authors retain the right of replication, subject only to crediting the original source of publication and receiving written permission from the publisher.

Authors guarantee that this manuscript contains no matter that is libelous or otherwise unlawful, invades individual privacy, or infringes any proprietary rights.

Authors understand that they will receive no royalty or other compensation from the American Roentgen Ray Society or the publisher.

Authors guarantee that the editor has been or will be informed of any proprietary or commercial interest or conflicts of interest the authors may have that relate directly or indirectly to the subject of this article.

All authors certify that they have made substantive and specific intellectual contributions to the article and assume public responsibility for its content.

Finally, the authors certify that none of the material in this manuscript has been published previously or is currently under consideration for publication elsewhere.

_____	_____	_____
First author/date	Second author	Third author
_____	_____	_____
Fourth author	Fifth author	Sixth author

This agreement must be signed by all authors in order for the manuscript to be published.



## Benjamin Felson Lecture

# Chronic Interstitial Lung Disease of Unknown Cause: A New Classification Based on Pathogenesis

James C. Hogg<sup>1</sup>

Chronic interstitial lung disease of unknown cause is usually classified on the basis of descriptive histology. In this lecture, a recently published series of 910 cases of chronic interstitial lung disease is used to show that these descriptive terms can be reorganized into a classification that is based on inflammatory and neoplastic processes. The proposed classification includes three major diagnostic categories, two of which are based on the chronic inflammatory response and a third that results from infiltration of the interstitial space by neoplastic cells of either a benign, borderline, or frankly malignant nature. An argument is presented that the steps involved in the development of the end-stage of chronic interstitial lung disease are similar in all three groups. The advantage of this new classification is that it shifts the emphasis from descriptive terminology to pathogenesis, which provides a more critical basis for investigation of the causes of these diseases.

Our current understanding of chronic interstitial lung disease of unknown cause is based on correlating clinical, physiologic, and radiologic observations with the descriptive histology of the lung. Although this approach has met with some success, it tends to emphasize differences rather than similarities and provides very little insight into origin. In this lecture, I will present a brief overview of the anatomy and physiology of the lung interstitial space and propose a classification of chronic interstitial lung disease that uses two diagnostic categories that are based on the chronic inflammatory response and a third category that is based on the neoplastic process.

The advantages of this classification are that it readily accommodates the majority of the commonly used descriptive terms, stresses pathogenesis, and provides a framework for a more critical appraisal of the causes of chronic interstitial lung disease.

### Anatomy and Physiology of the Interstitial Space

The lung interstitium can be divided into a central compartment that surrounds the bronchovascular bundle and a peripheral compartment that outlines the secondary lung lobules (Fig. 1). The central interstitial compartment contains the conducting airways, the pulmonary and bronchial arterial and venous systems, and the central lymphatics, whereas the peripheral compartment contains the lymphatics and veins that drain to the periphery of the secondary lobule (Fig. 1). The alveolar wall (Fig. 2) forms a third interstitial compartment, seen best with the electron microscope, in which the basement membranes of epithelium and capillary fuse on the thin side and separate to form an interstitial space on the thick side of the alveolar wall. An extracellular material produced by endogenous cells forms a three-dimensional collagen fiber network embedded in a gel-like matrix that fills the central, peripheral, and alveolar compartments of the interstitial space.

The interstitial fluid is formed by the difference between filtration and reabsorption by the microvessels and is returned to the venous circulation by the lymphatics. In a normal 70-kg man with a cardiac output of 5 l/min, approximately 1–2 l

Received June 29, 1990; accepted after revision August 20, 1990.

Presented at the annual meeting of the Society of Thoracic Radiology, Naples, FL, January 1990.

This work was supported by grants from the Medical Research Council of Canada and the British Columbia Lung Association.

<sup>1</sup> University of British Columbia Pulmonary Research Laboratory, St. Paul's Hospital, 1081 Burrard St., Vancouver, B.C., Canada V6Z 1Y6.

AJR 156:225–233, February 1991 0361–803X/91/1562–0225 © American Roentgen Ray Society

of fluid leaves the systemic vessels to enter the interstitial space each day [1]. Although the lung receives the same cardiac output, it generates only about 10% of the net fluid flux of the systemic circulation [2]. This ultrafiltrate of plasma percolates through the interstitial space and is drained back into the venous system via the lymphatic vessels. Receptors on the surface of the circulating cells and ligands on the endothelium provide the specificity for directing cell traffic through the interstitial space [3]. Although these receptor-

ligand interactions are only partially understood, they can account for the organ-specific recirculation of lymphocytes, monocytic migration from the vascular to the interstitial and alveolar spaces, and polymorphonuclear cell migration out of the microvessels in response to an inflammatory stimulus.

Pathology of Interstitial Lung Disease

In a series of 910 biopsy samples collected during 10 years at the Brompton Hospital in London, Corrin [4] was able to describe the histology of chronic interstitial lung disease of unknown origin by using a relatively small number of descriptive terms. These include cryptogenic fibrosing alveolitis (*n* = 339); sarcoidosis (*n* = 343); organizing pneumonia (*n* = 123); lymphoproliferative disease (*n* = 32); extrinsic allergic alveolitis (*n* = 25); eosinophilic granuloma (*n* = 12); organizing diffuse alveolar damage (*n* = 6); lymphangiomyomatosis (*n* = 5); and small numbers of cases such as asbestosis, hard metal disease, and berylliosis for which the cause was known. These data have been regrouped in Table 1 to show that these descriptive terms can be reclassified according to whether the disease is based on (1) a chronic nongranulomatous inflammatory process; (2) a chronic granulomatous inflammatory process; or (3) a neoplastic process in which the interstitial space is infiltrated by a proliferation of either benign, borderline, or frankly malignant neoplastic cells.

The category that accounts for the largest number of cases (Table 1) is due to a chronic nongranulomatous inflammatory reaction of unknown cause that has been referred to as the usual form of interstitial pneumonia (UIP) in North America [5] and fibrosing alveolitis in Europe [6]. A variant of this inflammatory response that is characterized by organization of the

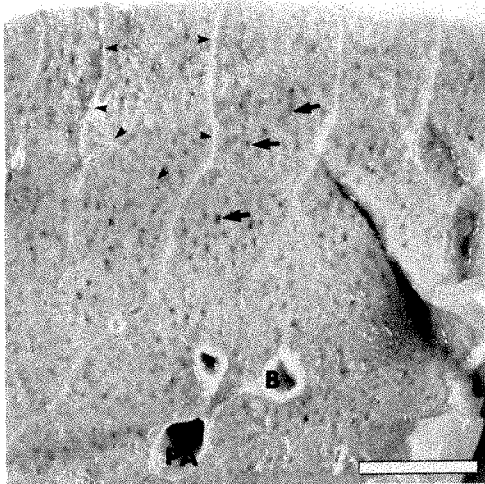


Fig. 1.—Cut surface of human lung in which connective tissue forming lobular septa (arrowheads) and surrounding airways and pulmonary vessels define two compartments of interstitial space. Arrows point to alveolar ducts. PA = pulmonary artery, B = bronchus. Scale bar = 500  $\mu$ m.

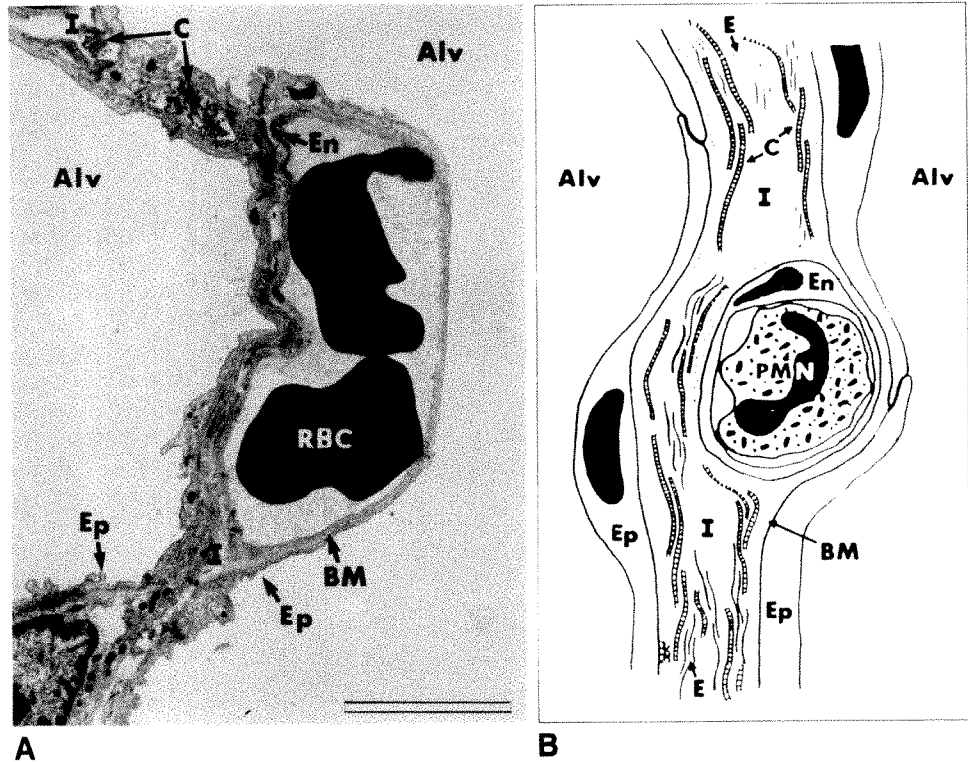


Fig. 2.—A and B, Electron micrograph of alveolar wall and accompanying diagram show third interstitial space located on thick side of capillary. I = interstitial space, C = collagen, ALV = alveolus, En = endothelium, BM = basement membrane, Ep = epithelium, E = elastin, PMN = polymorphonuclear leukocyte. Scale bar = 4  $\mu$ m.



inflammatory exudate within the distal airways is called cryptogenic organizing pneumonitis in Great Britain [7] and bronchiolitis obliterans with organizing pneumonia (BOOP) in the American literature [8]. A second variant desquamative interstitial pneumonia (DIP) has been described in the United States [9], but because it is included as a cellular form of cryptogenic fibrosing alveolitis in the British nomenclature, it does not appear as a separate group in Table 1. The descriptive category based on the chronic granulomatous form of inflammation is usually referred to as sarcoidosis or sarcoid-like granulomatous lung disease when no cause for the gran-

ulomatous process can be demonstrated. The third pathogenic pathway to the end-stage lung is a neoplastic process in which either benign, borderline, or frankly malignant neoplastic cells infiltrate and proliferate within the interstitial space. This category includes diagnoses such as eosinophilic granuloma in which histiocytes proliferate, lymphangiomyomatosis in which smooth muscle cells proliferate, lymphoproliferative disease such as lymphocytic interstitial pneumonia (LIP), and lymphangitic spread of carcinoma.

TABLE 1: Classification of Histologic Findings in Chronic Interstitial Lung Diseases of Unknown Cause

Classification	No. of Cases
Inflammatory reaction	
Nongranulomatous	
Cryptogenic fibrosing alveolitis (usual form of interstitial pneumonia)	339
Organizing pneumonia (bronchiolitis obliterans with organizing pneumonia)	123
Organizing diffuse alveolar damage	6
Granulomatous	
Sarcoidosis or sarcoidlike	343
Extrinsic allergic alveolitis	25
Neoplastic infiltration	
Eosinophilic granuloma (histiocytes)	12
Lymphangiomyomatosis (smooth muscle)	5
Lymphoproliferative disease (e.g., lymphocytic interstitial pneumonia)	32
Other (cases of known cause, such as asbestosis, berylliosis, hard metal disease)	25
Total	910

Note.—Data from Corrin [4] were reclassified into three groups on the basis of inflammatory and neoplastic processes. See text for further explanation.

Development of the End-Stage Lung

Figure 3 shows that the term end-stage lung is used to describe the final stages of all three of the diagnostic categories used in this classification. This section will outline the steps involved in progression toward the end-stage lung under the heading of Nongranulomatous Inflammation because this category contains the largest number of cases (Table 1). The pathology of the other two categories (i.e., granulomatous inflammation and neoplasia) also is discussed because the steps involved in the production of the end-stage lung are common to all three categories.

Nongranulomatous Inflammation

*Fibrosing alveolitis/UIP.*—An injury to the alveolar wall that disrupts the epithelial surface results in exudation of fluid and protein onto the air-tissue interface. This increases surface tension and causes alveoli to collapse on alveolar ducts because of the Laplace relationship:

$$\text{Pressure} = \frac{\text{Wall tension} + \text{surface tension}}{\text{Radii of curvature}}$$

Fig. 3.—Schema with three main pathogenetic pathways for development of end-stage lung. Pathways of chronic nongranulomatous inflammation (usual form of interstitial pneumonia [UIP]/fibrosing alveolitis) and chronic granulomatous inflammation can be subdivided and account for most cases of interstitial lung disease. The third pathway is produced by expansion of lung interstitial space by desmoplastic reaction to benign, borderline, or frankly malignant cells. Eos = eosinophilic, DIP = desquamative interstitial pneumonia, BOOP = bronchiolitis obliterans with organizing pneumonia.

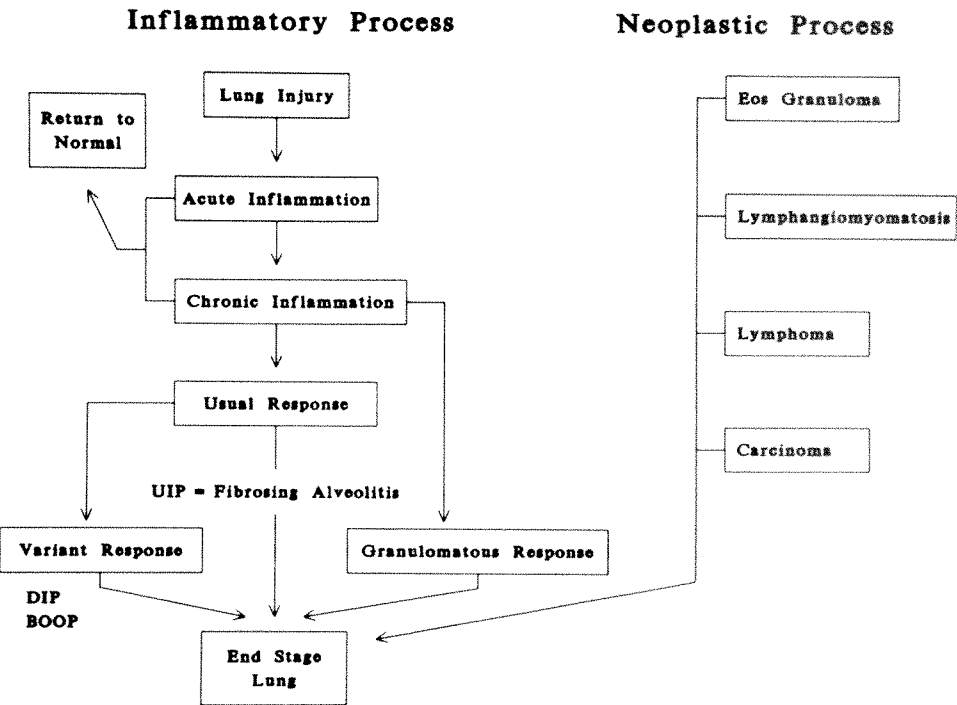


Figure 4 shows the result of an experiment in which wall tissue tension was increased by pressing on the surface of the lung [10]. The alveoli have collapsed while the alveolar ducts remain open in the deformed area. A similar change in anatomy occurs in acute lung injury when surface tension is increased by the exudation of plasma into the air spaces. If the injury is severe enough, hemorrhage is associated with this exudate, and large protein molecules such as fibrinogen escape onto the alveolar surface. The conversion of fibrinogen to fibrin traps the contents of the exudate on the surface of the lung to produce a hyaline membrane, which usually forms on the alveolar duct surface (Fig. 5) because the alveoli have collapsed. These changes (i.e., hemorrhage, edema, and hyaline membrane formation) are referred to as diffuse alveolar damage, which is the diagnostic term used to describe acute lung injury from any cause. This term was used infrequently in the series of Corrin [4] (Table 1) because all of the patients undergoing biopsy had chronic illness. Recently, Kuhn et al. [11] documented that organization of this exudate occurs within the air space rather than the interstitium (Fig. 6), which means that the increased tissue thickness seen in chronic interstitial disease (Fig. 7) is the result of epithelial growth over the surface exudate rather than true expansion of the interstitial space. The deposition of connective tissue in this exudate causes a further distortion of the alveolar ducts and

results in the formation of honeycomblike structures that characterize one form of end-stage lung (Figs. 8A and 8B). However, in situations in which the exudate fills the lumen, its subsequent organization obliterates the air space completely (Figs. 8C and 8D) and no honeycomblike structures are found.

When the lung surface is diffusely injured, the progression to end-stage lung can occur very rapidly. Pathologic studies [12] of lungs from patients in the National Institutes of Health multicenter membrane-oxygenator trial (Table 2) showed that the majority of patients dying within 1 week of the development of respiratory failure showed evidence of diffuse alveolar damage (i.e., hyaline membrane and hemorrhagic edema), whereas patients that survived more than 2 weeks showed marked fibrosis. This progression from acute injury to fibrosis suggests that the rapid clinical course of adult respiratory distress syndrome is the result of widespread initial injury, whereas the more usual, slowly progressive chronic interstitial lung disease is due to recurrent local injuries subtracting units from different lung regions over many years. Widespread initial injury also might have accounted for the rapid progression of the form of interstitial lung disease originally described by Hamman and Rich [13]. Furthermore, the dependence of chronic disease on multiple small sites of injury at different times is consistent with the conclusion of Spencer [14] that

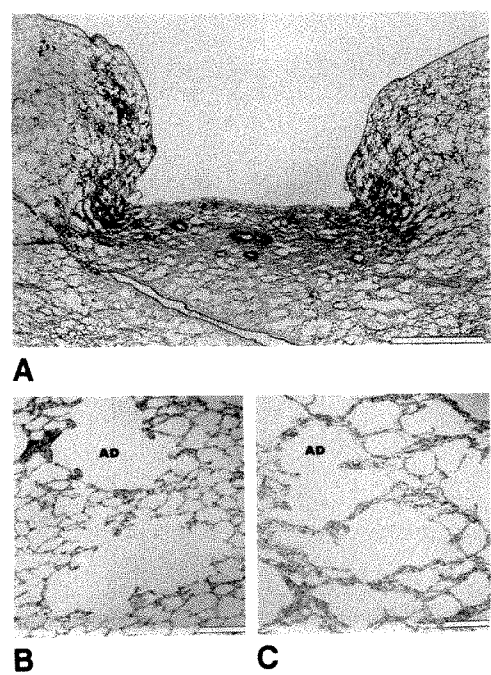


Fig. 4.—When pressure is applied to the lung to increase wall tension, alveoli collapse on alveolar ducts (AD) because they have smaller radii of curvature and behave according to the Laplace relationship (see text).  
A, Overview of pleural surface of lung, which has been compressed by application of a metal probe. Scale bar = 1 mm.  
B, Higher magnification of region at margin of compressed and noncompressed areas. Scale bar = 50 μm.  
C, Higher magnification of compressed area shows that only alveolar ducts are visible because many alveoli have collapsed. Scale bar = 50 μm. (Modified from Robertson et al. [10].)

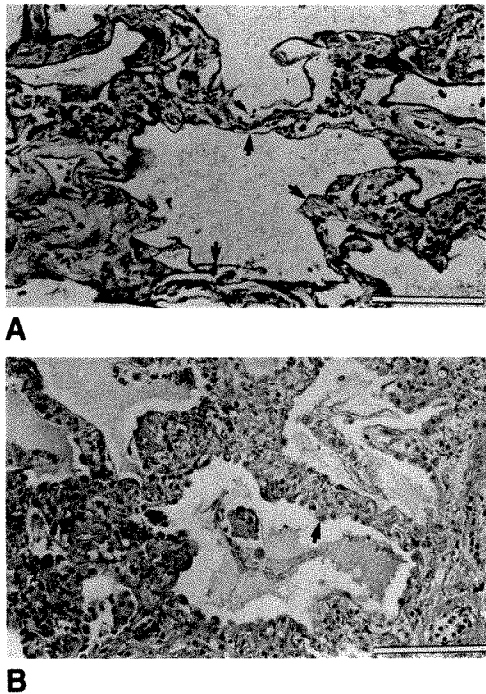


Fig. 5.—A, Early stage of lung injury in which hyaline membranes (arrows) have formed on alveolar ducts.  
B, Later stage in which type II epithelial cells (arrow) have proliferated over the surface, leaving a space that is the approximate size of an alveolar duct. The walls of this space are thickened owing to incorporation of surface exudate by overgrowth of epithelium rather than true expansion of interstitial space. Scale bar = 100 μm.



Fig. 6.—Organization of fibrinous exudate occurs within air space rather than interstitium. This means that increased tissue thickness (Fig. 5B) is result of epithelial growth over surface exudate (Fig. 5A) rather than true expansion of interstitial space.

A, Healthy parenchyma.  
B, Epithelial injury and air-space exudation.

C, Fibroblast proliferation and connective tissue synthesis.

(Reprinted with permission from Kuhn et al. [11].)

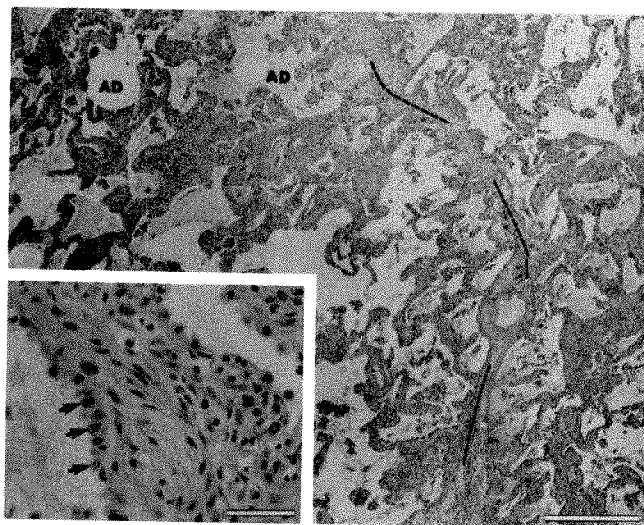
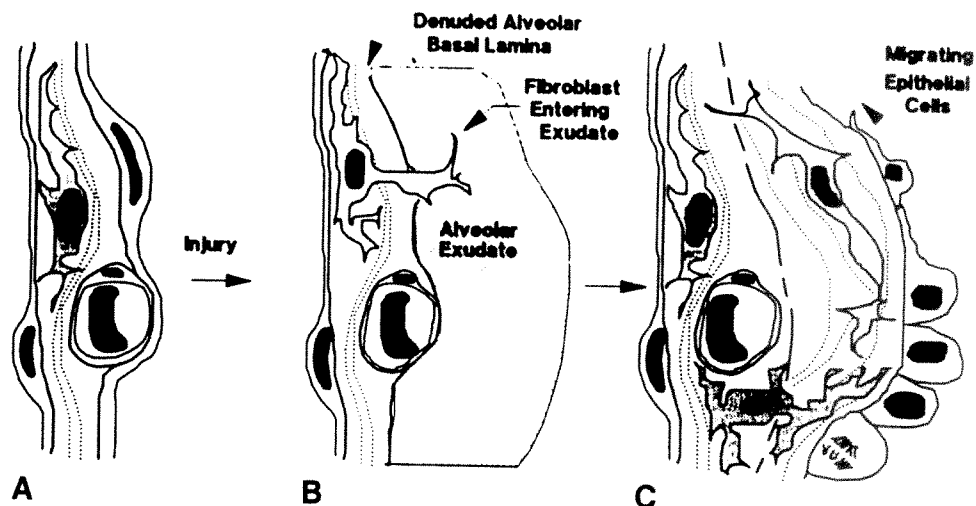


Fig. 7.—Low-power photomicrograph in a case of chronic interstitial disease shows lobular septa (broken line) and alveolar ducts (AD). Scale bar = 0.5 mm.

Inset shows an example of a thickened interstitium due to epithelial growth over a surface exudate (compare with Fig. 6). Scale bar = 50  $\mu$ m.

the outstanding pathologic change in chronic interstitial disease is that early, intermediate, and terminal stages are present in the same lung.

**Variant forms of nongranulomatous inflammation.**—When the inflammatory exudate fills the alveolar space completely rather than being limited to the surface of the alveolar ducts, the air spaces can be obliterated as the exudate is organized by connective tissue. This type of inflammatory response accounts for the cases that Epler et al. [8] referred to as BOOP in North America and Davison et al. [7] called cryptogenic organizing pneumonia in Great Britain. Epler et al. analyzed 2500 open-lung biopsy specimens and identified 67 adults in whom bronchiolitis obliterans was the prominent feature. In 85% (57/67) of these cases, the obliterating bronchiolitis was associated with organizing pneumonia and in the

majority of these (55/57), there was no obvious cause for the underlying disorder. Davison et al. [7] described a similar process in a smaller number of patients, which Corrin [4] applied to 129 of the 910 cases in his series (Table 1). The patients in this category have a reasonably homogeneous clinical course that frequently presents as a subacute illness with symptoms of cough, dyspnea, fever, sputum production, malaise, and weight loss, which are present for periods ranging from 3 to 6 months. Pulmonary function tests show a restrictive rather than an obstructive pattern and the majority have impaired gas exchange, particularly on exercise. The radiologic appearance is one of nodular opacities that progress in some areas and regress in others.

The pathologic descriptions provided by these two groups of authors are highly characteristic in that an exudate formed in the airways is organized in a way that results in the deposition of a large amount of connective tissue. This proliferation often occludes the lumen of the distal airways and is associated with interstitial pneumonia. The resultant histology is the same as that seen in postinfectious organizing pneumonia, except that no organisms could be demonstrated by either Epler et al. [8] or Davison et al. [7]. The clinical and radiologic features, faster course, and better initial response to steroids distinguish BOOP from UIP. The absence of physiologic evidence of airway obstruction when there is clear anatomic evidence of airway obliteration is puzzling. Guerry-Force et al. [15] have suggested that BOOP differs from the multiple conditions in which bronchiolitis obliterans is associated with airway obstruction [16–20] in that the lesions in BOOP are more scattered but are able to subtract enough peripheral lung units to cause lung restriction without producing obstruction.

A second variant form of nongranulomatous inflammatory response, DIP, was originally described by Liebow et al. [9] in 1965. These authors thought the histologic pattern of DIP differed from that of UIP in that the alveolar spaces were filled with cells that the authors interpreted as desquamating pneumocytes. Subsequent electron microscopic studies have shown that DIP is an inappropriate term because the cells thought to be desquamating pneumocytes are in fact alveolar macrophages. There is less deposition of connective tissue

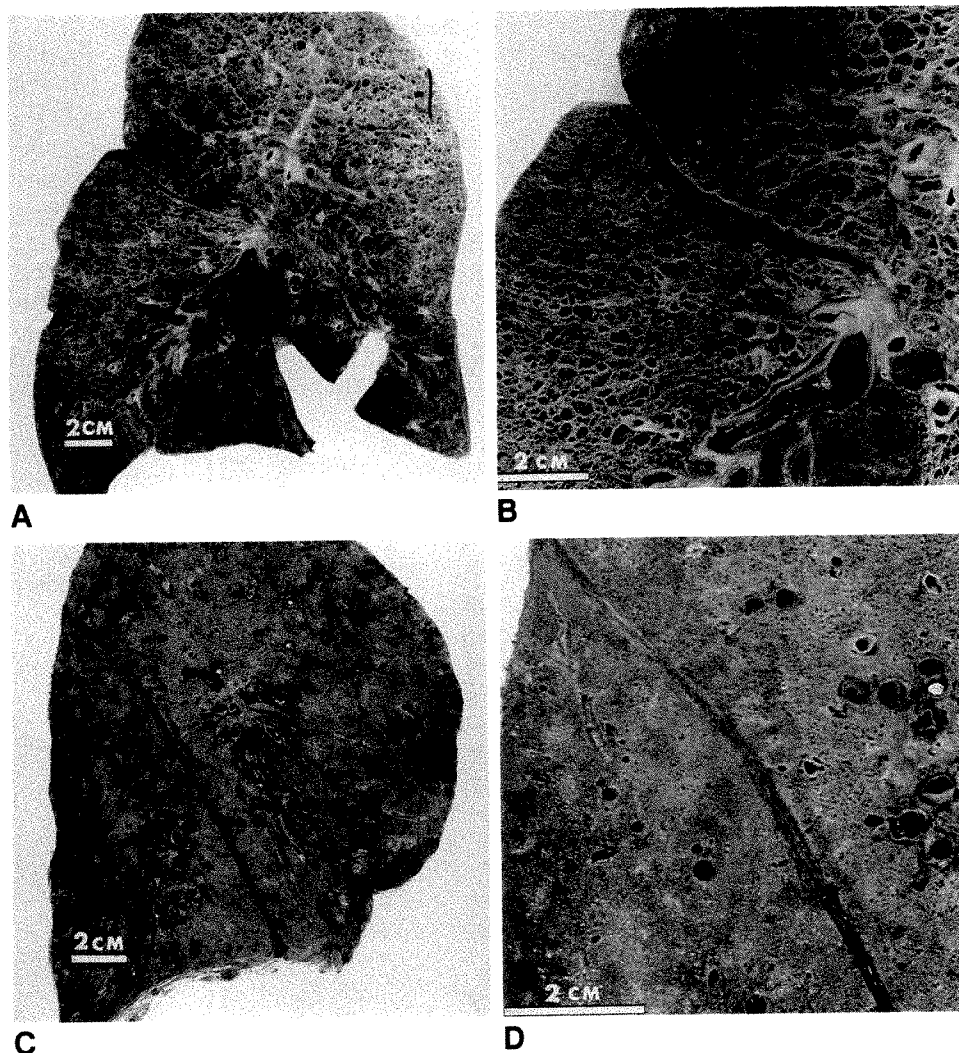


Fig. 8.—A, Overview of cut surface of entire lung with obvious honeycomb pattern.

B, Magnified view of honeycomb pattern. Comparison with Figs. 1, 4, and 5 suggests that honeycomb pattern is due to distortion of alveolar ducts by organization of inflammatory exudate.

C and D, Alternative pattern of end-stage lung in which proliferation of connective tissue has obliterated air space completely, leaving a solid lung architecture.

in DIP than in UIP, possibly because there is less exudation into the air spaces, and the cellular infiltrate in the interstitial space is a mixture of monocytes and lymphocytes, with occasional eosinophils and plasma cells.

The clinical importance of this histologic category is controversial. British researchers [6, 21] have suggested that DIP is an early phase of the usual response and included it in their overall concept of fibrosing alveolitis. American authors [5], on the other hand, have tended to think of UIP and DIP as separate entities and have argued that DIP has a different clinical presentation and subsequent course. However, examination of the data [5] used to support the argument that UIP and DIP have different clinical courses shows that the patients with DIP were about 10 years younger than those with UIP. Taking this age difference into account allows the survival data for DIP and UIP to fit a single continuous curve that supports the British opinion that DIP may be an early manifestation of UIP rather than a separate entity.

The histologic hallmarks of DIP and UIP are of interest with respect to this argument. The DIP pattern is one of air space filling by macrophages and cellular infiltration of the interstitial

space with little connective tissue deposition. It is conceivable that if this pattern were gradually replaced by a more exudative response, it might then organize in the manner described for UIP [11]. However, at the present time the argument as to whether UIP and DIP are separate or continuous processes cannot be resolved.

#### *Granulomatous Inflammation*

The second major histologic pattern leading to the end-stage lung is the result of a chronic granulomatous inflammatory response. This diagnostic category accounted for 368 of the 910 cases in the series of Corrin [4] (Table 1) and formed the second largest group in that report. Granulomatous inflammation is a process that is characterized by the formation of small (1–2 mm) collections of mononuclear inflammatory cells [22]. The predominant cell in the granuloma is a modified macrophage that, like all macrophages, is derived from blood monocytes. Activation of the macrophage gears it toward the production of lysosomal enzymes and abundant cytokines and causes it to take on the appearance



**TABLE 2: Pathologic Changes in Lung vs Survival Length After Development of Respiratory Failure**

Pathologic changes	No. of Patients by Duration of Survival		
	<1 Week	1-2 Weeks	>2 Weeks
Hyaline membranes	15	3	0
Mild duct fibrosis	2	6	5
Severe duct fibrosis	0	6	20
Total	17	15	25

Note.—Modified from Table 6 of Pratt et al. [12].

of an epithelial cell. This has resulted in the use of the term epithelioid cell as a synonym for an activated macrophage. Two types of giant cells are produced by the fusion of individual macrophages into multinucleated cells. In the Langhans type, the nuclei are arranged in a horseshoe pattern, whereas the nuclei form a ring in the foreign-body type of giant cell. In addition to the macrophages and giant cells, granulomas characteristically contain a rim of lymphocytes. In the tuberculous form of granulomatous inflammatory response, proteolytic enzymes released by the activated macrophages result in necrosis of the center of the granuloma. Because the gross appearance of many confluent granulomas undergoing this form of necrosis reminded early investigators of cheese, it is often referred to as caseous necrosis.

Two factors appear to be paramount in producing granulomatous inflammation [22]. The first is the presence of an inflammatory stimulus that the macrophage cannot completely digest and the second is a cell-mediated inflammatory response to this inciting agent. The known causes of granulomatous inflammation include infections with bacteria (tuberculosis), fungi (e.g., coccidiomycosis, cryptococcosis, histoplasmosis, and blastomycosis), chlamydia (psitticosis), and a variety of noninfectious agents including foreign bodies of an inorganic (beryllium) and organic (extrinsic allergic alveolitis) nature. The cause of this type of reaction frequently can be established by the intelligent use of case history, culture, serology, and histologic techniques. When the cause cannot be determined and there is an associated clinical syndrome involving the parotid glands, eye, lymph nodes, skin, bone, joints, and meninges, the term sarcoidosis is appropriate. However, in the absence of this characteristic clinicopathologic syndrome, the pathologist would be wise to use the term sarcoidlike rather than sarcoid to describe the pulmonary lesions. This simply reflects the incomplete knowledge of the nature of sarcoidosis and our ignorance of the causes of many other forms of granulomatous inflammation of the lung.

#### Neoplastic Response in Chronic Interstitial Lung Disease

The proliferation of benign, borderline, or frankly malignant neoplastic cells in the interstitial space is commonly associated with connective tissue deposition. This proliferation of connective tissue is part of the stromal reaction to the neoplastic cells and is not part of the neoplastic process [23]. Although far fewer cases of interstitial lung disease are due

to neoplasia than to chronic inflammation (Table 1), several of them are highly characteristic and easily recognized even though we are quite ignorant of their origin.

**Eosinophilic granuloma (histiocytosis X).**—Lichtenstein [24] grouped Letterer-Siwe disease, Hand-Schüller-Christian disease, and eosinophilic granuloma under the term histiocytosis X because they all involve a proliferation of histiocytes. Letterer-Siwe disease is an illness of infancy characterized by extensive histiocytic infiltration of the skin and reticuloendothelial system that is usually fatal. Hand-Schüller-Christian disease is a syndrome that progresses more slowly than does Letterer-Siwe disease and is characterized by the formation of disseminated histiocytic nodules containing many eosinophils in the skin, bones, lymph nodes, and abdominal viscera. Eosinophilic granuloma refers to a disease in which histiocytic nodules similar to those seen in Hand-Schüller-Christian disease are limited to either the lung or bone with both organs occasionally being involved at the same time. It is important to remember that the term eosinophilic granuloma is used because eosinophils accompany the proliferating histiocytes and not because the eosinophils are proliferating independently. The condition has no known cause and a variable natural history, with many patients living reasonably active lives into adulthood.

The histologic lesion frequently can be diagnosed at low power with the light microscope because the granulomatous nodules have a discrete fibrotic center with peripheral extensions that have a characteristic pattern. The proliferating histiocyte has an indented or bean-shaped nucleus that gives it a characteristic grooved appearance when viewed en face. These cells do not show significant phagocytosis and have a pale cytoplasm; electron microscopic examination shows that they contain tennis racket-shaped structures called Birbeck granules. However, because some airway epithelial cells also contain these granules, it is not wise to base a diagnosis on the presence of Birbeck granules in cells obtained by airway lavage.

**Lymphangiomyomatosis.**—This is a rare condition limited to women in the reproductive years. Some have thought it to be a variant of tuberous sclerosis [25, 26]. It is caused by the proliferation of spindle-shaped cells resembling immature smooth muscle in the lung interstitium and along the lymphatics in the thorax and abdomen. Most patients seek treatment, before age 50, because of the formation of large honeycomb cysts that rupture, resulting in pneumothorax. Pleural effusions are also common and are frequently chylous because the architecture of the lymph nodes is disrupted by the proliferating muscle cells, which interferes with lymphatic drainage to a degree that allows chylous fluid to accumulate in the pleural space.

The chest radiograph is usually abnormal on presentation and shows progressive lung enlargement and an increasing reticular nodular infiltrate due to expansion of the honeycomb cysts. This is one of the two conditions (the other being eosinophilic granuloma) in which honeycomb formation can be associated with an enlarging rather than a contracting lung.

**Lymphoproliferative disorders.**—Lymphocyte clusters are

normally found in the distal respiratory bronchioles, but true lymph nodes with a capsule and afferent and efferent drainage are seldom found much beyond the fourth-order bronchi. These peribronchial lymphatic collections drain centrally and become more numerous with progression toward the pulmonary hila. Lymphatic vessels are also found on the pleural surface in the lobular septa. Bienenstock et al. [27] introduced the term bronchial associated lymphoid tissue to describe the pulmonary mucosal lymphoid complex that is organized in a similar fashion in the gut and salivary and mammary glands.

Lymphoid hyperplasia can occur in either a nodular or diffuse pattern [28] and has an identical histologic appearance in both situations. The nodular form of lymphoid hyperplasia is an uncommon cause of a solitary pulmonary nodule and has been termed pseudolymphoma. The diffuse pattern of lymphoid hyperplasia is known as LIP and is characterized by a bilateral, diffuse, reticular nodular pattern. Microcystic changes consistent with end-stage lung form in advanced cases [29], but involvement of hilar or mediastinal lymph nodes is rare. LIP is seen in association with systemic disorders such as Sjögren syndrome, myasthenia gravis, pernicious anemia, chronic active hepatitis, diffuse lymphoid hyperplasia, and more recently AIDS. In both nodular and diffuse forms of lymphoid hyperplasia, the infiltrate is limited to the interstitial compartments of the alveolar wall, lobular septa, and peribronchial vascular regions. The lymphoid cells may extend into the bronchial mucosa and around vessel walls but usually do not infiltrate these structures and seldom cause necrosis.

Both pseudolymphoma and LIP have been considered premalignant conditions because conversion to frank lymphoma has been reported to be as high as 50% in some series [28]. The major differentiating features are that benign conditions have a polyclonal expression of both light and heavy chains, whereas the malignant conditions tend to be monoclonal; the infiltrate is polymorphous in the benign condition and monomorphous in the malignant; and the infiltrate surrounds blood vessels and bronchi and extends to the pleural surface in the benign condition. Malignant infiltrates, on the other hand, can aggressively invade these structures and frequently produce necrosis by causing thrombotic occlusion of invaded vessels. Involvement of the hilar and mediastinal lymph nodes is also much more common in the malignant than in the benign proliferations. The possibility that Epstein-Barr virus infection is an important cause of the lymphoid proliferation in LIP was suggested by Liebow and Carrington [29] and is being actively investigated at this time.

Intrapulmonary spread of carcinoma via the pulmonary lymphatics is common. The presence of the tumor cells may be associated with a pronounced desmoplastic reaction that may contribute substantially to the expansion of the interstitial space. The most common primary tumors associated with pulmonary lymphangitic spread arise in the breast, stomach, pancreas, and prostate. In a combined radiologic and autopsy study, Janower and Blennerhassett [30] divided their cases into three groups in which one had parenchymal nodules with a coarse reticular pattern on radiographs, the second showed a linear pattern without visible nodules on radiographs, and

the third showed no radiologic abnormality. The authors concluded that the cells reached the lungs by hematogenous spread in all cases and invaded through the blood vessels to the interstitium and proliferated in the lobular and peribronchial lymphatics. It is interesting to speculate that the cell transformation involved in the neoplastic process results in the expression of receptors for endothelial ligands similar to those that normal circulating cells use to migrate out of the vascular space and into tissue [3], but this remains to be proved.

## Conclusions

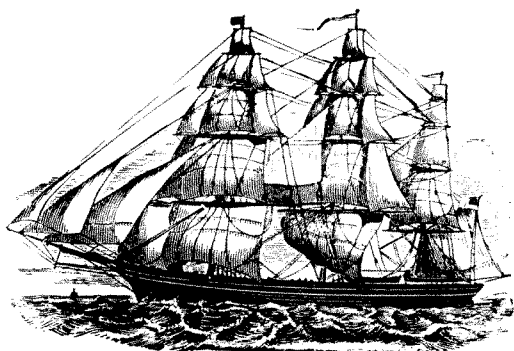
In summary, this overview is based on the premise that the pathogenesis of most cases of interstitial lung disease can be accounted for by inflammatory and neoplastic processes. The inflammatory process has two basic forms depending on whether the response takes on a nongranulomatous or granulomatous form. The third broad category of interstitial lung disease is attributed to the neoplastic process, in which the desmoplastic reaction associated with proliferation of either benign, borderline, or frankly malignant neoplastic cells is responsible for the interstitial process. The major roadblock to a more complete understanding of the pathology of individual cases of interstitial lung disease is our ignorance of the causative factors responsible for these inflammatory and neoplastic processes. The challenge to both radiologists and pathologists is to try to establish the causes of these processes by applying the newer techniques of imaging and molecular pathology to the diagnosis of this important group of lung diseases.

## REFERENCES

1. Landis EM, Pappenheimer JR. Exchange of substances through capillary walls. In: Hamilton WF, Dow P, eds. *Handbook of physiology*. Section 2: *Circulation*, vol. II. Washington, DC: American Physiological Society, 1963:961-1034
2. Michel RP, Inoue S, Hogg JC. Pulmonary capillary permeability in HRP in dogs: a physiologic and morphologic study. *J Appl Physiol* 1977;42:13-21
3. Butcher EC. Cellular and molecular mechanisms that direct leukocyte traffic. *Am J Pathol* 1990;136:3-11
4. Corrin B. Pathology of interstitial lung disease. In: Harasawa M, Fukuchi Y, Morinari H, eds. *Interstitial pneumonia of unknown etiology*. Tokyo: University of Tokyo Press, 1989:149-168
5. Carrington CB, Gaensler EA, Couti RE, FitzGerald MX, Gupta RG. Natural history and treated course of usual and desquamative interstitial pneumonia. *N Engl J Med* 1978;298:801-809
6. Scadding JG, Hinson KFW. Diffuse fibrosing alveolitis (diffuse interstitial fibrosis of the lungs). *Thorax* 1967;22:291-304
7. Davison AG, Heard BE, McAllister WAC, Turner-Warwick MEH. Organizing pneumonitis. *Q J Med* 1983;52(207):382-394
8. Epler GR, Colby TV, McLoud TC, Carrington CB, Gaensler EA. Bronchiolitis obliterans with organizing pneumonia. *N Engl J Med* 1985;312:152-158
9. Liebow A, Stear A, Billingsley JG. Desquamative interstitial pneumonia. *Am J Pathol* 1965;39:369-404
10. Robertson CH, Hall DL, Hogg JC. A description of lung distortion due to localized pleural stress. *J Appl Physiol* 1973;34:344-350
11. Kuhn C III, Boldt J, King ET, Crouch E, Vartio T, McDonald JA. An



- immunohistochemical study of architectural remodelling and connective tissue synthesis in pulmonary fibrosis. *Am Rev Respir Dis* **1989**;140:1693-1703
12. Pratt PC, Vollmer RT, Shelburne JD, Crapo JD. Pulmonary morphology in a multihospital collaborative extracorporeal membrane oxygenator project. *Am J Pathol* **1979**;95:191-214
  13. Hamman L, Rich AR. Acute diffuse interstitial fibrosis of the lung. *Johns Hopkins Med J* **1944**;74:177-212
  14. Spencer H. Pulmonary diseases of uncertain etiology. In: *Pathology of the lung*, 3rd ed, vol. 2. Philadelphia: Saunders, **1977**:697-772
  15. Guerry-Force ML, Muller NL, Wright JL, et al. A comparison of bronchiolitis obliterans with organizing pneumonia, usual interstitial pneumonia and small airways disease. *Am Rev Respir Dis* **1987**;135:705-712
  16. Geddes DM, Corrin B, Brewerton DA, Davies RJ, Turner-Warwick M. Progressive airway obliteration in adults and its association with rheumatoid disease. *Q J Med* **1977**;46:427-444
  17. Ralph D, Springmeyer SC, Sullivan KM, Hackman RC, Storb R, Thomas ED. Rapidly progressive air-flow obstruction in marrow transplant recipients. *Am Rev Respir Dis* **1984**;129:641-644
  18. Estenne M, Ketelbant P, Primo G, Yernault JC. Human heart-lung transplantation: physiologic aspects of the denervated lung and post-transplant obliterative bronchiolitis. *Am Rev Respir Dis* **1987**;135:976-978
  19. Wright JL, Churg A. Diseases caused by metals and related compounds, fumes and gases. In: Churg A, Green FHY, eds. *Pathology of occupational lung diseases*. New York: Igaku-shoin, **1988**:31-71
  20. Spencer H. Pneumonia due to rickettsiae, bedsoniae viruses and mycoplasma. In: *Pathology of the lung*, 3rd ed, vol. 1. Philadelphia: Saunders, **1977**:193-233
  21. Turner-Warwick M, Burrows B, Johnson A. Cryptogenic fibrosing alveolitis: response to corticosteroid treatment and its effect on survival. *Thorax* **1980**;35:593-599
  22. Cotran RS, Kumar V, Robbins SL. Inflammation and repair. In: *Pathologic basis of diseases*, 4th ed. Philadelphia: Saunders, **1989**:39-86
  23. Richie AC. The classification, morphology and behavior of tumors. In: Florey H, ed. *General pathology*. London: Lloyd Luke Medical Books, **1962**:551-597
  24. Lichtenstein L. Histiocytosis. *Arch Pathol Lab Med* **1953**;56:84-102
  25. Corrin B, Liebow AA, Friedman PJ. Pulmonary lymphangiomyomatosis. A review. *Am J Pathol* **1975**;79:348-382
  26. Malik SK, Neely P, Martin CJ. Involvement of the lungs in tuberous sclerosis. *Chest* **1970**;58:538-540
  27. Bienenstock J, Johnson N, Percy DYE. Bronchial lymphoid tissue. 1. Morphologic characteristics. *Lab Invest* **1973**;28:686-692
  28. Kradin RL, Mark EJ. Benign lymphoid disorders of the lung with a theory regarding their development. *Hum Pathol* **1983**;14:857-867
  29. Liebow AA, Carrington CB. Diffuse pulmonary lymphoreticular infiltrations associated with dysproteinemia. *Med Clin North Am* **1973**;57:809-843
  30. Janower ML, Blennerhassett JB. Lymphangitic spread of metastatic cancer to the lung: a radiologic pathologic classification. *Radiology* **1971**;101:267-273



Scientific Program (200 papers)  
Instructional Courses (60 hours)

Categorical Course on  
Body MR Imaging

The Caldwell Lecture

Award Papers

Scientific Exhibits

Social, Golf, and Tennis Programs

Guest Programs



Come to the  
American Roentgen  
Ray Society  
91<sup>st</sup>

ANNUAL MEETING

Boston, MA

Sheraton Boston Hotel  
May 5-10, 1991

## Book Review

**Christensen's Physics of Diagnostic Radiology**, 4th ed. By Thomas S. Curry III, James E. Dowdey, and Robert C. Murry, Jr. Philadelphia: Lea & Febiger, 504 pp., 1990. \$39.50

Radiology librarians know that when September comes, all the copies of *Christensen's Physics of Diagnostic Radiology* go. This text is used so widely for review for American radiology board examinations that many residents assume that the written physics questions are formulated from it.

Much of the third edition of this book is still present in the fourth edition. In chapter 1, "constant potential heat unit computation" is new, as is a description of the advantages of metal-enclosed X-ray tubes. A complete description of the use of semiconductors as rectifiers will be helpful for the questions on semiconductors that are now part of the written board examination questions for physicists. Chapter 2, "X-ray Generators," now includes the Delta and Wye methods of 12-pulse, three-phase generators and a clear explanation of 13-kHz high-frequency generators. Testing of exposure timers has been eliminated, and a description of solid-state phototimers has been included as new material in this chapter. Chapters 4-8 are substantially the same as those in the third edition except for a section on K-edge filters.

Chapter 9, "Luminescent Screens," has replaced a chapter titled "Intensifying and Fluoroscopic Screens." The two chapters are nevertheless similar, except that DuPont screens have been updated in the tables. A two-page section on photostimulable phosphors has been added because of their use in digital radiology. Chapter 10, "Physical Characteristics of X-ray Film and Film Processing," has expanded the section on film processing to include new data about the two components of developer, hydroquinone and phenidone. The inclusion of information about antioxidants and replenishment data is pertinent for radiologists in private practice who must cope with film-processing service companies. Chapter 11, "Photographic Characteristics of X-ray Film," includes a description of the effects of film-grain shape for tabular films and the use of dyes to prevent film print-through. The section on mammographic film has been eliminated.

The contents of chapters 12 and 13 in the third edition have been combined with magnification and moved to chapters 13 and 14 in this new edition. Because of this, modulation transfer function is not discussed in chapter 12, "Fluoroscopic Imaging," so that line pair/millimeter values for image intensifiers have been eliminated. This chapter combines fluoroscopy with image intensifiers and increases the material on cesium iodide image intensifiers. Chapter 13, "Viewing and Recording the Fluoroscopic Image," combines the third edition's chapters 16 and 17, "Cinefluorography" and "Television," respectively, and condenses the material in these chapters. Charge-coupled-device cameras are included now as well as a short section on optical disks. The whole section on processing cine film has been eliminated.

Chapter 16, "Body Section Radiography," is the same as the third edition's chapter 18, but sections on the book cassette and special tomographic techniques have been eliminated. Dental pantomography, a popular technique for oral board questions, is still present.

Chapter 17, "Stereoscopy," remains the same, as does chapter 18 on xeroradiography. As xeroradiography rapidly is being replaced by film-screen mammography, it is too bad that this chapter was not replaced, particularly as radiology board examinations now will include questions on mammography. An updated section on liquid-toner xerography and dose measurements has been added, but doses for xeromammography are lower than usually obtained.

A chapter on copying radiographs has been eliminated to make room for expanded chapters on CT and MR. Chapter 19, "Computed Tomography," has reduced the section on X-ray tubes and has updated the section on detectors. The sections on image display and quantum mottle have been rewritten, as have the ones on resolution and exposure of patients. Artifacts are described much more completely, and modern CT clinical scans illustrate this section. A single page has been added on three-dimensional and volumetric reconstruction. However, the chapter does not describe how CT is used for quantification of bone mineral. Chapter 20, "Ultrasound," still illogically occupies the space after CT and before X-ray protection (which is substantially the same). Because the physics of ultrasound bears no relationship to the physics of X-ray imaging, it is difficult to cover, even in this long chapter. This chapter still contains a number of disturbing compromises and inaccuracies. Despite the enormous changes in sonographic equipment during the last 6 years, this chapter remains singularly untouched. Short sections on pulsed Doppler sonography and color flow imaging have been added, but, unlike the rest of the chapter, no illustrations are included for this new material.

Chapter 22, "Digital Radiography," is virtually the same as it was in the third edition, despite enormous changes in the availability of expanded devices for storage of images and the decreased cost of all digital display and interface equipment, which make them more widely used than they were 6 years ago. Chapter 23, "Nuclear Magnetic Resonance," is the same as chapter 27 in the third edition, except that the last three pages have been replaced by an excellent new chapter on MR imaging that includes short sections on fast-imaging techniques and MR safety. This new chapter is illustrated with the type of figures we have come to expect in *Christensen's Physics of Diagnostic Radiology* and includes clinical MR images of the head.

Without question, this edition is still a *Christensen's*, with its wealth of detail, examples, and illustrations. Radiologists cannot get along without it, and we are indebted to the authors for continuing to update this text.

Carolyn Kimme-Smith  
University of California, Los Angeles, Medical Center  
Los Angeles, California 90024-1721



## Review Article

# Advances in Contrast-Enhanced MR Imaging

Sanjay Saini,<sup>1</sup> Michael T. Modic,<sup>2</sup> Bernd Hamm,<sup>3</sup> and Peter F. Hahn<sup>1</sup>

The 1980s witnessed vast technological gains in MR imaging. Imaging times were reduced from more than 15–20 min to a fraction of a second. Anatomic resolution in today's MR imagers is comparable to that in state-of-the-art CT scanners. As a result, in a relatively short time, MR imaging became an essential diagnostic tool for the practice of medicine. Yet, in countless clinical settings, especially when imaging the chest and abdomen, the usefulness of MR imaging remains suboptimal. As the rate of technical innovations in MR imaging plateaus, it is likely that pharmaceutical manipulation of tissue signal intensity will provide solutions to many of MR imaging's current shortcomings. MR contrast agents also may expand the horizon of MR imaging into areas of clinical medicine that are presently unaffected by the MR revolution.

A historical perspective on the potential use of contrast agents in MR imaging is of some interest. Initial reports that described the development of MR imaging invariably included in the list of advantages of MR over X-ray imaging the notion that because of superior intrinsic soft-tissue contrast, contrast

agents would not be necessary for diagnostic MR imaging. Today it is widely recognized that MR contrast agents will play an increasingly important role in clinical practice. Since receiving Food and Drug Administration (FDA) approval in June 1988, gadopentetate dimeglumine has already become indispensable in neuroradiologic practice. In short order, the diversity of MR contrast agents will approach that of radio-pharmaceuticals and the role of contrast-enhanced MR imaging will expand as more formulations receive governmental approval. Contrast-enhanced MR imaging can simultaneously provide dynamic physiologic information (anatomic and/or biochemical) and high anatomic detail, thereby overcoming the major limitations of both nuclear scintigraphy (poor anatomic resolution) and CT (limited physiologic information).

In this article, we examine recent advances in the development of MR contrast media and review the status of contrast-enhanced MR imaging. After briefly examining the spectrum of MR contrast agents and describing how they affect MR images, a review of clinical applications of MR contrast media will be provided.

Received April 20, 1990; accepted after revision August 27, 1990.

<sup>1</sup> Department of Radiology, Massachusetts General Hospital and Harvard Medical School, 32 Fruit St., Boston, MA 02114. Address reprint requests to S. Saini.

<sup>2</sup> Division of Radiology, Cleveland Clinic Foundation, 9500 Euclid Ave., Cleveland, OH 44195.

<sup>3</sup> Department of Radiology, Universitätsklinikum Steglitz and Freie Universität Berlin Medical School, Hindenburgdamm 30, D 1000 Berlin 45, Germany.

**AJR 156:235–254, February 1991** 0361–803X/91/1562–0235 © American Roentgen Ray Society

## Principles

Sanjay Saini

In this section, I briefly review the principles of pharmaceutical manipulation of soft-tissue contrast in MR images and outline the spectrum of MR contrast agents that are undergoing or are close to undergoing clinical evaluation. For a more detailed explanation, a recent review by Lauffer [1] is recommended.

### MR Contrast Agents and Proton Relaxation

Tissue relaxation times (T1 and T2) and proton density are the principal intrinsic factors that determine signal intensity on MR images. Stated simply, magnetopharmaceuticals manifest their effect on MR images by either decreasing proton relaxation times or by altering proton density. Most of the research effort has centered on the development of magnetopharmaceuticals that decrease proton relaxation times. This phenomenon was first reported more than 40 years ago by Bloch et al. [2], who described the use of paramagnetic ferric nitrate to shorten relaxation times of water protons. The ability of certain chemicals to enhance proton relaxation rates is based on their magnetic response to an external magnetic environment [3], because substances with large magnetic moments (compared with the nuclear magnetic moment of protons) influence relaxation behavior of nearby protons. When classified on the basis of magnetic properties, paramagnetic and ferromagnetic (of which superparamagnetic is a subvariety) materials are the two principal types of MR contrast media. The active ingredients in most paramagnetic contrast agents are paramagnetic ions that have unpaired outer shell electrons, and these contrast agents incorporate one or more paramagnetic metal ions. Of these, paramagnetic gadolinium (III)—with seven unpaired electrons—in gadopentetate dimeglumine is the most widely recognized. Ferromagnetic materials (or one of the subvarieties) consist of paramagnetic ions that are arranged in a crystalline matrix. Paramagnetic iron in crystalline iron oxide is a prototypic example of a superparamagnetic contrast agent. Superparamagnetic materials are potent contrast agents because their magnetization is several orders of magnitude greater than the magnetization of paramagnetic materials. Thus, for example, superparamagnetic contrast agents alter MR signal intensity in doses that are a fraction of doses required for paramagnetic contrast agents.

When MR contrast agents bearing large magnetic moments are found in the vicinity of tissue protons (proximity is essential because magnetic strength decreases with distance), they can stimulate nuclear relaxation and thereby decrease both T1 and T2 relaxation times. How do these powerful magnets alter proton relaxation? T2 shortening is easier to envision. Increases in local magnetic field inhomogeneities enhance

dephasing of nonstationary protons, resulting in decreased T2 or T2\*. On the other hand, enhanced T1 relaxation occurs when the frequency of time-varying magnetic fields produced by contrast agents (a result of molecular rotation or tumbling) is similar to protons' resonance (Larmor) frequency. This mechanism is often referred to as dipole-dipole interaction. As paramagnetic ion-chelate complexes increase magnetic field inhomogeneities and also have tumbling rates that approximate Larmor frequency, they produce both T2 and T1 shortening [4]. On the other hand, large particulate magnetized spheres of superparamagnetic contrast agents produce little T1 shortening but preferentially shorten tissue T2 [5].

### Instrument Factors

In MR imaging, reduced T1 increases tissue signal intensity whereas T2 shortening decreases tissue signal intensity. As T1 and T2 shortening have opposing effects on MR images, MR contrast agents are designed, or are administered in doses, so that the effect of one of these concurrent processes predominates. Several instrument factors play an important role in determining which of these effects predominates. These include pulse-sequence timing parameters and field strength. Of these, pulse-sequence timing parameters are of critical importance. For example, because superparamagnetic iron oxide preferentially shortens T2, tissue signal intensity decreases after iron oxide administration, an effect that is best seen on T2-weighted images. Conversely, at recommended doses paramagnetic gadopentetate dimeglumine produces a much larger effect on T1 than on T2. Thus tissue signal intensity increases after gadopentetate dimeglumine is administered, an effect that is best seen on T1-weighted images. However, in sufficiently high tissue concentrations (such as in the renal collecting system), T2 shortening from gadopentetate dimeglumine is of greater consequence than T1 shortening, which leads to a loss in signal intensity. This effect is best seen on T2-weighted images. Thus, MR contrast agents are often also classified according to their effect on MR images, namely T1 agents, which enhance signal intensity, or T2 agents, which diminish signal intensity. However, this classification is of limited usefulness because some magnetopharmaceuticals fall into either category depending on the MR imaging technique that is used.

The effect of static magnetic field on the relaxivity of MR contrast agents is of less practical significance because, in a given setting, this instrument parameter cannot be altered. However, it is important to recognize that the potencies of MR contrast agents depend on field strength. Nuclear magnetic relaxation dispersion (NMRD) studies have shown, for example, that the relaxivity of gadopentetate dimeglumine



diminishes by about one third as field strength is varied from 0.02 to 1.50 T [6]. Furthermore, at field strengths less than 0.15 T, Gd-DOTA (gadolinium tetra-azacyclododecane tetra-acetic acid) meglumine is a better T1 relaxation agent than is gadopentetate dimeglumine. Thus the application of contrast agents may not be readily transposed from one field strength to another [7].

### Classification of MR Contrast Agents

Because of the multitude of contrast agents being developed, a useful classification is one that is based on their physiologic behavior. In this section, the design and pharmacokinetics of MR contrast agents that have undergone or are approaching clinical evaluation is reviewed.

#### Extracellular Agents

Metal ions chelated to molecules make up a group of contrast agents that have no tissue specificity. Metal ions are chelated to reduce biologic toxicity, and it is the ligand's biodistribution that determines the pharmacokinetics of the contrast agent. Paramagnetic gadopentetate dimeglumine (Berlex Laboratories, Cedar Knolls, NJ) is the prototypic example of this category of MR contrast agents [8]. Others that have undergone clinical evaluation include Gd-DOTA meglumine (Guerbet Laboratories, Aulnay-sous-Bois, France) [9] and Ferrioxamine (Salutar, Sunnyvale, CA) [10]. The physiologic behavior (extracellular distribution) of these contrast agents differs slightly from one to another, except that Ferrioxamine has a slightly higher hepatic excretion [10]. However, some magnetic and biochemical differences are present. For example, Ferrioxamine is a weaker T1 agent than gadopentetate dimeglumine is (relaxivity at 20 MHz, 1.8 vs 4.5 mmol<sup>-1</sup> sec<sup>-1</sup>) [10], whereas Gd-DOTA meglumine has a stronger ion-chelate bond than gadopentetate dimeglumine does ( $K_s$  10<sup>28</sup> vs 10<sup>23</sup>), resulting in a higher LD<sub>50</sub> (5.5 vs 10.6 mmol/kg) [9]. In practice however, the imaging effects of extracellular contrast agents are similar, and in the discussions that follow, gadopentetate dimeglumine, Gd-DOTA meglumine, and other similar formulations may be interchanged.

Gadopentetate dimeglumine administered IV has a plasma half-life of 90 min, and over 90% is eliminated by the kidneys within 3 hr. Recommended dose in the United States is 0.1 mmol/kg, whereas in Europe it may be administered at up to 0.2 mmol/kg. In clinical studies to date, this magnetopharmaceutical has been extremely safe and very few moderate or severe reactions have been attributed to it [11]. Although it is suggested that gadopentetate dimeglumine should be infused slowly (over several minutes), anecdotal experience and animal studies have shown no increase in reactions with rapid bolus administration [12]. To reduce reactions attributable to the hyperosmolar nature of Gd-DTPA dimeglumine, isosmolar nonionic formulations (Gd-DTPA-bis-methylamide (Salutar) [13]; Gd-HP-DO3A (Squibb, Princeton, NJ) [14]) also have been designed, and clinical trials are in progress.

The imaging effects of extracellular contrast agents are identical to those of iodinated contrast media. They are rapidly redistributed from the vascular compartment into the extracellular space and undergo renal elimination by passive glo-

merular filtration. On T1-weighted images, they enhance tissue signal intensity by tissue perfusion or because of breakdown of the blood brain barrier (BBB). With fast T2-weighted gradient-echo (GRE) pulse sequences, decrease in tissue signal intensity from T2 effects can be seen during the first pass of a compact bolus [15] or after hyperconcentration in the renal collecting system. Among agents mentioned, Ferrioxamine has been investigated primarily in the urinary tract because of its less potent paramagnetic effect.

#### Hepatobiliary Contrast Agents

Efforts to design contrast agents for the hepatobiliary system are based on the chelation of paramagnetic ions to ligands having affinity for hepatocytes. Paramagnetic iron(III)ethylene-bis-(2-hydroxyphenylglycine) (Fe-EHPG) was the first such agent evaluated in animals [16]. However, because only a small percentage of Fe-EHPG is eliminated by hepatocytes, the agent never progressed to clinical trials. Ferrioxamine with less than 20% hepatic excretion has been evaluated clinically; however, it also does not appreciably enhance the liver or biliary tree [10]. Newer formulations, such as paramagnetic manganese dipyrrodoxal diphosphate (Mn-DPDP, Salutar [17]) and an octadentate chelate of gadolinium (B-19036, Bracco, Italy [18]), both of which have relatively greater hepatobiliary excretion, are more likely to achieve desirable levels of selective hepatobiliary enhancement. For example, approximately 40% B-19036 administered IV is excreted into the bile (vs <1% for gadopentetate dimeglumine), and therefore, the hepatic T1 relaxivity of B-19036 is 14.6 mmol<sup>-1</sup> sec<sup>-1</sup> in comparison to 7.6 mmol<sup>-1</sup> sec<sup>-1</sup> for gadopentetate dimeglumine [18]. Hepatobiliary contrast agents may thus prove superior to gadopentetate dimeglumine in MR imaging of liver cancer and also may be used for evaluation of hepatobiliary function [17].

#### Blood-Pool Agents

Contrast agents confined to the intravascular compartment may be useful for detecting tissues with decreased perfusion. Although for a brief period all pharmaceuticals administered IV act as markers of vascular perfusion, these small molecules rapidly redistribute out of the intravascular space, which limits their practical use as markers of tissue perfusion. Macromolecules that are impervious to capillary leakage and glomerular filtration are being developed as blood-pool agents. Of these, human serum albumin covalently bound to gadopentetate dimeglumine is the best known [19]. However, all studies to date have been limited to animals, and no clinical trials are presently foreseen. A unique feature of this material is that its T1 relaxivity is superior to that of gadopentetate dimeglumine alone. This effect has been attributed to its correlation time, and it is hypothesized that the larger albumin-gadopentetate dimeglumine molecule tumbles at rates that more closely approximate proton resonance frequency than gadopentetate dimeglumine does.

#### Reticuloendothelial Agents

Particulate materials administered IV are cleared by the body's reticuloendothelial system (RES), and numerous MR

contrast agents are being developed for targeting the RES. These include liposomes containing paramagnetic ions [20] and dextran-coated crystals of superparamagnetic iron oxide (Advanced Magnetix, Cambridge, MA) [21]. Of these, biodegradable superparamagnetic iron oxide has already undergone preliminary clinical evaluation [22, 23]. Superparamagnetic iron oxide is an aqueous colloid with a concentration of 200  $\mu\text{mol Fe/ml}$  (11.2 mg Fe/ml) and a median particle diameter of 80 nm. According to animal studies, approximately 80% of the administered dose localizes in the liver, about 6% in the spleen, and a very small amount goes to the bone marrow [24]. The material is rapidly cleared from circulation ( $t_{1/2} < 1$  hr) but clearance from the liver and spleen is slower ( $t_{1/2} = 3$  days and 4 days, respectively). Evidence for biodegradation is obtained from  $^{59}\text{Fe}$  studies, which show incorporation of labeled iron into hemoglobin of rats with iron-deficiency anemia.

Reports of adverse reactions associated with IV administration of iron preparations has tempered enthusiasm for this contrast agent. In clinical trials thus far, slow infusions have been free of adverse reactions, but more rapid infusions have produced severe hypotension even in relatively healthy patients. However, animal studies have not shown any acute or chronic toxicity in the liver [25].

In tissue (liver, spleen, bone marrow), iron oxides produce a dose-dependent decrease in signal intensity [21]. This offers an immediate advantage over paramagnetic contrast agents, which can either increase or decrease tissue signal intensity depending on their concentration in tissue and the imaging technique. The tissue signal-depletion effect of iron oxides is best seen on T2-weighted images but is also readily demonstrated on MR images with relatively less T2 information. Thus pulse sequences suitable for imaging with iron oxides are not necessarily the most heavily T2-weighted pulse sequences that have limited signal-to-noise ratios (SNR), but pulse sequences with mixed T1-T2 information that have relatively greater SNR [26]. Indeed Marchal et al. [23] showed that tumor-liver contrast was high on images obtained after iron oxide administration with a wide range of pulse-sequence timing parameters. In their present formulation, the predominant effect of RES-specific contrast agents is on the liver and spleen, and they are useful in imaging focal and diffuse diseases in both of these organs [27]. Newer formulations with smaller particles and concurrent RES blockade of the liver and spleen also may allow a more selective targeting to the bone marrow or even to cancer sites [20].

#### Lymphographic Agents

Superparamagnetic iron oxide administered in subcutaneous tissues has been shown to accumulate in draining lymph nodes [28]. The usefulness of this in pathologic conditions has not been demonstrated but it could be used to replicate iodinated X-ray lymphography, in which diseased lymph nodes do not trap the contrast media.

#### Oral Gastrointestinal Agents

Any of the magnetopharmaceuticals mentioned thus far can be used to demarcate the gastrointestinal tract. Additional

possibilities include materials with no (gas) or few (clay, barium) mobile protons and short-T1 preparations (oils and paramagnetic ferric ammonium citrate). However, design of gastrointestinal contrast agents requires consideration of issues such as suspension, dilution, and hyperconcentration [29]. Significant research effort is underway in this field because a suitable gastrointestinal contrast agent is a prerequisite for MR imaging to compete fully with CT scanning in the abdomen.

#### Tumor-Specific Contrast Agents

Paramagnetic contrast agents do not localize in sufficient quantity to produce signal-intensity changes in tumor foci even if the issue of poor antibody-antigen specificity is ignored. However, because of their more powerful magnetic properties, superparamagnetic contrast agents are more likely to be successful, and preliminary experimental studies are underway [30].

#### ACKNOWLEDGMENT

The author is grateful to Randall B. Lauffer for critically reviewing this manuscript.

#### REFERENCES

1. Lauffer RB. Paramagnetic metal complexes as water proton relaxation agents for NMR imaging: theory and design. *Chem Rev* **1987**;87:901-927
2. Bloch F, Hansen WW, Packard M. The nuclear induction experiment. *Phys Rev* **1948**;70:474-480
3. Saini S, Frankel RB, Stark DD, Ferrucci JT. Magnetism: a primer and review. *AJR* **1988**;150:735-743
4. Koenig SH, Brown RD. Relaxometry of paramagnetic ions in tissue. In: Sigel H, ed. *Metal ions in biological systems*, vol. 2. *Application of nuclear magnetic resonance to paramagnetic systems*. New York: Marcel Dekker, **1987**:229-269
5. Koenig SH, Gillis P. Transverse relaxation ( $1/T_2$ ) of solvent protons induced by magnetized spheres and its relevance to contrast enhancement in MRI. *Invest Radiol* **1988**;23[suppl 1]:S224-S228
6. Muller RN, Elst LV, Rinck PA, et al. The importance of nuclear magnetic relaxation dispersion (NMRD) profiles in MRI contrast media development. *Invest Radiol* **1988**;23[suppl 1]:S229-S231
7. Kormano M, Niemi P, Paajanen H, Maattanen H, Katevuo K. The utility of contrast media in MRI at 0.02 T. *Invest Radiol* **1988**;23[suppl 1]:S289-S291
8. Weinmann HJ, Brasch RC, Press WR, Wesby GE. Characteristics of Gd-DTPA complex: a potential NMR contrast agent. *AJR* **1984**;142:619-624
9. Allard M, Doucet D, Kien P, Bonnemain B, Caille JM. Experimental study of DOTA-gadolinium pharmacokinetics and pharmacologic properties. *Invest Radiol* **1988**;23[suppl 1]:S271-S274
10. Worah D, Berger AE, Burnett KR, et al. Ferrioxamine as a magnetic resonance contrast agent: preclinical studies and phase I and II human clinical trials. *Invest Radiol* **1988**;23[suppl 1]:S281-S285
11. Wolf GL. Current status of MR imaging contrast agents: special report. *Radiology* **1989**;172:709-710
12. Sullivan ME, Goldstein HA, Sansone KJ, Stoner SA, Holyoak WL, Wiggins JR. Hemodynamic effects of Gd-DTPA administered via rapid bolus or slow infusion: a study in dogs. *AJNR* **1990**;11:537-540.
13. Hayne LA, Maravilla KR, Cohen WA, Gerlach R. Gd-DTPA-BMA, a new nonionic MR contrast agent: preliminary clinical results and comparisons with Magnevist. *Radiology* **1989**;173(P):365
14. Tweedle MF, Eaton SM, Eckelman WC, et al. Comparative chemical structure and pharmacokinetics of MRI contrast agents. *Invest Radiol* **1988**;23[suppl 1]:S236-S239
15. Villringer A, Rosen BB, Belliveau JW, et al. Dynamic imaging with lanthanide



- chelates in normal brain: contrast due to magnetic susceptibility effects. *Magn Reson Med* **1988**;6:164-174
16. Lauffer RB, Grief WL, Stark DD, et al. Iron-EHPG as hepatobiliary contrast agents: initial imaging and biodistribution studies. *J Comput Assist Tomogr* **1985**;9:431-437
  17. Young SW, Simpson BB, Ratner AV, Matkin C, Carter EA. MRI measurement of hepatocyte toxicity using the new MRI contrast agent manganese dipyridoxal diphosphate, a manganese/pyridoxal 5-phosphate chelate. *Magn Reson Med* **1989**;10:1-13
  18. Vittadini G, Felder E, Tirone P, Lorusso V. B-19036, a potential new hepatobiliary contrast agent for MR proton imaging. *Invest Radiol* **1988**;23[suppl 1]:S246-S248
  19. Schmeidl U, Ogan M, Paaanen H, et al. Albumin labelled with Gd-DTPA as an intravascular, blood-pool enhancing agent for MR imaging. *Radiology* **1987**;162:205-210
  20. Seltzer SE. The role of liposomes in diagnostic imaging. *Radiology* **1989**;171:19-21
  21. Saini S, Stark DD, Hahn PF, et al. Ferrite particles: superparamagnetic MR contrast agent for the reticuloendothelial system. *Radiology* **1987**;162:211-217
  22. Stark DD, Weissleder R, Elizondo G, et al. Superparamagnetic iron oxide: clinical application as a contrast agent for MR imaging of the liver. *Radiology* **1988**;168:297-302
  23. Marchal G, Van Hecke P, Demaerel P, et al. Detection of liver metastases with superparamagnetic iron oxide in 15 patients: results of MR imaging at 1.5 T. *AJR* **1989**;152:771-778
  24. Weissleder R, Stark DD, Engelstad BL, et al. Superparamagnetic iron oxide: pharmacokinetics and toxicity. *AJR* **1989**;152:167-173
  25. Bacon BR, Stark DD, Park CH, et al. Ferrite particles: a new magnetic resonance imaging contrast agent. Lack of acute or chronic hepatotoxicity after intravenous administration. *J Lab Clin Med* **1987**;110:164-171
  26. Fretz CJ, Elizondo G, Weissleder R, et al. Superparamagnetic iron oxide-enhanced MR imaging: pulse sequence optimization for detection of liver cancer. *Radiology* **1989**;172:393-398
  27. Weissleder R, Elizondo G, Stark DD, et al. The diagnosis of splenic lymphoma by MR imaging: value of superparamagnetic iron oxide. *AJR* **1989**;152:175-180
  28. Weissleder R, Elizondo G, Josephson L, et al. Experimental lymph node metastases: enhanced detection with MR lymphography. *Radiology* **1989**;171:835-839
  29. Hahn PF, Stark DD, Saini S, et al. Ferrite particles for bowel contrast in MR imaging: design issues and feasibility studies. *Radiology* **1987**;164:37-41
  30. Patrizio G, Elizondo G, Fretz CJ, et al. Ferrosomes: tumor detection by selective enhancement of peritumoral macrophages. *Radiology* **1989**;173(P):254

## Neurologic Applications

Michael T. Modic

Gadopentetate dimeglumine is presently the only MR contrast agent approved by the FDA for MR imaging of the brain and spine. The current recommended dose is 0.1 mmol/kg, and studies performed with fractionated incremental amounts have shown that little additional information is obtained with doses above this level [1]. In fact, anecdotal evidence suggests that even half the recommended dose may be used without a noticeable diminution in tissue enhancement. In most imaging situations, precontrast T1-weighted (spin-echo [SE] or gradient-echo) and precontrast T2-weighted SE images are obtained first. The precontrast T1-weighted images are important for identifying blood and fat and for separating them from any subsequent enhancement with gadopentetate dimeglumine. The precontrast T2-weighted images are necessary because they are very sensitive to alterations in brain water content associated with breakdown of the blood brain barrier (BBB). In comparison, greater BBB breakdown is needed for leakage of contrast material, which has a relatively larger molecular size [2].

### Imaging of Normal Structures

In the head, some enhancement of normal structures can be seen on images obtained after gadopentetate dimeglumine administration. Owing to differences in perfusion, gray matter will enhance more than white matter, resulting in a loss of gray-white soft-tissue contrast on postcontrast images. The pituitary stalk, pituitary gland, cavernous sinus, choroid

plexus, and to a lesser degree, the periphery of the pineal gland enhance also. Mild enhancement may also be seen in the cranial nerves as they traverse the cavernous sinus. Dural structures such as the falx and tentorium show enhancement in only about 50% of cases, and when present the enhancement is usually less than that seen with CT [3]. Because of flow, vascular enhancement is more variable than it is with CT and is most obvious in the venous structures, where small veins enhance more than larger ones. Large arteries usually do not show significant enhancement unless there is pathologic slowing of blood flow.

During spinal imaging, the epidural venous plexus will show some enhancement, which persists for at least 20-30 min. This is most obvious in the regions of the neural foramen in the cervical region and posterior to the vertebral body in the lumbar area. Variable degrees of enhancement also can be noted in the region of the ventral and dorsal nerve root ganglion, especially in the lumbar region. The normal cord, nerve roots, and intervertebral disks do not enhance.

### Intracranial Applications

#### *Intraaxial Neoplasms*

The pattern of enhancement generally parallels CT contrast enhancement, but for most tumors it is usually superior to CT [4]. Although the overall sensitivity may not increase dramatically when compared with that on precontrast T2-weighted

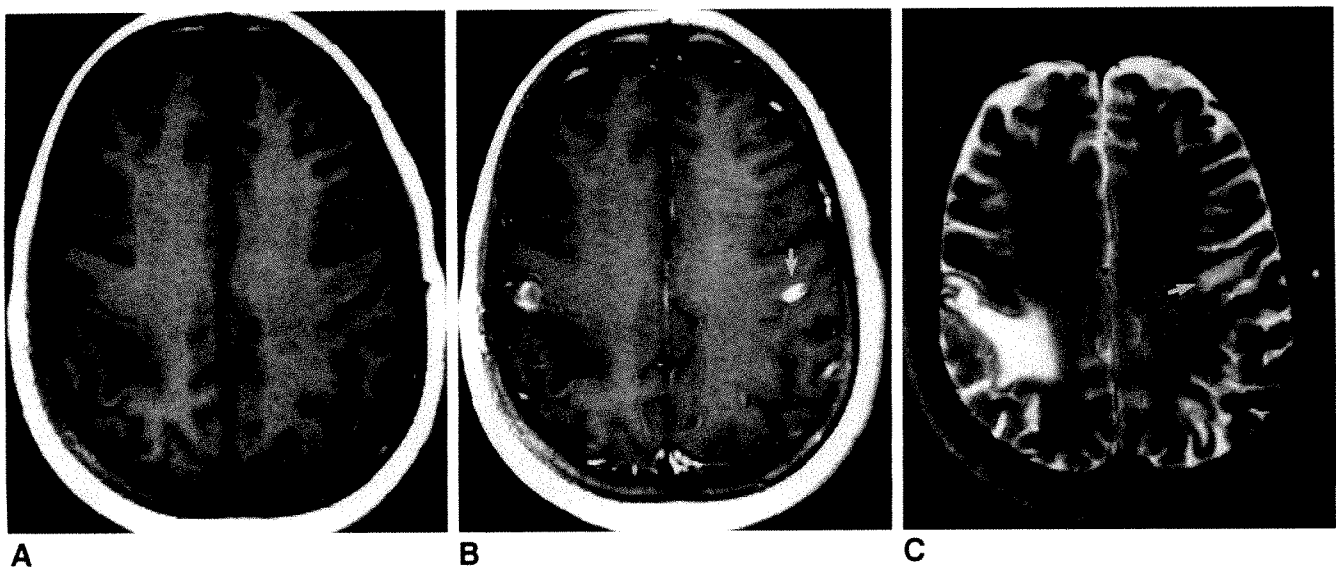


Fig. 1.—Breast carcinoma metastases.

A–C, T1-weighted (SE 500/15) MR images obtained at 1.5 T before (A) and after (B) gadopentetate dimeglumine administration and T2-weighted image obtained before gadopentetate dimeglumine administration (C). After gadopentetate dimeglumine administration, metastatic tumor nidus anterior to edema is enhanced. In addition, note unsuspected area of involvement in contralateral hemisphere (arrow). On T2-weighted image (C) area of vasogenic edema in right hemisphere is well appreciated, but edema due to lesion in left hemisphere (arrow) is poorly appreciated and could be confused with partial volume averaging with CSF.

images [2, 5], gadopentetate dimeglumine clearly improves the diagnostic sensitivity of T1-weighted pulse sequences. Gadopentetate dimeglumine is also helpful in identifying the nidus of tumor and separating it from surrounding edema [6]. However, it is important to remember that gadopentetate dimeglumine enhancement does not delineate the borders of tumors, but rather the site of maximal BBB breakdown [7].

Gadopentetate dimeglumine is most useful in patients with metastatic disease, in whom enhanced examinations have identified more lesions (Fig. 1) [2, 6, 8, 9]. This is primarily useful in increasing diagnostic confidence. Another important area in which gadopentetate dimeglumine has been useful is in the examination of patients who have had tumor resection. Enhancement of residual or recurrent tumor is readily separated from postoperative changes such as encephalomalacia and/or gliosis (which often have signal-intensity characteristics similar to tumor) (Fig. 2) [10]. The value of gadopentetate dimeglumine in separating radiation necrosis from residual tumor is unclear.

#### Extraaxial Neoplasms

In contradistinction to intraaxial lesions, studies to date indicate that gadopentetate dimeglumine enhancement increases the sensitivity of MR for detecting extraaxial lesions. Often these processes possess little intrinsic soft-tissue contrast differentiation from adjacent brain or CSF [11–13]. As these tumors do not have a BBB, lesion vascularity plays the primary role in determining the degree of enhancement. This is especially true of meningiomas. Other lesions reported to be seen with greater advantage after gadopentetate dimeglumine administration are acoustic neuromas and schwanno-

mas [14]. Favorable results also have been reported with pituitary tumors, especially microadenomas [15–18]. Pituitary tumors may be outlined when thin slices are used, because the tumors enhance less than the surrounding normal gland does on the immediate postgadopentetate dimeglumine image. In some cases a "flip-flop" phenomena is seen on delayed images, with the lesions becoming hyperintense relative to normal gland. Inhomogeneity is a normal pattern of enhancement of the pituitary gland and therefore a potential cause of confusion. Finally and perhaps most importantly is the increased sensitivity of postgadopentetate dimeglumine images to leptomeningeal disease [19].

#### Nonneoplastic Diseases

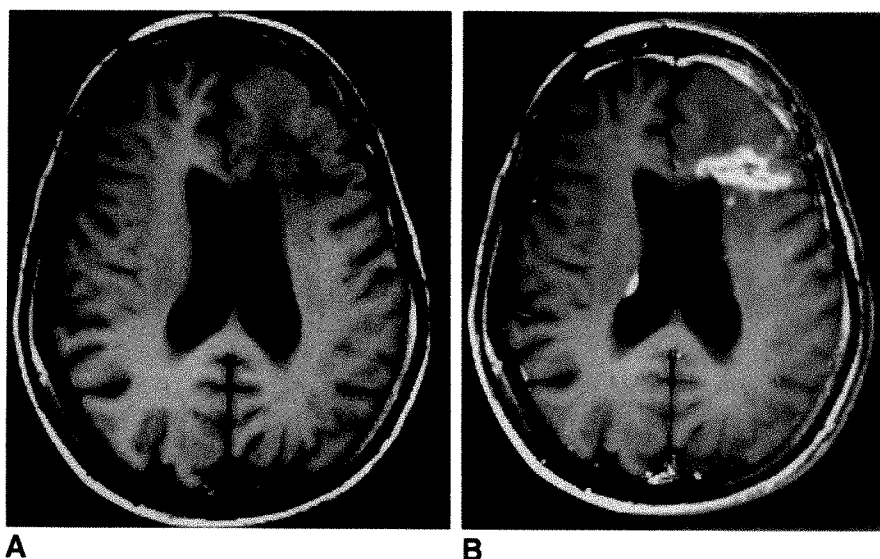
MR without gadopentetate dimeglumine has been shown to be highly sensitive to changes from inflammatory processes, but these may be difficult to separate from neoplastic disease. The major advantage of gadopentetate dimeglumine therefore appears to be in identifying enhancement around necrotic areas and in separating these regions from cerebral edema. Likewise, enhancement may be seen with meningitis, leptomeningitis, or changes involving the pia and arachnoid [20]. Similar enhancement also has been noted postoperatively and after subarachnoid hemorrhage. Postoperative changes within the surgical bed usually resolve within 1 year, but persistent enhancement in the overlying dura has been noted in 50% of cases after 2 years. These changes are probably associated with a meningeal and/or dural inflammatory response (Fig. 2) [21, 22].

Although T2-weighted images remain the most sensitive for identification of changes due to ischemia, enhanced MR



Fig. 2.—Postoperative glioblastoma recurrence.

A and B, T1-weighted (SE 600/20) MR images obtained at 1.5 T before (A) and after (B) gadopentetate dimeglumine administration. Note area of decreased signal intensity in left frontal lobe on unenhanced image. Some thickening of surface of brain is present in frontal region. After administration of gadopentetate dimeglumine, marked enhancement is seen in core of surgical bed, indicative of recurrent or residual tumor. Note also a metastatic nodule along lateral aspect of right ventricle. Dural-meningeal interface in frontal region is enhanced, presumably as a result of previous surgery, but is impossible to separate from metastatic disease.



is useful in studying the status of the BBB. This is particularly helpful in cortical lesions, in which the problem of proximity to the CSF spaces on T2-weighted images can be overcome on postcontrast T1-weighted images. Additionally, in patients with multiple white-matter lesions, active disruption of the BBB (or lack thereof) is important in differential considerations [23].

Multiple studies have shown that noncontrast MR imaging is very sensitive in detecting demyelinating diseases, especially on T2-weighted images. However, gadopentetate dimeglumine-enhanced MR has been shown to be more sensitive than contrast-enhanced CT is for identifying regions of abnormal BBB that may correlate with clinical activity [24, 25].

#### Summary, Intracranial Applications

Gadopentetate dimeglumine-enhanced MR imaging has important clinical applications. However, exact clinical indications remain to be determined. Initial clinical trials reported a somewhat optimistic view of the clinical efficacy of gadopentetate dimeglumine, showing improved diagnostic ability, or increased lesion demarcation or accounting. This in part was the result of highly selective trials with a preselection bias in favor of patients with lesions [6, 13, 26, 27]. More recently, Moody et al. [28] performed a prospective study of 500 consecutive children and adults referred for routine MR to determine if and when contrast material was radiologically helpful. Gadopentetate dimeglumine increased sensitivity in 15 (3%) of 500 cases. Although 99 (20%) showed contrast enhancement, it was considered helpful in only 74 patients (15% overall). Furthermore, lack of enhancement was considered helpful in 112 (22%). They concluded that gadopentetate dimeglumine was most helpful in older patients, those with clinically documented systemic or CNS disease, and when the patient had had a craniotomy for tumor. Specifically, gadopentetate dimeglumine was of use in delineating tumor nidus from edema, metastatic disease, residual tumor, the

subacute nature of infarcts, activity in multiple sclerosis, vasculitis, and inflammatory disease. Lack of enhancement was an important finding for assessing the integrity of the BBB, proving a surgical cure, and excluding meningeal involvement.

Despite the reduced influence of selection bias, this study may still remain overly optimistic because of its reliance on the concept of "radiologically helpful enhancement" rather than sensitivity. Even the 3% sensitivity figure may be overly optimistic when one subtracts interpretation error and clinically asymptomatic lesions such as incidental meningiomas.

#### Spinal Applications

The dosage and mode of examination in the spine are similar to those in the head except that in the spine, timing of the injection may be more critical, and a variety of disorders (especially in the extradural compartment) are studied only with T1-weighted images. Furthermore, in the evaluation of the intramedullary compartment, care must be taken to compensate for CSF motion on unenhanced T2-weighted images so that they are not degraded by artifacts, thus forcing greater reliance on contrast-enhanced T1-weighted images than may be necessary.

#### Intramedullary

Assuming good quality MR, unenhanced T1- and T2-weighted images are quite sensitive to intramedullary disease because they show changes in cord size and/or signal intensity. Despite the fact that gadopentetate dimeglumine does not appear to increase the sensitivity of the examination, most investigators feel it is critical for lesion characterization [29]. This is especially true in cases of neoplasm in which gadopentetate dimeglumine improves the localization of tumor nidus and separation from edema (particularly important with hemangioblastomas [Fig. 3] and metastasis). Furthermore, gadopentetate dimeglumine aids in differentiating be-

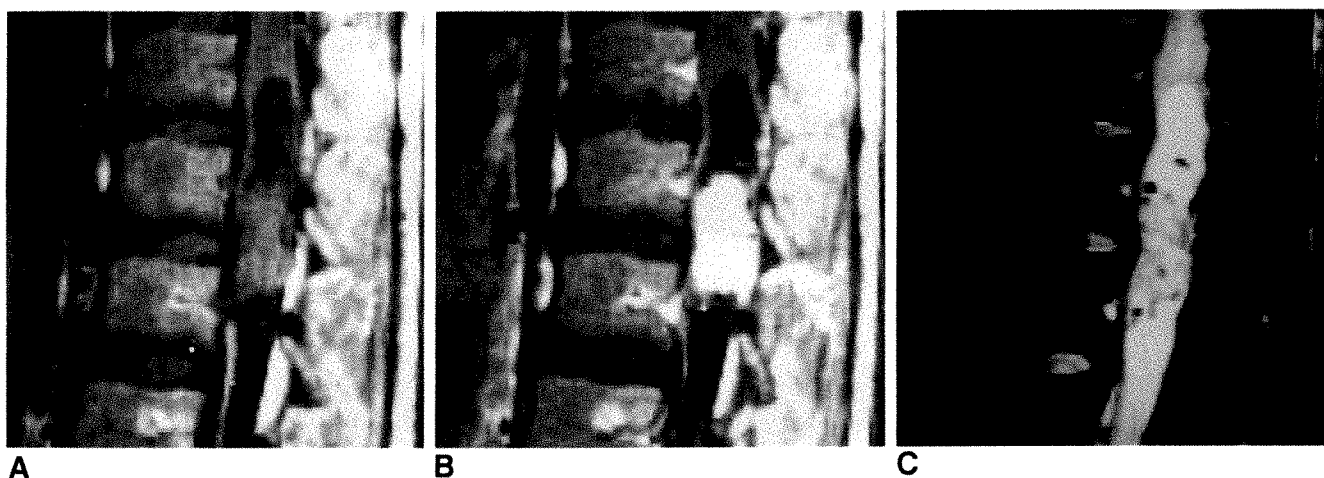


Fig. 3.—Spinal cystic hemangioblastoma.

A–C, Sagittal T1-weighted (SE 500/20) MR images obtained at 1.5 T before (A) and after (B) gadopentetate dimeglumine administration, and precontrast T2-weighted image (C) (SE 2800/90). A mixed solid cystic lesion is noted in region of conus. After administration of gadopentetate dimeglumine, a central soft-tissue density is seen to enhance. On T2-weighted image, note high signal intensity in region of lesion and in cord cranially. Decreased signal intensity on T1-weighted images, although appearing cystic, is probably edema, which is typical of reactive change in cord adjacent to hemangioblastomas.

nign or reactive processes from neoplasms. The lack of enhancement surrounding a hemorrhagic or cystic lesion may suggest a benign cause, as most neoplasms tend to enhance. Although benign syrinxes can show high signal in the adjacent cord on T2-weighted images, it is thought to be due to gliosis, which does not enhance. This is also true of rostral and caudal cysts (tumor cysts) associated with neoplasm, in which the lack of enhancement suggests these are reactive changes, in contradistinction to intratumoral cysts, which will usually show enhancement. Enhancement may be useful in following up patients who have undergone irradiation or surgery.

In addition to neoplasms, enhancement may be seen with other intramedullary disorders in which the BBB is disrupted and evidence is present of an active lesion. Examples would include inflammatory disorders such as AIDS myelopathy, sarcoidosis, and demyelinating disease, whereas in the brain, not all lesions with high signal on T2-weighted images will enhance.

#### *Intradural-Extramedullary*

Although large lesions such as meningiomas, neurofibromas, and schwannomas can usually be identified without difficulty on unenhanced scans, smaller or diffuse lesions may have signal-intensity characteristics similar to those of the surrounding CSF and neural structures (Fig. 4). This is especially true of lesions spreading via the subarachnoid space or via the leptomeninges. Lymphoma, primitive neuroectodermal tumors, ependymomas, glioblastomas, metastases, and inflammatory disease all enhance dramatically, markedly increasing their conspicuity [30, 31]. Occasionally, very mild enhancement will be noted of the traversing nerve roots that otherwise appear normal and in some cases of arachnoiditis, in association with disk herniations [32]. This is rarely a

differential problem because of the dramatic enhancement seen with neoplastic or active inflammatory processes.

#### *Extradural*

Experience to date has centered primarily on neoplastic and degenerative changes. Unlike the other compartments, routine T2-weighted images are not always obtained, and assessment has been primarily morphological. Gadopentetate dimeglumine is not routinely used for the evaluation of metastatic disease. Tumor involvement is usually predicted on the basis of marrow or epidural fat infiltration, and studies to date do not indicate that gadopentetate dimeglumine-enhanced MR improves the detection of tumors in the extradural compartment. In fact, some lesions become isointense when compared with surrounding bone marrow and become difficult to see [33, 34]. An exception may be the patient with a large extradural soft-tissue mass and adjacent bony changes in the contours of the lateral recess. Although uncommon, free disk fragments have been shown to be associated with bony changes, and an enhanced scan should separate a tumor, which would enhance diffusely, from a free fragment with surrounding granulation tissue [35].

In degenerative disease, gadopentetate dimeglumine was first applied to the postoperative spine. Current data suggest that gadopentetate dimeglumine has a 96% agreement with surgery in separating epidural fibrosis from disk material and suggests it should be used routinely in the postoperative spine [36, 37]. It seems likely that gadopentetate dimeglumine diffuses rapidly into the extravascular space through regions of endothelial discontinuity. Herniated disk, on the other hand, does not typically enhance early, but is often "wrapped in scar" and may enhance on delayed studies because of diffusion of contrast material from adjacent scar tissue (Fig. 5) [38].



Fig. 4.—Glioblastoma multiforme in right frontal lobe.

A and B, Sagittal T1-weighted (SE 500/22) MR images obtained at 1.5 T before (A) and after (B) gadopentetate dimeglumine administration. On unenhanced scan, note inhomogeneous increased signal intensity of a thecal sac. After contrast administration, linear and globular areas of enhancement are shown (arrows), indicative of CSF seeding.

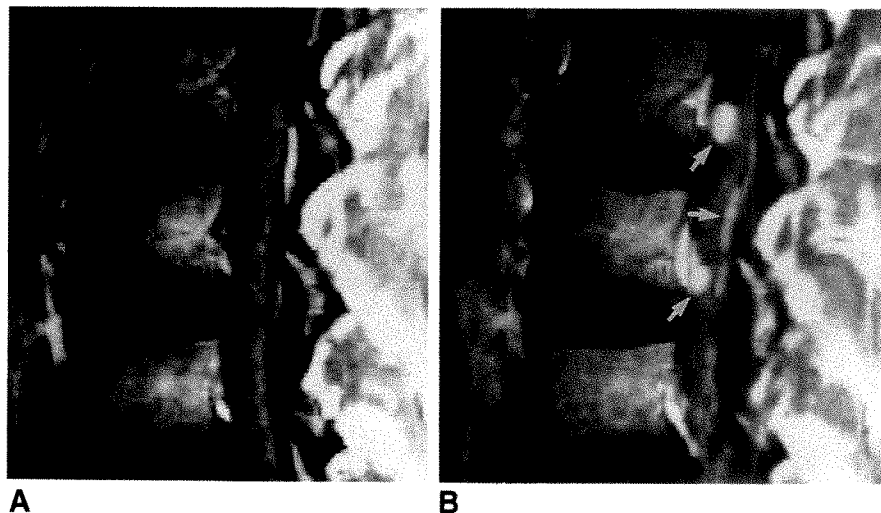
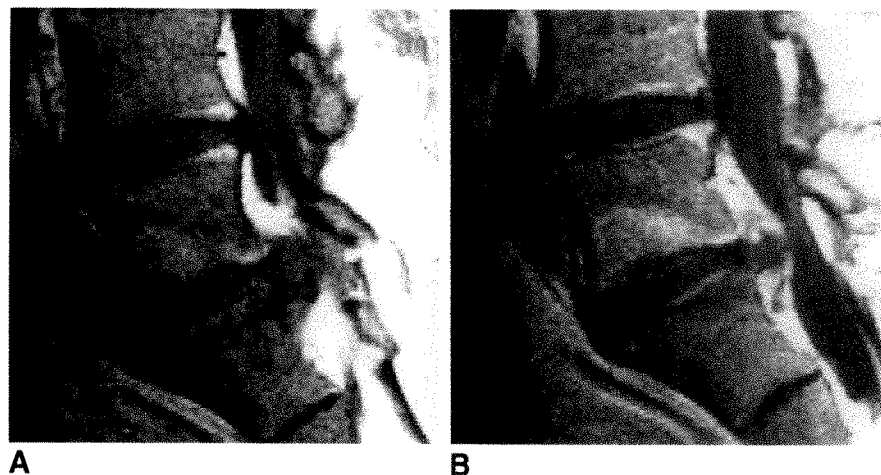


Fig. 5.—Postoperative disk.

A and B, T1-weighted (SE 500/15) MR images obtained at 1.5 T before (A) and after (B) gadopentetate dimeglumine administration. An aberrant soft-tissue mass is identified posterior to L5-S1 disk on precontrast image. After contrast administration, enhancement surrounds this mass, and margins of intervertebral disk are linearly enhanced. This case illustrates potential problems with partial volume averaging.



In both the operated and nonoperated spine, enhancement may be noted within some degenerative disks and is presumably caused by the ingrowth of granulation tissue. This may occur in a linear or, rarely, in a diffuse pattern. Probably by the same mechanism, enhancement is also seen with Type I vertebral body changes. Anular tears are another sequela of the degenerative process that may show enhancement based on the presence of granulation tissue, a component of the healing process [39]. Along these same lines, enhancement has been demonstrated surrounding herniated disks in the unoperated spine in over 50% of patients and may represent a significant portion of the mass. Histologically, these areas of enhancement again seem to be related to granulation tissue. Its presence is not surprising, because one would expect the body to respond to tissue disruption by attempted healing. In the cervical region, lateral disks and osteophytes are seen to better advantage because of enhancement of the epidural venous plexus. However, despite some degree of increased conspicuity of extradural disease with enhancement of granulation tissue and/or the epidural venous plexus,

contrast studies do not appear to alter significantly the diagnostic accuracy of noncontrast MR in the nonoperated spine [40].

Enhancement is noted in a variety of other disorders, and in the extradural space it is usually associated with some type of inflammatory or reparative (granulation tissue) response. This would include rheumatoid arthritis, especially in and about the dens, bone infarcts, vertebral osteomyelitis, and some primary bone tumors.

#### Summary, Spinal Applications

The literature suggests that a gadopentetate dimeglumine-enhanced T1-weighted sequence should be routinely performed in the evaluation of intramedullary and intradural extradural lesions and for the evaluation of the postoperative spine (for separating recurrent or residual disk from epidural fibrosis) in the extradural compartment.

## Future Directions

With respect to all neurologic applications, refinements in technique will no doubt occur. For example, fat-suppressed images may obviate routine acquisition of a precontrast T1-weighted image [41, 42]. The suboptimal sensitivity for intradural and parenchymal CNS disease on three-dimensional gradient-echo techniques, which allow rapid image acquisition and multiplanar reconstruction capability, may be overcome by using contrast agents [43]. Even more striking developments may occur with echo-planar imaging techniques that can provide dynamic imaging function while reducing the temporal resolution of sequential images to a fraction of a second. By use of both paramagnetic and superparamagnetic contrast agents, initial investigations have shown that it may be feasible to observe differences (normal and pathologic) in blood perfusion in various regions of the brain. During the first-pass phenomenon, T2 effects of contrast agents reduce signal intensity in perfused tissue [44]. The clinical usefulness of these observations is being investigated.

## REFERENCES

- Niendorf HP, Leniado M, Semmler W, Schorner W, Felix R. Dose administration of gadolinium DTPA in MR imaging of intracranial tumors. *AJNR* 1987;8:803-815
- Brant-Zawadzki M, Berry I, Osaki L, Brasch R, Murovic J, Norman D. Gadolinium DTPA in clinical MR of the brain: 1. Intraaxial lesions. *AJNR* 1986;7:781-788
- Kilgore DP, Breger RK, Daniels DL, Pojunas KW, Williams AL, Haughton VM. Cranial tissues: normal MR appearance after intravenous injection of gadolinium DTPA. *Radiology* 1986;160:757-761
- Price AC, Runge VM, Nelson KL. CNS: neoplastic disease. In: Runge VM, ed. *Enhanced magnetic resonance imaging*. St Louis: Mosby, 1989: 139-177
- Powers TA, Partain CL, Kessler RM, et al. Central nervous system lesions in pediatric patients: gadolinium DTPA enhanced MR imaging. *Radiology* 1988;169:723-726
- Russell EJ, Schaibel TJ, Dillon W, et al. Multi-center double blind placebo controlled study of gadopentetate dimeglumine as an MR contrast agent: evaluation of patients with cerebral lesions. *AJNR* 1989;10:53-63
- Lilja A, Bergstrom K, Spannare B, Olsson Y. Reliability of computed tomography in assessing histopathological features of malignant supratentorial gliomas. *J Comput Assist Tomogr* 1981;5:625-631
- Sze G, Shin J, Krol G, Johnson C, Liu D, Deck MDF. Intraparenchymal brain metastases: MR imaging versus contrast-enhanced CT. *Radiology* 1987;165:619-624
- Healy ME, Hesselink JR, Press GA, Middleton MS. Increased detection of intracranial metastases with intravenous gadolinium DTPA. *Radiology* 1987;165:619-624
- Bird CR, Drayer BP, Mudina M, Rekte HL, Flom RA, Hodak JA. Gadolinium DTPA enhanced MR imaging in the pediatric patients after brain tumor resection. *Radiology* 1988;69:123-126
- Berry I, Brant-Zawadzki M, Osaki L, Brasch R, Murovic J, Newton T. Gadolinium DTPA in clinical MR of the brain. 2. Extraaxial lesions and normal structures. *AJNR* 1986;7:789-793; *AJR* 1986;147:1231-1235
- Breger RK, Papke RA, Pionuas KW, Haughton VM, Williams AL, Daniels DL. Benign extraaxial tumors: contrast enhanced with gadolinium DTPA. *Radiology* 1987;163:427-429
- Haughton VM, Rimm AA, Czervionke LF, et al. Sensitivity of gadolinium DTPA enhanced MR imaging of benign extraaxial tumors. *Radiology* 1988;166:829-833
- Curati WL, Graif M, Kingsley DPE, Niendorf HP, Young IR. Acoustic neuromas: gadolinium DTPA enhancement in MR imaging. *Radiology* 1986;158:447-451
- Davis PC, Hoffman JC, Malko JA, et al. Gadolinium DTPA in MR imaging of pituitary adenoma: a preliminary report. *AJNR* 1987;8:817-823
- Doppman JL, Frank JA, Dwyer AJ, et al. Gadolinium DTPA-enhanced MR imaging of ACTH including microadenomas of the pituitary gland. *J Comput Assist Tomogr* 1988;12:728-735
- Dwyer AJ, Frank JA, Doppman JL, et al. Pituitary adenomas in patients with Cushing disease: initial experience with gadopentetate enhanced MR imaging. *Radiology* 1987;163:421-426
- Newton DR, Dillon WP, Norman D, Newton TH, Wilson CV. Gadolinium DTPA enhanced MR imaging of pituitary adenomas. *AJNR* 1989;10: 949-954
- Russell EJ, Geremia GK, Johnson DE, et al. Multiple cerebral metastases: detectability with gadolinium DTPA enhanced MR imaging. *Radiology* 1987;165:609
- Price AC, Runge VM, Nelson KL. CNS-non-neoplastic disease. In: Runge VM, ed. *Enhanced magnetic resonance imaging*. St. Louis: Mosby, 1989: 178-192
- Elster AD, DiPersio DA. Cranial postoperative site: assessment with contrast-enhanced MR imaging. *Radiology* 1990;174:93-98
- Burke JW, Podrasky AE, Bradley WG. Meninges: benign postoperative enhancement on MR images. *Radiology* 1990;174:99-102
- Virapongse CE, Mancuso A, Quisling R. Human brain infarcts: gadolinium DTPA enhanced MR imaging. *Radiology* 1986;161:785-794
- Grossman RI, Gonzales-Gorano F, Atlas SW, Gleda S, Silverberg DH. Multiple sclerosis: gadolinium enhancement of MR imaging. *Radiology* 1986;161:721-725
- Grossman RI, Braffman BH, Brorson JR, Goldberg HI, Silverberg DH, Gonzalez-Scarano F. Multiple sclerosis: serial study of gadolinium enhanced MR imaging. *Radiology* 1988;169:117-122
- Runge VM, Schaible TF, Goldstein JA, et al. Gadolinium-DTPA clinical efficacy. *RadioGraphics* 1988;8:147-179
- Felix R, Schorner W, Laniado M, et al. Brain tumors: MR imaging with gadolinium-DTPA. *Radiology* 1985;156:681-688
- Moody DM, Ball MR, Laster DW. Is gadolinium DTPA required for routine cranial MR imaging? *Radiology* 1989;173:231-238
- Sze G, Kro LG, Zimmerman RD, Deck MDF. Intramedullary disease of the spine: diagnosis using gadolinium DTPA enhanced MR imaging. *AJNR* 1988;9:847-858
- Berns DH, Blaser SI, Ross JS, Masaryk TJ, Modic MT. MR imaging with gadolinium DTPA in leptomeningeal spread of lymphoma. *J Comput Assist Tomogr* 1988;12:499-500
- Sze G, Abramson A, Krol G, et al. Gadolinium DTPA in the evaluation of intradural extramedullary spinal disease. *AJNR* 1988;9:153-163
- Johnson C, Sze G. Benign lumbar arachnoiditis: MR imaging with gadopentetate dimeglumine. *AJNR* 1990;11:763-770
- Stimac GK, Porter BA, Olsen DL, Gerlach R, Genton M. Gadolinium DTPA enhanced MR imaging of spinal neoplasms: preliminary investigation in comparison with unenhanced spin echo and STIR sequences. *AJNR* 1988;9:839-846
- Sze G, Krol G, Zimmerman RG, Deck MDF. Malignant extradural spinal tumors: MR imaging with gadolinium DTPA. *Radiology* 1988;167:217-223
- Schlesinger SD, Elkin C, Pinto RS, Firooznia H. Lumbar and cervical osseous erosions secondary to herniated disks: comparison of CT and MR imaging. *Radiology* 1989;172(P):44
- Jueffle MG, Modic MT, Ross JS, et al. Lumbar spine: postoperative MR imaging with gadolinium DTPA. *Radiology* 1988;167:817-824
- Ross JS, Modic MT, Masaryk TJ, Schrader M, Gentili A. Gd-DTPA in the postoperative spine: update. *Radiology* 1989;172(P):285
- Ross JS, Delamarter R, Hueffle MG, et al. Gadolinium DTPA enhanced MR imaging of the postoperative lumbar spine: time course and mechanism of enhancement. *AJNR* 1989;10:37-46
- Ross JS, Modic MT, Masaryk TJ. Tears of the annulus fibrosis: assessment of gadolinium DTPA enhanced MR imaging. *AJNR* 1989;10:1251-1254
- Ross JS, Modic MT, Masaryk TJ, Carter J, Marcus RE, Bohlman H. Assessment of extradural degenerative disease with gadolinium DTPA enhanced MR imaging: correlation with surgical and pathological findings. *AJNR* 1989;10:1243-1249
- Bobman S, Atlas SW, Listerud J, Grossman RI. Contrast-enhanced, chemical shift MR imaging of the postoperative lumbar spine. *Radiology* 1989;172(P):285-286
- Simon JH, Szumowski J, Ketonen L, Kido DK, Totterman S. Improved



detection of paramagnetic contrast enhancement by PEACH imaging for the diagnosis of disk versus scar in lumbar MR imaging. *Radiology* **1989**;172(P):286

43. Ross JS, Masaryk TJ, Modic MT. 3-Dimensional FLASH imaging applica-

tion with gadolinium DTPA. *J Comput Assist Tomogr* **1988**;13:547-552

44. Majumdar S, Zoghbi SS, Gore JC. Regional differences in rat brain displayed by fast MRI with superparamagnetic contrast agents. *Magn Reson Imag* **1988**;6:611-615

## Nonneurologic Applications

Bernd Hamm

Clinical studies investigating the use of contrast agents in MR imaging of the body are few in comparison to studies of contrast-enhanced MR imaging of the brain and spinal canal. This fact is attributable in part to the relatively greater complexity associated with contrast-enhanced MR imaging of nonneurologic disorders. For example, gadopentetate dimeglumine-induced signal enhancement can result in more pronounced motion artifacts, and the rapid diffusion of gadopentetate dimeglumine into the extracellular space may neutralize soft-tissue contrast between healthy and diseased tissue. As there is considerable organ-to-organ variation in the use of contrast agents, in this section we will present an organ-specific discussion on nonneurologic applications of MR contrast agents.

### Extracranial Head and Neck

Experience in MR imaging of the head and neck with gadopentetate dimeglumine suggests that contrast-enhanced MR imaging will be of variable usefulness. Although the exact role of gadopentetate-enhanced imaging of head and neck tumors is still evolving, CT is still required to evaluate bony changes. In normal persons, contrast enhancement is particularly striking in the well-perfused nasal mucosa. Thus, diagnostic improvement associated with contrast-enhanced MR imaging does not extend to all tumors of the nasopharynx and oropharynx, but mainly to those in the nasal and paranasal cavities [1-3]. The advantage of contrast-enhanced imaging results from improved demarcation of tumors from thickened mucosa, scar tissue, or sinus secretions, because tumors show only modest enhancement as opposed to the intense enhancement of mucosa and the nonenhancement of scar tissue or secretions [1, 2, 4]. Compared with T1-weighted precontrast images, there also may be better delineation of tumors from muscles and connective tissue, although the tumor enhancement reduces contrast with fatty tissue.

In the neck, good visualization of the highly vascularized paragangliomas of the carotid body is possible with dynamic contrast-enhanced MR imaging [5]. Maximal signal intensity is seen approximately 300 sec after bolus application of gadopentetate dimeglumine [6]. The sensitivity of contrast-

enhanced MR imaging is far superior to that of CT for detecting even small paragangliomas in the temporal bone and the carotid body. The usefulness of dynamic gadopentetate dimeglumine-enhanced MR imaging with gradient-echo pulse sequences is still being examined for differentiation between various histologic types.

### Mediastinum

Few reports are available on the use of gadopentetate dimeglumine in the chest. A major drawback is that gadopentetate dimeglumine reduces contrast between mediastinal fat and enhancing tumors (Fig. 1) [7, 8], although this limitation can be overcome with the use of fat-suppressed imaging techniques [9]. Our experience (unpublished data) shows that contrast-enhanced MR imaging does not improve the staging of esophageal carcinoma compared with unenhanced MR imaging or CT. Contrast-enhanced MR imaging, however, does permit differentiation between viable and necrotic tumor areas, which may be useful for the evaluation of mediastinal tumors (especially lymphomas) in patients undergoing chemotherapy or radiation treatment.

### Heart

Research on contrast-enhanced MR imaging of the heart has focused on the diagnosis of myocardial infarction, because congenital heart disease, acquired valvular defects, and cardiac function are adequately evaluated with unenhanced MR imaging. Assessment of myocardial infarction requires ECG-gated, T1-weighted, SE pulse sequences with gadopentetate dimeglumine being applied as a bolus [10-12]. Gadopentetate dimeglumine produces pronounced shortening of T1 in the infarcted area, thus enhancing the signal intensity of this area relative to unaffected myocardium [10, 13]. This observation is explained by the fact that the accumulation of gadopentetate dimeglumine in myocardial tissue is determined not only by the tissue blood volume and blood flow, but also by the size of the extracellular space and capillary permeability [14]. De Roos et al. [10] found the highest contrast between normal and infarcted myocardium to occur 20 to 30 min after the application of gadopentetate

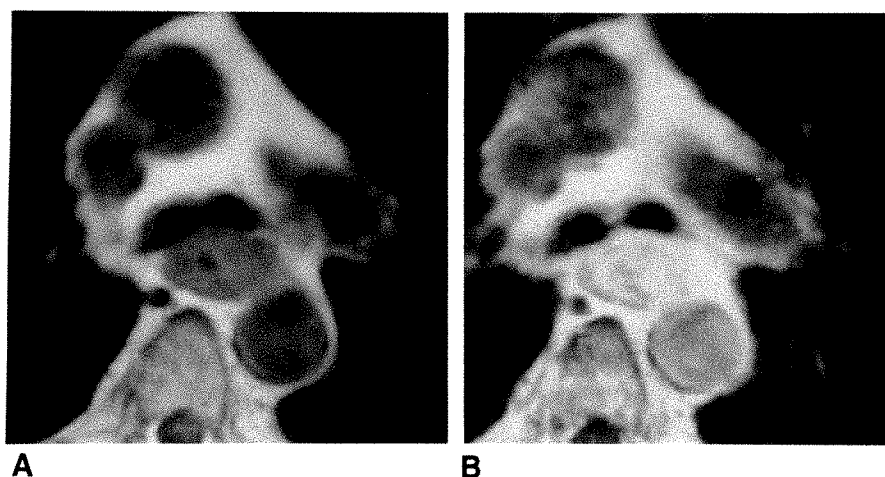


Fig. 1.—T1-weighted (SE 500/15) MR images of esophageal carcinoma obtained at 1.5 T before (A) and after (B) administration of gadopentetate dimeglumine. Note intense enhancement of tumor obscuring its border with adjoining fat.

dimeglumine, and the authors considered the delineation of infarcted area to be substantially improved in the postcontrast images. However, the interesting question of differentiation between reperfused and nonperfused myocardial infarction is presently insufficiently answered by contrast-enhanced MR imaging.

Gadopentetate dimeglumine may be used to distinguish between acute and chronic myocardial infarction. Although no significant uptake of gadopentetate dimeglumine occurs in chronic myocardial infarction, and the affected area is therefore delineated only indirectly on the basis of morphologic changes, such as thinning of the wall and aneurysm formation, gadopentetate dimeglumine also can be a positive marker of acute myocardial infarction [11, 15]. For instance, Nishimura et al. [11] found enhancement in the infarcted area in (82%) of 17 patients with acute myocardial infarction but only in three (21%) of 14 patients 90 days later.

The use of gadopentetate dimeglumine in the evaluation of the myocardium is limited by diffusion of the contrast agent into the extracellular space and rapid renal excretion [16]. Better results might be obtained by combining the use of gadopentetate dimeglumine as a myocardium-perfusion substance with fast imaging techniques. Additionally, intravascular contrast agents such as albumin-gadopentetate dimeglumine could further improve the diagnostic value of myocardial perfusion studies [17, 18].

### Breast

Gadopentetate dimeglumine-enhanced MR imaging may provide valuable information for tumor diagnosis in dense breasts, differentiation of scars from carcinoma, and screening for tumor recurrence between silicone implants and the thoracic wall. Dynamic contrast-enhanced MR imaging provides the key for improving the differential diagnosis [19–22]. Carcinomas are characterized by a strong increase in signal intensity of up to 100% within the first 2 min after contrast administration and a subsequent plateau [20]. The increase in signal intensity is strongest in mucinous carcinomas, followed by ductal and lobular carcinomas, whereas scirrhous

carcinomas show the lowest increase [22]. Normal glandular tissue and nonproliferating mastopathy as well as scars after 6 months show no or only insignificant uptake of the contrast agent [19]. Proliferating mastopathy displays considerable variation with respect to contrast uptake, but increasing enhancement is observed with higher degrees of proliferation [22]. The greatest variation in contrast behavior and signal enhancement is seen in fibroadenomas [19, 20]. Thus, because of the strong and early contrast enhancement of carcinomas of the breast as opposed to the delayed and less pronounced enhancement of most benign lesions, dynamic contrast-enhanced examination appears to be promising for MR imaging of the breast.

### Liver

Both paramagnetic gadopentetate dimeglumine and superparamagnetic iron oxide particles have been investigated in clinical studies of liver tumors. Results obtained so far indicate that these two substances do not compete with each other: dynamic gadopentetate dimeglumine-enhanced MR imaging yields important physiologic information for the differential diagnosis of liver tumors, whereas iron oxides are of particular interest for tumor screening.

Gadopentetate dimeglumine-enhanced MR imaging of liver tumors requires that fast imaging techniques be used in combination with bolus application of the contrast agent. An increase in contrast between liver and tumor occurs only in the first 2–3 min after administration of gadopentetate dimeglumine [23, 24]. Subsequent diffusion of the contrast agent into the tumor reduces tumor-liver contrast. As there is no significant hepatocyte excretion of gadopentetate dimeglumine, delayed MR imaging, unlike CT with iodinated contrast media, does not improve the detection of hepatic lesions [25]. Dynamic gadopentetate dimeglumine-enhanced MR imaging is most useful for studying perfusion of hepatic tumors. The enhancement patterns of benign and malignant liver tumors in MR imaging are similar to those seen in CT [26–30]. However, enhancement induced by gadopentetate di-

meglumine in MR imaging (on strongly T1-weighted fast pulse sequences) is more pronounced than enhancement with iodinated contrast media in dynamic CT [31]. The appearance of hemangiomas in dynamic gadopentetate dimeglumine-enhanced MR imaging is characterized by hyperintense peripheral enhancement followed by a fill-in phenomenon (Fig. 2). This is quite distinct from the enhancement behavior of liver metastases (Fig. 3) and hepatocellular carcinomas [32]. The difference in signal intensity between hemangiomas and metastases is most striking on delayed images [30]. Hypervascular metastases do not show the homogeneous high signal intensity typical of hemangiomas [31]. Focal-nodular hyperplasia is characterized in dynamic contrast-enhanced MR imaging by strong contrast enhancement, with a peak during the first 30 sec after contrast administration, and by a rapid decrease in signal intensity (Fig. 4) [31].

The effect of superparamagnetic iron oxide particles on MR imaging is fundamentally different from that of gadopentetate dimeglumine. Animal studies showed that IV iron oxide selectively reduces signal intensity of healthy liver tissue, whereas signal intensity of intrahepatic tumors remains constant. Thus contrast between the two tissues increases [33, 34]. Although

iron oxide-induced signal reduction of liver tissue is strongest on gradient-echo sequences [35], intermediately weighted spin-echo sequences are more suitable for liver imaging because they offer better anatomic resolution owing to their superior signal-to-noise ratios. Preliminary clinical evaluation of patients with liver cancer suggests that iron oxide-enhanced MR imaging may increase the conspicuity of liver lesions and lower the size threshold for lesion detection (Fig. 5) [36, 37]. More importantly, this contrast agent also appears to reduce the rigid scanning requirements associated with paramagnetic gadopentetate dimeglumine (Fig. 6). Discriminating benign from malignant lesions has been investigated also. Hahn et al. [38] showed that iron oxides produce prolonged diminution in signal intensity of cavernous hemangiomas and that this phenomenon was absent in hypovascular and hypervascular metastases. Difficulties in image interpretation after iron oxide administration arise from signal in blood vessels and perivascular fat. Although this problem has not been fully evaluated, possible solutions include the use of fat-suppressed techniques (to eliminate signal from lipid protons) and early dynamic imaging after iron oxide administration (to eliminate intravascular signal) (Fig. 7).

Fig. 2.—Dynamic gadopentetate dimeglumine-enhanced MR images (GRE 100/5, 80°) of hemangiomas at 1.5 T. Large hemangioma shows peripheral enhancement on early image (A, 5 min) and fill-in phenomenon on delayed image (B, 20 min). Smaller hemangiomas (arrows) show early and persistent homogeneous enhancement after gadopentetate dimeglumine administration. Thus hemangiomas show slow fill-in and slow washout of contrast agent.

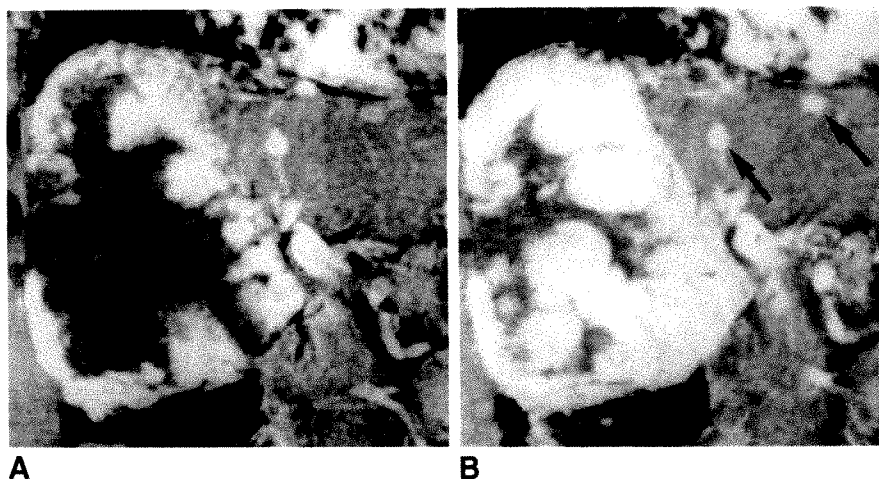
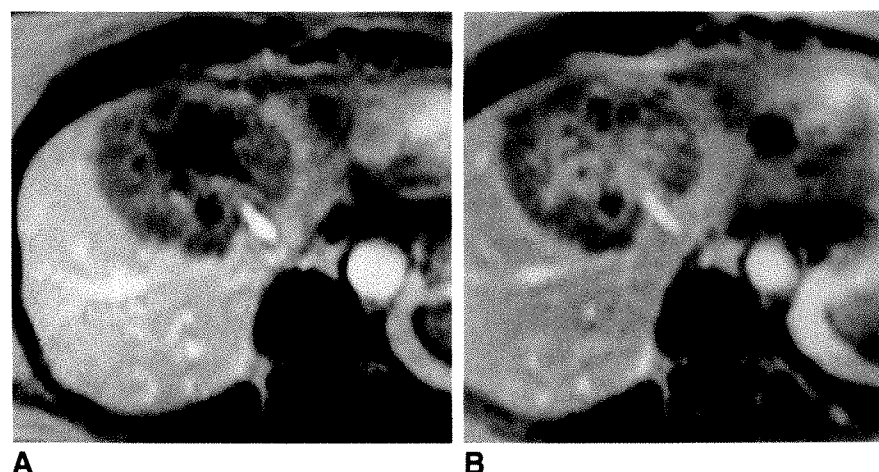


Fig. 3.—Dynamic gadopentetate dimeglumine-enhanced MR images (GRE 100/5, 80°) of adenocarcinoma metastasis at 1.5 T. Lesion shows inhomogeneous enhancement on immediate (30 sec) image (A) and remains hypointense relative to surrounding liver parenchyma at 5 min (B). Thus hypovascular metastases show limited enhancement with contrast agent.





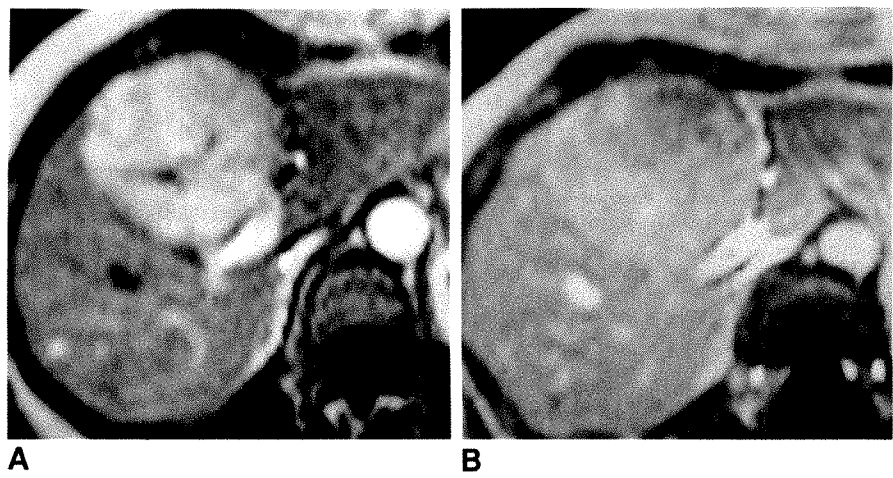


Fig. 4.—Dynamic gadopentetate dimeglumine-enhanced MR images (GRE 100/5, 80°) of focal nodular hyperplasia at 1.5 T. Note immediate (A, 30 sec) and strong enhancement of hyperperfused lesion, which subsequently becomes isointense on delayed scans (B, 4 min). Thus focal nodular hyperplasia shows rapid fill-in and rapid washout of contrast agent.



Fig. 5.—Iron oxide-enhanced MR imaging of liver metastases at 0.6 T. A–C, SE 275/14, precontrast T1-weighted (A), SE 500/30, postcontrast (B) and precontrast (C) mixed T1-T2 weighted images. Note increased number of lesions seen on postcontrast scan (B) compared with best precontrast image (A).



Fig. 6.—Iron oxide-enhanced MR imaging of liver metastases at 0.6 T. A–C, Precontrast T1-weighted SE 275/14 (A), postcontrast proton-density SE 1500/40 (B), and postcontrast T2-weighted SE 1500/80 (C) images. Note high lesion-liver contrast on postcontrast images. Compare with Fig. 5B. These post-iron oxide images illustrate that wide range of pulse-sequence timing parameters can be used to provide high tumor-liver contrast.

**Spleen**

The sensitivity of MR imaging in the detection of tumorous lesions of the spleen is low because relaxation times and signal intensities of normal spleen and intrasplenic tumors are

very similar. The size and extent of focal processes are therefore easily underestimated or lesions completely escape detection [39]. Contrast agents can dramatically improve tumor detection. For example, the early phase of dynamic gadopentetate dimeglumine-enhanced MR imaging is char-



Fig. 7.—Dynamic iron oxide-enhanced MR imaging (SE 1500/80) of normal liver at 0.6 T.

A–C, Precontrast (A), dynamic image at 1–10 min after contrast administration (B), delayed image at 60 min after contrast administration (C). High signal intensity in blood vessels (aorta and intrahepatic vessels) seen on precontrast and delayed postcontrast images is absent in dynamic phase. This effect can be exploited to assess tissue perfusion.

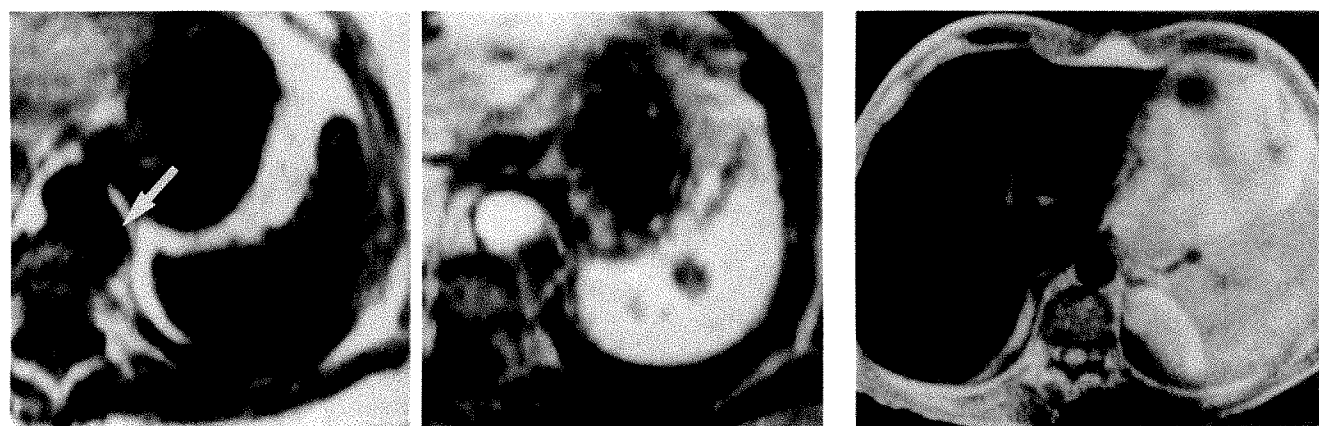


Fig. 8.—Dynamic gadopentetate dimeglumine-enhanced MR imaging at 1.5 T, GRE 100/5, 80°.

A and B, Precontrast image (A) shows paraaortic lymph node (arrow). Focus of nodular lymphoma in spleen is seen on 1-min postcontrast scan (B).

Fig. 9.—Iron oxide-enhanced MR image of splenic lymphoma at 0.6 T. Owing to lymphomatous infiltration, spleen does not trap iron oxide particles and therefore fails to turn black. Compare with signal decrease after iron oxide administration in normal spleen in Fig. 6. (Reproduced with permission from Weissleder et al. [41]).

acterized by improved contrast between the hypointense tumor and the surrounding hyperintense tissue. However, diffusion of the contrast agent into the lesion destroys this enhanced lesion-spleen contrast within a few minutes (Fig. 8). More promising results have been obtained with IV administered iron oxide particles. As in the liver, they reduce the signal intensity of normal splenic tissue. Clinical examinations of splenic tumors with iron oxide show that at a dose of 30  $\mu\text{mol Fe/kg}$ , a significant signal reduction in normal spleen occurs, while metastases remain unaffected, which results in improved visualization of metastases [40]. Iron oxide-enhanced MR imaging is also a promising procedure for distinguishing normal spleens from those diffusely infiltrated by lymphoma (Fig. 9) [41]. The diagnostic indicator in this case is the change in signal intensity after contrast administration (40  $\mu\text{mol Fe/kg}$ ), because lymphomatous spleens show a significantly higher signal intensity than do normal spleens or spleens that are enlarged because of benign diseases.

## Pancreas

In evaluating diseases of the pancreas, MR is still inferior to CT [42]. No concrete results have been published so far on the use of contrast-enhanced MR imaging of the pancreas, and it remains to be seen whether dynamic gadopentetate dimeglumine-enhanced MR imaging will yield better results in the future. However, development of oral contrast agents is a first step toward improving the usefulness of MR imaging of the pancreas, because first the pancreas must be differentiated from the gastrointestinal tract [43].

## Kidney

Gadopentetate dimeglumine has limited application in the kidney. This is due in part to the high accuracy of the less expensive contrast-enhanced CT in tumor identification and the competition of nuclear scintigraphy in the evaluation of



kidney function. Contrast-enhanced MR imaging, for both tumor diagnosis and functional assessment, is best achieved when dynamic studies are performed in combination with bolus injection of gadopentetate dimeglumine [44–46]. Contrast administration allows better visualization of tumor extension within the kidney than imaging without contrast material does, but it does not improve the assessment of extrarenal tumor extension because of the high signal intensity of perirenal fat [45]. T2 (susceptibility) effects resulting from accumulation of the contrast agent in the renal pyramids and pelvicaliceal system produce signal-free areas, which also impair the interpretation (Fig. 4) [46]. This effect also limits quantitative evaluation of renal function.

### Adrenal Glands

The results of a preliminary clinical study of adrenal masses with gadopentetate dimeglumine have given rise to optimism for increased reliability with tissue characterization [47]. Although malignant tumors and pheochromocytomas show a significantly greater signal intensity than adenomas do in precontrast images, after administration of gadopentetate dimeglumine, only moderate enhancement and quick washout is observed in adenomas, whereas malignant tumors and pheochromocytomas show strong enhancement and slower washout. This information may therefore be useful for differentiation between benign and malignant adrenal masses.

### Pelvis

For diagnostic assessment of urinary bladder tumors, gadopentetate dimeglumine can be applied either intravesically or IV. On T1-weighted images, intravesical administration (dilution 1:50) leads to a clear distinction of the hypointense tumor from the signal-rich fluid in the bladder [48]. However, no major additional information relative to T2-weighted images is obtained. MR examinations of patients with urinary bladder tumors also show significant contrast enhancement in the tumors after IV application of gadopentetate dimeglumine [49]. Dynamic studies show that the signal intensity of tumors peaks within 120 sec and remains elevated for up to 45 min. Because of the plateaulike course of the signal enhancement and the better spatial resolution, T1-weighted spin-echo sequences are to be preferred to T1-weighted fast gradient-echo pulse sequences for staging of bladder tumors. Contrast-enhanced MR imaging appears to allow better tumor staging than do precontrast T1- and/or T2-weighted pulse sequences. This is especially true for the distinction of superficial tumors from those infiltrating the muscle, because non-involvement of the muscle layer is visualized as an intact hypointense line in the region underlying the tumor [48]. However, transurethral resection may lead to overstaging, because contrast-enhanced MR imaging cannot differentiate between inflammation and tumor.

In the diagnosis of tumors of the uterus, gadopentetate dimeglumine-enhanced MR imaging can yield additional information in patients with endometrial carcinoma. Viable and necrotic areas are easier to distinguish on postcontrast than

on T2-weighted precontrast images. In the evaluation of ovarian masses, gadopentetate dimeglumine improves the visualization of the internal tumor structure and may allow better distinction of inflammatory adnexal processes from malignant tumors on the basis of the strong contrast enhancement in the former.

### Musculoskeletal System

The majority of clinical studies investigating gadopentetate dimeglumine-enhanced MR imaging concentrate on the diagnosis of bone and soft-tissue tumors [50–52]. Contrast-enhanced MR imaging with T1-weighted SE pulse sequences is more reliable in distinguishing different tumor components, in particular, necrosis and viable tumor tissue, than is precontrast imaging. Although marked improvement occurs after contrast application compared with the T1-weighted precontrast image (in which contrast between tumor and soft tissue is often absent), the contrast is never as strong as in T2-weighted precontrast sequences. However, IV application of gadopentetate dimeglumine reduces the contrast between enhancing tumor and signal-intensive fatty tissue and bone marrow. Contrast-enhanced MR imaging is therefore no substitute for precontrast spin-echo pulse sequences. More promising results are obtained with gadopentetate dimeglumine in distinguishing residual or recurrent sarcomas from posttherapy changes [53].

### Lymph Nodes

MR imaging has proved unreliable in the distinction of normal and neoplastic nodes by means of signal-intensity characteristics because relaxation times and proton densities of normal and metastatic nodes overlap [54]. Initial animal investigations have shown that iron oxide particles applied directly or via interstitial administration to a lymphatic vessel produce a loss of signal in normal lymph node tissue [55, 56]. Lymph node metastases, on the other hand, are characterized by a constant signal intensity and can thus be distinguished from unaffected lymph nodes. MR lymphography in combination with superparamagnetic iron oxide particles opens up promising future prospects for lymph node staging.

### Future Directions

The application of contrast agents in sites other than the CNS is still in its infancy. Considerable improvement in image quality is still needed to produce motion-free images. With novel formulations such as the nonionic isosmolar preparations, higher doses and/or prolonged infusion may further improve diagnostic information. Most importantly, without a gastrointestinal contrast agent, MR imaging will be unable to provide global examination of the abdomen. Once these technical hurdles have been overcome, the pace of development of contrast agents with organ and disease-specific applications will quicken.



## REFERENCES

- Robinson JD, Crawford SC, Teresi LM, et al. Extracranial lesions of the head and neck: preliminary experience with gadopentetate enhanced MR imaging. *Radiology* **1989**;172:165-170
- Crawford SC, Harnsberger HR, Lufkin RB, Hanafey WN. The role of gadolinium-DTPA in the evaluation of extracranial head and neck mass lesions. *Radiol Clin North Am* **1989**;27:219-242
- Vogl T, Markl AF, Bruening R, Greves G, Kang K, Lissner JA. MR imaging of oropharynx and oral cavity: gadopentetate and fast imaging technique. *Radiology* **1988**;169(P):308
- Vogl T, Dresel ST, Schedel H, Greves G, Lissner J. MR imaging of the nasopharynx: fast imaging technique and gadopentetate studies. *J Comput Assist Tomogr* **1988**;12:427-433
- Vogl T, Bruening R, Schedel H, et al. Paragangliomas of the jugular bulb and carotid body: MR imaging with short sequences and gadopentetate enhancement. *AJNR* **1989**;10:823-827
- Vogl T, Bruening R, Schedel H, et al. MR imaging of paragangliomas of the jugular bulb and carotid body: fast imaging technique and gadopentetate. *Radiology* **1988**;169(P):72
- Carr DH. Paramagnetic contrast media for magnetic resonance imaging of the mediastinum and lungs. *J Thorac Imaging* **1985**;1:74-78
- Nagele M, Hahn D, Seelos K, Lissner J. Gadopentetate-Kontrastverstärkung in der kernspintomographischen Diagnostik thorakaler Raumforderungen. *ROFO* **1988**;149:69-75
- Hahn D, Stelzer S, Schmidt H, Lissner J. MR imaging of the mediastinum: value of Gd-DTPA and fast MR imaging. *Radiology* **1988**;169(P):219
- de Roos A, Doornbos J, van der Wall EE, van Voorthuisen AE. MR imaging of acute myocardial infarction: value of Gd-DTPA. *AJR* **1988**;150:531-534
- Nishimura T, Kobayashi H, Ohara Y, et al. Serial assessment of myocardial infarction by using gated MR imaging and gadopentetate. *AJR* **1989**;153:715-720
- de Roos A, van Rossum AC, van der Wall E, et al. Reperfused and nonreperfused myocardial infarction: diagnostic potential of gadopentetate enhanced MR imaging. *Radiology* **1989**;172:717-720
- Rehr RB, Peshock RM, Malloy CR, et al. Improved in vivo magnetic resonance imaging of acute myocardial infarction after intravenous paramagnetic contrast agent administration. *Am J Cardiol* **1986**;57:864-868
- McNamara MT, Higgins CB, Ehman RL, Revel D, Sievers R, Brasch RC. Acute myocardial ischemia: magnetic resonance contrast enhancement with gadolinium-DTPA. *Radiology* **1984**;153:157-163
- Seiderer M, von Arnim T, Moser E, Riemmüller R, Hahn D. Gadopentetate in der kernspintomographischen Diagnostik chronischer Myokardinfarkte. *ROFO* **1986**;145:666-673
- Brown JJ, Higgins CB. Myocardial paramagnetic contrast agents for MR imaging. *AJR* **1988**;151:865-871
- Schmiedl U, Ogan MD, Paaßen H, et al. Albumin labeled with Gd-DTPA as an intravascular, blood pool enhancing agent for MR imaging: biodistribution and imaging studies. *Radiology* **1987**;162:205-210
- Moseley ME, White DL, Wang S, et al. Vascular mapping using albumin (gadopentetate), an intravascular MR contrast agent, and projection MR imaging. *J Comput Assist Tomogr* **1989**;13:215-221
- Heywang SH, Wolf A, Pruss E, Hilbertz T, Eiermann W, Permanetter W. MR imaging of the breast with gadopentetate: use and limitations. *Radiology* **1989**;171:95-103
- Kaiser WA, Zeitler E. MR imaging of the breast: fast imaging sequences with and without gadopentetate: preliminary observations. *Radiology* **1989**;170:681-686
- Heywang SH, Hilbertz TH, Pruss E, et al. Contrast material-enhanced MR imaging in patients with postoperative scarring and silicon implants. *Radiology* **1988**;169(P):352
- Hilbertz TH, Heywang SH, Fink U, Permanetter W, Eiermann W. Contrast material enhanced MR imaging of the breast with histopathologic correlation. *Radiology* **1988**;169(P):352
- Saini S, Stark DD, Brady TJ, Wittenberg J, Ferrucci JT Jr. Dynamic spin-echo MR imaging of liver cancer using gadolinium DTPA: animal investigations. *AJR* **1986**;147:357-362
- Hamm B, Wolf KJ, Felix R. Conventional and rapid MR imaging of the liver with gadolinium-DTPA. *Radiology* **1987**;164:313-320
- Nelson RC, Umpierrez ME, Chezmar JL, Bernardino ME. Delayed magnetic resonance hepatic imaging with gadolinium-DTPA. *Invest Radiol* **1988**;23:509-511
- Freeny PC, Marks WM. Hepatic hemangioma: dynamic bolus CT. *AJR* **1986**;147:711-719
- Freeny PC, Marks WM. Patterns of contrast enhancement of benign and malignant hepatic neoplasms during bolus dynamic and delayed CT. *Radiology* **1986**;160:613-618
- Mano I, Yoshida H, Nakabayashi K, Yashiro N, Iio M. Fast spin echo imaging with suspended respiration: gadolinium enhanced MR imaging of liver tumors. *J Comput Assist Tomogr* **1987**;11:73-80
- Ohtomo K, Itai Y, Yoshikawa K, et al. Hepatic tumors: dynamic MR imaging. *Radiology* **1987**;163:27-31
- Hamm B, Fischer E, Taupitz M. Differentiation of hepatic hemangiomas from hepatic metastases by using dynamic contrast enhanced MR imaging. *J Comput Assist Tomogr* **1990**;15:205-216
- Hamm B, Taupitz M, Felix R, Wolf KJ. Dynamic contrast enhanced MR imaging of benign and malignant liver tumors at 0.5 and 1.5 Tesla. In: *Book of Abstracts: Society of Magnetic Resonance in Medicine, 1989*. Berkeley, CA: Society of Magnetic Resonance in Medicine, 1989:91.
- Yoshida H, Itai Y, Ohtomo K, Kokubo T, Minami M, Yashiro N. Small hepatocellular carcinoma and cavernous hemangioma: differentiation with dynamic FLASH MR imaging with gadopentetate. *Radiology* **1989**;171:339-342
- Saini S, Stark DD, Hahn PF, et al. Ferrite particles: a superparamagnetic MR contrast agent for enhanced detection of liver carcinoma. *Radiology* **1987**;162:217-222
- Taupitz M, Hamm B, Wolf KJ. Efficacy of superparamagnetic iron oxide in MR imaging in liver tumors: in vivo and in vitro animal investigations. *Radiology* **1989**;173(P):174
- Fretz CJ, Elizondo G, Weissleder R, Hahn PF, Stark DD, Ferrucci JT. Superparamagnetic iron oxide enhanced MR imaging: pulse sequence optimization for detection of liver cancer. *Radiology* **1989**;172:393-397
- Stark DD, Weissleder R, Elizondo G, et al. Superparamagnetic iron oxide: clinical application as a contrast agent for MR imaging of the liver. *Radiology* **1988**;168:297-301
- Marchal G, van Hecke P, Demaerel P, et al. Detection of liver metastases with superparamagnetic iron oxide in 15 patients: results of MR imaging at 1.5 T. *AJR* **1989**;152:771-775
- Hahn PF, Stark DD, Weissleder R, Elizondo E, Saini S, Ferrucci JT. Clinical application of superparamagnetic iron oxide to MR imaging of tissue perfusion in vascular liver tumors. *Radiology* **1990**;174:361-366
- Hahn PF, Weissleder R, Stark DD, Saini S, Elizondo G, Ferrucci JT. MR imaging of focal splenic tumors. *AJR* **1988**;150:823-827
- Weissleder R, Hahn PF, Stark DD, et al. Superparamagnetic iron oxide: enhanced detection of focal splenic tumors with MR imaging. *Radiology* **1988**;169:399-403
- Weissleder R, Elizondo G, Stark DD, et al. The diagnosis of splenic lymphoma by MR imaging: value of superparamagnetic iron oxide. *AJR* **1989**;152:175-180
- Steiner E, Stark DD, Hahn PF, et al. Imaging of pancreatic neoplasms: comparison of MR and CT. *AJR* **1989**;152:487-491
- Laniado M, Kornmesser W, Hamm B, Clauss W, Weinmann HJ, Felix R. MR imaging of the gastrointestinal tract: value of Gd-DTPA. *AJR* **1988**;150:817-821
- Laniado M, Kornmesser W, Nagel R, et al. Spin echo, inversion recovery and fast imaging sequences with gadopentetate enhanced magnetic resonance imaging of renal tumors. In: Runge VM, Claussen C, Felix R, James AE, eds. *Contrast agents in magnetic resonance imaging*. Princeton, NJ: Excerpta Medica, **1986**:162-166
- Yashiro N, Suzuki M, Kishi H, Iio M. Is gadopentetate necessary to stage renal adenocarcinoma? *Radiology* **1988**;169(P):193
- Kikinis R, von Schulthess GK, Jager P, et al. Normal and hydronephrotic kidney evaluation of renal function with contrast enhanced MR imaging. *Radiology* **1987**;165:837-842
- Kresin GP, Steinbrich W, Friedmann G. Adrenal masses: evaluation with fast gradient-echo MR imaging and gadopentetate enhanced dynamic studies. *Radiology* **1987**;171:675-680
- Sparenberg A, Hamm B, Klien R, Wolf KJ. Contrast material-enhanced MR imaging of bladder neoplasms: correlation with CT and pathologic staging. *Radiology* **1989**;173(P):176
- Neuerburg JM, Bohndorf K, Sohn M, Teufel F, Guenther RW, Daus HJ. Urinary bladder neoplasms: evaluation with contrast enhanced MR imaging.

- ing. *Radiology* **1989**;172:739-743
50. Reiser M, Bohnndorf K, Niendorf HP, Friedmann G, Erlemann R, Kunze V. Preliminary results with gadolinium-DTPA in magnetic resonance tomography of bone and soft-tissue tumors. *Radiologie* **1987**;27:467-472
  51. Pettersson H, Eliasson J, Egund N, et al. Gadolinium-DTPA enhancement of soft tissue tumors in magnetic resonance imaging: preliminary clinical experience in five patients. *Skeletal Radiol* **1988**;17:319-323
  52. Erlemann R, Reiser MF, Peters PE, et al. Musculoskeletal neoplasms: static and dynamic gadopentetate enhanced MR imaging. *Radiology* **1989**;171:767-773
  53. Kim E, Abello R, Holbert JM, et al. Differentiation of therapeutic changes from recurrent or residual musculoskeletal sarcomas with gadopentetate enhanced MR imaging. *Radiology* **1989**;173(P):104
  54. Bottomley PA, Hardy RE, Argersinger RE, Allen-Moore G. A review of 1H nuclear magnetic resonance relaxation in pathology: are T1 and T2 diagnostic? *Med Phys* **1987**;14:1-37
  55. Weissleder R, Elizondo G, Josephson L, et al. Experimental lymph node metastases: enhanced detection with MR lymphography. *Radiology* **1989**;171:835-839
  56. Hamm B, Taupitz M, Wagner S, Hussmann P, Wolf KJ. MR lymphography: initial experimental results with superparamagnetic iron oxide. *Radiology* **1989**;173(P):274

## Gastrointestinal Contrast Agents

Peter F. Hahn

There is widespread agreement that development of a gastrointestinal contrast agent will be necessary for abdominal MR imaging to progress. For example, one reason that MR imaging of the liver has not been adopted more widely, despite evidence that it can compete favorably with CT in detecting and characterizing focal hepatic lesions, is that examinations performed to stage cancer in the liver routinely miss three times as many important extrahepatic lesions as CT does [1, 2]. Although issues of noise and spatial resolution must be confronted, bowel marking, with confident delineation of the pancreas and paraaortic area, seems an essential prerequisite for expanding the use of MR beyond the liver.

In general, MR contrast agents for use in the gastrointestinal tract may be classified according to whether they contribute signal to the bowel lumen (positive contrast agent) or reduce signal normally associated with the bowel lumen (negative contrast agent). This classification must be used cautiously, however, because changes in concentration, technical factors, and physiologic conditions can change a positive contrast agent into a negative agent. For example, although gadolinium compounds usually increase signal intensity by shortening T1, higher concentrations of these compounds and more heavily T2-weighted imaging can result in predominance of the T2-shortening effect, resulting in a decrease in signal intensity. Thus, an agent that began in the stomach as a positive agent might, after concentration in the colon by physiologic water resorption, become a negative agent. A second useful distinction can be made between contrast agents intended to mix with bowel contents, so-called *miscible* agents, and those intended to replace bowel contents, *immiscible* agents. Table 1 displays many of the materials that have been tested as gastrointestinal contrast agents, separated according to the positive-negative and miscible-immiscible characteristics.

### Positive Agents

Positive contrast agents for MR imaging include paramagnetic substances, which mix with bowel contents, and fats

and oils, which must replace bowel contents in order to mark the bowel. Although fatty materials, with inherently short T1, were among the earliest materials investigated for oral contrast in MR imaging [3], delivery of sufficient volume to replace all of the small-bowel contents has not been reported. Gadopentetate dimeglumine has been developed for use as an oral contrast agent (Fig. 1). With conventional spin-echo and gradient-echo techniques and doses on the order of 500-700 ml of 1 mmol/l solution, gadopentetate dimeglumine is a positive contrast agent that mixes with gastrointestinal tract contents, shortening T1 [4]. In order to ensure delivery deep into the small bowel, gadopentetate dimeglumine is given with a nonabsorbable sugar such as 15-30 g of mannitol. Positive contrast agents can increase image noise through motion of the bowel during imaging. Therefore, investigators using oral gadopentetate dimeglumine have obtained best results with fast gradient-echo imaging, abdominal compression, and pharmacologic reduction of bowel peristalsis.

Other paramagnetic substances have been investigated as oral contrast agents. The first proposed for this purpose was ferric ammonium citrate [5], widely available as the hematinic in Geritol (Beecham, Bristol, TN). Ferric ammonium citrate produces about one fifth as much T1 shortening as gadopentetate dimeglumine does at equal concentrations. At first only limited delivery of ferric ammonium citrate into the small bowel was achieved. Recently, a mixture of ice cream (30%), corn oil (20%), milk (38%), and ferric ammonium citrate (12%) has been found to be well tolerated and to achieve positive gastroduodenal and small-bowel marking [6].

### Negative Agents

Negative contrast agents include clays, barium sulfate, iron oxides, perfluorocarbons, and gas-evolving pellets. The clay mineral kaolin used to be in the nonprescription medication Kaopectate (Upjohn, Kalamazoo, MI). Kaolin is on the U.S. Food and Drug Administration list of substances generally recognized as safe for use as an indirect food additive. Kaolin produces diamagnetic T1 and T2 shortening in aqueous sus-

pension, the T2 effect predominating. Consequently, kaolin is a negative contrast agent, and oral administration of 950 ml Kaopectate has been shown to produce gastric and duodenal marking in humans [7]. Although kaolin is readily available, other clays may ultimately prove to be more effective for bowel contrast. Barium sulfate is another familiar and widely available material that can be used to produce a negative contrast effect. Concentrated bariums (60–70%) have been advocated as more effective oral gastrointestinal MR contrast agents [8]. Early experience with patients imaged after oral administration of barium indicates that this contrast agent marks the stomach and duodenum on MR images and can be useful for delineating the pancreas until a more favorable MR contrast agent becomes available [9].

TABLE 1: Classification of Gastrointestinal Tract Contrast Agents for MR Imaging

	Miscible Agents	Immiscible Agents
Positive agents	Gadopentetate dimeglumine Ferric ammonium citrate	Fats and oils
Negative agents	Barium sulfate Clays Superparamagnetic iron oxides	Perfluorocarbons Gas

Development of superparamagnetic iron oxide particles as gastrointestinal contrast agents followed their application in IV administration. Initial studies showed insufficient dynamic range, limited by artifacts produced by distortion of the magnetic field where particles concentrate in excess [10]. New preparations of iron oxide particles have been subjected to clinical trial as oral contrast agents (Fig. 2) [11, 12]. Careful particle design with particle size and other factors controlled to ensure prolonged homogeneous suspension is necessary to produce an agent that does not cause distortion [10]. Bowel loops containing iron oxide can be uniformly darkened with 100 mg of iron. T2-weighted images are more sensitive to the contrast agent than are T1-weighted images.

Perfluorocarbons also produce negative gastrointestinal tract contrast. Unlike the particulates, which are intended to mix with bowel contents, perfluorocarbons are immiscible. They act by replacing bowel contents with a material lacking protons and that therefore produces no proton MR signal. Perfluorooctylbromide (PFOB) has been studied in humans, producing readily identified loss of signal in the small bowel [13, 14]. PFOB transit time is rapid, so that the stomach may be nearly empty of contrast agent within 5 min of ingestion. Gas in the bowel produces a signal void that can be exploited to distend the gut and to produce contrast between bowel

Fig. 1.—Gadopentetate dimeglumine administered as oral contrast agent. SE 500/15 (1.5 T) MR images.  
A, Before contrast ingestion, stomach (S) is poorly distended; head of pancreas (arrow) is isointense with duodenum (D).  
B, After contrast ingestion, stomach and duodenum are distended and opacified by high-signal-intensity contrast material, producing good delineation of pancreatic head.

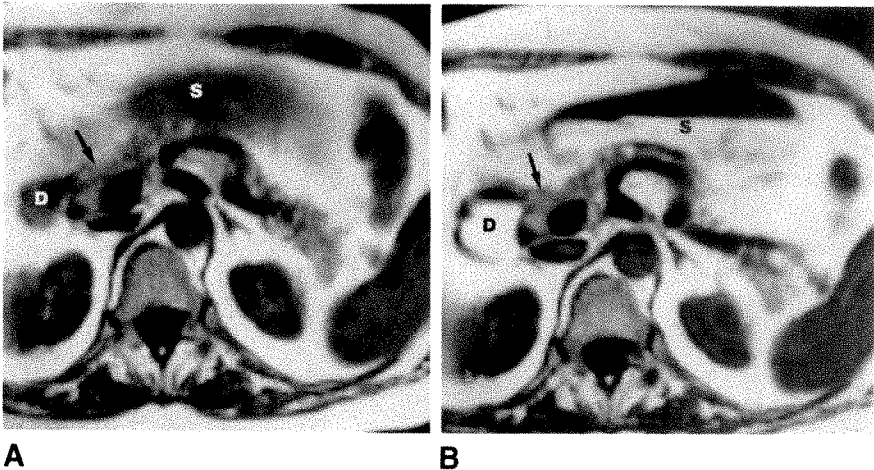
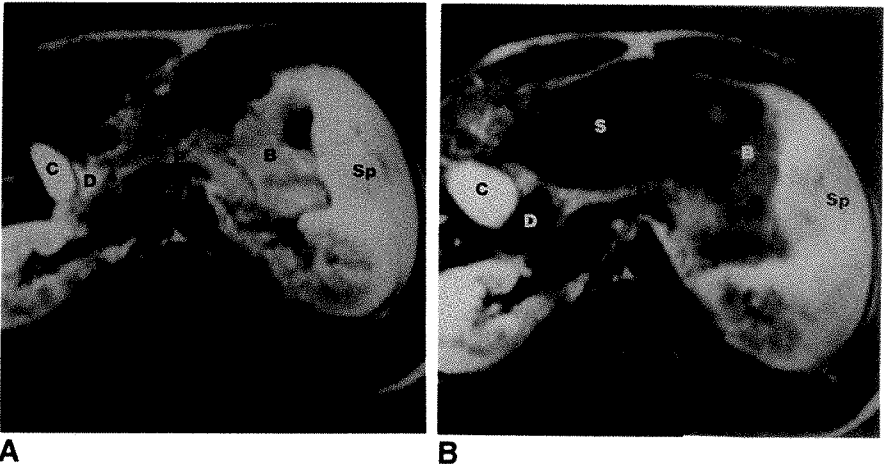


Fig. 2.—Superparamagnetic iron oxide administered as oral contrast agent. SE 2350/60 (1.5 T) MR images.  
A, Precontrast image shows pancreas (P) adjacent to nearly isointense duodenum (D) and small bowel (B).  
B, Postcontrast image shows signal void in stomach (S), duodenum, and small bowel created by iron oxide.  
Sp = spleen, C = gallbladder.





lumen and surrounding organs. Bowel gas can be associated with distortion of the signal from structures adjacent to the bowel through a magnetic susceptibility effect. Gas also may be introduced by oral ingestion of effervescent granules [15]. Pharmacologic paralysis of the bowel has been helpful in maintaining distension during imaging. This method has been advocated for outlining the pancreas [16, 17]. Air instilled through a rectal tube has proved useful in defining rectal carcinomas so that depth of invasion can be ascertained [18].

Several pediatric food formulas affect the signal in bowel. Although none has been developed systematically as a bowel contrast agent, administration of these materials before imaging has sometimes been found useful for imaging young children [19].

At present, no one MR contrast agent has been shown to be superior for gastrointestinal applications. Valid comparison studies will be extremely difficult to perform, particularly while the MR imaging parameters continue to change. As the protocols become better defined, indications for specific types of contrast material may emerge.

#### REFERENCES

- Chezmar JL, Rumancik WM, Megibow AJ, Hulnick DH, Nelson RC, Bernardino ME. Liver and abdominal screening in patients with cancer: CT versus MR imaging. *Radiology* **1988**;168:43-47
- Stark DD, Wittenberg J, Butch RJ, Ferrucci JT Jr. Hepatic metastases: randomized, controlled comparison of detection with MR imaging and CT. *Radiology* **1987**;165:399-406
- Newhouse JH, Pykett IL, Brady TJ, et al. NMR scanning of the abdomen: preliminary results in small animals. In: Witcofski RL, Karstaedt N, Partain CL, eds. *Proceedings of the Symposium on Nuclear Magnetic Resonance Imaging*. Winston-Salem, NC: Bowman Gray School of Medicine, Wake Forest University, **1981**;121-124
- Laniado M, Kornmesser W, Hamm B, Clauss W, Weinmann H-J, Felix R. MR imaging of the gastrointestinal tract: value of Gd-DTPA. *AJR* **1988**;150:817-821
- Wesbey GE, Brasch RC, Engelstad BL, Moss AA, Crooks LE, Brito AC. Nuclear magnetic resonance contrast enhancement study of the gastrointestinal tract of rats and a human volunteer using nontoxic oral iron solutions. *Radiology* **1983**;149:175-180
- Ang PGP, Li KCP, Tart RP, Storm B, Rolfes R. Geritol oil emulsion: ideal positive oral contrast agent for MR imaging. *Radiology* **1989**;172(P):522
- Listinsky JJ, Bryant RG. Gastrointestinal contrast agents: a diamagnetic approach. *Magn Reson Med* **1988**;8:285-292
- Tart RP, Li CPK, Fitzsimmons JR, Storm B, Mao J. Barium sulfate suspension as a negative oral contrast agent in MR imaging. *Radiology* **1989**;172(P):521
- Burton SS, Ros PR, Otto PM, et al. Barium MR imaging of the pancreas: initial experience. *Radiology* **1989**;172(P):517
- Hahn PF, Stark DD, Saini S, Lewis J, Wittenberg J, Ferrucci JT. Ferrite particles for bowel contrast in MR imaging: design issues and feasibility studies. *Radiology* **1987**;164:37-41
- Lönnemark M, Hemmingsson A, Bach-Gansmo T, et al. Effect of superparamagnetic particles as oral contrast medium at magnetic resonance imaging. *Acta Radiol* **1989**;30:193-196
- Hahn PF, Stark DD, Saini SS, et al. Clinical evaluation of superparamagnetic iron oxide particles as a gastrointestinal contrast agent for MR imaging. *Radiology* **1989**;172(P):160
- Mattrey RF, Hajek PC, Gyls-Morin VM, et al. Perfluorochemicals as gastrointestinal contrast agents for MR imaging: preliminary studies in rats and humans. *AJR* **1987**;148:1259-1263
- Mattrey RF. Perfluorooctylbromide: a new contrast agent for CT, sonography, and MR imaging. *AJR* **1989**;152:247-252
- Zerhouni EA, Brennecke CM, Fishman EK, Zimmer R, Soulen RL. Development of a gaseous contrast agent for MRI of the abdomen and pelvis. *Proceedings of the 34th annual meeting of the Association of University Radiologists*. Hartford, CT, **1986**;abstract no. 63
- Jenkins JPR, Braganza JM, Hickey DS, Isherwood I, Machin M. Quantitative tissue characterisation in pancreatic disease using magnetic resonance imaging. *Br J Radiol* **1987**;60:333-341
- Weinreb JC, Maravilla KR, Redman HC, Nunnally R. Improved MR imaging of the upper abdomen with glucagon and gas. *J Comput Assist Tomogr* **1984**;8:835-838
- Butch RJ, Stark DD, Wittenberg J, et al. Staging rectal cancer by MR and CT. *AJR* **1986**;146:1155-1160
- Gerscovich EO, McGahan JP, Buonocore MH, Ablin DS, Lindfors KK. The rediscovery of infant feeding formula with magnetic resonance imaging. *Pediatr Radiol* **1990**;20:147-151

## Review Article

## The Changing Epidemiology of Tuberculosis and Other Mycobacterial Infections in the United States: Implications for the Radiologist

C. Barry Buckner,<sup>1</sup> Richard E. Leithiser,<sup>2</sup> Craig W. Walker,<sup>1</sup> and Janice W. Allison<sup>1</sup>

Diseases consequent to infection with mycobacterial organisms, such as *Mycobacterium tuberculosis* and other mycobacterial species, remain a significant health problem in the United States. Over the past decade several new factors have amplified this problem, the most significant of which is the ongoing epidemic of infection with the human immunodeficiency virus. This review will discuss the changing epidemiology of mycobacterial disease and emphasize the significance of these changes to the radiologist.

Despite a dramatic decline over the past several decades, infections with *Mycobacterium tuberculosis* remain a significant public health problem in the United States. The previous steady decline in reported cases of tuberculosis (TB) ceased during the past few years, and cases actually have been increasing [1–3]. The major factor accounting for the recent resurgence of TB appears to be related to the epidemic of infection with the human immunodeficiency virus (HIV).

TB is becoming increasingly restricted to certain subsets of our society. Groups at inordinate risk include the homeless, IV drug abusers, immigrants and refugees from high-prevalence countries, HIV-infected persons, and residents of prisons and nursing homes [3]. Thus, efforts to reduce further the prevalence of TB will need to be targeted at these groups especially.

Additionally, care for TB patients has largely shifted from specialized institutions to the general medical community. Thus, much of the care for these patients is provided by physicians with relatively little experience in the management of TB. In view of this, it is incumbent that the radiologist assume an even greater responsibility for the prompt recognition of patients afflicted with this disorder.

Disease caused by mycobacterial species other than *M. tuberculosis* has become increasingly recognized. Numerous species, referred to as nontuberculous mycobacteria (NTMB), have been implicated in a broad spectrum of both pulmonary and extrapulmonary diseases [4, 5]. As with TB, the epidemic of infection with HIV has amplified the problem of diseases caused by NTMB.

### Epidemiology of Tuberculosis

Complete national reporting of TB first began in 1953 when 84,304 cases were reported, an incidence of 53 per 100,000. This represented a dramatic decline in the prevalence of TB in the United States from the beginning of this century, when TB was the leading cause of death in this country. Primarily because of improved public health measures and the advent of effective chemotherapy, further dramatic decrease occurred during the subsequent three decades. By 1985, the number of reported cases had declined to 22,201—an inci-

Received May 4, 1990; accepted after revision August 6, 1990.

<sup>1</sup> Department of Radiology, University of Arkansas for Medical Sciences, 4301 W. Markham St., Little Rock, AR 72205. Address reprint requests to C. B. Buckner.

<sup>2</sup> Department of Radiology, Arkansas Children's Hospital, Little Rock, AR 72205.

AJR 156:255–264, February 1991 0361–803X/91/1562–0255 © American Roentgen Ray Society

dence of approximately nine per 100,000. Between 1981 and 1984, the average rate of decline in TB cases was 6.7% per year [2].

The long-term steady decline of TB cases dramatically slowed in 1985, with only a very minimal (0.2%) further decline from 1984. In 1986, there was a 2.6% increase in the number of reported TB cases, the first increase in indigenous TB cases since national reporting began [1]. During 1987 and 1988, the last years for which complete data are available, the number of reported cases did not change significantly (Fig. 1). If the average annual rate of decline observed for the period between 1981 and 1984 had continued, there would have been almost 15,000 fewer reported cases of TB during the period from 1985 to 1988.

The increase in reported TB cases in recent years has largely been restricted to the age group of 25–44. Also, this increase has been primarily restricted to Hispanics and blacks. Likewise, there has been a change in the geographic distribution of TB such that a markedly disproportionate number of cases are reported from urban centers with large indigent populations. As is discussed later, this phenomenon probably relates primarily to the prevalence of HIV infection among subsets of these groups.

The recent trends in the pattern of increase in TB cases reflect a progressive polarization of the disease in the past several decades such that minority groups now suffer a markedly disproportionate burden of the reported cases. In 1987, 49% of reported TB cases were among minority groups exclusive of Hispanics (Fig. 2). If the latter group is included, then 64% of TB cases occurred among these racial and

ethnic minorities. Also, the median age of TB cases among non-Hispanic whites is 62 years as opposed to a median age of 39 years among members of minority groups [1].

#### Childhood Tuberculosis

Currently, about 5–6% of TB cases reported annually occur in children under 15 years of age, with 60% of these cases affecting children under 5 years of age [6, 7]. About 80% of pediatric TB cases currently occur in minority groups, with blacks and Hispanics accounting for the majority of these cases.

The vast majority of TB cases in children are related to primary infection. The radiologist frequently plays a key role in the recognition of such cases as the clinical presentation is often relatively benign and nonspecific. Thus, it is especially important to be alert to the most common radiologic presentation, namely, a focal area of parenchymal consolidation with associated hilar or mediastinal adenopathy (Fig. 3) [8]. Recovery of the tubercle bacillus may be difficult in the child with primary TB. Therefore, the diagnosis and management are often based on a positive tuberculin test in association with radiologic findings compatible with primary TB [7].

The prompt recognition of pediatric TB cases is especially important as other cases of TB frequently exist in the same environment. Usually the infectious source case is an adult in close contact with the child, such as a parent or grandparent. Transmission seldom occurs from one child to another (Fig. 3) [6]. Other children in the same environment should be tuberculin skin tested to detect occult primary infection so that appropriate prophylactic chemotherapy can be given.

Occasionally, in the very young child, primary TB may present as a serious life-threatening illness in which the diagnosis may be difficult to determine. The most severe cases are those caused by miliary dissemination of infection [9]. The radiologist frequently will be the initial physician to suspect this diagnosis, as the chest radiograph may be the most revealing examination performed in the evaluation of such a case. In 1979, for instance, it was noted that approximately 4% of childhood TB cases were miliary or meningeal [10]. Prognosis is generally good with prompt diagnosis and treatment unless meningeal TB, which has high morbidity and mortality rates, is present [9, 11]. The bacteriologic diagnosis of miliary TB may require invasive procedures such as transbronchial or even open lung biopsy (Fig. 4).

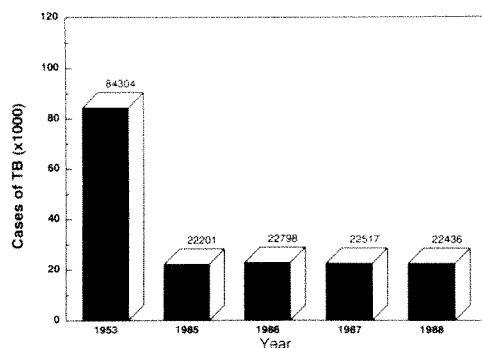
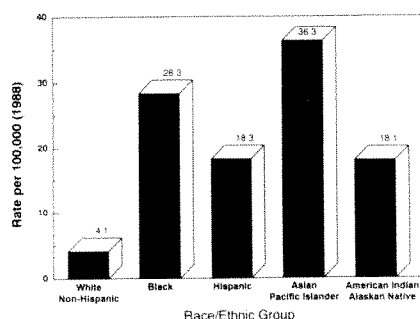
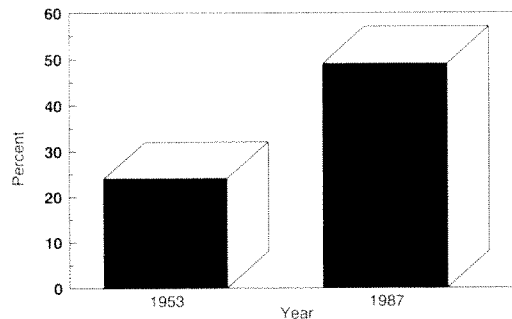


Fig. 1.—Annual number of tuberculosis (TB) cases during 1985–1988 compared with 1953. (Data obtained from [2].)



A



B

Fig. 2.—A, Racial/ethnic distribution of tuberculosis cases during 1988. (Data obtained from [2].)  
B, Change in proportion of tuberculosis cases occurring in minority groups.



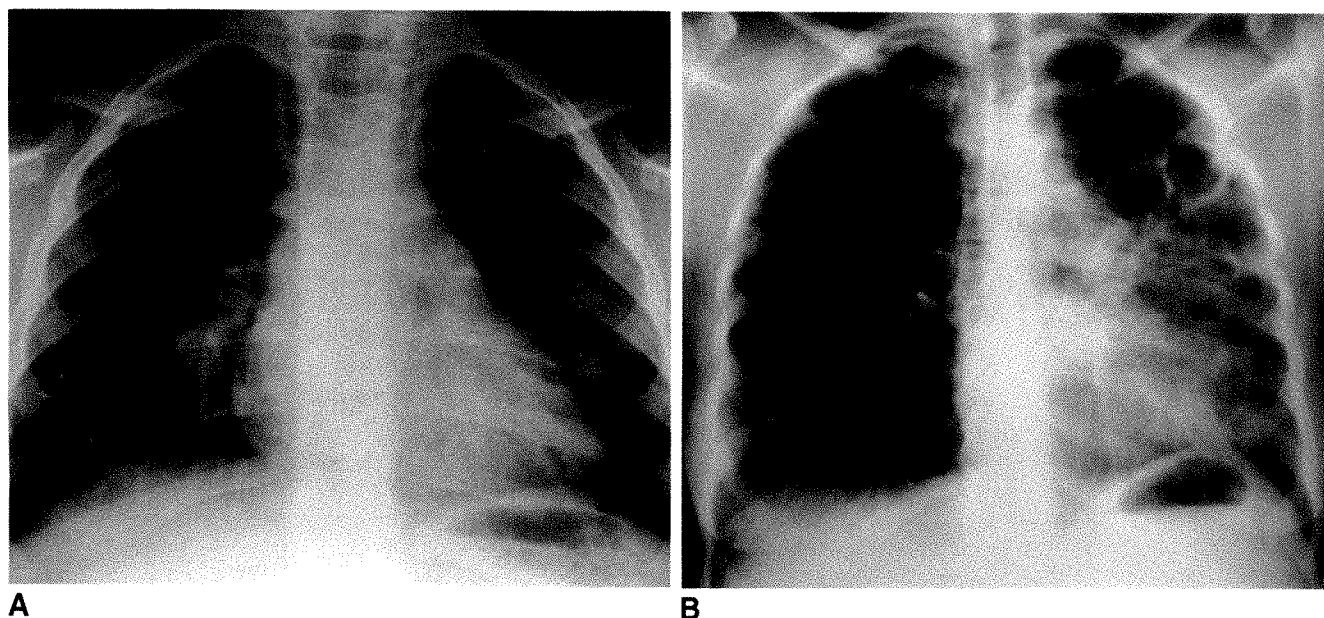


Fig. 3.—A, Anteroposterior chest radiograph reveals subtle alveolar disease in right lower lobe and hilar adenopathy in an asymptomatic 3-year-old child referred for evaluation of a positive purified protein derivative (PPD) skin test. The child's mother had been experiencing night sweats, weight loss, a productive cough, and fatigue for several months before she presented with pneumonia. Her sputum smear was positive for acid-fast bacilli.  
B, Posteroanterior chest radiograph of the mother shows left lung alveolar disease with cavitation. One other of her children also had a positive PPD test.

(Courtesy of R. Abernathy, Little Rock, AR.)

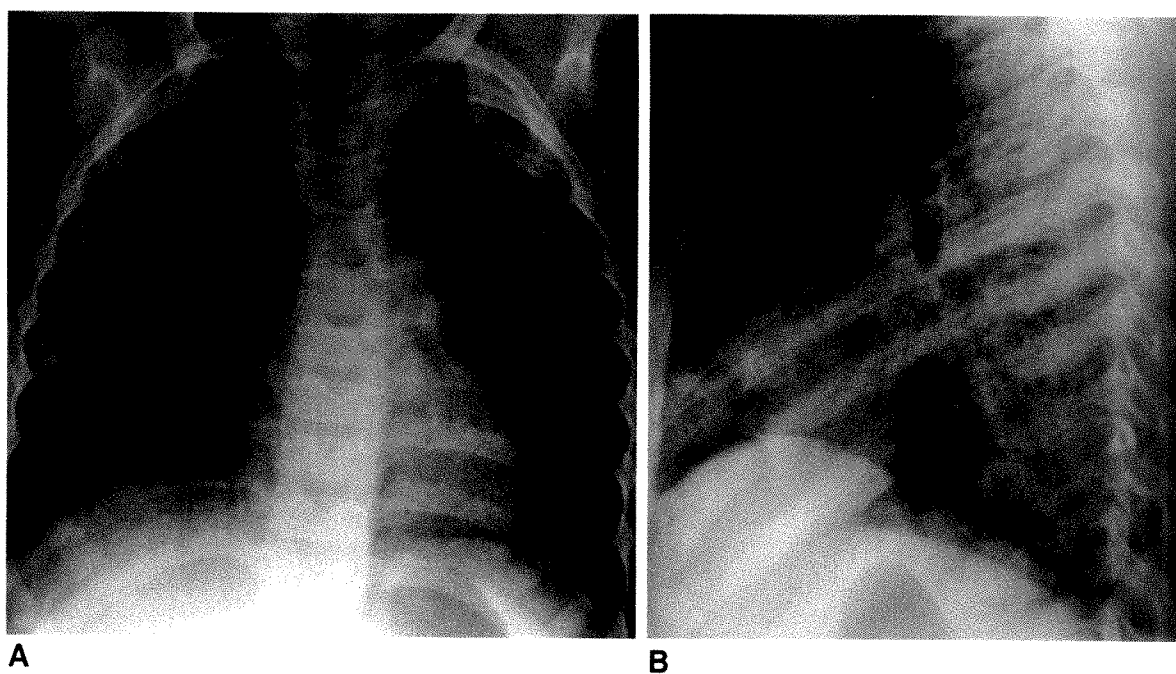


Fig. 4.—A and B, Anteroposterior (A) and lateral (B) chest radiographs of a 4-year-old black boy evaluated for fever, lethargy, and vomiting reveals numerous miliary nodules. Purified protein derivative (PPD) skin test was negative. Transbronchial biopsy and bone marrow aspirate failed to reveal acid-fast bacilli (AFB). Open lung biopsy finally revealed AFB and caseating granulomas. The patient's mother had occult cavitary tuberculosis, with a positive PPD test 10 years before and partial treatment. (Courtesy of R. Abernathy, Little Rock, AR.)

#### Adult Tuberculosis

At the present time more than 90% of TB cases occur in adults. As stated previously, TB in whites is heavily concen-

trated among the elderly. In minority groups, however, a high percentage of reported TB cases are in younger persons. In the latter group, certain subsets account for a disproportionate number of the cases. These include the indigent, the

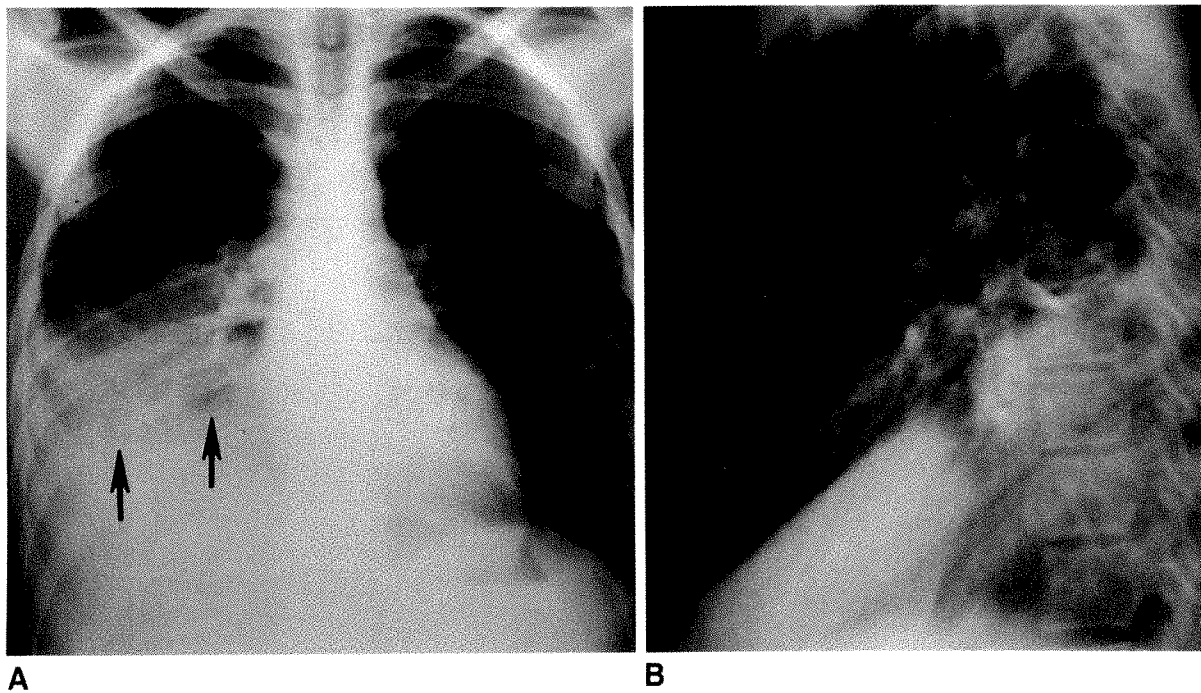


Fig. 5.—25-year-old black woman referred for presumed bacterial pneumonia unresponsive to antibiotics. The patient exhibited symptoms of a toxic reaction and fever (temperature, 40.6°C). Evaluation including percutaneous lung biopsy was negative. Sputum smears obtained several days after admission revealed acid-fast bacilli.

A and B, Posteroanterior (A) and lateral (B) chest radiographs show dense air-space consolidation with several cavities (arrows) involving right lower lobe. (Reprinted with permission from Euckner and Walker [12].)

homeless, persons in confined environments such as prisons, IV drug abusers, and especially HIV-infected persons.

Until recently, the vast majority of adult TB cases were due to postprimary disease. However, because of the declining prevalence of TB in the past several decades in our society, most adults now have negative purified protein derivative (PPD) skin tests, and are thus at risk for primary TB. Various reports now estimate that 10–30% of clinical TB in adults is due to primary infection [12–15].

The typical radiologic appearance of postprimary TB in the adult is widely known. Focal alveolar opacities, frequently with cavitation, in the apical and posterior segments of the upper lobes are the most typical pattern (Fig. 3). However, associated involvement of the anterior segments of the upper lobes and of the lower lobes is common, as has been recently emphasized by Woodring et al. [13]. Also, some adults with irregular nodular and linear opacities in the upper lung zones have active postprimary TB. Unfortunately, such changes may be dismissed as scarring indicative of healed TB. In such cases prior radiographs should be studied to assess for stability of the abnormalities [12, 13].

Primary TB in the adult may result in radiologic disease patterns that make the correct diagnosis of TB unlikely. Such patterns have been described in several articles as “atypical” manifestations of adult TB [14, 16]. Radiologic manifestations of primary TB in the adult include air-space disease restricted to the lower lobes, intrathoracic adenopathy, and pleural effusion.

When an adult patient presents with air-space disease

restricted to a lower lobe, TB is unlikely to be a prime diagnostic consideration. Most such cases will be presumed to have been caused by pyogenic bacterial infections. However, failure to respond to antimicrobial agents for common bacterial pneumonias should prompt concern that TB is a possible cause (Fig. 5). Also, application of a PPD skin test should be widely used to assist in the diagnosis of pulmonary infection (Fig. 6). As the prevalence of TB declines in our society, a positive PPD skin test becomes progressively more likely to indicate recent infection rather than merely being an index of remote infection.

Intrathoracic adenopathy related to primary TB in an adult patient is especially likely to result in an erroneous diagnosis (Fig. 7). Such patients often are considered more likely to have lymphoma, sarcoidosis, malignancy, or fungal disease. It is important to include TB in the differential diagnosis and to consider the results of the PPD skin test in the diagnostic evaluation.

Pleural effusion is a common manifestation of primary TB in the adult (Fig. 7). Such pleural effusions may be quite large. Particularly in elderly patients, the possibility of a tuberculous cause may be overlooked because of concern for such processes as malignant pleural effusion or congestive heart failure.

#### *Tuberculosis in the Elderly*

The highest case rate for TB in the United States currently is in the elderly, with the incidence of cases reported in patients over 65 years of age during 1988 nearly twice as

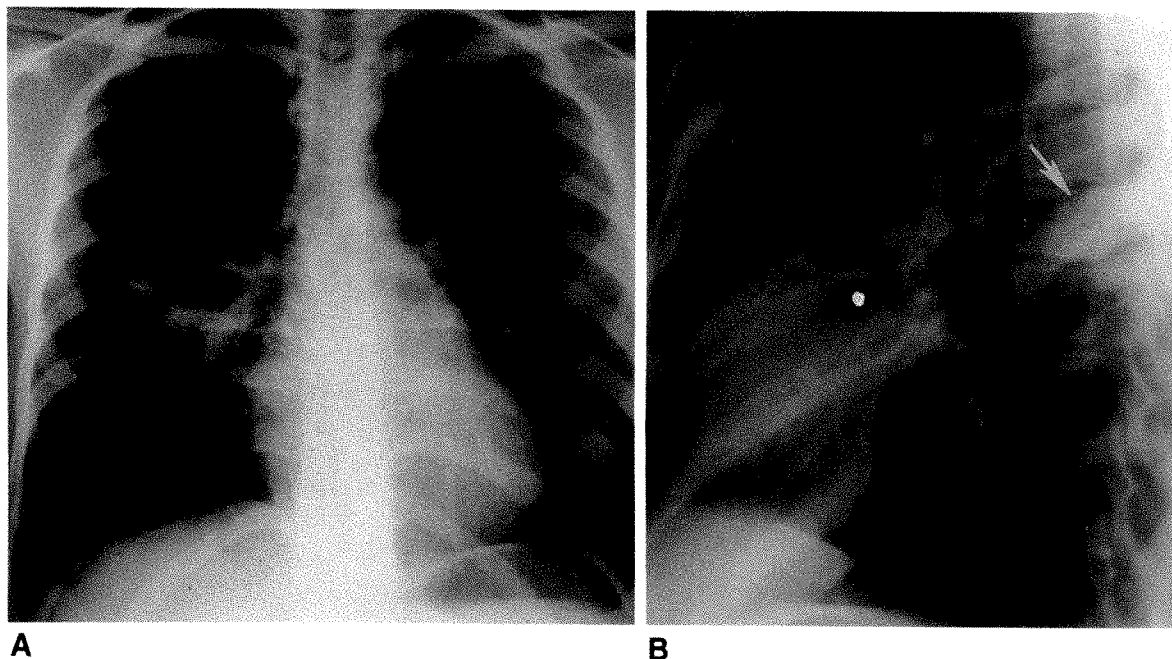


Fig. 6.—22-year-old white woman with conversion on routine purified protein derivative skin testing. A and B, Posteroanterior (A) and lateral (B) chest radiographs show focal air-space disease in superior segment of right lower lobe (arrow). Sputum smears and cultures were negative. Transbronchial biopsy showed granulomatous inflammation. The patient was treated with isoniazid and rifampin, although *Mycobacterium tuberculosis* was never cultured from biopsy specimens. Therapy resulted in subsequent clearing of radiologic abnormalities. (Reprinted with permission from Buckner and Walker [12].)

high as in any other age group (Fig. 8) [2]. Reports from the Centers for Disease Control (CDC) indicate that the national proportion of TB cases in persons over 65 years of age rose from 18.9% in 1960 to 29.7% in 1982, despite only a minimal increase in the proportion of the population within this age group during the same period [17]. The high rate of TB cases in the elderly largely relates to the prevalence of remote infection within this population that was acquired decades ago when TB was far more prevalent in our society [17–22]. Most active cases of TB in this group represent recrudescence of long-dormant infection, an event that may be promoted by waning immunocompetence with advanced age [20].

The diagnosis of TB in the elderly may be delayed because of the frequent coexistence of other medical problems within this population. The clinical and radiologic manifestations of other diseases prevalent in this population, such as malignancy, congestive heart failure, and nosocomial pneumonias, may divert attention away from TB as a diagnostic consideration. The presence of a large unexplained pleural effusion in an elderly patient may be attributed to congestive heart failure or malignancy, with little consideration of TB as a diagnosis. The radiologist may play an important role in such cases by raising the possibility of TB. An illustration of the problem of delayed diagnosis in this population is that currently 60% of TB cases first reported at death are within this group [1].

An additional problem regarding TB among the elderly relates to occasional outbreaks of this disease among members of this group confined to environments such as nursing homes. The recent work of Stead et al. [17, 18] has clearly

demonstrated this phenomenon. Outbreaks in such a setting may go unrecognized for long periods, as most persons infected by the source case do not manifest disease, and the small proportion that do develop clinically detectable TB do so only after a relatively long incubation period. Thus, surveillance programs that use tuberculin skin tests and chest radiographs are essential to monitor the undetected spread of TB in such settings.

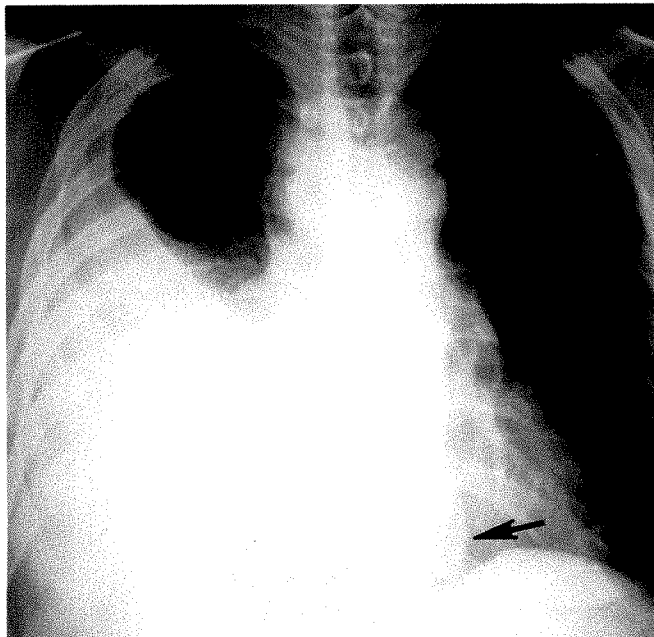
#### *Tuberculosis in Confined Populations*

Because of the infectious nature of TB, situations that involve large groups of people living in close proximity may result in outbreaks of TB within these populations [22]. Besides nursing homes, other closed populations in which such outbreaks may occur include mental hospitals, long-term-care hospitals, and prisons. Also, infections acquired in such environments may serve as vectors for infection of the general population. For example, a former prison inmate with infectious TB may have initially acquired the infection while incarcerated [23]. Thus, surveillance programs that use tuberculin skin tests are essential to monitor the possible undetected spread of TB in such settings.

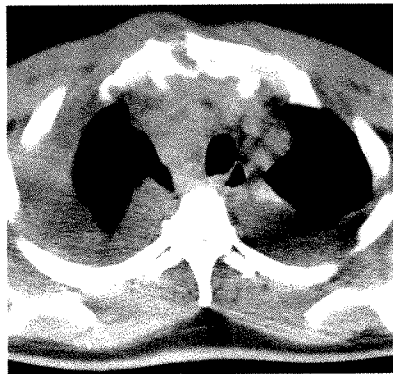
#### *Tuberculosis Among Immigrants and Minorities*

A disproportionate number of reported cases of TB arise among those who are foreign-born. In 1987, about one fourth

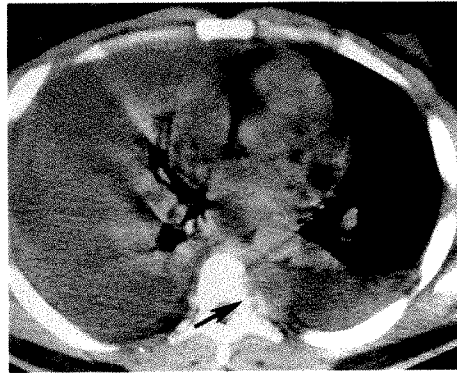




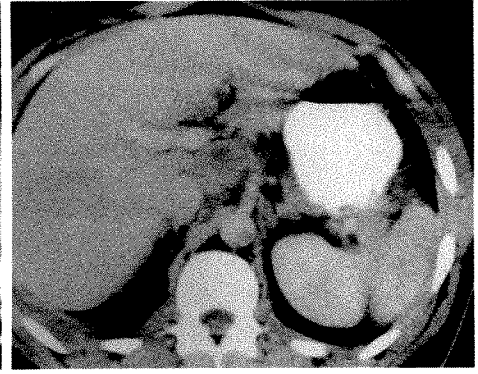
A



B



C



D

Fig. 7.—37-year-old black man (nonsmoker) who presented with fever and night sweats. Purified protein derivative skin test was positive.

A, Posteroanterior chest radiograph shows massive right pleural effusion, paratracheal adenopathy, and left paraspinal mass (arrow).

B–D, Chest CT scans show anterior mediastinal mass with sternal invasion, bilateral pleural effusions, left paraspinal mass with vertebral body erosion (arrow), and celiac lymphadenopathy.

Thoracentesis was nondiagnostic. Anterior mediastinotomy was performed after an inconclusive CT-directed biopsy of anterior mediastinal mass. Lymph nodes showing caseating necrosis and acid-fast bacilli were obtained. Subsequent culture revealed *Mycobacterium tuberculosis*.

(Reprinted with permission from Buckner and Walker [12].)

of reported TB cases occurred in these groups. Certain states report the majority of these cases, with California and New York accounting for about 50% [1]. Reported cases among foreigners tend to be in young persons, with the majority occurring in those who have recently arrived in this country [1, 24]. Thus, the magnitude of TB in this group relates largely to the influx of immigrants or refugees from countries with a high prevalence of TB. An additional problem with TB cases in foreigners is the relatively frequent resistance of their infections to commonly used antituberculous drugs.

#### *Tuberculosis in the Homeless*

TB is a common disease among the homeless population in this country [22, 25]. It has been estimated that the prevalence of latent TB among this group is 18–51% [25]. Factors explaining the high prevalence of infection in this group include low socioeconomic status and the frequent background of living in crowded, poorly ventilated environ-

ments or institutionalization in mental hospitals or other settings [25].

The frequent close contact of the homeless in a closed environment, such as a shelter, may promote widespread dissemination of TB from an active source case within the group. Contact tracing of infectious cases within this population may be especially difficult because of the transient and sometimes uncooperative nature of the individuals. Likewise, the extended chemotherapy necessary for clinical TB may be especially difficult to accomplish. Innovative outreach programs with social workers and other support staff are essential for successful management of TB in this segment of our population.

#### *Tuberculosis in HIV-Infected Patients*

Numerous reports in the past several years have shown an increased rate of TB in persons who are infected with HIV [26–34]. Early reports described a very high prevalence of

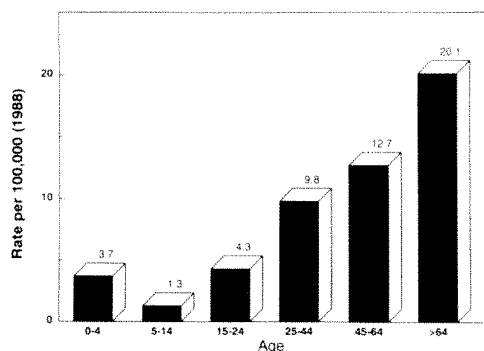


Fig. 8.—Incidence of tuberculosis by age during 1988. (Data obtained from [2].)

TB in Haitians who were afflicted with AIDS [26, 28, 29]. In 1984, Pitchenik et al. [26] reported that 60% of Haitians with AIDS in the group they studied had TB diagnosed during the course of their illness. In contrast, only 2.7% of non-Haitians with AIDS in their group had TB. Subsequent studies have shown a moderately high prevalence of TB in other populations of HIV-infected individuals [27–29]. In a report from New York in 1986, Louie et al. [27] noted that TB developed in 8.6% of 280 patients with AIDS, with a 7% rate of TB in male homosexuals and an 11% rate of TB in IV drug abusers. Other reports have shown a particularly high prevalence (about 20%) of TB among the subset of HIV-positive persons who are IV drug abusers [28].

It is now generally believed that the occurrence of clinical TB among HIV-infected populations is largely a reflection of the prevalence of latent TB among the various groups affected (Fig. 9) [30, 32–34]. For example, the prevalence of positive tuberculin skin tests (PPD) among Haitians living in Florida was reported to range from 78.5% to 91.2% [26]. Also, ethnic and racial minorities, as well as IV drug abusers, have a higher prevalence of remote TB than do non-Hispanic white male homosexuals [1].

Recent reports have emphasized that TB may develop during the course of HIV infection before the development of other illnesses indicative of AIDS [34]. Thus, it appears that the progressive immunologic deterioration that characterizes HIV infection predisposes patients with latent TB to develop clinical TB. In patients with HIV infection who have progressed to a clinical diagnosis of AIDS, up to 70% of patients with TB will show extrapulmonary manifestations. In fact, extrapulmonary TB is currently used by the CDC as an index infection for the diagnosis of AIDS in an HIV-infected patient [35].

In view of the high risk that clinical TB will develop in HIV-infected patients with occult TB, it is now recommended that all identified HIV-infected persons be tested with PPD skin tests [31]. During the early phases of HIV infection, cell-mediated immunity is often sufficiently intact that the PPD skin test will be a reliable index of previous infection with *M. tuberculosis*. Reactors should be given prophylactic antituberculous medication regardless of their age. In the later stages of HIV infection, particularly after a diagnosis of AIDS, the PPD skin test becomes less reliable owing to anergy.

Additionally, it is recommended that patients with clinical TB who are at known risk for HIV infection or who have atypical clinical and radiologic features be tested for HIV [31, 32].

Early in the course of HIV infection, the clinical and radiologic manifestations of TB may be similar to those of postprimary TB in patients without HIV infection [36]. As the patient's immunologic status deteriorates, the pattern of pulmonary involvement becomes more atypical, with coarse reticulonodular infiltrates a common manifestation. Also, intrathoracic adenopathy is a common feature of the disease at this stage. Pleural effusions may occur. It is often very difficult to discriminate between pulmonary manifestations of TB in AIDS patients and other infectious and noninfectious entities common in this disease. However, pleural effusion and adenopathy should suggest a cause other than *Pneumocystis carinii* pneumonia, which is the most common opportunistic infection in these patients [36].

A variety of extrapulmonary manifestations of TB have been seen in patients with AIDS. These include CNS manifestations, bone involvement, gastrointestinal involvement, and skin and soft-tissue involvement [35, 37]. *M. tuberculosis* has even been cultured from the blood of a patient with AIDS [38].

Infections with *M. tuberculosis* in patients with HIV infection respond well to standard antituberculous medication. Unfortunately, cure of TB in a patient with clinical AIDS does little to forestall death from other complications of the disease.

#### Epidemiology of Nontuberculous Mycobacteria

Although the existence of NTMB has long been known, it was not until the middle of this century that disease caused by these organisms was recognized [4]. Unlike TB, human-to-human transmission of NTMB occurs rarely, if ever. Also, diseases caused by NTMB are not reported to the CDC, making it difficult to determine the prevalence of disease resulting from these organisms. It has been estimated that

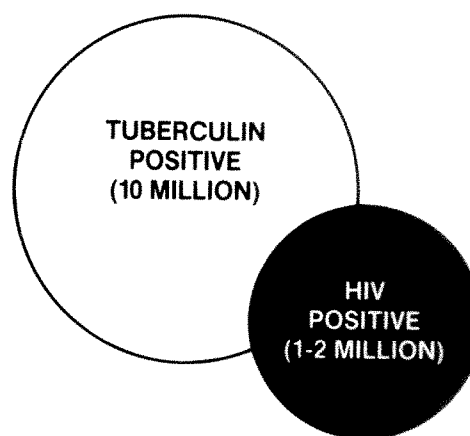


Fig. 9.—Relationship between infection with *Mycobacterium tuberculosis* and human immunodeficiency virus (HIV). Coinfection with *M. tuberculosis* and HIV places individuals at high risk for development of clinical tuberculosis. Groups at high risk for coinfection include IV drug abusers and racial/ethnic minorities.

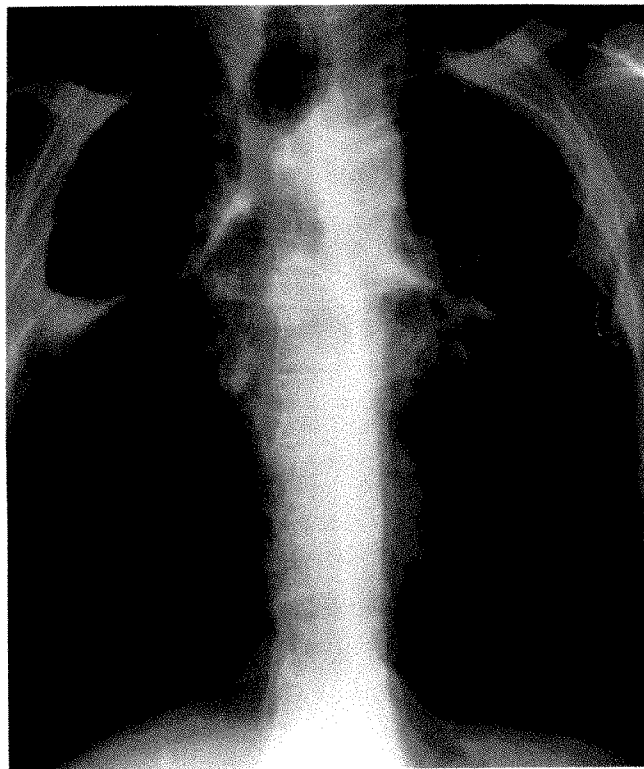


Fig. 10.—Posteroanterior chest radiograph reveals cavitary disease in upper lobes of a 59-year-old white male smoker with a history of chronic obstructive pulmonary disease. *Mycobacterium avium-intracellulare* pneumonia was diagnosed 2 years before by positive sputum cultures and was treated with isoniazid and rifampin for 1 year with poor response and continued positive sputum cultures. Weight loss, anorexia, fever, chills, and night sweats continued, and he became malnourished and cachectic. Purified protein derivative skin test remained negative.

disease caused by NTMB is about one fifth as common as TB [4].

Although many species of NTMB have been implicated in human disease, most clinically significant pulmonary or disseminated disease is caused by either *Mycobacterium kansasii* or *Mycobacterium avium-intracellulare* (MAI) [4, 39]. Geographic variations in the prevalence of *M. kansasii* and MAI infection have been noted, with the former more commonly seen in urban areas and the latter in rural areas [2, 17].

Before the epidemic of HIV infection, pulmonary disease due to NTMB was seen primarily in elderly patients with underlying chronic lung disease [4, 40]. Characterization of disease in these patients has been difficult because of the frequent colonization of the upper airways with NTMB in members of this patient population who have no demonstrable evidence of significant pulmonary disease [4, 5, 39, 40]. Repeatedly positive sputum cultures and failure to demonstrate other causes for chest radiologic abnormalities assist in defining true disease [39]. The radiologic manifestations of NTMB in this group overlap with and in general are similar to that seen in postprimary TB [5]. Cavitary upper lobe disease commonly is seen (Fig. 10). Disease caused by these organisms tends to be more indolent than that seen with TB. Disease caused by *M. kansasii* responds fairly well to antituberculous chemotherapy, whereas the response of MAI to regimens of four to five drugs is frequently poor.

Recent reports have shown that some patients with disease due to NTMB may have patterns of disease dissimilar to the upper lobe cavities described above [5, 40]. A pattern of patchy, nodular infiltrates without an upper lobe predominance has been described.

A new pattern of disease caused by NTMB, especially MAI, has emerged among HIV-infected populations. Several reports have shown evidence of disseminated MAI infection at autopsy in 50% or more of patients with AIDS [41, 42], with disseminated MAI infection diagnosed antemortem in approximately 20% of one large group of AIDS patients [42]. Unlike TB, which may be diagnosed early in the course of HIV infection before a clinical diagnosis of AIDS, MAI infection is usually diagnosed after AIDS develops [35].

Blood cultures are usually positive for MAI in affected persons. Also, stool, bone marrow, and urine cultures are frequently positive. Cultures of sputum or bronchial washings may be positive for MAI despite a normal chest radiograph [43].

A variety of abnormalities seen on chest radiographs have been associated with MAI infection in patients with AIDS. These include focal or diffuse coarse nodular opacities or areas of parenchymal consolidation. Hilar and mediastinal adenopathy also have been reported (Fig. 11) [43]. It is frequently difficult, if not impossible, to discriminate between radiologic manifestations due to MAI and any of a variety of other AIDS-related abnormalities seen on the chest radiograph. Treatment for MAI infection in AIDS patients is generally ineffective, although MAI infection is seldom the primary cause of death in these patients [42].

### Summary

After decades of steady decline, the number of reported TB cases in the United States has ceased to decline, and has actually increased slightly. The increase in TB cases has been restricted largely to minority groups in large urban areas. It has become increasingly apparent that the epidemic of HIV infection is largely responsible for this event.

Owing to the progressive polarization of TB into certain subsets of our society, the frequency with which radiologists encounter this disease will vary widely from one geographic location to another, and with the socioeconomic and racial constituency of different practices. Thus, in some practices even the more typical cases of adult TB will be encountered infrequently, whereas in other practices unusual presentations of TB will be sufficiently common to create difficulties in the differential diagnosis of individual cases. A knowledge of current epidemiologic trends, as well as a familiarity with both common and uncommon radiologic presentations of TB, will enhance the radiologist's ability to facilitate prompt and accurate diagnosis of TB cases.

The epidemic of HIV infection has also changed the spectrum of disease associated with NTMB. Characterization of clinical disease due to these organisms continues to be difficult, with no specific radiologic features to discriminate these infections from TB.



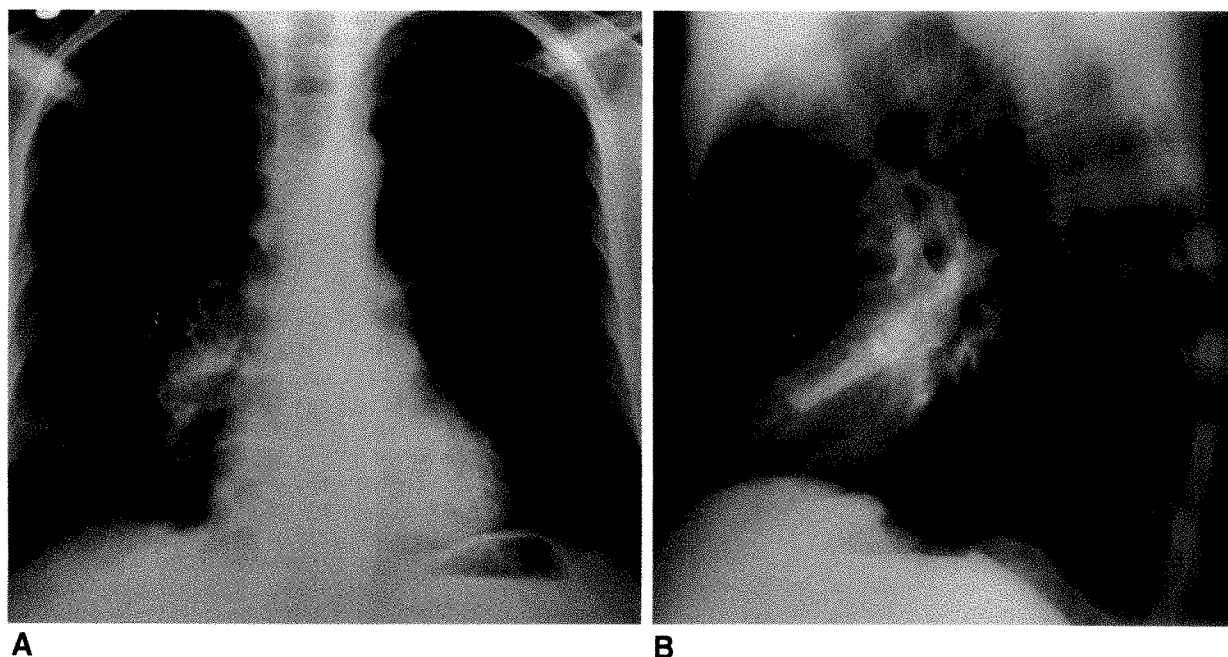


Fig. 11.—35-year-old homosexual man with established diagnosis of AIDS and history of *Pneumocystis carinii* pneumonia presented with cough and fever.

A and B, Posteroanterior (A) and lateral (B) radiographs at presentation reveal right hilar adenopathy and right middle lobe pneumonia. Bronchoscopy was performed and stains of bronchial washings were positive for acid-fast bacilli. Subsequent culture was positive for *Mycobacterium avium-intracellulare*.

#### REFERENCES

- Block AB, Rieder HL, Kelly GD, Cauthen GM, Hayden CH, Snider DE. The epidemiology of tuberculosis in the United States: implications for diagnosis and treatment. *Clin Chest Med* 1989;10(3):297-313
- Centers for Disease Control. Update: Tuberculosis elimination—United States. *MMWR* 1990;39:153-156
- Centers for Disease Control. A strategic plan for the elimination of tuberculosis in the United States. *MMWR* 1989;38:269-272
- O'Brien RJ. The epidemiology of nontuberculous mycobacterial disease. *Clin Chest Med* 1989;10(3):407-418
- Woodring JH, Vandiviere HM. Pulmonary disease caused by nontuberculous mycobacteria. *J Thorac Imaging* 1990;5(2):64-76
- Starke JR. Modern approach to the diagnosis and treatment of tuberculosis in children. *Pediatr Clin North Am* 1988;35(3):441-464
- Snider DE, Rieder HL, Combs D, Bloch AB, Hayden CH, Smith MHD. Tuberculosis in children. *Pediatr Infect Dis J* 1988;7:271-278
- Weber AL, Bird KT, Janower ML. Primary tuberculosis in childhood with particular emphasis on changes affecting the tracheobronchial tree. *AJR* 1968;103:123-132
- Schuit KE. Miliary tuberculosis in children. *Am J Dis Child* 1979;133:583-585
- Powell KE, Meador MP, Farer LS. Recent trends in tuberculosis in children. *JAMA* 1984;251(10):1289-1292
- Stansberry SD. Tuberculosis in infants and children. *J Thorac Imaging* 1990;5(2):17-27
- Buckner CB, Walker CW. Radiologic manifestations of adult tuberculosis. *J Thorac Imaging* 1990;5(2):28-37
- Woodring JH, Vandiviere HM, Fried AM, Dillon ML, Williams TD, Melvin IG. Update: the radiographic features of pulmonary tuberculosis. *AJR* 1986;146:497-506
- Miller WT, Mac Gregor RR. Tuberculosis: frequency of unusual radiographic findings. *AJR* 1978;130:867-875
- Khan MA, Kovnat DM, Bachus B, Whitcomb ME, Brody JS, Snider GL. Clinical and roentgenographic spectrum of pulmonary tuberculosis in the adult. *Am J Med* 1977;62:31-38
- Palmer PES. Pulmonary tuberculosis—usual and unusual radiographic presentations. *Semin Roentgenol* 1979;14:204-243
- Stead WW, Lofgren JP, Warren E, Thomas C. Tuberculosis as an endemic and nosocomial infection among the elderly in nursing homes. *N Engl J Med* 1985;312(23):1483-1487
- Stead WW. Tuberculosis among elderly persons: an outbreak in a nursing home. *Ann Intern Med* 1981;94:606-610
- Stead WW, To T. The significance of the tuberculin test in elderly persons. *Ann Intern Med* 1987;107:837-842
- Stead WW. Does the risk of tuberculosis increase in old age? *J Infect Dis* 1983;147(5):951-955
- Stead WW, To T, Harrison RW, Abraham JH. Benefit-risk considerations in preventive treatment for tuberculosis in elderly persons. *Ann Intern Med* 1987;107:843-845
- Stead WW. Special problems in tuberculosis: tuberculosis in the elderly and in residents of nursing homes, correctional facilities, long-term care hospitals, mental hospitals, shelters for the homeless, and jails. *Clin Chest Med* 1989;10(3):397-405
- Stead WW. Undetected tuberculosis in prison: source of infection for community at large. *JAMA* 1978;240(23):2544-2547
- Powell KE, Brown ED, Farer LS. Tuberculosis among Indochinese refugees in the United States. *JAMA* 1983;249(11):1455-1460
- Schieffelin CW, Snider DE. Tuberculosis control among homeless populations. *Arch Intern Med* 1988;148:1843-1846
- Pitcheik AE, Cole C, Russell BW, Fischl MA, Spira TJ, Snider DE. Tuberculosis, atypical mycobacteriosis, and the acquired immunodeficiency syndrome among Haitian and non-Haitian patients in south Florida. *Ann Intern Med* 1984;101:641-645
- Louie E, Rice LB, Holzman RS. Tuberculosis in non-Haitian patients with acquired immunodeficiency syndrome. *Chest* 1986;90(4):542-545
- Sunderam G, McDonald RJ, Maniatis T, Oleske J, Kapila R, Reichman LB. Tuberculosis as a manifestation of the acquired immunodeficiency syndrome (AIDS). *JAMA* 1986;256(3):362-366
- Pitcheik AE, Burr J, Suarez M, Fertel D, Gonzalez G, Moas C. Human T-cell lymphotropic virus-III (HTLV-III) seropositivity and related disease among 71 consecutive patients in whom tuberculosis was diagnosed. *Am Rev Respir Dis* 1987;135:875-879
- Chaisson RE, Schecter GF, Theuer CP, Rutherford GW, Echenberg DF, Hopewell PC. Tuberculosis in patients with the acquired immunodeficiency syndrome. *Am Rev Respir Dis* 1987;136:570-574

## Value of Sonography in Monitoring the Therapeutic Response of Mediastinal Lymphoma: Comparison with Chest Radiography and CT

Karl Wernecke<sup>1</sup>  
 Pierre Vassallo<sup>1</sup>  
 Gudula Hoffmann<sup>1</sup>  
 Peter E. Peters<sup>1</sup>  
 Richard Poetter<sup>2</sup>  
 Ernst Rummeny<sup>1</sup>  
 Peter Koch<sup>3</sup>

The aim of this retrospective study was to assess the diagnostic value of mediastinal sonography, compared with that of chest radiographs and CT, in the follow-up of patients with mediastinal lymphomas and in the prediction of clinical outcome. The sonograms, chest radiographs, and CT scans of 40 consecutive patients with Hodgkin ( $n = 29$ ) and non-Hodgkin ( $n = 11$ ) lymphoma obtained before and after completion of therapy were analyzed blindly and independently by three radiologists and compared with clinical outcome. Nine patients were treated with radiotherapy, 12 with chemotherapy, and 19 with combined therapy. Therapeutic response was assessed from all available clinical and biochemical findings as well as from the combined results of all imaging studies performed on further follow-up. The sonograms showed obvious changes in the size and echogenicity of the mediastinal lymphomas that corresponded closely with the response to therapy. Sonography showed complete regression of the lymphomas in 30 patients who had complete remission. In five patients with incomplete remission, sonographic diagnoses were correct. All lymph nodes, irrespective of size, detected with sonography after a phase of complete remission indicated recurrence (five patients). Sonographic findings corresponded with those of CT in 25 (81%) of 31 cases. Clinical outcome suggested that the sonographic findings were more reliable in the five cases in which CT and sonographic findings conflicted. Chest radiographs were inadequate for monitoring the response of mediastinal lymphomas to therapy; in 17 (43%) of 40 cases, a false impression was obtained of the extent and therapeutic response of mediastinal lymphomas.

The results of this study indicate that sonography is clearly superior to chest radiographs and comparable to CT for monitoring patients with mediastinal lymphomas.

*AJR* 156:265-272, February 1991

Chest radiographs are usually used to monitor the therapeutic response of patients with mediastinal lymphomas. In most countries, CT and MR imaging are reserved for cases with equivocal findings on chest radiographs because these studies are time-consuming and expensive [1, 2]. Lately, the question has arisen as to whether routine CT or MR should be performed on completion of therapy as a baseline study for subsequent correlation with follow-up studies [1-3]. The availability of mediastinal sonography [4, 5] offers an effective and inexpensive imaging method with a higher sensitivity than conventional radiographs for the detection of mediastinal tumors [6].

The aim of this retrospective study was to assess the diagnostic value of mediastinal sonography for the follow-up of patients with mediastinal lymphomas and for the prediction of clinical outcome in these patients as compared with chest radiographs and CT. A clinical follow-up of 12-38 months (average, 26 months) after therapy and histologic findings in patients with incomplete remission or recurrence were used as the gold standard to establish the results of treatment.

Received March 21, 1990; accepted after revision August 13, 1990.

<sup>1</sup> Institute of Clinical Radiology, University of Münster Medical School, Albert-Schweitzer-Str. 33, D-4400 Münster, Germany. Address reprint requests to K. Wernecke.

<sup>2</sup> Clinic of Radiotherapy, University of Münster Medical School, D-4400 Münster, Germany.

<sup>3</sup> Medical Clinic A, University of Münster Medical School, D-4400 Münster, Germany.

0361-803X/91/1562-0265  
 © American Roentgen Ray Society

## Materials and Methods

Sonograms were obtained in 40 patients undergoing treatment for Hodgkin ( $n = 29$ ) and non-Hodgkin ( $n = 11$ ) lymphomas for 8–48 months and the findings were compared retrospectively with the clinical course of the disease and with CT, chest film, and histologic findings. Sonography was performed before therapy and at least once on completion of therapy. CT was performed before therapy in all patients. Fourteen patients had one and 17 patients had two to six CT studies 1–48 months after therapy. In nine patients, CT had been performed only once before therapy. Chest radiographs were obtained in all cases before, during, and after therapy. A total of 194 sonograms (mean, five examinations per patient), 142 CT scans (mean, three examinations per patient), and 231 chest radiographs in two planes (mean, seven examinations per patient) were evaluated.

The patients included 22 women and 18 men 14–63 years old (mean, 31 years). Histologic confirmation of lymphoma was obtained in 36 patients with peripheral lymph node biopsy and in four patients with isolated mediastinal involvement at thoracotomy ( $n = 2$ ) or percutaneous biopsy ( $n = 2$ ). Nine patients with Hodgkin lymphoma were treated with radiotherapy alone, 12 patients (three Hodgkin lymphomas, nine non-Hodgkin lymphomas) received only chemotherapy, and 19 patients (17 Hodgkin lymphomas, two non-Hodgkin lymphomas) received combined therapy.

### *Radiologic and Clinical Evaluation of Therapeutic Response*

The criteria described by Glazer et al. [7] for the differentiation of pathologic from normal lymph nodes were used for the evaluation of the CT scans obtained before therapy. All lymph nodes with a short axis diameter greater than 1.0 cm were considered diseased. Mediastinal lymph nodes that regressed to a short axis diameter of less than 1.0 cm after therapy were considered indicative of full remission. These criteria referred only and specifically to CT.

When CT showed a residual lesion with a diameter greater than 1.0 cm after completion of therapy, these findings were classified as doubtful remission and were followed up with CT. If such lesions remained constant in size or showed further shrinkage without further therapy, they were considered to represent scar tissue.

The CT criteria for incomplete remission were fulfilled when a tumor showed incomplete regression (persistent lesion with a diameter greater than 1.0 cm) during therapy and when an increase in tumor size despite continuation of therapy was observed on further follow-up.

Tumor recurrence was diagnosed when renewed growth of the mediastinal tumor was observed after complete remission was documented with CT.

The chest radiographs were evaluated according to generally accepted criteria [8–13]. All pleuromediastinal lines were assessed and their displacement recorded as indicative of mediastinal tumor. A semiquantitative assessment of tumor regression during therapy was performed by using a method described by North et al. [14] for measuring the maximum transverse mediastinal diameter. A return of the pleuromediastinal lines to normal was assumed to indicate full remission. After treatment of large mediastinal tumors, residual widening was observed occasionally and was classified primarily as doubtful remission. Those cases showing no change or further mediastinal shrinkage over a period of at least 1 year were reclassified as residual mediastinal widening. Residual mediastinal widening was clearly distinguished from postirradiation changes occurring 2–3 months after radiotherapy as described by North et al. [15]. Those tumors showing incomplete regression after therapy and growth on further follow-up were assumed to be in incomplete remission.

The diagnosis of recurrence was assumed when mediastinal widening recurred on chest radiographs after a complete remission (normal chest radiograph).

The referring oncologists were responsible for the assessment of

the patients' clinical course. Clinical outcome was assessed from clinical findings (i.e., clinical history and examination) and biochemical tests (including erythrocyte sedimentation rate, blood count, differential count, LDH, alkaline phosphatase, serum iron, and ferritin levels), as well as from all imaging and histologic findings in patients with incomplete remission or recurrence. During the first 2 years after therapy, all patients were assessed clinically and radiologically at 3-month intervals. Thirty patients (23 Hodgkin lymphoma, seven non-Hodgkin lymphoma) went into complete remission as indicated by clinical and radiologic follow-up for 12–38 months (average, 26 months) after therapy. All five patients with incomplete remission (one Hodgkin lymphoma, four non-Hodgkin lymphoma) died of uncontrolled tumor growth, which was verified at autopsy. Of five patients with histologically confirmed recurrence (three Hodgkin lymphoma, two non-Hodgkin lymphoma), three were successfully treated and two died.

### *Sonographic Examination Technique and Image Analysis*

Sonography was performed with transducers of 3.5 and 5.0 MHz (LSC 7000, Picker International, Munich, Germany). A standard sonographic examination was performed in all patients. Each patient was examined in the supine position via the suprasternal approach, which allows visualization of the supraaortic, paratracheal, and aorticopulmonary regions to advantage [4]. Sonography was then performed via the parasternal approach, in both right and left decubitus positions, to assess the prevascular, pericardial, and subcarinal regions [5]. Suprasternal sonography was performed in all cases. The technique of parasternal sonography was developed in September 1986 and therefore was performed only in the second half of the study in 22 patients.

All structures delineated from mediastinal fat and connective tissue on initial sonograms were considered to be involved lymph nodes irrespective of their size and echogenicity; these criteria are identical to those used in abdominal lymph node sonography [16–18]. All mediastinal lymph nodes were classified according to their echogenicity as either hypoechoic, which were well delineated from surrounding connective tissue; echogenic, which were just delineated from surrounding connective tissue; and hyperechoic, which were difficult to delineate from surrounding connective tissue. Complete sonographic regression of mediastinal lymph nodes after therapy was interpreted as a complete remission. All mediastinal masses detected with sonography irrespective of size and echogenicity were interpreted as residual lymphomas. All new nodular lesions detected after an episode of complete remission were interpreted as mediastinal tumor recurrence.

The sonograms were evaluated prospectively by one experienced radiologist. The diagnostic value of the sonographic findings was assessed retrospectively by comparison with the patient's clinical outcome. The chest radiographs and CT scans were analyzed retrospectively by two independent radiologists without knowledge of the clinical outcome and sonographic findings. Each observer was asked to state whether a full remission had been reached after completion of therapy. Finally, the diagnostic information obtained from all three examinations regarding response of the mediastinal tumor to therapy was compared. Particular attention was given to the chronologic sequence of all examinations procedures, and the stage at which changes were detected with the criteria previously described.

## Results

### *Sonographic Findings*

In all 30 patients with complete remission, multiple lymph nodes 1–8 cm in diameter (mean, 3 cm) were evident in several mediastinal regions at initial investigation (supraaortic



region, 30 patients; paratracheal region, 28 patients; aortico-pulmonary window, four patients; prevascular region, 10 patients; subcarinal region, six patients; pericardial region, two patients).

The lymph nodes were hypoechoic in 18 cases, echogenic in six cases, and hyperechoic in six cases. In 27 of 30 patients, all lymphomas disappeared after therapy (Fig. 1). In 10 patients, in whom sonograms had been obtained frequently during therapy, changes in the echogenicity and size of the mediastinal lymph nodes were monitored closely. Halfway through the therapeutic protocol, a severe shrinkage of all lymph nodes was evident in all 10 cases: among the sonographically detected enlarged lymph nodes, the smaller nodes (diameter, <2.0 cm) had completely disappeared sonograph-

ically at this point, and larger lymph nodes showed a reduction in diameter of 30–60%. The echogenicity of all lymph nodes increased progressively during therapy to a stage at which no further delineation from surrounding connective tissue was possible. In 27 of 30 patients, complete remission with complete regression of all mediastinal lymphomas was correctly diagnosed with sonography.

In three patients with extensive prevascular masses before therapy (diameter, 5–10 cm), a large tumor (diameter, 2.5–4.0 cm) persisted after therapy that was considered a residual lymphoma (Figs. 2A and 2B). On further sonographic follow-up without therapy for 3–15 months, further shrinkage of the mass and the appearance of the typical thymic tongue configuration were observed (Fig. 2C). Owing to these morphologic

Fig. 1.—Sonograms of mediastinal lymphoma in complete remission.

A, Suprasternal sonogram shows multiple, paratracheal hypoechoic lymph nodes (L, arrowheads) up to 1.5 cm in diameter in a 35-year-old woman with Hodgkin lymphoma.

B, Complete regression of paratracheal lymph nodes after radiotherapy.

TR = brachiocephalic trunk, A = aorta, P = right pulmonary artery.

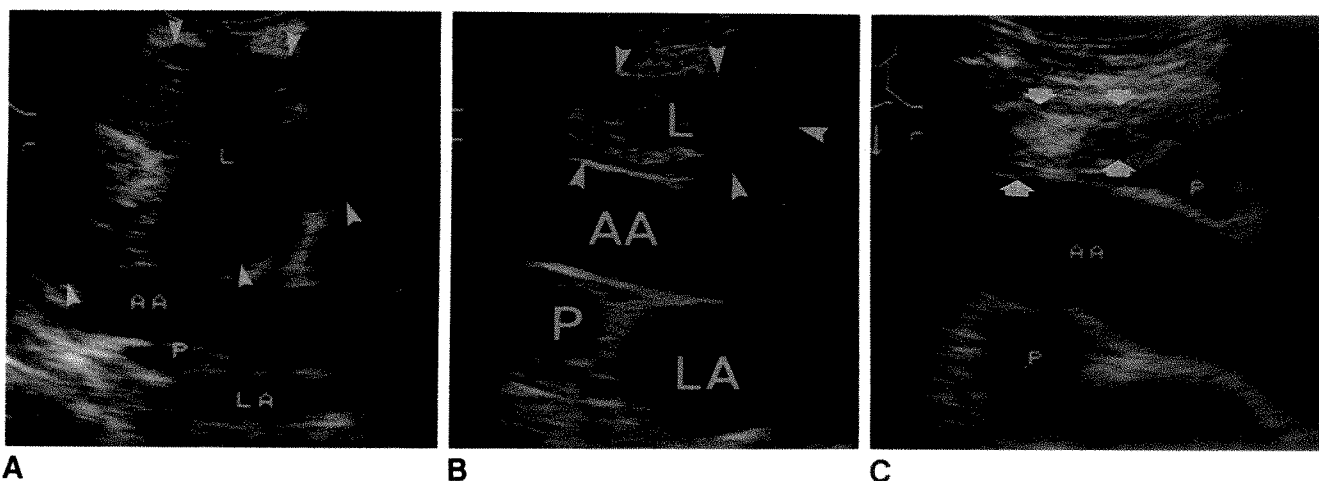
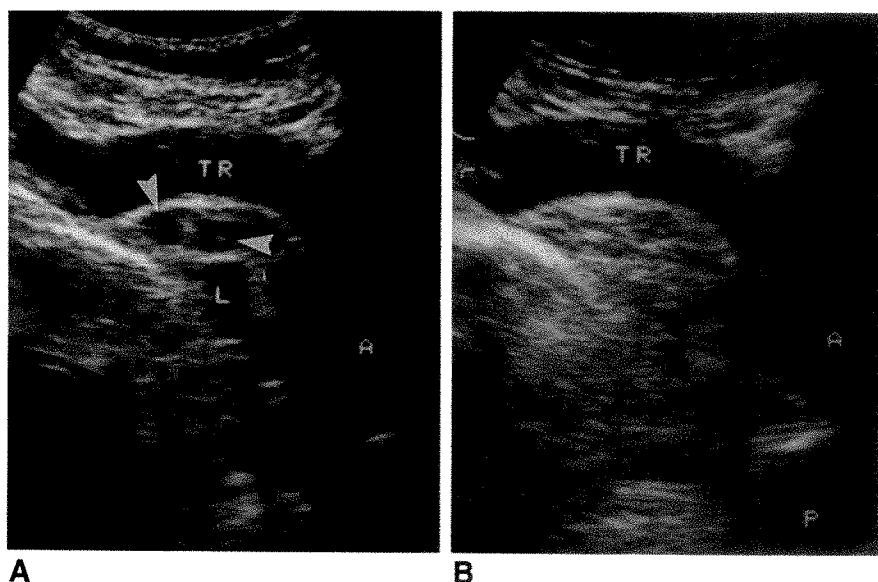


Fig. 2.—Follow-up sonograms in a 36-year-old man with extensive infiltration of thymus by Hodgkin lymphoma.

A, Initial right parasternal sagittal sonogram shows extensive, hyperechoic, prevascular tumor (L, arrowheads) with dorsal displacement of ascending aorta (AA) and compression of right pulmonary artery (P) and left atrium (LA).

B, At completion of therapy, sonogram shows persistence of hyperechoic prevascular nodular tumor (L, arrowheads) that was considered to be residual vital lymphoma.

C, Sonographic follow-up over a period of 15 months showed a further shrinkage of mass and typical thymic tongue configuration (arrows). Note further increase in echogenicity of residual tissue. AA = ascending aorta, P = pericardial recess/right pulmonary artery.

changes, we were able to attribute these lesions to residual thymic tissue.

In all five patients with incomplete remission, multiple lymph nodes between 1.5 and 8.0 cm in diameter (mean, 4.0 cm) were seen on sonography before therapy (supraaortic region, three patients; paratracheal region, three patients; prevascular region, two patients; subcarinal region, two patients; and pericardial region, three patients). In all five patients, incomplete remission with incomplete regression of mediastinal lymph nodes was correctly diagnosed by using sonography after therapy.

In three patients with hypoechoic lymph nodes with a maximal diameter of 5.0 cm, residual hypoechoic lymph nodes 0.8, 2.0, and 2.5 cm in diameter were evident on completion of therapy (Fig. 3). Further follow-up showed an increase in the size of these lymphomas. In two patients with large hyperechoic tumors between 5 and 10 cm in diameter, only a slight and temporary reduction in size (diameters of 3.5 and 6.0 cm, respectively) was observed.

All five patients with tumor recurrence had normal mediastinal sonograms on completion of initial therapy. Follow-up examinations detected small mediastinal lymph nodes (diameters of 1.0, 1.0–2.0, and 2.0 cm) (Fig. 4) in three patients, multiple large hypoechoic lymph nodes (diameter, 2.5–5.0 cm) in one patient, and a large hyperechoic lymphoma in the left cardiophrenic recess (diameter, 8.0 cm) in one patient. All lesions were correctly interpreted as recurrent tumor.

#### Correlation of Sonographic and CT Findings

In 31 patients, follow-up with both sonography and CT was available. In 25 (81%) of these cases, sonography and CT showed identical results regarding therapeutic response of mediastinal lymph nodes: complete regression of mediastinal lymphomas in 17 patients, doubtful remission in three patients, incomplete regression in two patients, and recurrent lymphoma in three patients.

In five patients (16%), conflicting results were obtained; in three of these, large residual masses 2–4 cm in diameter were seen in several mediastinal regions (supraaortic, paratracheal, and prevascular) on CT, whereas sonography showed no lymph nodes (Fig. 5). On further follow-up, regression of the mediastinal mass was evident on CT for a period of 5–20 months without therapy.

In one patient with incomplete remission who had multiple non-Hodgkin lymphomas up to 4.5 cm in diameter before therapy, only one residual nodular lesion 0.8 cm in diameter was observed on CT after three courses of chemotherapy, indicating full remission (Fig. 6B). However, the hypoechoic texture of the nodular lesion on sonography (Fig. 6C) suggested incomplete remission. This was confirmed on further follow-up by the recurrence of mediastinal lymphomas after six courses of chemotherapy.

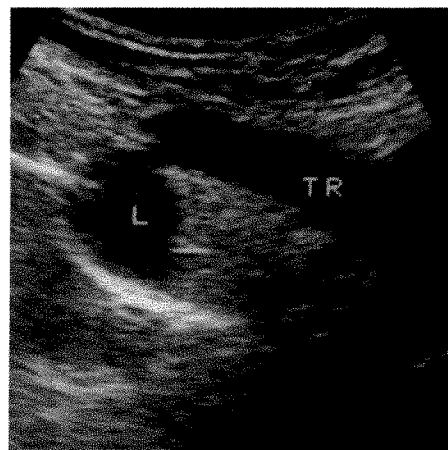


Fig. 4.—Tumor recurrence in a 28-year-old woman with Hodgkin lymphoma. This patient was treated for Hodgkin lymphoma 2 years before. Suprasternal sonogram shows a hypoechoic lymph node (L) with a diameter of 2.0 cm in right paratracheal region. TR = brachiocephalic trunk.

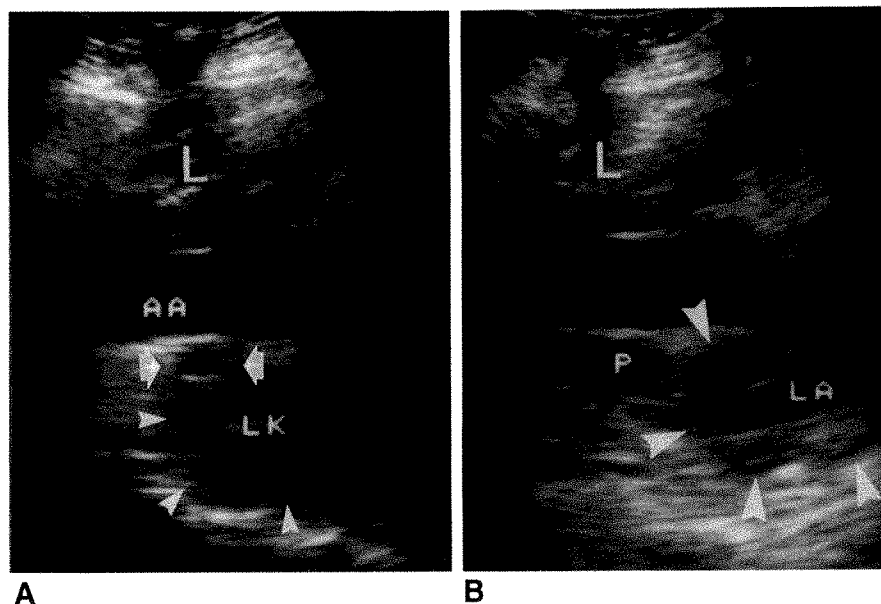


Fig. 3.—Sonograms in a 25-year-old man with incomplete remission of mediastinal lymphoma.

A, Initial right parasternal sagittal sonogram in non-Hodgkin lymphoma shows a prevascular lymphomatous tumor (L) and a large subcarinal lymph node (LK, arrowheads). The latter has compressed the right pulmonary artery (arrows). AA = ascending aorta.

B, After chemotherapy, complete regression of subcarinal lymph node is evident; right pulmonary artery (P) is normal. Left atrium (LA), however, is compressed and narrowed by hypoechoic tumor tissue (arrowheads). Prevascular lymphomatous tumor (L) shows only minimal regression.

Fig. 5.—CT and sonographic follow-up in a patient with unclear posttherapeutic paratracheal residual tumor on CT.

A, Initial CT scan in this 36-year-old man with Hodgkin disease shows a large paratracheal lymphoma 3.5 cm in diameter.

B, After therapy, right paratracheal region remains somewhat wide (approximately 2.0 cm in maximum diameter).

C, Initial suprasternal, semisagittal sonogram shows a large, hypoechoic, paratracheal lymphoma (L, arrowheads).

D, After therapy (40 Gy), sonogram shows no evidence of tumor despite paratracheal widening detected on CT scan. Arrowheads indicate homogeneous, hyperechoic tissue in right paratracheal region.

A = aorta, TR = brachiocephalic trunk, P = right pulmonary artery.

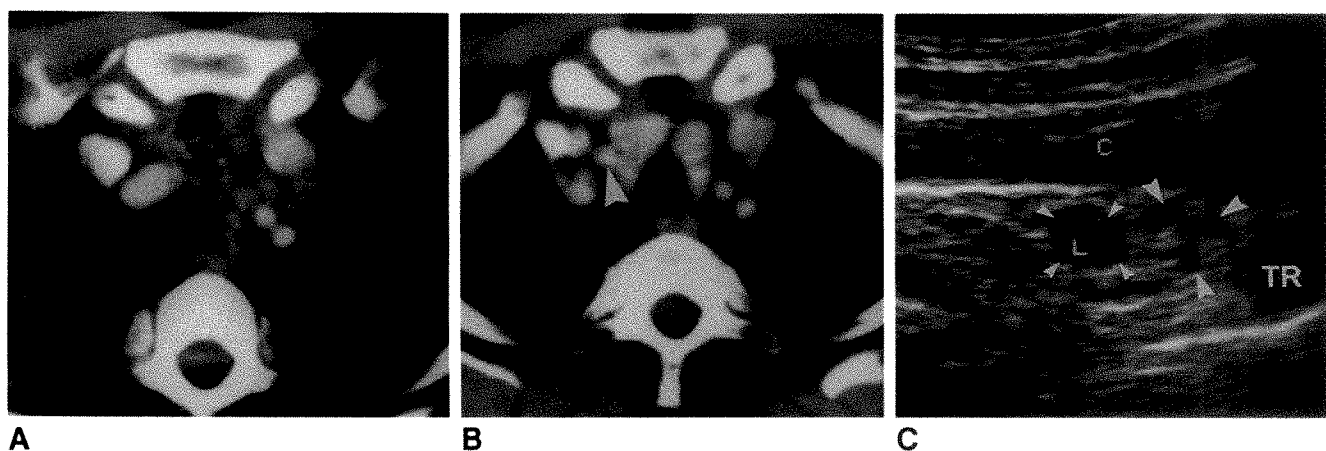
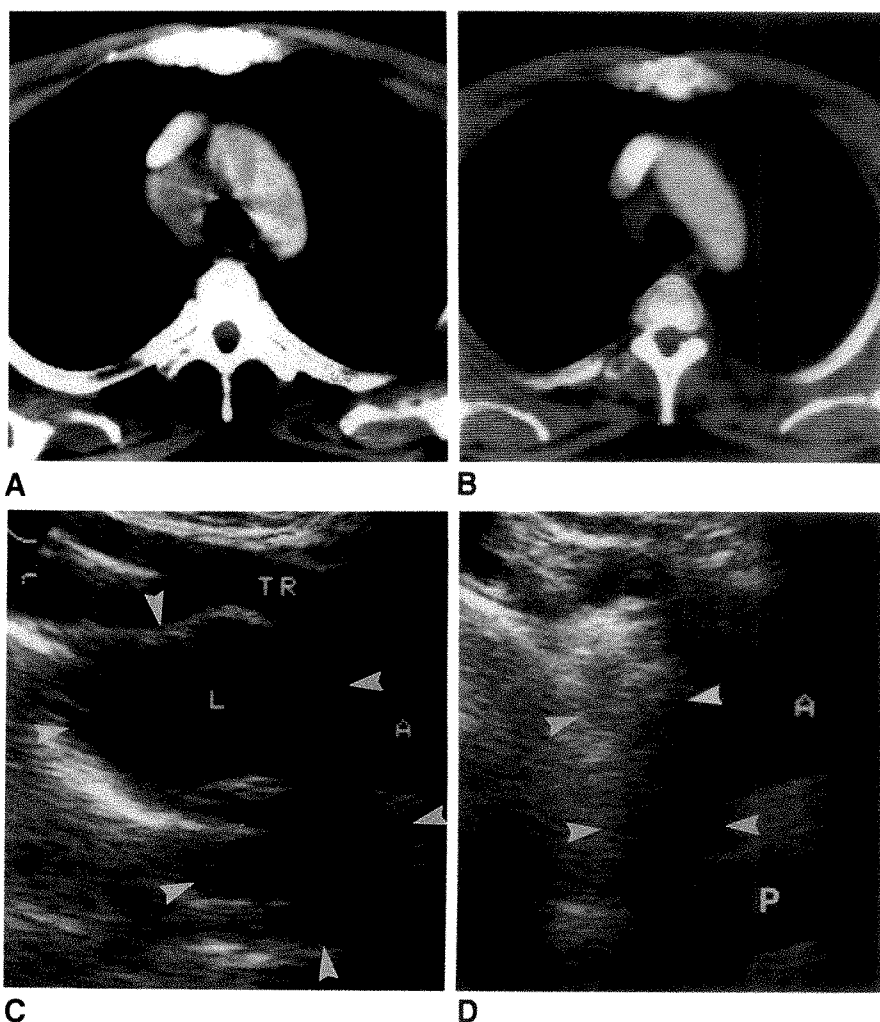


Fig. 6.—CT and sonographic follow-up in a 63-year-old woman with non-Hodgkin lymphoma and incomplete remission.

A, Initial CT scan shows multiple lymphomas around supraaortic vessels.

B, Follow-up CT scan after three cycles of chemotherapy shows marked regression of supraaortic lymphomas. A residual lesion 0.8 cm in diameter (arrowhead) lying between right lobe of thyroid gland and right carotid artery was considered to be within normal limits.

C, At same stage as B, suprasternal, semisagittal sonogram shows a hypoechoic residual lesion (L, small arrowheads) in right paratracheal region. Other hypoechoic lymph nodes (large arrowheads), 5 mm in diameter, are situated above pulmonary trunk (TR). These sonographic findings were interpreted as indicating incomplete remission, which was confirmed on further clinical course. C = left common carotid artery.



In one patient with recurrence, a hypoechoic, supraaortic lymph node 1.0 cm in diameter was detected with sonography 8 months after completion of chemotherapy (Fig. 7). According to CT criteria, this lymph node was considered to be within normal limits (Fig. 7B). Sonographic examination 3 months later indicated an increase in size (1.5 cm) and multiple, additional mediastinal lymph nodes (up to 1.8 cm in diameter), indicating recurrence.

In one patient, CT and sonographic findings of tumor recurrence could not be compared directly, as the two studies were performed at different times.

A major advantage of CT was the detection of mediastinal lymphomas in those regions that are difficult to assess with sonography. In six of 31 patients, CT detected nine additional lymphomas in various mediastinal regions (including two lymph nodes in the posterior mediastinum). However, the additional information offered by CT was of no major therapeutic significance, as sonography had produced overall true-positive results in all cases. Besides, all lymph nodes missed showed a therapeutic response similar to that of those detected with sonography, thus having no influence on the therapeutic regimen.

#### *Correlation Between Findings on Sonograms and Chest Radiographs*

A full correlation between findings on sonograms and chest radiographs in regard to the extent and response of mediastinal lymphomas to therapy was observed in only 23 (57%) of 40 cases: complete regression in 15 patients, doubtful remission in three patients, incomplete regression in three patients, and tumor recurrence in two patients.

In 12 (40%) of 30 patients with complete remission, conflicting results were obtained with sonography and chest radiographs during or after therapy. Eleven patients with evidence of multiple mediastinal lymphomas up to 4.0 cm in diameter on sonography and CT had normal chest radiographs (Fig. 8). Thus, in all these cases, chest radiographs incorrectly assessed the mediastinal therapeutic response. Sonography

and CT showed complete regression of all mediastinal lymphomas in all 11 cases after therapy.

In one patient with persistent widening of the right paratracheal stripe on radiographs after completion of therapy, sonography showed complete regression of all paratracheal lymph nodes detected before therapy. Return of the mediastinal lines to normal on chest radiographs was not evident until 14 months after completion of therapy.

In two of five patients with incomplete remission, incomplete regression of mediastinal lymphomas was indicated only with sonography. In these cases, lymphomas 0.8 and 2.5 cm in diameter were missed on chest radiographs, which only showed signs of renewed mediastinal tumor growth 4–6 months later.

Three of five mediastinal lymphoma recurrences (1.5, 2.0, and 2.5 cm in diameter) were detected with sonography only. Chest radiographs remained normal in one patient until the introduction of therapy 6 months later and in the second patient until death. In a third patient, rapid tumor growth was shown on sonograms; however, signs of mediastinal tumor recurrence were not detected on chest radiographs until 2 months later.

Chest radiographs were superior to sonograms in detecting extramediastinal intrathoracic manifestations of lymphoma. Hilar lymphomas were seen in six of 40 patients; in three of these, an additional pulmonary lymphomatous infiltration was seen on chest radiographs. All extramediastinal manifestations of lymphoma regressed concurrently with the mediastinal lymphomas during therapy. Pleural fluid was seen in one patient but disappeared during therapy.

#### **Discussion**

From the results of this study, it is evident that mediastinal lymphomas show typical sonographic changes during treatment depending on their response to therapy.

In all 30 patients with full remission, complete regression after therapy of all mediastinal lymph nodes was demonstrated sonographically (Fig. 1). Incomplete regression of

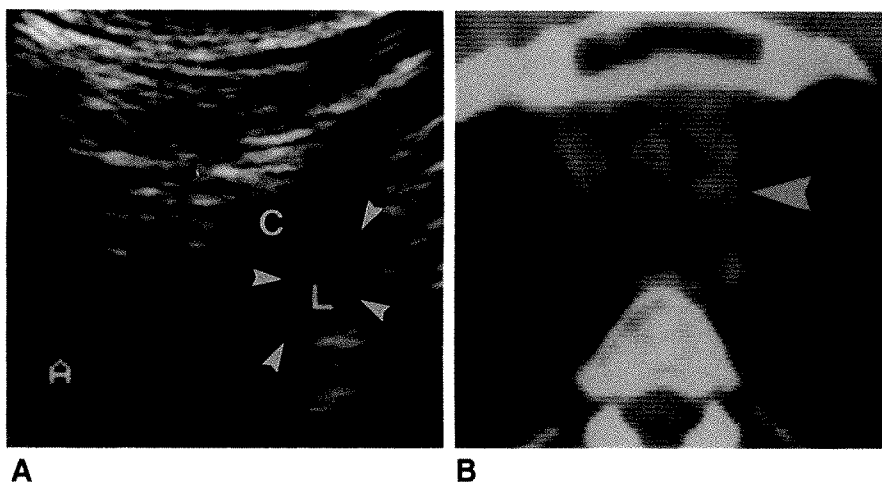


Fig. 7.—Sonogram and CT scan in 30-year-old man with recurrent lymphoma.

A, Suprasternal sonogram shows a hypoechoic lymph node (L, arrowheads), adjacent to origin of left common carotid artery (C), which was not evident on previous examination and was interpreted as indicating recurrence. A = aortic arch.

B, CT scan shows a small lymph node (arrowhead) lateral to left common carotid artery, which was considered to be within normal limits.

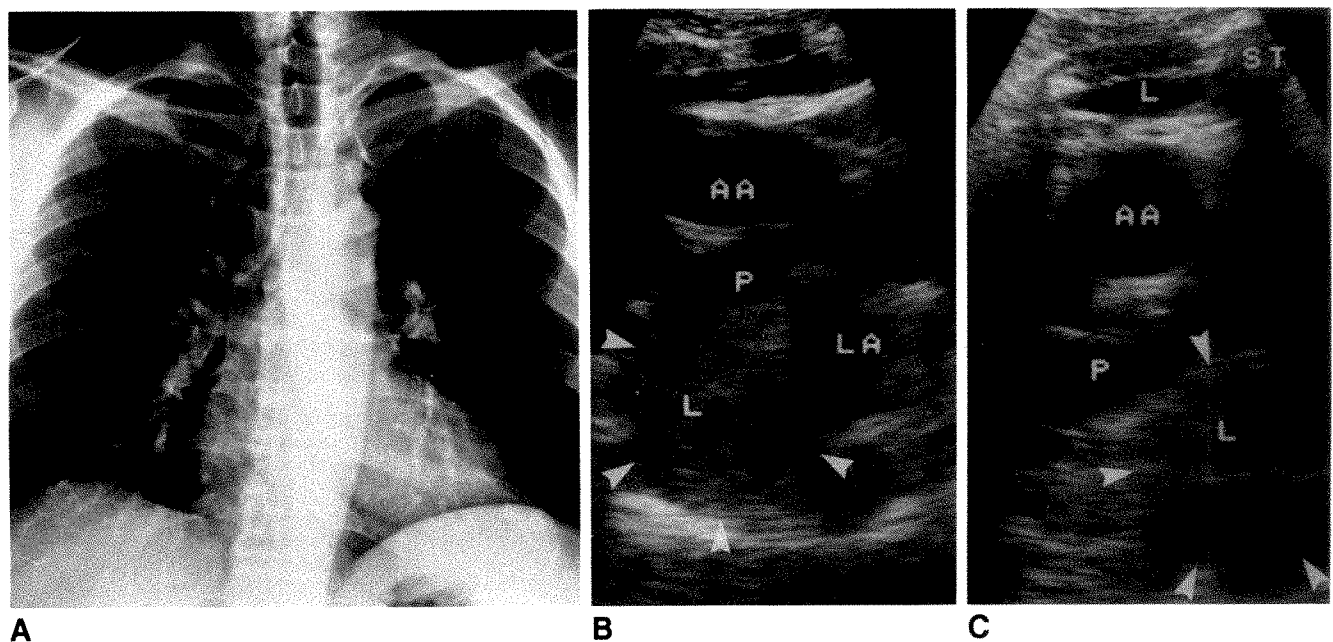


Fig. 8.—Initial findings on plain radiographs and sonograms in 54-year-old man with non-Hodgkin lymphoma.

A, Chest radiograph shows no evidence of mediastinal abnormality.

B, Right parasternal sagittal sonogram shows a hypoechoic, subcarinal lymphoma (L, arrowheads) 4 cm in diameter posterior to right pulmonary artery (P). Compression of superior wall of left atrium (LA) is evident.

C, Transverse sonogram shows the same subcarinal lymphoma (L, arrowheads) and a hypoechoic internal mammary lymphoma anterior to ascending aorta (AA). ST = sternum.

lymph nodes on sonography after therapy is highly indicative of an incomplete remission (Fig. 3). Persistence of even small mediastinal lymph nodes (with a diameter of less than 1.0 cm) strongly suggests incomplete remission, particularly when their hypoechoic structure remains unchanged. All new nodular lesions, irrespective of size, detected after an episode of complete remission should be interpreted as indicating mediastinal tumor recurrence (Fig. 4).

The results of this study also indicate that the changes in echogenicity observed in abnormal mediastinal lymph nodes are identical to those seen in the abdominal regions [16–18]. Normal mediastinal lymph nodes cannot be detected with sonography, and all mediastinal nodules detected with sonography—irrespective of size—should be considered pathologic (inflammatory or neoplastic). Infiltrated lymph nodes are almost always hypoechoic in relation to fat and connective tissue [16–18]. Presumably, edema and increased cellularity in diseased lymph nodes are responsible for this reduction in impedance [16].

Empirical experience has shown that inflammatory and neoplastic lymph nodes resume their hyperechoic structure and therefore cannot be detected sonographically after successful therapy [18, 19]. Our results confirm these observations. Meticulous sonographic follow-up of 10 patients indicated a progressively increasing echogenicity of mediastinal lymph nodes during therapy to a stage where no further delineation from surrounding tissue was possible (Fig. 1). In contrast, sonographically detectable residual thymic tissue of varying echogenicity persists over a long follow-up period in

cases of previous thymic lymphomatous infiltration despite complete remission (Fig. 2).

Sonographic and CT findings correlated in 25 (81%) of 31 cases in regard to the response of mediastinal lymphomas to therapy. In all five cases showing discrepancies between sonographic and CT findings, further follow-up indicated that the information obtained at sonography correlated more closely with the clinical outcome.

In three patients with large residual mediastinal masses on CT, lymphomas disappeared completely on sonograms, with a return of echogenicity to normal (equivalent to surrounding tissue), which seems to be a reliable indicator of good response to therapy (Fig. 5).

In two patients with normal CT findings, sonography was able to identify small hypoechoic nodes (less than 1.0 cm in diameter) within hyperechoic mediastinal connective tissue; with further radiologic and clinical follow-up, this could be classified retrospectively as residual (Fig. 6) or recurrent (Fig. 7) lymphomatous tissue.

The interpretation of residual mediastinal masses (scar tissue or tumor) occasionally observed after therapy of large mediastinal tumors remains a diagnostic problem [1, 3, 15, 20]. With the diagnostic imaging techniques available today (CT and MR), neoplastic, nonenlarged lymph nodes (smaller than 1.0 cm in diameter) cannot be identified correctly.

Mediastinal sonography may contribute to the solution of these two problems because the qualitative criterion (echogenicity) it offers may be a more reliable indicator for vital tumor tissue or clinical outcome than the quantitative criterion

(lymph node size) obtained with CT. The limited number of cases in this preliminary study supports this observation; however, further studies with larger patient groups are necessary to validate this hypothesis.

A comparison of sonographic and plain film findings indicated that chest radiographs were insensitive for the monitoring of therapeutic response of mediastinal lymphomas, because false results were obtained in 17 (43%) of 40 cases (Fig. 8).

The diagnostic advantage of mediastinal sonography over chest radiographs results from its capability to demonstrate deep central mediastinal lymph nodes tomographically long before a displacement of pleuromediastinal lines occurs [6]. Sonography also allows a reliable assessment of the mediastinum in those cases in which postirradiation fibrosis causes a distortion of mediastinal contours. Both supra- and parasternal sonography should be performed, because parasternal sonography allows assessment of mediastinal regions (prevascular, pericardial, and subcarinal regions) that cannot be assessed with suprasternal sonography [6].

As in other studies [3, 15, 20], no mediastinal lymph node biopsies were performed during follow-up, so that no histologic confirmation of the sonographic, CT, and plain film findings was available. We stress therefore that the imaging techniques described, together with clinical assessment, allow only prognostic evaluation and no histologic diagnosis.

From the results described, the following conclusions may be drawn: (1) Any mediastinal nodule detected by using sonography should be considered diseased. Mediastinal nodes that either remain or become hypoechoic after treatment should be viewed as highly suggestive of viable tumor. (2) Chest radiographs are insensitive to residual tumor and tumor progression. (3) Sonography offers a more accurate and subtle method for the monitoring of therapeutic response of mediastinal lymphomas than conventional radiographs do. (4) Sonography appears to offer better prognostic information than CT does because it provides information beyond the size of mediastinal lymph nodes.

At present and in the immediate future, the availability of CT and MR may be too limited, even in highly industrialized countries, to be implemented for the routine follow-up of lymphoma patients during therapy [1]. In contrast, sonography is a widely available, noninvasive, and inexpensive imaging method. The results of our study suggest that the combination of conventional chest radiographs and sonography could substantially improve the radiologic follow-up of lymphoma patients, because it may provide adequate evaluation

of all major intrathoracic compartments without the significant increase in cost and radiation exposure that would accompany routine follow-up CT scans of the thorax.

## REFERENCES

1. Castellino RA. Hodgkin disease: practical concepts for the diagnostic radiologist. *Radiology* 1986;159:305-310
2. Webb WR. MR imaging of treated mediastinal Hodgkin disease. *Radiology* 1989;170:315-316
3. Nyman RS, Rehn SM, Glimelius BLG, Hagberg HE, Hemmingsson AL, Sundström CJ. Residual mediastinal masses in Hodgkin disease: prediction of size with MR imaging. *Radiology* 1989;170:435-440
4. Wernecke K, Peters PE, Galanski M. Mediastinal tumors: evaluation with suprasternal sonography. *Radiology* 1986;159:405-409
5. Wernecke K, Pötter R, Peters PE, Koch P. Parasternal mediastinal sonography: sensitivity in the detection of anteriormediastinal and subcarinal tumors. *AJR* 1988;150:1021-1026
6. Wernecke K, Vassallo P, Pötter R, Lückener HG, Peters PE. Mediastinal sonography: sensitivity in the detection of mediastinal tumors compared to CT and chest radiography. *Radiology* 1990;175:137-143
7. Glazer GM, Gross BH, Quint LE, Francis IR, Bookstein FL, Orringer MB. Normal mediastinal lymph nodes: number and size according to American Thoracic Society mapping. *AJR* 1985;144:261-265
8. Blank N, Castellino RA. Patterns of pleural reflections of the left superior mediastinum. *Radiology* 1972;102:584-589
9. Blank N, Castellino RA. The intrathoracic manifestation of the malignant lymphomas and the leukemias. *Semin Roentgenol* 1980;15:227-243
10. Neufang KFR, Bulo W. Häufigkeit pleuromediastinaler Linien beim Gesunden. *ROFO* 1981;136:673-681
11. Müller NL, Webb WR, Gamsu G. Subcarinal lymph node enlargement: radiographic findings and CT correlation. *AJR* 1985;145:15-19
12. Müller NL, Webb WR, Gamsu G. Paratracheal lymphadenopathy: radiographic findings and correlation with CT. *Radiology* 1985;156:761-765
13. Sussman SK, Halvorsen RA, Silverman PM, Saeed M. Paracardiac adenopathy: CT. *AJR* 1987;149:20-34
14. North LB, Fuller LM, Hagemeister FB, Rodgers RW, Butler JJ, Shullenberger CC. Importance of initial mediastinal adenopathy in Hodgkin disease. *AJR* 1982;138:229-235
15. North LB, Fuller LM, Sullivan-Halley JA, Hagemeister FB. Regression of mediastinal Hodgkin disease after therapy: evaluation of time interval. *Radiology* 1987;164:599-602
16. Pirschel J, Rücker HC. Die Ultraschalldiagnostik des retroperitonealen Lymphsystems. In: Frommhold W, ed. *Erkrankungen des Lymphsystems. Klinisch-radiologisches Seminar*, Band 2. Stuttgart: Thieme, 1981:74-84
17. Heckemann R. Sonographische Tumordiagnostik im Retroperitoneum. *Therapiewoche* 1983;33:123-137
18. Beyer D, Friedmann G, Peters PE. Subdiaphragmales Lymphknotensystem. In: Bücheler E, Friedmann G, Thelen M, eds. *Real-time-Sonographie des Körpers*. Stuttgart: Thieme-Verlag, 1983:321-332
19. Brockmann WP, Maas R, Voigt H, Thomas G, Schweer S. Veränderungen peripherer Lymphknoten im Ultraschall. *Ultraschall Med* 1985;6:164-169
20. Jochelson MS, Mauch P, Balikian J, Rosenthal D, Canellos G. The significance of the residual mediastinal mass in treated Hodgkin's disease. *J Clin Oncol* 1985;3:637-640



# Value of CT in Determining the Need for Angiography When Findings of Mediastinal Hemorrhage on Chest Radiographs Are Equivocal

Patrice Richardson<sup>1</sup>  
 Stuart E. Mirvis<sup>1</sup>  
 Ronald Scorpio<sup>2</sup>  
 C. Michael Dunham<sup>2</sup>

The role of CT in determining the need for angiography in patients with possible thoracic vascular injury resulting from blunt trauma is controversial. During a 24-month period, we prospectively evaluated the results of CT to screen 90 patients with a history of decelerating thoracic trauma for evidence of mediastinal hemorrhage or great vessel abnormality. All patients either had equivocally abnormal mediastinal contours on chest radiographs (64%) or had technically suboptimal chest radiographs owing to body habitus or restriction to the supine projection (36%). Patients with unequivocal signs of mediastinal hemorrhage on chest radiographs underwent immediate arteriography without prior CT. Thoracic CT was interpreted as normal in 63 (77%) patients and no further imaging was performed. Five patients had technically suboptimal CT studies, and CT scans were interpreted as equivocal in six. These 11 patients had normal arteriograms. Sixteen CT scans (18%) demonstrated evidence of mediastinal hemorrhage and/or great vessel contour abnormality. Four (27%) of 15 patients who underwent arteriography had injury to the great vessels. One patient refused to undergo angiography. In 11 patients with CT evidence of mediastinal hemorrhage, major vascular injury was not seen on arteriography.

These results suggest a valuable role for CT in determining the need for arteriography to detect potential great vessel injury in patients with blunt decelerating thoracic trauma and equivocally abnormal mediastinal contours on chest radiographs.

*AJR* 156:273-279, February 1991

The diagnosis of injury to major arteries within the thorax after blunt decelerating trauma is difficult. Details concerning the precise mechanism of injury are often lacking, and even when available provide little predictive value in estimating the likelihood of major thoracic arterial injury [1]. In general, bedside clinical assessment also is acknowledged to be of little help in selecting patients for thoracic arteriography [1, 2]. Thus, the chest radiograph that is obtained on admission offers the best screening test for the presence of mediastinal hemorrhage and potential thoracic arterial injury [3-9].

A number of factors limit the value of the chest radiograph as a screening device for mediastinal hemorrhage and lead to obtaining an excessive number of thoracic arteriograms in patients with a history of decelerating thoracic trauma. In a previous prospective study of selected patients, we evaluated the potential role of thoracic CT as a screening test for mediastinal hemorrhage in an attempt to address the limitations of thoracic radiographs [10]. This study was limited to only 20 patients, but suggested that CT could safely obviate thoracic arteriography in some patients when chest radiographs are equivocal or technically unsatisfactory. Other limited studies have supported the role of CT in this capacity [11, 12], but some reports have cast doubt on the reliability of thoracic CT to detect significant vascular injury [13-15].

To better assess the possible role of thoracic CT in the evaluation of patients with acute decelerating thoracic trauma, we performed a prospective study over a

Received July 16, 1990; accepted after revision September 17, 1990.

<sup>1</sup> Department of Diagnostic Radiology, University of Maryland Medical Systems, 22 S. Greene St., Baltimore, MD 21201. Address reprint requests to S. E. Mirvis.

<sup>2</sup> Maryland Institute for Emergency Medical Services Systems, Baltimore, MD 21201.

0361-803X/91/1562-0273  
 © American Roentgen Ray Society

2-year period to evaluate the accuracy and usefulness of thoracic CT scans obtained on admission in 90 patients with a mechanism of injury consistent with that known to produce major thoracic arterial injury. This was done in an attempt to reduce the number of arteriograms obtained with normal results.

### Subjects and Materials

During a 24-month period from January 1988 through December 1989, 6181 patients were admitted to the Shock-Trauma Center of the University of Maryland Medical System. Of this total population, 1287 patients (21%) were entered into the trauma registry as having sustained principal blunt force trauma to the thorax. All patients in whom chest radiographs obtained on admission indicated unequivocal abnormality of the mediastinal contours consistent with mediastinal hemorrhage underwent immediate thoracic arteriography (Fig. 1). When technically satisfactory chest radiographs demonstrated normal mediastinal contours and the clinical suspicion of major thoracic injury was considered low to moderate, no further imaging studies were performed. If the clinical history was considered highly suggestive of major thoracic deceleration (e.g., high-speed impact, ejection from a vehicle, or falls from significant heights) or if the physical examination at admission detected findings consistent with major thoracic deceleration such as multiple anterior rib or sternal fractures or steering wheel contusion pattern on the chest wall, the trauma attending physician could request thoracic arteriography despite a normal chest radiograph or normal thoracic CT scan.

When chest radiographs obtained in either the supine and/or erect position were interpreted as equivocal and a technically adequate chest radiograph could not be obtained, or when a moderate or strong clinical suggestion of major thoracic vascular injury existed despite a normal radiologic appearance of the mediastinum, dynamic enhanced thoracic CT was the next imaging study (Fig. 1). The frequency and type of equivocal radiologic findings observed on the supine and/or erect chest radiographs were noted. In 32 (36%) of

the 90 patients in whom thoracic CT was performed, the radiographs were limited to the supine position only because of major skeletal injury (18 patients) or other clinical considerations (14 patients).

Chest radiographs were interpreted by the trauma-team attending surgeon and fellow in consultation with the radiology service resident. The interpretation of the chest radiograph findings used for this study was based on the interpretation at admission rather than on the official radiologist's report. Interpretation of thoracic CT scans was performed by the radiology resident on call (after 11 p.m.) or by an attending radiologist.

If the CT study revealed a normal mediastinum, no further imaging evaluation was performed (Fig. 1). The CT study was interpreted as abnormal if it showed either a contour abnormality of the thoracic aorta or proximal great vessels, intraluminal irregularity of these vessels suggestive of an intimal flap, or any evidence of mediastinal hemorrhage or focal hematoma. Thoracic arteriography was performed in these cases. If the initial interpretation of the CT scan was equivocal for any of these findings, thoracic arteriography was performed. All CT studies were reviewed retrospectively by two radiologists and their interpretation was compared with the CT interpretation made at the time of admission.

During the first 18 months of the study, CT scans were obtained with a Siemens DRH (Siemens Medical Systems, Iselin, NJ) or a GE 9800 (General Electric Medical Systems, Milwaukee, WI) unit. Patients received a rapid hand-injected 50-ml bolus of 60% contrast material at the level of the thoracic inlet. The scan time was 2.0 sec with a 3.5-sec (GE 9800) or 6.0-sec (DRH) interscan delay. Eight to 10 contiguous scans were obtained at 1-cm intervals to the carina. At the carina, an additional 50-ml contrast bolus was administered and eight to 10 additional scans were obtained at 1-cm intervals to the left hemidiaphragm. During the last 6 months of the study, all CT scans were obtained with a Siemens Hi-Q scanner and a power CT injector (Medrad Mark 4, Pittsburgh, PA) with contrast material delivered through a central or large (18 gauge or greater) peripheral catheter. Scanning was performed at 1-cm intervals from the level of the thoracic inlet to the diaphragm and was initiated after a bolus of 80 ml (at 2 ml/sec) of 60% contrast material. During scanning, a continuous infusion of 1.0 ml/sec of 60% contrast material for a total of 70 ml was administered. Nonionic contrast material (Omnipaque, Winthrop, New York, NY) was administered in some cases if there was a history of allergy or other relevant contraindications to ionic contrast material. Although patients were not routinely sedated or paralyzed for the CT examination, in very uncooperative or combative patients, sedation or intubation with paralysis was performed at the discretion of the attending physician. Whenever possible, ECG leads and other external devices were removed from the scanning field. Nasogastric tubes, if present, were usually left in place.

Thoracic arteriograms were obtained by digital subtraction with a General Electric CGR DG 200 unit using a pixel matrix of  $1024^2$  or a Siemens Digitron 3 unit using a pixel matrix of  $512^2$ . Arteriograms were obtained with a 5-French high-flow pigtail catheter placed in the proximal aorta. Images were acquired at three frames/sec for 6 sec after injection of 40 ml of 76% contrast material (DG 200) or 30% contrast material (Digitron 3) at 20 ml/sec. At least two radiologic projections (anteroposterior and left anterior oblique) were performed in all patients. All arteriograms were interpreted by an attending radiologist.

The frequencies at which thoracic angiography was performed in patients with any kind of blunt trauma and blunt thoracic trauma were analyzed for a 4-year period including the 2 years before the introduction of thoracic CT as an ancillary screening test for mediastinal hemorrhage. Follow-up chest radiographs of patients undergoing thoracic CT without angiography were available for review in 27 of the 63 cases.

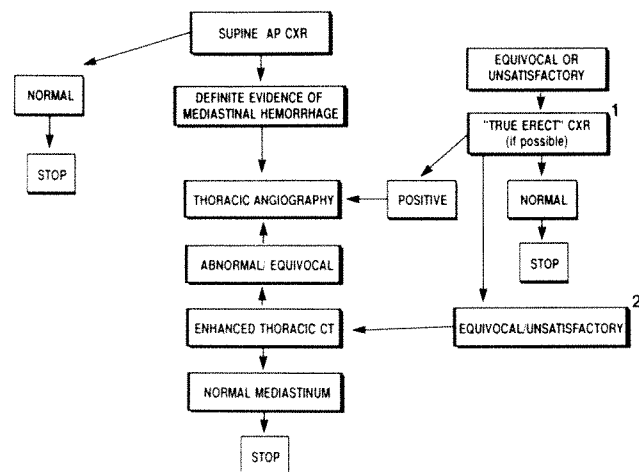


Fig. 1.—Suggested algorithm for evaluation of patients sustaining significant blunt decelerating thoracic trauma. If chest radiograph obtained with patient supine only is possible (1), choice of angiography or dynamic enhanced CT should be based on clinical level of suspicion for injury. When chest radiograph of erect patient is equivocal or unsatisfactory (2), choice of angiography or CT may be influenced by level of clinical suspicion for injury. AP = anteroposterior, CXR = chest radiograph.

## Results

CT scans were obtained in 90 patients (7% of blunt thoracic trauma admissions) over a 2-year period and were initially interpreted as showing no evidence of mediastinal hemorrhage or aortic contour abnormality in 63 (70%) (Table 1). Arteriography was not performed in any of these patients. Follow-up chest radiographs were obtained in 27 of these 63 patients at 2 days to 2 years after initial injury (mean, 7.5 weeks) and there was no evidence of delayed mediastinal abnormality. Thirteen patients have received only clinical follow-up at 2–27 months after injury (mean, 1 year) and there has been no evidence of adverse sequelae. No long-term clinical follow-up is available for 23 of these 67 patients, but no reports of adverse outcomes have been reported to date. In six patients (7%), CT scans were initially interpreted as equivocal; angiography was normal in all six. These six CT scans were interpreted as normal on retrospective review. Equivocal interpretations resulted from the presence of thymic tissue in the anterior mediastinum (two patients) or volume averaging of the rostral pulmonary artery with the proximal descending aorta (four patients). Thoracic CT scans were technically unsatisfactory in five patients (6%) because of excessive motion or inadequate vascular enhancement. Thoracic angiograms were normal in all five patients.

In 16 patients, thoracic CT scans were interpreted as showing evidence of mediastinal hemorrhage; two of these patients were diagnosed as having concomitant contour abnormality of the aortic contour. Thoracic arteriography was

normal in 11 (69%) of these 16 patients. One patient refused to undergo arteriography, but remained well at 27 months after injury. In four patients (25% of abnormal CT scans), thoracic arteriograms were positive for great vessel injury (Figs. 2 and 3). Evidence of both mediastinal hemorrhage and aortic contour abnormality was present on thoracic CT scans in two of these four, and both demonstrated pseudoaneurysms of the proximal descending aorta angiographically. One patient had a complete disruption of the proximal left subclavian artery, and one patient had a small laceration of the right sinus of Valsalva (Fig. 3). In this patient a sternal fracture, which was not recognized clinically, was also found on CT. The reasons for the inability to decide whether the mediastinum was normal on the chest radiographs are listed in Table 2. In 27 patients the thoracic CT scan clarified the reason for the abnormal radiologic finding (Table 3; Figs. 4–6). When thoracic CT demonstrated no abnormality, it was presumed that the abnormal radiographs were due to limitations of the supine projection and/or technically poor studies, often despite multiple repeated exposures.

The influence of including dynamic enhanced thoracic CT as a screening test for the evaluation of mediastinal hemorrhage on the frequency with which arteriography is performed in all blunt trauma and blunt thoracic trauma patients is shown in Table 4. A significant trend toward decreasing use of thoracic arteriography in patients with blunt impact trauma in general ( $p < .001$ ) and blunt thoracic trauma specifically ( $p < .01$ ) was observed after the introduction of contrast-enhanced thoracic CT for the evaluation of mediastinal hemorrhage.

TABLE 1: Thoracic CT Results in 90 Patients with Decelerating Thoracic Trauma

CT Finding	No. (%)	Angiographic Finding	
		Normal	Abnormal
Normal	63 (70)	NP	NP
Equivocal	6 (7)	6	0
Abnormal	16 (18)	11	4 <sup>a</sup>
Technically inadequate	5 (6)	5	0

Note.—NP = not performed.

<sup>a</sup> One patient refused to undergo angiography.

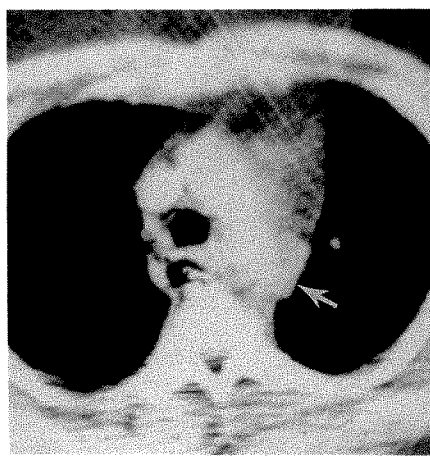
## Discussion

The diagnosis of injury to major arteries within the thorax is difficult. History and findings on physical examination provide little guidance in selecting patients for thoracic arteriography [1, 2]. For this reason some have advocated the use of thoracic arteriography when there is a history of decelerating thoracic impact and accept a substantial number of normal arteriograms in order to detect those patients with great vessel injury [16, 17]. Others select patients for thoracic arteriography based on combined information from clinical

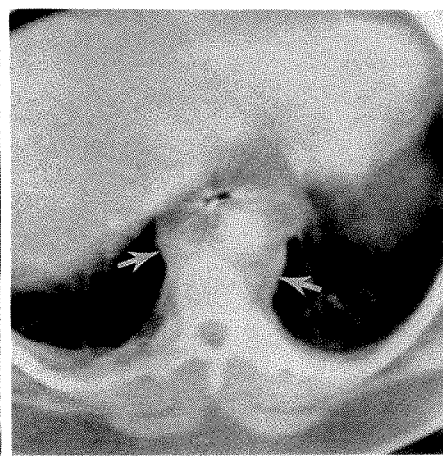
Fig. 2.—CT shows mediastinal hemorrhage and aortic contour irregularity. Chest radiographs obtained on admission in this obese 48-year-old man after a motor vehicle accident were equivocal because of body habitus and underexposure. A chest radiograph could not be obtained with patient erect because of concurrent orthopedic injuries.

A, CT scan shows irregularity and bulging of proximal descending aorta (arrow) and high density in anterior mediastinal fat suggestive of hemorrhage.

B, CT scan through lower thorax reveals high-density hemorrhage infiltrating and widening paraspinal lines (arrows). Arteriogram (not shown) revealed a pseudoaneurysm of proximal descending aorta just distal to origin of left subclavian artery, which was surgically confirmed and repaired.

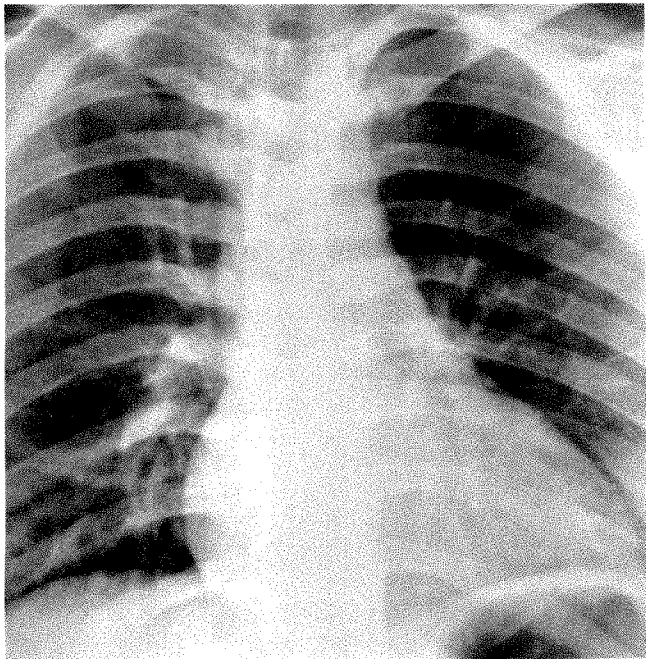


A



B





A

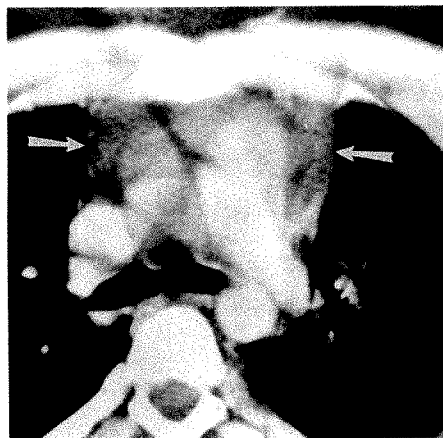
Fig. 3.—CT shows mediastinal hemorrhage and acute sinus of Valsalva aneurysm.

A, Chest radiograph obtained on admission in a standing 19-year-old man after a motor vehicle accident shows a narrowed superior mediastinum, but poorly defined aortic arch. Left paraspinal stripe is widened in superior mediastinum.

B, CT scan through level of root of aorta and pulmonary artery reveals high-density fluid distending lateral borders of mediastinum (arrows).

C, CT scan through superior mediastinum obtained with bone windows shows transsternal fracture that was not appreciated prior to CT.

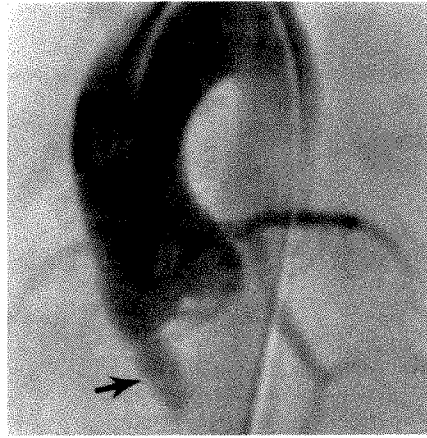
D, Digital subtraction arteriogram reveals a right sinus of Valsalva aneurysm (arrow), which was confirmed by cardiac catheterization. Non-surgical treatment was selected and the patient was well at clinical follow-ups.



B



C



D

TABLE 2: Reasons Cited for the Inability to Decide Whether the Mediastinum Was Normal on Chest Radiographs

Reason	No. (%)
Indistinct aortic arch/descending aorta	62 (69)
Widened mediastinum	15 (17)
Widened right paratracheal stripe	9 (10)
Rightward tracheal shift	9 (10)
Marked aortic ectasia	6 (7)
Other	10 (11)
Combined factors	20 (22)

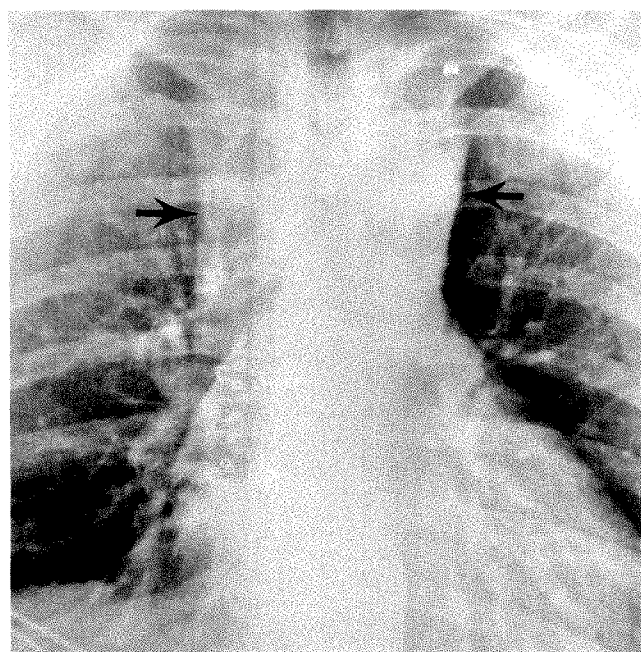
Note.—In 32 patients, only supine radiographs were obtained, 18 because of orthopedic injuries.

TABLE 3: Abnormal Findings on Contrast-Enhanced Dynamic CT Scans That Explained Abnormalities on Chest Radiograph(s)

Finding	No. (n = 27)
Left lung contusion or atelectasis adjacent to mediastinum	9
Medial left pleural effusion	7
Aortic ectasia	5
Increased mediastinal fat	4
Spine fracture with adjacent hematoma (cervical/lumbar)	2
Hiatal hernia	1
Periaortic adenopathy	1

history, physical findings, and assessment of the chest radiograph obtained on admission. While the chest radiograph occasionally provides substantial evidence of mediastinal hemorrhage and potential great vessel injury, the method

frequently is of marginal value owing to technical factors, as well as to the relatively low specificity of the radiologic observations made, particularly when chest radiographs are limited to the supine projection.



A

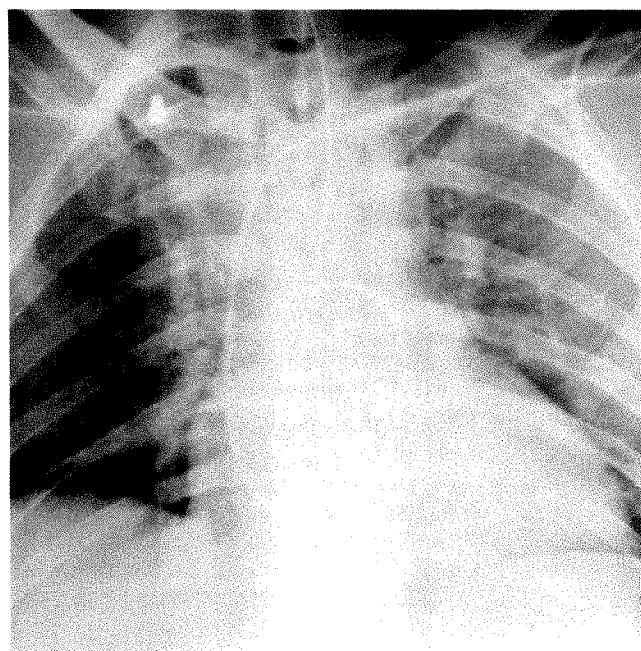


B

Fig. 4.—Mediastinal fat creating widened superior mediastinum.

A, Chest radiograph obtained on admission in a supine 46-year-old obese woman reveals bilateral straightening and widening of superior mediastinum (arrows). Chest radiograph with the patient erect could not be acquired because of orthopedic injuries.

B, CT scan through root of aorta and pulmonary artery reveals diffuse mediastinal fat widening lateral borders of mediastinum, but no evidence of vascular abnormality or mediastinal hemorrhage. No arteriogram was obtained, and the patient was still well 13 months after injury.



A

Fig. 5.—Lower cervical spine fracture producing superior mediastinal widening.

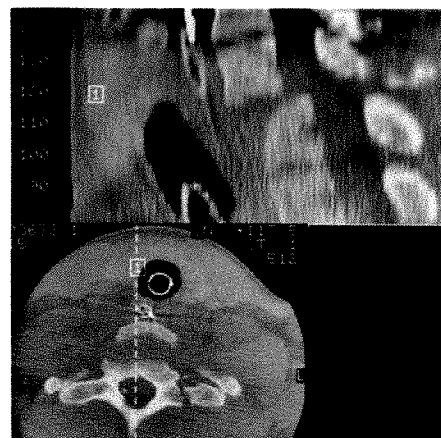
A, Chest radiograph obtained on admission in 37-year-old man after a motor vehicle accident reveals a widened and poorly defined superior mediastinum. An erect view could not be obtained because of a cervical spine injury.

B, CT scan through upper mediastinum reveals increased paraspinal density bilaterally (arrows), suggesting posterior mediastinal blood. More caudal CT sections revealed no evidence of mediastinal blood or abnormality of great vessel contours.

C, Sagittally reformatted CT scan of lower cervical spine shows fracture-dislocation of C7 on T1. Superior posterior mediastinal hemorrhage was attributed to cervical spine injury, and no arteriogram was obtained because remainder of mediastinum appeared normal.



B



C

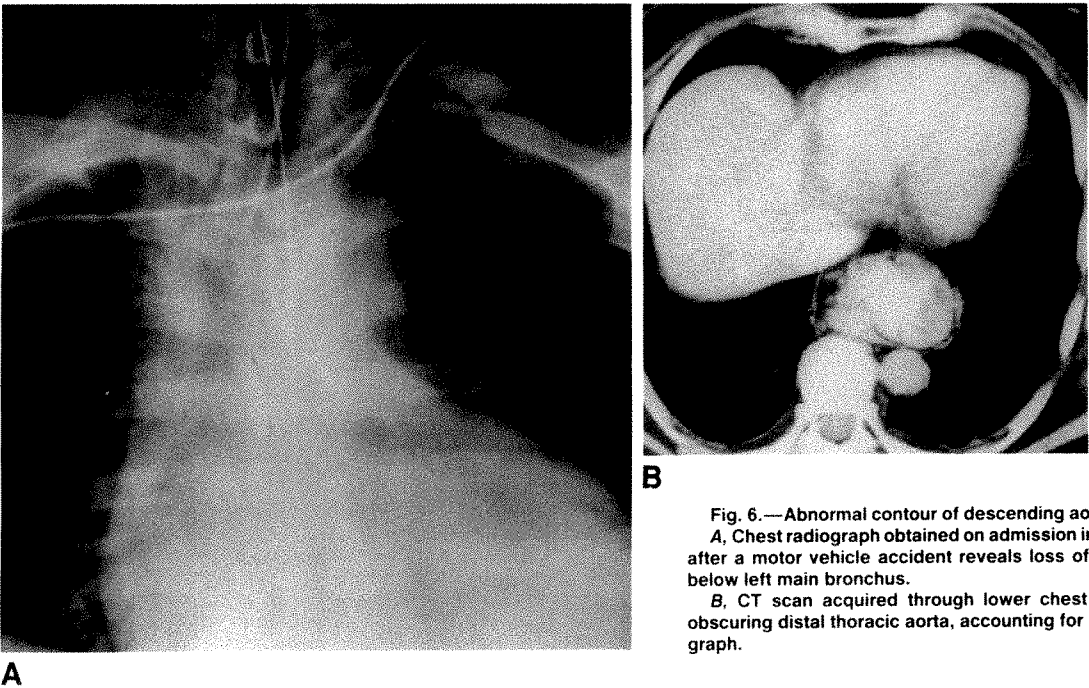


Fig. 6.—Abnormal contour of descending aorta created by hiatal hernia. A, Chest radiograph obtained on admission in supine 59-year-old woman after a motor vehicle accident reveals loss of descending aortic contour below left main bronchus. B, CT scan acquired through lower chest shows large hiatal hernia obscuring distal thoracic aorta, accounting for appearance on chest radiograph.

During the past two decades, numerous radiologic signs have been reported as having a significant association with major thoracic arterial injury, including widening of the mediastinum, loss of the smooth contours of the aortic arch and descending aorta, widening of the paraspinal soft-tissue stripes, rightward displacement of the nasogastric or endotracheal tube, and an apical extrapleural cap [1, 3–10, 18–23]. In actuality, the appearance of these various radiologic signs indicates the presence of mediastinal hemorrhage, which in a minority of patients is accompanied by major arterial injury [3, 22]. Thus, radiologic findings of mediastinal hemorrhage serve to select patients for thoracic arteriography. In our experience it is extremely rare for major vascular injury to occur without coincident mediastinal bleeding [3].

A number of factors compromise the value of the chest radiograph as a screening test for mediastinal hemorrhage. In many cases the radiograph must be obtained with the patient in the supine position, frequently because of concurrent injury. This projection tends to distort and magnify the mediastinal contours and is overly sensitive in suggesting the

presence of mediastinal hemorrhage [3, 9, 22, 23]. The radiologic evaluation of the mediastinum frequently is compromised by (1) poor exposure obtained with mobile radiographic units, a limitation accentuated in large or obese patients; (2) frequent inability of the patient to achieve full inspiration; (3) superimposed concurrent thoracic disease such as atelectasis, paramediastinal lung contusion, medial pleural effusion, and aspiration; (4) superimposition of devices such as backboard and physiologic support tubes and lines; and (5) acquired alterations in mediastinal anatomy, such as excessive mediastinal fat and vascular ectasia, and congenitally variant vascular anatomy.

The use of CT scanning as an adjunctive screening method in such cases has been investigated previously and remains controversial [10–17, 24]. In this study we examined a carefully selected group of patients for signs of mediastinal hemorrhage. Only those patients with equivocal signs of mediastinal hemorrhage on plain chest radiographs or technically unsatisfactory plain chest films were referred for CT study. Patients with unequivocal signs of mediastinal hemorrhage on radiographs were excluded from the study and underwent immediate thoracic angiography. Although for most patients in this prospective study there was low or moderate clinical suspicion of thoracic great vessel injury, patients for whom there was high clinical suspicion could also be evaluated by thoracic CT if the chest radiograph was normal or equivocal. However, patients for whom there was a high clinical suspicion for thoracic arterial injury could also be referred for arteriography directly at the discretion of the attending traumatologist when chest radiographs were equivocal or even normal. In this series, no patient with an unequivocally normal admission chest radiograph underwent thoracic arteriography.

The potential use of CT in the investigation of possible aortic injury was initially described by Heiberg et al. [11] in a small series of 10 patients. They were able to identify me-

TABLE 4: Trend in the Use of Thoracic Arteriography to Evaluate the Aorta After Blunt Trauma

Year	All Blunt Trauma		Blunt Chest Trauma	
	Total	% Undergoing Arteriography	Total	% Undergoing Arteriography
1986	518	12	1717	6
1987	539	15	1773	7
1988 <sup>a</sup>	619	10	2066	5
1989	668	10	2187	4

Note.—A comparison of the data from 1986 and 1987 with data from 1988 and 1989 shows a significant decrease in the use of thoracic angiography for all blunt trauma ( $p < .001$ ) and for blunt thoracic trauma ( $p < .01$ ).

<sup>a</sup> Year this study was initiated.



diastinal hemorrhage on CT with neither false-positive nor false-negative scans, as confirmed by aortography.

In our prospective study, dynamic enhanced thoracic CT was regarded as abnormal if either mediastinal hemorrhage was detected or a direct abnormality of the aorta or proximal great vessels was observed. On the basis of these criteria, 16 scans (18%) were abnormal out of a total of 90 scans. Of these 16 abnormal scans, great vessel injury was demonstrated in four (27%) of the 15 patients who underwent arteriography, and arteriography was normal in the other 11 patients. Direct aortic injury per se was visualized in only two (13%) abnormal CT studies, but evidence of mediastinal hemorrhage was seen in these and the other two angiographically abnormal studies.

The CT examination was technically suboptimal in five patients and was initially interpreted as equivocal in six patients. Thoracic angiography was normal in these 11 patients. However, in 63 patients (70%) CT scans revealed neither mediastinal hemorrhage nor abnormality of the aortic contour, thus sparing these patients the angiography that otherwise would have been performed. In addition, all six equivocal CT scans were retrospectively interpreted as normal by attending staff radiologists without knowledge of the ultimate clinical outcome. In this study, an improvement in resident interpretations was noted over the course of the study with most equivocal readings occurring early in the study period.

Our results conflict with those of Miller et al. [13], who reported five patients with arterial injury in whom CT did not show mediastinal hemorrhage. However, two of their patients had injuries involving the vertebral arteries and one had an injury to the subclavian artery. The two vertebral artery injuries required no surgical repair. One patient with a false-negative CT study had been imaged without administration of IV contrast material. The remaining CT scan in the group was thought in retrospect to show a mediastinal hemorrhage.

Godwin and Korobkin [14] also cautioned about the unreliability of CT scanning in this setting, but failed to cite any false-negative reports. Kubota et al. [15] reported a single case in which CT scanning failed to demonstrate a descending aortic injury. The scans were degraded by artifact in the area of injury, and, in retrospect, manipulation of CT window settings revealed an intimal flap in the aorta. No mention was made if an adjacent hematoma or mediastinal hemorrhage was present.

Thoracic arteriography is both time-consuming and invasive and should not be performed in an indiscriminate fashion. On the basis of our experience, we believe that patients in whom radiologic findings of mediastinal contour abnormality are uncertain and there is a low to moderate clinical suspicion of great vessel injury, based upon history and physical examination, are best evaluated by dynamic enhanced thoracic CT. Angiography should be reserved for those patients in whom CT reveals evidence of either mediastinal hemorrhage or direct signs of vascular injury. Patients with a good-quality thoracic CT result or CT observations that explain equivocal findings on chest radiograph should not undergo thoracic angiography.

Although our experience with thoracic CT scanning as an ancillary screening test to obtaining chest radiographs has been useful in our clinical setting, we believe that further

studies of this kind should be performed to verify this experience. In addition, institutions that receive a small number of patients with major trauma and have limited experience with both chest radiographs and CT of mediastinal hemorrhage may appropriately be more comfortable performing arteriography in patients admitted with a history of blunt decelerating thoracic trauma.

## REFERENCES

1. Kram HB, Wohlmuth MK, Appel PL, Shoemaker WE. Clinical and radiographic indications for aortography in blunt chest trauma. *J Vasc Surg* 1987;2:168-176
2. Rich NM, Spencer FC. *Vascular trauma*. Philadelphia: Saunders, 1978:425-440
3. Mirvis SE, Bidwell JK, Buddemeyer EU, et al. Value of chest radiography in excluding aortic rupture. *Radiology* 1987;163:487-493
4. Stark P. Traumatic rupture of the thoracic aorta: a review. *Crit Rev Diagn Imaging* 1984;21:239-255
5. Sturm JT, Olsen FR, Ceceio JJ. Chest roentgenographic findings in 26 patients with traumatic rupture of the thoracic aorta. *Ann Emerg Med* 1983;12(10):598-600
6. Gundry SR, Burney RE, Mackenzie JR, et al. Assessment of mediastinal widening associated with traumatic rupture of the aorta. *J Trauma* 1983;23:292-299
7. Marnocha KE, Maglinte DDT. Plain-film criteria for excluding aortic rupture in blunt chest trauma. *AJR* 1985;144:19-21
8. Gundry SR, Williams S, Burney RE, MacKenzie JR, Cleo KJ. Indications for aortography after blunt chest trauma: a reassessment of radiographic findings associated with traumatic rupture of the aorta. *Invest Radiol* 1983;18:230-237
9. Woodring JH, Loh FK, Kyrscio RJ. Mediastinal hemorrhage: an evaluation of radiographic manifestations. *Radiology* 1984;151:15-21
10. Mirvis SE, Kostrubiak I, Whitley NO, Goldstein L, Rodriguez A. Role of CT in excluding major arterial injury after blunt thoracic trauma. *AJR* 1987;149:681-685
11. Heiberg E, Wolverson MK, Sundaram M, Shields JB. CT in aortic trauma. *AJR* 1983;140:1119-1124
12. Egan TJ, Neiman HL, Herman JR, et al. Computed tomography in the diagnosis of aortic aneurysm, dissection, or aortic injury. *Radiology* 1980;136:147-151
13. Miller FB, Richardson JD, Hollis AT, Cujer HM, Willing SR. Role of CT in the diagnosis of major arterial injury after blunt thoracic trauma. *Surgery* 1989;106:596-603
14. Godwin JD, Korobkin M. Acute disease of the aorta. *Radiol Clin North Am* 1983;21:551-574
15. Kubota RT, Tripp MD, Tisnado J, Cho S. Evaluation of traumatic aortic rupture of the descending aorta by aortography and computed tomography: case report with follow-up. *J Comput Tomogr* 1985;9:237-240
16. Goodman PC. CT of chest trauma. In: Federle MP, Brant-Zawadzki M, eds. *Computed tomography in the evaluation of trauma*, 2nd ed. Baltimore: Williams & Wilkins, 1986:186-190
17. Charkravarty M. Utilization of aortography in trauma. *Radiol Clin North Am* 1986;24:383-396
18. Sturm JT, Marsh DG, Bodily KC. Ruptured thoracic aorta: evolving radiologic concepts. *Surgery* 1971;85:363-367
19. Wilson RF, Arbulu A, Bassett JS, Walt AJ. Acute mediastinal widening following blunt chest trauma. *Arch Surg* 1972;104:551-558
20. Seltzer SE, D'Orsi C, Kirshner R, DeWeese JA. Traumatic aortic rupture: plain radiographic findings. *AJR* 1981;137:1011-1014
21. Kirshner R, Seltzer S, D'Orsi C, DeWeese JA. Upper rib fracture and mediastinal widening: indications for aortography. *Ann Thorac Surg* 1983;35:450-454
22. Ayella RJ, Hankins JR, Turney SZ, Cowley RA. Ruptured thoracic aorta due to blunt trauma. *J Trauma* 1977;17:199-205
23. Schwab CW, Lawson RB, Lind JF, Garland LW. Comparison of supine and upright portable chest films to evaluate the widened mediastinum. *Ann Emerg Med* 1984;13:896-899
24. Brooks AP, Olsen LK, Shackford SR. Computed tomography in the diagnosis of traumatic rupture of the thoracic aorta. *Clin Radiol* 1989;40(2):127-132

## Book Review

**The Radiologic Clinics of North America. Lung Cancer.** Guest editor: John H. Woodring. Philadelphia: Saunders, May 1990;28(3):489-667. \$25; by subscription, 6 issues annually for \$93

In his preface to this issue of the *The Radiologic Clinics of North America*, Dr. Woodring describes his product "as a virtually complete treatise on the subject of imaging in lung cancer as of 1990." In most respects, the book nearly fulfills that billing.

The issue begins with an excellent and insightful discussion by David M. Epstein of the role of radiologic screening in lung cancer. Succeeding contributions include discussions of gallium imaging; the solitary pulmonary nodule; several discussions of staging the various portions of the thorax on the basis of findings on plain films, CT scans, and MR images; and a brief review of biopsy and ventilation-perfusion scanning. Coverage of the evaluation of mediastinal lymph nodes is particularly detailed. The one area of omission is the use of MR for evaluation of the chest wall. Many recent articles indicate that this may be the best method of evaluating soft-tissue extension of tumor, particularly in the region surrounding the apices and especially including the axilla and brachial plexus.

It would have been virtually impossible to avoid repetition and overlap among the various articles by different authors. Fortunately, however, the problem of contradiction is avoided. Self-contradictory articles within a single compilation often result in significant difficulty in understanding, but that is not the case in this book. Some overlap is clearly useful. A reader wishing a thorough discussion of a particular subject can find the relevant material more easily when it is repeated from several different points of view. Discussions of the size and CT appearance of lymph nodes, for example, can be found in four different articles within this issue. On the other hand, a reader attempting to peruse the book from cover to cover might find the repetition distracting and annoying. Two different articles, one by Frederick Stitik and one by Philip Templeton and associates, include slightly different versions of the same tables. These tables are noticeably more complete and understandable in Dr. Stitik's article, and the

brief versions in the other article easily could have been eliminated by giving a reference to the previous chapter.

The greatest problem, found throughout this issue, is the apparent reluctance of the authors and editor to recommend one study over another. Each chapter apparently has been written by a proponent of the technique being discussed. With the exception of the section on MR imaging, the authors understandably tend to highlight the value of the technique they have chosen to discuss. The reader thus is left with the impression that thorough imaging of bronchogenic carcinoma requires using virtually all techniques in virtually all cases. Neither the authors nor the editor indicates clearly when particular procedures are less useful than procedures discussed in other sections of this book.

The cover-to-cover reader is left in a quandary about the most efficient evaluation of patients with various initial images of lung cancer. How, for example, does the evaluation of a 1-cm peripheral mass differ from that of a larger, more central mass? Further, a reader will have great difficulty using this work for reference to the most efficient imaging workup of a specific patient. It would have been useful to have the editor, or one of the authors, critique the individual sections of this compilation.

Dr. Woodring has succeeded mostly in compiling an up-to-date collection of discussions of lung cancer. The book is thus an excellent source of information to increase our knowledge of this important subject. It is unfortunate that the nonjudgmental approach results in some confusion. This work nevertheless can be recommended as a convenient source of encyclopedic information.

David S. Feigin  
University of California, San Diego  
La Jolla, CA 92093

# Pathogenesis of Pulmonary Edema During Interleukin-2 Therapy: Correlation of Chest Radiographic and Clinical Findings in 54 Patients

Richard R. Saxon<sup>1</sup>  
 Jeffrey S. Klein<sup>1</sup>  
 Michael H. Bar<sup>2</sup>  
 Paul Blanc<sup>3</sup>  
 Gordon Gamsu<sup>1</sup>  
 W. Richard Webb<sup>1</sup>  
 Frederick R. Aronson<sup>2</sup>

The pathogenesis of pulmonary edema that occurs during interleukin-2 therapy has often been attributed to an increase in pulmonary capillary permeability. However, renal insufficiency, fluid overload, and hypotension also develop in many patients. These manifestations of systemic toxicity may contribute to the development of pulmonary edema during therapy. Understanding the cause of pulmonary edema during interleukin-2 therapy could directly affect patients' care. Therefore, we reviewed the chest radiographs and clinical course of 54 patients who received high-dose interleukin-2 therapy and lymphokine-activated killer cells for advanced carcinoma. The type, frequency, and course over time of pulmonary abnormalities were recorded and correlated with clinical measures of renal function, fluid status, and blood pressure. Focal or diffuse parenchymal lung opacities were found on radiographs in 43 (80%) of 54 patients. Findings of interstitial pulmonary edema were most common, occurring in 76% of patients. Weight gain, hypotension, and elevation of the serum creatinine level were not associated statistically with interstitial edema. Diffuse air-space disease developed in 20% of patients. Focal consolidation, which was associated with positive central venous catheter cultures ( $p < .03$ ), developed in 28% of patients. Pleural effusion occurred in 48% of patients and was associated with all types of parenchymal disease.

These data suggest that the frequent development of pulmonary edema during interleukin-2 therapy is not due to renal insufficiency, fluid overload, or hypotension, but is more likely the result of an interleukin-2-related increase in pulmonary capillary permeability.

*AJR* 156:281-285, February 1991

Interleukin-2 (IL-2), a glycoprotein secreted by activated T lymphocytes, is a promising drug used for immunotherapy in the treatment of advanced carcinoma [1-4]. It augments the tumoricidal activity of natural killer cells both in vitro and in vivo. Clinical trials have shown that IL-2, either alone or in combination with these lymphokine-activated killer (LAK) cells, can induce tumor regression. In animal models, and possibly in clinical trials, there is a dose-response relationship between antitumor activity and IL-2 dose. However, significant treatment-related pulmonary toxicity has been observed and often limits the amount of IL-2 a patient can receive [5-7].

It has been hypothesized that the pulmonary compromise occurring in these patients may be due to pulmonary edema from increased capillary permeability. Although the mechanism for increased capillary permeability is unknown, it may be due to an effect of IL-2-activated natural killer cells or IL-2-induced cytokines on vascular endothelium [6, 8]. The relationship of IL-2 therapy to pulmonary edema, however, has been obscured by the frequent concurrence of multiorgan system dysfunction manifested by hypotension, azotemia, oliguria, and weight gain due to fluid retention. Each of these factors could contribute to the pulmonary abnormalities observed during IL-2 therapy.

We reviewed the chest radiographs and clinical courses of 54 patients who received high-dose IL-2 in order to clarify further the pathogenesis of pulmonary

Received June 6, 1990; accepted after revision August 14, 1990.

Presented at the annual meeting of the American Roentgen Ray Society, Washington, DC, May 1990.

This work was supported in part by National Institutes of Health contract N01-CM73702 and National Institutes of Health Clinical Research Center Grant M01-RR0079.

<sup>1</sup> Department of Radiology, University of California, San Francisco, School of Medicine, 505 Parnassus Ave., San Francisco, CA 94143-0628. Address reprint requests to J. S. Klein in rm. M-396.

<sup>2</sup> Cancer Research Institute, University of California, San Francisco, School of Medicine, 505 Parnassus Ave., San Francisco, CA 94143-0128.

<sup>3</sup> Department of Medicine, University of California, San Francisco, School of Medicine, 505 Parnassus Ave., San Francisco, CA 94143-0128.

0361-803X/91/1562-0281  
 © American Roentgen Ray Society



edema in these patients. In addition, we characterized the type, frequency, and time course of parenchymal and pleural abnormalities that occur during therapy.

### Subjects and Methods

We treated 78 patients with one of 12 phase II, high-dose, IL-2 protocols at the University of California, San Francisco, Medical Center between April 1986 and March 1989. Protocols varied according to the dose of IL-2 and inclusion or exclusion of LAK cells. Fifty-four patients (37 men and 17 women) with both complete clinical and radiologic data available were evaluated. No apparent bias was introduced through the exclusion of the 24 patients with incomplete radiologic or clinical data. The mean age was 44 years, with a range from 19 to 67 years. The majority of patients had either melanoma (30 patients) or renal cell carcinoma (16 patients). The remaining eight patients had a variety of other malignant neoplasms. Eligibility criteria for inclusion in an IL-2 protocol included (but were not limited to): serum creatinine level of 1.5 mg/dl or less or a creatinine clearance greater than 60 ml/min, FEV<sub>1</sub> (forced expiratory volume in 1 sec) greater than 2 or greater than or equal to 75% of that predicted for age and height, no evidence of congestive heart failure, no history of myocardial infarction or serious arrhythmia, and no signs of myocardial ischemia on ECG and treadmill stress test. Other eligibility criteria have been presented in detail elsewhere [4]. Prior chemotherapy, radiation therapy, or immunotherapy was generally not a contraindication to IL-2 protocol enrollment. Investigational review board approval was obtained for each protocol, and all patients gave written, informed consent.

Each cycle of therapy with IL-2 lasted 15–16 days and was divided into three phases: an initial “priming” phase of IL-2 administration, a “rest” phase during which patients received no IL-2 treatment and leukapheresis was performed on those patients who were enrolled on protocols that used LAK cells, and a “final” phase during which patients received IL-2 either alone or in combination with LAK cell infusions. Recombinant human IL-2 [9] was provided by Cetus Corporation (Emeryville, CA).

All 12 protocols were designed to deliver the maximally tolerated dose of IL-2 and were therefore, by definition, associated with significant treatment-limiting toxicity. Toxicity was defined and graded according to previously described criteria [5]. A serum creatinine level of between 5 and 10 was defined as grade 3 renal toxicity. Hypotension requiring pressors for less than 48 hr was defined as grade 3 hypotension. Dyspnea at rest was defined as grade 3 pulmonary toxicity. Urine output of less than 80 ml over 8 hr was defined as grade 3 oliguria. Laboratory evaluations including serum levels of blood urea nitrogen and creatinine were obtained every other day during the “priming” phase and every day during the “final” phase of IL-2 administration. Vital signs, weight, and urine output were recorded daily.

All patients enrolled in an IL-2 study had a baseline posteroanterior and lateral chest radiograph within 2 weeks of initiating therapy. During the “priming” and “final” phases of therapy, patients underwent mandatory chest radiographs approximately every other day, and additional studies were performed as clinically indicated. These films were portable, anteroposterior radiographs obtained in the intensive care unit. Chest radiographs obtained immediately before and during therapy were collected and placed in chronological order. Two radiologists, blinded to the clinical data, scored each film for the presence of interstitial or air-space opacities, pleural effusion, pneumothorax, and endotracheal intubation.

Clinical data for each patient were retrieved from a computer data base audited and maintained by the Clinical Trials Monitoring Service

of the National Cancer Institute. Data items selected for review included the patient's age, sex, and underlying malignant neoplasm, as well as the maximal gain in body weight, peak serum creatinine level, and the presence of blood or central venous catheter cultures that were positive for any organism. In addition, we recorded whether or not oliguria, hypotension, or clinical pulmonary toxicity occurred during therapy.

The clinical and radiologic data were analyzed with a standard computer statistical package. Age, peak serum level of creatinine, and the time from initiation of therapy to the earliest findings on radiographs were entered as continuous variables; the remaining parameters were entered as dichotomous (yes/no) variables defined as follows: sex; presence or absence of renal cell carcinoma; presence or absence of melanoma; weight gain of 10% or more above baseline; oliguria, renal toxicity, pulmonary toxicity, or hypotension, all grades greater than or equal to 3; positive blood culture; positive central venous catheter culture; any abnormality on radiographs during therapy; development of interstitial pulmonary edema; development of focal air-space opacification; development of diffuse air-space opacification; development of a pleural effusion; development of a pneumothorax; and requirement for endotracheal intubation.

The difference in frequency of abnormalities on radiographs given the presence or absence of dichotomous predictor variables (such as oliguria) were tested with either a chi-square or Fisher exact test. Continuous potential predictor variables of radiologic abnormality (such as age) were analyzed by using logistic regression modeling. For both dichotomous and continuous variables, the association with radiologic abnormalities is described by the odds ratio together with its 95% confidence intervals. The odds ratio provides an estimate of the odds of abnormality among those with a specific risk factor compared with those without this risk factor. An odds ratio of 1.0 indicates no difference in risk. Ninety-five percent confidence intervals excluding 1.0 are associated with a *p* value less than .05. For certain associations of interest, we performed multiple logistic regression analysis also.

### Results

#### *Clinical and Laboratory Data*

Nineteen patients (35%) sustained a 10% or greater increase in weight above baseline, with a mean peak weight gain in all 54 patients of 7.4% (SD = 5%, range = 0–18). The mean peak serum creatinine level was 3.1 mg/dl (SD =  $\pm 1.9$ , range = 0.9–9.0). Forty-four patients (82%) developed oliguria (grade  $\geq 3$ ). Seven (13%) had blood cultures positive for any organism, and 11 (20%) had central venous catheter cultures positive for any organism. Six of the seven patients with positive blood cultures had simultaneous positive catheter cultures. Grade 3 or higher hypotension developed in 30 patients (56%). Grade 3 or higher pulmonary toxicity was seen in 16 patients (30%), including four (7%) who required intubation. Three patients developed pneumothoraces: two in association with acute respiratory distress syndrome and one after placement of a subclavian catheter. Two patients died within 4 weeks of initiation of therapy, one from gastrointestinal hemorrhage and one from an arrhythmia.

#### *Findings on Radiographs*

Forty-three patients (80%) developed focal and/or diffuse parenchymal opacities during the course of therapy. In 23

(53%) of the 43 patients, the radiologic abnormalities developed within 4 days of initiation of therapy, whereas 32 (74%) had abnormalities by 8 days. However, 11 (26%) developed radiologic findings 9 days or more after the initiation of therapy. Radiologic features of interstitial pulmonary edema including Kerley lines, indistinct vascularity, peribronchial cuffing, and hazy perihilar densities were most common, seen in 41 (76%) of 54 patients (Fig. 1). In 11 patients (20%), diffuse confluent air-space consolidation developed, generally 2 days after the onset of interstitial edema (Fig. 2). Diffuse air-space opacities were always preceded by, and never occurred more than 4 days after, the development of interstitial edema. Eight of 11 patients with diffuse air-space opacities had grade 3 or higher pulmonary toxicity. Focal lobar or segmental air-space consolidation was seen in 15 patients (28%) and occurred without antecedent interstitial pulmonary edema. Pleural effusion was a common finding, seen in 26 patients (48%, Fig. 3). In 23 patients, the effusion was associated with diffuse interstitial edema or air-space disease; in one patient a small effusion was present ipsilateral to focal air-space consolidation, and in two patients the effusion was an isolated finding.

#### Statistical Relationships

No statistical association was found between measures of hypotension, weight gain, or elevated levels of serum creatinine and the radiologic findings of interstitial pulmonary edema; for none of these was the odds ratio greater than 2.0, and none were statistically significant at less than the 0.15 level. A borderline statistically significant association existed between the frequency of interstitial pulmonary edema and oliguria (odds ratio = 2.9, 95% confidence interval = 0.96–9.00). The odds ratio was similar after taking into account

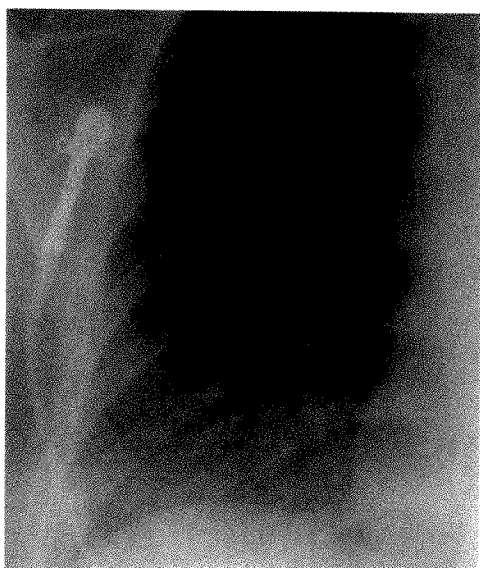


Fig. 1.—27-year-old woman with metastatic melanoma. Chest radiograph obtained 4 days after start of interleukin-2 therapy shows ground-glass opacities, peribronchial cuffing, and indistinct vascular margins indicative of interstitial pulmonary edema.

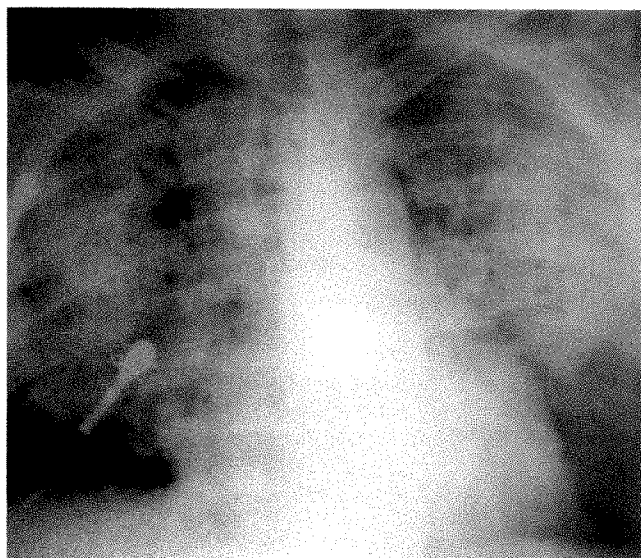


Fig. 2.—51-year-old man with metastatic renal cell carcinoma whose condition deteriorated 15 days after therapy was started. Chest radiograph shows diffuse air-space disease. Patient required intubation and bilateral chest tubes for pneumothoraces.

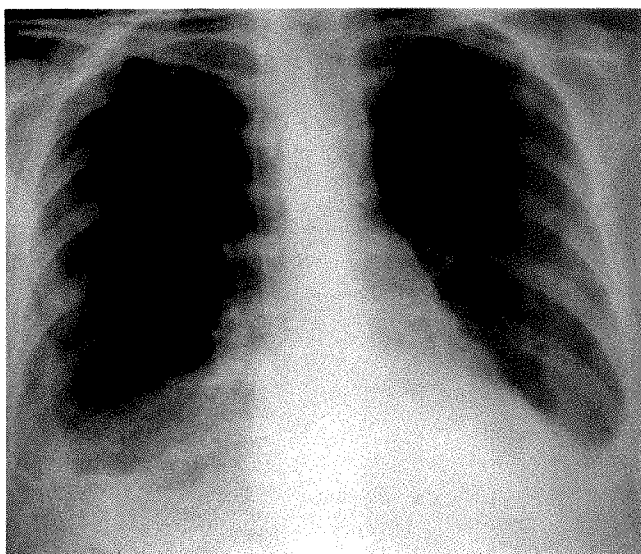


Fig. 3.—42-year-old woman with metastatic renal cell carcinoma. Radiograph obtained 5 days after treatment was started shows moderate bilateral pleural effusions. Interstitial pulmonary edema developed subsequently.

age, sex, type of malignancy, weight gain, and renal toxicity by multivariate logistic regression analysis (odds ratio = 2.5, 94% confidence interval = 0.83–7.50). A significant association existed between the presence of a positive central venous catheter culture and the development of focal air-space opacification ( $p < .03$ ). Although pulmonary toxicity diagnosed clinically (grade  $\geq 3$ ) was significantly ( $p < .007$ ) associated with findings of interstitial pulmonary edema on radiographs, no other statistically significant associations existed between

any of the findings on radiographs and either the dichotomous or continuous clinical variables.

## Discussion

During clinical trials in the last 5 years, interleukin-2 therapy in conjunction with LAK cells has produced objective tumor regression in 15–30% of patients, and sustained complete remissions in approximately 5–10% of patients with metastatic renal cell carcinoma and melanoma [1–4]. Severe pulmonary toxicity, however, occurs frequently in patients receiving IL-2 therapy. In our study, dyspnea at rest occurred in 30% and intubation was required in 7% of patients. Eighty percent of our patients had radiologic findings of diffuse or focal parenchymal disease, a prevalence similar to that (73%) reported by Vogelzang and colleagues (presented at the annual meeting of the Radiological Society of North America, November 1988). However, they reported a 47% prevalence of pulmonary edema, whereas the frequency of radiologically detectable interstitial pulmonary edema was 76% in our study. This discrepancy may relate to differences in treatment protocols, eligibility criteria, or criteria for the radiologic diagnosis of pulmonary edema.

The cause of pulmonary edema during IL-2 therapy remains a subject for debate. Increased capillary permeability may be responsible [10]. Rosenstein et al. [11] used  $^{125}\text{I}$ -labeled albumin to show a significant, dose-related increase in vascular permeability in the lungs and other organs of IL-2 treated mice. However, IL-2 does not appear to induce a vascular leak directly. Animals rendered immunoincompetent by prior exposure to cyclophosphamide have a very high tolerance to treatment with IL-2, suggesting that an intact immune system is necessary for the development of pulmonary toxicity [6].

Several mechanisms have been identified that could mediate a vascular leak and produce interstitial pulmonary edema during IL-2 therapy. For example, IL-2 promotes the adhesion of natural killer cells to endothelial cells and these IL-2-activated natural killer cells can lyse vascular endothelium in vitro [8, 12]. Thus, cell-mediated pulmonary vascular injury may produce an increase in capillary permeability. On the other hand, IL-2 induces pyogenic cytokines, such as tumor necrosis factor and interleukin-1, which may alter endothelial permeability and are thought to be mediators of the septic shock syndrome [6].

Factors other than increased capillary permeability, however, could contribute to the development of interstitial pulmonary edema, pleural effusions, and diffuse air-space disease during IL-2 therapy. Hypotension often develops during therapy, and patients consequently receive a significant amount of IV fluid. Additionally, oliguria, increases in serum creatinine level, and weight gain due to fluid retention routinely occur during therapy. We did not find an association between either increased serum creatinine level, weight gain, or hypotension and the radiologic manifestations of pulmonary toxicity during IL-2 therapy. Although we did find a borderline statistical association between oliguria and interstitial pulmonary edema, we consider oliguria an unreliable indicator of

systemic toxicity because of difficulties in accurately assessing decreased urine output in the clinical setting. Interstitial pulmonary edema, therefore, appears to be an independent toxic effect of IL-2 therapy.

Cardiac dysfunction also has been postulated as a cause of IL-2-related pulmonary edema [7]. IL-2 can induce a hemodynamic profile similar to that of septic shock: hypotension, decreased systemic vascular resistance, tachycardia, pre-renal azotemia, and a normal or increased cardiac output [13]. However, two groups evaluated hemodynamic variables in patients undergoing IL-2 therapy and found no increase in pulmonary capillary wedge pressure [10, 13]. Therefore, it seems unlikely that left ventricular failure is the predominant cause of the interstitial pulmonary edema that occurs during IL-2 therapy.

A more severe complication of IL-2 therapy is diffuse, confluent air-space disease. Twenty percent of our patients developed a syndrome similar to the adult respiratory distress syndrome, which is a form of increased capillary permeability edema. A combination of factors may be responsible. Four of the 11 patients with diffuse air-space disease had positive blood or central venous catheter cultures. Although this association was not statistically significant, treatment-related bacteremia may lead to diffuse air-space opacities in some patients. Of more importance is the fact that diffuse air-space disease always occurred 2–4 days after interstitial edema. In the majority of patients, therefore, diffuse air-space disease may represent the progression of IL-2-related increased capillary permeability edema, without concurrent infection.

Pleural effusion occurred in 48% of our patients. In 88% of these patients, the pleural effusion was associated with either diffuse air-space disease or interstitial pulmonary edema. Pleural effusion most likely represents another manifestation of increased capillary permeability. Pleural effusion has been described in patients with other types of capillary permeability edema, such as the adult respiratory distress syndrome [14].

The cause of focal air-space disease remains unclear. This finding is unlikely to be due to increased capillary permeability, because focal opacities would be an unusual manifestation of pulmonary edema. Nosocomial "sepsis" has been described in 19% of 107 patients receiving high-dose IL-2 therapy [15]. IL-2 induces an acquired defect in neutrophil chemotaxis that could be responsible for the high frequency of central venous catheter-associated bacteremia seen during therapy [16]. We identified a statistically significant association between positive central venous catheter cultures and the development of focal air-space disease. This association suggests that focal air-space disease may represent pneumonia caused by bacteremia.

In conclusion, our results support the hypothesis that pulmonary edema during IL-2 therapy is caused by increased capillary permeability; renal insufficiency, fluid overload, and hypotension are not contributing factors. Further investigation into the "capillary leak" syndrome seen with IL-2 therapy is needed to help develop methods for reducing the toxic effects of this promising therapy and may give new insight into the adult respiratory distress syndrome associated with septic shock.



## REFERENCES

1. Rosenberg SA. The development of new immunotherapies for the treatment of cancer using interleukin-2. *Ann Surg* **1988**;208:121-135
2. Lotze MT, Mule JJ, Rosenberg SA. New approaches to the immunotherapy of cancer using interleukin-2. *Ann Intern Med* **1988**;108:853-864
3. Rosenberg SA, Lotze MT, Muul LM, et al. A progress report on the treatment of 157 patients with advanced cancer using lymphokine-activated killer cells and interleukin-2 or high-dose interleukin-2 alone. *N Engl J Med* **1987**;316:889-897
4. Bar MH, Sznol M, Atkins MB, et al. Metastatic malignant melanoma treated with combined bolus and continuous infusion interleukin-2 and lymphokine-activated killer cells. *J Clin Oncol* **1990**;8:1138-1147
5. Margolin KA, Rayner AA, Hawkins MJ. Interleukin-2 and lymphokine-activated killer cell therapy of solid tumors: analysis of toxicity and management guidelines. *J Clin Oncol* **1989**;7:486-498
6. Mier JW, Aronson FR, Numerof RP, Vachino G, Atkins MB. Toxicity of immunotherapy with interleukin-2 and lymphokine-activated killer cells. *Pathol Immunopathol Res* **1988**;7:459-476
7. Conant EF, Fox KR, Miller WT. Pulmonary edema as a complication of interleukin-2 therapy. *AJR* **1989**;152:749-752
8. Mier JW, Brandon EP, Libby P, Janicka MW, Aronson FR. Activated endothelial cells resist lymphokine-activated killer cell-mediated injury. *J Immunol* **1989**;143:2407-2414
9. McGrogan M, Doyle M, Kawasaki E, et al. Biological activity of recombinant human interleukin-2 produced in *Escherichia coli*. *Science* **1984**;223:1412-1415
10. Lee RE, Lotze MT, Skibber JM, et al. Cardiorespiratory effects of immunotherapy with interleukin-2. *J Clin Oncol* **1989**;7:7-20
11. Rosenstein M, Ettinghausen SE, Rosenberg SA. Extravasation of intravascular fluid mediated by the systemic administration of recombinant interleukin-2. *J Immunol* **1986**;137:1735-1742
12. Aronson FR, Libby P, Brandon EP, Janicka MW, Mier JW. IL-2 rapidly induces natural killer cell adhesion to human endothelial cells. *J Immunol* **1988**;141:158-163
13. Gaynor ER, Vitek L, Sticklin L, et al. The hemodynamic effects of treatment with interleukin-2 and lymphokine-activated killer cells. *Ann Intern Med* **1988**;109:953-958
14. Weiner-Kronish JP, Goldstein R, Matthay MA. Pleural effusions are frequently associated with adult respiratory distress syndrome (abstr). *Am Rev Respir Dis* **1988**;13:227A
15. Snyderman DR, Sullivan B, Gill M, Gould JA, Parkinson DR, Atkins MB. Nosocomial sepsis associated with interleukin-2. *Ann Intern Med* **1990**;112:102-107
16. Klempner MS, Noring R, Mier JW, Atkins MB. An acquired chemotactic defect in neutrophils from patients receiving interleukin-2 immunotherapy. *N Engl J Med* **1990**;332:959-965

## Book Review

**Dr. Susan Love's Breast Book.** By Susan M. Love, Reading, MA: Addison-Wesley, 385 pp., 1990. \$18.95

This book could have been subtitled "All You Wanted to Know About Your Breasts, But Did Not Know Whom to Ask". Well, ask Dr. Susan Love, a well-known and well-respected surgeon in Boston. This book was written with the assistance of Karen Lindsey, who is a published author of many magazine articles and two novels (and who probably also deserves to have her photograph on the back cover for her contribution to this fine work).

As a collaboration aimed at the general mass market, the text appears to contain a measured amount of the "women vs the male medical establishment" theme. The introduction ends with, "Knowledge is power and most women have been denied real knowledge about their own breasts. With this book, I hope to give readers some of that power." Come on now. Enough male bashing! Magazines, newspapers, and radio and television talk shows have been graphically full of women's health topics for a long, long time. Many promoting doctors are selling books or their "new techniques" at their own personal offices, between other commercials for soap and cruises to the Caribbean. There is no lack of information (or misinformation) and no male conspiracy here.

That said, I still fully recommend this book to both patients and physicians. It has a lot of useful medical information, tempered by a historical perspective of enthusiasms for "breakthroughs." An overall review of breast problems is presented. The illustrations of surgical procedures are graphic enough for the general public to understand what may happen once disease is suspected or after treatment is needed. Medical terms are explained in clear English, without talking down to the reader. The book has a conversational tone.

Women have a lot of concerns about breasts: Too large. Too small. Breasts that hurt all the time or just a few days a month. Confusion about fibrocystic disease. Fear about the possibility of cancer. And what about life after the dreaded diagnosis is made? Small questions like applying for a new insurance policy, telling coworkers of "your problem." Herb diet? Big questions like chemotherapy or radiation treatment. Radical or partial mastectomy? Love and Lindsey address all these concerns, adding insights and personal knowledge while admitting that at times there are no good answers.

The detailed discussion of diagnosis may be of particular interest to radiologists who read this review. Love and Lindsey describe the various types of mammograms and reassure patients about the lower radiation dosages produced by modern mammographic units. The

patients also are warned about "part-time" mammographic radiologists and about "breast mills" set up to make a buck, rather than take care of patients. By looking for American College of Radiology accreditation and recommendations by the local American Cancer Society, the book suggests, patients may be more likely to find the best local radiologists for their needs. These radiologists may not be conveniently next door to the patient's referring physician. I wish that readers had been warned about the "in-office" operations of surgeons and other primary clinicians, too.

Love chastises the "inexperienced" radiologists who cannot state that a lesion is benign or malignant (page 182) and, at the same time, warns the patient that some radiologists use "words . . . as if they can see what the pathology is when they're looking at shadows on the mammogram" (page 180, discussion on fibrocystic changes). So it goes.

Two other points: Love also does not believe in the baseline mammogram at age 35 or 40, because the picture certainly will change at 50 years and again at 60, due to age alone. She also states that women should "ignore" the "Wolfe classifications" because mammograms cannot predict who is more likely to develop breast cancer. Do you experts out there agree?

The book is divided into six sections. The first two deal with normal development and the myth of fibrocystic disease. Part three deals with who is at risk for cancer and gives women both a critical review of how data are collected and insight into the meaning of what they may hear about risk factors. The remaining parts examine the issues of breast cancer, diagnosis, and treatments now available. The book refers to many up-to-date articles. It also includes a diet plan to reduce fat, a list of drugs commonly used in cancer treatment, recommended cancer centers by state, and a helpful glossary of medical terms.

I think this is a wonderful book. The thoughtfulness, knowledge, and caring come through on each page. It is quite well written. I encourage all radiologists involved in breast diagnosis, all residents, and anyone concerned about women's health issues to purchase it.

Michael Crade  
Long Beach Memorial Medical Center  
Long Beach, CA 90801-1428

## Pictorial Essay

# Abnormalities of the Breast Caused by Biopsy: Spectrum of Mammographic Findings

Kimberly B. Stigers,<sup>1</sup> Joseph G. King,<sup>1</sup> Diane D. Davey,<sup>2</sup> and Carol B. Stelling<sup>1</sup>

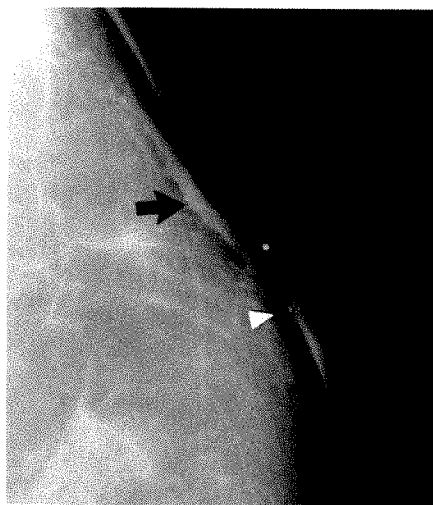
It is important for radiologists to be familiar with the spectrum of mammographic abnormalities caused by postbiopsy changes in the breast. Although many breast biopsies leave no residual abnormality, occasionally an atypical manifestation of a biopsy scar may produce a radiologic finding suspicious enough to mandate a biopsy. Problem-solving maneuvers recommended to increase confidence that a change is related to a recent biopsy include (1) skin markers; (2) comparison with preoperative films; (3) correlation with physical examination; (4) tailored mammographic views, including focal spot compression, magnification,

and tangential views; and (5) postoperative and follow-up mammograms.

### Skin Thickening

Excisional biopsy scars may produce various degrees of skin thickening (Fig. 1) and subcutaneous scarring [1]. Postoperative skin thickening generally is associated with a *localized* area of contour flattening. These changes may be more

Fig. 1.—Skin thickening 2 years after biopsy for a benign lesion. Craniocaudal view shows skin thickening and deformity (arrow) at biopsy site (metallic marker) and dystrophic calcification in areolar skin (arrowhead).



1

Fig. 2.—Skin retraction 28 years after biopsy for a benign lesion. Craniocaudal view shows long transverse radiolucency corresponding to air in a surgical deformity. Nipple retraction with flattening of areola is accentuated by compression applied during mammography. Note incidental benign secretory ductal calcifications.



2

Received June 18, 1990; accepted after revision August 28, 1990.

<sup>1</sup> Department of Diagnostic Radiology, Albert B. Chandler Medical Center, 800 Rose St., Lexington, KY 40536-0084. Address reprint requests to C. B. Stelling.

<sup>2</sup> Department of Pathology, Albert B. Chandler Medical Center, Lexington, KY 40536-0084.

AJR 156:287-291, February 1991 0361-803X/91/1562-0287 © American Roentgen Ray Society



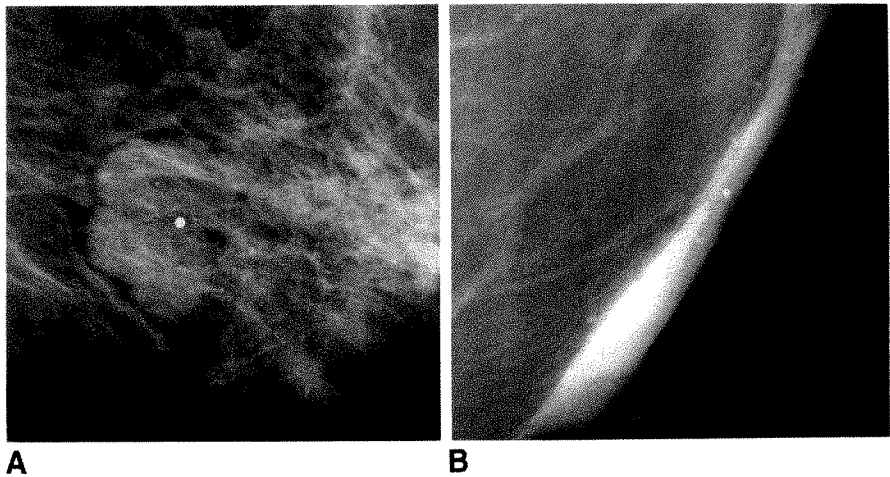


Fig. 3.—Keloid 15 years after biopsy for a benign lesion.  
A, Oblique view shows a large, smoothly lobulated density corresponding to keloid (metallic marker).  
B, Tangential view shows dystrophic calcifications in keloid.

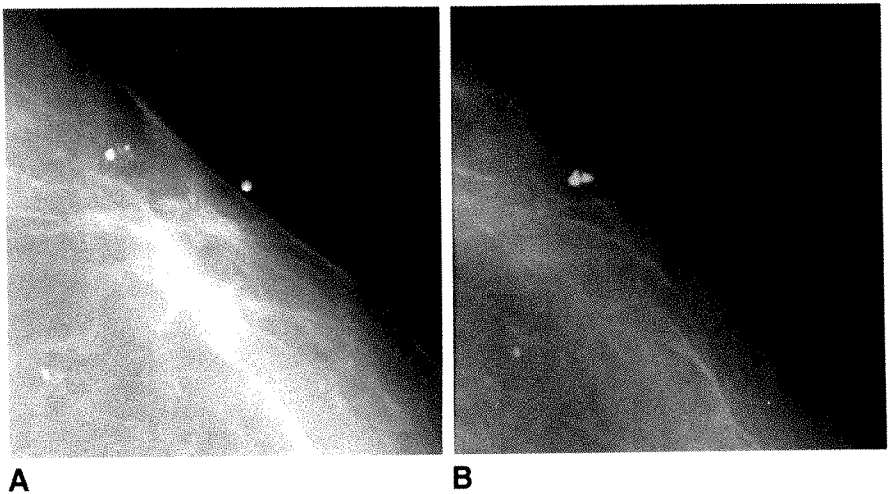


Fig. 4.—Parenchymal distortion 6 months after biopsy for a benign lesion.  
A, Tangential view shows skin thickening along scar (metallic marker) with focal retraction of the skin. New dense parenchymal stranding is seen in subcutaneous tissue.  
B, Tangential view 21 months after biopsy shows resolution of architectural distortion. Skin thickening and mild flattening of breast contour at biopsy site persist. Note incidental dystrophic calcifications.

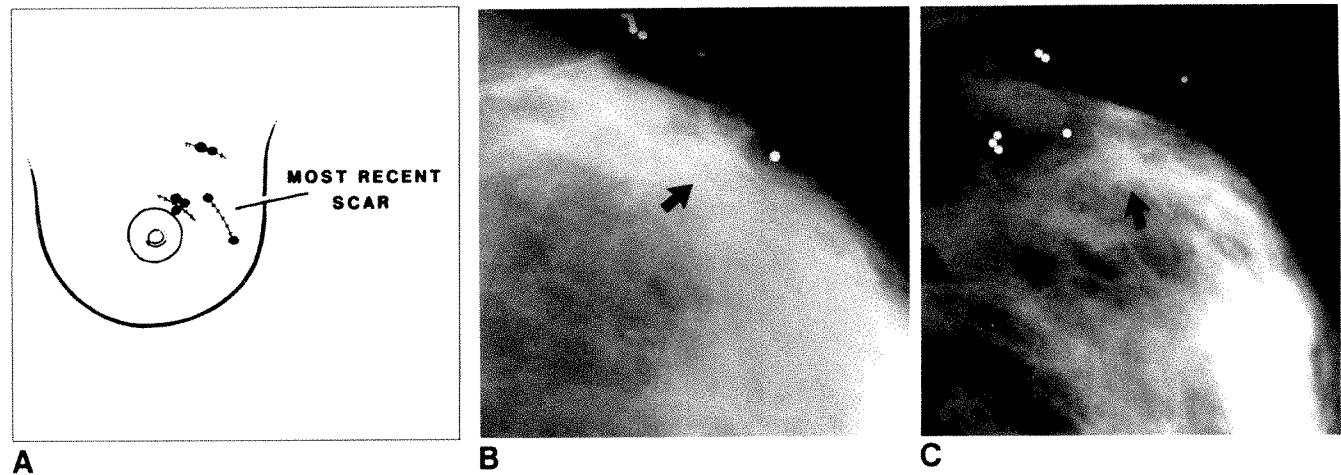
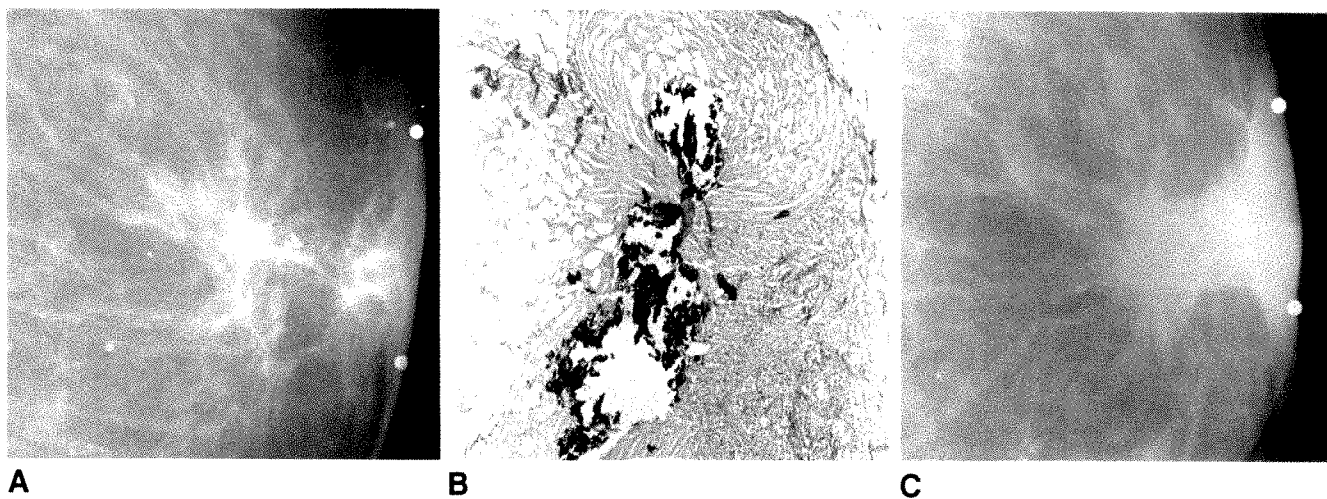
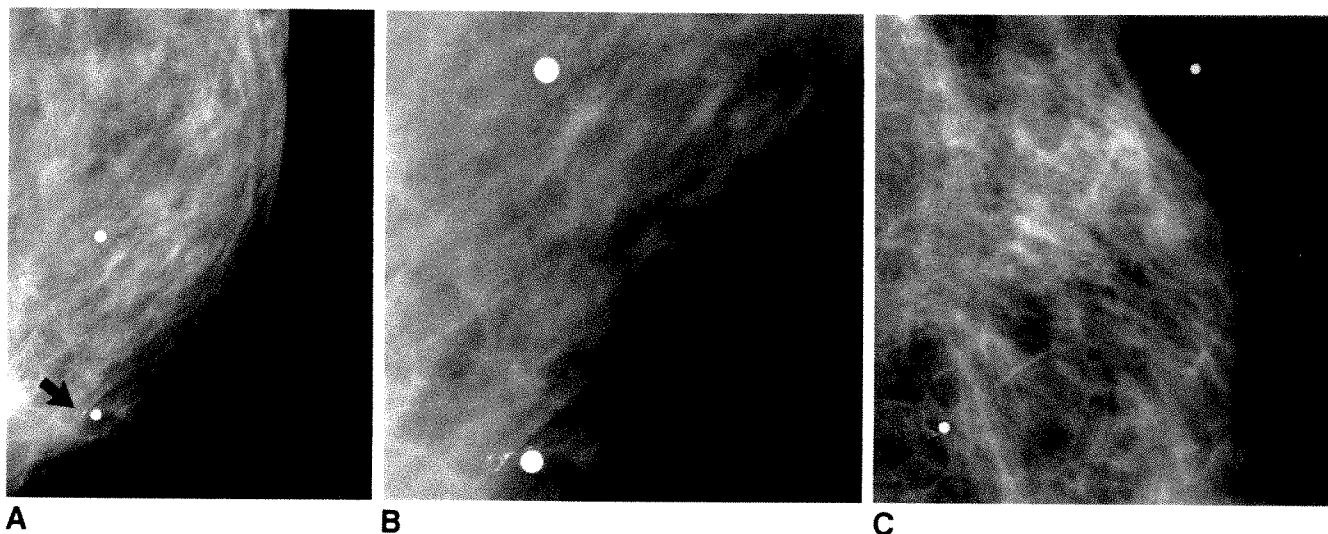


Fig. 5.—Parenchymal stellate scar 4 months after third biopsy for fibrocystic disease.  
A, Drawing shows where skin markers were taped on biopsy scars, with most recent scar marked by a single marker on each end.  
B and C, Craniocaudal (B) and oblique (C) views show new parenchymal stellate density (arrows). Because biopsy is recent and density is close to new scar, this stellate density is considered a postoperative change.



**Fig. 6.**—Parenchymal stellate scar 3 months after biopsy.  
**A**, Craniocaudal view shows stellate density and new suspicious microcalcifications in site of a biopsy that disclosed atypical ductal hyperplasia (markers on scar). A repeat biopsy was recommended.  
**B**, Histopathologic section shows dystrophic calcification and fibrous tissue composing the scar. (H and E,  $\times 13.2$ )  
**C**, Craniocaudal view 3 months after biopsy shows a stellate scar in latest biopsy site. A mammogram 3 months later showed further resolution of this density.



**Fig. 7.**—Dystrophic calcifications 6 months after lumpectomy and radiation therapy for cancer.  
**A–C**, Craniocaudal (**A**), coned (**B**), and oblique (**C**) views show a cluster of dense, irregular calcifications in inferior end of scar (arrow). These calcifications lie adjacent to the skin marker on all views, indicating a superficial location.

evident radiologically than clinically. Skin thickening may never resolve completely [1], particularly if the biopsy was complicated by infection.

#### Contour Deformity

Considerable postoperative deformity of the breast may occur, particularly after excision of large portions of tissue (Fig. 2) or if local infection complicated the biopsy.

#### Keloid

Hypertrophic scars and keloids (Fig. 3) are a result of abnormal wound healing in which collagen production ex-

ceeds collagen degradation. A hypertrophic scar is wide, reddened, and elevated. Keloids are similar, but continue to grow beyond the original dimensions of the wound, producing mounds of collagenous tissue. Keloids are seen most often in dark-skinned patients and are obvious on physical examination.

#### Architectural Distortion

Architectural distortion (Fig. 4) has been described as disordered trabecular pattern, fibrous stranding, and distortion of the normal fat-glandular interfaces [1]. This appearance is caused by subcutaneous fibrosis and shortening of Cooper ligaments. Architectural distortion is observed less frequently

3 years after biopsy than during the initial 6 months. Resolution over time aids in confirming the presence of a scar [1].

### Asymmetric Parenchyma

The area of previous biopsy often is less dense than other areas. Postbiopsy changes also can cause increased density at the biopsy site, without architectural distortion or stellate scar.

### Parenchymal Stellate Scar

Postbiopsy scarring with proliferation of connective tissue may lead to a parenchymal stellate scar that mimics scirrhous carcinoma. Skin markers are useful to delineate recent scars, particularly when several biopsies have been performed (Figs. 5 and 6). Comparison with old films and localization of the

new density within the most recent surgical bed indicate a benign scar.

Unfortunately, it is not always possible to differentiate mammographically a benign stellate scar from cancer. Biopsy or fine-needle cytology may be needed in some cases to establish a pathologic diagnosis [1].

### Dystrophic Calcification

Several types of benign calcifications within surgical scars have been described: (1) clustered or scattered smooth, round calcifications; (2) large streaks and clumps of calcifications oriented in the plane of the incision; (3) large globular calcifications; (4) small irregular calcifications mimicking malignancy; (5) knot-shaped calcifications (sutural); (6) plaquelike calcifications (dermal); and (7) calcifications of fat necrosis.

Scar calcifications may develop within 6 months after biopsy (Fig. 7) [2]. Coned/magnified/tangential views may confirm the benign nature or superficial location of the calcifications. In some cases, however, calcifications may be suspicious enough to warrant a repeat biopsy.

### Calcified Sutures

Calcified sutures are usually looped and may take the shape of small knots (Fig. 8). Sutural calcifications are usually few and correspond to the area of surgery. Most calcified sutures will be obvious. However, Figure 9 illustrates that some calcified sutures may produce thin, linear calcifications suggestive of malignancy, requiring biopsy.

### Fat Necrosis/Oil Cyst

Calcified oil cysts may be identified in the postsurgical breast. Tabar and Dean [3] separate these lesions into two entities on the basis of size. Fat necrosis (liponecrosis microcystica calcificans) is a small, ringlike calcification up to a few



Fig. 8.—Surgical sutures after biopsy for a benign lesion. Craniocaudal view shows evenly spaced knots, characteristic of calcified sutures.

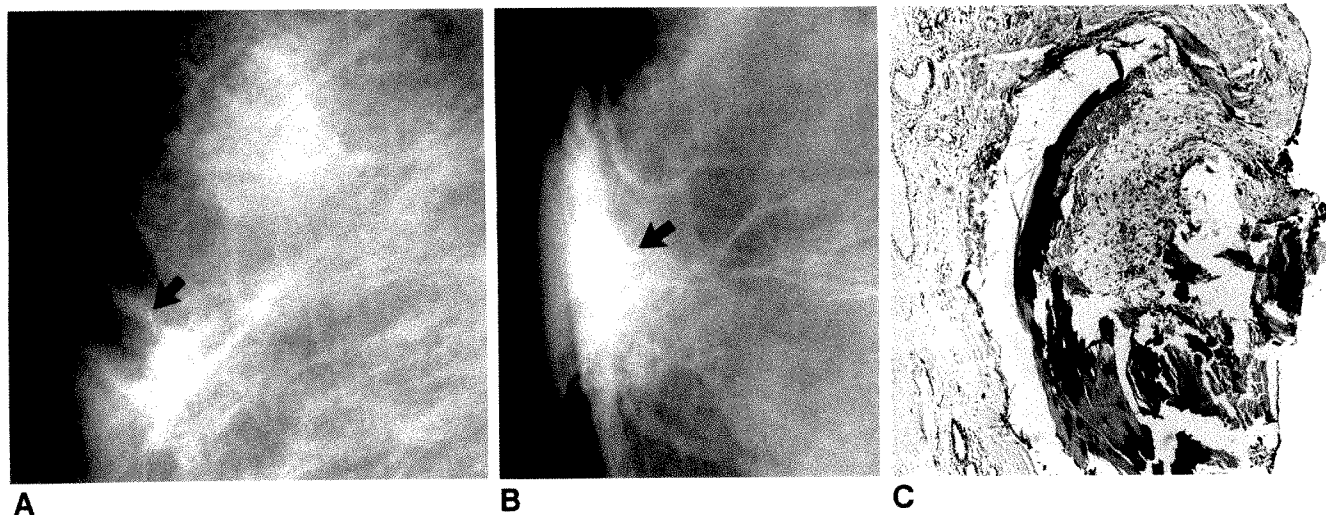


Fig. 9.—Surgical sutures 11 months after biopsy for a benign lesion. A and B, Oblique (A) and craniocaudal (B) views show a new cluster of linear microcalcifications (arrows) in retroareolar area near biopsy site. Another biopsy was recommended. Note associated flattening and thickening of skin contours at old biopsy site. C, Photomicrograph of new specimen shows calcified suture material. No evidence of malignancy was seen. (H and E,  $\times 20$ )



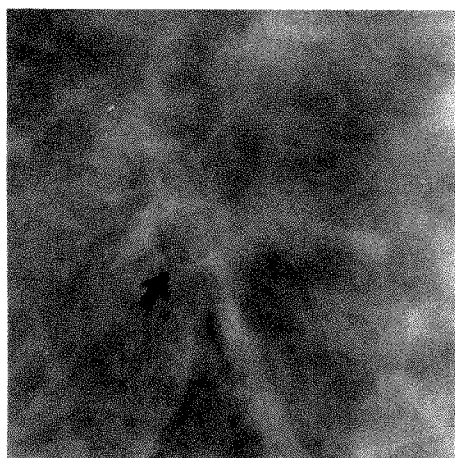
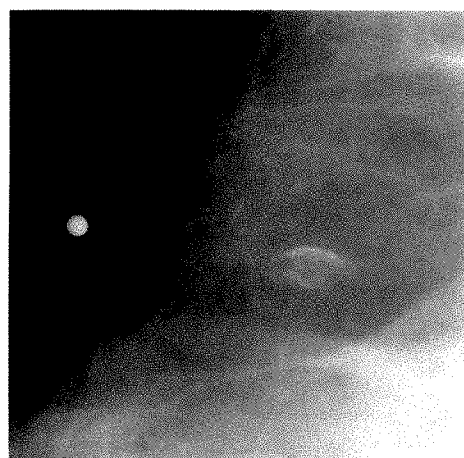


Fig. 10.—Oil cyst 6 months after biopsy for a benign lesion. Fibrous strands radiate toward a central lucency bounded by a thin smooth wall (arrow), characteristic of a postoperative oil cyst.



A

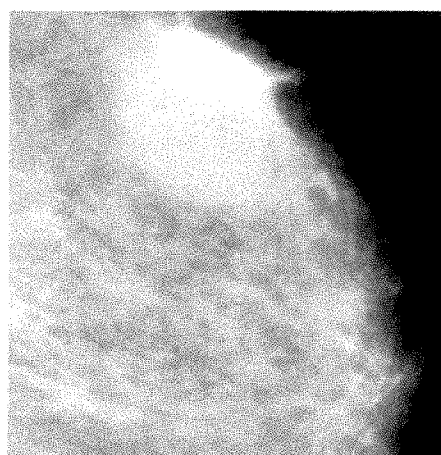


B

Fig. 11.—Fat necrosis/oil cyst 2 years after lumpectomy and radiation therapy for cancer.  
A, Two markers on the skin delineate extent of surgical defect. Flattening of skin contour is noted. Fat has filled glandular tissue defect.  
B, Photographic enlargement shows a 5-mm lucent lesion with calcified rim, characteristic of a calcified postoperative oil cyst.



A



B

Fig. 12.—Hematoma 6 weeks after biopsy for a benign lesion.

A and B, Craniocaudal (A) and oblique (B) views show relationship of hematoma to scar. A dense oval mass is seen in surgical bed. Incision is delineated by skin markers. Hematoma showed interval resolution on mammogram obtained 11 months later.

millimeters in size. Oil or lipid cysts are larger, up to 3 cm in diameter. Both may be caused by traumatic hemorrhage or biopsy.

Mammographic appearances of fat necrosis include (1) oval or rounded low-density area(s) that may gradually develop peripheral calcification, (2) angular microcalcifications that may resemble those in comedocarcinoma, and (3) a poorly defined or spiculated mass.

Although some of these radiologic appearances of fat necrosis may mimic breast cancer, the two cases shown (Figs. 10 and 11) represent the more typical appearances of postoperative oil cysts. These characteristic lesions with low-density centers can be monitored mammographically if associated with trauma or previous biopsy. In the absence of such a history, a spiculated lesion entrapping fat may suggest invasive ductal carcinoma [4].

## Hematoma

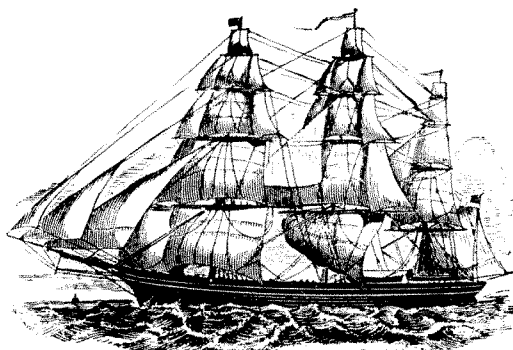
Hematomas in the breast (Fig. 12) are most often caused by open biopsy or needle-aspiration procedures. They may

appear either as an opaque mass with somewhat poorly defined margins or as small, poorly defined densities that cannot be differentiated from islands of residual malignancy [2]. Although hematomas usually do not have the spiculated or nodular margins of malignant lesions, they generally lack the sharply defined, smooth contour of a typically benign lesion.

Hematomas often resolve within 2–4 weeks, although some persist 8 weeks or longer [2]. As the hematoma regresses, residual distortion may occur. Some hematomas will evolve into oil cysts or fat necrosis.

## REFERENCES

1. Sickles EA, Herzog KA. Mammography of the postsurgical breast. *AJR* 1981;136:585–588
2. Peters ME, Fagerholm MI, Scanlan KA, Voegeli DR, Kelcz F. Mammographic evaluation of the postsurgical and irradiated breast. *RadioGraphics* 1988;8:873–899
3. Tabar L, Dean PB. *Teaching atlas of mammography*. New York: Thieme-Stratton, 1985:172
4. Mitnick JS, Vazquez MF, Harris MN, Roses DF. Differentiation of radial scar from scirrhous carcinoma of the breast: mammographic pathologic correlation. *Radiology* 1989;173:697–700



Come to the  
American Roentgen Ray Society

91<sup>st</sup>

ANNUAL MEETING

---

Boston, MA

---

Sheraton Boston Hotel  
May 5-10, 1991

---

---

Scientific Program (200 papers)

Instructional Courses (60 hours)

Categorical Course on Body MR Imaging

The Caldwell Lecture

Award Papers

Scientific Exhibits

Social, Golf, and Tennis Programs

Guest Programs



## Videofluoroscopy in Elderly Patients with Aspiration: Importance of Evaluating Both Oral and Pharyngeal Stages of Deglutition

Michael J. Feinberg<sup>1</sup>  
Olle Ekberg<sup>2</sup>

Oropharyngeal functional impairment increases with age so that radiologists frequently are asked to determine the cause of aspiration in elderly patients. Neuromuscular and cognitive impairment often make it difficult to perform and interpret videofluoroscopic deglutition examinations in these patients. We retrospectively reviewed the barium swallow examinations in 50 elderly patients (mean age, 87 years) who were known to aspirate. We looked for specific patterns of oropharyngeal dysfunction that resulted in bolus misdirection. Analysis revealed that aspiration was due to abnormalities of the oral stage in 23, pharyngeal stage in 10, and both stages in 17. Dysfunction in the oral stage was due to ingestion of large volumes or rapid acquisition rates in nine, failure of containment during processing (bolus manipulation) in 18, and dissociation of lingual delivery and swallowing initiation in the transitional phase in 13. Dysfunction in the pharyngeal stage was due to incomplete transport (bolus retention) in 21 and defective closure of the laryngeal vestibule in 11. No significant relationship between conditions known to cause oropharyngeal dysfunction (dementia, stroke, Parkinson disease, disuse deconditioning) and the specific pattern of dysfunction was identified.

These results indicate that an accurate and valid assessment of oropharyngeal dysfunction in elderly patients with aspiration is possible if specific patterns of dysfunction are sought. Our study indicates the importance of evaluating the oral and pharyngeal stages of deglutition in elderly patients who aspirate.

*AJR* 156:293-296, February 1991

Oropharyngeal impairment is now recognized as a frequent cause of morbidity, disability, and costly dependence in the elderly [1]. Videofluoroscopy has become the preferred diagnostic method for the routine evaluation of oropharyngeal function. Aspiration, or bolus misdirection into the airway, is perhaps the most significant abnormality routinely observed during radiologic examination. Critical management decisions regarding dietary alterations, degrees of oral intake, and institution of artificial feeding often depend on the videofluorographic assessment of aspiration.

We believe that the radiologic assessment of aspiration can be simplified by recognizing basic patterns of oral and pharyngeal stage dysfunction that directly cause or predispose to bolus misdirection. The purpose of the present investigation was to compare the frequency of these patterns in an elderly population of known aspirators.

### Materials and Methods

During a 7-month period, 71 consecutive patients were referred for videofluoroscopic deglutition examinations. Five uncooperative patients and 16 patients with no evidence of aspiration were excluded. The remaining 50 patients represented the study population and included 29 women and 21 men with a mean age of 87 years (range, 79-94 years). Each patient had been examined by a swallowing therapist within 2 weeks of the radiologic study and had medical records that allowed determination of the probable cause of oropharyngeal impairment. Twenty-one patients had a diagnosis of dementia, 15 had had strokes, six were

Received June 29, 1990; accepted after revision September 4, 1990.

<sup>1</sup> Department of Radiology, Albert Einstein Medical Center, York and Tabor Rds., Philadelphia, PA 19141. Address reprint requests to M. J. Feinberg.

<sup>2</sup> Department of Radiology, Hospital of the University of Pennsylvania, 3400 Spruce St., Philadelphia, PA 19104.

0361-803X/91/1562-0293  
© American Roentgen Ray Society



deconditioned owing to extended periods without oral intake, five had Parkinson disease, and three had no diagnosis that could directly affect deglutition. Eleven had subjective complaints of dysphagia, and 39 were noted by caregivers to choke on food and liquids.

Videofluorographic examination was performed according to a previously established protocol. Patients were examined while they were seated in a specially designed chair that provided adequate support and simulated mealtime or feeding conditions. A swallowing therapist fed the patients unless they were routinely accustomed to feeding themselves. Fluoroscopy was performed at 90 keV and recorded on a video recorder (Panasonic AG1830, Secaucus, NJ) with a 0.5-in. (1.3 cm) tape run at 30 frames/sec.

Initially, 1 teaspoon (6 ml) of a semisolid contrast material was administered, and swallowing was recorded in the lateral projection. This consistency was formulated by mixing equal amounts of E-Z-hd barium sulfate (E-Z-EM, Westbury, NY) and applesauce, pudding, or ice cream. This was followed with E-Z-hd liquid barium (250% wt/vol), administered in various ways and amounts depending on cooperation and degree of impairment. The choice of teaspoon, cup, or straw to deliver the bolus was determined by the swallowing therapist. The minimal study consisted of recording two uncontrolled administrations (patient determining bolus size and ingestion rate) and two controlled administrations (single 6-ml to 15-ml boluses) in the lateral projection. If the patient cooperated and aspiration was minor, the study was continued until a total of 8–16 swallows were recorded. If the patient could be adequately positioned, frontal projections were included.

Aspiration was diagnosed if contrast material entered the superior laryngeal inlet before, during, or after swallowing. The degree of aspiration was considered minor when small amounts of barium were aspirated inconsistently and major when large amounts were aspirated frequently. Oral stage abnormalities were classified into three types: ingestion of too large a bolus or too rapid an ingestion rate (Fig. 1A), failure to contain the bolus in the mouth during oral processing (Fig. 1B), and transitional phase dissociation due to lingual dysfunction or swallowing reflex delay (Fig. 1C). Pharyngeal stage abnormalities were classified as defective laryngeal closure (Fig. 2A) or incomplete bolus transport (retention) (Fig. 2B). Three specific pharyngeal functions also were evaluated: lingual propulsion, inversion of the epiglottis, and pharyngeal constrictor activity.

## Results

Analysis of the deglutition studies revealed that aspiration was caused by oral dysfunction in 23 patients (Fig. 1), pharyngeal dysfunction in 10 (Fig. 2), and combined dysfunction in 17. Of the 40 patients with oral stage abnormalities, 18 showed a failure to contain a bolus in the mouth consistently. Transitional phase dissociation was identified in 13 patients and large volume or very rapid bolus ingestion in nine. Each of the abnormal oral stage patterns resulted in bolus misdirection due to premature entry of barium into the pharynx relative to laryngeal closure. In a minority of cases, aspiration occurred before actual swallowing. The bolus either directly entered the open larynx or was aspirated as it accumulated in the pharynx. More commonly, the bolus was malpositioned in the pharynx, and aspiration occurred after reflex initiation.

A total of 27 abnormal pharyngeal stage patterns were observed. Incomplete bolus transport was seen in 16 patients, defective laryngeal closure in six, and both abnormal patterns in five. Bolus retained in the pharynx was aspirated during or

after laryngeal reopening or, alternatively, with delivery of the next bolus or initiation of the next swallow. Defective laryngeal closure was diagnosed when the arytenoid masses failed to completely appose the base of the epiglottis and contrast material entered the vestibule as it was transported through the pharynx.

A single dysfunction was associated with incomplete bolus transport in 12 of the 21 abnormal pharyngeal stages. Multiple abnormalities were detected in eight, and in one case, a Zenker diverticulum caused retention. Specific dysfunctions included abnormal lingual propulsion (11 patients), constrictor paresis (10), and incomplete inversion of the epiglottis (eight).

Liquid aspiration was judged to be minor in 42 of the patients and major in eight. None of the patients aspirated the semisolid bolus. Major aspiration was due to oral dysfunction in four, pharyngeal dysfunction in one, and combined dysfunction in three. A comparison of the frequency of oral and pharyngeal abnormalities and suspected causes is presented in Table 1. Although a history of stroke was present in 15 cases, in only six was the onset of the dysfunction directly related to an acute event. Of the eight patients who showed major aspiration, three had acute strokes and two had a history of strokes. Except for the overall high prevalence of oral stage dysfunction, specific abnormalities could not be correlated with the disorders thought to cause impairment.

## Discussion

Radiologic investigators have emphasized specific laryngopharyngeal morphodynamics that are associated with bolus misdirection [2, 3]. These observations are important, but complete analysis of aspiration requires a broader understanding of oropharyngeal function. Some have advocated a highly structured type of examination and an extensive "checklist" analysis of the recorded observations [4–6]. Radiologists may find it difficult to use such an approach, especially when examining elderly patients, who are often frail, debilitated, or unable to cooperate and demonstrate significant functional impairment.

Normal oral stage dynamics have been described recently [7, 8]; however, radiologic analysis of specific abnormalities has been limited [9]. Because of its voluntary nature, oral activity involving tongue, jaw, and palate movements is difficult to characterize consistently except when highly controlled. To evaluate the oral stage objectively, we divided it into three phases and identified patterns of dysfunction that caused aspiration in each. Our study showed that oral stage abnormalities alone were the most common cause of bolus misdirection and that combined oral and pharyngeal dysfunction was more common than pharyngeal dysfunction alone.

Normal ingestion behavior requires adequate oral motor function but is also influenced by individual preference and culturally prescribed norms. Contrary to others [5, 6, 10], our protocol reflects the belief that usual or routine oral intake should first be observed. Large bolus volumes and rapid ingestion rates caused aspiration during uncontrolled administration in 18% of our cases. It is important to identify these

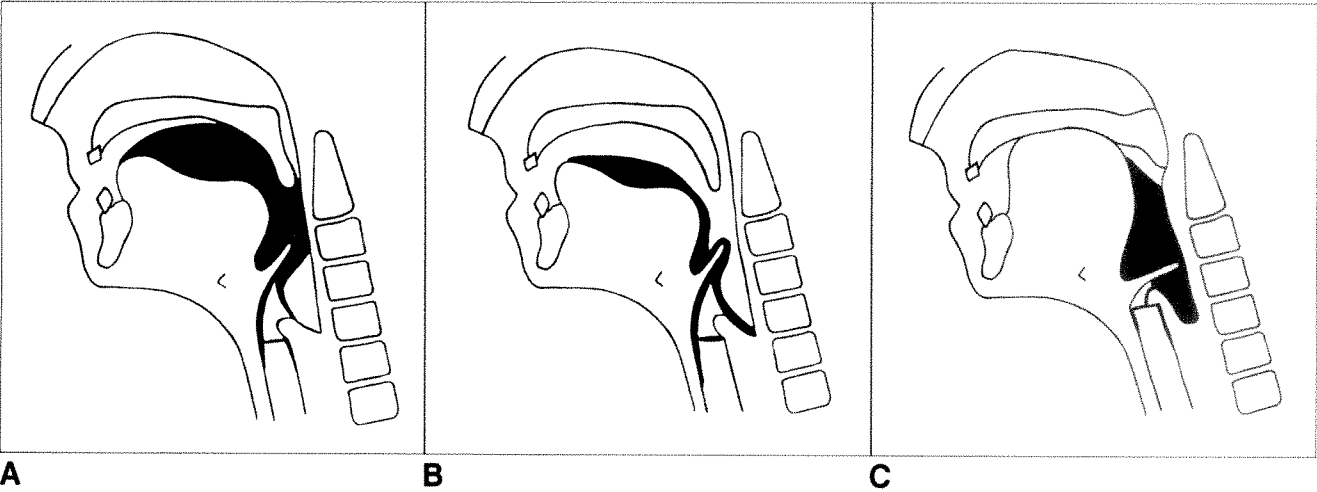


Fig. 1.—Schematic representations of oral stage abnormalities that cause aspiration.  
A, Ingestion of too large a bolus that cannot be adequately controlled and appropriately delivered into pharynx.  
B, Failure of oral containment allowing bolus to leak into pharynx and open larynx.  
C, Transitional phase dissociation resulting in premature bolus delivery into pharynx relative to swallowing initiation.

Fig. 2.—Schematic representations of pharyngeal stage abnormalities that result in bolus misdirection into airway.  
A, Defective laryngeal closure. Base of epiglottis fails to appose arytenoid masses, allowing filling of vestibule.  
B, Incomplete bolus transport (retention). Residual bolus enters larynx after swallowing is completed.

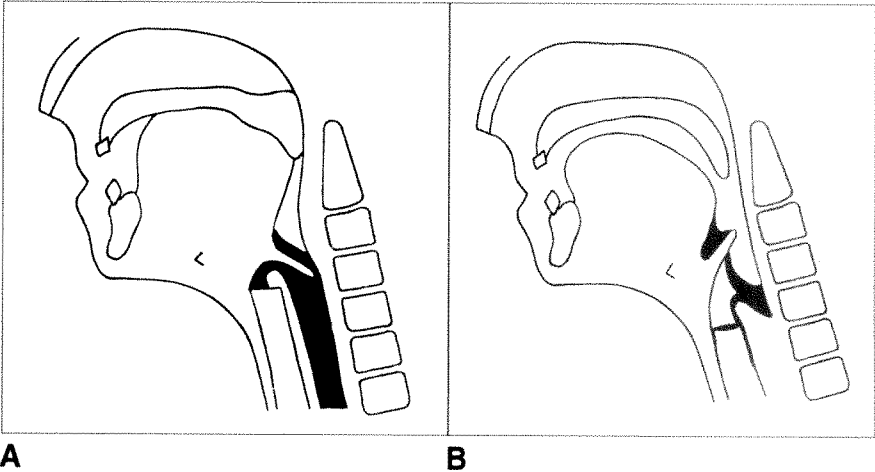


TABLE 1: Causes of Impairment and Patterns of Dysfunction in Elderly Patients Who Aspirate

Cause	Oral Abnormalities	Pharyngeal Abnormalities	Oral and Pharyngeal Abnormalities	Total No. of Patients
Dementia	13	2	6	21
Stroke	7	3	5	15
Deconditioning	1	2	3	6
Parkinson disease	2	1	2	5
None identified	0	2	1	3

patients because management strategies are relatively straightforward.

Failure of containment during oral processing was the most common cause of aspiration in the population. Abnormal lingual activity during this phase could best be described as purposeless, slow, or jerky. The lingual-palatal seal was intermittently disrupted by these movements, allowing bolus

leakage into the pharynx. At times, no oromotor activity was seen attempting to contain the bolus.

The oral transitional phase represents the integration of somatic and visceral neuromuscular activity. The swallowing mechanism can be elicited in a reflexive fashion [10, 11], but initiation during prandial swallowing is voluntary and we consider it part of the oral stage. The posterior tongue appears

to assume a specific configuration or position before triggering can occur [10]. Two basic types of transitional patterns are radiologically observed. An uninterrupted glossopalatal contact wave delivers the bolus into the posterior oral cavity or oropharynx and initiation immediately follows, resulting in a single ejection motion [7]. Alternatively, the bolus is delivered first into the pharynx, and a noticeable pause occurs before it is ejected. This two-step transitional phase is a prolongation of the delivery-initiation interval that is independent of bolus size and increases with age [12]. A number of our cases showed intervals as long as 1.5 sec. Frequently, this two-step pattern resulted in efficient and properly directed swallowing, and we believe this may represent a compensatory mechanism of aging.

Thirteen of our cases showed transitional phase dissociation. Prolonged, weak, or dyscoordinated tongue movements resulted in premature entry of the bolus into the pharynx and subsequent aspiration. When lingual activity was grossly abnormal, it was difficult to determine if patients were processing the bolus or attempting to initiate a swallow. Similarly, when bolus leaked from the posterior oral cavity as it was held for protracted periods, it was not always obvious if the patient was willfully holding the bolus or attempting to initiate. Such difficulties may have resulted in our classifying some cases as failure of containment instead of transitional dissociation.

The pharyngeal stage represents a relatively fixed sequence of events [13, 14]. However, voluntary factors such as bolus size [15, 16], ingestion rate [14], and head positioning [17] can influence pharyngeal dynamics. It may not be possible to control these variables and still obtain an examination that reflects current function. We therefore depended on just two observations to explain aspiration due to pharyngeal stage dysfunction. Incomplete bolus transport (retention) was diagnosed when bolus pooled in the pharynx consistently after swallowing was completed. Manofluorography has shown that the tongue is the major driving force for pharyngeal pressure generation [18]. It is not surprising that in 11 of the 21 examples of retention, lingual ejection motion appeared weak, incomplete, or dyscoordinated.

Laryngeal closure during swallowing is well described [19], but radiologic evaluation of all the components is usually not possible. In the lateral projection, vestibular closure can be evaluated by observing apposition of the arytenoid masses to the base of the epiglottis. When incomplete, aspiration occurs as the bolus is ejected through the pharynx, and this was seen intermittently in 11 of our cases. The mechanism was frequently adequate until the bolus was misdirected due to oral stage dysfunction (10 patients) or incomplete transport (one patient). It is possible that laryngeal dynamics are altered once aspiration occurs and that the abnormality we observed is a secondary and not a primary dysfunction. The glottic closure mechanism has been shown to be uniquely influenced by various sensory stimuli [20].

We frequently observed that oropharyngeal function varied considerably between swallows. This inconsistency made it difficult to apply previous descriptions of the timing and level of bolus misdirection [4, 21–24]. Oral stage abnormalities often caused aspiration before, during, and after swallowing

in the same patient. Similarly, retained bolus was aspirated not only immediately after swallowing but just before and during the subsequent swallow. Barium that initially only penetrated the supraglottic vestibule frequently passed into the trachea with continued drinking.

The radiologic assessment of aspiration in the elderly requires careful attention to both the oral and pharyngeal stages of deglutition. We believe that it is more important to identify the basic causes of bolus misdirection than to detail events that are often inconsistent when numerous bolus administrations are observed.

## REFERENCES

- Donner MW, Jones B. Editorial. *Gastrointest Radiol* **1983**;10:194–195
- Curtis DJ, Hudson T. Laryngotracheal aspiration: analysis of specific neuromuscular factors. *Radiology* **1983**;149:517–522
- Ekberg O. Defective closure of the laryngeal vestibule during deglutition. *Acta Otolaryngol* **1983**;93:309–317
- Dodds WJ, Logemann JA, Stewart ET. Radiologic assessment of abnormal oral and pharyngeal phases of swallowing. *AJR* **1990**;154:965–974
- Sonies BC, Baum BJ. Evaluation of swallowing pathophysiology. *Otolaryngol Clin North Am* **1988**;21:637–648
- Logemann JA ed. *Manual for the videofluorographic study of swallowing*. San Diego, CA: College-Hill Press, **1986**
- Shaker R, Cook IJS, Dodds WJ, Hogan WJ. Pressure-flow dynamics of the oral phase of swallowing. *Dysphagia* **1988**;3:79–84
- Dodds WJ, Taylor AJ, Stewart ET, Kern MK, Logemann JA, Cook IJ. Tipper and dipper types of oral swallows. *AJR* **1989**;153:1197–1199
- Ekberg O, Hillarp B. Radiologic evaluation of the oral stage of swallowing. *Acta Radiol [Diagn]* (Stockh) **1986**;27:533–537
- Dodds WJ, Stewart ET, Logemann JA. Physiology and radiology of the normal oral and pharyngeal phases of swallowing. *AJR* **1990**;154:953–963
- Miller A. Deglutition. *Physiol Rev* **1982**;62:129–184
- Tracy JF, Logemann JA, Kahrilas PJ, Jacob P, Kobara M, Krugler C. Preliminary observations on the effects of age on oropharyngeal deglutition. *Dysphagia* **1989**;4:90–94
- Curtis DJ, Cruess DF, Dachman AH, Maso E. Timing in the normal pharyngeal swallow: prospective selection and evaluation of 16 normal asymptomatic patients. *Invest Radiol* **1984**;19:523–528
- Miller AJ. Neurophysiological basis of swallowing. *Dysphagia* **1986**;1:91–100
- Dodds WJ, Man KM, Cook IJ, Kahrilas PJ, Stewart ET, Kern MK. Influences of bolus volume on swallow-induced hyoid movement in normal subjects. *AJR* **1988**;150:1307–1309
- Jacob P, Kahrilas PJ, Logemann JA, Shah V, Ha T. Upper esophageal sphincter opening and modulation during swallowing. *Gastroenterology* **1989**;97:1469–1478
- Logemann JA, Kahrilas PJ, Kobara M, Vakil NB. The benefit of head rotation on pharyngoesophageal dysphagia. *Arch Phys Med Rehabil* **1989**;70:767–771
- McConnel FMS, Cerenko D, Mendelsohn MS. Manofluorographic analysis of swallowing. *Otolaryngol Clin North Am* **1988**;21:625–635
- Curtis DJ. Laryngeal dynamics. *CRC Crit Rev Diagn Imag* **1982**;19:29–80
- Sasaki CT, Isaacson G. Functional anatomy of the larynx. *Otolaryngol Clin North Am* **1988**;21:595–611
- Logemann JA. *Evaluation and treatment of swallowing disorders*. San Diego, CA: College-Hill Press, **1983**:64–69
- Groher ME. Mechanical disorders of swallowing. In: Groher ME, ed. *Dysphagia: diagnosis and management*. Stoneham: Butterworth, **1983**:61–84
- Kramer SS. Radiologic examination of the swallowing impaired child. *Dysphagia* **1989**;3:117–125
- Linden P, Siebens A. Dysphagia: predicting laryngeal penetration. *Arch Phys Med Rehab* **1983**;64:281–284



## Carcinoma of the Esophagus: CT vs MR Imaging in Determining Resectability

Shodayu Takashima<sup>1</sup>  
 Noriyuki Takeuchi<sup>1</sup>  
 Hitoshi Shiozaki<sup>2</sup>  
 Kenji Kobayashi<sup>2</sup>  
 Shizuo Morimoto<sup>1</sup>  
 Junpei Ikezoe<sup>1</sup>  
 Noriyuki Tomiyama<sup>1</sup>  
 Koushi Harada<sup>1</sup>  
 Kin Shogen<sup>1</sup>  
 Takahiro Kozuka<sup>1</sup>

MR imaging and CT were performed prospectively in 35 patients with esophageal carcinoma to determine the resectability of the primary tumors, because at our institution patients with resectable tumors have surgery regardless of the presence of distant metastases. Tumors with evidence of aortic or tracheobronchial invasion on MR or CT were considered to be unresectable. Tracheobronchial invasion was diagnosed when the tumor extended into the lumen of the airway, and aortic invasion was diagnosed when the triangular fat space between the esophagus, aorta, and spine adjacent to the primary tumor was obliterated. Two patients were excluded because of suboptimal MR images produced by motion artifacts. Pathologic proof was obtained from either surgery or autopsy in 31 patients. Of these, six patients (19%) had proved unresectable tumors (three aortic invasion and three tracheobronchial invasion). In all six cases, these features were correctly detected with both MR and CT. One patient had false-positive findings on MR and CT. An indeterminate diagnosis was obtained with MR in three patients and with CT in four patients. These incorrect or indeterminate results were all related to the diagnosis of aortic invasion. No patient had a false-negative result. When indeterminate diagnoses were considered false-positive, sensitivity, specificity, and accuracy for resectability were 100%, 84%, and 87%, respectively, for MR and 100%, 80%, and 84%, respectively, for CT.

We conclude that MR and CT have nearly the same accuracy in predicting resectability of tumors in patients with esophageal carcinoma.

*AJR* 156:297-302, February 1991

Patients with carcinoma of the esophagus have a poor prognosis because the diagnosis is usually made at an advanced stage [1-5]. Proper therapy for the disease is controversial, and surgery, radiation therapy, and chemotherapy in various combinations have been proposed [2, 5-8]. However, the 5-year survival rate is only 4-9% [6, 7]. In our institution, regardless of the presence of distant metastases, patients with resectable tumors undergo esophagectomy. The key findings that preclude esophagectomy are aortic and/or tracheobronchial invasion. Local invasion of the pericardium, diaphragmatic crura, or stomach does not influence surgical management. In our hospital, therefore, preoperative prediction of resectability of the primary tumor is crucial.

Several reports comparing MR and CT results in staging and evaluating resectability of esophageal carcinoma have been published [9-11]. These studies support only a pessimistic view of the value of MR in this clinical setting. We report a prospective study of 35 patients with esophageal carcinoma that was designed to compare the value of CT and MR imaging in determining the resectability of the tumor.

### Subjects and Methods

Between November 1988 and February 1990, 35 consecutive patients with esophageal carcinoma proved by endoscopic biopsy had both MR and CT to determine the resectability

Received April 2, 1990; accepted after revision July 17, 1990.

<sup>1</sup>Department of Radiology, Osaka University Medical School, 1-1-50 Fukushima, Fukushima-ku, Osaka 553, Japan. Address reprint requests to S. Takashima.

<sup>2</sup>Second Department of Surgery, Osaka University Medical School, 1-1-50 Fukushima, Fukushima-ku, Osaka 553, Japan.

0361-803X/91/1562-0297  
 © American Roentgen Ray Society

of the tumor. Primary tumors without invasion of the aorta or tracheobronchial trees were regarded as resectable regardless of the presence of distant metastases. Each study was used to evaluate tumor invasion of aorta, tracheobronchial tree, pericardium, gastric tumor extension, distant metastases (liver, bone, and lung), and regional and distant lymphadenopathy. All patients had upper gastrointestinal radiographs and barium esophagograms obtained before CT and MR studies. The regional lymph nodes were the cervical or supraclavicular nodes or both for the cervical esophagus and the adjacent mediastinal nodes for the thoracic esophagus [12]. Involvement of more distant nodes except for celiac nodes was considered distant metastasis. Celiac nodes were considered distant in the case of cervical or midesophageal primary tumors but regional for distal neoplasms.

Mediastinal extension of the tumor was diagnosed on CT and MR when abnormal tissue extended from the primary tumor mass into the adjacent mediastinal fat. Lymph nodes larger than 1 cm in shortest diameter were considered metastatic. Tracheobronchial involvement was predicted when the tumor extended into the lumen of the airway. On CT, gastric extension was diagnosed when a soft-tissue mass extended from the esophageal tumor into the gastric fundus. On MR, gastric extension was diagnosed when T2-weighted images depicted a mass of high intensity relative to the gastric wall extending from the esophageal tumor into the gastric fundus. Pericardial invasion was present when a convex inward deformity of the heart with a loss of the normal fat plane was detected. Aortic invasion was diagnosed by obliteration of the triangular fat space between the esophagus, aorta, and spine adjacent to the primary neoplasm [13]. Surgical and pathologic proof of aortic, tracheobronchial, and pericardial invasion was established by the inability to dissect the tumor bluntly during surgery in addition to pathologic proof of tumor extension through the esophageal wall. Tumor extending through the wall was not considered evidence that adjacent structures were invaded.

Multisection spin-echo MR images were obtained on a 1.5-T MR unit (Magnetom; Siemens, Erlangen, Germany) with a 256 × 256 acquisition matrix. ECG-gated scans were made in all patients. T1-weighted images were obtained at repetition times (TR) of 450–850 msec and echo times (TE) of 15 msec, and T2-weighted images were obtained at TR of 1900–2400 msec and TE of 70 msec. Transaxial images with contiguous 1-cm sections were obtained from the pulmonary apices, including supraclavicular fossas, to the upper abdomen, including the entire liver. Coronal and sagittal images with contiguous 3- to 7-mm sections were obtained in 22 patients and in one patient, respectively. The number of excitations was two to four for T1-weighted imaging and one for T2-weighted imaging. Nothing

was administered to distend the stomach in the MR studies, and respiratory gating was not used.

In each patient, enhanced CT scans were obtained with 100 ml of 65% IV iodinated contrast material by using either an 8800 CT/T scanner (GE, Medical Systems, Milwaukee, WI), a CT 8600 scanner (Yokogawa Medical Systems, Tokyo), or a Quantex CT scanner (Yokogawa, Tokyo). Contrast enhancement was performed in a biphasic mode, with first a 40-ml bolus and then a 60-ml rapid-drip infusion in 30 patients, and with a rapid drip infusion in the remaining patients. Contiguous 1-cm sections were used for the chest and upper abdomen; usually the chest and abdomen were imaged on separate days. Unless patients had clinical or radiologic evidence of a significant esophageal obstruction, 300–400 ml of water was administered to the patients with distal neoplasms before the CT scanning in order to assess gastric tumor extension.

Of the 35 patients with esophageal carcinoma, two patients were excluded from the study because of suboptimal MR images produced by motion artifacts. The mean age of the 33 patients was 64 years, ranging from 43 to 77 years. Of these, 30 patients had squamous cell carcinoma (proximal third of the esophagus in two patients, middle third in 20, distal third in eight) and three had adenocarcinoma of distal esophagus and gastroesophageal junction. Pathologic proof of tumor invasion to surrounding structures and metastases to lymph nodes and other organs was obtained by surgery in 30 patients (20 by standard transthoracic esophagectomy, nine by blunt transhiatal esophagectomy, and one by retrosternal bypass surgery without mediastinal exploration), by autopsy in two, and by percutaneous liver biopsy in one. Of these, six patients received preoperative chemotherapy with or without radiotherapy. In each patient, MR and CT were done within a 10-day period; usually CT was the first study. Surgery was performed within 8 days after the MR studies. Autopsy was performed 15 days after the MR study in one case and 23 days later in the other. Thus, MR and CT findings were correlated with surgical and pathologic data in 33 instances. The MR and CT images were interpreted independently by two radiologists with knowledge only of the presence of esophageal cancer. Final interpretations were determined by consensus of both radiologists.

Results

Twenty-seven of the 33 primary tumors were identified with MR and CT; these tumors appeared as an area of isointensity relative to residual esophageal wall on T1-weighted MR im-

TABLE 1: MR and CT Findings vs Surgical-Pathologic Findings in 31 Patients with Esophageal Carcinoma

Surgical/Pathologic Findings	MR Findings/CT Findings			
	True-Positive	True-Negative	False-Positive	False-Negative
Aortic invasion	3/3	24/23	4/5 <sup>a</sup>	0/0
Tracheobronchial invasion	3/3	28/28	0/0	0/0
Pericardial invasion	1/0	24/25	6/5	0/1
Diaphragmatic crural invasion	0/0	29/29	0/0	2/2
Gastric extension	3/3	27/27	0/0	1/1
Liver metastasis (n = 32) <sup>b</sup>	4/4	28/28	0/0	0/0
Bone metastasis	1/0	30/30	0/0	0/1
Pulmonary metastasis	1/1	30/30	0/0	0/0
Regional node metastasis	11/10	10/10	2/2	8/9
Distant node metastasis (n = 32) <sup>c</sup>	5/5	22/22	0/0	5/5

<sup>a</sup> Indeterminate MR (n = 3) and CT studies (n = 4) were considered false-positive.  
<sup>b</sup> One patient who underwent percutaneous liver biopsy was included.  
<sup>c</sup> One patient who had bypass surgery without mediastinal exploration was included.

ages and generally as an area of high intensity on T2-weighted images.

MR and CT findings for tumor spread, distant metastases, and regional node involvement were compared with surgical-pathologic data (Table 1). Tracheobronchial invasion was found in three patients, which was correctly predicted on both CT and MR (Fig. 1); all these had tumor spread to the left main bronchus. Verification was by surgery in two cases and by autopsy in the other. Aortic invasion was found in three cases (Fig. 2); this was verified by surgery in one and by autopsy in the rest. Both MR and CT correctly predicted this feature in all three of these patients. One patient had a false-positive result for both MR and CT studies. No cases were false-negative. An indeterminate diagnosis was obtained with MR in three patients (10%) and with CT in four (13%); in these patients, effaced triangular fat space was seen not only at the level of the primary tumor but also at other levels of the esophagus. When indeterminate cases were considered false-positive, sensitivity, specificity, and accuracy for our criteria were 100%, 86%, and 87%, respectively, with the MR studies and 100%, 82%, and 84%, respectively, with the CT studies.

Four patients had liver metastases that were depicted on both CT and MR. Metastatic lesions in the liver were depicted as isointense or hypointense areas relative to the normal liver on T1-weighted images and as areas of hyperintensity on T2-weighted images (Fig. 3). In one of these four patients, CT detected only three of the five metastatic lesions, whereas T2-weighted MR imaging readily visualized all these lesions. In one patient, multiple metastases of the vertebrae that were not detected on CT were clearly shown as low-intensity areas on T1-weighted MR images (Fig. 4); this was subsequently confirmed by bone scintigraphy. Pulmonary metastases were detected in another patient by both techniques, but the number, size, and character of each nodule were shown far better on CT than on MR; proof was obtained by long-term follow-up.

Gastric extension of the esophageal tumor was correctly diagnosed both on CT and MR in three patients. A small isolated tumor in the stomach of one patient was found at surgery but was not detected on CT or MR. Pericardial invasion was found in one patient at surgery; this was correctly detected with MR, but not with CT. There were six false-positive diagnoses for MR studies and five for CT in

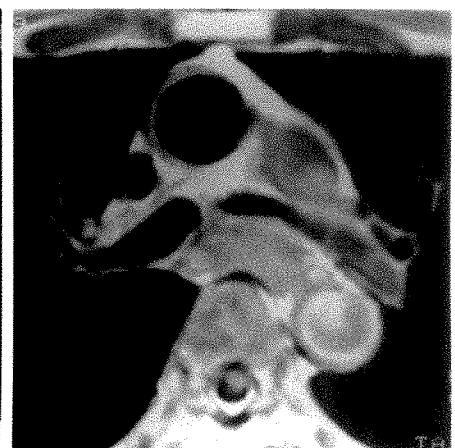
Fig. 1.—Bronchial invasion.

A, CT scan shows left main bronchus, which is displaced anteriorly, and tumor extending into lumen (arrow) of left main bronchus.

B, Bronchial invasion is depicted similarly on axial T1-weighted (700/15) MR image.



A



B

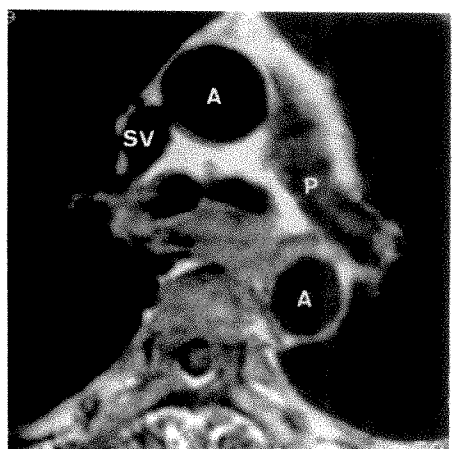
Fig. 2.—Aortic invasion.

A, CT scan shows obliteration of triangular fat space between esophagus, aorta, and spine, suggesting aortic invasion.

B, Aortic invasion was predicted by T1-weighted (500/15) MR image also. A = aorta, SV = superior vena cava, P = pulmonary artery.



A



B



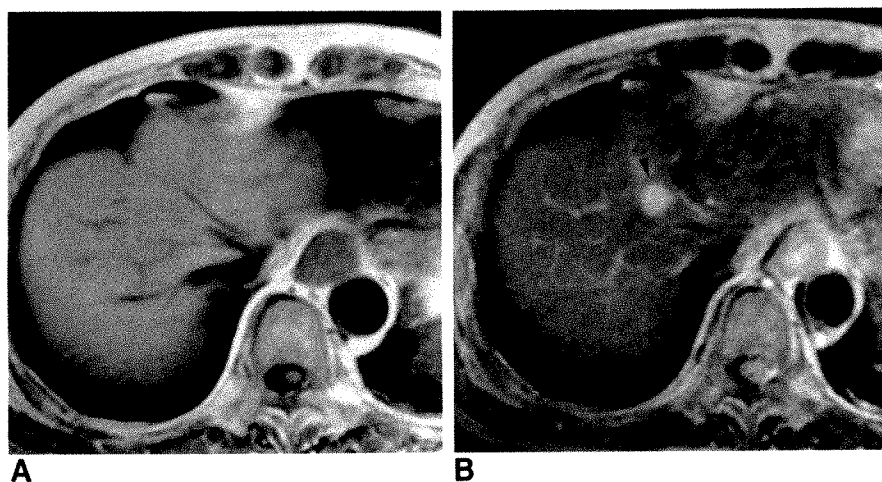


**Fig. 3.—Hepatic metastasis.**  
**A,** On axial T1-weighted (750/15) MR image, lesion is difficult to identify.  
**B,** On axial T2-weighted (2200/70) MR image, metastatic lesion stands out as high-intensity area (arrowheads).

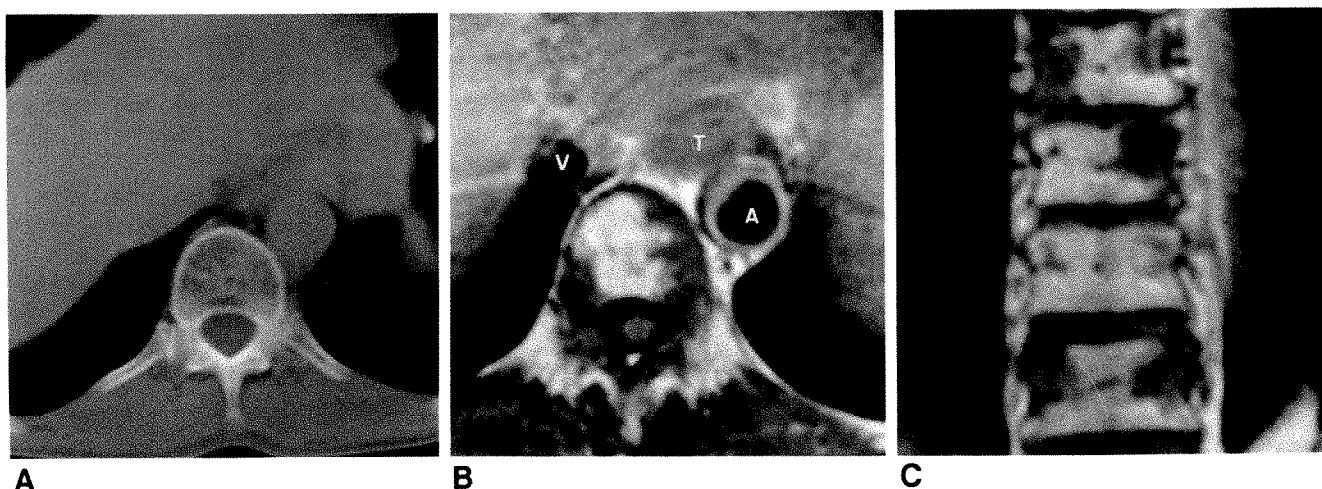


**Fig. 4.—Metastasis to vertebra.**  
**A,** CT scan shows no metastases.  
**B,** Axial T1-weighted (850/15) MR image shows low-intensity areas in vertebral column, suggesting metastatic tumor. V = inferior vena cava, T = primary tumor, A = aorta.  
**C,** Coronal T1-weighted (850/15) MR image shows multiple metastatic lesions in vertebral column.

predicting pericardial invasion. Tumor invasion of diaphragmatic crura was found in two patients at surgery; this was not detected with MR or with CT in these cases.

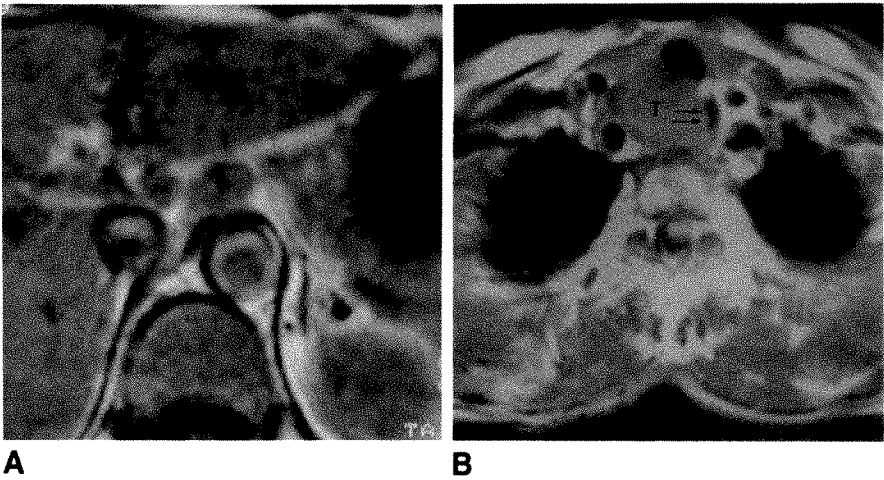
Metastatic disease in regional lymph nodes was correctly diagnosed with MR in 11 patients and with CT in 10. There were two false-positive MR and CT studies, one in the paratracheal region and the other in the aortopulmonary window; nodes in both cases proved to be reactive. Eight false-negative diagnoses were made by both MR and CT; each patient had normal-sized lymph nodes with metastatic deposits in various locations; two patients had nodes in the paraesophageal regions, three in the celiac region, two in the perigastric region, and one in both paratracheal and hilar regions. Another patient had a true-positive MR diagnosis and a false-negative CT diagnosis; metastatic paraesophageal nodes were correctly identified with MR but not with CT. Thus, sensitivity, specificity, and accuracy for regional nodes were 58%, 83%, and 68%, respectively, for MR and 53%,

83%, and 65%, respectively, for CT. Metastatic disease in the distant nodes was correctly diagnosed in five patients by both CT and MR (Fig. 5). There were five false-negative results for both studies; all these were due to the presence of normal-sized perigastric nodes with tumor deposits. Thus, sensitivity, specificity, and accuracy for distant node metastases were 44%, 100%, and 77%, respectively, for both MR and CT.

### Discussion

Although numerous reports about the clinical efficacy of CT in patients with esophageal carcinoma have been published [3, 4, 9, 14, 15], no consensus regarding the role of CT has been achieved. Moreover, several of the reports lack appropriate surgical and pathologic correlation with the CT findings. In our study rigorous radiologic-surgical-pathologic correlation was possible, because precise surgical and pathologic verifi-

Fig. 5.—Distant node metastasis.  
A, Axial T1-weighted (750/15) MR image shows enlarged perigastric lymph nodes (arrowheads). During pathologic study, these were found to contain metastatic tumors.  
B, Axial T1-weighted (650/15) MR image depicts a large tumor in tracheoesophageal groove. Air (arrows) in esophageal lumen is severely displaced to left. T = tumor.



cation was obtained by a vigorous attempt at surgical resection of the tumor in each case. However, currently most authorities believe that carcinoma of the esophagus should be treated for palliation only. Patients' survival depends on the biologic nature of the tumor and the extent of tumor spread at the time of surgery rather than on the extent of the resection performed [5]. Thus, the only importance that imaging has in evaluating these patients is to predict resectability of the primary tumor. Aortic or tracheobronchial involvement is the key finding because such involvement is the main reason not to perform esophagectomy.

Our criteria accurately predicted aortic invasion, because both sensitivity (100%) and specificity (86%) for the MR studies were high; CT had similar results. Lehr et al. [11] assessed aortic invasion in their comparative study of MR and CT by using the traditional criteria that predicted aortic invasion when contact between esophagus and aorta along 90° or more of the aortic circumference with loss of the intervening fat plane was present [14]. In their analyses, indeterminate cases were considered positive. They reported that both MR and CT had poor sensitivity and specificity in diagnosing this feature. However, their results differed from the high sensitivity and low specificity reported by others [10, 15]. Thus, we suggest that our criterion, which predicts aortic invasion by obliteration of the triangular fat space between the esophagus, aorta, and spine, will be useful in clinical practice. However, false-positive diagnoses, including indeterminate diagnoses, occurred in 13% of our 31 patients for MR studies and in 16% for CT. Such radiologic errors are unacceptable because they deny patients curative surgery.

In our study, tracheobronchial invasion was found in three cases at surgery and predicted with high accuracy (100%) by both CT and MR. Kijima et al. [10] reported that the same criteria used in our study for detection of this feature had accuracy of 73% for both MR and CT. They also included displacement or deformity of the tracheobronchial trees as an indication of tumor invasion. On the other hand, Gamsu and Webb [16] mentioned that adjacent posterior masses can produce concavity of the posterior portion of the trachea or main bronchi without invasion because the cartilage rings are incomplete in the posterior portion of the trachea and main

TABLE 2: MR and CT Detection of Unresectable Primary Tumors (n = 31)

	MR Findings	CT Findings
True-positive	6	6
True-negative	21	20
False-positive	4 <sup>a</sup>	5 <sup>a</sup>
False-negative	0	0
Sensitivity (%)	100	100
Specificity (%)	84	80
Accuracy (%)	87	84

Note.—Aortic or tracheobronchial invasion was considered nonresectable.  
<sup>a</sup> Aortic invasion was falsely predicted.

bronchi. However, no false diagnosis for tracheobronchial invasion occurred in our study.

In our series, neither MR nor CT was sensitive in detecting metastases to distant nodes, but the specificity was high (100%). False-negative results were frequently encountered because of failures to detect normal-sized perigastric nodes; such radiologic errors are documented in the literature [4, 11, 14]. Lehr et al. [11] reported that MR was more sensitive than CT was in predicting metastases in perigastric or celiac nodes. However, the presence or absence of metastases to the distant nodes does not influence surgical management because all patients with resectable tumors have surgery regardless of the presence of distant metastases.

Six (19%) of our 31 patients had unresectable primary tumors found at surgery or autopsy (Table 2). Both MR and CT accurately predicted such features in all these six cases. False-positive diagnosis occurred in four cases (13%) for MR studies and in five cases (16%) for CT; all these diagnoses were caused by erroneous prediction of aortic invasion. However, no patient had false-negative MR or CT findings related to resectability. Sensitivity, specificity, and accuracy for resectability were 100%, 84%, and 87%, respectively, for MR and 100%, 80%, and 84%, respectively, for CT. Thus, our study has shown that MR and CT have nearly the same accuracy for predicting resectability in patients with esophageal carcinoma.

## ACKNOWLEDGMENTS

We thank Seiichi Takasugi for valuable advice, Chieko Watanabe for secretarial assistance, and Reina Takashima for encouragement.

## REFERENCES

1. Daffner RH, Halber MD, Postlethwait RW, Korobkin M, Thompson WM. CT of the esophagus. II. Carcinoma. *AJR* **1979**;133:1051-1055
2. Drucker MH, Mansour KA, Hatcher CR Jr, Symbas PN. Esophageal carcinoma: an aggressive approach. *Ann Thorac Surg* **1979**;28:133-138
3. Moss AA, Schnyder P, Thoeni RF, Margulis AR. Esophageal carcinoma: pretherapy staging by computed tomography. *AJR* **1981**;136:1051-1056
4. Thompson WM, Halvorsen RA, Foster WL Jr, Williford ME, Postlethwait RW, Korobkin M. Computed tomography for staging esophageal and gastroesophageal cancer: reevaluation. *AJR* **1983**;141:951-958
5. Orringer MB. Transhiatal esophagectomy without thoracotomy for carcinoma of the thoracic esophagus. *Ann Surg* **1984**;200:282-288
6. Goodner JT. Surgical and radiation treatment of cancer of the thoracic esophagus. *AJR* **1969**;105:523-528
7. Gunnlaugsson GH, Wychulis AR, Roland C, Ellis FH Jr. Analysis of the records of 1,657 patients with carcinoma of the esophagus and cardia of the stomach. *Surg Gynecol Obstet* **1970**;130:997-1005
8. Nelson CS. Chemotherapy as the definitive form of therapy in esophageal carcinoma. *J Thorac Cardiovasc Surg* **1972**;63:827-837
9. Quint LE, Glazer GM, Orringer MB. Esophageal imaging by MR and CT: study of normal anatomy and neoplasms. *Radiology* **1985**;156:727-731
10. Kijima M, Kubo H, Nagao F, Sugimoto S, Tada S. MRI and CT findings of the paraesophageal organs and mediastinal lymph nodes with invasion or metastasis of esophageal carcinoma. In: Siewert JR, Holscher AH, eds. *Diseases of the esophagus*, 1st ed. New York: Springer-Verlag, **1987**: 149-151
11. Lehr L, Rupp N, Siewert JR. Assessment of resectability of esophageal cancer by computed tomography and magnetic resonance imaging. *Surgery* **1987**;103:344-350
12. Beahrs OH, Myers MH, eds. *Manual for staging of cancer*, 2nd ed. Philadelphia: Lippincott, **1983**:61-66
13. Ogawa Y, Nishiyama K, Ikezoe J, et al. Preoperative assessment of tumor invasion of the intrathoracic esophageal carcinoma. In: Siewert JR, Holscher AH, eds. *Diseases of the esophagus*, 1st ed. New York: Springer-Verlag, **1987**:203-206
14. Picus D, Balfe DM, Koehler RE, Roper CL, Owen JW. Computed tomography in the staging of esophageal carcinoma. *Radiology* **1983**;146: 433-438
15. Quint LE, Glazer GM, Orringer MB, Gross BH. Esophageal carcinoma: CT findings. *Radiology* **1985**;155:171-175
16. Gamsu G, Webb WR. Computed tomography of the trachea: normal and abnormal. *AJR* **1982**;139:321-326

**American Roentgen Ray Society  
Residents' Award Papers, 1991**

The ARRS announces competition for the 1991 President's Award and two Executive Council Awards for the best papers concerning the clinical application of the radiologic sciences.

**Awards**

The winner of the President's Award will receive a certificate and a \$2000 prize. The winners of the two Executive Council Awards will each be given a certificate and a prize of \$1000. The winners will be announced on March 15, 1991. Winning papers will be presented at the ARRS annual meeting at the Sheraton Boston Hotel, Boston, MA, May 5-10, 1991. Winning papers will be submitted for early publication in the *American Journal of Roentgenology*. All other papers will be returned to the authors.

**Regulations**

Eligibility is limited to residents or fellows in radiology who have not yet completed 4 years of approved training in a radiologic discipline. A letter from the resident's department chairman attesting to this status must accompany the manuscript. The resident must be the sole or senior author and be responsible for all or most of the project.

Submitted manuscripts must not exceed 5000 words and have no more than 10 illustrations. Four copies of the manuscript and illustrations are required. Submitted manuscripts should not contain previously presented or published material and should not be under consideration for publication elsewhere.

Deadline for submissions is February 15, 1991. Send papers to

Nancy O. Whitley, M.D.  
Chairman, Committee on Education & Research  
American Roentgen Ray Society  
Department of Radiology  
University of Maryland Medical Systems Hospital  
22 S. Greene St.  
Baltimore, MD 21201



## Expert Advice

# Radiologic Detection of Colonic Neoplasms: Benefits of a Systems-Analysis Approach

David W. Gelfand<sup>1</sup>, Yu Men Chen, and David J. Ott

Detection of carcinoma of the colon and precursor adenomatous polyps continues to be the most critical application of the barium enema examination. Beginning in 1975, we started a system analysis to optimize the barium enema examination for the detection of colonic neoplasms. In using this approach, we assumed that errors may be introduced by poor judgment or carelessness within all segments of the radiologic-diagnostic system comprising the barium enema examination and that optimal results are achieved only when the potential for error is stringently minimized at each stage of the diagnostic process. Systems analysis is widely used in manufacturing, where it is indispensable for product quality control, but to our knowledge has not been consciously applied to a complex radiologic examination. On the basis of this premise, we evaluated and altered as indicated each stage of the diagnostic process constituting the barium enema, including examination selection, patients' preparation, barium suspensions, use of adjuvant drugs, radiographic and fluoroscopic systems, and final quality controls.

### Accuracy of Examinations

Before presenting in detail the policies and technical factors eventually chosen, it is worth verifying the effectiveness of the systems-analysis approach. We recently reviewed all patients in our medical center who had surgical resection of a colonic carcinoma between 1980 and 1988 and had a barium

enema examination in our department within the 3 months preceding surgery. The study group comprised 172 patients, including 81 women and 91 men 25 to 93 years old, with 174 colonic carcinomas (Fig. 1). One hundred twenty-seven patients had single-contrast, and 45 had double-contrast studies. The lesions found at surgery ranged in size from a 1.0-cm polypoid lesion to a circumferential lesion of 13-cm axial length.

Of the 174 carcinomas, 173 (99%) were correctly identified as potential malignant neoplasms during the radiologic examination. The one cecal carcinoma not correctly identified as a malignant neoplasm was detected radiologically but was misdiagnosed as a benign polyp. These results verified four previous investigations of our single- and double-contrast examinations for the detection of endoscopically confirmed polypoid lesions, which had shown detection of 42 (100%) of the 42 polypoid lesions found histologically to contain carcinoma [1-4].

This high sensitivity for detection of colonic carcinoma is not entirely unique. Review of 19 English-language radiologic publications in the decade 1980-1989 showed 15 of the 19 publications reporting 90-100% sensitivity [1-19]. However, our results are unusual in that the sensitivity of 99% was achieved in a large series of 174 carcinomas during a 9-year period.

The techniques used in achieving these results vary somewhat from those most commonly used. The following sections

Received June 18, 1990; accepted August 27, 1990.

<sup>1</sup> All authors: Department of Radiology, Bowman Gray School of Medicine, 300 S. Hawthorne Rd., Winston-Salem, NC 27103. Address reprint requests to D. W. Gelfand.

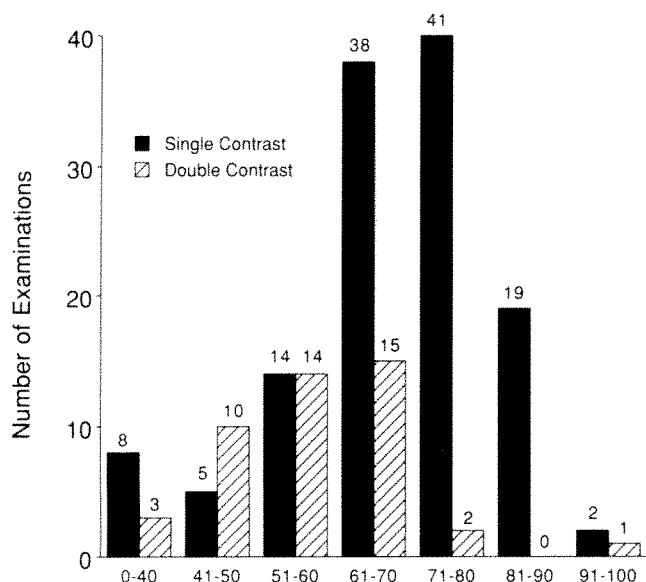


Fig. 1.—Bar graph of age distribution of single- and double-contrast examinations in 172 patients with colonic cancer. Preponderance of elderly patients determined that most examinations were performed with single-contrast technique.

indicate the methods used during our barium enema examinations and the published data and observations supporting those methods as determined by review and/or investigation of each element of the barium enema diagnostic process.

### Examination Selection

Selection of patients for a single- or double-contrast examination is based on the age-related prevalence of benign and malignant colonic neoplasms and on whether the patient is able to cooperate fully during the more demanding double-contrast examination. Review of the pertinent literature indicated that the prevalence of colonic neoplasms is minimal until age 40, when it undergoes a continuing increase in magnitude. Experience also showed that elderly and infirm patients often had difficulty with the double-contrast barium enema. However, our own investigation indicated that a properly performed single-contrast examination was appropriate for detection of neoplasms in such patients and would yield satisfactory results, demonstrating 80% of all polyps, 94% of those larger than 1.0 cm, and 100% of lesions larger than 2.0 cm [2].

On the basis of these considerations, all patients over age 40 who are mobile and able to cooperate receive double-contrast examinations. Patients with specific signs of colonic neoplasm, such as rectal bleeding, also receive double-contrast examinations even if under age 40. Despite our favoring the double-contrast examination for detection of neoplasms, particularly colonic polyps smaller than 1.0 mm in diameter [1-4], the majority of our 172 patients with colonic carcinoma were studied with single-contrast examinations (Fig. 1). Seventy percent of the carcinomas were found in patients more than 60 years old, and most of these patients were sufficiently

elderly or infirm that a double-contrast examination was not attempted.

### Patients' Preparation

Cleansing of the colon is achieved by a regimen suggested by H. Ichikawa of Tokyo. Each patient receives 300 ml of magnesium citrate at 4:00 p.m. and 2 oz. (60 ml) of castor oil or 4 oz. (120 ml) of emulsified castor oil at 8:00 p.m. In order to prevent dehydration and increase the effectiveness of the preparation, outpatients are asked to drink 8 oz. (240 ml) of water or other clear liquid each hour of the day preceding the examination. The morning of the examination, a cleansing enema of 1500 ml of tap water is administered in the radiology department and is repeated as necessary until the effluent is clear. In order to minimize the fluid retained in the colon during the examination, patients receiving a single-contrast enema wait 30 min after the cleansing enema, and those having double-contrast studies wait 60 min. In a study of 500 patients, this preparation was shown to produce a clean colon in 97% of patients [20].

### Barium Suspensions

When double-contrast examinations are performed on patients receiving a cleansing enema, the barium suspension must be of high viscosity to provide a thick, dense, easily discernible coating. Extensive testing performed for barium manufacturers indicated that three barium suspensions available in the United States coat the colonic mucosa well in the presence of small amounts of retained fluid: Liquid Polibar (E-Z-EM, Westbury, NY), Liquid Polibar Plus (E-Z-EM), and HD 85 (Lafayette Pharmacal, Lafayette, IN). Our examinations are currently performed with Liquid Polibar Plus. In our opinion, low-viscosity materials should be avoided. Their thinner, less easily seen coating greatly increases the chance for perceptive errors, which are the majority of errors found on barium enema examinations [5, 21].

Single-contrast examinations require a barium suspension that is stable at low densities. Laboratory testing of 15 barium suspensions at the low densities required for a single-contrast examination established that the most stable of these was Liquid Solopake (E-Z-EM) [22], which we currently use at 18% weight/volume. These tests also showed that the barium preparations sold as powder and preloaded into an enema kit are unstable. This was not surprising, because maximal suspension stability depends on (1) fine, uniform particle size; (2) a tenacious gum system; (3) vigorous mechanical mixing; and (4) long-term hydration. These qualities are best achieved in a factory premixed suspension, which can be diluted to the lower density needed for a single-contrast examination.

### Adjuvant Drugs

For many years, all patients having double-contrast examinations received 0.5 mg of IV glucagon immediately before the examination. Routine use of glucagon recently has been abandoned because little difference in discomfort was found for patients who did not receive glucagon. However, glucagon

is administered to those patients receiving single-contrast examinations who are found during the cleansing enema to have a marginal ability to retain the enema, because it relaxes the colon and diminishes the urge to evacuate the enema.

### Remote-Control Equipment

All examinations are performed with remote-control radiographic-fluoroscopic equipment [23]. Its major advantage is superior radiographic sharpness, which is the result of the long tube-film distance of 115 cm (Siemens Medical Systems, Iselin, NJ). Radiographic sharpness is maintained regardless of the patient's position, allowing greater fluoroscopic and radiographic flexibility. Another significant advantage is the ability to angle the tube, which is used mainly during fluoroscopy and radiography of the sigmoid colon and usually provides a clear view of redundant loops that might be difficult to see individually with a conventional fluoroscope. This is particularly helpful in the detection of neoplasms of the sigmoid colon, and indeed 53 (30%) of the 174 colonic carcinomas were in the sigmoid colon. Other direct advantages of remote-control fluoroscopy include virtually complete radiation protection for radiologists and technologists and the convenience of performing fluoroscopy without leaded aprons and gloves.

A further advantage of remote-control fluoroscopy is that very high quality can be maintained with reasonable speed and economy of personnel. Our four fluoroscopy rooms are operated by four or five technologists, two resident physicians, and a faculty radiologist, with first-year residents performing most examinations. The most recent annual volume of fluoroscopies performed in these rooms was 6530 studies.

The single-contrast barium enema performed with remote control is similar to that with a conventional fluoroscope. Filling of the colon is controlled by a remotely operated clamp (E-Z-EM). During and after filling, the entire colon is both viewed fluoroscopically and radiographed with carefully graded compression (the remote control table provides a 12 × 12 in. compression device). This is followed by fluoroscopically guided standard views that include a left lateral view of the rectum and both prone oblique views of the entire colon. The postevacuation film was found unnecessary for detection of neoplasms, and its elimination saves considerable time.

The double-contrast barium enema as performed on the remote-control fluoroscope is accomplished without decubitus films (Table 1) [23]. All films are obtained during fluoroscopy, which both provides optimal positioning and saves time, because the patient is placed in each position only once during the examination. Elimination of decubitus views also speeds the examination and determines that virtually all gastrointestinal studies can be obtained with the built-in tube of the remote-control fluoroscope, thus making a separate overhead tube stand unnecessary for gastrointestinal examinations.

### Film-Screen Combination

A high-resolution, moderately fast film-screen combination of 200 speed was identified, having characteristics specifically

**TABLE 1: Film Sequence for the Remote-Control Double-Contrast Enema**

1. Sigmoid, prone (table horizontal) 24 × 30 cm
2. Rectum, right lateral (table horizontal) 24 × 30 cm
3. Sigmoid, supine (table horizontal) 24 × 30 cm
4. Rectum, left lateral (table horizontal) 24 × 30 cm
Turn patient 360° twice away from examiner to coat entire colon
5. Entire colon (table upright) 35 × 43 cm
6. Hepatic flexure (table upright) 24 × 30 cm
7. Splenic flexure (table upright) 24 × 30 cm
8. Entire colon, prone (table horizontal) 35 × 43 cm
9. Entire colon, right posterior oblique (table horizontal) 35 × 43 cm
10. Entire colon, supine (table horizontal) 35 × 43 cm
11. Entire colon, left posterior oblique (table horizontal) 35 × 43 cm
12. Cecum, supine (table head down 20°) 24 × 30 cm

Note.—All positions listed are relative to the table surface.

desirable for gastrointestinal radiography. This film-screen combination (3M Company, Minneapolis, MN) uses both rare-earth and anti-crossover technology. It produces a spatial resolution of 13 line pairs per millimeter and high radiographic contrast. Rare-earth screens are relatively less sensitive at low energies and are thus less sensitive to scattered radiation than to the primary beam. This provides additional scatter rejection and allows high kilovoltages (110–130 kVp) to be used while preserving good radiographic contrast. The anti-crossover technology prevents light emitted by one screen from crossing over to and exposing the emulsion layer adjacent to the opposite screen, a process that normally degrades resolution.

### Fluoroscopic Image Chain

The importance of accurate fluoroscopic observation during single-contrast examinations has long been recognized. However, in an investigation of causes of error during barium studies, we found that accurate fluoroscopic observation during double-contrast examinations is similarly important in minimizing errors [21]. In order to help achieve this, the remote-control fluoroscopes have been equipped with 1023-line, 25-MHz bandwidth television systems. The television section of a fluoroscopic image chain typically has a much lower resolution than the image provided by the image intensifier, and is thus the limiting factor in determining fluoroscopic image clarity. Tests performed before and after changing from a 525-line, 6-MHz system to the 1023-line system indicated an increase in spatial resolution at fluoroscopy from 0.7 to 1.7 line pairs per millimeter. The increased image clarity allows fluoroscopic detection of almost all lesions eventually identified, including small colonic polyps, on both single-contrast and double-contrast examinations. Fluoroscopic detection of lesions ensures their radiographic documentation and removes uncertainty from the diagnostic process. This contributes greatly to both the high sensitivity of the examinations and the production of relatively few false-positive diagnoses [24].



## Quality Controls

On the basis of an analysis of errors occurring during gastrointestinal examinations [21], two routine quality controls are used. First, the films are developed during the examination and are reviewed while the patient remains on the examination table. This allows convenient resolution of any questions raised by potential lesions that may be poorly seen fluoroscopically or radiographically. Also, suboptimal parts of the examination can easily be repeated to ensure uniform quality.

Second, all films are read twice to minimize perceptive errors [5, 21]. The examination is first read when performed, and any necessary immediate report is rendered. On completion of the fluoroscopic schedule, the examinations are reinterpreted, and the final report is dictated. The second interpretation permits a more leisurely and thorough inspection of the films and results in recognition of a small percent of additional diagnoses.

Experience with a systems-analysis approach has, in our opinion, verified its usefulness as a means of minimizing the errors that may occur during a relatively complex radiologic process such as the barium enema, which is performed in substantial numbers. It is apparent to us that errors in the detection of colonic neoplasms can be introduced by lack of care or incorrect choice of policy or technique at any stage of the diagnostic process, which begins with preparation of the patient and ends with a written report. The individual technical factors used may vary from those described here. However, appropriate choices and careful attention to detail at each stage of the diagnostic process can produce barium enema examinations that are as accurate or more accurate than any competing method for examining the colon.

## REFERENCES

- Ott DJ, Chen YM, Gelfand DW, Wu WC, Munitz HA. Single-contrast vs. double-contrast barium enema in the detection of colonic polyps. *AJR* **1986**;146:993-996
- Gelfand DW, Chen YM, Ott DJ. Detection of colonic polyps on single-contrast barium enema study: emphasis on the elderly. *Radiology* **1987**;164:333-337
- Ott DJ, Scharling ES, Chen YM, Wu WC, Gelfand DW. Barium enema examination: sensitivity in detecting colonic polyps and carcinomas. *South Med J* **1989**;82:197-200
- Ott DJ, Gelfand DW, Wu WC, Kerr RM. Sensitivity of double-contrast barium enema: emphasis on polyp detection. *AJR* **1980**;135:327-330
- Kelvin FM, Gardiner R, Vas W, Stevenson GW. Colorectal carcinoma missed on double contrast barium enema study: a problem in perception. *AJR* **1981**;137:307-313
- Bloomfield JA. Reliability of barium enema in detecting colonic neoplasia. *Med J Aust* **1981**;1:631-633
- Kaude JV, Harty RF. Sensitivity of single contrast barium enema with regard to colorectal disease as diagnosed by colonoscopy. *Europ J Radiol* **1982**;2:290-292
- Thoeni RF, Petras A. Detection of rectal and rectosigmoid lesions by double-contrast barium enema examination and sigmoidoscopy. *Radiology* **1982**;142:59-62
- Johnson CD, Carlson HC, Taylor WF, Weiland LP. Barium enemas of carcinoma of the colon: sensitivity of double- and single-contrast studies. *AJR* **1983**;149:1143-1149
- Thoeni RF, Venbrux AC. The value of colonoscopy and double-contrast barium-enema examinations in the evaluation of patients with subacute and chronic lower intestinal bleeding. *Radiology* **1983**;146:603-607
- Fork FT, Lindstrom C, Ekelund G. Double contrast examination in carcinoma of the colon and rectum. *Acta Radiol Diagn* **1983**;24:177-188
- Beggs I, Thomas BM. Diagnosis of carcinoma of the colon by barium enema. *Clin Radiol* **1983**;34:423-425
- Myllyla V, Paivansalo M, Laitinen S. Sensitivity of single and double contrast barium enema in the detection of colorectal carcinoma. *Fortschr Röntgenstr* **1984**;140:393-397
- Baker SR, Alterman DD. False-negative barium enema in patients with sigmoid cancer and coexistent diverticula. *Gastrointest Radiol* **1985**;10:171-173
- Brekkan A, Kjartansson O, Tulinius H, Sigvaldason H. Diagnostic sensitivity of x-ray examination of the large bowel in colorectal cancer. *Gastrointest Radiol* **1983**;8:363-365
- Feczko PJ, Halpert RD. Reassessing the role of radiology in hemoccult screening. *AJR* **1986**;146:697-701
- Jensen J, Kewenter J, Haglund E, Lycke G, Svensson C, Ahren C. Diagnostic accuracy of double-contrast enema and rectosigmoidoscopy in connection with faecal occult blood testing for the detection of rectosigmoid neoplasms. *Br J Surg* **1986**;73:961-964
- Hallman JR, Howland WJ, Wolf BH. Retrospective review of the sensitivity of barium enema examination in a community hospital setting. *Ohio St Med J* **1986**;82:126-130
- Bolin S, Franzen L, Nilsson E, Sjö Dahl R. Carcinoma of the colon and rectum. *Cancer* **1988**;61:1999-2008
- Gelfand DW, Chen YM, Ott DJ. Colonic cleansing for radiographic detection of neoplasia: efficacy of the magnesium citrate-castor oil-cleansing enema regimen. *AJR* **1988**;151:705-708
- Ott DJ, Gelfand DW, Ramquist NA. Causes of error in gastrointestinal radiology. *Gastrointest Radiol* **1980**;5:99-105
- Gelfand DW, Ott DJ. Barium sulfate suspensions: an evaluation of available products. *AJR* **1982**;138:935-941
- Gelfand DW. *Gastrointestinal radiology*. New York: Churchill Livingstone, **1984**;11-12, 100-104
- Ott DJ, Scharling ES, Chen YM, Gelfand DW, Wu WC. Positive predictive value and posttest probability of diagnosis of colonic polyp on single- and double-contrast barium enema. *AJR* **1989**;153:735-739

## Fatty Infiltration of the Liver: Quantification with Phase-Contrast MR Imaging at 1.5 T vs Biopsy

Henry Levenson<sup>1</sup>  
Fred Greensite<sup>1</sup>  
John Hoefs<sup>2</sup>  
Louis Friloux<sup>1</sup>  
Gregory Applegate<sup>1</sup>  
Elzi Silva<sup>2</sup>  
Gary Kanel<sup>3</sup>  
Richard Buxton<sup>1</sup>

Quantification of hepatic fat content by application of MR phase-contrast imaging (Dixon method) at 1.5 T was compared with results of biopsy in 16 patients with a variety of liver abnormalities. Motion artifact was suppressed by employing six or eight averages of short TR in-phase (echo offset, 0 msec), out-of-phase (echo offset, 1.1 msec), and in-phase (echo offset, 2.2 msec) spin-echo pulse sequences. The 360° out-of-phase sequence was used to assess the impact of T2\* decay on this method of estimating fat fraction. A standard two-echo long TR sequence also was obtained in all patients. Histologic preparations from the biopsy specimens were examined by a pathologist who had no knowledge of the MR results and were graded according to overall visual assessment as belonging to one of four categories of fat fraction. Results of the MR-calculated apparent fat fraction were compared directly with biopsy category and were also placed in MR fat fraction categories, allowing estimation of the statistical correlation between the biopsy and MR grading systems. Eight of eight patients with biopsy categories indicating a fat fraction of less than 0.25 were computed by MR to have a fat fraction of less than 0.1. Seven of eight patients with biopsy categories indicating a fat fraction of greater than 0.25 were computed by MR to have a fat fraction of at least 0.24. The MR-calculated apparent fat fraction category correlated significantly with the histologic biopsy category ( $r = .86$ ,  $p < .01$ ). When compared with the in-phase image, decreased signal from liver was visually apparent on the 180° out-of-phase images in all cases in which the fat fraction was at least 0.24, but there was no indication of fatty liver on the standard T1- or T2-weighted images. Calculated T2 also showed no correlation with degree of fatty deposition. Correction for T2\* decay by using the 360° out-of-phase acquisition in addition to the standard 0° and 180° out-of-phase images had little effect on fat fraction computation.

Phase-contrast MR is a promising noninvasive method for quantitative assessment of fatty deposition in the liver.

*AJR* 156:307-312, February 1991

Quantification of the fat content in the liver is often of interest in the evaluation of patients with a variety of metabolic and hepatotoxic conditions. Definitive determination of the hepatic fat fraction generally requires percutaneous biopsy, but even this invasive technique is hampered by sampling errors. Thus, a noninvasive method involving tomographic imaging is desirable. The spectroscopic capabilities of nuclear magnetic resonance suggest that this should be possible with appropriate MR pulse sequences.

An elegant imaging sequence for discrimination between fat and water spins based on their resonant frequency difference was introduced by Dixon [1] in 1984. The quantitative accuracy of this phase-contrast method has been tested in phantoms at 0.6 [2] and 2.0 [3] T, and a hybrid version of the Dixon method combined with selective saturation has been tested at 1.5 T [4]. In clinical applications, the usefulness of the method in detecting fatty infiltration in the liver has been demonstrated at 0.35 T [5, 6], and the reproducibility of quantitative measurements of the fat fraction in vertebral bone marrow has been shown at 0.6 T [7].

Received April 13, 1990; accepted after revision July 10, 1990.

<sup>1</sup> Department of Radiological Sciences, Route 140, University of California-Irvine Medical Center, 101 The City Dr. S., Orange, CA 92668. Address reprint requests to F. Greensite.

<sup>2</sup> Department of Medicine, University of California-Irvine Medical Center, Orange, CA 92668.

<sup>3</sup> Department of Pathology, University of Southern California-Rancho Los Amigos Hospital, 7705 Golondrinas, 1200 Bldg., Downey, CA 90242.

0361-803X/91/1562-0307  
© American Roentgen Ray Society

In this article, we report our initial evaluation of the quantitative application of the Dixon method to the liver at 1.5 T in comparison with liver biopsy in patients with various degrees of fatty infiltration. A possible difficulty in the application of the Dixon method to the liver at high field strength is an increase in the confounding influence of magnetic susceptibility effects leading to systematic errors if the T2\* is short [2]. Accordingly, we have tested a simple correction scheme for eliminating these errors by producing a third image with a phase difference of 360° between fat and water spins. To assess the influence of respiratory motion on fat quantification, the reproducibility of the image measurements was tested in three normal volunteers and 10 patients.

Subjects and Methods

The study population consisted of seven men and nine women with known liver disease who were scheduled to undergo percutaneous liver biopsy as part of their routine medical workup. They were 21–66 years old. Their clinical diagnoses included the range of diseases listed in Table 1. Informed consent was obtained separately for liver biopsy and MR imaging after explanation of the procedures.

All imaging procedures were performed by using a 1.5-T clinical MR imaging system (Signa, General Electric Medical Systems, Milwaukee, WI). A standard spin-echo pulse sequence was modified to allow a shift of the 180° pulse by a user-selected time  $\tau$  without changing the frequency-encoding gradients (Fig. 1). Fat and water signals will then acquire a phase difference due to precession at their natural resonant frequencies for a time  $2\tau$ . For a chemical shift  $\delta$  (in parts per million) and a frequency  $\nu$  (in megahertz), the shift (in milliseconds) required to put the fat and water spins 180° out-of-phase is  $\tau = 1/(4\delta\nu)$ . At 1.5 T, a 180° shift between fat and water spins is produced during the readout time for  $\tau = 1.1$  msec. Apart from the phase difference, this offset can also lead to signal attenuation even in a tissue with no fat if there is significant field variation within a voxel—and this drop in signal would be misinterpreted as being due to a nonzero fat fraction. Local field variations within a voxel can result from iron accumulation or from gradients caused by magnetic susceptibility differences at tissue interfaces. The more

rapid signal decay when the 180° pulse is shifted is thus similar to the increased transverse decay characterized by T2\* in gradient-echo imaging. Note, however, that in gradient-echo imaging the decay with increasing TE is due to both T2 and to inhomogeneous fields (jointly characterized by T2\*), but that the decay with increasing  $\tau$  in phase-contrast imaging is due only to the inhomogeneous fields within a voxel. Despite this distinction, in this article we will refer to this as T2\* effect. To assess the impact of this T2\* attenuation we produced images with  $\tau = 0, 1.1$ , and 2.2 msec (fat and water spins out of phase by 0°, 180°, and 360°, respectively). Any drop in signal intensity between the 0° and 360° out-of-phase images should be due to T2\* effects only. Other pulse sequence parameters were TR = 300 msec, TE = 25 msec, and six or eight excitations with 128 phase-encoding steps. Multiple slices 1 cm thick with 1-cm gaps were obtained. The coronal imaging plane was used in the first three patients, after which the axial plane was used. Flow compensation, respiratory gating, and cardiac gating were not used. For each patient, the receiver attenuations were kept constant to facilitate arithmetic manipulation of the signal intensities in the different images for computation of fat fraction. In addition to these pulse sequences, a standard two-echo spin-echo pulse sequence, 1500/30, 60 or 2000/30, 80 (TR/TE), was also performed on each patient.

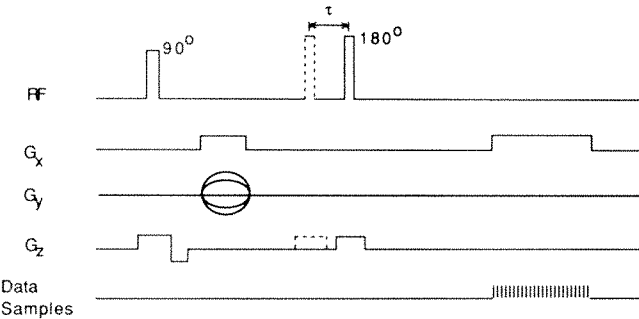


Fig. 1.—Diagram shows MR pulse sequence used to determine apparent fat fraction in liver. Time  $\tau$  is selected to produce phase offsets of 0°, 180°, and 360° between fat and water spins in three separate acquisitions. G<sub>x</sub>, G<sub>y</sub>, and G<sub>z</sub> = gradient magnetic field in the x, y, and z axes, respectively.

TABLE 1: Patients' Data and Amount of Liver Fat as Determined by MR and Biopsy

Age (yr)	Sex	Diagnosis	Fat Grade on Biopsy	% Fat by MR	T2 (msec)
27	F	Chronic active hepatitis, non-A, non-B	1	0	46
40	M	Cirrhosis, hepatitis B antigen positive	1	0	42
65	F	Congestive heart failure, diabetes	1	2	33
21	F	Sclerosing cholangitis	1	2	45
37	M	Alcoholic liver disease	1	5	38
38	F	Chronic active hepatitis, hepatitis B antigen positive	1	6	41
49	F	Chronic active hepatitis, hepatitis B antigen positive	1	8	25
53	M	Hemochromatosis	1	10	41
66	F	Primary biliary cirrhosis	2	9	33
32	M	Alpha <sub>1</sub> -antitrypsin deficiency	2	24	34
41	M	Diabetes	3	40	37
32	M	Hepatitis, hepatitis B antigen positive	3	40	36
37	F	Psoriasis	3	42	40
41	F	Alcoholic hepatitis	4	24	34
38	F	Alcoholic liver disease	4	29	43
38	M	Alcoholic liver disease	4	42	45

Note.—Fat content as assessed in biopsy material: grade 1 = 0–25%; grade 2 = 26–50%; grade 3 = 51–75%; grade 4 = >75%.



Data were analyzed by using regions of interest (ROIs) of 1–20 cm<sup>2</sup> from several positions in the liver, taking care to avoid regions obviously contaminated by partial-volume effects, chemical-shift artifact, and motion artifact. In these studies, flow and respiratory compensation were not used, and in seven of 23 studies the motion artifacts were insufficiently suppressed by averaging. Those scans that were grossly contaminated by motion artifact were not included in the study. Reproducibility of the image intensities was checked by repeating the pulse sequence several times in 10 of the patients and three normal volunteers.

The apparent fat fraction  $f$  was calculated as

$$f = (S_{in} - S_{out}) / (2 \times S_{in}), \quad (1)$$

where  $S_{in}$  is the in-phase image signal intensity and  $S_{out}$  is the 180° out-of-phase signal intensity from the same ROI. Two potential problems arise in using equation 1. First, because we are using a short TR,  $S_{in}$  and  $S_{out}$  will be somewhat T1-weighted, so that  $f$  is T1-weighted. Specifically, if  $f_0$  is the true fat fraction (the fractional spin density associated with the fat line), then

$$f = f_0 / \{1 / [(1 - f_0)\epsilon + f_0]\}, \quad (2)$$

where  $\epsilon = (1 + e^{-TR/T1(W)} - 2e^{-(TR-TE/2)/T1(W)}) / (1 + e^{-TR/T1(F)} - 2e^{-(TR-TE/2)/T1(F)})$  and the symbols W and F indicate liver water and fat, respectively. Equation 2 is plotted in Figure 2 for TR = 300 msec, T1(F) = 250 msec, and T1(W) = 400 and 500 msec. Although  $f$  will differ from  $f_0$ , it is not strongly sensitive to the exact value of T1 and so should still provide a useful measure of the fat content. Figure 2 also illustrates the second problem associated with equation 1. Because MR imagers typically display only the magnitude of the reconstructed image, there is an intrinsic ambiguity in applying equation 1 to data. Although  $S_{out}$  accurately reflects the difference in the water and fat signals, it is not possible to identify whether the fat or the water is the dominant signal. Mathematically, this means that we do not know the correct sign for  $S_{out}$  in equation 1. As a result, for  $f_0 > 0.5$ , we will in fact be calculating the water fraction,  $1 - f_0$  (shown as the dotted curves in Fig. 2). When this study was done, we did not have the

capability of determining the sign of  $S_{out}$  from the phase of the image [3, 7].

To correct for T2\* effects,  $S_{in}$  was taken as the average of the 0° and 360° out-of-phase signal intensities. For modest attenuation, this linear correction should be valid regardless of the exact form of the signal decay (e.g., exponential or gaussian [8]). The importance of this correction was assessed by also calculating the fat fraction without using the 360° out-of-phase signal. Finally, for each ROI the apparent T2 was calculated from the standard long TR two-echo spin-echo images from the same ROI position that was used for the fat fraction determinations.

Percutaneous liver biopsy was performed in all of the patients less than 2 weeks before the MR examination. The liver biopsy was obtained with a disposable Jamshidi aspiration needle (Baxter Health Care Corp., Valencia, CA) (16-gauge outer diameter) or with a Tru-cut needle (Travenol Laboratories Inc., Deerfield, IL) (18- by 1.5-mm core) and placed in B-5 solution. After routine processing and staining, the biopsy was graded by a pathologist not familiar with either the patients or the MR results. Fat content was scored subjectively as the overall impression of the percentage of fat in the hematoxylin and eosin-stained preparation, as previously reported [9]: grade 0 = <2%; grade 1 = 2–25%; grade 2 = 26–50%; grade 3 = 51–75%; grade 4 = >75%. To provide a linear scale more suitable for statistical comparison with the MR-calculated apparent fat fraction, grades 0 and 1 were combined into a single category termed grade 1. The correlation coefficient between the parameters measured with MR and the biopsy grade was calculated.

## Results

Patient data, biopsy grade, MR-calculated fat fraction, and calculated apparent T2 are summarized in Table 1.

Eight of eight patients with biopsy grade 0 or 1 (<25% fat content) were computed by MR to have a fat content of 10% or less. Seven of eight patients with at least grade 2 biopsy (>25% fat content) were computed by MR to have at least 24% fat. Results of the MR fat fraction category assignment showed a significant correlation with the biopsy grades ( $r = .86$ ,  $p < .01$ , with 5% confidence limits on  $r$  of .63 and .95). Figure 3A shows a plot of the mean and standard deviation of the MR categories vs the biopsy grade. Because of technical limitations, we did not try to resolve the intrinsic ambiguity of the Dixon method (i.e., whether the fat or the water signal is dominant in the out-of-phase image). Given their histologic grading (grades 3 and 4), it is likely that the fat fraction in the liver in six of the patients was greater than 50%. When the apparent fat fractions in these livers is taken as  $1 - f$  and then used for assignment to the MR fat categories, the correlation improves to  $r = .96$ , with 5% confidence limits of .88 and .99 (Fig. 3B).

Although one might expect a correlation between apparent T2 and fat fraction because of differences in the intrinsic T2 of the water and fat components, we found no significant correlation between them in this study with either the MR-calculated fat fraction (Fig. 4) or biopsy grading. The direct method for MR measurement of fat fraction is thus a much more sensitive indicator of fatty liver than the indirect effect of altered apparent T2.

The relative importance of using the 360° out-of-phase image in addition to the 0° and 180° out-of-phase images

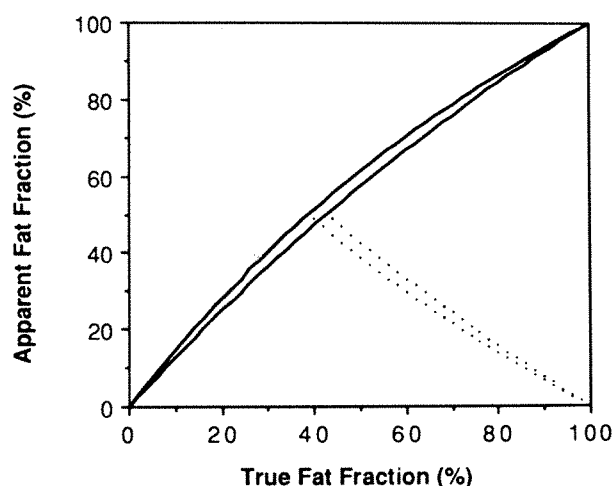


Fig. 2.—Graph shows theoretical curves of T1-weighted apparent fat fraction vs true fat fraction, calculated for TR = 300 msec, T1 (fat) = 250 msec, and T1 (liver water) = 400 and 500 msec. Dotted lines show fat fraction that would be calculated from equation 1 (see text) without correction for sign of  $S_{out}$  (180° out-of-phase signal intensity).

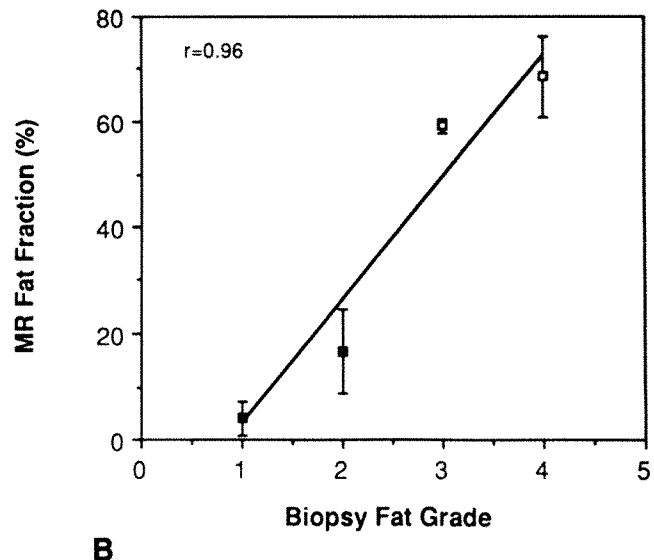
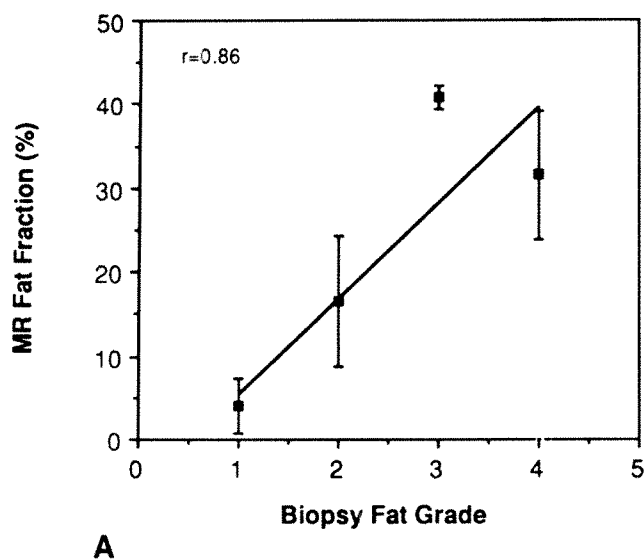


Fig. 3.—Graphs show apparent fat fraction determined by MR vs fat categorized by biopsy grade. Mean and standard deviations are plotted, as well as regression line from a scatterplot.

A, MR-apparent fat fraction ( $f$ ) is calculated with the formula from equation 1 (see text).

B, MR-apparent fat fraction is taken to be  $(1 - f)$  for histologic grades 3 and 4 biopsies.

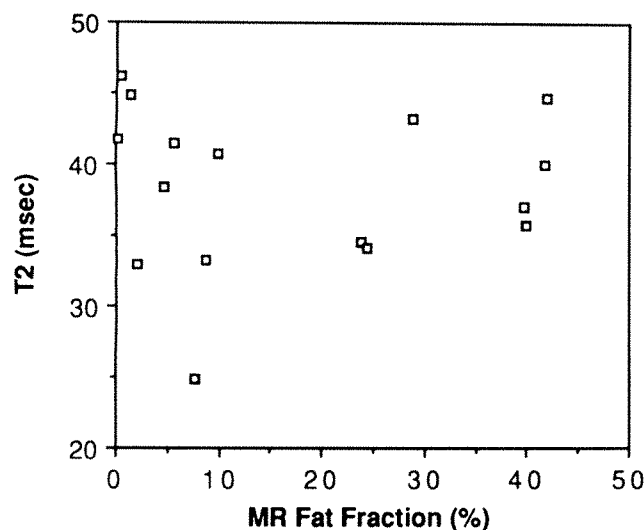


Fig. 4.—Graph shows apparent fat fraction vs calculated T2. There is no significant correlation between the two.

was evaluated by calculating the fat fraction with and without use of this additional image in all 16 patients. On average, the correction lowered the calculated fat fraction by only 1%, with a maximum correction of only 3%.

Visual appearance of the liver in the out-of-phase images compared with the in-phase images provided an immediate indication of the content of fat in the liver. In patients with high fat content (all seven patients with apparent fat fraction of at least 24%), the darkening of the liver on the 180° out-of-phase image was readily apparent when viewed with the same window and level as the in-phase image. This provided a good qualitative indication of fatty liver (Fig. 5 vs Fig. 6). There were no patients with apparent fat fractions between 10% and 24%, so we do not know the lower limit of the accuracy of this qualitative assessment.

Of concern was the reproducibility of the 180° out-of-phase

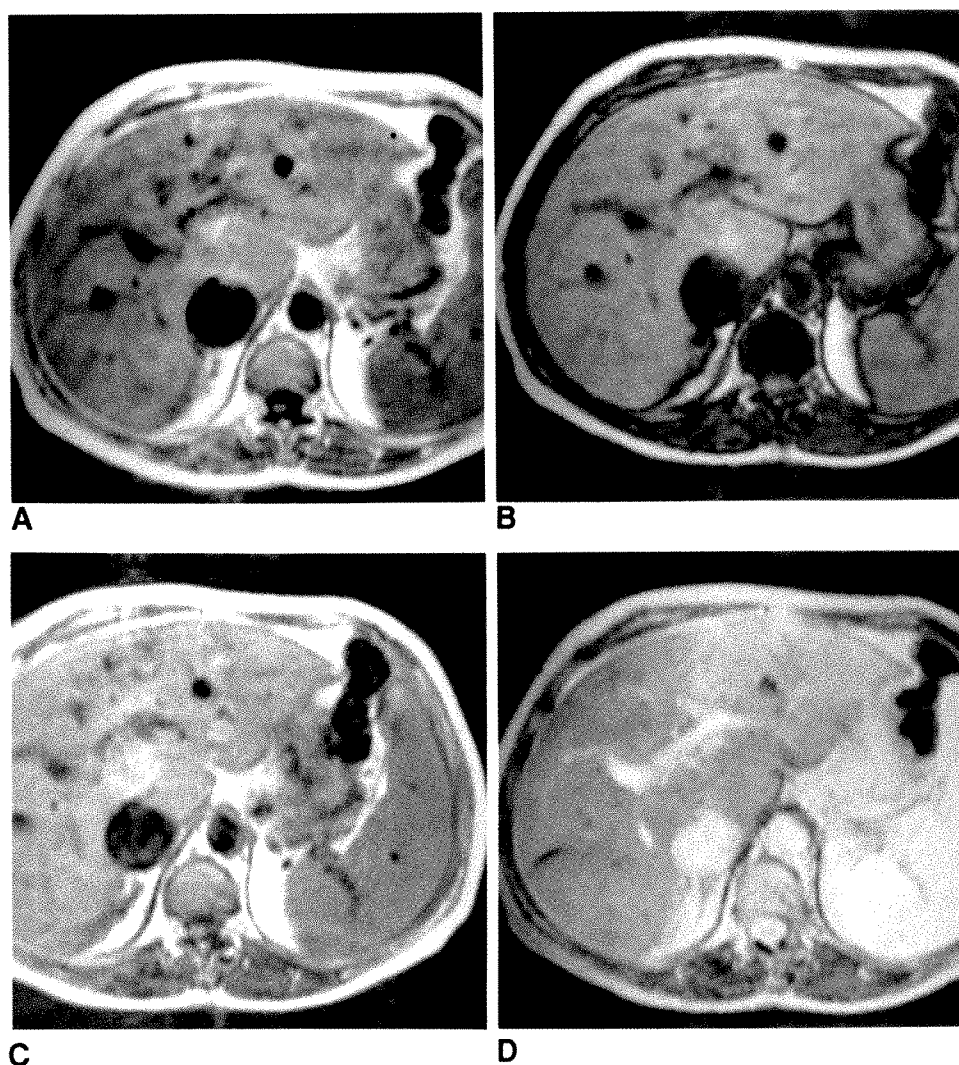
signal intensities due to the variable of respiratory motion. When these images were repeated in three volunteers and 10 patients, the variation in signal intensity from the ROIs used for determination of fat fraction was less than 5%. This would lead to a variation of less than 2.5% in the calculated fat fraction.

## Discussion

Fatty infiltration is a nonspecific response of liver to a variety of insults. Its quantification, generally via biopsy, can be an important factor in assessing disease status in the sizable population of patients with liver disease. However, biopsy is invasive and can have serious complications, especially in those patients with ascites and a bleeding diathesis due to the liver disease itself. Further, though multiple biopsy samples are generally taken, the sampling is blind, and quantification may be unduly influenced by sampling error resulting from inhomogeneity of the pathologic changes. Obviously, a reliable noninvasive method without sampling error would be a considerable improvement.

In this study we tested several aspects of the quantitative use of the Dixon method for measuring hepatic fat fraction, comparing the MR data with the semiquantitative histologic assessment of hepatic biopsy specimens routinely provided by the pathology department. The apparent fat fraction measured with the Dixon method will differ from the true fat fraction by weight for several reasons: (1) different proton densities of fat and water, (2) presence of a fat resonance near the water resonance (which thus will be interpreted as water), and (3) relaxation time weighting in the measured signals. The first two are inherent limitations of the method, and we have not tried to correct for them. The third depends on the chosen pulse sequence parameters. With a long TR the T1 sensitivity can be eliminated, but then less averaging can be done in the same imaging time. Averaging reduces somewhat the perceptible motion artifact, and for liver studies such artifacts are a persistent problem. In our studies a relatively short TR (300

Fig. 5.—A–D, MR images of patient with a small fat fraction determined by MR and biopsy. A–C are 0°, 180°, and 360° out-of-phase images, respectively. D is T2-weighted image. Little difference in signal intensity of liver is seen among A–C.



msec) was chosen, so that as a consequence the calculated fat fraction is somewhat T1 dependent. Also, with TE = 25 msec, some sensitivity to variations in T2 will exist. For clinical applications, our principal aim is to produce an index that can serve as a practical measure of the fat fraction, so we have not tried to correct the apparent fat fraction for these effects. The theoretical curves shown in Figure 2 suggest that the apparent fat fraction is close to the true fat fraction even for this heavily T1-weighted pulse sequence. As a result, variability in the apparent fat fraction due to variability in liver water T1 is likely to be small. In our studies with patients, the apparent fat fraction correlated significantly with the histologic assessment of biopsy material. In their study of fat quantification in bone marrow, Rosen et al. [7] similarly found that a T1-weighted apparent fat fraction was effective in discriminating between diseased and healthy tissue. When coupled with improved techniques for the suppression of respiratory artifacts, it may be possible to reduce the number of excitations and increase the TR to reduce the T1 weighting.

In using the  $f$  given by equation 1 as "fat fraction," we tacitly have assumed that the fat fraction is always less than the water fraction. On the basis of the biopsy results, it is likely that six of our patients had fat fractions greater than 0.5. As noted, this problem may have reduced our correlation coefficient from .96 to .86 (Fig. 3). A robust application of the

method clearly should include a phase-correction scheme (e.g., [3, 10]) so that the ambiguity is removed.

It is well known that in gross cases of generalized fatty infiltration, CT scans may reveal qualitatively decreased liver parenchymal attenuation clearly identifiable on clinical images. An analogous finding has not been noted with standard MR pulse sequences. Consistent with this is the finding in our study that there is no quantitative correlation between degree of fatty infiltration and apparent T2, which is in accord with observations by others [6]. This might be partly because fatty infiltration may be associated with other pathologic changes that tend to lower T2 (e.g., increased iron deposition). In any case, the out-of-phase images themselves seem to provide a qualitative gauge of the fatty infiltration (in this study, confirmed by biopsy), and thus address a deficiency of standard spin-echo liver imaging.

We have attempted to evaluate two possible sources of error in the uncritical application of the Dixon method to quantification of the liver fat fraction: reproducibility problems (due to respiratory artifact) and T2\* sensitivity (due to the interval between the RF and gradient-echo centers). We have found that in normal volunteers and patients, reproducibility of signal intensities was within 5% in studies not grossly contaminated by artifact. Although we think this degree of reproducibility is well within the boundaries of that necessary



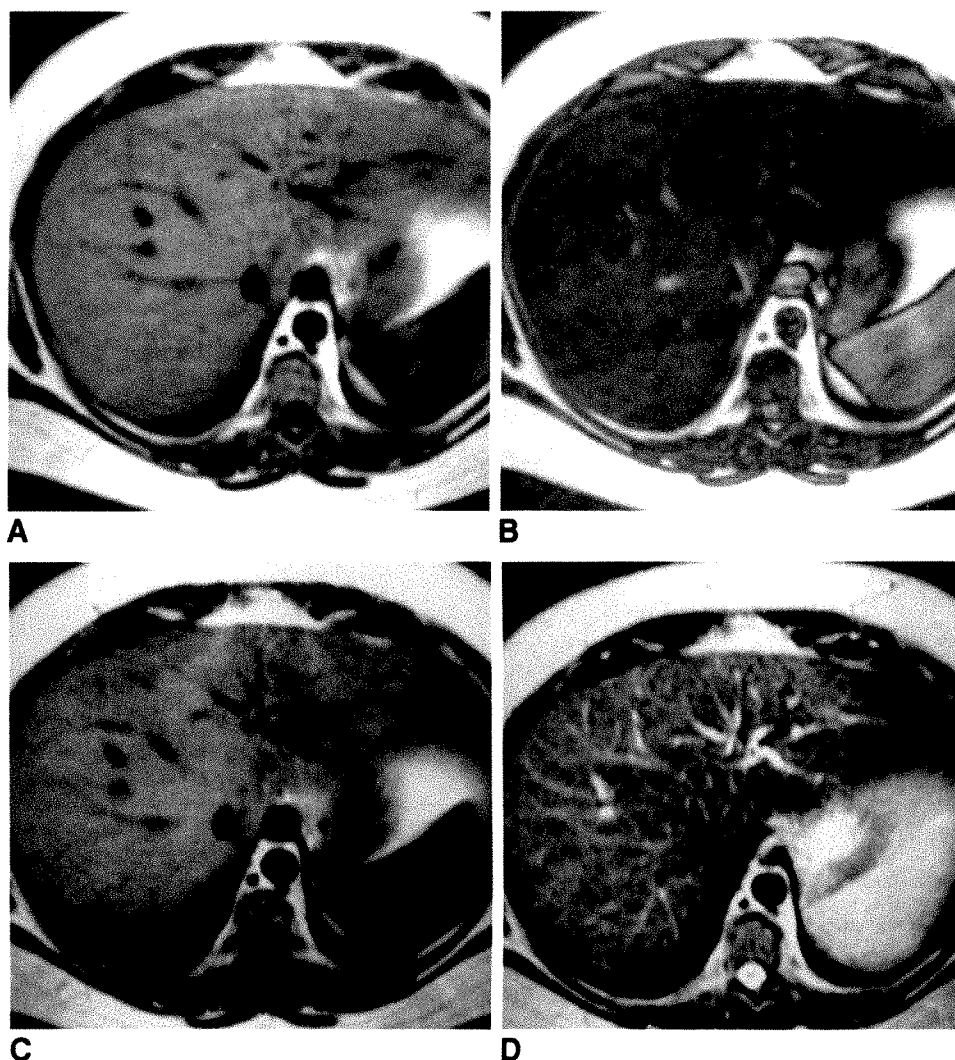


Fig. 6.—A–D, MR images of patient with MR-calculated fat percentage of 42% and biopsy grade 3. A–C are 0°, 180°, and 360° out-of-phase images, respectively. D is T2-weighted image. Note marked decrease in signal of liver on out-of-phase image B.

to make this a clinically viable method, it is likely it can be improved further by incorporating specific methods to suppress respiratory artifacts (which, apart from taking multiple averages, were not used in this study). Regarding the possible confounding influence of T2\* decay, we have used a scheme to detect and correct for such effects by using the 360° out-of-phase image signal intensities. The finding that fat fractions computed with and without the correction were typically within 1% of each other indicates that T2\* effects generally will not limit clinical application of this method. Nevertheless, there may be situations in which marked shortening of liver T2\* occurs (e.g., in a patient with liver disease who has had a large number of transfusions because of gastrointestinal bleeding and consequent increased liver deposition of iron). In these situations the correction scheme may be important.

In conclusion, this initial study of the quantitative application of the Dixon method of MR imaging of liver at 1.5 T shows reasonably good reproducibility and correlation with biopsy specimens. A correction for T2\* decay by using a 360° out-of-phase image produced only a small change in the calculated fat fraction. This noninvasive technique provides a rapid, safe procedure for evaluation of hepatic fat fraction.

#### ACKNOWLEDGMENTS

We thank Liesbeth Sotebeer, Gina Aldrich, and Diana Charlson for technical assistance.

#### REFERENCES

1. Dixon WT. Simple proton spectroscopic imaging. *Radiology* **1984**; 153:189–194
2. Buxton RB, Wismer GL, Brady TJ, Rosen BR. Quantitative proton chemical-shift imaging. *Magn Reson Med* **1986**;3:881–900
3. Aue WP, Lazeyras F, Terrier F. Quantitative proton chemical shift imaging. *J Magn Reson* **1988**;77:160–165
4. Poon CS, Szumowski J, Plewes DB, Ashby P, Henkelman RM. Fat/water quantitation and differential relaxation time measurement using chemical shift imaging technique. *Magn Reson Imag* **1989**;7:369–382
5. Lee JKT, Dixon WT, Ling D, Levitt RG, Murphy WA Jr. Fatty infiltration of the liver: demonstration by proton spectroscopic imaging. *Radiology* **1984**;153:195–201
6. Heiken JP, Lee JKT, Dixon WT. Fatty infiltration of the liver: evaluation by proton spectroscopic imaging. *Radiology* **1985**;157:707–710
7. Rosen BR, Fleming DM, Kushner DC, et al. Hematologic bone marrow disorders: quantitative chemical shift MR imaging. *Radiology* **1988**;169:799–804
8. Wismer GL, Buxton RB, Rosen BR, et al. Susceptibility induced MR line broadening: applications to brain. *J Comput Assist Tomogr* **1988**;12: 259–265
9. Duerinckx A, Rosenberg K, Hoefs J, et al. In vivo acoustic attenuation in liver: correlations with blood tests and histology. *Ultrasound Med Biol* **1988**;14:405–413
10. Borrello JA, Chenevert TL, Meyer CR, Aisen AM, Glazer GM. Chemical shift based true water and fat images: regional phase correction of modified spin echo MR images. *Radiology* **1987**;164:531–537

## Periportal Contrast Enhancement on CT Scans of the Liver

Albert M. Hammerman<sup>1</sup>  
Lawrence M. Kotner, Jr.  
Thomas B. Doyle

Periportal contrast enhancement relative to adjacent liver and portal blood has been reported on CT scans in cases of schistosomiasis and hepatic Kaposi sarcoma in AIDS patients. We observed this phenomenon in 10 (8%) of 130 consecutive, contrast-enhanced, nondynamic CT examinations of the abdomen. Thus, the occurrence is more common and less specific than previously reported. Seven of the 10 patients in our series were receiving chemotherapy for malignant disease, and three had abdominal pain with no definitive diagnosis. In four of the 10 patients, corresponding areas of periportal low attenuation or radiolucency were observed on initial dynamically enhanced scans. Periportal enhancement may be related to late diffusion of contrast material into periportal areas that were initially radiolucent. Such diffusion may occur because of endothelial insult.

Periportal contrast enhancement appears to be a nonspecific finding on nondynamic contrast-enhanced CT scans of the abdomen. Periportal enhancement is important to recognize because it can mimic the appearance of portal vein thrombosis and may also be used to differentiate intrahepatic biliary dilatation from periportal radiolucency.

*AJR* 156:313-315, February 1991

Interest in the periportal region on CT scans of the liver recently has concentrated on the occasional finding of linear bands of low attenuation or radiolucency parallel to the portal vessels (the periportal collar sign) [1]. We describe enhancement around the portal vessels on contrast-enhanced nondynamic CT scans. Periportal enhancement appears to be nonspecific and may be confused with thrombosis of the portal vein.

### Subjects and Methods

One hundred thirty consecutive CT examinations of the abdomen were reviewed. All scans were contrast-enhanced, nondynamic examinations—that is, they were not performed during bolus IV administration of contrast material. Of the 130 patients scanned, approximately 65% had received or were receiving chemotherapy for malignant disease.

The examinations were obtained either as a continuation of a combination chest/abdomen CT study or as delayed images of the liver after a standard dynamic examination of the abdomen. The average time was 15–20 min after administration of contrast material. In all cases, 180 ml of 60% iodinated contrast material (Berlex, Wayne, NJ) was administered. All examinations were performed on a GE 9800 Quick Scanner (General Electric, Milwaukee, WI).

### Results

Of the 130 cases imaged, 10 (8%) showed some degree of periportal enhancement relative to adjacent liver and portal blood (Figs. 1–3). Other than cysts in three patients, no other focal abnormalities of the liver were noted in these 10 patients.

Received May 14, 1990; accepted after revision August 14, 1990.

<sup>1</sup> All authors: Department of Radiology, The Jewish Hospital of St. Louis at Washington University, 216 S. Kingshighway, St. Louis, MO 63110. Address reprint requests to A. M. Hammerman.

0361-803X/91/1562-0313  
© American Roentgen Ray Society

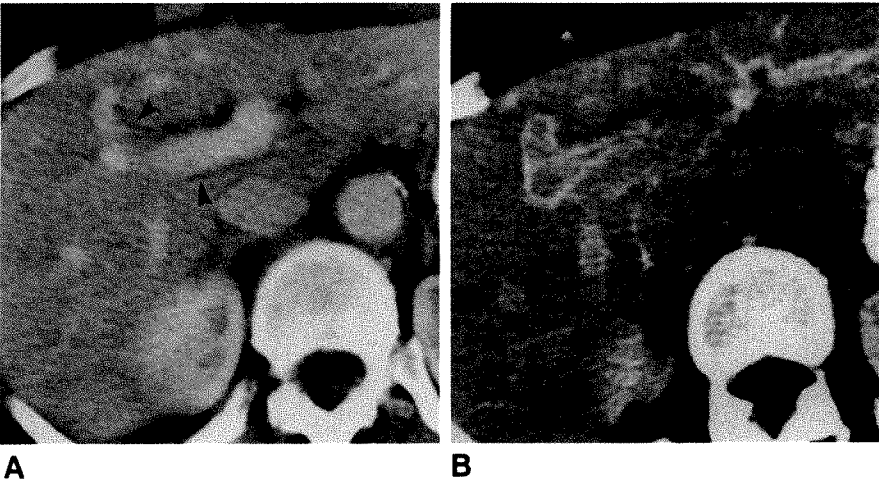


Fig. 1.—Patient receiving chemotherapy for lymphoma.  
A, Dynamic contrast-enhanced CT scan shows subtle periportal lucency (*arrowheads*).  
B, Nondynamic CT scan shows marked periportal enhancement.

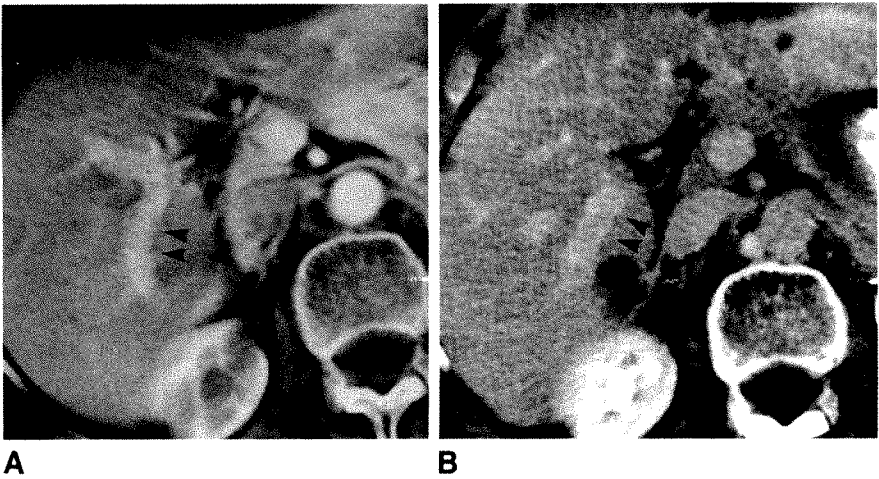


Fig. 2.—Patient receiving chemotherapy for adenocarcinoma of stomach.  
A, Dynamic contrast-enhanced CT scan shows subtle periportal lucency (*arrowheads*).  
B, Nondynamic CT scan at slightly different level shows periportal enhancement (*arrowheads*). Note cyst in right lobe of liver.

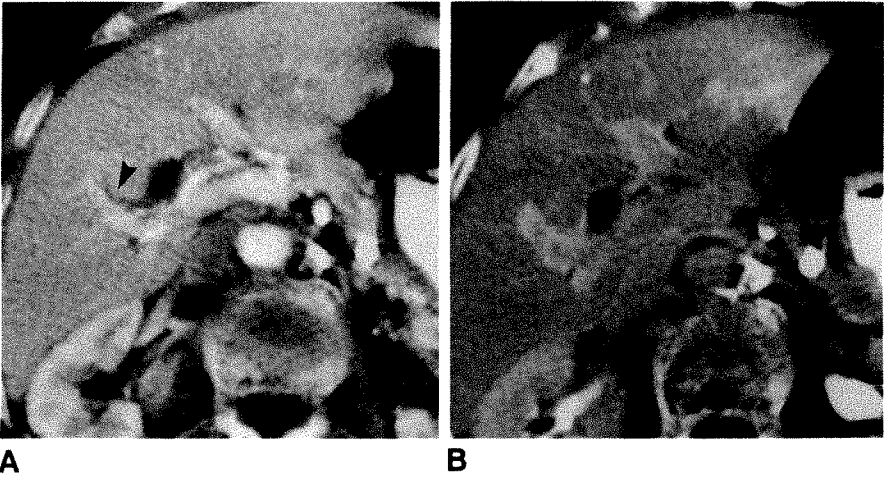


Fig. 3.—Patient with abdominal pain of unknown cause.  
A, Dynamic contrast-enhanced CT scan shows periportal lucency (*arrowhead*).  
B, Delayed CT scan shows marked periportal enhancement. Note cyst in right lobe of liver.

Four of the 10 patients had received chemotherapy for lymphoma, and three had received chemotherapy for other carcinomas. Two of the patients with malignant disease had retroperitoneal adenopathy, and one had mesenteric, celiac, and periportal adenopathy.

Of the 10 patients with periportal enhancement, three had

abdominal pain for which no definite cause was established, with clinical follow-up ranging from 8 months to 2 years. One of these three had congestive heart failure at the time of the examination.

In addition, five of the 10 patients with periportal enhancement had prior dynamic contrast-enhanced scans. In four of



these scans, corresponding areas of periportal lucency were observed. These dynamic scans were obtained 20 min earlier than the nondynamic contrast-enhanced scans in three cases, and in one case, 3 months earlier.

## Discussion

Low-density periportal bands on dynamic contrast-enhanced CT scans that enhance on delayed scans have been described in patients with schistosomiasis [2] and more recently in AIDS patients with Kaposi sarcoma [3]. Our findings suggest that this phenomenon is more common and less specific than previously thought.

Periportal enhancement was observed to some degree in 8% of the patients in our series undergoing nondynamic contrast-enhanced CT of the abdomen. The cause of this phenomenon is uncertain; it may be related to the low-attenuation linear bands that parallel the portal tracts on some CT scans, termed the periportal collar sign [1]. This association is suggested by the observation in several of our patients that areas of periportal enhancement on nondynamic contrast-enhanced scans correspond to areas of periportal low attenuation on dynamic contrast-enhanced scans of the same patient.

Wechsler et al. [1] were among the first to note the CT finding of low-attenuation bands paralleling the intrahepatic portal vessels. They thought this was an important clue to acute allograft rejection in patients with liver transplants. However, a subsequent study [4] concluded that this finding was of low specificity in the assessment of acute rejection. Low-attenuation bands around the portal veins also have been reported for many other conditions, including congestive hepatomegaly, malignant lymphatic obstruction, posttraumatic hematoma, cholangitis, and viral hepatitis [1, 4, 5].

Arrivé et al. [6] noted abnormal periportal signal intensity on nonenhanced MR images in patients receiving chemotherapy. This altered periportal appearance has been attributed to various causes, including lymphocytic portal infiltration, periportal hepatic fibrosis, lymphoma infiltration, lymphedema, and vascular endothelial damage [7, 8]. Many of the patients included in our study were receiving chemotherapy for malignant disease. Periportal enhancement in these cases may be the result of passive diffusion of contrast material into the periportal space because of vascular endothelial damage associated with chemotherapy. The high percentage of patients who were being followed up for malignancy in our study, however, may result in selection bias, adding to the relatively frequent occurrence of periportal enhancement in this series. Although dynamic CT scans of the abdomen are

routine in most patients at our institution, nondynamic scans of the abdomen often are obtained immediately after dynamic CT scans of the chest in patients being studied for malignant disease in whom both examinations are ordered for the same day.

Baker et al. [9] described a somewhat similar appearance of periportal enhancement in cases of metastatic periportal tumor and biliary carcinoma. The appearance of periportal enhancement in our cases, however, was more diffuse and less irregular. The periportal enhancement seen in cases of schistosomiasis [2] and hepatic Kaposi sarcoma [3] is similar to that seen in our cases. It appears, however, that this represents a less specific periportal response to disease or hepatic insult than has been suggested.

Several conditions may mimic or confuse the CT finding of portal vein thrombosis [10]. Periportal enhancement is one of these, as relatively less opacified portal blood surrounded by periportal enhancement could be mistaken for portal vein thrombosis. The late phase of periportal enhancement also can be helpful in cases in which initial periportal lucency on dynamic scans is difficult to differentiate from intrahepatic biliary dilatation.

## ACKNOWLEDGMENT

Special thanks to our administrative secretary, Janice Asher, for her assistance in manuscript preparation.

## REFERENCES

1. Wechsler RJ, Munoz SJ, Needleman L, et al. The periportal collar: a CT sign of liver transplant rejection. *Radiology* **1987**;165:57-60
2. Fataar S, Bassiony H, Satyanath S, et al. CT of hepatic schistosomiasis mansoni. *AJR* **1985**;145:63-66
3. Luburich P, Bru C, Ayuso MC, Azon A, Condom E. Hepatic Kaposi sarcoma in AIDS: US and CT findings. *Radiology* **1990**;175:172-174
4. Kaplan SB, Sumkin JH, Campbell WL, Zajko AB, Demetris AJ. Periportal low-attenuation areas on CT: value as evidence of liver transplant rejection. *AJR* **1989**;152:285-287
5. Koslin DB, Stanley RJ, Berland LL, Shin MS, Dalton SC. Hepatic perivascular lymphedema: CT appearance. *AJR* **1988**;150:111-113
6. Arrivé L, Hricak H, Goldberg HI, Thoeni RF, Margulis AR. MR appearance of the liver after partial hepatectomy. *AJR* **1989**;152:1215-1220
7. Hermann G, Lorenz M, Kirkowa-Reimann M, Hottenrott C, Hubner K. Morphological changes after intra-arterial chemotherapy of the liver. *Hepatogastroenterology* **1987**;34:5-9
8. Merine D, Fishman EK, Sitzmann JV, et al. Vascular abnormalities following radio and chemotherapy of hepatic neoplasms: CT angiographic findings. *J Comput Assist Tomogr* **1988**;12:584-587
9. Baker ME, Silverman PM, Halvorsen RA, Cohan RH. Computed tomography of masses in periportal/hepatoduodenal ligament. *J Comput Assist Tomogr* **1987**;11:258-263
10. Martin K, Balfe DM, Lee JKT. Computed tomography of portal vein thrombosis: unusual appearances and pitfalls in diagnosis. *J Comput Assist Tomogr* **1989**;13:811-816

## Book Review

**Aids to Radiological Differential Diagnosis**, 2nd ed. By Stephen Chapman and Richard Nakielny. Philadelphia: Baillière Tindall, 576 pp., 1990. \$24.95

At 541 pages, including a 52-page index that is wonderfully inclusive and thorough, this second edition is significantly longer than the popular first edition. The book is divided intelligently into two parts. The first consists of lists of differential diagnoses under categories that can best be described as both anatomic (e.g., spine) and physiologic according to organ systems (e.g., cardiovascular, respiratory). These lists, in contradistinction to another popular differential diagnostic reference (*Gamuts in Radiology*), are listed according to a "surgical sieve" classification presented in order of prevalence within the various pathologic classifications (e.g., neoplastic, inflammatory). The lists are presented in as interesting a manner as possible, considering the job at hand, with accompanying interesting and informative pathologic, physiologic, and descriptive information, admixed occasionally with rather helpful illustrations and line drawings to depict those aspects of the findings discussed in which a picture is truly worth a thousand words.

The second part consists of more detailed information on a seemingly randomly selected group of dozens of pathologic entities chosen both for their importance because they might be common or for their interesting features, be they pathologic, physiologic, or radiologic, if

they are more unusual. An example of each is the discussion of Paget disease, a common abnormality that is reviewed concisely yet usefully, and pseudopseudohypoparathyroidism, a fascinating syndrome about which all I ever wanted to know is included in seven succinct lines. Additions to the second edition of information in the fields of mammography, nuclear medicine, and obstetric and gynecologic sonography are important in the everyday practice of radiology, and credit is given to Michael Collins, Keith Harding, and Josephine McHugo for their contributions in these fields.

The authors are unduly modest in describing the book as one aimed primarily at those taking postgraduate examinations. Having practiced radiology for about 20 years, I think the book is aimed more directly at me. I intend to have it immediately available to me on a daily basis, and I recommend that everyone interested in radiology do likewise.

Hano A. Siegel  
Mercy Hospital  
San Diego, CA 92103

## Focal Nodular Hyperplasia of the Liver: MR Findings in 35 Proved Cases

Michael J. Lee<sup>1</sup>  
 Sanjay Saini<sup>1</sup>  
 Bernd Hamm<sup>2</sup>  
 Mathias Taupitz<sup>2</sup>  
 Peter F. Hahn<sup>1</sup>  
 Eric Seneterre<sup>1</sup>  
 Joseph T. Ferrucci<sup>1</sup>

MR images of 28 patients with 35 lesions of hepatic focal nodular hyperplasia were reviewed to determine the frequency of findings considered typical of this condition (isointensity on T1- and T2-weighted pulse sequences, a central hyperintense scar on T2-weighted images, and homogeneous signal intensity). Fifteen lesions were imaged at 0.6 T with T1- and T2-weighted spin-echo (SE) pulse sequences; 20 lesions were imaged at 1.5 T with T1-weighted SE and gradient-echo pulse sequences and T2-weighted SE pulse sequences. Diagnosis of focal nodular hyperplasia was made pathologically in 25 patients, with nuclear scintigraphy in four, and with follow-up imaging in six. Only seven lesions (20%) were isointense relative to normal liver on both T1- and T2-weighted images. On T1-weighted SE images, 21 lesions (60%) were isointense relative to normal liver, 12 (34%) were hypointense, and two (6%) were hyperintense. On T2-weighted SE images, 12 lesions (34%) were isointense and 23 (66%) were hyperintense relative to normal liver. A central scar was present in 17 lesions (49%) and was hypointense relative to the lesion on T1-weighted images and hyperintense on T2-weighted images. Twenty lesions (57%) were of homogeneous signal intensity throughout the lesion, except for the presence of a central scar. All three MR imaging characteristics were present in three cases (9%).

We conclude that hepatic focal nodular hyperplasia has a wide range of signal intensity on MR imaging.

*AJR* 156:317-320, February 1991

Recently, a number of small series have been published detailing the MR appearances of focal nodular hyperplasia (FNH) [1-4]. The largest of these [3] concluded that FNH has a fairly consistent MR appearance: (1) isointensity on T1- and T2-weighted sequences; (2) a central scar, which is hyperintense on T2-weighted sequences; and (3) homogeneous signal intensity except for the presence of a central scar. However, using improved pulse sequence timing parameters that provide better lesion-liver contrast than those used in previous studies, we noticed more variable signal intensities in our FNH cases. Therefore, we decided to analyze the MR findings in our patients with FNH by performing a retrospective analysis of 35 hepatic FNH lesions, imaged at high and mid field, to determine the prevalence and clinical usefulness of the aforementioned MR characteristics.

### Materials and Methods

Twenty-eight patients, six men and 22 women 20-55 years old (mean, 37 years), with 35 liver lesions detected by CT or sonography underwent MR imaging for the purpose of tissue characterization. In 12 patients with 15 lesions, MR imaging was performed with a 0.6-T superconducting imaging system (Teslacon, General Electric Medical Systems, Milwaukee, WI). With the 0.6-T unit, T1-weighted spin-echo (SE) images, 275/14 (TR/TE), and multiecho T2-weighted SE images, 2350/60, 120, 180, were acquired. Sixteen patients with 20 lesions were imaged on a 1.5-T superconducting system (Siemens Magnetom, Erlangen, Germany) with T1-weighted SE 500/15 and gradient-echo (GRE) 100/5/80° (TR/TE/flip angle) pulse

Received July 27, 1990; accepted after revision August 28, 1990.

<sup>1</sup> Department of Radiology, Massachusetts General Hospital and Harvard Medical School, 32 Fruit St., Boston, MA 02114. Address reprint requests to S. Saini.

<sup>2</sup> Department of Radiology, Freie Universität Berlin, Universitätsklinikum Steglitz, Hindenburgdamm 30, D 1000 Berlin 45, Germany.

0361-803X/91/1562-0317  
 © American Roentgen Ray Society



sequences and double-echo T2-weighted SE 2500/15,90 pulse sequences.

Pathologic proof of FNH was obtained with tissue histology in 25 of 35 lesions via percutaneous 14- or 16-gauge needle biopsy core specimens ( $n = 14$ ) or surgical resection ( $n = 11$ ). In the remaining 10 of 35 lesions, diagnosis of FNH was made with  $^{99m}\text{Tc}$  sulfur colloid nuclear scintigraphy ( $n = 4$ ), or typical radiologic features on MR imaging (three patients) and angiography (three patients), with an unchanged appearance over 6 months.

Qualitative analysis of liver lesions was performed in conference by three of the authors reaching a consensus on lesion signal intensity as compared with that of adjacent normal liver on each T1- and T2-weighted image, signal homogeneity, and the presence and signal intensity of central scars. Quantitative analysis could not be performed because of the retrospective nature of the study and the unavailability of magnetic storage tapes containing raw data for a large number of patients.

## Results

The mean size of all 35 FNH lesions was 5.7 cm (range, 1.5–12.0 cm). On T1-weighted SE images, 21 (60%) of 35 lesions were isointense relative to normal liver (Fig. 1A), 12 (34%) were hypointense relative to normal liver (Fig. 2A), and two (6%) were hyperintense relative to normal liver. The hyperintensity in one of these was shown at surgery to represent intralesional hemorrhage (Fig. 3). At 1.5 T, four of 20 lesions were isointense, whereas the remainder were hypointense relative to normal liver (Figs. 2B and 4) on the more heavily T1-weighted GRE pulse sequence. On T2-weighted SE images 12 (34%) of 35 lesions (11 were imaged at 0.6 T and one at 1.5 T) were isointense relative to normal liver (Fig. 1B); the remaining 23 (66%) of 35 (four were imaged at 0.6 T and 19 at 1.5 T) were hyperintense relative to normal liver (Figs. 2C and 4C). Only seven (20%) of 35 lesions were isointense on all pulse sequences. Further signal intensity classification for each field strength is given in Table 1.

In 17 (49%) of 35 lesions, a central scar was identified that was hypointense on T1-weighted and hyperintense on T2-weighted images (Figs. 1 and 4). Twenty (57%) of 35 lesions were of homogeneous signal intensity on all imaging sequences, except for the presence of the scar (Fig. 1). The

remainder had a heterogeneous appearance (Fig. 3). Only three (9%) of 35 FNH lesions demonstrated all three of the previously reported [3] typical MR features (Fig. 1) (isointensity on all pulse sequences, signal homogeneity throughout the lesion, and a central scar of increased signal intensity on T2-weighted images).

## Discussion

Hepatic FNH is a relatively uncommon benign tumor, occurring in approximately 3% of the adult population [5]. It is typically solitary (80%), occurs primarily in women (85%), and usually is asymptomatic and discovered incidentally. Pathologically, FNH is a nonencapsulated lesion with distorted liver architecture [6]. A central scar is a characteristic gross pathologic finding. Microscopically, stellate fibrous bands partially or completely encircle nodules of normal hepatocytes. Recently, several studies [2–4] have proposed that MR imaging may provide a noninvasive tissue-specific diagnosis of FNH, based on the findings of lesion homogeneity, isointensity on T1- and T2-weighted pulse sequences, and a hyperintense scar on T2-weighted images.

Our results, however, suggest that hepatic FNH has a wide range of signal-intensity appearances on MR imaging. Indeed, the isointensity noted in previous studies on T1- and T2-weighted images [2–4] was present in only 20% of our lesions. We believe that this discrepancy from previous reports is due to improvement in pulse sequence timing parameters, which provide increased tissue contrast on T1- and T2-weighted images. For example, Mattison et al. [3] used less heavily T1-weighted pulse sequences (500/28–60) and variable T2-weighted pulse sequences (2000/30–150) on a low-field system (0.35 T, Diasonics MT/S). Similarly, Schiebler et al. [4] used less heavily weighted T1 pulse sequences (600/25) on a high-field system (1.5 T, General Electric Signa). The usefulness of increased T1 weighting, as found by Edelman et al. [7], was evident in our patients when SE and GRE images were compared (1.5 T). In 13 of 20 lesions that were isointense relative to liver on T1-weighted SE images, nine became hypointense relative to liver on T1-weighted GRE

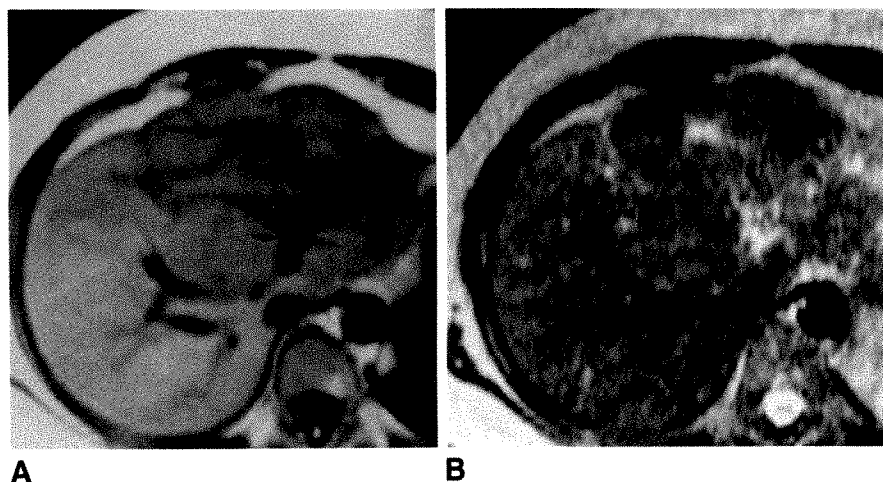
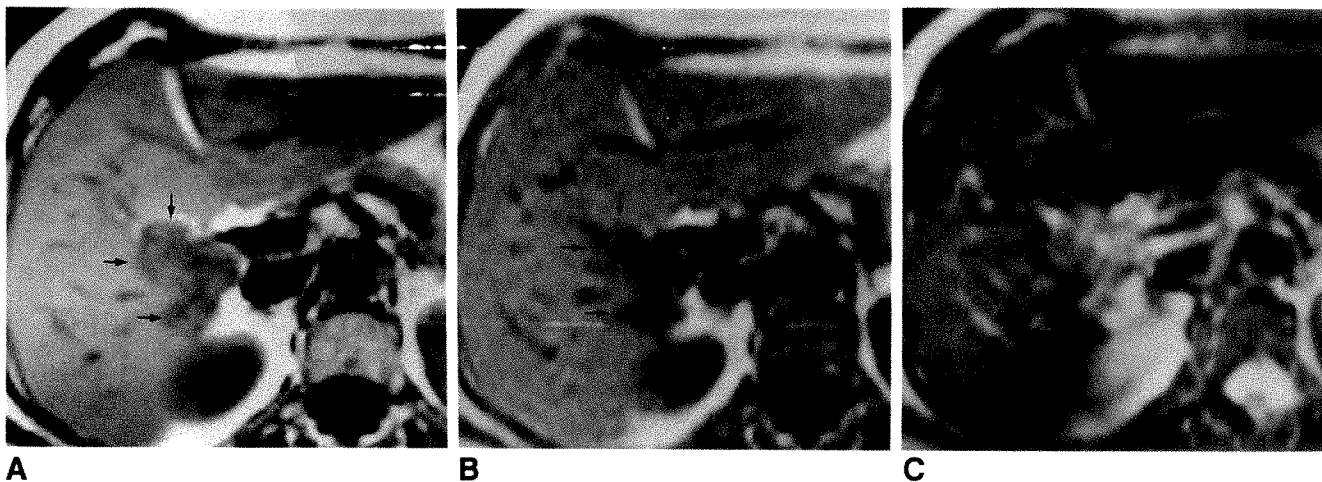


Fig. 1.—Typical MR findings of focal nodular hyperplasia (0.6 T).

A, T1-weighted MR image (275/14) shows a large, lobulated mass surrounding left portal vein (small arrows). Mass is isointense relative to normal liver, is of homogeneous signal intensity, and contains a central scar (large arrow).

B, T2-weighted MR image (2350/180) shows lesion has homogeneous signal intensity and is isointense relative to normal liver. This was true on all T2-weighted images (2350/60,120,180). Central scar (arrow) appears hyperintense on this image.



**Fig. 2.**—Atypical, nonisointense focal nodular hyperplasia (1.5 T).  
**A and B,** Periportal mass (arrows) is hypointense relative to normal liver on T1-weighted SE 500/15 pulse sequence (A) and T1-weighted GRE 100/5/80° pulse sequence (B).  
**C,** Lesion (arrows) is hyperintense relative to normal liver on T2-weighted SE images (2500/15,90).  
 Note absence of a central scar and lesion heterogeneity on both T1- and T2-weighted MR images.

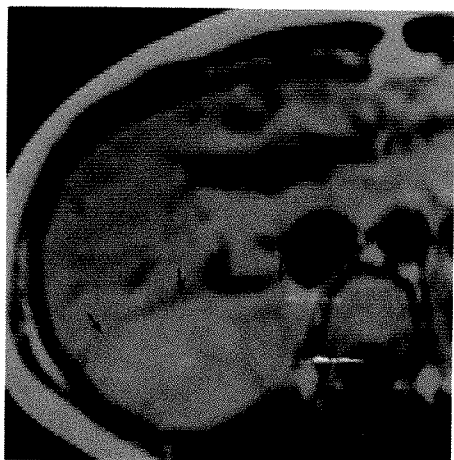


**Fig. 3.**—Atypical focal nodular hyperplasia (0.6 T) on T1-weighted MR image (275/14). There is no central scar. Large mass in right lobe (arrows) was hyperintense relative to normal liver on both T1- and T2-weighted pulse sequences, caused by intralesional hemorrhage.

images, because of increased lesion-liver contrast (Fig. 4; Table 1). When results were compared at different field strengths, a discrepancy was noted only on T2-weighted images. The majority of FNH lesions (19/20) imaged at 1.5 T were hyperintense relative to normal liver, whereas at 0.6 T most FNH lesions (11/15) were isointense relative to normal liver (Table 1). The reason for this discrepancy is not clear, but it may be due to population sampling errors or other unrecognized factors.

Central stellate scars were present in 49% of lesions in this series and were hypointense on T1-weighted images and hyperintense on T2-weighted images. Histopathologically, FNH scars contain bile ducts, blood vessels, and a few or many chronic inflammatory cells. These scars are not commonly detected on other imaging techniques, including CT

(14%) [8]. The MR findings indicate that these scars have a longer T1 and T2 than the body of the lesions, suggesting a higher fractional water content, which is compatible with pathologic observations. The signal intensity of the FNH scar is important, as it may prove to be a valuable differential diagnostic clue. Scars in liver hemangiomas also are watery [9], but on MR images, differences between hemangiomas and FNH are readily appreciated. Central scars in other tumors such as fibrolamellar hepatomas are generally hypointense on T1- and T2-weighted sequences, as might be expected from a true fibrous scar with poor vascularity [9]. A single report in the literature describes a central scarlike area in hepatocellular carcinoma, with increased signal intensity on T2-weighted images, mimicking FNH [10]. However, T1-weighted sequences were not performed and no pathologic proof was available, indicating that this scarlike area may have been due to central necrosis.

In this series, 20 of 35 lesions were of homogeneous signal intensity on all pulse sequences except for the presence of a scar. Homogeneity alone is unhelpful in distinguishing FNH from tumors, which tend to be heterogeneous and hyperintense on T2-weighted sequences, but may be useful when associated with other findings such as a central scar and isointensity on all sequences.

In conclusion, this series illustrates the varied appearance of hepatic FNH on MR imaging and stresses the development of appropriate differential diagnostic considerations. When the characteristic triad of isointensity on T1- and T2-weighted sequences, lesion homogeneity, and a central hyperintense scar on T2-weighted sequences is present, the diagnosis of FNH is almost certain. This triad was present in only 9% of patients in this series. However, because on MR images liver metastases are rarely isointense relative to liver, isointensity on either T1- or T2-weighted pulse sequences may be sufficient to discriminate FNH from liver metastases. By using this less rigid criterion of isointensity on either T1- or T2-weighted

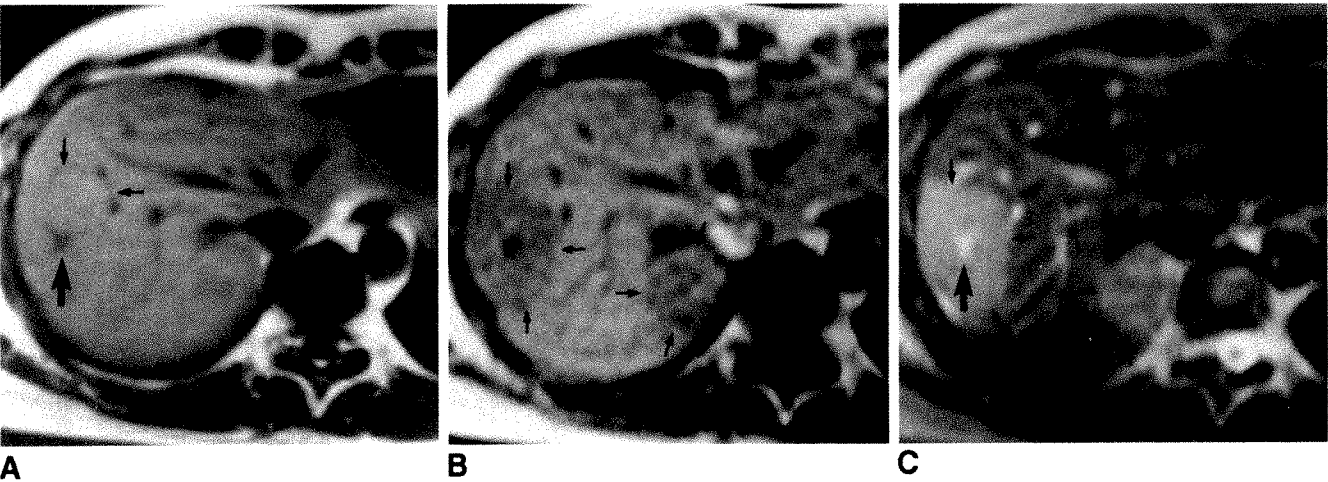


Fig. 4.—Effect of increasing T1 weighting (1.5 T) on MR imaging. Two lesions are present.  
A, On T1-weighted SE image (500/15), lesions are isointense relative to normal liver and are invisible, except for hypointense central scar (large arrow) and displacement of hepatic vessels (small arrows) in peripherally located lesion.  
B, On more heavily T1-weighted GRE image (100/5/80°), lesions become hypointense relative to normal liver (arrows).  
C, On T2-weighted SE images (2500/15,90), lesions appear hyperintense relative to normal liver (small arrows). Central scar (large arrow) in peripheral area of hyperplasia is hyperintense compared with remainder of lesion.

TABLE 1: MR Signal Intensities in Focal Nodular Hyperplasia

Sequence/Signal Intensity	1.5 T (n = 20)	0.6 T (n = 15)	Total (n = 35)
T1-Weighted SE			
Iso	13 (65)	8 (53)	21 (60)
Hypo/hyper	7 (35)	7 (47)	14 (40)
T1-Weighted GRE			
Iso	4 (20)	—	—
Hypo/hyper	16 (80)	—	—
T2-Weighted SE			
Iso	1 (5)	11 (73)	12 (34)
Hypo/hyper	19 (95)	4 (27)	23 (66)
T1- and T2-Weighted			
Iso	0	7 (47)	7 (20)
Hypo/hyper	20 (100)	8 (53)	28 (80)
T1- or T2-Weighted			
Iso	13 (65)	12 (80)	25 (71)
Hypo/hyper	7 (35)	3 (20)	10 (29)

Note.—Numbers in parentheses are percentages. Iso = isointense; hyper/hypo = hyper- or hypointense; SE = spin echo; GRE = gradient echo.

pulse sequences, we can increase diagnostic specificity to 71% (25/35) (Table 1). However, because of fatty change, tumors such as hepatomas also may appear isointense on T1-weighted images. In this situation, the presence of a typical central scar would increase diagnostic confidence. Further diagnostic specificity may require enhanced dynamic MR imaging [7, 11].

REFERENCES

1. Ferrucci JT, Freeney PC, Stark DD, et al. Advances in hepatobiliary radiology. *Radiology* **1988**;168:319-338  
2. Butch RJ, Stark DD, Malt RA. MR imaging of hepatic focal nodular hyperplasia. *J Comput Assist Tomogr* **1986**;10(5):874-877  
3. Mattison GR, Glazer GM, Quint LE, Francis IR, Bree RL, Ensminger WD. MR imaging of hepatic focal nodular hyperplasia: characterization and distinction from primary malignant hepatic tumors. *AJR* **1987**;148:711-715  
4. Schiebler ML, Kressel HY, Saul SH, Yeager BA, Axel L, Gefter WB. MR imaging of focal nodular hyperplasia of the liver. *J Comput Assist Tomogr* **1987**;11(4):651-654  
5. Karhunen PJ. Benign hepatic tumors and tumor-like conditions in man. *J Clin Pathol* **1986**;39:183-188  
6. Gold JH, Guzman IJ, Rosai J. Benign tumors of the liver: pathologic examination of 45 cases. *Am J Clin Pathol* **1978**;70(1):6-17  
7. Edelman RR, Siegel JB, Singer A, Dupuis K, Longmaid HE. Dynamic MR imaging of the liver with Gd-DTPA: initial clinical results. *AJR* **1989**;153:1213-1219  
8. Welch TJ, Sheedy PF, Johnson CM, et al. Focal nodular hyperplasia and hepatic adenoma: comparison of angiography, CT, US, and scintigraphy. *Radiology* **1985**;156:593-595  
9. Rummeny E, Weissleder R, Sironi S, et al. Central scars in primary liver tumors: MR features, specificity, and pathologic correlation. *Radiology* **1989**;171:323-326  
10. Wilbur WC, Gyi B. Hepatocellular carcinoma: MR appearance mimicking focal nodular hyperplasia. *AJR* **1987**;149:721-722  
11. Yoshida H, Itai Y, Ohtomo K, Kokubo T, Minami M, Yashiro N. Small hepatocellular carcinoma and cavernous hemangioma: differentiation with dynamic FLASH MR imaging with Gd-DTPA. *Radiology* **1989**;171:339-342



# Self-Expandable Stainless Steel Endoprostheses for Treatment of Malignant Bile Duct Obstruction

A. Adam<sup>1</sup>  
N. Chetty<sup>1</sup>  
M. Roddie<sup>1</sup>  
E. Yeung<sup>1,2</sup>  
I. S. Benjamin<sup>3</sup>

The Wallstent biliary endoprosthesis is a mesh of stainless steel that is delivered percutaneously over a 7-French catheter but expands to achieve a 1-cm lumen when released across a bile-duct stricture. The small transhepatic track required makes insertion easier, less painful, and probably safer when compared with plastic stents, and the large internal lumen reduces the rate of occlusion by encrusted bile. Wallstent endoprostheses were inserted under local anesthesia in 41 consecutive patients with malignant obstructive jaundice. Biliary drainage was considered the treatment of choice in all of these patients. The diagnosis was based on biopsy results in 32 patients and on radiologic appearances in nine. The patients were followed up in outpatient clinics for 16 months and had repeated radiologic examinations only if they had symptoms suggesting stent occlusion. No cases of hemobilia due to damaged hepatic vessels occurred. Two patients had septicemia treated with antibiotics. Three patients had recurrent jaundice due to growth of tumor below or above the stents. Endoprosthesis migration was not seen. No cases of stent occlusion due to encrustation of bile occurred. The median survival of patients was 105 days (range, 10–545 days).

Our experience shows that Wallstent endoprostheses can be inserted with little discomfort for the patient and with relatively few complications. They provide good palliation in patients with malignant obstructive jaundice.

*AJR* 156:321–325, February 1991

Biliary endoprostheses are of established value in the treatment of inoperable malignant tumors causing obstructive jaundice [1, 2]. They achieve satisfactory drainage of bile into the bowel without the physical and psychological problems associated with the use of external catheters [3]. The most frequent problems associated with the long-term use of such stents are migration and occlusion due to encrustation of bile. In addition, insertion can be traumatic, with resultant hemobilia, leakage of bile, and discomfort for the patient. Self-expandable stainless steel endoprostheses can be inserted by using catheters of relatively small caliber, but when they are released they expand to create a large lumen, which improves drainage and discourages bile encrustation [4–6].

Wallstent endoprostheses (Medinvent SA, Lausanne, Switzerland) have been used in the urinary tract, in peripheral and coronary arteries, and in the biliary tree [7–9]. They consist of a mesh of stainless steel, the wires of which are free to move over each other. Biliary Wallstent endoprostheses are inserted over 7-French catheters and expand to an unconstrained diameter of 1 cm. We have used this type of stent in 41 patients in the past 16 months. The patients were followed up during return visits to their family doctor's office or the hospital outpatient clinic and had appropriate imaging investigations if they developed symptoms of recurrent biliary obstruction.

Received May 29, 1990; accepted after revision July 16, 1990.

<sup>1</sup> Department of Diagnostic Radiology, Royal Postgraduate Medical School, Hammersmith Hospital, Du Cane Rd., London W12 0HS, England. Address reprint requests to A. Adam.

<sup>2</sup> Present address: Division of Gastrointestinal and Interventional Radiology, Toronto General Hospital, 200 Elizabeth St., Toronto, Ontario, Canada.

<sup>3</sup> Department of Surgery, Royal Postgraduate Medical School, Hammersmith Hospital, Du Cane Rd., London W12 0HS, England.

0361-803X/91/1562-0321  
© American Roentgen Ray Society

## Materials and Methods

Forty-one patients ranging in age from 22 to 89 years (median, 65 years) had Wallstent endoprostheses inserted during a period of 16 months. The level of obstruction was at the liver hilum in 24 cases, in the mid common bile duct in nine, and in the lower common bile duct in eight. In 21 patients, the clinical and radiologic findings suggested the diagnosis of cholangiocarcinoma, but this was confirmed by biopsy in only 15. Six patients had metastases to lymph nodes at the hilum of the liver from known colonic or gastric malignant neoplasms. One patient had carcinoma of the gallbladder, one had a recurrent hepatocellular carcinoma invading the left hepatic duct after an extended right hepatectomy, and 12 patients had carcinoma of the pancreas. Ten patients had had plastic stents removed before the insertion of a Wallstent endoprosthesis: in six cases, the plastic endoprosthesis in situ was the first one to be used; in three, the second one; and one patient had had seven plastic stents before. The duration of jaundice before the insertion of the metal endoprostheses ranged from 2 to 7 weeks. Six patients in whom stents were inserted successfully have been lost to follow-up and are excluded from our results.

Biliary Wallstent endoprostheses are available in lengths of 50 or 100 mm and are inserted over 7-French catheters. The method of release of the stent is shown in Fig. 1. Radiopaque metal markers indicate the proximal and distal ends of the endoprosthesis. Before insertion of the stent, the stricture is dilated with a high-pressure, low-profile angioplasty balloon 10 mm in diameter (Olbert, Meadox Limited, Dunstable, U.K.). After dilatation, the stent is appropriately positioned, and withdrawal of the rolling membrane allows the stent to expand gradually from its distal end. The endoprosthesis does not usually expand fully after its release, and it is necessary to dilate it. Use of a low-profile balloon is essential for this purpose, as a significant degree of friction during insertion or withdrawal of the balloon may result in distal or proximal displacement of the endoprosthesis. The final length of the stent depends on the extent of expansion; high inflation pressure and virtual elimination of the "waist" of the balloon ensures that the variation in caliber along the length of the stent is minimized and its final length is, therefore, more easily predictable.

Very occasionally, a defect in the rolling membrane may result in incomplete release of the stent and necessitate removal of a partially open stent. It is best to anticipate this malfunction by inserting a 9-French sheath over the stent; the sheath is not introduced into the biliary tree unless the rolling membrane malfunctions, in which case the sheath is advanced over the stent to protect the bile ducts and the liver parenchyma during withdrawal of the endoprosthesis. The sheath is then removed and a new stent inserted.

After successful deployment of the stent, a temporary external catheter is left through it for 24 hr. This is used to obtain a cholangiogram on the next day to check that the stent remains in a satisfactory position. If excessive shortening has taken place, a second stent can be inserted overlapping the first one.

In patients in whom it is necessary to drain both lobes of the liver, it is possible to have two stents passing through the confluence of the right and left hepatic ducts. If the obstructing lesion is in the lower common bile duct, the lower end of the stent is left slightly projecting through the papilla of Vater. In recurrent cholangiocarcinoma at the site of a surgical anastomosis, the distal end of the stent is allowed to project into the small bowel distal to the anastomosis.

In 31 patients, the stent was inserted in a two-stage procedure: an 8.3-French catheter providing internal/external drainage was inserted during the first session, and the endoprosthesis was inserted a few days later. In 10 patients, one-stage insertions were performed.

In 36 patients, only the right or left main hepatic ducts were drained. In most of these patients, one stent was sufficient to bypass the

malignant stricture but in a few cases two overlapping endoprostheses were necessary. In one patient, endoprostheses were inserted from both the right and the left side via separate transhepatic punctures (Fig. 2). In another case, an endoprosthesis was inserted from the right to the left lobe and a second endoprosthesis from the right lobe to the common bile duct (Fig. 3). One patient had separate segments of the right lobe drained, another had both segments of the left lobe drained, and a third patient had stents inserted in the right hepatic duct and both segmental ducts of the lateral part of the left lobe. In one case, a recurrent cholangiocarcinoma at the site of a previous hepaticojejunostomy was treated by the retrograde insertion of an endoprosthesis via a percutaneously punctured Roux-en-Y loop after the removal of an obstructed plastic endoprosthesis.

All procedures were performed with antibiotic prophylaxis (piperacillin 4 g and gentamicin 80 mg), which was given IV 1 hr before the procedure and 6 hr later. Continuous administration of antibiotics or choleretic agents was not done.

## Results

### Technical Aspects

The attempted percutaneous insertions of drainage catheters and placement of metal endoprostheses were successful in all patients. In some patients, mainly those having the left ducts drained, withdrawal of the membrane was difficult. In these cases a 9-French sheath was inserted into the biliary tree; this reduced the degree of friction and allowed release of the stent. In six patients the stent could not be released completely and had to be removed by withdrawing the introducing catheter through a 9- or 8-French sheath, which prevented any damage to the biliary tree. After the half-opened stent was removed, another endoprosthesis was inserted. These problems with stent release were encountered mainly at the beginning of the study. Changes in the design and technical composition of the plastic rolling membrane largely eliminated these problems in subsequent patients. In one patient (2%) an endoprosthesis was released inadvertently into the duodenum, with no ill effects. In another patient (2%) a partially deflated angioplasty balloon resulted in cephalic displacement of an endoprosthesis during with-

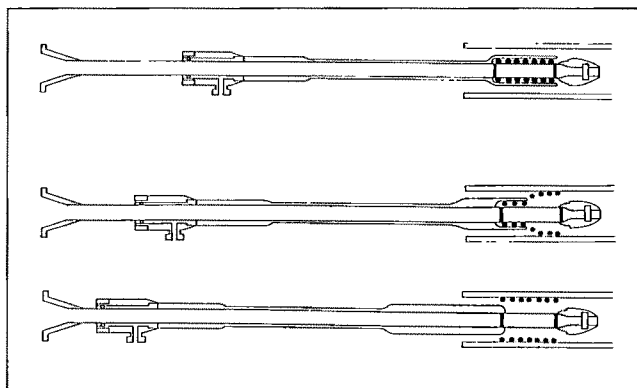


Fig. 1.—Diagram shows method of release of endoprosthesis. Black dots represent stent, which is held in a contracted state around a catheter by an outer plastic membrane. Withdrawal of membrane allows stent to expand gradually from its distal end.

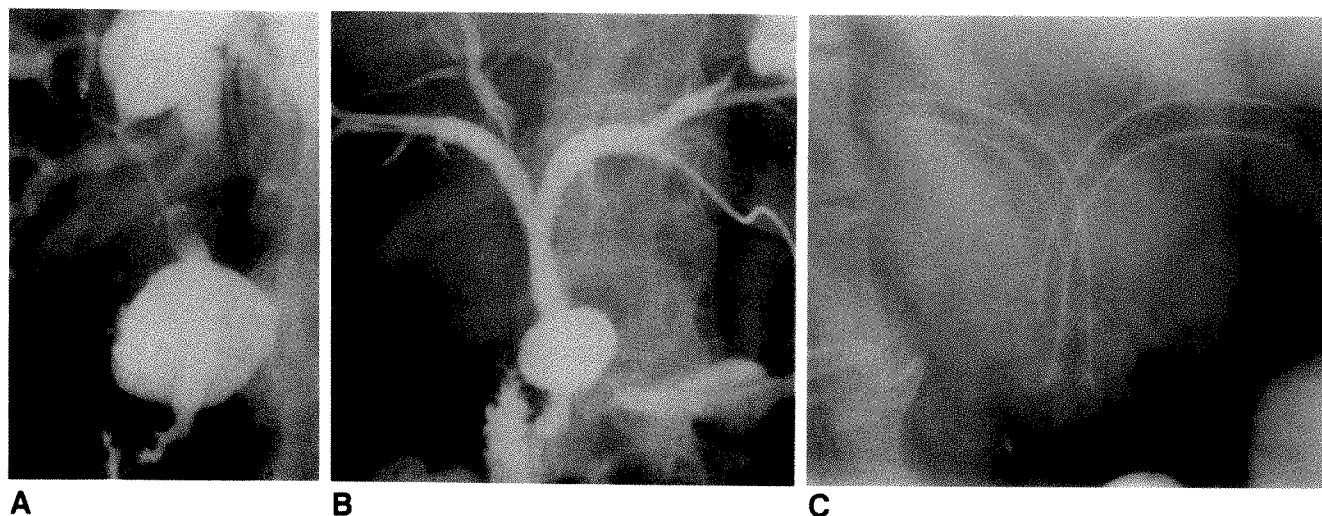


Fig. 2.—Radiographs of 58-year-old woman with cholangiocarcinoma.

A, Strictures of right and left hepatic ducts and of common hepatic duct caused by cholangiocarcinoma.

B, Contrast medium flows through stents inserted via separate punctures.

C, Steep left posterior oblique view. Endoprostheses do not compress each other significantly where they overlap.

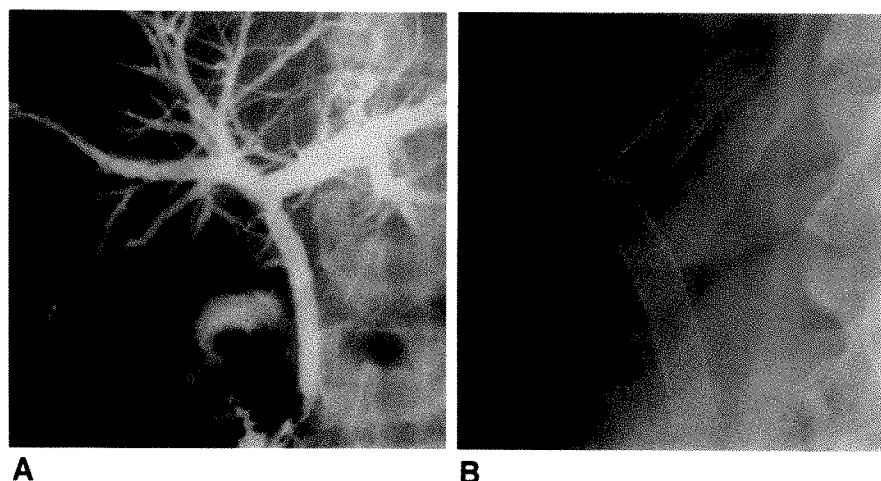


Fig. 3.—Radiographs of 76-year-old man with cholangiocarcinoma.

A, Contrast medium flows through stents inserted from same puncture on right side.

B, One stent extends from right to left and the other from right duct to common bile duct. Upper ends of stents have not expanded fully because of lack of space in right hepatic duct.

drawal of the balloon catheter. A second stent was inserted overlapping the first, and this ensured adequate biliary drainage.

#### Short-Term Complications

Blood entered the biliary tree in one patient (2%) after a small cutaneous blood vessel was punctured during securing of an internal/external catheter. No cases of hemobilia due to damage to hepatic blood vessels occurred. Two cases of septicemia (5%) responded to treatment with antibiotics. Leakage of bile via the transhepatic track and through the cutaneous puncture for a few days after stent introduction was seen in only one patient (2%). No procedure-related deaths occurred, but three patients (7%) died within 30 days; one had had a gastrectomy for carcinoma of the stomach; one had recurrent hepatocellular carcinoma after a right hepatic lobectomy, and one had carcinoma of the pancreas with

metastases to the liver. The overall short-term complication rate was 12% if problems encountered during stent insertion and mentioned under "Technical Aspects" are included.

#### Long-Term Complications

No cases of stent migration or occlusion due to bile encrustation resulted in recurrent jaundice and readmission to the hospital. Nevertheless, in three patients (7%) jaundice reoccurred because of progressive tumor growth: in one of these cases the stent remained patent but most of the right lobe was replaced by malignant tumor. In the second patient, tumor grew below the stent, and the resulting occlusion was relieved by the insertion of a plastic endoprosthesis through the metallic stent. In the third patient occlusion resulted from growth of tumor above the stent. External drainage was instituted, but the patient, who was extremely debilitated,



died within a few weeks. The overall long-term complication rate was 7%.

#### *Survival of Patients*

In four patients, jaundice persisted after successful insertion of an endoprosthesis. In all the other patients, the jaundice was improved significantly, and the serum bilirubin level reduced significantly. Nevertheless, in only 10 patients did the bilirubin level return to within normal range. The median survival of patients was 105 days (range, 10–545 days). Thirteen patients are still alive 20–545 days (median, 164 days) after the procedure. The median survival in 22 patients who died was 91 days (range, 10–330 days). Eleven of the 13 patients who are still alive are free of jaundice. The other two have some jaundice but are asymptomatic. Six patients have been lost to follow-up.

#### **Discussion**

The major problems associated with the use of conventional plastic biliary endoprostheses are stent migration and occlusion; these complications were seen in approximately 3–6% and 6–23% of cases, respectively, in two large series [2, 10]. The patency rate is approximately 25 weeks on average [10]. Occluded plastic stents protruding into the duodenum can be replaced by endoscopists. In recent years, various percutaneous methods have been described that allow relatively easy replacement of stents in cases where the distal end lies above the papilla of Vater [11–14]. Nevertheless, all methods of replacement involve an additional procedure for the patient, with its attendant inconvenience and discomfort.

It is often assumed, although not proved, that the large track necessary to introduce an endoprosthesis of a large-enough lumen to achieve satisfactory drainage and minimize the rate of bile encrustation is associated with an increased complication rate. Various methods have been devised to combat the problem of endoprosthesis migration, including the use of anchoring sutures [15] and a spiral shape [16]. The problem of occlusion has proved more difficult to solve. It is caused mainly by biliary sludge, and colonization of the stent by bacteria appears to play a major role [17–19].

Self-expandable metal endoprostheses attempt to deal with these problems. The constant outward radial force exerted by Wallstent endoprostheses and the firm anchorage afforded by the sharp ends of the steel filaments at the proximal and distal parts of the stents are very effective in preventing migration. None of the endoprostheses in our series migrated. The large internal lumen of the Wallstent endoprosthesis probably contributes to the low occlusion rate observed in this series. No cases of recurrent jaundice due to bile encrustation were seen. The occlusion due to tumor growth below a stent was caused by a combination of an error of judgment in leaving the distal end of the stent too close to the tumor and technical problems encountered with early models that

prevented ideal positioning. No cases of recurrent jaundice due to tumor ingrowth through the stainless steel mesh occurred. This may be because most of our patients had cholangiocarcinomas, which are relatively fibrous, acellular tumors and tend to grow in a concentric rather than an infiltrative fashion. Nevertheless tumor ingrowth has been observed by other investigators who have reported a higher overall rate of occlusion [20]. Our lower occlusion rate may be due to the relatively short follow-up in our series. Our series of patients is relatively small, and the median length of survival is too short to be certain that Wallstent endoprostheses have a lower occlusion rate than conventional plastic stents, although this may be the case. Nevertheless, if occlusion should occur, a second endoprosthesis can easily be introduced through the first one, and this was done in one of our patients with good results.

The difficulty experienced in withdrawing the rolling membrane in some patients in whom the stent was inserted via the left hepatic duct was probably caused by the acute angle between the distal left ducts and the left hepatic duct. In these cases, a 9-French sheath reduced the degree of friction and allowed release of the stent.

In our experience, leakage of bile from the cutaneous puncture site is observed in approximately 30% of cases when conventional endoprostheses are used. This stops after a few days when the track through the liver closes. This complication is not serious but is unpleasant for the patient. We observed this problem only once and only to a minor degree. The infrequent occurrence of this bile leakage is probably related to the excellent drainage achieved by the large lumen of the Wallstent endoprostheses. Hemobilia caused by injury to a hepatic blood vessel was not seen. In one patient, a small cutaneous artery was punctured when a temporary external drainage catheter was being secured to the skin and blood tracked around the catheter and entered the biliary tree. This is obviously not related to the use of the stent-introducing system. The small diameter of the introducing catheter and its great flexibility are likely to contribute to the relatively atraumatic insertion of the stents.

The procedure is much more comfortable for the patient than is the introduction of conventional endoprostheses. In almost all patients, the amount of analgesic medication necessary for stent insertion was reduced significantly compared with the anesthesia requirement during the insertion of plastic endoprostheses performed by the authors. These factors have allowed us to introduce these stents in a one-stage procedure with good results, even in one patient with cholangitic abscesses in the liver. Although manipulations of wires and catheters in an infected biliary tree carry significant risk, percutaneous biliary drainage is the treatment method of choice in cases of cholangitic abscesses unresponsive to antibiotics. Manipulations should be kept to a minimum in such patients, but if the catheter initially used for drainage passes the obstructing lesion easily, as it did in this patient's case, we consider it justifiable to release a Wallstent endoprosthesis across the stricture, because the stent can be introduced very easily with very few additional manipulations, and dilatation of the intrahepatic tract is unnecessary. This is

not the case with conventional stents, and we would normally await resolution of the abscesses after external drainage before introducing a plastic stent. Wallstent endoprostheses should probably be introduced in a one-stage procedure in most cases. The main reason most of our patients had two-stage procedures was the absence of a stock of Wallstent endoprostheses in the hospital; the devices were delivered from Switzerland on the day of insertion.

Wallstent endoprostheses are expensive when compared with conventional plastic stents. It can be argued that their use is not, therefore, indicated in patients with a relatively short life expectancy. We do not agree with this point of view. First, if their relatively low occlusion rate (5%) compared with the rate in plastic stents [2, 10] is confirmed in larger series, their cost disadvantage may not be as great as it first appears. Second, even if these stents eventually are proved to occlude as frequently as conventional endoprostheses do, their ease of insertion, the increased comfort of patients, and the very low rate of associated complications may justify their use. An additional advantage of these stents is that they can be inserted in a one-stage procedure, thereby shortening the patient's stay in the hospital and minimizing hospital costs.

Wallstent endoprostheses cannot be removed. Nevertheless we have not encountered a case in which it has been necessary to remove a stent, because we were dealing with nonresectable tumors. Should such an occasion arise, surgery would be necessary. In view of this, we would be very reluctant to use them in benign strictures unless no alternative existed because should stent occlusion occur, resection of the duct containing the stent would probably be made more difficult by the presence of the endoprosthesis.

The overall short-term complication rate was 12% (five patients), compared with 9% and 17% in two large series of plastic stent insertions [2, 10], but these figures disguise the fact that we have included as complications an inadvertent release of a stent into the duodenum and a cephalad stent displacement. These complications were clinically unimportant, and similar events when using plastic stents are usually unreported. A more representative complication rate in our series would be 7% (three patients). It is also of note that no hemobilia due to damage to hepatic blood vessels occurred.

Self-expandable metal biliary endoprostheses are still in their infancy, and they are bound to be improved and refined during the next few years. The principle underlying their use—the introduction of a large-lumen stent over a small introducing

catheter—is undoubtedly sound, and on the basis of our results they deserve further study.

#### REFERENCES

1. Ferrucci JT Jr, Mueller PR, Harbin WP. Percutaneous transhepatic biliary drainage: technique, results and applications. *Radiology* 1980;135:1-13
2. Lammer J, Neumayer K. Biliary drainage endoprostheses: experience with 201 placements. *Radiology* 1986;159:625-629
3. McLean GK, Burke DR. Role of endoprostheses in the management of malignant biliary obstruction. *Radiology* 1989;170:961-967
4. Coons HG. Self-expanding stainless steel biliary stents. *Radiology* 1989;170:979-983
5. Irving JD, Adam A, Dick R, Dondelinger RF, Lunderquist A, Roche A. Gianturco expandable metallic biliary stents: results of a European clinical trial. *Radiology* 1989;172:321-326
6. Rossi P, Bezzi M, Salvatori FM, Maccioni F, Porcaro ML. Recurrent benign biliary strictures: management with self-expanding metallic stents. *Radiology* 1990;175:661-665
7. Williams G, Jäger R, McLoughlin J, et al. Use of stents for treating obstruction of urinary outflow in patients unfit for surgery. *Br. Med J* 1989;298:1429-1430
8. Sigwart U, Puel J, Mirkovitch V, Jaffre F, Kappenberg L. Intravascular stents to prevent occlusion and restenosis after transluminal angioplasty. *N Engl J Med* 1987;316:701-706
9. Dick R, Gilliams A, Dooley JS, Hobbs KEF. Stainless steel mesh stents for biliary strictures. *J Intervent Radiol* 1989;4:95-98
10. Mueller PR, Ferrucci JT, Teplick SK, vanSonnenberg E, Haskin PH, Butch RJ, Papanicolaou N. Biliary stent endoprosthesis: analysis of complications in 113 patients. *Radiology* 1985;156:637-639
11. Brown AS, Mueller PR, Ferrucci JT. Transhepatic removal of obstructed Carey-Coons biliary endoprosthesis. *Radiology* 1986;159:555-556
12. Adam A. Use of the modified Cope introduction set for transhepatic removal of obstructed Carey-Coons biliary endoprosthesis. *Clin Radiol* 1987;38:171-174
13. Yeung E, O'Donnell C, Carvalho P, Adam A. A new technique for removal of double mushroom-tipped biliary endoprostheses. *AJR* 1989;152:527-528
14. Kadir S, Kauffmann GW. Technical note: percutaneous transhepatic removal of biliary endoprostheses using a snare. *Cardiovasc Intervent Radiol* 1988;11:39-41
15. Coons HG, Carey PH. Large-bore, long biliary endoprostheses (biliary stents) for improved drainage. *Radiology* 1983;148:89-94
16. Yeung E, Adam A, Gibson RN, Benjamin IS, Allison DJ. Spiral-shaped biliary endoprosthesis: initial study. *Radiology* 1988;168:365-369
17. Groen AK, Out T, Huibregtse K, Delzenne B, Hoek FJ, Tytgat GNJ. Characterization of the content of occluded biliary endoprostheses. *Endoscopy* 1987;19:57-59
18. Speer AG, Farrington H, Costerton JW, Cotton PB. Bacteria, biofilms and biliary sludge (abstr). *Gut* 1986;27:A601-A602
19. Leung JWC, Ling TKW, Kung JLS, Valance-Owen J. The role of bacteria in the blockage of biliary stents. *Gastrointest Endosc* 1988;34:19-22
20. Gilliams A, Dick R, Dooley JS, Wallsten H, El-Din A. Self-expandable stainless steel braided endoprosthesis for biliary strictures. *Radiology* 1990;174:137-140

## Book Review

**Computed Tomography of the Trunk. Normal and Pathological Anatomy.** By Jacques Hureau and Janine Pradel. (Translated by Gary Horn.) Padua, Italy: Piccin Nuova Libreria, 487 pp., 1988

A variety of comprehensive texts on CT of the body have been published, all of which include detailed descriptions of normal anatomy, and a number of atlases depict normal CT anatomy with correlation with gross anatomic drawings, axial cadaveric slices, and sonograms and MR images. Is this book by Hureau and Pradel just another in the lengthening list of atlases, or does it offer something new or unique?

The book, which is translated from the French by Gary Horn (more about this later), consists of 12 chapters. The first is a cursory chapter dealing with the physics and techniques of CT. This is followed by the atlas: a generous 219 pages packed with 767 figures (all of excellent quality) illustrating 103 axial CT scans and corresponding cadaveric anatomic levels (in both males and females) from the top of the chest to the bottom of the ischial rami. The atlas is good, but this material is already available in existing texts and other atlases.

Ten interesting chapters then follow the atlas: "Mediastinum," "Pulmonary Segmentation and CT: Fissures, Lobes and Segments," "Diaphragm," "Thoraco-Abdominal Walls—the Iliopsoas Muscle—the Gluteal Region," "Normal and Pathologic Posterior Interparieto-Peritoneal Spaces (Retroperitoneal Spaces)," "Lymphatics of the Abdomen and Pelvis," "Peritoneal Cavity and CT," "Hepatic Segmentation and CT," "Thoracic, Abdominal or Pelvic Residual Cavities after Surgical Exeresis: CT Exploration," and "Normal and Aneurysmal Abdominal Aorta in CT."

These 10 chapters represent what is unique about this book. First, although the anatomic information is not new, it is the most extensive discussion of normal and variant anatomy found in one place. To find the details presented in these chapters, a person would have to

search hard through a lot of old texts and papers. Second, the illustrations in these chapters (as well as in the atlas section) are drawn from 335 cases containing a variety of pathologic changes. Each case is listed at the end of the book, with a short history and description of the CT findings. Third, the general index is extensive and easy to use, plus the pathologic changes of the 335 cases also are indexed. Thus, the reader can look at normal anatomy of the thymus, or at a case of a thymic cyst, or at the normal inferior vena cava, or at a leiomyosarcoma of the cava.

Only one thing distracts from the book: the English translation of the French is quite disappointing. This makes reading the descriptions of normal anatomy, not an exciting subject to begin with, even more tedious. For example, the azygos fissure is described as "resulting from an *incrustation* of the vena azygos." Some sentences are really tough. Regarding hepatic anatomy, the translation states, "Actually, the correlations between the external morphology of the liver and the variations of portal segmentation are customary the unpredictable distortions are exceptional" and "The topographic diagnosis in hepatic pathology founded on clear, simple bases stereotyped from the modal diagram of the hepatic segmentation cannot be anything but far away from such a complex reality." On the other hand, if you enjoyed Chaucer in Old English in college, this just might be the book for you. The translation notwithstanding, this is a truly remarkable book.

Patrick C. Freeny  
The Virginia Mason Clinic  
Seattle, WA 98111



## Pictorial Essay

# Choledochal Cysts: Classification and Cholangiographic Appearance

Scott J. Savader,<sup>1</sup> James F. Benenati,<sup>1,2</sup> Anthony C. Venbrux,<sup>1</sup> Sally E. Mitchell,<sup>1</sup> David M. Widlus,<sup>1</sup> John L. Cameron,<sup>3</sup> and Floyd A. Osterman, Jr.<sup>1</sup>

A classification scheme for choledochal cysts is outlined and their appearance on cholangiograms is illustrated. Choledochal cysts are uncommon anomalies of the biliary system and are probably congenital in origin. They are manifested by cystic dilatation of the extra- or intrahepatic biliary tree or both. The classification system described here divides choledochal cysts into one of five main types. The most common, which is manifested by cystic or focal segmental dilatation of the common bile duct or fusiform choledochal dilatation, accounts for 80–90% of cases.

Choledochal cysts are an uncommon anomaly of the biliary system manifested by cystic dilatation of the extra- or intrahepatic biliary tree or both. Since Vater first described the entity in 1723, 3000 cases have been reported worldwide [1, 2]. Accounting for approximately one in 13,000 hospital admissions in the United States, choledochal cysts are three to four times more common in females than in males. Their origin is unknown; however, they are considered congenital because they occur in fetuses and neonates. Babbitt [3] theorized that an anomalous insertion of the common bile duct into the pancreatic duct results in chronic reflux of pancreatic enzymes into the biliary tree, which leads to inflammation, dilatation, and scarring (Fig. 1). This theory is supported by the occurrence of this anomalous insertion in 10–58% of cases [4].

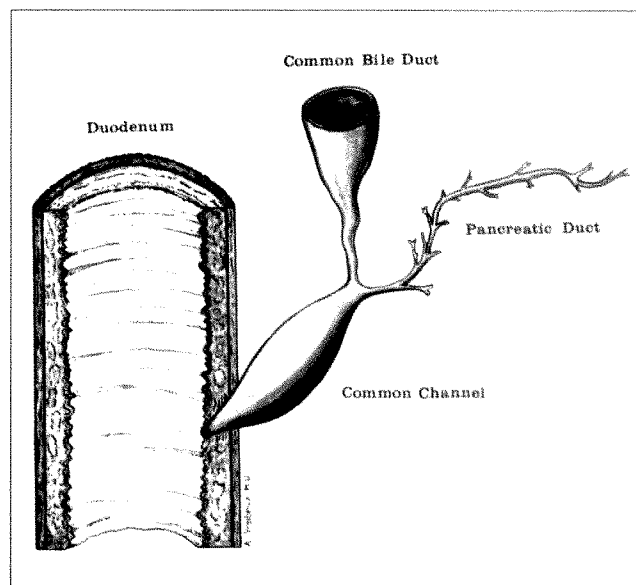


Fig. 1.—Diagram showing the long common channel and anomalous pancreaticobiliary junction proposed by Babbitt [3] to result in choledochal cyst formation.

Received July 23, 1990; accepted after revision August 30, 1990.

Presented at the annual meeting of the American Roentgen Ray Society, Washington, DC, May 1990.

<sup>1</sup> Russell H. Morgan Department of Radiology and Radiological Science, The Johns Hopkins Medical Institutions, 600 N. Wolfe St., Baltimore, MD 21205. Address reprint requests to S. J. Savader.

<sup>2</sup> Present address: Department of Radiology, Baptist Hospital, Miami, FL 33176.

<sup>3</sup> Department of Surgery, The Johns Hopkins Medical Institutions, Baltimore, MD 21205.

AJR 156:327–331, February 1991 0361–803X/91/1562–0327 © American Roentgen Ray Society

### Classification

The classification of Todani et al. (cited in [4]) is used most often, expanding the earlier one proposed by Alonzo-Lej et al. [5] by including intrahepatic cysts and further subdividing extrahepatic disease (Fig. 2). The type I cyst, accounting for 80–90% of cases, is most common. Type I is subdivided into type IA, cystic dilatation of the common bile duct; type IB, focal segmental common bile duct dilatation; and type IC, fusiform choledochal dilatation. Type II cysts account for about 2% of cases and consist of a true choledochal diverticulum. Type III cysts, accounting for 1.4–5.0% of cases, consist of a choledochoceles, involving only the intraduodenal portion of the duct. The type IV cyst is subdivided into type IVA, multiple intrahepatic and extrahepatic cysts, which accounts for 19% of cases, and type IVB, multiple extrahepatic cysts, which is much less common. The type V cyst, or Caroli disease, consists of either single or multiple intrahepatic cysts. Approximately two thirds of patients with Caroli disease also have extrahepatic disease [4, 5].

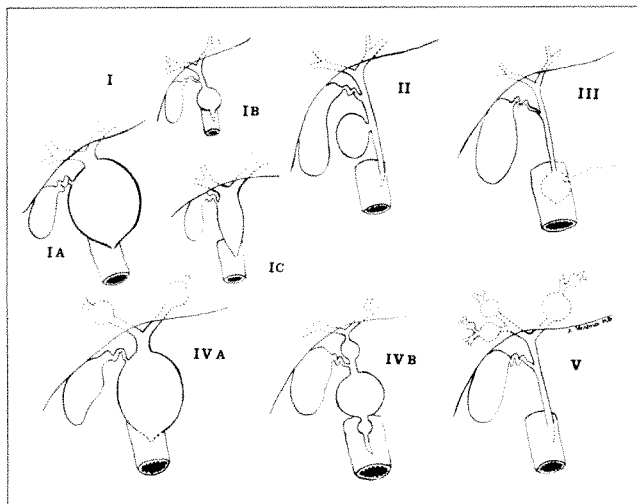


Fig. 2.—Todani's classification scheme of choledochal cysts [4].

### Findings on Percutaneous Transhepatic Cholangiography

Percutaneous transhepatic cholangiography provides detailed imaging of the choledochal cyst, the noninvolved portion of the extrahepatic biliary tree, and the intrahepatic biliary tree. In type IA choledochal cysts (Figs. 3 and 4), cholangiography shows marked dilatation of the extrahepatic biliary tree, partially or in its entirety. The gallbladder commonly arises from the choledochal cyst. The intrahepatic biliary tree is normal in appearance. Calculi may be visible within any portion of the biliary system. In type IB choledochal cysts (Fig. 5), there is focal dilatation of the most distal aspect of the common bile duct. A normal segment of common bile duct is usually present between the cyst and the cystic duct. The biliary tract proximal to the gallbladder is normal. In type IC choledochal cysts (Fig. 6), cholangiography shows smooth, fusiform dilatation of the common hepatic duct and common bile duct. The dilatation may be up to several centimeters wide. The gallbladder arises directly from the dilated common duct. The intrahepatic biliary system is not dilated. Type II choledochal cyst consists of a true diverticulum of the common bile duct. It may be as large as several centimeters in size. A type III choledochal cyst (Fig. 7) appears on (T-tube) cholangiograms as a focal dilated segment of the intraduodenal portion of the common bile duct. The proximal biliary tract is normal in appearance. The choledochoceles may be as small as 1–2 cm or, rarely, large enough to cause partial duodenal obstruction. It is analogous to the ureterocele. In type IVA choledochal cysts (Figs. 8–10), cholangiography shows gross cystic dilatation of the extrahepatic biliary tree (both common bile duct and common hepatic duct) with extension of the cystic process into the intrahepatic biliary tree. The intrahepatic disease may present as multiple focal segmental dilations, smooth fusiform ductal dilatation, or irregular nonuniform ductal dilatation. In type IVB choledochal cysts, cholangiography shows multiple cystic dilations of the common bile duct. This can have either a "string-of-beads" or a "bunch-of-grapes" (multiple diverticula) appearance. The intrahepatic biliary tree is normal. Type V choledochal cysts (Fig. 11), or Caroli disease, present as multiple saccular or cystic dilations of the intrahepatic biliary tree. The extrahe-

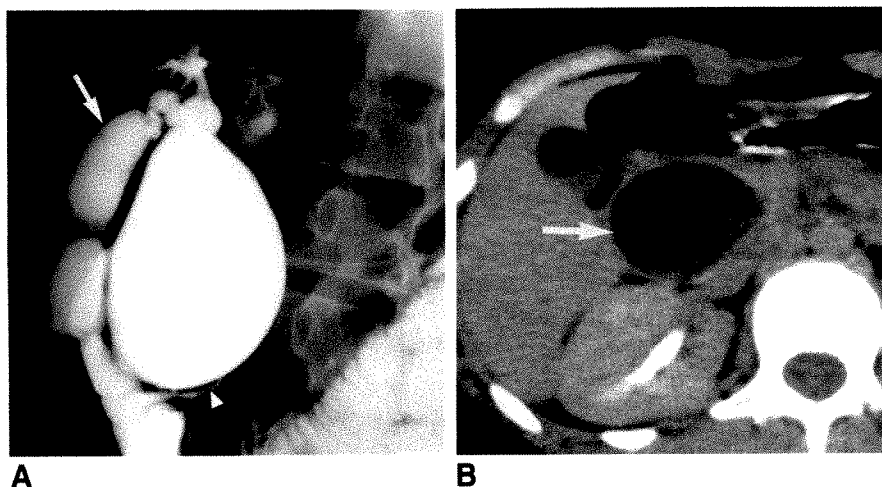
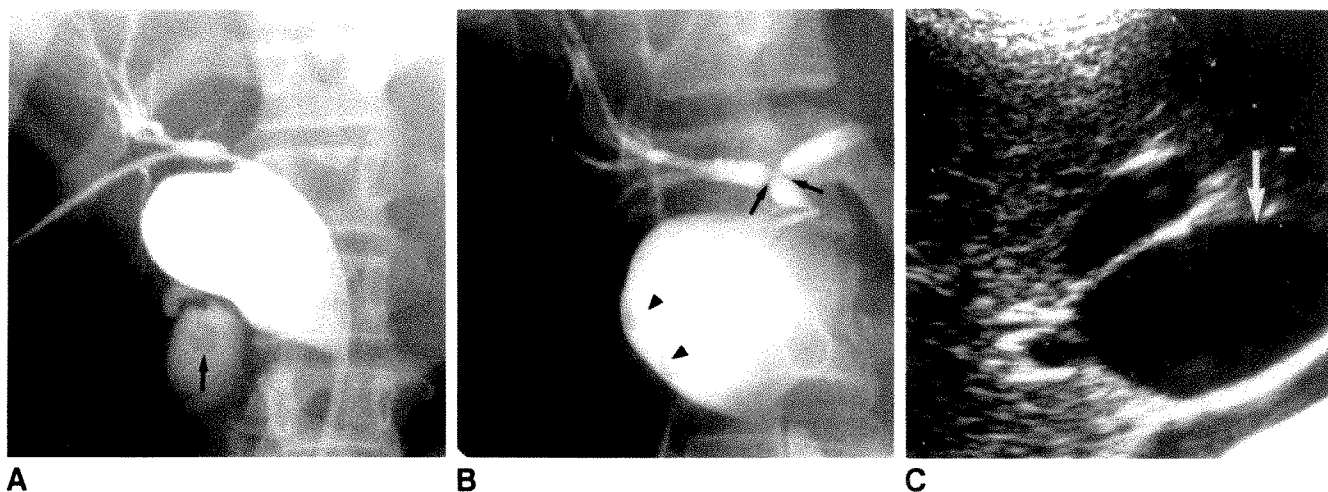


Fig. 3.—Choledochal cyst involving common bile duct (type IA).

A, Percutaneous transhepatic cholangiogram shows extrahepatic location of cyst. Gallbladder (arrow) and cystic ducts are proximal to cyst. Common duct (arrowhead) distal to cyst is small.

B, Enhanced CT scan shows low-density cyst (arrow) within pancreatic head.



**Fig. 4.**—Choledochal cyst involving common bile duct (type IA).  
**A,** Percutaneous transhepatic cholangiogram shows relationship of cyst to common bile duct (as marked by catheter). Note gallstone (*arrow*) in gallbladder.  
**B,** Another projection shows strictures (*arrows*) at confluence of common hepatic duct. Stones (*arrowheads*) are visible within cyst.  
**C,** Sonogram shows large cystic mass (*arrow*) between gallbladder (anterior) and inferior vena cava (posterior).

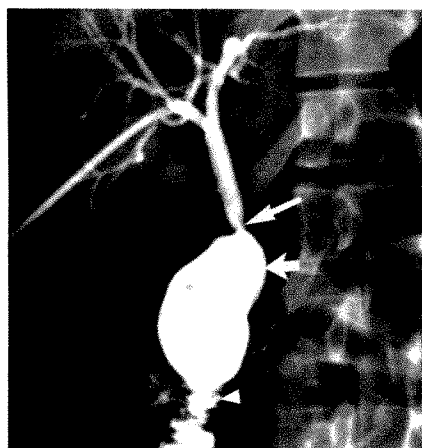


**Fig. 5.**—Focal choledochal cyst of distal common bile duct (type IB). The patient had symptoms of biliary obstruction after choledochocystojejunostomy. Percutaneous transhepatic cholangiogram shows focal dilatation of distal portion of common bile duct (*short arrow*) proximal to jejunal anastomosis (*arrowhead*). Note stricture of common bile duct (*long arrow*) at junction with cyst remnant.



**Fig. 6.**—Fusiform dilatation of common bile duct (type IC). Percutaneous transhepatic cholangiogram shows fusiform dilatation of common bile duct (*arrow*). Gallbladder (*arrowhead*) is opacified also.



**Fig. 7.**—T-tube cholangiogram shows focal dilatation of intrahepatic portion of common bile duct (choledochocoele, type III).

patic biliary tree usually is normal; however, repeated episodes of ascending cholangitis may result in stricture formation of the common bile duct or the intrahepatic ducts between areas of saccular dilatation.

#### Percutaneous Transhepatic Cholangiography vs ERCP

Both of these imaging techniques provide detailed analysis of the anatomy of the biliary tract and pancreaticobiliary junction [4–6]. The percutaneous transhepatic approach al-

lows detailed imaging of the intrahepatic ductal anatomy. This is important owing to the common occurrence of concomitant disease, such as ductal strictures and calculi. In addition, thorough evaluation of the cyst itself is possible, thus allowing cyst classification and surgical planning. The disadvantages of this technique are its invasive nature, the risk of liver injury, and its inability to clearly define the pancreaticobiliary junction. ERCP provides detailed evaluation of the anomalous arrangement of the pancreaticobiliary junction. The disadvantage of this technique is that it may not allow adequate evaluation of the cyst or intrahepatic biliary tree. In addition, retrograde



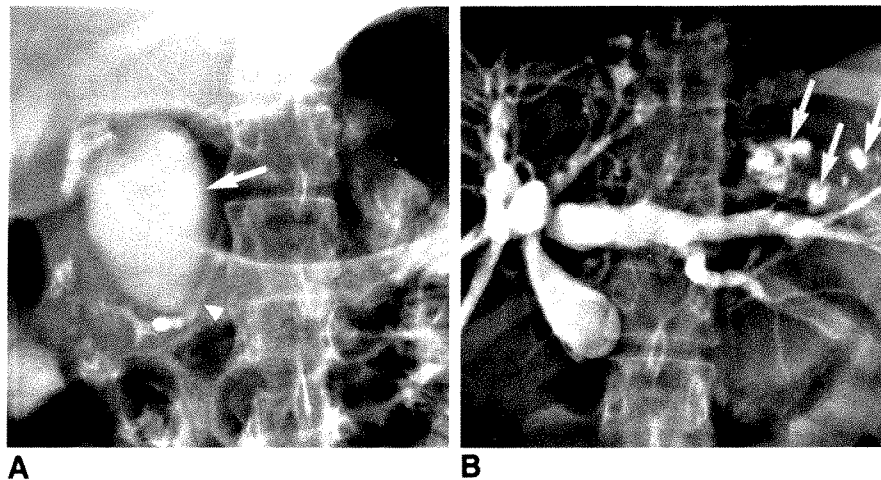


Fig. 8.—Choledochal cyst involving extra- and intrahepatic biliary tree (type IVA).

A, ERCP shows extrahepatic component of choledochal cyst (arrow). Note residual contrast material within pancreatic duct (arrowhead).

B, Percutaneous transhepatic cholangiogram shows cystic dilatation of intrahepatic bile ducts, particularly on left side. Multiple intrahepatic abscesses (arrows) arise from ducts.

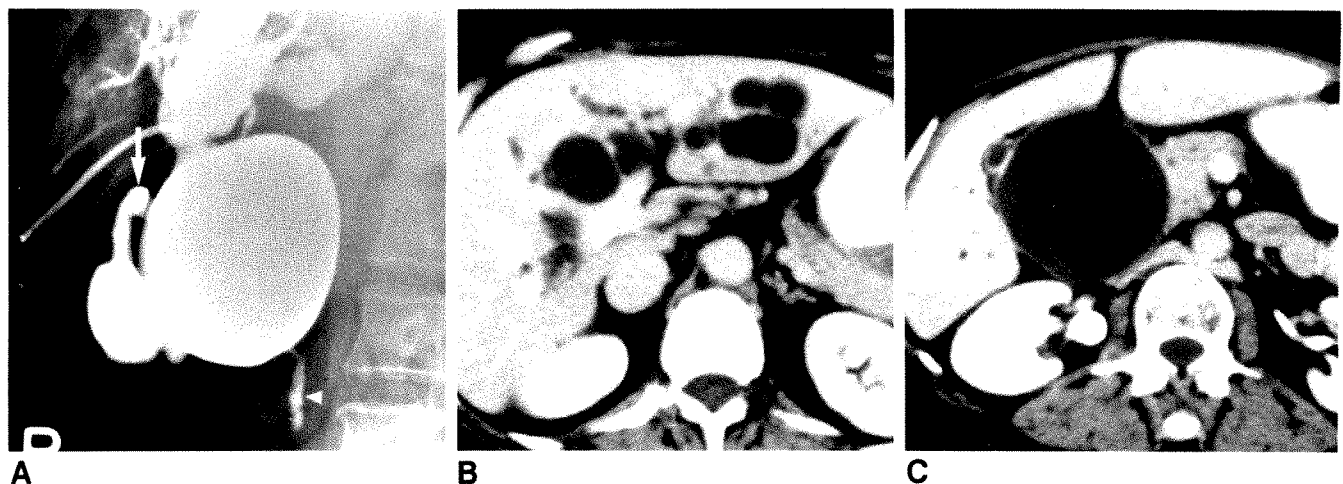


Fig. 9.—Choledochal cyst involving both extra- and intrahepatic ducts (type IVA).

A, Percutaneous transhepatic cholangiogram shows a large choledochal cyst with marked intrahepatic extension. Gallbladder (arrow) arises directly from cyst. Note small-caliber distal common bile duct (arrowhead).

B and C, Enhanced CT scans show intra- and extrahepatic extent of disease.

injections into a partially obstructed biliary system may result in ascending cholangitis.

## Discussion

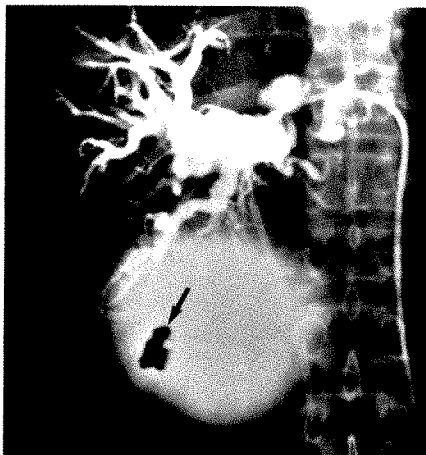
Choledochal cysts are an uncommon cause of obstructive jaundice. Many complications have been reported, including cholelithiasis, choledocholithiasis, cystolithiasis, pancreatitis, intrahepatic abscesses, biliary cirrhosis, portal hypertension, and hepatobiliary malignancy (4.2–28.0% total malignancy, 3.2% intracystic malignancy) [2, 4]. Associated hepatobiliary disease has occurred in six of 14 of our patients and included cholelithiasis (three cases), choledocholithiasis (two cases), common bile duct stricture (two cases), intrahepatic bile duct stricture (two cases), pancreatic duct stricture (one case),

intrahepatic abscesses (one case), ectopic pancreas (jejunum, one case), and cystolithiasis (one case).

In cases of suspected choledochal cyst, a wide variety of presurgical imaging techniques are available for evaluation of the patient. CT, MR imaging, sonography,  $^{99m}\text{Tc}$ -hepatobiliary scanning, ERCP, and percutaneous transhepatic cholangiography have all been reported to be useful [4]. Proper imaging is essential for classification and surgical planning. Because cyst types III and V do not have an anomalous pancreaticobiliary junction, some have believed they should not be included in the classification scheme. However, both are cystic malformations of the biliary tract, and their inclusion allows a succinct grouping of these anomalies in terms of presentation, treatment, and outcome.

In our experience, percutaneous transhepatic cholangiography allows the most thorough assessment of cyst anatomy,

Fig. 10.—Choledochal cyst involving both intra- and extrahepatic ducts (type IVA). Percutaneous transhepatic cholangiogram shows a large choledochal cyst with intraluminal filling defect (arrow) that proved to be a large blood clot. Note intrahepatic extent of disease.



10

Fig. 11.—Percutaneous transhepatic cholangiogram shows multiple intrahepatic cysts that communicate with biliary tree (Caroli disease, type V). Multiple strictures presumably are due to repeated episodes of cholangitis.



11

site of biliary origin, extent of both intra- and extrahepatic disease, and associated biliary tract anomalies and disease. Preoperative percutaneous biliary drainage can be performed in conjunction with percutaneous transhepatic cholangiography when necessary to relieve any component of biliary obstruction with subsequent improvement in liver function; symptoms such as jaundice, nausea, and vomiting; and the overall health of the patient. This serves both to decrease operative risk and shorten postoperative recovery time. Intraoperatively, percutaneously placed biliary stents provide the surgeon with easily palpated landmarks.

In conclusion, choledochal cysts are benign entities of the hepatobiliary tree that require surgical intervention because of their high potential risk for complications including malignant degeneration. Percutaneous transhepatic cholangiography is a valuable imaging technique that allows detailed anatomic definition. Percutaneous biliary drainage can be performed safely in these patients as a method of presurgical intervention and as an aid during surgical reconstruction.

#### ACKNOWLEDGMENTS

We thank Anthony C. Venbrux for the anatomic drawings.

#### REFERENCES

1. O'Neill JA, Templeton JM, Schnauffer L, Bishop HC, Ziegler MM, Ross AJ. Recent experience with choledochal cyst. *Ann Surg* 1987;205:533-540
2. Tan KC, Howard ER. Choledochal cyst: a fourteen-year surgical experience with 36 patients. *Br J Surg* 1988;75:892-895
3. Babbitt DP. Congenital choledochal cyst: new etiological concept based on anomalous relationships of common bile duct and pancreatic bulb. *Ann Radiol (Paris)* 1969;12:231-240
4. Crittenden SL, McKinley MJ. Choledochal cyst—clinical features and classification. *Am J Gastroenterol* 1985;80:643-647
5. Alonzo-Lej F, Revor WB, Pessagno DJ. Congenital choledochal cyst, with a report of 2, and an analysis of 94 cases. *Surg Gynecol Obstet Int Abstr Surg* 1959;108:1-30
6. Wiedmeyer DA, Stewart ET, Dodds WJ, Geenen JE, Vennes JA, Taylor AJ. Choledochal cyst: findings on cholangiopancreatography with emphasis on ectasia of the common channel. *AJR* 1989;153:969-972

## Book Review

**Disorders of the Patellofemoral Joint, 2nd Ed.** By John P. Fulkerson and David S. Hungerford. Baltimore: Williams & Wilkins, 294 pp., 1990. \$65

This monograph is a revision of a book first published by the late Dr. Paul Ficat and his colleague, Dr. Hungerford, in 1977. At that time, it was unusual to find a book dedicated to one portion of one joint. Orthopedic surgery had just begun the process of specialization that we find so common today. Advances in arthroscopy resulted in the patellar cartilage being the most thoroughly studied of any joint.

The knee joint is the most frequently traumatized major joint of the body. The function of the patella is to facilitate extension of the knee, primarily through elevating the extensor apparatus from the axis of flexion and extension and by increasing its length. Consequently, the patella is subject to a wide variety of disorders that range from direct trauma to the patellar cartilage itself to osteonecrosis, cracking disorders, and a variety of conditions that have been referred to generically as "chondromalacia." The purpose of the book, therefore, has been to collect in one easily readable source data from relevant anatomic, pathologic, and mechanical studies.

The book is organized into 11 chapters. The first chapter covers normal anatomy and discusses, in addition to gross anatomy, the embryology and the importance of the synovial musculotendinous appendages. The second chapter is the most important for understanding the pathophysiology of patellar disorders. It covers the biomechanics of the patellofemoral joint. The third chapter, which is of most interest to radiologists, deals with imaging of the patellofemoral joint. This chapter reviews standard radiography, tangential or axial views, tomography, CT, arthrography, MR imaging, and radionuclide imaging. Furthermore, the chapter gives a graphic description of the various angled techniques used for evaluating the patellofemoral joint. A special section on patellofemoral evaluation in children is included because of the radiologic changes that occur in the growing child. Radiologists who have a significant orthopedic practice will find

this chapter most interesting. This chapter concludes with a practical algorithm for imaging the patellofemoral joint.

The remainder of the book is divided into eight chapters that would be of more interest to orthopedic surgeons. The topics include dysplasias, evaluation and rehabilitation of nonarthritic anterior knee pain, patellar tilt/compression and the excessive lateral pressure syndrome, patellar subluxation, patellar dislocation, articular cartilage lesions, surgical treatment, and reflex sympathetic dystrophy.

The book is well illustrated with line drawings, radiographs, color illustrations, CT images, and a few MR images. The quality of the illustrations by and large is quite good. I did find that some of the radiographs are too "contrasty," however. The book is also well referenced, with citations as current as 1989. The main shortcoming of this book from a radiologic standpoint is the relative paucity of MR images. Although the authors cite several sources from the radiologic literature on the value of MR in evaluating patellar cartilage lesions, the only applicable illustration included is one of a patient with a hemangioma of the quadriceps muscle. The book also has fewer CT scans than I would have liked, particularly in view of the advances that have occurred in CT and near universal availability of this type of study.

Despite its deficiencies, I recommend this book to any radiologist who has a practice that includes large numbers of orthopedic patients. It will be particularly useful for those who deal with patients from sports medicine clinics. The book also might be useful in reference libraries of departments much in the same way as those books containing various roentgen measurements are used.

Richard H. Daffner  
Allegheny General Hospital  
Pittsburgh, PA 15212



## MR of the Knee: The Significance of High Signal in the Meniscus That Does Not Clearly Extend to the Surface

Phoebe A. Kaplan<sup>1</sup>  
 Nick L. Nelson<sup>1</sup>  
 Kevin L. Garvin<sup>2</sup>  
 David E. Brown<sup>2</sup>

On MR images of the knee it is sometimes impossible to determine with confidence if a focus of high signal in the meniscus is confined to the substance of the meniscus or if it extends to involve the surface. This is a critical differentiation because the latter represents meniscal tears that can be found and treated at arthroscopy, whereas the former represents degeneration, tears, or perhaps normal variants that cannot be detected or treated arthroscopically. We make an equivocal diagnosis of a tear when it is difficult to decide if signal in a meniscus involves the meniscal surface. We studied MR scans of the knee in 142 consecutive patients for the presence of such equivocal tears. Their prevalence was 14% (20/142); 17 were in the posterior horn of the lateral meniscus and three were in the posterior horn of the medial meniscus. In 13 cases with arthroscopy/arthrotomy correlation, no tears were found. In one of the 20 patients in whom the meniscus was removed during arthroplasty, histologic examination of the meniscus showed separation of collagen bundles, which was caused by meniscal degeneration confined to the substance of the meniscus.

These results suggest that a meniscal tear is unlikely when MR scans show a focus of high signal in a meniscus that does not unequivocally extend to involve the surface of the meniscus.

*AJR* 156:333-336, February 1991

The hallmark of a meniscal tear on MR imaging of the knee is increased signal intensity within the meniscus [1-14]. MR criteria have been established to differentiate surgically significant from insignificant meniscal abnormalities [1]. This entails a grading system with grades I and II signal (focal and linear regions of high signal, respectively) limited to the substance of the meniscus without communication with the meniscal surface (Fig. 1). Grade III signal is increased signal in the meniscus that communicates with the surface. Grades I and II types of signal are rarely associated with arthroscopically detectable tears. In grade III lesions, tears are found at arthroscopy in over 90% of cases [1-14].

It has been our experience that not all meniscal signal fits clearly into one of these categories. Some signals are neither clearly confined to the substance of the meniscus nor definitely extending through the meniscal surface (Figs. 2 and 3). The significance of these borderline findings, which we consider equivocal indications of meniscal tears, is uncertain. This dilemma led us to investigate the prevalence of equivocal meniscal tears on MR images and to correlate the MR and surgical findings in these patients.

### Materials and Methods

MR examinations of the knee in 142 consecutive patients were evaluated prospectively by two experienced radiologists for the presence and site of equivocal evidence of tears. The study population consisted of 80 men and 62 women 7-77 years old (average age, 28 years). All patients were referred by orthopedic surgeons for suspected internal derangements of the

Received June 1, 1990; accepted after revision August 13, 1990.

<sup>1</sup> Department of Radiology, University of Nebraska Medical Center, 42nd St. & Dewey Ave., Omaha, NE 68105. Address reprint requests to P. A. Kaplan.

<sup>2</sup> Department of Orthopedic Surgery, University of Nebraska Medical Center, Omaha, NE 68105.

0361-803X/91/1562-0333

© American Roentgen Ray Society

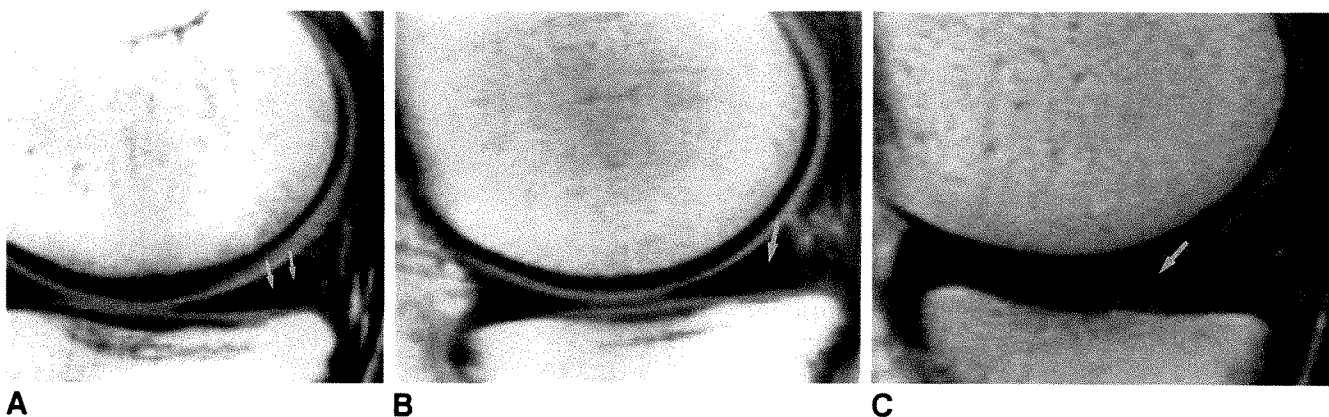


Fig. 1.—A and B, T1-weighted MR images (600/25) show focal (A) and linear (B) signal (arrows) confined to substance of meniscus. Diagnosis of meniscal tear is equivocal.

C, MR image shows linear area of high signal (arrow) clearly involving superior surface of the meniscus. This finding is diagnostic of a meniscal tear.



Fig. 2.—Proton-density MR image (2000/20) shows equivocal horizontal tear of posterior horn of lateral meniscus. One area of signal in meniscus does not positively involve inferior surface (arrow). Vague intermediate signal inferior to high signal makes it difficult to determine if a complete tear or a small amount of intact meniscus is present. Intrastance degeneration was found histologically after arthroplasty was performed for advanced degenerative joint disease. Subchondral sclerosis involves adjacent femoral and tibial condyles.

knee. When signal was identified within the meniscus, it was considered equivocal evidence of a tear if both radiologists were uncertain if the signal extended to involve the meniscal surface. In the rare instance in which the radiologists disagreed, it was not considered an equivocal tear. Equivocal tears were diagnosed if we could not determine if there was a small portion of normal intact meniscal tissue between the linear high signal in the meniscus and the articular surface abutting the meniscus. The results of arthroscopy were available in 92 of the 142 patients and were correlated with the MR findings. Arthroscopy was done if warranted by the patient's symptoms or because of other MR findings.

The MR pulse sequences we used changed with experience: either proton-density, 2000/20 (TR/TE), and T2-weighted, 2000/80, or T1-weighted, 600/25, and fast gradient-echo (multiplanar gradient recall [MPGR]), 600/25, with a 20° flip angle were used. Either 3- or 4-mm slice thicknesses were obtained in the sagittal and coronal planes. A

16-cm field of view was used. Scans were obtained with a 1.5-T Signa scanner (General Electric, Milwaukee, WI).

The meniscus of one patient with an equivocal tear was studied histologically after removal during a total knee arthroplasty.

## Results

Evidence of meniscal tears on MR images was equivocal in 20 (14%) of the 142 knees. The signal was horizontal in the midportion of the menisci and extended near the inferior meniscal surface in all cases. Only two locations were involved: the posterior horn of the lateral meniscus (17 cases) and the posterior horn of the medial meniscus (three cases). Twelve of the 20 patients had arthroscopy, and one had total-knee arthroplasty. In 12 of the 13 patients who had arthroscopy or surgery, MR showed equivocal evidence of tears in the posterior horn of the lateral meniscus; in one of the 13, MR showed equivocal evidence of a tear in the posterior horn of the medial meniscus. No tears found at arthroscopy were considered equivocal on MR.

Histologic examination of a meniscus removed during knee arthroplasty showed degeneration with separation of collagen bundles, but no tear.

Equivocal tears detected on MR images were always seen best on sagittal views. Images in the coronal plane added no additional information. All equivocal tears were detected on T1-weighted, proton-density, and gradient-echo sequences, but not on T2-weighted images. An equivocal tear on a T1-weighted image also was equivocal on the gradient-echo fast scans.

## Discussion

MR of the knee is an excellent examination for detection of meniscal tears, with a reported sensitivity and specificity of over 90% [1–14]. A meniscal tear on MR that can be detected by arthroscopy (and is therefore amenable to surgical therapy)

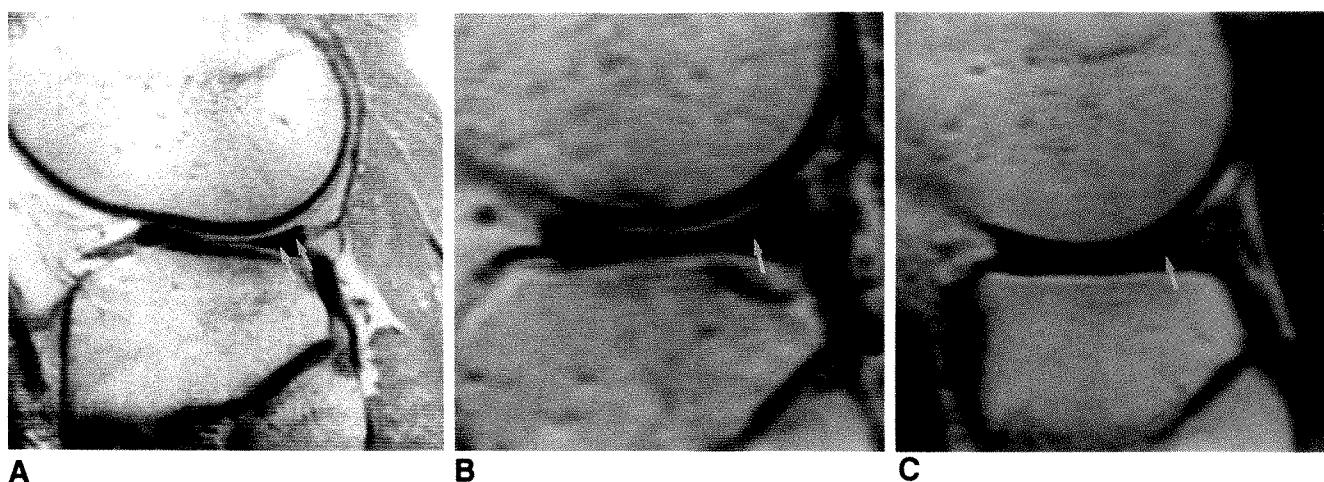


Fig. 3.—A-C, Three examples of T1-weighted (600/25) MR images showing equivocal tears of posterior horn of lateral meniscus (arrows). Linear areas of signal in meniscus do not definitely extend through inferior surface. No tears were found at arthroscopy.

is depicted as a focus of increased signal intensity that extends through the articular surface of the meniscus; this has been termed grade III signal [1]. Grades I and II signals are focal or linear areas of high signal that are confined to the substance of the meniscus with intact outer contour lines; these are not visible on arthroscopy (Fig. 1). However, it is not always possible to neatly categorize meniscal signal and determine if it is confined to the substance of the meniscus or extends through the surface. Published reports confirm a 10–40% rate of meniscal abnormalities on MR that were diagnosed as tears but were not confirmed at arthroscopy [4, 6, 7, 15]. Discrepancies between MR and arthroscopy have been explained partially by recognition that normal anatomic structures can simulate meniscal tears on MR images [15, 16]. Even with a full understanding of this pitfall, sometimes it is still impossible to determine if there is meniscal tissue between the intrameniscal high signal and the surface of the meniscus (Figs. 2 and 3). Another reason for the disparity between MR and arthroscopic findings is that tears may be missed at arthroscopy. The undersurfaces of menisci are difficult to examine arthroscopically, and the skill of the arthroscopist is a critical factor in the accuracy of the procedure.

It is well known that intrameniscal signal involving the surface of a meniscus represents a meniscal tear. The significance of high signal confined to the substance of the meniscus is less certain. It may represent microcyst formation and separation of collagen bundles [17, 18]. Others have reported it as a normal variation [19].

The equivocal tears were encountered with equal frequency on T1-weighted, proton-density, and gradient-echo fast scan (MPGR) images. We did not identify high signal in an equivocal tear on T2-weighted sequences, but this was of no significance because even complete meniscal tears seen on T1-weighted images may or may not be seen on T2-weighted images.

Signal that was neither clearly confined to the substance

of the meniscus nor definitely involved with the meniscal surface (equivocal meniscal tears) was encountered in 14% (20/142) of the MR examinations included in our study. Arthroscopy or open surgery in 13 of these patients did not show a tear. The MR findings in the majority of cases (17 of 20) were in the posterior horn of the lateral meniscus, whereas only three of 20 were in the posterior horn of the medial meniscus. It was not difficult to distinguish the high signal of the equivocal tears in the lateral meniscus from high signal associated with the popliteus tendon sheath. This sheath runs in a different, more vertical direction, and is a pitfall in MR interpretation that has been well described [17]. The direction of linear high signal is also incompatible with the more vertical appearance of the interface between the meniscofemoral ligaments (Humphry and Wrisberg) and the lateral meniscus. There is no normal anatomic structure to account for the position and appearance of equivocal tears. This possibility was considered initially because it occurred much more often in the lateral meniscus posteriorly. The orientation of the high signal is typical of horizontal cleavage tears. This fact also makes an anatomic variant less plausible as an explanation for the finding. One patient with an equivocal tear in the posterior horn of the lateral meniscus on MR had arthroplasty. Histologic analysis of the meniscus showed collagen degeneration with separation of collagen bundles without extension to either surface.

#### REFERENCES

1. Crues JV, Mink J, Levy TL, et al. Meniscal tears of the knee: accuracy of MR imaging. *Radiology* 1987;164:445–448
2. Mandelbaum BR, Finerman GAM, Reicher MA, et al. Magnetic resonance imaging as a tool for evaluation of traumatic knee injuries. *Am J Sports Med* 1986;14:361–370
3. Tyrrell RL, Gluckert K, Pathria M, Modic MT. Fast three-dimensional MR imaging of the knee: comparison with arthroscopy. *Radiology*



- 1988;166:865-872
4. Gallimore GW, Harms SE. Knee injuries: high resolution MR imaging. *Radiology* 1986;160:457-461
  5. Reicher MA, Hartzman S, Duckwiler GR, et al. Meniscal injuries: detection using MR imaging. *Radiology* 1986;159:753-757
  6. Burk DL Jr, Kanal E, Brunberg JA, Johnstone GF, Swensen HE, Wolf GL. 1.5-T Surface-coil MRI of the knee. *AJR* 1986;147:293-300
  7. Reicher MA, Hartzman S, Bassett LW, et al. MR imaging of the knee. Part I. Traumatic disorders. *Radiology* 1987;162:547-551
  8. Manco LG, Lozman J, Coleman ND, Kavanaugh JH, Bilfield BS, Dougherty J. Noninvasive evaluation of knee meniscal tears: preliminary comparison of MR imaging and CT. *Radiology* 1987;163:727-730
  9. Spritzer CE, Vogler JB, Martinez S, et al. MR imaging of the knee: preliminary results with a 3DFT GRASS pulse sequence. *AJR* 1988;150:597-603
  10. Hagger AM, Froelich JW, Hearshen DO, Sadasivan K. Meniscal abnormalities of the knee: 3DFT fast-scan GRASS MR imaging. *AJR* 1988;150:1341-1344
  11. Harms SE, Muschler G. Three-dimensional MR imaging of the knee using surface coils. *J Comput Assist Tomogr* 1986;10:773-777
  12. Mink JH, Levy T, Crues JV. Tears of the anterior cruciate ligament and menisci of the knee: MR imaging evaluation. *Radiology* 1988;167:769-774
  13. Polly DW, Callaghan JJ, Sikes RA, et al. The accuracy of selective magnetic resonance imaging compared with the findings of arthroscopy of the knee. *J Bone Joint Surg [Am]* 1988;70-A:192-198
  14. Glashow JL, Katz R, Schneider M, Scott WN. Double-blind assessment of the value of magnetic resonance imaging in the diagnosis of anterior cruciate and meniscal lesions. *J Bone Joint Surg [Am]* 1989;71-A:113-119
  15. Herman LJ, Beltran J. Pitfalls in MR imaging of the knee. *Radiology* 1988;167:775-781
  16. Watanabe AT, Carter BC, Teitelbaum GP, Seeger LL, Bradley WG Jr. Normal variations in MR imaging of the knee: appearance and frequency. *AJR* 1989;153:341-344
  17. Hajek PC, Gyls-Morin VM, Baker LL, et al. The high signal intensity meniscus of the knee: magnetic resonance evaluation and in vivo correlation. *Invest Radiol* 1987;22:883-890
  18. Stoller DW, Martin C, Crues JV III, Kaplan L, Mink JH. Meniscal tears: pathologic correlation with MR imaging. *Radiology* 1987;163:731-735
  19. Quinn SE. Meniscal tears: pathological correlation with MR imaging (letter). *Radiology* 1988;166:580-581

## Pictorial Essay

# MR Imaging of Synovial Sarcoma

Marilyn J. Morton,<sup>1</sup> Thomas H. Berquist,<sup>1</sup> Richard A. McLeod,<sup>1</sup> K. Krishnan Unni,<sup>2</sup> and Franklin H. Sim<sup>3</sup>

**The MR imaging findings in 12 cases of synovial sarcoma are illustrated. The MR appearance most indicative of the tumor is an inhomogeneous septated mass with infiltrative margins located close to a joint, a tendon, or bursae, especially if soft-tissue calcification can be seen on CT scans or plain radiographs.**

Synovial sarcoma constitutes approximately 10% of all soft-tissue sarcomas [1]. Although synovial sarcoma frequently occurs close to joints, tendons, and bursae, it rarely arises from the intraarticular synovial lining of these structures. Rather, it is considered to arise *de novo* from primitive mesenchymal cells that differentiate sufficiently to resemble synovial membrane. Synovial sarcoma may occur at any age but is most commonly seen between the ages of 20 and 40 years. Prognosis is generally poor (5-year survival rate, 55%) [2].

MR imaging is the most valuable imaging technique for the preoperative anatomic staging of soft-tissue tumors of the musculoskeletal system. MR imaging is less useful in predicting tumor histology and in differentiating benign from malignant soft-tissue masses [3]. Nevertheless, on the basis of combined clinical data and MR imaging features, the nature of a musculoskeletal mass often can be determined. We retrospectively reviewed the MR imaging features in 12 cases of synovial sarcoma and noted several MR imaging features that may contribute to a presumptive diagnosis of these soft-tissue sarcomas.

## Materials and Methods

Between January 1983 and August 1989, 12 patients with histologically documented synovial sarcoma underwent preoperative assessment by MR imaging at our institution. The clinical records, MR imaging studies, and pathologic specimens in these 12 patients were reviewed retrospectively. All images were obtained before any treatment. The group included 10 males and two females ranging in age from 11 to 73 years (mean age, 34 years). MR imaging studies were performed with a 1.5-T Signa magnet (General Electric, Milwaukee, WI) and a 0.15-T Picker magnet (Picker International, Highland Heights, OH). Images were obtained by using both T1-weighted, 400–800/20 (TR/TE), and T2-weighted, 2000/20–30, 60–80, spin-echo (SE) sequences.

The 12 synovial sarcomas included 11 untreated lesions and one local tumor recurrence. Three of the tumors were in an upper extremity (two wrists, one elbow) and nine were in a lower extremity or pelvic girdle (four thighs, two buttocks, two ankles, one knee). Eight synovial sarcomas were located within 5 cm of or adjacent to joints, tendons, or bursae, and one was intraarticular, arising from the anterior joint capsule of the ankle. The remaining three tumors were located in the thigh at a site removed from the adjacent joint. The mean diameter of the tumors was 9.2 cm (range, 2.5–15.0 cm).

## MR Imaging Appearance

On MR images, nine of the 12 synovial sarcomas had a heterogeneous, multilocular configuration with various degrees of internal septation (Figs. 1 and 2). Three of these multilocular lesions had a striking configuration of extensive loculations with multiple fluid-fluid levels (Figs. 3 and 4). In

Received June 4, 1990; accepted after revision August 27, 1990.

<sup>1</sup> Department of Diagnostic Radiology, Mayo Clinic and Mayo Foundation, Rochester, MN 55905. Address reprint requests to M. J. Morton.

<sup>2</sup> Division of Surgical Pathology, Mayo Clinic and Mayo Foundation, Rochester, MN 55905.

<sup>3</sup> Department of Orthopedics, Mayo Clinic and Mayo Foundation, Rochester, MN 55905.

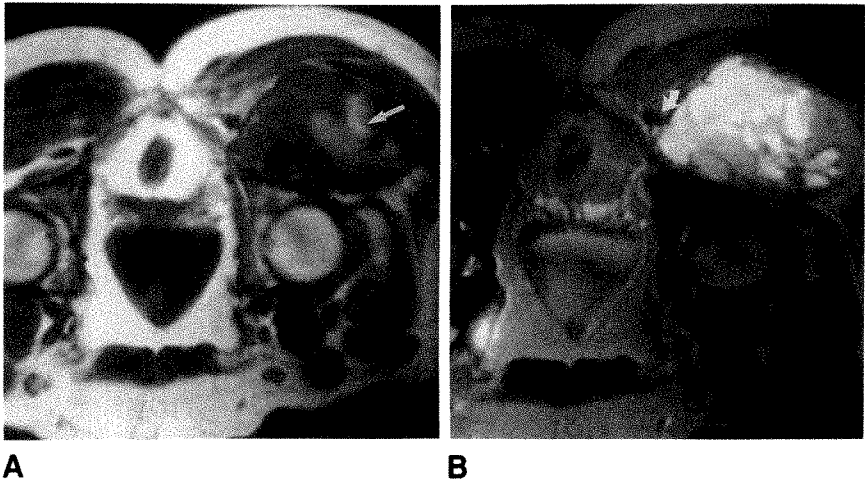


**Fig. 1.**—Multilocular synovial sarcoma of right posterior gluteal region.  
A, Axial MR image, SE 600/20, of prone patient shows large inhomogeneous tumor mass in right buttock posterior to hip joint. Central areas of bright signal intensity (arrow) (short T1) indicate subacute hemorrhage. Biopsy had not been performed before MR study.  
B, On T2-weighted MR image, SE 2000/60, inhomogeneous, septated configuration is more apparent. Tumor margin abuts gluteal neurovascular bundle (arrow). At surgery, vascular encasement was found.

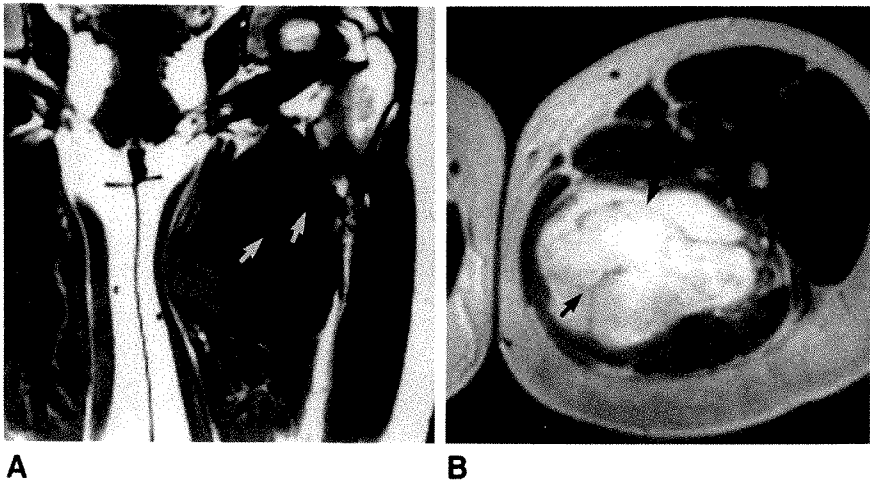


**Fig. 2.**—Multilocular synovial sarcoma of proximal left thigh.  
A, Coronal MR image, SE 650/20, shows lobulated, septated mass (arrows) in medial left thigh about 5 cm below hip joint.  
B, On transaxial MR image, SE 2000/60, tumor is detected within great adductor muscle. Lesion inhomogeneity and internal septa (arrows) are more conspicuous on T2-weighted image.

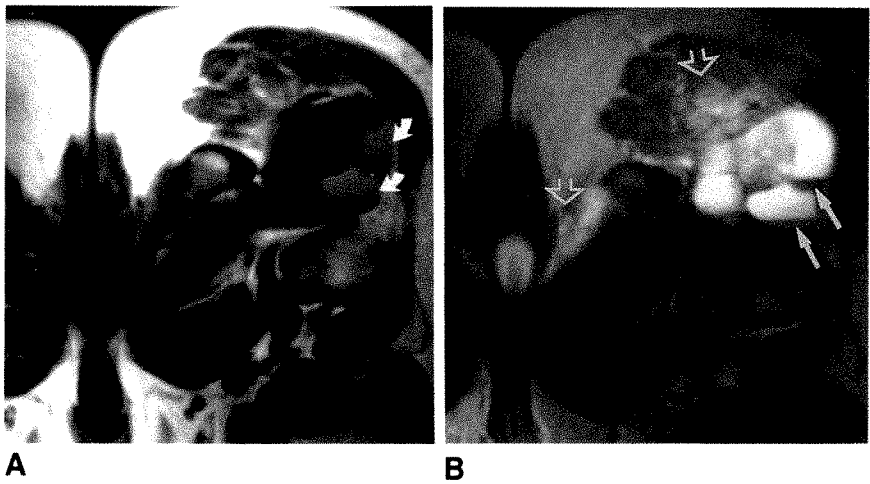


**Fig. 3.**—Multilocular synovial sarcoma with fluid-fluid levels.  
A and B, Axial SE 600/20 (A) and SE 2000/60 (B) MR images of prone patient (same patient as in Fig. 1 but at a more inferior scan level) show fluid-fluid levels adjacent to irregular tumor mass in right buttock. Signal intensities of fluid levels, notably short T1 of supernatant (curved arrows) and short T2 of sediment (straight solid arrows) are characteristic of diffusional and paramagnetic effects of degraded hemoglobin. Signal intensity of fluid levels indicated that hemorrhage had occurred within areas of necrosis or cyst formation. Infiltrative tumor margins and tumor extension along posterior ischium (open arrows) are evident on T2-weighted image.

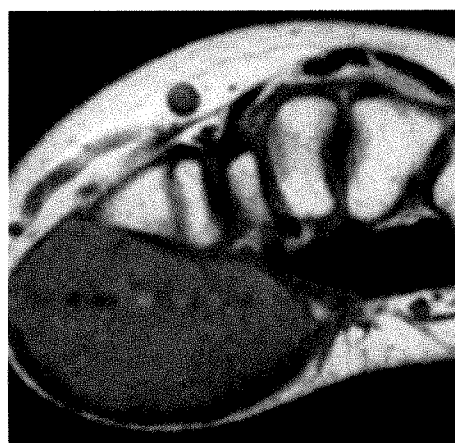
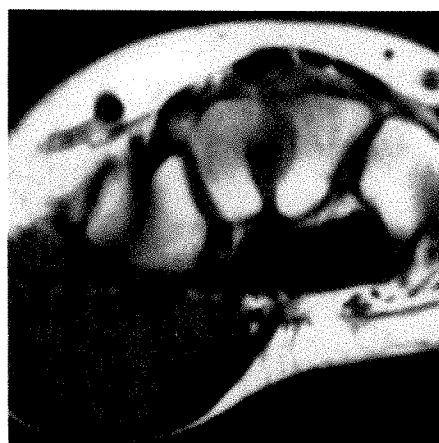
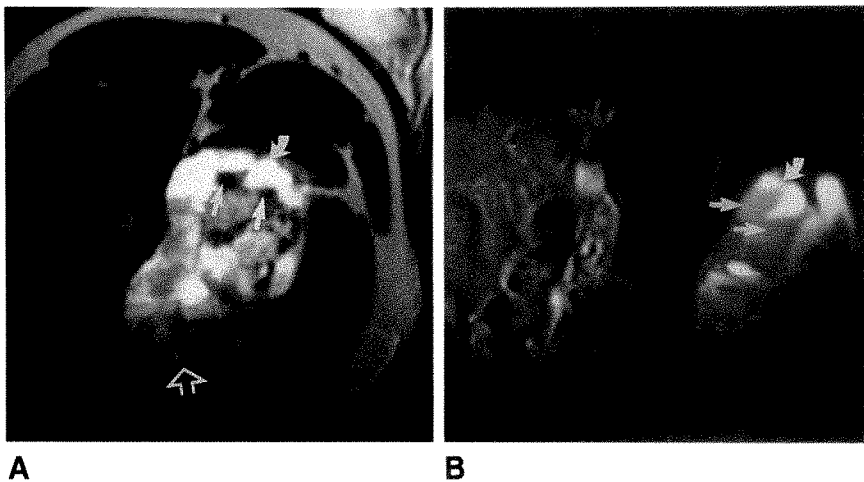
eight of the 12 synovial sarcomas, components of the tumor margins were poorly defined and infiltrative, which are MR imaging features more characteristic of malignant soft-tissue tumors. Eleven of the 12 lesions (including all nine multilocular

lesions) displayed a signal intensity similar to that of skeletal muscle on T1-weighted images and equal to or slightly greater than that of subcutaneous fat on T2-weighted images. In the one exception, the MR signal intensity was similar to that of



Fig. 4.—Synovial sarcomas in two patients have extensive loculations with multiple fluid-fluid levels.

A and B, Axial MR images, SE 2000/60, of proximal right thigh (A) and left gluteal region (B). Supernatant (curved arrows) and sediment (straight solid arrows) have signal intensities identical to those of lesion in Fig. 3. Lesion in A shows infiltrative tumor margins posteriorly (open arrow) obliterating neurovascular bundle. Sciatic nerve involvement was confirmed at surgery.



A

B

Fig. 5.—Small (5 cm) synovial sarcoma in thenar region of hand.

A and B, T1-weighted, SE 600/20 (A), and T2-weighted, SE 2000/60 (B), MR images both show homogeneous low signal intensity. Tumor margins are sharp, and lesion is circumscribed peripherally by low-signal-intensity rim. These combined morphologic features of lesion homogeneity and sharp margins are more characteristic of benign soft-tissue neoplasms. Absence of necrosis and hemorrhage in this small synovial sarcoma is most likely explanation for lesion homogeneity and absence of loculations.



Fig. 6.—Axial MR image, SE 2000/60, shows synovial sarcoma adjacent to ankle. Large lobulated mass with multiple septa has inhomogeneous signal intensity slightly greater than that of fat. Small focus of hyperintense signal (arrow) is most likely due to cyst formation or necrosis.

skeletal muscle on both T1- and T2-weighted images. This mass also had a uniform homogeneous signal intensity and well-defined margins (Fig. 5).

Neurovascular involvement was suspected in five cases in which the tumor margin abutted and displaced the neurovascular bundle. Neurovascular encasement was confirmed at operation in two of these cases. The MR studies in our series failed to show small punctate areas of soft-tissue calcification that were discernible on radiographs in three patients.

## Discussion

Synovial sarcoma is a rare, malignant mesenchymal neoplasm that occurs chiefly in the extremities of young adults. It occurs primarily in the paraarticular regions, usually close to tendon sheaths, bursae, and joint capsules. However,

origin from anatomic synovial lining is uncommon. The predominant feature on the MR images in these 12 cases of synovial sarcoma was the configuration of a heterogeneous, multilocular mass with internal septa (nine cases). Three tumors had a distinct feature of extensive loculations with multiple fluid-fluid levels. The signal intensities of these fluid levels were considered to be characteristic of sedimented blood products, indicating the presence of hemorrhage within areas of cyst formation or necrosis.

The MR studies showed that nine of the synovial sarcomas were inhomogeneous lesions, and eight of these had infiltrative tumor margins. In our experience, these combined morphologic features have been useful predictors of the malignant nature of soft-tissue neoplasms (Berquist TH et al., unpublished data). Only one tumor showed a homogeneous signal intensity and sharp margination, features more commonly seen in benign neoplasms. This same tumor was unique in

that it was the only synovial sarcoma to have low signal intensity on T2-weighted images. Pathologic examination of this lesion revealed the usual histologic components of synovial sarcoma, and a histologic basis for the decreased signal on the T2-weighted images could not be found—that is, hypocellularity and abundant fibrous elements were not evident.

A septated configuration has also been reported to be a characteristic MR feature in two types of benign soft-tissue masses: hemangiomas and synovial and ganglionic cysts [4, 5]. Typically, these soft-tissue masses are sharply marginated and have a homogeneous hyperintense signal that is much brighter than that of the subcutaneous fat on T2-weighted images [4, 5]. Homogeneous high signal intensity on T2-weighted images was not a feature in any of the synovial sarcomas in our series (Fig. 6).

An important feature of synovial sarcoma is the presence of focal calcification, which can be demonstrated on radiographs in up to 30% of patients [1]. Three synovial sarcomas in this series showed small punctate areas of calcification on CT scans or radiographs. These calcifications were not detectable by MR imaging. Because MR imaging is insensitive

to the presence of soft-tissue calcification, we believe that all MR images of bone and soft-tissue tumors should be interpreted with corresponding radiographs or CT scans.

Although these MR findings cannot be considered specific for synovial sarcoma, an awareness of the typical morphologic appearance may aid in the preoperative recognition of these lesions. The finding of an inhomogeneous, septated mass with infiltrative margins located close to a joint, a tendon, or bursae should suggest the presence of synovial sarcoma, especially if soft-tissue calcification can be identified on CT scans or plain radiographs.

#### REFERENCES

1. Cadman NL, Soule EH, Kelly PJ. Synovial sarcoma: an analysis of 134 tumors. *Cancer* **1965**;18:613-627
2. Wright PH, Sim FH, Soule EH, Taylor WF. Synovial sarcoma. *J Bone Joint Surg [Am]* **1982**;64-A:112-122
3. Kransdorf MJ, Jelinek JS, Moser RP Jr. Soft-tissue masses: diagnosis using MR imaging. *AJR* **1989**;153:541-546
4. Burk DL Jr, Dalinka MK, Kanal E, et al. Meniscal and ganglion cysts of the knee: MR evaluation. *AJR* **1988**;150:331-336
5. Kaplan PA, Williams SM. Mucocutaneous and peripheral soft-tissue hemangiomas: MR imaging. *Radiology* **1987**;163:163-166

## Case Report

# Fournier Gangrene Caused by a Perforated Retroperitoneal Appendix: CT Demonstration

Michele Gaeta,<sup>1</sup> Santi Volta,<sup>1</sup> Anselmo Minutoli,<sup>1</sup> Giovanni Bartiromo,<sup>1</sup> and Ignazio Pandolfo<sup>2</sup>

First described in 1883 by Fournier [1], gangrene of the male genitalia is recognized as a form of necrotizing fasciitis [2]. Although originally considered idiopathic, an underlying cause of the disease can be identified in the majority of patients [2]. Despite aggressive surgical and medical management, Fournier gangrene has a high mortality rate; however, the results of treatment can be improved by early recognition of the disease and its underlying cause.

We describe the imaging findings in a case of Fournier gangrene caused by perforated retroperitoneal appendicitis. To our knowledge, this is the first description of Fournier gangrene caused by appendicitis.

### Case Report

A 27-year-old man was admitted with a 2-day history of intermittent fever, vague pain in the right lumbar region, and a painful swelling of the scrotum. Clinical examination revealed massive swelling and erythema of the right side of the scrotum without skin necrosis. Abdominal tenderness in the right lower quadrant also was present. Temperature was 38.2°C and WBC count was  $6.0 \times 10^9/l$ . Other laboratory data was unremarkable. A presumptive diagnosis of right epididymitis was made. Sonography showed a normal right testis and gas in the subcutaneous tissue of the scrotum. Plain radiographs obtained after sonography confirmed the presence of scrotal gas extending into the pelvis (Fig. 1A). CT was performed in order to define better the extension of the disease (Fig. 1B-D). An extensive gas-forming infection of the retroperitoneal space in the right iliac

fossa and pelvis was seen. A 1-cm calcified appendicolith also was visible in the retrocecal retroperitoneum.

A diagnosis of Fournier gangrene caused by perforating appendicitis was made. During surgery, extensive necrotizing fasciitis of the wall of the scrotum was identified. The testes and their tunica vaginalis were free of gangrene. A diagnosis of perforated gangrenous retroperitoneal appendicitis with extensive retroperitoneal gangrene was confirmed. Debridement was performed, and several drains were placed. Antibiotic and hyperbaric oxygen therapy were started after surgery. The patient made a full recovery and was discharged 50 days after admission.

### Discussion

In 1883 Fournier [1] reported five cases of a syndrome characterized by abrupt onset in a healthy young male of rapid progressive gangrene of the scrotum and penis with no obvious cause. Fournier gangrene is a rare but life-threatening mixed anaerobic and aerobic infection [2]. The most common causes of the disease are periurethral and perianal infections [2]. Less commonly, gangrene can occur after scrotal skin disruption by trauma or local surgical procedures. Diabetes, immunodeficiency from chemotherapy, and advanced liver or kidney disease are predisposing factors.

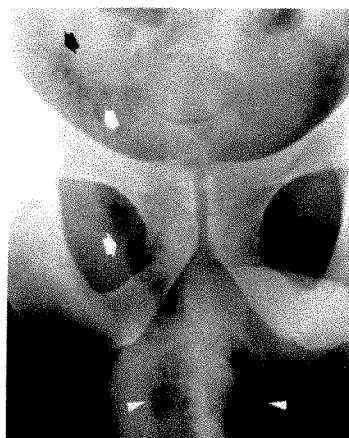
One case of Fournier gangrene was associated with perforating sigmoid diverticulitis [2] and a case of gangrene complicating a retroperitoneal infection has been reported [3]. Meyers [4] has described cases of retroperitoneal infec-

Received April 30, 1990; accepted after revision July 19, 1990.

<sup>1</sup> Service of Diagnostic Imaging, Piemonte Hospital, via Spadafora, 98124 Messina, Italy. Address reprint requests to S. Volta, Bordonaro, 98100 Messina, Italy.

<sup>2</sup> Institute of Radiologic Sciences, University of Messina, Policlinico Gazzi, 98100 Messina, Italy.



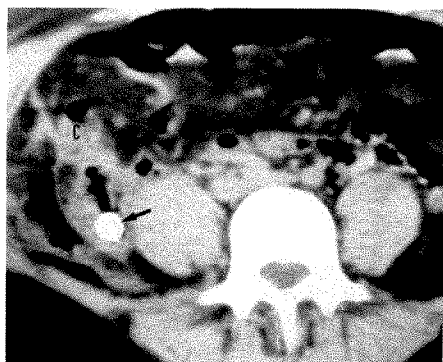


A

Fig. 1.—A, Plain radiograph shows mottled scrotal gas (arrowheads) extending upward into pelvis (arrows). B, CT scan through cecum (C) shows a 1-cm appendicolith (arrow), gas, and low-density inflammatory exudate in retroperitoneum.

C, CT scan through acetabular roofs reveals gas and inflammatory exudate in posterior pararectal space (P) and in right paravesical space along expected course of ductus deferens (arrowheads). Infection extends anteriorly to deep inguinal ring (long arrow). Note subcutaneous gas in right inguinal region (short arrow).

D, CT scan through perineum shows a normal perineum and gas in right spermatic cord (arrowheads) and scrotum (asterisk). Right testis (T) is displaced but not involved by gangrene.



B



C



D

tion spreading in the extraabdominal soft tissues. However, to our knowledge, our case is the first description of a retroperitoneal infection spreading to the scrotum and is the first reported case of Fournier gangrene caused by appendicitis. The cecum and retroperitoneal appendix lie in the anterior pararenal space, which is open inferiorly and in communication with extraperitoneal pararectal and paravesical spaces of the pelvis [4]. In our patient, the ductus deferens is the most likely pathway of spread of the gangrene into the scrotal wall. The ductus deferens lies in the extraperitoneal paravesical space and exits the pelvis through the inguinal canal surrounded by layers of extraperitoneal tissue. In our patient, surgery showed that the right ductus deferens was free of gangrene but surrounded by necrotic tissue at the level of the spermatic cord and inguinal canal.

Recently, Begley et al. [5] described a case of Fournier gangrene studied with sonography. The sonographic characteristics of Fournier gangrene include thickening of the

scrotal skin and gas in the subcutaneous tissue [5]. Scrotal subcutaneous gas is the hallmark of the disease and is well shown on plain radiographs [5]. In our patient, CT not only showed the scrotal involvement but also revealed the true extension and the underlying cause of the disease.

#### REFERENCES

1. Fournier AJ. Etude clinique de la gangrène foudroyante de la verge. *Semin Med* 1883;4:68-70
2. Spiranak JP, Resnick MI, Hampel N, Persky L. Fournier's gangrene: report of 20 patients. *J Urol* 1984;131:289-291
3. Cope JC, Bunler VB. Gangrene of the scrotum as complication of retroperitoneal infection. *J Urol* 1953;69:188-190
4. Meyers MA. Pathways of extrapelvic spread of disease. In: Meyers MA, ed. *Dynamic radiology of the abdomen: normal and pathologic anatomy*. New York: Springer Verlag, 1982:342-352
5. Begley MG, Shawker TH, Robertson CN, Bock SN, Wei JP, Lotze MT. Fournier gangrene: diagnosis with scrotal US. *Radiology* 1988;169:387-389

## Technical Note

### Two-Piece Wrist Surface Coil

Saara M. Totterman,<sup>1</sup> Robert Heberger,<sup>1</sup> Richard Miller,<sup>2</sup> Deborah J. Rubens,<sup>1</sup> and Judy S. Blebea<sup>1</sup>

In clinical MR imaging, the ideal surface coil is a coil whose geometry is optimized for inductive loading to the anatomy to be imaged [1]. In imaging of the wrist, this idealized geometry can be achieved by a coil that closely surrounds the wrist. Whole-volume and partial-volume coils surround the wrist and provide a relatively homogeneous signal over the imaged area but, as their size is dictated either by the size of the hand or by the distance between paired coils [2–8], their diameter is larger than necessary to fit the size of wrist. This is also true for the slip-over, circumferential, single-loop, receive-only coil.

To minimize the size of the coil, we developed a two-piece surface coil for wrist imaging. Its performance was tested against an identical continuous coil, and its usefulness was evaluated experimentally and clinically.

#### Materials and Methods

We first built a circumferential, single-loop, receive-only surface coil with a circumference slightly larger than that of an average-sized male wrist (7.5 × 5.6 mm). We then built a second coil of the same size, which was split into two sections for reassembly around the wrist. For this purpose, 10-gauge copper wire was formed into two halves of a rectangle. The insulation was stripped from the ends of each half. The corresponding ends of the two halves were connected to each other by a small Plexiglas box that had a strip of copper within it. This strip of copper formed a bridge over the gap between the two ends. The connections were secured by nylon screws. Both of the coils were tuned for 63.9 MHz and matched for loading of the male wrist.

Next, the signal-to-noise ratio of the two piece coil was measured against the continuous coil on a 1.5-T clinical imager (Signa, GE Medical System, Milwaukee, WI). Two different types of phantoms, one corresponding to the size and shape of the human wrist (7.5 cm in larger diameter) and the other to the size of the head (20 × 20 cm) were used for the test. Both phantoms were filled with saline solution doped with copper sulfate to simulate the loading effects of their respective anatomy. The slice thickness (3 mm), interslice interval (2.5 mm), field-of-view (FOV) (18 and 28 cm), number of excitations (NEX), TR/TE, and receiver attenuation value were all kept constant.

For both coils the signal intensity was measured along the shorter diameter of the coil in the wrist phantom and along the axis of the coil in the head phantom. The standard deviation of the signal intensity of background air was used for noise calibration.

Finally, the two-piece coil was tested on six cadaver wrists, and clinically tested on six normal volunteers and 18 patients with a variety of wrist abnormalities. The imaging parameters for patients with suspected soft-tissue tumors and for rheumatoid patients were 2000/20, 80; FOV of 8–10 cm; matrix of 256 × 128; slice thickness of 3 mm; and NEX of 1.00, 0.75, or 0.50. For patients with suspected soft-tissue injuries, the imaging parameters were 2000/25, 60; FOV of 8 cm; matrix of 256 × 256; slice thickness of 1.5 mm; and NEX of 1.00.

#### Results

On phantoms, the performance of the two-piece surface coil was almost identical to that of the same-size continuous coil (Fig. 1). In clinical use, the two-piece coil was easily assembled around the wrist and required no coil holder. When the circumferential coil is used for the wrist, the patient must be prone with the arm over head so that the hand is perpendicular to the gantry. Patients with rheumatoid disease did not tolerate this position well. For those patients, we found that the signal-to-noise ratio of the two-piece coil supported images acquired with 0.50 or 0.75 excitation, thereby minimizing imaging time.

Higher resolution images were found to be particularly useful in patients with suspected soft-tissue injury. Images obtained with 1.5-mm slice thickness and one excitation provided detailed visualization of the triangular fibrocartilage, articular cartilage, and intrinsic interosseous ligaments (Figs. 2A and 2B).

#### Discussion

Our tests show that a single-loop, receive-only surface coil can be divided into two separate sections without affecting

Received April 2, 1990; accepted after revision July 17, 1990.

<sup>1</sup> Department of Diagnostic Radiology, University of Rochester Medical Center, Rochester, NY 14642. Address reprint requests to S. M. Totterman.

<sup>2</sup> Department of Orthopedics, University of Rochester Medical Center, Rochester, NY 14642.

AJR 156:343–344, February 1991 0361–803X/91/1562–0343 © American Roentgen Ray Society

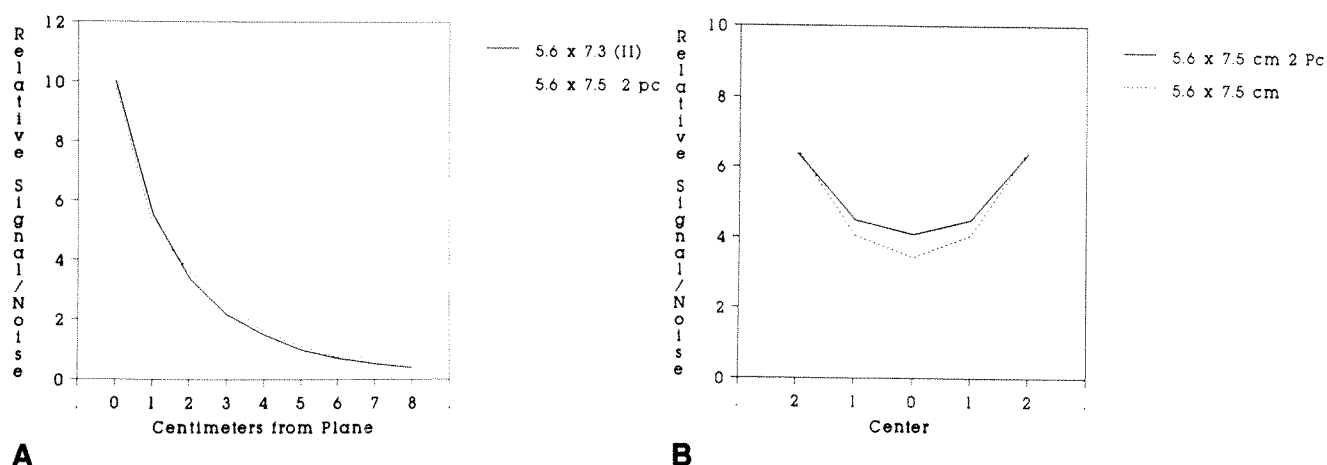


Fig. 1.—Relative signal-to-noise ratios of continuous coil and two-piece coil measured on head phantom (A) and on wrist phantom (B) are almost identical.

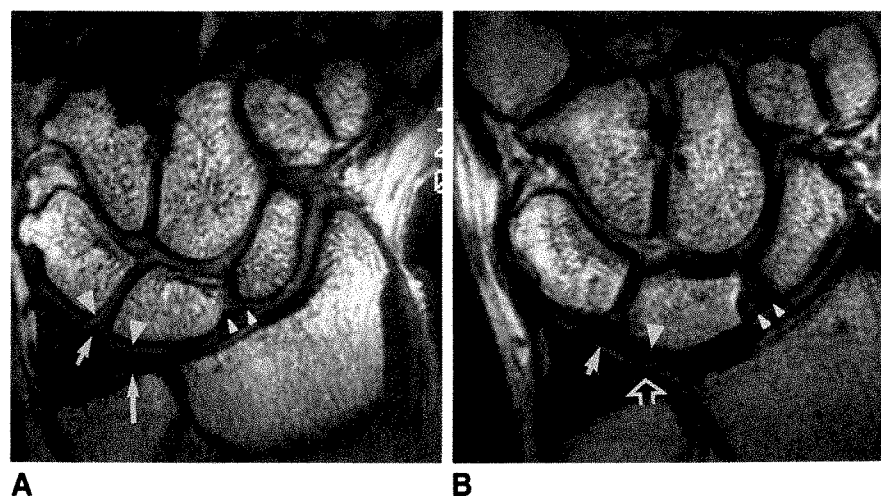


Fig. 2.—A and B, Coronal MR images of wrist at 1.5-mm slice thickness obtained with two-piece receiver coil. Normal volunteer (A), patient with chronic wrist pain (B). Note good visualization of intact triangular fibrocartilage (long arrow), torn triangular fibrocartilage (open arrow), lunotriquetral ligament (short arrow), scapholunate ligament (small arrowheads), and articular cartilages (large arrowheads).

the performance of the coil as a whole. The resulting coil, when used to image the wrist, can be made smaller than the conventional slip-over coil and therefore will have a higher signal-to-noise ratio close to the plane of the coil, but also will have a very steep sensitivity profile.

The steep sensitivity profile of the coil has both advantages and disadvantages. Because of this steep profile, it is important to align the highest signal-to-noise ratio area of the coil with the structures of particular interest. In soft-tissue injuries of the wrist, in which interest is focused on the evaluation of the extrinsic and intrinsic interosseous ligaments and triangular fibrocartilage, the optimal position of the coil is about 1 cm distal to the radiocarpal joint. In patients with rheumatoid disease, the optimal location is approximately 1 cm more distal. Although one of the potential drawbacks with the single-loop coil is the drop in signal proximal and distal to the plane of the coil, in practice this has not been a problem in the evaluation of wrist disease, in which the longitudinal extent of the region to be imaged is quite limited.

The very high signal-to-noise ratio close to the plane of the coil is beneficial in the evaluation of ligament injuries. The area in which the signal-to-noise ratio supports 1.5-mm slice thickness with in-plane resolution of 0.3 mm is large enough to cover the area of the triangular fibrocartilage and interosseous ligaments. In patients in whom high-resolution images are not required, the high signal-to-noise ratio can be used to de-

crease imaging time. With rheumatoid patients who find the imaging position uncomfortable, the short imaging time is important. In all patients, the shortened imaging time increases both patients' comfort and throughput.

## REFERENCES

1. Schenk JF, Hart HR Jr, Foster TH, Edelstein WA, Hussain MA. High resolution magnetic resonance imaging using surface coils. In: Kressel HY, ed. *Magnetic resonance annual*. New York: Raven, 1986:123-160
2. Weiss KL, Beltran J, Shamam OM, Stilla RF, Levey M. High-field MR surface-coil imaging of the hand and wrist. I. Normal anatomy. *Radiology* 1986;160:143-146
3. Weiss KL, Beltran J, Lubbers LM. High-field MR surface-coil imaging of the hand and wrist. II. Pathologic correlations and clinical relevance. *Radiology* 1986;160:147-152
4. Doornbos J, Grimbergen HAA, Booijsen PE, et al. Application of anatomically shaped surface coils in MRI at 0.5T. *Magn Reson Med* 1986;3:270-281
5. Koenig H, Lucas D, Meissner R. The wrist: a preliminary report on high-resolution MR imaging. *Radiology* 1986;160:463-467
6. Middleton WD, Kneeland JB, Kellman GM, et al. MR imaging of the carpal tunnel: normal anatomy and preliminary findings in the carpal tunnel syndrome. *AJR* 1987;148:307-316
7. Baker LL, Hajek PC, Björkengren A, et al. High-resolution magnetic resonance imaging of the wrist: normal anatomy. *Skeletal Radiol* 1987;16:128-132
8. Zlatkin MB, Chao PC, Osterman AL, Schnall MD, Dalinka MK, Kressel HY. Chronic wrist pain: evaluation with high-resolution MR imaging. *Radiology* 1989;173:723-729



## Comparison of Iohexol with Barium in Gastrointestinal Studies of Infants and Children

Mervyn D. Cohen<sup>1</sup>  
 Richard Towbin<sup>2</sup>  
 Sarah Baker<sup>1</sup>  
 Susan Davis<sup>1</sup>  
 C. Becker<sup>2</sup>  
 Daniel E. Eggleston<sup>2</sup>  
 M. Kehler<sup>2</sup>  
 John A. Smith<sup>1</sup>  
 David A. Cory<sup>1</sup>  
 Susan J. White<sup>1</sup>

This study evaluates iohexol as a contrast agent in the gastrointestinal tract in children. In the first part of the study, iohexol in concentrations of 180 and 300 mg I/ml was compared in a double-blind manner with barium. Sixty-four patients were studied. No significant difference in changes of blood pressure and pulse rate was found between the three groups of patients studied. Diarrhea was significantly more common in the children receiving iohexol than in children receiving barium. The diarrhea was not due to previously identified high-risk factors in the children, nor was it due to concurrent medication. When image quality was assessed in each anatomic region of the gastrointestinal tract, fewer nondiagnostic ratings occurred with barium than with iohexol. With barium, fewer ratings of poor mucosal coating and slightly fewer ratings of suboptimal contrast density occurred. The second part of the study was an open evaluation of iohexol 180 mg I/ml in 18 patients in whom barium was clinically contraindicated. Three of 53 assessments were nondiagnostic. Mucosal coating was poor in 6%, and contrast density was suboptimal in 8% of patients.

The results of this study indicate that barium is the preferred contrast agent for routine evaluation of the gastrointestinal tract in children. Good-quality images can be obtained, however, with iohexol in concentrations of 180 or 300 mg I/ml, and iohexol is an excellent contrast agent for evaluation of the gastrointestinal tract in those patients in whom barium is relatively or absolutely contraindicated.

*AJR* 156:345-350, February 1991

Three groups of contrast agents can be used to study the gastrointestinal tract [1]. These are barium, high-osmolality water-soluble contrast agents, and low-osmolality water-soluble contrast agents. Barium is a widely used, safe, and effective contrast agent, but both it and the high-osmolality water-soluble contrast agents have disadvantages. For example, barium is undesirable in patients with suspected bowel perforation, and high-osmolality agents are undesirable in the preterm infant or patients with inflammatory bowel diseases. These disadvantages have been reviewed in detail elsewhere [1].

The low-osmolality contrast agents offer some advantages over barium and high-osmolality water-soluble contrast agents [1]. Of the low-osmolality contrast agents, metrizamide has been studied most widely in the gastrointestinal tract [2-10]. Unfortunately, metrizamide is extremely expensive. For this reason, the efficacy of the newer, less expensive, low-osmolality water-soluble contrast agents in the gastrointestinal tract must be examined. Some reports of the use of iohexol, iopamidol, and ioxaglate describe the usefulness of these agents in the gastrointestinal tract [11-14]. Most of these reports are open studies without any blinded comparison. The objectives of the present study were twofold. In the first part, the safety of, tolerance of patients to, and quality of radiologic visualization with iohexol (180 and 300 mg I/ml) and barium were compared during and after examinations of the gastrointestinal tract in children. In the second part of the study, we evaluated the safety, tolerance, and efficacy of iohexol (180 mg I/ml) in patients in whom

Received June 11, 1990; accepted after revision September 12, 1990.

This work was supported in part by Sterling Drug Company.

<sup>1</sup> Department of Radiology, Indiana University Medical Center, Riley Hospital for Children, 702 Barnhill Dr., Indianapolis, IN 46202-5200. Address reprint requests to M. D. Cohen.

<sup>2</sup> Department of Radiology, Children's Hospital of Michigan, 3901 Beaubien Blvd., Detroit, MI 48201.

0361-803X/91/1562-0345  
 © American Roentgen Ray Society

barium is contraindicated (e.g., in a patient with possible bowel perforation) who were undergoing contrast examination of the gastrointestinal tract.

## Subjects and Methods

The study was performed at two centers. At each center, a study coordinator was designated to monitor patients' enrollment, randomization, contrast administration, adverse effects, and data collection.

Patients were considered eligible for inclusion in this study if they showed signs or symptoms that necessitated contrast-enhanced examination of the gastrointestinal tract and if they were younger than 18 years old. Patients were included in the study if their parent or guardian gave informed written consent. The study had two parts: the iohexol/barium study and the iohexol-only study. Patients in whom the use of barium was not contraindicated were included in the iohexol/barium study. This was a comparative double-blind study. In some patients (e.g., those with pneumoperitoneum or necrotizing enterocolitis) barium cannot be used. These patients were all studied with iohexol and formed the iohexol-only study. This was an open study.

Patients were excluded if they were pregnant or lactating, if they had had an enhanced examination or were scheduled for an enhanced examination within 48 hr, if they had received another investigational drug, if they had previously been entered into the study, or if they had conditions or suspected conditions that contraindicated the use of barium (iohexol/barium study only).

The study was approved by the institutional review board of the two participating institutions. Informed consent was obtained for every patient.

Patients were prepared according to routine hospital procedure. All patients had nothing orally for at least 3 hr before the contrast examination (older patients fasted for a longer period than younger patients did). All patients were permitted to receive routine prescribed medications (except for other investigational drugs), and all medications given within 24 hr before, during, and 24 hr after the examinations were recorded on the case report forms. All coexisting risk factors to contrast administration were recorded. These risk factors included previous reaction to contrast medium; diabetes; hypertension; severe cardiac, renal, or liver disease; sickle cell disease; asthma; hay fever; drug allergy; and food allergy. Previous contrast sensitivity was recorded on the data sheet but did not constitute exclusion from the study. The patient's age, sex, height, weight, race, and relevant medical history also were recorded. All of the images were acquired according to clinical need and routine departmental procedure. The total number of images acquired and therefore the radiation exposure was exactly the same as if the patient had not been in the study.

Randomization of patient allocation for the iohexol/barium study was achieved with a computer-generated randomized code. All patients were randomly allocated to receive either barium, iohexol 180 mg I/ml, or iohexol 300 mg I/ml. The investigator performing the examination and the patient were not told which contrast medium was being used. Cups, straws, bags, and tubing were either opaque or covered with tape. For single-contrast upper gastrointestinal examinations, the barium concentration was 60% weight per volume. For lower intestinal single-contrast barium studies, the concentration was 30% weight per volume. Patients in whom barium was contraindicated were allocated to the iohexol-only study. These patients received iohexol 180 mg I/ml.

The volume of contrast material given was determined by the radiologist performing the study and was based on clinical need. Each study was performed in exactly the same manner as it would

have been if the patient had not been entered in the study. The volume of contrast material given was therefore not influenced by the fact that the patient was in the study. Because of the large normal variation in the amount of contrast material given for any study, it was thought impossible to define a specific amount of contrast agent, based on weight, to be administered to each patient.

Recordings of blood pressure and pulse rate with the patient supine were obtained before, 1 hr after, and when possible at 6 and 24 hr after administration of contrast medium. Changes in vital signs from the baseline were evaluated. In addition, patients were observed for 1 hr after the examination for adverse events. All patients were either seen or their parents telephoned 24 hr after the examination to inquire further about the occurrence of adverse events.

Image quality was evaluated as follows: to facilitate patients' care, we made a radiologic diagnosis at the end of each study. Once all patients were enrolled, two radiologists at each center reviewed and graded the films obtained in both parts of the study in a blinded manner. An overall assessment of quality of radiologic visualization was recorded for each film series as well as individual assessments of the esophagus, stomach, duodenum, small bowel, and large bowel when seen. The quality of visualization was rated on a three-point scale (poor, good, and excellent). Poor visualization was considered nondiagnostic, whereas good and excellent visualizations were considered diagnostic.

For each segment assessed within the gastrointestinal tract, density of opacification and mucosal coating were recorded as well. The density of opacification was assessed on a three-point scale of not dense enough, optimal, and too dense. Mucosal coating was assessed on a three-point scale of poor, good, and excellent.

The iohexol-only study was an open study and therefore was not subject to statistical analysis. For the iohexol/barium study, safety and efficacy were summarized by using standard deviations and ranges. Safety was assessed by comparison of the proportion of patients experiencing any adverse event and efficacy as the proportion of patients with diagnostic overall evaluations. Both were analyzed by the standard contingency table method. Significant findings were followed with analyses considering each contrast medium pair. Additional testing was performed that examined differences in the quality of visualization among contrast media, with visualization considered either poor, good, or excellent. All analyses accounted for possible differences between centers.

## Results

Eighty-two patients were enrolled, 64 in the iohexol/barium study and 18 in the iohexol-only study (Table 1).

In the iohexol/barium study, patients from the three study groups are similar in terms of sex distribution, age, weight, and history of exposure to contrast medium. A few more patients with associated risk factors were in the barium group than in either of the other two groups (Table 1).

Twenty-nine (69%) of 42 patients receiving iohexol and 17 (77%) of 22 patients receiving barium from the iohexol/barium study and 14 (78%) of 18 patients in the iohexol-only study received one or more concomitant medications within 24 hr before and after the procedure. The most common medication classifications were antiasthma, anticonvulsant, antibiotic, and gastrointestinal.

Risk factors were present in over 60% of the patients (Table 1); no difference in frequency was seen between the groups ( $p = .144$ ). Allergy and age less than 1 year were the commonest risk factors.

**TABLE 1: Demographic Data, History of Prior Contrast Exposure, and Risk Factors**

Demographic Parameter	Iohexol/Barium Study			Iohexol-Only Study
	Iohexol (180 mg I/ml)	Iohexol (300 mg I/ml)	Barium	Iohexol (180 mg I/ml)
No. of patients	21	21	22	18
Sex (M/F)	11/10	12/9	15/7	9/9
Race				
White	19	20	20	12
Black	2	1	2	6
Age (years)	4.7 ± 4.8	5.4 ± 5.8	3.5 ± 4.5	1.2 ± 3.1
Weight (kg)	19.9 ± 19.3	19.2 ± 16.6	15.5 ± 14.9	4.7 ± 5.5
History of exposure to contrast medium (Y/N)	8/13	7/14	6/16	4/14
Associated risk factor(s) including sensitivity to allergens or contrast medium (Y/N)	12/9	9/12	16/6	15/3

No significant difference in the volume of contrast material administered was found between the three groups in the iohexol/barium study ( $p = .631$ ). The volumes given were  $5.2 \pm 5.9$  ml/kg (iohexol 180 mg I/ml),  $7.0 \pm 7.0$  (iohexol 300 mg I/ml), and  $6.5 \pm 3.3$  ml/kg (barium). The difference in the dose per kilogram between the iohexol 180 mg I/ml groups in the iohexol/barium study ( $5.2 \pm 5.9$  ml/kg) and in the iohexol-only study ( $9.2 \pm 5.6$  ml/kg) was statistically significant ( $p = .048$ ).

Comparing blood pressure and pulse rate recordings before and after contrast administration for patients in the iohexol/barium study, we noted that nine patients had systolic blood pressure changes of 30 mm Hg or greater; these systolic blood pressure changes ranged from  $-38$  to  $+63$  mm Hg. Three patients had diastolic blood pressure changes of 30 mm Hg or greater; these changes ranged from  $+30$  to  $+38$  mm Hg. Twenty-one patients had pulse rate changes of 30 beats per minute or greater; these changes ranged from  $-64$  to  $+98$  beats per minute. Most of the changes represented increases from relatively low baseline recordings or decreases from relatively high baseline recordings. Most of the changes were transient and many were thought to be due to an agitated state of the patient before or when the vital sign measurements were taken. No difference in the changes of blood pressure and pulse rate was seen between the three groups of patients. No clinical adverse effects were ascribed to the vital sign changes, and no child required treatment on the basis of changes in vital signs.

Adverse event information is summarized in Table 2. Eleven patients from the iohexol 180 mg I/ml group had a total of 17 adverse events, and nine patients from the iohexol 300 mg I/ml group had a total of 12 adverse events. One patient from the barium group had a single adverse event. The most common adverse event was mild to moderate diarrhea.

Overall none of the adverse events were serious or life threatening and all were followed up until they resolved. Allocation of a patient to a high-risk subgroup did not predict an adverse event, as adverse events were detected more frequently in the low-risk group than in the high-risk subgroup.

**TABLE 2: Summary of Adverse Events in Iohexol/Barium Study**

	Iohexol (180 mg I/ml)	Iohexol (300 mg I/ml)	Barium
No. of patients	20	20	22
Abdominal pain	1	0	0
Diarrhea	10	8	0
Fever	1	2	0
Nausea	1	2	0
Urticaria	1	0	0
Vomiting	3	0	1
Total <sup>a</sup>	17	12	1

<sup>a</sup> Barium vs iohexol 180 is significant ( $p \leq .005$ ); barium vs iohexol 300 is significant ( $p = .003$ ); iohexol 180 vs iohexol 300 is not significant ( $p = .75$ ).

The results of radiologic evaluation of the image quality for the various contrast agents are given in Tables 3–6. Tables 3, 4, and 5 give the analysis for radiologic visualization, mucosal coating, and contrast density for the three contrast agents used in the iohexol/barium study. The results are given separately for the duodenum, esophagus, stomach, small bowel, and large bowel. There are 64 separate evaluations for iohexol 180 mg I/ml, 63 for iohexol 300 mg I/ml, and 78 barium assessments for individual organs. Of these, only six with iohexol 180 mg I/ml, seven with iohexol 300 mg I/ml, and three with barium were considered nondiagnostic (poor rating on radiographic visualization). With regard to mucosal coating, the ratings were good or excellent for 52 (80%) of iohexol 180 mg I/ml, 57 (90%) of iohexol 300 mg I/ml, and 77 (99%) of barium evaluations. Contrast density was considered optimal in 58 (91%) of iohexol 180 mg I/ml, 57 (90%) of iohexol 300 mg I/ml, and 73 (94%) of barium evaluations.

Table 6 gives similar data for iohexol 180 mg I/ml for the iohexol-only study. Three of 53 iohexol 180 mg I/ml assessments were nondiagnostic (poor radiographic visualization). Mucosal coating was good or excellent in 50 cases (94%). Density was considered optimal in 49 evaluations (92%).



TABLE 3: Radiologic Efficacy by Anatomic Site for Barium in Barium/Iohexol Study

Site	Radiologic Visualization					Mucosal Coating					Density		
	Poor	Good	Excel- lent	Total	Percent Diag- nostic <sup>a</sup>	Poor	Good	Excel- lent	Total	Percent Diag- nostic <sup>a</sup>	Not Dense Enough (%)	Optimal (%)	Too Dense (%)
Duodenum	2	6	13	21	90	1	13	7	21	95	1 (5)	20 (95)	0
Esophagus	0	3	17	20	100	0	12	8	20	100	0	19 (95)	1 (5)
Stomach	0	12	9	21	100	0	16	5	21	100	0	19 (90)	2 (10)
Small Bowel	1	5	7	13	92	0	4	9	13	100	1 (7)	12 (93)	0
Large Bowel	0	2	1	3	100	0	2	1	3	100	0	3 (100)	0

<sup>a</sup> Good + excellent.

TABLE 4: Radiologic Efficacy by Anatomic Site for Iohexol (180 mg I/ml) in Iohexol/Barium Study

Site	Radiologic Visualization					Mucosal Coating					Density	
	Poor	Good	Excel- lent	Total	Percent Diagnostic <sup>a</sup>	Poor	Good	Excel- lent	Total	Percent Diagnostic <sup>a</sup>	Not Dense Enough (%)	Optimal (%)
Duodenum	2	13	1	16	88	5	11	0	16	69	2 (13)	14 (88)
Esophagus	1	14	4	19	95	2	17	0	19	89	2 (11)	17 (89)
Stomach	0	14	4	18	100	2	14	2	18	89	0	18 (100)
Small Bowel	3	4	1	8	63	3	4	1	8	63	2 (25)	6 (75)
Large Bowel	0	2	1	3	100	0	3	0	3	100	0	3 (100)

<sup>a</sup> Good + excellent.

TABLE 5: Radiologic Efficacy by Anatomic Site for Iohexol (300 mg I/ml) in Iohexol/Barium Study

Site	Radiologic Visualization					Mucosal Coating					Density	
	Poor	Good	Excel- lent	Total	Percent Diagnostic <sup>a</sup>	Poor	Good	Excel- lent	Total	Percent Diagnostic <sup>a</sup>	Not Dense Enough (%)	Optimal (%)
Duodenum	1	10	3	14	93	1	11	2	14	93	1 (7)	13 (93)
Esophagus	0	10	7	17	100	0	14	3	17	100	0	17 (100)
Stomach	1	9	5	15	93	0	11	4	15	100	1 (7)	14 (93)
Small Bowel	5	5	2	12	60	4	6	2	12	67	4 (34)	8 (65)
Large Bowel	0	1	4	5	100	1	0	4	5	80	0	5 (100)

<sup>a</sup> Good + excellent.

TABLE 6: Radiologic Efficacy by Anatomic Site for Iohexol (180 mg I/ml) in Iohexol-Only Study

Site	Radiologic Visualization					Mucosal Coating					Density	
	Poor	Good	Excel- lent	Total	Percent Diagnostic <sup>a</sup>	Poor	Good	Excel- lent	Total	Percent Diagnostic <sup>a</sup>	Not Dense Enough (%)	Optimal (%)
Duodenum	1	8	4	13	92	1	11	1	13	92	1 (8)	12 (92)
Esophagus	0	7	2	9	100	0	8	1	9	100	1 (11)	8 (89)
Stomach	0	11	3	14	100	0	14	0	14	100	0	14 (100)
Small Bowel	2	8	1	11	82	2	9	0	11	82	2 (18)	9 (82)
Large Bowel	0	3	3	6	100	0	5	1	6	100	0	6 (100)

<sup>a</sup> Good + excellent.

We evaluated the overall radiologic efficacy for each contrast agent. In the Iohexol/barium study, barium was rated as excellent in 12 cases and good in 10 cases; Iohexol 180 mg I/ml was rated as excellent in four cases, good in 14 cases,

and poor in three cases; Iohexol 300 mg I/ml was rated as excellent in seven cases, good in 12 cases, and poor in two cases. In the Iohexol-only study, Iohexol 180 mg I/ml was rated as excellent in six cases and good in 12 cases. These

data are for the radiologist's impression of the overall quality of the entire study, but are not broken down by anatomic region.

No statistical significant difference among the contrast media was found in the iohexol/barium study ( $p = .215$ ) with regard to diagnostic (good + excellent) vs nondiagnostic (poor) assessments. However, when the individual classifications of overall quality (poor, good, excellent) are considered, a significant ( $p = .024$ ) difference is seen among the contrast media owing to the greater frequency of excellent assessments in the barium group relative to the iohexol 180 mg I/ml group. No significant difference was observed between the iohexol 180 and 300 mg I/ml groups when individual assessments of specific organs were compared in the iohexol/barium study (Table 2).

### Discussion

In selected clinical situations, low-osmolality water-soluble contrast agents have definite advantages over other contrast agents for examination of the gastrointestinal tract in children [1]. Early attempts to achieve low osmolality involved dilution of high-osmolality contrast agents with resultant very low iodine concentrations [15]. For the past 10 years, metrizamide has been used in almost isotonic solutions and with an iodine concentration of 180 mg I/ml to achieve good-quality images for the diagnosis of a variety of disorders in children, including bowel perforation [6-8] and necrotizing enterocolitis [4-10]. Unfortunately metrizamide is expensive. Iohexol is similar to metrizamide, but less costly. Like metrizamide, it is extremely stable in bowel secretions [16] and has virtually no absorption from the normal bowel [16, 17].

Previous reports suggest that iohexol will have clinical usefulness similar to that of metrizamide in the intestinal tract, but unfortunately these reports do not include comparative double-blind evaluations of these agents [11-13, 18].

Evaluation of the radiologic visualization, mucosal coating, and density of the contrast agent showed that barium was the preferred contrast agent for each of these evaluations, although the difference between barium and iohexol was not great. The particulate nature of the barium probably accounts for its preference for mucosal coating. The greater attenuation of the X-ray beam by barium probably accounts for the fewer ratings of poor visualization with barium than with iohexol. The radiologists' overall rating of radiologic efficacy for each study showed that none of the barium studies was rated as poor, whereas five of the iohexol studies were assessed as poor. It should, however, be noted that 37 of the iohexol examinations in the iohexol/barium study were rated as good or excellent. Barium had more ratings of excellent than iohexol had. In summary, the results of the iohexol/barium study indicate that radiologic visualization with iohexol is good, but if the use of barium was not contraindicated, barium is the preferred agent.

The iohexol-only study evaluated iohexol 180 mg I/ml in an open manner in patients for whom barium was contraindicated. A comparison of Table 4 (iohexol 180 mg I/ml in the iohexol/barium study) and Table 6 (iohexol 180 mg I/ml in the iohexol-only study) indicates fewer poor evaluations with this concentration of iohexol in the iohexol-only study than in the

iohexol/barium study. For overall radiologic efficacy, three of 21 studies with iohexol 180 mg I/ml in the iohexol/barium study were rated as poor, whereas no studies with this concentration were rated as poor for the iohexol-only study. Two reasons are believed to account for this difference. The patients receiving iohexol 180 mg I/ml in the iohexol-only study received a greater volume of contrast material per kilogram of body weight ( $9.2 \pm 5.6$  ml) than did those patients in the iohexol/barium study ( $5.2 \pm 5.9$  ml/kg). Second, the age and weight of the patients in the iohexol-only study are very different from those of patients in the iohexol/barium study (Table 1). This is because many of the clinical conditions for which barium is contraindicated exist in the newborn. In the small patients in the iohexol-only study, the lower body weight may result in less scattering of the X-ray beam with less loss of contrast on the radiograph. The concentration of iodine is the same for each group of patients, but the image degradation from scatter is greater in the larger patients.

Both iohexol and barium were safe agents in that no major contrast reactions requiring therapeutic intervention or hospitalization were identified in either group. Table 2 shows, however, a much higher frequency of minor side effects with iohexol than with barium. In the iohexol/barium study, only one minor reaction occurred with barium, whereas 29 reactions occurred with iohexol. The frequency of these minor reactions did not correlate with the presence of high-risk factors in the patients' histories. Of these adverse events, diarrhea was by far the commonest. The diarrhea was slightly more common in the patients with the lower concentration of iohexol. Ten patients receiving iohexol 180 mg I/ml had diarrhea, compared with eight patients receiving iohexol 300 mg I/ml. The osmolality of the 180 mg I/ml iohexol concentration is 408 mOsm/l and that of the 300 mg I/ml iohexol is 798 mOsm/l. Although the differences in the frequency of diarrhea are not statistically significant, they do raise the possibility that the toxic effect of iohexol causing diarrhea may not be purely an osmotic effect but might be due to some other irritating effect of this agent on the bowel. The osmolality of iohexol 180 mg I/ml is only about 35% greater than that of normal blood, and the high frequency of diarrhea is somewhat surprising if one postulates that the diarrhea is due purely to an osmotic effect of the contrast agent. Unfortunately a review of the literature does not provide additional answers. In three European studies with iohexol, a combined total of 112 patients had no episodes of diarrhea [19]. In another study that used iohexol 350 mg I/ml in adults, diarrhea was reported as a common event [20]. In 11 fit adults, 150 ml of iohexol 350 mg I/ml caused diarrhea in 10 patients [21]. Finally, in a study of 115 patients receiving either iohexol, iopamidol, or ioxaglate, no evidence of toxicity was reported. The difference in frequency of diarrhea in patients receiving iohexol as compared with the patients receiving barium is highly significant. Although many of our patients were receiving concomitant medication, the medications received did not differ among the three groups of patients, and we therefore believe that the diarrhea is a result of the iohexol and not of the concomitant medication.

With regard to vital signs, the difference between the changes in blood pressure and pulse rate observed in the

three groups was not statistically significant, and we believe that all of these changes can be accounted for by variations in the calmness or agitation of the patients when the readings were made.

In summary, iohexol can be effectively used as a contrast agent in the gastrointestinal tract. The frequency of side effects is greater than that with barium, but these side effects are mild. Although iohexol is not as good as barium for bowel visualization, it should provide an excellent substitute for the more expensive metrizamide for those patients in whom barium is relatively or absolutely contraindicated. The radiologists' perception of image quality with iohexol is better in smaller than in larger patients.

These data have been submitted to the Food and Drug Administration for approval to label iohexol "for oral use in the gastrointestinal tract in children." Approval has not yet been obtained.

#### REFERENCES

1. Cohen MD. Choosing contrast media for the evaluation of the gastrointestinal tract of neonates and infants. *Radiology* **1987**;162:447-456
2. Cohen M, Smith WL, Smith JA, Gresham EL, Schreiner R, Lemons J. The use of metrizamide (Amipaque) to visualize the gastrointestinal tract in children: a preliminary report. *Clin Radiol* **1980**;31:635-641
3. Cohen MD. Prolonged visualization of the gastrointestinal tract with metrizamide. *Radiology* **1982**;143:327-328
4. Cohen MD, Smith JA, Slabaugh RD, Rust RJ. Neonatal necrotizing enterocolitis shown by oral metrizamide (Amipaque). *AJR* **1982**;138:1019-1023
5. Cohen MD, Schreiner R, Grosfeld J, Weber T, Lemons J, Jansen R. A new look at the neonatal bowel: contrast studies with metrizamide (Amipaque). *J Pediatr Surg* **1983**;18:442-448
6. Cohen MD, Weber TR, Grosfeld JL. Bowel perforation in the newborn: diagnosis with metrizamide. *Radiology* **1984**;150:65-69
7. Belt T, Cohen MD. Metrizamide evaluation of the esophagus in infants. *AJR* **1984**;143:367-369
8. Cohen MD, Jansen R, Lemons J, Schreiner R. Evaluation of the gasless abdomen in the newborn and young infant with metrizamide. *AJR* **1984**;142:393-396
9. Johansen JG. Assessment of a non-ionic contrast medium (Amipaque) in the gastrointestinal tract. *Invest Radiol* **1978**;13:523-527
10. Keller MS, Chawla HS. Neonatal metrizamide gastrointestinal series in suspected necrotizing enterocolitis. *Am J Dis Child* **1985**;139:713-716
11. Clarke EA, Dutton NE. Use of iohexol in the early determination of gastrointestinal perforation. *J Pediatr Surg* **1988**;23:1027-1028
12. Brick SH, Caroline DF, Lev-Toaff AS, Friedman AC, Grumbach K, Radecki PD. Esophageal disruption: evaluation with iohexol esophagography. *Radiology* **1988**;169:141-143
13. Ratcliffe JF. The use of ioxaglate in the paediatric gastrointestinal tract: a report of 25 cases. *Clin Radiol* **1983**;34:579-583
14. Ratcliffe JF. The use of low osmolality water soluble (LOWS) contrast media in the pediatric gastro-intestinal tract: a report of 115 examinations. *Pediatr Radiol* **1986**;16:47-52
15. Kuhns LR, Kanellitsas C. Use of isotonic water-soluble contrast agents for gastrointestinal examinations in infants. *Radiology* **1982**;144:411
16. Schwartzentruber DJ, Billmire DF, Cohen M, Block T, Gunter M, Grosfeld JL. Use of iohexol in the radiographic diagnosis of ischemic bowel. *J Pediatr Surg* **1986**;21:525-529
17. Mutzel W, Speck U. Pharmacokinetics and biotransformation of iohexol in the rat and dog. *Acta Radiol Suppl* **1980**;362:87-92
18. Bell KE, McKinstry CS, Mills OM. Iopamidol in the diagnosis of suspected upper gastro-intestinal perforation. *Clin Radiol* **1987**;38:165-168
19. Nycomed Clinical Report Nos. 120, 121, and 130. Rensselaer, NY: Sterling Research Group, **1989**
20. Sterling Research Group Clinical Study Report Nos. 137 and 632. Rensselaer, NY: Sterling Research Group, **1988**
21. Sterling Research Group Clinical Study Report No. 633. Rensselaer, NY: Sterling Research Group, **1988**



# Calcification of the Ligamentum Arteriosum in Children: A Normal Finding on CT

Michael Bisceglia<sup>1</sup>  
James S. Donaldson<sup>2</sup>

Calcification of the ligamentum arteriosum is a rare finding on plain radiographs. We commonly have seen the calcification on unenhanced CT scans of the chest, a finding not previously reported. A retrospective review of unenhanced CT scans of the chest was undertaken to determine the frequency of the described finding. Seven (13%) of 53 patients had a well-demarcated focus of calcification in the region of the ligamentum arteriosum. None of these patients had evidence of a patent ductus arteriosum.

Calcification within the ligamentum arteriosum was seen in 13% of routine CT examinations of the chest in children and should not be confused with a pathologic process producing mediastinal calcifications.

*AJR* 156:351-352, February 1991

Calcification of the ligamentum arteriosum as detected on plain radiographs has been described by several authors [1, 2]. Currarino and Jackson [1] reported 75 cases of ligamentum arteriosum calcification in children and suggest its presence may be used as evidence against patency of the ductus arteriosum. They found that ligamentum calcification was relatively common in children, developing from a few months to several years after the normal closure of the ductus and probably disappearing within a few years in many instances. Noting these calcifications frequently on unenhanced chest CT scans prompted our interest to define further the prevalence and appearance in normal children.

## Materials and Methods

We retrospectively reviewed consecutive unenhanced chest CT studies performed at The Children's Memorial Hospital in Chicago between May 1989 and April 1990. Excluded from the study population were all children with cardiovascular disease, mediastinal disease, and those whose scans had motion artifacts. This review yielded a total of 53 unenhanced CT scans of the chest on children ranging from 1 month to 20 years of age. Most patients were scanned for evaluation of metastatic disease to the lungs. All CT scans were performed on a GE 9800 CT scanner (Milwaukee, WI) by using 5-mm or 10-mm collimated contiguous slices through the lungs. Mediastinal and soft-tissue window settings were reviewed independently by both authors.

## Results

Seven (13%) of 53 cases reviewed had a punctate or curvilinear calcific density in the region of the ligamentum arteriosum (Figs. 1-3). The ligamentum appeared as a dense streak in some instances, because of cardiac motion artifact. These seven children ranged from 5 months to 14 years old. There were four boys and three girls. No mediastinal or cardiovascular disease was present, nor did it develop subsequently in any of these children. Specifically, none has clinical evidence of a patent ductus arteriosum.

## Discussion

Calcification of the ligamentum arteriosum is known to be a common finding on plain radiographs, but its appearance on CT has not been described. We observed the calcification frequently on unenhanced scans of the chest and recognized that it was seen much more commonly on CT scans than on plain radiographs. We thought that the calcification was within the ligamentum arteriosum on the basis of anatomic location, lack of associated soft-tissue mass, and lack of other evidence of mediastinal pathologic changes or congenital heart disease, specifically a patent ductus arteriosus.

Received December 18, 1989; accepted after revision August 13, 1990.

Presented at the annual meeting of the Society of Pediatric Radiology, Cincinnati, OH, April 1990.

<sup>1</sup> Department of Radiology, Rush-Presbyterian-St. Luke's Medical Center, Chicago, IL 60612.

<sup>2</sup> Department of Radiology, The Children's Memorial Hospital, 2300 Children's Plaza, Chicago, IL 60614. Address reprint requests to J. S. Donaldson.

0361-803X/91/1562-0351  
© American Roentgen Ray Society

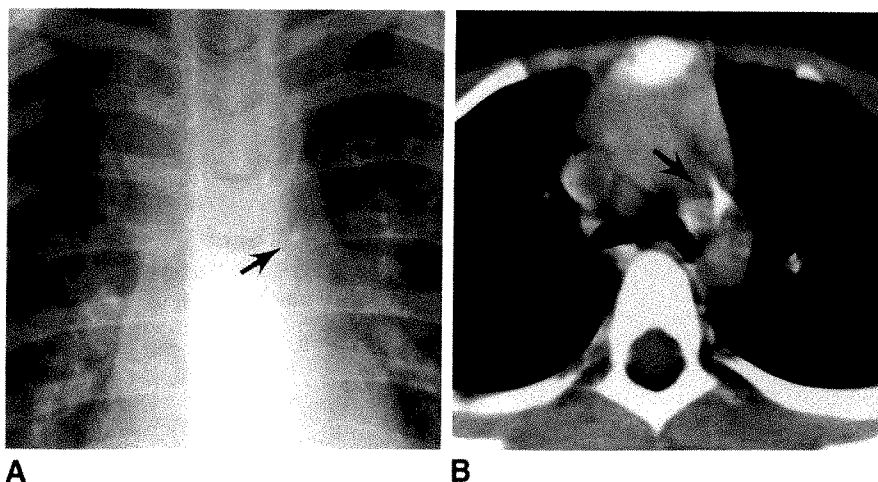


Fig. 1.—10-year-old child with punctate calcification (arrow) in ligamentum.  
A, Radiograph shows round calcification.  
B, CT scan at level of aortopulmonary window shows artifact around calcification (arrow) degraded slightly by motion artifact.



Fig. 2.—CT scan of chest of 8-year-old child shows a streaklike calcification (arrow). Other density with artifact is a central venous catheter in superior vena cava.



Fig. 3.—Despite administration of IV contrast material, CT scan readily shows calcified ligamentum arteriosum (arrow).

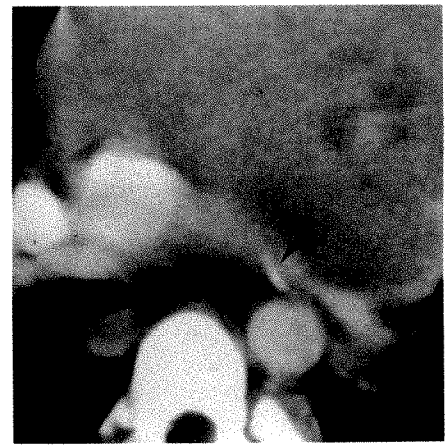


Fig. 4.—CT scan shows a small streak of calcification (arrow) in expected location of ligamentum arteriosum. This patient had newly diagnosed lymphoma; we originally had thought calcification was part of mediastinal mass.

Mediastinal calcifications in children usually are associated with disease and can be seen in granulomatous infections and neoplasms, such as neuroblastoma, teratoma, or, rarely, treated lymphoma. Other anatomic structures that may calcify include the pulmonary arteries in patients with longstanding pulmonary hypertension, the aorta with coarctation, an aneurysm of the ductus arteriosus, and the pericardium. We think that the ligamentum arteriosum calcification can be distinguished readily from these other entities.

On reviewing random cases with mediastinal masses, we found one patient with lymphoma whose mediastinum was thought to contain calcification within the mass (Fig. 4). We now believe the calcification is in the ligamentum arteriosum. Another child with calcified hilar nodes also had a calcified ligamentum arteriosum that we had initially misinterpreted as part of the calcified nodes.

The clinical significance of the calcification is uncertain because of conflicting studies in the literature [1–6]. Calcification of the ligamentum arteriosum is thought to be adequate proof of obliteration of the ductus in asymptomatic children, according to Currarino and Jackson [1]. No evidence of a patent ductus arteriosus was seen in any of our patients. In adults, calcification may be seen in both patent and obliterated

ductus arteriosi. Ruskin and Samuel [4] have reported calcification within patent ductus arteriosi in four adults. Conversely, an anatomic study of closure of the ductus arteriosus by Jager and Wollenmen [5] revealed that in the adult, closed ductus arteriosi occasionally contained calcification and ossification.

We report the CT appearance of calcification in the ligamentum arteriosum in children. It is a common finding on unenhanced CT scans and should not be confused with other mediastinal pathologic calcifications.

#### REFERENCES

1. Currarino G, Jackson JH Jr. Calcification of the ductus arteriosus and ligamentum Botalli. *Radiology* **1970**;94:139–142
2. Child AE, MacKenzie ER. Calcification in the ductus arteriosus. *AJR* **1945**;54:370–374
3. Swischuk LE. Patent ductus arteriosus. *Semin Roentgenol* **1985**;20:236–243
4. Ruskin H, Samuel E. Calcification in the patent ductus arteriosus. *Br J Radiol* **1950**;23:710–717
5. Jager BV, Wollenmen OJ, Jr. An anatomical study of the closure of the ductus arteriosus. *Am J Pathol* **1942**;18:595–613
6. Morrow AG, Clark WD. Closure of the calcified patent ductus. *J Thorac Cardiovasc Surg* **1966**;51:534–538

## Pictorial Essay

# Radiologic Evaluation of Limb-Lengthening Procedures

Craig W. Walker,<sup>1,2</sup> James Aronson,<sup>3</sup> Phoebe A. Kaplan,<sup>4</sup> W. Mark Molpus,<sup>1</sup> and Joanna J. Seibert<sup>1</sup>

**Limb-lengthening procedures are being performed at an increasing rate in the United States. A successful outcome relies heavily on serial radiologic evaluation. Therefore, it is important for radiologists to become familiar with the various techniques, their normal radiologic appearance, and associated complications. Lengthening by the Wagner method, distraction epiphysi-olysis, and the Ilizarov technique are illustrated. Chondrodiatasis and callotasis also are discussed.**

Limb-lengthening procedures are performed to correct significant length discrepancies in the upper or lower extremity that have resulted from various congenital or acquired abnormalities. The success of these procedures relies heavily on evaluation of serial radiographs to monitor progression and detect complications. Early detection of complications may allow prompt correction. A number of techniques that use a variety of external fixation devices are currently available. The biologic principles vary among the different procedures, resulting in different terminology and radiologic appearance. Unilateral fixators such as the Wagner (Synthes LTD, Paoli, PA) and Orthofix (EBI Medical Systems Inc., Fairfield, NJ) devices as well as the circular Ilizarov (Medical Plastic s.r.l., Milan, Italy) fixator are most commonly used (Fig. 1). The pertinent radiologic features of limb lengthening performed by the Wagner technique, distraction epiphysi-olysis, and the

Ilizarov method are illustrated. A discussion of chondrodiatasis and callotasis is included for completeness.

### Wagner Technique

Limb lengthening by the Wagner technique is a multistep process that requires three separate operations. At the initial surgery, an open middiaphyseal transverse osteotomy is performed by sawing across each bone layer, temporarily impairing new bone formation. An initial diastasis of 0.5–1.0 cm is created (Fig. 2A) and is immediately followed by daily distractions of 1.0–2.0 mm, depending on the patient's tolerance, in order to achieve the desired length as rapidly as possible (Fig. 2B). Partial weight bearing is permitted. When the desired length is achieved, a second operation is performed during which autogenous cancellous bone graft (usually from the iliac crest) is placed into the gap, the bone is plated, and the external fixator is removed (Fig. 2C). The patient is allowed partial weight bearing until the bone graft is incorporated into the distraction site, depicted radiologically as cortical remodeling. At a third operation, the bone plate is removed, and the patient must again limit weight bearing (Fig. 2D). The criterion used for full weight bearing is bony consolidation with a cortex and medullary canal that bridge the distraction gap [1].

Received June 27, 1990; accepted after revision August 20, 1990.

<sup>1</sup> Department of Radiology, University of Arkansas for Medical Sciences and Arkansas Children's Hospital, 4301 W. Markham St., Little Rock, AR 72205.

<sup>2</sup> Present address: Department of Radiology, University of Iowa Hospitals and Clinics, Iowa City, IA 52242. Address reprint requests to C. W. Walker.

<sup>3</sup> Department of Orthopaedic Surgery, University of Arkansas for Medical Sciences and Arkansas Children's Hospital, 4301 W. Markham St., Little Rock, AR 72205.

<sup>4</sup> Department of Radiology, University of Nebraska Medical Center, 600 S. 42nd St., Omaha, NE 68198–1045.

**AJR 156:353–358, February 1991** 0361–803X/91/1562–0353 © American Roentgen Ray Society



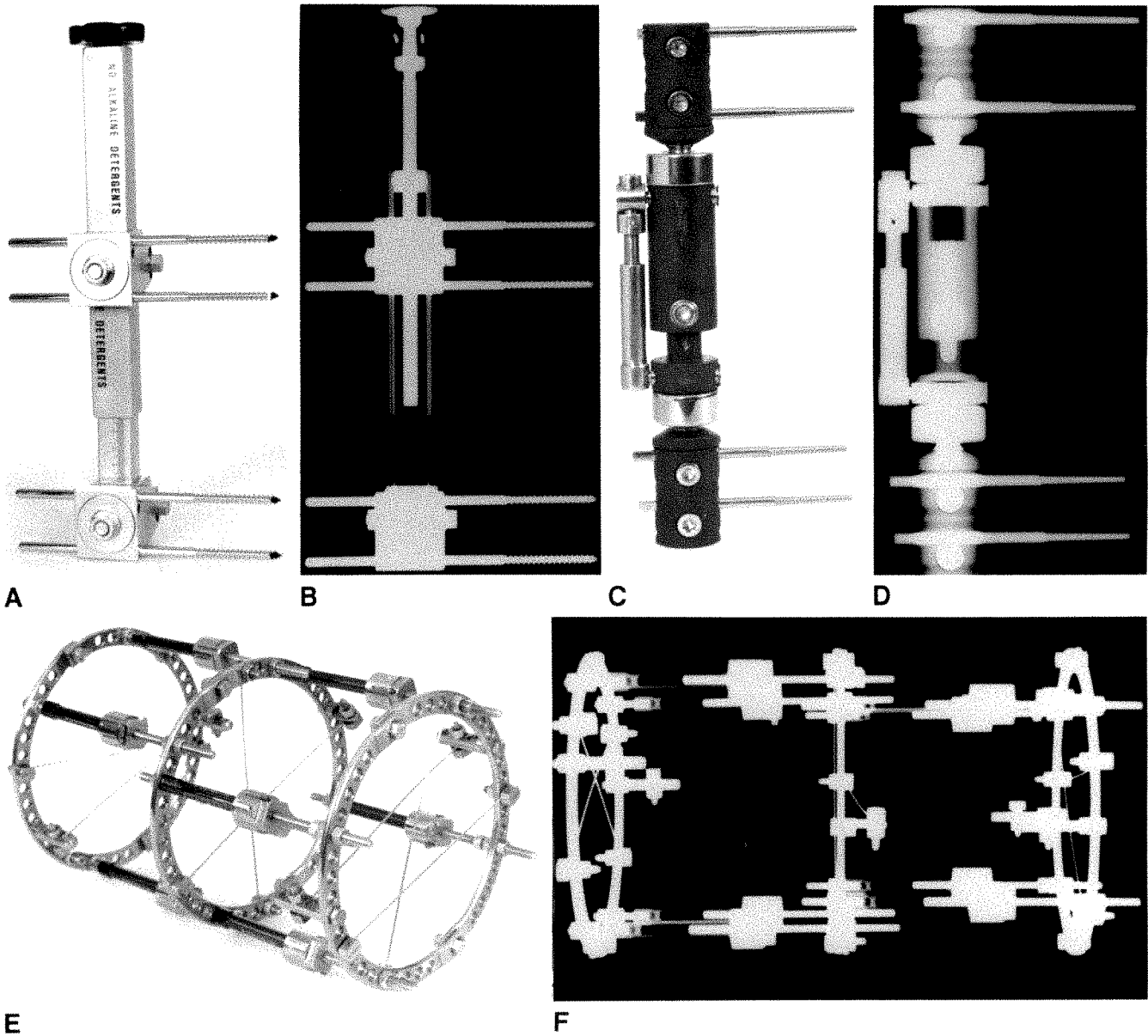


Fig. 1.—A–F, Photographs and radiographs of Wagner (A, B) and Orthofix (C, D) unilateral fixators and circular Ilizarov fixator with wires (E, F).

**Distraction Epiphysiolysis**

Distraction epiphysiolysis is a single-stage procedure that accomplishes limb lengthening through the application of tensile forces across an open growth plate. This method is best applied just before skeletal maturity, because growth plate fusion usually follows such a lengthening. After external fixator placement, distraction is begun immediately at a rate of 0.25 mm four times a day. A widening lucent zone between epiphysis and metaphysis occurs during distraction (Fig. 3A). Separation of the epiphysis from the metaphysis is heralded

by sudden and unpredictable pain, usually by the seventh day. New bone formation is first visible as a slight radiopacity about day 20–25 (Fig. 3B). Once the desired length is achieved, fixation is continued until a cortical shell is formed, approximately 2–3 months after treatment is begun (Fig. 3C). The fixator is then removed, a plaster cast placed, and gradual weight bearing allowed until cortical thickness is adequately developed (Fig. 3D) [2].

Chondrodiatasis is a modification of distraction epiphysiolysis whereby lengthening is achieved through slower distraction (0.25 mm twice daily) of the epiphyseal plate to avoid

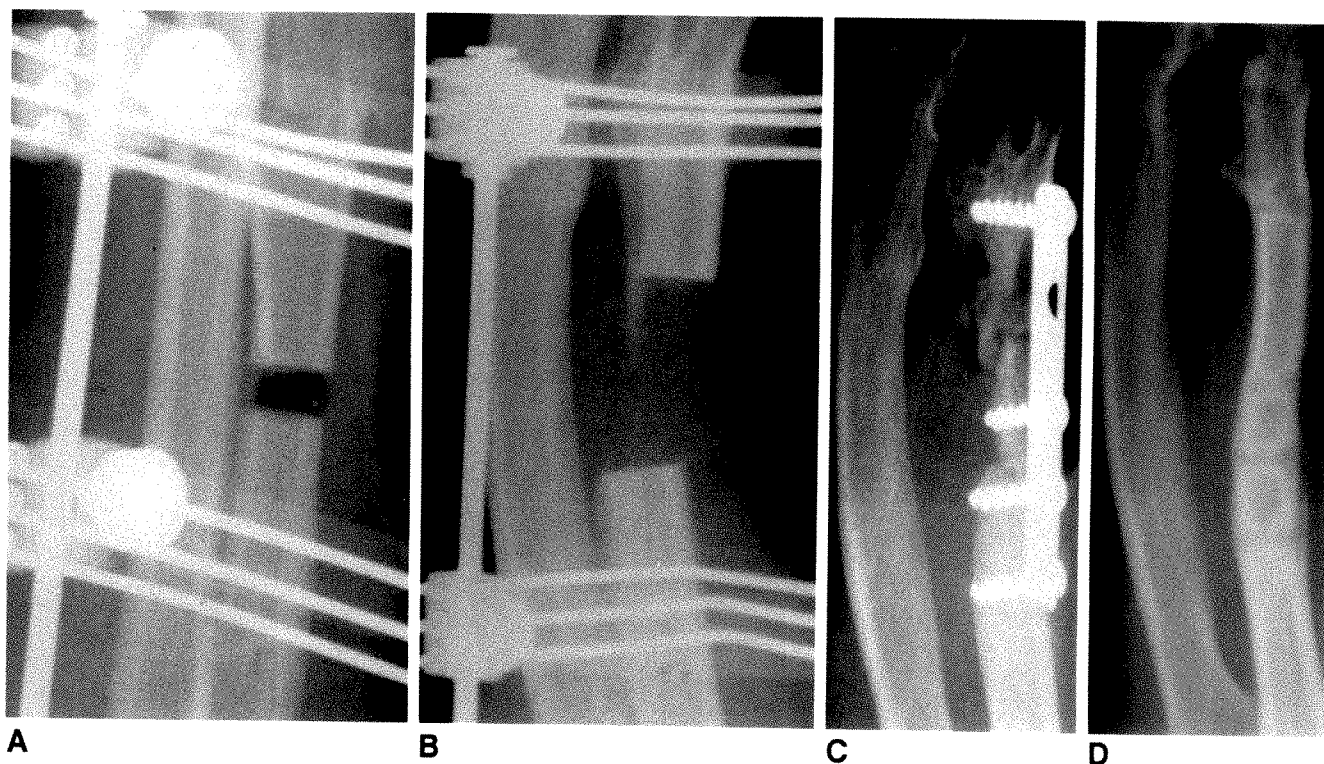


Fig. 2.—Serial radiographs show application of Wagner technique to lengthen a hypoplastic ulna.  
 A, Immediately after surgery, a 5-mm gap is present between cut bone ends.  
 B, 22 days after surgery, a 22-mm gap is present without significant new bone formation in distraction site.  
 C, 100 days after surgery, bone graft and plate have been placed across gap in a second operation.  
 D, 44 months after surgery, after incorporation of bone graft and cortical remodeling, metallic plate was removed in a third operation.

rupture or fracture. The goal is to preserve growth plate function. Total time for distraction is longer but the following period of corticalization is shorter. Physeal fracture and closure, however, may be unavoidable [3].

### Ilizarov Technique

Limb lengthening by the Ilizarov technique, also referred to as distraction osteogenesis, begins with a corticotomy, which is followed by controlled distraction. The corticotomy is usually performed through a small skin incision by using an osteotome to break the cortex along three quarters of the circumference. The remaining bone is fractured by twisting the osteotome (Fig. 4A). The goal of this procedure is to preserve the blood supply and the periosteum, allowing callus formation. Distraction typically begins 5–7 days after the corticotomy and proceeds at 0.25 mm every 6 hr (Fig. 4B). Callus formation is typically first seen approximately 28 days after corticotomy, appearing as well-formed columns of bone arising from each bone surface. A radiolucent central band initially separates the newly formed bone (Fig. 4C). When the lengthening goal is achieved, distraction is stopped, allowing new bone to bridge the gap. Remodeling of cortex and

medullary canal usually requires twice the distraction period (Figs. 4D–4F). Weightbearing is encouraged throughout treatment [1].

The versatility of the circular Ilizarov fixator can be exploited to decrease the duration of the lengthening procedure. This is accomplished by performing simultaneous distractions at separate sites on the same extremity (Fig. 5).

### Callotasis

Callotasis or callus distraction refers to a technique whereby limb lengthening is achieved through the slow distraction of callus formed in response to a submetaphyseal corticotomy. Distraction starts when callus formation is first observed on radiographs (usually between 10 and 15 days) and then proceeds at a rate of 0.25 mm every 6 hr. The rate of distraction is correlated closely with the radiologic progression of callus formation. If a radiolucent gap develops from excessive distraction, a short period of recompression is performed until callus continuity is reestablished. Distraction is continued until the desired length is obtained. The site is then maintained in rigid fixation until radiologic evidence of

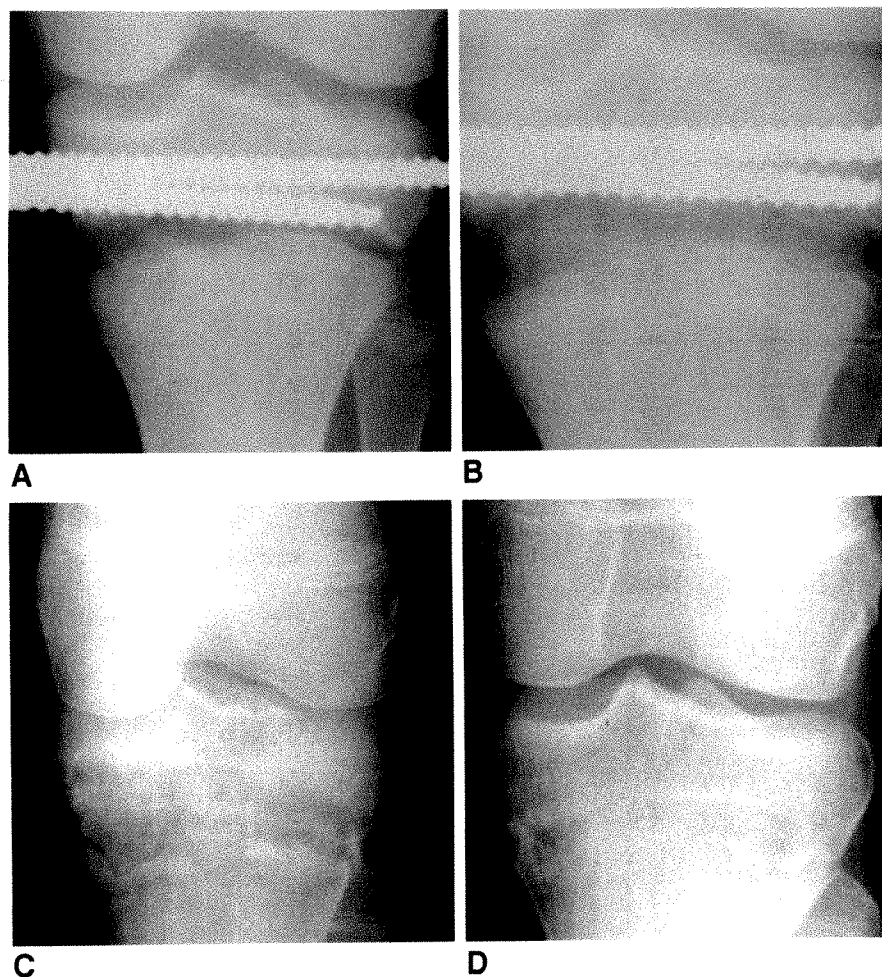


**Fig. 3.**—Sequential radiographs obtained during distraction epiphysiodesis performed across proximal tibial epiphysis.

**A**, 10 days after beginning of distraction, asymmetric gap was present measuring 10 mm medially without new bone formation.

**B**, 21 days after beginning of distraction, early new bone formation is visible in distraction site.

**C**, 71 days after beginning of distraction, pins were removed after development of cortical shell.

**D**, 410 days after beginning of distraction, good bone formation with fusion of tibial growth plate is visible.

adequate bone formation is observed. The use of dynamic axial loading helps promote corticalization [4].

### Complications and Comparisons

Although the reported rates of complications vary widely with these procedures, the potential complications are similar [1, 5, 6]. These include malalignment or angulation (Fig. 6), malunion (Fig. 7) or nonunion, infection (soft tissue and/or osseous), fracture (Fig. 8), joint deformity, pin osteolysis, and neurovascular problems.

Angulation at the distraction site is more problematic when a unilateral fixator is applied. These types of fixators do not provide the versatility inherent in the circular fixators, which provide three-dimensional control of the osseous structures. Circular fixators allow manipulation during distraction, which can correct for unwanted angulation or improve alignment in previously angulated bones.

Osteomyelitis is typically associated with fixators that use large pins and is almost unheard of with the smaller wires used with the Ilizarov fixator. Differentiating the radiologic

changes of osteomyelitis from the reactive changes due to the osteotomy or fixation device can be very difficult and may be possible only on subsequent radiographs.

Healing index, which refers to the number of days needed to gain 1 cm in length, is used to compare the duration of the different limb-lengthening procedures. The healing indexes for the Wagner, distraction epiphysiodesis, and callotasis techniques are similar, approximately 35–45 days. The healing time for distraction osteogenesis is typically around 30 days but can be reduced by performing bifocal lengthening with the Ilizarov fixator (Fig. 5) [1–5].

### Conclusion

The radiologist plays a critical role in the successful outcome of limb-lengthening procedures through the evaluation of serial radiographs and the early detection of complications. As more and more orthopedic surgeons begin to perform these highly specialized procedures, radiologists need to become familiar with the normal appearance of the most popular methods of limb lengthening and their inherent complications.



Fig. 4.—Ilizarov technique.

A, Immediately after ulnar corticotomy, irregular bone ends are without diastasis.

B, 11 days after corticotomy, a 5-mm gap is present with no new bone formation.

C, 32 days after corticotomy, early new bone formation is depicted as well-formed columns originating from bone ends with central lucency; gap is 26 mm.

D, 72 days after corticotomy, callus bridges distraction gap, allowing fixator removal.

E, 102 days after corticotomy, cortical remodeling continues with formation of medullary canal.

F, 529 days after corticotomy, a well-formed cortex and medullary canal are present.

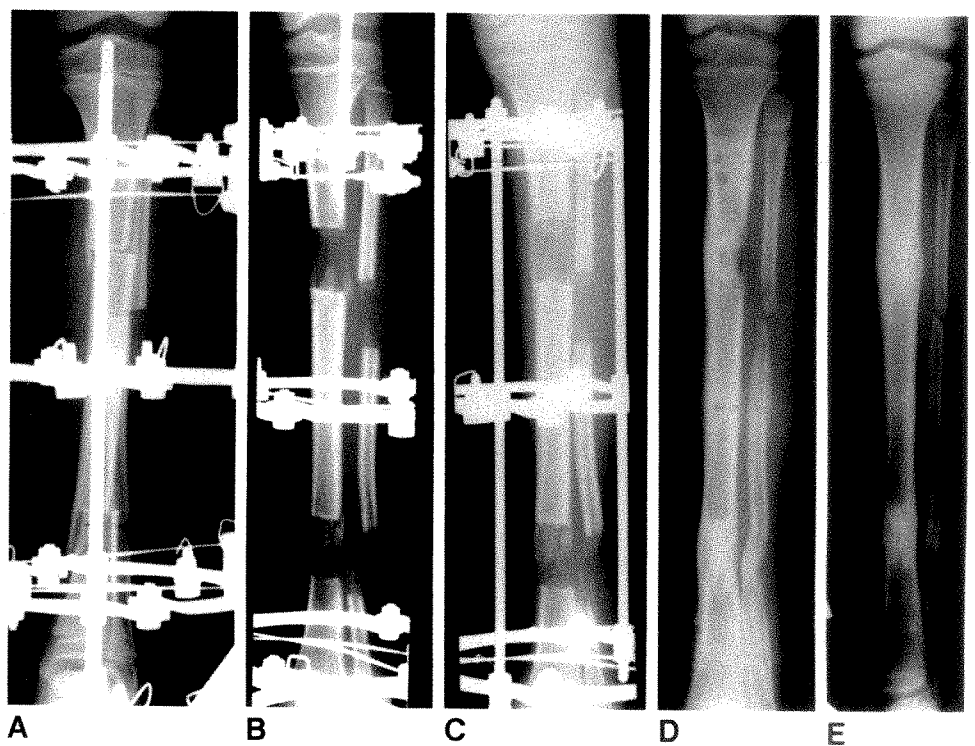
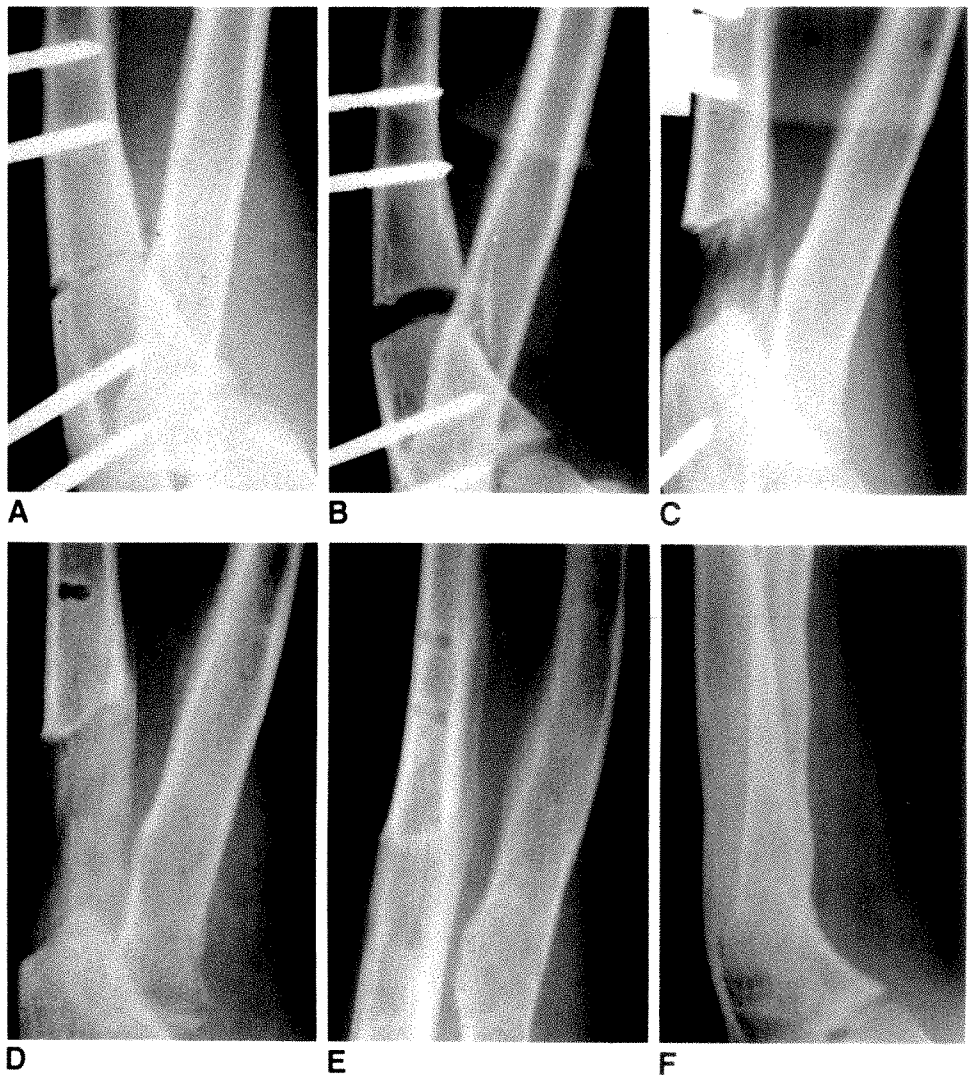


Fig. 5.—Bifocal tibial lengthening by using Ilizarov method and fixator to correct a 70-mm discrepancy in limb length that resulted from a neonatal infection.

A-E, Serial radiographs obtained immediately after surgery (A), 48 days later (B), 58 days later (C), 141 days later (D), and 254 days later (E) illustrate advantage of decreased procedure time when compared with other techniques that use solitary distraction sites.

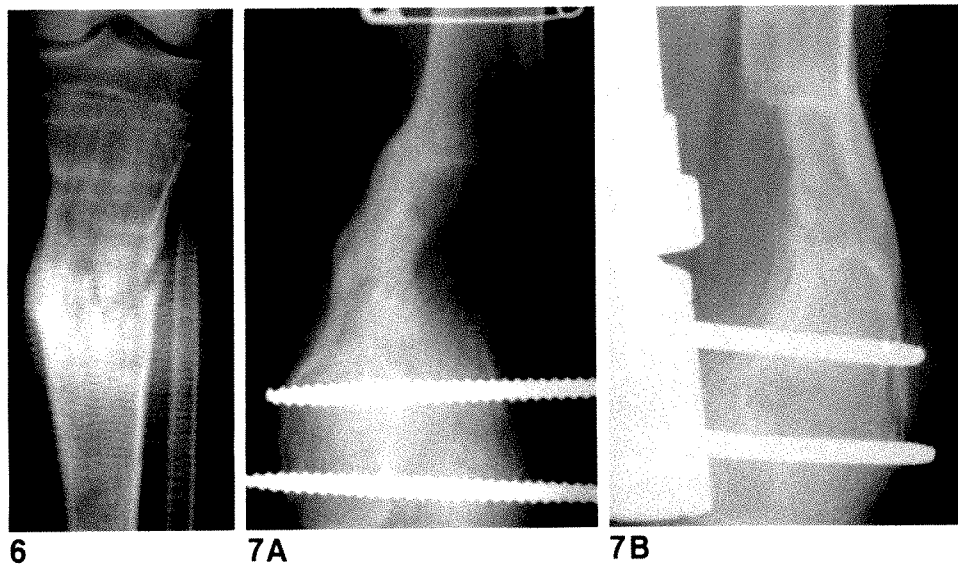


Fig. 6.—Radiograph obtained 191 days after distraction osteogenesis procedure involving proximal tibia shows loss of alignment with valgus angulation at distraction site due to cortical buckling after removal of external fixator.

Fig. 7.—A and B, Anteroposterior (A) and lateral (B) radiographs show inadequate bone formation along posterolateral aspect of distal femur during distraction osteogenesis. Also note posterior angulation of distal femur.

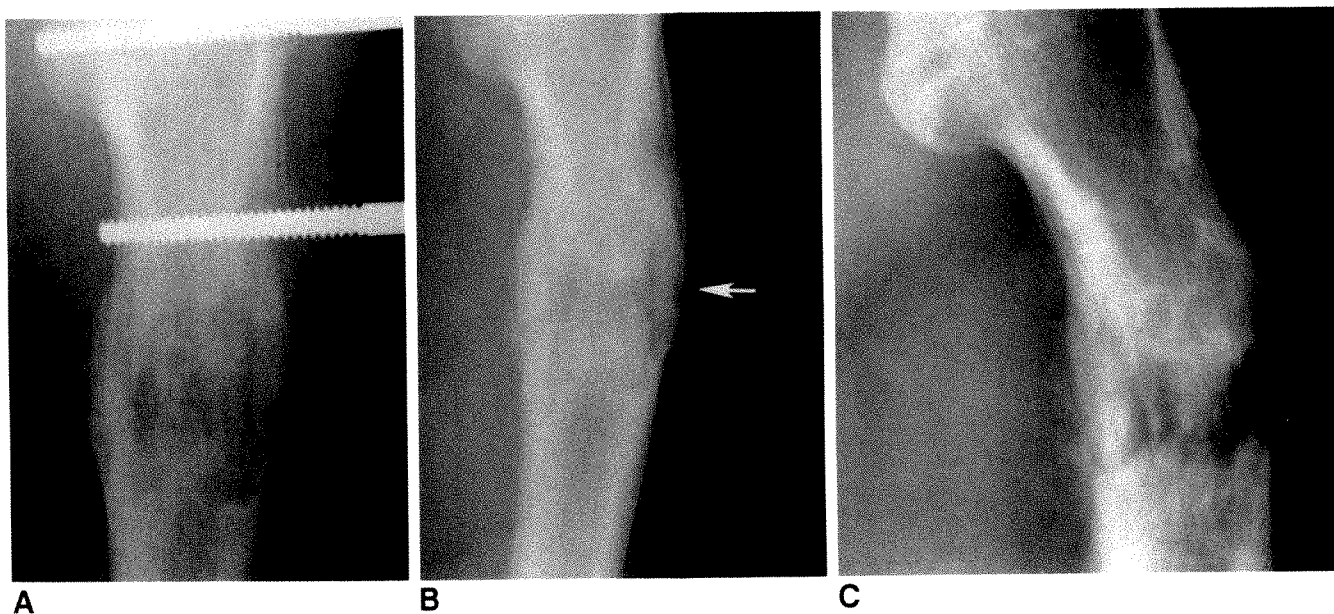


Fig. 8.—A–C, Serial anteroposterior radiographs before (A), and after (B, C) fixator removal. A subtle fracture (arrow) with slight varus angulation is present on first radiograph obtained after fixator removal (B). This was not recognized, and marked varus angulation developed (C).

#### REFERENCES

1. Paley D. Current techniques of limb lengthening. *J Pediatr Orthop* 1988;8:73–92
2. Monticelli G, Spinelli R. Limb lengthening by epiphyseal distraction. *Int Orthop* 1981;5:85–90
3. De Bastiani G, Aldegheri R, Renzi-Brivio L, Trivella G. Chondrodiastasis: controlled symmetrical distraction of the epiphyseal plate. *J Bone Joint Surg [Am]* 1986;68-A:550–556
4. De Bastiani G, Aldegheri R, Renzi-Brivio L, Trivella G. Limb lengthening by callus distraction (callotaxis). *J Pediatr Orthop* 1987;7:129–134
5. Dal Monte A, Donzelli O. Comparison of different methods of leg lengthening. *J Pediatr Orthop* 1988;8:62–66
6. Vade A, Eissenstat R. Radiographic features of bone-lengthening procedures. *Radiology* 1990;174:531–537

## Unilateral Hydrocephalus: Prenatal Sonographic Diagnosis

Randall M. Patten<sup>1,2</sup>  
 Laurence A. Mack<sup>1</sup>  
 Harris J. Finberg<sup>3</sup>

We studied six cases of unilateral hydrocephalus detected prenatally to analyze the sonographic features of the abnormality and to determine the cause and clinical outcome. In all cases, third-trimester sonograms showed marked unilateral lateral ventriculomegaly (mean atrial width, 4.4 cm) and normal contralateral lateral, third, and fourth ventricles. Five of the six cases had marked thinning of the cortical mantle on the affected side and shift of midline structures to the contralateral side. The causes of unilateral hydrocephalus were agenesis or stenosis of the foramen of Monro in three cases, transient obstruction of the foramen in one fetus with an intraventricular hematoma, underlying brain dysplasia in one fetus with a variant of holoprosencephaly, and undetermined in one case. All six neonates had placement of a ventriculoperitoneal shunt catheter; four of these have had normal cognitive development at follow-up. The remaining two infants have moderate to severe developmental impairment.

Unilateral hydrocephalus is a rare anomaly that can be recognized by prenatal sonography. Even though unilateral ventriculomegaly may be marked, early diagnosis and treatment may result in a favorable clinical outcome.

*AJR* 156:359-363, February 1991

Congenital hydrocephalus and ventriculomegaly can be diagnosed reliably with prenatal sonography. The prevalence (estimated to be between 0.5 and 1.8 per 1000 live births), the variable cause, the association with other CNS and extracranial abnormalities, and the relatively poor prognosis for congenital hydrocephalus have been well described. Because unilateral hydrocephalus is extremely uncommon, ventriculomegaly usually is assumed to be bilateral and symmetric, even if the near-field ventricle is obscured by artifact. However, the entity of unilateral hydrocephalus does exist and rarely may be diagnosed by prenatal sonography. Review of the literature revealed only two case reports documenting the prenatal sonographic diagnosis of unilateral hydrocephalus [1, 2]. We discuss the sonographic findings, causes, and clinical outcomes in a series of six fetuses with the prenatal diagnosis of unilateral hydrocephalus.

### Materials and Methods

We retrospectively reviewed maternal and infant medical records, prenatal sonograms, and postnatal diagnostic studies in six cases of unilateral hydrocephalus seen at two centers for high-risk obstetric sonography during a 4-year period. All fetuses in which prenatal sonography showed selective dilatation of one lateral ventricle (atrial diameter greater than 1.0 cm) and normal width of the contralateral, third, and fourth ventricles were identified. Cases of asymmetric but bilateral lateral ventriculomegaly were excluded from the study population.

The population of patients included three male and three female fetuses. Four cases were referred for evaluation after questionable ventriculomegaly was seen on sonograms at outside institutions; pregnancy-induced hypertension and gestational diabetes prompted referrals in one case each. Maternal age was 18-35 years (means, 25 years). Two of the mothers were primigravidas; the other four were multigravidas.

Received July 12, 1990; accepted after revision August 30, 1990.

Presented at the annual meeting of the American Roentgen Ray Society, Washington, DC, May 1990.

<sup>1</sup> Department of Radiology, SB-05, University of Washington Medical Center, 1959 N.E. Pacific St., Seattle, WA 98195.

<sup>2</sup> Present address: Rainier Medical Imaging Center, 11811 N.E. 128th, Kirkland, WA 98034. Address reprint requests to R. M. Patten.

<sup>3</sup> Phoenix Perinatal Associates, Edwards Medical Plaza, 1300 N. 12th St., Suite 320, Phoenix, AZ 85006.

0361-803X/91/1562-0359  
 © American Roentgen Ray Society



All sonograms were obtained with commercially available real-time sonographic scanners and 3.5- to 5.0-MHz electronically focused transducers. Fetal intracranial appearances were evaluated in both axial and coronal planes in all cases. Serial prenatal sonography was performed in four cases. All cases of unilateral hydrocephalus were confirmed after birth by CT, MR, sonography, ventriculography, or ventriculoscopy. Postnatal follow-up included chart review and telephone consultation with clinicians to assess outcome and prognosis.

## Results

Prenatal sonograms revealed moderate to marked unilateral ventriculomegaly in all cases. Maximal lateral ventricular atrial widths ranged from 2.0 to 6.2 cm (mean ventricular width, 4.4 cm); five (83%) of the six fetuses had moderate to severe thinning of cortex on the affected side (Fig. 1). Ventricular dilatation tended to be greatest in the region of the trigone and occipital horn in three cases (Fig. 2). Shift of midline structures to the contralateral side was seen in five cases (Fig. 3). After the detection of unilateral ventriculomegaly, serial sonograms showed that the degree of ventricular dilatation remained stable during 5- to 9-week follow-ups in three of four fetuses. In the fourth fetus, serial scans between 28 and 33 menstrual weeks showed progressive unilateral ventriculomegaly and inappropriately increasing fetal head circumference.

All cases were diagnosed in the third trimester. At the time of diagnosis, mean menstrual age was 32.8 weeks (range, 28.5–36.0 weeks). In two cases, intracranial appearances were normal at 9 and 18 menstrual weeks, respectively. In another case, the fetus was sonographically normal when scanned at 33.5 weeks. However, because of severe maternal hypertension and the onset of premature labor, sonography was repeated 2 days later. At that time, fetal intraventricular hemorrhage and unilateral ventriculomegaly were seen (Fig. 4).

No extracranial abnormalities were detected by prenatal sonography in any of the fetuses; none were found at birth. In one fetus, sonography showed additional cranial abnormalities, suggesting a complex dysplasia or variant of holoprosencephaly (Fig. 5). Fetal karyotype was normal in this case and in the two other cases in which chromosomal analysis was performed.

## Cause

In three cases, ventriculography or ventriculoscopy confirmed that the cause of unilateral hydrocephalus was either complete agenesis or severe stenosis of the foramen of Monro (Fig. 6). In one of these cases, marked cortical thinning, poor definition of the lateral ventricular wall, and lack of significant midline shift on sonography initially had suggested massive porencephaly from an in utero vascular accident. However, the findings of progressive ventriculomegaly and an enlarging head circumference in the neonatal period prompted both diagnostic reevaluation and therapeutic placement of a ventriculoperitoneal shunt catheter. Endoscopic assessment at the time of surgery showed that the choroid plexus entered blindly into an area where the foramen of Monro was closed completely.

In one case, unilateral ventriculomegaly was caused by an intraventricular thrombus that partially obstructed the foramen of Monro; underlying brain dysplasia was the cause in the fifth case. In the final case, the cause of unilateral hydrocephalus was not clearly established.

## Clinical Outcome

The prenatal detection of unilateral hydrocephalus altered the method of delivery in only two cases. To reduce the risk of cranial trauma during labor, one infant was delivered elec-

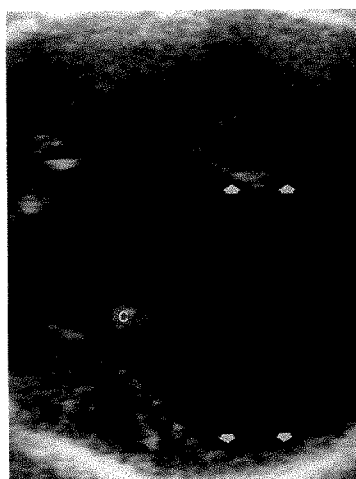


Fig. 1.—Axial prenatal sonogram at level of choroid plexus (C) in a 35-week-old fetus shows massive dilatation of dependent lateral ventricle (ventricular width marked by arrows).

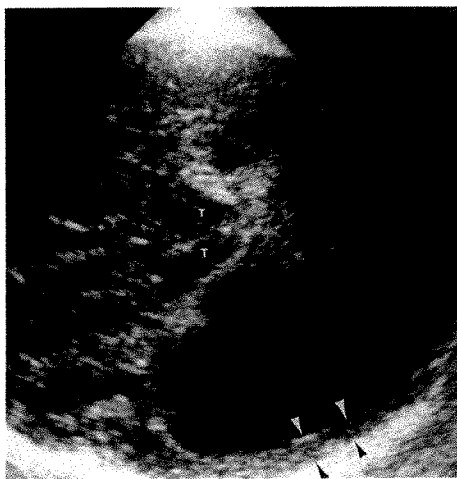


Fig. 2.—Sonogram of 34-week-old fetus shows unilateral ventricular dilatation to be greatest in occipital horn and atrium. Note thin residual cortical mantle (arrowheads). T = thalami.

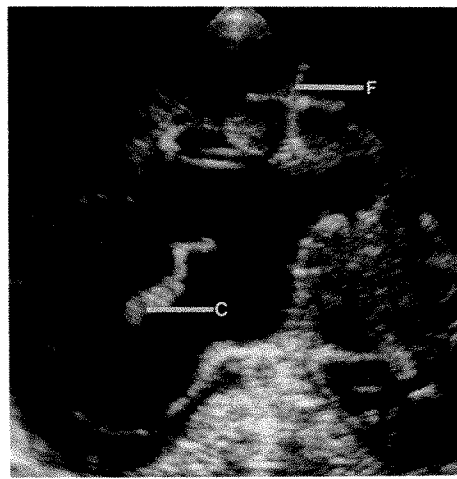


Fig. 3.—Neonatal cranial sonogram in coronal plane in a 2-day-old neonate confirms unilateral dilatation of right lateral ventricle and shows slight leftward shift of medial right ventricular wall. F = interhemispheric fissure, C = choroid plexus.

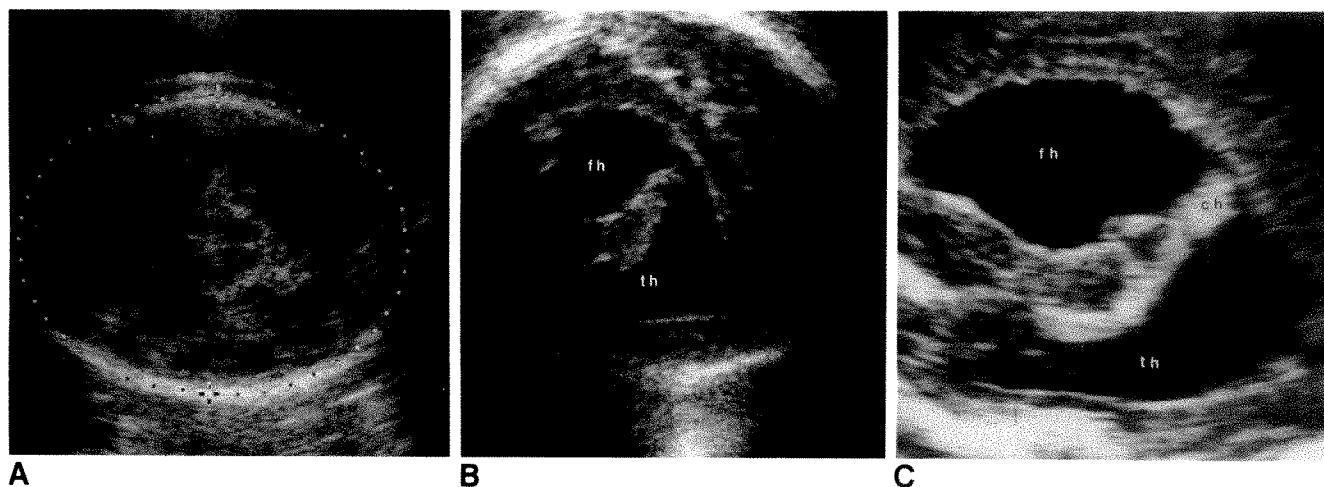


Fig. 4.—A, Sonogram of 33.5-week-old fetus shows normal intracranial appearances (cranial circumference outlined). B, Sonogram obtained 2 days later shows unilateral hydrocephalus. Intraventricular thrombus was seen on other images. C, Neonatal cranial sonogram in sagittal plane confirms unilateral lateral ventriculomegaly. fh = frontal horn, th = temporal horn, ch = choroid plexus. (B has been reoriented to correspond to neonatal sonogram.)

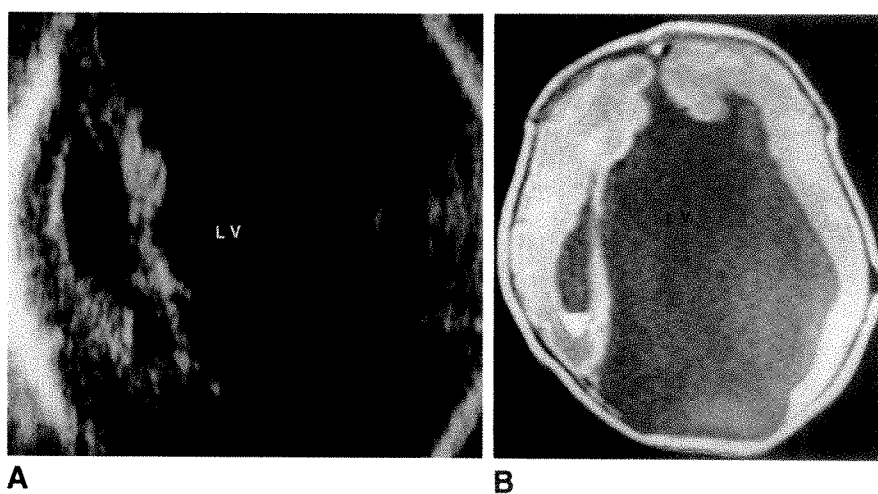


Fig. 5.—Brain dysplasia—probable variant of holoprosencephaly.

A and B, Prenatal sonogram (A) and postnatal T1-weighted cranial MR image, 600/20 (B), show irregular enlargement of left lateral ventricle (LV) associated with ipsilateral thinning of cortical mantle and contralateral midline shift. Fusion of thalami was seen at a more caudal level. (A has been reoriented to correspond to axial MR image.)

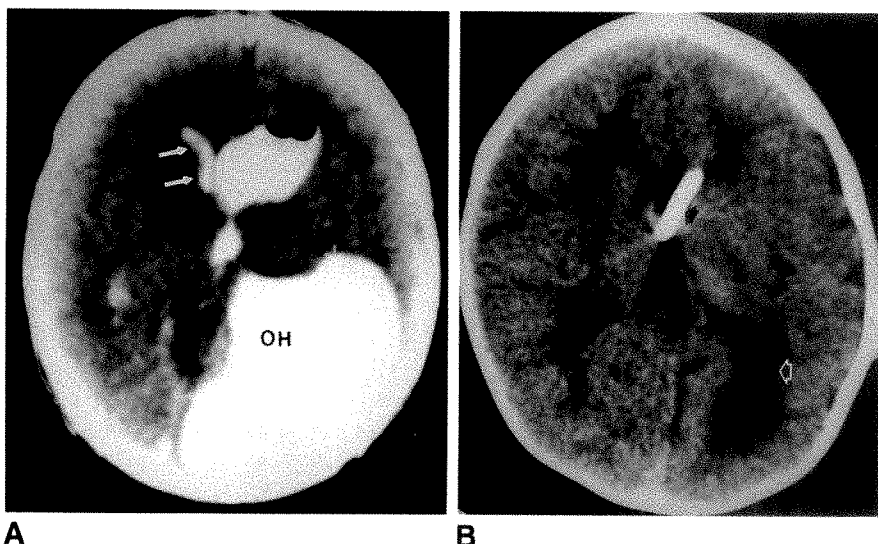


Fig. 6.—Severe stenosis of left foramen of Monro.

A, CT ventriculogram in 3-day-old neonate shows marked unilateral hydrocephalus, preferentially involving atrium and occipital horn (OH). Delayed appearance of a small amount of contrast medium within nondilated right lateral ventricle (arrows) confirmed interventricular communication.

B, CT scan after placement of a ventriculo-peritoneal shunt (solid arrow) shows minimal residual dilatation of left occipital horn (open arrow).

tively by cesarean section at 37 weeks after amniocentesis showed a mature lung profile. A second infant, with rapidly progressive unilateral ventriculomegaly, was delivered surgically at 33 weeks to facilitate neurosurgical care and to prevent possible birth dystocia from cranial enlargement.

Emergent cesarean section was performed in two patients for indications unrelated to the intracranial findings. One infant was delivered emergently at 34 weeks because of severe pregnancy-induced hypertension and intrauterine growth retardation; another was delivered surgically at term because of suspected placental abruption during labor. The two remaining infants were delivered vaginally at term. Mean age at delivery for the six infants was 37.2 menstrual weeks (range, 33–40 weeks). There were no prenatal or neonatal deaths.

All six neonates required ventriculoperitoneal shunt procedures in the first 3 months of life. Three of these six infants have reached appropriate developmental milestones at follow-up intervals ranging from 8 months to 2 years; an additional infant has normal mental development but mild left hemiparesis and motor delay, a result of prenatal intraventricular hemorrhage. Two of these infants have had follow-up CT studies; both showed almost complete decompression of ventriculomegaly and recovery of brain parenchymal thickness (Fig. 6B). Two remaining infants have moderate and severe developmental disabilities, respectively. The infant with brain dysplasia has a seizure disorder, mild hemiparesis, and mild to moderate developmental delay at 12 months of age. The infant with atresia of the foramen of Monro and massive porencephaly has an intractable seizure disorder, a markedly abnormal neurologic examination at 18 months, severe developmental delay, and a poor clinical prognosis.

## Discussion

Unilateral hydrocephalus is an uncommon entity, first reported by vonMohr in 1842 (cited in [3]). As of 1989, only 10 cases had been diagnosed within the first 2 months of life [2], and the prenatal sonographic detection of unilateral hydrocephalus had been documented in only two case reports [1, 2]. Nevertheless, early detection and treatment of this anomaly are stressed as important factors in limiting the extent of brain parenchymal damage [4].

Prenatal detection of unilateral hydrocephalus is difficult because common sonographic artifacts may obscure fetal intracranial detail, and in some cases may simulate the findings of unilateral hydrocephalus in either the normal or abnormal fetus. For example, the anechoicity of the normal developing cortical mantle in the dependent cerebral hemisphere frequently may suggest unilateral ventricular enlargement if the lateral ventricular wall is not delineated [5]. Conversely, in cases of congenital bilateral hydrocephalus, calvarial reverberation artifact and sonographic noise may prevent optimal examination of a dilated ventricle in the near field and suggest that the dependent ventricle is unilaterally enlarged [6]. Scanning the fetal cranium in both axial and coronal planes with properly focused high-resolution sonographic transducers and giving careful attention to scanning technique therefore are important to prevent diagnostic errors.

In all six cases in the current series, establishing the diagnosis of unilateral hydrocephalus was facilitated by scanning the fetal cranium in multiple anatomic planes to identify the normal contralateral lateral ventricle and to visualize the normal third and fourth ventricles. All cases were identified in the third trimester, when sonographic findings included moderate to marked unilateral ventriculomegaly. Such unilateral ventricular enlargement was associated with significant cortical thinning of the affected hemisphere and contralateral shift of midline structures in 83% of cases. Although these findings suggested increased intraventricular pressure, ventriculomegaly was progressive in utero in only one of four cases in which serial sonograms were obtained.

Thomas [7] in 1914 and Dandy [8] in 1919 experimentally produced unilateral hydrocephalus in animals by occluding one foramen of Monro, and abnormalities at or about this CSF pathway are cited as the major cause of both congenital and acquired forms of the anomaly [3]. Most reported cases of unilateral hydrocephalus are seen later in life, a result of obstruction of the foramen of Monro from inflammatory adhesions, ventriculitis, subependymal gliosis, membranous occlusions, and pedunculated tumors. Complete agenesis of the foramen of Monro is rare, and unilateral hydrocephalus may occur despite a patent foramen. In the current series of congenital lesions, three cases were attributed to atresia or severe stenosis of the foramen of Monro; one case resulted from transient obstruction of the foramen from intraventricular hemorrhage; and one case, in which ventriculography showed a patent foramen of Monro, was apparently the result of brain dysplasia.

In contrast to the 15–28% survival rates of fetuses and infants with congenital bilateral hydrocephalus [9, 10], all fetuses with unilateral hydrocephalus in our series survived the neonatal period. Undoubtedly, the improved survival in this population was related to the lack of iatrogenic intervention (i.e., termination or intrapartum cephalocentesis) and to the absence of significant associated life-threatening extracranial anomalies. Up to 84% of fetuses with congenital bilateral hydrocephalus have concurrent major CNS or extra-CNS anomalies [11, 12]; however, no extracranial abnormalities were found in the six fetuses with unilateral hydrocephalus.

The prenatal detection of unilateral hydrocephalus does not necessarily require emergent surgical intervention, but it should prompt careful sonographic examination to discover the potential cause of unilateral ventricular enlargement and to screen for possible additional anomalies. If unilateral hydrocephalus is an isolated finding, most authors advocate serial assessment by sonography and delay of delivery until full lung maturation has occurred [2]. Electively choosing the time, mode, and place of delivery may improve fetal prognosis. Sonographic demonstration of progressive increase in ventricular size, progressive thinning of the cortical mantle, and abnormally rapid intracranial growth might prompt more aggressive management.

After birth, all neonates had aggressive neurosurgical work-ups, and all required ventriculoperitoneal shunt procedures within the first 3 months. The degrees of ventriculomegaly



and thinning of the cortical mantle were moderate to marked in five of six fetuses, yet three of these five patients are considered developmentally normal at follow-up. Another infant with intraventricular hemorrhage in utero who had only mild unilateral ventriculomegaly has mild physical impairment but normal cognitive development. Thinning of the cortical mantle is known to correlate poorly with subsequent intelligence, and normal and even superior intelligence has been reported for some infants with hydrocephalus and aggressive neurosurgical care [11, 13], so such a favorable clinical outcome may not be surprising; however, such statistics contrast dramatically with studies of infants with bilateral congenital hydrocephalus, in which only 21–43% of the survivors develop normally [11, 14]. Final conclusions on the outcome in infants with unilateral hydrocephalus, of course, will require long-term follow-up.

On the basis of our small series and limited follow-up, we think that unilateral hydrocephalus is an entity separate from bilateral hydrocephalus, with reduced risk of perinatal death, fewer associated CNS or extra-CNS anomalies, and improved prognostic implications. Although unilateral ventriculomegaly may be marked, early diagnosis and treatment may result in a favorable clinical outcome. Awareness of this rare entity therefore is important to provide information and guidance to the referring clinician and family. Multiplanar scanning and attention to scanning technique are also important to facilitate the diagnosis of unilateral hydrocephalus and to prevent confusion caused by sonographic artifacts.

## REFERENCES

1. Hartnung RW, Yiu-Chiu V. Demonstration of unilateral hydrocephalus in utero. *J Ultrasound Med* 1983;2:369–371
2. Gaston BM, Jones BE. Perinatal unilateral hydrocephalus: atresia of the foramen of Monro. *Pediatr Radiol* 1989;19:328–329
3. Oi S, Matsumoto S. Pathophysiology of nonneoplastic obstruction of the foramen of Monro and progressive unilateral hydrocephalus. *Neurosurgery* 1985;17:891–896
4. Blatt ES, Berkmen YM. Congenital occlusion of the foramen of Monro. *Radiology* 1969;92:1061–1064
5. Reuter KL, D'Orsi DJ, Raptopoulos VD, Barber FE, Moss LG. Sonographic pseudoasymmetry of the prenatal cerebral hemispheres. *J Ultrasound Med* 1981;1:91–95
6. Schoenecker SA, Pretorius DH, Manco-Johnson ML. Artifacts seen commonly on ultrasonography of the fetal cranium. *J Reprod Med* 1985;30:541–544
7. Thomas WS. Experimental hydrocephalus. *J Exp Med* 1914;19:106–120
8. Dandy WE. Experimental hydrocephalus. *Ann Surg* 1919;70:129–142
9. Chervenak FA, Berkowitz RL, Tortora M, Hobbins JC. The management of fetal hydrocephalus. *Am J Obstet Gynecol* 1985;151:933–942
10. Pretorius DH, Davis K, Manco-Johnson ML, Manchester D, Meier PR, Clewell WH. Clinical course of fetal hydrocephalus: 40 cases. *AJR* 1985;144:827–831
11. Chervenak FA, Duncan C, Ment LR, et al. Outcome of fetal ventriculomegaly. *Lancet* 1984;2:179–181
12. Nyberg DA, Mack LA, Hirsch J, Pagon RO, Shepard TH. Fetal hydrocephalus: sonographic detection and clinical significance of associated anomalies. *Radiology* 1987;163:187–191
13. Lorber J. The results of early treatment of extreme hydrocephalus. *Dev Med Child Neurol [Suppl]* 1968;16:21–26
14. Cochrane DD, Myles ST, Nimrod C, Still DK, Sugarman RG, Wittman BK. Intrauterine hydrocephalus and ventriculomegaly: associated anomalies and fetal outcome. *Can J Neurol Sci* 1985;12:51–59

## Book Review

**Pocket Atlas of Pediatric Ultrasound.** By Carol M. Rumack, J. Gerard Horgan, Thomas C. Hay, and Deborah Kindsfater. New York: Raven, 118 pp., 1990. \$14.95

This book has two rare advantages: It is an excellent outline of normal anatomy of the child, and it really does slip into a normalized pocket. Each pair of facing pages contains three images. The left-hand page has a sonographic image and a small drawing of how and where the sonographic probe was placed in order to obtain the image. The right-hand page has a detailed drawing that closely simulates the sonogram and contains labels of the important anatomic landmarks seen on the sonogram. The concept is kept simple so that comparison between image and drawing can be done at a glance.

The brain, abdomen, hip, testis, and spine thus are outlined. The quality of sonograms and drawings is excellent. Typical features of the infant's anatomy (e.g., prominent adrenal glands, hyperechoic

renal cortex) are included, as well as a few pitfalls of sonography (e.g., reverberation echoes and their resultant images).

This is an excellent guide for the physician or technician who is not completely accustomed to pediatric sonography. I must admit that I slipped it into my laboratory coat pocket before performing a hip examination of an infant in front of a group of new residents. Alas, after the examination, the book was gone . . . into the pocket of a future pediatric sonographer?

Heidi Patriquin  
Hôpital Sainte-Justine  
Université de Montréal  
Montreal, Quebec, Canada H3T 1C5

## Case Report

# Occult Ectopic Ureter in Girls with Urinary Incontinence: Diagnosis by Using CT

Richard M. Braverman<sup>1</sup> and Robert L. Lebowitz

Girls with no other signs or symptoms but continuous dribbling of urine, despite successful toilet training, should be considered to have a ureter with an extravesical, infrasphincteric orifice. Usually, the ureter with an ectopic orifice drains the upper moiety of a double collecting system. Excretory urography is the imaging method of choice for confirmation, and it is usually diagnostic of both the condition and the affected side or sides. The two girls reported here had a provocative history but had normal findings on excretory urograms. Enhanced CT was then used to show the suspected poorly functioning upper moiety in each. Subsequent surgery resulted in complete relief of dribbling of urine.

### Case Report

A 9-year-old girl had a constantly wet perineum despite successful toilet training. Ectopia of the ureteral orifice draining the upper moiety of a duplex kidney was strongly suspected, and imaging was done to confirm this and to determine the side of the abnormality. Findings on excretory urography (EU) were normal, as were sonographic findings. Results of voiding cystourethrography (VCUG) also were negative.

Enhanced CT of the kidneys with contiguous 1-cm sections was performed to visualize the renal duplication strongly suggested by her history. The examination showed a small medially located left-upper-pole unit drained by a slightly dilated ureter (Figs. 1A and 1B).

Careful inspection of the vagina and perineum with the patient under general anesthesia failed to reveal the ectopic ureteral orifice. Left-upper-pole nephrectomy and partial ureterectomy were performed and her incontinence ceased.

### Discussion

Wetting is an exceedingly common pediatric complaint, and most children with urinary incontinence have no underlying structural abnormality. Their physical examination is normal, and their wetting is usually nocturnal. It is apparently due to immaturity of bladder and urethral sphincter function, is commonly hereditary, and is typically outgrown [1, 2]. Imaging is not recommended.

Anatomic abnormalities causing incontinence of urine include spinal dysraphism, sacral agenesis, and epispadias [3].

Such conditions are usually evident on careful physical examination of the back, perineum, and lower extremities. Plain films may show spinal anomalies or, in epispadias, an abnormal (>10 mm) interpubic distance.

In girls who are otherwise well and whose history is that of continuous wetting, day and night, despite successful toilet training, for as long as anyone can remember, an extravesical infrasphincteric ectopic ureteral orifice should be strongly suspected and imaging should be vigorously pursued. Ureteral ectopia with incontinence is uniquely female, because the most caudal location for an ectopic ureteral orifice in a male is always above the urethral sphincter.

Ectopia of the ureteral orifice is often associated with dysplasia of the kidney or of that portion of the kidney drained by the ectopic ureter. As a rule, the more ectopic the orifice the worse will be the dysplasia [4]. Thus, an infrasphincteric and therefore incontinent orifice often serves a very dysplastic unit; this dysplasia hinders radiologic detection. Excretory urography is the appropriate first study when ectopia is suspected and usually shows the abnormality. We commonly add nephrotomography to maximize our diagnostic sensitivity. Imaging, whether by urography, sonography, or CT, may be diagnostic by actually revealing the ectopic ureter coursing through the low pelvis to its infrasphincteric orifice. We believe, however, that the primary role of imaging is not to show the ectopic ureter itself, which is diagnosed by inference, but is to show directly or indirectly the abnormal moiety or kidney drained by the ectopic ureter.

When the ectopic ureter drains a kidney with a single collecting system (by far the minority of cases of ureteral ectopia) [5], urography and sonography often show the abnormal kidney easily. However, when the kidney is small, functions poorly, or is abnormally located, excretory urography and sonography may fail to detect it [6]. A solitary kidney may be incorrectly diagnosed in such girls, and their incontinence is not explained. CT has been used to detect the small, dysplastic, poorly functioning unit responsible for the wetting [7, 8].

In nearly all cases, excretory urography can be used to

Received July 11, 1990; accepted after revision September 12, 1990.

<sup>1</sup> Both authors: Department of Radiology, Children's Hospital and Harvard Medical School, 300 Longwood Ave., Boston, MA 02115. Address reprint requests to R. L. Lebowitz.

AJR 156:365-366, February 1991 0361-803X/91/1562-0365 © American Roentgen Ray Society



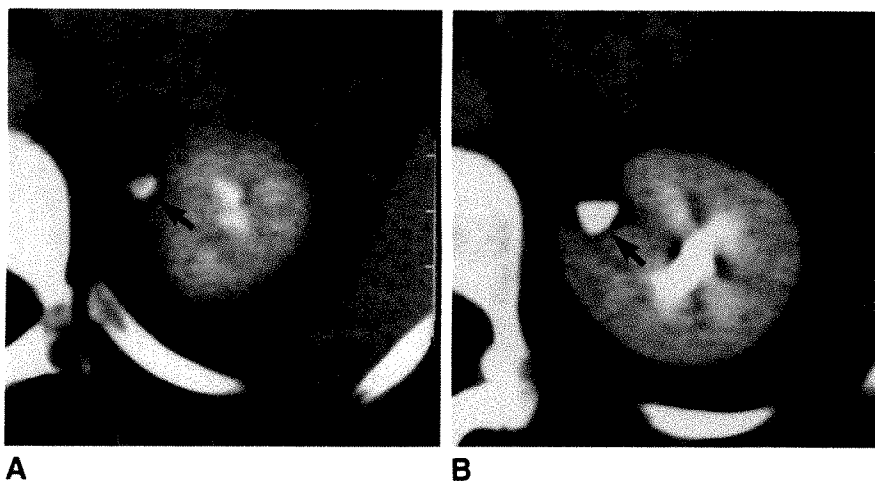


Fig. 1.—A and B, Enhanced CT scans show a medially located left-upper-pole ureter (arrows). Findings on excretory urogram and sonogram were normal.

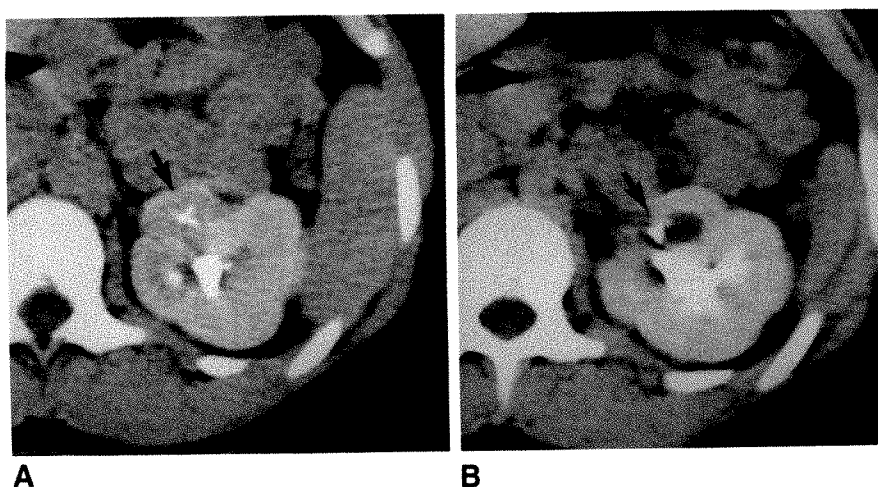


Fig. 2.—A and B, Enhanced CT scans show an anteriorly located left-upper-pole moiety (arrows). This 10-year-old girl with continuous dribbling of urine had had a normal urogram at age 5 and a normal urogram and sonogram at age 10.

detect ureteral duplication with upper-pole ureteral ectopia even when considerable dysplasia is present. Sonography may be diagnostic also. We have needed to perform CT for diagnosis of this entity in only two cases.

The urographic signs of renal duplication are well described. They include direct visualization of the offending upper moiety and its proximal ureter on excretory urography or sonography and indirect signs on excretory urography due to the effects of the upper-pole ureter on its lower-pole mate. Specifically, because the upper-pole ureter usually lies medial to the lower unit, the calices and ureter of the latter are displaced laterally and lie slightly farther from the spine than do those on the normal opposite side. In rare instances, even though the upper moiety makes enough urine to cause wetting, it is so small, so dysplastic, so poorly functioning, or so positioned that it escapes detection by urography.

In the case described earlier, it was the smallness of the upper moiety that hampered its urographic detection. In the only other patient in whom we used CT, the study showed a left duplex kidney with a tiny upper moiety lying anterior (and not medial) to the lower pole of the kidney (Figs. 2A and 2B). The anterior position of the dysplastic moiety negated the usual indirect urographic signs.

In summary, girls with continuous wetting should be considered to have an ectopic ureteral orifice until proved otherwise. Excretory urography with tomography is indicated to confirm the suspicion and to show the side or sides of

involvement. In most cases, excretory urography will be diagnostic. However, when the history is highly suggestive and the urographic findings seem normal, enhanced CT may show the abnormality, which is almost certainly present.

#### ACKNOWLEDGMENTS

N. Thorne Griscom made many helpful suggestions, and Donald Sucher prepared the illustrations.

#### REFERENCES

1. Perlmutter AD. Enuresis. In: Kelalis PP, King LR, Belman AB, eds. *Clinical pediatric urology*, 2nd ed. Philadelphia: Saunders, 1985:311-325
2. Smith DE. Diagnosis and management of the child with wetting. *Aust Paediatr J* 1967;3:193-205
3. Stannard MW, Lebowitz RL. Urography in the child who wets. *AJR* 1978;130:959-962
4. Mackie GG, Stephens FD. Duplex kidneys: a correlation of renal dysplasia with position of the ureteral orifice. *J Urol* 1975;114:274-280
5. Mandell J, Bauer SB, Colodny AH, Lebowitz RL, Retik AB. Ureteral ectopia in infants and children. *J Urol* 1981;126:219-222
6. Prewitt LH, Lebowitz RL. The single ectopic ureter. *AJR* 1976;127:941-948
7. Utsunomiya M, Itoh H, Yoshioka T, Okuyama A, Itatani H. Renal dysplasia with a single vaginal ectopic ureter: the role of computerized tomography. *J Urol* 1984;132:98-100
8. Korogi Y, Takahashi M, Fujimura N, Terasaki H, Ueno F. Computed tomography demonstration of renal dysplasia with a vaginal ectopic ureter. *CT* 1986;10:273-275

## Technical Note

# Limited-Slice CT in the Evaluation of Paranasal Sinus Disease in Children

George W. Gross,<sup>1,2</sup> Stephen J. McGeady,<sup>3,4</sup> Tim Kerut,<sup>3,4</sup> and Sandra M. Ehrlich<sup>1</sup>

Assessment of the status of the paranasal sinuses is important in the management of childhood sinusitis, which may occur as an isolated abnormality or as a concurrent finding and possible precipitating cause of recurrent episodes of asthma in children [1]. Conventional radiography, which has been the traditional method of imaging the paranasal sinuses in both children and adults, is generally less reliable in accurately evaluating the paranasal sinuses in children [2]. Although CT provides superior definition of both intrasinus disease and sinus bony margins, a complete CT examination has the disadvantages of higher cost and radiation dose compared with conventional sinus radiography.

To determine whether a substantial reduction in radiation dose is possible without significant loss of diagnostic accuracy, we compared "limited-slice" (e.g., maximum of four slices per examination) CT examinations with the corresponding complete CT examinations of the sinuses. Reducing overall radiation dose without loss of diagnostic accuracy could justify the use of CT in children for imaging the sinuses.

### Materials and Methods

Four diagnostic radiologists each interpreted coronal and axial CT examinations of the sinuses in 10 children with asthma. Initial review was of a limited (three- or four-slice) CT format, in which the slices preselected from a preliminary CT topogram were reviewed. Each complete examination, with all imaging slices included, was reviewed

separately by all radiologists. Both reviews consisted of evaluating intrasinus disease and any associated bony abnormality.

All studies were performed without contrast enhancement on a GE 9800 (16 cases) or Technicare HPS (four cases) CT scanner. The 20 examinations consisted of 5-mm-thick contiguous slices encompassing all paranasal sinuses in their entirety. Limits of imaging were determined from a preliminary lateral CT topogram. The number of slices per examination ranged from 11 to 21 (mean, 16); all slices were photographed and displayed in both soft-tissue and bony window formats.

For each complete examination, the lateral topographic image alone was viewed initially, and three or four slice levels were selected as follows: coronal images—slices chosen encompassed the estimated midpoint of each of the paired frontal, ethmoidal, maxillary, and sphenoidal sinuses; axial images—slices chosen passed through the midpoint of the ethmoidal, maxillary, and sphenoidal sinuses and through the lower third of the frontal sinuses (Fig. 1). When a single slice for either an axial or a coronal study was judged to encompass adequately the midportion of two sinus pairs (e.g., ethmoidal and sphenoidal sinuses for axial studies) only three slices were chosen; otherwise, four selected slices were included.

In a blinded and random-order review of all 20 limited studies, the radiologists were asked to evaluate frontal, ethmoidal, maxillary, and sphenoidal sinuses individually (total of eight paranasal sinus areas) and categorize them as follows: (a) not imaged, (b) not developed, (c) accurate evaluation not possible, (d) normal in appearance, and (e) three categories of sinus disease: mild, moderate, and severe. The presence of an air/fluid level within a sinus or demonstration of associated bony disease also was noted.

Received April 16, 1990; accepted after revision July 10, 1990.

<sup>1</sup> Department of Radiology, Jefferson Medical College and Thomas Jefferson University Hospital, 111 S. 11th St., Philadelphia, PA 19107. Address reprint requests to G. W. Gross.

<sup>2</sup> Department of Radiology, Children's Rehabilitation Hospital, Philadelphia, PA 19107.

<sup>3</sup> Department of Pediatrics, Jefferson Medical College and Thomas Jefferson University Hospital, Philadelphia, PA 19107.

<sup>4</sup> Department of Pediatrics, Children's Rehabilitation Hospital, Philadelphia, PA 19107.

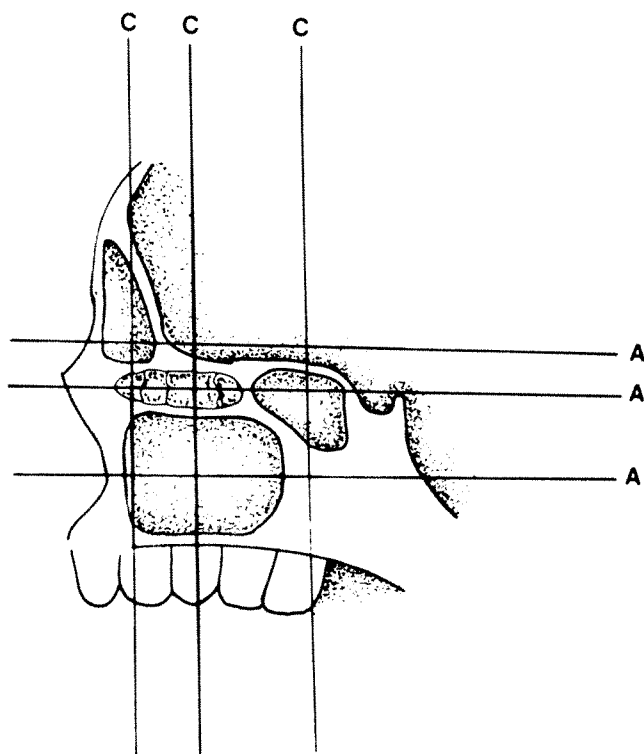


Fig. 1.—Diagram of paranasal sinuses, as viewed on lateral CT topographic image, shows location of suggested coronal (C) and axial (A) imaging planes for limited-slice paranasal sinus CT in children.

After a minimum 2-week interval, each radiologist reinterpreted all 20 CT studies in their complete form, without knowledge of the prior interpretation of the limited-slice studies. Results of the limited and complete examinations were compared with the complete CT examination, serving as the gold standard against which the limited examination was judged. Integral radiation doses for a three-film conventional radiographic examination, a complete CT examination, and a limited-slice CT examination were calculated.

## Results

The results are based on the evaluation of axial and coronal images of eight sinus regions (bilateral frontal, ethmoidal, maxillary, and sphenoidal) in 10 children. Comparison of limited- and complete-slice sinus CT studies yielded the following information.

### *Paranasal Sinus Development and Patterns of Disease*

Sinus disease involved the ethmoidal and maxillary sinuses most frequently, with less frequent involvement in the sphenoidal and frontal sinuses. Interpretations of "not developed" or "accurate evaluation not possible" were most often made regarding the frontal sinuses.

### *Comparison of Complete and Limited Sinus CT Examinations*

A 79% rate of agreement (range of 84% for sphenoidal and maxillary to 71% for frontal sinuses) is present between complete and limited CT evaluation of individual sinuses when any level of sinus disease is considered as a single option. In no instance did a limited study fail to image an individual sinus, and only a few studies (4%) were judged as "accurate evaluation not possible" when a more specific assessment was made on the corresponding study. The limited study was more likely to underestimate than to overestimate the severity of sinus disease.

### *Comparison of Coronal and Axial Imaging Planes*

No significant differences in the usefulness of axial and coronal imaging planes for detecting and quantifying sinus disease or identifying either bony disease or air/fluid levels were demonstrated.

### *Identification of Bony Abnormalities*

A bony abnormality was interpreted as present on 10 individual complete sinus studies (all maxillary). Bony abnormality was identified correctly in only five of the limited studies and was misidentified on the limited study when not present on the complete study at a 6% false-positive rate. Overall, the limited study was unreliable in identifying abnormalities involving the margins of the paranasal sinuses.

### *Identification of Air/Fluid Levels*

An air/fluid level was interpreted as present in 26 individual sinuses. In the limited study, air/fluid levels were identified correctly in only six cases and missed in 20 cases, giving a false-negative rate of 77%. The single false-positive air/fluid level determination was with a limited study. The limited study was generally unreliable in identifying air/fluid levels within the sinuses.

## Discussion

Knowledge of the presence and severity of pathologic changes in the paranasal sinuses is often an integral part of the treatment of children with uncontrolled asthma or persistent cough [3]. Asthma symptoms in many patients can be improved with accurate imaging assessment of the sinus disease followed by appropriate medical therapy [1, 3].

History and physical examination have been unreliable in the assessment of sinus disease in children [3]. Although identification of the sinus disease has traditionally relied on conventional radiography, typically consisting of between one and four projections, CT of the paranasal sinuses is superior for imaging and defining both bony structure associated with the paranasal sinuses and intrasinus disease [2].

Although widely available, CT has the disadvantages of higher examination cost and greater radiation dose. Integral dose range for conventional CT of the sinuses (assuming 3



rad per slice and 112-cm<sup>3</sup> slice volume) is approximately 53.6 mJ (3.35 mJ per slice  $\times$  16 slices per examination), vs 1.65–1.70 mJ for a three-view conventional radiographic study (Boone J, personal communication). Dose considerations are of greatest importance in infants and children, especially if repetitive examinations for chronic or recurrent diseases (e.g., chronic sinusitis, recurrent asthmatic attacks associated with or triggered by sinusitis) are required.

A limited-slice CT examination of the paranasal sinuses, providing both decreased radiation dose and imaging information comparable to that obtained via the complete CT study, would be of greatest potential value to children who, because of chronic asthma or recurrent sinusitis, are likely to undergo repetitive sinus imaging. Compared with conventional radiography, limited-slice CT provides superior imaging capability, although net radiation exposure is higher. In these children, CT could replace conventional radiography in the evaluation of sinus disease. Owing to better patient cooperation, CT is more readily used in children 4–5 years old or older (the age range in which both chronic sinusitis and asthma predominate). Achieving and maintaining proper head position (whether for axial or coronal scanning) for CT of the sinuses is much less of a problem in the older child (older than 4–5 years) and adolescent than in the infant and younger child.

Although the 79% rate of overall agreement between the complete and limited studies in identification of sinus disease was lower than expected, this discrepancy must be correlated with intraobserver variability, which has ranged up to 19% for radiographic and CT studies [4, 5]. In our study, expected

intraobserver variability is supplemented by examinations of differing scope (e.g., complete vs limited slices).

Because of the limited study's lack of sensitivity in identifying both air/fluid levels within the sinuses and associated bony abnormalities, we recommend a complete CT examination of the sinuses as the initial study in children with chronic asthma and/or recurrent sinusitis. However, on the basis of the data presented in this study, we advocate use of a three- or four-slice, limited CT examination for the follow-up assessment of sinus disease, thereby providing the superior anatomic definition of CT at a fourfold to fivefold reduction in net radiation exposure. Either an axial or a coronal imaging format could be used, with equivalent diagnostic accuracy in identifying intrasinus disease. The suggested locations of the imaging slices for the limited sinus CT examination are shown in Figure 1.

#### REFERENCES

1. Friday GA Jr, Fireman P. Sinusitis and asthma: clinical and pathogenetic relationships. *Clin Chest Med* 1988;9:557–565
2. McAlister WH, Lusk R, Muntz HR. Comparison of plain radiographs and coronal CT scans in infants and children with recurrent sinusitis. *AJR* 1989;153:1259–1264
3. Rachelefsky GS, Katz RM, Siegel SC. Chronic sinusitis in the allergic child. *Pediatr Clin North Am* 1988;35:1091–1101
4. Herschorn S, Hanley J, Wolkove N, Cohen C, Frank H, Palayew M. Measurability of non-small-cell lung cancer on chest radiographs. *J Clin Oncol* 1986;4:1184–1190
5. Warde P, Rideout DF, Herman S, et al. Computed tomography in advanced ovarian cancer. Inter- and intraobserver reliability. *Invest Radiol* 1986;21:31–33

# International Pediatric Radiology '91

## Conjoint Meeting: SPR and ESPR, Stockholm, Sweden, May 27-31, 1991

The members, officers, and program committee of the IPR Conjoint Meeting proudly announce the second conjoint meeting of the SPR and ESPR (European Society of Pediatric Radiology). Meeting registration and hotel reservation request forms will be available for **SPR members** from: Lynne Tiras, I.M.M., 4550 Post Oak Place, Ste. 248, Houston, TX 77027.

Further information about the meeting and registration can be obtained from Carol M. Rumack, M.D., Secretary, The Society for Pediatric Radiology, University of Colorado Health Sciences Center, 4200 E. 9th Ave., Box A030, Denver, CO 80262-0030; telephone (303) 270-4512.

**ESPR members** should contact: IPR'91 Congress, c/o Stockholm Convention Bureau, Box 6911, S-102 39, Stockholm, Sweden, for request forms.

### Sunday, May 26

1:00-7:00 p.m. Registration  
6:00-8:00 p.m. Early Bird Reception (wine and cheese)

### Monday, May 27

7:45-8:00 a.m. Opening Ceremony  
8:00-9:40 a.m. **Symposium** (1-5)  
9:40-10:20 a.m. Poster Session 1 (posters 1-10)  
10:20-12:20 p.m. **Scientific Session 1** (papers 1-12)  
12:20-1:20 p.m. Lunch  
1:20-3:20 p.m. **Scientific Session 2** (papers 13-24)  
3:40-5:00 p.m. **Scientific Session 3** (papers 25-32)  
5:00-5:40 p.m. Swedish Society of Medicine Pediatric Radiology Lecture  
8:00-5:40 p.m. Poster Exhibits  
7:00-9:00 p.m. Stockholm Town Hall Welcome Reception

### Tuesday, May 28

8:00-9:40 a.m. **Symposium** (6-10)  
9:40-10:20 a.m. Poster Session 2 (posters 11-20)  
10:20-12:20 p.m. **Scientific Session 4** (papers 33-44)  
8:00-12:20 p.m. Poster Exhibits  
Afternoon free Shopping, Sightseeing, Dining

### Wednesday, May 29

8:00-9:40 a.m. **Symposium** (11-15)  
9:40-10:20 a.m. Poster Session 3 (posters 21-30)  
10:20-12:20 p.m. **Scientific Session 5** (papers 45-56)  
12:20-1:20 p.m. Lunch  
1:20-3:20 p.m. **Scientific Session 6** (papers 57-68)  
3:40-5:40 p.m. **Scientific Session 7** (papers 69-76, short papers 1-8)  
8:00-5:40 p.m. Poster Exhibits  
7:00-8:30 p.m. Stockholm Concert Hall Reception & Concert

### Thursday, May 30

8:00-9:40 a.m. **Symposium** (16-20)  
9:40-10:20 a.m. Poster Session 4 (posters 31-40)  
10:20-12:20 p.m. **Scientific Session 8** (papers 77-88)  
12:20-1:20 p.m. Lunch  
1:20-3:00 p.m. Annual General Meetings  
3:20-4:30 p.m. Society for Pediatric Radiology (Room A)  
4:30-5:30 p.m. European Soc. of Pediatric Radiology (Berns' Lecture Hall)  
5:30-6:00 p.m. Australasian Society of Pediatric Imaging (Room C)  
8:00-6:00 p.m. **Scientific Session 9** (short papers 9-22)  
7:30-12:00 a.m. Neuhauser Lecture  
Awards Ceremony  
Poster Exhibits  
Dinner Dance Grand Hotel (Winter Garden Room)

### Friday, May 31

8:00-9:40 a.m. **Symposium** (21-25)  
9:40-10:20 a.m. Poster Session 5 (posters 41-50)  
10:20-12:20 p.m. **Scientific Session 10** (short papers 23-46)  
8:00-12:20 p.m. Poster Exhibits  
12:20 p.m. Closing Ceremonies & Post-Congress Tours (long/short)

## Technical Note

# CT Measurement of the Tracheal Lumen in Children and Adolescents

N. Thorne Griscom<sup>1</sup>

CT measurement of the cross-sectional area of the lumen of a child's trachea is useful, apart from investigations of respiratory physiology, chiefly in two circumstances. When a mediastinal mass such as a lymphoma is present, it may be necessary to determine if tracheal compromise is severe enough to make endotracheal intubation for biopsy or excision hazardous [1]. In primary tracheal stenosis, precise demonstration of the length of involvement and its severity can guide operative resection [2]. This report presents, in a form that can be used by radiologists who seldom deal with these illnesses, two techniques of tracheal measurement: first, when the magnetic tape is available and the General Electric 8800 or 9800 CT scanner is used and second, when CT images are reproduced on film.

### Determination of Tracheal Area from a CT Tape

At the General Electric 8800 or 9800 CT console (General Electric Medical Systems Division, Milwaukee, WI), the tracheal cross-sectional area is measured from a compatible tape as follows: The section of interest is displayed and magnified threefold to reduce imprecision. The CT number (about -1000) of the intraluminal air is determined. The CT number of the tracheal wall and paratracheal tissues is determined from three or four measurements; the mean will usually be about +50. Splitting the difference yields the full-width-half-maximum CT number, usually about -470; this is taken as the CT number of the wall/lumen interface. The image is

displayed, centered at this CT "level," with a narrow "window." The "blink" or "identify" mode causes pixels with this CT number to blink. A cursor is traced precisely through the blinking pixels, and the enclosed area is measured.

Elevation of the head often makes the trachea not quite perpendicular to the plane of the section. This elongates the tracheal lumen from front to back, and the area is falsely increased. To correct for this distortion, multiply by the cosine of the acute angle made by the trachea with the horizontal or (if that angle is unknown) subtract 2% [3].

The software used by the GE 8800 and GE 9800 for measuring area does not include the area of the interface pixels themselves. Precision requires that half the area of those interface pixels be counted. To make this correction, add 0.14 cm<sup>2</sup> to areas of 2.70–3.05 cm<sup>2</sup>, 0.13 cm<sup>2</sup> to areas of 2.35–2.70 cm<sup>2</sup>, 0.12 cm<sup>2</sup> to areas of 2.00–2.35 cm<sup>2</sup>, 0.11 cm<sup>2</sup> to areas of 1.65–2.00 cm<sup>2</sup>, 0.10 cm<sup>2</sup> to areas of 1.35–1.65 cm<sup>2</sup>, 0.09 cm<sup>2</sup> to areas of 1.05–1.35 cm<sup>2</sup>, 0.08 cm<sup>2</sup> to areas of 0.80–1.05 cm<sup>2</sup>, 0.07 cm<sup>2</sup> to areas of 0.60–0.80 cm<sup>2</sup>, 0.06 cm<sup>2</sup> to areas of 0.40–0.60 cm<sup>2</sup>, 0.05 cm<sup>2</sup> to areas of 0.20–0.40 cm<sup>2</sup>, and approximately 0.04 cm<sup>2</sup> to areas smaller than 0.20 cm<sup>2</sup>.

The area is then compared with standards for age and sex (Fig. 1) [4].

### Determination of Tracheal Area from CT Images on Film

If the GE 8800 or 9800 console cannot be used, cross-sectional area can be approximated from the hard copies

Received April 16, 1990; accepted after revision July 24, 1990.

<sup>1</sup> Department of Radiology, Harvard Medical School, 25 Shattuck St., Boston, MA 02115 and Department of Radiology, Children's Hospital, 300 Longwood Ave., Boston, MA 02115. Address reprint requests to N. T. Griscom at Children's Hospital.

AJR 156:371–372, February 1991 0361–803X/91/1562–0371 © American Roentgen Ray Society



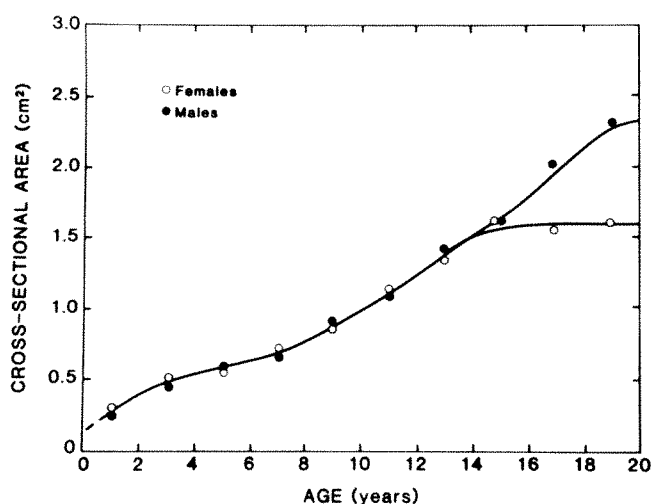


Fig. 1.—Graph shows mean tracheal cross-sectional area in control subjects, plotted against age. (Modified from Griscom and Wohl [4].)

[1], as follows: Identify the section of interest. To be usable, the section must have been photographed at two CT levels (for example, at +35 and -700), bracketing the full-width-half-maximum CT number assigned to the lumen/wall interface. It helps if the windows used for the images are narrow. A centimeter scale must be on the image.

The equation used for each setting is  $A = \pi \times \frac{1}{2}d_1 \times \frac{1}{2}d_2$  where A is area,  $d_1$  is the long diameter, and  $d_2$  is the largest diameter perpendicular to  $d_1$ . The diameters are measured with calipers and referred to the centimeter scale. In one example of tracheal compression by lymphoma,  $d_1$  was found to be 1.2 cm at a level of +35,  $d_2$  was 0.86 cm, and A at that setting was therefore 0.81 cm<sup>2</sup>. At a level of -700,  $d_1$  was 0.36 cm,  $d_2$  was 0.20 cm, and A was 0.06 cm<sup>2</sup>. Alternatively, the areas can be measured with a planimeter.

Straight-line arithmetical interpolation to a full-width-half-maximum CT number representing the lumen/wall interface (taken as -470) is then performed. If x is the area to be found, in the example just cited,

$$\frac{0.81 \text{ cm}^2 - x}{0.81 \text{ cm}^2 - 0.06 \text{ cm}^2} = \frac{35 - (-470)}{35 - (-700)}$$

$$x = 0.29 \text{ cm}^2.$$

From this a correction for elevation of the head and neck should be subtracted, as above; if the average 2% figure is used, the corrected area is 0.28 cm<sup>2</sup>. This number is then compared with standards for age and sex (Fig. 1).

This hard-copy method affords less precision and confidence than when the actual tape is used. Nevertheless, agreement between the two systems is good [1].

## Discussion

Postnatal tracheal growth is proportionately greatest early in infancy, when control values are relatively scanty [4]. Figure 1 shows an extrapolation of cross-sectional area back to the time of birth, based partly on the fact that tracheal dimensions 9 months before birth are necessarily zero. Furthermore, the tracheal dimensions of some males probably have not quite reached their adult plateaus by age 20. The last 5% of the male curve of Figure 1 is therefore also an extrapolation.

The published standards [4] give the mean area over the length of each trachea. When comparing a narrowed segment of the trachea with these standards, one needs to consider the amount by which a normal trachea varies in size along its length. This variation is quite small. The mean section-to-section coefficient of variation was 8.9% in reported control subjects [4] and ranged from 6.8% to 12.3% in subgroups of those control subjects.

The techniques described here are much more applicable to fixed tracheal narrowing, as in intrinsic stenosis or constriction by a mediastinal mass, than to the excessively variable caliber seen in tracheomalacia. Use of ultrafast CT and development of precise standards for changes in size of normal tracheas during tidal breathing and breathing from residual volume to total lung capacity (i.e., through the full range of intrapleural pressure) would overcome this limitation.

Standards for tracheal diameters also are available [4]. When diameter is in question, it can be analyzed in a similar fashion.

## REFERENCES

1. Shamberger RC, Holzman RS, Griscom NT, Tarbell NJ, Weinstein HJ. Quantitation of tracheal cross-sectional area as a guide to the surgical and anesthetic management of children with anterior mediastinal masses. *J Pediatr Surg* in press.
2. Jonas RA, Spevak PJ, McGill T, Castaneda AR. Pulmonary artery sling: primary repair by tracheal resection in infancy. *J Thorac Cardiovasc Surg* 1989;97:548-550.
3. Griscom NT, Wohl MEB. Dimensions of the growing trachea related to body height: length, anteroposterior and transverse diameters, cross-sectional area, and volume in subjects less than 20 years of age. *Am Rev Respir Dis* 1985;131:840-844.
4. Griscom NT, Wohl MEB. Dimensions of the growing trachea related to age and gender. *AJR* 1986;146:233-237.

# Intracranial Vascular Abnormalities: Value of MR Phase Imaging to Distinguish Thrombus from Flowing Blood

Lyn Nadel<sup>1</sup>  
Ira F. Braun<sup>2</sup>  
Kenneth A. Kraft<sup>3</sup>  
Panos P. Fatouros<sup>3</sup>  
Fred J. Laine<sup>4</sup>

The interpretation of conventional spin-echo and gradient-echo MR images of intracranial vascular lesions can be complex and ambiguous owing to variable effects on image intensity caused by flowing blood or thrombus. MR phase images, obtained simultaneously with conventional-magnitude images, are useful for evaluating proton motion (i.e., blood flow), and therefore can simplify the diagnosis of the presence or absence of thrombosis within a vascular structure or lesion. Fourteen patients with a variety of intracranial vascular abnormalities (aneurysms, superior sagittal sinus thrombosis, neoplasms adjacent to venous sinuses, and vascular malformations) were evaluated with conventional MR and phase imaging for the presence of blood flow. The phase images correlated with angiography in all cases. Phase imaging was not necessarily better than conventional spin-echo imaging in all cases, but it simplified the evaluation of thrombus vs blood flow in many. In three of five aneurysms, the phase images were diagnostic for evaluating lumen patency whereas the conventional images were ambiguous. Phase imaging was advantageous for detecting tumor invasion of the venous sinus when venous blood was enhanced by gadopentetate dimeglumine. A laminar flow phantom experiment determined the lower limits of sensitivity of phase imaging to be 0.5 cm/sec in the slice-select and 2.5 cm/sec in the read gradient directions.

Phase imaging is a simple, reliable technique that can distinguish thrombosis from flowing blood within intracranial lesions. It is easily performed and adds no additional time to the MR examination.

*AJNR* 11:1133-1140, November/December 1990; *AJR* 156:373-380, February 1991

The MR imaging evaluation of vascular abnormalities of the brain is a potentially complex subject because of separate phenomena that may occur simultaneously: (1) the clotting of blood and (2) the alteration of regional blood velocity. Each of these processes may individually exert profound and varied effects on MR image intensity [1, 2]; therefore, when they occur simultaneously, ambiguous image interpretation may result, particularly when using magnitude reconstructed images derived from either spin-echo or gradient-echo sequences. MR phase images are useful for revealing proton motion and are reconstructed from the same raw data used to generate conventional-magnitude images [3]. In the context of intracranial vascular abnormalities, phase imaging can simplify evaluation of the presence or absence of flow. This is because phase images are insensitive to certain parameters (e.g., relaxation times) that would normally dominate the intensity patterns on magnitude images. Thus, relaxation time changes caused by blood clot degradation, for example, which can profoundly affect the intensity of magnitude images, will exert little influence on spin-echo phase images. The simplicity of phase imaging makes it an appealing method to augment the diagnosis of various cerebrovascular abnormalities such as venous sinus thrombosis, aneurysms, or vascular malformations.

Received March 12, 1990; revision requested May 20, 1990; revision received June 8, 1990; accepted July 1, 1990.

<sup>1</sup> Department of Radiology, (R-109), University of Miami School of Medicine, P.O. Box 010960, Miami, FL 33101. Address reprint requests to L. Nadel.

<sup>2</sup> Department of Radiology, Baptist Hospital of Miami, 8900 N. Kendall Dr., Miami, FL 33176-2197.

<sup>3</sup> Division of Radiation Physics, Medical College of Virginia, Richmond, VA 23298.

<sup>4</sup> Department of Radiology, Division of Diagnostic Radiology, Medical College of Virginia, Richmond, VA 23298.

0361-803X/91/1562-0373  
© American Roentgen Ray Society

Phase imaging has been used elsewhere in the body to help ascertain the presence or absence of thrombus within blood vessels [4–10]. This study was undertaken to evaluate its utility intracranially. Fourteen patients with various intracranial vascular abnormalities were evaluated with conventional MR imaging and phase imaging of the brain. In addition, experiments were performed on a calibrated, constant-velocity laminar flow phantom to determine the threshold for reliable discrimination of motion-induced phase changes under conditions similar to those employed clinically.

## Materials and Methods

MR examinations were performed in 14 patients on a 1.0-T superconducting system (Siemens Magnetom). Abnormalities in the 14 patients comprised one idiopathic superior sagittal sinus thrombosis, five tumors adjacent to venous sinuses (three parasagittal meningiomas, one posterior fossa petrous meningioma, and one posterior parafalcine metastatic prostatic adenocarcinoma), two middle cerebral artery aneurysms (one 1.5-cm aneurysm with a large hematoma and one 5-cm giant aneurysm), two cavernous carotid aneurysms (one of 1.25 cm and one of 2.5 cm with a large hematoma), one 1.3-cm basilar tip aneurysm, two arteriovenous malformations, and one venous angioma. Four of the five neoplasms and four of the five aneurysms were surgically proved. The patients were 10–80 years old.

All patients had T1-weighted scans, 700/17–20/1–2 (TR/TE/excitations). Various imaging planes were used; many patients were studied in more than one plane (12 coronal, nine axial, nine sagittal). Slice thickness varied from 3 to 7 mm with 30% gaps between slices. In eight patients T1-weighted images were repeated with gadopentetate dimeglumine (0.1 mmol/kg IV). Proton-density T2-weighted scans (3000/45, 90/1) with a slice thickness of 3–5 mm were obtained in 12 patients, nine in the axial and three in the coronal planes. The one patient with superior sagittal sinus thrombosis had, in addition to the spin-echo study, a single-slice, 8-mm, coronal, gradient-echo study, 20/11/20° (TR/TE/flip angle).

The MR phase image reconstructions were derived from T1-weighted spin-echo data from all patients. The phase examinations were evaluated retrospectively, with all studies present, by two neuroradiologists for the presence or absence of blood flow within the area of interest. The results were compared with the spin-echo and gradient-echo magnitude images as well as with angiography and, in one case, CT.

A flow phantom was constructed in order to determine thresholds of sensitivity for reliable discrimination of slow flow from static tissue on MR phase maps. The flow apparatus consisted of two parallel tubes with inner diameters of 16 and 7 mm, respectively, which were connected in series and immersed in a static water bath. Gravity-driven steady flow was introduced through the tubes, and the flow rate was monitored continuously by using a calibrated in-line ultrasonic flowmeter (Transonic Systems Inc., Ithaca, NY). The recirculating fluid was a paramagnetically doped aqueous solution of high-molecular-weight dextran, having a viscosity and MR relaxation parameters similar to those of blood. The flow apparatus was placed within the same 1.0-T magnet used for the clinical studies such that the flow directions were parallel to the magnet bore. With an imaging sequence and associated parameters similar to those used clinically (700/20, 4-mm slice thickness), phase images were acquired in both transverse and parallel planes at several discrete flow rates through the flow tubes. Peak fluid velocities were calculated from the known flow rates and tube diameters, using the assumption of fully devel-

oped laminar flow. Using phase reconstructed images, thresholds of phase sensitivity were empirically chosen as the lowest velocities at which intraluminal phase variation was unambiguously present.

The MR signal is a vector quantity consisting of magnitude and direction (phase). Standard MR images are reconstructed by using only the magnitude information that is calculated for each pixel as the modulus of the real and imaginary signal components. A phase image is created by assigning directional values rather than magnitude values to a gray scale. This, mathematically, involves calculation of the arc tangent of the ratio of the imaginary to real signal elements for each pixel. Stationary protons will produce no imaginary signal component, and therefore the resulting phase angle will be zero for sequences having properly balanced gradients. Spins moving in the direction of a magnetic field gradient will experience a phase shift proportional to their velocity. In phase-reconstructed images, absent motion is represented by intermediate gray on the images, while moving protons are assigned shades of white or black depending on direction and velocity of motion [3, 7].

## Results

The patient with superior sagittal sinus thrombosis was imaged 15 days after the onset of symptoms (Fig. 1). The T1- and T2-weighted images showed high signal intensity within the superior sagittal sinus, torcular, and left transverse sinus. This is consistent with thrombus containing extracellular methemoglobin [2]. The gradient-echo coronal images showed increased signal intensity within the superior sagittal sinus; therefore, these images alone could be misinterpreted as showing flow-related enhancement, which could lead to a false-negative diagnosis [11]. The phase images show an intermediate shade of gray in the same vascular structures, which is indicative of nonflowing blood and corroborates the spin-echo diagnosis of thrombosis. Superior sagittal sinus thrombosis was confirmed angiographically; therefore, the increased signal seen on the gradient-echo image must have been from the altered relaxivity associated with extracellular methemoglobin.

Five patients had aneurysms ranging from 1.25 to 5.0 cm. Four aneurysms demonstrated patent lumens, although one was partially thrombosed. One aneurysm was totally thrombosed. All cases were confirmed angiographically.

The patient with a basilar tip aneurysm (Fig. 2) had an unenhanced CT scan that showed a hyperdense mass; with contrast material, the mass enhanced, suggesting an incompletely thrombosed aneurysm. A T1-weighted axial MR image showed a hypointense mass with an isointense left lateral aspect corresponding to the enhancing portion of the CT scan. The phase image demonstrated no motion, which correlated with a totally thrombosed aneurysm on angiography. All studies were performed within 24 hr of one another.

A 1.25-cm cavernous carotid aneurysm (Fig. 3) demonstrated isointensity on unenhanced T1-weighted images and homogeneously enhanced with gadopentetate dimeglumine. On T2-weighted images the mass was peripherally hyperintense with a hypointense center. These spin-echo MR characteristics were not diagnostic of an aneurysm and could be seen with a neoplastic or inflammatory lesion. Phase imaging demonstrated a white and black appearance to the area,



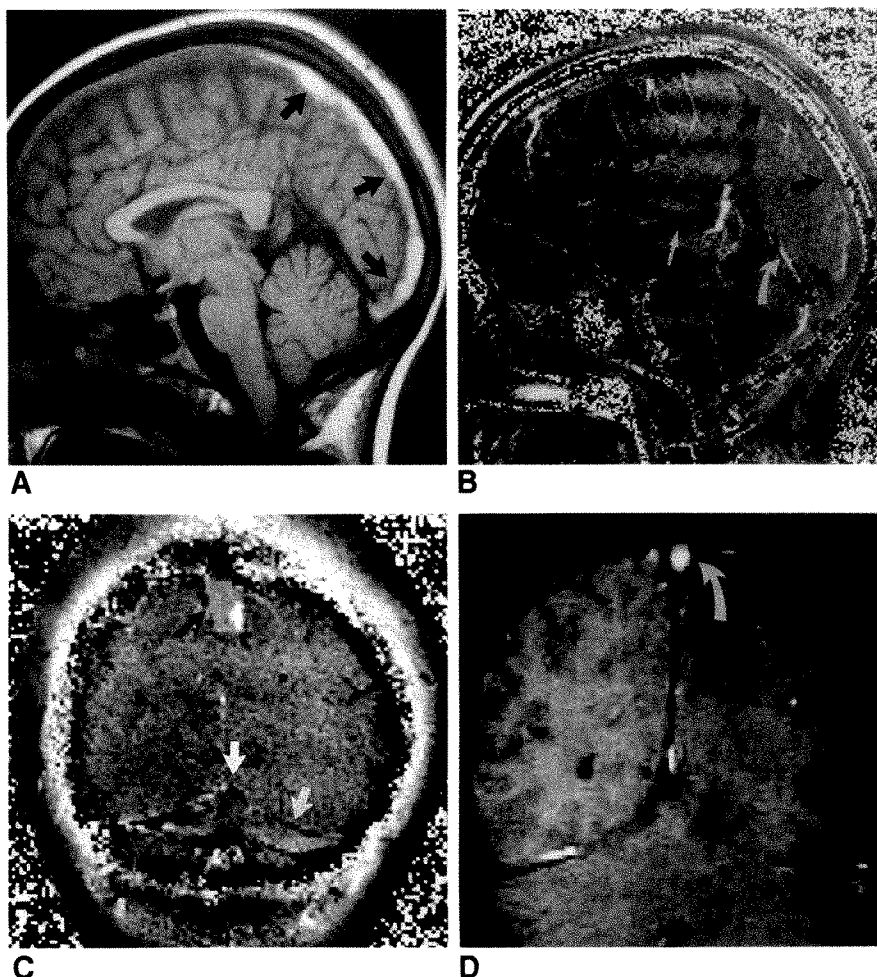
Fig. 1.—Superior sagittal sinus thrombosis.

A, Midsagittal T1-weighted image shows high-signal-intensity thrombus within superior sagittal sinus and torcular (arrows).

B, Corresponding phase image. Gray throughout extent of superior sagittal sinus and torcular (straight black arrows) indicates nonflowing blood. Note black appearance of internal cerebral veins (straight white arrow), white in vein of Galen (curved black arrow), and mixed black and white in straight sinus (curved white arrow), indicating flowing blood.

C, Coronal phase image. Gray signifies non-flowing blood in superior sagittal sinus (black arrow), torcular, and left transverse sinus (white arrows).

D, Coronal gradient-echo image (20/11/20°). High signal intensity in superior sagittal sinus (arrow) could be misinterpreted as patent sinus.



consistent with flowing blood within the lumen of an aneurysm.

Phase imaging was found to be accurate and simplified the evaluation of a patent lumen within a giant 5.0-cm middle cerebral artery aneurysm with associated parenchymal hemorrhage (Fig. 4). T1-weighted images showed that the majority of signal within the aneurysm was mixed hyper- and isointensity with a focal 1.5-cm area of marked hypointensity situated superolaterally. On T2-weighted images the signal characteristics of the aneurysm appeared as a mixture of marked hypo- and hyperintensity. The focal, peripheral area of hypointensity on T1-weighted images appeared hyperintense. This peripheral area was clearly shown to be the patent lumen within a mostly thrombosed aneurysm on phase images, and was corroborated by an angiogram.

The last two aneurysms were associated with large intraparenchymal hemorrhages. The lumens of the aneurysms that were seen on phase images as positive for proton motion appeared markedly hypointense (signal void) on both T1- and T2-weighted images. The large associated hematomas were essentially isointense on T1- and markedly hypointense on T2-weighted images with surrounding hyperintense edema on T2-weighted images. In these instances the spin-echo MR

characteristics were unambiguous and the phase images provided no new information.

Five patients with neoplasms adjacent to dural venous sinuses were imaged. The phase images were as sensitive as *unenhanced* T1- or T2-weighted images for tumor occlusion of the adjacent venous sinus in all five. Signal void was seen in the patent portion of the venous sinus on unenhanced magnitude reconstructed MR images. Three cases demonstrated partial or total occlusion of the superior sagittal sinus, one case demonstrated tumor invasion of the junction of the vein of Galen with the straight sinus, and one case had no invasion of the adjacent transverse and sigmoid sinus.

Four of the patients with neoplasms received gadopentetate dimeglumine. In one patient who had T1-weighted coronal images *only* with enhancement, tumor invasion of the superior sagittal sinus could not be completely excluded on the routine MR images owing to the high signal intensity within the sinus from IV gadopentetate dimeglumine (Fig. 5). Sagittal sinus patency was established by phase imaging. In the patient with a large parasagittal meningioma with extensive invasion of the superior sagittal sinus and torcular, a small signal void could be seen in a portion of the superior sagittal sinus on the T1-weighted images without gadopen-

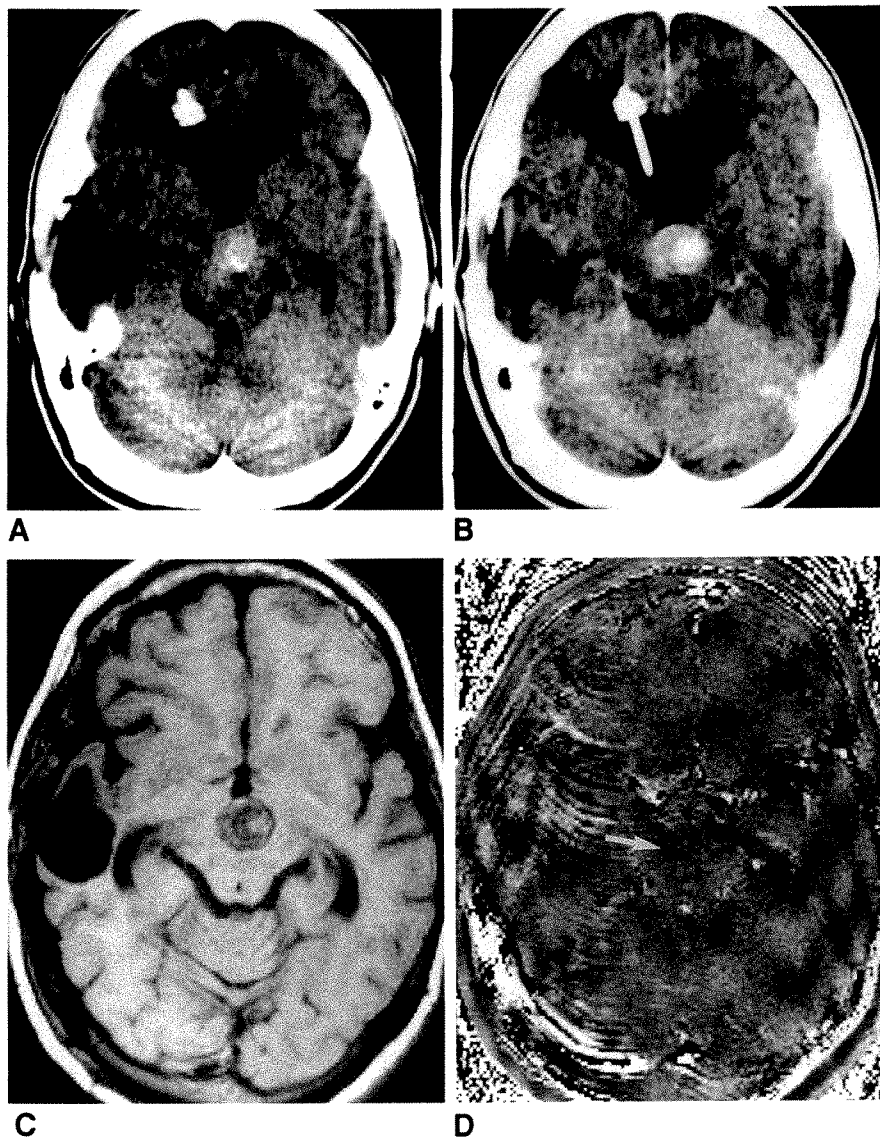


Fig. 2.—Thrombosed basilar tip aneurysm.

A, Axial unenhanced CT scan. Hyperdense mass is present in interpeduncular cistern (arrow).

B, Axial enhanced CT scan shows diffuse enhancement, greater on left aspect (arrow), suggesting patent lumen.

C, Axial T1-weighted MR image. Aneurysm is hypointense relative to brain with isointense area that corresponds to enhancing portion on CT.

D, Corresponding phase image shows no evidence of blood flow in region of the aneurysm (arrow), signifying total thrombosis.

E, Lateral subtraction arteriogram shows no evidence of aneurysm.

tetate dimeglumine. This small area of patency was also seen on phase imaging, but the signal void was obliterated on the enhanced T1-weighted magnitude images. In the remaining two patients, tumor occlusion of the superior sagittal sinus at the level of the tumor could be accurately diagnosed on the T1-weighted magnitude images with and without gadopentetate dimeglumine as well as on the phase images. However, posterior to the tumor on the enhanced T1-weighted images there was contrast enhancement of the venous sinus; therefore, posterior tumor extension into the venous sinus could not be excluded on the enhanced magnitude images alone. The phase images as well as the unenhanced magnitude images indicated flowing blood.

In the three patients with vascular malformations, signal voids could be seen easily on the routine T1- or T2-weighted images. The lesions were also seen easily on phase imaging as the black or white appearance of flowing blood.

*Flow phantom.*—For motion in the direction of the slice-select gradient (transaxial images), the lower limit of flow detection for either tube was found to be approximately 0.5 cm/sec for a 4-mm slice thickness. Conversely, the corresponding limit for motion in the read gradient direction (sagittal images) was determined to be 2.5 cm/sec. Hence, for the particular imaging parameters used, blood moving at velocities below these limits would be indistinguishable from thrombus on phase images. In general, the limits of sensitivity of phase imaging to slow proton motion are determined by the gradient strengths and their precise timing characteristics, and therefore are affected by the choice of imaging sequence and its associated parameters. In these phantom data, for example, the velocity sensitivity in the axial images was the highest, because the slice-select gradient was operating at its upper limit (6.0 mT/m). The strength of the read gradient, however, was lower (1.88 mT/m).

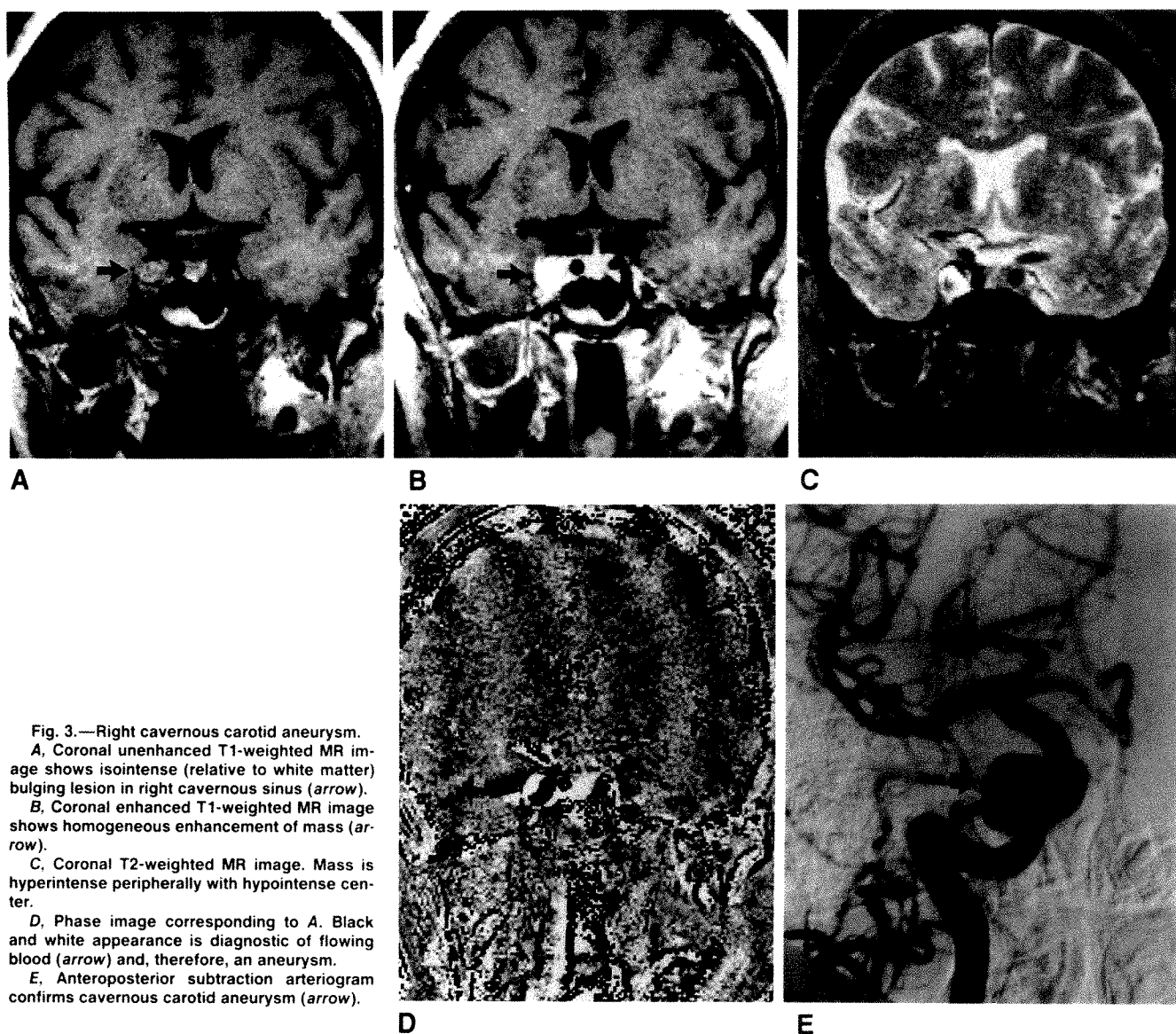


Fig. 3.—Right cavernous carotid aneurysm.  
 A, Coronal unenhanced T1-weighted MR image shows isointense (relative to white matter) bulging lesion in right cavernous sinus (arrow).  
 B, Coronal enhanced T1-weighted MR image shows homogeneous enhancement of mass (arrow).  
 C, Coronal T2-weighted MR image. Mass is hyperintense peripherally with hypointense center.  
 D, Phase image corresponding to A. Black and white appearance is diagnostic of flowing blood (arrow) and, therefore, an aneurysm.  
 E, Anteroposterior subtraction arteriogram confirms cavernous carotid aneurysm (arrow).

## Discussion

Evaluation of intracranial vascular lesions often can be confusing owing to the variable appearance of flowing and nonflowing blood on MR imaging. Many variables influence its appearance [1, 12, 13]. These include imaging sequence parameters (TR, TE, number of echoes), field strength, and whether motion-compensation techniques are used. The velocity of flowing blood will influence its appearance on MR images. A signal void may be produced by quickly flowing blood, whereas slowly flowing blood may simulate thrombus by appearing hyperintense. Even-echo rephasing and flow-related enhancement phenomena may cause high signal as a result of slow blood flow. Decreased signal may be seen owing to odd-echo dephasing or turbulence. Additionally, a blood clot or a thrombus will have varying appearances on MR as it undergoes multiple stages of hemoglobin breakdown, which has been well described [2].

MR phase imaging is well suited for the evaluation of blood flow since it is sensitive predominantly to proton motion [3]. It has been advocated for use outside the CNS. Phase imaging has been used successfully to study the aorta, vena cava, and heart [4–8]. Erdman et al. [9] found a sensitivity of 90% and specificity of 100% in evaluating deep venous thrombosis of the upper and lower extremities with MR phase images in comparison with contrast venography. Vessels of the thorax, abdomen, and pelvis were evaluated for occlusion by Tavares et al. [10], who concluded that magnitude images alone have a sensitivity of only 35% and a specificity of 90% while magnitude and phase images combined yield a sensitivity of 85% and a specificity of 90%.

MR imaging has been advocated for the evaluation of cerebral venous thrombosis with routine spin-echo sequences [14–21], but this can be confusing owing to variable signal intensities due to hemoglobin breakdown and flow effects on



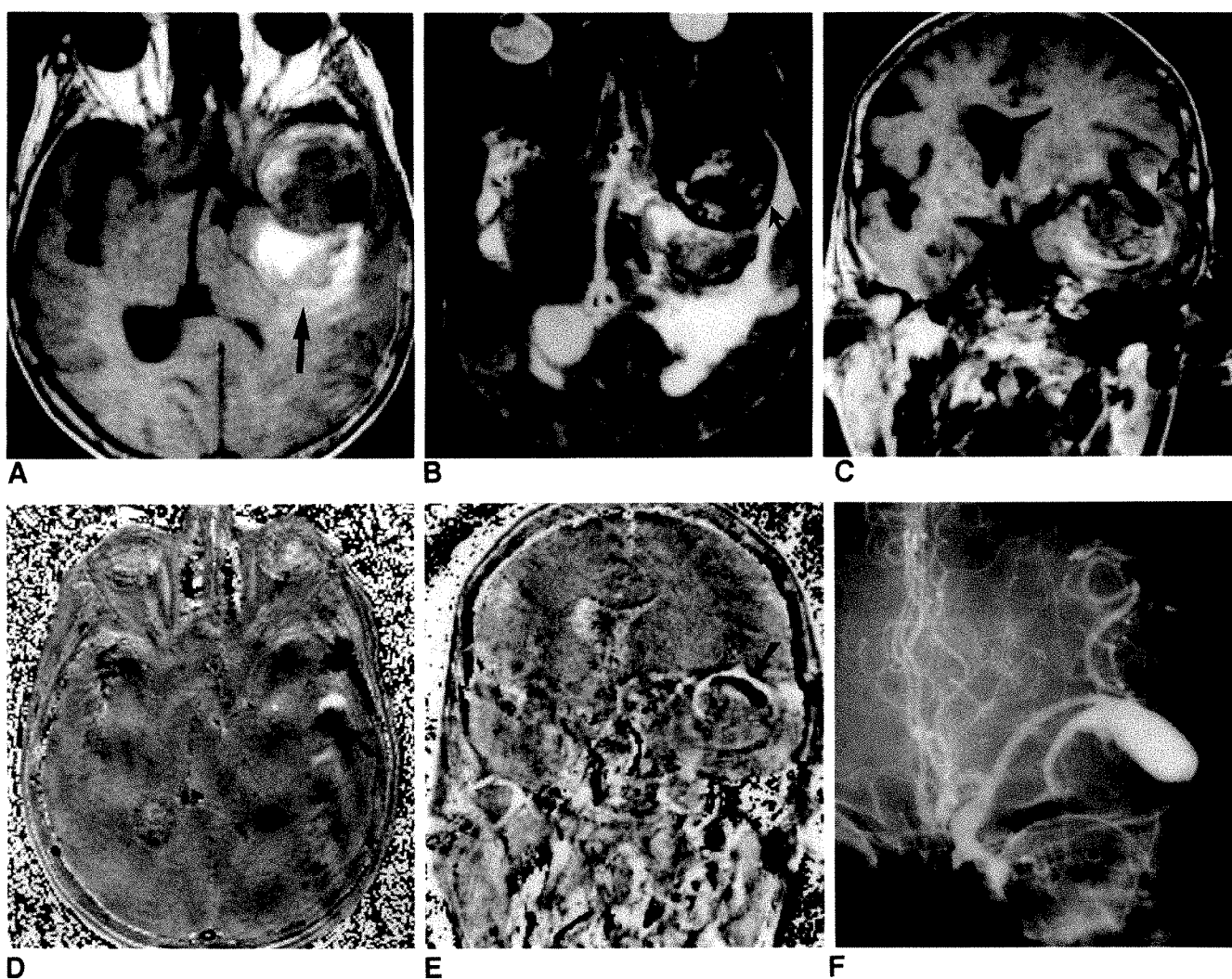


Fig. 4.—Partially thrombosed giant left middle cerebral artery aneurysm.

A, Axial T1-weighted MR image shows 5-cm mass of mixed hyper- and isointensity. Signal void is seen laterally (*curved arrow*). Hyperintense parenchymal hemorrhage is noted posteriorly (*straight arrow*).

B, Axial T2-weighted MR image. Signal within aneurysm is of mixed hypo- and hyperintensity pattern. Area of signal void on T1-weighted image appears hyperintense (*arrow*).

C, Coronal T1-weighted MR image shows signal void superiorly (*arrow*).

D and E, Phase images corresponding to A and C, respectively, simplify diagnosis of patent lumen (*arrows*) within partially thrombosed aneurysm.

F, Anteroposterior arteriogram shows lumen of aneurysm.

T1- and T2-weighted sequences. In our one patient with idiopathic thrombosis of the superior sagittal sinus, the diagnosis could be established, with relative confidence, from the routine spin-echo images, without the aid of phase images. The high signal intensity seen on both T1- and T2-weighted sequences was due to the presence of extracellular methemoglobin within the thrombus. However, there are potential pitfalls of spin-echo imaging. Slowly flowing blood can appear hyperintense owing to flow-related enhancement or even-echo rephasing [12]. A thrombus that is imaged within 24 hr may exhibit markedly decreased signal on T2-weighted sequences due to the presence of deoxyhemoglobin, and therefore be misinterpreted as signal void due to flowing blood in a patent venous sinus. Therefore, we believe that phase images are probably more reliable in this clinical situation.

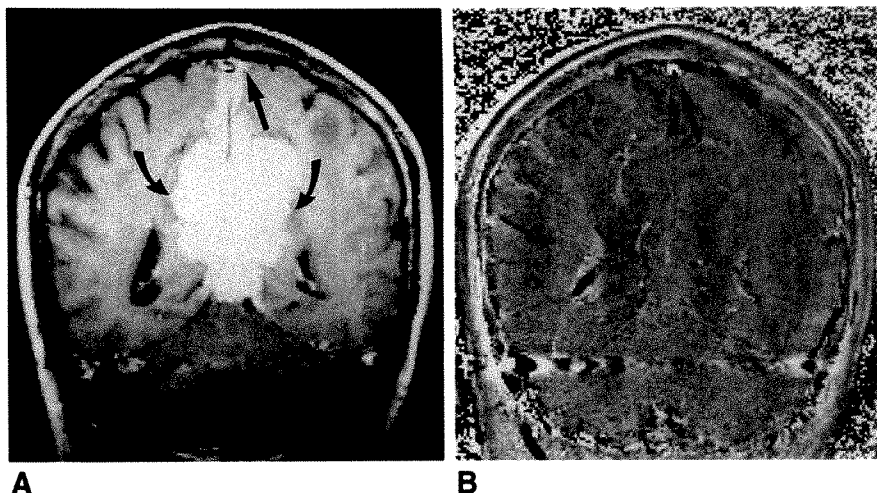
Gradient-echo MR imaging has been advocated to evaluate vascular lesions in the head and neck as well as the lower extremities [11, 22–27]. High signal intensity within the blood vessel is believed to be associated with flowing blood and therefore a patent blood vessel. Daniels et al. [23, 24] advocate its use for studying the cavernous sinus and jugular foramen [23, 24]. Tumoral invasion of the superior sagittal sinus has also been evaluated with gradient-echo MR imaging [25]. Intracranial aneurysms were evaluated by Tsuruda et al. [26] by using a cine MR technique.

Sixty-three patients with a variety of vascular intracranial lesions were studied by Atlas et al. [27], who found a potential pitfall of gradient-echo MR imaging in one patient with a thrombosed aneurysm. This was also reported by Yousem et al. [28] in four patients with arteriovenous malformations. A

Fig. 5.—Parafalcine metastatic adenocarcinoma of prostate.

A, Coronal enhanced T1-weighted MR image. Enhancing tumor is seen inferiorly (curved arrows) with extension superiorly on either side of falx. Hyperintensity within superior sagittal sinus (straight arrow) could be due to tumor invasion or normal enhancement of venous blood.

B, Corresponding phase image. Black and white appearance of superior sagittal sinus (arrow) confirms patency.



similar problem occurred in our case of superior sagittal sinus thrombosis. Specifically, if a blood clot contains substantial extracellular methemoglobin, it will appear hyperintense on gradient-echo images and therefore simulate flowing blood. Such ambiguity compromises the specificity of this technique.

Phase imaging augmented the MR evaluation of cerebral venous sinus thrombosis or occlusion. These six cases demonstrated that phase imaging was sensitive to flowing or nonflowing blood within the venous sinus. In the cases of neoplasm, the phase images were no more sensitive than the routine spin-echo images without IV gadopentetate dimeglumine, which demonstrated flow void in the patent venous sinus. Phase imaging was helpful for interpreting enhanced T1-weighted images because it was otherwise difficult to differentiate enhancing tumor within the sinus vs normal enhancement of the venous sinus.

Conventional spin-echo MR imaging has been advocated for the study of intracranial aneurysms [29–35]. The appearances of totally and partially thrombosed giant aneurysms have been described; a signal void on T1- and T2-weighted images indicates residual lumen patency. The signal intensity of the thrombus within these aneurysms is markedly variable depending on the interval between MR imaging and the onset of thrombosis.

Cine low-flip-angle gradient-refocused imaging has been described as a way of evaluating large aneurysms [26]. Regions of very high flow are accompanied by areas of signal dropout due to turbulence seen during systole. Thrombus was diagnosed by the signal intensity remaining unchanged during the cardiac cycle. A pitfall to this technique is that methemoglobin, which may be a component of intraluminal thrombus, appears as high signal intensity on cine MR and may mimic flowing blood. This indeed happened in one case and a small patent lumen within the aneurysm was missed. A similar phenomenon has been reported when imaging an aneurysm with gradient-recalled acquisition in the steady state [27]. This pitfall might have been avoided if phase imaging were employed.

Phase imaging was helpful in evaluating the five cases of aneurysms in this series. The phase images correctly indicated that a basilar tip aneurysm was totally thrombosed, whereas the CT data suggested a patent lumen, evidenced by contrast enhancement within the mass. Contrast enhancement of thrombosed aneurysms has been reported [36]. The

aneurysm in our patient had been known to be present for 5 years. CT, MR, and angiography were performed within 24 hr of one another with CT being performed first. Although unlikely, one might argue that the aneurysm thrombosed within that 24-hr period.

The routine T1- and T2-weighted images of a nonthrombosed cavernous carotid aneurysm did not exhibit signal intensities typical of a patent aneurysm, and in fact mimicked a neoplastic or possibly an inflammatory process. On the basis of phase images, however, the diagnosis was simple and agreed with angiography. In the case of the 5-cm giant aneurysm, phase images again proved to be more helpful in delineating the patent lumen than were the routine spin-echo images. The patent lumen was markedly hypointense on T1- and hyperintense on T2-weighted images. The lumen was difficult to discern within the markedly inhomogeneous signal intensities of the intraluminal thrombus. In the two patients with aneurysms adjacent to large intraparenchymal hematomas, signal void was seen on both T1- and T2-weighted sequences, indicating the presence of a lumen and obviating phase imaging.

Intracranial vascular malformations have been studied with spin-echo and gradient-echo techniques [22, 27, 37, 38]. Gradient-echo techniques have multiple limitations. One is the magnetic susceptibility-related artifact, which can be seen as a result of hemosiderin in an adjacent chronic hemorrhage or is produced by air/brain interfaces. The flow-related enhancement phenomenon that is used to make the diagnosis of flowing blood with gradient-echo imaging may be incomplete or absent when slow flow is encountered parallel to the imaging plane, such as in the case of a venous angioma or with very slow flow within a cavernous hemangioma [22]. There is also the potential pitfall of high signal intensity within a vascular malformation, caused by subacute thrombus after occlusion, simulating flow-related enhancement [28].

The three cases of vascular malformations in this study were not demonstrated any better with phase imaging than with routine spin-echo imaging. Phase imaging, however, may be helpful after embolic or surgical treatment or after treatment of aneurysms to evaluate for patency of vessel lumens.

There are certain limitations associated with MR phase imaging. These include volume averaging and extraneous sources of motion such as that caused by the patient or adjacent CSF pulsations. A potential problem would be a

phase shift of plus or minus 360°, which is indistinguishable from a phase shift of 0° and therefore may be interpreted as static blood flow. In practice, however, the parabolic velocity profile typical of laminar vessel flow results in a range of fluid velocities within the vessel lumen. In our experience, phase aliasing effects have not seriously affected our ability to differentiate thrombus from patent vessels.

From experiments performed on a calibrated, constant-velocity laminar flow phantom, we determined the limit of sensitivity of phase imaging to slow proton motion for the T1-weighted imaging sequence used with our patients. The limit of detection was found to be approximately 0.5 cm/sec for peak motion in the image slice direction and 2.5 cm/sec for motion along the image read gradient direction. Therefore, blood moving at velocities below these limits may be indistinguishable from thrombus when using phase maps. Peak flow velocity in the normal superior sagittal sinus has been determined to range from 20.1 to 45.5 cm/sec [39]. Tsuruda et al. (personal communication) found an average velocity of 14.4 cm/sec with phase imaging.

In conclusion, we believe that phase imaging is a simple, reliable technique that can distinguish thrombosis from flowing blood within intracranial vascular lesions. Phase imaging is based mainly on the presence or absence of proton motion and therefore unambiguously allows the differentiation between flowing blood and thrombus. It is an easily performed technique that adds no time to the MR evaluation, as it is acquired simultaneously with the routine spin-echo sequence. The complex variable spin-echo signal intensities associated with blood flow and blood clot degradation are eliminated in the phase image evaluation of vascular lumen patency.

Potential applications in the brain include evaluation of the deep venous sinuses, aneurysms, vascular malformations, and intracerebral arteries (i.e., internal carotid, vertebral, and basilar) for thrombosis vs patency. This technique may be particularly useful for the follow-up evaluation of therapeutic occlusion of aneurysms or vascular malformations.

## REFERENCES

- Bradley WG. Flow phenomena in MR imaging. *AJR* 1988;150:983-994
- Gomori JM, Grossman RI, Goldberg HI, Zimmerman RA, Bilaniuk LT. Intracranial hematomas: imaging by high-field MR. *Radiology* 1985;157:87-93
- Wedeen VJ, Rosen BR, Chesler D, Brady TJ. MR velocity imaging by phase display. *J Comput Assist Tomogr* 1985;9(3):530-536
- Wesbey GE, Higgins CB, Amparo EG, Hale JD, Kaufman L, Pogany AC. Peripheral vascular disease: correlation of MR imaging and angiography. *Radiology* 1985;756:733-739
- Von Schulthess GK, Augustiny N. Calculation of T2 values versus phase imaging for the distinction between flow and thrombus in MR imaging. *Radiology* 1987;164:549-554
- White RD, Ulyot DJ, Higgins CB. MR imaging of the aorta after surgery for aortic dissection. *AJR* 1988;150:87-92
- Rumancik WM, Naidich DP, Chandra R, et al. Cardiovascular disease: evaluation with MR phase imaging. *Radiology* 1988;166:63-68
- Dinsmore RE, Wedeen V, Rosen B, Wismer GL, Miller SW, Brady TJ. Phase-offset technique to distinguish slow blood flow and thrombus on MR images. *AJR* 1987;148:634-636
- Erdman WA, Jayson HT, Redman HC, Miller GL, Parkey RW, Peshock RW. Deep venous thrombosis of extremities: role of MR imaging in the diagnosis. *Radiology* 1990;174:425-431
- Tavares NJ, Auffermann W, Brown JJ, Gilbert TJ, Sommerhoff C, Higgins CB. Detection of thrombus by using phase-image MR scans: ROC curve analysis. *AJR* 1989;153:173-178
- Spritzer CE, Sussman SK, Blinder RA, Saeed M, Herfkens RJ. Deep venous thrombosis evaluation with limited-flip-angle, gradient-refocused MR imaging: preliminary experience. *Radiology* 1988;166:371-375
- Bradley WG, Waluch V. Blood flow: magnetic resonance imaging. *Radiology* 1985;154:443-450
- Mills CM, Brant-Zawadzki M, Crooks LE, et al. Nuclear magnetic resonance: principles of blood flow imaging. *AJR* 1984;142:165-170
- Bauer WM, Einhaupl K, Heywang SH, Vogl T, Seiderer M, Clados D. MR of venous sinus thrombosis: a case report. *AJNR* 1987;8:713-715
- McMurdo SK, Maj MC, Brant-Zawadzki M, et al. Dural sinus thrombosis: study using intermediate field strength MR imaging. *Radiology* 1986;161:83-86
- Hulcelle PJ, Doms GC, Mathurin P, Cornelis G. MRI assessment of unsuspected dural sinus thrombosis. *Neuroradiology* 1989;31:217-221
- Macchi PJ, Grossman RI, Gomori JM, Goldberg HI, Zimmerman RA, Bilaniuk LT. High field MR imaging of cerebral venous thrombosis. *J Comput Assist Tomogr* 1986;10(1):10-15
- McArdle CB, Mirfakhraee M, Amparo EG, Kulkarni MV. MR imaging of transverse/sigmoid dural sinus and jugular vein thrombosis. *J Comput Assist Tomogr* 1987;11(5):831-838
- Anderson SC, Shah CP, Murtagh FR. Case report: congested deep subcortical veins as a sign of dural venous thrombosis: MR and CT correlations. *J Comput Assist Tomogr* 1987;11(6):1059-1061
- Harris TM, Smith RR, Koch KJ. Case report: gadolinium-DTPA enhanced MR imaging of septic dural sinus thrombosis. *J Comput Assist Tomogr* 1989;13(4):682-684
- Sze G, Simmons B, Krol G, Walker R, Zimmerman RD, Deck MD. Dural sinus thrombosis: verification with spin-echo techniques. *AJNR* 1988;9:679-686
- Needell WM, Maravilla KR. MR flow imaging in vascular malformations using gradient recalled acquisition. *AJNR* 1988;9:637-642
- Daniels DL, Czervionke LF, Bonneville JF, et al. MR imaging of the cavernous sinus: value of spin echo and gradient recalled echo images. *AJNR* 1988;9:947-952
- Daniels DL, Czervionke LF, Pech P, et al. Gradient recalled echo MR imaging of the jugular foramen. *AJNR* 1988;9:675-678
- Daniels DL, Czervionke LF, Hendrix LE, et al. Gradient recalled echo MR imaging of superior sagittal sinus occlusion. *Neuroradiology* 1989;31:134-136
- Tsuruda JS, Halbach VV, Higashida RT, Mark AS, Hieshima GB, Norman D. MR evaluation of large intracranial aneurysms using cine low flip angle gradient-refocused imaging. *AJR* 1988;151:153-162
- Atlas SW, Mark AS, Fram EK, Grossman RI. Vascular intracranial lesions: applications of gradient-echo MR imaging. *Radiology* 1988;169:455-461
- Yousem DM, Balakrishnan J, Debrun GM, Bryan RN. Hyperintense thrombus on GRASS MR images: potential pitfall in flow evaluation. *AJNR* 1990;11:51-58
- Jaspan T, Wilson M, O'Donnell H, Worthington BS, Holland IM. Magnetic resonance imaging with even-echo rephasing sequences in the assessment and management of giant intracranial aneurysms. *Br J Radiol* 1988;61:351-357
- Olsen WL, Brant-Zawadzki M, Hodes J, Norman D, Newton TH. Giant intracranial aneurysms: MR imaging. *Radiology* 1987;163:431-435
- Atlas SW, Grossman RI, Goldberg HI, Hackney DB, Bilaniuk LT, Zimmerman RA. Partially thrombosed giant intracranial aneurysms: correlation of MR and pathologic findings. *Radiology* 1987;162:111-114
- Biondi A, Scialfa G, Scotti G. Intracranial aneurysms: MR imaging. *Neuroradiology* 1988;30:214-218
- Strother CM, Eldevik P, Kikuchi Y, Graves V, Partington C, Merlis A. Thrombus formation and structure and the evolution of mass effect in intracranial aneurysms treated by balloon embolization: emphasis on MR findings. *AJNR* 1989;10:787-796
- Brothers MF, Fox AJ, Lee DH, Pelz DM, Deveikis JP. MR imaging after surgery for vertebrobasilar aneurysm. *AJNR* 1990;11:149-161
- Kwan ES, Wolpert SM, Scott RM, Runge V. MR evaluation of neurovascular lesions after endovascular occlusion with detachable balloons. *AJNR* 1988;9:523-531
- Pinto RS, Cohen WA, Kricheff II, Redington RW, Berninger WH. Giant intracranial aneurysms: rapid sequential computed tomography. *AJR* 1982;139:973-977
- Kucharczyk W, Lemme-Pleghos L, Uske L, Brant-Zawadzki M, Doms G, Norman D. Intracranial vascular malformations: MR and CT imaging. *Radiology* 1985;156:383-389
- Smith HJ, Strother CM, Kikuchi Y, et al. MR imaging in the management of supratentorial intracranial AVMs. *AJR* 1988;150:1143-1153
- Mattle H, Edelman RR, Reis MA, et al. Cerebral venography and flow quantification with MR. *Radiology* 1989;173(p):187



## Paranasal Sinuses on MR Images of the Brain: Significance of Mucosal Thickening

Kevin M. Rak<sup>1</sup>  
John D. Newell II<sup>2</sup>  
Wayne F. Yakes<sup>1</sup>  
Melissa A. Damiano<sup>1</sup>  
James M. Luethke<sup>1</sup>

One hundred twenty-eight patients were examined prospectively to determine the significance of mucosal thickening seen in the paranasal sinuses during routine MR imaging of the brain. On the basis of responses to a questionnaire, each patient was categorized as symptomatic ( $n = 60$ ) or asymptomatic ( $n = 68$ ) for paranasal sinus disease. Patients were categorized further on the basis of the maximal mucosal thickening seen by MR in any paranasal sinus. A modified  $t$  test was used to compare the prevalence of various degrees of mucosal thickening between symptomatic and asymptomatic groups. Statistically significant differences between the groups were seen only in those patients with normal sinuses and in those with 4 mm or more of mucosal thickening.

We conclude that mucosal thickening of up to 3 mm is common and lacks clinical significance in asymptomatic patients. An ancillary finding is that 1- to 2-mm areas of mucosal thickening in the ethmoidal sinuses occur in 63% of asymptomatic patients. This minimal mucosal thickening in the ethmoidal sinuses is thought to be a normal variant, possibly a function of the physiologic nasal cycle.

*AJNR* 11:1211-1214, November/December 1990; *AJR* 156:381-384, February 1991

MR imaging is sensitive for detecting inflammation of the mucosa that occurs with sinusitis. In a prospective study of 128 patients, we attempted to determine the clinical significance of mucosal abnormalities seen in the paranasal sinuses during routine MR imaging of the brain.

### Subjects and Methods

We prospectively examined 128 random patients (age range, 15-85 years) who had MR imaging for intracranial disease. All patients were scanned on a 1.5-T unit (Signa, General Electric; Milwaukee, WI). Spin-echo axial MR images, 2800/45.90 (TR/TE), were obtained through the paranasal sinuses in all patients. T1-weighted sagittal images (600/20) also were obtained in all patients.

With the assistance of an otolaryngologist, we developed a questionnaire to delineate common presentations of paranasal sinus disease. Before the MR examination, each patient completed this questionnaire, commenting on the presence or absence of (1) facial or retroorbital pain, (2) rhinorrhea, (3) current symptoms of allergy/hay fever or of the common cold, and (4) current use of medications such as antihistamines. Patients with one or more positive responses to these questions were categorized as symptomatic for sinus disease, whereas patients with all negative responses were classified as asymptomatic. The MR examinations were blindly reviewed without knowledge of the questionnaires' results. Each paranasal sinus was evaluated for mucosal thickness, presence or absence of air/fluid level, and evidence of retention cyst/polyp. High signal intensity on the T2-weighted images was used to distinguish inflamed mucosa from the lower signal of bone in the sinus wall. Retention cysts and polyps could not be consistently distinguished from each other, but were reported as lobular intrasinus lesions of high signal intensity on T2-weighted images.

Each patient was categorized according to the maximal mucosal thickening present in any paranasal sinus. Thus, categories included normal, 1 mm of thickening, 2 mm, 3 mm, and 4

Received March 12, 1990; revision requested May 20, 1990; revision received June 11, 1990; accepted July 13, 1990.

The opinions or assertions contained herein are the private views of the authors and are not to be construed as official or as reflecting the views of the Department of the Army or Department of Defense.

<sup>1</sup> Department of Radiology, Fitzsimons Army Medical Center, Aurora, CO 80045-5001. Address reprint requests to K. M. Rak.

<sup>2</sup> Radiology Imaging Associates, Porter Memorial Hospital, Denver, CO 80210.

0361-803X/91/1562-0381

mm or more of mucosal thickening. Data from the asymptomatic and symptomatic groups were compared by using a modified t test. Significant differences were indicated by a two-tailed probability of .05 or less.

Results

In our initial analysis (Table 1), only two MR categories showed statistically significant differences between asymptomatic and symptomatic patients. Normal paranasal sinuses were more prevalent in the asymptomatic population, and 4 mm or greater mucosal thickening in any sinus was more common in the symptomatic group (Figs. 1 and 2). An interesting finding was that 63% of the asymptomatic patients (43 of 68) and 69% of all patients (88 of 128) had minimal, 1- to 2-mm, mucosal thickening in the ethmoidal sinuses. A second analysis was performed with this minimal ethmoidal thickening considered as normal. Ethmoidal abnormality was then categorized only if 3 mm or more of mucosal thickening was present. The results again showed statistical significance only in those patients with normal sinuses and in those with 4 mm or more of mucosal thickening (Table 2).

The prevalence of retention cysts/polyps was not significantly different between the symptomatic and asymptomatic patient groups. Four instances of air/fluid level or complete sinus opacification were seen in the symptomatic population; however, the absence of any cases in the asymptomatic

population precludes performance of statistical tests on this variable.

Discussion

MR imaging is highly sensitive for detecting mucosal thickening of the paranasal sinuses [1]. It has previously been reported with CT that abnormalities in one or more paranasal sinuses are seen in 42% of asymptomatic adults [2]. Similarly, various degrees of mucosal thickening in the paranasal sinuses are commonly seen during routine MR of the brain. Our goal was to delineate the significance of these abnormalities and to determine if there is a degree of mucosal thickening that helps distinguish a symptomatic from an asymptomatic population. Such a finding would be of obvious clinical importance regarding further medical workup and therapy.

An understanding of the normal nasal cycle is essential for interpreting our data. Zinreich et al. [3] report that, in a normal adult, changes in the nasal mucosal volume occur cyclically, alternating from side to side. The time course of each cycle varies from 50 min to 6 hr. Mucosal volume changes are observed in the mucosa of the turbinates, the nasal septum, lateral wall and cavity floor, nasolacrimal ducts, and ethmoidal sinuses. The frontal, maxillary, and sphenoidal sinuses are not affected [3].

Although our patients were scanned at only one time rather

TABLE 1: Comparison of Asymptomatic and Symptomatic Groups with All Mucosal Disease Reported

	Normal	Retention Cysts	Air/Fluid Level or Complete Opacification	Maximal Mucosal Thickening			
				1 mm	2 mm	3 mm	≥4 mm
Asymptomatic (n = 68)	21	8	0	11	30	4	2
Symptomatic (n = 60)	6	10	4	13	23	9	9
T value	2.95	0.80	—	0.73	0.69	1.66	2.37
Two-tailed probability	0.004	0.425	—	0.469	0.491	0.100	0.019

Note.—Absence of air/fluid level or complete opacification in asymptomatic group precluded statistical comparison of that factor.



1



2

Fig. 1.—MR image, SE 2800/90, shows typical appearance of diffuse 2-mm rim of mucosal thickening bilaterally in maxillary sinuses in an asymptomatic patient.

Fig. 2.—MR image, SE 2800/90, shows maximum of 5 mm mucosal thickening in right maxillary sinus in a clinically symptomatic patient.

than cyclically, we think that our findings corroborate those of Zinreich et al. We have found that in the asymptomatic group, 63% of patients had minimal ethmoidal "abnormality," with 1–2 mm of mucosal thickening. That this finding was limited to the ethmoidal sinuses and that the ethmoidal sinuses are the only paranasal sinuses to undergo cyclical mucosal volume changes suggests a direct relationship between these points. Furthermore, Zinreich et al. [3] reported that on T2-weighted images, the hyperintensity of the nasal cycle was similar to that shown by inflammatory mucosa. Given these facts and the prevalence of this mucosal thickening in the asymptomatic population, we postulate that minimal, 1- to 2-mm areas of high T2 signal in the ethmoidal sinuses are a physiologically normal variant, a function of mucosal volume changes occurring in the nasal cycle. Conversely, only two (3%) of 68 asymptomatic patients had areas of ethmoidal mucosal thickening greater than 2 mm. Thus, this degree of thickening is not thought to be a function of normal physiologic responses. The physiologic ethmoidal mucosal edema may be diffuse or focal (Figs. 3A and 3B). It is commonly bilateral, suggesting that in the nasal cycle, the resolution of mucosal edema may be somewhat delayed, such that edema may persist on one side while the contralateral mucosa has already become edematous.

Sinusitis is a nebulous disease, with subjective symptoms that are commonly vague or nonspecific. Clinical history is essential in the assessment of sinus disease [4], but symptoms may not reflect the true state of the paranasal sinuses

[5]. Our study is limited in that we have relied strictly upon clinical history to categorize patients as symptomatic or asymptomatic. Although such a categorization is not definitive of a pathologic diagnosis, it is certainly clinically relevant because only such symptomatic patients would seek medical attention.

In comparing abnormalities between the asymptomatic and symptomatic groups, statistically significant results were obtained only in those patients with normal sinuses and in those with 4 mm or more of mucosal thickening. We are not suggesting that mucosal disease of 3 mm or less is not clinically significant; however, our results show that up to 3 mm of mucosal thickening may commonly be seen in asymptomatic patients. As such, findings on radiographs and MR images may not match clinical symptoms. Thus, clinical correlation is required rather than blanket medical therapy.

The absence of any cases of air/fluid levels or complete sinus opacification in the asymptomatic group precludes statistical comparison with the symptomatic group. However, on the basis of the four cases in the symptomatic group, we suspect that extrapolation to a larger study population would show this factor to be significant.

Retention cysts are due to obstruction and dilatation of a duct of a minor seromucinous gland. They are typically asymptomatic [4], and their comparable prevalence in our two populations was expected.

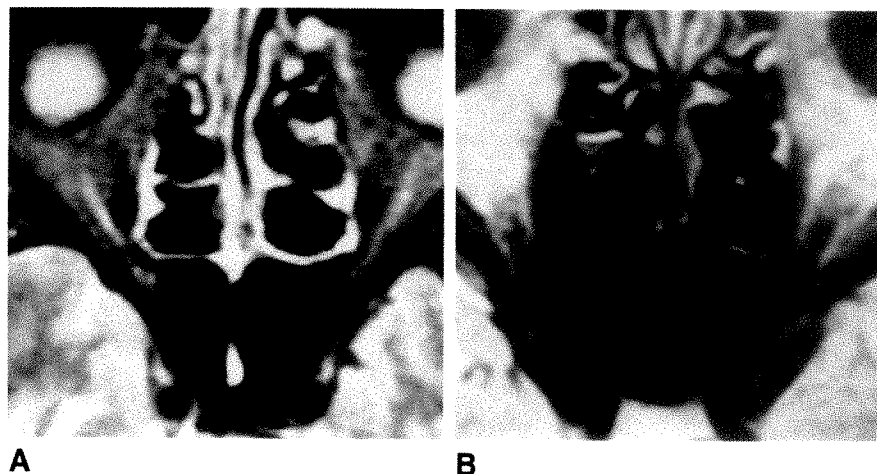
In conclusion, 1- to 2-mm areas of mucosal edema/thickening in the ethmoidal sinuses are thought to be a normal

**TABLE 2: Comparison of Asymptomatic and Symptomatic Groups with 1–2 mm of Mucosal Thickening in Ethmoidal Sinuses Classified as Normal**

	Normal	Maximal Mucosal Thickening			
		1 mm <sup>a</sup>	2 mm <sup>a</sup>	3 mm	≥4 mm
Asymptomatic (n = 68)	44	11	7	4	2
Symptomatic (n = 60)	24	5	13	9	9
T value	2.92	1.41	1.85	1.66	2.37
Two-tailed probability	0.004	0.160	0.066	0.100	0.019

<sup>a</sup> Exclusive of ethmoidal sinuses.

**Fig. 3.—A and B, MR images, SE 2800/90, show diffuse (A) and focal (B) mucosal edema in ethmoidal sinuses. Findings of this degree are thought to be physiologic. Both patients were asymptomatic.**





variant, due to the physiologic nasal cycle. With paranasal sinus inflammation, a significant difference in prevalence between symptomatic and asymptomatic patients is seen only with mucosal thickening of 4 mm or more. Although patients with less than 4 mm of mucosal thickening certainly may be symptomatic, our data suggest that this degree of abnormality is commonly not clinically significant. We intend to extend our study to a larger population to evaluate these findings further.

#### ACKNOWLEDGMENT

We acknowledge the advice and assistance of Janice L. Birney in the preparation of the questionnaire used in this study.

#### REFERENCES

1. Shapiro MD, Som PM. MRI of the paranasal sinuses and nasal cavity. *Radiol Clin North Am* **1989**;27:447-475
2. Havas TE, Motbey JA, Gullane PJ. Prevalence of incidental abnormalities on computed tomographic scans of the paranasal sinuses. *Arch Otolaryngol Head Neck Surg* **1988**;114:856-861
3. Zinreich SJ, Kennedy DW, Kumar AJ, Rosenbaum AE, Arrington JA, Johns ME. MR imaging of normal nasal cycle: comparison with sinus pathology. *J Comput Assist Tomogr* **1988**;12:1014-1019
4. Cummings CW, ed. *Otolaryngology—head and neck surgery*. St Louis: Mosby, **1986**:851-852, 1501-1502
5. Middleton E Jr, Reed CE, Ellis EF, Adkinson NF Jr, Yunginger JW, eds. *Allergy: principles and practice*. St. Louis: Mosby, **1989**:1295-1301



The Radiology Outreach Foundation (ROF) is a nonprofit corporation whose goal is to help disadvantaged countries improve their health care by providing radiology equipment, books, consultation, education, and training to their practitioners. This assistance is on an application basis that is independent of political, ethnic, or religious orientation of the grantee. It depends on the need of the people and the ability of the ROF to meet that need. The ROF is approved by the U.S. Internal Revenue Service as a tax-exempt organization. It is endorsed by the following radiologic societies: American Association of Women Radiologists, American College of Radiology, American Roentgen Ray Society, Association of University Radiologists, Radiological Society of North America, Society of Chairmen of Academic Radiology Departments, Society for Pediatric Radiology, European Society of Pediatric Radiology.

All donations to the ROF are tax deductible. Persons who would like to contribute financially to the ROF, would be interested in being a visiting professor, would like to send books or journals to any of the institutions supported by the ROF, or would like further information about the ROF should write to Charles A. Gooding, M.D., President, Radiology Outreach Foundation, 3415 Sacramento St., San Francisco, CA 94118 USA.

# Angiography Is Useful in Detecting the Source of Chronic Gastrointestinal Bleeding of Obscure Origin

Edward S. Rollins<sup>1,2</sup>  
 Daniel Picus<sup>1</sup>  
 Marshall E. Hicks<sup>1</sup>  
 Michael D. Darcy<sup>1</sup>  
 Bruce L. Bower<sup>1,3</sup>  
 Michael A. Kleinhoffer<sup>1</sup>

The treatment of patients with chronic gastrointestinal bleeding can be a frustrating diagnostic challenge. In the past 10–15 years, a variety of new diagnostic procedures (e.g., fiber-optic endoscopy, scintigraphy, and double-contrast barium studies) have become available to examine these patients. Despite these new procedures, a small number of patients continue to bleed without a defined cause. We sought to evaluate the role of visceral angiography in patients with chronic gastrointestinal bleeding in whom findings on an extensive noninvasive workup have been normal. Between 1983 and 1990, we obtained angiograms on 36 such patients. The cause of bleeding was established by angiography in 16 patients (44%). In 11 of these 16, angiography revealed only a structural abnormality without active bleeding. Twenty patients had normal angiographic findings. No angiograms were false-positive, but three were false-negative (8%). No complication occurred as a result of the angiographic procedures.

Our experience shows that visceral angiography can provide a positive diagnosis in a significant number of patients with chronic gastrointestinal bleeding of obscure origin in whom all other diagnostic measures have been unrevealing. Despite improvements in noninvasive diagnostic techniques, angiography still remains an important tool for examining this group of patients.

*AJR* 156:385–388, February 1991

Gastrointestinal bleeding is a common cause for hospitalization, particularly in the elderly. Fortunately, in 80–90% of patients, the source of bleeding can be determined quickly by conventional diagnostic investigations such as endoscopy or barium examinations. About half of the remaining 10–20% of patients in whom no bleeding source is identified spontaneously stop bleeding and never have bleeding again. However, about 5% of patients continue to bleed, chronically or intermittently, from an unidentified source [1–3]. These cases usually are defined as chronic gastrointestinal bleeding of obscure origin [4].

The treatment of these patients is a frustrating diagnostic challenge that can consume an inordinate amount of medical resources. These patients often require multiple hospitalizations and blood transfusions, in addition to a diagnostic workup that typically includes repeated endoscopies, barium examinations, and radio-nuclide scans [1–3]. Definitive therapy for these patients ultimately depends on locating the source of the bleeding.

In 1975, Sheedy et al. [5] showed the value of diagnostic angiography in a series of 88 patients with chronic gastrointestinal bleeding. Angiography was extremely helpful in these patients; a diagnosis was established in 45%. Nevertheless, it is our experience that angiography in such patients is often delayed until late in the diagnostic workup. This may be due to the presumption that angiography is too invasive or will not be helpful because the patient is not actively bleeding clinically. Alternatively, it is possible that the new techniques (e.g., flexible fiber-optic endoscopy, intraoperative endoscopy, double-contrast barium studies, and scintigraphy) that have been developed in the past 15 years have reduced the value of angiography in these patients.

Received June 28, 1990; accepted after revision August 29, 1990.

<sup>1</sup> Mallinckrodt Institute of Radiology, Washington University School of Medicine, 510 S. Kingshighway Blvd., St. Louis, MO 63110. Address reprint requests to D. Picus.

<sup>2</sup> Present address: Northside Hospital, P.O. Box 3726 CRS, 401 Princeton Rd., Johnson City, TN 37602.

<sup>3</sup> Present address: San Diego Diagnostic Radiology, P.O. Box 23540, San Diego, CA 92123.

0361-803X/91/1562-0385  
 © American Roentgen Ray Society

We sought to reevaluate the role of angiography in patients with chronic obscure gastrointestinal bleeding in light of the host of new noninvasive diagnostic techniques. To this end, we examined our experience during a 7-year period with elective angiography for occult gastrointestinal bleeding in patients for whom an extensive workup before angiography failed to establish the source of bleeding.

### Subjects and Methods

Between July 1983 and April 1990, 172 patients had angiography for gastrointestinal bleeding at our institution. Of these 172 patients, the following were excluded from further consideration: patients for whom the current bleeding episode was the first, patients with known gastroesophageal varices, patients with a chronic bleeding diathesis, and patients for whom a source of bleeding already had been determined and in whom angiography was being performed solely for therapeutic reasons (intraarterial embolization or infusion of vasopressin).

Of the 172 patients, 36 fit the criteria of having chronic gastrointestinal bleeding of obscure origin because they had had multiple episodes of bleeding with an extensive diagnostic workup that had failed to reveal the source. These 36 patients ranged in age from 27 to 84 years (mean, 68 years). Eleven patients had been chronically bleeding for less than six months, 10 patients for 6 months to 1 year, and 15 for longer than 1 year. Preangiographic procedures to diagnose the cause of bleeding in these 36 patients included barium studies of the entire gastrointestinal tract, esophagoduodenoscopy, sigmoidoscopy, and colonoscopy, as well as scintigraphy. Four of the 36 patients had undergone previous exploratory laparotomies for the diagnosis of obscure bleeding, and three of these had had intraoperative endoscopy. Seven patients had had visceral angiography. The total number of preangiographic procedures for each of the 36 patients ranged from three to 13, with a mean of 6.5.

Except for the radionuclide scans, the preangiographic studies were all normal or inconclusive. The radionuclide scans, although abnormal on one or more occasions in 16 patients, did not end the patient's diagnostic evaluation, but provided guidance for subsequent angiography. The 16 patients with abnormal findings on radionuclide scans were equally divided between those in whom angiography established a bleeding source (8/16 patients) and those in whom it did not (8/20 patients).

The hospital records of these 36 patients were reviewed to determine the chronicity and severity of bleeding and to determine which and how many preangiographic procedures had been performed and their results. The angiographic studies of all 36 patients were reviewed to establish the technical quality, angiographic findings, and any angiographically related complications.

All angiographic studies were performed via retrograde puncture of the femoral artery. Standard film-screen techniques were used in all patients. Subtraction techniques and magnification were used as adjuncts when appropriate. The superior mesenteric, inferior mesenteric, and/or celiac arteries were examined.

In three patients, provocative techniques were used when standard angiography failed to establish the source of bleeding [6]. Heparin (5000–10000 units) and tolazoline hydrochloride (25–50 mg) both were injected directly into the superior mesenteric artery in an effort to induce bleeding. This was followed by one or more additional diagnostic angiographic examinations.

The angiographic diagnosis was correlated with the long-term clinical outcome, particularly the recurrence of gastrointestinal bleeding. In those patients undergoing surgery, the results of pathologic examinations were compared with the angiographic interpretation.

### Results

Of the 36 patients undergoing diagnostic angiography, angiographic diagnoses were established in 16 (44%). In the remaining 20 patients, the angiographic findings were normal. No complications occurred from the angiographic procedures. Clinical follow-up on all 36 patients ranged from 3 to 78 months (mean, 32 months).

#### *Source of Bleeding Established with Angiography*

Of the 16 patients in whom angiography established a source of bleeding, 13 had surgical resection as a direct result of the angiographic findings. In 11 of these 13, pathologic findings confirmed the angiographic diagnosis. In the other two patients, both of whom were thought on angiography to have a cecal angiodysplasia, the pathologic findings were inconclusive or normal. Unfortunately, in neither of these two cases was the resected specimen examined with specimen-injection techniques [5]. Of the three patients who did not have surgery, two had active bleeding at the time of angiography, and intraarterial embolization was performed and was successful in both; the remaining patient spontaneously stopped bleeding, and because of severe underlying cardiac disease, had no further workup.

In 11 of the 16 patients, angiography revealed only a structural abnormality; active bleeding was not seen. These abnormalities, which were confined to the jejunum, ileum, and ascending colon, consisted of six cases of arteriovenous malformation or angiodysplasia; two cases of small-bowel leiomyoma; and one case each of new-onset Crohn disease, radiation injury to the ileum, and idiopathic portomesenteric venous thrombosis.

In five patients, active bleeding was observed at the time of angiography. The sites of bleeding were much more widespread than in the previously mentioned 11 patients; foci were detected from the stomach to the rectum. In one patient, the bleeding was thought to arise from a colonic diverticulum; in another, a cecal angiodysplasia was reported. In the remaining three patients, no specific cause for the active bleeding was detected.

In four patients, previous angiographic studies had failed to establish the source of bleeding. In two of these patients, the angiography had been performed at another hospital several months or years earlier; the other two patients had had angiography performed at our institution only a few days earlier. In these two patients, bleeding was intermittent and was observed during the second angiographic study only.

Fourteen of the 16 patients in this group are still living; the two other patients died from causes unrelated to gastrointestinal bleeding. None of the patients have had continued gastrointestinal bleeding.

#### *No Source of Bleeding Established with Angiography*

Of the 20 patients with normal angiographic findings, four had surgical resection during the same hospitalization. Three patients had surgery empirically, based on localization of



bleeding by the RBC scans, and one had a partial jejunectomy for a jejunal arteriovenous malformation detected at the time of exploratory laparotomy and intraoperative endoscopy. Two of these four patients have had recurrent bleeding despite the surgical resection; bleeding has ceased in the other two.

Two patients who continued to have bleeding after normal findings on angiography had surgical resection several months after the original hospitalization. One patient had small-bowel obstruction due to small-bowel adenocarcinoma 16 months later. After surgical resection of the tumor, no gastrointestinal bleeding has been observed. The other patient died of uremia and sepsis after right hemicolectomy, which was performed because of fulminant uremic colitis; this patient had not been uremic when the original angiography was performed 6 months earlier.

One patient who was seropositive for human immunodeficiency virus died of sepsis and pneumonia while hospitalized for the angiography. At autopsy, despite the presence of fresh blood throughout the bowel, no causative lesion could be found.

Of the remaining 13 patients who did not have surgery, no cause for the bleeding has been found. This group is equally divided. Seven have had complete resolution of the bleeding, and six have had recurrent, intermittent gastrointestinal bleeding.

In three patients, provocative measures were used during diagnostic angiography [6]. However, these provocative maneuvers did not show an occult lesion or induce active bleeding in any of these three patients.

## Discussion

In this series of 36 angiographic studies, a source of gastrointestinal bleeding was established in 44%, a yield essentially identical to the 45% figure reported by Sheedy et al. [5] in 1975. Despite innovations and improvements in noninvasive techniques during the past 15 years, angiography still can detect the cause of bleeding in a significant number of patients with obscure sources of chronic gastrointestinal bleeding.

Although our results and those of Sheedy et al. are similar in the percentage of cases for which a source was established angiographically, they differ in two important respects: the type and distribution of lesions discovered. In the study of Sheedy et al., the sources of bleeding included a wide variety of lesions, with arteriovenous malformations accounting for approximately 50%. In our series, however, the range of lesions was much more limited, so that, although the overall yield was the same, the spectrum of lesions detected was different. As before, arteriovenous malformations accounted for about half of the discovered lesions. However, in contrast, no gastrointestinal polyps or carcinomas (one false-negative) were discovered. Instead, a higher proportion of leiomyomas and other ileal diseases were seen. This change in the type of lesions found probably occurred because patients with polyps and carcinomas are examined more effectively with modern diagnostic tools (e.g., double-contrast barium studies

and endoscopy) and do not require angiography for ultimate diagnosis.

As a corollary to the type of lesion found, the distribution of these lesions within the gastrointestinal tract in our series was much more limited than that seen by Sheedy et al. In the 11 cases in which we found only a structural lesion (no active bleeding), the discovered lesions were confined entirely to the jejunum, ileum, cecum, and ascending colon. Most likely this change in distribution reflects the improved examination proximal and distal to these regions that is possible with modern flexible fiber-optic endoscopy; only lesions occurring in these difficult-to-reach regions escape detection before angiography.

Among the 16 patients in whom angiography established a source of bleeding, no false-positive diagnoses were made, which is identical to the results reported in 1975. Although two patients with presumed angiodysplasia had pathologic findings after surgery that were not confirmatory, failure to find an angiodysplasia at anatomic dissection, particularly when specimen-injection techniques are not used, is not uncommon [5]. Most importantly, neither of these patients has had recurrent gastrointestinal bleeding.

Of the 20 patients with normal angiographic studies, the diagnosis in three patients was falsely negative. Two of these patients had jejunal arteriovenous malformation, and the third had an adenocarcinoma of the ileum. Review of the angiographic studies in these patients revealed no technical cause for the erroneous interpretations; the films were of good technical quality, and a complete study had been performed. Presumably the abnormalities were simply below the threshold of detectability on angiography. None of these three patients showed signs of active bleeding on angiography, including one who received intraarterial heparin and tolazoline hydrochloride in an unsuccessful attempt to provoke bleeding or unmask a subtle lesion [6]. This false-negative rate of 8.3% is similar to the 6.8% recorded by Sheedy et al. [5] in 1975. Although this frequency is higher than would be desired, in these patients who frequently require numerous hospitalizations and extended diagnostic evaluations, it should not deter physicians from proceeding with angiography when appropriate.

It is noteworthy that four of the 16 patients in whom angiography established a source of bleeding had had a previous angiographic study that did not reveal the cause. A similar rate (six of 24 patients) for establishment of a source on repeated angiography has been reported by Lau et al. [7]. Although repeated angiographic studies usually are timed to coincide with clinically active bleeding, actual bleeding was seen in only two of our four patients and in two of six patients in Lau's series. In the remaining patients, a structural lesion was discovered that had not been detected earlier. Although our series contains too few patients for us to make a final conclusion, it appears that repeated angiography, particularly in difficult cases, can occasionally be diagnostic. We recommend that repeated angiography be considered for those patients in whom bleeding continues.

Angiography is often considered valuable only when the patient is actively bleeding. Radionuclide scans have become

a widely used noninvasive screening method to detect active bleeding, and many physicians are reluctant to perform angiography in a patient in whom radionuclide scans do not show bleeding. In our 36 patients, only 16 had had positive radionuclide studies. These 16 patients were equally divided between patients in whom angiography established a source of bleeding and those in whom it did not. Although radionuclide scans are extremely helpful in directing subsequent angiographic investigation, we believe our data support the performance of angiography in selected circumstances even if findings on a radionuclide scan are normal. In 11 of 16 patients, the source of bleeding was found despite the lack of active extravasation of contrast material. Angiography can detect structural abnormalities such as angiodysplasia, tumor, and inflammatory lesions that may cause chronic obscure gastrointestinal bleeding and that escape detection with other diagnostic procedures.

Current estimates suggest that approximately 5% of all patients with gastrointestinal bleeding ultimately will fall into the category of patients with chronic bleeding of obscure origin [4]. In the 1950s, roughly 15–25% of patients with gastrointestinal bleeding were so categorized [8]. This decline is certainly a result of the improved diagnostic techniques available today. However, although fewer patients with gastrointestinal bleeding ultimately fall into the category of patients with chronic bleeding of obscure source, angiography still establishes a source of bleeding in 44%.

In conclusion, in patients with chronic gastrointestinal bleeding of obscure origin, in whom all other diagnostic measures have been unrevealing, visceral angiography safely can establish the source of bleeding in a significant number of cases. This is true even if the patient is not actively bleeding. Despite improvements in noninvasive diagnostic techniques, angiography still remains an important tool in the examination of this group of patients. The use of angiography earlier in the workup of these patients may expedite the diagnosis.

#### REFERENCES

1. Spiller RC, Parkins RA. Recurrent gastrointestinal bleeding of obscure origin: report of 17 cases and a guide to logical management. *Br J Surg* **1983**;70:489–493
2. Lau WY, Fan ST, Wong SH, et al. Preoperative and intraoperative localization of gastrointestinal bleeding of obscure origin. *Gut* **1987**;28:869–877
3. Thompson JN, Slaem RR, Hemingway AP, et al. Specialist investigation of obscure gastrointestinal bleeding. *Gut* **1987**;28:47–51
4. Steger AC, Spencer J. Obscure gastrointestinal bleeding. *Br Med J* **1988**;296:3
5. Sheedy PF, Fulton RE, Atwell DT. Angiographic evaluation of patients with chronic gastrointestinal bleeding. *AJR* **1975**;123:338–347
6. Rosch J, Kozak BE, Keller FS. Interventional diagnostic angiography in acute lower-gastrointestinal bleeding. *Semin Intervent Radiol* **1988**;5:10–17
7. Lau WY, Ngan H, Chu KW, Yuen WK. Repeat selective visceral angiography in patients with gastrointestinal bleeding of obscure origin. *Br J Surg* **1989**;76:226–229
8. Jones FA, Read AE, Stubbe JL. Alimentary bleeding of obscure origin. *Br Med J* **1959**;1:1138–1142

# Iliac Artery Stenosis or Obstruction After Unsuccessful Balloon Angioplasty: Treatment with a Self-Expandable Stent

R. W. Günther<sup>1</sup>  
D. Vorwerk<sup>1</sup>  
F. Antonucci<sup>2</sup>  
B. Beyssen<sup>3</sup>  
A. Essinger<sup>4</sup>  
J. C. Gaux<sup>3</sup>  
F. Joffre<sup>5</sup>  
A. Raynaud<sup>3</sup>  
H. Rousseau<sup>5</sup>  
Ch. L. Zollkofer<sup>2</sup>

Obstruction or stenosis of the iliac artery was treated by placement of a self-expandable stent in 91 patients. A total of 100 lesions was treated. All patients had had poor results of balloon angioplasty including residual stenosis, iliac occlusion, and dissection. The stent used in all cases was a self-expandable stainless steel endoprosthesis mounted on a 7- or 9-French catheter and covered by an invaginated tubular rolling membrane. The diameter of the expanded stent varied from 7 to 12 mm. A total of 129 stents was placed. Technical success was 97%. Thromboses occurred immediately after placement in two patients and within the first month in six; these were mainly due to residual obstruction. Eighty-two (93%) of 88 patients with a follow-up longer than 3 months had no recurrent symptoms. Restenosis caused by intimal hyperplasia inside the stent occurred in 10 patients; these required repeated intervention in only four cases. In the remaining six patients, no further complications occurred.

Our results show that self-expanding endoprostheses are of value for improving the results of inadequate percutaneous transluminal angioplasty.

*AJR* 156:389-393, February 1991

Percutaneous transluminal angioplasty (PTA) for the treatment of stenoses of the iliac artery has a high rate of success [1]. However, in some patients PTA [2, 3] is either technically unsuccessful or restenosis occurs [1]. We studied the value of a self-expandable Wallstent type of endovascular prosthesis for treatment of such lesions in our first 100 consecutive patients.

## Materials and Methods

### Instrumentation

The Wallstent prosthesis (Medinvent Inc., Lausanne, Switzerland) is a tubular structure braided from surgical-grade spring stainless steel monofilaments. Because of the spring characteristics of the monofilaments and because the braided elements are free to pivot over each other, the prosthesis can be stretched elastically to an elongated format of small diameter. When released, the stent recoils to its shorter, preset unrestrained diameter.

The stents are selected so that the unrestrained diameter is between 1 and 2 mm larger than the target vessel. When implanted, the stent then can exert a residual radial pressure against the vessel wall, preventing collapse and holding the stent in place. The stent is premounted on a flexible delivery catheter, permitting access via tortuous and contralateral vessels. The distal catheter segment remains flexible despite the presence of the mounted prosthesis. The maximal external diameters of the delivery devices were 7-French for stents of 7- to 10-mm unrestrained diameter and 9-French for 12- to 14-mm unrestrained diameters. The catheters are coaxial; the inner shaft is joined to the external shaft by an invaginated tubular rolling membrane, which covers and retains the stent stretched on the inner shaft.

Hydraulic pressure of 3.5-4.0 atmospheres (350-400 kPa) applied to the anular space between the two layers of the rolling membrane facilitates rolling the membrane back off the stent. Peeling the membrane back like an inverted glove, therefore, allows the restrained prosthesis to open progressively. As long as the stent is deployed only partially, it can be

Received March 7, 1990; accepted after revision August 10, 1990.

<sup>1</sup> Department of Diagnostic Radiology, University of Technology, Aachen, Pauwelsstrasse, D-5100 Aachen, Germany. Address reprint requests to R. W. Günther.

<sup>2</sup> Department of Radiology, Kantonsspital Winterthur, Winterthur, Switzerland.

<sup>3</sup> Department of Radiology, Hôpital Broussais, Paris, France.

<sup>4</sup> Department of Diagnostic Radiology, Centre Hospitalier Universitaire Vaudois, Lausanne, Switzerland.

<sup>5</sup> Department of Radiology, Hôpital Universitaire Rangueil, Toulouse, France.

0361-803X/91/1562-0389

© American Roentgen Ray Society



retrieved by pulling out the delivery system. In order to avoid inadvertent further deployment of the stent during this maneuver, the hydraulic pressure must be released. Pushing the partially open stent will not result in repositioning, but must be avoided because the open end will engage the vessel wall.

#### Patients

Eighty men and 11 women with a mean age of 55 years (range, 36–88 years) and a total of 100 iliac lesions were included in this study. Of the lesions, 50 were located in the common iliac artery; 37 in the external iliac artery; and 13 in both the common and external iliac arteries, bridging the orifice of the internal iliac artery. According to Fontaine's classification, 11 patients had stage IIa claudication (walking distance 200 m and more), and 79 had stage IIb (walking distance less than 200 m). Six patients had pain at rest (stage III), and four had cutaneous necrosis (stage IV). Risk factors such as smoking ( $n = 84$ ), hypertriglyceridemia ( $n = 23$ ), hypercholesterolemia ( $n = 29$ ), hypertension ( $n = 38$ ), and diabetes ( $n = 9$ ) were found. All patients gave their informed consent to participate. Contraindications to stent placement were acute thrombosis, vascular rupture after

PTA, and severe coagulation defects. Stent placement was not considered after successful PTA.

Patients were considered for stent treatment only if their lesions did not respond well to angioplasty with respect to either immediate technical failure or poor results. Thus, patients with restenosis after previous angioplasty ( $n = 30$ ) or occlusions ( $n = 25$ ) were included. Thirteen patients were treated for flow-impairing dissections caused by previous angioplasty (Figs. 1 and 2). In 32 patients PTA was considered unsatisfactory, which was defined as a residual stenosis greater than 30% and/or a residual systolic pressure gradient of 20 mm Hg after administration of vasodilating drugs and reduced blood flow. Table 1 gives an overview of the reduction in vessel diameter before and after PTA and after placement of the stent.

The mean length of all 100 lesions was 42 mm (range, 10–180 mm; Table 2). One third of all lesions were longer than 5 cm. Lesions longer than 5 cm were found in 13% (4/30) of patients with restenosis, 72% (18/25) of patients with occlusion, 23% (3/13) of patients with dissection, and 25% (8/32) of patients with post-PTA recoil. A total of 129 stents was used in this study. Stents with implanted lengths of around 33 and 66 mm were available for implantation. Stents were selected to be longer than the target lesion, and the stented area

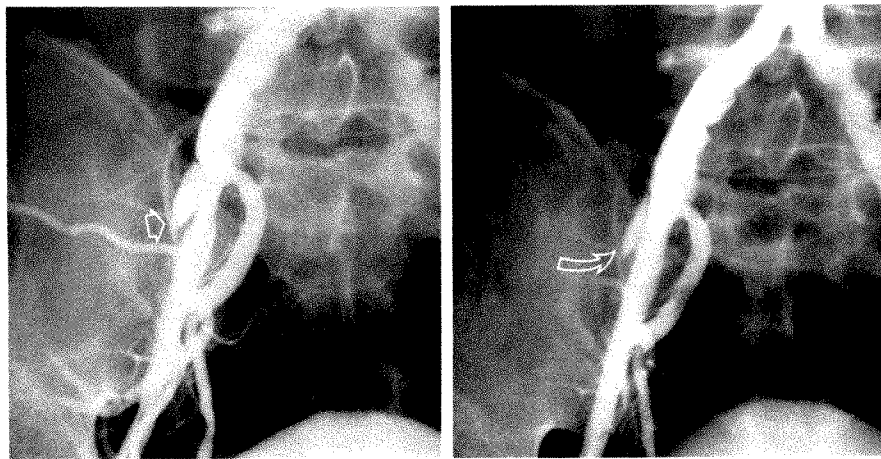


Fig. 1.—Complex lesion of right external iliac artery.

A, Angiogram obtained after dilatation with 8-mm balloon shows residual stenosis in short segment of proximal external iliac artery close to orifice of internal iliac artery. Note aneurysmal dissection (arrow) caused by angioplasty performed 4 months earlier.

B, Angiogram obtained after placement of an 8-mm stent shows normal vascular diameter and size of dissection (arrow) markedly decreased.

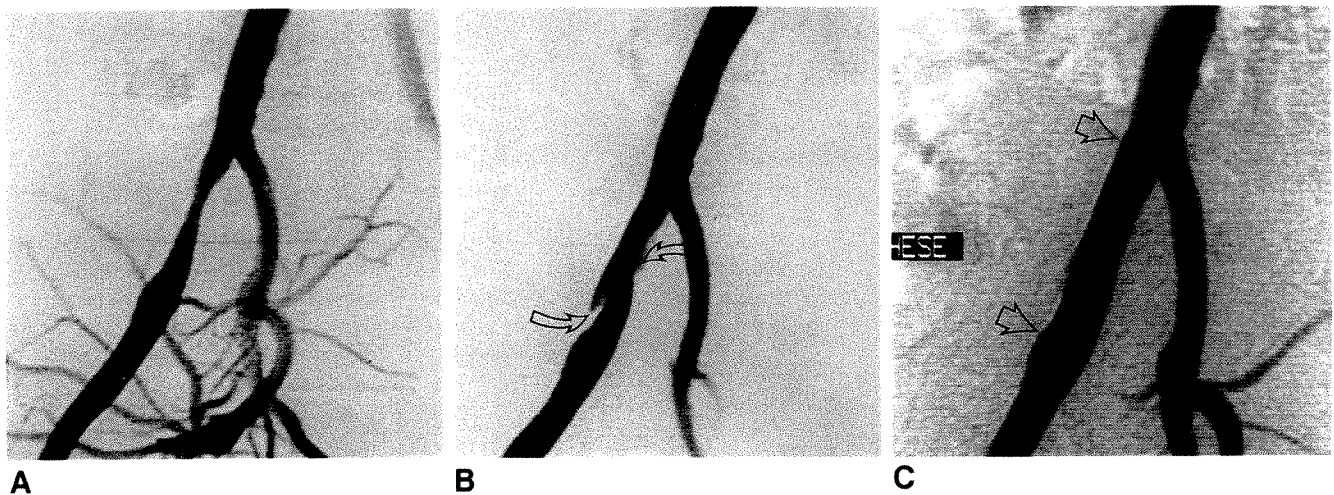


Fig. 2.—Acute complication treated by stent implantation.

A, Angiogram shows simple stenosis in a short segment of right external iliac artery that is amenable to balloon dilatation alone.

B, Angiogram obtained after dilatation with a 7-mm balloon shows marked dissection (arrows) compromising blood flow.

C, Angiogram obtained after immediate placement of a 8-mm Wallstent (arrows) shows restored vascular diameter.

**TABLE 1: Grade (%) of Stenosis or Obstruction Before and After Percutaneous Transluminal Angioplasty (PTA)**

	Restenosis (n = 30)	Occlusion (n = 25)	Dissection (n = 13)	Post-PTA Recoil (n = 32)
Before PTA	82 (60-90)	100	83 (50-90)	84 (60-90)
After PTA	46 (30-90)	62 (40-100)	46 (30-80)	51 (30-80)
After stent	9 (0-40)	4 (0-50)	10 (0-40)	17 (0-40)

**TABLE 2: Length (cm) of Stenosis or Obstruction Before and After Percutaneous Transluminal Angioplasty (PTA)**

	Restenosis (n = 30)	Occlusion (n = 25)	Dissection (n = 13)	Post-PTA Recoil (n = 32)
Minimum	1.0	3.0	1.0	1.0
Maximum	18.0	10.0	10.0	11.0
Mean	3.5	5.9	3.9	3.4

varied from 35 to 190 mm (mean, 61 mm). When a single lesion required two or more stents, the stents were placed with an overlap of approximately 10 mm, preferably from proximal to distal. In 76 lesions, one stent was implanted; in 19 lesions, two stents were used; and in five lesions, three stents were used. The unrestrained stent diameters were 7, 8, 10, and 12 mm. Vessel access was from the ipsilateral side in 88 lesions and from the contralateral approach in 12.

#### Medication

Acetylsalicylic acid was given 24 hr before the procedure and again on the day of the procedure. An intraoperative dose of 5000 IU of heparin was given; this was supplemented by a further 2000 IU if the procedure took longer than 1 hr. The protocol included postoperative heparin administration for 24 hr at a rate of 1000 IU/hr. Anticoagulation with warfarin for 3-6 months after treatment was used early in the study for a limited number of patients (30 lesions in 27 patients) who had an occlusion treated or outflow problems such as an occlusion of the ipsilateral superficial femoral artery.

#### Follow-up

Before being discharged, all patients underwent a postoperative clinical examination and Doppler evaluation. IV digital subtraction angiography was performed selectively. The follow-up protocol called for angiographic examination of all patients who were symptomatic and for clinical and, if possible, angiographic studies at 1 (or 3), 6, and 12 months. In cases in which the follow-up period exceeded 12 months, additional angiographic studies were performed at 24 months and later. For the purpose of reporting, restenosis was defined as recurrent luminal narrowing within or adjacent to the stent exceeding 20% of the previously restored diameter regardless of whether the patient was symptomatic.

#### Results

Primary technical success was achieved in 97 of 100 lesions. Complications occurred during treatment of 12 lesions and were severe in three (Table 3).

Two cases of acute thrombosis occurred. One happened

**TABLE 3: Complications (n = 100 Lesions)**

Severe complications	
Immediate thrombosis	2
Perforation of the vessel before stenting	1
Moderate complications	
Misplacement of a stent	7
corrected by an additional stent	5
Hemarthros, hematuria (due to warfarin)	2
Overall complication rate	12

during an implantation that was performed perioperatively as an adjunct procedure to a surgical crossover bypass. The thrombosis was caused by vascular clamping proximal to the implantation site. The other acute thrombosis occurred in a patient who had stage IV atherosclerotic disease, an iliac occlusion, and poor outflow conditions.

Technical complications developed in one patient (two lesions) with bilateral iliac disease after a successful stent implantation on one side. His contralateral vessel was to be treated, but a perforation of the artery was found after balloon angioplasty; the patient was transferred for bilateral reconstructive surgery.

Although misplacement occurred in seven (5%) of 129 stents implanted, it never had serious consequences. In four of these cases, a second stent was placed successfully during the same procedure to cover the lesion completely. In two cases, coverage by the stent remained incomplete, requiring reintervention: in one patient, an additional stent was implanted 2 months later; in the other, a proximal dissection was not sealed by the stent and was found thrombosed at follow-up. In all seven cases, misplacement was associated with lesions close to the aortic bifurcation or the origin of the internal iliac artery. The stent did not migrate in any case.

No groin hematoma requiring surgical intervention or retroperitoneal hematoma was observed. In two patients, complications due to warfarin therapy occurred—one had spontaneous hemarthrosis of the knee, the second had macrohematuria because of a small vesical tumor.

Six additional cases of reocclusion occurred within the first month after treatment. Prevalence of early thrombosis was almost the same, with 6% (4/70) in patients taking acetylsalicylic acid and 7% (2/30) in those taking anti-vitamin K. In three of those patients, a proximal dissection ( $n = 1$ ) or plaque ( $n = 2$ ) was covered incompletely by the stent, thereby causing an inflow obstruction. In one patient (stage IV disease, alcohol-induced hepatic insufficiency, acetylsalicylic acid medication), rethrombosis of the stent occurred 8 days after treatment. It was found after the patient had attempted suicide and probably was due to severe hypotension.

Thromboses occurred in two other cases without any obvious reasons. Medication included acetylsalicylic acid in one and warfarin in the other. Consequently, early patency at 3-month follow-up was seen in 90 of 100 lesions. Clinical benefit was seen in 88 of 100 lesions. Clinical symptoms improved for patients with Fontaine's stage I in 24, for stage II in 59, and for stage III in five lesions. No clinical change was seen in three patients without complications but with additional femoral lesions.



Eighty-two patients with 90 lesions were considered for follow-up studies longer than 3 months, which included clinical examination and Doppler evaluation for 26 lesions and clinical examination, angiographic studies and, if possible, Doppler imaging for 62 lesions. Two patients (two lesions) were lost to follow-up. Mean follow-up time was 13.5 months (range, 2–39 months). Ten lesions were followed up for 24 months or longer, 33 for 12–23 months, and 39 for 6–11 months. Six lesions were followed up for less than 6 months. In one patient, the stent was removed during bypass surgery for an aortic aneurysm 18 months after treatment [4]. One patient died 4 months after treatment.

Clinically, no recurrence or worsening of symptoms was found for 82 (93%) of 88 lesions during the reported period of follow-up. All patients who became symptomatic again underwent angiography. Symptomatic restenosis was diagnosed between 4.5 and 26.0 (mean, 11.5) months after treatment.

Restenosis was found within the endoprostheses of seven (11%) of 62 lesions with angiographic follow-up, but reintervention was required in only three symptomatic patients; this was done either by atherectomy or balloon dilatation (Fig. 3). Restenosis touching the extremities of the stent occurred in three patients; one of these required reintervention. In four cases, new lesions were detected that were unassociated with the stent in place. This means that recurrent symptoms were associated with restenosis within or close to a stent in four of six cases. Angiographic restenosis was related to the implant in 10 of 14 cases. Thus, the prevalence of clinically relevant restenosis inside the stent was 5% (4/88), and the angiographic prevalence of restenosis was 16% (10/62).

## Discussion

Early technical success and a long-term patency helped establish PTA [2, 3] of the iliac arteries as a widely accepted procedure [1]. A mean initial success rate of 92% and a 2-year patency rate of 81% were calculated by Becker and co-workers after analyzing the data from 2697 iliac procedures

[1]. A positively biased selection of the patients undergoing PTA must, however, be assumed because a subset of iliac lesions is known to respond poorly to this treatment. A poor result after angioplasty may be characterized by flow-obstructing dissection or recoil of the stenosis typified by the collapsing bifurcation lesion at the iliac orifice [1]. Significant residual stenosis after PTA complemented by a high-grade residual pressure gradient across the lesion is associated with a higher rate of recurrence [5]. Beyond this, controversy exists on the usefulness of PTA of iliac occlusions. Percutaneous treatment of iliac occlusions, especially those longer than 2 cm, is infrequent. Early papers [6, 7] reported a high rate of complications. The group of complex iliac lesions also may include iliac restenoses after previous PTA, long and eccentric lesions [1], and extensively ulcerated plaques. An innovative technique such as placement of a stent must prove its clinical benefit by improving both the initial technical success and the long-term patency of this subgroup of complex lesions.

Modern theories of the mechanism of balloon angioplasty favor fracture of plaque material and medial stretching [8]. Such controlled vascular injury, however, can cause severe changes in the intraluminal geometry, such as deep dissection, that increase the chances of early technical failure [1]. Implantation of a stent helps remodel the inner vascular surface by displacing an eccentric plaque or a dissecting membrane into the vessel wall. The implant is a foreign body, however, and thus poses additional problems, particularly thrombogenicity.

In our patients, early technical failure generally was due to acute or subacute occlusion and occurred in nine of 100 lesions. This rate is somewhat high compared with the results of simple balloon angioplasty. However, a negatively biased selection of lesions not primarily amenable to percutaneous treatment must be taken into consideration. Impaired blood flow combined with presence of a foreign body certainly predisposes to thrombotic reocclusion, and in five of our patients, obstruction of either the inflow or the outflow was still present despite implantation of a stent. Most of these

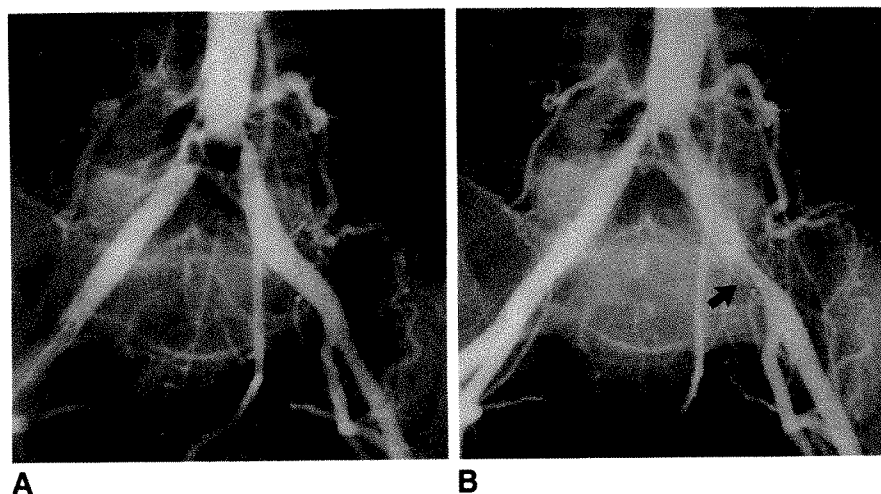


Fig. 3.—Restenosis after placement of stent. A, Angiogram shows high-grade eccentric stenosis in both common iliac arteries close to bifurcation.

B, Angiogram obtained 6 months after placement of stents shows symptomatic stenosis (solid arrow) in lower part of left endoprosthesis and another proximal stenosis on right side (open arrow). Lesions were treated successfully by balloon angioplasty and atherectomy.



cases occurred during an early stage of our study, and the rate of early reocclusion declined remarkably as the study progressed. Complete coverage of the lesion was difficult sometimes, such as in stenoses of the aortic bifurcation, in which a slight protrusion of the stent into the aortic lumen was sometimes required to accomplish adequate stenting. Proper selection of patients is important, and in cases of severe restricted outflow, special attention should be given to postprocedural anticoagulant therapy.

Progression of intraluminal hyperplasia within a stent can be monitored angiographically because of the clearly visible outline of the metallic endoprosthesis. Neointimal coverage of the stent surface corresponding to less than 20% of the stent's diameter was a normal finding. Excision of stenotic material inside implants with an atherectomy catheter showed neointimal hyperplasia [9, 10] similar to that seen after simple balloon dilatation [11]. Excessive growth of neointimal tissue has been reported in some patients with femoral stents [12, 13], so induction of neointimal growth by the stent cannot be excluded.

With iliac stents, the prevalence of restenosis due to intimal hyperplasia was notably lower than that reported in femoral arteries or hemodialysis shunts [12-17]. Moreover, in most cases restenosis was found only at angiography and was clinically insignificant. The follow-up period now extends to 3.5 years and, in most patients treated, stented iliac areas are completely patent and no stent-related late complications have been identified. Comparison with other types of stents, however, is still difficult because no larger series with comparable data have been published, and the composition of patient subgroups is heterogeneous. Additional follow-up data therefore are required for a definitive assessment.

Although the preliminary clinical experience with self-expandable stents, or stents in general [13, 16, 17], as an adjunct to balloon angioplasty in the iliac arteries is promising, the importance of a reasonable cost-benefit ratio should not be neglected. Placement of a stent is still a costly procedure, making PTA more expensive. A significant reduction of the rate of restenosis has not been proved. Balloon angioplasty, therefore, still remains the gold standard of percutaneous treatment. Consequently, insertion of a stent should be limited to the selected subset of lesions that we described. Too liberal an approach should be avoided, because it may compromise the use of this advanced new technique by decreasing the use of balloon angioplasty, which has striking advantages as a safe, successful, and inexpensive procedure for most iliac lesions.

#### ACKNOWLEDGMENTS

The authors thank Danielle Venderickx, Lausanne, for editorial assistance and Udo Buhl, Aachen, for the preparation of photographs.

#### REFERENCES

1. Becker GJ, Katzen BT, Dake MD. Noncoronary angioplasty. *Radiology* **1989**;170:921-940
2. Dotter CT, Judkins MP. Transluminal angioplasty of atherosclerotic obstructions: description of a new technique and a preliminary report of its application. *Circulation* **1964**;30:654-670
3. Grüntzig A, Hopff M. Perkutane Rekanalisation chronischer arterieller Verschlüsse mit einem neuen Dilatationskatheter: Modifikation der Dotter-Technik. *Dtsch Med Wochenschr* **1974**;99:2502-2510
4. Rousseau H, Joffre F, Raillat C, Dubouché C, et al. Iliac artery endoprosthesis: radiologic and histologic findings after 2 years. *AJR* **1989**;153:1075-1076
5. Leimgruber P, Roubin G, Anderson H, et al. Influence of intimal dissection on restenosis after successful coronary angioplasty. *Circulation* **1985**;72:530-535
6. Ring E, Freiman D, McLean G, Schwarz W. Percutaneous recanalization of iliac artery occlusions: an unacceptable complication rate. *AJR* **1982**;139:587-589
7. Pilla T, Peterson G, Tantana S, et al. Percutaneous recanalization of iliac artery occlusions: an alternative to surgery in the high-risk patient. *AJR* **1984**;143:313-316
8. Wolf G, LeVein R, Ring E. Potential mechanisms of angioplasty. *Cardiovasc Intervent Radiol* **1984**;7:11-17
9. Vorwerk D, Guenther RW. Removal of intimal hyperplasia in vascular endoprostheses managed by combined use of atherectomy and balloon dilatation. *AJR* **1990**;154:617-619
10. Zollikofer CL, Antonucci F, Thalmann R, Pfyffer M, Stuckmann G, Marty A. Early clinical experience with arterial stent placement with the Wallstent. *Radiology* **1989**;173(P):351
11. Giraldo AA, Esposito OM, Meis JM. Intimal hyperplasia as a cause of restenosis after percutaneous transluminal coronary angioplasty. *Arch Pathol Lab Med* **1985**;109:173-175
12. Triller J, Mahler F, Do D, Thalmann R. Die vaskuläre Endoprothese bei femoropoplitealer Verschlusskrankheit. *Fortschr Roentgenstr* **1989**;150:328-334
13. Guenther RW, Vorwerk D, Bohndorf K, et al. Iliac and femoral artery stenoses and occlusions: treatment with intravascular stents. *Radiology* **1989**;172:725-730
14. Guenther RW, Vorwerk D, Bohndorf K et al. Venous stenoses in dialysis shunts: treatment with self-expanding metallic stents. *Radiology* **1989**;170:401-405
15. Antonucci F, Zollikofer CL, Thalmann R, Stuckmann G, Redka F, Largiader J. Early clinical experience with the Wallstent in veins, grafts and dialysis shunts. *Radiology* **1989**;173(P):107
16. Palmaz JC, Richter GM, Noeldge G, et al. Intraluminal stent in atherosclerotic iliac artery stenosis: preliminary report of a multicenter study. *Radiology* **1988**;168:727-731
17. Palmaz JC, Garcia O, Schatz R, et al. Placement of balloon-expandable intraluminal stents in iliac arteries: first 171 procedures. *Radiology* **1990**;174:969-975

## Book Review

**Practical Nuclear Medicine.** Edited by P. F. Sharp, H. G. Gemmell, and F. W. Smith. New York: IRL Press, 349 pp., 1990. \$75, hardcover; \$40, softcover

*Practical Nuclear Medicine* is a small, thin, attractive text. The quality of the paper is excellent, and the book has clear figures, concise charts, and finely highlighted subheadings. Well-written introductory chapters present information on general principles, the gamma camera, quality control, and single-photon emission CT. These are followed by discussions on data processing, radiopharmaceuticals, and protection. The clinical part of the book is divided into sections on the brain; heart; vessels; lung; gastrointestinal, lymphatic, and urinary systems; bone; and the thyroid and parathyroid glands. The final chapters discuss tumors, infection scanning, and  $^{99m}\text{Tc}$ -technetium.

When the request came to review a British text, I was genuinely pleased. Each of us has certain prejudices, and one of mine is a fondness for British, Canadian, and Australian journals over the American. The foreign articles are lean and fact filled, whereas ours seem wordy and replete with effusive prose that detracts from the message. Australian articles are characteristically one or two pages long, whereas ours are five or 10 pages long. It was my hope that this text could do to American nuclear medicine texts what British articles do to American articles: cover the entire field in a few pages. However, I was disappointed. As I read along, I began to realize that attempts at brevity and clarity can sometimes, as here, lead to incompleteness or to omissions. As a simple example, in the discussion of the possible causes of foci of abnormally increased uptake of radionuclide on a bone scan, only metastasis and fracture are mentioned. One additional phrase including infection and primary tumor would have made this complete.

When noting the composition of gamma-camera crystals, the book refers to the inclusion of some thallium, but no comment is made about why thallium is included. In the part on pulmonary embolus, note is made that "arrhythmias are said to occur, but recent review

has not confirmed this as a reliable sign of PE." No reference is cited, and no note is made as to whose review included this statement. Also, bold opinions are stated as fact, without explanation, such as, "Failure to visualize the gall bladder by 3 h with normal passage of activity to the bowel is diagnostic of gall bladder disease and indicates cystic duct obstruction in virtually all cases." This, if adhered to, would have resulted in many unnecessary cholecystectomies in cachectic, bedridden patients in the hospital where I practice. Some of the figures are mislabeled. For example, the figure stated to show uptake by bone marrow on a colloid liver scan showed little to none, whereas the figure above it demonstrated the point quite well but was not included for that reason.

The authors state in the preface that they wish this text to be a practical manual of nuclear medicine, providing clear instruction on a wide variety of topics. It is not meant to be an academic approach, but aims to present the reader with practical experience, preference, and even the prejudices of a group of specialists working in nuclear medicine. It is just this statement that limits the readership to those able to sort through fact and opinion. If a reader fails to see this page or the implications in the statements in the preface or, because of a limited background, takes some of the conclusions in the book as the final word on a topic, problems could ensue. Thus, this is a book for those who have an interest in uncovering some new facts or for those who have strong opinions. My lament is that this could have been a truly complete, short, concise text. All it needs is a few additions, several more references, and a few lines explaining why opinions contrary to those of the authors are impractical.

James A. Usselman  
Scripps Clinic  
La Jolla, CA 92037

## Technical Note

# CT Analysis of a Safe Approach for Translumbar Access to the Aorta and Inferior Vena Cava

Francoise L. Cazenave,<sup>1</sup> Mark C. Glass-Royal,<sup>1</sup> George P. Teitelbaum,<sup>2</sup> Rebecca Zuurbier,<sup>1,3</sup> Robert K. Zeman,<sup>1</sup> and Paul M. Silverman<sup>1</sup>

The implications of normal anatomic structures being in the path of needle placement for interventional procedures such as percutaneous nephrostomy or diskectomy have been described [1, 2]. We reviewed 100 abdominal CT scans to determine, by analyzing cross-sectional anatomy, if the standard approach used for direct translumbar access to the aorta and inferior vena cava (IVC) is appropriate.

Translumbar aortography and direct translumbar access to the IVC are used when peripheral vascular approaches are not feasible. Translumbar aortography can be used when the direct femoral approach is contraindicated, for example, in cases of femoral occlusion or severe atherosclerotic disease, infection, or recent local surgery [3]. Direct translumbar access to the IVC has been proposed as an alternative approach for placing central venous catheters when traditional approaches are not possible [4]. Direct percutaneous access to the IVC has been described as a mirror image or "right-sided version" of translumbar aortography [5].

These two procedures are generally performed under fluoroscopic guidance rather than by cross-sectional imaging techniques such as sonography or CT. Although severe complications occur rarely (0.58% of cases), retroperitoneal hemorrhage occurs in almost all patients, and inadvertent laceration of the kidneys may result from the selection of an inappropriate approach [6]. We reviewed CT scans to assess whether the specific guidelines for entry site, angle, and depth

used for these procedures are consistent with an anatomically safe approach to these major vascular structures.

### Materials and Methods

One hundred randomly chosen abdominal CT scans were retrospectively reviewed. Scans were obtained on 43 males and 57 females, with an age range of 8 to 93 years (mean, 56 years).

Examinations were performed with a GE 9800 scanner (GE Medical Systems, Milwaukee, WI) with contiguous 10-mm sections of the patient in a standard supine position. We analyzed the level 1 cm below the confluence of the renal veins with the IVC, at approximately the L2 level, in order to determine three factors: (1) a "safe angle," defined as the highest possible angle from the sagittal plane that can be used to reach the posterior wall of the aorta or IVC without puncturing the kidney or interposed viscera; (2) a "safe distance," the distance between the skin entry site and the spinous process of L2 (body midline), for a given angle; (3) the "depth," the distance between the skin entry site and the posterior wall of the vessel (Fig. 1A).

For the last 30 patients, we noted the most lateral extent of the aorta and IVC with respect to the midline of the body, the vertebral spinous process, to determine if differences in approach angle to the aorta vs the IVC could be predicted on the basis of the vessel's position (Fig. 1B).

Ten CT scans obtained with the patient prone also were reviewed with respect to the same factors to test whether the measurements differed significantly from those made in the supine studies.

The measurements of angles and distance were statistically analyzed with the *t* test for paired data.

Received May 24, 1990; accepted after revision July 19, 1990.

<sup>1</sup> Department of Radiology, Georgetown University Hospital, 3800 Reservoir Rd., N. W., Washington, DC 20007. Address reprint requests to P. M. Silverman.

<sup>2</sup> Department of Radiology, LAC-USC Medical Center, 1200 N. State St., Los Angeles, CA 90033.

<sup>3</sup> Present address: Department of Radiology, Massachusetts General Hospital, 32 Fruit St., Boston, MA 02114.

AJR 156:395-396, February 1991 0361-803X/91/1562-0395 © American Roentgen Ray Society



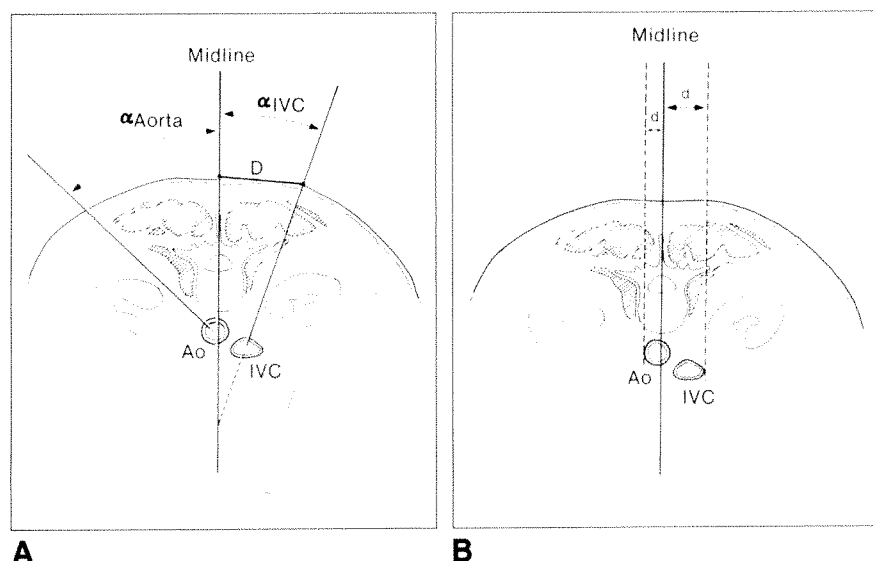


Fig. 1.—A, Diagram representing CT scan obtained with patient prone. Safe angles of approach to aorta (Ao) and inferior vena cava (IVC) are indicated, as is method of measuring distance (D) from midline.

B, Similar diagram shows method of measurement of lateral extent of aorta and inferior vena cava from midline (d).

## Results

The average safe angle was  $32 \pm 3^\circ$  for the aorta and  $16 \pm 9^\circ$  for the IVC ( $p < .001$ ). The average safe distance was  $8 \pm 2$  cm for the aorta and  $6 \pm 2$  cm for the IVC ( $p < .001$ ). The average measured depth was  $12.0 \pm 2$  cm for the aorta and  $10.3 \pm 2.8$  cm for the IVC ( $p < .001$ ).

No significant difference was found for any of these parameters between males and females or between the CT scans obtained with the patient prone and those obtained with the patient supine.

The projection of the lateral edge of the aorta and IVC was  $1.9 \pm 0.5$  cm lateral to the spinous process for the aorta and  $2.8 \pm 0.7$  for the IVC ( $p < .001$ ), demonstrating a slightly more lateral position for the IVC.

## Discussion

Translumbar aortography is widely used when safer, more traditional approaches are not feasible. The anatomic landmarks for this procedure are well known. For the standard "low translumbar aortography" technique, the abdominal aorta is entered at the lower border of L2, with the skin entry site approximately 10 cm to the left of the vertebral spinous process, midway between the 12th costal margin and the iliac crest. The needle is angled  $60$ – $70^\circ$  from the skin surface, equivalent to a  $30$ – $40^\circ$  angle from the sagittal plane [3]. Our results (approximately  $32^\circ$  and 8 cm) confirm the safety of this approach for translumbar aortography in terms of avoiding inadvertent renal or bowel puncture.

However, because of the more lateral position of the IVC, the approach parameters should be modified for safe percutaneous direct venous access. We recommend a more vertical angle (about  $17^\circ$ ), with a skin entry site closer to the spine (6 cm), if the puncture is at the L2 level.

A cranially angled approach, with a skin entry site just

above the iliac crest, and caval puncture at L3 level, has been advocated by some authors [7, 8]. This more oblique approach may allow easier catheter insertion, and decrease the risk of renal damage, because of the more lateral position of the lower pole of the kidney.

In conclusion, the general guidelines for low translumbar aortography are consistent with our analysis of a safe approach as evaluated by cross-sectional imaging by CT. Access to the IVC should not be considered an exact mirror-image technique of translumbar aortography. Modifications including a more vertical approach with a skin entry site closer to the midline or a more cranially angled lower approach (L3 level) is recommended for the IVC. In specific instances, CT guidance may be beneficial in defining the safest possible approach.

## REFERENCES

1. Helms CA, Munk PL, Witt WS, Davis GW, Morris J, Onik G. Retrorenal colon: implications for percutaneous discectomy. *Radiology* 1989;171:864–865
2. Hopper KD, Sherman JL, Luethke JM, Ghaed N. The retrorenal colon in the supine and prone patient. *Radiology* 1987;162:443–446
3. Kadir S. *Diagnostic angiography*, 1st ed. Philadelphia: Saunders, 1986:41–43, 682–683
4. Denny DF, Dorfman GS, Greenwood LH, Horowitz NR, Morse SS. Translumbar inferior vena cava Hickman catheter placement for total parenteral nutrition. *AJR* 1987;148:621–622
5. Robards JB, Jaques PF, Mauro MA, Azizkhan RG. Percutaneous translumbar inferior vena cava central line placement in a critically ill child. *Pediatr Radiol* 1989;19:140–141
6. Hessel SJ, Adams DF, Abrams HL. Complications of angiography. *Radiology* 1981;138:273–281
7. Denny DF, Greenwood LG, Morse SS, Lee GK, Baquero J. Inferior vena cava: translumbar catheterization for central venous access. *Radiology* 1989;170:1013–1014
8. Lund GB, Lieberman RP, Haire WD, Martin VA, Kessinger A, Armitage JO. Translumbar inferior vena cava catheters for long-term venous access. *Radiology* 1990;174:31–35

## Technical Note

### A New Percutaneous Access Set for Interventional Procedures

Garey L. McLellan<sup>1</sup>

Image-guided percutaneous interventional procedures have been enhanced by the development of introducer systems and techniques that permit safe, small-needle, single-puncture access into the renal collecting system, biliary tree, or abscess cavity [1, 2]. The development of double-guidewire techniques and equipment for the placement of a safety and working guidewire has further facilitated the procedures, ensuring site access, especially in complex or difficult cases [3, 4]. Although these developments have aided in the performance of percutaneous procedures, they do not provide a means of directly manipulating the introducer catheter selectively into a ureter, bile duct, or abscess track. Often a series of catheter and guidewire manipulations are necessary to achieve the desired guidewire and catheter placement.

The ability to place the introducer catheter and primary guidewire selectively may eliminate the need for these maneuvers. This paper describes a percutaneous access set that provides for the introduction of both working and safety guidewires and permits the introducer catheter to attain various degrees of distal curvature for selective placement of the primary guidewire and catheter.

#### Materials and Methods

The percutaneous access set (Cook Inc., Bloomington, IN) described in this report consists of a 21-gauge, 15-cm trocar puncture needle; a 0.018-in. (0.046 cm), 80-cm-long, curved-tip Cope-mandril guidewire with platinum alloy spring guide; a 0.020-in. (0.051 cm), 42.5-cm-long malleable mandril steering wire with a 5-cm, right-angle

handle; a 4.5-French, 40-cm-long catheter with a 0.018-in. end hole with a matching 19-gauge steel stiffening cannula; a 7.5-French, 20-cm-long straight catheter with a 4.5-French end hole back loaded and luer-locked to the 4.5-French catheter; and a 4.5-French, 20-cm fascial dilator with a 0.018-in. end hole (Fig. 1).

The procedure for using the access set is as follows: After the entry site is selected and prepared, make the initial puncture under fluoroscopic control with the 21-gauge trocar needle. When the needle is in the desired location and the site is opacified, pass the

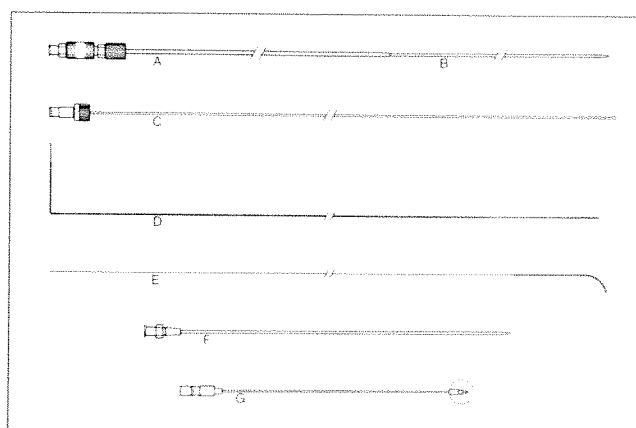


Fig. 1.—Access set contains the following components: 7.5-French sheath (A), backloaded over 4.5-French introducer catheter (B), 19-gauge stiffening cannula (C), 0.020-in. malleable steering wire (D), 0.018-in. Cope mandril guidewire (E), 4.5-French fascial dilator (F), and 21-gauge trocar needle (G).

Received June 18, 1990; accepted after revision August 6, 1990.

<sup>1</sup> Department of Radiology, University of Florida Health Science Center/Jacksonville, 655 W. Eighth St., Jacksonville, FL 32209. Address reprint requests to G. L. McLellan.

AJR 156:397-399, February 1991 0361-803X/91/1562-0397 © American Roentgen Ray Society

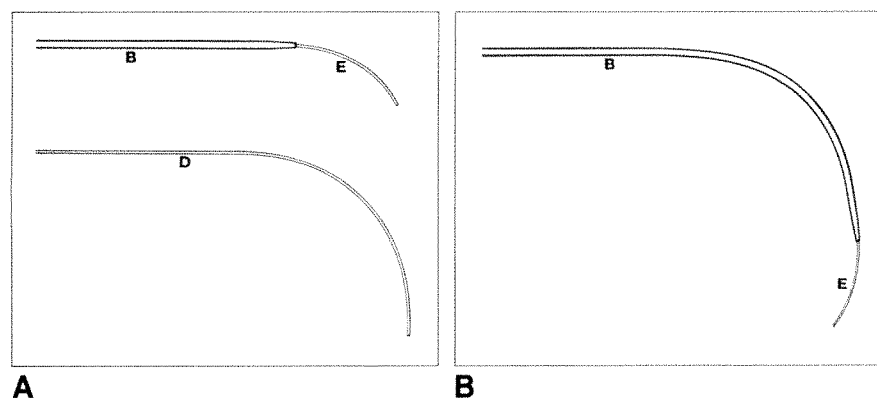


Fig. 2.—Demonstration of malleable steering wire with components labeled as in Fig. 1.

A, Curved end of Cope wire (E) is seen extending from tip of 4.5-French introducer catheter (B). End of steering wire (D) has been hand-shaped to desired curvature.

B, With Cope wire (E) and catheter (B) held in position, steering wire is placed coaxially into catheter and advanced completely to bend in wire. End of catheter and Cope wire have assumed shape of steering wire.

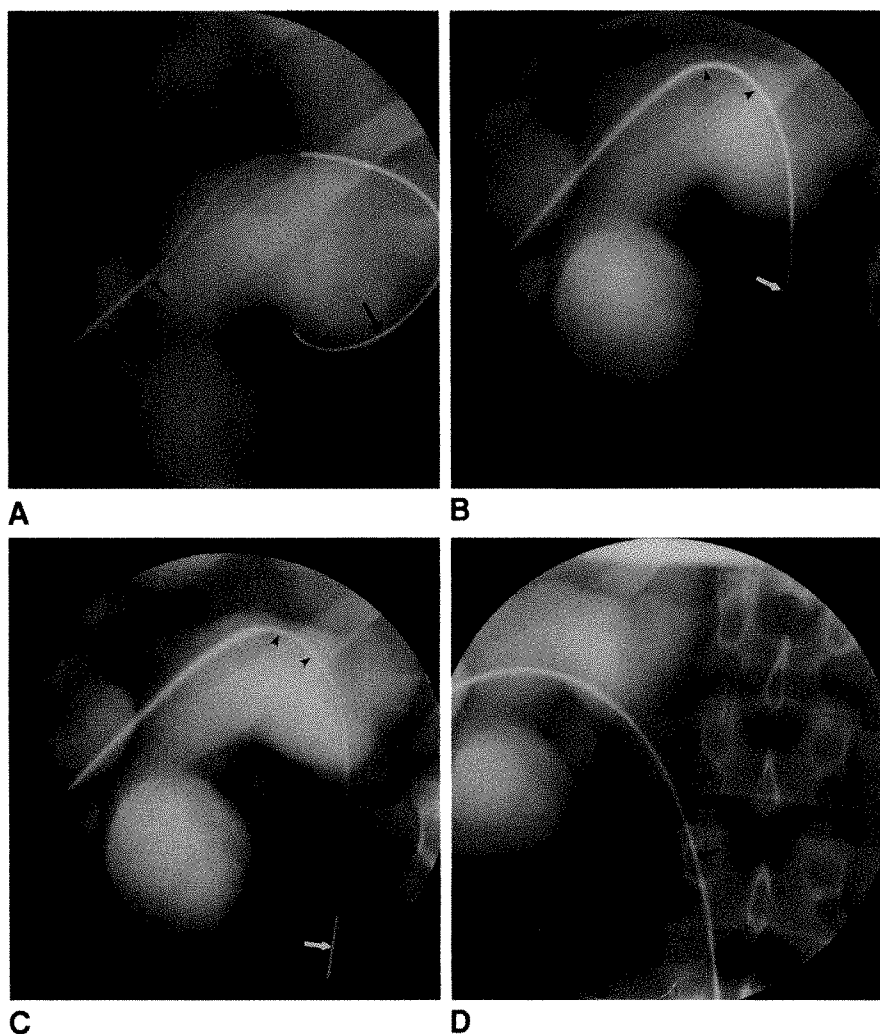


Fig. 3.—A, Spot radiograph shows a 21-gauge needle tip (small arrow) and proximal portion of a Cope wire (large arrow) within dilated renal pelvis. Note ureteropelvic junction (UPJ) strictures (arrowheads).

B, Spot radiograph shows curve (arrowheads) introduced into catheter by placing hand-shaped steering wire into it. Cope wire (arrow) has been manipulated across UPJ stricture.

C, A spot radiograph shows curved steering wire (arrowheads) without platinum portion of Cope wire (arrow) superimposed over it.

D, A 0.035-in. working guidewire (arrow) has been introduced through sheath (arrowheads) adjacent to Cope wire.

0.018-in. Cope guidewire through the needle. In biliary and renal cases, direct the guidewire distally to ensure adequate purchase within the mid-ureter or distal common duct. As there is an abrupt step-off at the weld of the tapered mandril and spring coil portion of the guidewire, do not withdraw this area of the wire through either the needle or metal cannula because the wire could shear [5]. Then

withdraw the needle, leaving the wire in place. Place the steel cannula in the introducer catheter and outer sheath and lock it in position. Advance this assembly over the guidewire into the desired position within the site, and unlock the outer sheath from the inner catheter. Hold the wire, cannula, and catheter stationary, and advance the sheath to the desired location. When other than minimal curvature of



the wire is encountered, unlock the steel cannula from the assembly, hold the cannula and wire in position, and advance the catheter and sheath into position. Observing this caveat will avoid kinking of the wire. Remove the inner catheter and cannula and leave the Cope wire and sheath in place. Then, advance a stiff, 0.035-in. (0.089 cm) guidewire through the sheath. Remove the sheath, leaving the Cope guidewire as the safety wire and the 0.035-in. (0.089 cm) guidewire as the working wire. Therapeutic maneuvers can then be performed. If a drainage catheter is to be left in position when the procedure is completed, overdilate the track 2- to 3-French to facilitate placement of the drain and removal of the safety wire.

In instances in which the Cope wire cannot be directed into the optimal location, the malleable steering wire and introducer catheter can be used to direct the guidewire and catheter into the desired location. After the 21-gauge needle has been removed, advance the introducer catheter assembly over the Cope wire into the site as noted earlier. Withdraw the wire until approximately 1–2 cm of the distal tip protrudes from the catheter tip. Estimate the desired curvature of the catheter tip fluoroscopically. Then, shape the distal portion of the 0.020-in. malleable steering wire by hand to the required curve (Fig. 2). Insert the curved steering wire coaxially beside the Cope guidewire and advance it completely to the handle of the wire under fluoroscopic control. The steering wire is 2–3 mm shorter than the catheter and will not extend from the tip. If sufficient space is available, the distal portion of the catheter and flexible Cope wire will assume the shape of the curved steering wire. The handle of the steering wire can be used to change the position of the distal catheter tip to select the desired direction. In order to aid in manipulation of the Cope wire, a steering handle (C. R. Bard, Billerica, MA) can be used to rotate the curved wire tip. The combination of curved catheter and Cope wire can then be used to probe the site, which aids in cannulation and guidewire placement. The possibility of spring-coil tip detachment from the mandril of Cope-type wires during withdrawal through catheters has been suggested [5]. Therefore, wire resistance should be monitored carefully during removal. No instances of wire detachment occurred in this series.

### Representative Case Report

A 25-year-old man was admitted with fever and pain in the right flank. Six years earlier, he had sustained stab wounds to the abdomen and chest without evidence of urologic injury. An excretory urogram and contrast-enhanced CT scan showed right hydronephrosis without filling of the ureter. A working diagnosis of proximal right ureteral obstruction with right pyelonephritis was made. Percutaneous nephrostomy and ureteral stent placement were requested. Antegrade pyelography via a 21-gauge needle puncture showed marked hydronephrosis with high-grade stricture at the ureteropelvic junction (UPJ). Initial attempts to cross the stricture failed. The curved steering wire technique described was then used successfully to advance both safety and working guidewires across the stricture (Fig. 3). A ureteral stent and nephrostomy catheter were then placed, and the patient quickly improved clinically.

### Results

The access set has been used successfully in 38 cases; 25 percutaneous urologic procedures, seven biliary drainage procedures, four abdominal abscess drainages, and two

empyema drainages. The malleable steering wire has been successfully used to shape the introducer catheter tip, enabling selective placement of the wire in all six procedures in which the technique was attempted. No complications occurred.

### Discussion

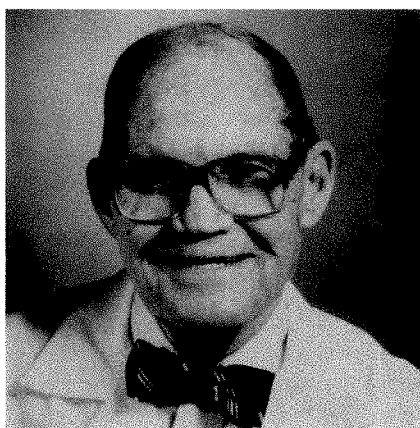
The access set provides a rapid means of establishing a percutaneous track into the desired space and placing a working guidewire as well as a safety wire by using a small-gauge needle and single-puncture technique. Entry into the original site is thus preserved in the event that access is lost during catheter and guidewire manipulations. A similarly priced set, the Accu-Stik introducer system (Medi-tech, Watertown, MA), also permits single-puncture placement of a safety and working guidewire by using a coaxial system. However, it and other similar systems [3, 4] are not designed to permit selective manipulation of the primary guidewire or introducer catheter/dilator as is the access set used in this series. In situations in which selective placement of the primary guidewire would gain greater purchase or is necessary to continue the procedure, the use of the access set's malleable steering wire provides a means to add a distal curve to the introducer catheter, which permits probing and selective cannulation. The maximum curvature used in this series was approximately 100 degrees. J-type curvatures of up to 180° with a minimum diameter of 4 cm have been achieved experimentally. Small tight J curves are not possible because of the length and rigidity of the catheter and sheath hubs. Passage through the hubs may partially straighten and broaden the curvature placed in the wire. This effect tends to increase when the curve is greater than 90° and when a narrow curvature is used. The changes in the curvature may be partially compensated for by increasing the tip angle 10–20° and shaping a narrower curve than estimated at fluoroscopy before initial insertion. The resulting curve after passage through the hubs will be maintained by the wire and catheter, if sufficient space is available at the target site. At our hospital, this set has been used successfully to gain excellent guidewire position in a wide variety of percutaneous interventional procedures, greatly facilitating their completion.

### REFERENCES

1. Cope C. Conversion from small (0.018") to large (0.038") guidewires on percutaneous drainage procedures. *AJR* 1982;138:170–171
2. Swartz W. New coaxial introducer system for percutaneous drainage. *AJR* 1985;144:1277
3. Dawson S, Papanicolaou N, Mueller PR, Ferrucci JT Jr. Preserving access during percutaneous catheterization using a double-guide-wire technique. *AJR* 1983;141:407
4. Jeffrey RB Jr. Modified Cope introducer set for rapid insertion of a safety wire. *AJR* 1986;147:828–829
5. Quinn SF, Morse S. Complications from 0.018-in. floppy platinum-tip guidewires. *AJR* 1990;154:1103–1104

## Memorial

### Hyman R. Senturia, 1909–1990



Hyman R. Senturia received his A.B. and M.D. degrees from Washington University. He was a gifted student and was elected to Phi Beta Kappa and Alpha Omega Alpha. After graduation from medical school, he served an internship, a year of medical residency, and a 2-year residency in radiology at the University of Cincinnati. There, as the senior resident, he was a mentor of the late Benjamin Felson, a dear friend, who became a giant in world academic radiology. Having been awarded a National Cancer Institute

fellowship as a trainee in cancer, Dr. Senturia spent the next 2 years on rotations at several cancer centers and a final year at the Chicago Tumor Institute under the direction of the renowned radiotherapists Henri Coutard and Max Cutler.

Starting in 1942, Dr. Senturia served a 4-year stint during World War II as a major in the Army Air Force. After discharge from the armed forces, he came back to St. Louis and became a radiologist at The Jewish Hospital, where he practiced radiology almost without missing a day, except for short vacations, until 2 weeks before his death. He was appointed director of radiology in 1953.

Dr. Senturia was a disciplined radiologist, blessed with a keen intellect and a discerning eye. His diagnostic talents were recognized immediately by his medical colleagues. His reading cubicle was one of the major diagnostic centers for the hospital: he was consulted on almost every puzzling diagnostic case. A significant portion of Dr. Senturia's training and career was spent in radiotherapy. His skill and compassion in treating malignant diseases were appreciated by his medical colleagues and by his patients.

Dr. Senturia was the author of several scientific papers, yet his greatest fulfillment and contribution were in teaching house staff

and medical students. Soon after his arrival at The Jewish Hospital, he began a residency program in radiology that since has trained more than 50 radiologists.

When Washington University medical students began rotating at The Jewish Hospital, Dr. Senturia organized a teaching elective in radiology for fourth-year students. Almost immediately, it became one of the most oversubscribed electives offered. He organized his entire weekly work schedule to optimize the course as a teaching experience for the students, who rarely left his side. The medical students elected him teacher of the year on at least four different occasions; Washington University named him professor of clinical radiology; and in 1988, he received the Washington University Medical School Alumni/Faculty Award in recognition of his teaching contributions.

He continued to practice radiology full-time and, to the best of his ability, almost until his death from cancer. Such controlled commitment brings majesty to mortal man. Having witnessed this *imitatio dei*, we are thankful that when it was time for him to be taken, it was without compromise of dignity and pride.

Noah Susman  
Ronald G. Evens  
St. Louis, MO 63110

## Technical Note

# Improved Needle-Tip Visualization by Color Doppler Sonography

Ulrike M. Hamper,<sup>1</sup> Barbara L. Savader, and Sheila Sheth

The usefulness of sonography for guidance of percutaneous aspiration biopsies of solid masses or fluid collections is well established [1–6]. Visualization of the needle tip can, however, be difficult at times, especially if a narrow angle technique is used or the needle is inserted parallel to the ultrasound beam. We describe the use of color Doppler flow imaging for enhancement of needle tip and shaft visualization and its application during aspiration biopsies.

### Materials and Methods

Spinal needles of four sizes (18-, 20-, 22-, and 25-gauge) were scanned after insertion into a Kitecko standoff pad (3M Company, St. Paul, MN). A color Doppler flow system with a 3.5-MHz sector probe and 5- and 7.5-MHz linear array transducers (Acuson 128, Mountain View, CA) was used to scan these devices in the gel block. Either the entire needle shaft or the inner stylet was moved slightly in order to produce a color image of the needle tip or shaft (Fig. 1).

Subsequently this technique was applied during percutaneous mass biopsy (renal mass, liver mass, thyroid nodule) in three patients. The aspiration biopsies were performed with 20-gauge needles in the liver and renal masses and with a 23-gauge needle in the thyroid nodule. Color flow imaging was performed during the biopsies with 2.25-MHz, 3.5-MHz sector, and 7-MHz linear array transducers (Acuson 128, Mountain View, CA), respectively. Needle-tip visualization was enhanced by gentle up and down motion of either the entire needle or the inner stylet (Fig. 2).

### Results

The needle tip and the entire shaft of the needle could be visualized much more easily with this technique than with conventional B-mode imaging during the in vitro and the in vivo applications. This was especially obvious when smaller gauge needles (23-gauge, 25-gauge) and narrow angle techniques (thyroid aspiration) were used. In the liver and renal masses, where an aspiration angle closer to 90° was attempted, we were easily able to delineate large portions of the needle shaft and the needle tip because of the color image produced by moving the needle shaft or inner stylet. In addition, we were able to avoid biopsy of vascular portions of the renal mass (renal cell carcinoma) by using color flow imaging.

### Discussion

In the past years, many different sonographically guided biopsy techniques have been developed coincident with technical advances in sonographic equipment. Aspiration techniques creating a distinct angle between the sonographic transducer and needle tip allow easier monitoring of the needle during aspirations than needle insertions parallel to the transducer beam do. In addition, dedicated biopsy transducers and needle guide attachments for transducers are available. Often, however, exact visualization of the needle

Received April 10, 1990; accepted after revision May 20, 1990.

<sup>1</sup>All authors: Russell H. Morgan Department of Radiology and Radiological Science, The Johns Hopkins Medical Institutions, 600 N. Wolfe St., Baltimore, MD 21205. Address reprint requests to U. M. Hamper.

AJR 156:401–402, February 1991 0361–803X/91/1562–0401 © American Roentgen Ray Society



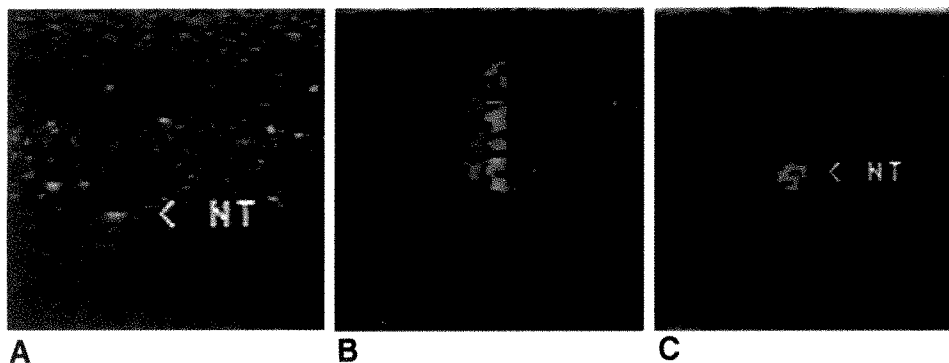


Fig. 1.—A, Tip (NT) of 22-gauge spinal needle produces faint echo within gel standoff pad on color Doppler sonogram.

B and C, Slight motion of needle tip shows distinct color artifact at site of needle tip (right), and slight motion of inner stylet of needle produces color outline of needle shaft and tip (left).

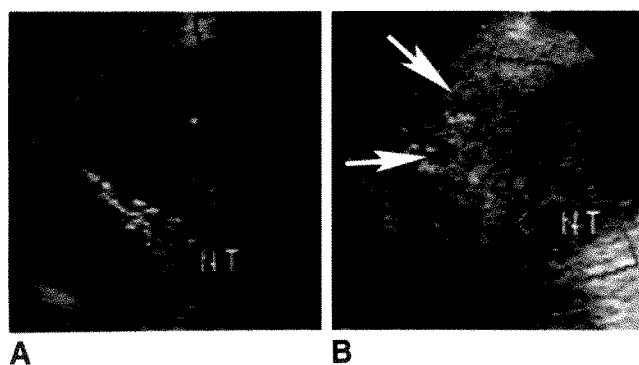


Fig. 2.—A, Color Doppler sonogram of aspiration of liver mass (hepatocellular carcinoma). 20-gauge needle and tip (NT) outlined by color image produced by gentle motion of needle.

B, Color Doppler sonogram of renal cell carcinoma biopsy with 20-gauge needle. Note needle-tip color artifact (NT) and needle insertion medial to tumor vascularity (arrows).

tip within a desired target is difficult. Visualization of the needle tip can be enhanced by using needles with special tips (echo-tips), which produce high-intensity echoes, or by injecting a tiny amount of air, which produces a very bright echogenic focus at the needle tip.

Color Doppler flow devices have recently become available for clinical use. Known artifacts of color flow Doppler systems are associated with motion and respiration (flash artifact) [7]. In color flow devices, any movement produces Doppler shifted frequencies and is modulated into color, producing an artifactual impression of flow expressed as a color signal on the

image [7]. When in motion, needles and other devices also produce such a color registration on the color Doppler image; this is much more easily discernible with color Doppler imaging than with conventional B-mode gray-scale imaging [8]. This technique might be useful for either difficult, deep biopsies of abdominal masses, superficial biopsies in which needle insertion parallel to the transducer or narrow angle techniques need to be used, or when small-gauge needles need to be used and the exact location of the needle tip is difficult to determine. In addition, biopsy of vascular portions of tumor masses can be avoided when color Doppler imaging is performed during aspiration biopsies.

#### REFERENCES

1. Gazelle GS, Haaga JR. Guided percutaneous biopsy of intraabdominal lesions. *AJR* 1989;153:929-935.
2. Bree RL, Jafri SZ, Schwab RE, et al. Abdominal fine needle aspiration biopsies with CT and ultrasound guidance: techniques, results and clinical implications. *Comput Radiol* 1984;8:9-15.
3. Taavitsainen M, Koivuniemi A, Bondestam S, et al. Ultrasonically guided fine-needle aspiration biopsy in focal pancreatic lesions. *Acta Radiol* 1987;28:541-543.
4. Martinez A, Martin V, Cáceres J. Fine-needle biopsy of the pancreas using real-time ultrasonography. *Gastrointest Radiol* 1984;9:231-234.
5. Fornage BD, Faroux MJ, Simatos A. Breast masses: US-guided fine needle aspiration biopsy. *Radiology* 1987;162:409-414.
6. Ravin CE. Thoracentesis of loculated pleural effusion using grey scale ultrasonic guidance. *Chest* 1977;71:666-668.
7. Taylor JW, Holland S. Doppler US. Part I. Basic principles, instrumentation, and pitfalls. *Radiology* 1990;174:297-307.
8. Kurohiji T, Sigel B, Justin J, et al. Motion marking in color Doppler ultrasound needle and catheter visualization. *J Ultrasound Med* 1990;9:243-245.

## Letters

### Reaction to Intrathecal Iohexol

A 21-year-old woman had a 1-year history of nonradiating low back pain. She had no other medical problems, had no known allergy, and was taking no medications. She had never been exposed to iodinated contrast material. She had a lumbar myelogram/CT scan in which 2 ml of 1% lidocaine, for local anesthesia, and 12 ml of iohexol (Omnipaque, Winthrop Pharmaceuticals, New York, NY) were used. Injection of iohexol, through a 22-gauge spinal needle, was observed fluoroscopically, and normal filling of the subarachnoid space occurred. No evidence of extrathecal extravasation was seen. One hour after the iodinated contrast material had been administered, pruritic, urticarial lesions developed on the patient's upper chest and neck. Respirations, blood pressure, and pulse were normal. No wheezing or angioedema was observed. The urticaria and pruritus responded promptly to 25 mg of IV diphenhydramine.

Reactions to contrast material during myelography are infrequent occurrences. One study [1] reported that urticarial reactions occurred in two of 1850 subarachnoid infusions with metrizamide. Reactions to intrathecal iohexol have not been reported in the literature; however, Winthrop Pharmaceuticals has knowledge of a previous case (personal communication). The potential for a reaction to iohexol during myelography with this agent supports the prophylactic pretreatment of any patient who has a history of a reaction to contrast material. This is the current practice at our institution.

Mark D. Stanley  
Jeffery E. Hull  
Naval Hospital  
San Diego, CA 92134

### REFERENCE

1. Nickel A, Salem J. Clinical experience in North America with metrizamide. *Acta Radiol Suppl* (Stockh) 1977;355:409-416

Note.—The Chief, Navy Bureau of Medicine and Surgery, Washington, DC. Clinical Investigation Program sponsored the preceding letter (case report #84-16-1968-241). The views expressed in this letter are those of the authors and do not reflect the official policy or position of the Department of the Navy, the Department of Defense, or the United States Government.

### Music Enhances Patients' Comfort During MR Imaging

Up to 35% of patients report anxiety during MR imaging [1]. Severe symptoms prevent imaging in approximately 4% [2]. These reactions

are costly because of nonrecoverable staff and equipment time. Unsuccessful attempts to image such distressed patients who because of chronic disorders require frequent MR follow-up consume some 13% of imaging time at our institution. Others have reported modifications of the MR imager, including communication devices, fans, and earphones, that result in improved tolerance by patients [3]. Similarly, patients who use relaxation strategies during imaging appear to experience less intense anxiety [4].

We investigated music as an aid to relaxation during imaging by building an air-tube earphone system for one of our imagers. Ninety-eight patients (14-79 years old) completed an 11-item Patient Comfort Questionnaire. Thirty-five patients (mean age, 41 years) selected music from a variety of available tapes and listened to it during imaging. The other 63 patients (mean age, 44 years) made up the no music group. Before imaging, the two groups did not differ in terms of anxiety (Fisher's exact test,  $p = 1.0$ ), confidence about coping with the examination ( $p = 1.0$ ), or number of previous procedures ( $p = 1.0$ ). Results indicated that significantly fewer of the patients listening to music reported extreme worry about their medical condition during imaging ( $p = .05$ ). These patients also showed a greater decrement in "nervousness" during imaging (compared with preimaging levels) than did the no music group (between groups  $t = 2.16$ ,  $p = .03$ ). Patients' postimaging written comments more often included symptoms of anxiety (5%) and somatic complaints (14%) in the no music group than in the music group (0% and 3%, respectively). No examinations were aborted entirely in either group.

Keith J. Slifer  
Keith Penn-Jones  
Michael F. Cataldo  
Robert T. Conner  
Elias A. Zerhouni  
The Kennedy Institute  
The Johns Hopkins University, School of Medicine  
Baltimore, MD 21205

### REFERENCES

1. Brennan SC, Redd WH, Jacobsen PB, et al. Anxiety and panic during magnetic resonance scans. *Lancet* 1988;1:512
2. Flahartey JA, Hoskinson K. Emotional distress during magnetic resonance imaging. *N Engl J Med* 1989;320:467-468
3. Weinreb JC, Maravilla KR, Peshock R, Payne J. Magnetic resonance imaging: improving patient tolerance and safety. *AJR* 1984;143:1285-1287
4. Quirk ME, Letendre AJ, Ciottone RA, Lingley JF. Evaluation of three psychologic interventions to reduce anxiety during MR imaging. *Radiology* 1989;173:759-762

### Pneumoperitoneum and Catamenial Pneumothorax

The interesting recent article in the *AJR* by Downey et al. [1] contains the statement that "pneumoperitoneum has never been described in association with catamenial pneumothorax." Actually, a patient with this combination was reported by Crutcher et al. [2], and the report of this association was cited later by Lillington et al. [3] in the paper that first used the term catamenial pneumothorax.

Failure of a diagnostic pneumoperitoneum to result in pneumothorax in a patient with a history of catamenial pneumothorax also was described by Crutcher et al. [2] and occurred in one of the five cases in our report [3]. The presence of right hemidiaphragmatic pores has been shown in many patients with catamenial pneumothorax, and it seems certain that this allows passage of endometrial tissue from the abdomen to the thorax [4]. The theory that air may pass through the genital tract, abdominal cavity, and diaphragmatic pores into the pleural cavity at the time of menses is not necessarily ruled out by these studies.

The case report by Downey et al. is also striking because there are virtually no other reports of catamenial pneumothorax involving the left hemithorax.

G. A. Lillington  
S. P. Mitchell

University of California, Davis, Medical Center  
Sacramento, CA 95817

#### REFERENCES

1. Downey DB, Towers MJ, Poon PY, Thomas P. Pneumoperitoneum with catamenial pneumothorax. *AJR* 1990;155:29-30
2. Crutcher RR, Waltuch TL, Blue ME. Recurring spontaneous pneumothorax associated with menstruation. *J Thorac Cardiovasc Surg* 1967;54:599-602
3. Lillington GA, Mitchell SP, Wood GA. Catamenial pneumothorax. *JAMA* 1972;219:1328-1332
4. Slasky BS, Siewers RD, Lecky JW, Zajko A, Burkholder JA. Catamenial pneumothorax: the roles of diaphragmatic defects and endometriosis. *AJR* 1982;138:639-643

#### Reply

We thank Drs. Lillington and Mitchell for their comments on our article [1] on catamenial pneumothorax, a term they introduced in 1972 [2]. Unlike our patient, the patient described by Crutcher et al. [3] was not shown to have had a pneumoperitoneum at the same time as her catamenial pneumothoraces. After three documented right-sided catamenial pneumothoraces and probably many more undocumented ones, she had a right-sided thoracotomy. An intact pleural bleb was resected, but no diaphragmatic defects were seen, though these were not looked for specifically. Subsequently, the patient's right-sided chest symptoms persisted intermittently at menstruation, but the pneumothoraces did not recur. Four years later, air was detected under the right hemidiaphragm at menstruation, but no associated pneumothorax occurred at that time.

We postulate that the reason no pneumoperitoneum was detected concurrent with the pneumothoraces in this patient, or in any other patient with catamenial pneumothorax, before our case [1] is that the difference in pressure between the peritoneal cavity and the pleural space causes air entering through the genital canal to move rapidly into the chest through diaphragmatic defects [1]. In the patient described by Crutcher et al. [3], postoperative changes probably blocked the diaphragmatic defects. When air subsequently entered the abdomen at menstruation, it presumably was stopped below the diaphragm, resulting in a pneumoperitoneum without an associated pneumothorax. The ability of CT to detect a few small bubbles of intraperitoneal air is the only reason we were able to detect the

pneumoperitoneum that complicated the last two episodes of pneumothorax in our patient. These tiny collections of air were not evident on chest radiographs.

As Drs. Lillington and Mitchell correctly point out, our case is unusual in that the catamenial pneumothorax occurred on the left side. In an extensive review of the literature, Gray et al. [4] found that 87% (60/69) of catamenial pneumothoraces were right sided, 7% (5/69) were left sided, and 6% (4/69) were bilateral.

Donal B. Downey  
Mark J. Towers  
Peter Y. Poon  
Peter Thomas  
St. Michael's Hospital  
University of Toronto  
Ontario M5B 1W8, Canada

#### REFERENCES

1. Downey DB, Towers MJ, Poon PY, Thomas P. Pneumoperitoneum with catamenial pneumothorax. *AJR* 1990;155:29-30
2. Lillington GA, Mitchell SP, Wood GA. Catamenial pneumothorax. *JAMA* 1972;219:1328-1332
3. Crutcher RR, Waltuch TL, Blue ME. Recurring spontaneous pneumothorax associated with menstruation. *J Thorac Cardiovasc Surg* 1967;54:599-602
4. Gray R, Cormier M, Yedlicka J, Moncada R. Catamenial pneumothorax: case report and literature review. *J Thorac Imaging* 1987;2(2):72-75

### A Different Opinion on the Tru-Close Thoracic Vent

In a recent technical note in the *AJR*, Molina et al. [1] describe their experience with the use of the Tru-Close Thoracic Vent manufactured by UreSil Corporation, Skokie, IL. They report 10 cases, nine of which were treated successfully with the device. We describe our experience with the device, which has not been as felicitous as theirs. We have stopped using the vent.

Over a period of several months, we placed five of these devices for the treatment of pneumothorax caused by percutaneous needle biopsy of the lung. Our method of placement was similar to that described by Molina et al. except that we used oblique C-arm fluoroscopy for direct visualization of the tube as it entered the pleural space. In all cases, we were able to aspirate large amounts of air from the pleural space without difficulty, and, fluoroscopically, we were able to see the size of the pneumothorax decrease. We used posteroanterior and lateral chest radiographs after placement to assess the position of the tube.

In four of the five cases, the tube backed out of the pleural space before it was to be removed. This was documented by obtaining lateral chest radiographs (Fig. 1). The first time the tube backed out, it occurred to us that the patient's raising her arms over her head for the chest radiograph might have caused the tube to shift position.

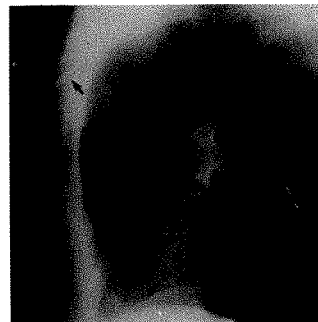


Fig. 1.—Lateral chest radiograph shows Tru-Close Thoracic Vent (arrow) is outside pleural space.



Thereafter lateral radiographs were obtained, with the patient's arms in neutral position or extended no more than 90° anteriorly. This did not seem to help; the tubes still backed out.

In four of the cases, no further treatment was needed for the pneumothorax. In one case, the tube backed out within 24 hr of placement, and the pneumothorax recurred. A 10-French chest tube connected to a Heimlich valve (Cook Inc., Bloomington, IN) was placed then, and the pneumothorax resolved without further incident.

We think that the failure of this chest tube to remain in the pleural space is related to its relatively short (7 cm) length. In our cases, thickness of the chest wall was between 2.0 and 3.5 cm, as measured at the second anterior interspace on supine chest CT scans. This means that when the tubes were placed with the patient supine, 3.5–5.0 cm of tube at most was present in the pleural space. The Tru-Close Thoracic Vent also has a side hole approximately 1 cm from its tip. In our patients, this meant that the tube could retract at most 2.5–4.0 cm before the side hole came out of the pleural space. With our patients, the tube did not seem to be long enough. Although all of our patients were hospitalized and were not engaged in any extraordinary activity, 80% of the tubes backed out. The only case in which the tube stayed in the pleural space was in a woman who had the tube removed after only 1 hr because of severe pleuritic pain. In three cases, the tube was out within 1 day; in the other case, within 2 days. This has led us to think that even the relatively sedate activities of an inpatient are sufficient to cause enough motion between the skin and the rib cage to cause the tube to back out.

Undoubtedly, treatment with this device was successful in four of our cases because the air leak was not sustained. This may account for the success of Molina et al. in treating 90% of their cases. However, we think that because of this device's inability to remain stable in the pleural space, its 7-cm version is inadequate for evacuation of pneumothorax. The 10-cm version may solve this problem.

Raymond E. Bertino

Terry M. Brady

St. Francis Hospital

University of Illinois, College of Medicine at Peoria  
Peoria, IL 61637

#### REFERENCE

1. Molina PL, Solomon SL, Glazer HS, Sagel SS, Anderson DJ. A one-piece unit for treatment of pneumothorax complicating needle biopsy: evaluation in 10 patients. *AJR* 1990;155:31–33

#### Reply

Unlike Drs. Bertino and Brady, we have not had a problem with the Tru-Close Thoracic Vent backing out of the pleural space before it is removed. In part, this may be due to our liberal use of tape, in addition to the adhesive backing of the thoracic vent, to fix the entire device securely to the chest wall.

As noted in our report [1] of our early experience with this vent, the manufacturer has increased the length of the catheter to 10 cm. This longer version should lessen the possibility of inadvertent withdrawal of the catheter from the pleural space. We have used the updated device successfully in five patients and have had no problem with the vent backing out.

Paul L. Molina

Steven L. Solomon

Harvey S. Glazer

Stuart S. Sagel

Dixie J. Anderson

Mallinckrodt Institute of Radiology  
Washington University, School of Medicine  
St. Louis, MO 63110

#### REFERENCE

1. Molina PL, Solomon SL, Glazer HS, Sagel SS, Anderson DJ. A one-piece unit for treatment of pneumothorax complicating needle biopsy: evaluation in 10 patients. *AJR* 1990;155:31–33

#### Papillomatosis of the Common Bile Duct Associated with Ampullary Carcinoma

A 60-year-old man with a history of cholecystectomy and cholecystostomy 4 months earlier had pain in the right upper quadrant, jaundice, and fever. An abdominal sonogram showed dilatation of the intra- and extrahepatic bile ducts and some small echogenic foci within the common hepatic duct without acoustic shadowing. ERCP showed multiple polypoid filling defects throughout the wall of the extrahepatic bile ducts (Fig. 1). In addition, a few polypoid lesions involved the ampulla of Vater. Biopsy specimens obtained under endoscopic and fluoroscopic guidance showed tubulopapillary adenomas with moderate dysplasia and an area of adenocarcinoma in the ampulla. Pathologic examination of a surgical specimen obtained during a Whipple procedure confirmed the diagnosis.

This patient initially had acute cholecystitis. Intraoperative cholangiography, done after cholecystectomy and extraction of stones from the common bile duct, showed the multiple filling defects, which were considered to be air bubbles. No visual or palpable abnormalities were found by the surgeons at the time of laparotomy.

Papillomatosis of the extrahepatic bile ducts is a rare disease and an unusual cause of obstructive jaundice. Obstruction probably occurs when papillomas involve the ampulla or the periampullary region, particularly if a superimposed malignancy or malignant degeneration is present. There is no agreement in the literature about association of biliary papillomas and carcinoma [1–4], but this possibility must be kept in mind, considering the frequent findings of dysplasia and atypia in the pathologic specimens. Awareness of this association has diagnostic, therapeutic, and prognostic implications.

Preoperative diagnosis should be possible by means of sonography and direct cholangiography. Small multiple echogenic lesions involving the wall of the extrahepatic bile ducts that appear as rounded filling defects on direct cholangiography are characteristic. ERCP is the method of choice because direct visualization of the ampulla and biopsies are mandatory to rule out carcinoma, especially if a distal obstruction of the common bile duct is suspected. CT is used for staging purposes only.

Mario Fava

Giancarlo Foradori

Francisco Cruz

Sergio Guzman

Hospital Clínico

Pontificia Universidad Católica de Chile

Santiago, Chile

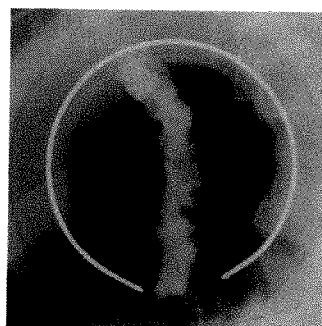


Fig. 1.—ERCP shows multiple polypoid filling defects within common bile ducts that were confirmed as papillomata by histologic examination.

## REFERENCES

1. Chu PT. Benign neoplasms of the extrahepatic bile ducts. *Arch Pathol* 1950;50:84-97
2. Shapiro PF, Livvendahl RA. Tumors of the extrahepatic bile ducts. *Ann Surg* 1931;94:61-79
3. Dowdy GS, Olin WG, Shelton EL, et al. Benign tumors of extrahepatic bile ducts. *Arch Surg* 1962;85:503-513
4. Eiss S, DiMaio D, Caedo JP. Multiple papillomas of the entire biliary tract: case report. *Ann Surg* 1960;152:320-324

### Scintigraphic Detection of Splenosis Causing Ureteral Compression and Hydronephrosis

Splenosis is the heterotopic autotransplantation of splenic tissue, invariably after splenic trauma. The entity was first described in the American literature in 1939 by Buchbinder and Lipkoff [1]. Splenosis easily is confused with more ominous processes. The condition may mimic metastatic carcinoma or endometriosis and, rarely, may cause bowel obstruction [2]. Patients frequently have had a splenectomy for traumatic rupture of the spleen. Technetium-99m-sulfur colloid scintigraphy is helpful in showing the reticuloendothelial nature of these nodules [3].

A 52-year-old man who had had a splenectomy after trauma when he was 9 years old was admitted with flank pain and hematuria. Excretory urography showed moderate dilatation of the left renal calices and ureter with distal ureteral narrowing and two small renal pelvic calculi. A left-sided retrograde pyelogram performed before extracorporeal shock-wave lithotripsy showed left-sided hydronephrosis and diffuse ureteral narrowing (Fig. 1A). The previously observed renal calculi were no longer visualized. A CT scan of the pelvis

after rectal administration of contrast material showed multiple soft-tissue nodules (Fig. 1B) at the base of the bladder. A scintigram with <sup>99m</sup>Tc sulfur colloid (Fig. 1C) showed intense uptake of the radionuclide by the soft-tissue nodules.

Surgery revealed multiple splenic implants compressing the left ureter. These were excised, and the ureter was freed up to the bladder. Histopathologic examination of the excised nodules confirmed the diagnosis of splenosis. No evidence of hydronephrosis was seen postoperatively or on sonograms obtained during a 1-year follow-up.

To our knowledge, this is the first reported case of obstructive uropathy due to splenosis. Although CT is effective in determining the exact location of splenic implants, scintigraphy shows the functional reticuloendothelial nature of the nodules.

D. G. K. Varma  
M. D. Anderson Cancer Center  
Houston, TX 77030  
Richard J. Campeau  
Zane A. Kartchner  
Tulane University Medical Center  
New Orleans, LA 70112  
Satish Karnik  
Chalmette Urology  
Chalmette, LA 70043

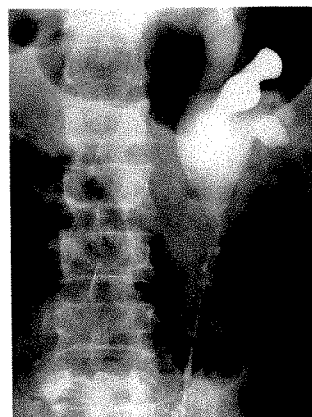
## REFERENCES

1. Buchbinder JH, Lipkoff CJ. Splenosis: multiple peritoneal splenic implants following abdominal injury. *Surgery* 1939;6:927-934
2. Sirinek KR, Livingston CD, Bova JG, Levine BA. Bowel obstruction due to infarcted splenosis. *South Med J* 1984;77:764-767
3. Derin H, Yetkin E, Ozkilic H, Ozekli K, Yaman C. Detection of splenosis by radionuclide scanning. *Br J Radiol* 1987;60:873-875

### Detection of Inadvertent Vaginal Filling During Cystography

We read with interest the pictorial essay, "Catheter Malposition During Cystography: A Cause of Diagnostic Errors," by Zerlin and Lebowitz [1] in the August 1989 issue of the *AJR*. We wish to share our observations on inadvertent vaginal filling during cystography.

It has been mentioned that this condition can be detected on the basis of the tubular shape of the vagina. Besides this finding, we have noticed that many times the vagina is rounded superiorly and tapers downward. The inferior end is poorly defined, and the vagina



A

Fig. 1.—Splenosis causing ureteral compression and hydronephrosis.

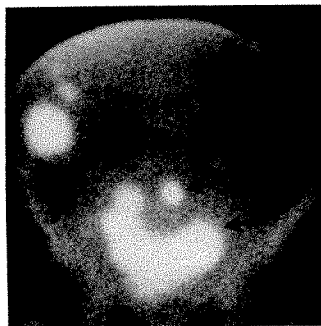
A, Left-sided retrograde pyelogram shows hydronephrosis and diffuse narrowing of ureter.

B, CT scan of pelvis performed with rectal, IV, and oral contrast shows multiple nodules adjacent to bowel loops indenting contrast-filled bladder (arrowheads).

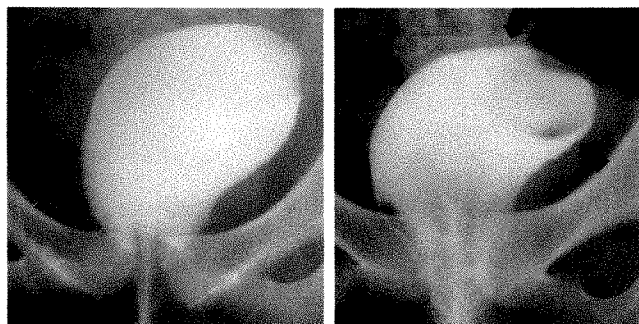
C, Anterior <sup>99m</sup>Tc-sulfur colloid scintigram of lower abdomen and pelvis obtained same day as B shows intense uptake of radio-colloid corresponding to splenic nodules (arrows) at base of bladder evident on CT and found at surgery. Other implants, including a large right paracolic nodule, are evident (arrowheads).



B



C



A

Fig. 1.—Inadvertent filling of vagina during cystography.

A, Cystogram shows "hot-air balloon" appearance of vagina filled with contrast material.

B, Voiding cystogram shows a spuriously wide "urethra" and a coiled catheter (arrows) preferentially filling left side of vagina.

B

looks not unlike a hot-air balloon, open at its lower end. Whatever the shape of the vagina, downward tapering and a poorly defined lower margin are good clues that it has been filled with contrast material (Fig. 1A). In addition, if the vagina is not too distended, the coiled catheter preferentially fills the lateral fornix in which it lies, thereby leading to a further oddity in vaginal shape (Fig. 1B). Finally, the voiding cystogram shows a spuriously wide "urethra" that merges with this cavity without the normal narrowing noted at the bladder neck.

Suleman Merchant  
Vimal Patel  
Hemant Morparia  
Rupal Someshwar  
King Edward Memorial Hospital  
Bombay 12, India

## REFERENCE

1. Zerwin JM, Lebowitz RL. Catheter malposition during cystography: a cause of diagnostic errors. *AJR* 1989;153:363-367

## Reply

Dr. Merchant et al. have suggested several more clues that might make it possible to recognize inadvertent catheterization of the vagina during attempted cystography. We agree with their suggestions. In addition, several other features may help in the differentiation: (1) Vaginal rugae may be visible after the introduction of contrast material. (2) The appearance of the vaginal outlet is quite different than that of the bladder base. The vaginal outlet is positioned below the pelvic floor and it has no sphincter to prevent the free efflux of contrast material from the vagina onto the perineum. (3) The malposition of the catheter may be apparent by inspection of the perineum.

J. Michael Zerlin  
University of Michigan Hospitals  
C. S. Mott Children's Hospital  
Ann Arbor, MI 48109-0252  
Robert L. Lebowitz  
The Children's Hospital  
Boston, MA 02115

## Bone Scintigraphy for Evaluation of Pelvic Pain

We would like to comment on the obvious bias in the comparative analysis of three standard imaging techniques for the evaluation of pelvic pain in cancer patients as presented by Beatrous et al. [1]. Not only was bone scintigraphy unreasonably expected to show soft-tissue metastases, which certainly are delineated better by MR imaging, but optimal state-of-the-art tomographic imaging of the pelvis and lumbar spine was not performed as part of the radionuclide study. Single-photon emission CT enhances lesion detection and localization and is particularly useful in the lumbosacral spine and pelvis [2-4]. In fact, in the Materials and Methods section, Beatrous et al. describe neither the bone scanning protocol (e.g., analog vs digital, total-body vs spot views) nor the instrumentation (e.g., camera/collimator). They do, however, provide complete technical details for the CT and MR imaging.

Meticulously acquired and carefully interpreted bone scintigrams are highly accurate for showing skeletal disease. Given the prevailing emphasis on medical cost containment, bone scintigraphy remains an excellent initial imaging technique in the evaluation of skeletal disease and may be complemented by CT and MR imaging in the appropriate clinical setting.

Elizabeth Oates  
Dwight Achong  
New England Medical Center  
Boston, MA 02111

## REFERENCES

1. Beatrous TE, Choyke PL, Frank JA. Diagnostic evaluation of cancer patients with pelvic pain: comparison of scintigraphy, CT, and MR imaging. *AJR* 1990;155:85-88
2. Gates GF. SPECT imaging of the lumbosacral spine and pelvis. *Clin Nucl Med* 1988;13:907-914
3. Fogelman I, Collier BD. *An atlas of planar and SPECT bone scans*. London: Martin Dunitz, 1989
4. Gates GF. Normal anatomy of the lumbosacral spine and pelvis: a correlation of SPECT and radiographic techniques. *Clin Nucl Med* 1988;13:327-330

## Reply

We thank Drs. Oates and Achong for their comments. They correctly point out some omissions in our description of the bone scanning technique. To set the record straight, we performed the studies on either a General Electric Starport or Maxicamera 500, both with low-energy all-purpose collimation, or on a Picker SX100, with high-resolution, low-energy collimation. In all instances, spot views were obtained in the analog or digital mode.

We agree that bone scanning is superior to MR imaging in the initial detection of bone metastases because of the broader scope and lower cost of scintigraphy. However, in criticizing our paper, Oates and Achong failed to consider the clinical context in which MR imaging was compared with bone scanning. We evaluated pelvic pain in cancer patients. Our study showed that osseous and extraosseous metastases are common in patients who have advanced malignancy. Although bone scanning is used frequently in this setting, the extent of disease is underestimated. Even if single-photon emission CT had been used, the extraosseous component would not have been detected. Thus, a second study is necessary regardless of the results of bone scanning. MR showed all the anatomic abnormalities, including soft-tissue and bony lesions, and, because of its multiplanar capabilities, was able to show their relationship with the nerve roots. Appreciation of the full extent of the neoplastic soft-tissue component has important implications for the choice of therapy, size of radiation port, and follow-up. We wish to reemphasize that our study was done on patients with advanced malignancy in whom nerve root involvement not only was likely but also was the major diagnostic issue. Recently, we have encountered two patients with advanced malignancy in whom bone scans were normal, pelvic CT showed herniated disks, and MR showed nerve root compression. This reinforces our conclusion that a single comprehensive study is preferable to multiple studies.

The comments of Oates and Achong underscore an important dictum: Statements about the superiority of one technique over another can be made only in the context of a given population of patients.

Peter L. Choyke  
National Institutes of Health  
Bethesda, MD 20892  
Thomas E. Beatrous  
Glenwood Regional Medical Center  
Monroe, LA 71294  
Joseph A. Frank  
National Institutes of Health  
Bethesda, MD 20892  
Georgetown University Medical Center  
Washington, DC 20007



## Doppler Velocity Waveforms of Blood Flow in the Fetal Renal Artery in a Case of Meckel Syndrome

Numerous reports have been published on the antenatal diagnosis of infantile polycystic renal disease [1]. However, the fetal renal hemodynamics of this condition has not been described. We used pulsed Doppler sonography to determine the velocity waveforms of blood flow in the renal artery in a fetus with Meckel syndrome at 21 weeks gestation.

A 24-year-old woman at 21 weeks gestation was referred because of suspected fetal anomalies and oligohydramnios. Real-time sonography showed a single fetus in vertex presentation that had severe oligohydramnios. The fetal head was extremely dolichocephalic (cephalic index, 56%), and an occipital encephalocele was noted. The fetal kidneys were enlarged and hyperechogenic. No evidence was present of a fetal bladder or stomach. The rest of the fetal structures appeared to be normal. The presence of the occipital encephalocele and bilateral polycystic kidneys suggested the diagnosis of Meckel syndrome.

Pulsed Doppler sonography showed an increased diastolic component in the velocity waveform of blood flow in the fetal renal artery (Fig. 1). The pulsatility index (0.81) was significantly low. The pulsatility indexes in the middle cerebral artery, descending aorta, and umbilical artery were within the normal range.

At 22 weeks gestation a male stillborn fetus weighing 554 g was delivered vaginally. Autopsy showed dolichocephaly with occipital encephalocele and bilateral infantile polycystic dysplastic kidneys. The diagnosis was Meckel syndrome.

Diagnosis of infantile polycystic kidney disease in utero depends on abnormal renal anatomy (kidney size and texture) and the consequences of renal failure (oligohydramnios and the absence of a fetal bladder) [1]. In our case, all four antenatal sonographic criteria were fulfilled. On pulsed Doppler sonography, the pulsatility indexes in the middle cerebral artery, descending aorta, and umbilical artery were normal. The interesting aspect of our case is the significantly low pulsatility index in the renal artery. This increase in the renal perfusion of the infantile polycystic dysplastic kidney was probably an expression of the enlarged kidney mass.

Toshiyuki Hata  
Giancarlo Mari  
Alexander A. Reiter  
Baylor College of Medicine  
Houston, TX 77030



Fig. 1.—Doppler image obtained prenatally shows velocity waveforms of blood flow in fetal renal artery (waveform above line) and vein (waveform below line). Arrows show diastolic venous reverse flows.

## REFERENCE

1. Romero R, Cullen M, Jeanty P, et al. The diagnosis of congenital renal anomalies with ultrasound. II. Infantile polycystic kidney disease. *Am J Obstet Gynecol* 1984;150:259-262

## An Uncommon Complication of Translumbar Aortography

Translumbar aortography largely has been replaced by angiographic procedures that use the Seldinger technique. In the last decade, however, the use of the translumbar approach has increased because many interventional radiologists wish to save femoral arteries for percutaneous transluminal angioplasty. The complication rate of translumbar aortography is equal to or perhaps even somewhat less than that of transfemoral aortography [1]. We describe an unusual complication associated with translumbar aortography that has not been reported before.

A 56-year-old man had a history of ischemic pain in the lower extremities. Translumbar aortography was performed. A Cook translumbar needle was inserted in the infrarenal segment of the aorta, and 90 ml of Omnipaque (iohexol) was injected with an angiographic pump. The aortogram was technically satisfactory (Fig. 1); the patient felt well, and he returned to his hospital room. Four hours later, lower back pain developed. In our experience, this is not an unusual symptom after translumbar aortography. The next hour, the patient felt worse. His hematocrit fell to 28%, his systolic blood pressure was about 100 mm Hg, and he showed signs of hypovolemic shock. At surgery, it was determined that the translumbar needle had entered the inferior mesenteric artery a few millimeters from its origin at the aorta and then had entered the aorta through the ostium of this artery. The inferior mesenteric artery was transected completely from the puncture site in the artery to the artery's origin at the aorta, a distance of 5 mm. The artery was ligated, and the ostium of the artery on the aortic wall was closed.

Goran Nikolic  
Svetozar Pervulov  
Miomir Stanojevic  
Vesna Pashu-Cerčina  
Mirko Draganic  
Slobodan Cirkovic  
Sinisa Kamenica  
Military Medical Academy  
11000 Belgrade, Yugoslavia

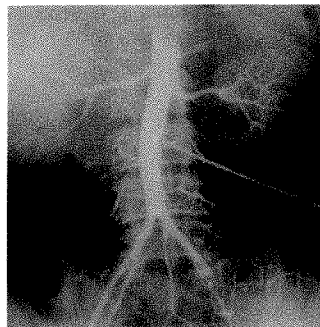


Fig. 1.—Successful aortogram shows no extravasation of contrast material.

## REFERENCE

1. Szilagyi DE, Smith RF, Elliot JR Jr, Hageman JH. Translumbar aortography: a study of safety and usefulness. *Arch Surg* 1977;112:399-342

Letters are published at the discretion of the Editor and are subject to editing.

Letters to the Editor must not be more than two *double-spaced*, typewritten pages. One or two figures may be included. Abbreviations should not be used. See Author Guidelines, page A5.

Material being submitted or published elsewhere should not be duplicated in letters, and authors of letters must disclose financial associations or other possible conflicts of interest.

Letters concerning a paper published in the *AJR* will be sent to the authors of the paper for a reply to be published in the same issue. Opinions expressed in the Letters to the Editor do not necessarily reflect the opinions of the Editor.

## Review of Current Literature

Initials and addresses of corresponding authors are provided in parentheses for each article so that the reader can obtain reprints directly. Abstracts are printed verbatim from each journal.

### The New England Journal of Medicine

**Aerosolized pentamidine for prophylaxis against *Pneumocystis carinii* pneumonia: the San Francisco Community Prophylaxis Trial.** Leoung GS, Feigal DW Jr, Montgomery AB, et al. (DWF, Dept. of Medicine, UCSD Medical Center, 225 Dickinson St., H811E, San Diego, CA 92103). *N Engl J Med* 323(12):769-775, Sept. 1990

**Background and Methods.** *Pneumocystis carinii* pneumonia (PCP) is the most frequent life-threatening opportunistic infection associated with human immunodeficiency virus (HIV) infection. To assess the possible value of aerosolized-pentamidine prophylaxis in different doses, a controlled clinical trial was begun in 1987 with 408 subjects at 12 treatment centers. The participants were randomly assigned to receive 30 mg of pentamidine every two weeks, 150 mg every two weeks, or 300 mg every four weeks.

**Results.** Eighteen months after randomization, the subjects in the 300-mg arm had had 8 confirmed episodes of PCP while receiving treatment, as compared with 22 in the 30-mg arm ( $P = 0.0008$ ). The 150-mg arm had intermediate results but ones not significantly different from those of the 300-mg arm. Participants with previous episodes of PCP and CD4-cell counts less than 100 per cubic millimeter were at the highest risk for PCP.

**Conclusions.** Aerosolized pentamidine was effective for prophylaxis against PCP in patients infected with HIV, according to the dose and schedule of administration. It and zidovudine were well tolerated together and had independent prophylactic benefits.

**Oral therapy for *Pneumocystis carinii* pneumonia in the acquired immunodeficiency syndrome: a controlled trial of trimethoprim-sulfamethoxazole versus trimethoprim-dapsone.** Medina I, Mills J, Leoung G, et al. (C. B. Wofsy, Ward 95, Bldg. 90, San Francisco General Hospital, 995 Potrero Ave., San Francisco, CA 94110). *N Engl J Med* 323(12):776-782, Sept. 1990

**Background.** Antimicrobial drugs that can be taken orally are needed for the treatment of *Pneumocystis carinii* pneumonia in patients with the acquired immunodeficiency syndrome (AIDS). Preliminary data indicate that dapsone with trimethoprim may be an effective alternative to trimethoprim-sulfamethoxazole, which is frequently toxic.

**Methods.** In a double-blind trial, 60 patients with AIDS and mild-to-moderately-severe first episodes of *P. carinii* pneumonia (partial pressure of oxygen in arterial blood,  $>60$  mm Hg while breathing room air) were randomly assigned to 21 days of treatment with either

trimethoprim-sulfamethoxazole (20 and 100 mg per kilogram of body weight per day, respectively) or trimethoprim-dapsone (20 mg per kilogram per day and 100 mg per day).

**Results.** The orally administered treatment failed because of progressive pneumonitis in 3 of the 30 patients assigned to trimethoprim-sulfamethoxazole and in 2 of the 30 assigned to trimethoprim-dapsone ( $P > 0.3$ ). Major toxic effects required a switch to intravenous pentamidine for 17 patients (57 percent) in the trimethoprim-sulfamethoxazole group, as compared with 9 (30 percent) in the trimethoprim-dapsone group ( $P < 0.025$ ). With trimethoprim-sulfamethoxazole, there were more instances of severe chemical hepatitis (six, as compared with one in the trimethoprim-dapsone group) and marked neutropenia (five vs. one). Intolerable rash (three in each treatment group) and severe nausea and vomiting (two in each group) occurred with equal frequency with both drug combinations. Methemoglobinemia occurred in most of the patients treated with trimethoprim-dapsone, but it was asymptomatic and the level exceeded 20 percent in only one patient. Mild hyperkalemia (serum potassium level, 5.1 to 6.1 mmol per liter) also occurred in 53 percent of the patients treated with trimethoprim-dapsone.

**Conclusions.** In patients with AIDS, oral therapy with trimethoprim-sulfamethoxazole and with trimethoprim-dapsone are equally effective for mild-to-moderate first episodes of *P. carinii* pneumonia, but with trimethoprim-dapsone there are fewer serious adverse reactions than with trimethoprim-sulfamethoxazole.

**A controlled trial of the effect of calcium supplementation on bone density in postmenopausal women.** Dawson-Hughes B, Dallal GE, Krall EA, Sadowski L, Sahyoun N, Tannenbaum S (BDH, U. S. Dept. of Agriculture Human Nutrition Research Center on Aging at Tufts University, 711 Washington St., Boston, MA 02111). *N Engl J Med* 323(13):878-883, Sept. 1990

**Background.** The effectiveness of calcium in retarding bone loss in older postmenopausal women is unclear. Earlier work suggested that the women who were most likely to benefit from calcium supplementation were those with low calcium intakes.

**Methods.** We undertook a double-blind, placebo-controlled, randomized trial to determine the effect of calcium on bone loss from the spine, femoral neck, and radius in 301 healthy postmenopausal women, half of whom had a calcium intake lower than 400 mg per day and half an intake of 400 to 650 mg per day. The women received placebo or either calcium carbonate or calcium citrate malate (500 mg of calcium per day) for two years.

**Results.** In women who had undergone menopause five or fewer years earlier, bone loss from the spine was rapid and was not affected by supplementation with calcium. Among the women who had been postmenopausal for six years or more and who were given placebo, bone loss was less rapid in the group with the higher dietary calcium intake. In those with the lower calcium intake, calcium citrate malate

prevented bone loss during the two years of the study; its effect was significantly different from that of placebo ( $P < 0.05$ ) at the femoral neck (mean change in bone density [ $\pm$ SE],  $0.87 \pm 1.01$  percent vs.  $-2.11 \pm 0.93$  percent), radius ( $1.05 \pm 0.75$  percent vs.  $-2.33 \pm 0.72$  percent), and spine ( $-0.38 \pm 0.82$  percent vs.  $-2.85 \pm 0.77$  percent). Calcium carbonate maintained bone density at the femoral neck (mean change in bone density,  $0.08 \pm 0.98$  percent) and radius ( $0.24 \pm 0.70$  percent) but not the spine ( $-2.54 \pm 0.85$  percent). Among the women who had been postmenopausal for six years or more and who had the higher calcium intake, those in all three treatment groups maintained bone density at the hip and radius and lost bone from the spine.

**Conclusions.** Healthy older postmenopausal women with a daily calcium intake of less than 400 mg can significantly reduce bone loss by increasing their calcium intake to 800 mg per day. At the dose we tested, supplementation with calcium citrate malate was more effective than supplementation with calcium carbonate.

**Evaluation of systemic amyloidosis by scintigraphy with  $^{123}\text{I}$ -labeled serum amyloid P component.** Hawkins PN, Lavender JP, Pepys MB (PNH, Immunological Medicine Unit, Royal Postgraduate Medical School, Hammersmith Hospital, Du Cane Rd., London W12 0NN, United Kingdom). *N Engl J Med* 323(8):508-513, Aug. 1990

**Background.** In systemic amyloidosis the distribution and progression of disease have been difficult to monitor, because they can be demonstrated only by biopsy. Serum amyloid P component (SAP) is a normal circulating plasma protein that is deposited on amyloid fibrils because of its specific binding affinity for them. We investigated whether labeled SAP could be used to locate amyloid deposits.

**Methods.** Purified human SAP labeled with iodine-123 was given intravenously to 50 patients with biopsy-proved systemic amyloidosis—25 with the AL (primary) type and 25 with the AA (secondary) type—and to 26 control patients with disease and 10 healthy subjects. Whole-body images and regional views were obtained after 24 hours and read in a blinded fashion.

**Results.** In the patients with amyloidosis the  $^{123}\text{I}$ -SAP was localized rapidly and specifically in amyloid deposits. The scintigraphic images obtained were characteristic and appeared to identify the extent of amyloid deposition in all 50 patients. There was no uptake of the  $^{123}\text{I}$ -SAP by the control patients and the healthy subjects. In all patients with AA amyloidosis the spleen was affected, whereas the scans showed uptake in the heart, skin, carpal region, and bone marrow only in patients with the AL type. Positive images were seen in six patients in whom biopsies had been negative or unsuccessful; in all six, amyloid was subsequently found on biopsy or at autopsy. Progressive amyloid deposition was observed in 9 of 11 patients studied serially.

**Conclusions.** Scintigraphy after the injection of  $^{123}\text{I}$ -SAP can be used for diagnosing, locating, and monitoring the extent of systemic amyloidosis.

**Swallowing dysfunction in nephropathic cystinosis.** Sonies BC, Ekman EF, Andersson HC, et al. (W. A. Gahl, Bldg. 10, Rm. 9S242, Human Genetics Branch, National Institute of Child Health and Human Development, 9000 Rockville Pike, Bethesda, MD 20892). *N Engl J Med* 323(9):565-570, Aug. 1990

**Background.** Nephropathic cystinosis causes renal failure in most patients at approximately 10 years of age. This can be prevented or retarded by cystine-depleting therapy with oral cysteamine. Many patients who do not receive adequate cysteamine therapy undergo renal transplantation, but the accumulation of cystine continues in other organs, resulting in various clinical abnormalities. We report age-related swallowing dysfunction in patients with nephropathic cystinosis.

**Methods.** We studied 43 patients with cystinosis (24 who had received a renal transplant and 19 who had not), 3 to 31 years of age. Oral motor function was assessed by a cranial-nerve oral sensorimotor examination, and an oral motor index was calculated for

each patient. The oral phase of swallowing was assessed by ultrasonography, and the pharyngeal and esophageal phases were evaluated by videofluoroscopy.

**Results.** Approximately half the patients were slow eaters. Oral motor dysfunction, reflected by a higher oral motor index, increased with age. Speech, oral structure and anatomy, and tongue and lip strength were particularly affected. Seven of nine patients 21 to 31 years old had abnormalities in all three phases of swallowing; the deficits were variable in younger patients. In 28 patients with cystinosis, the mean ( $\pm$ SD) duration of oropharyngeal swallowing for a dry swallow ( $3.06 \pm 1.06$  seconds) was longer than in 14 normal subjects ( $1.89 \pm 0.57$  seconds;  $P < 0.001$ ). This prolongation reflected impairment of the initiation phase of swallowing.

**Conclusions.** Swallowing dysfunction is a late complication of nephropathic cystinosis, probably related to muscular dysfunction. Changes in the consistency of foods, swallowing exercises, and long-term cysteamine therapy should be considered for patients with cystinosis who have difficulty in swallowing.

**Absence of need for amniocentesis in patients with elevated levels of maternal serum alpha-fetoprotein and normal ultrasonographic examinations.** Nadel AS, Green JK, Holmes LB, Frigoletto FD Jr, Benacerraf BR (ASN, Dept. of Obstetrics and Gynecology, Brigham and Women's Hospital, 75 Francis St., Boston, MA 02115). *N Engl J Med* 323(9):557-561, Aug. 1990

**Background.** Recent improvements in the accuracy of sonographic diagnosis of neural-tube and ventral-wall defects have raised a question about the wisdom of routinely offering amniocentesis to women who have elevated levels of maternal serum alpha-fetoprotein with a structurally normal fetus as determined by ultrasonography.

**Methods.** We reviewed the ultrasound findings in 51 consecutive fetuses with spina bifida, encephalocele, gastroschisis, or omphalocele that were delivered or aborted at a single hospital, to estimate the sensitivity of ultrasonography for these diagnoses. In all cases, the mothers had undergone prenatal sonography at one facility between 16 and 24 weeks after the last menstrual period. We used these data to calculate the probability of an affected fetus in a woman with a given level of maternal serum alpha-fetoprotein and a normal sonogram.

**Results.** These four types of anomalies were correctly identified in all 51 cases, yielding a sensitivity of 100 percent (95 percent confidence interval, 94 to 100 percent). Using the lower limit of this confidence interval, we calculated that the probability of an affected fetus ranges from 0.01 to 0.15 percent for maternal serum alpha-fetoprotein levels ranging from 2.0 to 3.5 times the median, respectively.

**Conclusions.** This level of risk is less than the reported risk of abortion due to amniocentesis and may lead some women with elevated levels of alpha-fetoprotein to decide not to proceed with amniocentesis.

## Chest

**Diagnostic value of nonfluoroscopic percutaneous lung needle aspiration in patients with pneumonia.** Torres A, Jiménez R, Puig de la Bellacasa J, Celis R, González J, Gea J (AT, Servei de Pneumologia, Hospital Clinic, Barcelona, Spain 08036). *Chest* 98(4):840-844, Oct. 1990

In forty-one patients (mean [ $\pm$ SD] age  $51 \pm 19$  years; range, 11 to 88 years; seven female and 34 male) with clinical signs and symptoms of pneumonia, we performed a nonfluoroscopic percutaneous lung needle (22 gauges) aspiration (PLNA) to investigate the diagnostic yield of this technique. All the patients were receiving antibiotics at the time of the study, and PLNA was performed either because of a lack of response to empiric antibiotic treatment or because of the severity of the pneumonia or the underlying condition of the patient. Eight patients were mechanically ventilated (MV) due



to acute respiratory failure. The PLNA was performed at bedside and without fluoroscopic guidance. Twenty-two microorganisms were identified by means of stains and/or cultures of PLNA samples. Sensitivity of PLNA was 43 percent (18/41). We detected three false-positive cultures probably due to contamination from the skin area punctured. In the eight MV patients studied, the sensitivity of PLNA was 37.5 percent, and the microbiologic findings turned out to be crucial for the outcome of the patients. Pneumothorax developed in three patients (7 percent) after PLNA. None of these three patients developed a pleural infection but two of them required thoracostomy drainage. None of the MV patients presented complications. Our results showed that nonfluoroscopic PLNA is a technique with moderately good sensitivity and with a low rate of false-positive cultures (8 percent) to diagnose pulmonary infections in patients with unresponsiveness to empiric antibiotic treatment or with severe pneumonia. Further evaluation of its diagnostic value and complications in MV patients is needed, although our preliminary results suggest that PLNA can be an alternative technique to other methods for diagnosing pulmonary infections in patients receiving artificial ventilatory support.

## Gastroenterology

**Biomechanics of cricopharyngeal bars.** Dantas RO, Cook IJ, Dodds WJ, Kern MK, Lang IM, Brasseur JG (ROD, Dept. of Radiology, Medical College of Wisconsin, Milwaukee, WI). *Gastroenterology* 99:1269-1274, 1990

Patients with a prominent cricopharyngeal bar visible on radiography are generally considered to have spasm of the cricopharyngeus, which is the major muscle component of the upper esophageal sphincter. This condition has been termed "cricopharyngeal achalasia." The aim of this study was to determine the pathogenesis of cricopharyngeal bars. Concurrent videofluoroscopic and manometric examinations of the pharynx and upper esophageal sphincter were performed in a cohort of six patients with prominent cricopharyngeal bars and in eight control volunteers. In each subject, swallows of 2-30 mL barium boluses were recorded. The patients with cricopharyngeal bars showed (a) normal peristaltic contraction in the pharynx, (b) normal axial upper esophageal sphincter pressure and relaxation, (c) normal flow rate across the upper esophageal sphincter, and (d) normal duration of upper esophageal sphincter opening for different bolus volumes. The major abnormalities in the patients with cricopharyngeal bars were (a) reduced maximal dimensions of the upper esophageal sphincter during the transsphincteric flow of barium and (b) increased intrabolus pressure upstream to the upper esophageal sphincter. Thus, the increase in intrabolus pressure preserved normal transsphincteric flow rates even though the upper esophageal sphincter did not open normally. Overall, the constellation of findings in the patients studied suggests that the underlying pathogenesis of their cricopharyngeal bar was reduced muscle compliance wherein the relaxed cricopharyngeus did not distend normally during swallowing.

Reprinted with permission by the American Gastroenterological Association.

**Piezoelectric lithotripsy: stone disintegration and follow-up results in patients with symptomatic gallbladder stones.** Ell C, Kerzel W, Schneider HT, et al. (CE, Dept. of Medicine I, University of Erlangen-Nuremberg, Erlangen, Federal Republic of Germany). *Gastroenterology* 99:1439-1444, 1990

One hundred symptomatic patients with radiolucent gallbladder stones were treated with a new piezoelectric lithotripter and oral chemolitholytic agents. Stone disintegration was achieved in 99 of these patients (99%) with a mean ( $\pm$ SD) maximum fragment size of  $5.1 \pm 4.1$  mm. Significant differences were found when the mean ( $\pm$ SD) fragment sizes of single stones  $\leq 20$  mm ( $4.2 \pm 2.5$  mm) were compared with those of single stones  $> 20$  mm ( $5.8 \pm 3.4$  mm;  $P < 0.05$ ) and multiple stones ( $6.2 \pm 3.8$  mm;  $P < 0.05$ ), respectively. None of the patients required anesthesia, analgesics, or sedatives before or during the treatment. The stone-free rates for all patients

followed up for up to 4-12 months (mean  $\pm$  SD,  $10.7 \pm 2.9$  months) were 18% (1 month), 25% (2 months), 38% (4 months), 52% (8 months), and 67% (12 months). Partly significant differences were obtained in stone-free rates for single stones ( $\leq 20$  mm) compared with larger stones ( $> 20$  mm) and multiple stones ( $P < 0.05$ ), respectively. Serious adverse reactions (i.e., cholestasis and pancreatitis) were observed in only 3 patients (3%). These conditions were induced by fragment impaction in the common bile duct. In 2 of these patients, endoscopic retrograde cholangiopancreatography with endoscopic sphincterotomy was required. It is concluded that piezoelectrically generated shock waves are suitable for the effective and safe disintegration of gallbladder stones in humans. The anesthesia-free and analgesia-free shock-wave application opens up the possibility to perform biliary lithotripsy as an outpatient procedure. The stone-free rate achieved in combination with oral bile acids is most promising for single stones ( $\leq 20$  mm).

Reprinted with permission by the American Gastroenterological Association.

**In vivo assessment of shock-wave pressures: implication for biliary lithotripsy.** Vergunst H, Terpstra OT, Schröder FH, Matura E (HV, Dept. of Surgery, University Hospital Dijkzigt, Erasmus University Rotterdam, Rotterdam, the Netherlands). *Gastroenterology* 99:1467-1474, 1990

During extracorporeal shock-wave lithotripsy, the pressure profile, which is generated by the lithotripter, determines the risk of tissue damage. In the present study, the pressure distribution of a lithotripter (Lithostar; Siemens A. G., Erlangen, Federal Republic of Germany) was investigated in 10 pigs, five of which had gallstones surgically implanted into the gallbladder. The in vivo values were compared with in vitro data. Measurements were carried out along the shock-wave transmission path at the focus within the gallbladder, the adjacent liver, the diaphragmatic surface of the right lung, and the shock-wave exit site from the skin. Interposition of ribs did not cause a significant decrease in focal positive pressure. However, a gallstone positioned in the focus caused a 30%-65% reduction in pressure, recorded immediately behind the stone. Pressures obtained in vivo were always 15%-25% lower than those measured in vitro. The spatial distributions of the positive pressure in vivo and in vitro were almost identical. There was a high correlation between the pressures in vitro and in vivo ( $r = 0.88$ ;  $P \leq 0.01$ ). This justifies assessment of shock-wave energies generated during biliary lithotripsy by extrapolation of in vitro data. It is concluded that it is possible to characterize different lithotripters by in vitro pressure profile measurements.

Reprinted with permission by the American Gastroenterological Association.

**Endoscopic retrograde brush cytology: a new technique.** Venu RP, Geenen JE, Kini M, et al. (RPV, Dept. of Gastroenterology, Medical College of Wisconsin, Milwaukee, WI). *Gastroenterology* 99:1475-1479, 1990

Endoscopic retrograde cholangiopancreatography has been shown to be a very valuable adjunct in the diagnosis of malignancy involving the biliary and/or pancreatic ductal system. However, characteristic endoscopic retrograde cholangiopancreatography radiographic findings associated with malignant strictures are frequently not specific and cytological confirmation becomes essential for the diagnosis. Unfortunately, the current overall diagnostic yield of positive cytology in such circumstances ranges from 18%-56% depending on the technique. A new brush device has been designed which is uniquely adapted to pancreaticobiliary strictures of varying anatomical configurations. This study shows results using this new cytology brush in a series of 53 patients with pancreaticobiliary malignancy. A significant improvement in the cytological yield of tumor confirmation was obtained with a diagnostic sensitivity of 70% and specificity of 100% using the new brush technique.

Reprinted with permission by the American Gastroenterological Association.

## Digestive Diseases and Science

**Gastric lesions secondary to long-distance running.** Gaudin C, Zerath E, Guezennec CY (CYG, CERMA, 5 bis, Avenue de la Porte de Sevres, 75731 Paris, 15 Air Cedex, France). *Dig Dis Sci* 35(10):1239-1243, Oct. 1990

Gastrointestinal disorders have been reported during long-distance running. The purpose of this study was to evaluate the effects of prolonged exercise on the upper digestive tract. Seven subjects were submitted to a standard endoscopic examination of the upper digestive tract before and after long-distance running (range 18-50 km). Mucosal biopsy specimens were taken during all endoscopies. After running, all runners had histologically pathological features in the stomach. Vascular lesions were present in the chorion in six subjects after running, with the intensity of the lesions ranging from congestion to hemorrhage. Postexercise histological examination also showed a decrease in mucosal secretion. These lesions secondary to prolonged exercise indicate the presence of hemodynamic perturbations in the upper digestive tract.

## Gastrointestinal Endoscopy

**Endoscopic retrograde cannulation of the gallbladder: direct dissolution of gallstones.** Foerster EC, Matek W, Domschke W (ECF, Medizinische Klinik mit Poliklinik I der Universität Erlangen-Nürnberg, Krankenhausstr. 12, D-8520 Erlangen, Federal Republic of Germany). *Gastrointest Endosc* 36(5):444-450, 1990

Percutaneous transhepatic catheterization of the gallbladder for dissolution of cholesterol stones by instillation of methyl tert-butyl ether (MTBE) is an invasive therapeutic procedure. The only non-invasive alternative available to now, endoscopic retrograde cannulation of the cystic duct, was difficult because of the cystic duct's tortuosity and spiral valves. We therefore developed a catheter system which, using conventional duodenoscopes during a routine endoscopic retrograde cholangiography (ERC) procedure, permits reliable and safe catheterization of the gallbladder without the need for endoscopic sphincterotomy. In 18 of 22 patients (82%) we were able to place a cysto-nasal catheter, and in 14 patients MTBE dissolution therapy was then performed. Eight patients (57%) were completely free of stones after treatment; the other six (43%) had residual debris. In 4 of 22 patients (18%) cannulation attempts failed, in 3 patients due to cystic duct blockage by a calculus. Endoscopic retrograde cannulation of the gallbladder (ERCg) represents a promising alternative to the invasive percutaneous transhepatic catheterization procedure.

**Expandable biliary metal stents for malignancies: endoscopic insertion and diathermic cleaning for tumor ingrowth.** Cremer M, Deviere J, Sugai B, Baize M (MC, Hopital Erasme, Hepato-gastroenterologie, Route de Lennik 808, Bruxelles, 1070, Belgium). *Gastrointest Endosc* 36(5):451-457, 1990

Seventeen patients with malignant biliary strictures have been treated by endoscopic insertion of self-expandable metallic prostheses. Two patients received two prostheses inserted simultaneously in both the left and right hepatic ducts for Klatskin tumor type III. Immediate results were satisfactory despite an operative mortality of 18%, and neither early nor late clogging was observed even in patients who presented previously with sludge above plastic stents that were removed. However, among five patients followed for more than 4 months, two presented with obstruction due to tumor ingrowth into the stent through the metallic mesh. Accordingly, initial enthusiasm concerning long-term patency of these stents has decreased. However, we describe a technique of "diathermic cleaning" of tumor ingrowth which can easily restore the stent patency. The advantages of these wire mesh 30 F stents are their easier insertion, better immediate drainage, and absence of dislocation or perforation.

**Sinacalide-aided ultrasonography of the common bile duct as a predictor of biliary obstruction determined by ERCP and biliary manometry.** Aronchick CA, Ritchie WGM, Kaplan SM, Wright SH, Retig JN, Lipshutz WH (CAA, Pennsylvania Hospital, Gastroenterology/Medicine, 8th and Spruce Sts., Philadelphia, PA 19107). *Gastrointest Endosc* 36(5):467-471, 1990

Sonographically observed changes in common bile duct caliber following intravenous sinacalide injection were correlated with distal common duct pathology as defined by endoscopic retrograde cholangiopancreatography and biliary manometry. Thirty-two patients, 17 with prior cholecystectomies, were studied. In post-cholecystectomy patients, a 1-mm or greater diminution of duct caliber within 5 min represented a normal response. When gallbladder contraction occurred in normal patients with an intact gallbladder, no change or a diminution in duct caliber was observed. When gallbladder contraction was not observed, a normal response was considered to be the same as that in post-cholecystectomy patients with a diminution in duct caliber occurring. By using these criteria two false negatives, both with hypertensive sphincters of Oddi that responded normally to sinacalide injection, were encountered. This technique was valuable in defining non-obstructed post-cholecystectomy dilated bile ducts which demonstrated a prompt diminution in caliber following sinacalide injection.

## The Journal of Bone and Joint Surgery

**Sequelae and reconstruction after septic arthritis of the hip in infants.** Choi IH, Pizzutillo PD, Bowen JR, Dragann R, Malhis T (PDP, Dept. of Medical Education, Alfred I. duPont Institute, P. O. Box 269, Wilmington, DE 19899). *J Bone Joint Surg [Am]* 72-A(8):1150-1165, Sept. 1990

We evaluated the residual deformity and late treatment of thirty-four hips of thirty-one children who had had septic arthritis when they were less than one year old. The hips were classified into four groups on the basis of radiographic changes. Type-I deformity (five hips) involved transient ischemia of the epiphysis, with or without mild coxa magna, and these hips did not need reconstruction. Type-II deformity (eleven hips) included deformity of the epiphysis, physis, and metaphysis, and these hips needed an operation to prevent subluxation; the goals of the operation included improvement in acetabular coverage, improvement in abductor efficiency by epiphyseodesis or transfer of the greater trochanter, and equalization of limb-length discrepancy by epiphyseodesis of the contralateral limb. Type-III deformity (five hips) involved malalignment of the femoral neck, with extreme anteversion or retroversion or with a pseudarthrosis of the femoral neck that necessitated a realignment osteotomy of the proximal part of the femur or bone-grafting of the pseudarthrosis. Type-IV deformity (thirteen hips) included destruction of the femoral head and neck, with persistence of only a remnant of the medial base of the femoral neck. In the hips that had a Type-IV deformity, the complex clinical problems, which included severe limb-length discrepancy and incompetent articulation of the hip, necessitated operations such as Pemberton osteotomy, trochanteric arthroplasty, arthrodesis, epiphyseodesis of the contralateral limb, and lengthening of the ipsilateral tibia. The functional result was satisfactory in all five hips that had a Type-I deformity, in seven of eleven that had a Type-II deformity, in three of four that had a Type-III deformity, and in only four of thirteen that had a Type-IV deformity.

## Pediatrics

**Open lung biopsy in the critically ill newborn.** Cheu HW, Lally KP, Clark R, Harrell S, Null D (KPL, Dept. of Surgery, Wilford Hall USAF Medical Center, Lackland AFB, TX 78236). *Pediatrics* 86(4):561-563, Oct. 1990

Experience with 17 open lung biopsies in critically ill premature neonates was reviewed. Despite their small size, prematurity, and

near maximal ventilation requirements, the infants suffered no significant complications. In three cases, an infectious agent was identified. In one case end-stage lung fibrosis associated with persistent (>3 months), severe respiratory failure prompted termination of support. In the remainder of the cases, definitively ruling out infection allowed the confident trial of a course of steroids in an attempt to treat bronchopulmonary dysplasia. Unlike older patients, the definitive diagnosis of no infection in the premature neonate is just as informative as the diagnosis of an infection. Used judiciously, open lung biopsy can be performed in the premature infant with acceptable morbidity and mortality.

Reprinted by permission of PEDIATRICS © 1990.

## The Journal of Nuclear Medicine

**McCune-Albright syndrome: the patterns of scintigraphic abnormalities.** Pfeffer S, Molina E, Feuillan P, Simon TR (TRS, Bldg. 10, Rm. 1C401, Warren G. Magnuson Clinical Center, Dept. of Nuclear Medicine, 9000 Rockville Pike, Bethesda, MD 20892. *J Nucl Med* 31(9):1474-1478, Sept. 1990

This study of 22 patients with the McCune-Albright syndrome examined the scintigraphic distribution of fibrous dysplasia. The most frequently affected areas were the base of the skull (82% of patients), mandible (50%), facial bones (45%), femora (59%), and legs (64%). The least frequently affected areas included the hands (none), wrists (none), ankles (none), feet (5%), sacrum (5%), and vertebrae (9%). The distribution varied somewhat from idiopathic fibrous dysplasia but generally agreed with the distributions reported in radiographic studies of patients with the McCune-Albright Syndrome. The serum alkaline phosphatase was not an accurate predictor of the extent of fibrous dysplasia.

**Intravenous erythromycin dramatically accelerates gastric emptying in gastroparesis diabeticorum and normals and abolishes the emptying discrimination between solids and liquids.** Urbain JLC, Vantrappen G, Janssens J, Van Cutsem E, Peeters T, De Roo M (JLCU, Nuclear Medicine Dept., U. Z. Gasthuisberg, Herestraat 49, 3000 Leuven, Belgium). *J Nucl Med* 31(9):1490-1493, Sept. 1990

Erythromycin, a macrolide antibiotic, has recently been shown to have a motilin like effect on gastrointestinal muscle strips. In this study, we have evaluated the effect of erythromycin on patients with delayed gastric emptying and healthy subjects using the dual radionuclide technique. Twelve patients with gastroparesis diabeticorum and ten healthy age- and sex-matched controls were studied. Gastric emptying of solids and liquids was determined using  $^{99m}\text{Tc}$ -SC scrambled egg and  $^{111}\text{In}$ -DTPA in water. Following a baseline study and on a separate day, each patient and control received a 15-min i.v. perfusion of erythromycin starting at meal ingestion. Eleven out of the 12 patients were restudied after a 3-wk oral administration. In patients and controls, i.v. erythromycin dramatically accelerated gastric emptying of both solids and liquids which were emptied at the same rate. After chronic oral administration, solid and liquid emptying remained significantly accelerated. Erythromycin appears to be a very powerful gastrokinetic drug. Derived compounds with the gastrokinetic effect and without the antibiotic activity could be useful in dyspeptic patients with delayed gastric emptying.

**Splenic accumulation of technetium-99m-methylene diphosphonate in a transfusion-dependent patient with chronic myelogenous leukemia.** Franceschi D, Nagel JS, Holman BL (DF, Dept. of Radiology, Brigham and Women's Hospital, 75 Francis St., Boston, MA 02115). *J Nucl Med* 31(9):1552-1553, Sept. 1990

Intense splenic activity was incidentally observed on a radionuclide bone scan, performed for the evaluation of cellulitis versus osteomyelitis, in a transfusion-dependent patient with chronic myelogenous leukemia.

**Three-phase radionuclide bone imaging in stress injury of the anterior iliac crest.** Rockett JF (JFR, Dept. of Nuclear Medicine, Baptist Hospital East, 6019 Walnut Grove Rd., Memphis, TN 38120). *J Nucl Med* 31(9):1554-1556, Sept. 1990

Two adolescents with stress-related avulsion injury of the anterior iliac crest apophysis are presented. Increased tracer concentration in the anterior iliac crest area is present on the blood-pool and delayed images. Increased iliac crest activity was demonstrated on the radionuclide angiogram in one patient. Scintigraphic detection of this injury is useful when clinical findings are atypical, if objective evidence of a fracture is required, or when the fracture is not readily apparent radiographically.



## FORTHCOMING ARTICLES

### GEORGE W. HOLMES LECTURE

Whose turf is imaging? Independent practice, academics, and research. *Hillman BJ*

### REVIEW ARTICLES

Breast sonography. *Bassett LW, Kimme-Smith C*

Gadolinium-enhanced MR imaging of the musculoskeletal system. *Beltran J, Chandnani V, McGhee RA Jr, Kursunoglu-Brahme S*

### CARDIOPULMONARY RADIOLOGY

Detection of bullous lung disease: conventional radiography versus digital storage phosphor radiography. *Buckley KM, Schaefer CM, Greene R, et al.*

Technical note. Percutaneous removal of transvenous pacing lead perforating the heart, pericardium, and pleura. *Deutsch L-S, Dang H, Brandon JC, Ott R, Allen B, Futerman C*

### BREAST RADIOLOGY

Commentary. Mammography and malpractice. *Potchen EJ, Bisesi MA, Sierra AE, Potchen JE*

### GASTROINTESTINAL RADIOLOGY

Pictorial essay. Extracolonic manifestations of the familial adenomatous polyposis syndromes. *Harned RK, Buck JL, Olmsted WW, Moser RP, Ros PR*

Intraabdominal *Mycobacterium tuberculosis* vs *Mycobacterium avium-intracellulare* infections in patients with AIDS: distinction based on CT findings. *Radin DR*

Gallstone fragmentation during biliary lithotripsy: effect of stone composition and structure. *Zeman RK, Marchand T, Davros WJ, Garra BS, Glass-Royal M, Soloway RD*

### GENITOURINARY RADIOLOGY

Natural history of acquired renal cystic disease in dialysis patients: a prospective longitudinal CT study. *Levine E, Slusher SL, Grantham JJ, Wetzel LH*

Arteriovenous fistulae complicating biopsy of renal allografts: treatment of bleeding with superselective embolization. *deSouza NM, Reidy JF, Koffman CG*

Carcinoma of the prostate: MR images made with body coils do not accurately reflect tumor volume. *Quint LE, Van Erp JS, Bland PH, et al.*

Case report. MR imaging in sclerosing mesenteritis. *Kronthal AJ, Kang YS, Fishman EK, Jones B, Kuhlman JE, Tempany CMC*

Case report. Retroperitoneal sarcoidosis. *Bach DB, Vellet AD*

Pictorial essay. CT appearance of the pelvis after cesarean section. *Twickler DM, Setiawan AT, Harrell RS, Brown CEL*

CT pelvimetry: the fovea are not an accurate landmark for the level of the ischial spines. *Aronson D, Kier R*

### MUSCULOSKELETAL RADIOLOGY

Review. Automated percutaneous lumbar discectomy. *Onik G, Helms CA*

MR imaging in fibromatosis: results in 26 patients with pathologic correlation. *Quinn SF, Erickson SJ, Dee PM, et al.*

Case report. CT appearance of angiosarcoma secondary to chronic lymphedema. *Kazerooni E, Hessler C*

Technical note. Aspiration of the hip in patients treated with Girdlestone arthroplasty. *Swan JS, Braunstein EM, Capello W*

### FETAL RADIOLOGY

Review. Sonography of the fetal heart: findings on the four-chamber view. *McGahan JP*

Pictorial essay. Sonographic diagnosis of the amniotic band syndrome. *Burton DJ, Filly RA*

Case report. CT amniography: a new technique used to confirm a monoamniotic pair in a triplet pregnancy. *Sargent SK, Young W, Crow P, Simpson W*

### PEDIATRIC RADIOLOGY

Deferoxamine-induced bone dysplasia in patients with thalassemia major. *Brill PW, Winchester P, Giardina PJ, Cunningham-Rundles S*

Aortic thrombosis after umbilical artery catheterization in newborns: incidence of complications on long-term follow-up. *Seibert JJ, Northington FJ, Miers JF, Taylor BJ*

Posterior fossa hemorrhage in infants treated with extracorporeal membrane oxygenation: sonographic findings. *Bulas DI, Taylor GA, Fitz CR, Revenis ME, Glass P, Ingram JD*

Case report. Schmid-like metaphyseal chondrodysplasia simulating child abuse. *Kleinman PK*

### NEURORADIOLOGY

Pictorial essay. MR anatomy and pathology of the hypothalamus. *Loes DJ, Barloon TJ, Yuh WTC, DeLaPaz RL, Sato Y*

Congenital nasal masses: CT and MR imaging features in 16 cases. *Barkovich AJ, Vandermarck P, Edwards MSB, Cogen PH*

Idiopathic growth hormone deficiency: MR findings in 35 patients. *Abrahams JJ, Trefelner E, Boulware SD*

MR imaging in chronic partial epilepsy: role of contrast enhancement. *Elster AD, Mirza W*

Diagnosis of carotid artery stenosis: comparison of 2DFT time-of-flight MR angiography with contrast angiography in 50 patients. *Litt AW, Eidelman EM, Pinto RS, et al.*

### VASCULAR RADIOLOGY

Pulsed-spray thrombolysis of arterial and bypass graft occlusions. *Valji K, Roberts AC, Davis GB, Bookstein JJ*

The importance of preoperative evaluation of the subclavian vein in dialysis access planning. *Surratt RS, Picus D, Hicks ME, Darcy MD, Kleinhoffer M, Jendrisak M*

### SPECIAL ARTICLE

Fate of manuscripts rejected for publication in the *American Journal of Roentgenology*. *Chew FS*

## News

### Severe Adverse Reactions to Barium Enema Procedures

Because of recent reports of severe allergic and anaphylactic reactions associated with barium enema procedures, the Food and Drug Administration (FDA) is requesting that radiologists and other health professionals report to the agency any such incidents that have occurred over the past 12 months. Some of the reactions have been fatal and have occurred within minutes of the start of the procedures. In some cases, the reactions occurred after the enema tip had been inserted but before the barium had been introduced. Although the cause of the reactions is unclear, health professionals should determine if patients who are about to have a barium enema have a history of allergy or known increased sensitivity to latex. For patients who do have such a history, noncuffed enema tips should be used. The FDA is particularly interested in the following: (1) the type of allergic reaction or adverse incident; (2) the time of onset of symptoms; (3) whether barium was introduced before the reaction; (4) whether the procedure was a single- or double-contrast study; (5) the type and brand of the enema kit and the type and brand of the lubricant; and (6) the age, sex, occupation, and allergy/asthma history of the patient. The FDA also is interested in incidents not related to barium enema procedures that involve the use of surgical lubricants or latex medical products. To report an adverse incident, call the FDA Problem Reporting Program through the U. S. Pharmacopeia's toll-free number: (800) 638-6725. (In Maryland, call collect (301) 881-0256). Reports can remain anonymous; the U. S. Pharmacopeia will act as intermediary for any future correspondence. For more information, write or call Tim Wells, Office of Compliance and Surveillance (HFZ-345), FDA's Center for Devices and Radiological Health, 1390 Piccard Dr., Rockville, MD 20850; (301) 427-1144.

### MR Imaging Fellowships at LAC/USC Imaging Science Center

The Los Angeles County/University of Southern California (LAC/USC) Imaging Science Center is offering a visiting fellowship program in MR imaging for physicians and experienced MR technologists. The 1991 schedule is as follows: Feb. 4-8, March 4-8, April 1-5, May 6-10, June 3-7, Aug. 5-9, Sept. 16-20, Oct. 7-11, and Nov. 4-8. The program offers a minimum of 20 hr of didactic teaching, detailed introduction to instrumentation, case reviews with senior staff members, and complete access to extensive teaching files. Course topics include basic principles of MR imaging; neurologic, abdominal, pelvic, obstetric, cardiovascular, and musculoskeletal imaging; MR spec-

troscopy; angiography; and cardiac imaging. Fee: physicians, \$1100; technologists, \$550. Information: Michael R. Terk, M.D., USC/MRI Visiting Fellowship Program, 1744 Zonal Ave., Los Angeles, CA 90033; (213) 221-1934.

### Fetal Assessment Practicums

The Dept. of Gynecology and Obstetrics Nurse-Midwifery Service, The Johns Hopkins Medical Institutions, is sponsoring two 1991 Fetal Assessment Practicums: (1) Biophysical Profile and Doppler Velocimetry and (2) Third Trimester Ultrasound, Feb. 4-8, March 4-8, and April 8-12, at The Johns Hopkins Hospital, Baltimore. The first practicum offers experienced nurses who do antepartum testing an opportunity to expand their skills into the areas of biophysical profiles and Doppler velocimetry. The second practicum is for nurse-midwives. It will cover ultrasound imaging in the third trimester for level 1 fetal evaluation and the fetal assessment tools of biophysical profiles and Doppler velocimetry. Participants in the practicums will attend a variety of medical and nursing conferences on high-risk pregnancies. The courses will include seminars, videotapes, and clinical performance of studies. Enrollment will be limited to two students per practicum. Continuing education credit: Biophysical Profile and Doppler Velocimetry: NAACOG, 42.5 contact hr; ACNM, 4 CEUs; Third Trimester Ultrasound: ACNM, 3.7 CEUs. Fee: \$1250. Information: Program Coordinator, The Johns Hopkins Medical Institutions, Office of Continuing Education, Turner Bldg., 720 Rutland Ave., Baltimore, MD 21205; (301) 955-2959.

### Annual Uroradiology Course

The Armed Forces Institute of Pathology, the American Registry of Pathology, and the American College of Radiology are sponsoring the 9th annual Uroradiology Course, Feb. 6-7, at the Hyatt Regency Bethesda, Bethesda, MD. The purpose of the course is to teach basic genitourinary radiology to radiologists, urologists, and urology residents. Particular emphasis will be given to differential diagnosis of abnormal urograms. Course directors: David S. Hartman and Alan J. Davidson. Guest faculty: E. S. Amis, Jr., J. L. Buck, F. L. Choyke, S. M. Goldman, W. S. Hayes, S. E. Mirvis, and Douglas Van Nostrand. Category 1 credit: 13.75 hr. Fee: nonfederal physicians, \$275; active-duty military personnel and other full-time federal salaried physicians, \$20. Information: Alan J. Davidson, M.D., Armed Forces Institute of Pathology, Washington, DC 20306-6000; telephone: (202) 576-0413; fax: (202) 576-2164.

### Postgraduate Course in Diagnostic Imaging

The Dept. of Radiology, Duke University Medical Center, is offering a postgraduate course in diagnostic imaging, Feb. 11–15, at the Buena Vista Palace, Orlando, FL. This lecture course is designed to update participants in a number of newer imaging techniques in diagnostic radiology, including CT, MR imaging, sonography, musculoskeletal radiology, genitourinary radiology, neuroradiology, pulmonary radiology, and digital imaging. Category 1 credit: 25 hr. Fee: \$495. Information: Duke Postgraduate Course, Barbara McLeod, CMP, Meeting Manager, c/o Matrix Meetings, Inc., P. O. Box 1103, Rochester, MN 55903; (507) 288-5620.

### Ultrasound in Obstetrics and Gynecology

The Dept. of Radiology, University of Michigan Medical School, is sponsoring Ultrasound in Obstetrics and Gynecology, April 10–12, at the Towsley Center, Ann Arbor, MI. The course is intended for those who have modest or no previous experience with sonography. A broad range of both introductory and advanced obstetric and gynecologic topics will be covered. Course director: Richard A. Bowerman. Category 1 credit: 21 hr. Information: Julie Jacobs, Office of Continuing Medical Education, G-1100 Towsley Center, Box 0201, University of Michigan Medical School, Ann Arbor, MI 48109-0201; (313) 763-1400.

### Skeletal Radiology Course

Allegheny General Hospital and the Allegheny campus of the Medical College of Pennsylvania in conjunction with Allegheny Associates, Ltd., will present the 8th annual course on skeletal radiology, April 13–18, at the Hyatt Regency Resort at Gainey Ranch, Scottsdale, AZ. Guest faculty: T. H. Berquist, M. E. Kricun, J. P. Lawson, W. Martel, D. I. Rosenthal, and B. N. Weissman. Category 1 credit: 20 hr. Fee: practicing physicians, \$495; residents, fellows, and retirees, \$295. Information: Sandra Johnston, Dept. of Continuing Education, Allegheny General Hospital, 320 E. North Ave., Pittsburgh, PA 15212-9986; (412) 359-4952.

### Society of Computed Body Tomography Annual Course

The 14th annual course of the Society of Computed Body Tomography will be held April 15–19 at the Grand Hyatt, Washington, DC. Lectures, workshops-seminars, case presentations, the CT Club, and research award papers will be used to provide timely and useful information on CT and MR of the body. Anatomy, techniques, advantages, drawbacks, and comparisons of CT and MR will be included. Category 1 credit: 28 hr. Fee: through March 15: physicians, \$600; residents and fellows, \$475; after March 15, physicians, \$650; residents and fellows, \$525. Information: Society of Computed Body Tomography, c/o Matrix Meetings, Inc., Barbara McLeod, Meeting Manager, P. O. Box 1103, Rochester, MN 55903; (507) 288-5620.

### Radiology Review Course

The Depts. of Radiology, Mount Sinai Medical Center of Greater Miami and the University of Miami School of Medicine, Miami, FL, are sponsoring Radiology Review Course, April 28–May 3, at the Fountainebleau Hilton, Miami Beach. The course is designed for residents who are completing their training and for physicians in practice. It will provide an up-to-date review of imaging of all the major organ

systems, including the chest, cardiovascular system, abdomen, retroperitoneum, pelvis, musculoskeletal system, and CNS. Didactic presentations will be augmented with audiovisual material, and informal case presentations will conclude each session. The Self-Study Center, which will be an integral part of the course, will give registrants an opportunity to review approximately 180 cases. Program directors: Manuel Viamonte, Jr., and Catherine Poole. Category 1 credit: 43 hr. Fee: \$390. Information: Lucy R. Kelley, Program Coordinator, Radiology Seminars, P. O. Box 143762, Coral Gables, FL 33114-3762; (305) 674-2810.

### Sonography Symposium

The Dept. of Radiology and Radiological Sciences and the Division of Continuing Medical Education, Vanderbilt University Medical Center, Nashville, TN, are sponsoring the 15th annual Sonography Symposium, May 24–25. The symposium will provide an update on new clinical applications of obstetric sonography and color Doppler imaging. Course director: Arthur C. Fleischer. Guest faculty: Beryl Benacerraf, Rajat Goswami, and Harvey Neiman. Fee (full registration/Friday only/Saturday only): physicians, \$350/\$250/\$150; Vanderbilt alumni, \$225/\$175/\$100; sonographers, \$200/\$150/\$100. Information: Brenda Boner, Course Coordinator, Division of Continuing Medical Education, CCC-5326 MCN, Vanderbilt University Medical Center, Nashville, TN 37232-2337; (615) 322-4030.

### Contemporary Medical Imaging VIII

The Dept. of Radiology and Radiological Sciences and the Division of Continuing Medical Education, Vanderbilt University Medical Center, are sponsoring Contemporary Medical Imaging VIII, June 19–23, at the Sandestin Hilton, Destin, FL. The purpose of the course is to provide an update on new clinical applications of contemporary imaging techniques, including MR imaging, CT, interventional radiology, and sonography. Course codirectors: Arthur C. Fleischer and Max I. Shaff. Guest faculty: J. J. Crittenden and Kathy Gill. Fee (full registration/Wednesday and Thursday only/Friday through Sunday only): physicians, \$550/\$300/\$400; Vanderbilt alumni, \$450/\$225/\$300; sonographers, \$300/\$175/\$225. Information: Brenda Boner, Course Coordinator, Division of Continuing Medical Education, CCC-5326 MCN, Vanderbilt University Medical Center, Nashville, TN 37232-2337; (615) 322-4030.

### Neuroradiology in the Rockies

The Colorado Neurological Institute and Medical Education Resources are sponsoring Neuroradiology in the Rockies, July 7–12, at the Silvertree Hotel, Snowmass at Aspen, CO. Category 1 credit: 17 hr. Fee (through March 31/after March 31): physicians, \$550/\$625; residents, \$325/\$400. Information: Medical Education Resources, Inc., 1500 W. Canal Ct., Ste. 500, Littleton, CO 80120-4528; telephone: (800) 421-3756 or (303) 798-9682; fax: (303) 798-5731.

### The American Board of Radiology Examinations

Written examinations for the American Board of Radiology (ABR) are scheduled for Oct. 3–4. Oral examinations will be held at the Executive West Hotel in Louisville, KY, June 3–7. The ABR will accept applications for admission to the examinations after July 1, but not later than Sept. 30, in the year *preceding* the year in which the examination is to be taken. For application forms and further information: Office of the Secretary, The American Board of Radiology, 300 Park, Ste. 440, Birmingham, MI 48009.



## Meeting and Course Review

For the reader's convenience, a summary of upcoming meetings and courses is provided. Detailed listings are given in the *AJR* issue given in parentheses.

**Cyanoacrylate Embolization Course**, times arranged, Baltimore (July 1990)

**Visiting Fellowships in Ultrasound**, times arranged, Baltimore (Aug 1990)

**Visiting Fellowships in Interventional Radiology**, times arranged, Baltimore (Oct 1990)

**Swallowing Center Preceptorship**, times arranged, Baltimore (Jan)

**Imaging Fellowship**, times arranged, Miami Beach (Jan)

**Society for Pediatric Radiology Research and Education Grants**, application deadline, Feb. 1 (Sept 1990)

**Midwinter Radiological Conference**, Feb. 1-3, Los Angeles (Nov 1990)

**Annual AFIP Neuroradiology Review Course**, Feb. 2-3, Bethesda, MD (Dec 1990)

**Practical Aspects of Diagnostic Radiology/Medical Imaging IV**, Feb. 2-8, Snowmass Village, CO (Nov 1990)

**Big Sky Radiology Conference**, Feb. 3-7, Big Sky, MT (Nov 1990)

**Practical Radiology 1991**, Feb. 3-8, near Vancouver, B.C. (Dec 1990)

**Angio-Interventional Radiology**, Feb. 4-5, Coronado (San Diego), CA (Oct 1990)

**Obstetrics and Gynecology**, Feb. 4-8, March 11-15, and April 22-26, Philadelphia (Dec 1990)

**Mid-Pacific Radiological Conference**, Feb. 5-9, Maui, HI (Nov 1990)

**Intraluminal Ultrasound Imaging**, Feb. 6, Coronado (San Diego), CA (Dec 1990)

**Duplex Imaging**, Feb. 6-9, Coronado (San Diego), CA (Dec 1990)

**Duplex Imaging Tutorial Conference and Exhibit**, Feb. 7-9, San Diego (Oct 1990)

**Computed Body Tomography 1991—The Cutting Edge**, Feb. 7-10, Orlando, FL (Nov 1990)

**Obstetric and Gynecology Sonographic Update**, Feb. 9-10, Coronado (San Diego), CA (Dec 1990)

**Annual Intermountain Imaging Conference**, Feb. 9-16, Steamboat Springs, CO (Nov 1990)

**Contemporary Diagnostic Imaging**, Feb. 11-15, Mauna Lani, HI (Oct 1990)

**Current Topics in Diagnostic Imaging**, Feb. 11-15, Cerrimar Beach, Puerto Rico (Dec 1990)

**Mammographically Detected Early Breast Cancer**, Feb. 14-17, Naples, FL (Dec 1990)

**Palm Beach Magnetic Resonance Imaging Update**, Feb. 17-20, Palm Beach, FL (Jan)

**Society of Gastrointestinal Radiologists Annual Meeting and Postgraduate Course**, Feb. 17-21, Carlsbad, CA (Oct 1990)

**Imaging the Head, Spine, and Musculoskeletal System**, Feb. 17-22, Kauai, HI (Oct 1990)

**MR Imaging Course at Disney World**, Feb. 17-22, Orlando, FL (Oct 1990)

**Skeletal Radiology Symposium**, Feb. 18-22, Sun Valley, ID (Jan)

**North American Society for Cardiac Imaging Annual Meeting**, Feb. 22-24, San Francisco (Jan)

**Sun Valley Imaging Meeting**, Feb. 23-March 2, Sun Valley, ID (Nov 1990)

**Positron Emission Tomography**, Feb. 24-27, Dana Point, CA (Dec 1990)

**Principles and Practice of Clinical MRI**, Feb. 28-March 3, Lake Buena Vista, FL (Nov 1990)

**Advanced Seminars in Diagnostic Imaging**, March 1-3, Laguna Niguel, CA (Nov 1990)

**Winter Congress on Diagnostic Imaging**, March 2-9, Val D'Isere, France (Dec 1990)

**Masters Diagnostic Radiology Conference**, March 3-8, Maui, HI (Dec 1990)

**Practicum in Diagnostic Ultrasound**, March 4-8 and April 22-26 (Oct 1990)

**Course on MR Imaging**, March 4-8, Coronado (San Diego), CA (Nov 1990)

**Musculoskeletal Imaging**, March 4-8, Barbados (Nov 1990)

**Update on Body Imaging and Neuroradiology**, March 4-8, Aca-pulco, Mexico (Dec 1990)

**Pediatric Radiology Course**, March 11-15, Park City, UT (Dec 1990)

**Advances in PET and SPECT Imaging**, March 14-16, Baltimore (Jan)

**Breast Imaging Conference**, March 21-24, Lake Buena Vista, FL (Dec 1990)

**Orthopedic Radiology 1991**, March 25-27, Boston (Nov 1990)

**1991 MRI Update at Vail**, March 25-29, Vail, CO (Jan)

**Ultrasound 1991**, April 2-5, Boston (Nov 1990)

**National Council on Radiation Protection and Measurements Annual Meeting**, April 3-4, Washington, DC (Nov 1990)

**CT Symposium**, April 5-6, Madison, WI (Jan)

**Differential Diagnosis in Radiology**, April 6-8, Ann Arbor, MI (Jan)

**MRI Fellowships at Johns Hopkins**, April 8-12 and June 17-21, Baltimore (Oct 1990)

**Society for Magnetic Resonance Imaging Annual Meeting**, April 13-17 (Nov 1990)

**San Diego Residents' Radiology Review Course**, April 21-26, La Jolla, CA (Dec 1990)

**Clinical Nuclear Medicine 1991**, April 22-25, Boston (Nov 1990)

**Introduction to Interventional Radiology**, April 27, La Jolla, CA (Dec 1990)

**International Radiopharmaceutical Dosimetry Symposium**, May 7-10, Oak Ridge, TN (Jan)

**Thoracic Imaging 1991**, May 13-17, Toronto (Jan)

**International Pediatric Radiology '91**, May 27-31, Stockholm (Aug 1990)

**Leeds Gastroenterology Course for Radiologists**, July 1-5, Leeds, England (Dec 1990)

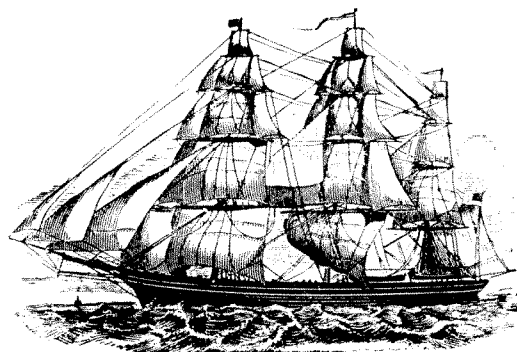
**International Congress of Radiation Research**, July 7-12, Toronto (May 1990)

**World Congress in Ultrasound**, Sept. 1-6, Copenhagen (Sept 1990)

**International Workshop on Hypertrophic Osteoarthropathy**, Sept. 8-11, Dubrovnik, Yugoslavia (Jan)

**European Congress of Radiology 1991**, Sept. 15-20, Vienna, Austria (Oct 1990)

*AJR* carries announcements of courses, symposia, and meetings of interest to its readers if received a minimum of 5 months before the event. There is no charge; receipt of items by the *AJR* Editorial Office is not acknowledged. Submit items for publication typed double-spaced. Provide title, date, location, brief description, sponsor, course directors, fees, category I credit, and address and telephone number for additional information. Faculty from the host institution will not be listed. Guest faculty names will appear **only** if initials are provided. Mail news items to *AJR* Editorial Office, 2223 Avenida de la Playa, Suite 103, La Jolla, CA 92037-3218.



Come to the  
American Roentgen Ray Society

91<sup>st</sup>

ANNUAL MEETING

---

Boston, MA

---

Sheraton Boston Hotel  
May 5-10, 1991

---

---

Scientific Program (200 papers)

Instructional Courses (60 hours)

Categorical Course on Body MR Imaging

The Caldwell Lecture

Award Papers

Scientific Exhibits

Social, Golf, and Tennis Programs

Guest Programs



# **Invitation to the 1991 American Roentgen Ray Society Meeting in Boston, MA, May 5–10, 1991**

I am pleased to extend an invitation to all radiologists to attend the 91st annual meeting of the American Roentgen Ray Society in Boston, MA, May 5–10, 1991. In keeping with the ARRS tradition, outstanding scientific and social programs will be provided.

The excitement of a meeting set in Boston, MA, in the spring requires no further description. The opportunity for busy radiologists to attend a major national meeting while enjoying all that Boston, MA, has to offer is ideal.

The scientific program, instructional courses, and categorical course are certain to be interesting and informative (see schedule below).

## **Scientific Program**

Two hundred scientific papers have been selected from more than 400 abstracts. Scientific sessions will be devoted to all major body systems, angiography, interventional techniques, sonography, and mammography, as well as technologies. Special emphasis has been placed on discussion of new developments.

The innovative and timely Friday morning minisymposium is entitled "Breast Imaging Update 1991." An outstanding faculty has been assembled for what I am sure will be a very stimulating program.

## **Instructional Courses**

Robert J. Stanley, Chairman, and Bruce McClennan, Associate Chairman of the Instructional Course Committee, have put together 60 instructional courses. Faculty members have been drawn from across the country. A superlative educational experience is anticipated, and advance registration is recommended.

## **Categorical Course**

An extraordinary categorical course on spine and body MR imaging has been fashioned. The course covers all aspects of the field, including equipment and principles of diagnosis. This course is certain to be popular, and advance registration is advised.

## **Summary of 1991 American Roentgen Ray Society Meeting**

Sunday May 5	Monday May 6	Tuesday May 7	Wednesday May 8	Thursday May 9	Friday May 10
	8:00–9:30 Instructional courses	8:00–9:30 Instructional courses	8:00–9:30 Instructional courses	8:00–9:30 Instructional courses	8:00–10:00 Symposium: breast imaging update
10:00–12:30 Categorical course: spine and body MR imaging	10:00–10:30 Opening cere- monies				
	10:30–12:30 Scientific programs	10:00–12:30 Scientific programs	10:00–12:30 Scientific programs	10:00–12:30 Scientific programs	10:30–12:30 Symposium: breast imaging update
2:00–3:00 Categorical course: spine and body MR imaging	1:30–3:30 Categorical course: spine and body MR imaging	1:30–3:30 Scientific programs	1:30–3:30 Caldwell lecture and award session	1:30–3:30 Scientific programs	
3:30–5:00 Categorical course: spine and body MR imaging	4:00–5:30 Instructional courses and cate- gorical course: spine and body MR imaging	4:00–5:30 Instructional courses and cate- gorical course: spine and body MR imaging	4:00–5:30 Instructional courses and cate- gorical course: spine and body MR imaging	4:00–5:30 Instructional courses and cate- gorical course: spine and body MR imaging	



### Scientific Exhibits

The more than 200 scientific exhibits coordinated by N. Reed Dunnick will cover the entire breadth of the field of diagnostic radiology. The technical exhibits will be integrated among the scientific exhibits to enhance the interaction of the attendees with technical exhibitors, a format that has proven to be very satisfactory.

### Caldwell Lecture

N. Thorne Griscom, M.D., has agreed to present the Caldwell Lecture at the 1991 meeting. This promises to be one of the highlights of the meeting and is concerned with pediatric pulmonary disorders encountered in the adult.

### Social Events

Boston, MA, offers an unlimited number of diversions, and Abner M. Landry, Jr., Chairman of the Annual Meeting Committee, has engaged a Boston-based tour consultant to plan a variety of tours. The annual golf and tennis tournaments for attendees and their companions are scheduled for Monday. The traditional cocktail party given by the society in the exhibit area for all registrants will be Sunday evening and will provide a convenient and early meeting place.

This promises to be a truly outstanding event in exceptional surroundings. I hope you will be able to accept our invitation. Plan now to attend.

John A. Kirkpatrick  
President-Elect, ARRS

### Forthcoming ARRS Meeting Information

Details of the American Roentgen Ray Society Meeting in Boston, MA, May 5–10, 1991, will appear in the **February**, **March**, and **April** 1991 issues of the *AJR*. Information about the scientific program, instructional programs, and social events and hotel and travel forms will be published in the Journal.

See pages 421–427 of this issue for more information concerning the meeting.

## 1991 ARRS Meeting Summary, May 5–10, 1991 Boston, MA

A comprehensive description of the meeting, including the instructional courses, categorical course, and the Friday symposium, appears in this issue of the *AJR*. Meeting and registration forms also will be found in the February and March issues. These may be photocopied. A special loose insert on the meeting also accompanies this issue.

### Accreditation

All courses and scientific sessions carry AMA Category 1 credit on an hour-for-hour basis.

### Meeting Format

**Scientific Program.** Sessions will be grouped in parallel sessions so that registrants may choose topics related to their interests. A total of 189 scientific papers will be presented, Monday–Thursday, May 6–9. In addition, on Wednesday, May 8, the afternoon session will feature award papers and the Caldwell Lecture, which will be delivered by N. Thorne Griscom, M.D. On Friday, May 10, there will be a special 4-hr symposium on breast imaging.

**Categorical Course on Spine and Body MR.** This 15.5-hr course will be held Sunday–Thursday.

**Luncheon Sessions.** Registrants may enroll in special luncheon sessions, Monday–Thursday. A box lunch will be provided.

### Exhibits

**Scientific and Technical Exhibits and Case of the Day** will be set up in the Hynes Convention Center, Hall A, adjacent to the Sheraton Boston Hotel, Monday–Thursday, May 5–9. The Case of the Day will be presented by John F. O'Connor of Boston University School of Medicine.

### Local Activities

**General Reception.** Sunday evening, May 5, for all registrants.

**Golf Tournament.** Monday, May 6 at a local country club.

**Men's and Women's Tennis Tournaments.** Monday, May 6, at the Winchester Tennis Club.

**Local Tours.** See pages 425–430 in this issue for a description of the activities and registration forms.

### Meeting Registration

Preregistration will be accepted until April 20. There will be on-site registration. Official badges and program books will be available at

the registration desk, Sheraton Boston Hotel. No confirmations will be mailed.

### Course Registration

Register early—enrollment is limited. List first, second, and third choices for each period. Also, indicate whether you wish to take the categorical course. Deadline for registration by mail is April 20. All ticket orders will be filled according to postmarked date. Course tickets *will not* be mailed. Tickets will be available beginning at 1:00 p.m. on Saturday, May 4, at the ARRS registration desk in the Sheraton Boston Hotel. There will be on-site registration for courses not already filled.

### Hotel Registration

Reservations are handled by the ARRS Housing Bureau, Sheraton Boston Hotel, Attn: Reservations Office, 39 Dalton St., Boston, MA 02199. These must be received by April 13. Make check payable to Sheraton Boston Hotel. See reservation form in this issue for prices and complete instructions.

### Fees

#### Meeting:

ARRS members and resident members	No fee
Nonmembers	\$250
Nonmember physicians in training (with verification)	25
Categorical course	75
Luncheon sessions/each	12
Local tours	20–75

### Cancellations and Fee Refunds (Excluding Hotel Fees)

Fees will be refunded only if cancellation is received by April 20, 1991. Send to American Roentgen Ray Society, 1891 Preston White Drive, Reston, VA 22091.

### Transportation Discounts

United Airlines is offering discounts of up to 40% on airfares. Call (800) 521-4041 and reference ARRS account number 429JW.

Hertz Rent-A-Car is offering special rates on car rentals. Reserve a Hertz car at these special rates through United Airlines when you make your plane reservations, or call Hertz directly at (800) 772-3773.

## **Categorical Course in Spine and Body MR Imaging**

### **American Roentgen Ray Society 91st Annual Meeting**

**May 5–9, 1991, Sheraton Boston Hotel, Boston, MA**

*Course Director, Anton N. Hasso, M.D.*

*Course Codirector, David D. Stark, M.D.*

#### **Sunday, May 5**

9:50–10:00 Welcome/Introduction (*Hasso/Stark*)  
10:00–10:30 Fundamental MRI (*Matwiyoff*)  
10:30–11:00 Fast Scanning (*Hendrick*)  
11:00–11:40 Sedation/Anesthesia/Patient Monitoring (*Hinshaw/Shellock*)  
11:40–12:20 MR Angiography  
Body (*Edelman*)  
Head and Neck (*Hasso*)  
12:20–2:00 Lunch Break

#### **Spine/Neck**

2:00–2:30 Flow/Spine CSF Flow (*Bradley*)  
2:30–3:00 Congenital/Developmental Lesions (*Naidich*)  
3:00–3:30 Mass Lesions/Myelopathy (*Sze*)  
3:30–4:00 Coffee Break  
4:00–4:30 Infective Spondylitis (*Sharif*)  
4:30–5:00 3D Spine/Degenerative/Postoperative (*Ross*)  
5:00–5:30 Neck Soft Tissues (*Vogl*)

#### **Monday, May 6**

1:30–2:00 MR Contrast Agents, Introduction (*Wolf*)  
2:00–2:30 Contrast Agents for Body MR (*Stark*)  
2:30–3:00 Motion Artifact Suppression (*Ehman*)  
3:00–3:30 Coffee Break

#### **Pediatric**

3:30–4:15 Pediatric Abdomen/Pelvis (*Dietrich*)  
4:15–5:00 Pediatric Musculoskeletal/Marrow (*Moore*)  
5:00–5:45 Pediatric Cardiovascular (*Higgins*)

#### **Tuesday, May 7**

3:45–4:15 Liver (*Mitchell*)  
4:15–5:00 Male Pelvis  
Prostate/Bladder (*Rifkin*)  
Testes/Scrotum (*Fritzsche*)  
5:00–5:45 Female Pelvis  
Neoplasms (*Hricak*)  
Non-neoplastic Disorders (*McCarthy*)

#### **Wednesday, May 8**

3:45–4:25 Neck/Musculoskeletal  
Infection and Avascular Necrosis (*Beltran*)  
4:25–5:05 Soft Tissue/Bone Neoplasms (*Seeger*)  
5:05–5:45 Knee (*Reiser*)

#### **Thursday, May 9**

3:45–4:15 Musculoskeletal  
Temporomandibular Joints (*Fulmer*)  
4:15–4:45 Wrist (*Kneeland*)  
4:45–5:15 Shoulder (*Crues*)  
5:15–5:45 Foot and Ankle (*Solomon*)



# 1991 American Roentgen Ray Society Instructional Courses and Symposium

Robert J. Stanley, Director, and Bruce L. McClennan, Associate Director

Sixty Instructional Courses will be presented during the 91st annual meeting of the American Roentgen Ray Society (ARRS) beginning Monday, May 6, and continuing through Thursday, May 9. Each of the Instructional Courses listed on the next page will be 90 min long. In addition, there will be a week-long Categorical Course in Spine and Body MR Imaging and a half-day Symposium, Current Topics in Breast Imaging.

The Categorical Course in Spine and Body MR Imaging will have 15.0 hr of instruction and will begin on Sunday, May 5, and conclude on Thursday, May 9. The Symposium, Current Topics in Breast Imaging, will be on Friday, May 10, from 8 a.m. to 12 noon. All courses carry Category 1 credit on an hour-to-hour basis.

## Registration Information

To register for courses, complete the meeting registration form in this section and mail promptly. Tickets also will be available at the Instruction Course Registration Desk, Sheraton Boston Hotel for courses that have not been sold out. All courses will take place in the headquarters' hotel.

After reviewing the course list, select three for each morning and afternoon session. Write the course number and name of the first instructor on the registration form. Please note that the -01 residents'-masters' tutorials are intended primarily for residents and that attendance will be limited.

All who register for the Categorical Course in Spine and Body MR Imaging (including ARRS members) must pay a fee of \$75 and must take the entire series of classes. The Categorical Course totals 15.0 hr of instruction and includes a syllabus.

## Course Schedule

### Sunday, May 5, through Thursday, May 9

The Categorical Course in Spine and Body MR Imaging will have 15.0 hr of instruction over 5 days. Topics and instructors are listed on p. 422.

### Monday, May 6, through Friday, May 10

A total of 60 courses will be offered (see next page) plus a symposium, Current Issues in Breast Imaging.

## ACR Luncheon Presentations on Socioeconomics of Radiology

A series of luncheon presentations on the socioeconomic of radiology will be arranged by the American College of Radiology (ACR). A box lunch will be provided. The presentations will be from 12:30 to 1:30 p.m. and do not conflict with other elements of the program. Advance registration is required. Cost per session is \$12.

### Date, Topic, Speaker

**Monday, May 6:** Governmental Issues for Radiology, Gary Price, ACR Director of Government Relations

**Tuesday, May 7:** Economic Issues of Radiology Practice, Emmett O. Templeton, M.D., Chairman, ACR Commission on Economics

**Wednesday, May 8:** Current Legal Issues in Radiology, Thomas W. Greeson, J.D., ACR Legal Counsel

**Thursday, May 9:** Update on ACR Activities, James M. Moorefield, M.D., Chairman, ACR Board of Chancellors

### Symposium: Current Issues in Breast Imaging Friday, May 10, 1991, 8:00 a.m. to 12:00 p.m.

Time	Topic (Presenter)
8:00 a.m.	Introduction and ACR accreditation (Kopans DB)
8:30 a.m.	Are the screening guidelines wrong? (Moskowitz M)
9:00 a.m.	Proper positioning—not just basic, but required (Eklund GW)
9:30 a.m.	Now that I've found it, what should I do about it? (Kopans DB)
10:00 a.m.	Questions and break
10:30 a.m.	The therapeutic implications of diagnostic findings—extensive intraductal component and the pre- and postirradiated breast (Sadowsky NL)
11:00 a.m.	How can you tell that you are screening at appropriate thresholds? (Sickles EA)
11:30 a.m.	Questions and panel discussion

Note.—There is no fee for this symposium. However, to facilitate planning, please register on the meeting registration form.

## American Roentgen Ray Society Instructional Courses: May 6–May 9, 1991

Topic	Monday	Tuesday	Wednesday	Thursday
Morning (all sessions begin at 8:00 a.m.)				
Residents'-masters' tutorial	101. Some basic signs of chest X-ray diagnosis including plain film/CT correlation. <i>Fraser RG, Heitzman ER</i>	201. Advances in imaging the brain and spine: impact on diagnosis and treatment of CNS abnormalities. <i>Quencer RM</i>	301. The role of ultrasound in pediatric gastrointestinal tract disease. <i>McAlister WH</i>	401. Angioplasty—past and present. <i>Tegtmeyer CJ</i>
Pediatrics	102. Evaluation of pneumonia in the pediatric patient. <i>Singleton EB</i>	202. A practical approach to pediatric abdominal diagnosis. <i>Wood BP, Senac MO</i>	302. Diagnostic imaging of child abuse. <i>Kleinman PK</i>	402. Musculoskeletal and cranial pediatric ultrasonography. <i>Teele RL, Share J</i>
Technique and technology	103. Ultrafast CT scanning—an update. <i>Sheedy PF</i>	203. CT and US guided biopsies: practical approaches, pitfalls and new techniques. <i>Charboneau JW, Reading CC</i>	303. Advances in abdominal CT examination techniques. <i>Berland LL, Megibow AJ</i>	403. Computer assisted 3-D imaging: state of the art. <i>Fishman EK, Ney D</i>
Chest	104. CT of the lung parenchyma. <i>Pugatch RD</i>	204. Pulmonary manifestations of the immunocompromised patient. <i>Vydareny KH, Gross BH</i>	304. Plain chest radiograph manifestations of esophageal and diaphragmatic diseases. <i>Stark P, Tarver RD</i>	404. Thoracic infections and their complications. <i>Choplin RH, Reed JC</i>
Gastrointestinal	105. Biliary diagnosis: a problem oriented approach. <i>Koehler RE, Balfe DM</i>	205. Inflammatory bowel disease from beginning to end. <i>Gore RM, Laufer I</i>	305. Radiologic screening for colorectal cancer. <i>Gelfand DW, Ott D</i>	405. Radiologic evaluation of the pharynx and esophagus. <i>Rubenstein SE, Levine MS</i>
Genitourinary/retroperitoneum	106. CT/MRI of the retroperitoneum. <i>Lee JKT, Heiken JP</i>	206. The radiologic evaluation of the adrenal. <i>Kenney PJ</i>	306. Imaging of acute renal inflammatory disease. <i>McClennan BL</i>	406. CT and MRI of the kidney. <i>Newhouse JH, Amis ES</i>
Body imaging/CT, MR imaging, sonography	107. Staging of lymphoma. <i>Gedgudas-McClees RK, Torres WE</i>	207. The peritoneum and mesentery: anatomy, pathology, and technique. <i>Halvorsen RA, Silverman PM</i>	307. Computed tomographic evaluation of the liver. <i>Moulton JS</i>	407. Sonographic evaluation of the adult acute abdomen. <i>Wilson SR</i>
Neuroradiology	108. Supratentorial neoplasms—MRI. <i>Leeds NE</i>	208. MRI and CT in the evaluation of head trauma. <i>Davis KR</i>	308. MRI of the sella and parasellar region. <i>El Gammal T, Brooks BS</i>	408. Imaging CNS vascular disease: radiologic-pathologic correlation. <i>Osborn AG</i>
Radiologic practice	109. The battle over turf: who has it and how to get it. <i>Hillman BJ</i>	209. Cost containment in radiology departments. <i>Janower ML</i>	309. Pointers on scientific manuscript preparation. <i>Berk RN, Levene M, Hilton S, Spiller KL</i>	409. The future of digital radiology: technical and clinical considerations. <i>Ovitt TW, Hunter TB</i>
Radiologic-pathologic correlation	110. Radiographic pathology of the GI mucosa. <i>Ghahremani GG</i>	210. Radiologic-pathologic correlation of GI tract tumors. <i>Lichtenstein JE, Olmsted WW</i>	310. Arthropathies: radiologic-pathologic correlations. <i>Made-well J</i>	410. Imaging and pathologic correlation of bone and soft-tissue neoplasms. <i>Hudson TM</i>
Afternoon (all sessions begin at 4:00 p.m.)				
Musculoskeletal	111. The analytic approach to the film (an imaging discipline). <i>Jacobson HG, Ed-eiken J</i>	211. Current practice in musculoskeletal ultrasonography. <i>Adler RS, Fornage BD</i>	311. The pelvis and hip: anatomic-clinical correlations. <i>Pitt MJ</i>	411. Evaluation of bone and marrow in osteoporosis and other metabolic conditions. <i>Rosenthal DI</i>
Body imaging/sonography	112. Imaging and biopsy of the prostate. <i>Papanicolaou N, Tung GA</i>	212. Transvaginal sonography in obstetrics and gynecology. <i>Fleischer AC, Rao BK</i>	312. Update on ultrasound in hepatobiliary imaging. <i>Kane RA</i>	412. Peripheral vascular ultrasound imaging. <i>Carroll BA</i>
Head and neck/nuclear medicine	113. Imaging of the sinonasal cavities. <i>Som PM</i>	213. Imaging of head and neck cancers. <i>Curtin HD</i>	313. SPECT brain imaging. <i>Mountz JM</i>	413. Nuclear cardiology in clinical practice. <i>Thrall JH</i>
Body imaging/CT, MR imaging, sonography	114. Use of diagnostic imaging for the follow-up of treated cancer patients. <i>Kagan AR, Steckel RJ</i>	214. Pitfalls in plain film and CT analysis of the mediastinum. <i>Glazer HS, Molina P</i>	314. Radiologic evaluation of the transplant kidney. <i>Baumgartner BR, Pozniak MA</i>	414. MRI of the thorax with CT correlation. <i>McLoud TC</i>
Angiography/interventional	115. New devices in peripheral vascular intervention: diagnosis and therapy. <i>Becker G, Katzen BT</i>	215. Biliary calculus disease: interventional management. <i>Mueller PR, vanSonnenberg E, Teplick SK</i>	315. Update on embolotherapy. <i>Keller FS, Waltman AC</i>	415. Plugging vessels and opening ureters: treating kids with catheters. <i>Fellows KE, Hoffer FA</i>

## 1991 ARRS Meeting: Local Activities and Tennis and Golf Tournaments

The 91st annual meeting of the American Roentgen Ray Society (ARRS) in Boston, MA, will feature activities for members, nonmembers, spouses, and guests. The social programs have been arranged by the ARRS, with the assistance of Uncommon Boston, Ltd. The tennis tournament will be arranged and supervised by Melvin E. Clouse of New England Deaconess Hospital. The golf tournament will be arranged and supervised by Roy Strand of Children's Hospital Medical Center. The chairman of the Annual Meeting Committee is Abner M. Landry, Jr. To register for any of these events, please complete the registration form in this issue.

### Golf Tournament

The annual golf tournament will be held at the Ferncroft Country Club on Monday, May 6. Buses will leave the Sheraton Boston at 11 a.m., after the opening ceremonies. There will be a buffet lunch, followed by a shotgun start. Participants must bring their own golf clubs and shoes. The pro shop and clubhouse will be open. The fee for the golf tournament is \$100, and includes transportation, luncheon, greens fees, cart, prizes, and hors d'oeuvres and drinks after play is completed. Buses will return immediately after the tournament and again after the cocktail hour.

### Men's and Women's Tennis Tournaments

The annual men's and women's tennis tournaments will be held at the Winchester Indoor Tennis Club on Monday, May 6. Buses will leave the hotel at 11:00 a.m., after the opening ceremonies. The fee of \$60 includes luncheon, court fees, balls, prizes, and transportation. Appropriate dress is required.

### Local Program

Reservations for the social program are limited. To avoid disappointment, send in the reservation form immediately. Reservations will be filled in the order in which they are received. Because guarantees are required for all events, reservations must be received by April 20, 1991. Tickets for all events will be included in the registration packet. Prices for these events include transportation, meals where indicated, escorts and guides, and all entrance fees, taxes, and gratuities. Prices do not include alcoholic beverages with meals unless indicated. On Sunday, May 5, from 2 to 5 p.m., and on Monday, May 6, from 8 to 11 a.m., remaining tickets for events will be sold at the meeting registration desk. These tickets may be sold at a slightly higher cost. Refunds are available if the ARRS office in Reston, VA, receives a written cancellation request by April 20, 1991. No cancellations will be accepted by telephone. The ARRS reserves the right to cancel an event if registration is insufficient. In that case, refunds will be issued.

This year the ARRS is offering a special spouse/companion program on Monday, May 6. The program is entitled "Breast Cancer: Early Detection—The Key to the Cure" and is offered by the Society at no charge to women accompanying registrants to the meeting. We urge you to register for this important program.

### Sunday, May 5

**Welcome to Boston, 1:30–4 p.m.** Begin your visit to Boston with an overview of the city and all it has to offer. A luxury motor coach will take you on an itinerary that includes stately Beacon Hill, Back Bay with its lovely Victorian homes, and the elegant beauty of the Boston Public Garden. You will also see Quincy Market, a restored warehouse with food emporiums, fabulous shops, and outdoor entertainment. Many sites along the Freedom Trail will be covered as well, including the Old North Church, where in 1775 two lanterns were hung by Paul Revere to warn the colonists that the British were coming. Lest you begin to think that Boston is living in its past, you will also see many new faces of the city, including the John Hancock and New England Life Towers, the restored waterfront, and Copley Place. Fee: \$20.00.



**Monday, May 6****Breast Cancer: Early Detection—The Key to the Cure**

Monday, May 6, 7:45–10 a.m.

Women today are talking about breast cancer and taking charge of their own health. The ARRS is sponsoring a program designed to continue to educate women about the importance of the early detection of breast cancer.

- 1 in 10 women will get breast cancer in her lifetime
- Breast cancer is the second leading cancer killer in women
- More than 150,000 women will be diagnosed with breast cancer this year
- More than 40,000 women are expected to die of breast cancer this year

These are alarming statistics, but there is something you can do!

The program will include:

- A short seminar in breast self-examination . . . the importance of knowing your body
- When, why, and where to arrange for your mammogram
- What are your choices if cancer is diagnosed?

A panel of experts will conduct brief presentations, answer your questions, and identify ways to cope with the anxieties associated with this disease.

This program is offered free of charge to all women accompanying registrants to the annual meeting. Join us at 7:45 a.m. for a continental breakfast, followed by the program. You must preregister, as attendance is limited.

**Welcome to Boston, 2–4:30 p.m.** See description in preceding Sunday section. Fee: \$20.00.

**Tour of Cambridge and Harvard University, 2:30–5:30 p.m.** Cambridge is in every sense a "town and gown" community, steeped in tradition, history, and academic life. Your tour will take you to Brattle Street, known as Tory Row for the homes of the British sympathizers during the Revolution. You will see where George Washington trained the militia, and visit the Henry Wadsworth Longfellow House, a beautiful example of Victorian architecture. Harvard Yard also will be visited, as well as the famed Widener Library, the hub of the largest private library system in the United States. You will walk the paths and see the sites familiar to the men and women educated here who have helped form America's past and present. Comfortable shoes recommended. Fee: \$25.

**Tuesday, May 7**

**In The Footsteps of JFK, 9 a.m.–12 noon.** Explore the famed John F. Kennedy Library and Museum, housed in a building designed by I. M. Pei and overlooking beautiful Dor-

chester Bay. The tour includes a 25-min retrospective film of the late President's life, and a visit to the multimedia exhibits that chronicle his political career and brief presidency. A replica of the Oval Office contains his famous antique desk and rocking chair. Also on display is JFK's beloved sailboat, the *Victura*. This museum also houses the papers of Ernest Hemingway. Fee: \$25.

**Newport, Rhode Island, 8:30 a.m.–5 p.m.** Home of the America's Cup sailing races, the famed Newport Jazz Festival, and countless socialites, millionaires, and artists lured by the picturesque waterfront, Newport is well worth the hour and a half trip from Boston. The city abounds in elegance, natural beauty, and historic landmarks. You will view the magnificent mansions built at the turn of the century in "Great Gatsby" style by the Astors and the Vanderbilts, and visit the beautiful galleries, unusual art and antique shops, and lovely boutiques. The trip includes a tour of one of Newport's lavish mansions, as well as a visit to Hammersmith Farm, former home of Jacqueline Bouvier Kennedy and now a working stud farm. Lunch at a favorite Newport restaurant is included. Fee: \$63.00.

**Wednesday, May 8**

**Lexington and Concord, 1:30–5:30 p.m.** A trip to Lexington takes you back more than 200 years to April 1775 as you visit Lexington Green, where the Minuteman Statue now stands, and cross the bridge where "the shot heard 'round the world" was fired. You will learn where the British headquarters were located, and where Samuel Adams and John Hancock were awakened by Paul Revere on his famous midnight ride from Boston's Old North Church. In Concord, you will learn about the giants of American literature who lived there—Louisa May Alcott, Nathaniel Hawthorne, and Ralph Waldo Emerson. Walden Pond, famed home of Henry David Thoreau, is located in nearby Lincoln. Fee: \$25.

**Antiques Through the Centuries, 2–4 p.m.** By special arrangement, you will visit the famed Skinner Gallery on Newbury Street, New England's foremost antiques auction house. A representative of the gallery will take you on a behind-the-scenes tour, and offer you an insider's tips on how to evaluate and purchase antiques at auction. Tea and cookies will be served. Fee: \$22.

**Thursday, May 9**

**North to the Sea: A Tour of Salem and Marblehead, 9 a.m.–3 p.m.** An hour's drive north of Boston takes you to the splendid homes of early sea captains and merchants. Your first stop will be Salem, where you will learn about witchcraft and visit one of the several museums for which Salem is famous. With appetites piqued by the wealth of history, architecture, and antiques, time will be allotted for browsing the shops on Pickering Wharf. Lunch will be served at the Peabody Museum, which offers a special tour of unique memorabilia from the days when spices from India, objets d'art, and porcelains from China came to the wealthy from abroad. Following lunch, you will tour picturesque Marblehead

Neck and visit Abbott Hall, home of the famous painting "Spirit of '76." A seacoast tour of Salem and Marblehead is truly a trip back in time. Fee: \$45, including lunch.

**Beacon Hill Tour, 1:30–4 p.m.** This tour visits the stately neighborhood of Beacon Hill, touching on its fascinating literary, architectural, and historical highlights. En route, you will pass by the Public Garden, with its beautiful parklike environment and famed Swan Boats. Your walking tour of the Hill will include access to two stately and historic homes. The remarkable detail of these Federal buildings, with their wooden mouldings, spindle staircases, distinctive mantels, windows, and chandeliers bring to life this historically and architecturally preserved neighborhood. Visitors will be personally greeted by caretakers and given the opportunity to

view family heirlooms, collections, and memorabilia. Comfortable shoes recommended. Fee: \$28.

#### **Friday, May 10**

**Filene's Basement Shopping Trip, 8 a.m.–12 noon.** Start the day with a continental breakfast in the hotel, while a representative of Boston's famed department store presents a history of Filene's Basement, where unbelievable mark-downs on quality clothing from exclusive shops and designers can be found. You will then be escorted by motorcoach to Filene's Basement, where you will have plenty of time to experience this shopping phenomenon for yourself. Fee: \$25, including breakfast.

### **Transportation Discounts**

United Airlines is offering special airfares to the 1991 ARRS meeting for travel to and from Boston, MA, between May 1 and 14 inclusive. To obtain a 5% discount from any United available/applicable fare (MaxSavers and first class included) or a 40% discount off standard coach fares, telephone (toll-free) 1-800-521-4041 between the hours of 8:00 a.m. and 11:00 p.m. EST and immediately reference special ARRS account number 429JW. For travel to and from Canada, United will offer published Canadian meeting fares in selected markets. This discount can be as much as 35% off normal coach fares. No discounts are permitted from Mexico, the Bahamas, or the Orient. In addition, ARRS attendees who fly on United as outlined above will be eligible for a special drawing. The prize is one complimentary round-trip ticket good for travel in the continental United States before February 28, 1992 (holiday periods excluded).

Hertz Rent-A-Car service also can be arranged at discounted rates by calling United Airlines reservations at 1-800-521-4041.

# American Roentgen Ray Society: Officers, Committees, and Membership Information

## Officers

**President:** M. Paul Capp

**President-elect:** John A. Kirkpatrick, Jr.

**1st Vice-president:** A. Everette James, Jr.

**2nd Vice-president:** Andrew K. Poznanski

**Secretary:** Joseph T. Ferrucci, Jr.

**Treasurer:** Beverly P. Wood

**Executive Council:** R. J. Alfidi, R. N. Berk, M. P. Capp, W. J. Casarella, N. R. Dunnick, R. G. Evens, J. T. Ferrucci, Jr., A. E. James, Jr., J. A. Kirkpatrick, Jr., A. M. Landry, Jr., J. E. Madewell, A. A. Moss, A. K. Poznanski, L. F. Rogers, R. J. Stanley, J. H. Thrall, K. H. Vydareny, N. O. Whitley, B. P. Wood, G. R. Leopold, chairman

## Committees

**Editorial Policy:** R. N. Berk, E. Buonocore, Melvin M. Figley, S. v. W. Hilton, M. S. Huckman, C. A. Rohrmann, Jr., R. J. Stanley, R. I. White, W. J. Casarella, chairman

**Education and Research:** C. B. Higgins, B. J. Hillman, R. A. McLeod, R. J. Stanley, W. M. Thompson, N. O. Whitley, chairman

**Finance and Budget:** R. J. Alfidi, R. K. Gedgaudas-McClees, J. R. Thornbury, K. H. Vydareny, J. H. Thrall, chairman

**Nominating:** G. A. W. Gooding, L. F. Rogers, K. H. Vydareny, chairman

**Publications:** E. Buonocore, C. A. Rohrmann, Jr., R. J. Stanley, R. I. White, W. J. Casarella, chairman

**Membership:** J. E. Madewell, A. A. Moss, K. H. Vydareny, R. J. Alfidi, chairman

## Representatives to Other Organizations

**American Board of Radiology:** J. A. Kirkpatrick, Jr., E. C. Klatte, L. F. Rogers

**American College of Radiology:** J. M. Dennis, R. A. Gagliardi, J. E. Madewell, B. L. McClennan, R. J. Stanley

**American Medical Association:** S. F. Ochsner, delegate; K. L. Krabbenhoft, alternate; K. L. Kidd, CPT Advisory Committee

**American National Standards Institute:** M. E. Haskin

**National Council on Radiation Protection and Measurements:** F. Miraldi, E. L. Saenger

**Armed Forces Institute of Pathology:** J. E. Madewell

## Meeting Arrangements

**Annual Meetings:** May 5–10, 1991, Sheraton Boston, Boston; May 10–15, 1992, Marriott's World Center, Orlando, FL

**Annual Meeting Committee:** H. C. Carlson, J. K. Crowe, N. R. Dunnick, R. R. Lukin, R. J. Stanley, R. D. Steele, Jr., A. M. Landry, Jr., chairman

**Instructional Courses:** Bruce L. McClennan, associate chairman; R. J. Stanley, chairman

**Scientific Program:** P. Arger, E. Buonocore, D. O. Davis, K. B. Hunter, D. Kushner, T. C. McLoud, W. A. Murphy, Jr., L. B. Talner, J. H. Thrall, J. A. Kirkpatrick, chairman

**Scientific Exhibits:** J. R. Haaga, R. G. Ramsey, N. R. Dunnick, chairman

## ARRS Membership

An application form is printed in this issue of the Journal. For consideration at the 1991 ARRS meeting, send completed forms before February 1, 1991, to American Roentgen Ray Society, 1891 Preston White Dr., Reston, VA 22091. Active members are graduates of an approved medical or osteopathic school or hold an advanced degree in an allied science. They must practice radiology or work in an associated science in the United States or Canada and be certified by the American Board of Radiology, American Osteopathic Board of Radiology, or Royal College of Physicians of Canada or otherwise adequately document training and credentials. Corresponding members are foreign radiologists or scientists who are active in radiology or an allied science. Members-in-training are residents or fellows in radiology or postgraduate students in an allied science. Additional application forms can be obtained from the ARRS offices in Reston, VA.

## Business Office

Paul Fullagar, Executive Director, American Roentgen Ray Society, 1891 Preston White Dr., Reston, VA 22091; (703) 648-8992.



# Meeting and Local Activities Registration Form: ARRS 91st Annual Meeting May 5–10, 1991, Boston, MA

If you plan to attend, please complete this form. Official badges and program booklets will be available at the ARRS Registration Desk, Sheraton Boston Hotel. **There will be no confirmations before the meeting.** Preregistration by mail will be accepted until April 20. On-site registration will be available.

Make all checks payable to: American Roentgen Ray Society

Mail to: American Roentgen Ray Society  
1891 Preston White Drive  
Reston, VA 22091

Please type or print:  
Registrant

Last Name

First Name or Initials

Street

City

State

ZIP Code

Accompanying Guest

Name

(Accompanying person's name to be printed on badge)

Street

City

State

ZIP Code

Check appropriate categories:      Registration fee:

☐ Member ARRS

None

☐ Nonmember

\$250

☐ Nonmember physician in training (please complete section below)

\$25

☐ Course faculty, presenter of scientific paper, scientific exhibitor, technical exhibitor (circle one)

None

☐ ACR luncheon course, Monday, May 6

\$12

☐ ACR luncheon course, Tuesday, May 7

\$12

☐ ACR luncheon course, Wednesday, May 8

\$12

☐ ACR luncheon course, Thursday, May 9

\$12

☐ Categorical course

\$75

☐ Social programs (see next page)

Total enclosed

## Instructional Courses

Please register early for Instructional Courses. Attendance is limited. List first, second, and third choices for each day by course number. Ticket orders are filled according to postmark. ARRS members, nonmembers, and those in radiology training may take all courses without charge except the categorical course, **for which all registrants must pay \$75. Nonmembers also must pay the meeting registration fee. All who wish to attend courses must complete this section.**

Course tickets will be available at the ARRS Registration Desk at the Sheraton Boston Hotel beginning Saturday, May 4, at 1 p.m.

Complete section at right for courses other than the categorical course. Be sure to fill out second and third choices for each day.

Course Choices	Morning			Afternoon		
	1st	2nd	3rd	1st	2nd	3rd
Monday						
Tuesday						
Wednesday						
Thursday						

Friday \_\_\_\_\_ Check if you wish to attend the breast imaging symposium (only course offered this day).

For Nonmember Physicians in Training:

\_\_\_\_\_ is in training in my department.

Training Program Director \_\_\_\_\_

Institution \_\_\_\_\_ Date \_\_\_\_\_

(OVER)

Local Activities

No refunds after April 20

Sunday, May 5, 1:30–4 p.m., Welcome to Boston	_____ tickets @ \$20	\$ _____
Monday, May 6, 7:45–10 a.m., Breast Cancer Screening Program	_____ tickets @ no charge	
Monday, May 6, 2–4:30 p.m., Welcome to Boston	_____ tickets @ \$20	\$ _____
Monday, May 6, 2:30–5:30 p.m., Cambridge and Harvard University	_____ tickets @ \$25	\$ _____
Tuesday, May 7, 9 a.m.–12:00 noon, In the Footsteps of JFK	_____ tickets @ \$25	\$ _____
Tuesday, May 7, 8:30 a.m.–5 p.m., Newport, Rhode Island	_____ tickets @ \$63	\$ _____
Wednesday, May 8, 1:30–5:30 p.m., Lexington and Concord	_____ tickets @ \$25	\$ _____
Wednesday, May 8, 2–4 p.m., Antiques Through the Centuries	_____ tickets @ \$22	\$ _____
Thursday, May 9, 9 a.m.–3 p.m., Salem and Marblehead	_____ tickets @ \$45	\$ _____
Thursday, May 9, 1:30–4 p.m., Beacon Hill Tour	_____ tickets @ \$28	\$ _____
Friday, May 10, 8 a.m.–12 noon, Filene’s Basement	_____ tickets @ \$25	\$ _____

Preregistration is required.

Annual ARRS Golf Tournament, Monday, May 6

The tournament will be at the Ferncroft Country Club, Danvers, MA. Transportation, luncheon, greens fee, cart, prizes and hors d’oeuvres and drinks after play is completed are included in the \$100 fee. Preregistration is important.

Name: \_\_\_\_\_ Telephone: \_\_\_\_\_

Address: \_\_\_\_\_

Handicap (if any): \_\_\_\_\_

My foursome includes (list handicaps): \_\_\_\_\_

\_\_\_\_\_ tickets @ \$100 \$ \_\_\_\_\_

Men’s and Women’s Tennis Tournaments, Monday, May 6

The tournaments will be at the Winchester Indoor Tennis Club. Tennis attire is required. Fee of \$60 includes transportation, luncheon, court fees, and balls.

Name: \_\_\_\_\_ Telephone: \_\_\_\_\_

Address: \_\_\_\_\_

\_\_\_\_\_ tickets @ \$60 \$ \_\_\_\_\_

# Hotel Registration Form: ARRS 91st Annual Meeting

## May 5–10, 1991, Sheraton Boston Hotel

### Boston, MA

Mail to:

**ARRS Housing Bureau**  
Sheraton Boston Hotel  
Attention: Reservations Office  
39 Dalton St.  
Boston, MA 02199

(PLEASE MAKE CHECKS PAYABLE TO THE SHERATON BOSTON HOTEL—NOT TO THE ARRS)

Individual guest name \_\_\_\_\_

Address \_\_\_\_\_

City & State \_\_\_\_\_ ZIP \_\_\_\_\_

Arrival date/time \_\_\_\_\_ Departure date/time \_\_\_\_\_

Individual requesting reservation \_\_\_\_\_

Address \_\_\_\_\_

City & State \_\_\_\_\_ ZIP \_\_\_\_\_

Please forward with your reservation a deposit of one night's room rate to be applied to the last night of your scheduled stay, or provide credit card information to guarantee your reservation. The hotel accepts American Express, Diners Club, Carte Blanche, Visa, and Master Card credit cards. The deposit will hold your room until 6 a.m. of the morning following your scheduled arrival date. In the event of an early departure, the deposit is nonrefundable unless the hotel is notified prior to or at the time of check-in. Cancellation notice of 14 days is required for a deposit refund.

Check accommodations desired

Room Category	Main House	Towers
Single	\$144, \$172	\$200
Double	\$160, \$188	\$216
Executive suite	\$260	\$300
Mini suite	\$260	—
1-bedroom suite	\$340	\$400
2-bedroom suite	\$460	\$540

Deposit amount (1 night's rate) \$\_\_\_\_\_

☐ Check enclosed

☐ Credit card: \_\_\_\_\_  
Type of card Exp. date

\_\_\_\_\_  
Card number

\_\_\_\_\_  
Signature

- Important Information:
- Reservations must be received by the Sheraton Boston Hotel/ARRS Housing Bureau no later than April 6 to be assured of written confirmed accommodation. Reservations after that time are subject to availability. We urge you to make your reservations promptly.
  - Written confirmation of your reservation will be sent to you by the hotel.
  - To change or cancel reservations, please call the hotel directly at (617) 236-2000.
  - If you plan to share a room, please send in only one housing form. Be sure to list all names of occupants of rooms. Assignment is delayed until complete information is received.
  - Check-in is after 3 p.m., or earlier if the room is available. Check-out time is 1 p.m.
  - Parking is available at the hotel.



# Information and Application for Membership in the American Roentgen Ray Society

## General Information

The American Roentgen Ray Society, founded in 1900, has been a forum for progress in radiology since shortly after the discovery of X-rays. From its beginning and continuing to today, the ARRS has been guided by dedication to the goal of the advancement of medicine through the science of radiology and its allied sciences.

The goal of the ARRS is maintained through an annual scientific and educational meeting, and through publication of the *American Journal of Roentgenology*.

The annual meeting consists of instructional courses, scientific sessions, a symposium, scientific exhibits, and commercial exhibits. A special categorical course is also offered. Category I CME credits are available on an hour-for-hour basis.

The monthly *American Journal of Roentgenology* is a highly respected peer review journal with a worldwide subscription base. For over 75 years the *AJR* has been accepted as one of the best specialty journals available in the world, and this reputation grows each month.

A recently developed quarterly ARRS newsletter keeps members informed of events and general Society news.

## Application Instructions

### Candidates for Active Membership

1. An Active member must be a graduate of an approved medical school or hold an advanced degree in one of the physical, chemical or biological sciences and be certified by the American Board of Radiology, the American Osteopathic Board of Radiology, the Royal College of Physicians of Canada, or document training and credentials that are adequate to qualify for membership. Active members shall actively practice radiology or one of its branches in the United States or Canada. Such members are eligible to participate in all activities of the Society, including membership on committees, and have full voting privileges.
2. Application must be on an official form, signed by the applicant and at least two members of the American Roentgen Ray Society, active or emeritus, in good standing, who endorse the applicant.
3. Application fee is \$50 (payable when billed for dues).
4. Annual dues are \$150, payable on January 1 of each year following the initial year. First year dues will be invoiced following candidate election at the annual meeting. Of this amount, \$50 is for a 1-year subscription to the *American Journal of Roentgenology*, beginning with the July issue following election to membership.
5. Application must be received by February 1 for action during the current year's meeting.

### Candidates for In-Training Membership

1. In-training members must be serving in a radiology residency program approved by the Radiology Residency Review Committee, the American Osteopathic Board of Radiology, or the Royal College of Physicians of Canada, or in an approved post-residency fellowship, or be a postgraduate student in an allied science. Training status must be verified by the program director. In-training members have special consideration in fees and subscription rates to the Society journal. Such members cannot hold Society offices or vote.
2. Application must be on an official form and signed by the applicant and by the applicant's training or residency program director.
3. In-training status is limited to a maximum of five years starting with the entrance date into the radiology residency. In the last year, each in-training member will receive an application for active membership from the Society. Those who do not apply for transfer to active membership shall be dropped from membership at the end of the fifth year, but can later apply as a new member through the process outlined for active status.
4. There is no application fee. Annual dues are \$25. Membership includes a subscription to the *American Journal of Roentgenology* and admission to the annual meeting without payment of the registration fee.
5. Membership applications will be acted on when received.

### Corresponding Membership

A corresponding member must meet the qualifications of active membership, but reside and practice in a foreign country. Corresponding members shall pay dues and fees, but shall not have the privileges of voting nor of holding elective office.

#### All Applicants

1. Do not remit application fee or dues until requested.
2. Send completed forms to: American Roentgen Ray Society  
1891 Preston White Drive  
Reston, Virginia 22091

For ARRS  
Office Use

Date Rec'd \_\_\_\_\_

I.D.# \_\_\_\_\_

AMERICAN ROENTGEN RAY SOCIETY

APPLICATION FOR MEMBERSHIP

Date: \_\_\_\_\_

Category of Membership: ☐ Active  
(Check One) ☐ Corresponding  
☐ In-Training

Name (Please Print) \_\_\_\_\_  
First Initial Last

Degree(s) \_\_\_\_\_

Mailing Address \_\_\_\_\_  
Street/Box

Date of Birth \_\_\_\_\_

City/State/Country \_\_\_\_\_ Zip Code

Telephone ( ) \_\_\_\_\_

A. Education: (List name of institution, years attended, and degree and type received.)

Undergraduate: \_\_\_\_\_  
\_\_\_\_\_

Graduate (Medical School, Graduate School, etc.):  
\_\_\_\_\_  
\_\_\_\_\_

Postgraduate (Internship, Residency, Fellowship, etc.):  
\_\_\_\_\_  
\_\_\_\_\_  
\_\_\_\_\_

B. Licensure:

Licensed to practice \_\_\_\_\_ in \_\_\_\_\_ since \_\_\_\_\_  
(Type) (State, Province, etc.)

C. Appointments/Memberships: (In-Training applicants: skip to Section F on reverse.)

Present Appointments: Academic \_\_\_\_\_  
\_\_\_\_\_

Hospitals \_\_\_\_\_  
\_\_\_\_\_

Memberships in Scientific Societies: \_\_\_\_\_  
\_\_\_\_\_

Offices or Committee Assignments: \_\_\_\_\_  
\_\_\_\_\_

Government Service (Military or Civilian) \_\_\_\_\_  
(Position) (Years)

**D. Credentials:**

(To be completed by Active and Corresponding applicants only.)

I hereby certify that I was issued a certificate of qualification in \_\_\_\_\_  
(Specialty)  
in \_\_\_\_\_ by the \_\_\_\_\_  
(Year) (Name of Qualifying Board)  
Other Credentials: \_\_\_\_\_

Signature: \_\_\_\_\_

**E. References:**

(To be completed by Active and Corresponding applicants only.)

We, active or emeritus members in good standing of the American Roentgen Ray Society, and acquainted with the applicant, do recommend him/her for membership in the Society. (Two references are required.)

Name (Please Print) 1. \_\_\_\_\_ 2. \_\_\_\_\_

Address \_\_\_\_\_  
\_\_\_\_\_

Signatures: \_\_\_\_\_

**F. IN-TRAINING APPLICANTS MUST COMPLETE THIS SECTION**

**Credentials:**

I certify that I am serving as a Resident/Fellow in \_\_\_\_\_  
(Specialty)  
at \_\_\_\_\_ Date program began (begins): \_\_\_\_\_  
(Name of Institution)  
date program to end: \_\_\_\_\_ I understand that in-training membership is limited to a  
maximum of 5 years.

Applicant Signature: \_\_\_\_\_

**Verification:** (Program Director or Department Chairman *only*)

I certify that the applicant is in training at the institution named and qualifies for enrollment as a member-in-training of the American Roentgen Ray Society.

Name (Please Print) \_\_\_\_\_

Address: \_\_\_\_\_  
\_\_\_\_\_

Signature \_\_\_\_\_

Send completed form to: **American Roentgen Ray Society**  
**1891 Preston White Drive**  
**Reston, Virginia 22091**



# Classified Advertisements

## Positions Available

**MEMPHIS, TENNESSEE**—Immediate opening for a board-certified, general radiologist to join a 5-person group currently performing 80,000 exam/yr in a diversified practice. MRI experience preferable. Excellent salary, benefits, and full partnership within 3 yr with no buy-in. Practice covers 3 community hospitals (250 beds) and 2 outpatient offices. No angiography duties and minimal interventional radiology. Democratically run, fee-for-service practice made up of young, academically oriented radiologists. Send CV to Robert A. Duke, M.D., Diagnostic Imaging, P.C., 1068 Cresthaven Rd., Ste. 100, Memphis, TN 38119; (901) 682-5053. 2-3ap

**RADIOLOGIST, BRIGHAM AND WOMEN'S HOSPITAL**—The Dept. of Radiology at the Brigham and Women's Hospital/Harvard Medical School wishes to recruit a staff person in ultrasound. This position offers diverse clinical work and extensive opportunities for research in abdominal, obstetric, vascular, and other areas of ultrasound. Rank and salary commensurate with experience. Evidence of interest in academic radiology and certification by the American Board of Radiology are preferred. Please send CV to B. Leonard Holman, M.D., Chairman, Dept. of Radiology, Brigham and Women's Hospital, 75 Francis St., Boston, MA 02115. Brigham and Women's Hospital/Harvard Medical School is an affirmative action/equal opportunity educator and employer. 2-4a

**MINNEAPOLIS, MINNESOTA**—Private practice opportunity for a neuroradiologist with procedural orientation to join an expanding group of 5 radiologists; 2 are ASNR members. Practice is primarily based at growing, free-standing, outpatient imaging centers and includes two 1.5-T Signa MR units, 3 GE 9800 CT scanners, and accompanying fluoroscopic-radiography equipment. A third MR unit is being installed in the Twin Cities and should be operational in early spring 1991. We are heavily oriented toward spine and musculoskeletal imaging and related procedures. Candidates must be interested in spine imaging and related procedures, such as myelography, nerve blocks, facet arthrograms/therapeutic procedures, and diskography. We are also affiliated with a 750-bed, tertiary hospital in Minneapolis. The practice is academically oriented and encourages clinical research and publication, although this is not required. No calls please. Send letters of inquiry and complete CV to Kurt P. Schellhas, M.D., Center for Diagnostic Imaging, 5775 Wayzata Blvd., Ste. 190, St. Louis Park, MN 55416. 2-4ap

**DIAGNOSTIC RADIOLOGIST**—Two young, progressive radiologists seek a third, recently trained, BC/BE, general radiologist to join in a rapidly growing practice in a 100-bed hospital. 31,000 exams/yr, including ultrasound, nuclear medicine, mammography, and CT. No angiography. An MR rotation is available at a free-standing center. Call will be shared equally. 9-wk vacation. The Oneida City Hospital is located in the scenic eastern Finger Lakes, with a 4-season climate, near a medical school. Excellent starting salary, with full partnership following 2 yr; no buy-in. Please send CV with letter to Ralph Stevens, M.D., Dept. of Radiology, Oneida City Hospital, 321 Genesee St., Oneida, NY 13421. 2-4ap

**NEURORADIOLOGIST, BIG SKY COUNTRY**—Group of 5 radiologists seek a BC, fellowship-trained colleague. Hospital and busy clinical practice. Must be a capable, general diagnostic radiologist. One yr to partnership. Send letter/CV to Bruce Pinkerton, M.D., Dept. of Diagnostic Radiology, Deaconess Medical Center, P.O. Box 2547, Billings, MT 59103. 2-7ap

## DUKE UNIVERSITY MEDICAL CENTER/STAFF

**RADIOLOGISTS**—Duke University Medical Center is seeking qualified candidates for staff positions in the Dept. of Diagnostic Radiology. A limited number of staff positions currently are available in the following sections: general diagnostic, pediatric, chest, vascular/interventional, and musculoskeletal radiology. We offer an excellent salary and benefits package. The radiology dept. is state-of-the-art in diagnostic imaging with diverse resources available for clinical, teaching, and academic pursuits. Staff members have guaranteed academic time and research support. Interested board-certified radiologists with appropriate experience should phone Robert Vandemark, M.D. at (919) 681-3711 ext. 5233, for additional information. Letters of inquiry should be sent to Carl E. Ravin, M.D., Dept. of Radiology, Box 3808, Duke University Medical Center, Erwin Rd., Durham, NC 27710. AA/EOE. 2-7a

**DEPT. OF RADIOLOGICAL SCIENCES, UCLA** Professorships available for qualified candidates who have extensive experience in image processing, picture archiving and communications systems, teleradiology, medical imaging instrumentation, radiographic detector technology, and communication theory. Applicants must have an excellent track record in research, experience in industrial collaboration, teaching, and administration. The successful applicants are expected to provide research guidance to junior faculty members, postdoctoral fellows, and graduate students; develop research programs through extramural funding agencies; and participate in the administration of the dept. teaching program. Please send CV and 3 reference letters to H. K. Huang, M.D., Professor and Chief, Medical Imaging Division, Dept. of Radiological Sciences, University of California, Los Angeles, CA 90024-1721. 2-3a

**CHAIR, DEPT. OF RADIOLOGY**—Applications and nominations are invited for Chairperson of the Dept. of Radiology at the University of Virginia School of Medicine in Charlottesville, VA. This person will also be Radiologist-in-Chief, University of Virginia Health Sciences Center. Candidates should hold an M.D. or equivalent degree and have evidence of scholarly accomplishment and leadership in radiology and the radiologic sciences. Minority and women applicants are especially encouraged. Applications and nominations should be sent to Irving L. Kron, M.D., Professor of Surgery, University of Virginia Health Sciences Center, Box 181, Charlottesville, VA 22908. 2a

**RADIOLOGIST, WESTERN MASSACHUSETTS** Large radiology group in western MA is seeking a general diagnostic radiologist with experience and interest in body imaging, and expertise in nonvascular interventional procedures. Primary assignment at 868-bed, tertiary-care hospital with radiology residency program. Practice also includes 3 community hospitals and 6 private offices. Full partnership after 1 yr. Available on or before July 1, 1991. Send CV to Director of Recruiting, Radiology & Imaging, Inc., 130 Maple St., Springfield, MA 01103. 2-4ap

**ABDOMINAL IMAGING**—A staff position is available at The Cleveland Clinic Foundation in the section of abdominal imaging. The Cleveland Clinic is a 1000-bed, tertiary-care facility with a large outpatient population and an international referral base. The section of abdominal imaging encompasses body CT, ultrasound, body MR, gastrointestinal radiology, and mammography. Applicants should be fellowship-trained, or possess equivalent experience. Send CV to David M. Paushter, M.D., Head, Section of Abdominal Imaging, Hospital Radiology, Cleveland Clinic Foundation, One Clinic Center Dr., Cleveland, OH 44195-5103. The Cleveland Clinic is an equal opportunity employer. (M-F-H-V). 2-3ap

**RADIOLOGIST, HOUSTON, TEXAS**—Large, well-established, multispecialty group is seeking a full-time, BC/BE radiologist due to growth in practice. Our group consists of over 100 physicians, including 5 radiologists. In addition to plain film interpretation, the practice includes fluoroscopy, urography, tomography, ultrasound, and mammography totaling 75,000 studies/yr. We are in the process of acquiring CT capability. Four-and-a-half-day work-wk and no call gives you time to enjoy the variety of activities Houston has to offer. We provide excellent benefits, including malpractice with tail coverage and a very competitive financial package. Interested candidates should send CV to MacGregor Medical Association, 2550 Holly Hall, Houston, TX 77054. Attn: Karen Aszman, Professional Relations Specialist. 2-3ap

**ARIZONA**—VA Medical Center imaging service, Prescott, AZ, is accepting applications for a full-time radiologist. Competence and proficiency in interpreting CT scans is required. Prescott is a 217-bed, general medicine hospital with a busy combined radiology and nuclear medicine service. Prescott is located in the mountains of north-central AZ with a population of 25,000. Commitment and selection is dependent upon obtaining and installing a CT scanner. Salary, approximately \$80,000, is dependent on qualifications. Send CV to Sharon K. Harneson, Personnel Service, VA Medical Center, Prescott, AZ 86313; (602) 445-4860 ext. 214. An equal opportunity employer. 2a

## PENN STATE UNIVERSITY, THE MILTON S. HERSHEY MEDICAL CENTER, FACULTY POSITION IN NUCLEAR MEDICINE

—The Division of Nuclear Medicine of the Dept. of Radiology at the Penn State University's Milton S. Hershey Medical Center is recruiting a physician with board certification in nuclear medicine (ABNM) for a full-time academic position. Board certification in diagnostic radiology (ABR) is desirable but not essential. Penn State University Hospital is a 350-bed, tertiary-care facility (currently expanding to 500 beds) in Hershey, PA, near Harrisburg, the state capital. Nuclear Medicine is a division of the Dept. of Radiology, which has an academic faculty of 20 physicians and 6 Ph.D.'s. The Nuclear Medicine Division currently performs 5000 exams/yr and is expected to increase as renovations and expansion are completed in subsequent years. There are currently 5 gamma cameras and a Hologic QDR 1000W bone-density unit in place, with 1 additional camera being added in 1991 or 1992. Four or 5 of the 6 will be tomographic. Areas of emphasis currently include cardiac and pediatric nuclear medicine. An interest in neuro-nuclear medicine and brain tomography is desirable but not essential. An interest in clinical and/or basic research is desirable. Applicants should respond as soon as possible with a letter of interest and current CV. Please direct inquiries to Douglas F. Eggli, M.D., Chief, Division of Nuclear Medicine, Dept. of Radiology, Penn State University/Hershey Medical Center, P.O. Box 850, Hershey, PA 17033. Penn State University is an affirmative action, equal opportunity employer. Women and minorities are encouraged to apply. 2-4a

**FAIRBANKS, AK**—Four diagnostic radiologists seek fifth partner for diversified practice including general radiology, ultrasound, nuclear medicine, MRI (GE 1.5-T), and CT (GE 9800). Hospital and office practice. Desirable life-style advantages in a university town. Unlimited access to the outdoors. Excellent salary, benefits, retirement, and vacation. One yr to full partnership. Contact Douglas Hutchinson, M.D., 1919 Lathrop #5, Fairbanks, AK 99701; (907) 452-5092. 2-4ap

**TWO DIAGNOSTIC RADIOLOGISTS** with recent training are sought for growing hospital practice of 3 BC radiologists in Elizabethtown, KY. Fellowship training in body imaging and intervention welcome. Modern, well-equipped radiology dept. at 300-bed regional hospital that includes 2 GE 9800 CT, GE 1.5-T MR, GE LU dedicated angiographic suite with DSA, ultrasound, nuclear medicine, and ACR-certified, dedicated mammography. Position available immediately. Send letters of inquiry with CV to Elizabethtown Radiology, P.S.C., P.O. Box 2489, Elizabethtown, KY 42701; (502) 765-4144. 2-4ap

**THE PENN STATE UNIVERSITY, MILTON S. HERSHEY MEDICAL CENTER, CHIEF OF MRI**  
The Pennsylvania State University Dept. of Radiology is seeking a full-time faculty chief of the section of Magnetic Resonance Imaging (MRI). The MRI section performs over 3000 MRI scans/yr on our 1-T Siemens system. We have just purchased a second magnet (1.5-T Toshiba MRI-150A). Both our in-house and outpatient magnet systems have significant research capacity for clinical and applications projects. A Nuclear Magnetic Resonance (NMR) Imaging/Spectroscopy center, directed by Michael B. Smith, Ph.D., with over 6500 sq. ft., is completed. It is connected to our outpatient MRI system. In this NMR center, we have 3 magnets: a 9.4-T Bruker AM-400 widebore spectrometer with micro imaging; a 1.9-T Oxford 26-cm-bore horizontal magnet interfaced to a Nicolet 1280 computer; and a 3.0-T Bruker 90-cm-bore spectrometer/imager which will be the first of its kind and 100% dedicated to research. The NMR center will also be completely equipped with surgical and animal preparation area, biochemistry laboratory, radio-frequency and electronics laboratory, full machine shop, computer resources, and office space for faculty, staff, postdoctorates, and students. The successful candidate must be experienced in both clinical and research MR, and have publications that confirm his/her experience. The chief of MRI will be responsible for developing further our clinical MRI service and integrating it with our new NMR research center. Clinical responsibility will be in MRI, either in neuroradiology, body imaging, or both, depending on the successful candidate's experience and certification. Independent original research is expected and is amply funded both in time and money. The academic rank will depend upon the candidate's achievement. The salary is dependent on the achieved rank and experience. The position is open to individuals who have completed an accredited residency program in radiology; can obtain a Pennsylvania medical license; can obtain medical staff privileges at University Hospital; and are board certified by the American Board of Radiology or its equivalent. Applicants should respond as soon as possible with a letter of interest and current CV. Please direct inquiries to John E. Madewell, M.D., Professor and Chairman, Dept. of Radiology, The Penn State University, Milton S. Hershey Medical Center, P.O. Box 850, Hershey, PA 17033. Penn State University is an affirmative action, equal opportunity employer. Women and minorities are encouraged to apply. 2-4a

**OREGON**—Group of 13 radiologists in Salem, OR, seeks BC/BE radiologist with general radiology skills. Practice includes 454-bed community hospital, large out-patient office, and multispecialty clinic. Near ideal family community and recreational amenities. Send CV to John Eyre, M.D., Salem Radiology, 919 Oak St., S.E., Salem, OR 97301. 2-5ap

**THE UNIVERSITY OF LOUISVILLE, DEPARTMENT OF DIAGNOSTIC RADIOLOGY** is seeking applications from BC/BE diagnostic radiologists to fill full-time faculty positions in the following areas in its 400-bed, teaching hospital: (1) cross-sectional body imaging and (2) general radiology (GI, GU, bone, chest). Candidates must be willing to participate in undergraduate and graduate teaching and in research activities in their respective areas. These are fine opportunities in a growing and busy dept. with excellent equipment. Both tenure and non-tenure track appointments are available, and academic rank will be commensurate with training and experience. Compensation negotiable and competitive. Louisville continues to be ranked one of the top 10 places to live in America by Rand McNally. Send inquiries with CV and 3 references to Hollis A. Thomas, M.D., Professor and Chairman, Dept. of Diagnostic Radiology, Humana Hospital-University of Louisville, 530 S. Jackson St., Louisville, KY 40202. An equal opportunity/affirmative action employer. 2-3a

**RADIOLOGIST NEEDED** with experience in CT, ultrasound, nuclear medicine, mammography, and general radiology to provide vacation coverage for 2 practices in rural western Montana. One practice requires some traveling. Position would be excellent for person who wishes to semiretire in a pleasant scenic area. Great opportunity for recreational activities. Send inquiries to Tyler H. Gill, M.D., 1200 Westwood Dr., Hamilton, MT 59840; (406) 363-2211. 1ap

**SEATTLE AND SUBURBS** — BC associate needed immediately for rapidly growing practice dedicated to mammography and breast diagnosis. Four offices; 2 also have general ultrasound. 85% OB-GYN. Mammography or ultrasound fellowship or extensive experience helpful. Association leading to partnership. Send letter and CV to Irwin Schiller, D.O. and Marita Acheson, M.D., c/o Breast Diagnostic Center, 411 Strander Blvd., #303, Seattle, WA 98188; (206) 575-9123. 1-3ap

**MUSCULOSKELETAL / MRI RADIOLOGIST, THOMAS JEFFERSON UNIVERSITY HOSPITAL**  
We are recruiting a faculty musculoskeletal radiologist (either junior or senior level) for an important and challenging position in our dept. The position encompasses MRI of the musculoskeletal system and other body applications, plain film musculoskeletal radiology, tomography, and arthrography. Jefferson currently operates 4 GE 1.5-T Signa MRI units and 3 CT scanners. Close relationships are maintained with busy orthopedic, rheumatology, trauma, and spinal cord injury services. A thriving clinical practice, active teaching program, and well-equipped research facilities all combine to make this an outstanding career opportunity. Excellent faculty incomes and many other benefits are provided. Interested applicants should contact David C. Levin, M.D., Chairman, Dept. of Radiology, Thomas Jefferson University Hospital, 11th and Walnut Sts., Philadelphia, PA 19107; (215) 955-7265. Jefferson is an equal opportunity/affirmative action employer. 1-4a

**SAN FRANCISCO BAY AREA** — Progressive BC/BE diagnostic radiologist sought to join 5 BC radiologists serving a 200-bed, acute-care hospital and outpatient clinic. Special competency in MRI and cross-sectional imaging desired. Quality practice in desirable suburban setting. We offer a competitive salary and generous benefits package. Send CV to Martin Portnoff, M.D., Dept. of Radiology, Kaiser Permanente Medical Center, 200 Muir Rd., Martinez, CA 94553; (415) 372-1100. EOE. 1-2a

**BC RADIOLOGIST, KANSAS CITY, MO**—Seven radiologists currently covering a 600-bed, tertiary medical center seek a radiologist with a special competency or fellowship in nuclear medicine. The position, open immediately, includes competitive salary and fringe benefits, and leads to full partnership. Send CV and letter of inquiry to J. M. Speckman, M.D., 6400 Prospect, Ste. 310, Kansas City, MO 64132. 1-4ap

**FACULTY OPENING IN THORACIC IMAGING**  
The Johns Hopkins University Hospital has an opening at the junior faculty level in the Division of Thoracic Imaging. The division is fully integrated across all modalities including MRI, CT, and interventional procedures. Research opportunities are exceptional with protected research time available to rapidly establish an academic career. Academic rank and salaries will be determined by previous experience. The candidate must be board-certified. Contact Elias A. Zerhouni, M.D., Director, Thoracic Imaging & MRI Divisions, Dept. of Radiology, Johns Hopkins Hospital, Baltimore, MD 21205; (301) 955-4062. 1-6a

**MAMMOGRAPHY FACULTY POSITION** — The Dept. of Radiology at Johns Hopkins University Hospital has a faculty position available in mammography. The mammography section is part of the thoracic imaging division. The section offers a strong potential for academic growth with emphasis on original research and teaching. Protected academic time is available for candidates interested in developing a strong academic career. Support, resources, and opportunities are available for creative research. The candidate can also participate in all other aspects of diagnostic imaging as desired. Academic rank and salary will be determined by previous experience. Candidate must be board-certified. Contact Elias A. Zerhouni, M.D., Director, Thoracic Imaging and MRI Divisions, Dept. of Radiology, Johns Hopkins Hospital, Baltimore, MD 21205; (301) 955-4062. 1-6a

**DIAGNOSTIC RADIOLOGIST IMMEDIATE OPENING AT ROSE MEDICAL CENTER (RMC), DENVER, CO**—A 7-person radiology group is recruiting a radiologist with fellowship training in interventional radiology. The practice involves all imaging modalities. Highly competitive first yr salary and generous fringe benefit package. Position leads to offer of equal shares in the professional corporation after 1 yr, if mutually agreed upon. RMC is affiliated with the University of Colorado. Contact David W. Wilder, M.D. or Jeffrey A. Levy, M.D.; (303) 320-2256. 1-3a

**FLORIDA, STAFF RADIOLOGIST**—Opportunity for board-certified/eligible diagnostic radiologist with experience in reading plain films, fluoroscopy, ultrasound, CT, nuclear medicine, and some angiography in the radiology service at this progressive, GM&S, Dept. of Veterans Affairs (VA) Medical Center. Potential academic appointment and affiliation in surgery with the University of Florida. Competitive salary plus incentive pay commensurate with qualifications. Excellent employment benefits including 30 days paid vacation and 15 days sick leave per yr; liberal life and health insurance benefits; malpractice insurance; and retirement program. Moving expenses paid. "Florida's new gateway city" is located in northern Florida with a mild climate yr round. Extensive outdoor recreational activities, reasonable cost of living, no state income tax, and fine schools and nearby universities provide opportunity for continuing education and cultural diversion. Florida license not required. Contact or send CV to Richard Parker, M.D., Chief of Radiology, VA Medical Center, Lake City, FL 32055-5898; (904) 755-3016, ext. 2543. An equal opportunity employer. 2-4a

**MUSCULOSKELETAL RADIOLOGIST**—The Dept. of Radiology, University of Texas Health Science Center at San Antonio, seeks a musculoskeletal radiologist. Salary and academic rank are commensurate with the candidate's experience. Excellent research opportunities are available in a new 30,000 sq. ft. research imaging center. The Health Science Center lies in the northern suburbs of San Antonio adjacent to excellent living areas and schools. Replies and CVs should be sent to Stewart R. Reuter, M.D., Chairman, Dept. of Radiology, 7703 Floyd Curl Dr., San Antonio, TX 78284-7800. Equal opportunity/affirmative action employer. 1-3a

**CONNECTICUT**—Expanding group of 8 radiologists has a position available for an additional angio/interventional, BC/BE radiologist with expertise in general radiology also. Practice includes a 435-bed, fully equipped, university-affiliated, community hospital and a 47-physician, multispecialty clinic. Excellent salary and benefits leading to full partnership after second yr. For information, send CV to Paul C. Lakin, M.D., Dept. of Radiology, New Britain General Hospital, 100 Grand St., New Britain, CT 06050. 1-4ap

**VASCULAR/INTERVENTIONAL RADIOLOGIST** Large radiology group in western Massachusetts is seeking a BC vascular/interventional radiologist to join existing 5-person vascular/interventional team. Fellowship or equivalent experience required. Must also have expertise in CT and general diagnostic radiology. Primary assignment at 868-bed, tertiary-care hospital with radiology residency program. Practice also includes 3 community hospitals and 6 private offices. Full partnership after 1 yr. Available July 1991. Send CV to Director of Recruiting, Radiology and Imaging, Inc., 130 Maple St., Springfield, MA 01103. 1-3ap

**SALEM, MA**—July 1991 position available for BC, recently trained radiologist with strong interest in general diagnostic radiology and expertise in mammography and OB-GYN ultrasound for Women's Imaging Center to open next yr. Eleven radiologists practicing in a large, community teaching hospital on Boston's beautiful North Shore. Contact Courtney Neff, M.D.; (508) 741-1200, ext. 4420. 1-2ap

**BOSTON, IMMEDIATE OPENING**—Radiologist wanted to join busy, well-established, private-practice group with 4 outpatient facilities. Expertise in ultrasound and mammography. No evening or weekend call. Excellent life-style, partnership opportunity. Send letter and CV to Box E49, AJR (see address this section). 9-2ap

**BC/BE DIAGNOSTIC RADIOLOGIST** with skills in all aspects of radiology, including CT, ultrasound, nuclear medicine, interventional, MR, and mammography sought to join a dynamic group of 6 BC radiologists covering a busy, progressive, community hospital, 2 private offices, and an outpatient women's center. Modern dept., state-of-the-art equipment, attractive vacation, CME, and benefits package. 30 min west of Philadelphia. Position available immediately but will wait for right person. Reply with CV to L. Griska, M.D., Dept. of Radiology, Montgomery Hospital, Powell and Farnance Sts., Norristown, PA 19401. 11-2ap

**IMMEDIATE OPENING, DIAGNOSTIC RADIOLOGIST**—Excellent opportunity for a young, dynamic, preferably board-certified radiologist to join an active, 9-member group. Growing practice includes a 700-bed hospital system with state-of-the-art equipment and excellent working facilities. Skills in all phases of diagnostic radiology desired. Attractive and competitive benefits package leading to full partnership. Contact Sanford E. Rabushka, M.D., 11133 Dunn Rd., Ste. 1017, St. Louis, MO 63136; (314) 653-4300. 11-4ap

**DIAGNOSTIC RADIOLOGIST**—Excellent opportunity in well-established, South Carolina hospital-based practice for BC/BE radiologist. Competitive salary. Full partnership in 1 yr. Send CV to Box H87, AJR (see address this section). 12-3ap

**THE UNIVERSITY OF TEXAS HEALTH SCIENCE CENTER AT SAN ANTONIO** announces formation of a Research Imaging Center. This center is designed to use modern imaging methods in evaluating pharmaceutical therapies in both animal and human models. Thirteen new positions are available in 1990/1991 and an equal number are anticipated the following yr. Applications are invited for the following faculty or administrative positions: Director of PET Facility—An M.D.- or Ph.D.-level scientist to provide overall direction of the PET facility operation, supervise personnel, and conduct an independent research program. Appointment at the assistant or associate professor level will depend on experience. Radiochemist—A Ph.D.-level scientist to direct operation of the cyclotron and radiochemistry hot lab in support of the PET operations and conduct an independent research program. Appointment at the assistant or associate professor level will depend on experience. Associate Radiochemist/Physicist—A Ph.D.-level scientist to be responsible for the operation of the cyclotron and related radiochemistry developments. Appointment as assistant professor or lecturer will depend on experience. Radiopharmacist—A Master's (or Ph.D.) level radiopharmacist who is licensed and certified to prepare, test, and certify radiopharmaceuticals for human use. The appointment will be at the assistant professor level. NMR Physicist or Chemist—A Master's (or Ph.D.) level scientist with a minimum of 2 yr experience operating and assisting others in the use of a 2-T (45-cm bore) MRI/MRS unit. The appointment will be at the level of lecturer. NMR Chemist or Biologist—A Master's (or Ph.D.) level scientist to operate high resolution NMR spectrometers and assist others in using these instruments. The appointment will be at the level of lecturer. All of the above faculty will have the opportunity to participate in both medical and graduate school (radiological sciences) educational programs with appointments depending on the interests and experience of the successful candidates. The University of Texas Health Science Center at San Antonio is an equal opportunity employer. Send cover letter/CV to Gary D. Fullerton, Ph.D., Dept. of Radiology, UTHSCSA, 7703 Floyd Curl Dr., San Antonio, TX 78284-7800. 12-2ap

**MAINE**—Excellent opportunity for BC/BE, fellowship-trained neuroradiologist with progressive, well-established, small group. Live and work in college community in southern region close to coast, mountains, and lakes. Competitive compensation package leading to partnership. Affiliated with 200-bed, modern community hospital. Send CV to New England Health Search, 63 Forest Ave., Orono, ME 04473; (207) 866-5680 or (207) 866-5685. 11-2ap

**GENERAL DIAGNOSTIC RADIOLOGIST**—Position available to join 11-member, private-practice group in 500-bed, university-affiliated, tertiary-care hospital in Allentown, PA. The position offers a competitive salary benefit package commensurate with training leading to full partnership. The Radiology Dept. offers a fellowship in CT, ultrasound, and angiography/interventional. The hospital has active residency programs in medicine and surgery. Allentown is located in the Lehigh Valley (population 250,000) and is 2 hr from New York City, 1 hr from Philadelphia, and 1 hr from the Pocono Mountains. For information, please contact Robert Kricun, M.D., or Alan Wolson, M.D., Lehigh Valley Hospital Center, 1200 S. Cedar Crest Blvd., P.O. Box 689, Allentown, PA 18105; (215) 776-8088. 12-2ap

**BROAD SPECTRUM RADIOLOGIST/UPSTATE NEW YORK**—Radiologist wanted for hospital-based practice 90 mi. northwest of New York City. Excellent recreational activities and easy access to metropolis. All modalities available. Excellent salary and benefits leading to early partnership. Immediate availability, but can wait for right applicant. Call G. Bilick; (914) 794-3300, ext. 2216 or send CV to P.O. Box 144, Harris, NY 12742. 11-2ap

**NUCLEAR MEDICINE OR INTERVENTIONAL RADIOLOGIST**—Progressive, 7-person group seeks to add an interventional radiology or nuclear medicine (special competency preferred) fellowship-trained radiologist for spring 1991. This busy, expanding practice is hospital- and recently full-service imaging center-based. Both institutions use leading edge technology. The proximity of Lake Tahoe, the gaming industry, the state capitol, and a major university provides many cultural, entertainment, and sporting opportunities. Send CV to Colby Laughlin, M.D., Reno Diagnostic Center, 590 Eureka Ave., Reno, NV 89512. 12-3a

**PHILADELPHIA, PA**—Temple University Hospital and School of Medicine seeks the following board-certified radiologists: Vascular/Interventional Radiologists (2)—Section Head and staff positions available. Positions involve responsibilities in patient care and teaching. Candidates with fellowship training and research skills preferred. Abdominal imaging radiologist—Strong clinical skills in ultrasound, CT, MRI, urography, and gastrointestinal radiology. Fellowship training is preferred. An interest in medical student and radiology resident teaching is required. Interest in abdominal imaging research desirable. Pulmonary radiologist—Candidate should be a senior-level radiologist at the professor or associate professor level with a primary interest in pulmonary radiology. Ideal candidate will have fellowship training in pulmonary radiology and proficiency in all areas of radiologic practice. Candidates should have demonstrated skills as a teacher and an interest in research. Applicants should send current CV (indicate position of interest), bibliography, and 3 letters of recommendation to Temple University School of Medicine, Attn: Francis J. Shea, M.D., Deputy Chairman, Dept. of Diagnostic Imaging, Broad and Ontario Sts., Philadelphia, PA 19140. An equal opportunity/affirmative action employer. 2xa

**CHIEF RADIOLOGIST AND RADIOLOGISTS**—In anticipation of the opening of our clinical addition, we are actively seeking BC radiologists for chief and staff positions. Facilities include fluoroscopy, tomography, diagnostic ultrasound, general radiology, CT, and angiography. Joint faculty appointment with our major affiliate, the Marshall University School of Medicine, dependent on candidate's clinical and academic experience. Our medical center is currently expanding to 250 beds and doubling facility size with a clinical addition. Radiology service will be located in new state-of-the-art facilities in the addition. Work with a rotating staff of radiologists, a chief technician, a permanent technical staff, and transitional residents in radiology. For more information on these challenging opportunities, please call or send your CV to Ms. R. Bookwalter, Office of the Chief of Staff, VA Medical Center, 1540 Spring Valley Dr., Huntington, WV 25704; (304) 429-6755, ext. 2517. 12-2a

**IMMEDIATE OPENING**—Radiologist needed to join 1 other in a 60-bed, hospital-based practice with GE 1.5-T MRI, 9800 CT, Doppler ultrasound, SPECT, nuclear, and biplane angio. Excellent salary leading to early partnership. Unique opportunity to join a sophisticated practice while living among the redwoods in a northern California coastal city with a referral population of over 100,000. Send CV to Dr. Jackson, 3560 N. St., Eureka, CA 95501; (707) 445-5993. 12-2ap



**DIAGNOSTIC RADIOLOGIST**—Eight board-certified radiologists in expanding, hospital-based private practice seek BC/BE general radiologist to associate. Competence in all modalities expected with need for MRI training emphasized for 2 MRI facilities in practice. Opportunity in midwestern city of 72,000 people offers generous compensation/vacation. Full partnership after 2 yr. Reply to Box H89, *AJR* (see address this section). 12-3ap

**DIAGNOSTIC RADIOLOGIST** needed in Conway Hospital, a community hospital located 10 mi. west of the resort/seaside community of Myrtle Beach, SC. The dept. performs 44,000 exams/yr including CT, MRI, nuclear medicine, ultrasound, mammography, and special procedures. All exams are done on state-of-the-art equipment. Our 3-person group offers a very strong financial package with all benefits including 17-wk vacation. Lovely, rapidly growing resort area includes 60 mi. of sandy beaches, 70 golf courses, and beautiful seaside homes. Contact Gary Rike, M.D., P.O. Box 917, Conway, SC 29526; (803) 347-7277. 12-5ap

**PART-TIME MAMMOGRAPHY / ULTRASOUND RADIOLOGIST** — Immediate opening for a half-time diagnostic radiologist with a 12-member group in a Pacific Northwest city of 60,000+. BC/BE with expertise/interest in mammography and ultrasound. Equipment is state-of-the-art. Competitive salary and benefits. Located amidst the recreational activities of the Puget Sound and Cascade Mountains. Send letter, personal sketch, and CV to J. W. Little, M.D., 3822 Colby Ave., Everett, WA 98201; (206) 259-3256. 12-2ap

**DIAGNOSTIC RADIOLOGIST, SAN FRANCISCO BAY AREA**—The Permanente Medical Group is seeking a progressive BC/BE diagnostic radiologist with special competency in MRI and cross-sectional imaging to join 5 other BC radiologists serving a 200-bed, acute-care hospital and outpatient clinic. This quality practice, located in a desirable suburban setting, offers all imaging modalities. Competitive salary and generous benefits. Send CV to Martin Portnoff, M.D., Kaiser Permanente Center, 200 Muir Rd., Martinez, CA 94553; (415) 372-1110. EOE. 12-2a

**RADIOLOGY / NEURORADIOLOGY, GEORGIA** Group of 5 radiologists seeks individual with neuroradiology fellowship training and interest in continuing to practice other aspects of radiology. Well-established, private practice in 300-bed, acute-care hospital with neuro intensive care unit and private office. All imaging modalities are represented including MRI. Excellent benefits with full partnership in 2 yr. This is an opportunity to join an expanding practice in a beautiful coastal city with excellent recreational and cultural advantages. Send CV to Don Starr, M.D., Savannah Radiologists, P.A., 503 Eisenhower Dr., Savannah, GA 31499. 12-2ap

**RURAL RADIOLOGY PRACTICE**—Interested in being an extremely busy general radiologist in a rural midwest setting? We are seeking a fourth board-certified general radiologist to replace our recently retired senior partner. Hays is a town of 25,000 (5000 students at Fort Hays State University) in central Kansas, and functions as a regional medical center with 40-50 physicians. We are the sole radiology practice in northwest Kansas, reading about 70,000 exams/yr in Hays and surrounding towns. Equipment is state-of-the-art including 2 GE 9800 CT, a GE Signa MRI, 2 Acuson 128 color Doppler, angiography with DSA, nuclear medicine, and fluoro and plain films. The practice is egalitarian, with identical work schedules, call, and vacation times. Contact Robert F. Bowerman, M.D., Ph.D., for more details at Radiology Associates of Hays, P.A., P.O. Box 833, Hays, KS 67601; (913) 625-6521. 12-2ap

#### VASCULAR / INTERVENTIONAL RADIOLOGIST

The University of Texas Southwestern Medical School, Dept. of Radiology, is seeking BC/BE vascular/interventional radiologists at the rank of assistant/associate professor who have had a CVI fellowship or extensive experience in the subspecialty. Responsibilities will include clinical work in all aspects of the subspecialty at Parkland Memorial Hospital, Zale-Lipsby Hospital, and the VA Hospital as well as teaching of medical students, residents, and fellows. Clinical and basic research opportunities abound at this rapidly growing medical school complex. Salary negotiable and competitive and is dependent on the level of experience. Interested individuals should contact Helen C. Redman, M.D., Dept. of Radiology, The University of Texas Southwestern Medical School, 5323 Harry Hines Blvd., Dallas, TX 75235. UT Southwestern is an equal opportunity/affirmative action employer. 12-2a

**IMMEDIATE OPENING** — BC/BE radiologist to join medium-size group in Austin, TX. Practice covers major trauma center and outpatient radiology facility. In addition to general diagnostic services, outpatient facility also provides CT and MRI services on 2 GE 9800 scanners and on GE 1.5-T and 0.5-T MR units. Applicants are requested to contact Drs. Boyd, Gray, or Lava at 711 W. 38th St., Ste. B-8, Austin, TX 78705; (512) 454-8718. 12-5ap

**RADIOLOGIST**—Seven-person group seeks general radiologist with fellowship training and special interest in MRI for 92-bed hospital and several imaging centers. Practice in the rapidly growing north San Diego and Temecula Valley areas. Send CV to North Coast Imaging Radiology Medical Group, Inc., 1582 W. San Marcos Blvd., Ste. 104, San Marcos, CA 92069; (619) 744-6442. 11-2ap

**TEN-PERSON RADIOLOGY GROUP** located in Corpus Christi is seeking a new associate to start July 1990 or as late as July 1991. Must be board-certified or eligible. Will perform all diagnostic studies, including interventional, CT, MRI, nuclear medicine, and ultrasound. Please send CV to Search Committee, P.O. Box 5608, Corpus Christi, TX 78465-5608. 2xa

**INDIANAPOLIS, IN**—Practice opportunity for a radiologist to serve as medical director of a new, freestanding, privately owned, high-field MR imaging center. Facility will be managed by and affiliated with the Center for Diagnostic Imaging in Minneapolis, MN. MR experience mandatory. Subspecialty experience in MR desirable. Board certification and licensure in Indiana required. Please send inquiries with CV to Cooper R. Gundry, M.D., Center for Diagnostic Imaging, 5775 Wayzata Blvd., Ste. 190, Minneapolis, MN 55416. All inquiries entirely confidential. No telephone calls please. 12-2a

**RADIOLOGISTS** — New York City, combined private radiology practice, and fee-for-service hospital practice has an immediate opening for a board-certified radiologist with experience in CT, ultrasound, and interventional radiology. In addition, MRI and mammography experience is preferred. This well-established practice has 3 private offices on the upper East Side of Manhattan as well as operations in 2 hospitals in Manhattan. Other studies performed in the practice are diagnostic radiology, nuclear imaging, and vascular duplex imaging. The practice continues to expand in all imaging modalities with its recent opening of a second state-of-the-art MRI unit. Excellent benefit package includes health, life, disability, and malpractice insurance; profit sharing plan; continuing medical education; and a travel and entertainment account for professional use. Send CV to Box F67, *AJR* (see address this section). 1-3ap

#### ULTRASOUND SECTION CHIEF, UNIVERSITY OF MARYLAND

—The University of Maryland Hospital seeks a chief for the ultrasound section of the Dept. of Radiology. Although already well-equipped, this position offers a great opportunity for expansion and development, both with the new all-digital Dept. of Radiology under construction at the adjoining VA Hospital and in a new planned all-digital Dept. of Radiology to be constructed at the University Hospital. Applicants should have specialist training and fellowship in ultrasound and a willingness to be involved in the teaching of residents and students. Academic rank and salary are commensurate with experience. The radiologists are organized as a professional corporation, offering excellent fringe benefits. Baltimore is a superb place to live and work. It has all the amenities of a large metropolitan center, yet is small enough to avoid most of the problems (traffic, inflated property values, etc.) of our largest cities. It is only 3 hr from the ocean and Washington, Philadelphia, and New York are readily accessible. Submit CV to Gerald S. Johnston, M.D., Dept. of Diagnostic Radiology, 22 S. Greene St., Baltimore, MD 21201; (800) 866-8667, ext. 3477. Affirmative action/equal opportunity employer encourages applications from members of minority groups. 9-2ap

#### THE DEPT. OF RADIOLOGY AT TRIPLER ARMY MEDICAL CENTER, HONOLULU, HI

is recruiting academic radiologists for several divisions of the dept. including ultrasound, chest, skeletal, neuro, and general diagnostic radiology. Our dept. offers a fully accredited residency program with 20 residents and 16 attending full-time staff. Numerous consultants from across the country lecture on a continuing and regular basis. The hospital is a modern, tertiary-care center serving Hawaii and the entire Pacific Basin. A strong residency program, diverse and interesting patient population, excellent equipment, and a tropical lifestyle are positive aspects of the practice. Academic credentials and/or experience are necessary. Recently graduated fellows are encouraged to apply. Board certification is mandatory. Candidates should be particularly interested in patient care, teaching, and research. Salary and benefits are competitive and generous. Tripler is an EO/EEO employer. Please contact Mark F. Hansen, M.D., Col., MC, Chief, Dept. of Radiology, TAMC, HI 96859-5000; (808) 433-6393. 8-7a

#### FACULTY ULTRASOUND RADIOLOGIST, THOMAS JEFFERSON UNIVERSITY HOSPITAL

Jefferson's Dept. of Radiology wishes to recruit a faculty radiologist to work in our division of diagnostic ultrasound. Candidates at all levels will be considered. This division is housed in 1 of the largest and best equipped facilities in the world and is extensively involved in the full range of ultrasound studies including obstetrical, vascular, echocardiography, invasive, endoluminal, and both biliary and kidney stone lithotripsy. A new outpatient ultrasound facility is under construction adjacent to the main campus. The position provides excellent salary and benefits, protected research time each wk, and an opportunity to become associated with 1 of the most academically productive ultrasound groups anywhere. Interested individuals should contact either Barry Goldberg, M.D. (Director of Ultrasound), or David C. Levin, M.D. (Dept. Chairman), at the Dept. of Radiology, Thomas Jefferson University Hospital, Philadelphia, PA 19107. Jefferson is an equal opportunity/affirmative action employer. 2xa

**FULL-TIME BC RADIOLOGIST** needed to staff outpatient women's diagnostic center in suburban Dallas. Experience in mammography and OB/GYN sonography preferred. No call responsibilities. Attractive compensation package. Send CV to Box Y56, *AJR* (see address this section). 2xa

**VASCULAR/INTERVENTIONAL RADIOLOGIST**

Progressive, private-practice group is seeking a second fellowship-trained vascular and interventional radiologist for its expanding interventional radiology service. We are currently performing more than 1000 procedures/yr. We are budgeted for 2 state-of-the-art vascular suites, the first to be installed early in 1991. We will break ground soon on a new imaging center to include 2 MRI and 2 CT (including a cine CT) scanners. We have a noninvasive lab and retain admitting privileges for our interventional service. We are located in Fresno, CA, at Saint Agnes Medical Center. Saint Agnes is a tertiary-referral center for the San Joaquin Valley, and Fresno is one of the fastest growing cities in CA. We are located 90 mi. from Yosemite National Park and less than 2 hr from excellent winter skiing and 2 hr from the coast. We offer 2 yr to full partnership with excellent salary and benefits. Please contact Art Fontaine, M.D., Dept. of Imaging, Saint Agnes Medical Center, 1303 E. Herndon, Fresno, CA 93710; (209) 449-3210. 10-3ap

**SALT LAKE CITY, UT**—Opportunity for board-certified diagnostic radiologist, with recent MRI fellowship training, to join group of 7 board-certified radiologists. Experience in all aspects of general radiology required. Practice includes 2 hospitals, 2 private offices, and a freestanding MRI center. Send letter and CV to Neel E. Bennett, M.D., Medical Director and Chairman, Dept. of Radiology, Holy Cross Hospital, 1050 E. S. Temple, Salt Lake City, UT 84102; (801) 350-4636. 2xa

**DIAGNOSTIC RADIOLOGIST** sought to join a fee-for-service group practice at 2 mid-Bronx hospitals. Board-certification with expertise in imaging and in special procedures/interventional radiology preferred. Please send CV to Arthur Avenue Radiology, P.C., P.O. Box 4332, Great Neck, NY 11027. 10-3ap

**DIAGNOSTIC RADIOLOGIST**—A 4-member radiology group located in beautiful southwestern Montana is currently seeking an additional board-certified/eligible radiologist. Expertise in MRI preferred. Hospital-based and office practice. Excellent school system and outstanding, year-round recreational activities. Approximately 35,000 exams last yr. Hospital is acquiring MRI and updating CT services. One yr to full partnership. Contact Dennis L. Rich, M.D., 300 N. Willson, Bozeman, MT 59715; (406) 587-8631. 10-3ap

**ULTRASOUND/CT/MRI**—Opportunity for a board-certified radiologist specializing in ultrasound, body CT, and body MRI to pursue an academic career at the New York Hospital-Cornell Medical Center. Dept. provides state-of-the-art equipment, including Acuson ultrasound, GE 9800 CT, and GE Signa 1.5-T MR. Wide variety of ultrasound exams include abdominal, OB-GYN, color Doppler, small parts, neonatal head, transvaginal, and transrectal. Prefer candidate with prior fellowship in sectional imaging or ultrasound. Responsibilities include clinical practice, teaching, and research. Position available 7/1/91 or earlier. Please send CV to Elias Kazam, M.D., Dept. of Radiology, The New York Hospital-Cornell Medical Center, 525 E. 68th St., New York, NY 10021. 1-4ap

**RADIOLOGIST**—Full-time; nice, small, well-located North Carolina town. Join active, hospital-based, service-oriented practice. General diagnostic, nuclear medicine, ultrasound, CT, and mobile MRI. No arteriography. Reply with CV to Box 195, AJR (see address this section). 2-4ap

**NORTHERN CALIFORNIA/SAN FRANCISCO BAY AREA**

—The Permanente Medical Group is seeking a BC radiologist with multimodality interests and fellowship training in MR or interventional radiology to join a 10-person group serving a 337-bed acute-care hospital and 2 outpatient clinics. Teaching opportunities are available with residents of subspecialty services on rotation from Stanford University Hospital and our own medical residents. We are currently siting a GE 1.5-T MRI system and installing a new LU arm. Competitive salary and excellent benefits. Please send inquiries and CV to Bruce Baker, M.D., Chief, Dept. of Radiology, Kaiser-Permanente Medical Center, 900 Kiely Blvd., Santa Clara, CA 95051; (408) 236-4444. EOE. 2-4a

**DENVER, CO**—Group of 8 diagnostic radiologists engaged in a predominantly hospital-based practice is seeking a new member on or about 10-1-90. The group provides diagnostic imaging services for a 565-bed, tertiary-care teaching hospital. The new member should be trained in diagnostic radiology and have fellowship training, and/or additional experience beyond residency level, in nuclear medicine. The new member will be primarily responsible for nuclear medicine but must be willing to participate in other modalities of diagnostic imaging. Salary, benefits, vacation time, and time to partnership are all competitive for the Rocky Mountain region. Interested parties should send their CV to Steve A. Holt, M.D., Western Radiologists, P.C., 3665 Cherry Creek Dr., N., Ste. 350, Denver, CO 80209. 2-4ap

**Fellowships and Residencies**

**DUKE UNIVERSITY MEDICAL CENTER FELLOWSHIP POSITIONS**—Duke University Medical Center is seeking qualified candidates for fellowship positions in the Dept. of Diagnostic Radiology. Currently there are positions available in the following areas: chest, musculoskeletal, and vascular/interventional radiology, ultrasound, advanced diagnostic imaging, MRI, neuroradiology, abdominal imaging, mammography, and research fellowships. The radiology dept. is state-of-the-art in diagnostic imaging with diverse resources available for clinical, teaching, and academic pursuits. Fellowship training is generally organized by organ systems, although experience can be individualized to accommodate special interests. Salary and benefits are competitive and academic time is guaranteed. For additional information, please phone Richard Leder, M.D. at (919) 681-2711 ext. 5310. Applications are due Feb. 1 of the preceding yr and can be obtained by writing to N. Reed Dunnick, M.D., Dept. of Radiology, Duke University Medical Center, Erwin Rd., Box 3808, Durham, NC 27710. AA/EOE. 2-7c

**FELLOWSHIP POSITIONS**—The University of Texas, M. D. Anderson Cancer Center, Dept. of Diagnostic Radiology, is currently accepting applications for fellowships in different subspecialties in diagnostic imaging, including oncologic radiology, body imaging, and vascular/interventional radiology for the academic yr 1992. The dept. is equipped with state-of-the-art ultrasonography, CT, MRI, PET, angiography, routine fluoroscopy, radiography, and mammography. Candidates interested in these positions should write to Chusilp Charnsangavej, M.D., Professor and Deputy Chairman for Academic Affairs, Dept. of Diagnostic Radiology, Box 57, University of Texas M. D. Anderson Cancer Center, 1515 Holcombe Blvd., Houston, TX 77030. An employer equal opportunity affirmation action. 2-4c

**FELLOWSHIP IN ULTRASOUND AND BODY CT-MRI**

—Unexpected position available July 1, 1991. A 1-yr body imaging fellowship at the Dept. of Radiology, University of Rochester Medical Center, a 750-bed, tertiary-care hospital. State-of-the-art equipment is available, including a free-standing MR center. Applicants must have completed an approved residency in diagnostic radiology and must be board-eligible or certified. For inquiries, please contact Deborah J. Rubens, M.D., Dept. of Radiology, Box 648, University of Rochester Medical Center, Rochester, NY 14642; (716) 275-8365. EO/AA/M-F employer. 2-4c

**FELLOWSHIP POSITIONS**—The Dept. of Radiology and Radiological Sciences of Vanderbilt University School of Medicine has 1-yr fellowship positions for 1991-92 in the following areas: musculoskeletal (2), ultrasound (1), and angiography (1). Research opportunities are available and encouraged. Candidates must be board-certified or board-qualified in diagnostic radiology, and obtain a Tennessee medical license. Address inquiries and CV to Martin P. Sandler, M.D., Director, Fellowship Committee, Dept. of Radiology, Medical Center North, Vanderbilt University, Nashville, TN 37232-2675. An equal opportunity/affirmative action employer. 2-3c

**WINTHROP FELLOWSHIP IN ABDOMINAL IMAGING**

—The Cleveland Clinic Foundation is offering 2 fellowship positions, each encompassing 1-yr of advanced training in body CT, ultrasound, and body MR, beginning July 1, 1992. One of these positions is supported by the Winthrop Corporation in order to advance expertise and research in the field of abdominal imaging. The Cleveland Clinic Foundation is a 1000-bed, tertiary-care hospital, with an international referral source, and a large outpatient population. The fellowship positions allow subspecialty training on state-of-the-art equipment, including ultrasound and CT-guided interventional procedures. Please submit CV and 2 letters of reference to David M. Paushter, M.D., Head, Section of Abdominal Imaging, Hospital Radiology, Cleveland Clinic Foundation, One Clinic Center Dr., Cleveland, OH 44195-5103. 2-3cp

**FELLOWSHIP IN GENERAL RADIOLOGY/MAMMOGRAPHY 1991**

—A fellowship is being offered in the Dept. of Radiology of the New England Medical Center Hospitals, Tufts University School of Medicine. This yr, the fellowship will provide experience in general radiology with a special emphasis on breast and GI radiology. The breast imaging portion of the fellowship includes training in all aspects of mammographic interpretation, breast ultrasound, and percutaneous needle localization for nonpalpable breast lesions. The dept. has 2 Senographe Units, an automated breast ultrasound scanner, and a small parts scanner. There will be involvement with the multidisciplinary Breast Health Center, which serves as a regional referral center as well as a resource for second opinions. Weekly conferences with the other disciplines involved in breast care, including surgery, hematology-oncology, radiation therapy, and pathology, guarantee close clinical-radiographic-pathologic correlation. Participation in clinical research will be available. The rotation through GI radiology will provide training in the performance and interpretation of double-contrast upper GI series and barium enema studies. Responsibility will include all areas of GI radiology. Attendance at a weekly GI-Radiology Correlative Conference is an integral part of the program. There will be opportunity for participation in clinical investigative projects. For further information, please contact Marc J. Homer, M.D., at (617) 956-0045. 2-3cp

**FELLOWSHIP IN ULTRASOUND / CT / ANGIO / INTERVENTIONAL**—A 1-yr fellowship program available beginning July 1992 at Lehigh Valley Hospital Center in Allentown, PA. LVHC is a 492-bed, acute-care, university-affiliated hospital. The fellowship program offers training in CT (head and body), ultrasound, angiography (neuro and visceral), and interventional radiography. MRI experience is also available. For further information, contact Robert Kricun, M.D., Dept. of Radiology, Lehigh Valley Hospital Center, P.O. Box 689, Allentown, PA 18105. 2-7c

**THE RADIOLOGY DEPT. AT NEW ENGLAND MEDICAL CENTER** (the major teaching hospital of Tufts University School of Medicine) has added a body imaging fellowship position available as of July 1, 1991. The fellowship program consists of 6 mo of CT, 4 mo of MRI (including neuro MRI), and 2 mo of ultrasound. Candidates must have completed an accredited diagnostic radiology residency program and be eligible for temporary licensure in Massachusetts. The radiology dept. is very active, providing a broad experience in CT, ultrasound, and MRI. Please send CV and/or contact Mark Bankoff, M.D., New England Medical Center, Box 180, 750 Washington St., Boston, MA 02111; (617) 956-0043. 2cp

**BODY IMAGING FELLOWSHIP JULY 1991**—The Dept. of Radiology at the University of Pittsburgh Medical Center has expanded the body imaging fellowship program, resulting in an available position beginning July 1991. Training is provided in all aspects of CT/MRI/ultrasound, with access to 9 GE 9800 CT Scanners, 5 1.5-T GE Signa MRI Scanners, and 8 state-of-the-art ultrasound machines providing body and OB-GYN imaging. Research time will be provided. Applicants must have completed an approved residency program in diagnostic radiology and be board-eligible/certified. For further information, contact Richard L. Baron, M.D., Dept. of Radiology, Presbyterian-University Hospital, DeSoto at O'Hara Sts., Pittsburgh, PA 15213; (412) 647-7886. The University of Pittsburgh is an equal opportunity/affirmative action program. 2c

**IMMEDIATE UNEXPECTED OPENING FOR RESIDENCY IN DIAGNOSTIC RADIOLOGY, PRESBYTERIAN MEDICAL CENTER OF PHILADELPHIA**—Sudden resignation from our program at the 2nd-yr level leaves us with an opening starting Feb. 1, 1991. The required start date is between Feb. 1 and July 1, 1991. The program includes intensive exposure to all modalities, a rich conference schedule, opportunities for and encouragement of clinical research and publication. Full approval of the applicant's current program is required. Send CV, and phone David B. Freiman, M.D., Dept. of Medical Imaging, Presbyterian Medical Center of Philadelphia, 39th & Market Sts., Philadelphia, PA 19104; (215) 662-9138. 2-3cp

**INTEGRATED CHEST RADIOLOGY FELLOWSHIP AT JOHNS HOPKINS UNIVERSITY HOSPITAL**—The Dept. of Radiology, Division of Thoracic Imaging, Johns Hopkins University is offering a 1- to 2-yr academically oriented fellowship in chest radiology. The fellowship offers an integrated experience in cross-sectional imaging, including over 4000 chest CT and 1000 thoracic MRI exams/yr. Strong research interests in high-resolution CT, MRI, digital imaging methods, and interventional thoracic radiology offer the candidate an exciting environment to work in. The fellowship is available starting July 1, 1991. Contact Elias A. Zerhouni, M.D., Director of Thoracic Imaging and MRI, Dept. of Radiology, Johns Hopkins Hospital, Baltimore, MD 21205; (301) 955-4062. 1-6c

**UNIVERSITY OF WASHINGTON FELLOWSHIP IN DIAGNOSTIC IMAGING SCIENCES**—The Diagnostic Imaging Sciences Center of the Dept. of Radiology at the University of Washington in Seattle is recruiting for 2 fellowship positions in radiology science research. The research fellowship program is funded by NCI Training Grant T32 CA 096552 and combines a 2-yr, fully funded, laboratory-based, educational and research program with a guaranteed clinical fellowship after successful completion of the radiology science program. Candidates should have successfully completed 2 or 3 yr of a diagnostic radiology residency and must have a strong interest and commitment to a career in academic radiology. The research fellowship program will combine academic courses and a thesis project that will lead to a masters degree in biomedical imaging at the University of Washington. A portion of each fellow's time will be spent in clinical subspecialty radiology training to keep the fellows clinically astute and to provide additional clinical experience. The Radiology Imaging Research Laboratory at the University of Washington consists of over 20,000 sq. ft. of dedicated research and includes more than 25 full-time scientists, state-of-the-art equipment in MRI, NMR spectroscopy, PET, SPECT, DIN/PACS, angiography, ultrasound, and image processing. Four MRI instruments, including a GE Signa system, are dedicated to research use. Candidates interested in the Radiology Research Sciences Program should contact James A. Nelson, M.D., Dept. of Radiology, SB-05, University of Washington, Seattle, WA 98195; (206) 543-3757. The University of Washington is an equal opportunity employer. 1-2c

**FELLOWSHIP IN ABDOMINAL IMAGING AND INTERVENTIONS**—The Dept. of Radiology, Massachusetts General Hospital and Harvard Medical School, offers a 2-yr fellowship in abdominal imaging and interventions beginning July 1, 1992. Training covers all aspects of abdominal imaging (radiography, fluoroscopy, ultrasound, CT, and MR) and nonvascular interventions in the GI and GU tracts. Research is active and participation is encouraged. Candidates should be ABR-eligible or certified. Address inquiries to Peter R. Mueller, M.D. or Nicholas Papanicolaou, M.D., Dept. of Radiology, Massachusetts General Hospital, Boston, MA 02114. An equal opportunity employer. 1-3cp

**NEURORADIOLOGY FELLOWSHIP**—The Dept. of Radiology, Strong Memorial Hospital, University of Rochester School of Medicine and Dentistry offers a 1- or 2-yr neuroradiology fellowship to begin July 1, 1991. Training is offered in MRI, CT, and special procedures, with the opportunity to perform both pediatric and carotid ultrasound. Assistance in teaching of medical students and residents is expected. Additional training in maxillofacial, dental, and ENT radiology also is available, as is the opportunity to perform both clinical and laboratory research. A very strong neuroscience community exists. The dept. consists of 25 radiologist faculty, 16 residents, and 3-5 fellows. State-of-the-art equipment is available in all modalities including new single and biplane angiographic systems, 3 third-generation CT, a 1.5-T MRI, and a midfield MR. Strong Memorial Hospital is a 750-bed, tertiary-care hospital with 100 beds dedicated to pediatric diseases. Candidates must have completed an accredited diagnostic radiology residency program, be board-certified or eligible, and have a New York state medical license by July 1, 1991. Send inquiries to Robert E. O'Mara, M.D., Box 648, University of Rochester Medical Center, Rochester, NY 14642; (716) 275-2733. EO/AA/M-F employer. 1-6c

**PEDIATRIC RADIOLOGY FELLOWSHIP**—The Dept. of Radiology at Children's Hospital of Philadelphia (CHOP) offers a 1- or 2-yr pediatric radiology fellowship beginning July 1, 1992. A 1-yr pediatric neuroradiology fellowship program is also offered and may be taken separately or in combination with a second yr adult neuroradiology fellowship at Jefferson University Medical Center in Philadelphia. A special (1-yr) cross-sectional imaging (CT, ultrasound, and MRI) fellowship may be arranged. CHOP is a 294-bed pediatric hospital affiliated with the University of Pennsylvania. Radiology has an attending faculty of 11 and performs 90,000 cases/yr (plain films, fluoroscopy, ultrasound, CT, nuclear medicine, neuroradiology, angiography/interventional radiology, and MRI). Our equipment is state-of-the-art and new since 1988 and includes ATL ultrasound equipment with duplex and color flow Doppler; gamma camera with SPECT; a high-resolution fast Siemens Somatom Plus CT scanner; and a 1.5-T Siemens Magnetom MRI installation with spectroscopy. A pediatric outpatient radiology facility has recently opened. We have an active teaching program for radiology residents and fellows. The patient population is large and varied, from routine emergencies to complicated tertiary care problems. The fellowship provides not only a broad clinical experience with subspecialty training, but offers opportunities for clinical and basic research and scholarship. Applicants must have completed a diagnostic radiology residency, be board-certified or eligible, and be able to obtain a Pennsylvania medical license. Salary and fringe benefits are highly competitive. Address inquiries to Sandra S. Kramer, M.D., Dept. of Radiology, The Children's Hospital of Philadelphia, 34th St. and Civic Center Blvd., Philadelphia, PA 19104; (215) 590-2575. The Children's Hospital of Philadelphia and the University of Pennsylvania are equal opportunity/affirmative action employers. 1-3cp

**DUKE UNIVERSITY, DEPT. OF RADIOLOGY** offers 1- or 2-yr fellowship positions in chest radiology, neuroradiology, vascular/interventional radiology, musculoskeletal radiology, CT, ultrasound, MRI, abdominal imaging, mammography, pediatric radiology, and nuclear medicine beginning July 1991. The dept. runs an active clinical service with top quality equipment including 5 GE 9800 Quick CT scanners, 3 GE 1.5-T MRI units, and 4 fully equipped vascular/interventional laboratories. In addition to their clinical responsibilities, fellows are provided academic time to pursue investigational interests. Applications are due March 1, 1991, and interviews will be scheduled in the spring. For further information and application material, please contact Ms. Debbie Sykes at the Dept. of Radiology, Box 3808, Duke University Medical Center, Durham, NC 27710; (919) 660-2711, ext. 5228. Duke University is an equal opportunity/affirmative action employer. 12-2c

**VASCULAR / INTERVENTIONAL RADIOLOGY FELLOWSHIP, ST. LOUIS VASCULAR INSTITUTE AT THE CHRISTIAN HOSPITAL, ST. LOUIS, MO**—A 1- to 2-yr fellowship in vascular and interventional radiology is offered beginning July 1, 1991. Training includes all aspects of diagnostic angiography and vascular and non-vascular interventional techniques. Candidates must have completed a diagnostic radiology residency in an accredited training program, must be certified by or eligible for certification by the ABR, and must be able to obtain a Missouri license. Direct inquiries to Saadoon Kadir, M.D., Dept. of Radiology, Christian Hospital Northeast, 11133 Dunn Rd., Ste. 1017, St. Louis, MO 63136. 11-4cp



**THE DEPT. OF RADIOLOGY, UNIVERSITY OF ARKANSAS FOR MEDICAL SCIENCES, LITTLE ROCK, AR**, has openings for fellowships to begin July 1991. Positions are available in body imaging/intervention, neuroradiology, vascular and interventional radiology, and pediatric radiology. Interested candidates should contact these program directors: imaging/intervention - Teresita L. Angtuaco, M.D., or Steven K. Teplick, M.D.; neuroradiology - Edgardo A. Angtuaco, M.D.; vascular and interventional radiology - Timothy C. McCowan, M.D.; pediatric radiology - Joanna J. Seibert, M.D. All program directors listed above can be contacted at the Dept. of Radiology, University of Arkansas for Medical Sciences, Slot 556, 4301 W. Markham St., Little Rock, AR 72205; (501) 686-5740. 2c

**FELLOWSHIP IN ULTRASOUND AND BODY CT/MRI**—July 1, 1992, to June 30, 1993, at the New York Hospital-Cornell Medical Center. Dept. provides state-of-the-art equipment including Acuson ultrasound, GE 9800 CT, and GE Signa 1.5-T MR. Wide variety of ultrasound exams include abdominal, OB-GYN, color Doppler, small parts, neonatal head, transvaginal, and transrectal. Applicant should be ABR eligible or certified. Send CV to Elias Kazam, M.D., Dept. of Radiology, The New York Hospital-Cornell Medical Center, 525 E. 68th St., New York, NY 10021. 1-4cp

**WOMEN'S IMAGING FELLOWSHIP**—A 1- or 2-yr comprehensive experience in women's imaging modalities is offered in Tucson, AZ. Procedures in which we expect the fellow to gain expertise include high-volume, low-cost screening mammography and its associated administrative, financial, and epidemiological aspects; problem-solving diagnostic mammography, including invasive mammographic procedures (e.g., stereotactic guided cytology and galactography); high-volume obstetric and gynecologic sonography. Annual stipend is \$50,000. Contact Arizona State Radiology, 7250 E. Ventana Canyon Dr., Tucson, AZ 85715; (602) 620-4911. 10-3cp

**FELLOWSHIPS AT THOMAS JEFFERSON UNIVERSITY HOSPITAL**—The Dept. of Radiology at Thomas Jefferson University Hospital in Philadelphia offers the following fellowship programs each yr. Ultrasound/CT/MRI — Jefferson's ultrasound division is 1 of the largest in the world and performs all currently available exams including obstetric, vascular, lithotripsy, invasive, and endoluminal. We also operate 4 GE 1.5-T MRI units and 3 CT scanners. Contact Barry Goldberg, M.D., regarding this program. Cardiovascular/interventional — this division is housed in a new suite containing Philips angio units with DSA and performs the full range of vascular and non-vascular interventional procedures. Contact Geoffrey Gardiner, Jr., M.D. Neuro/ENT radiology — very active clinical services supply a wealth of material to this division, which is housed in a neurosciences imaging center containing all imaging modalities. Contact Carlos Gonzalez, M.D. Breast imaging — Jefferson's new breast imaging center performs approximately 85 studies/day including ultrasound and needle localizations. Contact Stephen Feig, M.D. Chest — includes biopsies and CT. Contact Robert Steiner, M.D. MRI — a dedicated body MRI program including excellent research opportunities in addition to a large clinical case load. Contact Matthew Rifkin, M.D. Ultrasound — a dedicated ultrasound program. Contact Barry Goldberg, M.D. Musculoskeletal — includes MRI of the musculoskeletal system. Contact David Karasick, M.D. All program directors listed above can be contacted at the Dept. of Radiology, Thomas Jefferson University Hospital, Philadelphia, PA 19107. Jefferson is an equal opportunity/affirmative action employer. 2xc

**ABDOMINAL IMAGING FELLOWSHIP** — The Dept. of Radiology at the University of Florida is offering 1-yr fellowships in abdominal imaging beginning July 1, 1991, and July 1, 1992. Minimum requirements include successful completion of an accredited radiology residency. The fellowship includes training in all aspects of abdominal imaging (gastrointestinal and genitourinary radiology, CT, ultrasound, and MRI) by a 3-person subspecialty faculty. The program offers full clinical experience and research opportunities. Applicants must be eligible to obtain a license in the state of Florida. For additional information, contact Pablo R. Ros, M.D., Professor, Dept. of Radiology, Box J-374, Gainesville, FL 32610-0374; (904) 395-0288. The University of Florida is an equal opportunity/affirmative action employer and encourages applications from women and minorities. 10-6c

**Tutorials/Courses**

**ALASKA 91/CRUISE THE INLAND PASSAGE** MRI at sea, July 6-13, 1991. For information, contact Medical Seminars International, Inc., 18981 Ventura Blvd., Ste. 303, Tarzana, CA 91356; (818) 774-9077, fax (818) 774-0244. 1-5d

**NINTH WINTER DIAGNOSTIC IMAGING CONGRESS, VAL D'ISERE, FRANCE** — March 2-9, 1991. MRI, CT, ultrasound. Medical Seminars International, 18981 Ventura Blvd., #303, Tarzana, CA 91356; (818) 700-9821. 10-2d

**Other**

**VISITING PROFESSORSHIPS, THOMAS JEFFERSON UNIVERSITY HOSPITAL**—The Dept. of Radiology at Thomas Jefferson University Hospital in Philadelphia is offering visiting professorships over the next several yr, while some of our faculty members are on sabbatical leave. These positions can have either a 6-mo or 1-yr term. In particular, we are seeking candidates with expertise in either ultrasound or general diagnostic radiology, but emphasis in other areas may be acceptable as well. Funding for these positions is appropriate for a senior faculty member from another institution on sabbatical with partial funding of his/her own, or for a junior faculty member. These positions are also open to highly qualified foreign radiologists with current academic appointments at prestigious foreign medical schools. Visiting faculty members will do some clinical work in our dept. and also have access, for research or educational purposes, to state-of-the-art imaging modalities of all types, as well as well-equipped physics and physiology research laboratories. Interested persons should contact David C. Levin, M.D., Chairman, Dept. of Radiology, Thomas Jefferson University Hospital, Philadelphia, PA 19107. Jefferson is an equal opportunity/affirmative action employer. 2xc

**AJR Classified Advertisements Information**

**Box Responses and Address for Ad Placement**

Write Box \_\_\_\_\_, *AJR*, 2223 Avenida de la Playa, Suite 103, La Jolla, CA 92037-3218; Telephone: (619) 459-2229; FAX: (619) 459-8814.

**How to Place an Ad**

*AJR* accepts classified advertising for Positions Available, Positions Desired, Fellowships and Residencies, and Tutorials/Courses. Ads are accepted by mail or FAX.

**Rates:** \$6.00/line with a \$30 minimum charge. Box service is \$10 additional for each month the ad appears. There are discounts for multiple insertions: 10% for 2-3 insertions; 20% for 4 or more. To estimate lines, count all words and divide by 7.

**Billing:** Ads *must* be prepaid, or advertisers will be billed after the ad appears *providing* a purchase order number is submitted with the advertising copy. Terms are net 30 days.

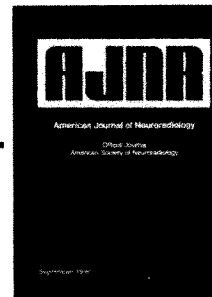
**Deadlines:** 6 weeks prior to issue date. For specific deadlines, telephone the *AJR* editorial office.

**Estimating Ad Charges**

Line charge: divide total words by 7 and multiply by \$6.00 . . . . .	\$
Multiple insertions? If so, multiply by number . . . . .	×
Subtotal . . . . .	\$
Discount applies to two or more insertions. Subtract 10% if ad appears 2-3 months; 20% if 4 months or more . . . . .	-
Subtotal . . . . .	\$
Box response requested? If so, multiply number of months by \$10.00 . . . . .	+
Approximate advertising charge . . . . .	\$

# Increase your expertise in evaluating CNS lesions

## AJNR American Journal of Neuroradiology



Editor: **Michael S. Huckman, MD**, Rush-Presbyterian-St. Luke Medical Center

Outstanding clinical papers on every aspect of CNS imaging, including spinal diagnosis...informed coverage of head and neck radiology...clear, readable CTs, angiographs, MR imaging and ultrasound studies. These are the features you demand of a quality professional journal. You'll find them in every issue of **AJNR: American Journal of Neuroradiology**.

As you are called upon to perform and interpret more and more sophisticated diagnostic tests — from myelography to CT to newborn ultrasound studies — you need a comprehensive, reliable journal that can keep you abreast of all the latest developments. Each bimonthly issue of **AJNR** brings you timely, clinically pertinent information, as well as important clinical research presented with an eye toward immediate practical application.

Here's a brief sampling of the variety of articles you'll find in **AJNR**:

The Anatomic Basis of Vertebrogenic Pain and the Autonomic Syndrome Associated with Lumbar Disk Extrusion. *Jenkins JR, Whittemore AT, Bradley WG*

MR Imaging Determination of the Location of the Normal Conus Medullaris Throughout Childhood. *Wilson DA, Prince JR*

Closed Spinal Dysraphism: Analysis of Clinical, Radiological, and Surgical Findings in 104 Consecutive Patients. *Scatliff JH, Kendall BE, Kingsley DPE, Britton J, Grant DN, Hayward RD*

Alzheimer's Disease: Longitudinal CT Studies of Ventricular Change. *de Leon MJ, George AE, Reisberg B, et al*

Congenital Absence of the Cervical and Petrous Internal Carotid Artery with Intercavernous Anastomosis. *Quint DJ, Boulos RS, Spera TD*

### Bimonthly

**Personal** \$133/yr **Institutions** \$160/yr

**In-training** \$65/yr

(add \$45.00 outside the US; in Canada, also add 7% GST.)



ORDER FREE BY PHONE. Just call  
**1-800-638-6423** from anywhere in the US  
or Canada.

or clip and return coupon to:



**Williams & Wilkins**

P.O. Box 23291 Baltimore, Maryland 21203-9990

## Subscribe to AJNR for 3 years and SAVE

Avoid future rate increases and ensure uninterrupted service by placing a multi-year subscription at current rates.

☐ 3 yrs ☐ 2 yrs ☐ 1 yr

☐ **Personal** \$133 ☐ **Institutions** \$160 ☐ **In-training\*** \$65  
(add \$45.00 outside the US; in Canada, also add 7% GST.)

☐ Also send me the **1991 Bound Volume** at \$87.00 (\$102.00 outside the US; in Canada, also add 7% GST). \$2.00 discount for orders placed before October 31, 1991 and for prepaid orders. I understand that the bound volume is *in addition* to my regular subscription and is available only to subscribers. (To be shipped in early 1992. Bound volumes for years prior to 1991 are unavailable.) *All bound volume orders must be received by December 31, 1991.*

☐ Check enclosed (payable to Williams & Wilkins) ☐ Bill me  
☐ VISA ☐ MasterCard ☐ American Express

printed in USA

AJNR 52705

Card # \_\_\_\_\_ Exp. \_\_\_\_\_

Signature/P.O. # \_\_\_\_\_

Name \_\_\_\_\_

Address \_\_\_\_\_

City/State/Zip \_\_\_\_\_

MD residents, please add 5% sales tax. Subscription orders from outside the US must be prepaid in US dollars only. Rates valid through October 31, 1991.

\*Residents, Fellows, Interns, and Students: when applying for the in-training rate, available for 3 years, please specify name of institution and training status:

Please allow 8 weeks for order processing and delivery of your first issue. Surface mail delivery to countries outside the US may take up to 16 weeks. Airmail rates available upon request.

J1043S01

**New look.  
New shape.**

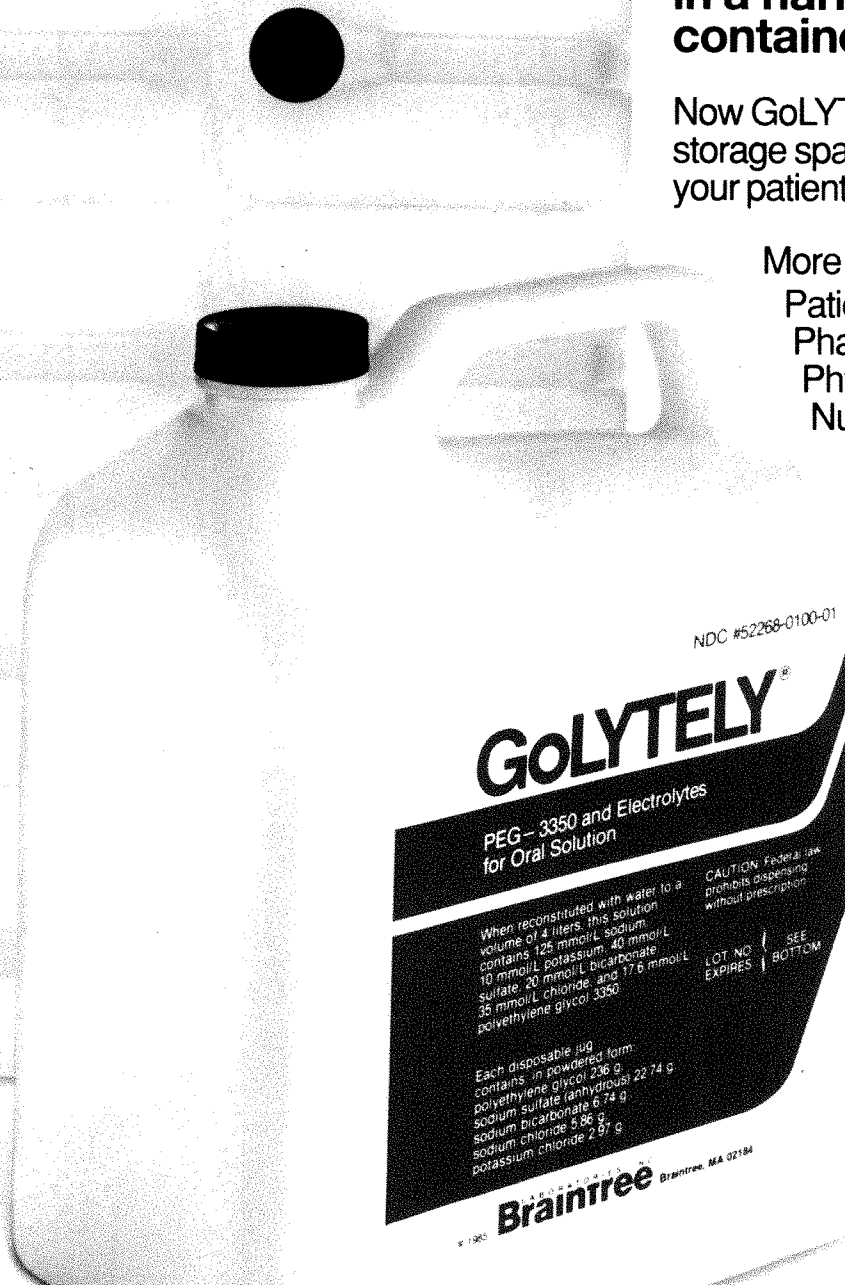
**GoLYTELY<sup>®</sup>**

PEG-3350 and Electrolytes for Oral Solution

**The name that started  
a revolution now comes  
in a narrow, stackable  
container.**

Now GoLYTELY takes up less  
storage space and less space in  
your patient's refrigerator.

More convenient for  
Patients  
Pharmacists  
Physicians  
Nurses



**New look.  
New shape.  
GoLYTELY.**

Made by Lyne Laboratories, Stoughton, MA  
02072, for BRAINTREE LABORATORIES, INC.,  
P.O. Box 361, Braintree, MA 02184.

**Braintree** LABORATORIES, INC.

© 1989 BRAINTREE LABORATORIES, INC.  
TRE-1039



## BENJAMIN FELSON LECTURE

- 225 Chronic interstitial lung disease of unknown cause: a new classification based on pathogenesis. *Hogg JC*

## REVIEW ARTICLES

- 235 Advances in contrast-enhanced MR imaging. *Saini S, Modic MT, Hamm B, Hahn PF*  
 255 The changing epidemiology of tuberculosis and other mycobacterial infections in the United States: implications for the radiologist. *Buckner CB, Leithiser RE, Walker CW, Allison JW*

## CHEST RADIOLOGY

- 265 Value of sonography in monitoring the therapeutic response of mediastinal lymphoma: comparison with chest radiography and CT. *Wernecke K, Vassallo P, Hoffmann G, et al*  
 273 Value of CT in determining the need for angiography when findings of mediastinal hemorrhage on chest radiographs are equivocal. *Richardson P, Mirvis SE, Scorpio R, Dunham CM*  
 281 Pathogenesis of pulmonary edema during interleukin-2 therapy: correlation of chest radiographic and clinical findings in 54 patients. *Saxon RR, Klein JS, Bar MH, et al*

## BREAST RADIOLOGY

- 287 Pictorial essay. Abnormalities of the breast caused by biopsy: spectrum of mammographic findings. *Stigers KB, King JG, Davey DD, Stelling CB*

## GASTROINTESTINAL RADIOLOGY

- 293 Videofluoroscopy in elderly patients with aspiration: importance of evaluating both oral and pharyngeal stages of deglutition. *Feinberg MJ, Ekberg O*  
 297 Carcinoma of the esophagus: CT vs MR imaging in determining resectability. *Takashima S, Takeuchi N, Shiozaki H, et al*  
 303 Expert advice. Radiologic detection of colonic neoplasms: benefits of a systems-analysis approach. *Gelfand DW, Chen YM, Ott DJ*  
 307 Fatty infiltration of the liver: quantification with phase-contrast MR imaging at 1.5 T vs biopsy. *Levenson H, Greensite F, Hoefs J, et al*  
 313 Periportal contrast enhancement on CT scans of the liver. *Hammerman AM, Kotner LM Jr, Doyle TB*  
 317 Focal nodular hyperplasia of the liver: MR findings in 35 proved cases. *Lee MJ, Saini S, Hamm B, Taupitz M, Hahn PF, Ferrucci JT*  
 321 Self-expandable stainless steel endoprosthesis for treatment of malignant bile duct obstruction. *Adam A, Chetty N, Roddie M, Yeung E, Benjamin IS*  
 327 Pictorial essay. Choledochal cysts: classification and cholangiographic appearance. *Savader SJ, Benenati JF, Venbrux AC, et al*

## MUSCULOSKELETAL RADIOLOGY

- 333 MR of the knee: the significance of high signal in the meniscus that does not clearly extend to the surface. *Kaplan PA, Nelson NL, Garvin KL, Brown DE*  
 337 Pictorial essay. MR imaging of synovial sarcoma. *Morton MJ, Berquist TH, McLeod RA, Unni KK, Sim FH*  
 341 Case report. Fournier gangrene caused by a perforated retroperitoneal appendix: CT demonstration. *Gaeta M, Volta S, Minutoli A, Bartiromo G, Pandolfo I*  
 343 Technical note. Two-piece wrist surface coil. *Totterman SM, Heberger R, Miller R, Rubens DJ, Blebea JS*

## FETAL AND PEDIATRIC RADIOLOGY

- 345 Comparison of iohexol with barium in gastrointestinal studies of infants and children. *Cohen MD, Towbin R, Baker S, et al*  
 351 Calcification of the ligamentum arteriosum in children: a normal finding on CT. *Bisceglia M, Donaldson JS*  
 353 Pictorial essay. Radiologic evaluation of limb-lengthening procedures. *Walker CW, Aronson J, Kaplan PA, Molpus WM, Seibert JJ*  
 359 Unilateral hydrocephalus: prenatal sonographic diagnosis. *Patten RM, Mack LA, Finberg HJ*  
 365 Case report. Occult ectopic ureter in girls with urinary incontinence: diagnosis by using CT. *Braverman RM, Lebowitz RL*  
 367 Technical note. Limited-slice CT in the evaluation of paranasal sinus disease in children. *Gross GW, McGeady SJ, Kerut T, Ehrlich SM*  
 371 Technical note. CT measurement of the tracheal lumen in children and adolescents. *Griscom NT*

## NEURORADIOLOGY

- 373 Intracranial vascular abnormalities: value of MR phase imaging to distinguish thrombus from flowing blood. *Nadel L, Braun IF, Kraft KA, Fatouros PP, Laine FJ*  
 381 Paranasal sinuses on MR images of the brain: significance of mucosal thickening. *Rak KM, Newell JD II, Yakes WF, Damiano MA, Luetheke JM*

## ANGIOGRAPHY

- 385 Angiography is useful in detecting the source of chronic gastrointestinal bleeding of obscure origin. *Rollins ES, Picus D, Hicks ME, Darcy MD, Bower BL, Kleinhoffer MA*  
 389 Iliac artery stenosis or obstruction after unsuccessful balloon angioplasty: treatment with a self-expandable stent. *Günther RW, Vorwerk D, Antonucci F, et al*  
 395 Technical note. CT analysis of a safe approach for translumbar access to the aorta and inferior vena cava. *Cazenave FL, Glass-Royal MC, Teitelbaum GP, Zuurbier R, Zeman RK, Silverman PM*

## TECHNICAL NOTES

- 397 A new percutaneous access set for interventional procedures. *McLellan GL*  
 401 Improved needle-tip visualization by color Doppler sonography. *Hamper UM, Savader BL, Sheth S*

## OTHER CONTENT

- Book reviews 234, 280, 286, 316, 326, 332, 364, 394  
 302 ARRS 1991 resident award papers information  
 400 Memorial, Hyman R. Senturia  
 403 Letters  
 409 Review of current literature  
 414 Forthcoming articles  
 415 News  
 419 Invitation to the 1991 ARRS meeting  
 421 1991 ARRS meeting summary  
 423 1991 ARRS meeting courses and symposium  
 425 1991 ARRS meeting local activities  
 428 American Roentgen Ray Society information  
 429 1991 ARRS meeting registration forms  
 432 ARRS membership information and application  
 435 Classified advertisements  
 A8 AJR business and subscriber information  
 A16 Guidelines for authors